

Spatial Tessellations

Second Edition

WILEY SERIES IN PROBABILITY AND STATISTICS

Established by WALTER A. SHEWHART and SAMUEL S. WILKS

Editors: *Vic Barnett, Noel A. C. Cressie, Nicholas I. Fisher,
Iain M. Johnstone, J. B. Kadane, David G. Kendall, David W. Scott,
Bernard W. Silverman, Adrian F. M. Smith, Jozef L. Teugels,*
Editors Emeritus: *Ralph A. Bradley, J. Stuart Hunter*

A complete list of the titles in this series appears at the end of this volume

Spatial Tessellations: Concepts and Applications of Voronoi Diagrams

Second Edition

ATSUYUKI OKABE

University of Tokyo, Japan

BARRY BOOTS

Wilfrid Laurier University, Ontario, Canada

KOKICHI SUGIHARA

University of Tokyo, Japan

SUNG NOK CHIU

Hong Kong Baptist University, China

With a Foreword by

D.G. KENDALL

JOHN WILEY & SONS, LTD

Chichester • New York • Weinheim • Brisbane • Singapore • Toronto

Copyright © 1992, 2000 by John Wiley & Sons Ltd
Baffins Lane, Chichester,
West Sussex, PO19 1UD, England

National 01243 779777
International (+44) 1243 779777

e-mail (for orders and customer enquiries): cs-books@wiley.co.uk

Visit our Home Page on <http://www.wiley.co.uk> or <http://www.wiley.com>

All rights reserved. No part of this publication may be reproduced, stored in a retrieval system, or transmitted, in any form or by any means, electronic, mechanical, photocopying, recording, scanning or otherwise, except under the terms of the Copyright, Designs and Patents Act 1988 or under the terms of a licence issued by the Copyright Licensing Agency, 90 Tottenham Court Road, London W1P 9HE, UK, without the permission in writing of the Publisher.

Other Wiley Editorial Offices

John Wiley & Sons Inc., 605 Third Avenue,
New York, NY 10158-0012, USA

Wiley-VCH Verlag GmbH, Pappelallee 3,
D-69469 Weinheim Germany

Jacaranda Wiley Ltd, 33 Park Road, Milton,
Queensland 4064, Australia

John Wiley & Sons (Asia) Pte Ltd, 2 Clementi Loop #02-01,
Jin Xing Distripark, Singapore 129809

John Wiley & Sons (Canada) Ltd, 22 Worcester Road,
Rexdale, Ontario, M9W 1L1, Canada

Library of Congress Cataloguing-in-Publication Data

Okabe, Atsuyuki, 1945-

Spatial tessellations: concepts and applications of Voronoi
diagrams / Atsuyuki Okabe . . . [et al.] ; with a foreword by D.G. Kendall — 2nd ed.

p. cm. — (Wiley series in probability and statistics)

Includes bibliographical references and index.

ISBN 0-471-98635-6 (alk. paper)

1. Voronoi polygons. 2. Spatial analysis (Statistics). 3. Geometry—Data processing.

I. Title. II. Series.

QA278.2.036 1999

519.5'36—dc21

99-13149

CIP

British Library Cataloguing in Publication Data

A catalogue record for this book is available from the British Library

ISBN 0-471-98635-6

Typeset in 10/12pt Times by Florence Production Ltd, Stoodleigh, Devon

Contents

Foreword to the First Edition	xi
Preface to the Second Edition	xiii
Acknowledgements (First Edition)	xv
Acknowledgements (Second Edition)	xvi
Chapter 1 Introduction	1
1.1 Outline	3
1.2 History of the concept of the Voronoi diagram	6
1.3 Mathematical preliminaries	12
1.3.1 Vector geometry	12
1.3.2 Graphs	24
1.3.3 Spatial stochastic point processes	31
1.3.4 Efficiency of computation	41
Chapter 2 Definitions and Basic Properties of Voronoi Diagrams	43
2.1 Definitions of the ordinary Voronoi diagram	43
2.2 Definitions of the Delaunay tessellation (triangulation)	52
2.3 Basic properties of the Voronoi diagram	57
2.4 Basic properties of the Delaunay triangulation	70
2.5 Graphs related to the Delaunay triangulation	97
2.6 Recognition of Voronoi diagrams	103
2.6.1 The geometric approach	104
2.6.2 The combinatorial approach	106
Chapter 3 Generalizations of the Voronoi diagram	113
3.1 Weighted Voronoi diagrams	119
3.1.1 The multiplicatively weighted Voronoi diagram	120
3.1.2 The additively weighted Voronoi diagram	123
3.1.3 The compoundly weighted Voronoi diagram	127
3.1.4 The power diagram	128
3.1.5 The sectional Voronoi diagram	131
3.1.6 Applications	133

3.2 Higher-order Voronoi diagrams	134
3.2.1 The order- k Voronoi diagram	135
3.2.2 The ordered order- k Voronoi diagram	144
3.2.3 Applications	150
3.3 The farthest-point Voronoi diagram and the kth nearest-point Voronoi diagram	151
3.3.1 The farthest-point Voronoi diagram	151
3.3.2 The k th nearest-point Voronoi diagram	155
3.3.3 Applications	157
3.4 Voronoi diagrams with obstacles	158
3.4.1 The shortest-path Voronoi diagram	158
3.4.2 The visibility shortest-path Voronoi diagram	163
3.4.3 The constrained Delaunay triangulation	165
3.4.4 SP- and VSP-Voronoi diagrams in a simple polygon	168
3.4.5 Applications	168
3.5 Voronoi diagrams for lines	169
3.5.1 Voronoi diagrams for a set of points and straight line segments	171
3.5.2 Voronoi diagrams for a set of points, straight line segments and circular arcs	176
3.5.3 Voronoi diagrams for a set of circles	178
3.5.4 Medial axis	181
3.5.5 Applications	184
3.6 Voronoi diagrams for areas	186
3.6.1 The area Voronoi diagram	186
3.6.2 Applications	188
3.7 Voronoi diagrams with V-distances	189
3.7.1 Voronoi diagrams with the Minkowski metric L_p	189
3.7.2 Voronoi diagrams with the convex distance	194
3.7.3 Voronoi diagrams with the Karlsruhe metric	201
3.7.4 Voronoi diagrams with the Hausdorff distance	202
3.7.5 Voronoi diagram with the boat-on-a-river distance	204
3.7.6 Voronoi diagrams on a sphere	206
3.7.7 Voronoi diagrams on a cylinder	209
3.7.8 Voronoi diagrams on a cone	210
3.7.9 Voronoi diagrams on a polyhedral surface	211
3.7.10 Miscellany	212
3.7.11 Applications	215
3.8 Network Voronoi diagrams	218
3.8.1 The network Voronoi node diagram	219
3.8.2 The network Voronoi link diagram	220
3.8.3 The network Voronoi area diagram	221
3.8.4 Applications	224
3.9 Voronoi diagrams for moving points	224
3.9.1 Dynamic Voronoi diagrams	224
3.9.2 Applications	227

Chapter 4 Algorithms for Computing Voronoi Diagrams	229
4.1 Computational preliminaries	229
4.2 Data structure for representing a Voronoi diagram	235
4.3 The incremental method	242
4.4 The divide-and-conquer method	251
4.5 The plane sweep method	257
4.6 Practical techniques for implementing the algorithms	264
4.6.1 Inconsistency caused by numerical errors	264
4.6.2 Construction of an error-free world	265
4.6.3 Topology-oriented approach	269
4.7 Algorithms for higher-dimensional Voronoi diagrams	275
4.8 Algorithms for generalized Voronoi diagrams	280
4.9 Approximation algorithms	287
Chapter 5 Poisson Voronoi Diagrams	291
5.1 Properties of infinite Voronoi diagrams	295
5.2 Properties of Poisson Voronoi diagrams	299
5.3 Uses of Poisson Voronoi diagrams	300
5.4 Simulating Poisson Voronoi and Delaunay cells	306
5.5 Properties of Poisson Voronoi cells	311
5.5.1 Moments of the characteristics of Poisson Voronoi cells	311
5.5.2 Conditional moments of the characteristics of Poisson Voronoi cells	315
5.5.3 Conditional moments of the characteristics of the neighbouring cells of a Poisson Voronoi cell	324
5.5.4 Distributional properties	331
5.6 Stochastic processes induced by Poisson Voronoi diagrams	350
5.6.1 Point processes of centroids of faces	350
5.6.2 Voronoi growth models	357
5.6.3 The Stienen model	360
5.6.4 Percolation on Poisson Voronoi diagrams and Poisson Delaunay tessellations	361
5.7 Sectional Voronoi diagrams	363
5.8 Additively weighted Poisson Voronoi diagrams: the Johnson–Mehl model	374
5.9 Higher order Poisson Voronoi diagrams	385
5.10 Poisson Voronoi diagrams on the surface of a sphere	389
5.11 Properties of Poisson Delaunay cells	389
5.12 Other random Voronoi diagrams	404

Chapter 6 Spatial Interpolation	411
6.1 Polygonal methods	416
6.1.1 Nearest neighbour interpolation	417
6.1.2 Natural neighbour interpolation	418
6.2 Triangular methods	427
6.3 Modifying Delaunay triangulations	434
6.4 Approximating surfaces	437
6.5 Delaunay meshes for finite element methods	439
6.5.1 Two-dimensional Delaunay meshes	440
6.5.2 Three-dimensional Delaunay meshes	442
6.6 Ordering multivariate data	446
Chapter 7 Models of Spatial Processes	453
7.1 Assignment models	454
7.2 Growth models	476
7.3 Spatial-temporal processes	482
7.3.1 Spatial competition models: the Hotelling process	482
7.3.2 Adjustment models	489
7.4 Two-species models	491
Chapter 8 Point Pattern Analysis	495
8.1 Polygon-based methods	498
8.1.1 Direct approach	498
8.1.2 Indirect approaches	502
8.2 Triangle-based methods	506
8.3 Nearest neighbour distance methods	512
8.3.1 Nearest neighbour distance method for point-like objects	514
8.3.2 Nearest neighbour distance method for line-like objects	517
8.3.3 Nearest neighbour distance method for area-like objects	520
8.3.4 Multi nearest neighbour distance method	521
8.4 The shape of a point pattern	521
8.4.1 Internal shape	521
8.4.2 External shape	523
8.5 Spatial intensity	525
8.6 Segmenting point patterns	527
8.7 Modelling point processes	529

Chapter 9 Locational Optimization Through Voronoi Diagrams	531
9.1 Preliminaries	532
9.1.1 The non-linear, non-convex programming problem	532
9.1.2 The descent method	534
9.1.3 The penalty function method	538
9.2 Locational optimization of points	541
9.2.1 Locational optimization of point-like facilities used by independent users	542
9.2.2 Locational optimization of points in a three-dimensional space	548
9.2.3 Locational optimization of point-like facilities used by groups	549
9.2.4 Locational optimization of a hierarchical facility	551
9.2.5 Locational optimization of observation points for estimating the total quantity of a spatial variable continuously distributed over a plane	555
9.2.6 Locational optimization of service points of a mobile facility	558
9.2.7 Locational optimization of terminal points through which users go to the central point	559
9.2.8 Locational optimization of points on a continuous network	563
9.3 Locational optimization of lines	564
9.3.1 Locational optimization of a service route	564
9.3.2 Locational optimization of a network	567
9.3.3 Euclidean Steiner minimum tree	570
9.4 Locational optimization over time	575
9.4.1 Multi-stage locational optimization	575
9.4.2 Periodic locational optimization	578
9.5 Voronoi fitting and its application to locational optimization problems	581
9.5.1 Method of fitting a Voronoi diagram to a polygonal tessellation	581
9.5.2 Locational optimization for minimizing restricted areas	584
References	585
Index	657

Foreword to the First Edition

I was delighted to be asked to write a preface to this beautiful and outstandingly original book. It is the unique treatise on its subject, it fills a serious gap in the literature and it covers the theory and the huge range of applications in a masterly way.

The authors are right to distinguish Voronoi *diagrams* and Delone *tesselations*. The Delone construction decomposes a Euclidean space of m dimensions, containing a given set of points, into non-overlapping space-filling *simplexes* (not, of course, all of the same shape and size), so that it tessellates the space using tiles that are identical with one another up to linear transformations. The Voronoi construction also splits up the space into polyhedral cells, but now they are much less uniform in character – the number of faces will vary from one cell to another, so that it would be wrong to call the result a tessellation.

These mutually dual procedures give fascinating but different insights into the structure of a set of points in m dimensions, and they have found numerous applications. At the time of writing there is a new application on the largest of all possible scales which throws light on the structure of the Universe as we see it. This will be seen as a particularly interesting development when one recalls that most of the earlier applications (for example, to the study of the structure of metallic composites, and other such aggregates) were on the microscopic scale. The reader of this book is strongly urged to look at a review paper just published by Icke and van de Weygaert (*Quarterly Journal, Royal Astronomical Society*, **32**, 85–112). There it is shown that the Voronoi construction not only gives insight into the distribution of galaxies, but also permits a new approach to the dynamics that mould the shape of the universe we live in.

My own contributions have been in the Delone tradition, and are concerned (for example) with the way in which high-dimensional Delone simplexes pack together around a common vertex. Thus in 15 dimensions the number of such locally associated simplexes turns out to be of the order of 44 million million. This implies a related statement about the Voronoi polyhedra, and there tells us something about the number of faces of an individual cell. It seems likely that the huge number of Delone simplexes in such a local ‘fan’ can be roughly partitioned into a moderate number of

'chunky' simplexes (substantial faces in the Voronoi case), and a vast number of 'needle-like' ones (tiny faces), but we have no precise information on this matter at the moment.

It is a great pleasure to welcome this book to the Wiley series.

David Kendall

Preface to the Second Edition

The First Edition of this book was published in 1992. In 1995, it was reprinted. At that time, we suggested to the publishers that, given the continuing interest in Voronoi diagrams in so many quarters, rather than consider further reprints they allow us to prepare a new, revised, Second Edition. We were pleased to receive a positive reply and so this volume was born.

While this edition maintains the overall structure of the first, there are substantial changes in the content. In particular, on-going growth in research relating to Voronoi diagrams is reflected in the addition of much new material to this volume. Although such additions occur throughout the book, they are most visible in new generalizations of the ordinary Voronoi diagram, new and revised results relating the Poisson Voronoi diagram, and new applications of all forms of Voronoi diagrams. The growth in Voronoi diagram research is also manifest in several other ways. One is the presence of a fourth author, Sung Nok Chiu, without whose contribution the original three authors would probably still be labouring over the revisions. Another is the increase in the number of references from 677 in the First Edition to 1680, 523 of which have appeared since the First Edition was published.

In order to accommodate the new developments we have omitted some material from the First Edition. This is most obvious in the mathematical preliminaries in Chapter 1 where we have omitted the sections relating to matrices, derivatives, integration and probability.

This book is accompanied by a World Wide Web site (<http://okabe.t.u-tokyo.ac.jp/okabelab/Voronoi/index.html>) which provides additional material such as pointers to available Voronoi diagrams and related geometric software and other Web sites featuring Voronoi diagrams. Our WWW page can also be used to notify us of any errors. Although the text has been proofread many times by ourselves and others, it is inevitable that some logical and typographical errors will not have been detected. We will correct any errors we become aware of and provide an Errata list on our WWW page.

Acknowledgments (First Edition)

So many people helped in so many ways during the preparation of this book that it is only possible to acknowledge a few of them individually. First, we are deeply grateful to D.G. Kendall, who read through the draft and encouraged its publication; and to Y. Asami, C.M. Hoffmann, M. Iri, K. Murota and A. Suzuki, who suggested or commented on parts of the draft. Our special thanks also go to D.A. Aboav, F. Aurenhammer, H. Edelsbrunner, S. Egginton, J.D. Embury, M.F. Goodchild, M. Hori, H.-C. Imhof, G. Le Caër, U. Lorz, J. Mecke, R.E. Miles, J. Møller, L. Muche, Y. Ohsawa, N. Rivier, Y.M. Seoung, D. Stoyan, T. Suzuki, M. Tanemura, G. Toussaint, D.S. Wilkinson, H. Yomono and L. Zaninetti, who provided material. We must also express our debt to A. Dawkins, S. Henry H. Honkers, J. Horton, T. Kaneko, O. Kurita, R. Metcalfe, P. Schaus, M. Stone and T. Yoshikawa, among others, who assisted in production. For the help that they have given us, we are indebted to the staff of the publisher, in particular, C. Farmer, S. Gale, J. Narain and H. Ramsey. We should also acknowledge the award of a Book Preparation Grant from Wilfrid Laurier University which helped meet costs incurred during the preparation of the manuscript. Finally we are grateful for academic e-mail networks which made us feel as if we had been working in the same office.

Acknowledgments (Second Edition)

As with the First Edition, so many people helped us in different ways in the preparation of this edition that it is impossible to acknowledge all of them individually. However, we are especially indebted to two individuals who exposed us to significant applications which were either overlooked or received only passing reference in the first edition. Initially by means of a footnote in Oden *et al.* (1993) and later by direct communication, H. Goebl revealed the use of Voronoi diagrams in linguistics, while E. Agrell, by way of his book (Agrell, 1997), showed us how much we had missed on the use of Voronoi diagrams in coding. For their comments and suggestions on the First Edition or drafts of this edition we would like to thank H. Imai, K. Imai, R. Klein, R.C. Lindenbergh, U. Lorz, M. McAllister, L. Muche, T. Roos, M. Schlather, N. Shiode, and C.A. Wang. We would also like to thank those who generously shared their unpublished research or other material with us, C. Gold, U. Lorz, K. McLeod, C. Moukarzel, L. Muche, K. Ohnishi, M. Schlather, D. Stoyan, and D. Watson. Thanks are also due to those who assisted in the production of this edition, especially P. Churcher, S. Horiike, J. Horton, C. Kanasaki, T. Kuroiwa, M. Lefebvre, H. Rayner, P. Schaus, and C. Yoshimoto. Finally, it is again a pleasure to acknowledge the help and guidance we have received from the staff of the publisher, in particular, S. Clutton, S. Corney, and H. Ramsey, who dealt with the idiosyncrasies of four authors scattered around the globe with both patience and good humour.

CHAPTER 1

Introduction

On initial consideration the following problems, which concern a variety of phenomena at disparate scales, would appear to have little in common:

- an astronomer studying the structure of the Universe;
- an archaeologist attempting to identify the parts of a region under the influence of different neolithic clans;
- a meteorologist estimating precipitation at a gauge which has failed to operate;
- an urban planner locating public schools in a city;
- a physicist studying the behaviour of liquid argon;
- a physiologist examining capillary supply to muscle tissue.

However, these problems (all of which, together with many others, are dealt with below) can be resolved by approaches developed from a single concept which forms the subject of this book.

The concept is a simple but intuitively appealing one. Given a finite set of distinct, isolated points in a continuous space, we associate all locations in that space with the closest member of the point set. The result is a partitioning of the space into a set of regions. Figure 1.0.1 shows a simple instance for two-dimensional Euclidean space. Given its widespread occurrence it is not surprising that this concept has been ‘discovered’ many times in many different places and as a result both the diagram and its constituent regions are known by a plethora of aliases. One immediate problem we faced in writing this book was the choice of an appropriate name which would be recognized by those interested in the concept. We selected the terms Voronoi diagram and Voronoi region, which seem to be the most extensively used, although equivalent terms are identified in Section 1.2.

A second diagram can be constructed from the Voronoi diagram in m -dimensional space by joining those points whose regions share an $(m-1)$ -dimensional face (see Figure 1.0.1). We refer to this dual diagram as the Delaunay tessellation, although it too has a number of aliases (see Section 1.2). The Delaunay tessellation may also be constructed directly from the point set by taking each $(m+1)$ -ad of points and examining its circumsphere. If the interior of this does not contain a point of the set, we construct the simplex determined by the $(m+1)$ points, but if it is not empty we do nothing.

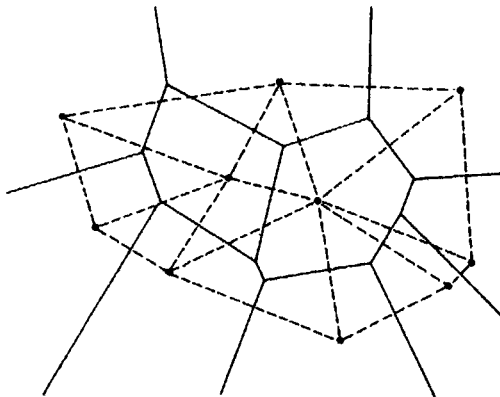


Figure 1.0.1 A planar Voronoi diagram (solid lines) and its dual Delaunay tessellation (dashed lines).

After all possible $(m+1)$ -ads have been considered in this way, the result is the Delaunay tessellation.

Voronoi diagrams and Delaunay tessellations are two of a few truly interdisciplinary concepts with relevant material to be found in, but not limited to, anthropology, archaeology, astronomy, biology, cartography, chemistry, computational geometry, crystallography, ecology, forestry, geography, geology, linguistics, marketing, metallography, meteorology, operations research, physics, physiology, remote sensing, statistics, and urban and regional planning. An unfortunate consequence of this is that the material is extremely diffused, of varying mathematical sophistication and quite often idiosyncratic. The amount of material relating to Voronoi diagrams has also been growing steadily since the early 1980s as witnessed by the dominance of recent references in the References. This proliferation results in part from the opening up of new areas of application and in part from the basic concept being extended in a variety of ways (see Chapter 3). Consequently, our major motive for writing this book was to synthesize and to unify as much of the material as possible and to present it in a structured form. This seemed particularly important at the time we wrote the First Edition because no other book had appeared which was devoted exclusively to the topic. The one which came closest was Aurenhammer (1988a) (also published as Aurenhammer, 1990a, 1991) but this was a short (87 pages), highly selective survey which emphasized computational algorithms and only offered brief descriptions of applications. A number of contemporary books also provided limited treatments of Voronoi diagrams as part of more extensive coverage, for example, Ahuja and Schachter (1983), Preparata and Shamos (1985), Iri and Koshizuka (1986), and Stoyan *et al.* (1987) but in most cases Voronoi diagrams accounted for less than ten percent of the books' contents. In addition, the second-last work was in Japanese, which restricted its exposure to an English language audience.

While texts which devote part of their contents to Voronoi diagrams continue to be published (e.g. de Berg *et al.*, 1997) and others focusing on a particular kind of Voronoi diagram (e.g. Møller, 1994) or a particular area of application (e.g. Agrell, 1997) are starting to appear, we believe that our text remains the only one which attempts to provide a comprehensive and balanced treatment of all aspects of Voronoi diagrams including their definition, history, computation, statistical properties and applications. It is our hope and intention that the book should appeal equally to those whose concern with Voronoi diagrams is theoretical, practical or both. However, in view of the continuing development of Voronoi diagrams, we feel that, like the First Edition, this one should be regarded as a report on the current state of affairs from a most dynamic area rather than an exhaustive study.

1.1 OUTLINE

We have already noted that the concept of the Voronoi diagram is used extensively in a variety of disciplines and has independent roots in many of them. In Section 1.2 we begin our treatment of the Voronoi diagram by tracing its origins and that of the Delaunay tessellation from the nineteenth century up to the present. In the course of this exploration we identify the other names by which both structures are known. Before proceeding further, in order to make the book as self-contained as possible, in Section 1.3 we briefly review some basic features of several topics involved in the subsequent discussion of Voronoi diagrams. These are vector geometry, graphs, stochastic point processes and computational efficiency. The material in this section is not intended to be exhaustive but rather to provide a sufficient introduction for those who may be unfamiliar with such topics.

Chapter 2 begins with a formal definition of both the Voronoi diagram (Section 2.1) and the Delaunay tessellation (Section 2.2). Sections 2.3 and 2.4 present properties of both structures, most of which are exploited in applications described elsewhere in the book. A number of other spatial structures which are related to the Delaunay tessellation and which have been used in a variety of applications including diffusion modelling, numerical taxonomy and the exploratory display and analysis of data are described in Section 2.5. The chapter concludes by considering techniques for determining if a given structure is a Voronoi diagram and, if not, the extent to which it approximates one.

A major reason for the continuing success of the Voronoi diagram is that it can be generalized in a variety of ways. Such generalizations are the subject of Chapter 3 and include weighting the points in various ways (Section 3.1), considering regions associated with subsets of points rather than individual points (Sections 3.2 and 3.3), including obstacles in the space (Section 3.4), considering regions associated with sets of geometric features other than points (Sections 3.5 and 3.6), examining Voronoi diagrams

in non-Euclidean spaces (Section 3.7), on networks (Section 3.8), and for moving points (Section 3.9). Accompanying each extension is a discussion of its applications.

In Chapter 4, after considering some computational preliminaries (Section 4.1), we examine data structures for representing the Voronoi diagram (Section 4.2). Then we present major algorithms for constructing it (Sections 4.3–4.5). For application purposes it is necessary to be able to implement these algorithms and in Section 4.6 we consider various practical techniques for doing this. Up to this point in the chapter the discussion concentrates on the planar Voronoi diagram but in Section 4.7 we consider Voronoi diagrams in higher dimensions and in Sections 4.8 and 4.9 we examine algorithms for generating the various generalized diagrams introduced in Chapter 3.

The Poisson Voronoi diagram (PVD) refers to the situation in which points are located in space ‘at random’ according to the homogeneous Poisson point process (Section 1.3.3). This diagram has been used extensively both as a descriptive and a normative model in the investigation of a wide range of empirical situations in both the natural and social sciences (Section 5.3) as diverse as galaxies, nesting territories of Royal Terns and mouthbreeder fish, and carbon particles in steels. Since the PVD is an infinite Voronoi diagram, Chapter 5 begins with a consideration of the properties of such structures (Section 5.1). We then focus on the major properties of the PVD (Section 5.2) and its constituent regions (Section 5.5), as well as those of the dual Poisson Delaunay tessellation (Section 5.11), sections of the three-dimensional PVD (Section 5.7) and generalizations of the PVD produced by weighting the points (Section 5.8), considering subsets of points rather than individual points (Section 5.9) and the PVD on the surface of a sphere (Section 5.10). We also consider stochastic processes induced by the PVD (Section 5.6) and briefly examine other types of ‘random’ Voronoi diagrams (Section 5.12). In view of the importance of the PVD and associated Voronoi diagrams to applications, the emphasis in this chapter is on the presentation of results relating to characteristics of Voronoi regions in such structures. Although some of these are exact results derived analytically, the majority are estimates obtained from Monte Carlo simulation procedures, the different types of which are described in Section 5.4.

In the remaining chapters the emphasis shifts towards applications of Voronoi diagrams. We identify four major areas, spatial interpolation, models of spatial processes, point pattern analysis, and locational optimization, each of which is the subject of a separate chapter. In Chapter 6, under the general heading of spatial interpolation, we consider how the Voronoi diagram has been used to facilitate the presentation and analysis of spatial data (values of one or more variables observed at a set of data sites in space). Such uses include employing Voronoi diagrams and Delaunay tessellations for defining various types of neighbour relationships (Section 6.1), creating meshes for finite element methods (Section 6.5), ordering multivariate data (Section 6.6), and constructing continuous surfaces from a set of data values observed at

punctiform data sites (Sections 6.1–6.3), including the approximation of such surfaces (Section 6.4).

Chapter 7 considers how, by equating the procedures involved in defining the Voronoi diagram with assumptions involved in spatial processes, we may produce simple spatial models. At least four types of spatial processes, assignment (Section 7.1), growth (Section 7.2), some spatial temporal processes (Section 7.3) and spatial competition (Section 7.4) can be represented in this way. The application of such models is extensive and examples from areas as diverse as crystallography, solid state physics, biology, astronomy, physiology, archaeology and urban economics are presented.

Use of the Voronoi diagram and the Delaunay tessellation in point pattern analysis is described in Chapter 8. Section 8.1 considers different methods using the Voronoi diagram while Section 8.2 examines those methods which make use of the Delaunay tessellation. In both of these sections our concern is with how the points in a given set are positioned with respect to each other and the space in which they are located. In Section 8.3 our attention shifts to a consideration of how the members of the point set are located with respect to other objects, not members of the set, which are also located in the same space. These objects may be other points, lines or areas, or a combination of all three. We also examine how Voronoi concepts can be used to describe the shape of a point pattern (Section 8.4), estimate its spatial intensity (Section 8.5) and divide it into sub-units (Section 8.6). Section 8.7 echoes Section 5.6 by considering some stochastic point processes that are induced by Voronoi diagrams.

Finally, Chapter 9 deals with the various ways in which the Voronoi diagram can be applied in solving locational optimization problems. Although problems relating to locational optimization on a network have been the subject of extensive investigation, less work has been undertaken on problems in the plane and it is such problems which are emphasized in this chapter. Planar optimization problems are important in a number of natural and social sciences. Examples range from locating observation sites for estimating a continuous spatial random variable to the location of various types of public facilities such as health clinics, fire stations and public transportation stops. All of these problems involve objects which can be represented as points and they, and other situations, form the subject matter of Section 9.2. Section 9.3 considers problems relating to the location of linear features, while Section 9.4 extends the discussion to situations where the objects under study are not located synchronously in the space. The final section (Section 9.5) illustrates how locational optimization procedures relate to fitting a Voronoi diagram to a given tessellation, a topic which is treated more generally in Section 2.6.

1.2 HISTORY OF THE CONCEPT OF THE VORONOI DIAGRAM

It is quite possible that the concept of the Voronoi diagram is of considerable antiquity. As we show elsewhere in the book (but especially in Chapter 7), many different kinds of natural structures closely resemble Voronoi diagrams and it seems unlikely that such structures would have gone unnoticed by early scientists and observant laymen alike. In his treatment of cosmic fragmentation in both *Le Monde de Mr Descartes, ou Le Trait de la Lumière* published in 1644 (but written between 1629 and 1633) and in Part III of *Principia Philosophiae*, also published in 1644, Descartes uses Voronoi-like diagrams to show the disposition of matter in the solar system and its environs (see Figure 1.2.1). Since these diagrams are not accompanied by any special commentary relating to their construction, it is possible that such figures were not uncommon at that time. In fact, diagrams such as that in Figure 1.2.1 are actually more akin to a generalized version of a Voronoi diagram, known as a weighted Voronoi diagram (see Section 3.1).

The first undisputed comprehensive presentations of the concept that we are aware of appear in the work of Peter Gustav Lejeune Dirichlet (1805–1859) and Georgy Fedoseevich Voronoy (Georges Voronoï) (1868–1908) who, in their studies on positive definite quadric forms (Dirichlet, 1850; Voronoï, 1907, 1908, 1909) considered a special form of the Voronoi diagram. Dirichlet treated two- and three-dimensional cases whereas Voronoï examined the general m -dimensional case. Their concern was with the distribution of points with integer coordinates that give minima of the values of a given quadric form. In that context, they considered the set of points regularly placed in the m -dimensional space generated by linear combinations of m linearly independent vectors with integer coefficients. This set contains infinitely many points, and the Voronoi diagram generated by this set of points gives the partition of the space into mutually congruent polyhedra. Using this concept Voronoï, for example, extended the work of Minkowski (1897) to give a simple proof of the upper bound $2(2^m - 1)$ of the number of $(m-1)$ -dimensional facets of an m -dimensional polyhedron, the translational repetition of which can fill the whole space without overlap. As far as we can determine, it was the Russian number theorist, Boris Nikolaevitch Delone (1890–1980) (see below), who was the first to associate the names of Dirichlet and Voronoï with such polyhedra. He coined both the term *domaine de Dirichlet* (Dirichlet domain) (Delaunay, 1929a, b) and *Voronoi'schen Bereich* (Voronoi region) (Delaunay, 1932) which have subsequently become the two most frequently encountered terms.

Given that the initial developments of the Voronoi diagram concept involved sets of points which were regularly placed in space, it is not surprising that some of its first applications were in crystallography. Work in this area began in the late nineteenth and early twentieth centuries (see Nowacki, 1933, 1976, for reviews) and was dominated by German and Russian researchers. At this time Voronoi regions were known by a number of names.

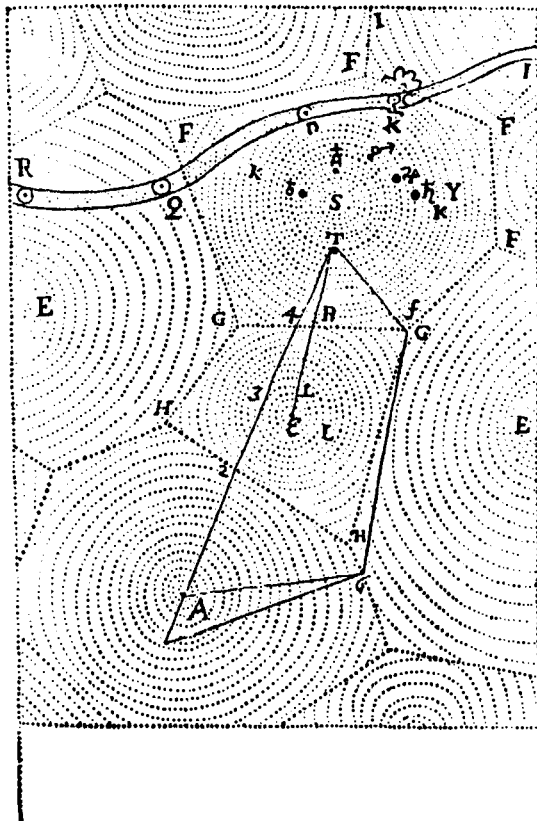


Figure 1.2.1 The disposition of matter in the Solar System and its environs by Descartes (S is the sun; ϵ is a star; RQD represents the path of a comet; polygonal areas represent heavens). (Source: Copy of the original in Descartes, 1644, reproduced in Mahoney, 1979.)

For example, Fedorov (1885), who was the first to determine the five combinatorial types of space-filling parallelohedra in \mathbb{R}^3 (see Section 7.1), called such regions *stereohedra*, while Schoenflies (1891), Steinitz (1906) and Speiser (1927) used the term *Fundamentalbereich* (fundamental area), and Wulff (1908) used *Wirkungssphäre* (sphere of influence). Later Schoenflies (1923) and Niggli (1927) independently introduced the term *Wirkungsbereich* (domain of action, field of activity, area of influence). The line of research originating in the early work concerned with identifying congruent space-filling domains has continued to the present (see Section 7.1) and Grünbaum and Shephard (1980) have coined the term *plesiohedra* for Voronoi regions encountered in this context.

At the same time as the Voronoi diagram concept was being applied in crystallography, it appears to have been developed independently in at least two other areas, both involving spatial interpolation. The first of these

occurred in meteorology when Thiessen (1911) used Voronoi regions as an aid to computing more accurate estimates of regional rainfall averages (see Section 6.1.1). While acknowledging Thiessen's paper, Horton (1917) claims to have developed the procedure independently in exactly the same context. Notwithstanding this, Whitney (1929) refers to the procedure as 'Thiessen's method' and since then the term *Thiessen polygon* has remained a popular one in two-dimensional applications in meteorology, geography and related social science disciplines.

The second area involved the estimation of ore reserves in a deposit using information obtained from bore holes (see Section 6.1.1). The earliest work on this topic by Boldyrev appeared in Russia in 1909 (Smirnov *et al.*, 1960) and was independently developed in the United States by Davis and Harding (Harding, 1920–21, 1923). Here the Voronoi regions are termed simply *area of influence polygons*, a name which remains current in this area of application (Hayes and Koch, 1984).

Despite this expansion of the use of Voronoi diagrams, further independent rediscoveries continued. In their study of the chemical properties in metallic sodium the physicists Wigner and Seitz (1933) described Voronoi regions for points arranged on a lattice in three-dimensional space. Although they did not label these polyhedra, the term *Wigner–Seitz regions* has come into quite common usage amongst physicists even when they are aware of the precedence of Voronoi diagrams, with the former term being used when the regions are regular polytopes and the latter when they are not. Somewhat ironically, over twenty years later, Voronoi diagrams were rediscovered in a similar context by Frank and Kasper (1958) modelling complex alloy structures as packings of spheres. Their concern focused on the neighbour relationships defined by the Voronoi polyhedra of atoms contiguous to that of the Voronoi polyhedron of a given atom, which they labelled the *domain of an atom*. Later still, Venables and Ball (1971) defined the equivalent of Voronoi regions to approximate capture zones of xenon crystals growing on graphite.

Meijering (1953) also appears to have been unaware of Voronoi concepts since he developed a crystal aggregate model which is a specific instance of the Voronoi Growth Model (see Section 7.2). In his *cell model*, crystals start to grow simultaneously and isotropically from nuclei randomly distributed in space so that the resulting structure is equivalent to a Poisson Voronoi diagram (see Chapter 5).

Voronoi regions were also developed independently in the study of codes. In the communication model introduced by Shannon (1948a,b, 1949), one of C equally likely messages is presented for communication to a transmitter containing a code book with C code words, each of which can be represented by a vector in \mathbb{R}^3 . A received signal is represented by a vector consisting of the sum of the sent vector (code word) and a noise vector whose components are independent Gaussian variates. The ideal receiver for such a communication system is one which chooses the code word nearest to the received vector, since it can be shown that such a strategy minimizes

the average error probability of the transmitted code words. This operation is equivalent to defining the Voronoi diagram of the set of code words and noting in which Voronoi region a transmitted message is located. Since this type of decoding scheme was labelled minimum distance decoding or maximum likelihood decoding (Shannon, 1959), the resulting Voronoi regions have been labelled *maximum likelihood regions* (Slepian, 1965, 1968). Later still, in the same context Conway and Sloane (1992, p.56) refer to the Voronoi diagram as the *Voronoi honeycomb*.

In a span of only two years in the 1960s, Voronoi diagrams were rediscovered not once but twice more in the field of ecology. First, when estimating the intensity of trees in a forest, Brown (1965) defined a Voronoi region for an individual tree, calling it the *area potentially available (APA)* to a tree. One year later Mead's paper appeared (Mead, 1966) using the same concept for plants and labelling the resulting Voronoi regions as *plant polygons*. This name has remained reasonably common in this area of application despite the early recognition by Jack (1967) that such polygons are equivalent to Voronoi regions.

The final rediscovery that we are aware of is by Hoofd *et al.* (1985) who defined Voronoi regions with respect to the centres of capillaries in sections of tissue, labelling the resulting polygons capillary domains. However, as late as 1987 Icke (Icke and van de Weygaert, 1987) admits to developing them yet again, this time in an astronomical context, only to be saved from claiming such work as novel by his co-author's discovery of the vast field of literature on Voronoi diagrams.

Given the continuing integration of Voronoi concepts into so many fields of application (and the sales of the first edition of this book!), we do not anticipate that there will be any future rediscoveries of the Voronoi diagram. However, since most of its generalizations have a much shorter history and more specialized applications (and some individuals did not contribute to our sales!), it seems almost inevitable that many of these generalizations will inherit the trait of rediscovery. Indeed, weighted Voronoi diagrams (see Section 3.1) are already witness to this, with the additively weighted Voronoi diagram (see Section 3.1.2) being rediscovered by Medvedev (1994) and Goede *et al.* (1997) and the multiplicatively weighted diagram (see Section 3.1.1) by Aparicio and Cocks (1995), Moukarzel (1993), and Gerstein *et al.* (1995), and both diagrams by Parr (1995a,b, 1997a,b).

Although much of the development and many of the initial applications of Voronoi diagrams occurred in the natural sciences, the earliest application of Voronoi concepts known to us appears in a map included in the *Report on the Cholera Outbreak in the Parish of St. James, Westminster, During the Autumn of 1854* (Cholera Inquiry Committee, 1855). This map shows a continuous broken line, described as the 'Boundary of equal distance between Broad Street Pump and other Pumps', which encloses an area around the Broad Street Pump. Although there is no attribution associated with this map, it is most likely the work of John Snow whose map showing the spatial distribution of cholera deaths around the Broad Street Pump in

1854 (Snow, 1855) has become 'the most famous 19th century disease map' (Meade *et al.*, 1988) being reproduced in a variety of forms in many texts in both epidemiology and cartography (e.g. Stamp, 1964; Longmate, 1966; Thrower, 1972; Monmonier, 1996). The remarkable thing about the boundary defined on the map in the *Report* is that distance is not measured in terms of the Euclidean metric but in terms of distance along the street network of Westminster (including allowances for the presence of culs-de-sac), making this a network Voronoi-area diagram (see Section 3.8.3), a concept which would not reappear for nearly one hundred and fifty years.

The next social science application appears in the work of the German dialectologist Carl Haag (1860–1946) who used the Voronoi diagram as a means of visualizing dialect variation and identifying linguistic divides (isoglosses). In his study of dialects in south-west Germany (Haag, 1898), he defined the equivalent of the Voronoi diagram of a set of localities at which dialect data had been collected. He then decorated the Voronoi edge shared by two localities if those localities differed in terms of a dialect feature. Highly decorated edges thus signified the presence of isoglosses. The basis of this approach was adopted by the three main German dialectical institutes and variants are still in current use (see Section 7.1). Although Carl Haag made no mention of this, it is likely that his ideas were influenced by the work of the early chemists, one of whom was his brother, F. Haag, who wrote quite extensively on Voronoi diagrams of point sets in two dimensions (Haag, 1911, 1923, 1924, 1925).

Despite these early studies, most social science applications have been developed only in the last fifty years. The first of these was by Bogue (1949) who used the Voronoi polygons defined about US metropolitan centres (represented as points on a map) as surrogates for their market areas. Aided by other early studies by Snyder (1962) and Dacey (1965), this has remained the main area of application with work extending down to the level of individual retail stores, although geographers, anthropologists and archaeologists have also used the concept to model other types of human territorial systems. Related antecedents to such applications, some dating back to the mid-nineteenth century (see Shieh, 1985, for a review) can be found in spatial economics in the 'law of market areas'. This law considers the form of the boundary between the market areas of two competing centres under various conditions of market prices and transportation costs. Similar considerations are used in the definition of various kinds of weighted Voronoi diagrams (see Section 3.1). Following the suggestion of Evans (1967), geographers were also the first to use Voronoi (and Delaunay) concepts in the analysis of two-dimensional point patterns (Boots, 1974).

So by the 1960s knowledge of the Voronoi concept was current in both the natural and social sciences. However, empirical applications remained somewhat limited because of the lack of a simple and efficient means of constructing them, with practitioners relying on methods involving compass and ruler and fraught with ambiguities (Kopec, 1963). This situation motivated solutions from the rapidly developing area of computer science and by

the early 1970s a number of algorithms had been developed to construct Voronoi diagrams in both two and three dimensions. In turn, this work stimulated other developments in computer science which contributed to the now flourishing field of computational geometry. This endeavour is typified by the seminal paper of Shamos and Hoey (1975). Not only did they present an algorithm for constructing the Voronoi diagram, they also illustrated how it could be used to solve a series of what were then seen as essentially independent problems relating to a finite set of distinct points in Euclidean space, such as finding the minimum spanning tree, identifying the nearest neighbour of each point, and finding the largest circle, containing no points of the set, whose centre is inside the convex hull of the point set (see Section 2.3). In addition, they also suggested ways of generalizing the Voronoi diagram by considering Voronoi regions associated with subsets of k points of the entire point set rather than individual points (see Section 3.2). As a consequence of this and other contemporary initiatives, in the past twenty-five years the basic concept has been extended in a great variety of ways which are detailed in Chapter 3.

The dual concept of the Delaunay tessellation also has a history marked by rediscoveries, although these are not as frequent as in the case of the Voronoi diagram. The concept originated with Voronoï (1908) who defined it by way of the neighbour relationships in the Voronoi diagram, referring to the resulting structure as *l'ensemble (L) de simplexes*. However, it was Delone who first defined the tessellation using the empty sphere method. Delone's initial paper on this topic was included in an International Mathematical Congress held in Toronto, Canada, in 1924. Both this paper and its follow-up (which was dedicated to the memory of Voronoï) were written in French under the name of Delaunay (Delaunay, 1928, 1934), as were other of his earlier papers written in French (Delaunay, 1929a,b) and German (Delaunay, 1932). These circumstances may help to explain why Delaunay is often encountered misspelt Delauney (e.g. Baranyai and Ruff, 1986; Lingas, 1986a,b; Kermode and Weaire, 1990; Cressie, 1991; Finney, 1991; Voigtmann *et al.*, 1994; Blatov *et al.*, 1995) and why Davies and Bell (1996) mistakenly label him as a French mathematician. Delone did not propose a term for the tessellation and followed Voronoï's lead by calling it *la partition de l'espace en tétraèdres L* . The term *L -partition* is still in current use in some quarters (e.g. Gruber and Lekkerkerker, 1987).

One of the properties of the Delaunay tessellation in two dimensions is that the individual triangles are as equilateral as possible (see Section 2.4, Property D15). Thus, when Whitney (1929) adopted this criterion to select triangles for a triangulation for use in spatial interpolation, he unknowingly constructed a Delaunay tessellation.

Smith (1964) seems to have rediscovered the concept in his work on three-dimensional aggregates, labelling the structure the *simplicial graph*. Nevertheless, a year later he recognized the precedence of Delaunay's work and re-labelled the constituent regions as *Delaunay simplices* (Smith, 1965), a term which appears to have been coined by Rogers (1964) in his com-

hensive work on tessellations. Since then, the term Delaunay tessellation has been increasingly used which, given Delone's pivotal role in developing the concept, seems entirely appropriate.

There has been at least one recent rediscovery of the structure since this naming, that of Christ *et al.* (1982a) in the context of random lattice field theory. Although they recognized that the structure is the dual of the Voronoi diagram, they did not give a name to it.

1.3 MATHEMATICAL PRELIMINARIES

In this text, the reader is assumed to be familiar with basic mathematical notions related to sets, matrices, derivatives, geometry, integration, probability and statistics (such as Bartle, 1964 (real analysis); Feller, 1957 (probabilities) and Freund, 1962 (statistics)). For the reader's convenience, this section presents some basic geometrical notions that will be commonly used in this text. The major notions are those related to vector geometry, graphs, spatial stochastic point processes and computational efficiency. Since space is limited, some developments may not be in full detail. The reader who wishes to understand these notions with full formal derivations should consult the relevant mathematical textbooks (such as Royden, 1963 (real analysis); Busacker and Saaty, 1965 (graph theory); Wilks, 1962 (statistics); Karlin, 1969 (stochastic processes); Knuth, 1968 (algorithms)).

1.3.1 Vector Geometry

Consider an m -dimensional real Cartesian space, denoted by \mathbb{R}^m (\mathbb{R}^2 in Figure 1.3.1). In this space an m -tuple or the Cartesian coordinates (x_1, \dots, x_m) indicate a *point*, denoted by p ($p = (x_1, x_2)$ in Figure 1.3.1). If there are n points in \mathbb{R}^m , these points are denoted by p_1, \dots, p_n with Cartesian coordinates (x_{i1}, \dots, x_{im}) , $i = 1, \dots, n$ (for brevity, $i = 1, \dots, n$ will be referred to as $i \in I_n$ hereafter, where $I_n = \{1, \dots, n\}$ is a set of integers from 1 to n). Points p and p_i may also be represented by vectors

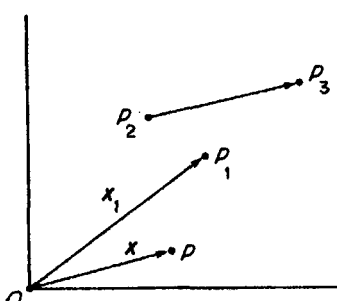


Figure 1.3.1 Vectors.

$$\mathbf{x} = \begin{bmatrix} x_1 \\ \vdots \\ x_m \end{bmatrix} \text{ and } \mathbf{x}_i = \begin{bmatrix} x_{i1} \\ \vdots \\ x_{im} \end{bmatrix}, \quad (1.3.1)$$

respectively. Note that the corresponding row vectors are indicated by $\mathbf{x}^T = (x_1, \dots, x_m)$ and $\mathbf{x}_i^T = (x_{i1}, \dots, x_{im})$, respectively, where T is a transpose operator; by definition, $\mathbf{x}_i = (x_{i1}, \dots, x_{im})^T$. In some contexts, it is more convenient to represent a point p as the arrow from the origin o of \mathbb{R}^m to the point p , denoted by \overrightarrow{op} . The length of the arrow in \mathbb{R}^2 is, using the Pythagorean theorem, given by $\sqrt{x_1^2 + x_2^2}$. Similarly, in \mathbb{R}^m , the length of the arrow, or the *norm* of a vector \mathbf{x} , denoted by $\|\mathbf{x}\|$, is given by

$$\|\mathbf{x}\| = \sqrt{\mathbf{x}^T \mathbf{x}} = \sqrt{\sum_{i=1}^m x_i^2} \quad (1.3.2)$$

(generally, $\mathbf{x}_1^T \mathbf{x}_2 = (x_{11}x_{21} + \dots + x_{1m}x_{2m})^T$ indicates the *inner product* of vectors \mathbf{x}_1 and \mathbf{x}_2). If a vector is designated as an arrow, it may be shifted provided that its length and direction are maintained; that is, an arrow may be shifted in a parallel way. In Figure 1.3.1, for example, $\overrightarrow{p_2p_3}$ and \overrightarrow{op} have the same length and the same direction, and so these two arrows indicate the same vector. It should be noted, however, that if a vector is designated as a point, then the point cannot be shifted. For example, in Figure 1.3.1 a point p is indicated by \overrightarrow{op} but not by $\overrightarrow{p_2p_3}$. We sometimes call a vector indicating a point a *location vector* or a *point vector*.

The scalar multiplication of \mathbf{x} by a positive scalar λ , i.e. $\lambda\mathbf{x} = (\lambda x_1, \dots, \lambda x_m)^T$, is represented by the arrow obtained from extending (shrinking) \overrightarrow{op} λ times in the same direction (Figure 1.3.2(a)). The scalar multiplication of \mathbf{x} by a negative scalar $-\lambda$, i.e. $-\lambda\mathbf{x}$, is represented by the arrow obtained from extending (shrinking) \overrightarrow{op} λ times in the opposite direction (Figure 1.3.2(a)). The vector addition, $\mathbf{x}_1 + \mathbf{x}_2 = (x_{11} + x_{21}, \dots, x_{1m} + x_{2m})^T$, is represented by the diagonal $\overrightarrow{op_3}$ of the parallelogram constructed from $\overrightarrow{op_1}$ and $\overrightarrow{op_2}$ (Figure 1.3.2(b)). The vector subtraction, $\mathbf{x}_1 - \mathbf{x}_2$, is obtained from the addition $\mathbf{x}_1 + (-\mathbf{x}_2) = (x_{11} - x_{21}, \dots, x_{1m} - x_{2m})^T$, where the vector $-\mathbf{x}_2$ is obtained from the vector \mathbf{x}_2 multiplied by a negative scalar -1 ; that is, $\mathbf{x}_1 - \mathbf{x}_2$ is indicated by the diagonal $\overrightarrow{op_5}$ of the parallelogram constructed from $\overrightarrow{op_1}$ and $\overrightarrow{op_4}$ (Figure 1.3.2(c)). Alternatively, the vector subtraction, $\mathbf{x}_1 - \mathbf{x}_2$, is represented by the diagonal $\overrightarrow{p_2p_1}$ of the parallelogram constructed from $\overrightarrow{op_1}$ and $\overrightarrow{op_2}$ (observe that $\overrightarrow{op_5}$ and $\overrightarrow{p_2p_1}$ represent the same vector $\mathbf{x}_1 - \mathbf{x}_2$).

Suppose that two vectors \mathbf{x}_1 and \mathbf{x}_2 are given by those in Figure 1.3.3(a). Then, we can find a scalar λ that satisfies $\mathbf{x}_2 = \lambda\mathbf{x}_1$. On the other hand, we cannot find such a λ for the vectors shown in Figure 1.3.3(b). We say that the vectors in panel (a) are *linearly dependent* and those in panel (b) are *linearly independent*. This notion can be extended to n vectors in \mathbb{R}^m . We say that vectors $\mathbf{x}_1, \dots, \mathbf{x}_n$ are *linearly dependent* in \mathbb{R}^m if there exists a set $\Lambda = \{\lambda_1, \dots, \lambda_n\}$ of n scalars which are not all zero such that

$$\lambda_1 \mathbf{x}_1 + \dots + \lambda_n \mathbf{x}_n = \mathbf{0}. \quad (1.3.3)$$

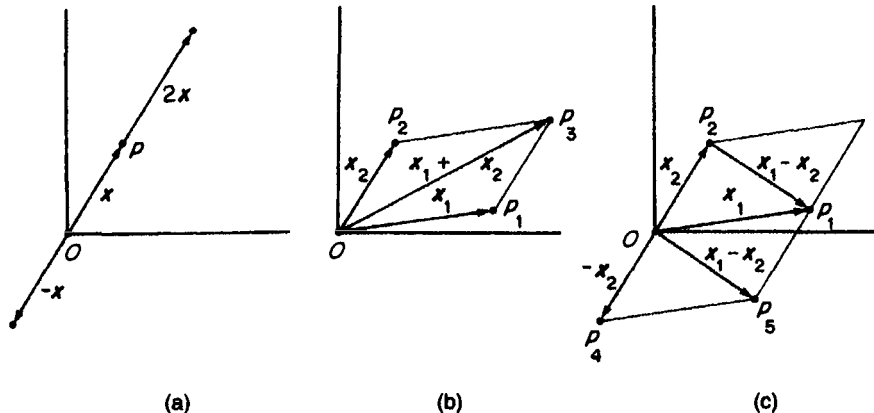


Figure 1.3.2 Vector operations: (a) scalar multiplication; (b) addition; (c) subtraction.

On the other hand, if the only λ for which equation (1.3.3) holds is $\lambda_1 = \dots = \lambda_n = 0$, then the vectors are said to be *linearly independent*. The number of linearly independent vectors in \mathbb{R}^m is at most m . For example, in \mathbb{R}^2 , as is shown in Figure 1.3.3(c), two vectors x_1 and x_2 are linearly independent, but three vectors x_1 , x_2 and x_3 are linearly dependent, because, as is indicated by the broken arrows in Figure 1.3.3(c), $\lambda_1 x_1 + \lambda_2 x_2 - x_3 = 0$ holds.

When two vectors x_1 and x_2 form the right angle as in Figure 1.3.4(a), we say that the vectors x_1 and x_2 are *orthogonal*, and denote it by $x_1 \perp x_2$. From Figure 1.3.4(a) it is evident that vectors x_1 and x_2 are orthogonal if and only if $\|x_1 + x_2\|$ equals $\|x_1 - x_2\|$, i.e. $(x_1 + x_2)^T(x_1 + x_2) = (x_1 - x_2)^T(x_1 - x_2)$. After a few steps of calculation, we obtain the following relation:

$$x_1 \perp x_2 \text{ if and only if } x_1^T x_2 = 0. \quad (1.3.4)$$

In Figure 1.3.4(b) we perpendicularly project p_2 or the line containing \overrightarrow{op} . Let p'_2 be the projected point and x'_2 be its location vector. Then we say that p'_2 is the *perpendicular projection* or *orthogonal projection* of p_2 on the line containing \overrightarrow{op}_1 . Since $x'_2 = \lambda x_1$, and $(\lambda x_1 - x_2)^T(\lambda x_1) = 0$, from equation (1.3.4), the vector x'_2 is written as

$$x'_2 = \frac{x_2^T x_1}{\|x_1\|} x_1. \quad (1.3.5)$$

Equation (1.3.5) becomes simpler when p_i with coordinates (x_{i1}, x_{i2}) in \mathbb{R}^2 is projected orthogonally onto the x_1 -axis. In this case the orthogonal projection of p_i onto the x_1 -axis is given by $(x_{i1}, 0)$. Similarly, the orthogonal projection of p_i with coordinates (x_{i1}, x_{i2}, x_{i3}) in \mathbb{R}^3 onto the x_1-x_2 plane is given by $(x_{i1}, x_{i2}, 0)$. Furthermore, we can project a set S in \mathbb{R}^3 orthogonally onto the x_1-x_2 plane by $S' = \{(x_1, x_2, 0) \mid (x_1, x_2, x_3) \in S\}$ (note that a set of elements constrained by conditions is denoted by {elements | conditions}). In this case we say that S' is the *orthographic projection* of S onto the x_1-x_2

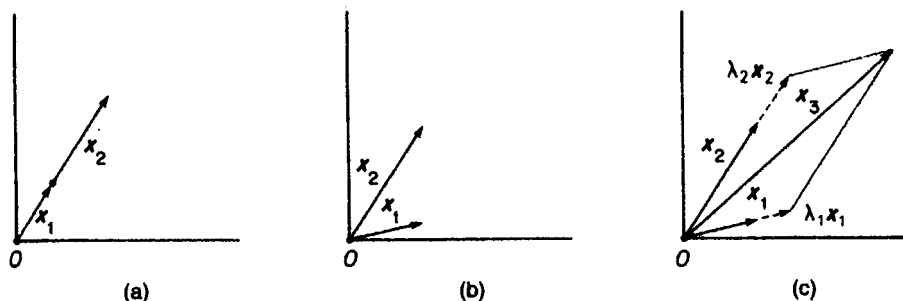


Figure 1.3.3 (a) Two vectors being linearly dependent; (b) linearly independent vectors; (c) three vectors being linearly dependent.

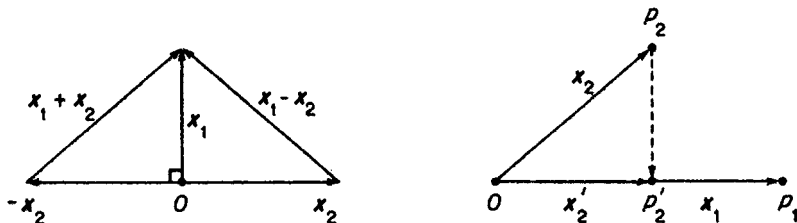


Figure 1.3.4 (a) Orthogonal vectors; (b) an orthogonal projection.

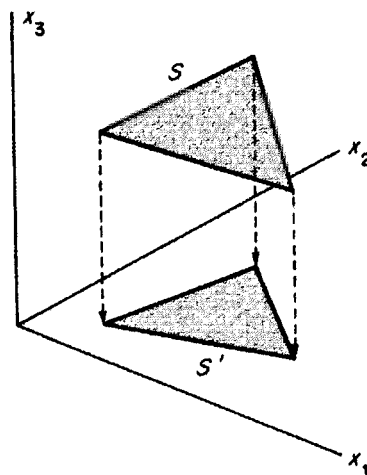


Figure 1.3.5 Orthographic projection.

plane. Figure 1.3.5 depicts the orthographic projection of a triangle placed in \mathbb{R}^3 onto the x_1 - x_2 plane.

As is seen in Figure 1.3.2(c), $\overrightarrow{p_2 p_1}$ and $\overrightarrow{o p_3}$ both represent the vector $\mathbf{x}_2 - \mathbf{x}_1$. Since the length of $\overrightarrow{o p_3}$ is given by equation (1.3.2), where $\mathbf{x} = \mathbf{x}_2 - \mathbf{x}_1$, we understand that the *Euclidean distance* between a point $\mathbf{x}_i = (x_{i1}, \dots, x_{im})^T$ and a point $\mathbf{x}_j = (x_{j1}, \dots, x_{jm})^T$ is given by

$$\begin{aligned}\|\mathbf{x}_i - \mathbf{x}_j\| &= \sqrt{(\mathbf{x}_i - \mathbf{x}_j)^T (\mathbf{x}_i - \mathbf{x}_j)} \\ &= \sqrt{\sum_{k=1}^m (x_{ik} - x_{jk})^2}.\end{aligned}\tag{1.3.6}$$

We call the m -dimensional real Cartesian space with the Euclidean distance the m -dimensional *Euclidean space*.

In the Euclidean space, we now show a few topological concepts. For a point \mathbf{c} in \mathbb{R}^m and $\varepsilon > 0$, we define the set

$$N_\varepsilon(\mathbf{c}) = \{\mathbf{x} \mid \|\mathbf{x} - \mathbf{c}\| < \varepsilon\},\tag{1.3.7}$$

which is called an *open ball* (in particular, an *open disk* for $m = 2$, as in Figure 1.3.6(a)) with radius ε centred at \mathbf{c} . Using this term, we say that a set A in \mathbb{R}^m is *open* if every point in A is the centre of some open ball entirely contained in A (Figure 1.3.6(c)); a set A in \mathbb{R}^m is *closed* if $\mathbb{R}^m \setminus A$ is open in \mathbb{R}^m where \setminus means a complement operator (i.e. for two sets A and B , $A \setminus B$ means a set of points which are included in A but not in B); a point \mathbf{x} in \mathbb{R}^m is a *boundary point* of A if every open ball centred at \mathbf{x} contains a point of A and a point of $\mathbb{R}^m \setminus A$ (Figure 1.3.6(d)). The set of all boundary points of A is called the *boundary* of A , and is denoted by ∂A . If a set A includes the boundary of A , then every point in $\mathbb{R}^m \setminus A$ is the centre of some open ball entirely contained in $\mathbb{R}^m \setminus A$. Thus a set A is closed if it contains its boundary. A point \mathbf{x} in \mathbb{R}^m is called an *interior point* of a set A if there exists an open ball centred at \mathbf{x} that contains only points in the set A (point \mathbf{x} in Figure 1.3.6(c)). If \mathbf{c} is a point in \mathbb{R}^m ($\mathbf{c} \in \mathbb{R}^m$), then any set that contains an open set containing \mathbf{c} is called a *neighbourhood* of \mathbf{c} in \mathbb{R}^m (generally, $a \in A$ means that a is an element of the set A). The open ball defined by equation (1.3.7) is a neighbourhood of \mathbf{c} , and is sometimes referred to as an ε -*neighbourhood*. For a set A , the intersection of all closed sets including A is called a *closure* of A .

In conjunction with an open ball, we define the sets

$$\bar{N}_\varepsilon(\mathbf{c}) = \{\mathbf{x} \mid \|\mathbf{x} - \mathbf{c}\| \leq \varepsilon\} \quad \text{for } \mathbf{c} \in \mathbb{R}^m, \varepsilon > 0\tag{1.3.8}$$

(notice that $<$ in equation (1.3.7) is replaced by \leq), and

$$\partial\bar{N}_\varepsilon(\mathbf{c}) = \{\mathbf{x} \mid \|\mathbf{x} - \mathbf{c}\| = \varepsilon\} \quad \text{for } \mathbf{c} \in \mathbb{R}^m, \varepsilon > 0,\tag{1.3.9}$$

which is a hypersphere in \mathbb{R}^m (specifically, a circle in \mathbb{R}^2 , a sphere in \mathbb{R}^3). The set $\partial\bar{N}_\varepsilon(\mathbf{c})$ is the boundary of $\bar{N}_\varepsilon(\mathbf{c})$. Since the set $\bar{N}_\varepsilon(\mathbf{c})$ includes its boundary, the set $\bar{N}_\varepsilon(\mathbf{c})$ is a closed set. Thus we call $\bar{N}_\varepsilon(\mathbf{c})$ a *closed ball* (specifically, a *closed disk* for $m = 2$, as in Figure 1.3.6(b)) centred at \mathbf{c} with radius ε .

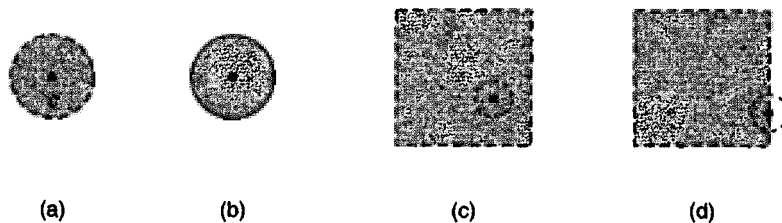


Figure 1.3.6 (a) An open disk; (b) a closed disk; (c) an open set; (d) a closed set.

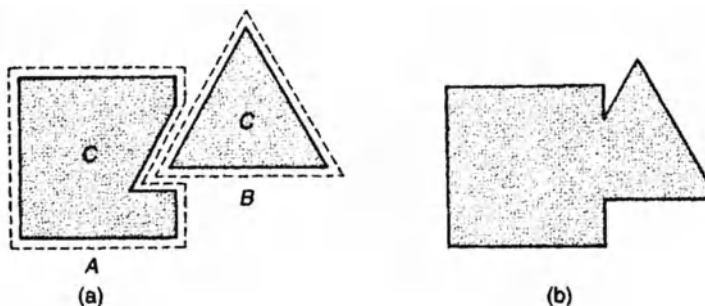


Figure 1.3.7 (a) A disconnected set C ; (b) a connected set C .

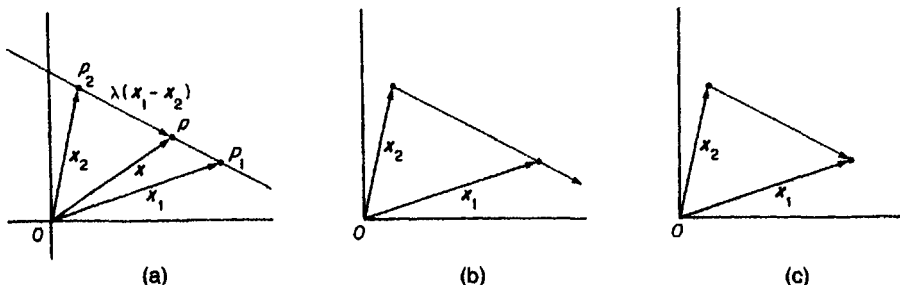


Figure 1.3.8 Lines (bold lines) defined by vectors: (a) a line; (b) a half line; (c) a line segment.

For a set C , if there exist two open sets A and B such that $(A \cap C) \cap (B \cap C) = \emptyset$ and $(A \cap C) \cup (B \cap C) = C$, then the set C is said to be *disconnected* (Figure 1.3.7(a); note that \cap is an intersection operator, i.e. for two sets A and B , $A \cap B$ means a set of points that are included in A and B ; \cup is a union operator, i.e. $A \cup B$ means a set of points that are included in A or B ; \emptyset denotes a set of no elements or an empty set). If a set is not disconnected, then the set is said to be *connected* (Figure 1.3.7(b)).

As we showed in Figure 1.3.2(c), $\overrightarrow{p_2p_1}$ represents the vector $x_1 - x_2$. We extend or shrink this arrow by multiplying by a scalar λ keeping its initial point at p_2 (Figure 1.3.8(a)). This extended or shrunken arrow represents the

vector $\lambda(\mathbf{x}_1 - \mathbf{x}_2)$. Let \mathbf{x} be the location vector indicating the head point, p , of this vector. Recalling the vector addition depicted in Figure 1.3.2(b), we notice that \overrightarrow{op} is obtained by adding $\overrightarrow{op_2}$ and $\overrightarrow{p_2 p}$ (Figure 1.3.8(a)). Since these arrows represent the vectors \mathbf{x} , \mathbf{x}_2 and $\lambda(\mathbf{x}_1 - \mathbf{x}_2)$, respectively, we obtain the equation $\mathbf{x} = \lambda(\mathbf{x}_1 - \mathbf{x}_2) + \mathbf{x}_2 = \lambda\mathbf{x}_1 + (1 - \lambda)\mathbf{x}_2$. From this equation the (*straight*) *line* passing through p_1 and p_2 ($p_1 \neq p_2$) is written as

$$L_1 = \{\mathbf{x} \mid \mathbf{x} = \lambda\mathbf{x}_1 + (1 - \lambda)\mathbf{x}_2, \lambda \in \mathbb{R}\}. \quad (1.3.10)$$

Observing that $\mathbf{x} = \mathbf{x}_2$ if $\lambda = 0$, and $\mathbf{x} = \mathbf{x}_1$ if $\lambda = 1$, we notice that the *half-line* radiating from p_2 passing through p_1 (Figure 1.3.8(b)) is given by the set

$$L_2 = \{\mathbf{x} \mid \mathbf{x} = \lambda\mathbf{x}_1 + (1 - \lambda)\mathbf{x}_2, \lambda \geq 0\}, \quad (1.3.11)$$

and the (*straight*) *line segment* connecting p_1 and p_2 (Figure 1.3.8(c)) is given by the set

$$L_3 = \{\mathbf{x} \mid \mathbf{x} = \lambda\mathbf{x}_1 + (1 - \lambda)\mathbf{x}_2, 0 \leq \lambda \leq 1\}. \quad (1.3.12)$$

The points p_1 and p_2 are called the *end points* of L_3 . The line segment L_3 contains its end points p_1 and p_2 .

Let us next consider a plane in \mathbb{R}^3 passing through points p_1, p_2 and p_3 which are not all on the same line, or equivalently, $\mathbf{x}_2 - \mathbf{x}_1$ and $\mathbf{x}_3 - \mathbf{x}_1$ are linearly independent. A point v on the line passing through p_1 and p_2 is, from equation (1.3.10), given by $v = \alpha\mathbf{x}_1 + (1 - \alpha)\mathbf{x}_2$; a point w on the line passing through p_1 and p_3 is given by $w = \beta\mathbf{x}_1 + (1 - \beta)\mathbf{x}_3$ (Figure 1.3.9). Thus a point x on the plane is given by $\mathbf{x} = \gamma v + (1 - \gamma)w = (\alpha\gamma + (1 - \gamma)\beta)\mathbf{x}_1 + \gamma(1 - \alpha)\mathbf{x}_2 + (1 - \beta)(1 - \gamma)\mathbf{x}_3$ (Figure 1.3.9). It follows from this equation that if we define the set by

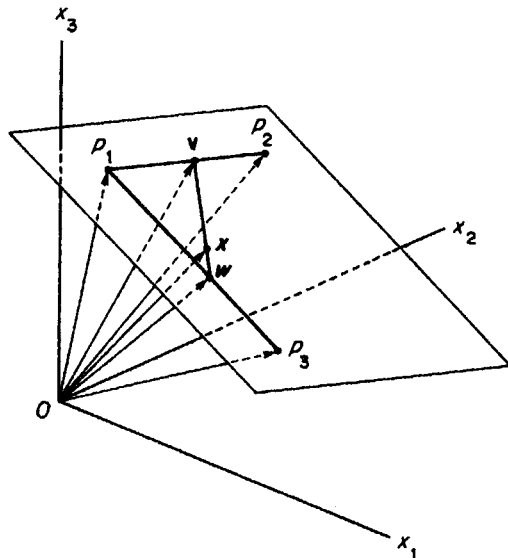


Figure 1.3.9 A plane in \mathbb{R}^3 .

$$A_1 = \{x \mid x = \lambda_1 x_1 + \lambda_2 x_2 + (1 - \lambda_1 - \lambda_2) x_3, \lambda_1, \lambda_2 \in \mathbb{R}\}, \quad (1.3.13)$$

then the set A_1 represents a plane. More generally, we define the set in \mathbb{R}^m by

$$A_2 = \left\{ x \mid x = \sum_{i=1}^{m-1} \lambda_i x_i + \left(1 - \sum_{i=1}^{m-1} \lambda_i\right) x_m, \lambda_i \in \mathbb{R}, i \in I_{m-1} \right\}, \quad (1.3.14)$$

where $x_2 - x_1, \dots, x_m - x_1$ are linearly independent. We call the set A_2 a *hyperplane* in \mathbb{R}^m .

In the Cartesian plane \mathbb{R}^2 , a line is given by equation (1.3.10). The equation on the right-hand side of equation (1.3.10) is written as $x_1 = \lambda x_{11} + (1 - \lambda)x_{12}$ and $x_2 = \lambda x_{21} + (1 - \lambda)x_{22}$. Cancelling λ from these equations, we obtain $(x_{21} - x_{22})x_1 + (x_{11} - x_{12})x_2 = (x_{21} - x_{22})x_{12} + (x_{11} - x_{12})x_{22}$. Thus, a line is alternatively written as $L_1 = \{(x_1, x_2) \mid a_1 x_1 + a_2 x_2 = b\}$, where a_1 and a_2 are constants, at least one of which is non-zero, and b is a constant. Similarly, in \mathbb{R}^3 , a plane is alternatively written as $A_1 = \{(x_1, x_2, x_3) \mid a_1 x_1 + a_2 x_2 + a_3 x_3 = b\}$, where a_1, a_2 and a_3 are constants, at least one of which is non-zero. Extending this expression to \mathbb{R}^m , we can alternatively write the hyperplane A_2 as

$$A_2 = \{x \mid a^T x = b, a, x \in \mathbb{R}^m, \|a\| \neq 0\}. \quad (1.3.15)$$

A line splits a plane into two disjoint regions (Figure 1.3.8(a)); a plane splits a space into two disjoint regions (Figure 1.3.9); generally, a hyperplane splits a space into two disjoint regions. We call one of the regions with the hyperplane, i.e. the region defined by

$$H = \{x \mid a^T x \leq b, a, x \in \mathbb{R}^m, \|a\| \neq 0\} \quad (1.3.16)$$

a (*closed*) *half space* (in particular, a (*closed*) *half plane* for $m = 2$; Figure 1.3.10(a)).

Observing Figure 1.3.10(a), we readily understand that the line segment between any two points in a half plane is included in the half plane. This

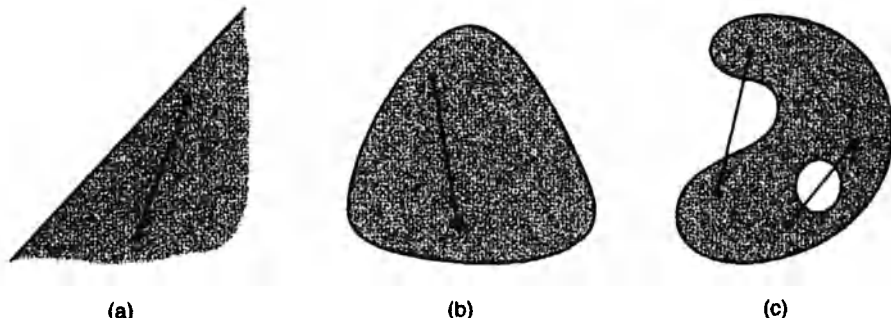


Figure 1.3.10 Convex and non-convex sets: (a) a half plane; (b) a convex set; (c) a non-convex set.

property holds not only for a half plane but also for other figures, such as Figure 1.3.10(b). Unlike Figure 1.3.10(c), Figure 1.3.10(b) does not have holes or its boundary does not bend into the figure. In such a case we say that a geometrical figure is *convex*. Formally, if for any two points \mathbf{x}_1 and \mathbf{x}_2 in A the line segment joining the points is contained in A , i.e.

$$\lambda \mathbf{x}_1 + (1 - \lambda) \mathbf{x}_2 \in A \text{ for all } 0 \leq \lambda \leq 1, \quad (1.3.17)$$

then we call the set A a *convex set*; otherwise, a *non-convex set*. In particular, if for any two points \mathbf{x}_1 and \mathbf{x}_2 in A the relation

$$\lambda \mathbf{x}_1 + (1 - \lambda) \mathbf{x}_2 \in A \setminus \partial A \text{ for all } 0 \leq \lambda \leq 1 \quad (1.3.18)$$

holds, we call the set A a *strictly convex set*.

A half space (equation (1.3.16)) is convex, because $\mathbf{a}^T(\lambda \mathbf{x}_1 + (1 - \lambda) \mathbf{x}_2) = \lambda \mathbf{a}^T \mathbf{x}_1 + (1 - \lambda) \mathbf{a}^T \mathbf{x}_2 \leq \lambda b + (1 - \lambda)b = b$ for $\mathbf{x}_1, \mathbf{x}_2 \in H$ and $0 < \lambda < 1$. The intersection of two convex sets is also convex. To prove it, let \mathbf{x}_1 and \mathbf{x}_2 be arbitrary points in the intersection of two convex sets A_1 and A_2 . Then, $\mathbf{x}_1, \mathbf{x}_2 \in A_1$ and $\mathbf{x}_1, \mathbf{x}_2 \in A_2$. Since A_1 and A_2 are convex sets, from relation (1.3.17) the line $\lambda \mathbf{x}_1 + (1 - \lambda) \mathbf{x}_2$, $0 \leq \lambda \leq 1$, is in A_1 and in A_2 . Therefore, the line $\lambda \mathbf{x}_1 + (1 - \lambda) \mathbf{x}_2$, $0 \leq \lambda \leq 1$, is in $A_1 \cap A_2$. Applying this proof, we can see that the intersection of convex sets is also convex. It is left as an exercise to show that a convex polygon A with vertices $\mathbf{x}_1, \dots, \mathbf{x}_n$ is given by

$$A = \left\{ \mathbf{x} \mid \sum_{i=1}^n \lambda_i \mathbf{x}_i \text{ where } \sum_{i=1}^n \lambda_i = 1, \lambda_i \geq 0, i \in I_n \right\} \quad (1.3.19)$$

(recall the derivation leading to equation (1.3.13)).

A type of convex sets which is of particular interest is the so-called convex hull. To be explicit, consider the geometric figure in Figure 1.3.11(a) and suppose that this figure is encircled by a rubber band. Then the rubber band becomes like the heavy line in Figure 1.3.11(b). We fill the inside of this rubber band with points. Then we obtain Figure 1.3.11(c), which we call a *convex hull*. To give a formal definition of the convex hull of a set A , consider

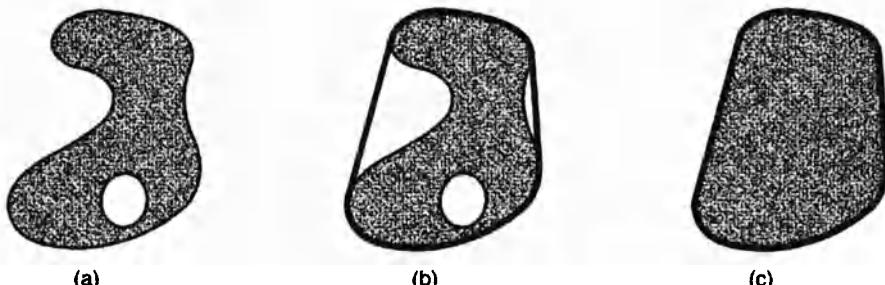


Figure 1.3.11 A convex hull: (a) a non-convex figure A ; (b) the boundary of the convex hull of A (the heavy line); (c) the convex hull of A .

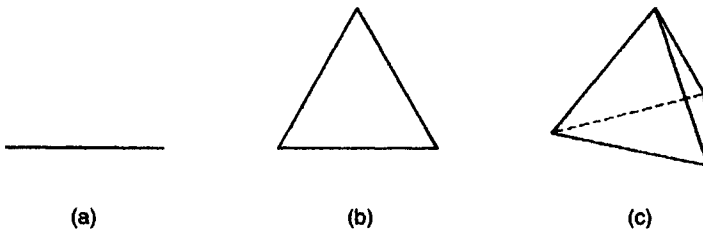


Figure 1.3.12 Simplices.

all possible convex sets that contain the set A . The number of such sets is infinite. We take the intersection of all such convex sets. Then the resulting set is called the *convex hull* of the set A . Since the intersection of convex sets is a convex set, the convex hull of the set A is a convex set. Moreover, it is the ‘smallest’ convex set that contains the set A . Obviously, if the set A is a convex set, then the convex hull of A is A itself.

As a special type of a convex hull, we define a simplex. A *simplex* in \mathbb{R}^m is the convex hull of any set of $m+1$ points which do not all lie on one hyperplane in \mathbb{R}^m . If $m = 0$, the simplex is a point itself, called the *zeroth-order simplex*; if $m = 1$, the simplex is the straight line segment connecting two points, called the *first-order simplex* (Figure 1.3.12(a)); if $m = 2$, the simplex is a triangle, called the *second-order simplex* (Figure 1.3.12(b)); if $m = 3$, the simplex is a tetrahedron, called the *third-order simplex* (Figure 1.3.12(c)), and so forth. The first-order simplex is written as equation (1.3.12). Similarly, the second-order simplex is written as equation (1.3.19), where $n = 3$ and $x_2 - x_1$ and $x_3 - x_1$ are linearly independent. In general, the m th-order simplex is written as equation (1.3.19), where $x_2 - x_1, \dots, x_{m+1} - x_1$ are linearly independent. If a set is contained in a simplex, we say that the set is *bounded*; otherwise *unbounded*. We sometimes say that the region given by a bounded set is a *finite region* and the region given by an unbounded set is an *infinite region*.

Let A be a subset of \mathbb{R}^m . We call an element a_u in \mathbb{R}^m an *upper bound* of A if $a_u > x$ for all x in A . Similarly, we call an element a_l in \mathbb{R}^m a *lower bound* of A if $a_l < x$ for all x in A . When the set A has an upper bound, we say that A is *bounded above*. Similarly, if the set A has a lower bound, we say that A is *bounded below*. If the set A is bounded above in \mathbb{R}^m , we say that an upper bound of A is a *supremum* of A if it is less than any other upper bound of A . Similarly, we say that a lower bound of A is an *infimum* of A if it is greater than any other lower bound of A .

The concept of convexity can be introduced into a function. Let $f(x)$ be a function from \mathbb{R}^n to \mathbb{R} , and $\{(x, y) | y \geq f(x), x \in S\}$, where S is the domain of the function f . This set is called the *epigraph* of the function f . Two examples of the epigraph are shown in Figure 1.3.13. If the epigraph of the function f is convex, we call the function f a *convex function* (Figure 1.3.13(a)); otherwise, a *non-convex function* (Figure 1.3.13(b)).

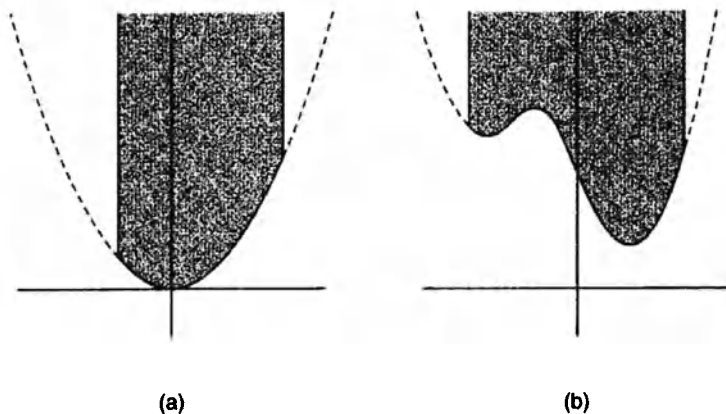


Figure 1.3.13 (a) The epigraph of a convex function, and (b) that of a non-convex function.

Suppose, as is shown in Figure 1.3.14, that five half planes, H_1, \dots, H_5 , are given. Using a finite number of intersection and union operations with respect to these half planes, we may construct a connected region. For example, $(H_1 \cap H_2 \cap H_3) \cup (H_1 \cap H_4 \cap H_5)$ in Figure 1.3.14(a). We call this region a *polygon*. Stated a little more generally, if a region constructed from a finite number of intersection and union operations with respect to a finite number of half planes is a non-empty connected set, then we call the region a *polygon*. The boundary of a polygon consists of straight line segments. These line segments are called *edges* and their end points are called *vertices*. If a polygon does not have a hole in it, and each vertex of a polygon has exactly two edges and every edge intersects only at vertices, we call the polygon a *simple polygon*. The polygon in Figure 1.3.14(a) is a simple polygon, but that in Figure 1.3.14(b) is not.

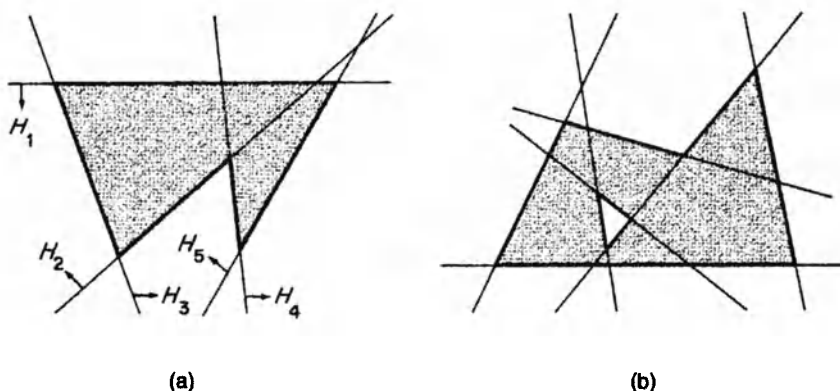


Figure 1.3.14 A polygon constructed from half planes: (a) a simple polygon; (b) a polygon that is not simple.

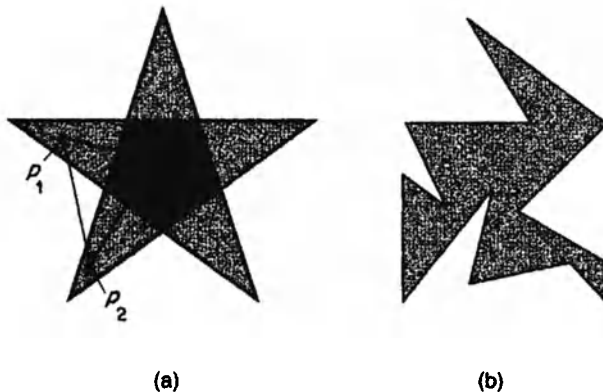


Figure 1.3.15 (a) A star-shaped polygon (the shaded region) and its kernel (the densely shaded region); (b) a polygon that is not star-shaped.

The notion of a polygon defined in \mathbb{R}^2 can be extended to \mathbb{R}^m . If a set constructed from a finite number of intersection and union operations on a finite number of half spaces is a non-empty connected bounded set, we call the set a *polyhedron*. A polyhedron (polygon) may be convex or non-convex. If a polyhedron is convex and bounded, it is sometimes called a *polytope*. A simplex (for example, the tetrahedron shown in Figure 1.3.12(c)) is a polytope.

The boundary of a polyhedron in \mathbb{R}^3 consists of polygons, which are called *faces*. Generally, the boundary of a polyhedron in \mathbb{R}^m consists of polyhedrons in \mathbb{R}^{m-1} , which are called $(m-1)$ -faces; the boundary of an $(m-1)$ -face consists of polyhedrons in \mathbb{R}^{m-2} , which are called $(m-2)$ -faces; and so forth. Note that 0-faces are *vertices*, and 1-faces are *edges*, and that $(m-1)$ -faces are sometimes called *facets*.

Recalling the definition of a convex set (equation (1.3.17)), we notice that the sets shown in Figure 1.3.15 are non-convex, because the line segment connecting points p_1 and p_2 is not contained in the set. However, if we fix one end point at p_0 , as in Figure 1.3.15(a), the line connecting p_0 and any point in the set is contained in the set. We call a set with this geometric property *star-shaped*. Stated precisely, the set A is *star-shaped* if there exists a point x_0 in A for which $\lambda x_0 + (1 - \lambda)x \in A$ holds for all $0 \leq \lambda \leq 1$ and for all $x \in A$. The set of such points, $\{x | \lambda x_0 + (1 - \lambda)x \in A, 0 \leq \lambda \leq 1, x \in A\}$, is called the *kernel* of the set A . The kernel of the star-shaped polygon of Figure 1.3.15(a) is shown by the densely shaded region. Obviously, a convex polygon is star-shaped, and its kernel is the convex polygon itself.

Let S be a closed subset of \mathbb{R}^m , S_i be a closed subset of S and $\mathcal{S} = \{S_1, \dots, S_n\}$ (when we deal with an infinite n , we assume that only finitely many S_i hit a bounded subset of \mathbb{R}^m). If elements in the set \mathcal{S} satisfy

$$[S_i \setminus \partial S_i] \cap [S_j \setminus \partial S_j] = \emptyset, \quad i \neq j, i, j \in I_n, \quad (1.3.20)$$

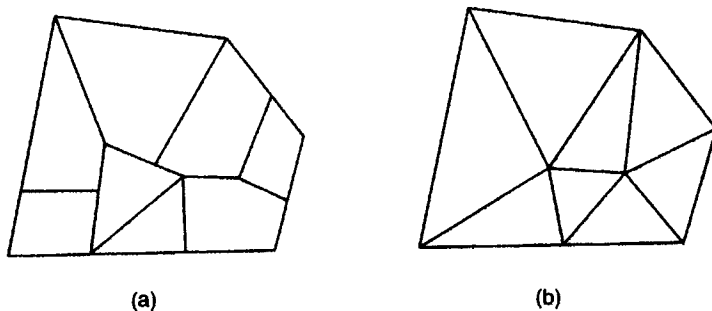


Figure 1.3.16 Tessellations: (a) a tessellation that is not a triangulation; (b) a triangulation.

and

$$\bigcup_{i=1}^n S_i = S_1 \cup \dots \cup S_n = S, \quad (1.3.21)$$

then we call the set \mathcal{S} a *tessellation* of S . Specifically, we call a tessellation in \mathbb{R}^2 a *planar tessellation* of S . Figure 1.3.16 shows two planar tessellations. The tessellation in panel (a) consists of polygons with three or more vertices, whereas that in panel (b) consists of only triangles. We call a planar tessellation like panel (b), i.e. a tessellation in which S_i in \mathcal{S} is a triangle for all $i \in I_n$, a *triangulation* of S .

1.3.2 Graphs

Suppose, as is shown in Figure 1.3.17(a), that there are four towns p_{g1}, \dots, p_{g4} (indicated by the filled circles) in a region and those towns are connected by roads L_{g1}, \dots, L_{g4} (indicated by line segments). We are living in the town p_{g1} and wish to visit towns p_{g3} and p_{g4} in this order without going through the other towns, and return to the town p_{g1} . To examine this type of trip feasibility, the distance between towns or the shape of roads are not essential; the essential information is whether or not there exists a direct road

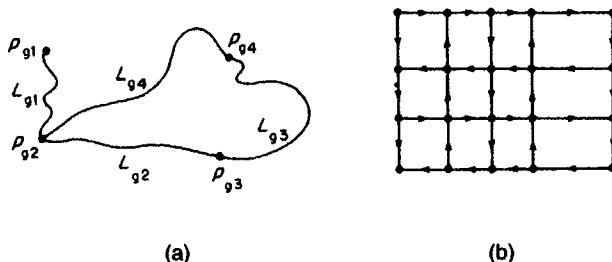


Figure 1.3.17 (a) Towns and roads between towns, and (b) one-way streets, which can be regarded as geometric graphs.

Table 1.3.1 Roads and their incident towns

Roads L_{g_i}	Towns incident with road L_{g_i}
L_{g_1}	p_{g_1}, p_{g_2}
L_{g_2}	p_{g_2}, p_{g_3}
L_{g_3}	p_{g_3}, p_{g_4}
L_{g_4}	p_{g_4}, p_{g_2}

between towns. This information is summarized in Table 1.3.1. Mathematically, we can treat the incidence of roads with towns listed in Table 1.3.1 using graph theory, which is to be introduced here.

To define a graph formally, let $P = \{p_1, \dots, p_{n_p}\}$ be a non-empty set, and $\{p_i, p_j\}$ be an unordered pair, where $p_i, p_j \in P$. The set of all distinct unordered pairs $\{\{p_i, p_j\} | p_i, p_j \in P\}$ is called the *unordered product* of P , and denoted by $P * P$ (note that $\{p_i, p_i\}$ is allowed). Let $L = \{L_1, \dots, L_{n_L}\}$ be a set which is possibly empty, and f be a mapping of L into $P * P$, i.e. $\{p_j, p_k\} = f(L_i)$. Just for notational simplicity, we write $L_i \sim \{p_j, p_k\}$ for $\{p_j, p_k\} = f(L_i)$. We call the paired sets P and L with the mapping f an (*undirected*) *abstract graph*, or simply a(n) (*undirected*) *graph*, and denote it by $G(P, L, f)$, $G(P, L)$ or G . To distinguish a geometric graph to be defined below, we sometimes use G_a for an abstract graph. An example of an abstract graph is given by

$$G_a(P, L, f) = G_a(\{p_1, p_2, p_3, p_4\}, \{L_1, L_2, L_3, L_4\}, \\ \{L_1 \sim \{p_1, p_2\}, L_2 \sim \{p_2, p_3\}, L_3 \sim \{p_3, p_4\}, L_4 \sim \{p_2, p_4\}\}). \quad (1.3.22)$$

If the sets P and L in G are finite, we call the graph a *finite graph*. In this text, we shall deal with only finite graphs.

Given a graph $G(P, L, f)$, we can construct a graph, called a *subgraph*, consisting of selected links and nodes of G with the same incidences as those of G satisfying that the selected nodes include all of the end points of the selected links. Mathematically, we call $G(P_s, L_s, f_s)$ a *subgraph* of G if and only if $G(P_s, L_s, f_s)$ satisfies the following three conditions: (i) $P_s \subset P$ and $L_s \subset L$; (ii) $f(L_i) = f_s(L_i)$ for every $L_i \in L_s$; (iii) if $L_i \in L_s$ and $\{p_j, p_k\} = f(L_i)$, then $p_j \in P_s$ and $p_k \in P_s$.

Inspecting the similarity between the function f of equation (1.3.22) and Figure 1.3.17(a) or Table 1.3.1 (which actually shows a function), we notice that the above abstract graph may be represented by a set of geometric points, and a set of geometric line segments connecting those points. For this representation, let us introduce the notion of a geometric graph.

Let $P_g = \{p_{g1}, \dots, p_{gn_p}\}$ be a set of n_p distinct points in the m -dimensional Euclidean space and $L_g = \{L_{g1}, \dots, L_{gn_l}\}$ be a set of n_l non-self-intersecting line segments with end points in P_g . The line segments in L_g may be straight or may be curved, but they should satisfy the following three properties.

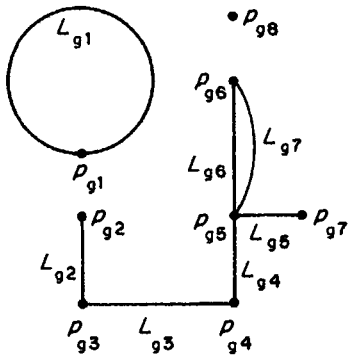


Figure 1.3.18 A geometric graph $G_g = G_g(\{p_{g1}, \dots, p_{g8}\}, \{L_{g1}, \dots, L_{g7}\})$.

- (i) Every line segment that forms a loop (a non-self-intersecting line segment whose end points coincide) contains exactly one point of P_g (for example, a loop with p_{g1} in Figure 1.3.18).
- (ii) Every line segment that does not form a loop contains exactly two points of P_g , and these points agree with its end points (for example, L_{g2} with p_{g2} and p_{g3} in Figure 1.3.18).
- (iii) Every line segment in L_g has no common points except for points of P_g (for example, L_{g2} and L_{g3} share p_{g3} in Figure 1.3.18).

We call the paired sets (P_g, L_g) satisfying the above properties a *geometric graph* and denote it by $G(P_g, L_g)$ or G . In particular, when L_g is a set of open straight line segments, $G(P_g, L_g)$ is called a *planar straight-line graph* and abbreviated to PSLG (Preparata and Shamos, 1985). When we distinguish a geometric graph from an abstract graph G_a , we sometimes use G_g . As is noticed from this definition, the end points of every line segment in L_g are included in P_g , but a point in P_g is not necessarily an end point of a line segment in L_g (such as p_{g8} in Figure 1.3.18).

From the definition of a geometric graph, we notice that the geometric points and the geometric line segments shown in Figure 1.3.16(a) actually form a geometric graph, i.e.

$$\begin{aligned} G_g(P_g, L_g, f_g) = & G_g(\{p_{g1}, p_{g2}, p_{g3}, p_{g4}\}, \{L_{g1}, L_{g2}, L_{g3}, L_{g4}\}, \\ & \{L_{g1} \sim \{p_{g1}, p_{g2}\}, L_{g2} \sim \{p_{g2}, p_{g3}\}, L_{g3} \sim \{p_{g3}, p_{g4}\}, L_{g4} \sim \{p_{g2}, p_{g4}\}\}). \end{aligned} \quad (1.3.23)$$

Moreover, we notice that there is a one-to-one correspondence between the vertices in the abstract graph G_a of equation (1.3.22) and those in the geometric graph G_g of equation (1.3.23) such that the adjacency relations are preserved.

To state this correspondence more precisely, let us consider two graphs $G(P_\alpha, L_\alpha, f_\alpha)$ and $G(P_\beta, L_\beta, f_\beta)$. First, when $G(P_\alpha, L_\alpha, f_\alpha)$ is an abstract graph and $G(P_\beta, L_\beta, f_\beta)$ is an abstract graph or a geometric graph, if there exist a one-to-one mapping φ_p of P_α onto P_β , and a one-to-one mapping φ_L of L_α onto L_β such that $\{p_j, p_k\} = f_\alpha(L_i)$, $L_i \in L_\alpha$, $p_j, p_k \in P_\alpha$, if and only if $\{\varphi_p(p_j), \varphi_p(p_k)\} = f_\beta(\varphi_L(L_i))$, then we say that the graphs $G(P_\alpha, L_\alpha, f_\alpha)$ and

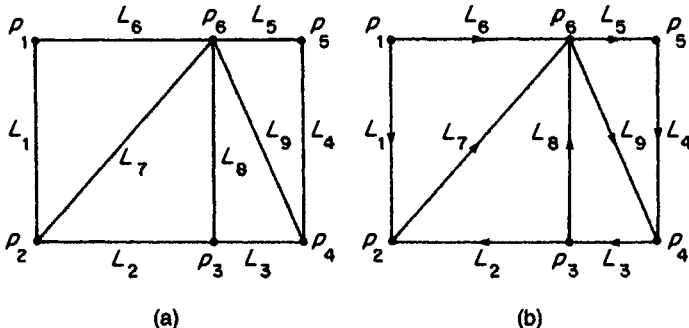


Figure 1.3.19 (a) An undirected graph and (b) a directed graph.

$G(P_\beta, L_\beta, f_\beta)$ are *isomorphic*. If an abstract graph G_a is isomorphic to a geometric graph G_g , then we say that graph G_g is a *geometric realization* of the abstract graph G_a . If a graph has a geometrical realization in \mathbb{R}^2 , we call the graph a *planar graph*; otherwise, a *non-planar graph*. Although graphs are not always planar graphs, every finite graph has a geometric realization in \mathbb{R}^3 . Comparing equations (1.3.22) and (1.3.23), we readily notice that the abstract graph G_a and the geometric graph G_g are isomorphic, and hence the geometric graph G_g is a geometric realization of the abstract graph G_a . Moreover, since the geometric graph G_g can be drawn on a plane (Figure 1.3.17(a)), it is a planar graph.

Second, when two graphs $G_g(P_\alpha, L_\alpha, f_\alpha)$ and $G_g(P_\beta, L_\beta, f_\beta)$ are both geometric graphs, the notion of isomorphic becomes a little stronger than the above. If $G_g(P_\beta, L_\beta, f_\beta)$ is obtained by deforming $G_g(P_\alpha, L_\alpha, f_\alpha)$ by moving the vertices continuously in \mathbb{R}^2 in such a way that the edges are also moved as their end points are moved (the edges may be extended or shrunken) and that no edges hit a vertex other than its own end points, then we say that graphs $G_g(P_\alpha, L_\alpha, f_\alpha)$ and $G_g(P_\beta, L_\beta, f_\beta)$ are *isomorphic*.

In the example of Figure 1.3.17(a) we implicitly assume that every road is two-way; we can drive, say, from p_{g1} to p_{g2} as well as from p_{g2} to p_{g1} . In the downtown of a city, however, streets are often one-way, such as in Figure 1.3.17(b). To take this directional feature into account in a graph, we introduce a direction on links in L .

Let $P = \{p_1, \dots, p_{n_p}\}$ be a non-empty set, (p_i, p_j) be an ordered pair, where $p_i, p_j \in P$ (cf. $\{p_i, p_j\}$), $L = \{L_1, \dots, L_{n_L}\}$ be a set which is possibly empty. The set of all distinct ordered pairs $\{(p_i, p_j) | p_i, p_j \in P\}$ is called the *ordered product* of P , and denoted by $P \times P$. Let f be a mapping of L into $P \times P$, i.e. $(p_i, p_j) = f(L_k)$, which is simply written as $L_k \sim (p_i, p_j)$. We call the paired sets P and L with mapping f a *directed graph*, which should be distinguished from the undirected graph defined above. The graphs in Figures 1.3.19(a) and 1.3.19(b) are an undirected graph and a directed graph, respectively.

The elements of P and L in G are called *nodes* and *links*, respectively, and f is called an *incidence mapping*. In particular, in a directed graph, p_i and p_k

in $L_i \sim (p_j, p_k)$ are called an *initial node* and a *terminal node*, respectively. For example, in the directed graph in Figure 1.3.19(b), p_1 is the initial node of L_1 , and p_2 is the terminal node of L_1 . If $L_i \sim \{p_j, p_k\}$ (for an undirected graph) or $L_i \sim (p_j, p_k)$ (for a directed graph), then L_i is said to be *incident* with each of p_j and p_k . In particular, in a directed graph, L_i is said to be *positively incident* with p_j and *negatively incident* with p_k . The nodes incident with a link are called *end points*. For $L_i \sim \{p_j, p_k\}$ or $L_i \sim (p_j, p_k)$, if $p_j = p_k$, then L_i is called a *loop* (L_{g1} in Figure 1.3.18 is a loop). If $L_i \sim \{p_j, p_k\}$ or $L_i \sim (p_j, p_k)$ and $L_i \sim \{p_j, p_k\}$ or $L_i \sim (p_j, p_k)$, then L_i and L_i are called *parallel links* (L_{g6} and L_{g7} are parallel links in Figure 1.3.18).

If $L_i \sim \{p_j, p_k\}$ or $L_i \sim (p_j, p_k)$, then p_j and p_k are called *adjacent nodes* (for example, p_2 and p_3 in Figure 1.3.19(a),(b) are adjacent nodes). If L_i and L_j share at least one common end point, then L_i and L_j are called *adjacent links* (for example, L_2 and L_3 in Figure 1.3.19(a),(b) are adjacent links). The number of links incident with p_i is called the *degree* of p_i , and denoted by $\delta(p_i)$ (for example, $\delta(p_2) = 3$ in Figure 1.3.19(a),(b)). In particular, in a directed graph, the number of positively incident links with p_i , denoted by $\delta^+(p_i)$, is called the *positive degree* of p_i , and the number of negatively incident links with p_i , denoted by $\delta^-(p_i)$, is called the *negative degree* of p_i (for example, $\delta^+(p_2) = 1$ and $\delta^-(p_2) = 2$ in Figure 1.3.19(b)). Obviously, the equation $\delta(p_i) = \delta^+(p_i) + \delta^-(p_i)$ holds. A node in P whose degree is zero is called an *isolated node* (for example, p_{g8} in Figure 1.3.18).

The adjacency of nodes may be indicated in terms of a matrix, called an *adjacency matrix*. To be explicit, consider a graph $G(\{p_1, \dots, p_n\}, L)$ and let C be an $n \times n$ matrix (n columns and n rows),

$$C = \begin{bmatrix} c_{11} & \cdots & c_{1n} \\ \vdots & \ddots & \vdots \\ c_{n1} & \cdots & c_{nn} \end{bmatrix}, \quad (1.3.24)$$

which is sometimes written as $[c_{ij}]$ for short. When G is an undirected graph, c_{ij} denotes the number of links incident with both nodes p_i and p_j . When G is a directed graph, let c_{ij} be the number of links directed from a node p_i to a node p_j . Then, the adjacency of nodes in graph G can be indicated by the matrix C , which we call an *adjacency matrix* of nodes. The adjacency matrices C_1 of the undirected graph shown in Figure 1.3.19(a) and C_2 of the directed graph shown in Figure 1.3.19(b) are given by

$$C_1 = \begin{bmatrix} 0 & 1 & 0 & 0 & 0 & 1 \\ 1 & 0 & 1 & 0 & 0 & 1 \\ 0 & 1 & 0 & 1 & 0 & 1 \\ 0 & 0 & 1 & 0 & 1 & 1 \\ 0 & 0 & 0 & 1 & 0 & 1 \\ 1 & 1 & 1 & 1 & 1 & 0 \end{bmatrix}, \quad C_2 = \begin{bmatrix} 0 & 1 & 0 & 0 & 0 & 1 \\ 0 & 0 & 1 & 0 & 0 & 1 \\ 0 & 1 & 0 & 0 & 0 & 1 \\ 0 & 0 & 1 & 0 & 0 & 0 \\ 0 & 0 & 0 & 1 & 0 & 0 \\ 0 & 0 & 0 & 1 & 1 & 0 \end{bmatrix},$$

respectively.

From the definition of c_{ij} and that of $\delta(p_i)$, it follows that the equation $\delta(p_i) = \sum_{j=1}^n c_{ij}$ holds for an undirected graph, and the equations $\delta^+(p_i) = \sum_{j=1}^n c_{ij}$ and $\delta^-(p_i) = \sum_{j=1}^n c_{ji}$ hold for a directed graph.

For a given graph, if we can traverse from node to node on successively adjacent links without visiting the same links more than once, we call such a set of links a *chain* in an undirected graph, and a *path* in a directed graph (note that in a directed graph, we are supposed to follow directions). For example, L_7, L_9, L_4, L_5, L_6 in Figure 1.3.19(a) is a chain, and L_7, L_9, L_3, L_8, L_5 in Figure 1.3.19(b) is a path. In traversing a chain or a path, if we visit every node only once, the chain or the path is called a *simple chain* or a *simple path*. The chain or the path in the above example is not a simple chain nor a simple path, because we visit p_6 twice. An example of a simple chain in Figure 1.3.19(a) is L_7, L_9, L_3 , and that of a simple path in Figure 1.3.19(b) is L_7, L_9, L_3 . Note that we allow a chain or a path that returns to the same node, for example $L_1, L_7, L_9, L_4, L_5, L_6$ in Figure 1.3.19(a), and L_7, L_9, L_3, L_2 in Figure 1.3.19(b). Such a chain and a path are called a *circuit* and a *cycle*, respectively. If we can traverse a circuit and a cycle visiting every node only once, we call them a *simple circuit* and a *simple cycle*, respectively. The circuit in the above example is not a simple circuit because we visit p_6 twice, but the cycle in the above example is a simple cycle.

In the graph of Figure 1.3.19(a) we can traverse from any node in P to any node in P through links. In this sense, the graph is connected. Stated a little more precisely, an undirected graph $G(P, L)$ is *connected* if there exists at least one chain between every pair of nodes in P ; the graph G is *disconnected* if there exists no chain between at least one pair of nodes in P . For example, the graph in Figure 1.3.19(a) is connected; the graph in Figure 1.3.18 is disconnected. In a directed graph $G(P, L)$, if there exists at least one path from any node to any node in P , we say that the graph is *strongly connected*. The directed graph in Figure 1.3.19(b) is not strongly connected because there is no path from node p_2 to node p_1 . A connected subgraph which is not contained in any larger connected subgraph is called a *component*. The graph in Figure 1.3.18(a) consists of three components.

The graph shown in Figure 1.3.20 is a connected graph, which looks like a tree (we shall often show a tree upside down). Obviously, an actual tree does not have looped twigs. In graph theory, if a graph is connected and does not have circuits, the graph is called a *tree (graph)*. When a graph is a tree, the following equation holds:

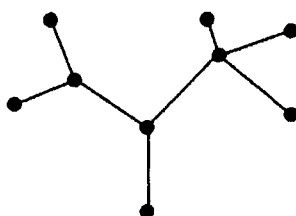


Figure 1.3.20 A tree graph

$$n_p - n_l = 1, \quad (1.3.25)$$

where n_p is the number of nodes and n_l the number of links in a tree.

When a graph is not a tree, equation (1.3.25) does not necessarily hold, but we have a more general equation, called Euler's formula. When a graph is a planar graph, links of the graph may partition the plane into disjoint regions one of which is unbounded. Let n_r be the number of those regions. Note that when a graph is a tree, the links of the tree do not partition the plane and hence we have only one (unbounded) region ($n_r = 1$). In terms of n_p , n_l and n_r , *Euler's formula* is stated as follows.

Euler's formula For a connected planar graph with n_p nodes, n_l links and n_r regions, the equation

$$n_p - n_l + n_r = 2 \quad (1.3.26)$$

holds.

Euler's formula can be generalized in \mathbb{R}^m .

The Euler–Poincaré formula (the Euler–Schlaefli formula) Let \mathcal{S} be a tessellation of a bounded set S in \mathbb{R}^m , and n_i be the number of i -faces in \mathcal{S} . Then the equation

$$\sum_{i=0}^m (-1)^i n_i = 1 + (-1)^m \quad (1.3.27)$$

holds.

We call this equation the *Euler–Poincaré formula* or the *Euler–Schlaefli formula*.

A planar graph is always associated with a 'dual graph'. To define it explicitly, let $G_g(P_g, L_g)$ be a planar graph with k regions R_i , $i \in I_k$. We take a point q_i in each region R_i (the unfilled circles in Figure 1.3.21(a)) and let $P_g^* = \{q_i, i \in I_k\}$. For each link which is shared by regions R_i and R_j , we generate a line segment combining q_i and q_j which crosses the common link only once and has no point in common with any other links of L (the broken

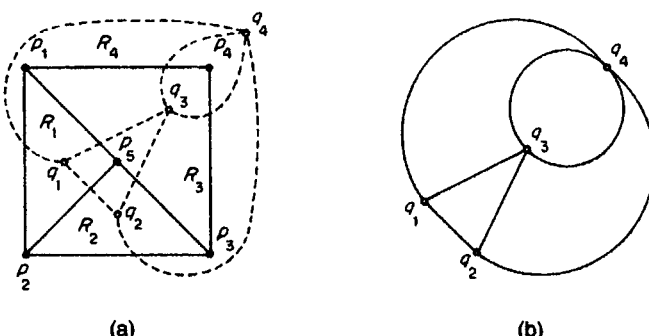


Figure 1.3.21 The primal and its dual graph.

line in Figure 1.3.21(a)). Let L_g^* be the set of resulting links. Then we obtain the new geometric graph G_g^* with P_g^* and L_g^* (Figure 1.3.21(b)). We call $G_g(P_g, L_g)$ the *dual graph* of $G_g(P_g, L_g)$. For the dual graph G_g^* , G_g is called the *primal graph*. Note that the dual graph and the primal graph are a relative notion. We can say that the dual graph of G_g^* is G_g . In this case, the primal graph is G_g^* .

1.3.3 Spatial stochastic point processes

A *stochastic point process* is a probabilistic generation of points in a space according to a probability distribution function defined over the space. From the term ‘process’, the reader might call to mind a process over time. In the study of *spatial stochastic point processes*, however, a time process is usually implicit. When we explicitly deal with a spatial stochastic point process over time, we call it a *spatial-temporal stochastic point process*.

Let f be a probability density function defined over S . The meaning of $f(x)$ is that the probability of a point being placed in a very small volume (area), ΔS , around x is given by $f(x) \Delta S$. An example of f is the *uniform distribution* given by

$$f(x) = \begin{cases} \frac{1}{|S|}, & x \in S, \\ 0, & x \notin S, \end{cases} \quad (1.3.28)$$

where $S \subset \mathbb{R}^m$ and $|S|$ is the area or volume of S ($|S| < \infty$). We call the process in which points are generated over S according to the uniform distribution a *binomial point process*. Figure 1.3.22 shows the binomial point process with $n = 50$ points in a unit square.

The reader may be curious to know why the above point process is called the binomial point process. To see the reason, let A be a subset of S , and $N(A)$ be the number of points placed in A when n points are generated according to the uniform distribution. Since the probability of a point being placed in A is given by $|A|/|S|$, the probability, $\Pr(N(A) = x)$, that x points are placed in A is given by

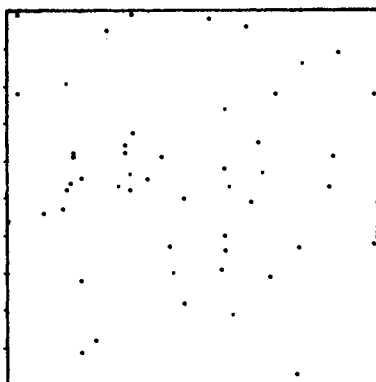


Figure 1.3.22 A binomial point process ($n = 50$).

$$\Pr(N(A) = x) = \binom{n}{x} \left(\frac{|A|}{|S|} \right)^x \left(1 - \frac{|A|}{|S|} \right)^{n-x}. \quad (1.3.29)$$

This distribution is the *binomial distribution* with the parameter values n and $\theta = |A|/|S|$, after which the above process is named.

In the above we defined the binomial point process by the uniform distribution. Alternatively, we can directly define the binomial point process by the binomial distribution. The *binomial point process* is defined by the process in which, for any subset A in S , the probability distribution of $N(A)$ is given by equation (1.3.29).

In a similar way, we can define a general stochastic point process. Let S be a non-empty subset of \mathbb{R}^m , and $N(A)$ be the number of points in a subset, A , of S . Then a *stochastic point process* is defined by the process in which points are generated according to a probability distribution $\Pr(N(A) = x)$, $x = 0, 1, \dots$, for any A in S . Specifically, if $m = 2$, the process is called a *planar stochastic point process*. If the probability of two points being coincident is zero under a stochastic point process, we say that the process is *simple*. If any finite region A in \mathbb{R}^m contains a finite number of points under a stochastic point process, the process is said to be *locally finite*. In this text, we deal with stochastic point processes that satisfy these two conditions.

Among many simple and locally finite stochastic point processes, the most fundamental process is the *Poisson point process*, which is defined by the process in which for any subset A in $S = \mathbb{R}^m$, $\Pr(N(A) = x)$ is given by

$$\Pr(N(A) = x) = \frac{\lambda^x |A|^x e^{-\lambda|A|}}{x!}, \quad x = 0, 1, 2, \dots \quad (1.3.30)$$

We can also define the Poisson point process as a limit of the binomial point process. The limit means the expansion of the finite region S to an infinite region keeping $n/|S|$ constant. Since $\lambda = n/|S|$ is the density of points, this expansion implies the expansion of the region S keeping the density of points constant. In the limit, the binomial distribution of equation (1.3.29) approaches the Poisson distribution of equation (1.3.30). We understand from this derivation that the parameter λ in the Poisson point process shows the density of points in a unit volume. The density λ is sometimes referred to as *intensity*.

In the above, we derived the Poisson point process directly from the Poisson distribution. More fundamentally, we can derive the Poisson point process from the following four postulates, through which we can see the characteristics of the Poisson point process explicitly.

Postulate PO1 $0 < \Pr(N(A) = 0) < 1$ if $0 < |A| < \infty$.

Postulate PO2 The probability distribution of $N(A)$ depends on $|A|$ and $\Pr(N(A) \geq 1)$ approaches zero as $|A|$ approaches 0.

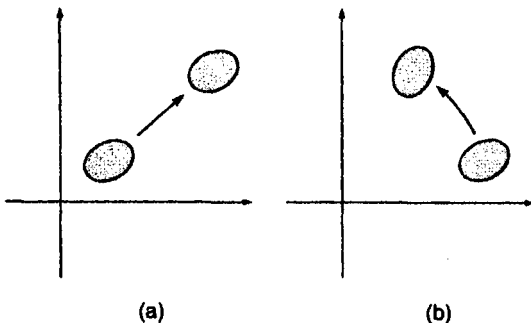


Figure 1.3.23
(a) Translation; (b)
rotation.

Postulate PO3 If A_1, \dots, A_n are disjoint, then $N(A_1), \dots, N(A_n)$ are mutually independent and $N(A_1 \cup \dots \cup A_n) = N(A_1) + \dots + N(A_n)$.

Postulate PO4

$$\lim_{|A| \rightarrow 0} \frac{\Pr(N(A) \geq 1)}{\Pr(N(A) = 1)} = 1. \quad (1.3.31)$$

Postulate PO1 asserts that if a region A has a positive volume, then the probability of a point being placed in the region A is not zero. Postulate PO2 asserts that $\Pr(N(A) = x)$ does not depend upon the location of A but only upon its volume (or its area for $m = 2$). There is no tendency for points to occupy particular regions in \mathbb{R}^m . Postulate PO3 means no interactions between points. We call this property *independent scattering*. It should be noted that the binomial point process is not independent scattering, because if x points are placed in A , then $n-x$ points are inevitably placed in $S \setminus A$. Postulate PO4 implies that the process is simple. If the random variable $N(A)$ satisfies the above four postulates for $A \subset \mathbb{R}^m$, then $N(A)$ is proved to follow the distribution of equation (1.3.30). Since this proof requires much space, we omit it here; the reader should consult a textbook on stochastic processes, for example Karlin (1969, pp. 337–43).

As is seen in Postulate PO2, the Poisson point process has the invariance property in the sense that $\Pr(N(A_1) = x) = \Pr(N(A_2) = x)$ for $|A_1| = |A_2|$. Generally, we can examine the characteristics of stochastic point processes in terms of invariance properties. First, let us consider the transformation of A in S defined by

$$\phi_c(A) = \{x + c \mid x \in A\}, \quad A \subset S, \quad \phi_c(A) \subset S, \quad (1.3.32)$$

where $c \in \mathbb{R}^m$ is a constant vector. If we regard A as a figure in \mathbb{R}^m , we may say that $\phi_c(A)$ moves the figure A without rotation in \mathbb{R}^m (see Figure 1.3.23(a), $m = 2$). We call such a transformation a *translation*. In observing equation (1.3.30), we readily notice that $\Pr(N(A) = x) = \Pr(N(\phi_c(A)) = x)$ holds; that is, the Poisson point process is invariant under translation.

Generally if a stochastic point process satisfies

$$\Pr(N(A_1) = x_1, \dots, N(A_k) = x_k) = \Pr(N(\varphi_c(A_1)) = x_1, \dots, N(\varphi_c(A_k)) = x_k), \quad (1.3.33)$$

$$A_i \subset S, \varphi_c(A_i) \subset S, \quad i = 1, \dots, k, \quad k = 1, 2, \dots,$$

we say that the stochastic point process is *homogeneous* or *stationary*. The binomial point process and the Poisson point process are homogeneous. This may be intuitively understood from the fact that the processes are derived from the uniform distribution.

We next consider the transformation of A in S defined by

$$\varphi_\theta(A) = \{Bx \mid x \in A, |B| = 1, B^T B = 1\}, \quad A \subset S, \varphi_\theta(A) \subset S, \quad (1.3.34)$$

where B is an $m \times m$ matrix and $|B|$ is its determinant. The transformation φ_θ rotates the figure A around the origin in \mathbb{R}^m as is shown in Figure 1.3.23(b) ($m = 2$). We call such a transformation a *rotation*. Since $|A| = |\varphi_\theta(A)|$ holds, $\Pr(N(A) = x) = \Pr(N(\varphi_\theta(A)) = x)$ holds for equation (1.3.30). Generally, if a stochastic point process satisfies

$$\Pr(N(A_1) = x_1, \dots, N(A_k) = x_k) = \Pr(N(\varphi_\theta(A_1)) = x_1, \dots, N(\varphi_\theta(A_k)) = x_k), \quad (1.3.35)$$

$$A_i \subset S, \varphi_\theta(A_i) \subset S, \quad i = 1, \dots, k, \quad k = 1, 2, \dots,$$

we say that the stochastic point process is *isotropic*. If a stochastic point process is homogeneous and isotropic, we call the stochastic point process *motion-invariant*. The binomial point process and the Poisson point process are motion-invariant.

The binomial point process and the Poisson point process have a stronger property than the motion-invariant property. If a transformation, φ_v , of A in S satisfies

$$|\varphi_v(A)| = |A|, \quad A \subset S, \varphi_v(A) \subset S, \quad (1.3.36)$$

we call φ_v the *volume-preserving transformation* (*area-preserving transformation* for $m = 2$). Obviously, translation and rotation are volume-preserving transformations. Generally, if a stochastic point process satisfies

$$\Pr(N(A_1) = x_1, \dots, N(A_k) = x_k) = \Pr(N(\varphi_v(A_1)) = x_1, \dots, N(\varphi_v(A_k)) = x_k), \quad (1.3.37)$$

$$A_i \subset S, \varphi_v(A_i) \subset S, \quad i = 1, \dots, k, \quad k = 1, 2, \dots,$$

we say that the stochastic point process is *volume-preserving*. From equation (1.3.29), we notice that the binomial point process is volume-preserving. The Poisson point process is also volume-preserving because Postulate PO2 is satisfied in that process.

The volume-preserving transformation can be extended to a measure-preserving transformation. To be explicit, consider a set S and a set \mathcal{A} of

subsets of S which satisfy the following three conditions: (i) $S \in \mathcal{A}$; (ii) if $A_i \in \mathcal{A}$, then $S \setminus A_i \in \mathcal{A}$; (iii) if $A_i \in \mathcal{A}$, $i = 1, 2, \dots$, then $\bigcup_{i=1}^{\infty} A_i \in \mathcal{A}$. We call the pair (S, \mathcal{A}) satisfying these conditions a *measurable space*. If a function, m , from \mathcal{A} to a non-negative real number satisfies $m(\emptyset) = 0$ and $m(\bigcup_{i=1}^{\infty} A_i) = \sum_{i=1}^{\infty} m(A_i)$, where A_1, A_2, \dots are mutually disjoint, we say that m is a *measure* on (S, \mathcal{A}) . A measurable space (S, \mathcal{A}) with a measure m is called a *measure space* and is denoted by a triple (S, \mathcal{A}, m) . In particular, if $m(S) = 1$, we call (S, \mathcal{A}, m) a *probability space*. If a transformation φ satisfies $\varphi^{-1}(A_i) \in \mathcal{A}$ for $A_i \in \mathcal{A}$, we say that φ is *measurable* (φ^{-1} is the inverse function of φ). If φ is one-to-one, if $\varphi(S) = S$ and if $A_i \in \mathcal{A}$ implies $\varphi^{-1}(A_i) \in \mathcal{A}$, then we say that φ is *invertible*. For a measurable transformation φ in (S, \mathcal{A}, m) , if

$$m(\varphi^{-1}(A)) = m(A), \quad A \in \mathcal{A}, \quad (1.3.38)$$

we say that φ is a *measure-preserving transformation* and a point process which satisfies equation (1.3.37) for all measure-preserving transformations is a *measure-preserving stochastic point process*; if φ is invertible, equation (1.3.38) is equivalent to $m(\varphi(A)) = m(A)$. In the following exposition, we assume, for simplicity, that a measure-preserving transformation is invertible. Obviously the volume-preserving transformation is a measure-preserving transformation. Thus the binomial point process and the Poisson point process are measure-preserving point processes.

To sum up, the Poisson point process is simple, independent scattering and invariant under the measure-preserving transformation; consequently it is motion-invariant, i.e. it is homogeneous and isotropic. Because of these properties, we sometimes say that a pattern of points resulting from the Poisson point process is a *complete spatial random pattern* or *complete spatial randomness*, and abbreviated to CSR (Diggle, 1983; note that Daley and Vere-Jones, 1988, refer to independent scattering as complete randomness).

We next introduce another important property of the Poisson point process, called *ergodicity*, which plays an important role in deriving the properties of the Poisson Voronoi diagram in Chapter 5. In the above discussion we regard a point process as a counting process (i.e. counting the number $N(A)$ of points in a region A). Alternatively we may regard a point process as a ‘random set’ of points. To be explicit, we consider the collection, \mathbb{M} , of all simple and locally finite sets of points in \mathbb{R}^m , and a collection, \mathcal{M} , of subsets of \mathbb{M} that satisfies (i), (ii) and (iii) above. Namely we consider a measurable space, $(\mathbb{M}, \mathcal{M})$. Let U be an element of \mathcal{M} (i.e. a set of sets of points), and Θ be a random variable of which each realization is an element of \mathbb{M} (i.e. a set of points). We call such a set of points Θ a *random set* of points. Let $P(U)$ be the probability of a random set Θ being an element of U , i.e.

$$P(U) = \Pr(\Theta \in U), \quad U \in \mathcal{M}. \quad (1.3.39)$$

Then $(\mathbb{M}, \mathcal{M})$ with P forms a measure space, or more specifically a probability space, $(\mathbb{M}, \mathcal{M}, P)$. In this context we may regard a *stochastic point*

process as a random set Θ determined by the probability distribution P over \mathcal{M} .

Let φ_x be the translation transformation, i.e.

$$\varphi_x(U) = \{\mathbf{x}_1 + \mathbf{x}, \mathbf{x}_2 + \mathbf{x}, \dots \mid \{\mathbf{x}_1, \mathbf{x}_2, \dots\} \in U\}, \quad U \in \mathcal{M}, \quad (1.3.40)$$

where $\mathbf{x} \in \mathbb{R}^m$. The set $\varphi_x(U)$ implies the set of sets of points that are translated by \mathbf{x} . For the sets $\varphi_x(U)$ and U , if the following equation holds,

$$P(U) = P(\varphi_x(U)) \text{ for any } \mathbf{x} \in \mathbb{R}^m \text{ and } U \in \mathcal{M}, \quad (1.3.41)$$

we say that a point process Θ is *stationary*. This definition is found to be equivalent to the definition given by equation (1.3.33) above.

Let $[-a, a]^m$ be a hyper-cube in \mathbb{R}^m whose edge is given by $[-a, a]$. For any sets U and W in \mathcal{M} , if the following relation holds,

$$\frac{1}{2^m a^m} \int_{[-a,a]^m} P(U \cap \varphi_x(W)) dx - P(U)P(W) \rightarrow 0 \text{ as } a \rightarrow 0, \quad (1.3.42)$$

we say that a stationary point process Θ determined by the distribution P is *ergodic*. A homogeneous Poisson point process, Θ_P , is ergodic.

To give an alternative definition of ergodicity, we define a set U , called an *invariant set*, as

$$P(U \setminus \varphi_x(U) \cup \varphi_x(U) \setminus U) = 0 \text{ for all } \mathbf{x} \in \mathbb{R}^m. \quad (1.3.43)$$

In this term, we may alternatively say that a stationary point process Θ is *ergodic* if $P(U)$ is 0 or 1 for any invariant set $U \in \mathcal{M}$. Stated differently, a stationary point process Θ determined by the distribution P is *ergodic* if P is not a mixture of two distinct stationary distributions, i.e. there do not exist two distinct stationary distributions P' and P'' such that $P = pP' + (1-p)P''$ for any $0 < p < 1$. Intuitively, this implies that P is not decomposable.

The ergodicity of a spatial stochastic point process enables us to find the spatial averages in individual realizations of the stochastic point process. To be explicit, consider a stationary point process Θ with intensity $\lambda > 0$ in which its distribution is given by P . For a set U in \mathcal{M} , we consider a point p_i satisfying that the point is an element of a set θ of points and is included in the cube $[0, 1]^m$ (i.e. $\mathbf{x}_i \in \theta \cap [0, 1]^m$) and that the set θ is an element of the set $\varphi_{x_i}(U)$ of sets of points (i.e. $\{\mathbf{x}_1, \mathbf{x}_2, \dots\} \in \varphi_{x_i}(U)$, where \mathbf{x}_i is the location vector of p_i). We consider the number of such points p_i , i.e. $\#\{i \mid \mathbf{x}_i \in \{\mathbf{x}_1, \mathbf{x}_2, \dots\} \cap [0, 1]^m \text{ and } \{\mathbf{x}_1, \mathbf{x}_2, \dots\} \in \varphi_{x_i}(U)\}$, where $\#(\text{a set})$ means the number of elements in the set. Then the sum of this number for θ in \mathcal{M} divided by λ is written as

$$P_0(U) = \frac{1}{\lambda} \int_{\mathcal{M}} \#\{i \mid \mathbf{x}_i \in \{\mathbf{x}_1, \mathbf{x}_2, \dots\} \cap [0, 1]^m \text{ and } \{\mathbf{x}_1, \mathbf{x}_2, \dots\} \in \varphi_{x_i}(U)\} P(d\theta), \quad U \in \mathcal{M}. \quad (1.3.44)$$

(Note that there are various expressions for $P(d\theta)$; see Stoyan *et al.*, 1995, p.101.) We call this distribution the *Palm distribution*, P_0 , of P . This

distribution implies that the point process, Θ_0 , determined by the distribution P_0 is a random shift of Θ such that Θ_0 has a point at the origin.

The ergodicity and the Palm distribution defined above have an important relation, which is shown in the following theorem (Daley and Vere-Jones, 1988, Proposition 12.4.I).

Theorem V1 Let P be the distribution of a stationary ergodic point process in \mathbb{R}^m with finite intensity $\lambda > 0$ and P_0 the corresponding Palm distribution. Denote by E_P and E_{P_0} the expectations under the distributions P and P_0 , respectively. For non-negative functions f and g defined on \mathcal{M} such that $E_P(f(\Theta))$ and $E_{P_0}(g(\Theta_0))$ are finite, we have the following relations with probability 1.

$$\begin{aligned} \frac{1}{2^m a^m} \int_{[-a,a]^m} f(\varphi_{-x}(\Theta_0)) dx &\rightarrow E_P(f(\Theta)) \text{ as } a \rightarrow \infty, \\ \frac{1}{n} \sum_{i=1}^n g(x_{N_i}) &\rightarrow E_{P_0}(g(\Theta_0)) \text{ as } a \rightarrow \infty, \end{aligned} \quad (1.3.45)$$

where x_{N_i} is the i th nearest point in Θ to the origin.

Equation (1.3.45) implies that the averages along an individual realization converge to the theoretical mean, which, loosely speaking, is the average of infinitely many realizations. Equation (1.3.45) is particularly important for the study of the Poisson Voronoi diagram (see Chapter 5). Suppose that $g(\Theta)$ is a characteristic of the Voronoi cell (see Chapter 2) containing the origin. Then the left-hand side of equation (1.3.45) means the average of the characteristic of n distinct Voronoi cells in an individual realization. If Θ is ergodic, the limit of the averages exists and is defined to be the mean of the characteristic of a *typical Voronoi cell* called by Cowan (1978, 1980; see Chapter 5). Equation (1.3.45) enables us to calculate the mean by using the Palm distribution (see Chapter 5).

The following theorem is quite useful to simplify the expectation calculation under the Palm distribution of a Poisson point process (Slivnak, 1962).

Theorem V2 A stationary point process Θ is a Poisson point process if and only if $\Theta \cup \{o\}$ has the same distribution as Θ_0 where o is the origin.

The Poisson point process satisfies a stronger property than ergodicity. A stationary point process Θ determined by the distribution P is said to be:

(i) *strongly mixing (α -mixing)* if for any subsets U and V in \mathcal{M} ,

$$P(U \cap \varphi_c(W)) - P(U)P(W) \rightarrow 0 \text{ as } \|c\| \rightarrow 0; \quad (1.3.46)$$

(ii) *weakly mixing* if for any subsets U and V in \mathcal{M} ,

$$\frac{1}{2^m a^m} \int_{[-a,a]^m} |P(U \cap \varphi_x(W)) - P(U)P(W)| dx \rightarrow 0 \text{ as } a \rightarrow 0. \quad (1.3.47)$$

Strong mixing implies weak mixing, which in turn implies ergodicity.

In addition to the above mixing conditions, there are many other mixing conditions which are different in their so-called *mixing coefficients*. Let \mathcal{U} and \mathcal{W} be two collections of subsets of \mathbb{M} . Then the α -mixing coefficients and the β -mixing coefficients are defined as:

$$\alpha(\mathcal{U}, \mathcal{W}) = \sup_{U \in \mathcal{U}, V \in \mathcal{W}} |\Pr(U \cap V) - \Pr(U)\Pr(V)|, \quad (1.3.48)$$

$$\beta(\mathcal{U}, \mathcal{W}) = E \sup_{W \in \mathcal{W}} |\Pr(W| \mathcal{U}) - \Pr(W)|, \quad (1.3.49)$$

where E is an expectation operator under the probability \Pr and $\Pr(W| \mathcal{U})$ is the conditional probability of W given \mathcal{U} . If $\alpha(\mathcal{U}, \mathcal{W})$ or $\beta(\mathcal{U}, \mathcal{W})$ goes to zero as the ‘distance’ (to be defined) between \mathcal{U} and \mathcal{W} tends to infinity, then we say that the α -mixing condition or the β -mixing (*absolute regularity*) condition is satisfied, respectively. Other mixing coefficients such as $\psi(\mathcal{U}, \mathcal{W})$, $\phi(\mathcal{U}, \mathcal{W})$ and $\varrho(\mathcal{U}, \mathcal{W})$ have also been defined in the literature (see, for example, Lin and Lu, 1996).

If \mathcal{U} and \mathcal{W} are the collections of subsets of \mathbb{M} which involve Θ and $\varphi_{-c}(\Theta)$, respectively, and the distance between them is defined to be $\|c\|$, then the point process Θ is α -mixing or β -mixing if the mixing coefficient $\alpha(\mathcal{U}, \mathcal{W}) \rightarrow 0$ or $\beta(\mathcal{U}, \mathcal{W}) \rightarrow 0$, respectively, as $\|c\| \rightarrow \infty$.

Finally, let us mention one more useful mixing condition. Suppose that \mathcal{U} and \mathcal{W} are collections of subsets of \mathbb{M} which involve $\Theta \cap [-a, a]^m$ and $\Theta \cap \{\mathbb{R}^m \setminus [-b, b]^m\}$, respectively, and the distance between them is defined to

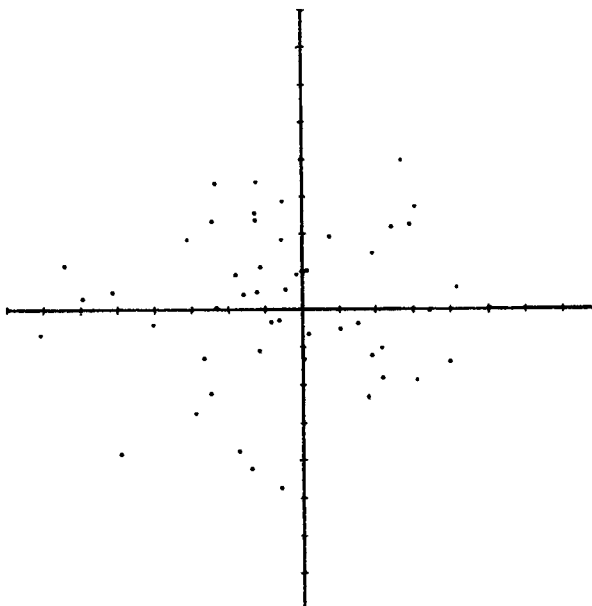


Figure 1.3.24 A general Poisson point process with $\lambda(x) = c_1 \exp(-c_2 \sqrt{x_1^2 + x_2^2})$.

be $b - a$. Heinrich (1994) established various theorems for Voronoi diagrams generated by a point process Θ (e.g. a homogeneous Poisson point process) for which $\beta(\mathcal{U}, \mathcal{W}) \rightarrow 0$ as $b - a \rightarrow \infty$ (see Section 5.6.1).

The Poisson point process may be extended in several directions. First, we may relax homogeneity, and define the point process by

$$\Pr(N(A) = x) = \frac{\lambda(A)! A^x e^{-\lambda(A)A}}{x!}, \quad x = 0, 1, 2, \dots, \quad (1.3.50)$$

where

$$\lambda(A) = \int_A \lambda(x) dx. \quad (1.3.51)$$

We call this point process the *general Poisson point process* with the intensity function $\lambda(x)$. An example is shown in Figure 1.3.24, where $\lambda(x) = c_1 \exp(-c_2 \sqrt{x_1 + x_2})$, $c_1, c_2 > 0$.

The general Poisson point process reduces to the Poisson point process of equation (1.3.30) if $\lambda(x) = \lambda$ (a constant). Since λ in equation (1.3.30) indicates the density of points, $\lambda(x)$ implies that the density depends upon where A is placed. Thus the density of points may vary from location to location in a general Poisson point process. This property distinguishes from that of the Poisson point process defined by equation (1.3.30) which we call the *homogeneous Poisson point process*.

In the homogeneous Poisson point process the parameter λ is deterministic. We may relax this assumption, and regard it as probabilistic. We call the Poisson point process with a probabilistic parameter λ a *doubly stochastic Poisson point process*, a *compound Poisson point process*, or a *Cox point process*. Such a point process is in general not ergodic.

We may also relax the property of independent scattering. Examples include the Poisson cluster processes, hard core processes and Gibbs point processes. We briefly mention these point processes here (in Section 5.12, we deal with Voronoi diagrams generated by these point processes).

Poisson cluster processes are point processes in which a cluster of points are independently scattered around a point of a Poisson point process; the clusters are independent and finite with probability 1; points of the Poisson point process are then deleted. If the clusters are not only independent but also identically distributed, such Poisson cluster processes are called the *Neyman–Scott processes*. *Hard core processes* are point processes in which there is a minimum interpoint distance. *Gibbs point processes* are a class of point processes in which interaction between points exists. A rigorous treatment of Gibbs point processes is rather mathematically involved. Here we present the simplest case: a Gibbs point process with a non-random total number of points in a bounded subset of \mathbb{R}^m . The distribution P of such a point process (see equation (1.3.39)) is in the form:

$$P(U) = \int \dots \int_{|x_1, \dots, x_n| \in U} f(x_1, \dots, x_n) dx_1 \dots dx_n, \quad U \in \mathcal{M}, \quad (1.3.52)$$

where the probability density function is given by

$$f(x_1, \dots, x_n) \propto \exp(-C(x_1, \dots, x_n)) \quad (1.3.53)$$

The function C , which does not depend on the order of its arguments, is called the *interaction energy function*. In statistical physics C is usually assumed to be the sum of pair potentials given by

$$C(x_1, \dots, x_n) = \sum_{1 \leq i < j \leq n} h(\|x_i - x_j\|). \quad (1.3.54)$$

If the pair potential function is

$$h(\|x_i - x_j\|) = \begin{cases} \infty & \text{if } \|x_i - x_j\| \leq r, \\ -b & \text{if } r < \|x_i - x_j\| \leq R, \\ 0 & \text{if } \|x_i - x_j\| > R, \end{cases} \quad (1.3.55)$$

then the corresponding Gibbs point process is a hard core point process with minimum interpoint distance r . If $b > 0$ or $b < 0$, there is attraction or repulsion, respectively, between points within a distance R . When the bounded subset is replaced by \mathbb{R}^m , the formulation is more sophisticated and so we do not discuss it here. The reader who is interested in general point processes, including the Gibbs point processes, should consult Bartlett (1975), Haggett *et al.* (1977, Chapter 13), Pielou (1977), Getis and Boots (1978), Matthes *et al.* (1978), Cliff and Ord (1981), Diggle (1983), Kallenberg (1983), Upton and Fingleton (1985), Daley and Vere-Jones (1988), Ripley (1988), Cressie (1991), Snyder and Miller (1991), Kingman (1993), Reiss (1993), and Stoyan *et al.* (1995), among others.

A random set of points or a stochastic point process may be generalized to a random set of lines or a stochastic line process. Stated precisely, a *stochastic line process* is a random collection of lines in \mathbb{R}^m and there are only finitely many lines that hit each bounded subset of \mathbb{R}^m . A line is uniquely determined by its perpendicular distance to the origin and the angle between the line and the x_1 -axis measured in a counterclockwise direction. Thus a line can be represented by a point in $\mathbb{R}^m \times (0, \pi]$. The *Poisson line process* in \mathbb{R}^m has the same distribution as the Poisson point process in $\mathbb{R}^m \times (0, \pi]$. Similarly, a random set of k -dimensional hyperplanes in \mathbb{R}^m ($1 \leq k \leq m$) forms a *hyperplane process*, which can be regarded as a point process in $\mathbb{R}^m \times (0, \pi]$. The *Poisson hyperplane process* is a stochastic hyperplane process the distribution of which is the same as the Poisson point process in $\mathbb{R}^m \times (0, \pi]$. A Poisson m -dimensional hyperplane process divides the space \mathbb{R}^m into polytopes. The resultant structure is known as the *Poisson hyperplane tessellation*. In particular, the Poisson m -dimensional hyperplane process (tessellation) is known as the *Poisson line process (tessellation)* if $m = 2$ and the *Poisson plane process (tessellation)* if $m = 3$. Details of the Poisson hyperplane tessellations can be found in Santaló (1976), Miles (1964a,b, 1972a, 1973, 1995), Matheron (1975), Crain and Miles (1976), Mecke (1995, 1999), and Stoyan *et al.* (1995).

In a stochastic line process we consider a random set of lines. Naturally, we can consider a random set of line segments. For example, at each point

of a Poisson point process we put a line segment the length of which is random and the angle between the line segment and the x_1 -axis is uniformly distributed on $(0, \pi]$. A line segment can be further generalized to a fibre, which is a segment of a curve. A random set of fibres in \mathbb{R}^2 is called a *stochastic fibre process*. Just as a line process in \mathbb{R}^2 can be generalized to a hyperplane process in \mathbb{R}^m , a stochastic fibre process can be generalized to a *stochastic manifold process* (Mecke, 1981), which is a random set of fragments of manifolds of fixed dimension. A *manifold* is the solution of a system of equations $f_1(x) = 0, \dots, f_k(x) = 0$. Thus, a random set of fragments of hyperplanes is a stochastic manifold process.

1.3.4 Efficiency of computation

When we carry out a computation using an algorithm with a set of input data, we wish to evaluate how ‘efficiently’ the algorithm runs. A standard method for evaluating the efficiency is to observe the asymptotic behaviour of the time required by the algorithm with respect to the size of input data (Knuth, 1968; Aho *et al.*, 1974). Let $T(n)$ denote the time required by an algorithm to process input data of size n . In general there are many different input data of the same size and they require different processing times. Hence we usually consider the worst case or the average case. In the worst case, $T(n)$ is the maximum time over all possible inputs of size n , whereas in the average case $T(n)$ is the average time over them. For some positive function $f(n)$ if there exists a constant C such that

$$\frac{T(n)}{f(n)} < C \text{ for all } n, \quad (1.3.56)$$

we write $T(n) = O(f(n))$ and say that $T(n)$ is of *order* $f(n)$. If $T(n) = O(f(n))$, we also say that the *time complexity* of the algorithm is of $O(f(n))$. Intuitively, $T(n)$ being of $O(f(n))$ implies that $T(n)$ does not increase more rapidly than $f(n)$ does as n grows. Hence the algorithm can be considered as being efficient if it admits a slowly increasing function $f(n)$ satisfying equation (1.3.56).

We say, for example, an algorithm with $T(n) = O(1)$ is ‘ideally fast’, and an algorithm with $T(n) = O(\log n)$ is ‘very fast’. An algorithm with $T(n) = O(n)$ is called a *linear time* algorithm, and an algorithm with $T(n) = O(n^q)$ is called a *polynomial time* algorithm.

Turing proposed an abstract model of a computer, which is called a *Turing machine*. There are two types of Turing machines. One is a *deterministic Turing machine*; it corresponds to an actual computer in which the machine behaves deterministically according to a given sequence of instructions (i.e. a program). The other type is a *non-deterministic Turing machine*. It does not correspond to an actual computer; it is more powerful in the sense that this machine can choose one of any possible branches of instruction sequences non-deterministically. See Aho *et al.* (1974), for example, for the strict definition of the Turing machine.

A problem whose answer is either ‘yes’ or ‘no’ is called a *decision problem*. For example, for a given set V of vectors, to judge whether V is linearly independent is a decision problem, whereas to find a maximal linearly independent subset of V is not a decision problem. The set of all decision problems that can be solved in polynomial time by a deterministic Turing machine is called a *class P*. On the other hand, the set of all decision problems that can be solved in polynomial time by a non-deterministic Turing machine is called a *class NP*. Since the non-deterministic Turing machine is more powerful than the deterministic one, the class NP includes the class P. It is a big open problem to judge whether the class P is a proper subset of the class NP.

A decision problem p is called *NP-complete* provided that p satisfies the following two conditions:

- (i) p belongs to the class NP.
- (ii) If p belongs to the class P, all the problems in the class NP belong to the class P.

Condition (ii) intuitively means that if someone finds an algorithm for solving p in polynomial time, then all the problems in the class NP can be solved using this algorithm. Hence, an NP-complete problem can be regarded as one of the most difficult problems in the class NP. The set of all NP-complete problems is called *class NP-complete*.

For a given graph, a cycle visiting all the vertices exactly once is called a *Hamilton cycle*. To judge whether a given graph has a Hamilton cycle is a decision problem belonging to the class NP-complete.

A general problem (i.e. a problem which is not necessarily a decision problem) is said to be *NP-hard* if it contains an NP-complete problem as a subproblem.

For a given geometric graph, finding the Hamilton cycle whose total length is minimum is called the *travelling salesperson problem*. The travelling salesperson problem is NP-hard, because if we solve this problem, we can also judge whether the graph has a Hamilton cycle.

CHAPTER 2

Definitions and Basic Properties of Voronoi Diagrams

In Chapter 1 we discussed the concept of a Voronoi diagram from a historical viewpoint. In this chapter we wish to fully develop this concept from a geometric viewpoint.

The chapter consists of six sections. In Section 2.1 we define a Voronoi diagram and introduce notations to be commonly used in this text. In Section 2.2 we define a Delaunay tessellation, in particular a Delaunay triangulation in terms of the ‘dual tessellation’ of a Voronoi diagram. Voronoi diagrams and Delaunay tessellations are, as we overviewed in Section 1.2, quite useful in various fields because of their nice geometric properties. In Sections 2.3 and 2.4 we show the basic geometric properties of Voronoi diagrams and Delaunay triangulations, respectively (specific properties only used in each chapter will be shown in that chapter). In Section 2.5 we refer to geometric graphs closely related to a Delaunay triangulation, such as a Gabriel graph, a relative neighbourhood graph and a minimum spanning tree. In Section 2.6 we show how to judge whether or not a given diagram is a Voronoi diagram.

2.1 DEFINITIONS OF THE ORDINARY VORONOI DIAGRAM

For ease of exposition, we first give a fairly intuitive definition of a Voronoi diagram in a plane. We next restate this definition more precisely in mathematical terms. Lastly, extending the definition in \mathbb{R}^2 to \mathbb{R}^m , we define an m -dimensional Voronoi diagram.

Suppose that a set of points is given in the Euclidean plane (for example, the filled circles in Figure 2.1.1). The number of points is assumed to be two or more but finite and they are all distinct in the sense that no points coincide in the plane. Given this point set, we assign every location in the plane to the closest member in the point set (in Figure 2.1.1, for example, the point p is assigned to the filled circle incident to the heavy broken line). If a location happens to be equally close to two or more members of the point set,

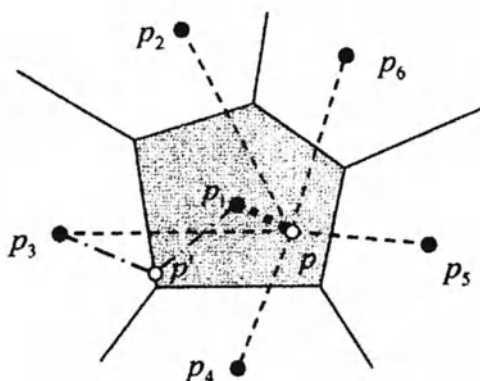


Figure 2.1.1 A planar ordinary Voronoi diagram.

we assign the location to those members (point p' in Figure 2.1.1 is assigned to the two filled circles incident to the dash-dot lines in Figure 2.1.1). As a result, the set of locations assigned to each member in the point set forms its own region (the shaded region in Figure 2.1.1). The resulting regions are collectively exhaustive in the plane because every location is assigned to at least one member in the point set. The set of locations assigned to two or more members in the point set forms the boundaries of the regions (the continuous lines in Figure 2.1.1). Hence adjacent regions overlap only on their boundaries. Thus the set of the regions is collectively exhaustive and mutually exclusive except for boundaries; namely, the set of the regions forms a tessellation. We call this tessellation a *planar ordinary Voronoi diagram*, and the regions constituting the Voronoi diagram *ordinary Voronoi polygons*.

To sum up, we have the following definition of a Voronoi diagram.

Definition V1 (a planar ordinary Voronoi diagram) Given a set of two or more but a finite number of distinct points in the Euclidean plane, we associate all locations in that space with the closest member(s) of the point set with respect to the Euclidean distance. The result is a tessellation of the plane into a set of the regions associated with members of the point set. We call this tessellation the *planar ordinary Voronoi diagram* generated by the point set, and the regions constituting the Voronoi diagram *ordinary Voronoi polygons*.

Note that when the Euclidean plane (space) is understood, or when there is no confusion with generalized Voronoi diagrams (to be shown in Chapter 3), we shall often refer to a planar ordinary Voronoi diagram simply as a *Voronoi diagram* and an ordinary Voronoi polygon as a *Voronoi polygon*. Also note that we exclude from our discussion the point set consisting of only one member, because such a Voronoi diagram is too trivial (it consists of only one Voronoi polygon which is the whole plane).

In the above definitions we define the Voronoi diagram for a set of finitely many points, but we can also define a diagram for a set of infinitely many points in the same manner. We also call the resulting diagram a Voronoi diagram (which is referred to as an *infinite Voronoi diagram* in Chapter 5). One diagram of this kind, the Poisson Voronoi diagram, is the subject of Chapter 5. In other chapters, however, we deal with only the former Voronoi diagram (which may be called a *finite Voronoi diagram*) because it is consistent with the applications to be presented throughout the book and, moreover, we want to avoid lengthy treatments resulting from the distinction between finite and infinite.

Let us now restate Definition V1 in mathematical terms. We consider a finite number, n , of points in the Euclidean plane, and assume that $2 \leq n < \infty$. The n points are labelled by p_1, \dots, p_n with the Cartesian coordinates $(x_{11}, x_{12}), \dots, (x_{n1}, x_{n2})$ or location vectors $\mathbf{x}_1, \dots, \mathbf{x}_n$. The n points are distinct in the sense that $\mathbf{x}_i \neq \mathbf{x}_j$ for $i \neq j$, $i, j \in I_n = \{1, \dots, n\}$. Let p be an arbitrary point in the Euclidean plane with coordinates (x_1, x_2) or a location vector \mathbf{x} . Then the Euclidean distance between p and p_i is given by $d(p, p_i) = \|\mathbf{x} - \mathbf{x}_i\| = \sqrt{(x_1 - x_{i1})^2 + (x_2 - x_{i2})^2}$. If p_i is the nearest point from p or p_i is one of the nearest points from p , we have the relation $\|\mathbf{x} - \mathbf{x}_i\| \leq \|\mathbf{x} - \mathbf{x}_j\|$ for $j \neq i$, $i, j \in I_n$ (recall the heavy broken and dash-dot lines in Figure 2.1.1). In this case, p is assigned to p_i . Therefore, Definition V1 is written mathematically as follows.

Definition V2 (a planar ordinary Voronoi diagram) Let $P = \{p_1, \dots, p_n\} \subset \mathbb{R}^2$, where $2 < n < \infty$ and $\mathbf{x}_i \neq \mathbf{x}_j$ for $i \neq j$, $i, j \in I_n$. We call the region given by

$$V(p_i) = \{\mathbf{x} \mid \|\mathbf{x} - \mathbf{x}_i\| \leq \|\mathbf{x} - \mathbf{x}_j\| \text{ for } j \neq i, j \in I_n\} \quad (2.1.1)$$

the *planar ordinary Voronoi polygon* associated with p_i (or the Voronoi polygon of p_i), and the set given by

$$\mathcal{V} = \{V(p_1), \dots, V(p_n)\} \quad (2.1.2)$$

the *planar ordinary Voronoi diagram* generated by P (or the Voronoi diagram of P). We call p_i of $V(p_i)$ the *generator point* or *generator* of the i th Voronoi polygon, and the set $P = \{p_1, \dots, p_n\}$ the *generator set* of the Voronoi diagram \mathcal{V} (in the literature, a generator point is sometimes referred to as a *site*).

For brevity we may write V_i for $V(p_i)$. Also, we may use $V(x_{i1}, x_{i2})$ or $V(\mathbf{x}_i)$ when we want to emphasize the coordinates or location vector of the generator point p_i . In addition, we may use $\mathcal{V}(P)$ when we want to explicitly indicate the generator set P of \mathcal{V} .

In Definition V2 the reader should notice that the relation in equation (2.1.1) is defined in terms of \leq , but not $<$. A Voronoi polygon is hence a closed set. Alternatively, we may define a Voronoi polygon as

$$V^\circ(p_i) = \{\mathbf{x} \mid \|\mathbf{x} - \mathbf{x}_i\| < \|\mathbf{x} - \mathbf{x}_j\| \text{ for } j \neq i, j \in I_n\}, \quad (2.1.3)$$

which is an open set. Both definitions are acceptable, but in this text we

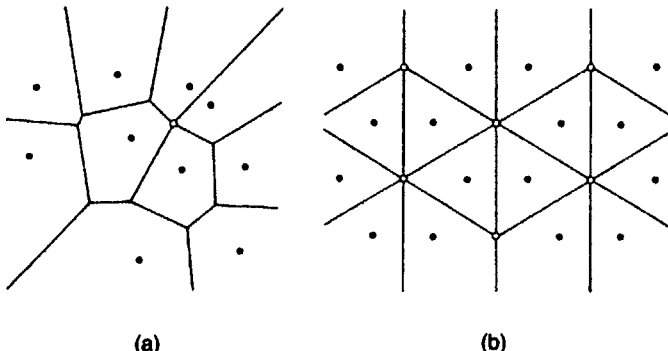


Figure 2.1.2 Degenerate Voronoi diagrams.

define a Voronoi polygon as a closed set. When we want to emphasize this property, we call $V(p_i)$ a *closed Voronoi polygon*, and $V^\circ(p_i)$ an *open Voronoi polygon*.

Since a Voronoi polygon is a closed set, it contains its boundary, which is denoted by $\partial V(p_i)$. The boundary of a Voronoi polygon may consist of line segments, half lines or infinite lines, which we call *Voronoi edges*. We denote a Voronoi edge by e_i . Note that a Voronoi diagram is sometimes defined by the union of Voronoi edges, i.e. $\cup_{i=1}^n \partial V(p_i)$ in place of the set $\{V(p_1), \dots, V(p_n)\}$. Since the union of Voronoi edges may be regarded as a network, it is sometimes called a *Voronoi network* (Medvedev *et al.*, 1988; Bartkowiak and Mahan, 1995).

Noticing that e is included in the relation of equation (2.1.1), we may alternatively define a Voronoi edge as a line segment, a half line or an infinite line shared by two Voronoi polygons with its end points. Mathematically, if $V(p_i) \cap V(p_j) \neq \emptyset$, the set $V(p_i) \cap V(p_j)$ gives a Voronoi edge (which may degenerate into a point). We use $e(p_i, p_j)$ for $V(p_j) \cap V(p_i)$, which is read as the Voronoi edge generated by p_i and p_j . Note that $e(p_i, p_j)$ may be empty. If $e(p_i, p_j)$ is neither empty nor a point, we say that the Voronoi polygons $V(p_i)$ and $V(p_j)$ are *adjacent*.

An end point of a Voronoi edge is called a *Voronoi vertex*. Alternatively, a Voronoi vertex may be defined as a point shared by three or more Voronoi polygons. We denote a Voronoi vertex by q_i . When there exists at least one Voronoi vertex at which four or more Voronoi edges meet in the Voronoi diagram \mathcal{V} (the unfilled circle in Figure 2.1.2(a)), we say that \mathcal{V} is *degenerate*; otherwise, we say that \mathcal{V} is *non-degenerate*. The Voronoi diagram in Figure 2.1.2(a) is degenerate and that in Figure 2.1.1 is non-degenerate. A degenerate Voronoi diagram often appears when generator points are regularly spaced, such as in Figure 2.1.2(b). In some derivations, a degenerate Voronoi diagram requires special lengthy treatments which are not always essential. To avoid this difficulty, we shall often make the following assumption.

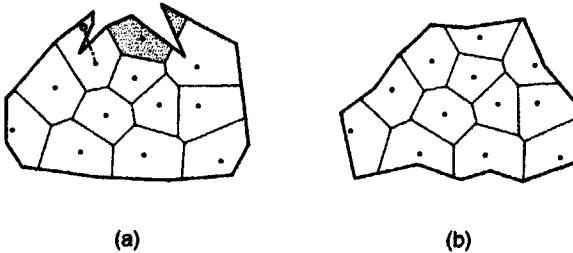


Figure 2.1.3 Bounded Voronoi diagrams: (a) a disconnected boundary Voronoi region (the shaded region) and a non-star-shaped boundary Voronoi polygon with respect to its generator (the broken line segment); (b) star-shaped boundary Voronoi polygons with respect to their generator points.

Assumption V1 (the non-degeneracy assumption) Every Voronoi vertex in a Voronoi diagram has exactly three Voronoi edges.

In Definition V1 or V2, we defined a Voronoi diagram in an unbounded plane. In practical applications, however, we often deal with a bounded region S where generator points are placed (the heavy lines in Figure 2.1.3). In this case we consider the set, $\mathcal{V}_{\cap S}$, given by

$$\mathcal{V}_{\cap S} = \{V(p_1) \cap S, \dots, V(p_n) \cap S\}. \quad (2.1.4)$$

We call this set a *bounded Voronoi diagram* or the *Voronoi diagram bounded by S* (which should be distinguished from the bounded Voronoi diagram defined by Wang and Schubert, 1987; see Section 3.4). If a Voronoi polygon $V(p_i)$ shares the boundary of S , we call the region $V(p_i) \cap S$ a *boundary Voronoi polygon* or *region* (the term ‘region’ is used when ∂S is curved or when $V(p_i) \cap S$ is not connected).

We should note that a boundary Voronoi region may be disconnected (the shaded region in Figure 2.1.3(a)), and that the line segment joining a point in $V(p_i)$ and p_i may not be contained in $V(p_i) \cap S$ (the broken line segment in Figure 2.1.3(a)). In practical applications, such boundary Voronoi polygons are often problematic, and so we have to define a more appropriate Voronoi diagram. We shall show such an alternative Voronoi diagram in Section 3.4. A bounded Voronoi diagram may be meaningful in practice if every boundary Voronoi region is star-shaped with respect to its generator point (Figure 2.1.3(b); recall Figure 1.3.15). In practice, we usually treat such a well-formed bounded Voronoi diagram.

As we observed in Figure 2.1.1, the ordinary Voronoi diagram consists of polygons. Recalling that a polygon is defined in terms of half planes (Section 1.3), we may alternatively define a Voronoi diagram in terms of half planes. To show this alternative definition, we consider the line perpendicularly bisecting the line segment $\overline{p_i p_j}$ joining two generator points p_i and p_j (Figure 2.1.4). We call this line the *bisector* between p_i and p_j and denote it by

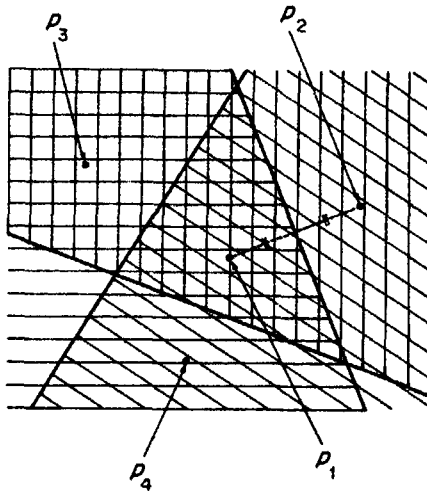


Figure 2.1.4 A Voronoi polygon obtained from half planes.

$b(p_i, p_j)$. Since a point on the bisector $b(p_i, p_j)$ is equi-distant from the generator points p_i and p_j , $b(p_i, p_j)$ is written as

$$b(p_i, p_j) = \{x \mid \|x - x_i\| = \|x - x_j\|\} \quad j \neq i. \quad (2.1.5)$$

The bisector divides the plane into two half planes and gives

$$H(p_i, p_j) = \{x \mid \|x - x_i\| \leq \|x - x_j\|\} \quad j \neq i. \quad (2.1.6)$$

We call the region $H(p_i, p_j)$ the *dominance region* of p_i over p_j . In Figure 2.1.4 we indicate the dominance regions of p_1 over p_2, p_3 and p_4 by the horizontally, diagonally and vertically hatched regions, respectively. Obviously, in the dominance region $H(p_i, p_j)$ the distance to the generator p_i is shorter than or equal to the generator p_j . In Figure 2.1.4, therefore, the distance from a point p in the intersection of the vertically, horizontally and diagonally hatched regions to the generator p_1 is shorter than or equal to the distance from p to the generator $p_j, j = 2, 3, 4$. This relation is equivalent to equation (2.1.1), and hence the intersection $H(p_1, p_2) \cap H(p_1, p_3) \cap H(p_1, p_4)$ gives the Voronoi polygon associated with p_1 . From this example, we understand that the following definition is an alternative to Definition V2.

Definition V3 (a planar ordinary Voronoi diagram defined with half planes)
Let $P = \{p_1, \dots, p_n\} \subset \mathbb{R}^2$, where $2 \leq n < \infty$ and $x_i \neq x_j$ for $i \neq j, i, j \in I_n$. We call the region

$$V(p_i) = \bigcap_{j \in I_n \setminus \{i\}} H(p_i, p_j) \quad (2.1.7)$$

the *ordinary Voronoi polygon* associated with p_i and the set $\mathcal{V}(P) = \{V(p_1), \dots, V(p_n)\}$ the *planar ordinary Voronoi diagram* generated by P .

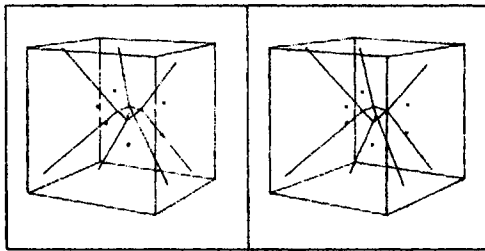


Figure 2.1.5 A stereographic view of a three-dimensional Voronoi diagram (view the left panel with the left eye and the right panel with the right eye at the same time, or use a stereographic viewer). (Source: Gen, 1983, p. 178.)

The equivalence of Definition V3 to Definition V2 is apparent, because $\|\mathbf{x} - \mathbf{x}_i\| \leq \|\mathbf{x} - \mathbf{x}_j\|$ if and only if $\mathbf{x} \in H(\mathbf{p}_i, \mathbf{p}_j)$ for $j \neq i$.

We can readily extend the above definition to the m -dimensional Euclidean space.

Definition V4 (an ordinary Voronoi diagram in \mathbb{R}^m) Let $P = \{\mathbf{p}_1, \dots, \mathbf{p}_n\} \subset \mathbb{R}^m$, where $2 \leq n < \infty$ and $\mathbf{x}_i \neq \mathbf{x}_j$ for $i \neq j$, $i, j \in I_n$. We call the region

$$V(\mathbf{p}_i) = \{\mathbf{x} \mid \|\mathbf{x} - \mathbf{x}_i\| \leq \|\mathbf{x} - \mathbf{x}_j\| \text{ for } j \neq i, j \in I_n\} \quad (2.1.8)$$

$$= \bigcap_{j \in I_n \setminus \{i\}} H(\mathbf{p}_i, \mathbf{p}_j) \quad (2.1.9)$$

the m -dimensional ordinary Voronoi polyhedron associated with \mathbf{p}_i , and the set $\mathcal{V}(P) = \{V(\mathbf{p}_1), \dots, V(\mathbf{p}_n)\}$ the m -dimensional ordinary Voronoi diagram generated by P , where $H(\mathbf{p}_i, \mathbf{p}_j)$ is given by equation (2.1.6) for $\mathbf{p}_i, \mathbf{p}_j \in \mathbb{R}^m$.

Note that when \mathbb{R}^m is understood, we may simply call $\mathcal{V}(P)$ an *ordinary Voronoi diagram* or just a *Voronoi diagram*, and that Voronoi polyhedra (polygons) are sometimes called *Voronoi cells*.

For the three-dimensional Voronoi diagram, the boundaries of a Voronoi polyhedron consists of facets, which we call *Voronoi facets*. The boundaries of a Voronoi facet consist of line segments, half lines or infinite lines, which we call *Voronoi edges*. The boundaries of a Voronoi edge consist of points, which we call *Voronoi vertices*. Figure 2.1.5 shows a stereographic view of a three-dimensional Voronoi diagram obtained by Gen (1983) (see also Bowyer, 1981). In astronomy, realized Voronoi polyhedra in a three-dimensional space are sometimes called *Voronoi foams* (Icke and van der Weygaert, 1987). In winner-take-all type neural networks, the Voronoi polyhedron $V(\mathbf{p}_i)$ is called the *receptive field* of a neural unit i with \mathbf{x}_i being the synaptic weight vector of this neural unit (Martinetz and Schulten, 1994).

A visual presentation of an m -dimensional Voronoi diagram becomes difficult when $m \geq 4$. Formally, we call the boundaries of an m -dimensional

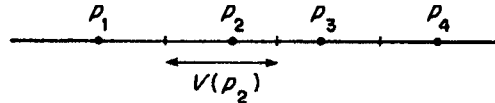


Figure 2.1.6 A Voronoi diagram on a line.

Voronoi polyhedron ($m-1$)-dimensional Voronoi faces; the boundaries of an ($m-1$)-dimensional Voronoi face ($m-2$)-dimensional Voronoi faces etc.; the boundaries of a three-dimensional Voronoi face two-dimensional Voronoi faces or simply Voronoi faces; the boundaries of a two-dimensional Voronoi face one-dimensional Voronoi faces or Voronoi edges; the boundaries of a one-dimensional Voronoi face zero-dimensional Voronoi faces or Voronoi vertices. An ($m-1$)-dimensional Voronoi face is also called a Voronoi facet.

Obviously we allow $m = 1$, a one-dimensional Voronoi diagram, or a Voronoi diagram on a line (Figure 2.1.6). In this case, a ‘one-dimensional Voronoi polyhedron’ is a half line or a line segment called a Voronoi line, and Voronoi vertices are end points of Voronoi lines. We easily notice that the boundary point between two adjacent Voronoi lines is the midpoint of the generator points of those Voronoi lines; the number of unbounded Voronoi lines is always two; the number of Voronoi lines adjacent to a Voronoi line is one or two. Because of these simple geometric properties, a Voronoi diagram on a line is often adopted in a simplified theoretical context to avoid complicated geometric arguments (for example, the original Hotelling model in Section 7.3). In this text we shall mainly treat a Voronoi diagram whose dimension is two or more.

In the above definitions, a space is represented by a continuous plane. This representation, however, may not be acceptable in some contexts, for instance raster image analysis. In such an analysis a space is represented by a set of square cells forming a grid lattice, and a geometrical figure is represented in terms of these cells. To be explicit, let $c_{ij} = \{(x, y) \mid i \leq x \leq i + 1, j \leq y \leq j + 1\}$, $i, j = \dots, -n, \dots, -1, 0, 1, \dots, n, \dots$. For a set of points representing a geometrical figure, G , we define $\text{Im}(G) = \{c_{ij} \mid c_{ij} \cap G \neq \emptyset\}$, called the image of G . In terms of $\text{Im}(G)$, we give the following definition (Dehne, 1989; Dehne *et al.*, 1991).

Definition V5 (a planar digitized Voronoi diagram) Let $\mathcal{V} = \{V(p_1), \dots, V(p_n)\}$ be the Voronoi diagram defined in Definitions V1–V3. We call the set $\text{Im}\mathcal{V} = \{\text{Im}(V(p_1)), \dots, \text{Im}(V(p_n))\}$ the (planar ordinary) digitized Voronoi diagram of \mathcal{V} , $\text{Im}(V(p_i))$ a digitized Voronoi region, and $\text{Im}(\partial V(p_i))$ the border of a digitized Voronoi region $\text{Im}(V(p_i))$.

An example is shown in Figure 2.1.7. Dehne (1989) shows a computational method for the planar ordinary digitized Voronoi diagram. Dehne (1989) also shows a computational method for a planar digitized Voronoi diagram generated by a set of objects with convex distance functions (see Section

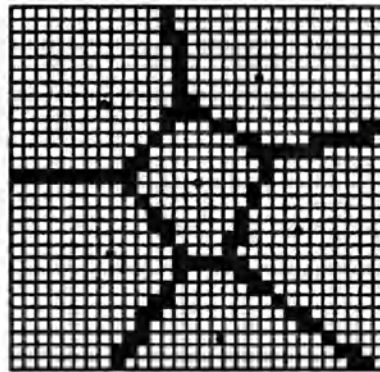


Figure 2.1.7 A planar ordinary digitized Voronoi diagram.

3.7). Embrechts and Roose (1996) develop a parallel algorithm using the Euclidean transformation. Also see Adamatzky (1994, 1996).

Alternatively we may define a Voronoi diagram by assigning cells to their nearest cells (Melkemi and Vandorpe, 1994; Watanabe and Murashima, 1996).

Definition V6 (a planar digital Voronoi diagram) Let $C = \{c_{ij}, i = 1, \dots, n_h, j = 1, \dots, n_v\}$ and $P_c = \{p_{ci}, \dots, p_{cn}\}$ be a subset of C , where $2 \leq n \leq n_v, n_h < \infty$, and $p_{ci} \neq p_{cj}$ for $i \neq j, i, j \in I_n$, and $d(c_{ij}, p_{ck})$ denotes the Euclidean distance between the centre of c_{ij} and that of p_{ck} . We call the region

$$\begin{aligned} V(p_{ci}) &= \{c_{kl} \mid d(c_{kl}, p_{ci}) < d(c_{kl}, p_{cj}) \text{ for } j \neq i; \\ &\quad d(c_{kl}, p_{ci}) = d(c_{kl}, p_{cj}) < d(c_{kl}, p_{cm}) \\ &\quad \text{for } i < j \neq m, k \in I_{n_k}, l \in I_{n_l}\} \end{aligned} \quad (2.1.10)$$

the *digital Voronoi polygon* associated with p_{ci} and the set $\mathcal{V}(P_c) = \{V(p_{ci}), \dots, V(p_{cn})\}$ the *digital Voronoi diagram* generated by P_c . Note that the second condition in equation (2.1.10) means that if a cell c_{kl} is equally distant from the generator cells p_{ci} and p_{cj} , we assign, for convenience, the cell c_{kl} to the generator that has a smaller index, i.e. p_{ci} where $i < j$ (not both as in the ordinary Voronoi diagram). Toriwaki and Yokoi (1988), Schwarzkopf (1989), Melter and Stojmenović (1995), and Watanabe and Murashima (1996) call the digital Voronoi diagram the *discrete Voronoi diagram*.

Recalling Definition V2, we notice that $V(p_i)$ is alternatively written in terms of a function $f_i(\mathbf{x}) = \|\mathbf{x} - \mathbf{x}_i\|$ as

$$V(p_i) = \{\mathbf{x} \mid f_i(\mathbf{x}) = \min_{j \in I_n} \{f_j(\mathbf{x})\}\}. \quad (2.1.11)$$

Geometrically, $z = f_i(\mathbf{x})$ shows the cone centred at \mathbf{x}_i in the three-dimensional space $\{(x_1, x_2, z)\}$, and hence $z = f_{\min}(\mathbf{x}) = \min_{j \in I_n} \{f_j(\mathbf{x})\}$ shows the lower envelope of the n cones, $z = f_1(\mathbf{x}), \dots, z = f_n(\mathbf{x})$. This envelope forms

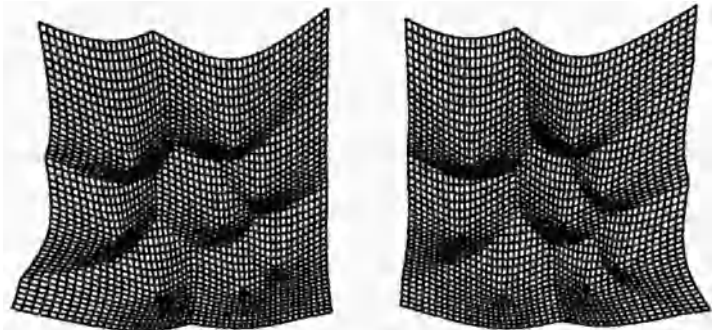


Figure 2.1.8 A Voronoi surface (look at the left-hand figure with the right eye and the right-hand figure with the left eye).

a surface, which we call the *Voronoi surface* of \mathcal{V} (Huttenlocher *et al.*, 1993). An example is shown in Figure 2.1.8 (also see Figure 2 in Webster, 1998). Alternatively we may replace $f_i(\mathbf{x}) = \|\mathbf{x} - \mathbf{x}_i\|$ with $f_i(\mathbf{x}) = \|\mathbf{x} - \mathbf{x}_i\|^2$, and obtain another surface $z = f_{\min}(\mathbf{x})$. This surface is differentiable except at points on the boundaries $\cup_{i=1}^n \partial V(p_i)$. Siersma (1998) examines the differential topology of this surface through the Morse theory.

2.2 DEFINITIONS OF THE DELAUNAY TESSELLATION (TRIANGULATION)

In the same way that a planar graph has its dual graph, a Voronoi diagram has its ‘dual tessellation’, called a Delaunay tessellation. In this section we define a Delaunay tessellation, in particular a Delaunay triangulation.

We consider a Voronoi diagram in the Euclidean plane, and assume that generator points of the Voronoi diagram are not on the same line as in Figure 2.2.1(a). Since this assumption will be adopted often in this text, we shall refer to it as:

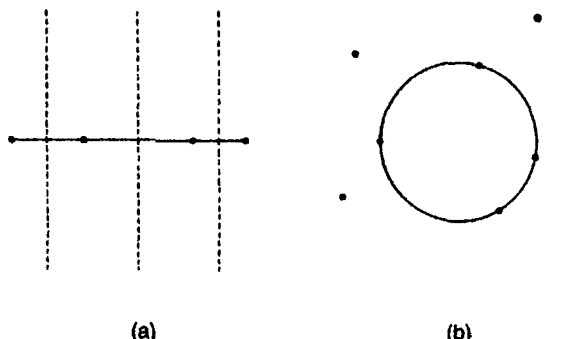


Figure 2.2.1 (a) Collinear generator points; (b) cocircular generator points.

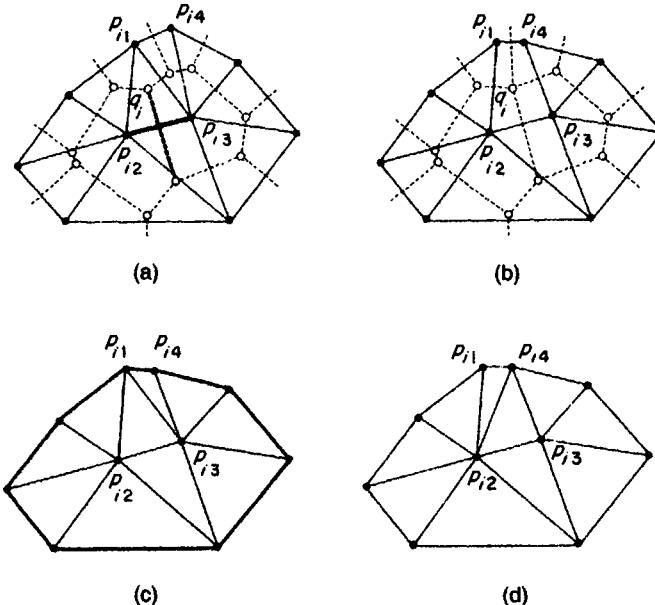


Figure 2.2.2 Voronoi diagrams (the broken lines) and triangulations (the solid lines): (a) a Delaunay triangulation; (b) a Delaunay pretriangulation; (c) a Delaunay triangulation obtained from (b); (d) another Delaunay triangulation obtained from (b).

Assumption D1 (the non-collinearity assumption) For a given set $P = \{p_1, \dots, p_n\}$ of points, the points in P are not on the same line.

Note that Elbaz and Spehner (1990) show an approximation test for collinearity, which is useful in numerical computation with finite digits.

In addition to this assumption we assume that the number of points is three or more but finite. Note that the non-collinearity assumption implicitly implies $n \geq 3$, because two points are always on the same line. Also note that this assumption was not made in the preceding section, but it is made here because, as will be shown later, without these assumptions we cannot obtain a triangulation. Also note that we can obtain a Voronoi diagram even when $n = 2$ or when generator points are collinear (the broken lines in Figure 2.2.1(a)).

Under the non-collinearity assumption and $3 \leq n < \infty$, we now show how to obtain a Delaunay triangulation from a Voronoi diagram (the broken lines in Figure 2.2.2). First we choose a Voronoi edge in a Voronoi diagram (the heavy broken line in Figure 2.2.2(a)). This Voronoi edge is shared by two Voronoi polygons. We join the generator points (the filled circles) of these Voronoi polygons by a line segment (the heavy solid line in Figure 2.2.2(a)). We carry out this line generation with respect to all Voronoi edges in the Voronoi diagram. As a result, we obtain a second tessellation of the convex hull of the generator points (the solid lines in Figure 2.2.2(a)). In Figure

2.2.2(b) we have another tessellation of the convex hull of the generator points (the solid lines) obtained from another Voronoi diagram (the broken lines). These two tessellations are different in that the tessellation in panel (a) consists of only triangles, whereas the tessellation in panel (b) contains a quadrangle. We call the former tessellation a *Delaunay triangulation*. The latter is not a triangulation, but since it is to be triangulated, we call it a *Delaunay pretriangulation*. Inspecting the Voronoi diagram indicated by the broken lines in Figure 2.2.2(b), we notice that a Delaunay pretriangulation occurs when the Voronoi diagram is degenerate (this condition will be proved in Property V7 in Section 2.3).

A Delaunay pretriangulation has polygons having four or more vertices. We partition these non-triangular polygons into triangles by non-intersecting line segments joining the vertices. For example, we partition the quadrangle with vertices $p_{i1}, p_{i2}, p_{i3}, p_{i4}$ in Figure 2.2.2(b) by the line segment $\overline{p_{i1}p_{i3}}$. As a result, the Delaunay pretriangulation becomes a tessellation consisting of only triangles (Figure 2.2.2(c)). We also call this tessellation a *Delaunay triangulation* (and sometimes a *degenerate Delaunay triangulation* to distinguish it from the above Delaunay triangulation). We should note that, as can be seen in Figures 2.2.2(c) and 2.2.2(d), a Delaunay triangulation obtained from a Delaunay pretriangulation is not unique; the quadrangle $p_{i1}p_{i2}p_{i3}p_{i4}$ can be triangulated either by the line segment $\overline{p_{i1}p_{i3}}$ or the line segment $\overline{p_{i2}p_{i4}}$. Both triangulations are acceptable.

A Delaunay triangulation should consist of at least one triangle, and this condition is guaranteed by the non-collinearity assumption. If the non-collinearity assumption and $3 \leq n < \infty$ are not satisfied, as in Figure 2.2.1(a), the above procedure does not produce triangles but line segments, or triangles which degenerate into line segments. To sum up, we have the following definition.

Definition D1 (a Delaunay triangulation) Given a Voronoi diagram where generator points are not collinear and their number is three or more but finite, we join all pairs of generator points whose Voronoi polygons share the common Voronoi edge. As a result, we obtain a second tessellation. If this tessellation consists of only triangles, we call it a *Delaunay triangulation*. If not, we call it a *Delaunay pretriangulation*. For the Delaunay pretriangulation, we partition non-triangular polygons into triangles by non-intersecting line segments joining the vertices. As a result, the Delaunay pretriangulation becomes a triangulation. We also call it a *Delaunay triangulation*.

Note that in the same procedure in Definition D1, we can construct a diagram from a Voronoi diagram defined for a set of infinitely many points. We also call it a Delaunay triangulation, but such a Delaunay triangulation is treated only in Chapter 5 (where it is called an *infinite Delaunay triangulation*).

In Definition D1 we constructed a tessellation by generating line segments with respect to every Voronoi edge. Alternatively, we may construct a tessellation by generating line segments with respect to every Voronoi vertex.

Although a Delaunay triangulation can be obtained from a Voronoi diagram constructed by the former method as well as the latter method, we employ the latter method here because it will be easily extended to the definition in \mathbb{R}^m (Definition D3).

We consider a Voronoi diagram $\mathcal{V}(P)$ generated by a set of distinct points $P = \{p_1, \dots, p_n\}$ ($3 \leq n < \infty$) which satisfies the non-collinearity assumption. Consider a Voronoi vertex q_i and let $V(p_{i1}), \dots, V(p_{ik_i})$ be the Voronoi polygons sharing the Voronoi vertex q_i . Note that the generator points p_{i1}, \dots, p_{ik_i} are indexed counterclockwise (or clockwise) around q_i (Figure 2.2.2(a)). For these generator points, we construct the polygon with line segments $\overline{p_j p_{j+1}}, j = 1, \dots, k_i$ (p_{ik_i+1} is read as p_{i1}). If the resulting polygon is a triangle (such as $\Delta p_{i1}p_{i2}p_{i3}$ in Figure 2.2.2(a)), we leave it as it is. If it is not a triangle (such as the quadrangle $p_{i1}p_{i2}p_{i3}p_{i4}$ in Figure 2.2.2(b)), we partition the polygon into triangles by non-intersecting line segments joining the vertices (Figures 2.2.2(c) and 2.2.2(d)). In this manner we construct triangles with respect to all Voronoi vertices in $\mathcal{V}(P)$. As a result, we obtain the set of triangles that forms a tessellation of the convex hull $\text{CH}(P)$ of P . We call this tessellation the *Delaunay triangulation* of $\text{CH}(P)$ spanning P . Stated a little more mathematically, we have the following definition.

Definition D2 (a Delaunay triangulation) Let $\mathcal{V}(P)$ be a Voronoi diagram generated by a set of n distinct points $P = \{p_1, \dots, p_n\} \subset \mathbb{R}^2$, ($3 \leq n < \infty$) that satisfies the non-collinearity assumption (D1); $Q = \{q_1, \dots, q_{n_v}\}$ be the set of Voronoi vertices in \mathcal{V} ; and x_{i1}, \dots, x_{ik_i} be the location vectors of the generator points whose Voronoi polygons share a vertex q_i . We define the set by

$$T_i = \left\{ x \mid x = \sum_{j=1}^{k_i} \lambda_j x_{ij}, \text{ where } \sum_{j=1}^{k_i} \lambda_j = 1, \lambda_j \geq 0, j \in I_{k_i} \right\} \quad (2.2.1)$$

(recall equation (1.3.19)) and let

$$\mathcal{D} = \{T_1, \dots, T_{n_v}\}. \quad (2.2.2)$$

If $k_i = 3$ for all $i \in I_{n_v}$, we call the set \mathcal{D} the *Delaunay triangulation* of $\text{CH}(P)$ spanning P . If there exists at least one $k_i \geq 4$, we call the set \mathcal{D} the *Delaunay pretriangulation* of $\text{CH}(P)$ spanning P . We partition T_i having $k_i \geq 4$ into $k_i - 2$ triangles by non-intersecting line segments joining the vertices, and denote the resulting triangles by $T_{i1}, \dots, T_{ik_i-2}$ (note that $T_{ik_i-2} = T_{i1} = T_i$ for $k_i = 3$). Let

$$\mathcal{D} = \{T_{i1}, \dots, T_{ik_i-2}, \dots, T_{n_v 1}, \dots, T_{n_v k_{n_v}-2}\}. \quad (2.2.3)$$

We call the set \mathcal{D} the *Delaunay triangulation* of $\text{CH}(P)$ spanning P , and triangles in \mathcal{D} *Delaunay triangles*.

As is seen in equation (2.2.1), a Delaunay triangle is defined as a closed set, and it contains the boundary consisting of line segments. We call these line segments *Delaunay edges*. Specifically, if a Delaunay edge is shared by

two Delaunay triangles, we call it an *internal Delaunay edge* (the light lines in Figure 2.2.2(c)); otherwise, we call it an *external Delaunay edge* (the heavy lines in Figure 2.2.2(c)). When \mathcal{V} is non-degenerate, a Voronoi edge and a Delaunay edge are in one-to-one correspondence. Hence the number of Voronoi edges in \mathcal{D} is the same as the number of Voronoi edges in \mathcal{V} . Unlike a Voronoi edge, a Delaunay edge is always finite. We call the end points of a Delaunay edge *Delaunay vertices*. Obviously, every Delaunay vertex is a generator of $\mathcal{V}(P)$, and hence the set of Delaunay vertices in \mathcal{D} is given by P .

In Definitions D1 and D2 we defined a Delaunay triangulation using a Voronoi diagram. This does not imply that a Delaunay triangulation should always be defined with a Voronoi diagram. In fact, we shall show in Section 2.3 that a Delaunay triangulation can be defined without a Voronoi diagram. We can define a Delaunay triangulation once a set P of points is given. To indicate this property explicitly, we sometimes write \mathcal{D} as $\mathcal{D}(P)$ in the same way that we write \mathcal{V} as $\mathcal{V}(P)$.

Since triangulation is a two-dimensional geometric notion, a Delaunay triangulation is defined only in \mathbb{R}^2 . We can, however, extend this notion (Definition D2) to the m -dimensional Euclidean space as follows.

Definition D3 (an m -dimensional Delaunay tessellation) Let $\mathcal{V}(P)$ be a Voronoi diagram generated by $P = \{p_1, \dots, p_n\} \subset \mathbb{R}^m$ ($m+1 \leq n < \infty$), where the generator points satisfy the non-collinearity assumption (D1); $Q = \{q_1, \dots, q_{n_v}\}$ be the set of Voronoi vertices (0-faces) in $\mathcal{V}(P)$; $V(p_{i1}), \dots, V(p_{ik_i})$ be Voronoi $(m-1)$ -faces sharing q_i ; and T_i be the m -dimensional convex hull spanning generator points p_{i1}, \dots, p_{ik_i} . If $k_i = m+1$ for all $i \in I_{n_v}$, the set $\mathcal{D}(P) = \{T_1, \dots, T_{n_v}\}$ consists of m -dimensional simplices. We call the set $\mathcal{D}(P)$ the *m -dimensional Delaunay tessellation* of $\text{CH}(P)$ spanning P . If there exists at least one $k_i \geq m+2$, we call the set $\mathcal{D}(P)$ the *m -dimensional Delaunay pretessellation* of $\text{CH}(P)$ spanning P (note that the pretessellation is a tessellation). We partition T_i having $k_i \geq m+2$ into $k_i - m$ simplices by non-intersecting hyperplanes passing through the vertices of T_i . Let $T_{i1}, \dots, T_{ik_i-m}$ be the resulting simplices ($T_{ik_i-m} = T_{i1} = T_i$ for $k_i = m+1$), and $\mathcal{D}(P) = \{T_{i1}, \dots, T_{ik_1-m}, \dots, T_{n_v1}, \dots, T_{n_vk_{n_v}-m}\}$. We call the set $\mathcal{D}(P)$ the *m -dimensional Delaunay tessellation* of $\text{CH}(P)$ spanning P , and a simplex in $\mathcal{D}(P)$ an *m -dimensional Delaunay simplex*. When the notion of a simplicial complex is the main concern, m -dimensional Delaunay tetrahedrization is sometimes called the *Delaunay simplicial complex* (Edelsbrunner and Shah, 1994).

As defined in Definition D1 or D2, a two-dimensional Delaunay tessellation is called a *Delaunay triangulation*. A three-dimensional Delaunay tessellation is called a *Delaunay tetrahedrization*. Figure 2.2.3 shows a stereographic view of a Delaunay tetrahedrization. Higher dimensional ($m \geq 3$) Delaunay tessellations have been investigated by many: Watson (1981), Bowyer (1981), Tanemura *et al.* (1983), Avis and Bhattacharya (1983), Field

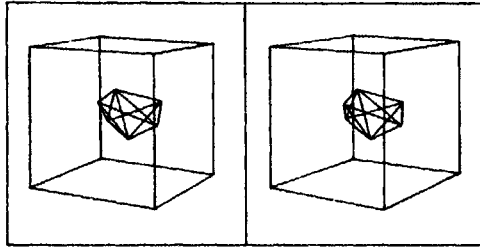


Figure 2.2.3 A stereographic view of a Delaunay tetrahedrization (view the left panel with the left eye and the right panel with the right eye, or use a stereographic viewer). (Source: Gen, 1983, p.78.)

(1986), Edelsbrunner *et al.* (1990a), Joe (1991a, 1993, 1995a), Dey *et al.* (1992b), Mohan and Lee (1993), Bertin *et al.* (1993), Teng *et al.* (1993), Rajan (1994), Weatherill and Hassan (1994), Borouchaki and Lo (1995), Lee and Jou (1995), Fang and Piegl (1995), Cignoni *et al.* (1995), Golias and Dutton (1997) and others. Escobar and Montenegro (1996) define a ‘*nearly*’ Delaunay tetrahedrization considering round-off errors made by the computer when working with floating arithmetic. In general the round-off errors are problematic in practical computations. Dey *et al.* (1992b), and Jünger *et al.* (1991) discuss this problem in depth with respect to a Delaunay triangulation and Minkowski Voronoi diagrams (Section 3.7.1). We also discuss this problem in Chapter 4.

2.3 BASIC PROPERTIES OF THE VORONOI DIAGRAM

Having defined a Voronoi diagram in Section 2.1, we now wish to observe their geometric properties. We deal mainly with the properties of a planar Voronoi diagram, but some of them may be readily extended to an m -dimensional Voronoi diagram. (Note that in what follows, fairly technical or lengthy derivations are shown in Proof . . . \square . The reader who wishes to know the properties first may skip those derivations without losing the main stream.)

Although we have already stated in Definition V2 that the region $V(p_i)$ given by equation (2.1.1) is a polygon, this property is readily seen from Definition V3 which defines a Voronoi polygon in terms of half planes (equation (2.1.7)). Since a half plane is a convex set and the intersection of convex sets is a convex set (Section 1.3.1), a Voronoi polygon is a convex set. Since generator points are distinct, a Voronoi polygon is non-empty. Since every point in \mathbb{R}^2 is assigned to at least one of the generator points (Definition V1), the Voronoi polygons in $\mathcal{V}(P)$ are collectively exhaustive in \mathbb{R}^2 . Moreover, noticing that Definition V3 implies $V(p_i) \subset H(p_i, p_j)$, $V(p_j) \subset H(p_j, p_i)$ and $[H(p_i, p_j) \setminus \partial H(p_i, p_j)] \cap [H(p_j, p_i) \setminus \partial H(p_j, p_i)] = \emptyset$, we understand that Voronoi polygons are mutually exclusive except for boundaries. These properties are quite obvious for an ordinary Voronoi diagram,

but some of them may not hold for generalized Voronoi diagrams (shown in Chapter 3). To draw attention to this contrast, we sum up these properties in Property V1.

Property V1 Let $P = \{p_1, \dots, p_n\} \subset \mathbb{R}^2$ ($2 \leq n < \infty$) be a set of distinct points. The set $V(p_i)$ defined by

$$V(p_i) = \{x \mid \|x - x_i\| \leq \|x - x_j\| \text{ for } j \neq i, j \in I_n\} \quad (2.3.1)$$

is a non-empty convex polygon, and $\mathcal{V}(P) = \{V(p_1), \dots, V(p_n)\}$ satisfies

$$\bigcup_{i=1}^n V(p_i) = \mathbb{R}^2, \quad (2.3.2)$$

$$[V(p_i) \setminus \partial V(p_i)] \cap [V(p_j) \setminus \partial V(p_j)] = \emptyset, \quad i \neq j, i, j \in I_n. \quad (2.3.3)$$

The Voronoi diagram $\mathcal{V}(P)$ is thus a unique tessellation of \mathbb{R}^2 for P .

It is straightforward to see that Property V1 also holds in \mathbb{R}^m if a polygon is replaced by a polyhedron and \mathbb{R}^2 is replaced by \mathbb{R}^m . Since a Voronoi polyhedron is a convex set, a bounded Voronoi polyhedron is sometimes called a *Voronoi polytope*. Since Voronoi polygons cover the Euclidean plane, it is obvious that at least one Voronoi polygon is unbounded. From the assumption that $n \geq 2$, we have two or more Voronoi polygons, some of which may be bounded. When generator points are collinear, we readily notice from Figure 2.2.1(a) that all Voronoi polygons are unbounded. When generator points are non-collinear, we have Property V2.

Property V2 For a Voronoi diagram generated by a set of distinct points $P = \{p_1, \dots, p_n\} \subset \mathbb{R}^2$ ($2 \leq n < \infty$), a Voronoi polygon $V(p_i)$ is unbounded if and only if p_i is on the boundary of the convex hull of P , i.e. $p_i \in \partial \text{CH}(P)$.

Proof Under the non-collinearity assumption, assume that some generator points are in the interior of $\text{CH}(P)$. We shall show that a Voronoi polygon whose generator is an interior point of $\text{CH}(P)$ is bounded. First, consider an interior generator point, p_i (p_i in Figure 2.3.1(a)). For p_i we can construct a triangle such that its vertices are generator points on the boundary of $\text{CH}(P)$, say $p_{i1}, p_{i2}, p_{i3} \in P$, and it contains p_i in its interior (see Figure 2.3.1(a)). We next construct the triangle by the intersection of the half planes $H(p_i, p_{i1}), H(p_i, p_{i2})$ and $H(p_i, p_{i3})$ (the dash-dot lines in Figure 2.3.1(a)). Since p_i is an interior point of $\triangle p_{i1}p_{i2}p_{i3}$, this triangle is bounded and $H(p_i, p_{i1}) \cap H(p_i, p_{i2}) \cap H(p_i, p_{i3}) \supset \bigcap_{j \in I_n \setminus \{i\}} H(p_i, p_j) = V(p_i)$. The Voronoi polygon $V(p_i)$ is thus bounded.

Conversely, assume that the Voronoi polygon $V(p_i)$ is bounded by Voronoi edges $e(p_i, p_j)$ generated by p_i and $p_j, i \neq j, j \in J_i$, where J_i is the set of indices of Voronoi polygons adjacent to $V(p_i)$ (Figure 2.3.1(b)). It is then obvious that p_i is in the interior of $\text{CH}(\{p_j, j \in J_i\})$ (the dash-dot lines in Figure

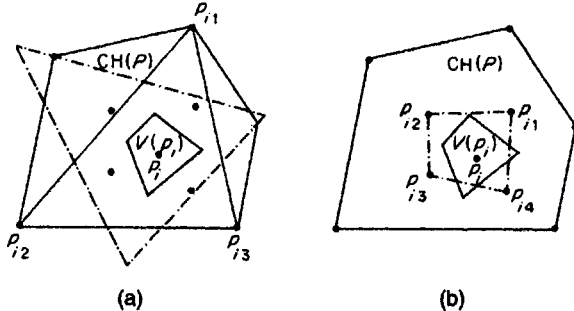


Figure 2.3.1 Illustration of the proof of Property V2.

2.3.1(b)). Since $\text{CH}(\{p_j, j \in J_i\}) \subset \text{CH}(P)$, p_i is not on the boundary of $\text{CH}(P)$. When generator points are collinear, all generator points are on $\text{CH}(P)$ which degenerates into a line segment, and all Voronoi polygons are unbounded. \square

Note that almost in the same manner, we can prove that Property V2 holds for an m -dimensional Voronoi polyhedron.

When a Voronoi diagram $\mathcal{V}(P)$ is given, we can obtain the convex hull of P using Property V2; line segments joining generator points whose Voronoi polygons are unbounded and share the boundary give $\text{CH}(P)$.

It follows from Property V2 that:

Property V3 For the Voronoi diagram generated by a set of distinct points $P = \{p_1, \dots, p_n\}$ ($2 \leq n < \infty$):

- (i) Voronoi edges are infinite straight lines if and only if P is collinear.
- (ii) A Voronoi edge $e(p_i, p_j)$ ($\neq \emptyset$) is a half line if and only if P is non-collinear and p_i and p_j are consecutive generator points of the boundary of $\text{CH}(P)$.
- (iii) Suppose that p_i and p_j give a Voronoi edge $e(p_i, p_j)$. Then this edge is a finite line segment if and only if the line segment $\overline{p_i p_j}$ is not an edge of $\text{CH}(P)$.

From Definition V3 we notice that Voronoi edges are parts of bisectors, but bisectors do not always generate Voronoi edges. The following property shows a sufficient condition for the generation of a Voronoi edge.

Property V4 The nearest generator point of p_i generates a Voronoi edge of $V(p_i)$.

Proof Let p_j be the nearest generator of p_i , and suppose that the bisector $b(p_i, p_j)$ does not generate a Voronoi edge. Let r_m be the midpoint of $\overline{p_i p_j}$ ($r_m \in b(p_i, p_j)$; Figure 2.3.2). Since $b(p_i, p_j)$ does not generate a Voronoi edge,

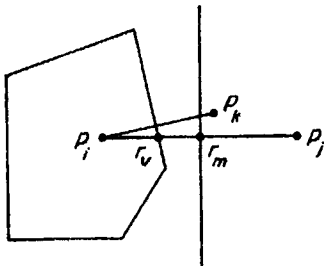


Figure 2.3.2 Illustration of the proof of Property V4.

r_m is outside of $V(p_i)$. Hence $\overline{r_m p_i}$ intersects a Voronoi edge, say $e(p_i, p_k)$, of $V(p_i)$, and let r_v be this intersection point. Since $\overline{p_i p_k}/2 \leq \overline{p_i r_v} < \overline{p_i r_m} = \overline{p_i p_j}/2$, we have $\overline{p_i p_k} < \overline{p_i p_j}$, but this contradicts that p_j is the nearest point of p_i . Thus, $b(p_i, p_j)$ generates the Voronoi edge $e(p_i, p_j)$. \square

From Property V4, we readily notice Property V5.

Property V5 The nearest generator point from p_i exists in the generator points whose Voronoi polygons share the Voronoi edges of $V(p_i)$.

This property is useful in solving the following well-known problems (Shamos and Hoey, 1975; Bentley *et al.*, 1980).

Problem V1 (the closest pair problem) For a finite set P of distinct points, if the distance between $p_i \in P$ and $p_j \in P$ is the minimum among the distances between all possible pairs of points in P , we say that the pair $\{p_i, p_j\}$ is the *closest pair*. Given P , find the closest pair.

Problem V2 (the all nearest neighbour problem) Given a finite set P of distinct points, find the nearest neighbour point of p_i for every $p_i \in P$.

Property V5 suggests that when we want to solve the above problems, we need not compare all distances from p_i with the rest of the generator points; we just compare the distances from p_i with the generator points whose Voronoi polygons share the Voronoi edges of $V(p_i)$. Once Problem V2 is solved with this comparison, it is easy to find reciprocal pairs. A pair $\{p_i, p_j\}$ is a *reciprocal (nearest) pair* when p_i is the nearest neighbour point of p_j , and p_j is the nearest neighbour point of p_i . The closest pair is found in the reciprocal pairs.

Properties V4 and V5 are concerned with the nearest generator point from a generator point. The next property is concerned with the nearest generator point from an arbitrary point.

Property V6 The generator p_i is the nearest generator point from point p if and only if $V(p_i)$ contains p .

Although this property is quite obvious (almost the definition of a Voronoi polygon itself), we state it in the above because it is very useful in solving the following problem.

Problem V3 (the nearest-search problem) Given a finite set P of distinct points, find the nearest neighbour point among P from a given point p (p is not necessarily a point in P).

This problem is often referred to as the *post office problem* (Knuth, 1973). A naive method for solving Problem V3 is to find the minimum distance among n distances, $\{\|x - x_i\|, i \in I_n\}$. When we have only one probe point, this calculation is not so arduous. However, if the number of probe points becomes fairly large, the calculation with this naive method becomes time consuming. To unburden this computational load, Property V6 is useful. In general, when a tessellation is given, the problem of finding a region in which a given probe point is placed is called the *point-location problem*. Using efficient methods developed in computational geometry, such as the bucketing technique in Chapter 4 (or Mücke *et al.*, 1996), we can efficiently search to find in which Voronoi polygon a probe point exists. Once this polygon is known, say $V(p_i)$, then we immediately know from Property V6 that p_i is the nearest generator point.

In conjunction with Problem V3, we note the following problem (Dickerson and Drysdale, 1990; Dickerson *et al.*, 1992; Dickerson and Eppstein, 1996).

Problem V4 (the fixed-radius nearest neighbour search problem) Given a finite set P of distinct points on the plane and a given distance δ , find all pairs of p_i and p_j in P that satisfy $\|x_i - x_j\| \leq \delta$.

To solve this problem, we first construct the Delaunay triangulation spanning P . Second, we choose the Delaunay edges $\bar{p}_i\bar{p}_j$ that satisfy $\|x_i - x_j\| \leq \delta$. The chosen edges form the graph $G(P_g, L_g)$, where P_g is the set of end points of the chosen edges and L_g is the set of the chosen open edges. Third, from each point $p_i \in P_g$, we do a depth-first search on $G(P_g, L_g)$, halting each branch of the search at the first point p_k such that $\|x_i - x_k\| \geq \delta$, and report all pairs $\{p_i, p_k\}$ with $\|x_i - x_k\| \leq \delta$ (Dickerson and Drysdale, 1990).

A Voronoi vertex also has interesting properties. Let $Q = \{q_1, \dots, q_n\}$ be the set of Voronoi vertices of $\mathcal{V}(P)$. Then we have the following property.

Property V7 For every Voronoi vertex, $q_i \in Q$, in a Voronoi diagram, there exists a unique circle C_i centred at q_i which passes through three or more generator points and contains no points in its interior. Under the non-degeneracy assumption, C_i passes through exactly three generator points.

Note that a circle which does not contain any points in its interior is called an *empty circle*; thus the circle C_i in Property V7 is an empty circle.

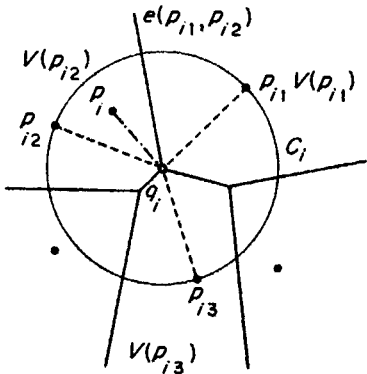


Figure 2.3.3 Illustration of the proof of Property V7.

Proof Since a Voronoi vertex q_i is shared by three or more Voronoi polygons, $V(p_{il}), \dots, V(p_{ik})$, $k \geq 3$, $p_{ij} \in P$, $j \in I_k$, where j is indexed counter-clockwise (Figure 2.3.3), three or more Voronoi edges, $e(p_{il}, p_{ij}), \dots, e(p_{ik}, p_{il})$, meet at q_i . Recalling that $e(p_{ij}, p_{ij+1})$ is contained in the bisector $b(p_{ij}, p_{ij+1})$, we see that the Voronoi vertex q_i is equally distant from p_{ij} and p_{ij+1} , i.e. $\overline{q_i p_{ij}} = \overline{q_i p_{ij+1}}$. Since this holds for $j \in I_k$ ($k+1$ is read as 1), we have $\overline{q_i p_{il}} = \dots = \overline{q_i p_{ik}}$ (the broken lines in Figure 2.3.3). The points p_{il}, \dots, p_{ik} are hence on the same circle, which is denoted by C_i .

We next show that the circle C_i is an empty circle. Suppose that point $p_j \in P \setminus \{p_{il}, \dots, p_{ik}\}$ is inside C_i . Then $\overline{q_i p_j} < \overline{q_i p_{ij}}$ for $j = 1, \dots, k$ (the dash-dot line in Figure 2.3.3), implying that q_i should be assigned to $V(p_j)$. This contradicts that q_i is shared only by $V(p_{il}), \dots, V(p_{ik})$. Hence C_i is an empty circle. \square

From Property V7, the non-degeneracy assumption is equivalent to the following assumption.

Assumption V2 (the non-cocircularity assumption) Given a set of points $P = \{p_1, \dots, p_n\} \subset \mathbb{R}^2$ ($4 \leq n < \infty$), there does not exist a circle, C , such that points $p_{il}, \dots, p_{ik} \in P$ ($k \geq 4$) are on C and all points in $P \setminus \{p_{il}, \dots, p_{ik}\}$ are outside C .

Note that Elbaz and Spehner (1990) show an approximation test for cocircularity.

This assumption can be extended to the assumption in \mathbb{R}^m if we replace a circle with a (hyper)sphere and 4 with $m+2$. In this case, we may call the assumption the *non-cosphericity assumption*. In the literature of Poisson Voronoi diagrams (Chapter 5), the configuration of P satisfying this assumption and the non-collinearity assumption (D1) is referred to as the *general quadratic position* (Møller, 1994) (note that Huttenlocher *et al.*, 1992b, refer to the configuration of P satisfying only the non-cosphericity assumption as the *general position*).

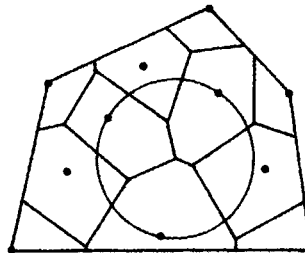


Figure 2.3.4 The largest empty circle whose centre is inside the convex hull of a set of points.

Immediately from Property V7, we obtain Property V8.

Property V8 The circle C_i in Property V7 is the largest empty circle among empty circles centred at the Voronoi vertex q_i .

Using this property with a slight modification, we can solve the following problem.

Problem V5 (the largest empty circle problem) Given a set P of distinct points, find the largest empty circle whose centre is in the convex hull of P .

Let Q' be the vertices of the Voronoi diagram \mathcal{V} bounded by $\text{CH}(P)$ (here Q' also includes the vertices formed at the points of the intersection between Voronoi edges and the boundary of the $\text{CH}(P)$), and C_i be the largest empty circle centred at $q_i \in Q'$. Then the largest circle among $\{C_i \mid q_i \in Q'\}$ gives the answer to Problem V5. An example is shown in Figure 2.3.4. This circle is useful to find the largest ‘empty area’ (an example is given in Section 7.3).

A Voronoi diagram has certain topological properties with respect to the number of Voronoi vertices, Voronoi edges and Voronoi polygons. To see them, we first induce a planar graph from a two-dimensional Voronoi diagram, $\mathcal{V}(P)$. Let $Q = \{q_1, \dots, q_{n_v}\}$ be the set of Voronoi vertices and $E = \{e_1, \dots, e_{n_e}\}$ be the set of Voronoi edges in $\mathcal{V}(P)$ in which the first n_c edges are infinite. Since infinite edges are not allowed in a geometric graph, a Voronoi diagram cannot be regarded as a geometric graph; we have to modify infinite Voronoi edges. To make this modification, we place a dummy point q_0 sufficiently far from $\text{CH}(P)$. We cut every infinite Voronoi edge at a certain point, and join its end point and q_0 with a line segment (Figure 2.3.5). Let $e_{b1}, \dots, e_{b n_c}$ be the edges obtained from e_1, \dots, e_{n_c} with this modification, and $E_b = [E \setminus \{e_1, \dots, e_{n_c}\}] \cup \{e_{b1}, \dots, e_{b n_c}\}$. Then, the pair of sets $Q_{+1} = Q \cup \{q_0\}$ and E_b actually forms a planar graph, $G(Q_{+1}, E_b)$. We call $G(Q_{+1}, E_b)$ the *Voronoi graph* induced from $\mathcal{V}(P)$. For a Voronoi graph, the Euler formula (equation (1.3.26)) holds, and hence we have the equation $(n_v + 1) - n_e + n = 2$ (n_v in equation (1.3.26) is n in \mathcal{V}), which is written as Property V9.

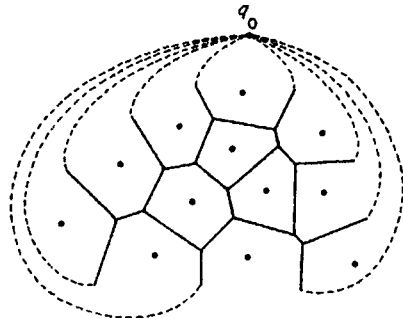


Figure 2.3.5 A Voronoi graph induced from a Voronoi diagram.

Property V9 Let n , n_e and n_v be the number of generator points, Voronoi edges and Voronoi vertices of a Voronoi diagram in \mathbb{R}^2 , respectively ($2 \leq n < \infty$). Then

$$n_v - n_e + n = 1. \quad (2.3.4)$$

As an extension of this property, we obtain Property V10 from the Euler–Poincaré formula (equation (1.3.26)).

Property V10 Let n_k be the number of k -dimensional Voronoi faces in an m -dimensional Voronoi diagram. Then,

$$\sum_{k=0}^m (-1)^k n_k = (-1)^m. \quad (2.3.5)$$

Under the non-collinearity assumption and $3 \leq n < \infty$, every vertex in the Voronoi graph $G(Q_{+1}, E_b)$ has at least three edges. Hence the number of edges in $G(Q_{+1}, E_b)$ is not less than $3(n_v + 1)/2$ (the 2 in the denominator implies that every edge is counted twice), i.e.

$$n_e \geq \frac{3}{2}(n_v + 1). \quad (2.3.6)$$

Substituting this relation into equation (2.3.4), we obtain Property V11.

Property V11 Let n , n_e and n_v be the number of generator points, Voronoi edges and Voronoi vertices of a Voronoi diagram in \mathbb{R}^2 , respectively, and assume that $3 \leq n < \infty$. Then

$$n_e \leq 3n - 6, \quad (2.3.7)$$

$$n_v \leq 2n - 5. \quad (2.3.8)$$

Although we derived this property under the non-collinearity assumption, Property V11 does not require it, because if generator points are collinear, then $n_v = 0$ and $n_e = n$, for which relations (2.3.7) and (2.3.8) hold for $n \geq 3$.

When a finite set P of generator points satisfies the non-collinearity assumption with $n \geq 3$, every bounded Voronoi polygon has at least three Voronoi edges, and every unbounded Voronoi polygon has at least two Voronoi edges. From these facts and recalling that the number of bounded Voronoi polygons is $n - n_e$ and that of unbounded Voronoi polygons is n_e ,

we notice that the number of edges is not less than $[3(n - n_c) + 2n_c]/2$ (the 2 in the denominator implies that every edge is counted twice), i.e.

$$n_e \geq \frac{3(n - n_c) + 2n_c}{2}. \quad (2.3.9)$$

Substituting equation (2.3.4) into this relation, we obtain Property V12.

Property V12 Let n, n_e, n_v and n_c be the numbers of Voronoi polygons, Voronoi edges, Voronoi vertices and unbounded Voronoi polygons of a planar Voronoi diagram $\mathcal{V}(P)$, respectively, where $3 \leq n < \infty$ and P satisfies the non-collinearity assumption. Then the following relations hold:

$$n_v \geq \frac{1}{2}(n - n_c) + 1, \quad (2.3.10)$$

$$n_e \leq 3n_v - n_c - 3. \quad (2.3.11)$$

A Voronoi polygon is given by the intersection of $n-1$ half planes (equation 2.1.9)). A Voronoi polygon thus has $n-1$ Voronoi edges at the maximum. At the minimum when generator points are collinear (Figure 2.2.1(a)), the leftmost and the rightmost Voronoi polygons have only one Voronoi edge. So, what is the average number of Voronoi edges of a Voronoi polygon? From relation (2.3.7) and the fact that every Voronoi edge is shared by exactly two Voronoi polygons, we notice that the average number of Voronoi edges per Voronoi polygon is less than or equal to $2(3n - 6)/n$ (also see Table 5.5.1 and equation (5.5.6)). We hence obtain Property V13.

Property V13 The average number of Voronoi edges per Voronoi polygon does not exceed six.

Relation (2.3.8) shows that the maximum possible number of Voronoi vertices in a two-dimensional Voronoi diagram is $2n - 5$. For an m -dimensional Voronoi diagram, we have the following property.

Property V14 The maximum number, $n_{\max}(i, m)$, of i -dimensional Voronoi faces of an m -dimensional Voronoi diagram generated by n distinct generator points is given by:

for $n \leq m + 1$,

$$n_{\max}(i, m) = \binom{n}{m+1-i}; \quad (2.3.12)$$

for $1 \leq m+1 \leq n$,

$$n_{\max}(i, m) = \begin{cases} C(m - i, m + 1) - 1, & i = 0, \\ C(m - i, m + 1), & 0 < i \leq m, \end{cases} \quad (2.3.13)$$

where

$$C(j, m+1) = \begin{cases} \sum_{i=1}^s \frac{n}{i} \binom{n-i-1}{i-1} \binom{i}{j-i+1}, & m+1=2s, \\ \sum_{i=1}^s \frac{j+2}{i+1} \binom{n-i-1}{i} \binom{i+1}{j-i+1}, & m=2s. \end{cases} \quad (2.3.14)$$

The proof of this property is shown in Seidel (1991) (also see Klee, 1980). This property is closely related to *Crum's problem*: what is the maximum number of non-overlapping convex polyhedra such that any pair of them has a common boundary of positive area? (Dewdney and Vranch, 1977.)

When a generator set is given, we can of course construct Voronoi edges. Conversely, when Voronoi edges are given without generator points, can we determine the locations of generator points? This problem is referred to as the *generator recognition problem* or the problem of *inverting the Voronoi diagram* (Adamatzky, 1993).

Problem V6 (the generator recognition problem) Provided that the Voronoi edges of a non-degenerate Voronoi diagram $\mathcal{V}(P)$ are given, recover the locations of generator points P .

Note that this problem can be extended to generalized Voronoi diagrams (Chapter 3; see Ash and Bolker, 1985), and degenerated cases are discussed in depth in Section 2.6.

To consider this problem, see Figure 2.3.6. Let q_i be a Voronoi vertex, p_{i1}, p_{i2}, p_{i3} be generator points whose Voronoi polygons share q_i , and q_{i1}, q_{i2}, q_{i3} be Voronoi vertices of the Voronoi edges incident to q_i . From Property V7, q_i is the centre of the circle that passes through p_{i1}, p_{i2}, p_{i3} . Since the Voronoi edges $e(p_{i1}, p_{i2}), e(p_{i2}, p_{i3})$ and $e(p_{i3}, p_{i1})$ perpendicularly bisect the Voronoi edges $\overline{q_{i2}q_i}, \overline{q_{i3}q_i}$, and $\overline{q_{i1}q_i}$, respectively, we have the equations $\angle p_{i1} q_i p_{i1} = \alpha_i, \angle p_{i2} q_i p_{i2} = \beta_i, \angle p_{i3} q_i p_{i3} = \gamma_i$. Hence

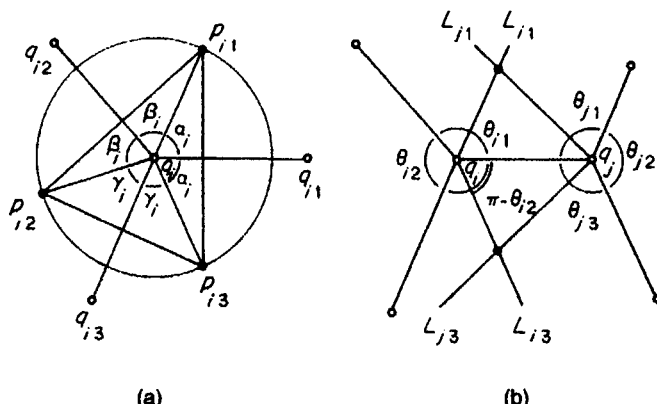


Figure 2.3.6 Recognition of generator points from Voronoi edges.

$2\alpha_i + 2\beta_i + 2\gamma_i = 2\pi$, i.e. $\alpha_i = \pi - \beta_i - \gamma_i = \pi - \angle q_{i2} q_i q_{i3}$. From this equation, we obtain Property V15.

Property V15 Let $\overline{q_i q_j}$ be a Voronoi edge in a non-degenerate Voronoi diagram, and θ_{ik} and θ_{jk} , $k = 1, 2, 3$, be acute angles at q_i and q_j , respectively, where k is indexed counterclockwise from $\overline{q_i q_j}$ at q_i and clockwise at q_j (Figure 2.3.6(b)). Let L_{ik} (L_{jk}) be the half line radiating from q_i (q_j) with angle $\pi - \theta_{iz}$ ($\pi - \theta_{jz}$) with $\overline{q_i q_j}$ in the sector of θ_{ik} (θ_{jk}), $k = 1, 3$. Then the intersection point made by L_{ii} and L_{jj} , and that by L_{i3} and L_{j3} give the generator points of the Voronoi diagram sharing $\overline{q_i q_j}$.

This property can be developed into a more general property with which we can examine whether or not a given planar tessellation, $\mathcal{T} = \{S_1, \dots, S_n\}$, is a Voronoi diagram. Suppose that the tessellation \mathcal{T} consists of convex polygons and every vertex has exactly three edges. Let q_{i1}, \dots, q_{ik_i} be the vertices of a polygon S_i indexed counterclockwise. Let p_{ij} be the intersection point in S_i obtained through the same procedure stated in Property V15, where $\overline{q_i q_j}$ is replaced by $\overline{q_{ij} q_{ij+1}}$, $j = 1, \dots, k_i$ (k_i+1 should be read as 1). Then we have the following property.

Property V16 A planar tessellation consisting of convex polygons whose vertices are all degree three is a Voronoi diagram if and only if $p_{i1} = p_{i2} = \dots = p_{ik_i}$ holds for $i \in I_n$, where p_{ij} is defined in the above.

The proof of this property is provided by Ash and Bolker (1985). Degenerated cases are shown in Section 2.6.

A closely related problem to Problem V6 was raised by Heath and Kasif (1993). Consider a planar tessellation \mathcal{T} consisting of k regions and a planar Voronoi diagram \mathcal{V} generated by a finite set P of n distinct points (Figure 2.3.7). We say that \mathcal{V} is *finer* than \mathcal{T} if every region in \mathcal{T} is partitioned into one or more regions of \mathcal{V} , or every edge which forms part of the boundary of \mathcal{T} is covered by a union of Voronoi edges of \mathcal{V} (Heath and Kasif, 1993).

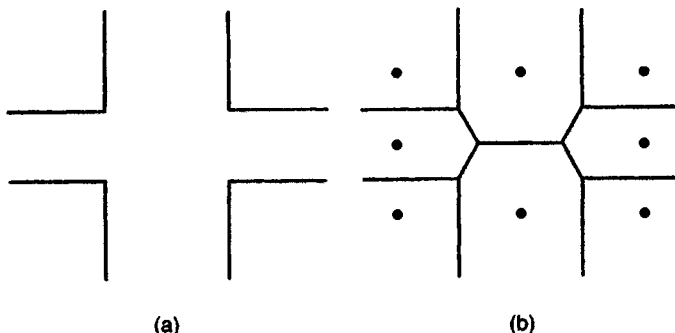


Figure 2.3.7 (a) A tessellation \mathcal{T} , and (b) a Voronoi diagram \mathcal{V} that is finer than \mathcal{T} .

(obviously, $k \leq n$). We call the set P a *Voronoi cover* of \mathcal{T} or, more specifically, n -*Voronoi cover* if \mathcal{V} is finer than \mathcal{T} .

Problem V7 (the Voronoi cover problem) For a given tessellation \mathcal{T} consisting of k regions and an integer n ($k \leq n$), is there a Voronoi cover $P = \{p_1, \dots, p_n\}$ of \mathcal{T} that contains no more than n points? If there is, find the locations of such generator points P .

Note that if $k = n$, the Voronoi cover problem is equivalent to the generator recognition problem (Problem V6). Heath and Kasif (1993) show that this problem is NP-hard (Section 1.3.4).

A planar Voronoi diagram is of course defined in \mathbb{R}^2 , but interestingly we can construct this Voronoi diagram through a polyhedron in \mathbb{R}^3 . This construction uses a transformation from a point in \mathbb{R}^2 to a point in \mathbb{R}^3 , which is illustrated in Figure 2.3.8. Let p_i be a point on the x - y plane with coordinates (x_i, y_i) . We lift this point vertically by height $z_i = x_i^2 + y_i^2$, and denote the lift-up point by p_i^* . The coordinates of p_i^* are given by $(x_i, y_i, x_i^2 + y_i^2)$. Recalling that the set $A = \{(x, y, z) \mid z = x^2 + y^2\}$ represents the paraboloid of the revolution along the z -axis, we notice that the point p_i^* is on the paraboloid A . Thus the above transformation is to lift a point p_i on the x - y plane vertically to the point p_i^* on the paraboloid A . We call this transformation the *lift-up transformation*; that is, we call the transformation from (x_i, y_i) to (x_i, y_i, z_i) by $z_i = x_i^2 + y_i^2$ the *lift-up transformation* from p_i to p_i^* , and call p_i^* the *lift-up* of p_i . For a set $P = \{p_1, \dots, p_n\}$ of points, we also say that $P^* = \{p_1^*, \dots, p_n^*\}$ is the *lift-up* of P .

For a given finite generator set P on the x - y plane, let P^* be the lift-up of P , and A_i be the plane tangential to the paraboloid A at p_i^* (Figure 2.3.9). Then the plane A_i is given by

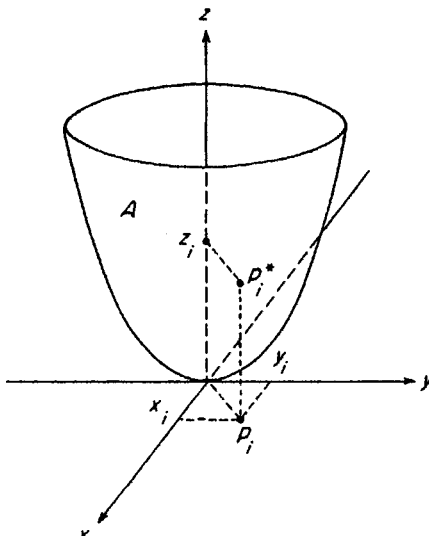


Figure 2.3.8 The lift-up transformation (p_i^* is the lift-up of p_i).

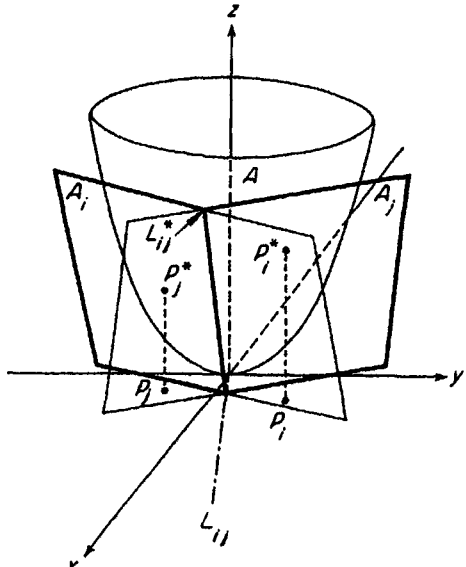


Figure 2.3.9 The construction of a planar Voronoi diagram through a polyhedron in \mathbb{R}^3 .

$$z = 2x_i x + 2y_i y - (x_i^2 + y_i^2). \quad (2.3.15)$$

Notice that p_i^* is on the plane A_i and the points of P^* , other than p_i^* , are all above the plane A_i .

We next consider the intersection of two planes A_i and A_j , $i \neq j$ (Figure 2.3.9). Obviously this intersection, denoted by L_{ij}^* , is a line in \mathbb{R}^3 . We project the line L_{ij}^* on the x - y plane orthographically, and let L_{ij} be the projected line (the dash-dot line in Figure 2.3.9). The line L_{ij} is algebraically obtained by eliminating z from the equations of (2.3.15) for i and j . As a result, we obtain

$$2(x_i - x_j)x + 2(y_i - y_j)y - (x_i^2 + y_i^2 - x_j^2 - y_j^2) = 0. \quad (2.3.16)$$

This equation represents the line perpendicularly bisecting $\overline{p_i p_j}$, namely the bisector $b(p_i, p_j)$ between p_i and p_j .

The plane A_i divides \mathbb{R}^3 into two half spaces. Let H_i be the half space given by the region above the plane A_i with the boundary A_i , i.e.

$$H_i = \{(x, y, z) \mid z \geq 2x_i x + 2y_i y - (x_i^2 + y_i^2)\}. \quad (2.3.17)$$

For two half spaces H_i and H_j ($i \neq j$), we construct the intersection $H_i \cap H_j$ (the heavy solid lines in Figure 2.3.9), which forms a polyhedron in \mathbb{R}^3 . Since the orthographic projection of the edge of the polyhedron $H_i \cap H_j$ onto the x - y plane is the bisector between p_i and p_j , the orthographic projection of the facet of $H_i \cap H_j$ containing A_i onto the x - y plane gives the half plane $H(p_i, p_j)$. From this property we understand that the orthographic projection of the surface of the polyhedron given by $\bigcap_{i=1}^n H_i$ onto the x - y plane gives $\mathcal{V}(P)$. To sum up, we obtain the following property.

Property V17 The Voronoi diagram $\mathcal{V}(P)$ is obtained as the orthographic projection of the facets of the polyhedron made by the intersection of all upper half spaces $H_i, i \in I_n$, onto the x - y plane, where the upper half space H_i is the region above the plane tangential to the paraboloid at the lift-up point of the generator p_i .

We note that a planar Voronoi diagram can also be obtained through the inversion transformation in \mathbb{R}^3 , which will be referred to in Section 2.4 (Property D7), and that the Delaunay triangulation obtained through the lift-up transformation is linked to a certain matroid, called the *Delaunay oriented matroid* (Santos, 1996).

2.4 BASIC PROPERTIES OF THE DELAUNAY TRIANGULATION

Corresponding to Property V1 of a Voronoi diagram, we first state the following basic property which is almost obvious from Definition D2.

Property D1 The set T_i defined by equation (2.2.1) is a unique non-empty polygon, and the set $\mathfrak{D}(P) = \{T_1, \dots, T_{n_v}\}$ given by equation (2.2.2) satisfies

$$\bigcup_{i=1}^{n_v} T_i = \text{CH}(P), \quad (2.4.1)$$

$$[T_i \setminus \partial T_i] \cap [T_j \setminus \partial T_j] = \emptyset, \quad i \neq j, i, j \in I_{n_v}. \quad (2.4.2)$$

Hence the set $\mathfrak{D}(P)$ forms a unique tessellation spanning P . If P satisfies the non-cocircularity assumption, $\mathfrak{D}(P)$ is a Delaunay triangulation; otherwise, $\mathfrak{D}(P)$ is a Delaunay pretriangulation. A Delaunay triangulation obtained from the Delaunay pretriangulation through the procedure mentioned in Definition D2 is not unique.

Although implicitly stated in equation (2.4.1) (and the heavy lines in Figure 2.2.2(c)), it follows from Definition D1 and Property V2 that:

Property D2 The external Delaunay edges in $\mathfrak{D}(P)$ constitute the boundary of the convex hull of P .

Thus the Delaunay triangulation spanning P is a triangulation of $\text{CH}(P)$ spanning P . Since $\text{CH}(P)$ is bounded, all Delaunay triangles and Delaunay edges are finite. This property is in contrast to Properties V2 and V3 of a Voronoi diagram.

In Properties V4–V6 we showed the properties concerning the nearest neighbour point in a Voronoi diagram. To find a similar property for a Delaunay triangulation, let us inspect the Delaunay triangulations in Figure

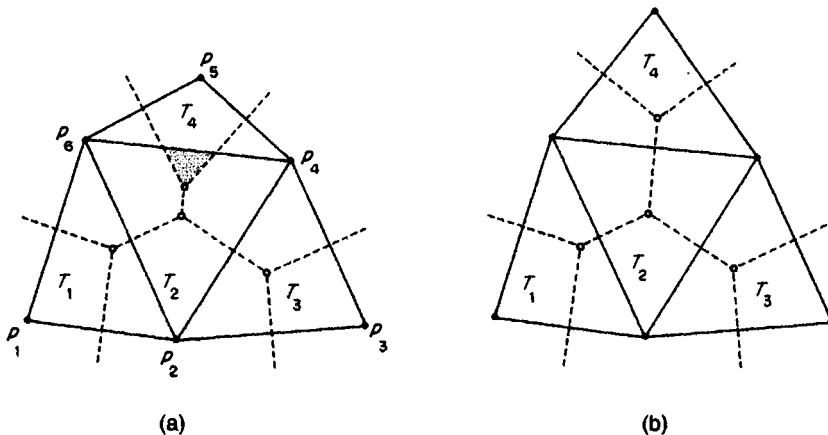


Figure 2.4.1 Delaunay triangulations: (a) is not a Pitteway triangulation, while (b) is a Pitteway triangulation.

2.4.1, where the unfilled circles, the broken lines and the solid lines represent Voronoi vertices, Voronoi edges and the Delaunay triangulation spanning six generator points p_1, p_2, \dots, p_6 , respectively. In observing the Delaunay triangles T_1, T_3, T_4 in panel (a), we notice that the nearest generator from any point in a triangle is one of the three vertices of the triangle, because the whole triangle is covered by the three Voronoi polygons whose generator points are the vertices of the triangle. On the other hand, the nearest generator from some points in T_2 (points in the shaded area) is a generator other than the three vertices of T_2 , because T_2 is not exhaustively covered by the three Voronoi polygons whose generator points are the vertices of T_2 . If a triangulation consists of only the former type triangles, such as in Figure 2.4.1(b), we call the triangulation a *Pitteway triangulation*. More generally, for a triangulation $\mathcal{T}(P)$ of $\text{CH}(P)$ spanning P , if for any point P in $\text{CH}(P)$ the closest generator point from p is one of the three vertices of the triangle containing p , we call the triangulation $\mathcal{T}(P)$ a *Pitteway triangulation* spanning P (cf. McLain, 1976). The triangulation in Figure 2.4.1(b) is a Pitteway triangulation.

Between a Delaunay triangulation and a Pitteway triangulation, we have the following relationship.

Property D3 (the Pitteway triangulation theorem) The Delaunay triangulation spanning P is a Pitteway triangulation spanning P if and only if every internal Delaunay edge crosses the associated Voronoi edge of the Voronoi diagram generated by P .

Proof First, assume that $\mathcal{D}(P)$ is a Pitteway triangulation spanning P . Then, any Delaunay triangle is covered by the three Voronoi polygons whose generator points are the vertices of the triangle. Let $\overline{p_i p_j}$ be an internal

Delaunay edge shared by Delaunay triangles $\Delta p_i p_j p_k$ and $\Delta p_i p_j p_l$. Assume, contrary to the property, that $\overline{p_i p_j}$ does not cross the associated Voronoi edge. This means that if the four generator points p_i, p_j, p_k and p_l are not cocircular, the Voronoi vertices generated by p_i, p_j, p_k and by p_i, p_j, p_l are both on the same side of $\overline{p_i p_j}$. If the four generator points are cocircular, the Voronoi vertex shared by $V(p_i), V(p_j), V(p_k)$ and $V(p_l)$ (in other words, the length-zero Voronoi edge associated with the Delaunay edge $\overline{p_i p_j}$) is not on $\overline{p_i p_j}$. Hence the midpoint of $\overline{p_i p_j}$ belongs to $V(p_k)$ or $V(p_l)$ but not to the both, which contradicts that $\mathcal{T}(P)$ is a Pitteway triangulation. Thus, any internal Delaunay edge crosses the associated Voronoi edge.

Assume next that any internal Delaunay edge crosses the associated Voronoi edge. Let p_i, p_j and p_k be the three vertices forming a Delaunay triangle. The proof varies according to which edges are internal edges among $\overline{p_i p_j}, \overline{p_j p_k}$ and $\overline{p_k p_i}$.

Case 1. Suppose that $\overline{p_i p_j}, \overline{p_j p_k}$ and $\overline{p_k p_i}$ are all internal edges (such as T_2 in Figure 2.4.1(b)). Then, because of the above assumption, the triangle contains the Voronoi vertex generated by p_i, p_j and p_k , but does not contain any other Voronoi vertex. Since the line segment connecting the generator p and a point on the boundary of $V(p)$ belongs to $V(p)$, the triangle is covered by $V(p_i), V(p_j)$ and $V(p_k)$.

Case 2. Suppose that $\overline{p_i p_j}, \overline{p_j p_k}$ and $\overline{p_k p_i}$ are all external Delaunay edges. This implies that there are exactly three generator points in P , and hence the triangle (actually the whole plane) is covered by $V(p_i), V(p_j)$ and $V(p_k)$.

Case 3. Suppose that one edge, say $\overline{p_i p_j}$, is an external Delaunay edge while the other two edges are internal. Then, the Voronoi vertex generated by p_i, p_j and p_k is either in the triangle or on the side opposite to the triangle with respect to $\overline{p_i p_j}$. In the former case, the external Delaunay edge $\overline{p_i p_j}$ also crosses the associated Voronoi edge, and hence the triangle is covered by $V(p_i), V(p_j)$ and $V(p_k)$, as we saw in Case 1. In the latter case, the triangle contains no Voronoi vertex, and the Voronoi edge generated by p_i and p_k crosses both $\overline{p_j p_k}$ and $\overline{p_i p_j}$; the Voronoi edge generated by p_j and p_k crosses both $\overline{p_i p_k}$ and $\overline{p_i p_j}$. No other Voronoi edge traverses the triangle. This means that the triangle is covered by the three Voronoi polygons generated by its vertices.

Case 4. Suppose that two edges, say $\overline{p_i p_j}$ and $\overline{p_j p_k}$, are external edges and the other is an internal edge (such as T_1 in Figure 2.4.1(b)). Then, the Voronoi vertex generated by p_i, p_j and p_k is either in the triangle or on the side opposite to the triangle with respect to one of the external edges. In both cases the configuration is the same as in Case 3, and hence the triangle is covered by the three Voronoi polygons generated by its vertices. \square

Property D3 gives the necessary and sufficient condition for $\mathcal{D}(P)$ to be a Pitteway triangulation. The next question is: If the point set P admits a Pitteway triangulation, does it necessarily coincide with $\mathcal{D}(P)$? The answer is ‘no’. A counterexample is shown in Figure 2.4.2, where P consists of four points forming a rhombus; (a) is $\mathcal{D}(P)$ whereas (b) is not. However, both (a)

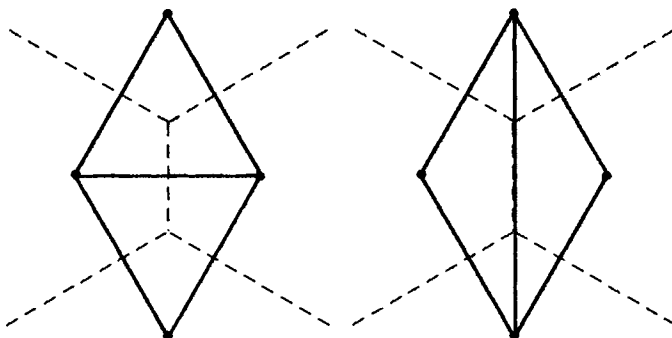


Figure 2.4.2 Two Pitteway triangulations spanning four points forming a rhombus (the solid lines) and Voronoi diagrams (the broken lines): (a) is the Delaunay triangulation while (b) is not.

and (b) are Pitteway triangulations. Thus, a Pitteway triangulation spanning P , if it exists, is not necessarily unique, and does not necessarily coincide with $\mathcal{D}(P)$.

As we observed in Definitions D1 and D2, we have nice relationships between $\mathcal{V}(P)$ and $\mathcal{D}(P)$ that share the same point set P . First, from Definition D1, the Delaunay vertices of $\mathcal{D}(P)$ are the generator points of $\mathcal{V}(P)$; conversely, the generator points of $\mathcal{V}(P)$ are the Delaunay vertices of $\mathcal{D}(P)$. Second, from Property V7, the Voronoi vertices of $\mathcal{V}(P)$ are the circumcentres of Delaunay triangles in $\mathcal{D}(P)$; conversely, the circumcentres of Delaunay triangles in $\mathcal{D}(P)$ are the Voronoi vertices in $\mathcal{V}(P)$. Lastly, the number of Delaunay edges of $\mathcal{D}(P)$ is greater than or equal to that of Voronoi edges (recall a Delaunay pretriangulation); under the non-degeneracy assumption, both numbers are the same. To sum up, we have the following property.

Property D4 For the Voronoi diagram $\mathcal{V}(P)$ generated by a finite set P of distinct points, and the Delaunay triangulation spanning P , let Q and Q_d be the set of Voronoi vertices and that of Delaunay vertices, respectively; E and E_d be the set of Voronoi edges and that of Delaunay edges, respectively; C_d be the set of circumcentres of Delaunay triangles. Then,

- (i) $Q_d = P$;
- (ii) $C_d = Q$;
- (iii) $|E_d| \geq |E|$; $|E_d| = |E|$ if and only if $\mathcal{V}(P)$ is non-degenerate, where $|E|$ indicates the number of elements in the set E .

From Property D4 and Property V7, all Delaunay triangles have the next property which corresponds to Property V8.

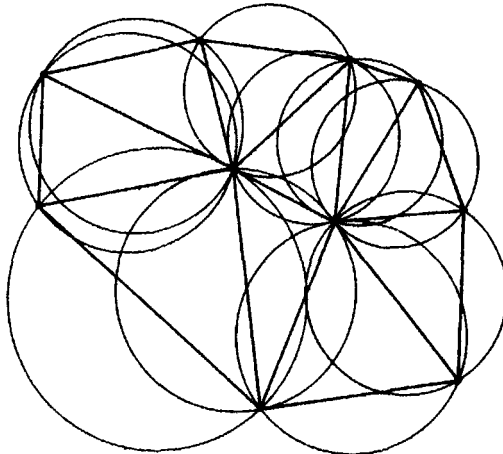


Figure 2.4.3 Empty circumcircles of Delaunay triangles (i.e. Delaunay circles) in a Delaunay triangulation.

Property D5 All circumcircles of Delaunay triangles are empty circles.

Note that the circumcircle of a Delaunay triangle is sometimes called a *Delaunay circle* and points on a Delaunay circle are called *natural neighbours* (Watson, 1985). An example is shown in Figure 2.4.3. The notion of a Delaunay circle can be extended in \mathbb{R}^3 , and we call the circumsphere of a Delaunay tetrahedron a *Delaunay sphere*. Using Property D5, we can solve the largest empty circle problem (Problem V5) (a slight modification is necessary, as we remarked below Property V8).

Having observed Figure 2.4.3, the reader may question whether or not the converse relation in Property D5 holds; that is, if the circumcircles of all triangles in a triangulation are empty circles, then the triangulation is a Delaunay triangulation. To answer this question, we first introduce the following criterion.

The empty circumcircle criterion Given a triangulation of $\text{CH}(P)$ spanning a finite set P of distinct points, if the circumcircle of a triangle in the triangulation is an empty circle, we say that the triangle satisfies the *empty circumcircle criterion*.

With this criterion, we can now show Property D6.

Property D6 (the empty circumcircle theorem) Every triangle in a triangulation spanning a finite set P of distinct points satisfies the empty circumcircle criterion if and only if the triangulation is the Delaunay triangulation spanning P .

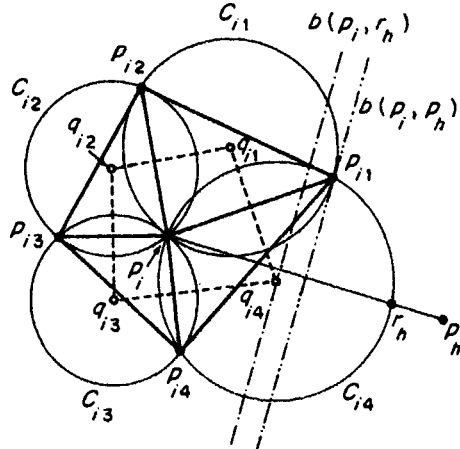


Figure 2.4.4 Illustration of the proof that a triangulation in which every triangle satisfies the empty circumcircle criterion is a Delaunay triangulation.

Proof Since we have already obtained Property D5, what is left is to prove that a triangulation in which every triangle satisfies the empty circumcircle criterion is a Delaunay triangulation.

Consider triangles sharing a point $p_i \in P$ in a triangulation \mathcal{T} spanning P (Figure 2.4.4). Let p_{i1}, \dots, p_{ik} be the vertices of these triangles where the points are indexed counterclockwise, and q_{i1}, \dots, q_{ik} be the centres of the circumcircles, C_{i1}, \dots, C_{ik} , of triangles $\Delta p_i p_{i1} p_{i2}, \dots, \Delta p_i p_{ik} p_{i1}$ (the heavy solid lines in Figure 2.4.4). Since $\overline{p_i p_{ij}}$ is orthogonal to $\overline{q_{ij} q_{ij-1}}$, $j = 1, \dots, k$ (0 is read as k), the polygon with vertices q_{i1}, \dots, q_{ik} is given by $\cap_{j=1}^k H(p_i, p_{ij})$ (the broken lines in Figure 2.4.4). From the assumption, all points of P other than $p_i, p_{ij}, j = 1, \dots, k$, are outside the circumcircles C_{i1}, \dots, C_{ik} . We take a point, say p_h , from $P \setminus \{p_i, p_{ij}, \dots, p_{ik}\}$, and draw the line segment $\overline{p_i p_h}$. Then $\overline{p_i p_h}$ intersects the arc of the circumcircle on the boundary of $\text{CH}(\cup_{j=1}^k C_{ij})$, say the arc $p_{ij} p_{ij+1}$ of C_{ij} ($j + 1 = 5$ is read as 1). Let r_h be this intersection point. Then the boundary of $H(p_i, r_h)$ (the dash-dot line in Figure 2.4.4) passes through q_{ij} because r_h is on the circumcircle, and $\cap_{i=1}^k H(p_i, p_{ij}) \subset H(p_i, r_h) \subset H(p_i, p_h)$. This relation holds for all p_h in $P \setminus \{p_i, p_{ij}, \dots, p_{ik}\}$. Therefore

$$\bigcap_{j=1}^k H(p_i, p_{ij}) = \bigcap_{j \in I_i \setminus \{i\}} H(p_i, p_j) = V(p_i). \quad (2.4.3)$$

Thus the polygon with q_{i1}, \dots, q_{ik} is the Voronoi polygon of p_i . If we carry out the above procedure for every p_i in P , we obtain $\mathcal{V}(P)$. Since \mathcal{T} is the same as the Delaunay triangulation obtained from $\mathcal{V}(P)$ (Definition D2), the given triangulation is the Delaunay triangulation spanning P . \square

A Delaunay triangulation is of course a tessellation in \mathbb{R}^2 , but like Property V17 we can also construct a Delaunay triangulation through a polyhedron in \mathbb{R}^3 . Here we show two methods: one using the inversion transformation (to be defined below), and one using the lift-up transformation adopted in

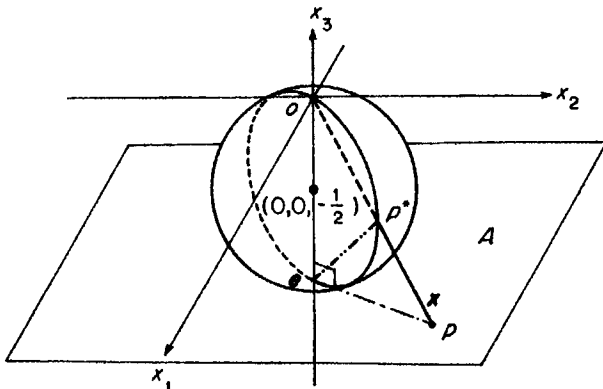


Figure 2.4.5 The inversion transformation.

Property V17. The *inversion transformation* with the inversion centre at the origin o and the inversion radius 1 is defined by

$$F(\mathbf{x}) = \frac{\mathbf{x}}{\|\mathbf{x}\|^2}, \quad \mathbf{x} \in \mathbb{R}^m \quad (2.4.4)$$

(Dodge, 1972, Chapter 5). This function has the property that $\|F(\mathbf{x})\| = 1/\|\mathbf{x}\|$, that is, the direction of the vector $F(\mathbf{x})$ is the same as that of the vector \mathbf{x} ; the length of the vector $F(\mathbf{x})$ is the inverse of the length of the vector \mathbf{x} . We now consider the three-dimensional Euclidean space \mathbb{R}^3 with the Cartesian coordinate system (x_1, x_2, x_3) , and let A be the plane parallel to the x_1-x_2 plane passing through the point $(0, 0, -1)$ whose location vector is given by e (see Figure 2.4.5). Suppose that p is on the plane A and \mathbf{x} is the location vector of p . Then the vectors e and $\mathbf{x}-e$ are orthogonal (observe that the x_3 -axis and the dash-dot line in Figure 2.4.5 are orthogonal) which is mathematically written as $e^T(\mathbf{x} - e) = 0$ or $e^T\mathbf{x} = 1$. Let $\mathbf{x}^* = F(\mathbf{x}) = \mathbf{x}/\|\mathbf{x}\|^2$. Then $\mathbf{x}^{*T}(\mathbf{x}^* - e) = (\mathbf{x}^T/\|\mathbf{x}\|^2)(\mathbf{x}/\|\mathbf{x}\|^2 - e) = (1/\|\mathbf{x}\|^2)(1 - \mathbf{x}^Te) = 0$, showing that the vectors \mathbf{x}^* and $\mathbf{x}^* - e$ are orthogonal (observe that the heavy broken line and the dash-dot-dot line in Figure 2.4.5 are orthogonal). This means that the point p^* indicated by the location vector \mathbf{x}^* is on the circle centred at $(0, 0, -1/2)$ with radius $1/2$ (see the great circle in Figure 2.4.5). Since this property holds for any point on the plane A , the set $S = \{\mathbf{x}^* | \mathbf{x}^* = F(\mathbf{x}), \mathbf{x} \in A\}$ forms a sphere without the point o . Thus, the inversion transformation of equation (2.4.4) maps the plane A onto $S \setminus \{o\}$. Stated more specifically, the image of a point p on the plane A under the inversion transformation is the point p^* given by the intersection point of the sphere S and the line joining the point p and the origin o (Figure 2.4.5). This mapping is indicated by $p^* = F(p)$.

The inversion transformation is a one-to-one function, and hence the inverse function F^{-1} exists. To obtain F^{-1} explicitly, we solve $\mathbf{x}^* = \mathbf{x}/\|\mathbf{x}\|$ with respect to \mathbf{x} using the property $\|\mathbf{x}^*\| = 1/\|\mathbf{x}\|$. As a result, we get

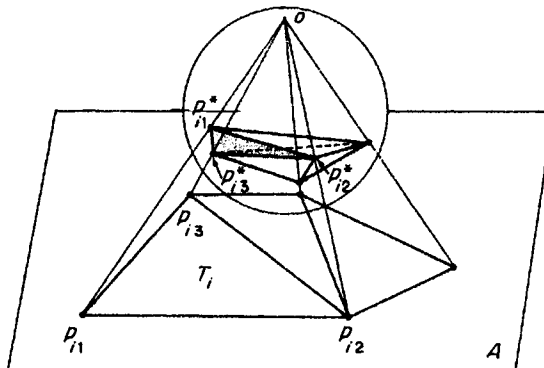


Figure 2.4.6 A Delaunay triangulation obtained through the inversion transformation.

$$F^{-1}(x^*) = \frac{x^*}{\|x^*\|^2} \quad (2.4.5)$$

We notice from equations (2.4.4) and (2.4.6) that $F^{-1} = F$. The inverse inversion transformation (i.e. the inversion transformation) maps $S \setminus \{o\}$ onto the plane A .

Using the inversion transformation, we now construct a triangulation according to the following procedure (Brown, 1979).

In \mathbb{R}^3 with the Cartesian coordinates (x_1, x_2, x_3) we consider the plane A which is parallel to the x_1-x_2 plane passing through $(0, 0, -1)$, and place a set of n distinct points $P = \{p_1, \dots, p_n\}$ ($3 \leq n < \infty$) on A , where P satisfies the non-collinearity assumption (this assumption can be easily relaxed). Let $P^* = \{p_1^*, \dots, p_n^*\} = \{F(p_1), \dots, F(p_n)\}$, where F is given by equation (2.4.4) ($m = 3$) (the filled circles on the sphere in Figure 2.4.6). Then, $\text{CH}(P^*)$ (the polyhedron in Figure 2.4.6) consists of triangular faces T_i^* , $i \in I_r$. These triangles can be classified into ‘near-side’ triangles and ‘far-side’ triangles. A *near-side triangle* T_i^* is a triangle that satisfies the condition that $\text{CH}(P^*)$ and the origin are in the same half space produced by the plane containing T_i^* (the shaded face in Figure 2.4.6). We reindex T_i^* so that the first n_v triangles are near-side triangles. Let p_{ij}^* , $j = 1, 2, 3$, be vertices of a near-side triangle T_i^* , $i \in I_{n_v}$, where $j = 1, 2, 3$ are indexed counterclockwise on the surface of $\text{CH}(P^*)$, and let $p_{ij} = F^{-1}(p_{ij}^*)$, $j = 1, 2, 3$. On the plane A , we construct the triangle by $\overline{p_{ij}p_{ij+1}}$, $j = 1, 2, 3$ (where 4 is read as 1), and denote it by T_i . Then the set $\mathcal{T}(P) = \{T_1, \dots, T_{n_v}\}$ gives a triangulation of $\text{CH}(P)$ spanning P . We now demonstrate that this triangulation satisfies the next property.

Property D7 The triangulation obtained through the above inversion transformation procedure is a Delaunay triangulation.

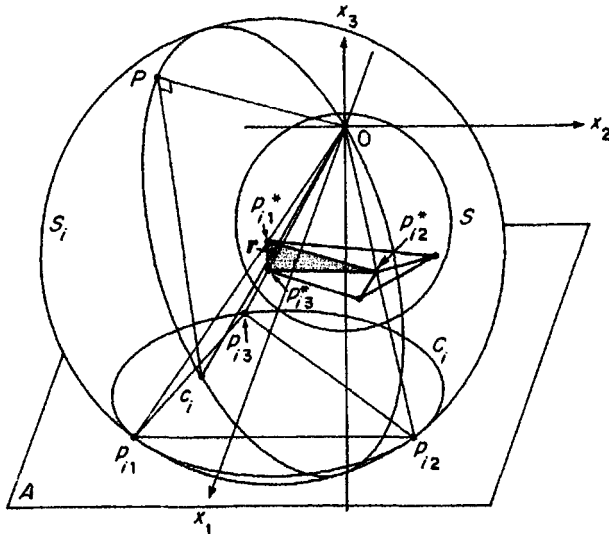


Figure 2.4.7 Illustration of the proof of Property D7.

Proof Let $x_{ij}^* = F(x_{ij}) = x_{ij}/\|x_{ij}\|^2, j = 1, 2, 3$, be the location vectors of the vertices $p_{i1}^*, p_{i2}^*, p_{i3}^*$ of a near-side triangular face T_i^* (the shaded face in Figure 2.4.7) of $\text{CH}(P^*)$, where $P^* = \{p_1^*, \dots, p_n^*\}$, $p_i^* = F(p_i)$, $p_{ij}^* = F^*(p_{ij})$, $p_{ij} \in P$ and x_{ij} is the location vector of p_{ij} . Let A_i^* be the plane containing the face T_i^* , i.e.

$$\begin{aligned} A_i^* &= \{z^* \mid \lambda_1 x_{i1}^* + \lambda_2 x_{i2}^* + \lambda_3 x_{i3}^*, \text{ where } \lambda_1 + \lambda_2 + \lambda_3 = 1\} \\ &= \left\{ z^* \mid z^* = \lambda_1 \frac{x_{i1}}{\|x_{i1}\|^2} + \lambda_2 \frac{x_{i2}}{\|x_{i2}\|^2} + \lambda_3 \frac{x_{i3}}{\|x_{i3}\|^2}, \text{ where } \lambda_1 + \lambda_2 + \lambda_3 = 1 \right\}. \quad (2.4.6) \end{aligned}$$

Let S_i be the sphere passing through points $p_{i1}, p_{i2}, p_{i3}, o$; r be the location vector of the centre of the sphere S_i ; and c_i be the point indicated by $2r$. If a point p (indicated by the location vector x) is on S_i , points o, c_i, p are on the great circle of S_i (the great circle in Figure 2.4.7) whose diameter is given by the line segment joining o and c_i , and so $\angle opc_i = \pi/2$, i.e. the vectors x and $x - 2r$ are orthogonal. Thus S_i is represented by the set of points

$$S_i = \{x \mid x^T(x - 2r) = 0, x \in \mathbb{R}^3\}. \quad (2.4.7)$$

Since points p_{i1}, p_{i2}, p_{i3} are on S_i , the equation $x_{ij}^T(x_{ij} - 2r) = 0$, i.e. $x_{ij}^T x_{ij} = 2x_{ij}^T r$, holds for $j = 1, 2, 3$.

We now prove that points on the plane A_i^* are mapped on the sphere S through the (inverse) inversion transformation, i.e. we prove $S_i = \{z \mid z = F^{-1}(z^*), z^* \in A_i^*\}$. From $F^{-1}(z^*) = z^*/\|z^*\|^2$ and equation (2.4.6), we obtain:

$$\begin{aligned}
 F^{-1}(z^*)^T (F^{-1}(z^*) - 2r) &= \frac{z^{*T}}{\|z\|^2} \left(\frac{z^{*T}}{\|z\|^2} - 2r \right) \\
 &= \frac{z}{\|z^*\|^2} \left(1 - \sum_{j=1}^3 \frac{2\lambda_j x_{ij}^T r}{\|x_{ij}\|^2} \right).
 \end{aligned} \tag{2.4.8}$$

Upon substituting $x_{ij}^T x_{ij} = 2x_{ij}^T r$ into this equation, we obtain:

$$F^{-1}(z^*)^T (F^{-1}(z^*) - 2r) = \frac{1}{\|z^*\|^2} (1 - \lambda_1 - \lambda_2 - \lambda_3) = 0. \tag{2.4.9}$$

Thus $F^{-1}(z^*)$ satisfies the equation in equation (2.4.7), showing that the plane A_i^* is mapped onto S_i , and that the closed half space, H^* , produced by A_i^* which contains the origin is mapped onto the space outside the sphere S_i (recall that the distance is reversed by the inversion transformation of equation (2.4.4)). The intersection of S_i with the plane parallel to the x_1-x_2 plane passing through $(0, 0, -1)$ is the circle C_i passing through points p_{i1}, p_{i2}, p_{i3} . Obviously the circle C_i is the circumcircle of the triangle T_i . Since all points in P^* are in H^* , all points in $P = F^{-1}(P^*)$ are on or outside C_i , indicating that the circumcircle C_i is an empty circle. Thus the set $\{T_1, \dots, T_n\}$ of triangles forms a triangulation in which circumcircles of the triangles are all empty circles. From the empty circumcircle theorem (Property D6), we notice that this triangulation is the Delaunay triangulation spanning P . \square

In Definition D2 we remarked that \mathcal{D} was not necessarily defined with \mathcal{V} . In fact, Property D7 shows that once a set of points P is given, we can define \mathcal{D} as the triangulation obtained from the above procedure (which does not require a Voronoi diagram). We can also use Property D7 to give a definition of \mathcal{V} alternative to Definition V1 or V2. When \mathcal{D} is given, it is straightforward

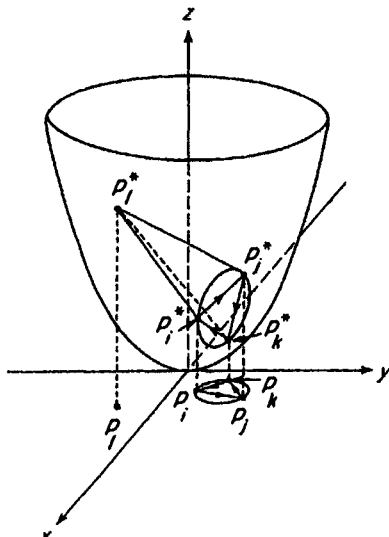


Figure 2.4.8 A Delaunay triangulation obtained through the lift-up transformation.

to construct \mathcal{V} by inverting the procedure mentioned in Definition D1. Thus we may define \mathcal{V} via \mathcal{D} obtained from the inversion transformation procedure. We also note that we can construct \mathcal{V} directly through the inversion transformation. We leave it as an exercise.

In Property D7 we obtained the Delaunay triangulation $\mathcal{D}(P)$ from the convex hull of $P^* = F(P)$ in \mathbb{R}^3 through the inversion transformation F . This method can be extended to \mathbb{R}^m . We can construct an m -dimensional Delaunay tessellation $\mathcal{D}(P)$ or an m -dimensional Voronoi diagram $\mathcal{V}(P)$ from the convex hull of $F(P)$ in \mathbb{R}^m through the inversion transformation (Brown, 1979, 1980).

We next show another correspondence between a Delaunay triangulation and a convex hull in \mathbb{R}^3 (Edelsbrunner and Seidel, 1986; O'Rourke *et al.*, 1986; Edelsbrunner, 1987; Agarwal *et al.*, 1989a).

Let P^* be the lift-up of $P = \{p_1, \dots, p_n\}$ (where $p_i \in \mathbb{R}^2$) and $\text{CH}(P^*)$ be the convex hull of P^* . A facet of $\text{CH}(P^*)$ is called a *lower facet* if the plane containing the facet passes through or below any point in P^* . The surface formed by all the lower facets of $\text{CH}(P^*)$ is called the *lower boundary* of $\text{CH}(P^*)$.

Suppose without loss of generality that three points p_i, p_j, p_k are placed on the x - y plane so that the cycle p_i, p_j, p_k, p_i has a counterclockwise direction when it is viewed from a point far above the x - y plane (see Figure 2.4.8). Let

$$H(p_i, p_j, p_k, p) = \begin{vmatrix} 1 & x_i & y_i & x_i^2 + y_i^2 \\ 1 & x_j & y_j & x_j^2 + y_j^2 \\ 1 & x_k & y_k & x_k^2 + y_k^2 \\ 1 & x & y & x^2 + y^2 \end{vmatrix}. \quad (2.4.10)$$

It is left as an exercise to see that the circle passing through p_i, p_j, p_k is represented by $H(p_i, p_j, p_k, p) = 0$, and that this circle is an empty circle if and only if $H(p_i, p_j, p_k, p_l) \geq 0$ for any point $p_l \in P \setminus \{p_i, p_j, p_k\}$. In this connection, recall that the three points p_i, p_j, p_k form a Delaunay triangle if and only if the circle passing through these points is an empty circle (Property D6).

$H(p_i, p_j, p_k, p)$ gives another implication. The value of $H(p_i, p_j, p_k, p)/6$ can be interpreted as the signed volume of the tetrahedron with vertices p_i, p_j, p_k, p . Since we choose p_i, p_j, p_k so that the cycle p_i, p_j, p_k, p_i has a counterclockwise direction, the volume of the tetrahedron is positive if and only if p_l^* is above the plane containing p_i^*, p_j^*, p_k^* (see Figure 2.4.8). This means that p_i, p_j and p_k form a Delaunay triangle if and only if p_i^*, p_j^* and p_k^* give a facet of the lower boundary of $\text{CH}(P^*)$. Thus we obtain the following property.

Property D8 The Delaunay triangulation $\mathcal{D}(P)$ is obtained as the orthographic projection of the lower boundary of $\text{CH}(P^*)$ onto the x - y plane, where P^* is the lift-up of P .

This property gives an interesting implication to the interpolation problem (Chapter 6). Suppose that we are given the height $z_i = x_i^2 + y_i^2$ at each site $p_i = (x_i, y_i)$, and that we want to interpolate these data by a collection of triangles whose vertices are the given points p_1^*, \dots, p_n^* , where p_i^* is the lift-up of p_i . Every triangulation spanning P gives such an interpolation, but among them, $\mathcal{D}(P)$ is the only one that gives the surface of interpolation convex downward. Recall that the points in P^* lie on the paraboloid of revolution (Figure 2.4.8), which is convex downward. It is hence desirable that the interpolant is also convex downward. This requirement is satisfied only by $\mathcal{D}(P)$. Since this property is a distinct property, we state it as Property D9.

Property D9 The Delaunay triangulation spanning a finite set P of distinct points is the only triangulation $\mathcal{T}(P)$ spanning P such that the lift-up transformation of $\mathcal{T}(P)$ gives a surface convex downward.

Property D9 gives a justification for the use of a Delaunay triangulation as a tool for interpolation. Applications of Voronoi diagrams and Delaunay triangulations to interpolation are discussed in detail in Chapter 6.

Unlike a Voronoi diagram, a Delaunay pretriangulation or a Delaunay triangulation has edges of finite length. Thus we can regard a Delaunay pretriangulation or a Delaunay triangulation as a geometric graph. This graph is a connected planar graph consisting of the set of Delaunay vertices, P , and the set of Delaunay edges, E_d . We call this graph the *Delaunay graph* of $\mathcal{D}(P)$ and denote it by $G(P, E_d)$. It is easy to see from Definition D2 that the Voronoi graph $G(Q_{+1}, E_d)$ and the Delaunay graph $G(P, E_d)$ have the following relation.

Property D10 The Delaunay graph $G(P, E_d)$ is the dual graph of the Voronoi graph $G(Q_{+1}, E_d)$.

Because of this property, we sometimes say that the Delaunay triangulation is the *dual tessellation* of the Voronoi diagram. Alternatively, we can view the duality between a Voronoi diagram and a Delaunay triangulation in terms of Legendre dual functions (Chynoweth and Sewell, 1990; Chynoweth, 1996). In Section 2.3 (Figure 2.3.9) we constructed a Voronoi diagram through the polyhedron consisting of planes tangential to the paraboloid at the lift-up points of the generator points. Earlier in this section (Figure 2.4.8) we constructed a Delaunay triangulation through the convex hull of the lift-up points of the same generator points. The relationship between the polyhedron and the convex hull forms Legendre dual functions (a precise and general definition of the Legendre dual functions is found in Chapter 2 of Sewell, 1987). Chynoweth (1996) calls this relationship the *generalized Voronoi/Delaunay duality*.

Recalling Definitions V3 and D1, we notice that a Voronoi edge and its corresponding Delaunay edge are orthogonal under the non-degeneracy

assumption. When two geometric figures form the primal–dual graphs, and their corresponding edges are orthogonal, these two figures are called *reciprocal figures* (Maxwell, 1864). The Voronoi diagram generated by P and the Delaunay triangulation spanning P are hence reciprocal figures. This property is strongly related to the realizability of polyhedra from a Delaunay triangulation and a Voronoi diagram (Properties D8 and V17). The relation between realizability and reciprocity is discussed in depth by Sugihara (1986). Note that the topological stability of a Delaunay graph with respect to the location of nodes is examined by Abellanas *et al.* (1994).

From Properties D4 and D10 we can obtain a few relationships among the numbers of Delaunay triangles, Delaunay edges, external Delaunay edges and Delaunay vertices, denoted by n_v , n_e , n_c and n , respectively (equivalently n_c is the number of unbounded Voronoi polygons in $\mathcal{V}(P)$). First, since the Delaunay graph is a planar graph, Euler's formula (equation (1.3.26)) holds, i.e. $n - n_e + (n_v + 1) = 2$, which is equivalent to Property V9. Second, more generally, for an m -dimensional Delaunay tessellation, the Euler–Poincaré formula (equation (1.3.27)) holds, which corresponds to Property V10. Third, since every internal edge is shared by two Delaunay triangles and every external edge belongs to only one Delaunay triangle, the number of Delaunay edges is given by

$$n_e = \frac{1}{2}(3n_v + n_c) \quad (2.4.11)$$

Upon substituting equation (2.4.11) into $n - n_e + n_v = 1$, we have the following property.

Property D11 For the Delaunay triangulation $\mathcal{D}(P)$ spanning a finite set P of distinct points, which satisfies the non-cocircularity assumption, let n_e be the number of Voronoi or Delaunay edges, n_v be the number of the triangles in $\mathcal{D}(P)$ and n_c be the number of the vertices on the boundary of $\text{CH}(P)$. Then, the following equations hold:

$$n_v = 2n - n_c - 2, \quad (2.4.12)$$

$$n_e = 3n - n_c - 3. \quad (2.4.13)$$

Recalling Property D4, we notice that the above equations hold for a non-degenerate $\mathcal{V}(P)$, where n_e , n_v and n_c are the number of Voronoi edges, Voronoi vertices and unbounded Voronoi polygons, respectively.

For the non-degenerate Delaunay tetrahedrization spanning a finite set P of n distinct points, the Euler–Poincaré equation, $n_0 - n_1 + n_2 - n_3 = 1$, holds, where n_i is the number of i th dimensional faces, or more specifically, n_0 , n_1 , n_2 and n_3 are the number of vertices, edges, triangular faces, and tetrahedra, respectively. Since the vertices are points in P , we have $n_0 = n$. Since every tetrahedron is bounded by four triangular faces and every triangular face bounds at most two tetrahedra, we have $2n_3 \leq n_2$. Substituting this relation and $n_0 = n$ into $n_0 - n_1 + n_2 - n_3 = 1$, we obtain the following property (Chazelle *et al.*, 1990).

Property D12 For the Delaunay tetrahedrization $\mathcal{D}(P)$ spanning a finite set P of n distinct points satisfying the non-cosphericity assumption, the following relations hold:

$$n_3 \leq n_1 - n + 1, \quad (2.4.14)$$

$$n_2 \leq 2n_1 - 2n + 2. \quad (2.4.15)$$

These relations imply that n_1 is a good measure of the combinatorial complexity of $\mathcal{D}(P)$. Chazelle *et al.* (1990) call it the *size* of $\mathcal{D}(P)$. The maximum size of $\mathcal{D}(P)$ is $\binom{n}{3}$. Chazelle *et al.* (1990) show that no matter how badly P is distributed, there is always a small set, A , of points such that $\mathcal{D}(P \cup A)$ has the size at most $O(n^{3/2} \log^3 n)$. Bern *et al.* (1990) give an algorithm that adds a set A of $O(n)$ new points such that $\mathcal{D}(P \cup A)$ has size $O(n)$.

For a Delaunay vertex p_i of the m -dimensional Delaunay tessellation, consider Delaunay spheres B_{i1}, \dots, B_{ik_i} incident to p_i . Bern *et al.* (1991) call the boundary of $B_{i1} \cup \dots \cup B_{ik_i}$ the *Delaunay surface* of p_i . They show that the $(m-1)$ -dimensional volume of the Delaunay surface is of order $O(r^{m-1})$, where r is the maximum radius of the balls B_{i1}, \dots, B_{ik_i} (Lemma 7 in Bern *et al.*, 1991).

In the same way that a Delaunay triangulation can be regarded as a geometric graph, any triangulation can be regarded as a geometric graph with the vertices and edges of the triangles. Figure 2.4.9(a) shows an example in which the geometric graph $G(P, L)$ consists of a set $P = \{p_0, p_1, \dots, p_4, p'_1, \dots, p'_4\}$ of nine points and a set $L = \{L_1, \dots, L_8, L'_1, \dots, L'_8\}$ of 16 line segments (they are labelled as in Figure 2.4.9(a)). We now ask whether or not there exists a non-degenerate Delaunay triangulation whose geometric graph is isomorphic to the geometric graph $G(P, L)$ in Figure 2.4.9(a). More generally, we ask whether or not there exists a non-degenerate Delaunay triangulation whose geometric graph is isomorphic to the geometric graph of a given triangulation.

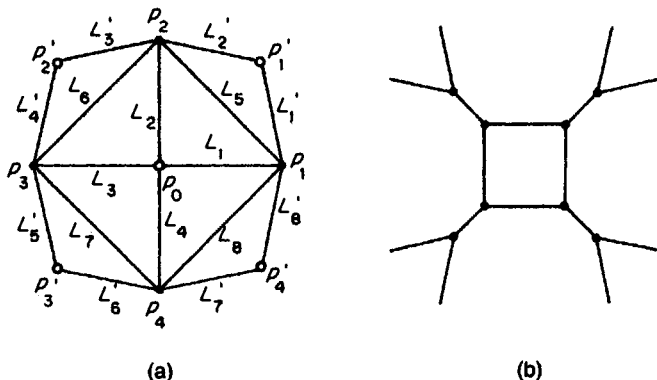


Figure 2.4.9 (a) A triangulation whose geometric graph is not isomorphic to any non-degenerate Delaunay triangulation, and (b) its dual diagram whose geometric graph is not isomorphic to any non-degenerate Voronoi diagram.

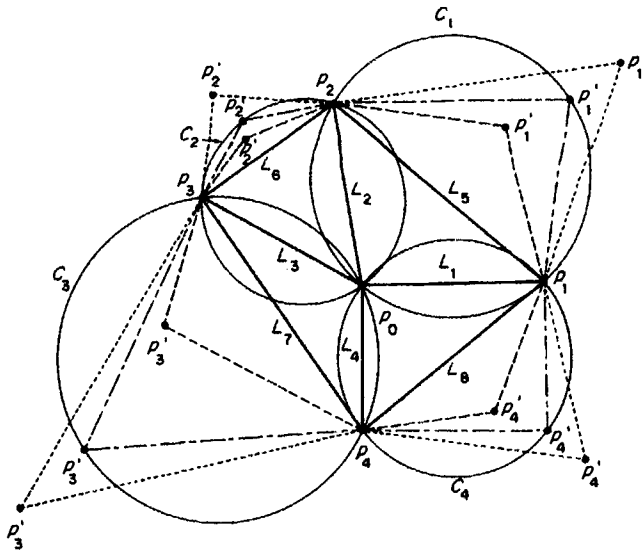


Figure 2.4.10 Three triangulations (the solid lines with the broken lines, the dash-dot lines, or the dot lines).

To answer the first question we construct a geometric subgraph, $G_s(P_s, L_s)$, consisting of $P_s = \{p_0, p_1, \dots, p_4\}$ and $L_s = \{L_1, \dots, L_8\}$ in such a way that L_5, \dots, L_8 and p_1, \dots, p_4 form an arbitrary convex quadrangle and the point p_0 is placed in its interior (Figure 2.4.10). Obviously the subgraph $G_s(P_s, L_s)$ is isomorphic to the corresponding subgraph in Figure 2.4.9(a). We next add four points p'_1, \dots, p'_4 and eight line segments L'_1, \dots, L'_8 to $G_s(P_s, L_s)$ so that the resulting geometric graph is isomorphic to the geometric graph $G(P, L)$ in Figure 2.4.9(a). The number of such geometric graphs is infinitely many. To examine which geometric graph is a Delaunay triangulation, we construct the circle C_i which passes through p_0, p_i, p_{i+1} for $i = 1, \dots, 4$ (p_5 is read as p_1), and consider the following three possible cases relative to the circle C_i .

First, suppose that we place p'_i in the region encircled by $\overline{p_ip_{i+1}}$, and the arc from p_i to p_{i+1} of C_i that does not contain p_0 , and let $L'_{2i-1} = \overline{p_ip'_i}, L'_{2i} = \overline{p'_ip_{i+1}}, i = 1, \dots, 4$ (the broken lines in Figure 2.4.10). Then $\triangle p_ip'_ip_{i+1}$ does not satisfy the empty circle criterion. Thus, the resulting triangulation is not a Delaunay triangulation.

Second, suppose that p_i is on the arc of C_i from p_j to p_{j+1} that does not contain p_0 (the dash-dot lines in Figure 2.4.10). Then the triangles in the resulting triangulation satisfy the empty circle criterion. If the octagon with vertices $p_1, p'_1, \dots, p_4, p'_4$ is convex, this triangulation is a Delaunay triangulation. At first glance the convexity is not satisfied in general, but it may be satisfied in a special case. To examine the convexity, we construct a triangulation by adding $p'_1, \dots, p'_4, L'_1, \dots, L'_4$ in the following way.

Choose a point p'_1 on C_1 such that p_0 and p'_1 are on mutually opposite sides of the line $\overline{p_1p_2}$ (Figure 2.4.11). For $i = 2, \dots, 4$, let p'_i be the point

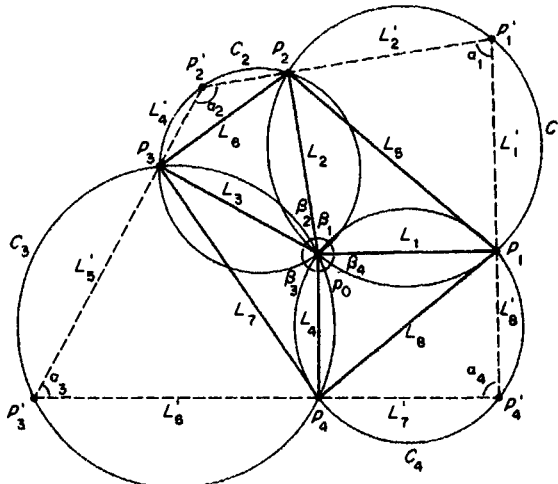


Figure 2.4.11 The degenerate Delaunay triangulation isomorphic to the geometric graph in Figure 2.4.9(a).

(other than p_i) of intersection between C_i and the line $\overline{p'_{i-1}p_i}$ (the broken lines), $i = 2, \dots, 4$. We now show that p_1 is on the line $\overline{p'_1p'_4}$. Let $\alpha_i = \angle p_ip_i p_{i+1}$ and $\beta = \angle p_ip_o p_{i+1}$ for $i = 1, \dots, 4$, where $p_5 = p_1$. Since p_o, p_i, p'_i, p_{i+1} are on C_i , we get $\alpha_i + \beta_i = \pi$ for $i = 1, \dots, 4$. Substituting these equations into $\beta_1 + \dots + \beta_4 = 2\pi$, we obtain $\alpha_1 + \dots + \alpha_4 = 2\pi$. On the other hand, the sum of the inner angles of the pentagon with vertices $p'_1, p'_2, \dots, p'_5, p_1$ is 3π , i.e. $\alpha_1 + \dots + \alpha_4 + \angle p'_4 p_1 p'_1 = 3\pi$. From these equations we have the equation $\angle p'_4 p_1 p'_1 = \pi$. Hence p_1, p'_1 and p'_4 are on the same line (note that this property can be easily generalized for m -gons p_1, \dots, p_m and p'_1, \dots, p'_m obtained in the same manner). Thus the polygon with vertices $p_1, p'_1, p_2, p'_2, \dots, p_4, p'_4$ is a convex quadrangle. Since the triangulation in Figure 2.4.11 is a triangulation spanning the convex quadrangle p'_1, \dots, p'_4 and every triangle satisfies the empty circle criterion, the triangulation in Figure 2.4.11 is a Delaunay triangulation. The graph $G(P, L)$ in Figure 2.4.9(a) is hence isomorphic to the Delaunay triangulation in Figure 2.4.11. However, the Delaunay triangulation is degenerate because every circle C_i has four points in P on it.

Last, suppose that p_i is placed outside C_i in such a way that the geometric graph of the resulting triangulation is isomorphic to the geometric graph $G(P, L)$ (the dot lines in Figure 2.4.10). In this case every triangle in the triangulation satisfies the empty circle criterion, but using the triangulation in Figure 2.4.11 we can show that the octagon with vertices $p_1, p'_1, \dots, p_4, p'_4$ cannot be convex.

To sum up, we come to the conclusion that there does not exist a non-degenerate Delaunay triangulation whose geometric graph is isomorphic to the geometric graph of the triangulation in Figure 2.4.9(a). This conclusion

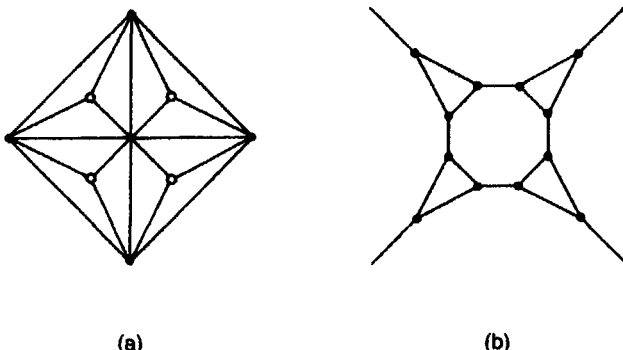


Figure 2.4.12 (a) A triangulation whose geometric graph is not isomorphic to any Delaunay triangulation, and (b) its dual diagram whose geometric graph is not isomorphic to any Voronoi diagram.

in turn implies that the diagram shown in Figure 2.4.9(b), which is the dual of the diagram in Figure 2.4.9(a), is not isomorphic to any non-degenerate Voronoi diagram. Similarly, using the triangulation shown in Figure 2.4.11, we can show that there does not exist a Delaunay triangulation whose geometric graph is isomorphic to the geometric graph shown in Figure 2.4.12(a). Consequently, the diagram shown in Figure 2.4.12(b), which is the dual of the diagram shown in Figure 2.4.12(a), is not isomorphic to any Voronoi diagram.

Dillencourt (1990a,b) investigated these unrealizability properties more generally, and showed the following two properties.

Property D13 A triangulation \mathcal{T} spanning P is not isomorphic to a non-degenerate Delaunay triangulation if there exists a subset $P' \subset P$ such that the subgraph of \mathcal{T} induced by the vertex set $P \setminus P'$ contains more than $|P|$ connected components (where $|P|$ indicates the number of points in P).

Property D14 A triangulation \mathcal{T} spanning P is not isomorphic to a Delaunay triangulation if there exists a subset $P' \subset P$ such that the subgraph of \mathcal{T} induced by the vertex set $P \setminus P'$ contains more than $|P| - 2$ connected components that do not contain any vertex on the boundary of \mathcal{T} .

The proofs are provided by Dillencourt (1990a).

We can recognize the unrealizability of the triangulation in Figure 2.4.9(a) by Property D13. Indeed, if we remove the four vertices represented by the filled circles, we obtain five connected components, each consisting of an isolated vertex represented by an unfilled circle. We can also recognize the unrealizability of the triangulation in Figure 2.4.12(a) by Property D14. If we remove the five vertices represented by the filled circles, we obtain four connected components each of which consists of an isolated vertex (represented by an unfilled circle) that is not on the boundary of the triangulation.

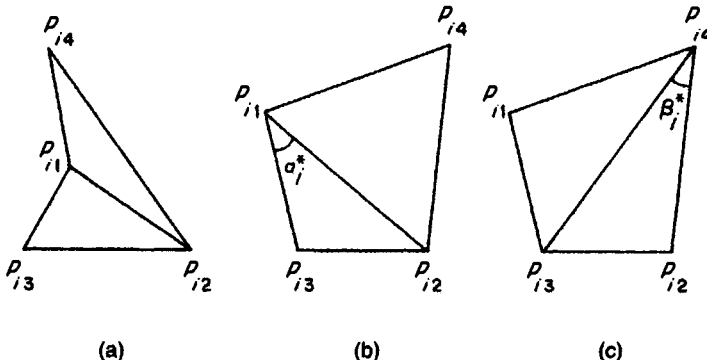


Figure 2.4.13 The local max-min angle criterion.

Properties D12 and D13 present only the sufficient conditions for a triangulation not to be isomorphic to a Delaunay triangulation. Characterization of the necessary and sufficient conditions in combinatorial terms, however, is still an open problem (Dillencourt, 1990a,b).

For a given finite set P of distinct points we have many possible triangulations of $\text{CH}(P)$ spanning P . In some applications we want to choose a triangulation in which triangles are as closely equiangular as possible (practical examples will be shown in Chapter 6). One of the criteria is to choose a triangulation in which the minimum angle in each triangle is as large as possible. To state this criterion more explicitly, let us consider an internal edge $\overline{p_{i1}p_{i2}}$ in a triangulation \mathcal{T} , and let $\Delta p_{i1}p_{i2}p_{i3}$ and $\Delta p_{i1}p_{i2}p_{i4}$ be triangles sharing the edge $\overline{p_{i1}p_{i2}}$ (Figure 2.4.13(a), (b)). The quadrangle $p_{i1}p_{i3}p_{i2}p_{i4}$ may be non-convex (Figure 2.4.13(a)) or convex (Figure 2.4.13(b)). If it is convex and it does not degenerate into a triangle (p_{i1} is on $\overline{p_{i3}p_{i4}}$ or p_{i2} is on $\overline{p_{i3}p_{i4}}$), we have another possible triangulation, i.e. $\Delta p_{i1}p_{i3}p_{i4}$ and $\Delta p_{i2}p_{i3}p_{i4}$ (Figure 2.4.13(c)). We are concerned with which triangulation is locally better ('locally' in the sense that a triangulation is made in a local area, i.e. the quadrangle $p_{i1}p_{i3}p_{i2}p_{i4}$). In the triangulation in panel (b), the minimum angle among the six angles in $\Delta p_{i1}p_{i2}p_{i3}$ and $\Delta p_{i1}p_{i2}p_{i4}$ is $\angle p_{i2}p_{i1}p_{i3} = \alpha_i^*$. In the triangulation in panel (c), the minimum angle among the six angles in $\Delta p_{i1}p_{i3}p_{i4}$ and $\Delta p_{i2}p_{i3}p_{i4}$ is $\angle p_{i2}p_{i4}p_{i3} = \beta_i^*$. Comparing α_i^* and β_i^* in Figures 2.4.13(b) and 2.4.13(c), we notice that $\alpha_i^* > \beta_i^*$, or $\alpha_i^* = \max\{\alpha_i^*, \beta_i^*\}$. We may thus conclude that the triangulation in panel (b) is locally better than that in panel (c), because the minimum angle is maximized in the triangulation in panel (b). This criterion may be written generally as follows.

The local max-min angle criterion For a triangulation \mathcal{T} of $\text{CH}(P)$ spanning P , let $\overline{p_{i1}p_{i2}}$ be an internal edge in $\text{CH}(P)$, and $\Delta p_{i1}p_{i2}p_{i3}$ and $\Delta p_{i1}p_{i2}p_{i4}$ be two triangles sharing the edge $\overline{p_{i1}p_{i2}}$. For the convex quadrangle $p_{i1}p_{i3}p_{i2}p_{i4}$ which does not degenerate into a triangle, let $\alpha_{ij}, j \in I_6$, be the

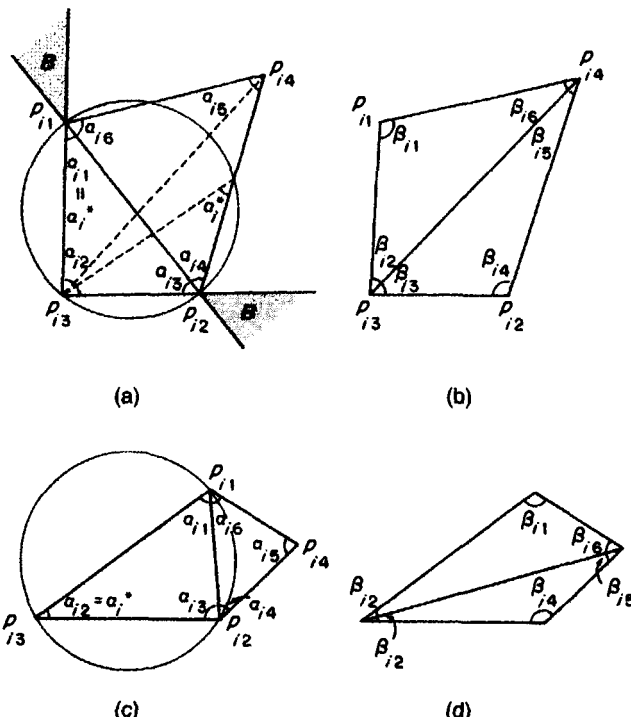


Figure 2.4.14 Conditions for the local max-min angle criterion.

six angles in $\triangle p_{i1}p_{i2}p_{i3}$ and $\triangle p_{i1}p_{i2}p_{i4}$; and $\beta_{ij}, j \in I_6$, be the six angles in $\triangle p_{i1}p_{i3}p_{i4}$ and $\triangle p_{i2}p_{i3}p_{i4}$. If the quadrangle $p_{i1}p_{i3}p_{i2}p_{i4}$ is non-convex or it degenerates into a triangle, or if it is a convex quadrangle which does not degenerate into a triangle and the relation

$$\min_j \{\alpha_{ij}, j \in I_6\} \geq \min_j \{\beta_{ij}, j \in I_6\} \quad (2.4.16)$$

holds, then we say that the edge $\overline{p_{i1}p_{i2}}$ satisfies the *local max-min angle criterion*.

In Figure 2.4.13 the edge $\overline{p_{i1}p_{i2}}$ in panels (a) and (b) satisfies the local max-min angle criterion, but the edge $\overline{p_{i3}p_{i4}}$ in panel (c) does not.

At first glance the practical operation in equation (2.4.16) (measuring angles and finding the minimum angles among them) appears a little complicated. In practice, we do not carry out such an operation but use the following relation.

Let $\alpha_i^* = \min_j \{\alpha_{ij}, j \in I_6\}$, and suppose, without loss of generality, that α_i^* is one of the angles of $\triangle p_{i1}p_{i2}p_{i3}$. Let C_i be the circumcircle of $\triangle p_{i1}p_{i2}p_{i3}$; H be the open half plane made by the line containing $\overline{p_{i1}p_{i2}}$ that does not contain $\triangle p_{i1}p_{i2}p_{i3}$; and B be the region indicated by the shaded region

(including the boundary) in Figure 2.4.14(a). Obviously, p_{i4} is in H . The quadrangle $p_{i1}p_{i2}p_{i3}p_{i4}$ may be convex or non-convex. If p_{i4} is in B , the quadrangle $p_{i1}p_{i2}p_{i3}p_{i4}$ is non-convex or it degenerates into a triangle ($\triangle p_{i4}p_{i2}p_{i3}$). The quadrangle $p_{i1}p_{i2}p_{i3}p_{i4}$ is a convex quadrangle which does not degenerate into a triangle if $p_{i4} \in H \setminus B$. Now suppose that p_{i4} is in $H \setminus [B \cup \text{CH}(C_i)]$ and the minimum angle α_i^* is either $\angle p_{i3}p_{i1}p_{i2}$ (Figure 2.4.14(a)) or $\angle p_{i3}p_{i2}p_{i1}$. Let $\triangle p_{i1}p_{i3}p_{i4}$ and $\triangle p_{i2}p_{i3}p_{i4}$ be triangles constituting another triangulation of the quadrangle $p_{i1}p_{i2}p_{i3}p_{i4}$, and $\beta_{ij}, j \in I_6$, be angles of those triangles indicated in Figure 2.4.14(b). Using the theorem of equiangles on a circle (see the two α_i^* 's in Figure 2.4.14(a)), we notice that $\alpha_i^* = \min_j \{\alpha_{ij}, j \in I_6\} = \alpha_{i1}$ (or $\alpha_{i3} > \beta_{i5}$ (or $\beta_{i6} \geq \min_j \{\beta_{ij}, j \in I_6\} = \beta_i^*$). If the minimum angle α_i^* is $\angle p_{i1}p_{i3}p_{i2}$ as in Figure 2.4.14(c), $\alpha_i^* = \min_j \{\alpha_{ij}, j \in I_6\} = \alpha_{i2} > \beta_{i2} \geq \min_j \{\beta_{ij}, j \in I_6\} = \beta_i^*$. Therefore the edge $\overline{p_{i1}p_{i2}}$ satisfies the local max-min angle criterion. Almost in the same manner, we can show that if $p_{i4} \in H \cap C_i$, then $\alpha_i^* = \beta_i^*$ holds, and if $p_{i4} \in H \cap [\text{CH}(C_i) \setminus C_i]$, then $\alpha_i^* < \beta_i^*$ holds. Therefore we obtain the following relations:

$$\begin{aligned} \min_j \{\alpha_{ij}, j \in I_6\} &> \min_j \{\beta_{ij}, j \in I_6\} && \text{if } p_{i4} \text{ is outside } C_i, \\ \min_j \{\alpha_{ij}, j \in I_6\} &= \min_j \{\beta_{ij}, j \in I_6\} && \text{if } p_{i4} \text{ is on } C_i, \\ \min_j \{\alpha_{ij}, j \in I_6\} &< \min_j \{\beta_{ij}, j \in I_6\} && \text{if } p_{i4} \text{ is inside } C_i \end{aligned} \quad (2.4.17)$$

(Lawson, 1977; Kishimoto, 1978; Sibson, 1978; Lee and Schachter, 1980; Lee and Lin, 1986). Note that the choice of a triangle from the two triangles $\triangle p_{i1}p_{i2}p_{i3}$ and $\triangle p_{i1}p_{i2}p_{i4}$ does not affect the result (it is an exercise of elementary geometry to prove that the circumcircle of $\triangle p_{i1}p_{i2}p_{i3}$ does not contain p_{i4} if and only if the circumcircle of $\triangle p_{i1}p_{i2}p_{i4}$ does not contain p_{i3}). Using relation (2.4.17), we can prove the following property.

Property D15 (the local max-min angle theorem) Let $P = \{p_1, \dots, p_n\} \subset \mathbb{R}^2$ ($3 \leq n < \infty$) be a finite set of distinct points satisfying the non-cocircularity assumption, and \mathcal{T} be a triangulation of $\text{CH}(P)$ spanning P . Every internal edge in $\mathcal{T}(P)$ satisfies the local max-min criterion if and only if $\mathcal{T}(P)$ is the Delaunay triangulation spanning P .

Proof From relation (2.4.17) it is obvious that if $\mathcal{T}(P)$ is $\mathfrak{D}(P)$, every internal edge satisfies the local max-min criterion, because if the circumcircle of $\triangle p_{i1}p_{i2}p_{i3}$ is an empty circle, p_{i4} is outside of the circumcircle. We shall prove that if every internal edge in $\mathcal{T}(P)$ satisfies the local max-min angle criterion, $\mathcal{T}(P)$ is $\mathfrak{D}(P)$. Since the edge $\overline{p_{i1}p_{i2}}$ satisfies the local max-min angle criterion, p_{i4} is outside C_i . What is left to prove is that all other vertices of the triangles are outside C_i (Figure 2.4.15). Since the edges $\overline{p_{i2}p_{i4}}$ and $\overline{p_{i1}p_{i4}}$ satisfy the local max-min angle criterion, there are no points in the horizontally and vertically hatched regions in Figure 2.4.15. Similarly, since the edges $\overline{p_{i1}p_{i3}}$ and $\overline{p_{i2}p_{i3}}$ satisfy the local max-min angle criterion, there are no points in the diagonally hatched regions. Obviously there are no points

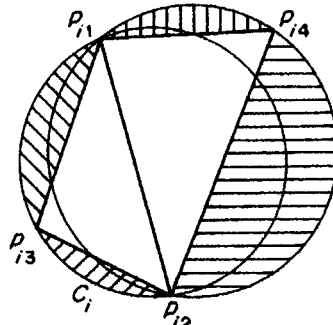


Figure 2.4.15 Illustration of the proof of Property D14.

in $\triangle p_{i1}p_{i2}p_{i3}$ and $\triangle p_{i1}p_{i2}p_{i4}$. Therefore there are no points in the circumcircle of $\triangle p_{i1}p_{i2}p_{i3}$. Applying the same procedure to every triangle, we can prove that every circumcircle is an empty circle. From the empty circumcircle theorem (Property D6), we see that the triangulation spanning P is $\mathcal{D}(P)$. \square

Having understood Property D15 in theory, let us now consider a practical method for finding a triangulation satisfying the condition in Property D15 with an example shown in Figure 2.4.16.

We first construct an arbitrary triangulation of $\text{CH}(P)$ spanning P , which is indicated by the continuous lines in Figure 2.4.16(a). Let E be the set of edges in this triangulation. We choose an edge, say $\overline{p_3p_5}$ (the heavy continuous lines in Figure 2.4.16(a)), from $E \setminus \partial\text{CH}(P)$ and examine if this edge satisfies the local max-min angle criterion. Since $\alpha^* > \beta^*$ in Figure 2.4.16(a), the edge satisfies it. We next choose another edge, $\overline{p_2p_5}$ (the heavy continuous line segment in Figure 2.4.16(b)), from $E \setminus \text{CH}(P)$, and examine if this edge satisfies the local max-min angle criterion. Since $\alpha^* < \beta^*$ in Figure 2.4.16(b), the edge does not satisfy it. In this case we swap $\overline{p_2p_5}$ (the heavy continuous line in Figure 2.4.16(b)) for $\overline{p_1p_3}$ (the broken line in Figure 2.4.16(b)), and replace E with $(E \setminus \{\overline{p_3p_5}\}) \cup \{\overline{p_1p_3}\}$. We next choose an edge, say $\overline{p_3p_5}$ (the heavy continuous line in Figure 2.4.16(c)), from $E \setminus \text{CH}(P)$. Since $\alpha^* < \beta^*$ in Figure 2.4.16(c), we swap $\overline{p_3p_5}$ (the heavy line in Figure 2.4.16(c)) for $\overline{p_1p_4}$ (the broken line in Figure 2.4.16(c)), and replace E with $(E \setminus \{\overline{p_3p_5}\}) \cup \{\overline{p_1p_4}\}$. We continue this procedure until we do not have to swap any edge in E . In the example of Figure 2.4.16(d), both internal edges satisfy the local max-min angle criterion, and so we stop. From Property D15, we notice that this triangulation is $\mathcal{D}(P)$.

We now state the above procedure in a general form as follows.

The swapping procedure Let $P = \{p_1, \dots, p_n\} \subset \mathbb{R}^2$ ($3 \leq n < \infty$) be a finite set of n distinct points satisfying the non-cocircularity assumption.

Step 0. Construct an arbitrary triangulation of $\text{CH}(P)$ spanning P , and let E be the set of edges in the triangulation.

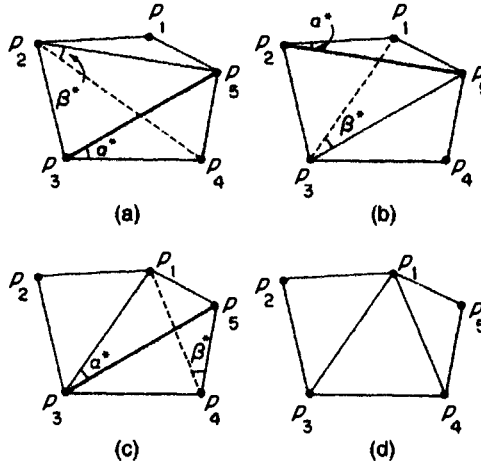


Figure 2.4.16 The swapping procedure.

- Step 1. If all the edges in E satisfy the local max-min angle criterion, report E and stop; otherwise go to Step 2.
- Step 2. Choose and delete from E an edge e that does not satisfy the local max-min angle criterion, and add to E the other diagonal edge of the quadrangle formed by the two triangles containing e , and go to Step 1.

We call this procedure the *swapping procedure*. Note that the above procedure is alternatively called the *local(ly) optimal procedure* in Lee and Schachter (1980), the *locally equiangular triangulation* in Sibson (1978), and the *Delaunay diagonal flips* in Fortune (1993).

The process of the swapping procedure can be easily understood by the lift-up transformation (Edelsbrunner, 1988). As shown in Figure 2.4.17, let $\mathcal{T} = \{T_1, \dots, T_n\}$ be an arbitrary triangulation spanning P , and let $\mathcal{T}^* = \{T_1^*, \dots, T_n^*\}$ be the surface formed by the collection of triangles obtained from \mathcal{T} by the lift-up transformation (T_i^* is the lift-up of T_i). As we saw in Property D9, if \mathcal{T} is not a Delaunay triangulation, the surface \mathcal{T}^* is not convex downward. Let T_i^* and T_j^* be two triangles in \mathcal{T}^* such that the triangles share the edge $\overline{p_i^* p_j^*}$ and they bend downward along the edge $\overline{p_i^* p_l^*}$ as in Figure 2.4.17(a). Such triangles make the surface \mathcal{T}^* non-convex.

Let p_i, p_j, p_k be the vertices of T_i , and p_i, p_j, p_l be the vertices of the triangle T_j . Let T'_i and T'_j be two triangles created by swapping the edge $\overline{p_i p_j}$ with the other diagonal edge $\overline{p_k p_l}$. By this swapping, we get a new pair of triangles T'_i^* and T'_j^* in \mathbb{R}^3 that bend upward along the edge $\overline{p_k^* p_l^*}$, as in Figure 2.4.17(b). Such triangles contribute to the convex surface \mathcal{T}^* . It is easy to see that by this swapping the edge shared by the resulting triangles satisfies the local max-min angle criterion. Hence swapping an edge according to the local max-min angle criterion corresponds to the procedure for

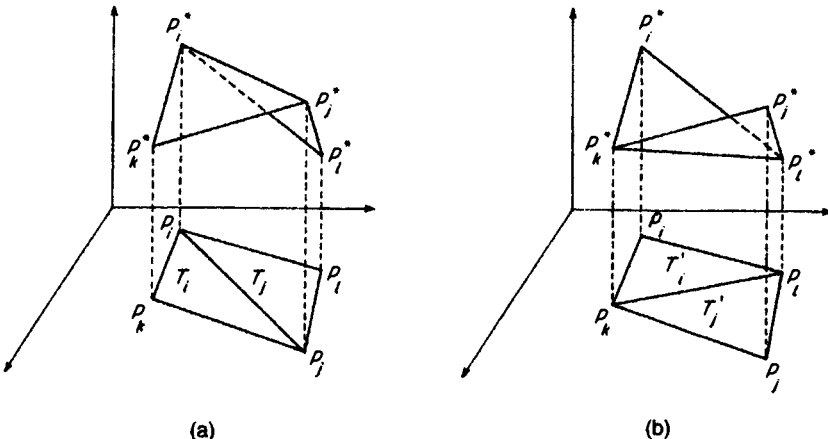


Figure 2.4.17 Two triangles: (a) bending downward along the common edge and (b) those bending upward along the common edge.

changing the surface from \mathcal{T}^* to \mathcal{T}'^* by replacing two upper facets of the tetrahedron having the vertices $p_i^*, p_j^*, p_k^*, p_l^*$ with two lower facets. Intuitively, this procedure corresponds to gluing the tetrahedron onto the surface \mathcal{T}^* from below; the new lower surface gives \mathcal{T}'^* . We apply this replacement to any edge on the surface \mathcal{T}^* . Consequently, the swapping procedure terminates only when the lift-up surface \mathcal{T}^* becomes convex downward. From this property and Property D9 we obtain the following property.

Property D16 The swapping procedure based upon the local max-min angle criterion always terminates with a Delaunay triangulation.

We know that the number of tetrahedra in the three-dimensional tessellation spanning n points is of order n^2 (Edelsbrunner, 1987). Consequently, a Delaunay triangulation is obtained from any initial triangulation by at most of order n^2 repetitions of the swappings.

We may extend the idea of the swapping procedure to the construction of a Delaunay tetrahedrization in \mathbb{R}^3 . Joe (1989, 1991a) develops this extension and calls the procedure the *local transformation procedure* in which faces are swapped according to a certain criterion. It is shown by Joe (1991a) that the local transformation procedure can be used to construct a Delaunay tetrahedrization under a certain condition.

A Delaunay triangulation satisfies a little stronger property than Property D16. Let $\alpha_i^*(\mathcal{T}_j)$ be the minimum angle in a triangle T_i , $i \in I_{n_v}$, in a triangulation \mathcal{T}_j of $\text{CH}(P)$ spanning P . We reindex $\alpha_1^*(\mathcal{T}_j), \dots, \alpha_{n_v}^*(\mathcal{T}_j)$ as $\alpha_{(1)}^*(\mathcal{T}_j), \dots, \alpha_{(n_v)}^*(\mathcal{T}_j)$, where $(\alpha_{(1)}^*(\mathcal{T}_j)) \leq \dots \leq (\alpha_{(n_v)}^*(\mathcal{T}_j))$, and call $\mathbf{a}(\mathcal{T}_j)^T = (\alpha_{(1)}^*(\mathcal{T}_j), \dots, \alpha_{(n_v)}^*(\mathcal{T}_j))$ the *ordered minimum angle vector* of \mathcal{T}_j or briefly the *angle vector* of \mathcal{T}_j . For two angle vectors $\mathbf{a}(\mathcal{T}_1)$ and $\mathbf{a}(\mathcal{T}_2)$, if there exists $k \leq n_v$ such that

$$\begin{aligned}\alpha_{(i)}^*(\mathcal{T}_1) &= \alpha_{(i)}^*(\mathcal{T}_2), \quad i = 1, \dots, k-1, \\ \alpha_{(k)}^*(\mathcal{T}_1) &< \alpha_{(k)}^*(\mathcal{T}_2),\end{aligned}\tag{2.4.18}$$

we say that \mathcal{T}_2 is *lexicographically greater* than \mathcal{T}_1 , and denote this relation by $\mathcal{T}_1 \leq \mathcal{T}_2$. In terms of this relation, we can now state the following property.

Property D17 (the lexicographically maximum triangulation theorem) A triangulation spanning a finite set P of distinct points is lexicographically maximum with respect to the ordered minimum angle vector if and only if the triangulation is the Delaunay triangulation spanning P .

Proof Suppose that an edge is swapped according to the local max-min angle procedure, and the triangulation changes from \mathcal{T}_1 to \mathcal{T}_2 . By this swapping, suppose that two triangles sharing the edge, say T_1 and T_2 in \mathcal{T}_1 , change into T_1^* and T_2^* in \mathcal{T}_2 (the other triangles remain the same), and that $\alpha_1^*(\mathcal{T}_1)$ and $\alpha_2^*(\mathcal{T}_1)$ are $\alpha_{(k)}^*(\mathcal{T}_1)$ and $\alpha_{(h)}^*(\mathcal{T}_1)$ in the ordered minimum angle vector $\alpha(\mathcal{T}_1)$, $k < h$. Since the edge is swapped according to the local max-min angle procedure, the relation

$$\min \{\alpha_1^*(\mathcal{T}_1), \alpha_2^*(\mathcal{T}_1)\} < \min \{\alpha_1^*(\mathcal{T}_2), \alpha_2^*(\mathcal{T}_2)\}\tag{2.4.19}$$

holds (recall relation (2.4.17)), where $\alpha_i^*(\mathcal{T}_2)$ is the minimum angle in the triangle T_i^* , $i = 1, 2$. Hence $\alpha_{(j)}^*(\mathcal{T}_2) = \alpha_{(j)}^*(\mathcal{T}_1)$, $j = 1, \dots, k-1$, and $\alpha_{(k)}^*(\mathcal{T}_1) < \alpha_{(k)}^*(\mathcal{T}_2)$, from which we obtain $\mathcal{T}_1 \leq \mathcal{T}_2$. Whenever an edge is swapped, the new triangulation becomes lexicographically greater than the old triangulation. Moreover, Property D16 shows that the swapping procedure always terminates with $\mathcal{D}(P)$ for any initial triangulation. Therefore $\mathcal{D}(P)$ is lexicographically maximum. \square

As is shown in Property D17, $\mathcal{D}(P)$ is the triangulation with the lexicographically largest angle vector. This intuitively means that $\mathcal{D}(P)$ avoids thin and elongated triangles as much as possible. Noticing this property, we might expect that the length of the shortest path on $\mathcal{D}(P)$ between two points in P is a good approximation to the Euclidean distance. This expectation is indeed true. To be precise, let $D(p_i, p_j)$ be the length of the shortest chain connecting p_i and p_j composed of Delaunay edges in $\mathcal{D}(P)$, where the length of a Delaunay edge is the Euclidean distance between the two endpoints of the edge and the length of the chain is the sum of the length of the edges on the chain. Then the following property holds.

Property D18 For any p_i and p_j in a finite set $P = \{p_1, \dots, p_n\}$ of distinct points,

$$D(p_i, p_j) \leq c d(p_i, p_j)\tag{2.4.20}$$

holds, where $d(p_i, p_j)$ is the Euclidean distance between p_i and p_j , and $c = 2\pi/(3 \cos(\pi/6)) \approx 2.42$.

This is proved by Keil and Gutwin (1989); a little weaker result, where $c = (1 + \sqrt{5}) \pi/2 \approx 5.08$, is proved by Dobkin *et al.* (1990).

Recall that for n points there are $O(n^2)$ pairs of points whereas there are only $O(n)$ edges in $\mathcal{D}(P)$. Hence, the network composed of $O(n^2)$ direct routes between points and the points of their intersection can be efficiently approximated by the Delaunay triangulation, which requires only $O(n)$ storage.

Having noticed that $\mathcal{D}(P)$ satisfies the optimal criteria shown in Properties D14, D15 and D16, we might expect that $\mathcal{D}(P)$ satisfies more optimal criteria. We refer to two notable criteria for optimal triangulations (a general review is provided by Tan, 1996).

The minimax length criterion For a given finite set P of distinct points, if a triangulation spanning P minimizes the length of its longest edge, we say that the triangulation satisfies the *minimax length criterion*, and call the triangulation satisfying the minimax criterion the *minimax length triangulation*.

The minimum weight (minimum length) criterion For a given finite set P of distinct points, if a triangulation spanning P minimizes the total length of its edges, we say that the triangulation satisfies the *minimum weight (minimum length) criterion*, and call the triangulation satisfying the minimum weight criterion the *minimum weight (minimum length) triangulation*.

It is shown that $\mathcal{D}(P)$ neither satisfies the minimax length criterion (Edelsbrunner and Tan, 1993) nor the minimum weight criterion (Lloyd, 1977; Kirkpatrick, 1980). In comparison with $\mathcal{D}(P)$, Edelsbrunner and Tan (1993) and Levcopoulos and Lingas (1989, 1992) examine the lower bound for the minimax triangulation; Manacher and Zobrist (1979), Kirkpatrick (1980) and Levycopoulos and Krznaric (1996) examine that for the minimum weight triangulation.

We also note a few more optimal triangulations. A *minimum energy triangulation* is a triangulation for which the finite element solution has the minimum energy. Rippa and Schiff (1990) show that the Delaunay triangulation is a minimum energy triangulation for the energy functional associated with the non-homogeneous Laplace equation (the proof is given by Rippa and Schiff, 1990; see also Corollary 3.3 in Rees and Morton, 1991). Rippa (1990, Theorem 2.1) shows that the Delaunay triangulation is a ‘minimum roughness triangulation’ (also see Power, 1992, and Section 2.6). Rajan (1994) shows that the maximum min-containment radius of the Delaunay triangulation of a point set is less than or equal to the maximum min-containment radius of any other triangulation of the point set (Theorem 2); the weighted sum of squares of the edge lengths is the smallest for a Delaunay triangulation (Theorem 4).

Noticing that Manacher and Zobrist (1979), Kirkpatrick (1980) and Levycopoulos and Krznaric (1996) tend to avoid thin and elongated triangles as much as possible (Property D17), we might expect that a Delaunay tetrahedrization also has a similar property. This expectation is not always true.

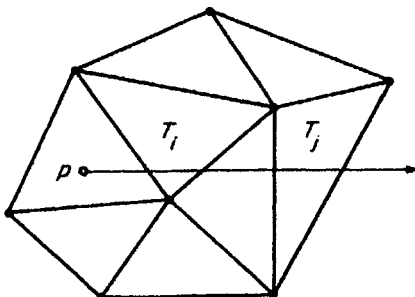


Figure 2.4.18 Monotonicity with respect to ray shooting.

Joe (1991a) reports that a Delaunay tetrahedrization tends to contain poorly shaped sliver tetrahedra with four nearly co-planar vertices lying near an equator of the circumsphere (see Figure 2.8 in Ruppert, 1995). To avoid poorly shaped sliver tetrahedra, Joe (1995a) proposes an alternative method for constructing a tetrahedrization using ‘combined local transformations’ (see Section 6.5.2).

The Delaunay triangulation has an interesting monotonicity property with respect to ray shooting. To illustrate it, let us consider a triangulation spanning P , and let p be a point in \mathbb{R}^2 . For any triangles T_i and T_j in \mathcal{T} , we write $T_i \leq_p T_j$ if there exists a ray starting at p such that a traveller traversing along the ray from p passes through T_i and T_j in this order (Figure 2.4.18). If there is no cyclic sequence $(T_1, T_2, \dots, T_k, T_1)$ of triangles satisfying $T_1 \leq_p T_2 \leq_p \dots \leq_p T_k \leq_p T_1$, $k \geq 2$, we say that \mathcal{T} is *monotone with respect to ray shooting* at p . If \mathcal{T} is monotone with respect to ray shooting at any point in \mathbb{R}^2 , we say that \mathcal{T} is *ray-shoot monotone*.

The ray-shoot monotonicity is not necessarily satisfied by any triangulation. A counterexample is shown in Figure 2.4.19. For the ray r_1 , $T_1 \leq_p T_2$ holds; for the ray r_2 , $T_2 \leq_p T_3$ holds; for the ray r_3 , $T_3 \leq_p T_1$ holds. Thus $T_1 \leq_p T_2 \leq_p T_3 \leq_p T_1$, showing that the triangulation in Figure 2.4.19 is not monotone with respect to ray shooting at p . The Delaunay triangulation, however, has the following property.

Property D19 The Delaunay triangulation is ray-shoot monotone.

To show the outline of the proof, let p be any point in \mathbb{R}^2 . For convenience, we transform the (x, y) coordinate system in such a way that p is at the origin, and construct the lower boundary of the convex hull of the lift-up of P , i.e. $\text{CH}(P^*)$. For a Delaunay triangle T_i in \mathbb{R}^2 , let T_i^* be the corresponding triangular facet on the boundary of $\text{CH}(P^*)$, and α_i be the z coordinate of the intersection point between the z -axis and the plane containing T_i^* (see Figure 2.4.20). Using the value of α_i , we define a binary relation, $<_p$: $T_i <_p T_j$ if and only if $\alpha_i \leq \alpha_j$. The binary relation $<_p$ gives a total order in the set of Delaunay triangles in $\mathcal{D}(P)$.

Next consider a ray in \mathbb{R}^2 starting at the origin and passing through T_i and T_j in this order. Since the lower boundary of $\text{CH}(P^*)$ lies on the paraboloid

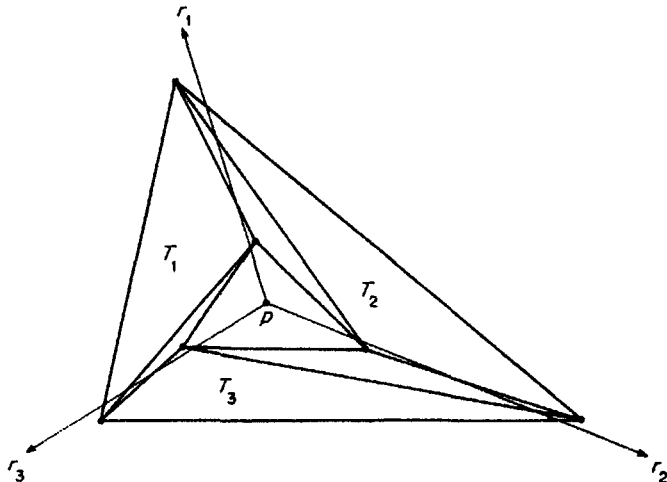


Figure 2.4.19 A triangulation not satisfying ray-shoot monotonicity.

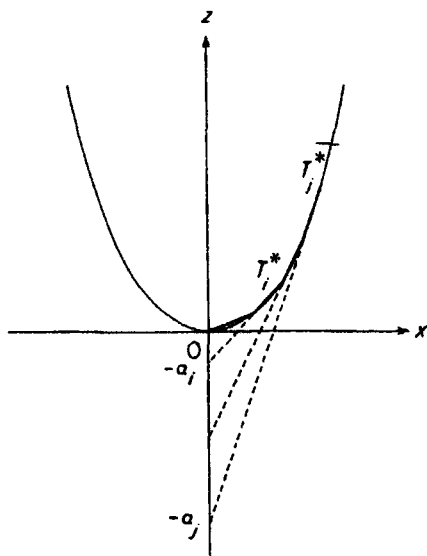


Figure 2.4.20 Monotonicity and order.

of revolution with the bottom at $(0, 0, 0)$, the plane containing T_i^* cuts the z -axis at the higher point than the plane containing T_j^* , as shown in Figure 2.4.20. Thus, $T_i \leq_p T_j$ implies $T_i <_p T_j$. Since $<_p$ is a total order, we notice that $\mathcal{T}(P)$ is monotone with respect to ray shooting at p . This property holds for an arbitrary point p , and hence we obtain Property D19.

The ray-shoot property is a useful property when we consider problems related to visibility (De Floriani, 1989b), and ordering multivariate data (see Section 6.6).

2.5 GRAPHS RELATED TO THE DELAUNAY TRIANGULATION

As we mentioned in Section 2.4 (Property D10), the Delaunay triangulation $\mathcal{D}(P)$ spanning P can be regarded as the connected geometric graph that consists of the set of nodes given by P and the set of links given by the edges E_d of the Delaunay triangles. We call this graph a *Delaunay graph* and denote it by $G(P, E_d)$. The graph $G(P, E_d)$ contains many subgraphs. Among them, notable subgraphs are the Gabriel graph, the relative neighbourhood graph, the Euclidean minimum spanning tree and the nearest neighbour graph. In this section we show the definitions of these graphs together with their geometric properties. Note that we assume throughout this section that P satisfies the non-cocircularity assumption, so that $G(P, E_d)$ is defined uniquely for the set P of points.

First of all we notice from Property D2 that the boundary $\partial\text{CH}(P)$ of the convex hull $\text{CH}(P)$ is a subgraph of $G(P, E_d)$. Figure 2.5.1 represents an example, where (a) shows a Delaunay triangulation for 12 points and (b) shows $\partial\text{CH}(P)$ of the same points.

In Property D6 we characterized $\mathcal{D}(P)$ or $G(P, E_d)$ in terms of an empty circle. Similarly, we can characterize a subgraph of $G(P, E_d)$, called the Gabriel graph, in terms of another type of empty circle. The *Gabriel graph*, denoted by $\text{GG}(P)$, of P is defined by the graph in which $\overline{p_i p_j}$ is an edge of $\text{GG}(P)$ if and only if the circle having $\overline{p_i p_j}$ as a diameter is an empty circle, that is, if and only if it contains no point of P in its interior (Gabriel and Sokal, 1969). Figure 2.5.1(c) presents the Gabriel graph for the same set of points as in (a). If $\overline{p_i p_j}$ is an edge of the Gabriel graph, p_i and p_j are said to be *Gabriel neighbours* of each other. Obviously, an edge of $\text{GG}(P)$ is a Delaunay edge of $G(P, E_d)$. It should be noted, however, that a Delaunay edge of $G(P, E_d)$ is not necessarily an edge of $\text{GG}(P)$.

To derive a necessary and sufficient condition for an edge of $\text{GG}(P)$ to be a Delaunay edge, let $\overline{p_i p_j}$ be an edge of $\text{GG}(P)$, and C be the circle with diameter $\overline{p_i p_j}$, as shown in Figure 2.5.2. Let C' be the empty circle that passes through p_i, p_j and one more point, say p_k , in P . Since C' contains no point of P in its interior, the centre of C' is a Voronoi vertex shared by the Voronoi polygons of p_i, p_j and p_k (Property V7). Let C'' be the empty circle passing through p_i, p_j and one more point other than p_k , say p_l , such that the centre of C' is on the other side of $\overline{p_i p_j}$ (see Figure 2.5.2). Then, the centre of C'' is also a Voronoi vertex, and the line segments connecting the centre of C' and that of C'' is a Voronoi edge shared by the two Voronoi polygons $V(p_i)$ and $V(p_j)$. Since the centres of C' and C'' are both on the perpendicular bisector of $\overline{p_i p_j}$, the line segment $\overline{p_i p_j}$ crosses the Voronoi edge shared by $V(p_i)$ and $V(p_j)$. In the above argument we implicitly assume that both C' and C'' exist. If C' or C'' does not exist (which happens when p_i and p_j are consecutive vertices on the boundary of the convex hull of P), we can consider that the centre of C' or C'' is at infinity, and hence the above property still holds. Thus we get the next property.

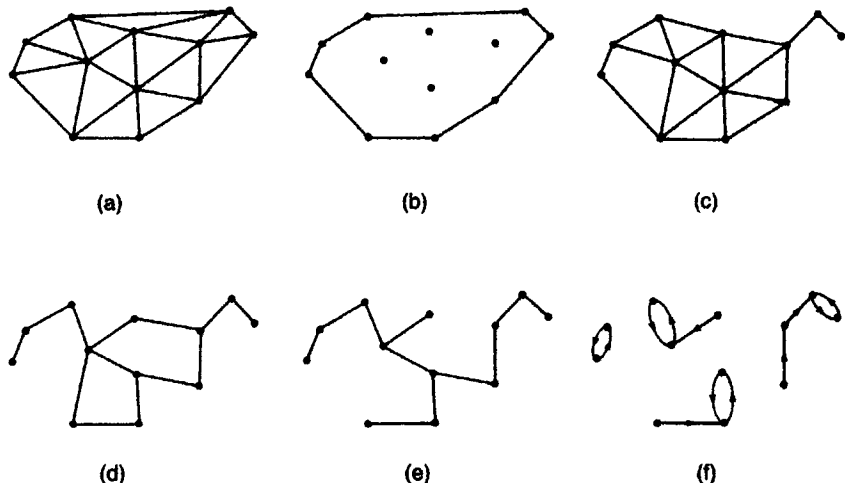


Figure 2.5.1 Graphs related to the Delaunay triangulation: (a) Delaunay triangulation; (b) convex hull; (c) Gabriel graph; (d) relative neighbourhood graph; (e) Euclidean minimum spanning tree; (f) nearest neighbourhood graph.

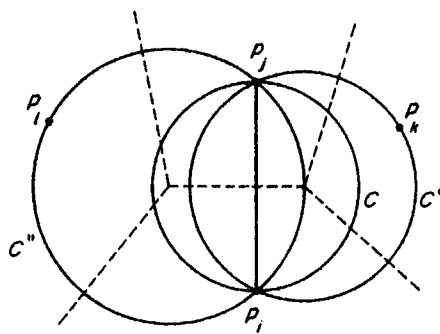


Figure 2.5.2 An edge of a Gabriel graph.

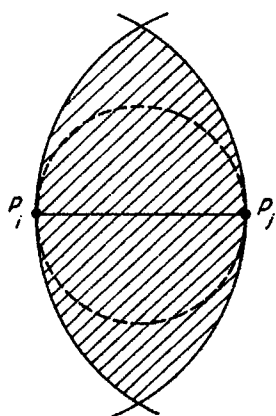


Figure 2.5.3 An edge of a relative neighbourhood graph.

Property D20 $\overline{p_i p_j}$ is an edge of $\text{GG}(P)$ if and only if $\overline{p_i p_j}$ is a Delaunay edge of $G(P, E_d)$ and $\overline{p_i p_j}$ crosses the corresponding Voronoi edge.

Note that the condition stated in Property D19 is similar to the condition imposed on each interior edge of the Pitteway triangulation (recall Property D3). Actually in the Pitteway triangulation, every edge is an edge of $\text{GG}(P)$. Hence we get the next property.

Property D21 If the Delaunay triangulation $\mathcal{D}(P)$ is a Pitteway triangulation, $\text{GG}(P)$ is exactly the same as $G(P, E_d)$.

We can use $\text{GG}(P)$ in defining adjacency in point patterns (Gabriel and Sokal, 1969; Matula and Sokal, 1980; Urquhart, 1982).

As is illustrated in Figure 2.5.3, the Gabriel graph is defined with the empty circle indicated by the broken lines. Modifying this empty circle, we may define a subgraph of $G(P, E_d)$, called the relative neighbourhood graph, with an ‘empty spindle’, indicated by the shaded area in Figure 2.5.3. To be precise, the *relative neighbourhood graph*, denoted by $\text{RNG}(P)$, is defined as a geometric graph in which $\text{RNG}(P)$ has an edge between p_i and p_j if and only if

$$d(p_i, p_j) \leq \min_{k(\neq i, j)} \max\{d(p_i, p_k), d(p_j, p_k)\} \quad (2.5.1)$$

(Toussaint, 1980a; Supowit, 1983; Urquhart, 1982). In other words, $\overline{p_i p_j}$ is an edge of $\text{RNG}(P)$ if and only if there is no other point of P in the interior of the intersection of the disk with the centre at p_i and the radius $d(p_i, p_j)$ and the disk with the centre at p_j and the same radius (i.e. the open region represented by the shaded area in Figure 2.5.3). This region contains the interior of the circle (represented by the dashed line in Figure 2.5.3) having $\overline{p_i p_j}$ as a diameter, and hence we get the next property.

Property D22 An edge of $\text{RNG}(P)$ is an edge of $\text{GG}(P)$.

Figure 2.5.1(d) represents the relative neighbourhood graph for the same set of points as in (a). We can use $\text{RNG}(P)$ as well as $\text{GG}(P)$ for the analysis of point patterns (Toussaint, 1980a; Urquhart, 1982; Lefkovitch, 1984, 1985, 1987; Ichino and Sklansky, 1985; Dearholt *et al.*, 1988).

The subgraphs of the graph $G(P, E_d)$ include tree graphs. One of the most frequently referred to tree graphs is the Euclidean minimum spanning tree. The *Euclidean minimum spanning tree*, denoted by $\text{EMST}(P)$, is defined as the tree having a vertex set P in which the sum of the Euclidean length of all the edges attains the minimum over all trees having the vertex set P . Regarding the relationship between an edge of $\text{EMST}(P)$ and that of $\text{RNG}(P)$, we can show the following property.

Property D23 An edge of $\text{EMST}(P)$ is an edge of $\text{RNG}(P)$.

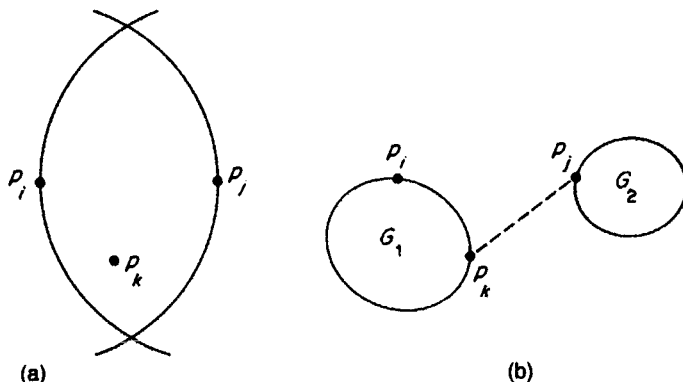


Figure 2.5.4 An edge in the $\text{EMST}(P)$.

To prove this property, assume, contrary to Property D23, that $\overline{p_i p_j}$ is an edge of $\text{EMST}(P)$ but that there is a point, say p_k , in the intersection of the two disks with radius $d(p_i, p_j)$ centred at p_i and p_j , as shown in Figure 2.5.4(a). If we remove the edge $\overline{p_i p_j}$ from $\text{EMST}(P)$, the tree is divided into two subtrees, G_1 and G_2 ; one contains p_i and the other contains p_j . Without loss of generality, suppose that G_1 contains p_i and p_k and G_2 contains p_j . Then we can obtain a new tree G' from G_1 and G_2 by adding a new edge $\overline{p_i p_k}$, as shown in Figure 2.5.4(b). Since $d(p_j, p_k) < d(p_i, p_j)$, the total length of the edges in G' is smaller than the total length of the edges in $\text{EMST}(P)$, which is a contradiction. Thus, we get Property D23.

Figure 2.5.1(e) represents the Euclidean minimum spanning tree for the same set of points as in (a).

Minimum-cost spanning trees, $\text{EMST}(P)$ in particular, have many applications such as clustering (Gower and Ross, 1969; Rohlb, 1973; Friedman and Rafsky, 1979, 1981; Johnson, 1967; Kayser *et al.*, 1992; Martinetz *et al.*, 1990; McIntosh, 1988), pattern recognition (Osteen and Lin, 1974), natural pattern analysis (Billia *et al.*, 1991; Bhavsar and Line, 1988; Dussert *et al.*, 1986), biological pattern analysis (Dussert *et al.*, 1987; Kayser and Stute, 1989; Choi *et al.*, 1995) and approximation algorithms for the travelling salesman problem (Rosenkrantz *et al.*, 1977).

The geometric subgraphs of $\mathcal{D}(P)$ discussed above are all non-directed graphs. If we introduce a direction in a subgraph of $G(P, E_d)$, we can define a directed subgraph, called the nearest neighbour graph. The *nearest neighbour graph*, denoted by $\text{NNG}(P)$, is defined as the directed graph having a vertex set P such that $\overrightarrow{p_i p_j}$ is an edge of $\text{NNG}(P)$ if and only if

$$d(p_i, p_j) = \min_{k (\neq i)} d(p_i, p_k).$$

In other words, $\overrightarrow{p_i p_j}$ is an edge of $\text{NNG}(P)$ if and only if p_j is the nearest neighbour of p_i . Note that the nearest neighbour relation is not symmetric; p_j being the nearest neighbour of p_i does not necessarily imply that p_i is the nearest

neighbour of p_i . Every point has its nearest neighbour unless P consists of only one point. However, the nearest neighbour is not necessarily unique; there may be two or more points whose distances from p_i attain the minimum. Hence, in general, every vertex in NNG(P) has one or more edges going out from that vertex. The next property follows directly from the definition.

Property D24 If $\overrightarrow{p_i p_j}$ is an edge of NNG(P), then $\overline{p_i p_j}$ is an edge of RNG(P).

Furthermore, we may derive a little stronger property than Property D24.

Property D25 If $\overrightarrow{p_i p_j}$ is an edge of NNG(P) and there is no other edge in NNG(P) that has the same initial vertex p_i , then $\overline{p_i p_j}$ is an edge of EMST(P).

To prove this property, assume, contrary to Property D25, that (p_i, p_j) is an edge of NNG(P) but $\overline{p_i p_j}$ is not an edge of EMST(P). If we add an edge $\overline{p_i p_j}$ to EMST(P), the resulting graph has exactly one cycle, and $\overline{p_i p_j}$ belongs to this cycle. Let $\overline{p_i p_k}$ be the other edge that is on this cycle and that has p_i as one of the terminal points. Let G be the graph obtained from EMST(P) by replacing the edge $\overline{p_i p_k}$ with the edge $\overrightarrow{p_i p_j}$. Then G is a spanning tree. Moreover, since $\overrightarrow{p_i p_j}$ is the only edge starting at p_i in NNG(P), $\overline{p_i p_j}$ is shorter than $\overline{p_i p_k}$. Hence, the total length of the edges in G is smaller than that in EMST(P), which is a contradiction. Thus we get Property D25.

Property D25 implies that if no two pairs of points in P have the same distance, NNG(P) is a subgraph of the directed graph that is obtained from EMST(P) by replacing each edge with two parallel edges having opposite directions. Figure 2.5.1(f) represents the nearest neighbour graph for the same set of points as in (a). NNG(P) can be applied to geographic analysis (Kolars and Nystuen, 1974). The properties of NNG(P) are studied by Saaty (1970) and Pielou (1977).

For a set P of points in the plane, we have considered six graphs $G(P, E_d)$, $\partial\text{CH}(P)$, GG(P), RNG(P), EMST(P) and NNG(P). The relations of the first five undirected graphs are shown in Figure 2.5.5, where the lower graph is a subgraph of the upper graph. These relations come from Properties D2 and D20–D25. $\partial\text{CH}(P)$ is a subgraph of $G(P, E_d)$ (Property D2). EMST(P) is a subgraph of RNG(P) (Property D23). RNG(P) is a subgraph of GG(P)

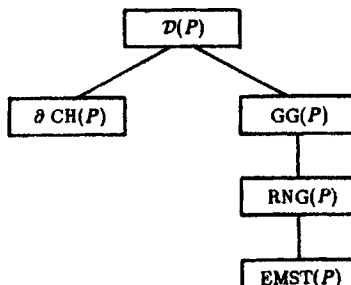


Figure 2.5.5 Relations among the Delaunay triangulation and the related graphs.

(Property D22). $GG(P)$ is a subgraph of $G(P, E_d)$ (Property D20). $NNG(P)$ is a subgraph of the directed graph obtained from $RNG(P)$ by replacing each edge with two parallel edges having opposite directions (Property D24). If no two pairs of points in P have the same distance, $NNG(P)$ is a subgraph of the directed graph obtained from $EMST(P)$ by replacing each edge with two parallel edges having opposite directions (Property D25). In particular, $\overrightarrow{p_i p_j}$ or $\overleftarrow{p_i p_j}$ can be a candidate for an edge of these graphs only when $\overrightarrow{p_i p_j}$ is a Delaunay edge. As we will see in Chapter 4, $G(P, E_d)$ can be constructed efficiently. Hence, the above relationships give us methods for constructing these graphs through $G(P, E_d)$; we first construct $G(P, E_d)$ and next delete superfluous edges from $G(P, E_d)$.

The construction of $\partial CH(P)$ from $G(P, E_d)$ is straightforward; indeed, what we have to do is simply gather the outermost Delaunay edges in $G(P, E_d)$. The construction of $GG(P)$ from $G(P, E_d)$ is likewise straightforward, because whether or not a Delaunay edge is an edge of $GG(P)$ can be checked locally according to Property D20. Similarly, the construction of $NNG(P)$ from $G(P, E_d)$ is straightforward; all we have to do is to select, for each point in P , the shortest Delaunay edge incident to the point. The construction of $RNG(P)$ and $EMST(P)$ requires a more global check. See Toussaint (1980a) and Supowit (1983) for the construction of $RNG(P)$. Prim (1957) showed some principles for finding the minimum-cost spanning tree, and those principles were used in many algorithms proposed thereafter. An efficient algorithm for finding the minimum-cost spanning tree for a planar graph is known (Cheriton and Tarjan, 1976). Since $G(P, E_d)$ is a planar graph, this algorithm can be used for finding $EMST(P)$ from $G(P, E_d)$.

Historically there is another graph that was believed to be a subgraph of the Delaunay graph. For a vertex set P , a route visiting all the vertices in P exactly once and returning to the start vertex is called a *Hamilton cycle*. A minimum length Hamilton cycle for P is called a Euclidean travelling salesman cycle for P . It was once conjectured that every Delaunay diagram for P has a Euclidean travelling salesman cycle for P (Shamos, 1978). However, this conjecture was refuted by Kantabutra (1983); actually he found a Delaunay diagram that does not have even a Hamilton cycle. While Kantabutra's counterexample is a degenerate Delaunay diagram, Dillencourt (1987a) found a non-degenerate Delaunay diagram that does not have a Hamilton cycle. He also showed that it is very hard to judge whether or not a given Delaunay diagram has a Hamilton cycle (Dillencourt, 1996a). Cimikowski (1990) found a subclass of the Delaunay diagrams that have Hamilton cycles.

The graphs considered in this section are all defined on the basis of proximity relations. Hence these graphs are called *proximity graphs*. The graph theoretical properties of the proximity graphs together with their construction algorithms are studied by Devroye (1988), Jaromczyk and Kowaluk (1987), Katajainen (1988), Katajainen and Nevalainen (1986) and Chang *et al.* (1992).

The proximity graphs have many applications in engineering, particularly to morphological problems. For example, Radke (1988) applied the proximity

graphs to point pattern analysis; the proximity graphs define structures among unstructured collections of points that are useful for pattern recognition. Toussaint (1988) used these proximity graphs together with another proximity graph called a 'sphere-of-influence graph' for constructing a so-called primal sketch to capture the low-level perceptual structure of visual scenes consisting of dot patterns. Tüceryan and Chorzempa (1991) studied the stability of the proximity graphs against noise points in the context of line extraction using Hough transformation, and observed that the Delaunay triangulation is more stable than other types of proximity graphs. Toriwaki and Yokoi (1988) applied the Delaunay triangulation and the Gabriel graph to the recognition of the structure of texture in digital images, and showed that they are useful for the decomposition of images into meaningful regions. ElGindy and Toussaint (1988) applied the relative neighbourhood graph to the decomposition of polygons into perceptually meaningful points. Beasley and Goffinet (1994) used the Delaunay triangulation for finding the Euclidean minimum Steiner tree. Dickerson and Drysdale (1991) used the Delaunay triangulation to enumerate k smallest distances. Other applications can also be found in a survey by Jaromczyk and Toussaint (1992).

The proximity graphs have been generalized in many directions. O'Rourke (1982) studied the proximity graphs with respect to L_1 and L_∞ norms. The relative neighbourhood graph is generalized to ' k -relative neighbourhood graphs', in which two points are connected by an edge if and only if the spindle in Figure 2.5.3 contains less than k points (Su and Chang, 1991b; Chang *et al.*, 1990b, 1992). The Gabriel graph can be generalized to the ' k -Gabriel graph' similarly (Su and Chang, 1990). Proximity graphs with constraints are also defined; they admit an inclusion relationship similar to Figure 2.5.5 (Su and Chang, 1991a; Jennings and Lingas, 1992); refer to the next chapter for the constrained Delaunay triangulation. The proximity graphs are also defined and studied in higher dimensional spaces (Agarwal *et al.*, 1990b; Jaromczyk and Kowaluk, 1991; Agarwal and Matousek, 1992; Smith *et al.*, 1995).

2.6 RECOGNITION OF VORONOI DIAGRAMS

Sometimes we want to judge whether a given diagram is a Voronoi/Delaunay diagram or not. Here we consider methods for this judgement.

The problems can be divided into three types. The first type, given a diagram actually drawn in the plane, is to judge whether it is a Voronoi/Delaunay diagram. This problem is called the *geometric recognition problem*. The second type, given a graph embedded in the plane, is to judge whether it is isomorphic to a Voronoi/Delaunay diagram. This problem is called the *combinatorial recognition problem*. The third type, given a diagram drawn in the plane, is to find the Voronoi/Delaunay diagram that is closest to the given diagram. This problem is called the *approximation problem*.

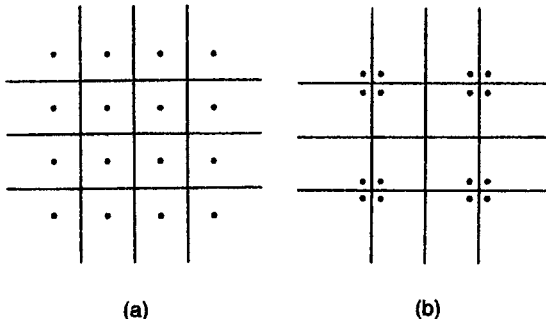


Figure 2.6.1 Voronoi diagram whose generators are not unique.

In this section we consider the first and second types of problems. The approximation problem will be considered in Section 9.5.

2.6.1 The geometric approach

As before, let $P = \{p_1, p_2, \dots, p_n\}$ be a set of n points in the plane. Suppose that we are given a triangulation \mathcal{T} with the vertex set P . The first problem we consider is the following.

Problem V8 Given a triangulation \mathcal{T} with the vertex set P , judge whether \mathcal{T} is the Delaunay diagram for P .

This problem can be solved easily. What we have to do is to check whether the circumcircle of each triangle in \mathcal{T} is an empty circle. \mathcal{T} is the Delaunay diagram if and only if all the circumcircles are empty circles. Recall Property D5 in Section 2.4.

Next, suppose that we are given a partition Q of the plane into n convex polygons q_1, q_2, \dots, q_n and their boundaries. We are interested in judging whether Q is the Voronoi diagram for some set P of n points. Thus the problem is as follows.

Problem V9 Given a partition Q of the plane into n convex polygons, judge whether Q is the Voronoi diagram for some P .

This problem is less trivial because we have to search for the locations of the generators. Suppose that Q is the Voronoi diagram, and that the location of any one generator, say p_i , is known. Then, we can find the locations of the neighbouring generators uniquely, because they are the mirror images of p_i with respect to the mirrors at the Voronoi edges on the boundary of $V(p_i)$. The locations of their neighbours are determined in a similar way. In this way, starting with p_i , we can locate all the generators from neighbour to neighbour.

Keeping this fact in mind, let us first consider the case where Q has at least one edge, say e , both end vertices of which are incident to exactly three edges (including e). Then, Property V15 tells us the unique locations of the generators on both sides of e . Consequently, we can locate all the generators by taking the mirror images with respect to other edges. Let the resultant set of generators be P . We construct the Voronoi diagram $\mathcal{V}(P)$ and compare it with Q . We can judge that Q is the Voronoi diagram if $Q = \mathcal{V}(P)$, and Q is not otherwise. This direction of analysis was given by Loeb (1976), Stoyan and Stoyan (1980) and Ash and Bolker (1985); see also Problem V6, Property V15 and Property V16.

Next, let us consider the case where there is no edge both end vertices of which are incident to exactly three edges. In this case, even if Q is the correct Voronoi diagram, the locations of the generators are not necessarily unique. An example is shown in Figure 2.6.1; the generators in (a) are different from those in (b), but both sets of generators give the same Voronoi diagram.

Hartvigsen (1992) solved Problem V9 by reducing it to the satisfiability of a system of linear equations and linear inequalities in the following way.

Let $\mathbf{x}^T = (x_1, y_1, x_2, y_2, \dots, x_n, y_n)$ be the $2n$ -dimensional unknown vector. We search for the locations $(x_1, y_1), (x_2, y_2), \dots, (x_n, y_n)$ of n generators whose Voronoi diagram coincides with Q . The generators should satisfy the following conditions.

- (1) Each generator should be in the associated Voronoi region.
- (2) An edge in Q should be on the perpendicular bisector of the two side generators.

Let e be an edge of Q shared by two polygons q_i and q_j . Without loss of generality, we assume that the line containing e does not contain the origin of the coordinate system. Then, the line containing e can be expressed by the equation

$$ax + by = 1. \quad (2.6.1)$$

Suppose that q_i and the origin lie in the same side of e . Then we get

$$ax_i + by_i > 0 \text{ and } ax_j + by_j < 0. \quad (2.6.2)$$

We obtain similar inequalities for each edge of Q . Collecting them all, we get the system of linear inequalities. Let us denote this system by

$$A\mathbf{x} > 0. \quad (2.6.3)$$

This is the mathematical expression of condition (1).

Next, let us consider condition (2). The line containing e should contain the midpoint of (x_i, y_i) and (x_j, y_j) . Hence we get

$$a \frac{x_i + x_j}{2} + b \frac{y_i + y_j}{2} = 1. \quad (2.6.4)$$

Furthermore, since the line connecting (x_i, y_i) and (x_j, y_j) should be perpendicular to e , we get

$$a(y_i - y_j) - b(x_i - x_j) = 0. \quad (2.6.5)$$

Note that the above two equations are linear in the unknown coordinates.

We get similar equations for each edge. Collecting them all, we obtain a system of linear equations, which we denote by

$$Bx = c. \quad (2.6.6)$$

This system of equations represents condition (2). We now state the following theorem.

Theorem V1 (Hartvigsen, 1992) The partition Q of the plane is the Voronoi diagram if and only if the system of equations (2.6.6) and inequalities (2.6.5) has a solution.

The satisfiability of the system of linear equations and inequalities can be checked by the linear programming techniques. Hence, if the vertices and the edges of Q are represented by rational numbers, Problem V9 can be solved in time represented by a polynomial function of n (Khachian, 1979, 1980).

Usually the given diagram contains numerical errors in the coordinates of the vertices, and hence equations (2.6.6) do not hold strictly. Evans and Jones (1987) proposed to

$$\text{minimize } \|Bx - c\|^2$$

instead of searching for the exact solution of equations (2.6.6).

The above theorem was generalized to the n -dimensional space by Hartvigsen (1992). Aurenhammer (1987b) also gave another method for recognizing the Voronoi diagram in the n -dimensional space; he also studied the recognition of a weighted Voronoi diagram.

2.6.2 The combinatorial approach

Suppose that G is a simple, connected, and planar graph embedded in the plane, where the graph G being simple means that G has no self-loop or no parallel edges, and hence any cycle of G contains at least three edges. In this subsection we assume that every vertex in G is incident to three or more edges. Let $V = \{v_1, v_2, \dots, v_n\}$ be the set of vertices of G , and let E be the set of edges of G . The edges of G divide the plane into connected regions. These regions are called *cells* generated by the embedded graph G . The outermost cell is unbounded while the other cells are bounded. The bounded cells are called *inner cells*. We call the embedded graph G a *triangulation graph* if all the inner cells are bounded by exactly three edges.

Let G be a triangulation graph, and C be the set of all the cycles of G that bound the inner cells counterclockwise. We represent this triangulation graph by $G(V, E, C)$. When we write $G(V, E, C)$, we concentrate our

attention on the combinatorial structure of the embedded graph; we do not care about the actual locations at which the vertices are placed.

For a triangulation graph $G(V, E, C)$, let ψ be a mapping from V to \mathbb{R}^2 such that $\psi(v_i) \neq \psi(v_j)$ whenever $i \neq j$. Placing the vertices v_i of G at $\psi(v_i)$ and representing the edges of G by the straight line segments connecting the two terminal vertices, we get a diagram. If this diagram realizes the triangulation graph G (i.e. both if no edges intersect except at the end points, and if the set of all the cycles that bound the inner cells coincides with C), then this diagram is called a *triangulation* and is denoted by $\mathcal{T} = (G, \psi)$ or $\mathcal{T} = (V, E, C, \psi)$.

Triangulation $\mathcal{T} = (V, E, C, \psi)$ is a Delaunay triangulation if

1. the boundary of the outermost cell forms a convex polygon, and
2. the circumcircle of each inner cell (i.e. triangle) does not contain a vertex in its interior.

The triangulation graph $G(V, E, C)$ is called a *Delaunay-triangulation-realizable graph* (*DT-realizable graph* for short) if there is a mapping ψ such that $\mathcal{T} = (G, \psi)$ is a Delaunay triangulation.

The triangulation graph $G(V, E, C)$ is called a *non-degenerate DT-realizable graph* if there exists a mapping ψ such that $\mathcal{T} = (G, \psi)$ is a non-degenerate Delaunay triangulation.

The graph G is said to be *2-connected* if deletion of any one vertex and all the edges incident to it from G does not make the resultant graph disconnected. The Delaunay triangulation gives a 2-connected graph. Hereafter we assume that G is 2-connected. The problem we consider is the following.

Problem V10 Given a triangulation graph $G(V, E, C)$, judge whether G is a (non-degenerate) DT-realizable graph.

As we have already seen, Property D13 gives a sufficient condition for G to be a non-degenerate DT-realizable graph, and Property D14 gives a sufficient condition for G to be a DT-realizable graph (Dillencourt, 1990a,b). On the other hand, Hodgson *et al.* (1992) gave a necessary and sufficient condition for a graph to be the vertex-edge graph of a convex polyhedron with all the vertices on a common sphere. As we have seen in Property D7, the Delaunay triangulation and a convex polyhedron inscribed in a sphere have a one-to-one correspondence through the inversion transformation. Hence, Hodgson *et al.*'s result (1992) together with Property D7 gives a solution of Problem V10.

Hiroshima and Sugihara (1994, 1996) also gave a necessary and sufficient condition for G to be a DT-realizable graph. Their condition is represented by a system of linear equations and linear inequalities. Hence, Problem V10 can be solved by linear programming techniques. They assigned variables to the angles of all the triangles, and formulated the condition in the following way.

For the triangulation graph $G(V, E, C)$, let the elements of C be $c_1, c_2, \dots, c_{|C|}$. Each cycle c_i has three vertices; we assign three variables x_{3i-2}, x_{3i-1}

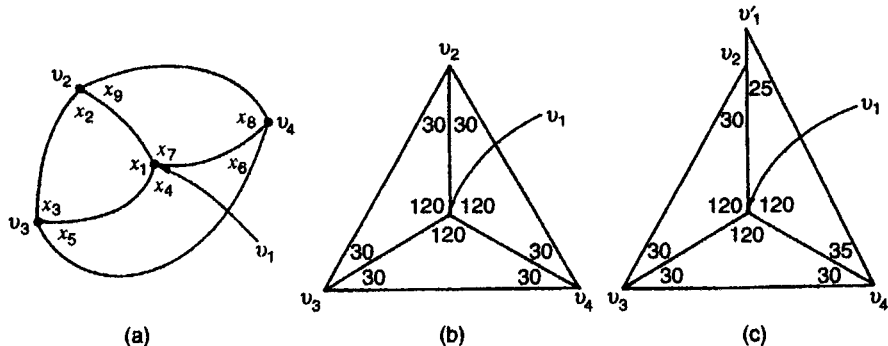


Figure 2.6.2 Triangulation graph and angle variables.

and x_{3i} , one to each vertex of c_i . We interpret these variables as angles at the corresponding corners of the triangle. So let us call these variables *angle variables*. In total we have $3|C|$ angle variables, each corresponding to a corner of a triangle. For the triangulation graph in Figure 2.6.2(a), for example, we assign nine angle variables x_1, x_2, \dots, x_9 as shown in this figure.

We call a vertex of G an *outer vertex* if it is on the boundary of the outermost cell, and an *inner vertex* otherwise. Similarly, we call an edge of G an *outer edge* if it is on the boundary of the outermost cell, and an *inner edge* otherwise.

For a given triangulation graph $G(V, E, C)$, we generate the following five types of constraints; they should be satisfied if G is realized as a Delaunay triangulation.

- (C1) For each cycle in C , the sum of the associated three angle variables is equal to 180.
- (C2) For each inner vertex, the sum of all the associated angle variables is equal to 360.
- (C3) For each outer vertex, the sum of all the associated angle variables is equal to or less than 180.
- (C4) For each inner edge, the sum of the associated pair of facing angle variables (i.e. the angle variables corresponding to the vertices that are on the same cycle as, but are not incident to, the inner edge) is equal to or less than 180.
- (C5) Each angle variable is positive.

Let us denote by $S(G)$ the system consisting of all the constraints.

For example, for the triangulation graph in Figure 2.6.2(a), (C1) implies

$$x_1 + x_2 + x_3 = 180, \quad x_4 + x_5 + x_6 = 180, \quad x_7 + x_8 + x_9 = 180. \quad (2.6.7)$$

(C2) implies

$$x_1 + x_4 + x_7 = 360. \quad (2.6.8)$$

(C3) implies

$$x_3 + x_5 \leq 180, \quad x_6 + x_8 \leq 180, \quad x_9 + x_2 \leq 180. \quad (2.6.9)$$

(C4) implies

$$x_2 + x_6 \leq 180, \quad x_5 + x_9 \leq 180, \quad x_3 + x_8 \leq 180. \quad (2.6.10)$$

(C5) implies

$$x_1 > 0, x_2 > 0, \dots, x_9 > 0. \quad (2.6.11)$$

Thus $S(G)$ consists of four equations, six improper inequalities and nine proper inequalities.

For any Delaunay triangulation $\mathcal{T} = (G, \psi)$, the realized values of the angle variables (measured in degrees) satisfy the constraints. Indeed, (C1), (C2) and (C5) are satisfied by any triangulation, whereas (C3) means that the outermost cycle of \mathcal{T} forms a convex polygon, and (C4) means that the circumcircle of any triangle is an empty circle. An example of a Delaunay triangulation realizing the graph in Figure 2.6.2(a) is shown in Figure 2.6.2(b).

However, the converse is not true. That is, the values of the angle variables that satisfy all the constraints in $S(G)$ do not necessarily correspond to a Delaunay triangulation. For example, for the graph G in Figure 2.6.2(a), the angle values

$$\begin{aligned} x_1 = x_4 = x_7 = 120, \quad x_2 = x_3 = x_5 = x_6 = 30, \\ x_8 = 35, x_9 = 25 \end{aligned}$$

satisfy $S(G)$, but they do not correspond to a triangulation; if we try to draw the diagram using these angle values, we come across inconsistency, as shown in Figure 2.6.2(c). Indeed, we can choose the size of the first triangle $\Delta v_1 v_2 v_3$ arbitrarily, but next we must glue the second triangle $\Delta v_1 v_3 v_4$ along the edge $\overline{v_1 v_3}$, and finally glue the third triangle $\Delta v_1 v_4 v_2$ along the edge $\overline{v_1 v_4}$, ending up with an inconsistent position of the vertex v_2 . In order to avoid such inconsistency we need still more constraints.

Let x_i, x_j and x_k be three angle variables corresponding to the three vertices v_α, v_β and v_γ , counterclockwise in this order, of a cell. Then, we say that x_j is *cc-facing* (meaning ‘facing counterclockwise’) around v_α , and x_k is *c-facing* (meaning ‘facing clockwise’) around v_α . In Figure 2.6.2(a), x_2, x_5 and x_8 are cc-facing around v_1 , while x_3, x_9 and x_6 are c-facing around v_1 .

For two mutually adjacent vertices v_i and v_j , there is a unique angle variable x_k such that x_k is cc-facing around v_i and c-facing around v_j . We denote the angle variable x_k by μ_{ij} . For the triangulation graph in Figure 2.6.2(a), $\mu_{12} = x_8$ because x_8 is the unique angle variable that is cc-facing around v_1 and c-facing around v_2 . Note that $\mu_{ij} \neq \mu_{ji}$. In Figure 2.6.2(a), $\mu_{21} = x_3, \mu_{32} = x_1$ and μ_{23} is undefined.

Suppose that v_i is an inner vertex of G . Let $d(i)$ denote the number of edges incident to v_i , let $\phi_1^{(i)}, \phi_2^{(i)}, \dots, \phi_{d(i)}^{(i)}$ be the cc-facing angle variables around v_i , and let $\theta_1^{(i)}, \theta_2^{(i)}, \dots, \theta_{d(i)}^{(i)}$ be the c-facing angle variables around v_i . Furthermore, we define

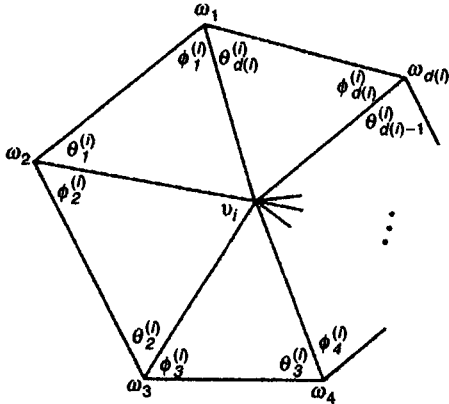


Figure 2.6.3 Angles cc-facing and c-facing around the vertex \$v_i\$.

$$F(v_i) = \frac{\sin\phi_1^{(i)} \sin\phi_2^{(i)} \dots \sin\phi_{d(i)}^{(i)}}{\sin\theta_1^{(i)} \sin\theta_2^{(i)} \dots \sin\theta_{d(i)}^{(i)}}. \quad (2.6.12)$$

We consider only positive angle values, and hence we get \$0 < F(v_i) < \infty\$.

Lemma 2.6.1 Any triangulation \$\mathcal{T} = (V, E, C, \psi)\$ satisfies the next constraint.

(C6) \$F(v_i) = 1\$ for any inner vertex \$v_i\$.

Proof Let \$v_i\$ be an inner vertex of \$\mathcal{T}\$. As shown in Figure 2.6.3, let \$w_1, w_2, \dots, w_{d(i)}\$ be the vertices incident to \$v_i\$ counterclockwise, let \$\phi_j^{(i)}\$ and \$\theta_j^{(i)}\$ be the cc-facing angle and the c-facing angle, respectively, around \$v_i\$ associated with the triangle \$\Delta v_i w_j w_{j+1}\$, where \$w_{d(i)+1}\$ is to be read as \$w_1\$. Let \$l(v_i, w_j)\$ denote the length of the edge \$\overline{v_i w_j}\$. Then we get

$$l(v_i, w_j) \sin\phi_j^{(i)} = l(v_i, w_{j+1}) \sin\theta_j^{(i)} \quad \text{for } j = 1, 2, \dots, d(i). \quad (2.6.13)$$

Substituting these equations in \$F(v_i)\$, we obtain

$$F(v_i) = \prod_{j=1}^{d(i)} \frac{\sin\phi_j^{(i)}}{\sin\theta_j^{(i)}} = \prod_{j=1}^{d(i)} \frac{l(v_i, w_{j+1})}{l(v_i, w_j)} = 1. \quad (2.6.14)$$

□

Theorem V2 A 2-connected triangulation graph \$G(V, E, C)\$ is a DT-realizable graph if and only if the set of constraints (C1)–(C6) is satisfiable.

Proof First suppose that \$G\$ is a DT-realizable graph. Then there exists a Delaunay triangulation \$\mathcal{T} = (G, \psi)\$. Let us assign the values of the angles realized by \$\mathcal{T}\$ to the corresponding angle variables. Then, they satisfy (C1), (C2), (C5) and (C6) because \$\mathcal{T}\$ is a triangulation. Moreover, they satisfy (C3) and (C4) because \$\mathcal{T}\$ is a Delaunay triangulation.

Next suppose that there exist angle values for G that satisfy (C1)–(C6). Then, we can construct the triangulation using these angle values. First, we choose an arbitrary cell of G and draw it as a triangle of arbitrary size with the given angle values. Next we augment the triangulation by adding adjacent triangles one by one. Since a new triangle added at each step is adjacent to at least one old triangle, its size is determined automatically in such a way that the edges common to the old and the new triangles coincide. Even if the new triangle is adjacent to two or more triangles, it can be glued to the old part of the triangulation consistently because the constraint (C6) is satisfied. Hence we can complete the triangulation $\mathcal{T} = (G, \psi)$. The constraint (C3) implies that the outermost edges form a convex polyhedron, and hence the triangulation is the partition of the convex hull of the vertices whose locations are specified by ψ . The constraint (C4) directly implies that the circumcircle of a triangle does not contain the vertices of the adjacent triangles. This fact, in turn, implies that the circumcircle of a triangle does not contain a vertex, because we can always obtain the Delaunay triangulation by flipping the diagonals of the quadrilaterals that do not satisfy (C4). Thus, the constraints (C3) and (C4) altogether guarantee that \mathcal{T} is a Delaunay triangulation. \square

If we restrict the Delaunay triangulations to non-degenerate ones, constraints (C3) and (C4) are respectively changed in the following way.

- (C3') For each outer vertex, the sum of all the associated angle variables is less than 180.
- (C4') For each inner edge, the sum of the associated pair of the angle values facing the edge is less than 180.

Namely, the constraints (C3) and (C4) are represented by inequalities allowing equalities, while the constraints (C3') and (C4') are represented by inequalities without allowing equalities.

Thus, we get a non-degenerate version of Theorem V2 as follows.

Theorem V3 A 2-connected triangulation graph $G(V, E, C)$ is a non-degenerate DT-realizable graph if and only if the set of constraints (C1), (C2), (C3'), (C4'), (C5) and (C6) is satisfiable.

Proof The proof of this theorem is straightforward because the addition of the constraints (C3') and (C4') simply implies the deletion of the equality symbols from the improper inequalities generated by (C3) and (C4). \square

Thus, we get the necessary and sufficient condition for a triangulation graph to be a DT-realizable graph or a non-degenerate DT-realizable graph. Battista and Vismara (1993) pointed out that if actual values are assigned to the angle variables, the constraints (C1)–(C6) can be used to judge whether the given set of angle values corresponds to the actual Delaunay triangula-

tion. However, the condition stated in Theorem V2 or V3 is not useful for the recognition of a DT-realizable graph, because the angle values are unknown variables in our problem, and we do not know a finite-step algorithm for judging the satisfiability of the condition.

If we happen to be able to delete the constraint (C6), we can judge the satisfiability in finite steps because the constraints (C1)–(C5) are linear in the variables and the method for checking their satisfiability has been established in linear programming. Indeed we can delete the constraint (C6). The next two theorems hold.

Theorem V4 (Hiroshima and Sugihara, 1994) A 2-connected triangulation graph $G(V, E, C)$ is a DT-realizable graph if and only if the set of constraints (C1)–(C5) is satisfiable.

Theorem V5 (Hiroshima and Sugihara, 1994) A 2-connected triangulation graph $G(V, E, C)$ is a non-degenerate DT-realizable graph if and only if the set of constraints (C1), (C2), (C3'), (C4') and (C5) is satisfiable.

As we have already seen in Figure 2.6.2(c), the angle values satisfying (C1)–(C5) cannot be used directly for the construction of a Delaunay triangulation. However, we can show that once we obtain the angle values that satisfy (C1)–(C5), then we can change them so as to satisfy (C6) while (C1)–(C5) are kept unviolated. This is the main story of the proofs of Theorems V4 and V5. The details of the proof are shown in Hiroshima and Sugihara (1994, 1996).

CHAPTER 3

Generalizations of the Voronoi Diagram

Since the early 1970s the ordinary Voronoi diagram has been extended or generalized in many directions, and those generalized Voronoi diagrams facilitate many practical applications in various fields. In this chapter we show the definitions of those generalized Voronoi diagrams together with their major geometric properties. First, to give a perspective of this section, we fix a general framework for possible generalizations and make general comments. (If the reader is interested in only a specific generalized Voronoi diagram, he or she may skip this introduction and go directly to the section on that Voronoi diagram.)

We notice from the definition of the ordinary Voronoi diagram (Definition V1) that an abstract idea for defining a Voronoi diagram is that every point in a space is assigned to at least one of the generators according to a certain assignment rule, and that the resulting sets of points associated with the generators are collectively exhaustive and mutually exclusive except for boundaries. To formalize this abstract idea, we consider a non-empty space S and a set, $A = \{A_1, \dots, A_n\}$, of n distinct subsets of S ($2 \leq n < \infty$) satisfying $A_i \cap A_j = \emptyset$, $i \neq j$, which we shall call a *generator set*. In the ordinary Voronoi diagram the space S is the Euclidean space, and the generator set A is a set of points $P = \{p_1, \dots, p_n\}$ ($A = P$, $A_i = p_i$). In general the space S may be the Euclidean space or a non-Euclidean space, and an element A_i in A may be a point, a set of points, a line, an area, a polyhedron, etc.

Given a space S and a set A , we consider an assignment of a point p in S to at least one element of A according to a certain rule. If we assign p to A_i , we put 1 for (p, A_i) ; if we do not assign p to A_i , we put 0 for (p, A_i) , $p \in S$, $A_i \in A$. Then this assignment can be regarded as a mapping from $S \times A$ to $\{1, 0\}$. Mathematically, we consider a mapping, δ_A , from $S \times A$ to $\{0, 1\}$ such that

$$\delta_A(p, A_i) = \begin{cases} 1 & \text{if } p \text{ is assigned to } A_i \text{ in } A, \\ 0 & \text{otherwise.} \end{cases} \quad (3.0.1)$$

We call the mapping δ_A an *assignment rule*. In the ordinary Voronoi diagram, for example, the assignment rule δ_A is given by

$$\delta_A(p, A_i) = \begin{cases} 1, & \text{if } \|x - x_i\| \leq \|x - x_j\|, \quad j \neq i, j \in I_n, \\ 0, & \text{otherwise,} \end{cases} \quad (3.0.2)$$

where x and x_i are the location vectors of p and p_i in \mathbb{R}^m , respectively.

Under an assignment rule δ_A , we consider the closure (see Section 1.3.1) of the set of points assigned to A_i , i.e.

$$V(A_i) = \text{Closure}[\{p \mid \delta_A(p, A_i) = 1, \quad p \in S\}]. \quad (3.0.3)$$

In terms of $V(p_i)$ we define

$$e(A_i, A_j) = V(A_i) \cap V(A_j), \quad i \neq j, \quad (3.0.4)$$

and

$$\mathcal{V}(A, \delta_A, S) = [V(A_1), \dots, V(A_n)]. \quad (3.0.5)$$

The mapping δ_A of equation (3.0.1) allows many assignment rules. Among them, we are concerned with a family of assignment rules that satisfy the following four conditions.

(i) Every point p in S is assigned to at least one element of A , i.e.

$$\sum_{i=1}^n \delta_A(p, A_i) \geq 1, \quad p \in S. \quad (3.0.6)$$

This condition guarantees that $V(A_1), \dots, V(A_n)$ are collectively exhaustive, i.e.

$$\bigcup_{i=1}^n V(A_i) = S. \quad (3.0.7)$$

Condition (i) implies that there exists at least one non-empty set $V(A_i)$ in \mathcal{V} , but if the whole space consists of only one $V(A_i)$, i.e. $\mathcal{V}(A, \delta_A, S) = V(A_i) = S$, such a \mathcal{V} does not constitute a tessellation. Thus δ_A is supposed to satisfy

(ii) There exists at least two non-empty sets, $V(A_i)$ and $V(A_j)$, in $\mathcal{V}(A, \delta_A, S)$.

Under Conditions (i) and (ii), it may happen that a non-empty set $V(A_i)$ may be degenerate, i.e. the Lebesgue measure of $V(A_i)$ may be zero (for example, the area of $V(p_i) \in \mathbb{R}^2$ is zero, i.e. $V(A_i)$ is given by a point or a line (Figure 3.0.1(a)); the volume of $V(A_i) \in \mathbb{R}^3$ is zero, i.e. $V(A_i)$ is given by a point, a line and a surface). It is arguable whether or not such a $V(A_i)$ constitutes a tessellation as a special case. In this text we mainly consider non-degenerate $V(A_i)$. To be explicit, δ_A is supposed to satisfy

(iii) For all $i \in I_n$, if $V(A_i)$ is non-empty and connected, the measure of $V(A_i)$ is positive; if $V(A_i)$ is non-empty and disconnected, the measure of every disconnected subset of $V(A_i)$ is positive.

In some cases, however, we relax this condition, and suppose that δ_A satisfies (iii').

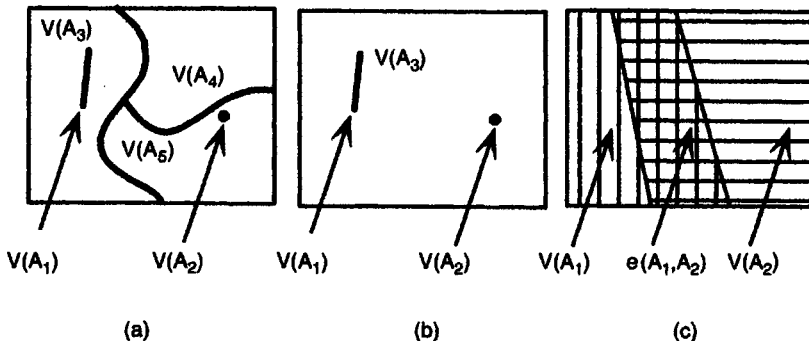


Figure 3.0.1 (a) Sets $V(A_i, A_j)$ that do not satisfy condition (iii); (b) a set $e(A_i, A_j)$ that does not satisfy condition (iv); (c) $e(A_i, A_j)$ that has a positive measure.

(iii') There exist at least two regions, $V(A_i)$ and $V(A_j)$, that satisfy condition (iii) (observe that panel (a) in Figure 3.0.1 satisfies condition (iii'), but panel (b) does not).

Generally $e(A_i, A_j)$ may be empty or not; if it is not empty, its measure may positive or zero (an actual example will be shown in Section 3.7). If the measure of $e(A_i, A_j)$ is positive (as in Figure 3.0.1(c)), then $V(A_i)$ and $V(A_j)$ share an overlapped region and \mathcal{V} does not form a tessellation. To exclude such an $e(A_i, A_j)$, we suppose

(iv) If $e(A_i, A_j)$ is not empty, $e(A_i, A_j)$ coincides with the intersection of the boundary of $V(A_i)$ and that of $V(A_j)$, i.e.

$$e(A_i, A_j) = \partial V(A_i) \cap \partial V(A_j) \text{ for } \partial V(A_i) \cap \partial V(A_j) \neq \emptyset, i \neq j. \quad (3.0.8)$$

From equations (3.0.4) and (3.0.8), the equation

$$[V(A_i) \cap V(A_j)] \setminus [\partial V(A_i) \cap \partial V(A_j)] = \emptyset, \quad i \neq j. \quad (3.0.9)$$

holds. This implies that $V(A_i)$ and $V(A_j)$ are exclusive except for boundaries. Therefore, under the assignment rule δ_A satisfying conditions (i), (ii), (iii) and (iv), the sets in $\mathcal{V}(A, \delta_A, S)$ are collectively exhaustive and mutually exclusive except for boundaries, that is, $\mathcal{V}(A, \delta_A, S)$ forms a tessellation of S . We designate this tessellation the *generalized Voronoi diagram* generated by the generator set A with the assignment rule δ_A in S , and $V(A_i)$ the *generalized Voronoi region* associated with A_i . We call the assignment rule δ_A that generates a generalized Voronoi diagram the *Voronoi generation assignment rule*, or briefly the *V-assignment rule*. As we remarked above, condition (iii) may be too strict in some cases. In those cases, we consider a weaker assignment rule than the above, i.e. δ_A is supposed to satisfy conditions (i), (ii), (iii') and (iv). When distinction is necessary, we call the resulting diagram obtained under these assumptions the *generalized weak Voronoi diagram*.

In the literature, the generalized Voronoi diagram sometimes is used to refer to more specific Voronoi diagrams than the above generalized Voronoi diagram. For example, the generalized Voronoi diagrams referred to by Drysdale and Lee (1978), Miles and Maillardet (1982) and Ó'Dúnlaing *et al.* (1986) are what we call the higher-order Voronoi diagram, the line Voronoi diagram and the area Voronoi diagram, respectively, in what follows. The generalized Voronoi diagram used in this text is much wider than their generalized Voronoi diagrams. In spirit, our generalization is similar to Leven and Sharir (1987), Klein (1988), Lavender *et al.* (1992), Melkemi and Chassery (1992), and Hamann and Tsai (1996).

The definition of the generalized Voronoi diagram by equation (3.0.3) is a generalization of Definition V2 of the ordinary Voronoi diagram. In Section 2.1 we defined the ordinary Voronoi diagram with half planes (Definition V3) as an alternative to Definition V2. When we examine the properties of Voronoi diagrams, we often find this definition more convenient and more operational. Motivated by this advantage, we next consider a generalization of Definition V3.

In the ordinary Voronoi diagram, the half plane $H(p_i, p_j)$ is alternatively called the *dominance region* of p_i over p_j (recall equation (2.1.6)). To emphasize this notion, we may write $\text{Dom}(p_i, p_j)$ for $H(p_i, p_j)$. We notice that the dominance region $\text{Dom}(p_i, p_j)$ is the same as $V(p_i)$ of $\mathcal{V}(P)$ generated by $P = \{p_i, p_j\}$ (two generator points). Keeping this property in mind, let us extend $\text{Dom}(p_i, p_j)$ to $\text{Dom}(A_i, A_j)$ for A in S .

For a pair $\{A_i, A_j\} \subset A = \{A_1, \dots, A_n\}$ ($2 \leq n < \infty$), we consider an assignment rule, $\delta_{\{A_i, A_j\}}$, given by

$$\delta_{\{A_i, A_j\}}(p, A) = \begin{cases} 1 & \text{if } p \text{ is assigned to } A_i \text{ in } \{A_i, A_j\}, \\ 0 & \text{otherwise} \end{cases} \quad (3.0.10)$$

(note that $\delta_{\{A_i, A_j\}}$ is a special case of δ_A , i.e. $A = \{A_i, A_j\}$). If $\delta_{\{A_i, A_j\}}$ satisfies conditions (i), (ii), (iii) and (iv), we can obtain the generalized Voronoi diagram $\mathcal{V}(\{A_i, A_j\}, \delta_{\{A_i, A_j\}}, S) = \{V(A_i), V(A_j)\}$. We call $V(A_i)$ the *dominance region* of A_i over A_j , and denote it by $\text{Dom}(A_i, A_j)$. Let

$$b(A_i, A_j) = \text{Dom}(A_i, A_j) \cap \text{Dom}(A_j, A_i). \quad (3.0.11)$$

We call this set the *bisector* between A_i and A_j . The sets $\text{Dom}(A_i, A_j)$ and $\text{Dom}(A_j, A_i)$ are collectively exhaustive and mutually exclusive except for the common boundary $b(A_i, A_j)$.

In terms of $\text{Dom}(A_i, A_j)$ we define

$$V(A_i) = \bigcap_{j \in I_n \setminus \{i\}} \text{Dom}(A_i, A_j), \quad (3.0.12)$$

and

$$\mathcal{V}(A, \text{Dom}, S) = \{V(A_1), \dots, V(A_n)\}. \quad (3.0.13)$$

In general, the resulting set $\mathcal{V}(A, \text{Dom}, S)$ may not coincide with $\mathcal{V}(A, \delta_A, S)$ of equation (3.0.5) under conditions (i), (ii), (iii), and (iv), because

$$\delta_A(p, A_i) = \prod_{j=1}^n \delta_{[A_i, A_j]}(p, A_i) \quad (3.0.14)$$

may not hold. For example, if δ_A is given by the assignment rule in which a point p is assigned to the k th nearest point ($3 \leq k \leq n$), then $\delta_{[A_i, A_j]}$ becomes meaningless, because there is no k th point in two generator points. When $\delta_{[A_i, A_j]}$ satisfies conditions (i), (ii), (iii), (iv) and equation (3.0.14) holds, we say that $\text{Dom}(A_i, A_j)$ and $b(A_i, A_j)$ are *well-behaving*.

In the above we defined the bisector $b(A_i, A_j)$ in terms of $\text{Dom}(A_i, A_j)$. Conversely, we may define $\text{Dom}(A_i, A_j)$ in terms of a bisector. Klein (1988, 1989) proposed this method in \mathbb{R}^2 (a similar method was also proposed by Hamann and Tsai, 1996). Let $b(A_i, A_j)$ be a simple (i.e. not self-intersecting) and continuous curve tending to infinity at both ends (or mathematically, $b(A_i, A_j)$ is homeomorphic to the open interval (0,1)). Klein (1989) calls $b(A_i, A_j)$ a *bisecting curve*. The bisecting curve $b(A_i, A_j)$ bisects \mathbb{R}^2 into two open unbounded domains, $D(A_i, A_j)$ and $D(A_j, A_i)$, each of which has $b(A_i, A_j)$ as its complete boundary. For convenience, $b(A_i, A_j)$ is to be assigned to one of $D(A_i, A_j)$ and $D(A_j, A_i)$. To this end, a total order is introduced in A , that is, for any pair $\{A_i, A_j\}$ in A , either $A_i < A_j$ or $A_j < A_i$ holds, but not both. Let

$$\text{Dom}^*(A_i, A_j) = \begin{cases} D(A_i, A_j) \cup b(A_i, A_j) & \text{if } A_i < A_j, \\ D(A_i, A_j) & \text{if } A_j < A_i. \end{cases} \quad (3.0.15)$$

In terms of $\text{Dom}^*(A_i, A_j)$, $V^*(A_i)$ is defined as

$$V^*(A_i) = \bigcap_{j \in I_n \setminus \{i\}} \text{Dom}^*(A_i, A_j). \quad (3.0.16)$$

Klein (1988) calls $\bigcup_{i=1}^n \partial V^*(A_i)$ an *abstract Voronoi diagram*. It should be noted that the abstract Voronoi diagram does not always result in a tessellation. The conditions that produce a tessellation are examined in depth by Klein (1989) and Mehlhorn *et al.* (1991). The reader who is interested in this derivation should consult those papers. Amato and Ramos (1996) specify the abstract Voronoi diagram by assuming that bisecting curves are simple curves consisting of a constant number of algebraic pieces of bounded degree, and call it an *algebraic planar Voronoi diagram*.

To construct a generalized Voronoi diagram in practice, we have to specify the assignment rule δ_A in terms of algebraic relations such as equation (3.0.2) or, more broadly, logical relations. In the literature, V-assignment rules are often specified in terms of a distance relation or a set of distance relations. One of the simplest and most frequently adopted V-assignment rules is that a point p is assigned to the closest generator(s), i.e.

$$\delta_A(p, A_i) = \begin{cases} 1 & \text{if } d(p, A_i) \leq d(p, A_j) \text{ for any } j \in I_n \setminus \{i\}, \\ 0 & \text{otherwise,} \end{cases} \quad (3.0.17)$$

where $d(p, A_i)$ is a ‘distance’ from a point p to an element A_i in A . Aurenhammer (1991) calls this rule the *nearest-neighbour rule*. The assignment rule of equation (3.0.2) is a special case of the assignment rule of

equation (3.0.17). When a generator is a point (i.e. $A_i = p_i$), the distance $d(p, p_i)$ usually implies a distance metric. The *distance metric* or *metric* for points in S is defined as a mapping, $d(p_i, p_j)$, of $S \times S$ into non-negative reals satisfying the following four axioms: for points $p_i, p_j, p_k \in P$, Axiom (i) $d(p_i, p_i) = 0$; Axiom (ii) $d(p_i, p_j) \leq d(p_i, p_k) + d(p_k, p_j)$; Axiom (iii) $d(p_i, p_j) = d(p_j, p_i)$; Axiom (iv) if $p_i \neq p_j$ then $d(p_i, p_j) > 0$. In the ordinary Voronoi diagram, the distance $d(p, A_i) = d(p, p_i)$ is given by the Euclidean distance, $d(p, p_i) = \|x - x_i\|$. Obviously the Euclidean distance is a distance metric. In general, however, the 'distance' $d(p, p_i)$ in the assignment rule of equation (3.0.17) for $A = P$ is not necessarily a distance metric. The distance metric $d(p_i, p_j)$ is defined for any point p_i in S and any point p_j in S , but when we define the assignment rule of equation (3.0.17) for $A = P$, it is sufficient to define $d(p, p_i)$ for any point p in S and any point p_i in P (not S). More generally, $d(p, A_i)$ in equation (3.0.17) is defined as a mapping of $S \times A$ (not $S \times S$) into \mathbb{R} . If the assignment rule δ_A of equation (3.0.17) with this mapping is a V-assignment rule, we call the mapping $d(p, A_i)$ a *Voronoi generation distance* or a *V-distance* (or just a *distance*) for short. The assignment rule of equation (3.0.17) with a V-distance produces a generalized Voronoi diagram, and we write it symbolically as $\mathcal{V}(A, d, S)$. The ordinary Voronoi diagram is written as $\mathcal{V}(P, \|x - x_i\|, \mathbb{R}^m)$.

An example of a non-metric V-distance is given by

$$d(p_i, p_j) = \|x - x_i\| - w, \quad w \neq 0. \quad (3.0.18)$$

This distance does not satisfy $d(p_i, p_i) = -w \neq 0$, i.e. Axiom (i) is not satisfied. We notice, however, that the set $\text{Dom}(p_i, p_j) = \{x \mid \|x - x_i\| - w \leq \|x - x_j\| - w\}$ produces exactly the same dominance region defined with the Euclidean distance; consequently, the distance given by equation (3.0.18) is a V-distance. This example shows that a V-distance allows many more forms than a distance metric.

We should note, however, that some of these are trivial. To show which generalizations are trivial, let F be a strictly increasing function of a V-distance, i.e. $F(d(p, A_i)) \leq F(d(p, A_j))$ if and only if $d(p, A_i) \leq d(p, A_j)$. It follows from this relation that $\text{Dom}(A_i, A_j)$ defined with $F(d(p, A_i))$ is the same as $\text{Dom}(A_i, A_j)$ defined with $d(p, A_i)$, and hence $\mathcal{V}(A, F(d), \mathbb{R}^m) = \mathcal{V}(A, d, \mathbb{R}^m)$. In this case we say that the distance $F(d(p, A_i))$ is *transformable* to the distance $d(p, A_i)$, and that the Voronoi diagram with $F(d(p, A_i))$ is a *trivial generalization* of the Voronoi diagram with $d(p, A_i)$.

In applications, we often use the exponential distance $d(p, p_i) = \exp(\|x - x_i\|)$, the logarithmic distance $d(p, p_i) = \log(\|x - x_i\|)$ and the power distance $d(p, p_i) = \|x - x_i\|^a$ ($a > 0$). Apparently, these distances are transformable to the Euclidean distance. Thus, Voronoi diagrams with these distances are trivial generalizations of the ordinary Voronoi diagram.

In the following sections we show several generalized Voronoi diagrams defined with V-distances that are not transformable to the Euclidean distance. Stated a little more specifically, we show $\mathcal{V}(P, d, \mathbb{R}^m)$, where $d(p, p_i)$ is the weighted distance (Section 3.1), the shortest-path distance, the visibility-

shortest-path distance (Section 3.4), the Minkowski metric, the Karlsruhe metric, the convex distance, the boat-on-a-river distance, and the Hausdorff distance (Section 3.7).

In the above generalized Voronoi diagrams, the generator set A is restricted to a set of points and the space S is restricted to the Cartesian space. Recalling the definition of equation (3.0.1), we can of course relax these restrictions. Regarding the generalizations with respect to a generator set A , we shall show $\mathcal{V}(A, d, \mathbb{R}^m)$, where the set A is a set of sets of points (Sections 3.2 and 3.3), a set of lines (Section 3.5), a set of areas (Section 3.6), and a set of moving points (Section 3.9). Regarding generalized Voronoi diagrams with respect to a space S , we show $\mathcal{V}(P, \text{the length of the shortest path on } S, S)$, where S is a sphere, a cylinder, a cone, a polyhedral surface (Section 3.7), and a network (Section 3.8).

As is noticed from the notation $\mathcal{V}(A, \delta_A, S)$, we can generalize the ordinary Voronoi diagram with respect to a generator set A , an assignment rule δ_A and a space S . This implies that the number of generalizations is potentially as many as the product of the numbers of generalizations of each factor. In the following sections, however, to avoid complicated exposition, we mainly deal with a single factor keeping the other factors the same as those of the ordinary Voronoi diagram. The reader may attempt to formulate a new generalized Voronoi diagram by combining those generalized Voronoi diagrams. We also note that the reader who wishes to understand generalized Voronoi diagrams from a more computational view point should consult Edelsbrunner and Seidel (1986), Klein (1989) and Mehlhorn *et al.* (1991); for an axiomatic approach, consult Stifter (1991).

3.1 WEIGHTED VORONOI DIAGRAMS

In the ordinary Voronoi diagram we implicitly assume that generator points are identical (except for their locations) or that each generator point has the same weight. In some practical applications, however, this assumption may not be appropriate. Rather, it is more appropriate to assume that generator points have different weights reflecting the variable property of the generator points; for example, the population size of a settlement, the number of functions in a shopping centre, the amount of emissions from a polluter, the size of an atom in a crystal structure, and so forth. In this section we show the family of generalized Voronoi diagrams that take these different weights into account in terms of the 'weighted distance'.

We consider a set of distinct points, $P = \{p_1, \dots, p_n\} \subset \mathbb{R}^m$ ($2 \leq n < \infty$) ($A = P, S = \mathbb{R}^m$) and assign a weight to each p_i which relates to some variable property of the phenomenon, such as those mentioned above. We represent this weight by a set of parameters $W_i = \{w_{i1}, \dots, w_{in_w}\}$ (if $n_w = 1$, we write w_i for W_i). With this weight we define a distance, $d_w(p, p_i)$, from p to p_i , called a *weighted distance*, which will be specified in the following

subsections. The dominance region of p_i over p_j with the weighted distance is written as

$$\text{Dom}(p_i, p_j) = \{p \mid d_w(p, p_i) \leq d_w(p, p_j)\}, \quad j \neq i. \quad (3.1.1)$$

Let

$$V(p_i) = \bigcap_{j \in I_p \setminus \{i\}} \text{Dom}(p_i, p_j), \quad (3.1.2)$$

and $\mathcal{V}(P, d_w, \mathbb{R}^m) = \mathcal{V}_w = \{V(p_1), \dots, V(p_n)\}$. If the dominance region given by equation (3.1.1) is well-behaving, \mathcal{V}_w gives a generalized Voronoi diagram. We call \mathcal{V}_w the *weighted Voronoi diagram* generated by P with the weight $\{W_1, \dots, W_n\}$, and the set $V(p_i)$ the *weighted Voronoi region* associated with p_i .

Since the weighted distance allows many functional forms, many weighted Voronoi diagrams are possible. In the following subsections we show four types of weighted Voronoi diagrams that often appear in the related literature. We mainly deal with \mathbb{R}^2 , but conceptually the extension to \mathbb{R}^m is straightforward.

3.1.1 The multiplicatively weighted Voronoi diagram

The first type of the weighted Voronoi diagram is characterized by the weighted distance given by

$$d_{mw}(p, p_i) = \frac{1}{w_i} \|x - x_i\|, \quad w_i > 0. \quad (3.1.3)$$

We call this distance the *multiplicatively weighted distance* or the *MW-distance* for short. After a few steps of calculation, we obtain the bisector as

$$b(p_i, p_j) = \left\{ x \mid \left\| x - \frac{w_i^2}{w_i^2 - w_j^2} x_j + \frac{w_j^2}{w_i^2 - w_j^2} x_i \right\| = \frac{w_i w_j}{w_i^2 - w_j^2} \|x_j - x_i\| \right\}, \quad (3.1.4)$$

$w_i \neq w_j, i \neq j$.

This bisector is the locus of a point p satisfying that the distance from p to the fixed point, $w_i^2 x_j / (w_i^2 - w_j^2) - w_j^2 x_i / (w_i^2 - w_j^2)$, is constant. Obviously, this locus is a circle in \mathbb{R}^2 . This circle passes through the interior and exterior division points (denoted by p_{ij1} and p_{ij2}) of $\overline{p_i p_j}$ with ratio w_i/w_j , and its diameter is given by $\overline{p_{ij1} p_{ij2}}$ (Figure 3.1.1). In classic geometry this circle is known as the *Apollonius circle*. Figure 3.1.1 shows the Apollonius circles representing the bisector defined with the MW-distance for several ratios $\alpha = w_i/w_j$ (where $w_i/w_j \geq 1$ is assumed without loss of generality). In the special case of $\alpha = 1$ ($w_i = w_j$), the bisector becomes a straight line, or a circle with an infinite radius.

In equation (3.1.3) we use $1/w_i$, but mathematically w_i is also acceptable. In equation (3.1.3) we adopt the former, because, as can be seen from Figure 3.1.1, the dominance region of p_i over p_j becomes larger as the weight w_i (or α) increases.

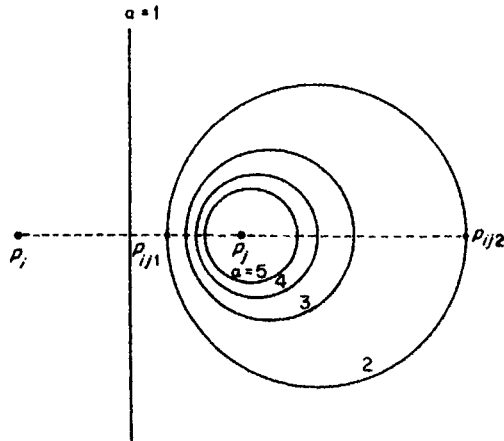


Figure 3.1.1 The bisectors with a multiplicatively weighted distance for several ratios $\alpha = w_i/w_j = 1, 2, 3, 4, 5$, or multiplicatively weighted Voronoi diagrams for $n = 2$.

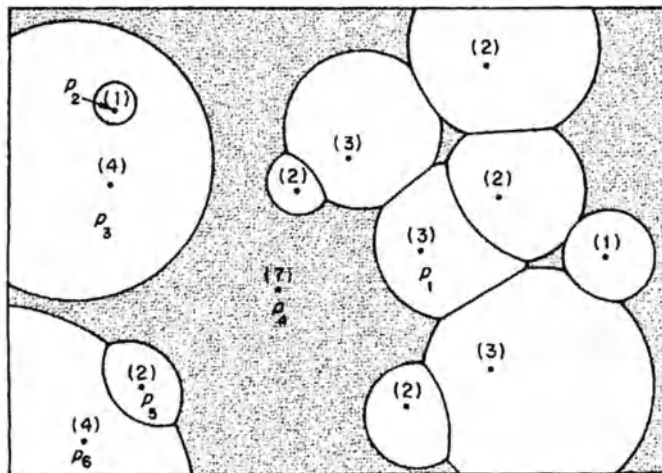


Figure 3.1.2 A multiplicatively weighted Voronoi diagram in \mathbb{R}^2 (the numbers in parentheses represent weights associated with the generators).

Since the Apollonius circle divides \mathbb{R}^2 into two disjoint regions, the bisector with the MW-distance is well-behaving. Thus the set $\mathcal{V}(P, d_{\text{mw}}, \mathbb{R}^2) = \mathcal{V}_{\text{mw}} = \{V(p_1), \dots, V(p_n)\}$ gives a generalized Voronoi diagram, where $V(p_i)$ is given by equation (3.1.2) with equation (3.1.3). We call \mathcal{V}_{mw} the *multiplicatively weighted Voronoi diagram* generated by P with the MW-distance or the *MW-Voronoi diagram* of P with $d_{\text{mw}}(p, p_i)$ (Aurenhammer and Edelsbrunner, 1984; Aurenhammer, 1988a). Ash and Bolker (1986) call \mathcal{V}_{mw} the *circular*

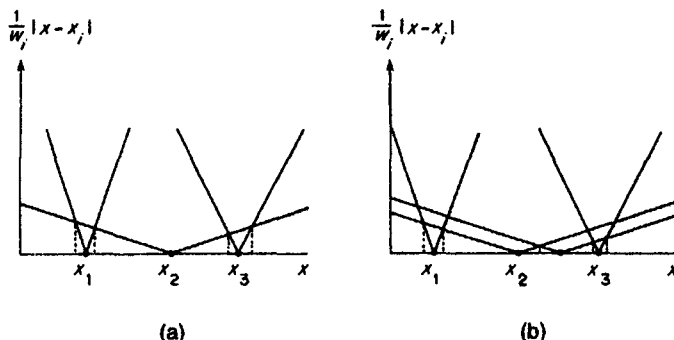


Figure 3.1.3 MW-Voronoi diagrams in \mathbb{R}^2 .

Dirichlet tessellation, and in crystallography, \mathcal{V}_{mw} is sometimes referred to as the *Apollonius model*. We call the set $V(p_i)$ the *multiplicatively weighted Voronoi region* associated with p_i , or briefly the *MW-Voronoi region* of p_i . Figures 3.1.1 and 3.1.2 show planar MW-Voronoi diagrams. The MW-Voronoi diagram reduces to the ordinary Voronoi diagram when w_i is the same constant for all $i \in I_n$. Thus the MW-Voronoi diagram includes the ordinary Voronoi diagram.

To observe the geometric properties of \mathcal{V}_{MW} , let us inspect Figure 3.1.2, where the numbers in the parentheses represent weights associated with the generators. First, $V(p_1)$ is not convex. Second, $V(p_2)$ is contained in $V(p_3)$ or $V(p_4)$, has a hole. Third, $V(p_4)$ indicated by the shaded area is not connected. Fourth, the weights of the MW-Voronoi regions adjacent to a convex MW-Voronoi region, say $V(p_5)$, are not smaller than the weight of the convex MW-Voronoi region ($w_5 < w_4, w_6$). We can understand this convexity property from the dominance region in Figure 3.1.1 and the fact that $V(p_i)$ is the intersection of the dominance regions. Fifth, from the same figure and the same equation, we notice that $V(p_i)$ is not empty because the weights are finite. To sum up, we have the following property.

Property MW1 An MW-Voronoi region is a non-empty set; it need not be convex, or connected; and it may have a hole(s). An MW-Voronoi region $V(p_i)$ is convex if and only if the weights of adjacent MW-Voronoi regions are not smaller than w_i .

To observe another geometric property, we depict a one-dimensional MW-Voronoi diagram in Figure 3.1.3 where the value of $|x - x_i|/w_i$ is shown on the vertical axis. Obviously, the slope of $|x - x_i|/w_i$ becomes flatter as the weight w_i increases. From Figure 3.1.3(a) we readily notice that the generator whose weight is the largest eventually dominates the places far from the locations of the generators; consequently, the MW-Voronoi region of the largest weight is infinite. When two or more generators have the same largest

weight as in Figure 3.1.3(b), however, the rightmost and leftmost Voronoi regions are infinite. Generalizing these properties in \mathbb{R}^2 , we obtain the following property.

Property MW2 Let $w_{\max} = \max_j \{w_j, j \in I_n\}$ and P_{\max} be the subset of P given by $P_{\max} = \{p_j \mid w_j = w_{\max}\}$. An MW-Voronoi region $V(p_i)$ is unbounded if and only if $p_i \in P_{\max}$ and p_i is on the boundary of $\text{CH}(P_{\max})$.

If the generator with the maximum weight is unique, we have only one unbounded MW-Voronoi region. An example is shown by the shaded MW-Voronoi region in Figure 3.1.2.

We observe in Figure 3.1.1 that the bisector $b(p_i, p_j)$ is either a circle or a straight line. In Figure 3.1.2 we find that the Voronoi edge shared by $V(p_4)$ and $V(p_6)$ is disconnected. From these findings we notice the following property with respect to edges.

Property MW3 Two MW-Voronoi regions may share disconnected edges. An edge is a circular arc if and only if the weights of the MW-Voronoi regions sharing the edge are different; an edge is a straight line if and only if the weights of the MW-Voronoi regions sharing the edge are the same.

3.1.2 The additively weighted Voronoi diagram

The second type of the weighted Voronoi diagram is characterized by the weighted distance

$$d_{aw}(p, p_i) = \|x - x_i\| - w_i. \quad (3.1.5)$$

We call this distance the *additively weighted distance* or briefly the *AW-distance*. The dominance region of p_i over p_j with the AW-distance is written as

$$\text{Dom}(p_i, p_j) = \{x \mid \|x - x_i\| - \|x - x_j\| \leq w_i - w_j\}, \quad i \neq j. \quad (3.1.6)$$

The shape of the dominance region varies according to the parameter values $\alpha = \|x_i - x_j\|$ and $\beta = w_i - w_j$ (where $w_i - w_j \geq 0$ is assumed without loss of generality). First, if $0 < \alpha < \beta$, then the generator p_i dominates the whole plane or the dominance region of p_j disappears, i.e. $\text{Dom}(p_i, p_j) = \mathbb{R}^2$ (which is not well-behaving). Such a case never happens for the dominance region defined with the MW-distance.

Second, if $\alpha = \beta$, then the dominance region is the whole plane except for the half line radiating from p_i in the direction from p_i to p_j (Figure 3.1.4, $\beta = 10$). This dominance region is also not well-behaving.

Third, if $\alpha > \beta$, then the boundary of the dominance region or the bisector is given by

$$b(p_i, p_j) = \{x \mid \|x - x_i\| - \|x - x_j\| = \beta\} \quad \text{if } \alpha > \beta, i \neq j. \quad (3.1.7)$$

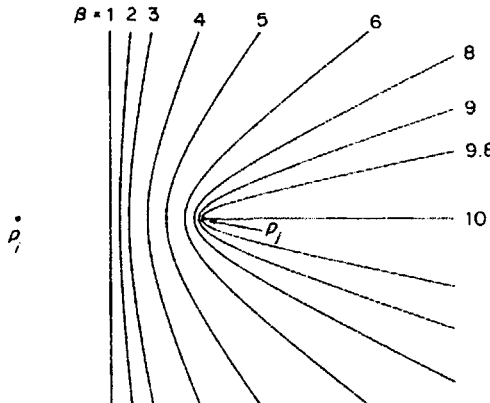


Figure 3.1.4 The bisectors with the additively weighted distance for parameter values $\alpha = \|x_i - x_j\| = 10$ and $\beta = w_i - w_j = 0, 1, 2, 3, 4, 5, 6, 8, 9, 9.8, 10$, or additively weighted Voronoi diagrams for $n = 2$.

This bisector is the locus of a point p satisfying that the difference between the distance from p to p_i and that from p to p_j is constant. This locus is known as a branch of the hyperbolic curve with foci p_i and p_j (Figure 3.1.4, $\beta = 1-9.8$). Note that if $\beta = 0$, the bisector becomes the straight line perpendicularly bisecting $\overline{p_i p_j}$ (Figure 3.1.4, $\beta = 0$). Figure 3.1.4 shows the bisectors for several parameter values.

In equation (3.1.5) we do not restrict the sign of w_i . Usually we assume a positive w_i because, as can be seen in Figure 3.1.4, the dominance region of p_i over p_j becomes larger as the weight w_i increases. Obviously, both $-w_i$ and $+w_i$ are acceptable in equation (3.1.5); in some applications (for example, in the market area analysis in Section 7.3), the latter form is used.

Since the bisector defined with the AD-distance is well-behaving for $\alpha > \beta$, we can obtain a generalized Voronoi diagram $\mathcal{V}(P, d_{aw}, \mathbb{R}^n) = \mathcal{V}_{aw} = \{V(p_1), \dots, V(p_n)\}$ for $\alpha > \beta$, where $V(p_i)$ is given by equations (3.1.1), (3.1.2) and (3.1.5). We call $V(p_i)$ the *additively weighted Voronoi region* associated with p_i , or briefly the *AW-Voronoi region* of p_i , and \mathcal{V}_{aw} the *additively weighted Voronoi diagram* generated by P with the AW-distance, or briefly the *AW-Voronoi diagram* of P with $d_{aw}(p, p_i)$ (Aurenhammer, 1988a). Ash and Bolker (1986) call \mathcal{V}_{aw} the *hyperbolic Dirichlet tessellation*. Figures 3.1.4 and 3.1.5 show planar AW-Voronoi diagrams.

The AW-Voronoi diagram reduces to the ordinary Voronoi diagram when w_i is the same constant for all $i \in I_n$ and so \mathcal{V}_{aw} includes the ordinary Voronoi diagram. Like the dual relationship between the ordinary Voronoi diagram and the ordinary Delaunay triangulation, we may define the (*additively*) *weighted Delaunay diagram* as the dual of the AW-Voronoi diagram, but note that a few modifications are necessary (Mirzaian, 1993). Having noticed this diagram, we might consider the possibility of the multiplicatively weighted

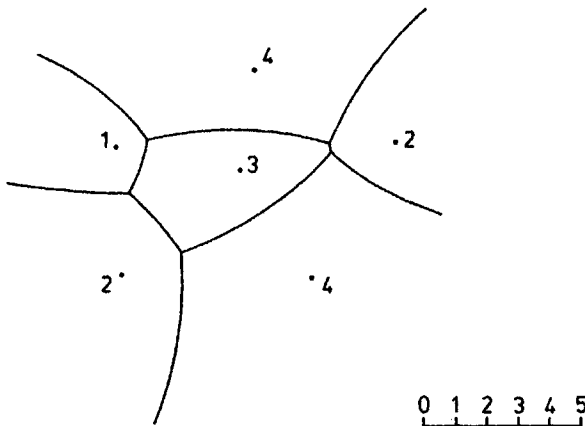


Figure 3.1.5 An additively weighted Voronoi diagram (the numbers indicate weights, w_i).

Delaunay diagram. Figure 3.1.2 shows that such a diagram is difficult to define because the line segments connecting generators whose AW-Voronoi regions share the common boundaries may cross.

The AW-Voronoi diagram is often discussed in conjunction with a special case of the (general) Voronoi growth model (see Section 7.2 for details), which is called the *Johnson-Mehl model* (Section 5.8). Suppose that a finite number of points or disks with zero radius are placed on a plane. Each disk grows with the same constant growth rate keeping its centre at the initial point but the growth of each disk starts at a different time. In the early stages disks do not overlap, but after a certain time a disk may touch another. The growth of a disk ceases whenever two or more disks impinge. Eventually, every disk is deformed into a certain shape in the region, which is an AW-Voronoi region. We might consider that in the above process, if the same constant growth rate is replaced with a different growth rate and starting at a different time is replaced with one starting at the same time, then the process eventually leads to the MW-Voronoi diagram. This is not true because the MW-distance may not be applicable due to obstacles made by grown disks. Considering this fact, Schaudt and Drysdale (1991) modify the growth process in that the distance between points is replaced by the shortest path distance. We may call the resulting tessellation the *shortest-path multiplicatively weighted Voronoi diagram* (see Section 3.4).

The properties of the AW-Voronoi diagram are different from those of the MW-Voronoi diagram. In particular, we first note the following property.

Property AW1 The set $V(p_i)$ is empty if and only if

$$\min \{ \|x - x_j\| - w_j, j \in I_n \} < -w_i. \quad (3.1.8)$$

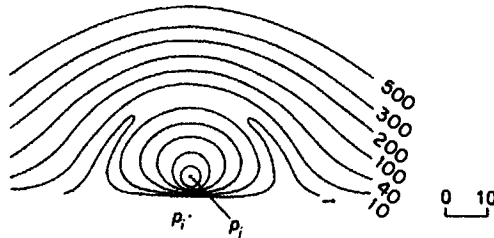


Figure 3.1.6 The bisectors with the generalized AW-distance given by $\phi(\|x - x_i\|) = (\|x - x_i\| - 3)^3 - w_i$, $\alpha = w_i - w_j = 1, 10, 40, 100, 200, 300, 500$, or additively weighted Voronoi diagrams with the generalized AW-distance for $n = 2$.

The set $V(p_i)$ is a half line or a line segment if and only if

$$\min_{j \neq i} \{\|x - x_j\| - w_j, j \in I_n\} = -w_i. \quad (3.1.9)$$

The set $V(p_i)$ has a positive area if and only if

$$\min_{j \neq i} \{\|x - x_j\| - w_j, j \in I_n\} > -w_i. \quad (3.1.10)$$

The properties of equations (3.1.8) and (3.1.9) contrast with those of the ordinary Voronoi diagram (Property V1) and the MW-Voronoi diagram (Property MW1). In those Voronoi diagrams a Voronoi region is neither empty nor degenerates into a line.

From equation (3.1.7) we understand the following property.

Property AW2 An edge of an AW-Voronoi region is either a hyperbolic arc or a straight line segment.

As a consequence of Property AW2, we notice the following property.

Property AW3 If at least one weight, w_i , is different from the others and relation (3.1.10) holds, then there exists at least one non-convex AW-Voronoi region. Every non-convex AW-Voronoi region is star-shaped with respect to its generator.

Besides these properties, Ash and Bolker (1986) show the properties related to the generator recognition problem (recall Problem P5) of the AW-Voronoi diagram (as well as the MW-Voronoi diagram).

We may generalize the AW-Voronoi diagram slightly by replacing equation (3.1.5) with

$$d_{g,aw}(p, p_i) = \phi(\|x - x_i\|) - w_i, \quad (3.1.11)$$

where ϕ is usually a strictly increasing function (Ash and Bolker, 1986; Hanjoul *et al.*, 1989). We call this distance the *generalized AW-distance*. The generalized AW-distance is general in the sense that it includes not only the

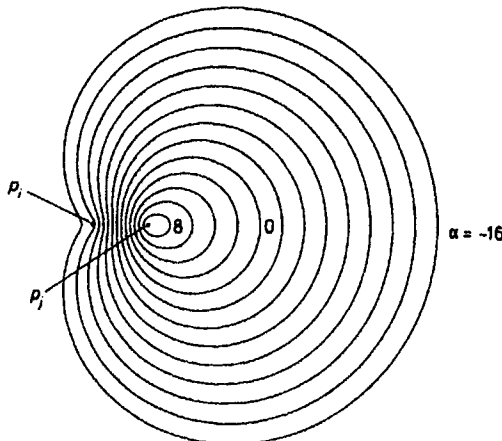


Figure 3.1.7 The bisectors with the compoundly weighted distance for several parameter values, $w_{i1}/w_{j1} = 1.5$, $\alpha = w_{i1}(w_{i2} - w_{j2}) = -16, \dots, -2, 0, 2, \dots, 8$ or compoundly weighted Voronoi diagrams for $n = 2$.

AW-Euclidean distance but also the MW-distance (the former is obtained by setting $\phi(t) = t$ and the latter is obtained by setting $\phi(t) = \log t$). Figure 3.1.6 shows planar AW-Voronoi diagrams with generalized AW-distances for $n = 2$.

3.1.3 Compoundsly weighted Voronoi diagram

The third type of weighted Voronoi diagram is obtained by compounding the MW-distance and the AW-distance, i.e.

$$d_{cw}(p, p_i) = \frac{1}{w_{i1}} \|x - x_i\| - w_{i2}, \quad w_{i1} > 0, \quad (3.1.12)$$

which we call the *compoundsly weighted distance* or simply the *CW-distance*. The CW-distance becomes the AW-distance if $w_{i1} = 1, i \in I_n$; it becomes the MW-distance if $w_{i2} = 0, i \in I_n$. The bisector with the CW-distance is given by the fourth-order polynomial function, and its shape is fairly complex, as is shown in Figure 3.1.7.

Although the shape of the bisector is fairly complex, it is easy to see that the bisector is well-behaving for $\|x_i - x_j\| > w_{i2}/w_{i1} - w_{j2}/w_{j1}$ (recall $\alpha > \beta$ in Section 3.1.2). Thus we can obtain a generalized Voronoi diagram, $\mathcal{V}(P, d_{cw}, \mathbb{R}^m) = \mathcal{V}_{cw} = \{V(p_i), \dots, V(p_n)\}$, where $V(p_i)$ is given by equations (3.1.1), (3.1.2) and (3.1.12). We call this generalized Voronoi diagram the *compoundsly weighted Voronoi diagram* generated by P , or the *CW-Voronoi diagram* of P . We call the set $V(p_i)$ the *compoundsly weighted Voronoi region* associated with p_i , or briefly the *CW-Voronoi region* of p_i . Figure 3.1.8 shows planar CW-Voronoi diagrams for different parameter values. The CW-Voronoi diagram reduces to the ordinary Voronoi diagram when

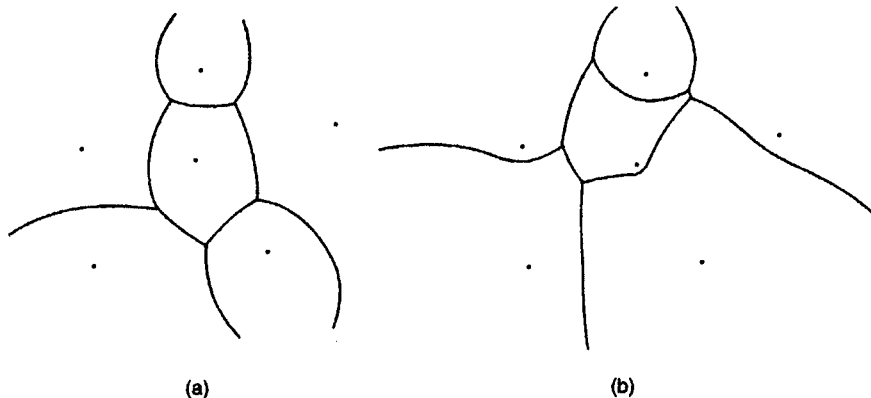


Figure 3.1.8 Compoundly weighted Voronoi diagrams in \mathbb{R}^2 .

$w_{i1} = 1, w_{i2} = 0, i \in I_n$. Thus, the CW-Voronoi diagram can be regarded as a generalization of the ordinary Voronoi diagram.

Since the CW-Voronoi diagram becomes the MW-Voronoi diagram if $w_{i1} = 0$ for $i \in I_n$ and it becomes the AW-Voronoi diagram if $w_{i2} = 1$ for $i \in I_n$, the CW-Voronoi diagram shows the properties of the AW-Voronoi diagram and the MW-Voronoi diagram for these specific cases. In other cases its proper properties appear. We show one example.

Property CW1 An edge of a CW-Voronoi region is part of the fourth-order polynomial curve (a proper property), a hyperbolic arc (Property AW2), a circular arc (Property MW3) or a straight line (Properties AW2 and MW3).

3.1.4 The power diagram

The fourth type of the weighted Voronoi diagram is characterized by the weighted distance

$$d_{pw}(p, p_i; w_i) = \|x - x_i\|^2 - w_i, \quad (3.1.13)$$

which we call the *additively weighted power distance* or, following Aurenhammer (1988a), the *power distance*. For simplicity, we usually employ the latter term, but the power distance should be distinguished from the ordinary power distance, $\|x - x_i\|^2$. Recalling the MW-distance, we might consider the multiplicatively weighted power distance $\|x - x_i\|^2/w_j$ (where $w_j > 0$). This distance, however, is transformable to the MW-distance, and hence it is a trivial extension.

The bisector with the MW-distance is, after a few steps of calculation, written as

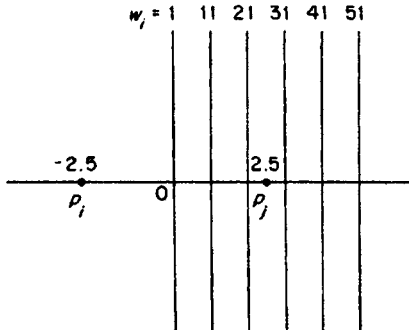


Figure 3.1.9 The bisectors with the additively weighted power distance for several parameter values, $\mathbf{x}^T = (-2.5, 0.0)$, $\mathbf{x}^T = (2.5, 0.0)$, $w_j = 1$, $w_i = 1, 11, 21, 31, 41$, or a power diagram for $n = 2$.

$$b(p_i, p_j) = \{ \mathbf{x} \mid (\mathbf{x}_j - \mathbf{x}_i)^T \mathbf{x} = \frac{1}{2} (||\mathbf{x}_j||^2 - ||\mathbf{x}_i||^2 + w_i - w_j) \}, \quad j \neq i. \quad (3.1.14)$$

We notice from this equation that the bisector is the straight line perpendicular to $\overline{p_i p_j}$ passing through the point \mathbf{x}_{ij}^* given by

$$\mathbf{x}_{ij}^* = \frac{||\mathbf{x}_j||^2 - ||\mathbf{x}_i||^2 + w_i - w_j}{2||\mathbf{x}_j - \mathbf{x}_i||^2} (\mathbf{x}_j - \mathbf{x}_i). \quad (3.1.15)$$

As w_i increases, the dominance region becomes larger. Because of this property, we usually use a positive weight for w_i . Mathematically, however, we may replace $-w_i$ with $+w_i$ in equation (3.1.13). Figure 3.1.9 shows $\text{Dom}(p_i, p_j)$ for several parameter values. As is seen in this figure, the generator p_i may not be in $\text{Dom}(p_i, p_j)$, for example, $w_i = 31, 41, 51$.

Since the line of equation (3.1.15) splits \mathbb{R}^2 into two disjoint half planes, the bisector of equation (3.1.14) is well-behaving. Thus, equation (3.1.2) with (3.1.1) and (3.1.13) gives a generalized Voronoi diagram $\mathcal{V}(P, d_{pw}, \mathbb{R}^m) = \mathcal{V}_{pw} = \{V(p_1), \dots, V(p_n)\}$. We call this generalized Voronoi diagram the *additively weighted power diagram* generated by P or simply the *power diagram* of P (Aurenhammer, 1988), and call the set $V(p_i)$ the *power Voronoi polygon* associated with p_i . As we shall show in Section 3.6, the power diagram can be regarded as a Voronoi diagram of circles or a Voronoi diagram with Laguerre geometry (called the Laguerre Voronoi diagram). Also, as we shall discuss in the next subsection, the power diagram can be regarded as a sectional Voronoi diagram. The power diagrams in \mathbb{R}^3 and \mathbb{R}^4 are investigated by Chan *et al.* (1995) and Amato and Ramos (1996), respectively.

We find in Figure 3.1.10 that some power polygons are unbounded. Imai *et al.* (1985) derive the conditions for a bounded or an unbounded region as follows.

Property PW1 (i) The set $V(p_i)$ defined by equations (3.1.1), (3.1.2) and (3.1.13) is non-empty and unbounded if p_i is a vertex of $\text{CH}(P)$.

(ii) The set $V(p_i)$ is either unbounded or empty if p_i is on the boundary of $\text{CH}(P)$ except the vertices (at least three generators are on a boundary line segment of $\text{CH}(P)$).

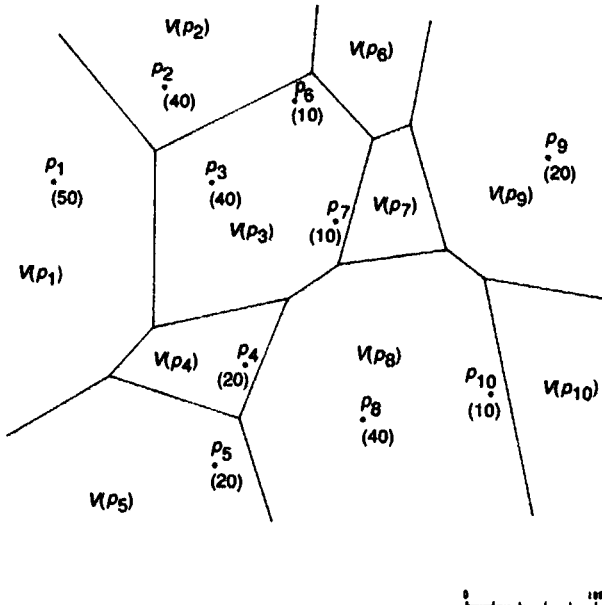


Figure 3.1.10 A(n) (additively weighted) power diagram.

(iii) The set $V(p_i)$ is either bounded or empty if p_i is an interior point of $\text{CH}(P)$.

The proof is provided by Imai *et al.* (1985, Lemma 3).

From the fact that the dominance region is a half plane and that $V(p_i)$ is the intersection of half planes, we note the following property.

Property PW2 If the set $V(p_i)$ is not empty, it is a convex polygon.

In Figure 3.1.9, we observe that the dominance region $\text{Dom}(p_i, p_j)$ with the parameter values $w_i = 31, 41, 51$ includes not only p_i but also p_j . From this property, we notice the following property.

Property PW3 The generator of $V(p_i)$ may not be in $V(p_i)$.

Similar to how we obtained the Delaunay triangulation as the dual of the ordinary Voronoi diagram, we can define a Delaunay diagram of the power diagram by connecting two generator points by a line segment if and only if their regions are adjacent. We refer to it as the *Delaunay power diagram*.

The Delaunay power diagram may be defined in the context of a more general tessellation. For a set $P = \{(x_1, y_1), \dots, (x_n, y_n)\}$ of points in \mathbb{R}^2 , we construct a set $P^* = \{(x_1, y_1, a_1), \dots, (x_n, y_n, a_n)\}$ of points in \mathbb{R}^3 with a set $A = \{a_1, \dots, a_n\}$ in such a way that every lower facet of $\text{CH}(P^*)$ (see the

proof of Property D7) is a triangle (a simplex). The orthographic projection of the lower facets of $\text{CH}(P^*)$ onto the x - y plane produces a triangulation of the convex hull of P . We call this resulting triangulation the *regular triangulation* spanning P induced by A (Edelsbrunner and Shah, 1996; Masada *et al.*, 1996a). We can easily extend the definition of the regular triangulation in \mathbb{R}^2 to that in \mathbb{R}^m (Edelsbrunner, 1986; Schlottmann, 1993).

Suppose that a_i is given by $a_i = x_i^2 + y_i^2 - w_i$. Then we notice that the Delaunay power diagram is a regular triangulation. More strongly, we have the following property.

Property PW4 A triangulation, \mathcal{T} , spanning P is a regular triangulation if and only if there are weights w_1, \dots, w_n such that \mathcal{T} is the Delaunay power diagram for P with these weights.

Since the Delaunay power diagram is a generalization of the Delaunay triangulation, it shares many properties with the Delaunay triangulation, some of which are shown below (Aurenhammer, 1991).

Property PW5 An edge of the regular triangulation spanning P is perpendicular to the corresponding edge of the power diagram generated by P .

3.1.5 The sectional Voronoi diagram

In the literature the sectional Voronoi diagram to be shown here is usually not subsumed under the family of weighted Voronoi diagrams. We refer to it here, however, because it can be regarded as a weighted Voronoi diagram.

Let $\mathcal{V} = \{V(p_1), \dots, V(p_n)\}$ be the three-dimensional ordinary Voronoi diagram generated by P , and K be a plane in \mathbb{R}^3 . Let J_s be the set of indices of i that satisfy $V(p_i) \cap K \neq \emptyset$,

$$V_{\text{sec}}(p'_i) = V(p_i) \cap K \neq \emptyset, \quad (3.1.16)$$

and $\mathcal{V}_{\text{sec}} = \{V_{\text{sec}}(p'_1), \dots, V_{\text{sec}}(p'_n)\}$, where p'_i is the orthogonal projection of p_i onto the plane K . The set $V_{\text{sec}}(p_i)$ is the intersection of polyhedron $V(p_i)$ with the plane K . We call $V_{\text{sec}}(p'_i)$ a *sectional Voronoi polygon*. Obviously, the collection of resulting sectional Voronoi polygons covers the plane K and they are not overlapping, except at the boundaries. Thus the set \mathcal{V}_{sec} forms a tessellation. We call this tessellation the *sectional Voronoi diagram* obtained as the intersection of \mathcal{V} with the plane K (Ash and Bolker, 1986; Aurenhammer, 1988a; Imai *et al.*, 1985; Sibson, 1980a). An example is shown in Figure 3.1.11, where generators are placed at $(1, 0, 1)$, $(-1, 0, 0)$ and $(0, -1, 0)$ in \mathbb{R}^3 . The ordinary Voronoi diagram of those generator points are indicated by the heavy lines (to make visual perception easy, the intersection of \mathcal{V} with the rectangle parallelopipedon is shown). The intersection of \mathcal{V} with the x_1 - x_2 plane (the plane K) is shown by the diagram on the x_1 - x_2 plane. We might expect that the resulting diagram is an ordinary Voronoi diagram, but this expectation is false. Chiu *et al.* (1996) prove that a sectional

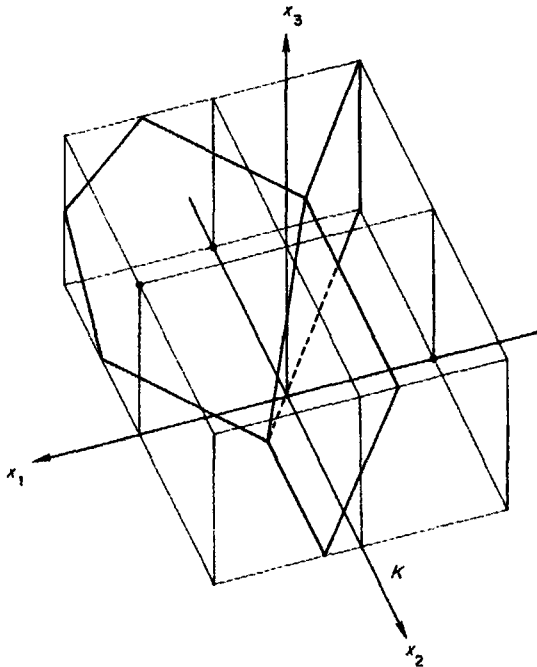


Figure 3.1.11 A sectional Voronoi diagram obtained from the three-dimensional ordinary Voronoi diagram with the x_1-x_2 plane, $n = 3$.

Voronoi diagram for points generated by the Poisson point process (see the sectional Poisson Voronoi diagrams in Section 5.7) is not the ordinary Voronoi diagram.

The sectional Voronoi diagram is related to the power diagram. To show this relation, suppose, for simplicity, that the plane K is the x_1-x_2 plane (we can place the plane K on the x_1-x_2 plane by rotating the plane K with P). Then $V_{\text{sec}}(p'_i)$ is written as

$$\begin{aligned} V_{\text{sec}}((x_i, x_n)) &= \left\{ (x_1, x_2) \mid \sqrt{(x_1 - x_{i1})^2 + (x_2 - x_{i2})^2 + x_{i3}^2} \right. \\ &\leq \sqrt{(x_1 - x_{j1})^2 + (x_2 - x_{j2})^2 + x_{j3}^2}, j \neq i, j \in I_n \}. \end{aligned} \quad (3.1.17)$$

If we write $\|x - x_i\|^2$ for $(x_1 - x_{i1})^2 + (x_2 - x_{i2})^2$, then equation (3.1.17) is written as

$$V_{\text{sec}}(x_i) = \{x \mid \|x - x_i\|^2 + x_{i3}^2 \leq \|x - x_i\|^2 + x_{j3}^2, j \neq i, j \in J_s\}. \quad (3.1.18)$$

Recalling the power distance of equation (3.1.13), we notice that this sectional Voronoi diagram is indeed the power diagram with the weight $\{-x_{i3}^2, j \in J_s\}$.

Extending the concept of the sectional Voronoi diagram in \mathbb{R}^3 , we can define a sectional Voronoi diagram of an m -dimensional ordinary Voronoi

diagram with a hyperplane in \mathbb{R}^m . Modifying it, we may consider a k -dimensional polytope Q defined by hyperplanes and a k -flat in \mathbb{R}^m , $k \leq m$, and define a Voronoi diagram by the collection of all non-empty intersections of the Voronoi polytopes with Q . Chan *et al.* (1995) call this diagram the *Voronoi diagram clipped to Q* or a *clipped Voronoi diagram*. Furthermore, we can define a *generalized sectional Voronoi diagram* by the intersection between a hyperplane in \mathbb{R}^m and a generalized Voronoi diagram in \mathbb{R}^m . A notable one is the *sectional multiplicatively weighted Voronoi diagram* defined by the intersection of a plane and the three-dimensional multiplicatively weighted Voronoi diagram (Moukarzel, 1995). Similarly we can define the *sectional additively weighted Voronoi diagram*, which is alternatively called the *sectional Johnson–Mehl Voronoi diagram* (Møller, 1992).

3.1.6 Applications

The family of weighted Voronoi diagrams is often adopted in market area analysis to determine the market areas of firms or stores, where the weights w_{i1} and w_{i2} in equation (3.1.12) correspond to a transportation cost and a mill price of goods or products, respectively. According to Shieh (1985), the earliest study dates back to Rau (1841). Launhardt (1882) and Fetter (1924) are also forerunners, followed by Tuominen (1949), Hyson and Hyson (1950), Gambini *et al.* (1967), Beckmann (1971), Boots (1980), Von Hohenbalken and West (1984), Aurenhammer (1987a), Hanjoul and Thisse (1987), Sakamoto and Takagi (1987), Hanjoul *et al.* (1989), O’Kelly and Miller (1989) and many others.

Gambini *et al.* (1967), Huff and Jenks (1968) and Huff (1973) studied national urban systems with the MW-Voronoi diagram. Huff and Lutz (1979) also used the same diagram to discuss a geographical delivery system for serving public interest in the Republic of Ireland. Illeris (1967) adopted the same diagram to determine functional regions of urban centres in Denmark; Hubbard (1970) and Wood (1974) carried out similar studies in Jamaica and Kenya, respectively. Cox and Agnew (1974) used the MW-Voronoi diagram to produce a partition of all Ireland into theoretical counties, which are compared with the actual counties (note that their map contains an error pointed by Weaire and Rivier, 1984). Archaeologists have used the MW-Voronoi diagram to define territories for various sites. Their work in this regard is reviewed by Hodder and Orton (1976, pp. 187–95). The most extensive of such studies is that of Hogg (1971) who used the MW-Voronoi diagram as a surrogate for territories of Neolithic hillforts south of the River Thames in England. Melachrinoudis and Smith (1995) uses the MW-Voronoi diagram to find the location that achieves the maximum distance to the nearest facility (imagine obnoxious facilities) where the facilities are characterized by their weights (Melachrinoudis and Cullinane, 1986). This problem is an extension of the largest empty circle problem in the ordinary Voronoi diagram discussed in Section 2.3. Billia *et al.* (1991) statistically analyze defects and disorder in two-dimensional cellular arrays in the

directional solidification of binary alloys using the MW-Voronoi diagram. Moukarzel (1993) examines the equilibrium state of foams represented by the MW-Voronoi diagram. Boots (1994) illustrates how the cross-product form of most spatial autocorrelation models, such as those of Geary and Moran, is equivalent to the form of the MW-Voronoi diagram and show a method of visualizing spatial autocorrelation in point data. Gerstein *et al.* (1995) models a cell structure of globular proteins in terms of the MW-Voronoi diagram. Billia *et al.* (1991) investigate the disorder of cellular arrays where the weight reflects the diameter of a cell. Siersma (1998) examines the Voronoi surface of the MW-Voronoi diagram (recall Section 2.1) in terms of the Morse theory. Inaba *et al.* (1994) apply the MW- and AW-Voronoi diagrams to a variance-based clustering.

The AW-Voronoi diagram is a special case of the Johnson–Mehl model (Johnson and Mehl, 1939; see Sections 5.8 and 7.2), which provides many diverse applications, such as crystal growth, cell structures of plants and foams made out of soap bubbles (Matzke and Nestler, 1946; Smith, 1954; Williams, 1968). Lesley (1976), Vaughan and Cousins (1977) and Wirasinghe and Ghoneim (1981) represented service areas of bus stops in terms of the AW-Voronoi diagram. Tao and Huang (1996) and Hai and Huang (1996) apply the AW-Voronoi diagram to warping, widely used in image distortion correction, special animation effects and human expression synthesis.

The sectional Voronoi diagram, which is regarded as the power diagram, may be utilized in stereology, which attempts to recover three-dimensional information from one- or two-dimensional samples. In the same fashion, van de Weygaert (1994) shows how to infer information on the actual three-dimensional galaxy distribution from a survey confined to two dimensions (i.e. slices), or one dimension (i.e. pencil beams). Moukarzel (1995) shows that equilibrium configurations of two-dimensional foams are well represented by the sectional multiplicatively weighted Voronoi diagram.

The power diagram is also used in modelling the crystal structure of organic compounds (Fischer and Koch, 1979), grain growth in a two-dimensional polycrystal (Telly *et al.*, 1992), metallic glass (Gellatly and Finney, 1982a), globular proteins (Gellatly and Finney, 1982b), and muscle fibres (Venema, 1991) (see also the applications in Sections 3.5.5 and 7.1). Aurenhammer (1987) refers to the power diagram in conjunction with the problem called the *illumination of balls* (Linhart, 1981): the union of n balls in a space can be illuminated by the vertices of the power diagram for the corresponding spheres. The power diagram is also applied to the grain boundary structure of polycrystalline materials (Ogawa *et al.*, 1996b).

3.2 HIGHER-ORDER VORONOI DIAGRAMS

In the ordinary Voronoi diagram, a generator is a point p_i , or a generator set is a set $P = \{p_1, \dots, p_n\}$ of points. In this section, which extends a point to a set of points, we consider the family of generalized Voronoi diagrams

generated by a set of all possible subsets consisting of k points out of P , i.e. $A^{(k)}(P) = \{\{p_{11}, \dots, p_{1k}\}, \dots, \{p_{l1}, \dots, p_{lk}\}\}$, where $p_{ij} \in P$ and $l = n!/(k!(n-k)!)$. We shall call this family the ‘higher-order’ Voronoi diagram. Here the ‘order’ means the number of points constituting a generator and ‘higher’ means more than one point. Note that ‘higher’ does not refer to the dimension of a space. In this section we deal with only \mathbb{R}^2 , but conceptually the extension from \mathbb{R}^2 to \mathbb{R}^m is straightforward.

The higher-order Voronoi diagram has been studied by many researchers, including Miles (1970a), Shamos and Hoey (1975), Shamos (1978), Bentley and Maurer (1979), Sibson (1980a), Dehne (1982), Lee (1982b), Miles and Maillardet (1982), Edelsbrunner (1986), Chazelle *et al.* (1986), Chazelle and Edelsbrunner (1987), Aurenhammer (1990b), Aurenhammer and Schwarzkopf (1991) and Agarwal *et al.* (1994). This section is based upon the results obtained by those researchers.

3.2.1 The order- k Voronoi diagram

Suppose, as is illustrated in Figure 3.2.1, that a set of distinct points (the filled circles) is placed in the Euclidean plane. We consider the Euclidean distances from a location, say the location indicated by the unfilled circle in the figure, to all points in the point set. As can be seen from the dashed lines in Figure 3.2.1, the first and the second nearest points from the location are p_1 and p_4 . In this case we assign the location to the set $\{p_1, p_4\}$. In general, if a set of the first and the second nearest points from a location is $\{p_i, p_j\}$, we assign the location to $\{p_i, p_j\}$. If the set is not only $\{p_i, p_j\}$ but also other sets of two points, we assign the location to those sets. Note that we are not

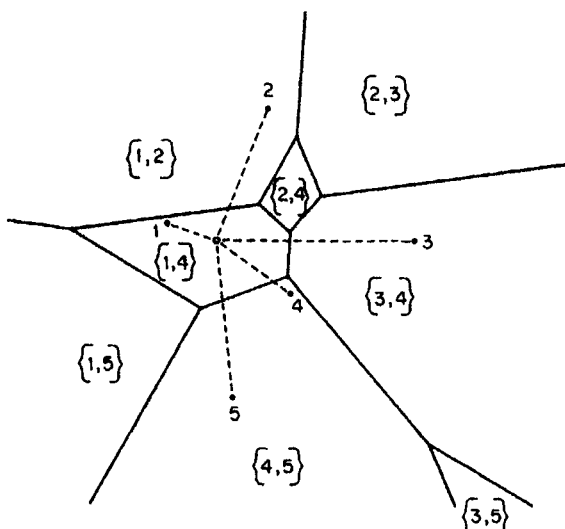


Figure 3.2.1 An order-2 Voronoi diagram ($n = 5$).

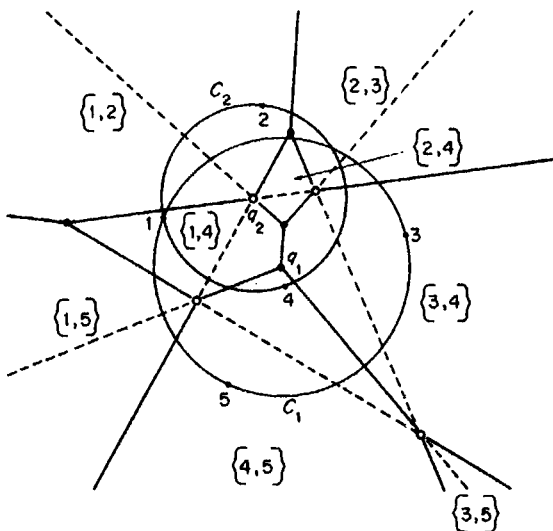


Figure 3.2.2 The ordinary Voronoi diagram (the dashed lines) and the order-2 Voronoi diagram (the solid lines) generated by the same set of generator points ($n = 5$; the locations of generator points are the same as those in Figure 3.2.1).

concerned with which point is the first nearest point in $\{p_i, p_j\}$; p_i may be the first or the second nearest point. Following this assignment rule, we assign all locations in the plane to at least one of the sets of two points. As a result, locations assigned to $\{p_i, p_j\}$ form a region, which we call the *order-2 Voronoi polygon* associated with $\{p_i, p_j\}$. A collection of the resulting order-2 Voronoi polygons is depicted in Figure 3.2.1, where the region with symbol $\{i, j\}$ indicates the order-2 Voronoi polygon associated with $\{p_i, p_j\}$ and i associated with a filled circle indicates the point p_i . This collection forms a tessellation, which we call the *order-2 Voronoi diagram* generated by the set of points.

Having understood the order-2 Voronoi diagram, the reader may be curious to know what the configurational relationship is between this diagram and the ordinary Voronoi diagram. Figure 3.2.2 shows this relationship. The dashed lines indicate the ordinary Voronoi diagram and the solid lines indicate the order-2 Voronoi diagram generated by the same generator set. We notice from this figure that the two Voronoi diagrams do not share edges but share some vertices (the unfilled circles). These vertices have an interesting property. To show it precisely, we first give the mathematical definition of the order-2 Voronoi diagram.

Let $P = \{p_1, \dots, p_n\}$ be a set of distinct points in \mathbb{R}^2 , where $2 \leq n < \infty$; $A^{(2)}(P) = \{P_1^{(2)}, \dots, P_i^{(2)}, \dots, P_l^{(2)}\}$, where $P_i^{(2)} = \{p_{i1}, p_{i2}\}$, $p_{i1}, p_{i2} \in P$, and $l = n!/(2!(n - 2)!)$ (the number of all possible subsets consisting of two points out of P); and $d(p, p_{ij})$ be the Euclidean distance from p to p_{ij} . The points p_{i1} and p_{i2} are the first and the second nearest points from p if and only if

the distances from p to p_{i1} and p_{i2} are both shorter than or equal to the distances from p to the other points (i.e. points in $P \setminus \{p_{i1}, p_{i2}\}$). Thus the set, $V(P_i^{(2)})$, of points assigned to $\{p_{i1}, p_{i2}\}$ is written as

$$\begin{aligned} V(P_i^{(2)}) &= \{p \mid d(p, p_{i1}) \leq d(p, p_j) \\ &\quad \text{and } d(p, p_{i2}) \leq d(p, p_j), \text{ for } p_j \in P \setminus P_i^{(2)}\}. \end{aligned} \quad (3.2.1)$$

The assignment rule in equation (3.2.1) is equivalent to the assignment rule that the longest distance among the distances from p to p_{i1} and p_{i2} is shorter than or equal to the shortest distance among the distances from p to the other points (i.e. points in $P \setminus \{p_{i1}, p_{i2}\}$). Thus $V(P_i^{(2)})$ is alternatively written as

$$\begin{aligned} V(P_i^{(2)}) &= \{p \mid \max_{p_h} \{d(p, p_h) \mid p_h \in P_i^{(2)}\} \\ &\leq \min_{p_j} \{d(p, p_j) \mid p_j \in P \setminus P_i^{(2)}\}\}. \end{aligned} \quad (3.2.2)$$

The extension of the order-2 Voronoi diagram to the order- k Voronoi diagram is straightforward. Let $A^{(k)}(P)$ be the set of all possible subsets consisting of k points out of P , i.e. $A^{(k)}(P) = \{P_1^{(k)}, \dots, P_i^{(k)}, \dots, P_l^{(k)}\}$, where $P_i^{(k)} = \{p_{i1}, \dots, p_{ik}\}$, $p_{ij} \in P$ and $l = n!/(k!(n - k)!)$. In these terms, we define

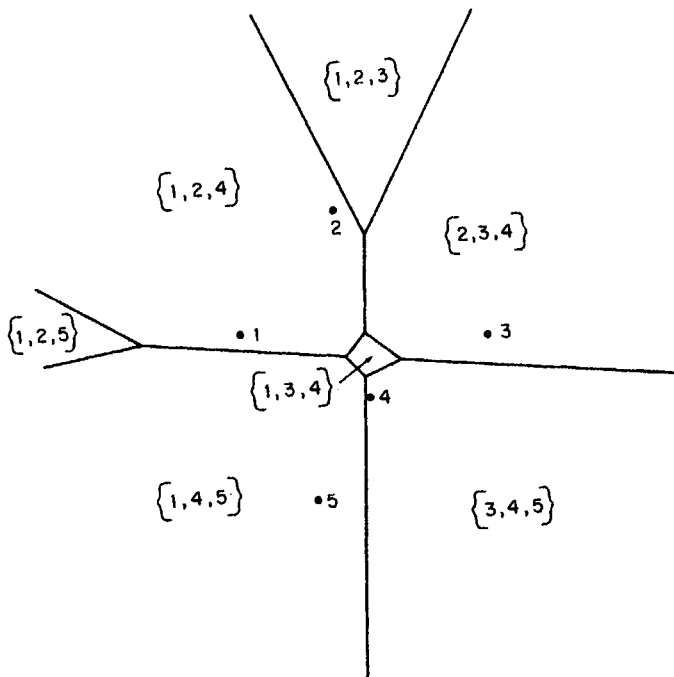
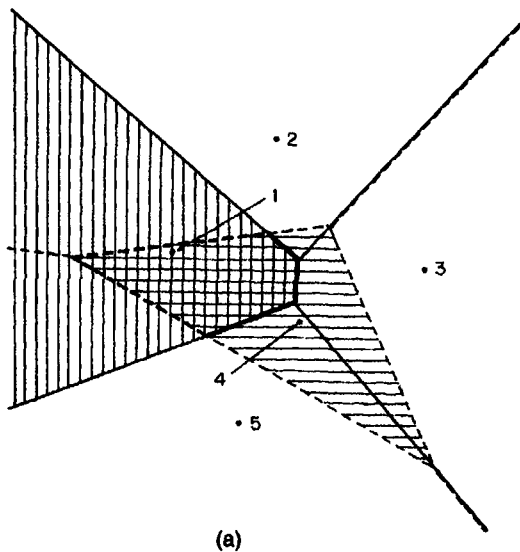
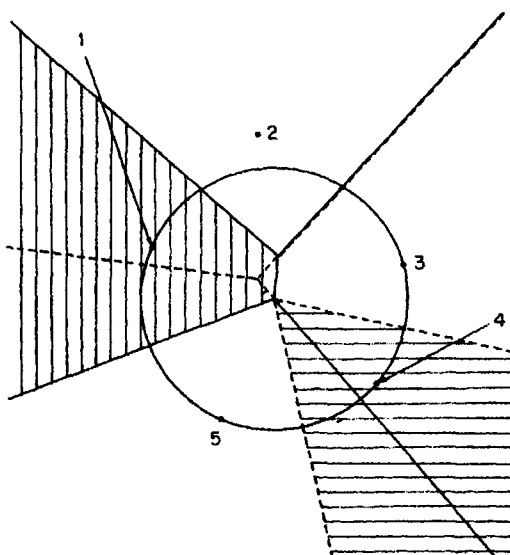


Figure 3.2.3 An order-3 Voronoi diagram ($n = 5$, the locations of points are the same as those in Figure 3.2.1).



(a)



(b)

Figure 3.2.4 An order-2 Voronoi polygon obtained from the intersection of two ordinary Voronoi polygons: (a) the intersection has a non-zero area; (b) the intersection is a point.

$$\begin{aligned} V(P_i^{(k)}) &= \{ p \mid \max_{p_h} \{ d(p, p_h) \mid p_h \in P_i^{(k)} \} \\ &\leq \min_{p_j} \{ d(p, p_j) \mid p_j \in P \setminus P_i^{(k)} \}. \end{aligned} \quad (3.2.3)$$

We call the set $V(P_i^{(k)})$ the *order- k Voronoi polygon* associated with $P_i^{(k)}$, and the set of order- k Voronoi polygons, $\mathcal{V}(A^{(k)}(P), d, \mathbb{R}^m) = \mathcal{V}^{(k)} = \{V(P_1^{(k)}), \dots, V(P_n^{(k)})\}$, the *order- k Voronoi diagram* generated by P . In the literature, $\mathcal{V}^{(k)}$ is sometimes called the *generalized Voronoi diagram*, the *k th order Voronoi diagram* and the *Voronoi diagram of order k* . Figure 3.2.3 shows an order-3 Voronoi diagram in which the region with the symbol $\{i, j, k\}$ indicates the order-3 Voronoi polygon of $\{p_i, p_j, p_k\}$.

In addition to the definitions of $V(P_i^{(2)})$ and $V(P_i^{(k)})$ by equations (3.2.1) and (3.2.3), we give one more definition. Since the set of points satisfying $d(p, p_{i1}) \leq d(p, p_j)$ and $d(p, p_{i2}) \leq d(p, p_j)$ is given by $H(p_{i1}, p_j) \cap H(p_{i2}, p_j)$, equation (3.2.1) is alternatively written as

$$V(P_i^{(2)}) = \bigcap_{p_j \in P \setminus \{p_{i1}, p_{i2}\}} [H(p_{i1}, p_j) \cap H(p_{i2}, p_j)], \quad (3.2.4)$$

where $H(p_{i1}, p_j)$ is the half plane used in defining the ordinary Voronoi diagram. Generalizing this definition for a general k , we obtain:

$$V(P_i^{(k)}) = \bigcap_{p_j \in P \setminus P_i^{(k)}} [H(p_{i1}, p_j) \cap \dots \cap H(p_{ik}, p_j)]. \quad (3.2.5)$$

This definition is useful in examining the properties of the order- k Voronoi diagram.

The order, k , varies from one to n . An order-1 Voronoi diagram is the ordinary Voronoi diagram; thus an order- k Voronoi diagram includes the ordinary Voronoi diagram. If $k = n$, then $A^{(n)}(P) = \{P\}$, and $\mathcal{V}^{(k)} = \{\mathbb{R}^2\}$. Since this diagram is too trivial, we exclude it from our discussion. If $k = n - 1$, an order- $(n-1)$ Voronoi diagram has a special name, which we shall discuss in the next subsection.

As we remarked in the introduction to this chapter, we may generalize the order- k Voronoi diagram with respect to a distance. Among many possible distances, the order- k Voronoi diagram with the additively weighted power distance (equation (3.1.13)) is notable. In the literature this Voronoi diagram is called the *order- k power diagram* (Aurenhammer, 1987). The reader who wishes to understand this Voronoi diagram in depth should consult Aurenhammer (1988a).

Having defined $\mathcal{V}^{(k)}$, we now wish to examine its geometric properties. From the definition of equation (3.2.4) we obtain:

$$V(P_i^{(2)}) = \left[\bigcap_{p_j \in P \setminus P_i^{(2)}} H(p_{i1}, p_j) \right] \cap \left[\bigcap_{p_j \in P \setminus P_i^{(2)}} H(p_{i2}, p_j) \right]. \quad (3.2.6)$$

Let $V(p_{i1}|P \setminus \{p_j\})$ denote the Voronoi polygon of p_{i1} in the ordinary Voronoi diagram generated by $P \setminus \{p_j\}$, i.e. $\mathcal{V}(P \setminus \{p_j\})$. Then, equation (3.2.6) is written as

$$V(P_i^{(2)}) = V(p_{i1} | P \setminus \{p_{i2}\}) \cap V(p_{i2} | P \setminus \{p_{i1}\}). \quad (3.2.7)$$

Figure 3.2.4(a) illustrates equation (3.2.7). The solid lines show $V(P \setminus \{p_4\})$ and the vertically hatched region indicates $V(p_1 | P \setminus \{p_4\})$. The vertically hatched region consists of the region in which the first nearest point is p_1 and the region in which the first and second nearest points are p_4 and p_1 . The dashed lines show $V(P \setminus \{p_1\})$ and the horizontally hatched region indicates $V(p_4 | P \setminus \{p_1\})$. The horizontally hatched region consists of the region in which the first nearest point is p_4 and the region in which the first and second nearest points are p_1 and p_4 . Thus the intersection of the vertically and horizontally hatched regions is the region in which the first and the second nearest points are p_1 and p_4 , respectively, or they are p_4 and p_1 , respectively. Thus the intersection gives $V(\{p_1, p_4\})$. In panel (a), the intersection is non-empty, but in some cases it may be empty. In a very special case, the intersection may be a point. In fact, panel (b) shows this example. This special case occurs when points in P are cocircular.

We can generalize equation (3.2.7) for a general k (Miles and Maillardet, 1982, Lemma on p. 102). From equation (3.2.5), we obtain the following property.

Property OK1

$$V(P_i^{(k)}) = \bigcap_{h=1}^k V(p_{ih} | [P \setminus P_i^{(k)}] \cup \{p_{ih}\}). \quad (3.2.8)$$

From this property we can derive a few important properties. First, as we mentioned above, the set $V(P_i^{(k)})$ may be empty. If $V(P_i^{(k)})$ is not empty, it is a point or an area. If it is a point, $V(P_i^{(k)})$ does not constitute a tessellation. If $V(P_i^{(k)})$ is an area, it is a polygon and, moreover, it is convex, because $V(p_{ih} | [P \setminus P_i^{(k)}] \cup \{p_{ih}\})$ is, from Property V1, a convex polygon and the intersection of convex polygons is a convex polygon. To sum up, we obtain the following property.

Property OK2 The set $V(P_i^{(k)})$ given by equation (3.2.3) may be empty, a point or an area. Under the non-cocircularity assumption, a non-empty $V(P_i^{(k)})$ is a convex polygon.

In observing Figure 3.2.2 we notice that every order-2 Voronoi polygon is split by one Voronoi edge of the ordinary Voronoi polygon. We can intuitively understand this property from the fact that the first nearest point from a point in $V(\{p_i, p_j\})$ is p_i or p_j , i.e. $V(\{p_i, p_j\})$ consists of part of $V(p_i)$ and part of $V(p_j)$ which share one Voronoi edge. From this property and Property D7, the number, $n_f^{(2)}$, of non-empty order-2 Voronoi polygons is equal to the number of Voronoi edges in the ordinary Voronoi diagram, i.e. $n_f^{(2)} = n_e = 3n - 3 - n_u$. Generalizing this equation for k , Lee (1982b, Theorem 2 and Corollary 3) proves the following property.

Property OK3 If P satisfies the non-cocircularity assumption, the number, $n_f^{(k)}$, of non-empty Voronoi polygons in $\mathcal{V}^{(k)}$ is given by

$$n_f^{(k)} = (2k - 1)n - (k^2 - 1) - \sum_{i=1}^k n_u^{(i-1)}, \quad (3.2.9)$$

where $n_u^{(i-1)}$ is the number of unbounded order- $(i-1)$ Voronoi polygons ($n_u^{(0)} = 0$). Consequently, $n_f(k)$ is $O(k(n - k))$.

When we use equation (3.2.9), we have to count $n_u^{(i-1)}$. To this end, let us obtain the necessary and sufficient condition for an order- $(i-1)$ Voronoi polygon to be unbounded. Let P_1 and P_2 be two disjoint sets of points in the plane. We say that a line L separates P_1 and P_2 if the points in P_1 and the points in P_2 lie in mutually opposite open half planes defined by L . In these terms the necessary and sufficient condition is written as follows.

Property OK4 The order- k Voronoi polygon $V(P_i^{(k)})$ is unbounded if and only if either (i) there is a line that separates $P_i^{(k)}$ (the filled circles in Figure 3.2.5(a), (b)) and $P \setminus P_i^{(k)}$ (the unfilled circles in Figure 3.2.5(a), (b)) or (ii) there are two consecutive points p_j, p_l ($\in P \setminus P_i^{(k)}$) on $\partial\text{CH}(P \setminus P_i^{(k)})$ such that the points in $P_i^{(k)} \setminus \overline{p_j p_l}$ are in the open half plane defined by the line passing through p_j and p_l opposite to $\text{CH}(P \setminus P_i^{(k)})$ (Figure 3.2.5(c)).

Proof First, suppose that either (i) or (ii) holds. If (i) holds, we transform the coordinate system in such a way that the separating line L is vertical and $\text{CH}(P \setminus P_i^{(k)})$ is to the left of L (Figure 3.2.5(a)). If (ii) holds, we transform the coordinate system in such a way that $\overline{p_j p_l}$ is vertical, the midpoint of $\overline{p_j p_l}$ lies on the x -axis, and $\text{CH}(P \setminus P_i^{(k)})$ is to the left of $\overline{p_j p_l}$ (Figure 3.2.5(c)). In both cases the point at infinity on the x -axis in the positive x direction belongs to the region $V(p_{ih} \mid [P \setminus P_i^{(k)}] \cup \{p_{ih}\})$ for any $p_{ih} \in P_i^{(k)}$. Hence we see from Property OK1 that if either (i) or (ii) holds, the Voronoi polygon $V(P_i^{(k)})$ is unbounded.

Next, suppose that $V(P_i^{(k)})$ is unbounded. Then, there exists at least one ray X such that the point at infinity on X belongs to $V(P_i^{(k)})$. We transform the coordinate system in such a way that X lies on the x -axis facing toward

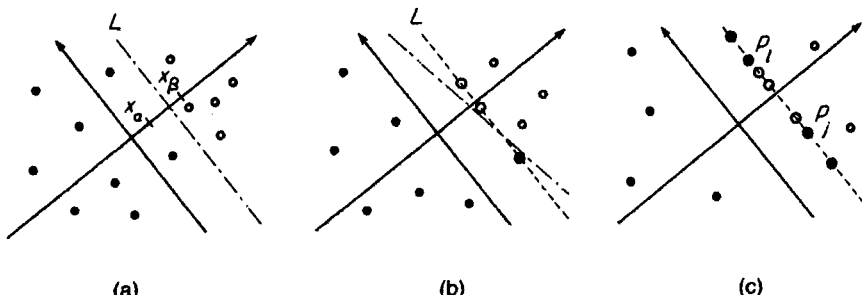


Figure 3.2.5 Illustration of the proof of Property OK4.

the positive x direction. Let x_α be the maximum value of the x coordinates of the points in $P \setminus P_i^{(k)}$, and x_β be the minimum value of the x coordinates of the points in $P_i^{(k)}$ (Figure 3.2.5(a), (b)). Then we get $x_\alpha \leq x_\beta$; this is because if $x_\alpha > x_\beta$, then for the point p_{ih} with the x coordinate x_β , the polygon $V(p_{ih} | [P \setminus P_i^{(k)}] \cup \{p_{ih}\})$ does not contain the point at infinity on the x -axis in the positive x direction.

Case 1. Suppose that $x_\alpha < x_\beta$ (Figure 3.2.5(a)). Then the vertical line defined by $x = (x_\alpha + x_\beta)/2$ separates $P_i^{(k)}$ and $P \setminus P_i^{(k)}$; hence (i) holds.

Case 2. Suppose that $x_\alpha = x_\beta$ (Figure 3.2.5(b), (c)). Let P_α be the set of points in $P \setminus P_i^{(k)}$ whose x coordinates are equal to x_β (the large filled circles in Figure 3.2.5(b), (c)), and let P_β be the set of points in $P_i^{(k)}$ whose x coordinates are equal to x_β ($= x_\alpha$) (the large unfilled circles in Figure 3.2.5(c)).

Case 2.1. Suppose that P_α contains exactly one point: $P_\alpha = \{p_j\}$. Then either all the points in P_β are above p_j or all the points in P_β are below p_j , because if $p_{ih} \in P_i^{(k)}$ is above p_j and $p_{ii} \in P_i^{(k)}$ is below p_j , the regions $V(p_{ih} | [P \setminus P_i^{(k)}] \cup \{p_{ih}\})$ and $V(p_{ii} | [P \setminus P_i^{(k)}] \cup \{p_{ii}\})$ have no point in common. If the points in P_β are above p_j , we rotate the coordinate axes counter-clockwise slightly (the dash-dot line in Figure 3.2.5(b)), and get the situation where $x_\alpha < x_\beta$ and the point at infinity on the new x -axis in the positive x direction still belongs to $V(P_i^{(k)})$; thus we get (i). If the points in P_β are below p_j , we rotate the coordinate axes clockwise and get (i) similarly.

Case 2.2. Suppose that P_α contains two or more points. Then for any $p_j \in P_\alpha$ either all the points in P_β are above p_j or all the points in P_β are below p_j , because otherwise $V(P_i^{(k)})$ becomes empty, as we saw in Case 2.1. If all the points in P_β are above the highest point in P_α or below the lowest, we reduce the situation to Case 2.1 by slightly rotating the coordinate axes counter-clockwise or clockwise, respectively, as we did in Case 2.1. Hence, the only remaining case is that there are two points p_j and p_l in P_α such that $\overline{p_j p_l}$ contains no other points in P_α and $\overline{p_j p_l}$ contains all the points in P_β , which implies (ii). Thus, in all cases either (i) or (ii) holds. \square

In inspecting Figure 3.2.1 we notice that $V(\{p_1, p_5\})$ contains no points of P ; $V(\{p_1, p_2\})$ contains one point of P ; $V(\{p_4, p_5\})$ contains two points of P . In general, we notice the following property.

Property OKS A non-empty order- k Voronoi polygon contains 0, 1, . . . , or k points of P .

In an ordinary Voronoi diagram, every Voronoi vertex has the empty circle (Property V7). To find the corresponding property in an order- k Voronoi diagram, let us first examine a vertex, say q_1 , shared by $V(\{p_1, p_4\})$, $V(\{p_3, p_4\})$ and $V(\{p_4, p_5\})$ in Figure 3.2.2. We notice that p_1, p_3 and p_5 are equally distant from the vertex q_1 , and hence we can draw the circle C_1 centred at q_1 which passes through p_1, p_3 and p_5 . This circle contains p_4 . From this inspection and recalling Property V7, we might expect that for every vertex in an order-2 Voronoi diagram, there exists a circle which passes through three points of P .

and contains exactly one point of P in its interior. This expectation is, however, false. A counterexample is given by the circle C_2 centred at the vertex q_2 shared by $V(\{p_1, p_2\})$, $V(\{p_2, p_4\})$ and $V(\{p_1, p_4\})$ (Figure 3.2.2). The circle C_2 does not contain any point of P in its interior. If we draw circles at all vertices in Figure 3.2.2, we can see that the circles centred at the unfilled circles (which are called ‘old vertices’ in Lee, 1982b) have no points of P in their interiors, and the circles centred at the large filled circles (which are called ‘new vertices’) have exactly one point of P in their interiors. This result can be proved theoretically and is generalized by Lee (1982b, Lemma 6) as follows.

Property OK6 Under the non-cocircularity assumption, for every vertex q_i of an order- k Voronoi polygon, there exists a unique circle centred at q_i which passes through three points of P and contains $k-2$ or $k-1$ points of P in its interior.

The condition for $k-2$ or $k-1$ is explicitly stated in Lee (1982b, Lemma 6).

Applying almost the same derivation used for Property D11, we obtain the following property.

Property OK7 Let $n_v^{(k)}$, $n_e^{(k)}$, $n_f^{(k)}$ and $n_u^{(k)}$ be the number of vertices, edges, order- k Voronoi polygons and unbounded order- k Voronoi polygons, respectively. Then under the non-cocircularity assumption, the following equations hold:

$$n_v^{(k)} = 2(n_t^{(k)} - 1) - n_u^{(k)}, \quad (3.2.10)$$

$$n_e^{(k)} = 3(n_t^{(k)} - 1) - n_u^{(k)}. \quad (3.2.11)$$

These equations with $k = 1$ are, of course, the same as equations (2.4.13) and (2.4.14) in Property D11. The proof is shown by Lee (1982b, Lemma 11).

In addition to these properties, the statistical properties of the order- k Voronoi diagram are investigated in spatial statistics. We show these properties in Chapter 5. Regarding the properties of the order- k power diagram, see Aurenhammer (1988a).

We may define an order- k Voronoi diagram with the additively weighted distance (Section 3.1.2). We call a set of regions $V(P_i^{(k)})$ defined by equation (3.2.5) with the distance between x and x_i given by $\|x - x_i\| - w_i$ the *additively weighted order- k Voronoi diagram* generated by P (Rosenberger, 1991). The additively weighted order- k Voronoi diagram has the following property.

Property OK8 For the additively weighted order- k Voronoi diagram generated by P , let D_i be a disk centred at $p_i \in P$ with radius $|w_i|$, and assume that no disk is contained in another and $1 \leq k < n$. Then the relations

$$n_v^{(k)} \leq (4k - 2)(n - k) - \min\{k, n - k\} - 1, \quad (3.2.12)$$

$$n_e^{(k)} \leq (6k - 2)(n - k) - \min\{k, n - k\} - 1 \quad (3.2.13)$$

hold.

The proof is shown by Rosenberger (1991, Theorem 5).

We may also define an order- k Voronoi diagram by extending a generator set of points to a generator set of points, lines and polygons (Roos, 1989; regarding Voronoi diagrams for a set of lines and a set of polygons, see Sections 3.5 and 3.6, respectively).

3.2.2 The ordered order- k Voronoi diagram

The order- k Voronoi diagram has a closely related tessellation which we call the ‘ordered’ order- k Voronoi diagram. In the order- k Voronoi diagram, points in a generator set are not ordered (recall that in $\mathcal{V}^{(k)}$ we were not concerned with which point was the first nearest point in a generator set), whereas in the ordered order- k Voronoi diagram, they are ordered. To show this contrast, let us begin our discussion with the same example used in Figure 3.2.1.

Suppose that a set of distinctive points (the filled circles in Figure 3.2.6) is placed in the Euclidean plane. We consider the Euclidean distances from a location, say the location indicated by the unfilled circle in Figure 3.2.6, to all points in the point set. The dashed lines in Figure 3.2.6 show that the first nearest point from the location is p_1 and the second nearest point from the location is p_4 . In this case we assign this location to the ordered pair (p_1, p_4) (note that $(p_1, p_4) \neq (p_4, p_1)$). In general, if an ordered pair of the first and the second nearest points from a location is (p_i, p_j) , we assign the location to (p_i, p_j) . If the ordered pairs are not only (p_i, p_j) but also other ordered pairs, then we assign the location to those ordered pairs. In this manner we

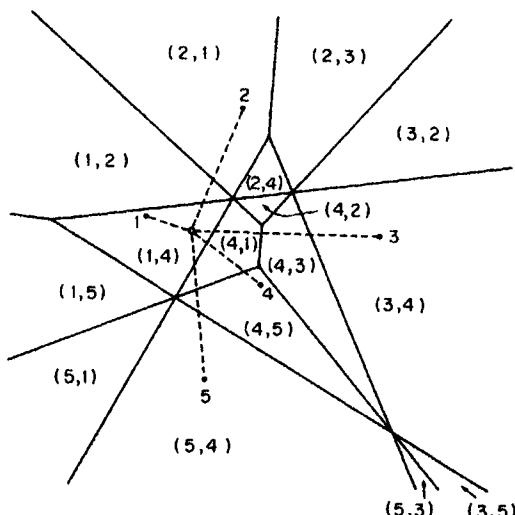


Figure 3.2.6 An ordered order-2 Voronoi diagram ($n = 5$; the locations of the generator points are the same as those in Figure 3.2.1).

assign all locations in the plane to at least one ordered pair. As a result, locations assigned to each pair form a region, which we call the *ordered order-2 Voronoi polygon* associated with (p_i, p_j) . The collection of ordered order-2 Voronoi polygons is shown in Figure 3.2.6 in which the region with the symbol (i, j) indicates the ordered order-2 Voronoi polygon associated with (p_i, p_j) . This collection forms a tessellation, which we call the *ordered order-2 Voronoi diagram* generated by the set of points.

To observe the geometric properties of an ordered order- k Voronoi diagram, it is instructive to compare this diagram with the ordinary Voronoi diagram, \mathcal{V} , generated by the same set of generator points. In Figure 3.2.7 the dashed lines show \mathcal{V} , and the solid lines show the ordered order-2 Voronoi diagram. In this figure, consider a Voronoi polygon, for example $V(p_4)$ in \mathcal{V} . Since the first nearest point of P from a location in $V(p_4)$ is p_4 , the ordered order-2 Voronoi polygons associated with $(p_4, p_j), j = 1, 2, 3, 5$, are included in $V(p_4)$, and these polygons constitute $V(p_4)$. Thus the Voronoi edges in \mathcal{V} are the edges of the order-2 Voronoi diagram. To deepen this analysis, let us restate the above verbal definition in mathematical terms.

Let $A^{(2)}(P)$ be the set of all ordered pairs of points obtained from $P = \{p_1, \dots, p_n\}$, i.e. $A^{(2)}(P) = \{P_1^{(2)}, \dots, P_i^{(2)}, \dots, P_l^{(2)}\}$, where $P_i^{(2)} = (p_{i1}, p_{i2})$, $p_{i1}, p_{i2} \in P$, and $l = n(n - 1)$. For a set $P_i^{(2)}$ in $A^{(k)}(P)$, we define

$$V(P_i^{(2)}) = \{p \mid d(p, p_{i1}) \leq d(p, p_{i2}) \leq d(p, p_j), p_j \in P \setminus \{p_{i1}, p_{i2}\}\}. \quad (3.2.14)$$

We call the set $V(P_i^{(2)})$ the *ordered order-2 Voronoi polygon* associated with $P_i^{(2)}$.

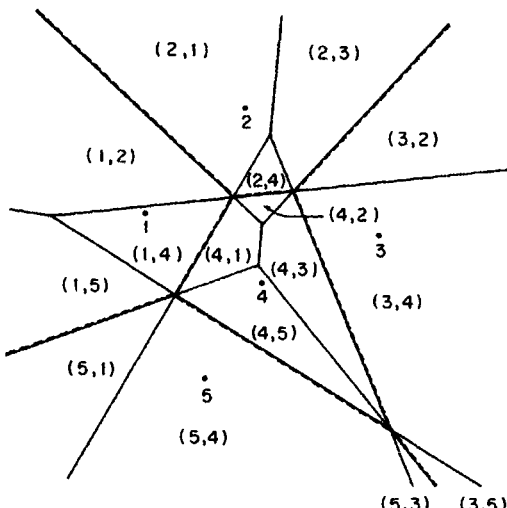


Figure 3.2.7 The ordered order-2 Voronoi diagram (the solid lines) and the ordinary Voronoi diagram (the broken lines) generated by the same set of points ($n = 5$; the locations of the generator points are the same as those in Figure 3.2.1).

The extension to a general k is immediate. Let $A^{(k)}(P)$ be the set of all ordered k -tuples of points obtained from P , i.e. $A^{(k)}(P) = \{P_1^{(k)}, \dots, P_i^{(k)}, \dots, P_l^{(k)}\}$, where $P_i^{(k)} = (p_{i1}, \dots, p_{ik})$, $p_{ij} \in P$, $j \in I_k$, and $l = n(n-1) \dots (n-k+1)$. For a set $P_i^{(k)}$ in $A^{(k)}(P)$, we define

$$V(P_i^{(k)}) = \{p \mid d(p, p_{i1}) \leq d(p, p_{i2}) \leq \dots \leq d(p, p_{ik}) \leq d(p, p_j), \\ p_j \in P \setminus \{p_{i1}, \dots, p_{ik}\}\}. \quad (3.2.15)$$

We call the set $V(P_i^{(k)})$ the *ordered order- k Voronoi polygon* associated with $P_i^{(k)}$ and $\mathcal{V}(A^{(k)}(P), d, \mathbb{R}^m) = \mathcal{V}^{(k)} = \{V(P_1^{(k)}), \dots, V(P_l^{(k)})\}$ the *ordered order- k Voronoi diagram* generated by P . Figure 3.2.8 shows an ordered order-3 Voronoi diagram.

To analyse the geometric properties of the ordered order- k Voronoi diagram, the following alternative definition is more useful. The set of points satisfying $d(p, p_{i1}) < d(p, p_{i2}) < d(p, p_j)$ is given by $H(p_{i1}, p_{i2}) \cap H(p_{i2}, p_j)$. Thus, equation (3.2.14) is written as

$$V(P_i^{(2)}) = \bigcap_{p_j \in P \setminus \{p_{i1}, p_{i2}\}} H(p_{i1}, p_{i2}) \cap H(p_{i2}, p_j). \quad (3.2.16)$$

Similarly, for a general k , equation (3.2.15) is written as

$$V(P_i^{(k)}) = \bigcap_{p_j \in P \setminus \{p_{i1}, \dots, p_{ik}\}} H(p_{i1}, p_{i2}) \cap \dots \cap H(p_{ik-1}, p_{ik}) \cap H(p_{ik}, p_j). \quad (3.2.17)$$

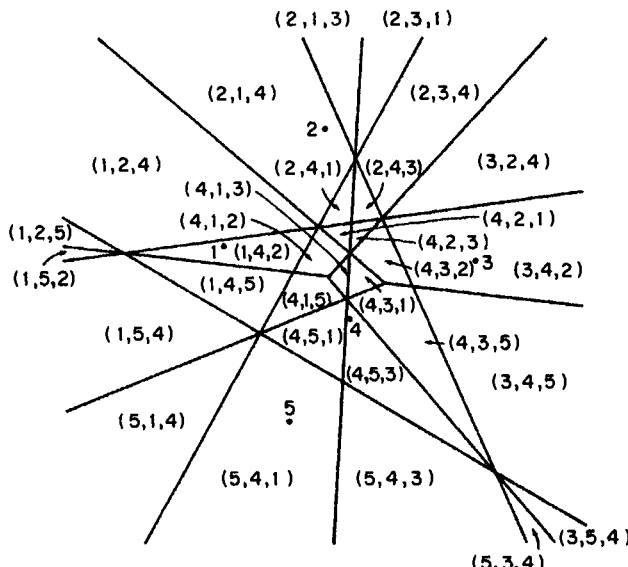


Figure 3.2.8 An ordered order-3 Voronoi diagram ($n = 3$; the locations of generator points are the same as those in Figure 3.2.1).

Having defined the ordered order- k Voronoi diagram $\mathcal{V}^{(k)}$ mathematically, we are now ready to examine its geometric properties. From equation (3.2.16) we can write $V(P_i^{(2)})$ as

$$\begin{aligned} V(P_i^{(2)}) &= \bigcap_{p_j \in P \setminus \{p_n, p_n\}} H(p_n, p_n) \cap H(p_n, p_j) \cap H(p_n, p_j) \\ &= \left[\bigcap_{p_j \in P \setminus \{p_n\}} H(p_n, p_j) \right] \cap \left[\bigcap_{p_j \in P \setminus \{p_n, p_n\}} H(p_n, p_j) \right] \\ &= V(p_n) \cap V(p_n | P \setminus \{p_n\}). \end{aligned} \quad (3.2.18)$$

Let us confirm this equation with $V((p_1, p_4))$ in Figure 3.2.7. Since the first nearest point in $V((p_1, p_4))$ is p_1 , $V((p_1, p_4))$ is included in $V(p_1)$. The second nearest point in $V((p_1, p_4))$ becomes the first nearest point if p_1 is deleted from P . Thus $V((p_1, p_4))$ is given by $V(p_1) \cap V(p_4 | P \setminus \{p_1\})$. Generalizing equation (3.2.18), we obtain the following equation.

Property OOK1 An ordered order- k Voronoi polygon is written in terms of ordinary Voronoi polygons as

$$V(P_i^{(k)}) = \bigcap_{h=1}^k V(p_{ih} | P \setminus \{p_{i1}, \dots, p_{ih-1}\}), \quad (3.2.19)$$

where $\{p_{i1}, \dots, p_{ih-1}\} = \emptyset$ for $h = 1$.

In Figure 3.2.7 we observe that $V(p_4)$ consists of $V((p_4, p_2))$, $V((p_4, p_1))$, $V((p_4, p_5))$ and $V((p_4, p_3))$. We can generalize this property for a general k as follows.

Property OOK2 Let $A^{(k-1)}(P \setminus \{p_{i1}\})$ be all possible ordered $(k-1)$ -tuples obtained from $P \setminus \{p_{i1}\}$. Then

$$V(p_{i1}) = \bigcup_{(p_{i2}, \dots, p_{ik}) \in A^{k-1}(P \setminus \{p_{i1}\})} V((p_{i1}, p_{i2}, \dots, p_{ik})). \quad (3.2.20)$$

This property implies that the ordered order- k Voronoi diagram $\mathcal{V}^{(k)}$ generated by $A^{(k)}(P)$ is a refinement of the ordinary Voronoi diagram generated by P . Figure 3.2.6 shows the refinement of $\mathcal{V}(P)$ by $\mathcal{V}^{(2)}(A^{(2)}(P))$.

An ordered order- k Voronoi diagram also refines the order- k Voronoi diagram. The region in which the first and the second nearest points are $\{p_i, p_j\}$ consists of the region in which the first and second nearest points are p_i and p_j , respectively, and the region in which the first and the second nearest points are p_j and p_i , respectively (observe this relation in Figure 3.2.9). Thus $V(\{p_i, p_j\}) = V((p_i, p_j)) \cup V((p_j, p_i))$. More generally, we have the following property.

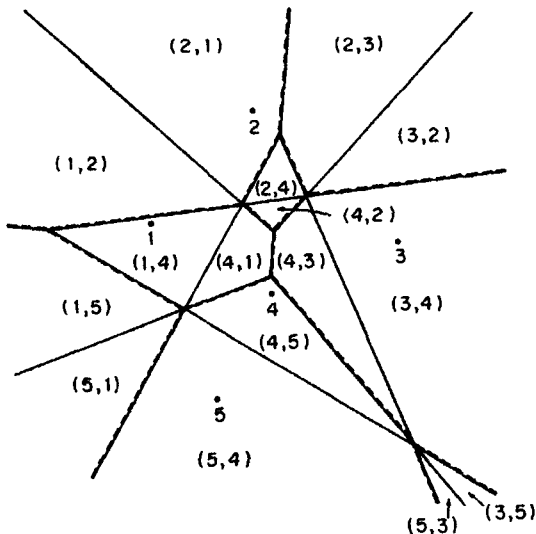


Figure 3.2.9 The order-2 Voronoi diagram (the dashed lines) and the ordered order-2 Voronoi diagram (the solid lines) generated by the same set of points; the ordered order-2 Voronoi diagram is a refinement of the order-2 Voronoi diagram.

Property OOK3

$$V(P_i^{(k)}) = \bigcup_{P_j^{(k)} \in A^{(k)}(P_i^{(k)})} V(P_j^{(k)}), \quad (3.2.21)$$

where $A^{(k)}(P_i^{(k)})$ is the set of all possible k -tuples made of p_{i1}, \dots, p_{ik} .

Equation (3.2.21) says that $\mathcal{V}^{(k)}$ generated by P is a refinement of $\mathcal{V}^{(k)}$ generated by P . An example is shown in Figure 3.2.9.

From Property OOK1, we obtain the next property.

Property OOK4 The set $V(P_i^{(k)})$ given by equation (3.2.15) may be empty. If $V(P_i^{(k)})$ is not empty, it is a point or an area. Under the non-cocircularity assumption, a non-empty $V(P_i^{(k)})$ is a convex polygon.

In Property OK4 we saw the necessary and sufficient condition for an order- k Voronoi polygon to be unbounded. A similar condition is obtained for an ordered order- k Voronoi polygon. To avoid unnecessary complication, we next state the condition that is valid only when no two lines passing through two points in P are parallel to each other.

Property OOK5 Suppose that no two lines passing through two points in P are mutually parallel. Let $P_i^{(k)} = (p_{i1}, p_{i2}, \dots, p_{ik})$ be an ordered k -tuple of elements of P . Then the ordered order- k Voronoi polygon $V(P_i^{(k)})$ is

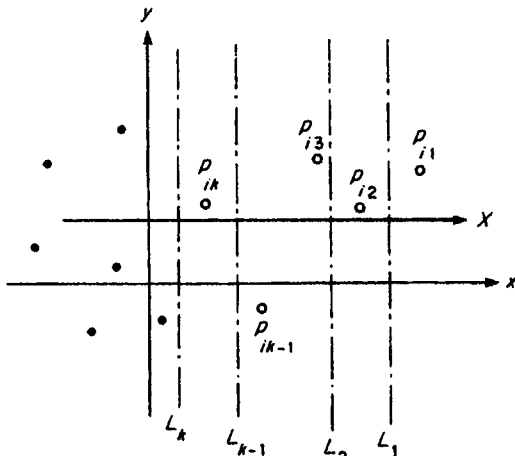


Figure 3.2.10 Illustration of the proof of Property OOK5.

unbounded if and only if there are k mutually parallel lines L_1, L_2, \dots, L_k such that L_h separates $\{p_{i1}, p_{i2}, \dots, p_{ih}\}$ and $P \setminus \{p_{i1}, p_{i2}, \dots, p_{ih}\}$ for $h = 1, 2, \dots, k$ (Figure 3.2.10).

Proof First, suppose that there exist k mutually parallel lines L_1, \dots, L_k specified in Property OOK5 (Figure 3.2.10). We transform the coordinate system in such a way that L_1, \dots, L_k are vertical and p_{i1} is the rightmost point in P . Then the point at infinity in the positive x direction is contained in the region $V(p_{i1} | P \setminus \{p_{i1}, \dots, p_{ih-1}\})$ for any k . Hence it follows from Property OOK1 that $V(P_i^{(k)})$ contains the point at infinity in the positive x direction; that is, $V(P_i^{(k)})$ is unbounded.

Next, suppose that $V(P_i^{(k)})$ is unbounded. Then there exists a ray X such that the point at infinity on X belongs to $V(P_i^{(k)})$. Since no two lines passing through two points in P are mutually parallel, the perpendicular bisectors of two points in P are not parallel to each other. In particular, no two edges on the boundary of $V(P_i^{(k)})$ are parallel, and hence we can choose the ray X in such a way that X is not perpendicular to any line passing through two points in P .

Now we transform the coordinate system in such a way that X is parallel to the x -axis (Figure 3.2.10). Let x_{ih} be the x coordinate of p_{ih} for $h = 1, 2, \dots, k$. Property OOK1 implies that x_{ih} is greater than the x coordinate of any point in $P \setminus \{p_{i1}, \dots, p_{ih-1}\}$ and consequently we get $x_{i1} > x_{i2} > \dots > x_{ik}$ and all the points in $P \setminus P_i^{(k)}$ have smaller x coordinates than p_{ik} . Let L_h be the vertical line defined by $x = (x_{ih} + x_{ih+1})/2$ for $h = 1, \dots, k$, where x_{ik+1} is the x coordinate of the rightmost point in $P \setminus P_i^{(k)}$. Then L_1, \dots, L_k are mutually parallel (actually they are vertical) and L_{ih} separates $\{p_{i1}, \dots, p_{ih}\}$ and $P \setminus \{p_{i1}, \dots, p_{ih}\}$. \square

Corresponding to Property D7 and Property OK7, the following equations hold for the numbers of vertices, edges and polygons.

Property OOK6 Let $n_v^{(2)}$, $n_e^{(2)}$, $n_f^{(2)}$ and $n_u^{(2)}$ be the number of vertices, edges, ordered order-2 Voronoi polygons and unbounded ordered order-2 Voronoi polygons, respectively, in the ordered order-2 Voronoi diagram generated by P ; $n_v^{(2)}$, $n_e^{(2)}$, $n_f^{(2)}$ and $n_u^{(2)}$ be those in the order-2 Voronoi diagram generated by P ; and n_v , n_e , n_f and n_u be those in the ordinary Voronoi diagram generated by P which satisfies the non-cocircularity assumption. Then

$$n_v^{(2)} = n_v^{(2)}, \quad (3.2.22)$$

$$n_e^{(2)} = n_e^{(2)} + n_e, \quad (3.2.23)$$

$$n_f^{(2)} = 2n_f^{(2)} = 2n_e = 6n - 6 - 2n_u. \quad (3.2.24)$$

Equation (3.2.22) may be understood visually from Figure 3.2.9 in which vertices of $\mathcal{V}^{(2)}$ are coincident with vertices of $\mathcal{V}^{(2)}$. Also equation (3.2.23) is understandable from Figures 3.2.6 and 3.2.8 in which the edges of $\mathcal{V}^{(2)}$ consist of the edges of \mathcal{V} and $\mathcal{V}^{(2)}$. The first equation in equation (3.2.24) is obtained from the fact that $V(\{p_{i1}, p_{i2}\})$ consists of $V((p_{i1}, p_{i2}))$ and $V((p_{i2}, p_{i1}))$ (Figure 3.2.9). The second equation is obtained from $n_f^{(2)} = n_e$ (see the equation obtained below Property OK2), and the third equation is obtained from equation (3.2.9). Substituting equations (3.2.9), (3.2.10) and (3.2.11) into the above equations, we can write $n_v^{(2)}$, $n_e^{(2)}$ and $n_f^{(2)}$ in different terms, some of which are shown in Shamos (1978).

Last, it is worth noting an interesting property found by Sibson (1980a), called the *local coordinates property*, and extended by Piper (1993).

Property OOK7 The equation

$$\mathbf{x}_i = \frac{\sum_{j \in I_n \setminus \{i\}} |V((p_i, p_j))| \mathbf{x}_j}{\sum_{j \in I_n \setminus \{i\}} |V((p_i, p_j))|} \quad (3.2.25)$$

holds if the denominator is greater than zero and less than infinity, i.e. if p_i is the interior of the convex hull of $P \setminus \{p_i\}$.

This equation says that the location of the point p_i is the centroid of the locations of points of $p_j \in P \setminus \{p_i\}$ weighted with the area $|V((p_i, p_j))|$ of the ordered order-2 Voronoi polygon associated with (p_i, p_j) . Sibson (1980a) proves this property in a little more general context. Since the proof requires a few pages, it is omitted here (see the proof on pp. 153–154 in Sibson, 1980a). This property is useful for interpolation (Sibson, 1980b), which is discussed in Chapter 6.

3.2.3 Applications

A natural application is found in a facility location problem in which the k th nearest facility is critical, for instance in the case of a single unit emergency depot when more than one unit is required or when the first nearest unit is in use (Keeney, 1972).

We can find other applications in multivariate density estimation (Loftsgaarden and Quesenberry, 1965), classification (Cover and Hart, 1967) and information retrieval systems (Fukunaga and Narendra, 1975; Chazelle, 1985). In the study of waves and crystals, the k th nearest-point Voronoi diagram gives an important concept called the Brillouin zone (Brillouin, 1953). As we shall see in Chapter 6, the ordered order- k Voronoi diagram can be used for spatial interpolation (Sibson, 1980a), which is applied in statistical estimation (Ripley, 1981, Chapter 4) as well as in cartography (isoline generation). The multiplicatively weighted order- k Voronoi diagram has been used for retail trade area analysis (Boots and South, 1997).

3.3 THE FARTHEST-POINT VORONOI DIAGRAM AND k TH NEAREST-POINT VORONOI DIAGRAM

The nearest generator point from a point in an ordinary Voronoi polygon is of course the generator point of the Voronoi polygon (Property V6). To emphasize this property, we alternatively call the ordinary Voronoi diagram the *nearest-point Voronoi diagram*. In opposition to the nearest point Voronoi diagram, we can consider the ‘farthest-point’ Voronoi diagram. More generally, we can consider the ‘ k th nearest-point’ Voronoi diagram. In this section we show these generalized Voronoi diagrams.

3.3.1 The farthest-point Voronoi diagram

The definition of the farthest-point Voronoi diagram is almost the same as that of the nearest-point Voronoi diagram (Definition V1) except that ‘closest’ is replaced with ‘farthest’.

Given a set of distinct points in the Euclidean plane, we assign all locations in that plane to the farthest member(s) of the point set. The result is a tessellation of the plane into a set of regions associated the members in the point set. We call this tessellation the *farthest-point Voronoi diagram* generated by the point set, and the regions constituting the Voronoi diagram *farthest-point Voronoi polygons*. Figure 3.3.1(a) shows a farthest-point Voronoi diagram.

To restate the above verbal definition mathematically, let $P = \{p_1, \dots, p_n\} \subset \mathbb{R}^2$ ($2 \leq n < \infty$), $p_i \neq p_j$ for $i \neq j$. Then the *farthest-point Voronoi polygon*, $V_{fp}(p_i)$, associated with p_i is written as

$$V_{fp}(p_i) = \{p \mid d(p, p_i) \geq d(p, p_j), p_j \in P \setminus \{p_i\}\}, \quad (3.3.1)$$

$$= \{p \mid d(p, p_i) \geq \max_{p_j} \{d(p, p_j), p_j \in P \setminus \{p_i\}\}\}. \quad (3.3.2)$$

Alternatively, in terms of the dominance region $\text{Dom}(p_i, p_j) = \{p \mid d(p, p_i) \geq d(p, p_j)\} = H(p_j, p_i)$, the set $V_{fp}(p_i)$ is written as

$$V_{fp}(p_i) = \bigcap_{p_j \in P \setminus \{p_i\}} H(p_j, p_i). \quad (3.3.3)$$

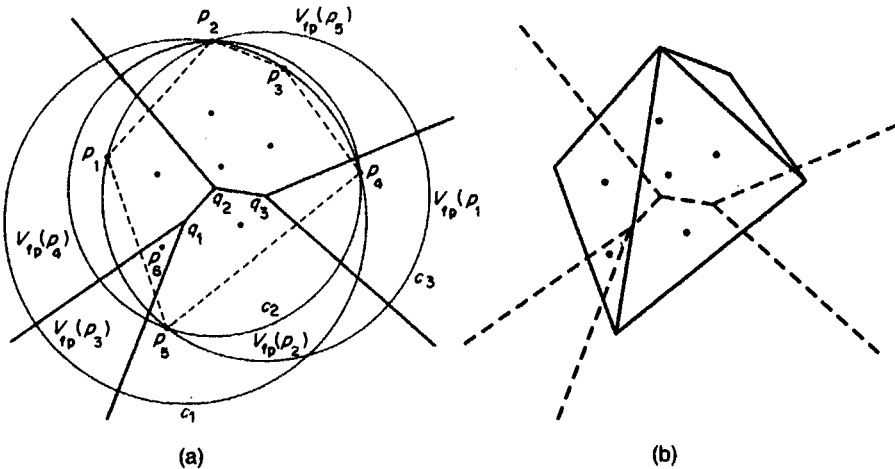


Figure 3.3.1 (a) A farthest-point Voronoi diagram and (b) its farthest-point Delaunay triangulation.

For brevity, we call the region $V_{fp}(p_i)$ the *FP-Voronoi polygon* of p_i . Since $\text{Dom}(p_i, p_j)$ is a half plane, it is well-behaving. Thus the set of FP-Voronoi polygons, $\mathcal{V}_{fp} = \{V_{fp}(p_1), \dots, V_{fp}(p_n)\}$, forms a tessellation of \mathbb{R}^2 . We call this tessellation the *farthest-point Voronoi diagram* generated by P , or briefly the *FP-Voronoi diagram* of P .

The FP-Voronoi diagram is, in fact, an order- k Voronoi diagram. If p_i is the farthest point from p , then the set $P \setminus \{p_i\}$ is the set of the first, the second, ..., the $(n-1)$ th nearest point from p_i . Thus the $V_{fp}(p_i)$ of \mathcal{V}_{fp} is the same as the order- $(n-1)$ Voronoi polygon associated with $P \setminus \{p_i\}$ of the order- $(n-1)$ Voronoi diagram generated by P . Following the notation of the order- k Voronoi diagram, we can write $V_{fp}(p_i)$ as $V(P_i^{(n-1)})$.

Since the FP-Voronoi diagram is the order- $(n-1)$ Voronoi diagram, the properties of the FP-Voronoi diagram are implicitly stated in the properties of the order- k Voronoi diagram. We, however, explicitly state some of them here adding slightly stronger properties.

From Properties OK2 and OK4, we obtain the following property.

Property FP1 The set $V_{fp}(p_i)$ given by equation (3.3.1) may be empty. If $V_{fp}(p_i)$ is not empty, the set $V_{fp}(p_i)$ is always an unbounded convex polygon.

Observe that there is no FP-Voronoi polygon associated with p_6 in Figure 3.3.1(a). Note too that the above property holds even if points in P are cocircular. The condition for a non-empty FP-Voronoi polygon is stated in Property FP2.

Property FP2 $V_{fp}(p_i)$ is not empty if and only if p_i is at a vertex of the convex hull of P . A non-empty FP-Voronoi polygon need not contain generator points.

Observe the broken lines in Figure 3.3.1(a). The proof is given by Seidel (1982, pp. 25–26).

In Section 2.3.1 we solved the closest pair problem (Problem P1) with the ordinary Voronoi diagram (Property V6). Similarly, we can solve the farthest-pair problem corresponding to the closest-pair problem with the FP-Voronoi diagram.

Problem FP1 (the reciprocal farthest-pair problem and the farthest-pair problem) For a given set P of distinct points in \mathbb{R}^2 , if p_j is the farthest point from p_i and in addition p_i is the farthest point from p_j , we say that the pair $\{p_i, p_j\}$ is a *reciprocal farthest pair*. If the distance between p_i and p_j is the farthest among the distances between all possible pairs of points in P , we say that the pair $\{p_i, p_j\}$ is the *farthest pair*. Given P , find the reciprocal farthest pairs and the farthest pair.

It follows from the definition of the FP-Voronoi diagram that:

Property FP3 $\{p_i, p_j\}$ is a reciprocal farthest pair if and only if $p_j \in V_{fp}(p_i)$ and $p_i \in V_{fp}(p_j)$.

Using this property and Property FP2, we can solve Problem FP1. Let us solve, for example, the reciprocal farthest-pair problem in Figure 3.3.1. We notice from Property FP2 that reciprocal farthest pairs are found at points on the boundary of the convex hull of P , i.e. $\{p_1, \dots, p_5\}$. First, consider p_1 . This point is included in $V_{fp}(p_4)$, and p_4 is included in $V_{fp}(p_1)$. Thus $\{p_1, p_4\}$ is a reciprocal farthest pair. Second, consider p_2 . This point is included in $V_{fp}(p_5)$, and p_5 is included in $V_{fp}(p_2)$. Thus $\{p_2, p_5\}$ is also a reciprocal farthest pair. Third, consider p_3 . This point is included in $V_{fp}(p_5)$, but p_5 is not included in $V_{fp}(p_3)$. Thus $\{p_3, p_5\}$ does not give a reciprocal farthest pair. Consequently the reciprocal farthest pairs are $\{p_1, p_4\}$ and $\{p_2, p_5\}$. The farthest pair is given by the reciprocal pair whose distance is the greatest among the obtained reciprocal farthest pairs. Hence $\{p_2, p_5\}$ is the farthest pair. Note that the farthest pair gives the diameter of P . The *diameter* of P is defined by the greatest distance among the distances between any two points in P . Thus the diameter is given by the farthest pair. In the example of Figure 3.3.1, $\overline{p_2 p_5}$ is the diameter. This method, however, is not the most efficient when we want to obtain only the diameter of P (Preparata and Shamos, 1985; Clarkson and Shor, 1989). Also note that to obtain the farthest pair, we should solve the point location problem (Section 2.3, Problem V3).

In Section 2.3 we considered the largest empty circle problem (Problem P4). Its counterpart problem is written as follows.

Problem FP2 (the smallest enclosing circle problem) Given a set of distinct points P , find the smallest circle, called the *smallest enclosing circle*, which contains all points of P in its interior or on it.

This problem is alternatively called the *minimum (radius) spanning circle* or the *short minimum spanning circle* (Bass and Schubert, 1967; Nair and Chandrasekaran, 1971; Hearn and Vijay, 1982; Melville, 1985; and Datta, 1996). We can solve this problem with the aid of the following property.

Property FP4 For every vertex q_i of FP-Voronoi polygons of the FP-Voronoi diagram generated by P , there exists the unique circle C_i centred at q_i which passes through three or more points of P , and in addition, which encloses all other points of P .

The smallest enclosing circle is determined either by the diameter of P or by three points of P . First, we examine if the circle whose diameter is given by the diameter of P encloses all points of P . If so, that circle is the smallest enclosing circle. If not, we draw the circles $\{C_i\}$ defined in Property FP4. Then the smallest enclosing circle is given by the smallest circle among $\{C_i\}$. In the example of Figure 3.3.1, since the circle with diameter $\overline{p_7p_5}$ does not include p_4 , we draw circles C_1 , C_2 and C_3 , and notice that C_2 is the smallest enclosing circle. Note that an alternative simple algorithm is proposed by Skyum (1991).

In conjunction with Property FP4, it may be worth recalling the definition of the Delaunay triangulation with the inversion transformation (Property D7 in Chapter 2). We defined there ‘near-side’ and ‘far-side’ triangles and defined a Delaunay triangulation with near-side triangles. In the same manner, we can define a triangulation with far-side triangles. As we showed in Section 2.4 (in the derivation from equation (2.4.6) to equation (2.4.9)), the circumcircle of the triangle mapped from a near-sided triangle through the inversion transformation does not contain any points of P in its interior. In the same manner, we can show that the circumcircle of the triangle mapped from a far-side triangle through the inversion transformation contains all points of P in its interior or on the boundary. This circumcircle indeed corresponds to the circle referred to in Property FP4.

From Properties OK7 and FP1 (non-empty FP-Voronoi polygons are all unbounded), we obtain the following property.

Property FP5 Let $n_v^{(n-1)}$, $n_e^{(n-1)}$ and $n_f^{(n-1)}$ be the numbers of vertices, edges and FP-Voronoi polygons in \mathcal{V}_{fp} . Then

$$n_v^{(n-1)} = n_f^{(n-1)} - 2 \leq n - 2, \quad (3.3.4)$$

$$n_e^{(n-1)} = 2n_f^{(n-1)} - 3 \leq 2n - 3. \quad (3.3.5)$$

In the above we treated \mathcal{V}_{fp} in \mathbb{R}^2 , but \mathcal{V}_{fp} can be defined in \mathbb{R}^m , $m \geq 2$. For this diagram, we have the following property which corresponds to Property V14 in Chapter 2 (Seidel, 1991).

Property FP6 The maximum number, $n_{\max}(i, m)$, of i -dimensional Voronoi faces of an m -dimensional farthest-point Voronoi diagram is given by:

for $n \leq m + 1$,

$$n_{\max}(i, m) = \binom{n}{m+1-1}; \quad (3.3.6)$$

for $1 \leq m + 1 \leq n$,

$$n_{\max}(i, m) = \begin{cases} C(m-i, m+1) - n+m, & i=0, \\ C(m-i, m+1) - n+m+1, & i=1, \\ C(m-i, m+1), & 2 \leq i \leq m, \end{cases} \quad (3.3.7)$$

where $C(m-i, m+1)$ is given by equation (2.3.14).

The proof is shown in Section 4 in Seidel (1991). The FP-Voronoi diagram in \mathbb{R}^3 is used for finding the farthest point from a point in P , but Edelsbrunner and Sharir (1985) show an alternative method.

In a similar fashion to how we defined the Delaunay triangulation as the dual diagram of the ordinary Voronoi diagram, we can define the dual diagram of the FP-Voronoi diagram by joining generator points p_i and p_j whose FP-Voronoi polygons $V_{fp}(p_i)$ and $V_{fp}(p_j)$ share the common FP-Voronoi edge by the line segment $\overline{p_i p_j}$ (Figure 3.3.1(b)). We call the resulting dual diagram the *farthest-point Delaunay triangulation* (Eppstein, 1992). This diagram has the following property that contrasts to Property D17.

Property FP7 Consider triangulations of the convex hull $\text{CH}(P)$ of a finite set P of distinct points satisfying the non-cocircularity assumption. The triangulation that lexicographically minimizes the sequence of angles, sorted from sharpest to the least sharp, of its triangles is the farthest-point Delaunay triangulation spanning P .

We note the contrast between ‘lexicographically maximized’ in Property D16 and ‘lexicographically minimized’ in Property FP7 (see Property D16). The proof is shown by Eppstein (1992, Theorem 2).

3.3.2 The k th nearest-point Voronoi diagram

The definition of the k th nearest-point Voronoi diagram is similar to that of the order- k Voronoi diagram.

Given a set of distinct points in the Euclidean plane, $P = \{p_1, \dots, p_n\}$ ($2 \leq n < \infty$), we assign a location p in the plane to a point p_i in the point set P if p_i is the k th nearest point from p ; if the k th nearest points are not only p_i but also other points in P , we assign the location to those points. Following this assignment rule, we assign all locations in the plane to at least one point in P . As a result, we obtain a collection of regions associated with points in P , denoted by $\mathcal{V}^{[k]} = \{V^{[k]}(p_1), \dots, V^{[k]}(p_n)\}$, which forms a tessellation.

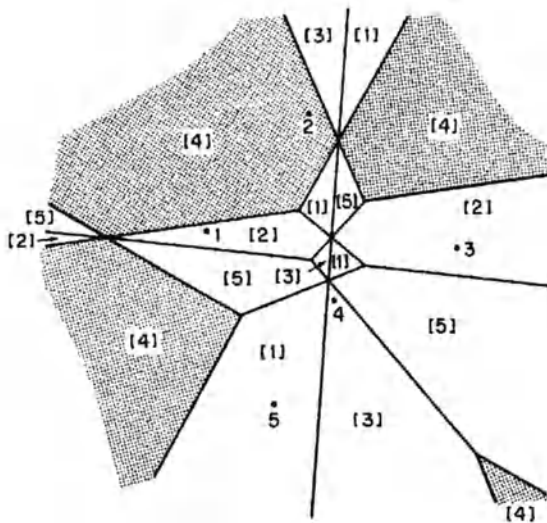


Figure 3.3.2 A third nearest-point Voronoi diagram ($[i]$ indicates $V^{[3]}(p_i)$).

We call the tessellation $\mathcal{V}^{[k]}$ the *kth nearest-point Voronoi diagram* generated by P , or briefly the *KNP-Voronoi diagram* of P , and the region $V^{[k]}(p_i)$ the *kth nearest-point Voronoi region* or the *KNP-Voronoi region* for short. An example is shown in Figure 3.3.2 where $k = 3$.

The definition of the KNP-Voronoi diagram with the dominance region $\text{Dom}(p_i, p_j)$ encounters a difficulty, because it is meaningless to consider the k th nearest point for only two points p_i and p_j . This difficulty is not so crucial because we usually define the KNP-Voronoi diagram through the ordered order- k Voronoi diagram. As a simple example, consider $V^{[2]}(p_1)$ in Figure 3.2.6. The region in which the second nearest point is p_1 is given by $V((p_2, p_1)), V((p_4, p_1))$ and $V(p_5, p_1)$, i.e. $V^{[2]}(p_1) = V((p_2, p_1)) \cup V((p_4, p_1)) \cup V(p_5, p_1)$. Generalizing this equation, we obtain the following property.

Property KNP1

$$V^{[k]}(p_i) = \bigcup_{(p_{j1}, \dots, p_{jk-1}) \in A^{(k-1)}(P \setminus \{p_i\})} V((p_{j1}, \dots, p_{jk-1}, p_i)), \quad (3.3.8)$$

where $A^{(k-1)}(P \setminus \{p_i\})$ is the set of all possible $(k-1)$ -tuples consisting of $k-1$ elements out of $P \setminus \{p_i\}$.

Since this property holds, it is an exercise to derive the properties of the KNP-Voronoi diagram from those of the ordered order- k Voronoi diagram. Here we mention only one distinctive property.

Property KNP2 For $k \geq 2$, a KNP-Voronoi region is not necessarily convex, and may be disconnected.

In fact, $V^{[3]}(p_4)$ in Figure 3.3.2 is disconnected (observe the shaded region).

Generalizing the nearest neighbour problem (Problem P2) in Chapter 2, we have the following problem.

Problem KNP1 (the k th nearest neighbour problem) Given a set of distinct points P , find the k th nearest neighbour point of p_i for all $p_i \in P$.

Once the KNP-Voronoi diagram is given, we immediately obtain the solution. If $p_j \in V^{[k]}(p_i)$, then the k th nearest point is p_j .

3.3.3 Applications

A natural application of the FP-Voronoi diagram is found in a facility location problem in which the k th nearest facility is critical, for instance in the case of a single unit emergency depot when more than one unit is required or when the first nearest unit is in use (Keeney, 1972). The FP-Voronoi diagram is also used for facility location problems of the min-max criteria (Okabe and Suzuki, 1997; Ohsawa and Imai, 1997), for determining the position of a specific object in an image (Ninomiya and Nakagawa, 1991), and finding the minimum radial separation centre which measures out-of-roundness (Le and Lee, 1991; Roy and Zhang, 1994).

An interesting application of the FP-Voronoi diagram is found in an industrial robot attaching a pin-grid array LSI (Large Scale Integrated circuit) to a board (Imai *et al.*, 1989). A print board has a set of holes centred at square grid points; pins of a LSI are fixed in the near neighbourhoods of square grid points (Figure 3.3.3). We wish to know the minimum radius of the holes which contain all the pins.

Problem FP3 (the pin-grid fitting problem) Let $P = \{p_{ij}, i \in I_n, j \in I_m\}$ be a configuration of points exactly placed on square grid points (Figure 3.3.3(b)), and $Q = \{q_{ij}, i \in I_n, j \in I_m\}$ be a configuration of points (Figure 3.3.3(c)) where p_{ij} and q_{ij} have a one-to-one correspondence. Fit P to Q by moving the configuration P through translation and rotation in such a way that the maximum distance between a point in P and its corresponding point in Q is minimized.

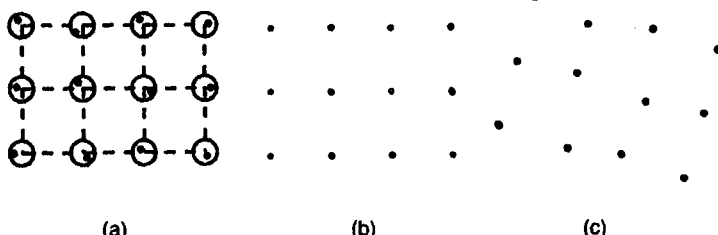


Figure 3.3.3 (a) Fitting holes (the big unfilled circles) of a print board to pins (the filled circles) of a LSI; (b) P ; (c) Q .

This problem can be solved using the FP-Voronoi diagram when the configuration P moves only through translation. To be explicit, let $p_{ij} = (x + a(i - 1), y + a(j - 1))$ and $q_{ij} = (u_{ij}, v_{ij})$. Then the Euclidean distance between p_{ij} and q_{ij} is given by

$$d(p_{ij}, q_{ij}) = \sqrt{(x + a(i - 1) - u_{ij})^2 + (y + a(j - 1) - v_{ij})^2}, \quad (3.3.9)$$

which is written alternatively as

$$d(p_{ij}, q_{ij}) = \sqrt{(x - (u_{ij} - a(i - 1)))^2 + (y - (v_{ij} - a(j - 1)))^2}. \quad (3.3.10)$$

Thus $d(p_{ij}, q_{ij})$ may be regarded as the distance between (x, y) and $(u_{ij} - a(i - 1), v_{ij} - a(j - 1))$. Let $o_{ij} = (u_{ij} - a(i - 1), v_{ij} - a(j - 1))$ and $O = \{o_{ij}, i \in I_{n_1}, j \in I_{n_2}\}$. Then the problem is re-stated as: find the point (x, y) from which the distance to the farthest point in O is the shortest. This problem is exactly the same as the smallest enclosing circle problem referred to above. When the configuration moves not only through translation but also rotation, we need a modification, which will be discussed in Section 3.9. In this connection it is worth noting a similar problem in which we find the minimum Hausdorff distance between two sets of points or line segments under translation. Huttenlocher *et al.* (1993) show how to solve this problem in terms of Voronoi surfaces.

We can find other applications of the KNP-Voronoi diagram in multivariate density estimation (Loftsgaarden and Quesenberry, 1965), classification (Cover and Hart, 1967) and information retrieval systems (Fukunaga and Narendra, 1975; Chazelle, 1985).

3.4 VORONOI DIAGRAMS WITH OBSTACLES

The ordinary Voronoi diagram is defined with the Euclidean distance. The assumption underlying the Euclidean distance is that we can take a straight path between any two points in a region. In some applications, however, this assumption is not acceptable. For example, consider a region in which there exist obstacles, such as rivers and lakes, that prevent traversal. If obstacles lie on the line between an origin and a destination, we cannot traverse straight; we have to make a detour around the obstacles. To deal with such obstacles in a Voronoi diagram, we develop two types of generalized Voronoi diagrams, called the ‘shortest-path’ Voronoi diagram and the ‘visibility-shortest-path’ Voronoi diagram. We also refer to a closely related diagram, called the ‘constrained Delaunay triangulation’.

3.4.1 The shortest-path Voronoi diagram

We consider a generator set consisting of n distinct generator points, $P = \{p_1, \dots, p_n\}$, $p_i \in \mathbb{R}^2$, $i \in I_n$ ($2 \leq n < \infty$), and a set of n_0 closed regions,

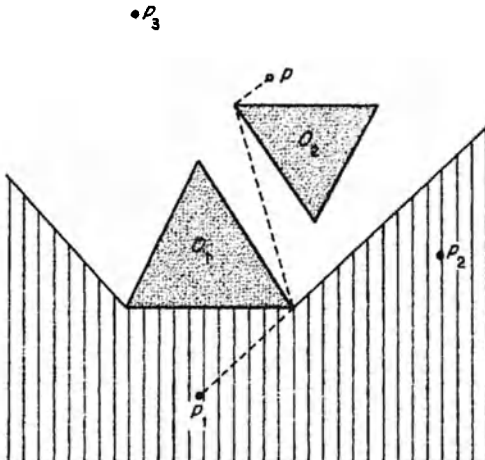


Figure 3.4.1 Generators (the filled circles), obstacles (the shaded areas), the visibility polygon with respect to p_1 (the hatched area) and the shortest path between p and p_1 (the dashed lines).

$O = \{O_1, \dots, O_{n_0}\}$, $(1 \leq n_0 < \infty)$. The set O represents a set of obstacles, which are neither transparent nor traversable. We assume that obstacles do not overlap each other; points of P are not allowed to locate in the obstacles; each obstacle is connected and has no holes. In addition, for analytical as well as computational convenience, we assume that O_i is a polygon (not necessarily convex); O_i may be connected line segments or a line segment; in general, O_i may be represented by a planar straight-line graph). Figure 3.4.1 shows an example of generator points (the filled circles) and obstacles (the shaded area) placed in the plane. The assumption of no holes can be easily relaxed. If a hole has no generator points, points in the hole are not assigned to any generator point. If there are some generator points in the hole, the Voronoi diagram in the hole can be treated as a Voronoi diagram in a simple polygon to be discussed in Section 3.4.3.

In the region $S = \mathbb{R}^2 \setminus O$, we define the distance between a point p and a point p_i in P by the length of the shortest path among all possible continuous paths connecting p and p_i , that do not intersect obstacles $O_i \setminus \partial O_i$, $i \in I_{n_0}$ (note that a path can pass through points on the boundary of O_i). We call this distance the *shortest-path distance* between p and p_i , and denote it by $d_{sp}(p, p_i)$. Alternatively, this distance is sometimes referred to as a *geodesic distance* in the computational geometry literature (Asano and Toussaint, 1987) or the *shortest obstacle-free path* (Mitchell, 1993). In practice, we obtain the shortest-path distance with the aid of a ‘visibility polygon’ and a ‘visibility graph’ (Sharir and Schorr, 1984).

A *visibility polygon*, denoted by $VIS(p_i)$, with respect to p_i is the set of points that are visible from p_i . Mathematically $VIS(p_i)$ is defined by

$$\text{VIS}(p_i) = \{p \mid \overline{p_i p} \cap [O_j \setminus \partial O_j] = \emptyset, \quad p \in \mathbb{R}^2, j \in I_{n_0}\}. \quad (3.4.1)$$

An example is shown in Figure 3.4.1, where the visibility polygon with respect to p_1 is indicated by the hatched area. If p is visible from p_i , there are no obstacles between p and p_i , and hence the shortest-path distance between p and p_i is given by the Euclidean distance, i.e. $d_{sp}(p, p_i) = \|x - x_i\|$ if $x \in \text{VIS}(p_i)$.

Computational methods for constructing a visibility polygon were developed by El Gindy and Avis (1981), Lee (1983), Lee and Chen (1985), Imai et al. (1985), Chazelle and Guibas (1985), Franklin et al. (1985) and others.

A 'visibility graph' is defined for a given geometric graph (Section 1.3). Let $G(Q, L)$ be a given geometric graph, where Q is a set of n_q nodes and L is a set of links (Figure 3.4.2(a)). We assume that links are not transparent. Let L_{vis} be the set of line segments $\overline{q_i q_j}$ satisfying that q_j is visible from q_i , i.e.

$$L_{\text{vis}} = \{\overline{q_i q_j} \mid q_j \in \text{VIS}(q_i), \quad i < j, \quad j \in I_{n_0}\} \quad (3.4.2)$$

(all lines in Figure 3.4.2(b) where $Q = \{q_1, \dots, q_6, p, p_1\}$). Note that line segments in L_{vis} may intersect. The *visibility graph* of $G(Q, L)$ is defined by the graph consisting of Q and L_{vis} , denoted by $G(Q, L_{\text{vis}})$. The computational methods for constructing the visibility graph were developed by Asano et al. (1986), Ghosh and Mount (1991), and Welzl (1985; for line obstacles).

With the aid of a visibility graph we can find the shortest path. As an example, let us obtain the shortest path between p and p_1 in Figure 3.4.1. We first consider the geometric graph $G(Q, L)$ in which Q is given by vertices of the obstacles O , p and p_i , and L is given by the edges of the obstacles O (Figure 3.4.2(a)). Second, we construct the visibility graph $G(Q, L_{\text{vis}})$ of the graph $G(Q, L)$ (Figure 3.4.2(b)). Third, we solve the shortest-path problem on this visibility graph (using, for example, the Dijkstra, 1959, method). Then, the shortest path between p and p_1 on $G(Q, L_{\text{vis}})$ gives the shortest path between p and p_1 in Figure 3.4.1. Note that Guibas et al. (1987) develop an

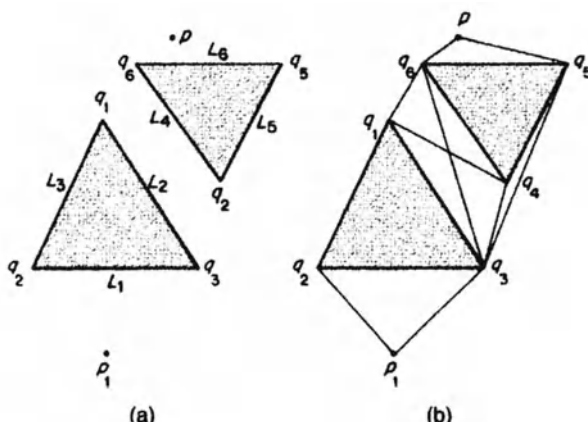


Figure 3.4.2 A shortest-path Voronoi diagram.

alternative efficient method for the shortest path in a simple polygon, Lee and Preparata (1984) for the shortest path in the presence of rectilinear barriers, Wu *et al.* (1987) for the rectilinear shortest path (the shortest path with the Manhattan metric) in the presence of rectilinear obstacles and Storer and Reif (1994) for the shortest path in the presence of polygonal obstacles. Also note that a new method, the 'continuous Dijkstra method' is developed by Mitchell *et al.* (1987) and Mitchell (1991, 1992, 1993, 1996) applying the analogy to wavefront propagation, and that Rajasekaran and Ramaswami (1995) develop a fast algorithm using a mesh-connected computer.

With the shortest path we define

$$V(p_i) = \{p \mid d_{sp}(p, p_i) \leq d_{sp}(p, p_j), j \neq i, j \in I_n\}. \quad (3.4.3)$$

We call this set the *shortest-path Voronoi region* associated with p_i , or briefly the *SP-Voronoi region* of p_i , and the set of SP-Voronoi regions, $\mathcal{V}(P, d_{sp}, \mathbb{R}^2) = \mathcal{V}_{sp} = [V(p_1), \dots, V(p_n)]$, the *shortest-path Voronoi diagram* generated by P with obstacles O , or the *SP-Voronoi diagram* of P with O for short. Alternatively \mathcal{V}_{sp} is called the *geodesic Voronoi diagram* (Asano and Asano, 1987; Aronov, 1989; Papadopoulou and Lee, 1995), or the *nearest-site geodesic Voronoi diagram* (Asano and Toussaint, 1987) (note that they define their diagrams for points in a simple polygon; see Section 3.3). Figure 3.4.3 shows \mathcal{V}_{sp} generated by p_1, p_2 and p_3 with the obstacles O_1 and O_2 in Figure 3.4.1. Tsin and Wang (1996) deal with a SP-Voronoi diagram with a set O of parallel line segments. Mitchell (1992) deals with a SP-Voronoi diagram with the Manhattan metric.

To observe the geometric properties of \mathcal{V}_{sp} , consider the bisector defined in terms of d_{sp} . Figure 3.4.4 shows $b(p_1, p_3)$ with O_1 and O_2 given by the triangles $\Delta q_1 q_2 q_3$ and $\Delta q_4 q_5 q_6$. If a point p is in the region given by $VIS(p_1) \cap VIS(p_3)$ (the hatched region), then the shortest-path distances $d(p, p_1)$ and

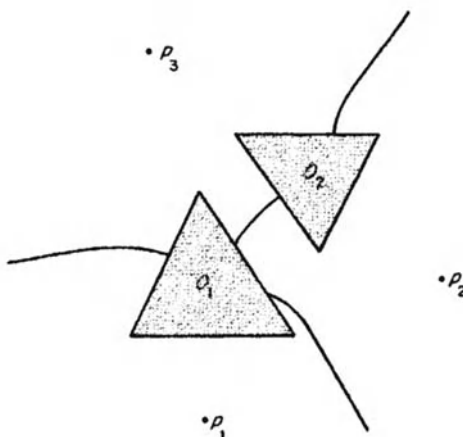


Figure 3.4.3 A geometric graph and its visibility graph.

$d(p, p_3)$ are given by the Euclidean distances. Thus the bisector between p_1 and p_3 in $\text{VIS}(p_1) \cap \text{VIS}(p_3)$ is given by

$$\begin{aligned} b(p_1, p_3) \cap [\text{VIS}(p_1) \cap \text{VIS}(p_3)] \\ = \{x \mid \|x - x_1\| = \|x - x_3\|\} \cap [\text{VIS}(p_1) \cap \text{VIS}(p_3)] \end{aligned} \quad (3.4.4)$$

(the half lines radiating from r_1 and r_7 in Figure 3.4.4). Second, in the region $\text{VIS}(q_2) \cap \text{VIS}(p_3)$ the shortest-path distance $d_{sp}(p, p_3)$ is given by the Euclidean distance, but the shortest-path distance $d_{sp}(p, p_1)$ is given by $\|x - u_2\| + \|u_2 - x_1\|$, where u_2 is the location vector of q_2 . This distance can be regarded as the additively weighted distance with the weight $-\|u_2 - x_1\|$ (equation (3.1.5)). The bisector in $\text{VIS}(q_2) \cap \text{VIS}(p_3)$ is hence given by

$$\begin{aligned} b(p_1, p_3) \cap [\text{VIS}(q_2) \cap \text{VIS}(p_3)] \\ = \{x \mid \|x - u_2\| + \|u_2 - x_1\| = \|x - x_3\|\} \cap [\text{VIS}(q_2) \cap \text{VIS}(p_3)], \end{aligned} \quad (3.4.5)$$

which is a hyperbolic arc (the curved line segment between r_1 and r_2 in Figure 3.4.4). Similarly, the bisector $b(p_1, p_3)$ in $\text{VIS}(q_3) \cap \text{VIS}(p_3)$, $\text{VIS}(q_3) \cap \text{VIS}(q_5)$ and $\text{VIS}(p_1) \cap \text{VIS}(q_5)$ is given by the hyperbolic arcs r_3 and r_4 ; r_5 and r_6 ; and r_6 and r_7 , respectively, in Figure 3.4.4. From this examination we notice that \mathcal{V}_{sp} is closely related to the additively weighted Voronoi diagram.

Like the farthest-point Voronoi diagram shown in Section 3.3, we may define the *farthest-point SP-Voronoi diagram* by replacing $d(p, p_i)$ with $d_{sp}(p, p_i)$ in equation (3.3.1). Alternatively this diagram is called the *geodesic*

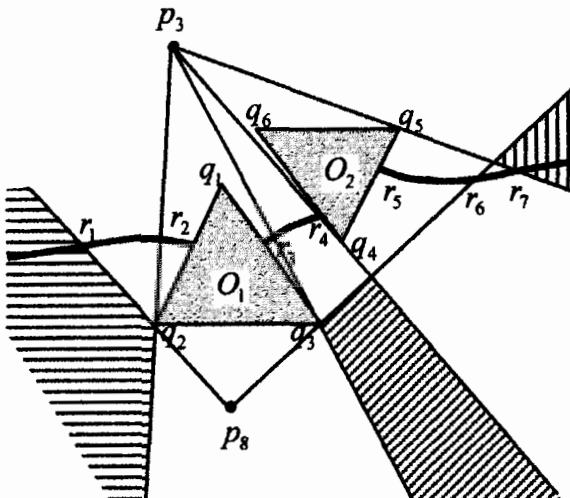


Figure 3.4.4 The bisector between p_1 and p_3 , where the distance is given by the shortest-path distance.

farthest-point Voronoi diagram (Asano and Toussaint, 1987), the *farthest-site Voronoi diagram with the geodesic distance* (Bhattacharya and Toussaint, 1985; Pollack *et al.*, 1989), and the *farthest-site geodesic Voronoi diagram* (Aronov *et al.*, 1993). Guha and Suzuki (1997) formulate the SP-Voronoi diagram with the shortest Manhattan metric avoiding rectangular obstacles.

3.4.2 The visibility-shortest-path Voronoi diagram

In the SP-Voronoi diagram we assumed that obstacles were polygons. Here we assume, for simplicity, that obstacles in O are all line segments that do not intersect each other at their interior points (possibly at their end points). In addition, we assume that the end points of the line segments in O are all generator points of P . Generator points in P are not necessarily end points of the line segments in O ; some points may be isolated. An example is shown in Figure 3.4.6, where generator points are indicated by the filled circles.

Given a set $P = \{p_1, \dots, p_n\}$ of generator points and a set $O = \{O_1, \dots, O_n\}$ of line obstacles, we define a distance by

$$d_{\text{vsp}}(p, p_i) = \begin{cases} \|x - x_i\|, & \text{if } p_i \in \text{VIS}(p), \\ \infty, & \text{otherwise} \end{cases} \quad (3.4.6)$$

This distance implies that if a point p is visible from p_i , the distance is given by the Euclidean distance; if it is not visible, the distance is infinite. We call this distance the *visibility-shortest-path distance* and abbreviate it to the *VSP-distance*, which is sometimes called the *bounded distance* (Aurenhammer, 1988a).

With the VSP-distance, we define the set $V(p_i)$ by equation (3.4.3), where $d_{\text{sp}}(p, p_i)$ is replaced by $d_{\text{vsp}}(p, p_i)$. We call the set $V(p_i)$ the *visibility-shortest-*

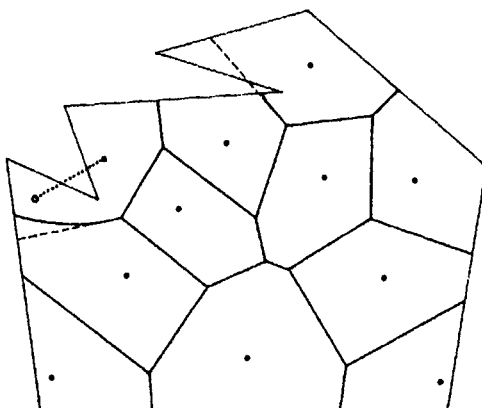


Figure 3.4.5 A Voronoi diagram in a simple polygon (a modification of the bounded Voronoi diagram (the dashed lines) with its SP-Voronoi diagram).

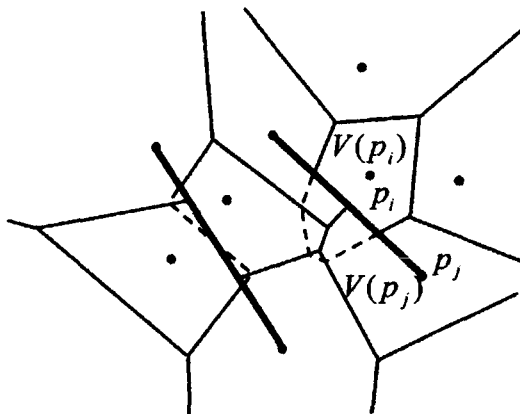


Figure 3.4.6 A visibility-shortest-path Voronoi diagram.

path Voronoi polygon associated with p_j , or briefly the *VSP-Voronoi polygon* of p_j ; the set of VSP-Voronoi polygons the *visibility-shortest-path Voronoi diagram*, \mathcal{V}_{vsp} , generated by P with obstacles O , or the *VSP-Voronoi diagram* of P with O for short. Alternatively, \mathcal{V}_{vsp} may be called the *bounded Voronoi diagram* (Wang and Schubert, 1987; Aurenhammer, 1988a; Djidjev and Lingas, 1991 (generated by vertices of a simple polygon); Klein and Lingas, 1992 (with the L_1 metric)), the *Voronoi diagram with barriers* (Lingas, 1989), or the *constrained Voronoi diagram* (Joe and Wang, 1993; Wang and Chin, 1995) (note that generators of those diagrams are slightly different from those of the VSP-Voronoi diagram defined above). An example of \mathcal{V}_{vsp} is illustrated in Figure 3.4.6 (the continuous lines).

As is seen in Figure 3.4.6, some edges of $\mathcal{V}_{\text{vsp}}(P)$ are the same as those of the corresponding ordinary Voronoi diagram $\mathcal{V}(P)$ and some are not (the broken lines and the continuous lines). A method for finding the difference between $\mathcal{V}_{\text{vsp}}(P)$ and $\mathcal{V}(P)$ is shown by Wang and Schubert (1987). This difference produces different properties, two of which are noted here.

Property VSP1 A VSP-Voronoi polygon may be non-convex (for example, the VSP-Voronoi polygon associated with p_j in Figure 3.4.6).

Property VSP2 Some edges of \mathcal{V}_{vsp} may not be part of a perpendicular line between generators (the boundary formed by an obstacle line); thus a point on an edge of \mathcal{V}_{vsp} may not be equally distant from two (or more) generators.

We note that \mathcal{V}_{vsp} has a special name when O is given by a line with a window and generators are placed on one side of the half plane produced by the line (Figure 3.4.7). This Voronoi diagram is called the *peeper's Voronoi diagram* (Aurenhammer, 1991). We may generalize the VSP-Voronoi diagram

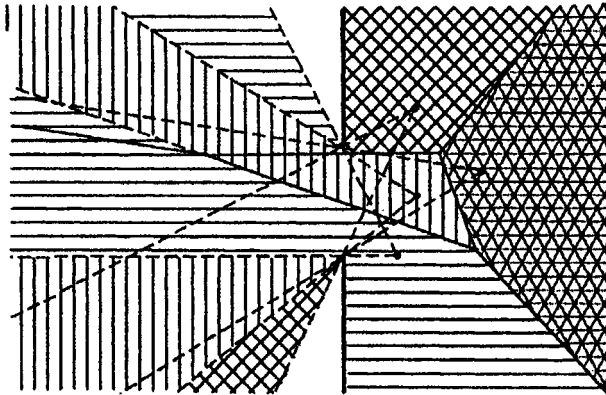


Figure 3.4.7 A peeper's Voronoi diagram.

by replacing the Euclidean distance in equation (3.4.6) with the weighted distance given by equation (3.1.3). We call the resulting diagram the *weighted visibility-shortest-path Voronoi diagram* (Wang and Tsin, 1990, call it the *constrained and weighted Voronoi diagram*).

3.4.3 The constrained Delaunay triangulation

In a similar fashion to how we obtained the Delaunay triangulation from the Voronoi diagram, we may obtain the dual diagram of \mathcal{V}_{vsp} by joining by line segments generators whose VSP-polygons share the common boundaries (note that VSP-polygons sharing obstacle boundaries are not considered as adjacent polygons). An example is shown in Figure 3.4.8(b). This dual diagram is closely related to a diagram, called the ‘constrained Delaunay triangulation’, which has been studied by many: Lee and Lin (1986), Chew (1989a,b), de Floriani and Puppo (1988), Agarwal *et al.* (1989a), Cline and Renka (1990), Jian-ming *et al.* (1990), Lu and Dai (1991), Dai (1991), Renka and Cline (1992), Baker (1992), de Floriani and Puppo (1992b), Sloan (1993), Wang (1993), Joe and Wang (1993), Loze and Saunders (1993), Fang and Piegl (1994), Guha (1994), Anglada (1997), and others. See also Section 6.3.

To be explicit, let $G(P_g, L_g)$ be a planar straight-line graph consisting of a set L_g of straight open line segments, and P_g be a set of end points of the line segments in L_g . Let Q be a set of points that are distinct from those in P_g , and $P = P_g \cup Q$. Note that Q may be empty.

Definition D4 (the constrained Delaunay triangulation) For a given planar straight-line graph $G(P_g, L_g)$ representing obstacles and a set Q of points, the *constrained Delaunay triangulation* is a triangulation spanning $P = P_g \cup Q$ satisfying the condition that the circumcircle of each triangle does not contain in its interior any other vertex which is visible from the vertices of the triangle.

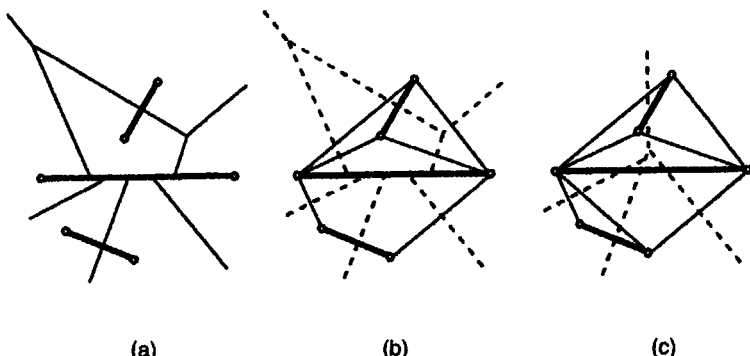


Figure 3.4.8 (a) A VSP-Voronoi diagram, (b) its dual and (c) the corresponding constrained Delaunay triangulation (the heavy lines indicate obstacles).

The constrained Delaunay triangulation is alternatively called the *generalized Delaunay triangulation* (Lee and Lin, 1986), the *obstacle triangulation* (Chew, 1986), and the *restricted Delaunay triangulation* (Sheng and Hirsch, 1992; Anglada, 1997). An example is shown in Figure 3.4.9 where the heavy lines indicate obstacles. Note that software for constructing a constrained Delaunay triangulation is provided by Renka (1996).

The constrained Delaunay triangulation is very useful for interpolation. Suppose that the heavy lines in Figure 3.4.9 are ridges of mountains, and the filled circles are points at which the height is known. In this case, we often want to obtain a triangulation spanning the filled circles whose edges coincide with the ridges. The constrained Delaunay triangulation can provide such a triangulation. Note that the constrained Delaunay triangulation is different from the ordinary Delaunay triangulation, but it is ‘as close as possible’ to the ordinary Delaunay triangulation (Chew, 1989a,b).

One might consider that the dual of the \mathcal{V}_{vsp} is the constrained Delaunay triangulation. This is not true, as is seen in Figure 3.4.8 where panel (b) shows the dual of \mathcal{V}_{vsp} , and panel (c) shows the corresponding constrained Delaunay triangulation. Although both are not completely the same, Joe and Wang (1993) prove that the dual of \mathcal{V}_{vsp} is a subgraph of the corresponding constrained Delaunay triangulation.

The constrained Delaunay triangulation is generally different from the ordinary Delaunay triangulation, but if we add a set S of points on L_g , then the constrained Delaunay triangulation spanning $P \cup S$ may coincide with the ordinary Delaunay triangulation spanning $P \cup S$ (Boissonnat *et al.*, 1988; Weatherill, 1990). We define such a special Delaunay triangulation as follows (Boissonnat *et al.*, 1988; Edelsbrunner and Tan, 1993).

For a given planar straight-line graph $G(P_g, L_g)$ representing obstacles and a set Q of points, we consider a set S of additional points and construct the ordinary Delaunay triangulation $\mathfrak{D}(P_g \cup Q \cup S)$ spanning $P_g \cup Q \cup S$. If all line segments in L_g are the union of the edges of $\mathfrak{D}(P_g \cup Q \cup S)$, we

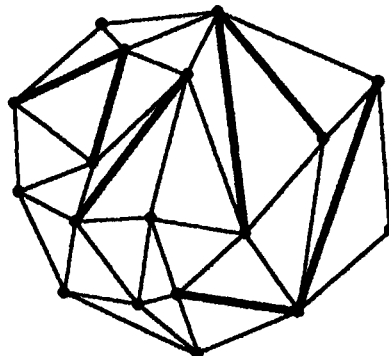


Figure 3.4.9 A constrained Delaunay triangulation (the heavy lines indicate obstacles). (Source: Lee and Lin, 1986, Figure 1.)

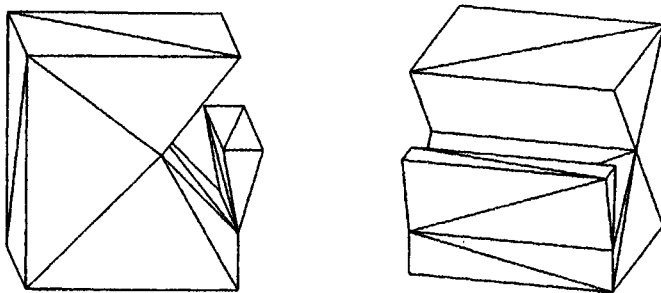


Figure 3.4.10 A domain Delaunay tetrahedrization. (Source: part of Figure 1 in Sapidis and Perucchio, 1991a).

call $\mathcal{D}(P_g \cup Q \cup S)$ the *conforming Delaunay triangulation* (Olooufa, 1991; Saalfeld, 1991; Sapidis and Perucchio, 1991a,b, 1992; Nackman and Srinivasan, 1994; see also Section 6.5.1). Ruppert (1995) calls a similar procedure a *Delaunay refinement*.

We readily notice that if we add many points on L_g , we can obtain the conforming Delaunay triangulation, but we wish to find a small set S . Edelsbrunner and Tan (1993) show an upper bound of such a set.

The constrained Delaunay triangulation can be extended to \mathbb{R}^3 , but its construction becomes harder, because the topology of faces forming a solid becomes complicated. To construct a topologically and geometrically valid Delaunay tetrahedrization, consider a solid S in \mathbb{R}^3 whose faces are given by F_1, \dots, F_k , which may be curved. We construct a triangulation $T(F_i)$ of F_i spanning points placed on F_i such that each edge of F_i corresponds to a unique boundary edge of $T(F_i)$. We call this triangulation the *domain triangulation* of F_i , and $\bigcup_{i=1}^k T(F_i)$ the *domain triangulation* of the boundary of S , denoted by $T(\partial S)$. We next construct a tetrahedrization of S spanning points placed on the surface of S such that its surface triangles are the domain

triangulation of the boundary of S . We call this tetrahedrization the *domain tetrahedrization* of S . Finally, if the domain tetrahedrization of S includes the Delaunay tetrahedra only, the domain tetrahedrization is called the *domain Delaunay tetrahedrization* of S . Sapidis and Perucchio (1991a,b, 1992) develop a computational method for constructing a domain Delaunay tetrahedrization. An example is shown in Figure 3.4.10. Hazlewood (1993) shows a method for approximating constrained tetrahedrization.

De Floriani *et al.* (1996) propose a triangulation using constrained Delaunay triangulations in a hierarchical manner. Let \mathcal{D} be a Delaunay triangulation consisting of triangles $\{T_1^{(0)}, \dots, T_n^{(0)}\}$. For each triangle $T_i^{(0)}$, we construct a constrained Delaunay triangulation of $T_i^{(0)}$ spanning points in $T_i^{(1)}$, i.e. $T_i^{(0)} = T_{i1}^{(1)} \cup \dots \cup T_{in_i}^{(1)}$. Note that this construction is achieved under the condition that adjacent subdivisions are matching. Applying the same procedure successively, we obtain a hierarchical set of Delaunay triangulations. We call this set the *hierarchical Delaunay triangulation*.

3.4.4 SP- and VSP-Voronoi diagrams in a simple polygon

We assumed in Section 2.1 that the boundary Voronoi polygons of a bounded Voronoi diagram, \mathcal{V}_{BS} (equation (2.1.4)), are star-shaped with respect to their generator points in terms of the Euclidean distance. This assumption is made because in many applications the shortest path that traverses outside of S is unrealistic (the dotted line in Figure 3.4.5). If we relax the star-shaped assumption with the Euclidean distance, we should consider the shortest path that is embedded in S (Franklin *et al.*, 1985; Asano and Asano, 1987; Seoung and Asano, 1987; Aronov, 1989). Recalling the SP-Voronoi diagram, the reader may notice that the bounded Voronoi diagram \mathcal{V}_{BS} can be regarded as an SP-Voronoi diagram with the obstacle given by $\mathbb{R}^2 \setminus S$. Figure 3.4.5 shows a modification of the bounded Voronoi diagram (the dashed lines) with its SP-Voronoi diagram. Note that every Voronoi polygon in this modified bounded Voronoi diagram is star-shaped with respect to its generator point in terms of the SP-distance (Aronov, 1989).

We may also consider the VSP-Voronoi diagram in a simple polygon. This diagram is treated by Klein and Lingas (1993) (generator points are vertices of a simple polygon) as an extension of Agarwal *et al.* (1989a). Klein and Lingas (1992, 1993) formulate a VSP-Voronoi diagram in a simple polygon with the Manhattan metric (also see Section 3.7).

3.4.5 Applications

Since an actual space often contains obstacles, Voronoi diagrams with obstacles are useful for relaxing the problems formulated in an ideal space (no obstacles) in the preceding sections. For example, imagine the sea in which there exist islands with ports. The nearest search problem in Chapter 2 in this context is written as: find the nearest port from a given point in the sea avoiding islands. This problem can be solved using the SP-Voronoi diagram.

The constrained Delaunay triangulation can be applied to the triangulation of geological surfaces. Since such surfaces often have faults, the triangulation is restricted by the discontinuity, which can be treated by the constrained Delaunay triangulation (Fowler and Little, 1979; Cline and Renka, 1990). The constrained Delaunay triangulation can also be applied to surface triangulation (Baker, 1992; Zhou *et al.*, 1992; Voigtmann *et al.*, 1994; Park and Kim, 1995), triangulation in a multiply connected region (Weatherill, 1988; Taniguchi *et al.*, 1992; Zhou *et al.*, 1993), cartographic generalization (Ware *et al.*, 1995), robot routing path planning (Chew, 1989a,b; Xie, 1990; Takizawa *et al.*, 1996; Hama and Etoh, 1997), patrol robot planning (Yamamoto *et al.*, 1995), object reconstruction (Boissannat, 1988; Bruzzone *et al.*, 1991), stereo data interpolation (Faugeras *et al.*, 1990; Bruzzone *et al.*, 1992; Takizawa *et al.*, 1996; Lechat *et al.*, 1997), image warping (Ruprecht and Müller, 1995) and multichip module layout (Lu and Dai, 1991; Dai, 1991).

The farthest-point SP Voronoi diagram is utilized to find the *geodesic centre* of points in a simple polygon or that of vertices of a simple polygon (i.e. the centre of points in terms of the SP-distance), and the *geodesic diameter* of a polygon (i.e. the diameter of a polygon in terms of the SP-distance) (Suri, 1989; Pollack *et al.*, 1989). It is shown by Asano and Toussaint (1987) that the geodesic centre of the vertices of a polygon is either the geodesic centre of the polygon or a vertex of the farthest-point SP-Voronoi diagram generated by the vertices of the polygon.

3.5 VORONOI DIAGRAMS FOR LINES

In the preceding four sections, a generator is a point or a set of points. In this section, extending a generator from a point to a line, we consider a generalized Voronoi diagram generated by a set of lines. In theory we can consider a general line, but in practice we deal with points (as a special case of lines), straight lines, chains of straight line segments, circular arcs, chains of circular arcs and full circles. Curved lines may not be exactly represented by those lines, but this restriction is not crucial in practice because we can approximate a curved line by a chain of small straight line segments. In computational geometry a generalized Voronoi diagram for lines has been intensively studied since the late 1970s by Drysdale and Lee (1978), Drysdale (1979), Kirkpatrick (1979), Lee and Drysdale (1981), Imai *et al.* (1985), Kokubo (1985), Sharir (1985), Fortune (1986), Yap (1987), Clarkson and Shor (1989), Goodrich *et al.* (1993), Burnikel *et al.* (1994), Rajasekaran and Ramaswami (1994, 1995), and Deng and Zhu (1996), among others. In this section we mainly follow their results.

We consider a generator set $L = \{L_1, \dots, L_n\} \subset \mathbb{R}^2$ ($1 \leq n < \infty$), where L_i is a point, a line segment (which may be curved) or a geometric element consisting of line segments that are connected. We assume that elements in L do not intersect each other. Under this assumption, we define the distance

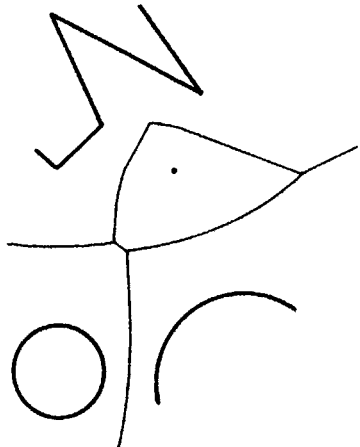


Figure 3.5.1 The line Voronoi diagram generated by the set of a point, a chain of straight line segments, a circular arc and a full circle.

from $p (=x)$ to L_i by the shortest Euclidean distance between p and a point $p_i (=x_i)$ on L_i , i.e.

$$d_s(p, L_i) = \min_{x_i} \{ \|x - x_i\| \mid x_i \in L_i \}. \quad (3.5.1)$$

With this distance, we define

$$V(L_i) = \{ p \mid d_s(p, L_i) \leq d_s(p, L_j), j \neq i, j \in I_n \}. \quad (3.5.2)$$

Alternatively, let

$$\text{Dom}(L_i, L_j) = \{ p \mid d_s(p, L_i) \leq d_s(p, L_j) \}, j \neq i, \quad (3.5.3)$$

Then the set $V(L_i)$ is written as

$$V(L_i) = \bigcap_{j \in I_n \setminus \{i\}} \text{Dom}(L_i, L_j). \quad (3.5.4)$$

Since the dominance region $\text{Dom}(L_i, L_j)$ is well-behaving, the resulting set $\mathcal{V}(L, d_s, \mathbb{R}^2) = \mathcal{V}(L) = \{V(L_1), \dots, V(L_n)\}$ gives a generalized Voronoi diagram. We call this generalized Voronoi diagram the *line Voronoi diagram* generated by L , and the set $V(L_i)$ the *line Voronoi region* associated with L_i . If L_i degenerates into a point for all i , the line Voronoi diagram reduces to the ordinary Voronoi diagram. Figure 3.5.1 shows the line Voronoi diagram generated by the set consisting of a point, a chain of straight lines, a circular arc and a full circle.

The line Voronoi diagram can be defined in the three-dimensional space. Chew *et al.* (1995) examine the combinatorial complexity of the line Voronoi diagram in \mathbb{R}^3 with a polyhedral convex distance (see Section 3.6.2). More generally, Dwyer (1997) examines the Voronoi diagram of random lines and flats in \mathbb{R}^m , $m \geq 3$.

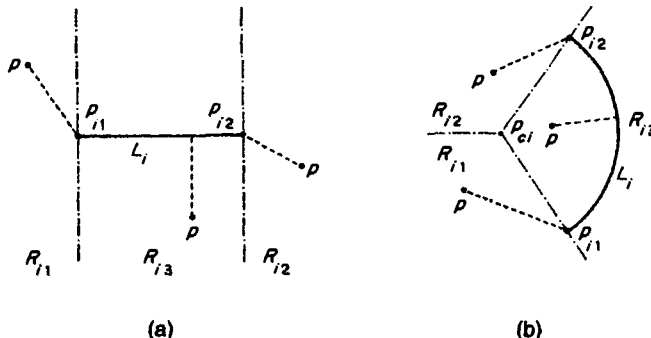


Figure 3.5.2 (a) The distance from a point to a straight line segment; (b) the distance from a point to a circular arc.

3.5.1 Voronoi diagrams for a set of points and straight line segments

In the above definition we consider a general line, but in this subsection we assume that a generator L_i is a point, a straight line segment, or a chain of straight line segments. We also assume that a straight line segment L_i contains both end points. Under these assumptions the shortest distance of equations (3.5.1) is explicitly written as

$$d_s(p, L_i) = \begin{cases} \|x - x_{i1}\| & \text{if } p \in R_{i1}, \\ \|x - x_{i2}\| & \text{if } p \in R_{i2}, \\ \left\| (x - x_{i1}) - \frac{(x - x_{i1})^T(x_{i2} - x_{i1})}{\|x_{i2} - x_{i1}\|}(x_{i2} - x_{i1}) \right\| & \text{if } p \in R_{i3} = \mathbb{R}^2 \setminus [R_{i1} \cup R_{i2}], \end{cases} \quad (3.5.5)$$

where x_{i1} and x_{i2} are the end points of L_i , and $R_{i1} = \{x \mid (x_{i2} - x_{i1})^T(x - x_{i1}) < 0\}$, $R_{i2} = \{x \mid (x_{i1} - x_{i2})^T(x - x_{i2}) < 0\}$ (see Figure 3.5.2(a)).

The bisectors between L_i and L_j with this distance are depicted in Figure 3.5.3, where L_i and L_j are: (a) a point and a point; (b) a point and a straight line segment; and (c) a straight line segment and a straight line segment. In any case, the bisector splits \mathbb{R}^2 into two disjoint regions, and so the dominance region is well-behaving. Thus the set $\mathcal{V}(L, d_s, \mathbb{R}^2)$ with the distance of equation (3.5.5) gives a line Voronoi diagram.

Figure 3.5.4 illustrates the line Voronoi diagram generated by the set L consisting of points, straight line segments and chains of straight line segments (the heavy lines). When we construct this Voronoi diagram, we add a modification to the generator set L to gain analytical and computational tractability. To be explicit, suppose that the first l elements in L are points, i.e. $L_1 = p_1, \dots, L_l = p_l$, and the rest of the elements are straight line segments. As we assumed in the above, a straight line segment or a chain of straight line segments L_i includes both end points, but now we decompose

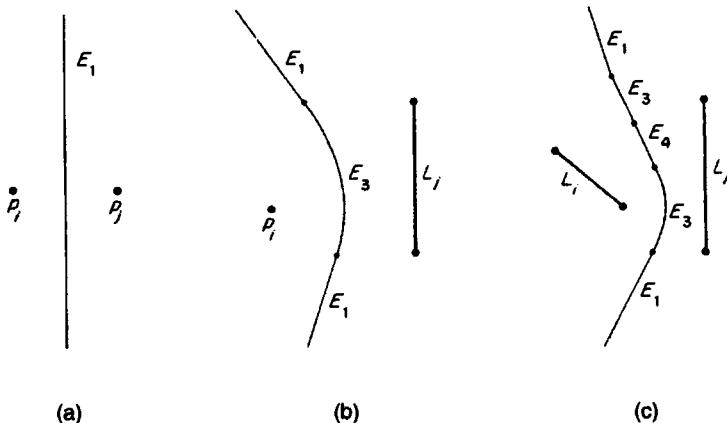


Figure 3.5.3 The bisectors between L_i and L_j , where L_i and L_j are (a) a point and a point; (b) a point and a straight line segment; (c) a straight line segment and a straight line segment.

this line segment into the end points, intermediate points and straight line segments without end points. The set of the points is denoted by $\{p_{ij}, j \in I_{n_i+1}\}$ and the set of the lines is denoted by $\{L_{ij}^o, j \in I_{n_i}\}$ ($n_i = 1$ for a straight line segment). As a result, the generator set L is decomposed into

$$L^{(d)} = \{p_i, i \in I_i\} \cup \left[\bigcup_{i=l+1}^n \{p_{ij}, j \in I_{n_i+1}\} \right] \cup \left[\bigcup_{i=l+1}^n \{L_{ij}^o, j \in I_{n_i}\} \right]. \quad (3.5.6)$$

We call this set the *decomposed generator set* of L . If we decompose the generator set of L in Figure 3.5.4, we obtain the decomposed generator set depicted by the filled circles and the heavy lines in Figure 3.5.5 (where a line segment with small gaps at both ends symbolically indicates a line segment without end points). Since L_i^o does not include end points, the distance of equation (3.5.1) is alternatively defined by

$$d_s(p, L_i^o) = \inf_{x_i} \{\|x - x_i\| \mid x_i \in L_i^o\}, \quad (3.5.7)$$

where ‘inf’ is an infimum operator (Section 1.3). Using this decomposed generator set with this distance, we generate the line Voronoi diagram $\mathcal{V}(L^{(d)})$, which is indicated by the light solid lines and the broken lines in Figure 3.5.5 (Reddy and Turkiyyah, 1995, call $\mathcal{V}(L^{(d)})$ the generalized Voronoi diagram of a *mixed dimensional set*.) Obviously, the edges of $\mathcal{V}(L)$ are included in $\mathcal{V}(L^{(d)})$. We can hence obtain $\mathcal{V}(L)$ from $\mathcal{V}(L^{(d)})$ by deleting the unnecessary edges indicated by the broken lines in Figure 3.5.5.

Like the ordinary Delaunay triangulation defined as the dual of the ordinary Voronoi diagram, we may consider the dual of $\mathcal{V}(L^{(d)})$ for separated line segments (Figure 3.5.6; Dehne *et al.*, 1991, Figure 13). Reddy and Turkiyyah (1995) call this dual diagram the *generalized Delaunay triangulation*. It should be noted, however, that the vertices of the generalized

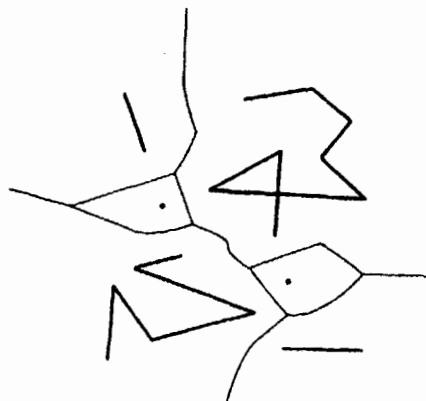


Figure 3.5.4 A line Voronoi diagram generated by the set consisting of points, two straight lines and two chains of straight line segments.

Delaunay triangulation do not have a specific geometric meaning; a Delaunay edge merely indicates the existence of a non-redundant edge.

As is noticed from Figures 3.5.4 and 3.5.5, the line Voronoi diagram $\mathcal{V}(L^{(d)})$ of the decomposed set $L^{(d)}$ is a refinement of the line Voronoi diagram $\mathcal{V}(L)$ of L . This refinement is fundamental in the sense that every edge in $\mathcal{V}(L^{(d)})$ is part of a unique conic curve. For this reason, we examine the geometric properties of $\mathcal{V}(L)$ through $\mathcal{V}(L^{(d)})$.

From equation (3.5.4) with Figure 3.5.3, we notice the following property.

Property L1 No line Voronoi region in $\mathcal{V}(L^{(d)})$ is empty. A line Voronoi region of a point to which three or more lines are incident is a point.

Substituting equation (3.5.5) into equation (3.5.3), we obtain the following property.

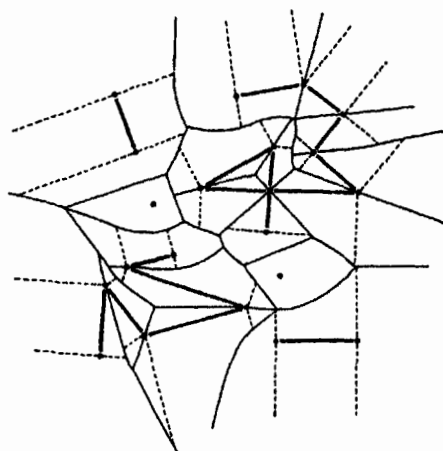


Figure 3.5.5 The line Voronoi diagram generated by the decomposed generator set obtained from the generator set in Figure 3.5.4.

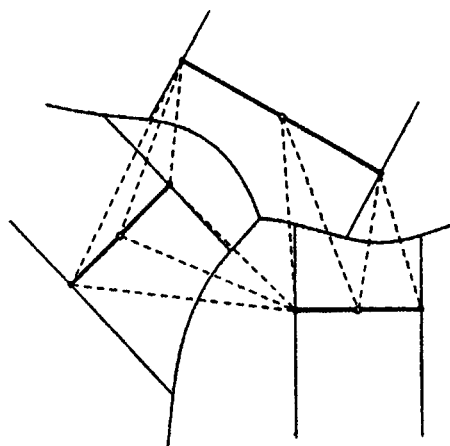


Figure 3.5.6 The dual of a line Voronoi diagram, called the generalized Delaunay triangulation (the broken lines).

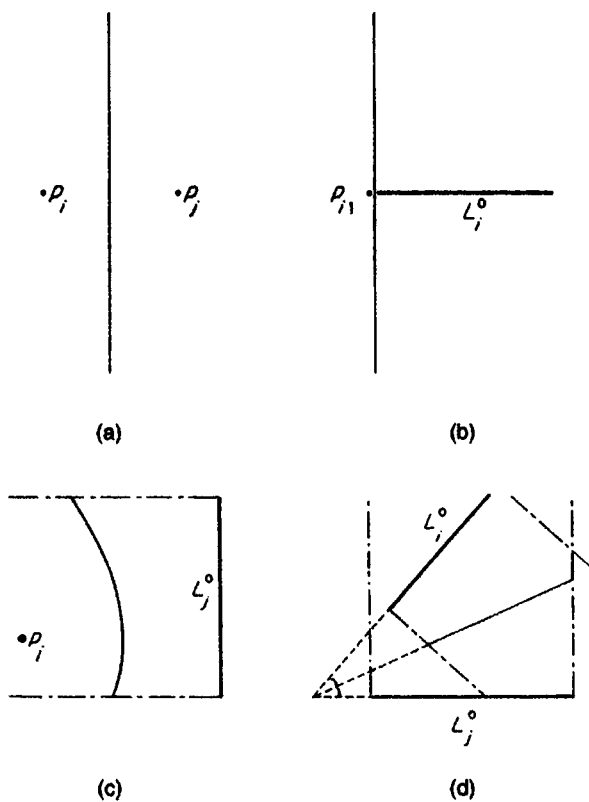


Figure 3.5.7 Four types of edges in a line Voronoi diagram: (a) type E1; (b) type E2; (c) type E3; (d) type E4.

Property L2 Edges in $\mathcal{V}(L^{(d)})$ are straight lines or parabolic arcs. These edges can be classified into the following four types according to the types of generators generating the edges.

Type E1. An edge generated by points p_i and p_j . The edge is the straight line perpendicularly bisecting $\overline{p_i p_j}$ (Figure 3.5.7(a)).

Type E2. An edge generated by a straight line segment L_i^o , and its end point $p_{i1} \in \partial L_i$. The edge is the straight line perpendicular to L_i^o passing through p_{i1} (Figure 3.5.7(b)).

Type E3. An edge generated by a point p_i and a straight line segment L_j^o ($p_i \notin \partial L_j$). The edge is the locus of a point p satisfying the condition that the distance from p to p_i is equal to the distance from p to the line L_j . This locus is known as a parabolic arc whose focus is p_i and whose directrix is L_j^o (Figure 3.5.7(c)).

Type E4. An edge generated by straight line segments L_i^o and L_j^o . The edge is the straight line dividing the angle made by L_i^o and L_j^o (Figure 3.5.7(d)).

The reader should not confuse Figures 3.5.7(c) and (d) with Figures 3.5.3(b) and (c). The bisectors in Figure 3.5.3 are generated by the generators that are not decomposed. Using Property L2, the reader should confirm that the bisectors in Figures 3.5.3(b) and (c) consist of edges of types E1, E3 and E4. In Figure 3.5.3 we indicate the type of each edge by E1–E4.

As a consequence of Property L2, we obtain the following property.

Property L3 A line Voronoi region $V(L_i)$ is not necessarily convex.

When exactly three edges are incident at every vertex in a line Voronoi diagram, we say that the line Voronoi diagram is *non-degenerate*. Regarding a non-degenerate line Voronoi diagram $\mathcal{V}(L^{(d)})$, we obtain the following property from Property L2.

Property L4 Vertices $\{q_i\}$ in a non-degenerate line Voronoi diagram can be classified into the following six types according to the types of three edges, e_{i1} , e_{i2} and e_{i3} , which are generated by three generators.

Type V1. A vertex q_i generated by points p_i , p_j and p_k . The edges e_{i1} , e_{i2} and e_{i3} are all type E1 (Figure 3.5.8(a)).

Type V2. A vertex q_i generated by a point p_i , a straight line segment L_i^o , and its end point $p_{i1} \in \partial L_i$. The edges are types E1, E2 and E3. The edge of type E1 and that of type E3 are tangent at the Voronoi vertex q_i (Figure 3.5.8(b)).

Type V3. A vertex q_i generated by a straight line segment L_i^o and two points p_j and p_k which are not the end points of L_i . The edges are types E1 and E3. The edges of type E3 have the common directrix L_i^o (Figure 3.5.8(c)).

Type V4. A vertex q_i generated by two straight line segments L_i^o and L_j^o , and its end point $p_{i1} \in L_i^o$. The edges are types E2, E3 and E4. The edges of type E3 and E4 are tangent at q_i (Figure 3.5.8(d)).

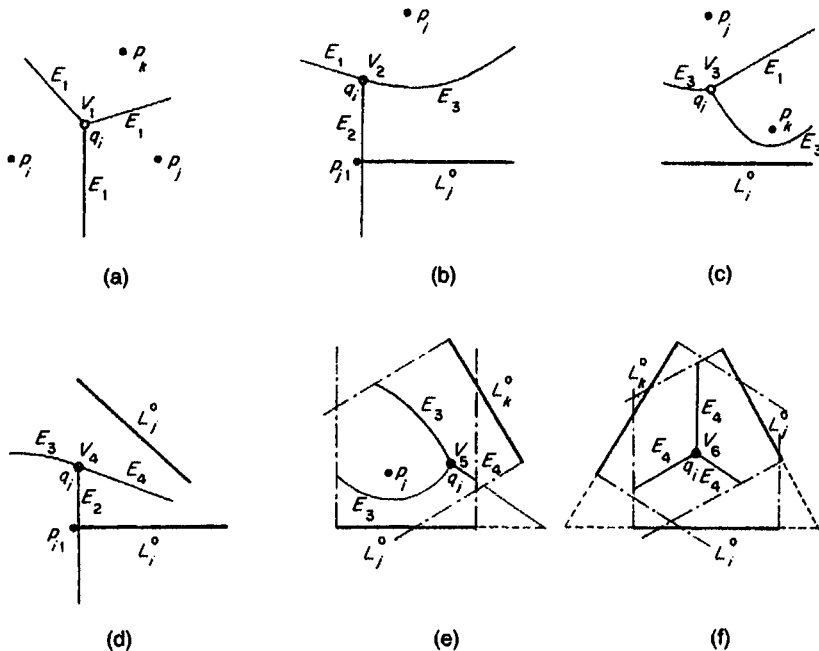


Figure 3.5.8 Types of vertices in a line Voronoi diagram: (a) type V1; (b) type V2; (c) type V3; (d) type V4; (e) type V5; (f) type V6.

Type V5. A vertex q_i generated by a point p_i and two straight line segments L_j^o and L_k^o ($p_i \notin \partial L_j$, $p_i \notin \partial L_k$). The edges are types E3 and E4 (Figure 3.5.8(e)).

Type V6. A vertex q_i generated by straight line segments L_j^o , L_k^o and L_l^o . The edges are type E4. The extended lines of L_j^o , L_k^o , and L_l^o form a triangle. If q_i is inside this triangle, q_i is its inscribed centre. If q_i is outside the triangle, q_i is one of its excentres (Figure 3.5.8(f)).

In Figure 3.5.8, types of vertices are indicated by V1–V6 with edge types. Finally, almost the same derivation used in Property V2 leads to the following property.

Property L5 A line Voronoi region $V(L_i^o)$ is unbounded if and only if L_i^o is on the boundary of the convex hull of $L^{(d)}$.

3.5.2 Voronoi diagrams for a set of points, straight line segments and circular arcs

We now add circular arcs to the generator set examined in the preceding subsection. For computational convenience we assume that a circular arc is less than or equal to a semicircle. We treat a circular arc greater than a semicircle as two circular arcs connected at a point, and a full circle as two

semicircles connected at two points. For a circular arc with radius r_i centred at \mathbf{x}_{ci} , the shortest distance of equation (3.5.1) is explicitly written as

$$d_s(p, L_i) = \begin{cases} \|\mathbf{x} - \mathbf{x}_{ii}\| & \text{if } \mathbf{x} \in R_{ii}, \\ \|\mathbf{x} - \mathbf{x}_{iz}\| & \text{if } \mathbf{x} \in R_{iz}, \\ |\|\mathbf{x} - \mathbf{x}_{ci}\|| - r_i & \text{if } \mathbf{x} \in R_{iz} = \mathbb{R}^2 \setminus [R_{ii} \cup R_{iz}], \end{cases} \quad (3.5.8)$$

where R_{ii} , R_{iz} and R_{iz} are the regions defined in Figure 3.5.2(b).

Since the dominance region is well-behaving, a generator set consisting of points, straight line segments and circular arcs gives a line Voronoi diagram. An example is depicted in Figure 3.5.1. We construct this Voronoi diagram in the same manner as we employed in the preceding subsection. First, we decompose a given generator set L and next construct the line Voronoi diagram for the decomposed generator set $L^{(d)}$. The line Voronoi diagram $\mathcal{V}(L)$ is obtained from the line Voronoi diagram $\mathcal{V}(L^{(d)})$ by deleting superfluous edges.

To observe the geometric property of the line Voronoi diagram, let $L_{pl}^{(d)}$ be the decomposed generator set consisting of points and straight lines, and $L_{plc}^{(d)}$ be the decomposed generator set consisting of points, straight lines and circular arcs (the subscript ‘plc’ indicates points, lines and circles). Since the line Voronoi diagram $\mathcal{V}(L_{pl}^{(d)})$ is a special case of the line Voronoi diagram $\mathcal{V}(L_{plc}^{(d)})$, some properties of $\mathcal{V}(L_{pl}^{(d)})$ mentioned in Section 3.5.1 hold in such a special case. In fact, Properties L1, L3 and L5 of $\mathcal{V}(L_{plc}^{(d)})$ hold for $\mathcal{V}(L_{pl}^{(d)})$. Also Property L2 of $\mathcal{V}(L_{pl}^{(d)})$ holds for $\mathcal{V}(L_{plc}^{(d)})$, but we should add the following six types.

Property L7 Edges in $\mathcal{V}(L_{plc}^{(d)})$ are straight line segments, parabolic arcs, elliptic arcs and hyperbolic arcs. Those edges can be classified into ten types according to the types of generators generating the edges. The first four types are given by E1–E4 in Property L2.

Type E5. An edge generated by a circular arc L_i^o and a point $p_j \notin \partial L_i$ which is inside the circle containing L_i^o centred at p_{ci} . The edge is the locus of a point p satisfying the condition that the total distance from p to two fixed points p and p_{ci} is constant, which is known as an elliptic arc whose foci are p_{ci} and p_j (Figure 3.5.9(a)).

Type E6. An edge generated by a circular arc L_i^o and a point $p_j \notin \partial L_i$ which is outside the circle containing L_i^o centred at p_{ci} . The edge is the locus of a point p satisfying the condition that the difference between the distances from p to p_{ci} and p_j is constant. This locus is known as a branch of a hyperbolic curve whose foci are p_{ci} and p_j (Figure 3.5.9(b)).

Type E7. An edge generated by a circular arc L_i^o and its end point $p_{i1} \notin \partial L_i$. The edge generated by these generators is a straight line radiating from the centre of the circle containing L_i^o to p_{i1} (Figure 3.5.9(c)).

Type E8. An edge generated by a circular arc L_i^o and a straight line containing L_j^o , which intersects the circle containing L_i^o centred at p_{cj} with radius r_i (note that $L_i^o \cup L_j^o = \emptyset$). The edge is the locus of a point p satisfying the

condition that the sum of the distances from p to the line L_i^o and to the fixed point p_{ci} is constant. This locus is known as a parabolic arc whose focus is p_{ci} and whose directrix is the line parallel to L_i at distance r_i (Figure 3.5.9(d)).

Type E9. An edge generated by two circular arcs L_i^o and L_j^o where the circle containing L_i^o centred at p_{ci} is contained in the circle containing L_j^o centred at p_{cj} . The edge is an elliptic arc whose foci are p_{ci} and p_{cj} (Figure 3.5.9(e)).

Type E10. An edge generated by two circular arcs L_i^o and L_j^o where the circle containing L_i^o centred at p_{ci} intersects the circle containing L_j^o centred at p_{cj} or the former circle is outside of the later circle. The edge is a branch of a hyperbolic curve whose foci are p_{ci} and p_{cj} (Figure 3.5.9(f)).

Note that the types of a bisector between a point and a parametric curve are classified by Farouki and Johnstone (1994), and those of a bisector between a point and a curve and that between a curve and a curve are classified by Kim *et al.* (1995) using rational quadratic Bézier curves. Also note that Haladar and Patnaik (1990) examine the bisector between monotone algebraic curve segments.

3.5.3 Voronoi diagrams for a set of circles

In the literature, special attention is paid to a line Voronoi diagram generated by a set L_c of full circles. To generate this special Voronoi diagram, we have to define a distance from a point to a circle. In the literature, several distances are proposed. Probably the most natural distance is given by the shortest distance of equation (3.5.1), which is explicitly written as

$$d_{cl}(p, L_i) = \left| \|x - x_{ci}\| - r_i \right|, \quad (3.5.9)$$

where L_i is the circle centred at p_{ci} with radius r_i . A line Voronoi diagram $\mathcal{V}(L_c)$ generated by a set of circles with this distance is a special case of the line Voronoi diagram $\mathcal{V}(L_{plc})$ defined in the above subsection (the generator set is a set of paired semicircles). Hence the line Voronoi diagram $\mathcal{V}(L_c)$ shares the properties of $\mathcal{V}(L_{plc})$ mentioned above. In Figure 3.5.10 we depict the line Voronoi diagram generated by two intersecting circles. The reader should confirm the types of edges using Property L7.

Lee and Drysdale (1981) and Sharir (1985) employ a similar but slightly different distance given by

$$d_{c2}(p, L_i) = \|x - x_{ci}\| - r_i. \quad (3.5.10)$$

This distance is not a metric because it may take a negative value. The difference between $d_{cl}(p, L_i)$ and $d_{c2}(p, L_i)$ appears when $d_{cl}(p, L_i)$ and $d_{c2}(p, L_i)$ have different signs. We can observe this difference in Figure 3.5.10 where panel (a) uses $d_{cl}(p, L_i)$ and panel (b) uses $d_{c2}(p, L_i)$. The elliptic curve does not appear if we employ $d_{c2}(p, L_i)$. The properties of this line Voronoi diagram are examined in detail by Sharir (1985). We also note that if the

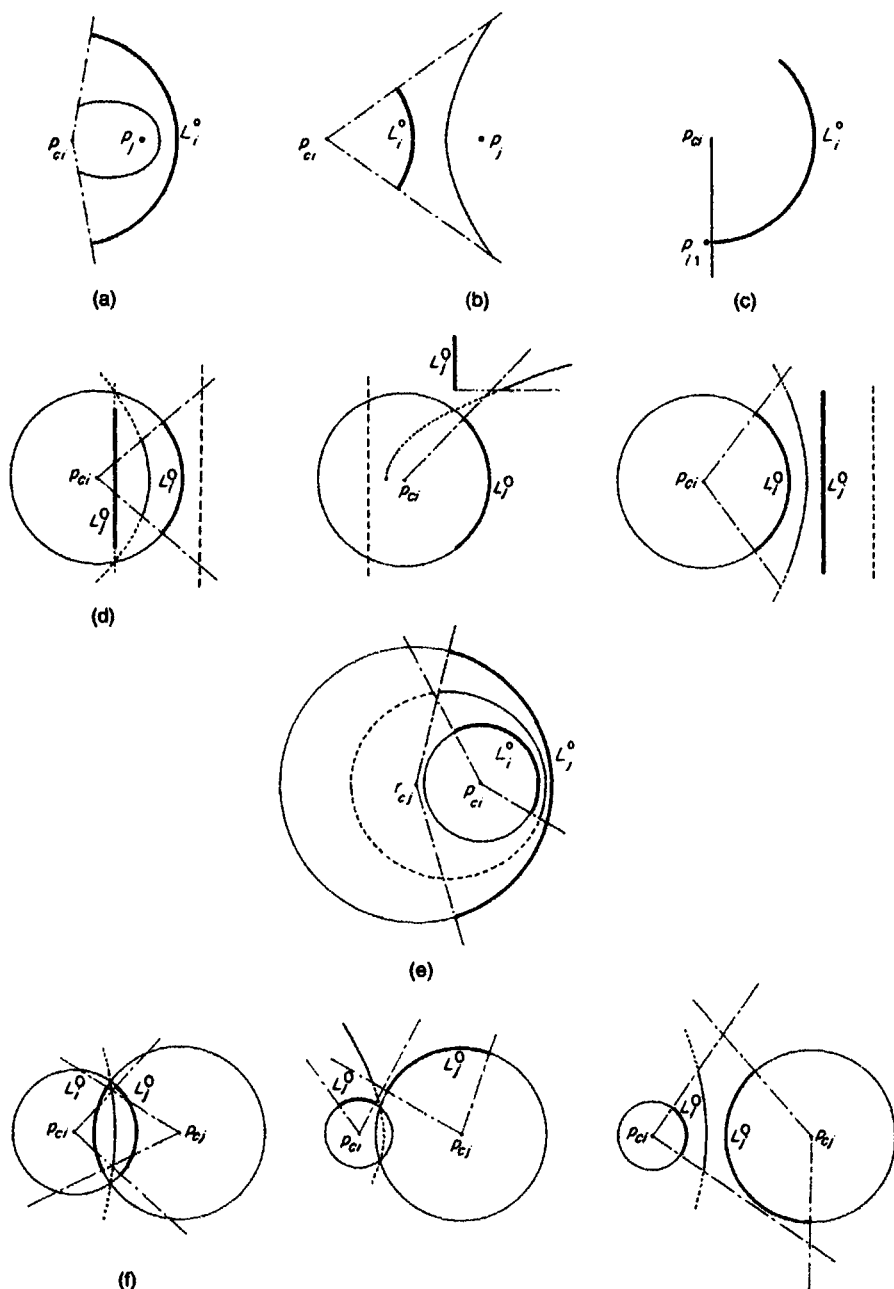


Figure 3.5.9 Types of edges generated by a circular arc and a point, a straight line or a circular arc: (a) type E5; (b) type E6; (c) type E7; (d) type E8; (e) type E9; (f) type E10.

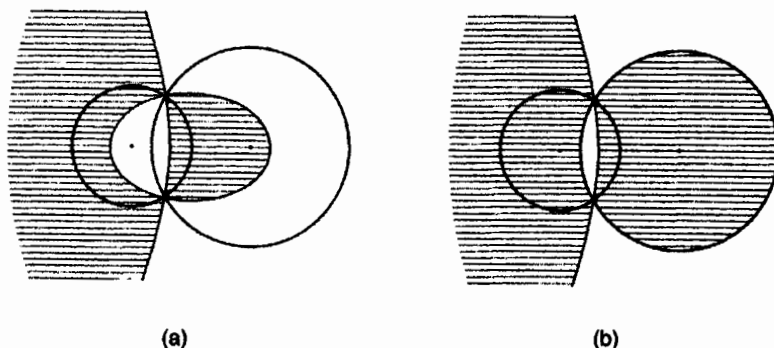


Figure 3.5.10 The line Voronoi diagrams generated by two intersecting circles with (a) the distance given by equation (3.5.9), and (b) the distance given by equation (3.5.10).

circles do not overlap, the distance $d_{c1}(p, L_i) = d_{c2}(p, L_i) = \|x - x_{ci}\| - r_i$ is the additively weighted distance (equation (3.1.5) in Section 3.1); thus $\mathcal{V}(L_c)$ reduces to the AW-Voronoi diagram.

A fairly different distance is employed by Aurenhammer (1988a,b), Imai *et al.* (1985), Telly *et al.* (1992, 1996), which is given by

$$d_{c3}(p, L_i) = \|x - x_{ci}\|^2 - r_i^2. \quad (3.5.11)$$

If p is outside the circle, $\sqrt{d_{c3}(p, L_i)}$ indicates the distance from point p to the point p_i on L_i , where $\overline{pp_i}$ is tangential to L_i at p_i (the broken line in Figure 3.5.11). We call the line Voronoi diagram with this distance the *Laguerre Voronoi diagram* or *Laguerre diagram*. This term is named after Laguerre geometry in which a point $(x, y, z) \in \mathbb{R}^3$ corresponds to a directed

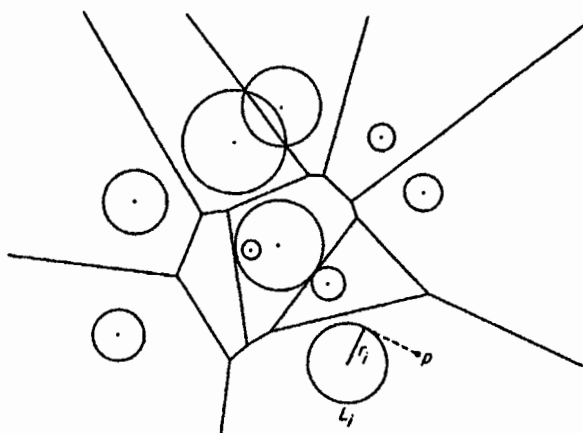


Figure 3.5.11 The Laguerre Voronoi diagram.

circle centred at (x, y) with radius $|z|$ on \mathbb{R}^3 . The bisector with this distance is given by a radical axis in \mathbb{R}^2 and a radical plane in \mathbb{R}^3 , and hence the Laguerre Voronoi diagram may be called the *radical axis Voronoi diagram* or *radical axis tessellation* (Gellatly and Finney, 1982c; Weaire and Rivier, 1984; Venema, 1991). Note that Venema (1991) also defines the *radical axis triangulation* as the dual of the radical axis Voronoi diagram. Also note that since the distance of equation (3.5.11) is the power distance, the Laguerre Voronoi diagram is exactly the same as the power Voronoi diagram (Section 3.1.4).

Extending the closest pair problem for a set of points (Problem V1 in Section 2.3), we may consider the closest problem for a set of circles. In fact, Sharir (1985) develops a computational method for this problem.

3.5.4 Medial axis

In conjunction with the line Voronoi diagram, we refer to a ‘medial axis’ which is often applied in shape analysis (Blum, 1967). The medial axis can be defined for a connected geometric figure C (disconnected regions can be treated separately; a polygon C may have holes, called the *multiply connected polygonal domain* (Srinivasan and Nackman, 1987; Meshkat and Sakkas, 1987; Srinivasan *et al.*, 1992; Mayya and Rajan, 1996)). The *medial axis* is defined as the locus of all points that have at least two closest points on the boundary of C . Alternatively, the *medial axis* can also be defined as the locus of the centres of all the interior maximal disks of C , where a *maximal disk* is a disk which is not contained by any other disks that are included in C (the disks in Figure 3.5.12(a)) (Pfaltz and Rosenfeld, 1967; Peleg and Rosenfeld, 1981; Held, 1993, calls it a *clearance disk*). The medial axis may be intuitively understood if we imagine a grassfire in a prairie. The set C represents a region covered with grass and the region C is surrounded by a wetland. Suppose that the border of the region C is set on fire. Then the subsequent internal quenching points of the fire represent the medial axis (Blum, 1973; Blum and Nagel, 1978; Leymarie and Levine, 1992; Dehne and Klein, 1997 (who generalize this idea)). Stated a little more precisely, the *medial axis* of C is

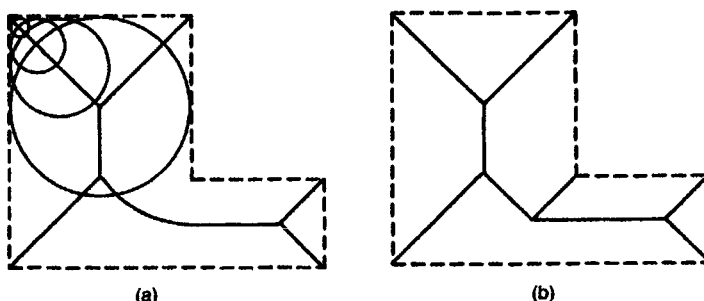


Figure 3.5.12 A medial axis with a maximal disk (a) and a straight skeleton (b).

the set $M(C)$ of points x in C for which there exist at least two distinct points, x_i and x_j , on the boundary of C such that the distance between x and x_i is the same as that between x and x_j , and these distances are both the minimum distance between x and a point on the boundary of C . Mathematically,

$$M(C) = \left\{ x \mid \|x - x_i\| = \|x - x_j\| = \min \{ \|x - y\| \mid y \in \partial C \}, \begin{array}{l} x_i \neq x_j, x_i, x_j \in \partial C, x \in C \end{array} \right\}. \quad (3.5.12)$$

A point $x \in M(C)$ is called a *skeletal point* (Mayya and Rajan, 1996). The medial axis of C is alternatively called the *symmetric axis* (Blum 1973), (*continuous*) *skeleton* (Montanari, 1968, 1969; Kirkpatrick, 1979) or *stick figure* (Blum, 1967) of C . An example is illustrated in Figure 3.5.12(a). The transform from C into $M(C)$ is called the *medial axis transform* (Blum, 1967), *symmetric axis transform* (Blum, 1973), *skeletonization* (Smith, 1987) or *Blum's transform* (Aurenhammer, 1991). Fukushima and Okumura (1991) and Fukushima (1997) propose a modified symmetric axis transform, called the *division-based analysis of symmetry*.

Let $R(x) = \min_u \{ \|x - u\| \mid u \in \partial C, x \in M(C)\}$, which is the radius of the maximal disk, $D_{\max}(x)$, centred at a point x on the medial axis $M(C)$. The function $R(x)$ is called the *radius function* of the maximal disk (in the analogy to the grassfire, the time of quenching for unity velocity propagation is the radius function). From the definitions of the medial axis and the radius function, we note the following property (Gürsoy and Patrikalakis, 1991, 1992).

Property L8 The medial axis is unique for a given figure C . The figure C can be exactly reconstructed by taking the union of all maximal disks with radius equal to the radius function $R(x)$ on the medial axis $M(C)$, i.e. $C = \bigcup_{x \in M(C)} D_{\max}(x)$.

Note that other theoretical properties of $M(C)$ are discussed in depth by Calabi and Hartnett (1968) and Chou (1995).

The definition of $M(C)$ by equation (3.5.12) is applicable to \mathbb{R}^3 . In this case, however, $M(C)$ is called the *medial (axis) surface* and $D_{\max}(x)$ is called the *maximal sphere*. An example is shown in Figure 3.5.13. Computational methods for constructing medial surfaces are developed by many: Nackman and Pizer (1985), Goldak *et al.* (1991), Sherbrooke *et al.* (1996), Reddy and

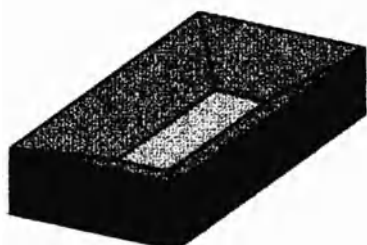


Figure 3.5.13 A medial surface of a rectangular parallelepiped.

Turkiyyah (1995), Sheehy *et al.* (1996), Turkiyyah *et al.* (1997), Näf *et al.* (1997), and others.

The medial axis method can treat a polygonal figure as well as a curved figure C . When a figure C is a polygon, we can obtain its medial axis by the use of the line Voronoi diagram (Kirkpatrick, 1979; Lee, 1982a). First, we decompose a set, L , of line segments forming the boundary of C (the dashed line in Figure 3.5.12(a)) into $L^{(d)}$ as we did in Section 3.5.1. Second, we generate the line Voronoi diagram $\mathcal{V}(L^{(d)})$ by the decomposed generator set $L^{(d)}$. Recalling the property that points on the edges of line Voronoi regions are equally distant from generator lines (the boundaries of the geometric figure), we notice that the medial axis is included in the edges in $\mathcal{V}(L^{(d)})$. Deleting unnecessary edges in $\mathcal{V}(L^{(d)})$, we obtain the medial axis of C (the solid line in Figure 3.5.12(a)). Because of this, the medial axis is sometimes called the *Voronoi skeleton* (Ogniewicz and Ilg, 1992; Näf *et al.* (1997)) or *Voronoi medial axis* (Ogniewicz and Kübler, 1995).

The detailed computational methods for vector data (i.e. C is represented by vectors) are shown in Preparata (1977), Kirkpatrick (1979), Lee (1982a), Yao and Rokne (1991), Devillers (1992), Klein and Lingas (1995) and Imai (1996). When C is represented by raster data as in image analysis, some special treatments are necessary, and alternative computational methods are developed by Rosenfeld and Pfaltz (1966), Pfaltz and Rosenfeld (1967), Montanari (1968), Peleg and Rosenfeld (1981), Smith (1987; a review), Xia (1989), Brandt and Algazi (1992), and Arcelli and Baja (1993).

When the boundary of C is curved, we usually approximate C by a polygon C' , and obtain the medial axis for C' by applying the line Voronoi diagram (Montanari, 1968; Lee, 1982a). This method, however, may suffer from computational burden because C' has many edges to approximate to C . To overcome this burden, a simple method was proposed by Blum and Nagel (1978), which has been developed by Boissonnat and Kofakis (1985), Yun (1989), Brandt and Algazi (1991, 1992), Goldak *et al.* (1991), Brandt (1994) and Sheehy *et al.* (1996). First, we approximate C by C' . Second, we construct the Delaunay triangulation spanning the vertices of C' . Third, we classify the resulting triangles into inside triangles and outside triangles (the triangles that are not included in C'). Last, we join the centres of any two Delaunay disks by line segments if they are adjacent. We call the resulting set of line segments the *discrete medial axis* of C (Goldak *et al.*, 1991; Yu *et al.*, 1991; Ogniewicz and Kübler, 1995). Obviously, the discrete medial axis of C is not exactly the same as the true medial axis. Schmit (1988), Goldak *et al.* (1991), Brandt and Algazi (1992), and Brandt (1994) examine the degree of this approximations theoretically. Roughly speaking, if the shape of C is ‘nice’ (r -nice in Brandt, 1994), increasingly dense vertices of the polygon C' give rise to increasingly accurate approximations of the true medial axis. Marston and Shih (1995) develop a multi-scale representation for the approximation levels of C' .

As is seen in Figure 3.5.12(a), the medial axis may include a curved line. Alternatively, Aichholzer and Aurenhammer (1996) propose the axis of a

polygonal figure C consisting of only straight line segments, called the *straight skeleton* (for more general figures, see Aichholzer and Aurenhammer, 1996). Intuitively the straight skeleton is given by the ridges of roofs that rise from the edges of the figure C at the same slant. An example is shown in Figure 3.5.12(b).

The Voronoi diagram may be alternatively defined in terms of the medial axis (Ó'Dúnlaing and Yap, 1985). If we replace ∂C by $P = \{p_1, \dots, p_n\}$, and C by \mathbb{R}^2 in equation (3.5.12), i.e.

$$\begin{aligned} M(P) = \{x \mid \|x - x_i\| = \|x - x_j\| = \min_y \{\|x - y\| \mid y \in P\}, \\ x_i \neq x_j, x_i, x_j \in P, x \in \mathbb{R}^2\}, \end{aligned} \quad (3.5.13)$$

then, $M(P)$ coincides with the Voronoi edges of the planar ordinary Voronoi diagram generated by P . Similarly, for a set L of line segments, we may modify $M(C)$ as

$$\begin{aligned} M(L) = \{x \mid \|x - x_i\| = \|x - x_j\| = \min_y \{\|x - y\| \mid y \in L_1 \cup \dots \cup L_n\}, \\ x_i \neq x_j, x_i, x_j \in L_1 \cup \dots \cup L_n, x \in \mathbb{R}^2\}. \end{aligned} \quad (3.5.14)$$

We might expect that $M(L)$ coincides with the Voronoi edges of the line Voronoi diagram generated by L (or $L^{(d)}$). This is true when L consists of separated line segments, but it is not always true in general. For example, when L is a set of connected line segments or a set of curved line segments, $M(L)$ does not always form a tessellation. An example of the former case is shown in Figure 3.5.14 (or Figure 4 in Lavender *et al.*, 1992), and the latter case by Alt and Schwarzkopf (1995, Figure 1).

3.5.5 Applications

Okabe and Fujii (1984) showed a possible application of the line Voronoi diagram for testing the effect of car emissions on withered trees along expressways. The same method was used by Okabe and Yoshikawa (1989) and Yoshikawa and Okabe (1991) to test the effect of arterial streets on the

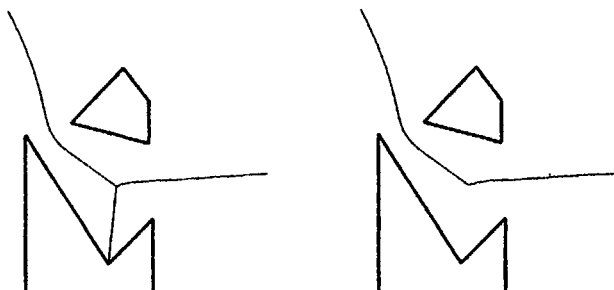


Figure 3.5.14 (a) The modified medial axis for a set L of lines defined by equation (3.5.14) and (b) the line Voronoi diagram generated by L .

distribution of apartment buildings in the Setagaya and Kohto-Sumida districts in Tokyo (see Section 8.3.2).

In converting contour lines in a raster format to those in a vector format, we often have a problem of inconsistent contour lines, such as crossing contour lines and broken contour lines. To search for such errors, Mizutani *et al.* (1993) use the line Voronoi diagram. Using the topology of the line Voronoi diagram they suggest how to correct these errors. A closely related method is also proposed by Kawashima *et al.* (1994), Gold *et al.* (1996) and Gold (1997).

Zaninetti (1991b) uses the line Voronoi diagram in \mathbb{R}^3 to analyse the distribution of galaxies. Medvedev (1994) and Anishchik and Medvedev (1995) apply the Voronoi diagram for circles to a packing problem found in dense granular systems. This problem dates back to the *Appollonian packing problem*: find the circle inscribed among three given circles in a plane. Rounse *et al.* (1990) deal with particles on a two-dimensional section in terms of the Voronoi diagram for ellipsoids. The same diagram is also used for directional clustering (Reyes and Adjouadi, 1997).

Gellatly and Finney (1982c) use the radical axis Voronoi diagram for the characterization of crystalline structures when atoms have different sizes, and Venema (1991) uses the same diagram to examine muscle fibre patterns. Telly *et al.* (1992) use the Laguerre Voronoi diagram as geometric idealization of two dimensional polycrystals. Gerstein *et al.* (1995) propose a similar diagram with a slightly different distance which reflects the size of atoms. See also the related applications shown in Section 7.1.

The medial axis associated with the line Voronoi diagram in a simple polygon is applied to shape analysis (Blum, 1967, 1973; Philbrick, 1968; Blum and Nagel, 1978; Lee, 1982a; Brady, 1983; Rosenfeld, 1979), pattern recognition (Calabi and Hartnett, 1968; Fujii, 1976), character recognition or font generation (Hobby, 1993), object identification of overlapping objects (Kübler *et al.*, 1990; Ogniewicz and Ilg, 1992), image processing (Smith, 1987; Lantuejoul and Maisonneuve, 1984; Tam and Armstrong, 1991), mesh generation (Srinivasan *et al.*, 1992 (a review); Gürsoy and Patrikalakis, 1992, among others), pocket machining (Held, 1991, 1993; Lambregts *et al.*, 1996), design rule checking (Meshkat and Sakkas, 1987), documentation analysis (Ilg, 1990), segmentation (Chassery and Melkemi, 1990), motion planning (see the Voronoi diagram with convex distances in Section 3.7.2), and so forth.

Applications of the straight skeleton are found in architecture (Recuero and Gutiérrez, 1993), a data structure for finding pairwise interactions (Eppstein and Erickson, 1998), and origami constructions (Lang, 1996).

The line Voronoi diagram is closely related to the buffer zones of lines often used in geographical information systems. The boundaries of the buffer zone give parallel lines to generator lines, which may be used in spatial analysis (Okabe and Fujii, 1984). The problem of determining lines that are parallel to the edges of a polygon is called the *offset problem*, and is studied by Tiller and Hanson (1984), Sutherland (1990) and Hoschek (1985). The line Voronoi diagram can also be applied to the optimization of service lines (Takeda, 1985; see Chapter 9).

3.6 VORONOI DIAGRAMS FOR AREAS

Noticing that the preceding subsection has extended a generator from a point to a line, the reader might expect that the next extension would be from a line to an area. This extension is actually possible and useful in many applications.

3.6.1 The area Voronoi diagram

We consider a set of areas, $A = \{A_1, \dots, A_n\}$ ($2 \leq n < \infty$), in \mathbb{R}^2 . We assume that A_i is a connected closed set and areas do not overlap each other. An area A_i is not necessarily convex, and may have holes in which another area may exist. Under these assumptions, we define a distance from a point to an area A_i as the shortest Euclidean distance from p to A_i , i.e.

$$d_s(p, A_i) = \min_{x_i} \{ \|x - x_i\| \mid x_i \in A_i \}, \quad (3.6.1)$$

where x and x_i are the location vectors of p and p_i , respectively. With this distance, we define a set by

$$V(A_i) = \{p \mid d_s(p, A_i) \leq d_s(p, A_j), j \neq i, i, j \in I_n\}. \quad (3.6.2)$$

We call this set the *area Voronoi region* associated with A_i , and the set of area Voronoi regions, $\mathcal{V}(A) = \{V(A_1), \dots, V(A_n)\}$, the *area Voronoi diagram* generated by the generator set A . Mathematically, an area includes a line and a line includes a point. Thus the area Voronoi diagram includes the line Voronoi diagram, which includes the ordinary Voronoi diagram. Figure 3.6.1(a) shows an area Voronoi diagram. We may restrict the set A to a set of special figures. Rappaport (1992) deals with the area Voronoi diagram generated by a set of disks.

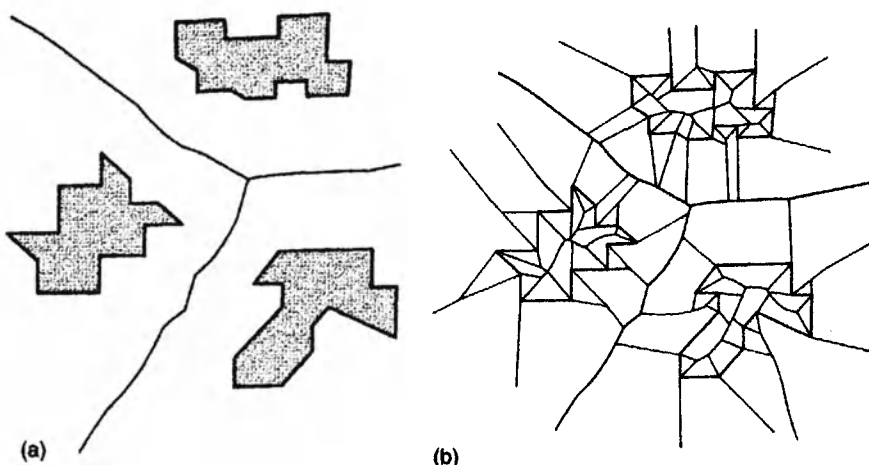


Figure 3.6.1 (a) An area Voronoi diagram and (b) its corresponding line Voronoi diagram.

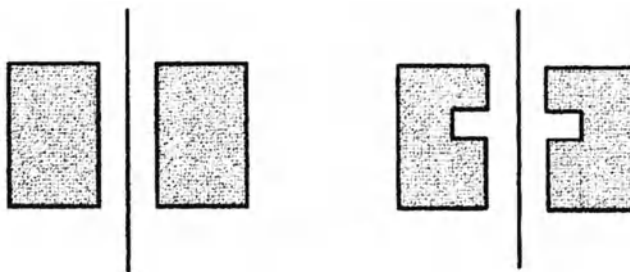


Figure 3.6.2 The same area Voronoi diagrams generated by two different sets of areas.

The area Voronoi diagram is unique for a given set of areas, but the converse is not true (Jones, 1991). Different sets of areas may give the same area Voronoi diagram. An example is shown in Figure 3.6.2.

An area (which does not degenerate into a line) appears different from a line, but computationally the area Voronoi diagram is quite similar to the line Voronoi diagram. As a matter of fact, we construct an area Voronoi diagram from its corresponding line Voronoi diagram. To be explicit, let $L(A)$ be the set of the boundaries of A , i.e. $L(A) = \{\partial A_1, \dots, \partial A_n\}$. We first construct the line Voronoi diagram with $L(A)$ (Figure 3.6.1(b)). We next delete the superfluous edges. Then the remaining edges form the area Voronoi diagram (Figure 3.6.1(a)). As is noticed from this procedure, some properties of the area Voronoi diagram are similar to those of the line Voronoi diagram. It should be noted, however, that the properties of the line Voronoi diagram that are related to the inside of a circuit chain or a circle are not applicable to those of the area Voronoi diagram. For instance, an elliptical curve does not appear in the area Voronoi diagram because the curve only appears inside a circle.

We may extend the order- k Voronoi diagram for points (Section 3.2) to that for areas. If we replace p_i with A_i and $d(p, p_i)$ with $d_s(p, A_i)$ in equation (3.2.3), we obtain a tessellation, which we call the *order- k area Voronoi diagram* (Roos, 1989). We present two properties similar to Property OK7 shown in Roos (1989).

Property OKA1 Let $n, n_a^{(k)}, n_v^{(k)}, n_e^{(k)}, n_u^{(k)}$, and $n_c^{(k)}$ be the number of generator polygons, Voronoi polygons, Voronoi vertices, Voronoi edges, unbounded Voronoi polygons, and connected components of Voronoi edges, respectively. For $1 \leq k \leq n - 1$, the following equations hold:

$$n_e^{(k)} = 3n_a^{(k)} - n_u^{(k)} - n_c^{(k)} - 2, \quad (3.6.3)$$

$$n_v^{(k)} = 2n_a^{(k)} - n_u^{(k)} - n_c^{(k)} - 1. \quad (3.6.3)$$

Property OKA2 For $2 \leq k \leq n - 1$, the following relation holds:

$$n_a^{(k)} \leq (2k - 1)n - (k^2 - k) - \sum_{i=1}^{k-1} (n_u^{(k)} + n_c^{(k)}). \quad (3.6.5)$$

An extension of the area Voronoi diagram in \mathbb{R}^3 is a Voronoi diagram generated by three-dimensional solid objects (which may be represented by polyhedra). We may call it a *solid object Voronoi diagram*.

3.6.2 Applications

Yoshikawa *et al.* (1987) and Okabe *et al.* (1988) examined the effect of large parks on the distribution of high-class apartment buildings in Tokyo using the area Voronoi diagram (see Section 8.3.3). Fujii (1983), Fujii and Oikawa (1986) and Oikawa (1986) determine the sphere of influence of parks with the weighted area Voronoi diagram, where the weights reflect the area of a park. Boggs (1951) and Ricketts (1986) dealt with the delimitation of seaward areas under national jurisdiction which implicitly uses the area Voronoi diagram, where areas correspond to national domains. Tagare *et al.* (1995) use the area Voronoi diagram to evaluate the similarity of tomographic sections. Edwards (1993) clarifies the linguistic structure of space (such as ‘inside’–‘outside’, ‘near’–‘far’) in terms of the area Voronoi diagram; similarly Gold (1992) interprets the meaning of neighbour. Edwards *et al.* (1996) apply the line and area Voronoi diagram to route descriptions expressed in natural language. Burge and Monagan (1995a,b) apply the area Voronoi diagram to grouping words and multi-part symbols in documents. Gold (1989a) shows that the area Voronoi diagram is useful to determine the spatial adjacency between objects in a map, e.g. the spatial adjacency between a house and a road. Lam and Ip (1994) and Ip and Lam (1995) examine the structural texture using the area and solid object Voronoi diagrams.

The area Voronoi diagram is often used in robot path planning (Lozano-Pérez, 1981). Consider a region in which obstacles are placed and a disk-shaped robot is supposed to move avoiding these obstacles (Ó'Dúnaing and Yap, 1985; Krozel and Andrisani II, 1989 (who approximate an area Voronoi diagram by a Voronoi diagram for a set of vertices of generator polygons); Rao *et al.*, 1991). The area in which the robot can move without collision is called the *free placements* (Kedem and Sharir, 1985) or *free configuration space* (Aronov and Sharir, 1994) or *free space* for short. The free space is readily obtained by the complement of the area enclosed by the parallel lines at distance r from the obstacles, where r is the radius of the disk robot.

Voronoi edges of an area Voronoi diagram included in the free space may be regarded as *collision-free paths* along which the robot can move without collision. Recalling the property of a Voronoi edge, we notice that a point on a Voronoi edge is equally distant from at least two polygons, A_i and A_j , and that the minimum distance in $\{d_s(q, A_i), d_s(q, A_j)\}$ for points q in a sufficiently small neighbourhood of p achieves maximum when $q = p$. In this sense, we may say that the collision-free paths given by Voronoi edges in the free space are the safest paths.

When we determine the size (radius) of a disk robot, the critical size is given by the minimum distance between the polygonal objects, which is called

the *bottleneck width*. We can find the bottleneck width by using the area Voronoi diagram, because the centre of the critical disk is found in a Voronoi vertex of the area Voronoi diagram generated by the polygonal objects.

The problem of robot motion planning occurs in a three-dimensional space where objects are solid objects. In this case, we may use the solid object Voronoi diagram. Such an application is discussed in Meng (1987), Latombe (1991) and Quin *et al.* (1995). The solid object Voronoi diagram is also used to analyse patterns of capillary blood vessels in the human liver (Saito and Toriwaki, 1992).

When the shape of a robot is not a disk, we have to use another area Voronoi diagram, which is discussed in depth in the next section.

3.7 VORONOI DIAGRAMS WITH V-DISTANCES

As we mentioned in the introduction of Chapter 3, we can define a generalized Voronoi diagram with any distance as long as the distance is a V-distance. The distance is not necessarily the Euclidean distance. In fact, we showed in the preceding sections that the multiplicatively weighted distance, the additively weighted distance, the compoundly weighted distance, the power distance and the shortest-path distance, which are not the Euclidean distance, produced generalized Voronoi diagrams. In this section we show other generalized Voronoi diagrams defined with various kinds of V-distances. First, we deal with V-distances defined in \mathbb{R}^m (in particular, $m = 2$) and next V-distances defined on surfaces in \mathbb{R}^3 .

3.7.1 Voronoi diagrams with the Minkowski metric L_p

We begin with a Voronoi diagram defined with the Minkowski metric in \mathbb{R}^m . The *Minkowski (power) metric* from a point p to a point p_i in \mathbb{R}^m is defined by

$$d_{L_p}(p, p_i) = \left[\sum_{j=1}^m |x_j - x_{ij}|^p \right]^{1/p}, \quad (3.7.1)$$

where (x_1, \dots, x_m) and (x_{i1}, \dots, x_{im}) are the Cartesian coordinates of p and p_i , respectively. Customarily, the symbol L_p is used for the Minkowski metric, where p refers to the degree of the power. The reader should not confuse the symbol p for a point with p of the degree of the power. The parameter p varies in the range of $1 \leq p < \infty$. If $p = 1$, equation (3.7.1) becomes

$$d_{L_1}(p, p_i) = \sum_{j=1}^m |x_j - x_{ij}|, \quad (3.7.2)$$

which is called the *Manhattan metric*, the *city-block distance* or the *taxi-cab distance*. If $p = 2$, the Minkowski metric is the Euclidean distance. If $p = \infty$, the Minkowski metric is called the *supremum metric* or *dominance metric*, which is alternatively written as

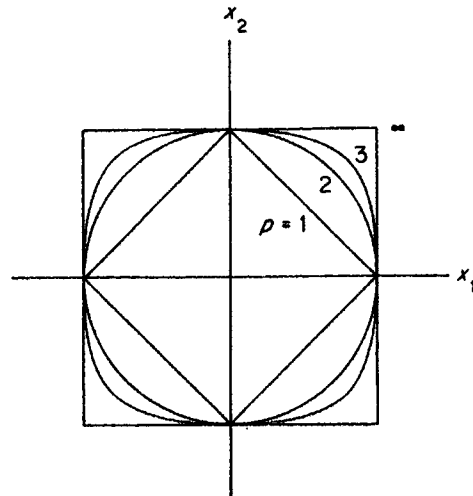


Figure 3.7.1 The contour lines of the Minkowski metric L_p for $p = 1, 2, 3, \infty$.

$$d_{L_\infty} = \max_j \{ |x_j - x_{ij}|, j \in I_m \}. \quad (3.7.3)$$

Figure 3.7.1 shows the contours of the Minkowski metric from the origin for $p = 1, 2, 3, \infty$.

The geometric properties of Voronoi diagrams with the Minkowski metrics L_p vary drastically according to the value of p ($1 \leq p \leq \infty$). We first consider a planar Voronoi diagram defined with the Manhattan metric. To see its geometric properties, let us observe the bisector defined with the Manhattan metric. From equation (3.7.2) ($p = 1$), we notice that the shape of the bisector varies according to the parameter value $\alpha = (x_{j2} - x_{i2})/(x_{j1} - x_{i1})$, where $x_{j1} \geq x_{i1}$ is assumed without loss of generality. We have eight possible types: (i) $-\infty < \alpha < -1$; (ii) $-1 < \alpha < 0$; (iii) $0 < \alpha < 1$; (iv) $1 < \alpha < \infty$; (v) $\alpha = \pm\infty$; (vi) $\alpha = 0$; (vii) $\alpha = -1$; and (viii) $\alpha = 1$. However, those types are essentially grouped into three types: I = (i)–(iv); II = (v) and (vi); and III = (vii) and (viii), which are shown in Figure 3.7.2. The bisector of type I consists of three straight lines as depicted in Figure 3.7.2(a). The diagonal line segment has angle $\pi/4$ or $3\pi/4$ with the x_1 -axis. This bisector is well-behaving. The bisector of type II is a straight line (Figure 3.7.2(b)), which is also well-behaving. The bisector of type III, however, is not well-behaving. In this case, as is indicated by the shaded area in Figure 3.7.2(c), the bisector consists of not only a straight line but also an area. To avoid this indeterminacy, we usually define the bisector as the straight perpendicular line bisecting $\overline{p_i p_j}$ (the solid and dashed lines in Figure 3.7.2(c)).

Once the above modification is made, the bisector becomes well-behaving, and hence the set $\mathcal{V}_M = \{V(p_1), \dots, V(p_n)\}$ defined in terms of $V(p_i) = \bigcap_{j \in I_M \setminus \{i\}} \text{Dom}(p_i, p_j)$ with equation (3.7.2) ($p = 1$) gives a generalized Voronoi diagram. We call the set \mathcal{V}_M the *Manhattan-metric Voronoi diagram* generated

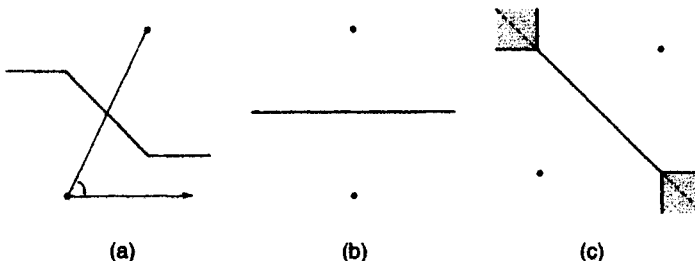


Figure 3.7.2 The bisector $b(p_i, p_j)$ defined with the Manhattan metric: (a) the bisector of type I ($\infty < \alpha < -1$, $-1 < \alpha < 0$, $0 < \alpha < 1$, $1 < \alpha < \infty$); (b) the bisector of type II ($\alpha = \pm\infty, 0$); (c) the bisector of type III ($\infty = \pm 1$); where $\alpha = (x_{j2} - x_{i2})/(x_{j1} - x_{i1})$ and where $x_{j1} \geq x_{i1}$ is assumed without loss of generality.

by P or the *Manhattan Voronoi diagram* in brief, and the set $V(p_i)$ the *Manhattan(-metric) Voronoi polygon* associated with p_i (Carter *et al.*, 1972; Hwang, 1979; Lee, 1980; Lee and Wong, 1980; Guha, 1993). An example is illustrated in Figure 3.7.3. Jeong (1991) and El Gindy and Wetherall (1995) develop computational methods with parallel computing, and Melter and Stojmenović (1995) develop a parallel computational method for the discrete Manhattan Voronoi diagram (see the discrete Voronoi diagram in Section 2.1).

From the properties of the bisector mentioned above with Figure 3.7.2, we note the following properties.

Property M1 The set $V(p_i)$ defined by $V(p_i) = \bigcap_{j \in I_n \setminus \{i\}} \text{Dom}(p_i, p_j)$ with the Manhattan metric (equation (3.7.2)) is not empty, and forms a (Manhattan Voronoi) polygon. The Manhattan Voronoi polygon $V(p_i)$ is not necessarily convex, but it is always star-shaped with respect to the generator p_i .

Property M2 Every edge of a Manhattan Voronoi polygon consists of at most three straight lines which are parallel to the x_1 -axis, x_2 -axis, or diagonal lines with angle $\pi/4$ or $3\pi/4$.

Property M3 The Manhattan Voronoi polygon $V(p_i)$ is unbounded if p_i is on the boundary of the convex hull of P , but not conversely.

Compared with Property V2 of the ordinary Voronoi diagram, the converse relation in Property M3 should be noted. An actual example is found in the Manhattan Voronoi polygon of p_1 in Figure 3.7.3. In addition to the above properties, Guha (1993) shows several properties that are utilized for parallel computing. Boissonnat *et al.* (1995) show the combinatorial complexity properties of \mathcal{V}_M in \mathbb{R}^3 .

A quite similar Voronoi diagram to the Manhattan Voronoi diagram is the Voronoi diagram defined with the supremum metric, which we call the

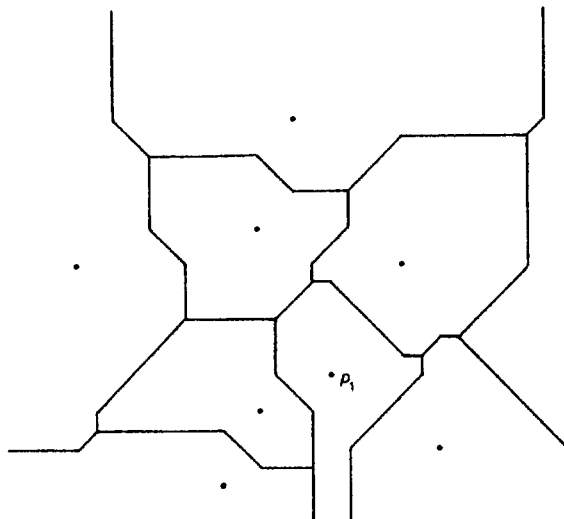


Figure 3.7.3 A Manhattan-metric Voronoi diagram.

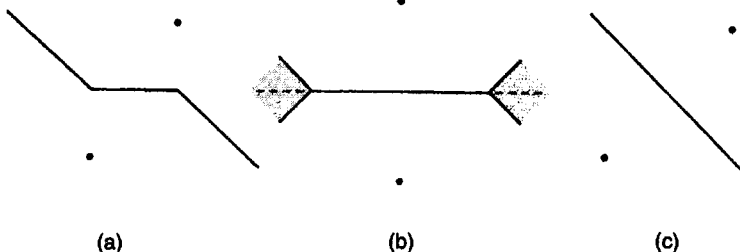


Figure 3.7.4 The bisector defined with the supremum metric: (a) the bisector of type I ($\infty < \alpha < -1$, $-1 < \alpha < 0$, $0 < \alpha < 1$, $1 < \alpha < \infty$); (b) the bisector of type II ($\alpha = \pm \infty$); (c) the bisector of type III ($\alpha = \pm 1$); where $\alpha = (x_{j2} - x_{i2})/(x_{j1} - x_{i1})$ and where $x_{ji} \geq x_{ii}$ is assumed without loss of generality.

supremum-metric Voronoi diagram. To see this similarity, we depict the bisector of the supremum metric in Figure 3.7.4 in which the locations of the generators are the same as those of the bisector of the Manhattan metric in Figure 3.7.2.

Comparing Figure 3.7.4(b) with Figure 3.7.2(c), we notice that if we rotate the x_1-x_2 plane in Figure 3.7.2(c) with generators counterclockwise by $\pi/4$, we obtain Figure 3.7.4(b). Generally, if we rotate the bisector defined with the Manhattan metric counterclockwise by $\pi/4$, we obtain the bisector defined with the supremum metric. From this property, we obtain the following property.

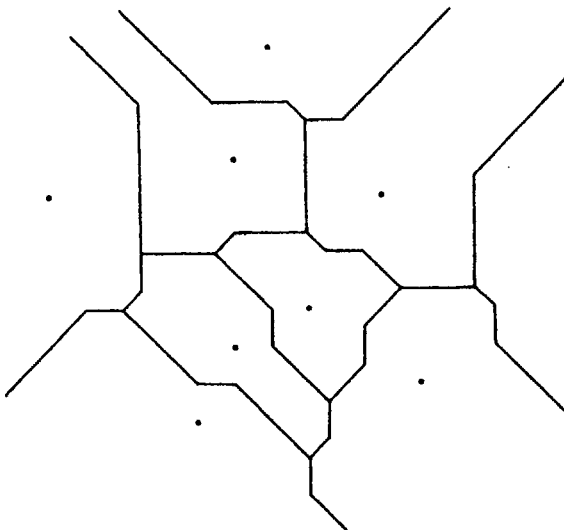


Figure 3.7.5 The supremum-metric Voronoi diagram generated by the generators whose locations are the same as those in Figure 3.7.3.

Property SUP1 The supremum-metric Voronoi diagram of P is obtained by first rotating P counterclockwise by $\pi/4$, next constructing the Manhattan Voronoi diagram for the rotated set of points, and finally rotating the resultant diagram clockwise by $\pi/4$.

We should note that Property SUP1 does not say that the supremum-metric Voronoi diagram of P is the same as the Manhattan Voronoi diagram of P . As we notice from Figures 3.7.3 and 3.7.5, these two Voronoi diagrams are different. The properties of the combinatorial complexity of the diagram in \mathbb{R}^m are shown in Boissonnat *et al.* (1995).

In the above, we focused on the Voronoi diagrams with L_1 and L_∞ in \mathbb{R}^2 , but we can define the Voronoi diagram with L_p , $1 \leq p \leq \infty$, in \mathbb{R}^m , which we call the *Minkowski (metric) Voronoi diagram*. Lê (1996) examines the Minkowski Voronoi diagram in \mathbb{R}^m , $m \geq 2$, from a combinatorial viewpoint.

We may construct a dual diagram of the Minkowski Voronoi diagram as we constructed the Delaunay triangulation from the ordinary Voronoi diagram. In fact, Shute *et al.* (1991) define a Delaunay triangulation as a dual diagram of the Minkowski Voronoi diagram for L_1 and L_∞ . We call it the *Minkowski Delaunay triangulation*. Note that their procedure is slightly different from the procedure employed in Section 2.2 (see Section 2 of Shute *et al.*, 1991).

In conjunction with the Manhattan Voronoi diagram, it may be worth noting a similar diagram, called the ‘rectangular Voronoi diagram’. For points $p_i, p_j \in P$, we define the half plane $H(p_i, p_j)$ by

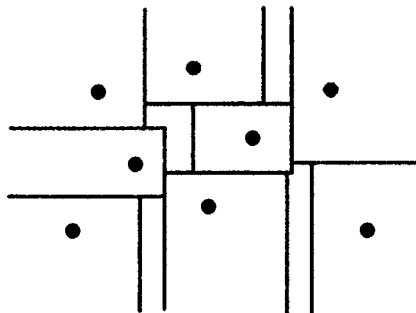


Figure 3.7.6 A rectangular Voronoi diagram.

$$H(p_i, p_j) = \begin{cases} \{(x_1, x_2) \mid x_2 \leq (x_{i1} + x_{j1})/2\} & \text{if } |x_{ii} - x_{jj}| \leq |x_{ii} - x_{jj}|, \\ \{(x_1, x_2) \mid x_1 \leq (x_{i2} + x_{j2})/2\} & \text{otherwise.} \end{cases} \quad (3.7.4)$$

Let $V(p_i) = \cap_{j \in I_n \setminus \{i\}} H(p_i, p_j)$, and $\mathcal{V}_{\text{rec}} = [V(p_1), \dots, V(p_n)]$. We call \mathcal{V}_{rec} the *rectangular Voronoi diagram* (Choi and Kyung, 1991). An example is shown in Figure 3.7.6. Note that, as is noticed in this figure, \mathcal{V}_{rec} is not a tessellation, because \mathcal{V}_{rec} does not cover the whole plane.

3.7.2 Voronoi diagrams with the convex distance

As is seen in Figure 3.7.1, the contour lines of the Minkowski metric are convex. This property is shared not only by the Minkowski metric but also by other distances, and those distances are subsumed under the ‘convex distance’. To be explicit, let us consider a closed convex figure, C , in \mathbb{R}^2 and choose an arbitrary interior point of C as the reference point of C (say, a triangle with its interior point in Figure 3.7.7). The figure C moves in \mathbb{R}^2 under a translational motion (without rotation). To indicate the position of C , we use the notation $C(p)$, implying that the reference point of C is placed at p (Figure 3.7.7). When p of $C(p)$ is placed at the origin o , we call $C(o)$ the *standard position* of $C(p)$. Mathematically, if p is represented by its location vector x , $C(p)$ is written as $C(p) = \{u + x \mid u \in C(o)\}$. The figure $C(p)$ may be scaled up (down) by $\lambda > 0$ fixing the similarity centre at p . The scaled up (down) figure is denoted by $C(p, \lambda)$ (Figure 3.7.7). Mathematically, $C(p, \lambda) = \{\lambda u + x \mid u \in C(o)\}$. Note that $C(p) = C(p, 1)$.

In terms of $C(p, \lambda)$, we define the *convex distance (function)* from a point p to a point p_i as the minimum value of λ that satisfies the condition that p_i is included in $C(p, \lambda)$ (the arrow from p to p_i in Figure 3.7.7). Mathematically, the *convex distance (function)*, $d_{\text{conv}}(p, p_i)$, from p to p_i is defined by

$$d_{\text{conv}}(p, p_i) = \min \{\lambda \mid p_i \in C(p, \lambda), \lambda > 0\}. \quad (3.7.5)$$

In terms of this distance, the convex distance from p to a polygon A_i is defined by

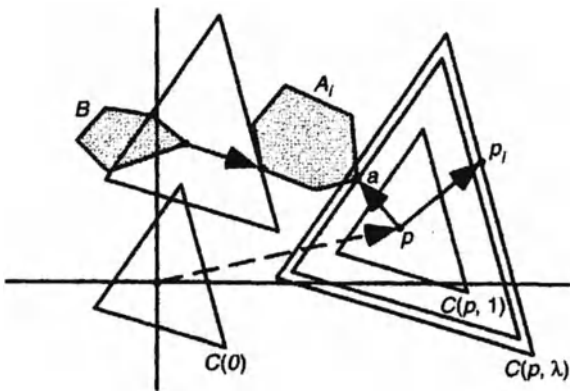


Figure 3.7.7 A convex distance from a point to a polygon, from a point to a polygon, and from a polygon to a polygon (points on the boundary of the triangle $C(o)$ are equally distant from o ; a is an attachment point).

$$d_{\text{conv}}(p, A_i) = \min_q \{ d_{\text{conv}}(p, q), q \in A_i \} \quad (3.7.6)$$

(the arrow from p to A_i in Figure 3.7.7). More generally, the convex distance from a polygon B to a polygon A_i is defined by

$$d_{\text{conv}}(B, A_i) = \min_{p, q} \{ d_{\text{conv}}(p, q), p \in B, q \in A_i \} \quad (3.7.7)$$

(the arrow from B to A_i in Figure 3.7.7).

Three remarks should be made. First, all points on the boundary of $C(p, \lambda)$ are at the same convex distance from p ; hence the boundary of $C(p, \lambda)$ indicates an equi-distant line (a contour line) from p (three equi-distant lines (triangles) from p in Figure 3.7.7). Second, when C is given by a disk, the convex distance becomes the Euclidean distance. Third, the convex distance does not satisfy $d_{\text{conv}}(p, q) = d_{\text{conv}}(q, p)$ when $C(p)$ is not symmetric with respect to p .

For ease of exposition, from now on we assume that A_i is convex and that the edges of C and those of A_i are not parallel (this assumption is relaxed, for example, in Leven and Sharir, 1987). Under these assumptions, there exists a unique point, a , for which the convex distance from p to A_i is equal to the convex distance from p to a , i.e. $d_{\text{conv}}(p, A_i) = d_{\text{conv}}(p, a)$ (Figure 3.7.7). We call the point a an *attachment point*, and the line segment \overline{pa} a (*finite*) *spoke* (McAllister *et al.*, 1996, p.77).

For two polygons A_i and A_j , we define the bisector $b(A_i, A_j)$ between A_i and A_j by $b(A_i, A_j) = \{p \mid d_{\text{conv}}(p, A_i) = d_{\text{conv}}(p, A_j)\}$. This bisector, however, may not be well-behaving, as is seen in Figure 3.7.8(a), where the convex distance from any point in the hatched area to A_1 is the same as that to A_2 . To avoid this indeterminacy, McAllister *et al.* (1996, p.78) propose the following rule. The boundary edges of the convex polygon $C(p, \lambda)$ are

directed, say counterclockwise, and each directed edge is supposed to include the end vertex but not the start vertex (Figure 3.7.8(a)). In terms of this directed polygon, we define the bisector $b(A_i, A_j)$ with the condition that the attachment point for A_i and that for A_j are not on the same edge. When this rule is adopted, the bisector becomes well-behaving. Note that this rule intuitively means that we rotate the convex polygon $C(p, \lambda)$ clockwise infinitesimally. In the hatched region in Figure 3.7.8(a), only the points on the heavy line form part of the bisector. Figure 3.7.8(b) shows the bisector between A_1 and A_2 obtained under the above rule. Since this bisector becomes well-behaving, it divides the plane into two half regions, and let $H(A_i, A_j)$ be the half region including A_i with $b(A_i, A_j)$. For a set $A = \{A_1, \dots, A_n\}$ of disjoint closed polygons, we define $V(A_i) = \bigcap_{j \in I_n \setminus i} H(A_i, A_j)$, and let $\mathcal{V}_{\text{conv}} = \{V(A_1), \dots, V(A_n)\}$. We call the diagram $\mathcal{V}_{\text{conv}}$ the *convex distance Voronoi diagram*. Chew and Drysdale (1985) call $\mathcal{V}_{\text{conv}}$ the *Voronoi diagram based on a convex distance function*, and Leven and Sharir (1987) call $\mathcal{V}_{\text{conv}}$ the *B-Voronoi diagram*. An example is shown in Figure 3.7.9. As we noted above, since the Euclidean distance is included in the convex distance, the ordinary Voronoi diagram is included in $\mathcal{V}_{\text{conv}}$. Also, the Manhattan-metric Voronoi diagram and the supremum metric Voronoi diagram are subsumed under $\mathcal{V}_{\text{conv}}$.

In addition to those diagrams, we refer to a specific $\mathcal{V}_{\text{conv}}$ where C is given by an ellipse. To be explicit, $C(o) = \{x \mid x^T G x \leq 1\}$ or the distance between x and x_i is given by

$$d_{\text{ellip}}(x, x_i) = \sqrt{(x - x_i)^T G (x - x_i)}, \quad (3.7.8)$$

where G is a positive definite symmetric matrix. We call the convex distance Voronoi diagram specified by d_{ellip} the *elliptic distance Voronoi diagram*, $\mathcal{V}_{\text{ellip}}$.

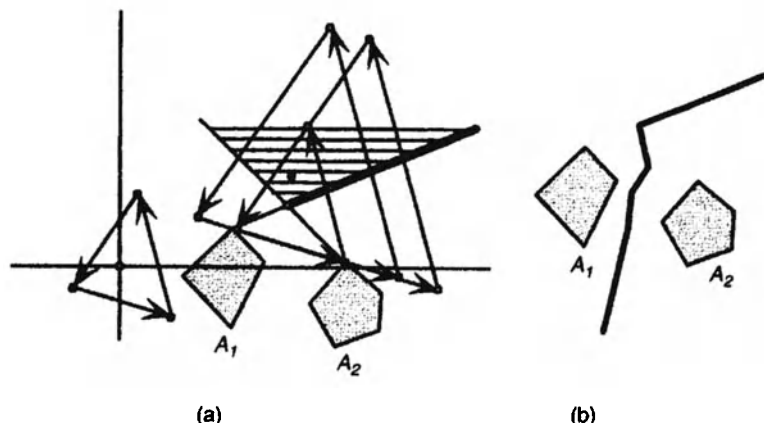


Figure 3.7.8 A bisector with a convex distance: (a) the indeterminant region in which the distances from any point in the hatched region to A_1 and A_2 are equal; (b) the well-behaving bisector between A_1 and A_2 defined in terms of the directed triangle C in panel (a).

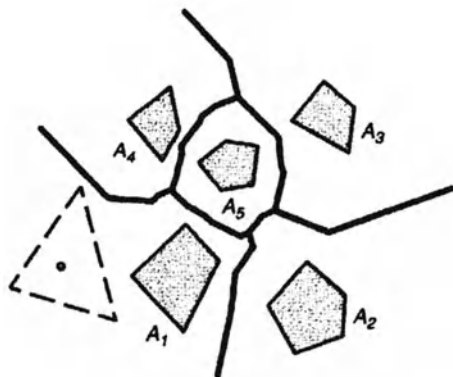


Figure 3.7.9 A convex distance Voronoi diagram (the heavy lines) generated by a set of polygons (the shaded polygons) with a convex distance specified by a triangle (the broken lines) $C(o)$.

(Scheike, 1994 calls it the *Voronoi-G tessellation*). Examples are shown in Figure 3.7.10.

It should be noted that $\mathcal{V}_{\text{ellip}}$ is easily obtained from the ordinary Voronoi diagram through an affine transformation. In Figure 3.7.10, $\mathcal{V}_{\text{ellip}}$ in panel (b) is obtained by shrinking $\mathcal{V}_{\text{conv}}$ in panel (c) in the vertical direction; $\mathcal{V}_{\text{ellip}}$ in panel (a) is obtained by rotating $\mathcal{V}_{\text{conv}}$ in panel (b). Thus the construction of $\mathcal{V}_{\text{ellip}}$ is straightforward once the corresponding ordinary Voronoi diagram is obtained (Scheike, 1994).

Recalling the nearest search problem (V3) solved by the ordinary Voronoi diagram, we notice that that problem can be generalized for polygons and readily solved by $\mathcal{V}_{\text{conv}}$.

Problem C1 (the nearest polygon search problem with the convex distance) Given a finite set $A = \{A_1, \dots, A_n\}$ of disjoint polygons, find the nearest polygon among A from a given point in terms of the convex distance.

Obviously, this problem reduces to Problem V3 when polygons degenerate into points and C is given by a disk.

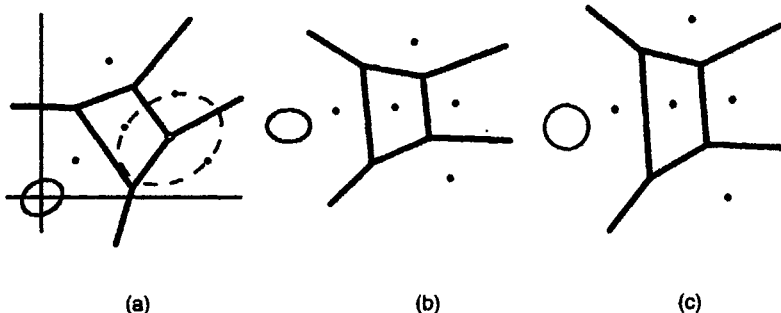


Figure 3.7.10 Elliptic distance Voronoi diagrams, $\mathcal{V}_{\text{conv}}$, with C : (a) $\mathcal{V}_{\text{conv}}$ with a tilted ellipse C (the broken ellipse is the largest ellipse whose centre is within the convex hull of the generator points); (b) $\mathcal{V}_{\text{conv}}$ with an upright ellipse C ; (c) $\mathcal{V}_{\text{conv}}$ with a disk C .

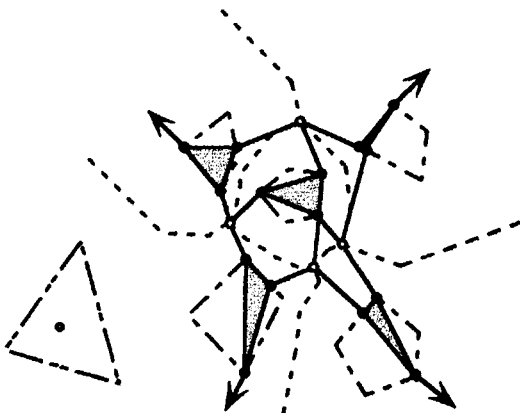


Figure 3.7.11 A core diagram (the continuous lines) and its corresponding convex distance Voronoi diagram (the broken lines) (the shaded regions are cores, the unfilled circles are Voronoi vertices, the filled circles are attachment points of the spokes from the Voronoi vertices, the dash-dot lines are generator polygons, the dash-dot-dot lines indicate a convex distance specified by a triangle, $C(o)$, at the standard position (the shaded circle)).

When our purpose is only to solve this problem, we may use a simplified $\mathcal{V}_{\text{conv}}$ to save memory space. Such a diagram is proposed by McAllister *et al.* (1996), which is constructed in the following manner. First, we obtain attachment points (the filled circles in Figure 3.7.11) of the spokes spanning from each Voronoi vertex of $\mathcal{V}_{\text{conv}}$. In addition to the ordinary Voronoi vertices (the unfilled circles in Figure 3.7.11), we suppose a fictitious Voronoi vertex placed at the farthest point at which all infinite Voronoi edges meet. From this fictitious Voronoi vertex, we span spokes and obtain attachment points (the filled circles connected to the arrows in Figure 3.7.11). As a result, each polygon A_i has a set of attachment points (the filled circles in Figure 3.7.11). For this set of attachment points, we construct a convex hull (the shaded triangle in Figure 3.7.11), which is called the *core* of A_i . The edges of cores and spokes from Voronoi vertices (the heavy continuous lines in Figure 3.7.11) partition \mathbb{R}^2 and form a tessellation. We call this tessellation the *compact piecewise-linear Voronoi diagram* (McAllister *et al.*, 1996) or the *compact Voronoi diagram* for short (McAllister and Snoeyink, 1994, call it the *spoke diagram*). The resulting polygons, except for cores, are called the *spoke regions*. If a probe point is included in a spoke region, the nearest polygon from the point is found in one of the polygons whose cores share the edges of the spoke region.

Each spoke region includes one Voronoi edge, and has at most six vertices regardless of the number of vertices of polygons in A and the number of line segments forming Voronoi edges (McAllister *et al.*, 1996). Thus the compact Voronoi diagram requires less memory space than the convex distance Voronoi diagram (regarding the search time, see McAllister *et al.*, 1996).

In a similar fashion to how we extended the nearest search problem (V3) to the nearest polygon search problem, we can extend the largest empty circle problem (V5) in Section 2.3 to the following problem.

Problem C2 (the largest empty polygon problem) Given a finite set P of distinct points, find the largest empty polygon, $C(p, \lambda)$, which is homothetic to a given polygon C and whose reference point p is included in the convex hull $\text{CH}(P)$ of P .

The position p^* of the largest $C(p^*, \lambda^*)$ is found in one of the Voronoi vertices of $\mathcal{V}_{\text{conv}}$, or cross points between the edges of $\mathcal{V}_{\text{conv}}$ and the boundary of $\text{CH}(P)$, or vertex of $\text{CH}(P)$. An example is shown in Figure 3.7.10 where the largest empty ellipse is indicated by the broken lines. A slightly more generalized probem is that given a convex polygon and an environment consisting of polygonal obstacles, we need to find the placement of the largest similar copy of the poygon that does not intesect any of the obstacles. This problem is solved by Chew and Kedem (1993).

In conjunction with the largest empty polygon problem, it may be worth noting the following problems (Chazelle, 1983; Fortune, 1985).

Problem C3 (the polygon containment problem) Find a position p , if it exists, of a polygon, $C(p, \lambda)$, contained in a simple polygon B (indicated by the light continuous lines in Figure 3.7.12) where $C(p, \lambda)$ is homothetic to a given polygon C .

Problem C4 (the largest convex polygon contained in a simple polygon) For a given simple polygon B , find the largest polygon $C(p, \lambda^*)$ contained in B , where $C(p, \lambda^*)$ is homothetic to a given polygon C .

To solve these problems, we construct $\mathcal{V}_{\text{conv}}$ for a set of line segments constituting the edges of B . Fortune (1985) calls $\mathcal{V}_{\text{conv}} \cap B$ the *C-diagram* (the heavy continuous lines in Figure 3.7.12). The position p^* of the largest $C(p^*, \lambda^*)$ contained in B can be found among one of the Voronoi vertices

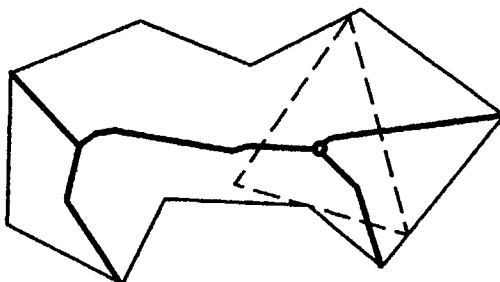


Figure 3.7.12 The largest triangle contained in a simple polygon where the triangle moves under translation and it may be scaled up or down.

(the broken line triangle in Figure 3.7.12), which is the solution to Problem C4. $C(p^*, \lambda^*)$ is called the *largest convex polygon contained in a simple polygon*.

If $C(p^*, \lambda^*)$ is not greater than $C(p^*, \bar{\lambda})$, i.e. $\lambda^* \leq \bar{\lambda}$, then there is no solution. If $C(p^*, \lambda^*)$ is smaller than $C(p^*, \bar{\lambda})$, i.e. $\lambda^* > \bar{\lambda}$, then p^* is a solution to Problem C3. This solution is optimal in the sense that the position p^* of $C(p^*, \bar{\lambda})$ is the farthest point from the edges of the polygon B in terms of the convex distance.

Note that Chazelle (1983), Aonuma *et al.* (1990) and Imai *et al.* (1998) deal with the case in which $C(p, \lambda)$ is allowed to rotate.

As in equation (3.7.5), the convex distance $d_{\text{conv}}(p, p_i)$ from a point p to a point p_i is defined by the minimum value of λ that satisfies the condition that p_i is included in $C(p, \lambda)$. Extending this definition, we may define an alternative convex distance, d_{conv^*} , from a point p to a polygon A_i by the minimum value of λ that satisfies the condition that A_i is included in $C(p, \lambda)$ (the arrow in the broken line triangle in Figure 3.7.13), i.e.

$$d_{\text{conv}^*}(p, A_i) = \min \{ \lambda \mid A_i \subset C(p, \lambda), \lambda > 0 \}. \quad (3.7.9)$$

Note that $d_{\text{conv}}(p, A_i) \neq d_{\text{conv}^*}(p, A_i)$ in general. With this distance, we can construct a Voronoi diagram for A . The resulting Voronoi diagram, $\mathcal{V}_{\text{conv}^*}$, is called the *closest covered set Voronoi diagram* (Abellanas *et al.*, 1995, 1997). An example is shown in Figure 3.7.13.

This diagram is used to prove the following interesting theorem: for a strictly compact convex set C and a family of disjoint compact convex sets, $A = \{A_1, \dots, A_n\}$, there exist two elements $A_i, A_j \in A$ such that any set homothetic to C containing A_i and A_j contains $[n/c]$ (the upper integer of n/c) elements of A , where c is a constant. The proof and the value of c are shown in Abellanas *et al.* (1995, 1997). Note that this problem is an extension of a similar problem defined for a set of points and a circle C (Neumann-Lara and Urrutia, 1988).

We may extend the convex distance Voronoi diagram in \mathbb{R}^2 to that in \mathbb{R}^3 . In fact, Icking *et al.* (1995) define such a diagram and show that the properties

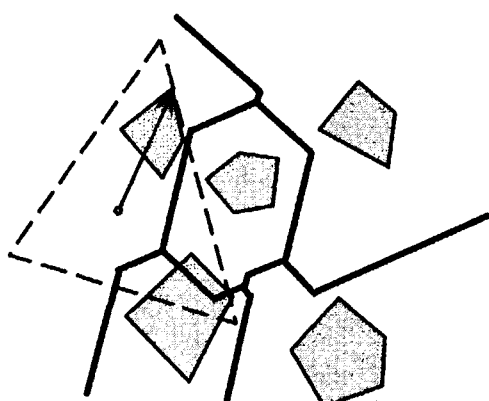


Figure 3.7.13 A closed covered set Voronoi diagram.

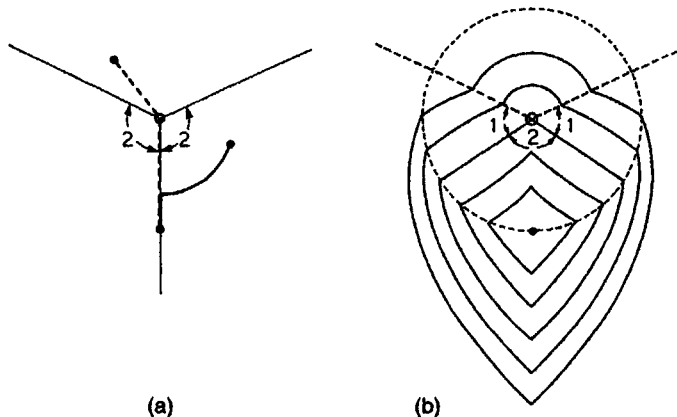


Figure 3.7.14 The contour lines of the Karlsruhe metric.

of that diagram are quite different from those in \mathbb{R}^2 . Chew *et al.* (1995) formulate the convex distance Voronoi diagram for lines in \mathbb{R}^3 .

3.7.3 Voronoi diagrams with the Karlsruhe metric

In Manhattan, we can move along either north–south avenues or east–west streets. In Karlsruhe, we can move along either radiating streets from the centre or circular avenues around the centre. We call the shortest distance in Karlsruhe the *Karlsruhe metric* (Klein, 1988). To be precise, let (r, θ) and (r_i, θ_i) be the polar coordinates of p and p_i , respectively, where $0 \leq \theta, \theta_i < 2\pi$, $r, r_i > 0$, and $\delta(\theta, \theta_i) = \min\{|\theta - \theta_i|, 2\pi - |\theta - \theta_i|\}$. Then, the *Karlsruhe metric* or *Moscow metric* from p to p_i is defined by

$$d_K(p, p_i) = \begin{cases} \min\{r, r_i\} \delta(\theta, \theta_i) + |r - r_i| & \text{for } 0 \leq \delta(\theta, \theta_i) < 2, \\ r + r_i & \text{for } 2 \leq \delta(\theta, \theta_i) < \pi \end{cases} \quad (3.7.10)$$

(Koshizuka and Kurita, 1986; Klein, 1988, 1989). In Figure 3.7.14(a) the shortest path for $0 \leq \delta(\theta, \theta_i) < 2$ is indicated by the heavy solid line and that for $2\delta(\theta, \theta_i) \leq \pi$ is indicated by the broken line. In Figure 3.7.14(b) the contour lines of the Karlsruhe metric from the point indicated by the filled circle (θ is measured from the line radiating from the unfilled circle (the origin) to the filled circle counterclockwise). In the fan-shaped region bounded by the lines radiating from the origin with 2 radians and $2\pi - 2$ radians, the contour lines are circular arcs centred at the origin, and the contour lines radiating from the origin with 1 radian and $2\pi - 1$ radians are straight lines in the dashed circle in Figure 3.7.14(b).

In most cases the bisector with the Karlsruhe metric is well-behaving, as is shown in Figure 3.7.15(a). In a special case (Figure 3.7.15(b)), however, the bisector is not well-behaving. The indeterminacy occurs when two

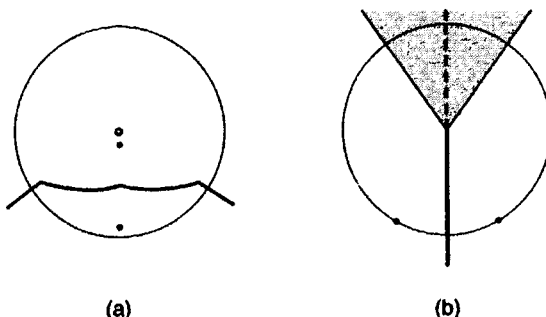


Figure 3.7.15 The bisectors defined with the Karlsruhe metric: (a) a well-behaving bisector; (b) not a well-behaving bisector and its modified bisector (the dashed line and heavy solid line).

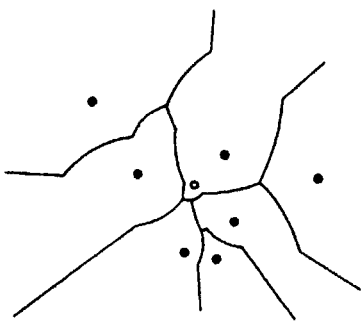


Figure 3.7.16 A Karlsruhe-metric Voronoi diagram (the unfilled circle is the centre). (Source: Klein, 1988, Figure 12.)

points p_i and p_j have the same distance from the origin ($r_i = r_j$) and $\delta(\theta_i, \theta_j) < 2\pi - 4$. In this case, as we did for the bisector of the Manhattan metric (Figure 3.7.2(c)), we define the bisector as the perpendicular line bisecting $\overline{p_i p_j}$ (the heavy solid and dashed lines in Figure 3.7.15(b)).

If we add the above modification to the bisector of the Karlsruhe metric, the set $V_K = \{V(p_1), \dots, V(p_n)\}$ gives a generalized Voronoi diagram. We call V_K the *Karlsruhe-metric Voronoi diagram*, or simply the *Karlsruhe Voronoi diagram*, and the regions constituting the Karlsruhe Voronoi diagram *Karlsruhe(-metric) Voronoi regions*. An example is shown in Figure 3.7.16.

3.7.4 Voronoi diagrams with the Hausdorff distance

The *Hausdorff distance* from a point p to a closed set A is defined by

$$d_H = \max_{x_i} \{\|x - x_i\| \mid x_i \in A_i\}. \quad (3.7.11)$$

This distance is useful in applications when we are concerned with the farthest distance. For instance, if we are concerned with the location of a fire station in a rural region where A_i represents the area of a village, the crucial house is the farthest house in each village from the fire station.

Aurenhammer (1988a) employs the Hausdorff distance to define a line Voronoi diagram. This line Voronoi diagram is quite different from the ordinary line Voronoi diagram in Section 3.4. To see this difference, let $b(L_i, L_j)$ be the bisector generated by two straight line segments L_i and L_j ; p_{ik} and p_{jk} be the end points of L_k , $k = i, j$; and $H(p_i, p_j)$ be the half plane made by the perpendicular line bisecting $\overline{p_ip_j}$ that includes p_i . If a point p is in $H(p_{i2}, p_{i1}) \cap H(p_{j2}, p_{j1})$, then the farthest point in L_i from p is p_{i1} , and the farthest point in L_j from p is p_{j1} . Thus the bisector $b(L_i, L_j)$ in $H(p_{i2}, p_{i1}) \cap H(p_{j2}, p_{j1})$ is given by the line perpendicularly bisecting $\overline{p_{i1}p_{j1}}$. Generally, the bisector $b(L_i, L_j)$ in $H(p_{ik}, p_{i\bar{k}}) \cap H(p_{jh}, p_{j\bar{h}})$ is written as

$$\begin{aligned} & b(L_i, L_j) \cap [H(p_{ik}, p_{i\bar{k}}) \cap H(p_{jh}, p_{j\bar{h}})] \\ &= \{x \mid \|x - x_{ik}\| = \|x - x_{jh}\|\} \cap [H(p_{ik}, p_{i\bar{k}}) \cap H(p_{jh}, p_{j\bar{h}})] \quad k, h = 1, 2, \end{aligned} \quad (3.7.12)$$

where $\bar{k} = 1$ if $k = 2$ and $\bar{k} = 2$ if $k = 1$, and the same for h . An example is shown in Figure 3.7.17.

From Figure 3.7.17 we notice that the bisector consists of straight lines. A curved bisector observed in the ordinary line Voronoi diagram never appears here. The bisector is well-behaving and hence we can obtain a line Voronoi diagram with the Hausdorff distance. We call this diagram the *Hausdorff line Voronoi diagram*. An example is shown in Figure 3.7.18.

From equation (3.7.11) or (3.7.12) the reader may notice that the Hausdorff line Voronoi diagram can be constructed with the help of the farthest-point Voronoi diagram. The role of the farthest-point Voronoi diagram becomes more explicit when we construct a Hausdorff Voronoi diagram generated by a set of polygons, called a *Hausdorff area Voronoi diagram*. Consider a set of polygons $A = \{A_1, \dots, A_n\}$ and let $P_i = \{p_{il}, l \in I_{n,i}\}$ be the vertices of the polygon A_i , $i \in I_n$. To obtain the bisector $b(A_i, A_j)$ between polygons A_i and A_j , we first construct the farthest-point Voronoi diagrams for P_k , $k = i, j$ (the dashed lines in Figure 3.7.19). Let $V_{fp}(p_{kl} | P_k)$ be the farthest-point Voronoi polygon of p_{kl} in the farthest-point Voronoi diagram generated by P_k , $k = i, j$. Then part of the bisector is given by

$$\begin{aligned} & b(A_i, A_j) \cap \{V_{fp}(p_{il} | P_i) \cap V_{fp}(p_{jh} | P_j) \setminus [A_i \cup A_j]\} \\ &= \{x \mid \|x - x_{il}\| = \|x - x_{jh}\|\} \cap \{V_{fp}(p_{il} | P_i) \cap V_{fp}(p_{jh} | P_j) \setminus [A_i \cup A_j]\} \end{aligned} \quad (3.7.13)$$

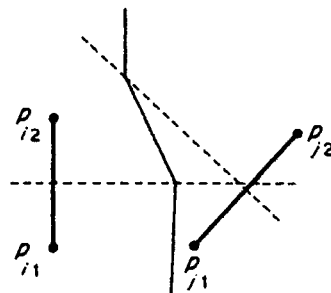


Figure 3.7.17 The bisector of two line segments defined with the Hausdorff distance.

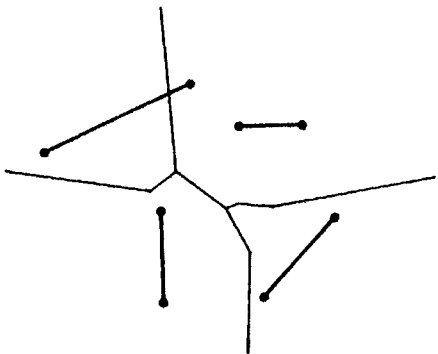


Figure 3.7.18 A Hausdorff line Voronoi diagram generated by a set of straight line segments.

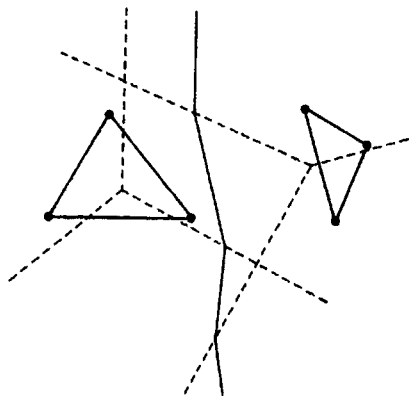


Figure 3.7.19 The bisector of two polygons with the Hausdorff distance, or a Hausdorff area Voronoi diagram generated by a set of two polygons (the dashed lines show the farthest-point Voronoi diagrams generated by the vertices of the polygons).

(the fine solid lines in Figure 3.7.19). Using this equation, we can construct a Hausdorff area Voronoi diagram.

3.7.5 Voronoi diagram with the boat-on-a-river distance

Imagine a wide river where lifeboats are moored at mooring posts and a lookout tower stands. When a watcher in the tower finds a boat driven on a rock, the watcher asks the lifeboat that can reach the boat in the shortest time to rescue the people in the boat. In this rescue system, the lifeboats have their own rescue regions covering the river, which may form a tessellation. We call this tessellation the *Voronoi diagram on a river* (Sugihara, 1992a).

To formulate this tessellation mathematically, let $P = \{p_1, \dots, p_n\}$ be a set of points (mooring posts) in the x - y plane; $w \geq 0$ be the flow velocity of a river running from west to east (which coincides with the x -axis); $v > 0$ be the velocity of a lifeboat; and $\alpha = w/v$, called the *relative flow velocity*. We measure the closeness from $p_i = (x_i, y_i)$ to a point $p = (x, y)$ by the shortest time, $t(p_i, p)$, spent in sailing from p_i to p . To be explicit, let θ be the angle

of the heading direction of a lifeboat measured from the x -axis. Then, $x - x_i = t(p_i, p) v \cos \theta + t(p_i, p) w$ and $y - y_i = t(p_i, p) v \sin \theta$ hold (Figure 3.7.20(a)). Eliminating θ from these equations, we obtain:

for $\alpha < 1$,

$$t(p_i, p) = \frac{-\alpha(x - x_i) + \sqrt{(x - x_i)^2 + (1 - \alpha^2)(y - y_i)^2}}{v(1 - \alpha^2)}; \quad (3.7.14)$$

for $\alpha = 1$,

$$t(p_i, p) = \begin{cases} \frac{(x - x_i)^2 + (y - y_i)^2}{2v(x - x_i)} & \text{for } x > x_i, \\ 0 & \text{for } x = x_i \text{ and } y = y_i, \\ \infty & \text{for } x \geq x_i \text{ and } y \neq y_i, \end{cases} \quad (3.7.15)$$

for $\alpha > 0$,

$$t(p_i, p) = \begin{cases} \frac{-\alpha(x - x_i) + \sqrt{(x - x_i)^2 + (1 - \alpha^2)(y - y_i)^2}}{v(1 - \alpha^2)} & \text{for } |x - x_i| \leq |y - y_i| \sqrt{\alpha^2 - 1}, \\ \infty & \text{otherwise.} \end{cases} \quad (3.7.16)$$

We call $t(p_i, p)$ the *boat-on-a-river distance*. The contour lines of the boat-on-a-river distance from the mooring pole p_i are shown in Figure 3.7.20, where the shaded regions (which correspond to $t(p_i, p) = \infty$ in equations (3.7.15) and (3.7.16)) indicate the regions which the lifeboat moored at p_i cannot reach (because the lifeboat cannot sail against the faster flow).

The dominance region of p_i over p_j is obtained from $\text{Dom}(p_i, p_j) = \{p \mid t(p_i, p) \leq t(p_j, p)\}, j \neq i$. When $0 < \alpha < 1$, this dominance region is well-behaving, and the boundary of $\text{Dom}(p_i, p_j)$ or the bisector between p_i and p_j is given by a hyperbolic curve. When $\alpha \geq 1$, the dominance region is not well-behaving, because there exists a region whose points are neither assigned to p_i nor p_j (recall Figure 3.7.20(b), (c)). The shape of the dominance region varies according to the value of α and the relative configuration of p_i and p_j (see Sugihara, 1992a).

When $0 \leq \alpha < 1$, the set $V(p_i) = \bigcap_{j \neq i, j=1}^n \text{Dom}(p_i, p_j)$ gives a region, and the set $\mathcal{V}_{\text{river}} = \{V(p_1), \dots, V(p_n)\}$ forms a tessellation (Figure 3.7.21(a)). Stated a little more formally, we have the following property.

Property RV1 The Voronoi regions $V(p_1), \dots, V(p_n)$ cover the whole plane \mathbb{R}^2 if and only if $0 \leq \alpha < 1$.

We call $\mathcal{V}_{\text{river}}$ the *Voronoi diagram on a river* generated by P . Note that in the specific case of $\alpha = 0$, $\mathcal{V}_{\text{river}}$ is reduced to the ordinary Voronoi diagram, because the boat-on-a-river distance becomes the Euclidean distance. When

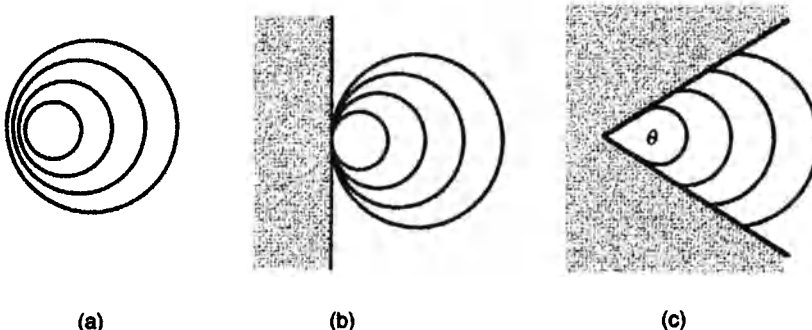


Figure 3.7.20 Contour lines of the boat-on-a-river distance from p_i : (a) $0 < \alpha < 1$; (b) $\alpha = 1$; (c) $\alpha > 1$.

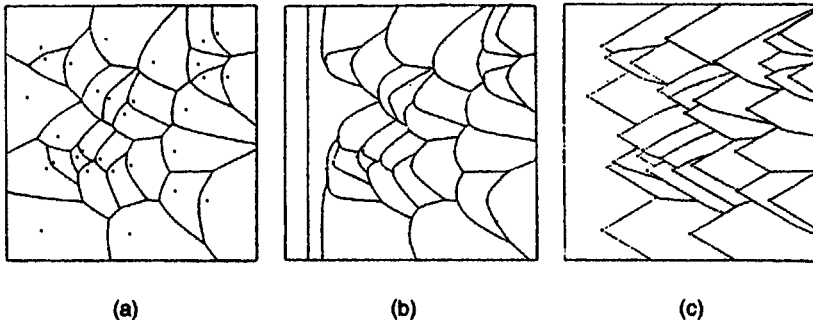


Figure 3.7.21 Voronoi diagrams on a river: (a) $\alpha = 0.5$; (b) $\alpha = 1$; (c) $\alpha = 2.0$.

$\alpha \geq 1$, $\mathcal{V}_{\text{river}}$ does not exhaust \mathbb{R}^2 , as shown in Figure 3.7.21(b), (c), but $\mathcal{V}_{\text{river}}$ may be regarded as a tessellation of $\bigcup_{i=1}^n V(p_i)$, which we also call the Voronoi diagram on a river.

We note one more important property.

Property RV2 For $0 \leq \alpha < 1$, the two generators of $\mathcal{V}_{\text{river}}$ are neighbours if and only if they are neighbours on the ordinary Voronoi diagram.

The proof is shown in Sugihara (1992a).

3.7.6 Voronoi diagrams on a sphere

In a military district problem, the dominance regions or coverage areas of air bases in the world is often discussed. We may treat this problem by a Voronoi diagram defined on a sphere.

Let $P = \{p_1, \dots, p_n\}$ ($2 \leq n < \infty$) be distinct points on a sphere S with the unit radius centred at the origin, and \mathbf{x} and \mathbf{x}_i be the location vectors of $p \in S$ and $p_i \in S$, respectively. The shortest distance from p to p_i on S is defined by the length of the lesser arc on the great circle (the circle whose centre is at the centre of S) passing through p and p_i . Mathematically, this distance is written as

$$d_{gc}(p, p_i) = \arccos(\mathbf{x}^T \mathbf{x}_i) \leq \pi. \quad (3.7.17)$$

We call this distance the *great circle distance*. The bisector defined with the great circle distance is given by the great circle that ‘perpendicularly’ passes through the mid-point of the great circular arc combining p_i and p (‘perpendicularly’ means that sufficiently small segments of the two great circles around the mid-point are orthogonal). This bisector divides the sphere S into two disjoint hemispheres. Thus the bisector defined with the great circle distance is well-behaving, and

$$V(p_i) = \{d_{gc}(p, p_i) \leq d_{gc}(p, p_j), j \in I_n \setminus \{i\}, p \in S\} \quad (3.7.18)$$

gives a non-empty set in S . We call this set the *spherical Voronoi polygon* associated with p_i . The set of resulting spherical Voronoi polygons gives a generalized Voronoi diagram, which we call the *spherical Voronoi diagram* generated by P on S (Miles, 1971; Brown, 1980; Paschinger, 1982; Ash and Bolker, 1985; Renka, 1984b; Augenbaum and Peskin, 1985; Sugihara, 1997). Figure 3.7.22 shows a spherical Voronoi diagram. Renka (1984b) provides software for constructing the spherical Voronoi diagram.

In a similar fashion to how we defined the Delaunay triangulation as the dual of the ordinary Voronoi diagram, we can define the *spherical Delaunay triangulation* as the dual of the spherical Voronoi diagram (Renka, 1984a,b).

The term ‘spherical polygon’ mentioned above is a ‘polygon’ on a sphere S . To be precise, let S_i be a hemisphere on S . Then, a spherical polygon is defined by the set of points on S which is obtained from the combination of intersections and/or unions of S_i , $i = 1, 2, \dots$. Like a convex polygon in \mathbb{R}^2 , we can define a *convex spherical polygon* by the spherical polygon in which the lesser arc of a great circle passing through any two points in the spherical polygon is embedded in the spherical polygon. From the definition of a spherical Voronoi polygon, we understand the following properties.

Property S1 The set $V(p_i)$ defined by equation (3.7.18) is a unique bounded non-empty convex spherical polygon.

Property S2 An edge of a spherical Voronoi polygon is an arc of a great circle.

These properties correspond to Properties V1–V3 of the ordinary Voronoi diagram. Properties V4–V7 of the ordinary Voronoi diagram also hold for the spherical Voronoi diagram by replacing relevant terms. Property V9,

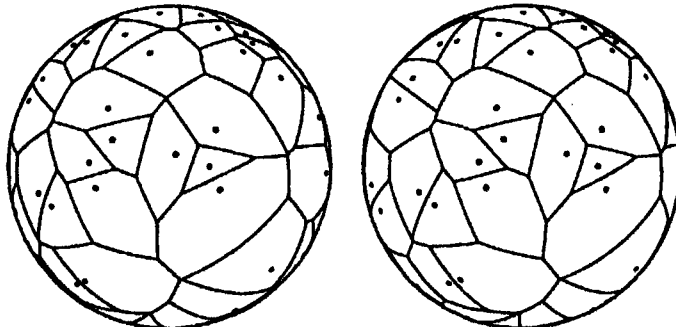


Figure 3.7.22 A stereographic view of a spherical Voronoi diagram.

however, becomes slightly different, because the ordinary Voronoi diagram is formulated in an unbounded space, whereas the spherical Voronoi diagram is formulated in a bounded space. From Euler's theorem, we obtain the following property.

Property S3 Let n_v and n_e be the number of vertices and edges in the spherical Voronoi diagram generated by $P = \{p_1, \dots, p_n\}$. Then the following equation holds:

$$n_v - n_e + n = 2. \quad (3.7.19)$$

Replacing equation (2.3.4) with equation (3.7.19) in the derivations used for Properties V11–V13, we can obtain the properties corresponding to Properties V11–V13 of the ordinary Voronoi diagram.

We may define a spherical Voronoi diagram by replacing the great circle distance with another distance. Sugihara (1997) shows the Voronoi diagram with the spherical Laguerre distance, called the *spherical Laguerre Voronoi diagram* or *spherical power (Voronoi) diagram*, following the power (Voronoi) diagram in Section 3.1. An example is shown in Figure 3.7.23.

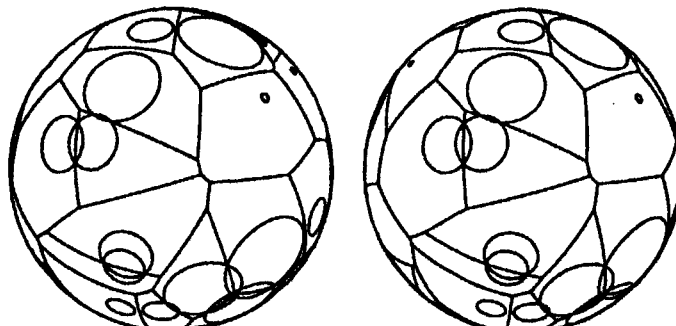


Figure 3.7.23 A spherical Laguerre Voronoi diagram.

3.7.7 Voronoi diagrams on a cylinder

When we meet phenomena in which the same configuration of generator points appears in cycles, we can analyse them with the aid of a Voronoi diagram on a cylinder.

Suppose that the axis of a cylinder S with unit radius is placed at an axis in \mathbb{R}^3 , and that a set $P = \{p_1, \dots, p_n\}$ of distinct points ($2 \leq n < \infty$) is placed on the cylinder S (Figure 3.7.24(a)). The location of p_i on S can be indicated by (x_i, y_i, z_i) , where $x_i^2 + y_i^2 = 1$, and the distance between p and p_i is defined by the length of the shortest path on S connecting p and p_i . At first glance this measurement appears difficult in practice, but if we notice that a cylinder can be developed on a plane, this measurement becomes quite easy. If we cut the cylinder S along the line parallel to the z -axis passing through $(1, 0, 0)$ (the dash-dotted line in Figure 3.7.24(a)), then S can be developed into S' on the plane, as is seen in Figure 3.7.24(b). The developed region S' is the region bounded by parallel lines at a distance 2π on \mathbb{R}^2 . To treat the location of a point p'_i on S' which corresponds to p_i on S , let θ_i be the counterclockwise angle (viewed from above the x - y plane, i.e. $z > 0$) from the x -axis to the half line radiating from the origin to the point $(x_i, y_i, 0)$, then we can indicate the point p'_i by (θ_i, z_i) (Figure 3.7.24(b)). Since the shortest path on S is represented by the straight line on S' , the distance between p and p_i on S is the same as the distance between $p' = (\theta, z)$ and $p'_i = (\theta_i, z_i)$ on S' (where $\theta \leq \theta_i$ is assumed without loss of generality), which is given by

$$d_{cy}(p, p_i) = \begin{cases} \sqrt{(\theta - \theta_i)^2 + (z - z_i)^2} & \text{for } \theta_i - \theta \leq \pi, \\ \sqrt{(\theta + 2\pi - \theta_i)^2 + (z - z_i)^2} & \text{for } \theta_i - \theta > \pi. \end{cases} \quad (3.7.20)$$

Since the bisector $b(p_i, p_j)$ defined with the distance of equation (3.7.20) splits S into two disjoint regions (Figure 3.7.25(a)), the dominance region is well-behaving. We can thus define a Voronoi diagram on S with this distance,

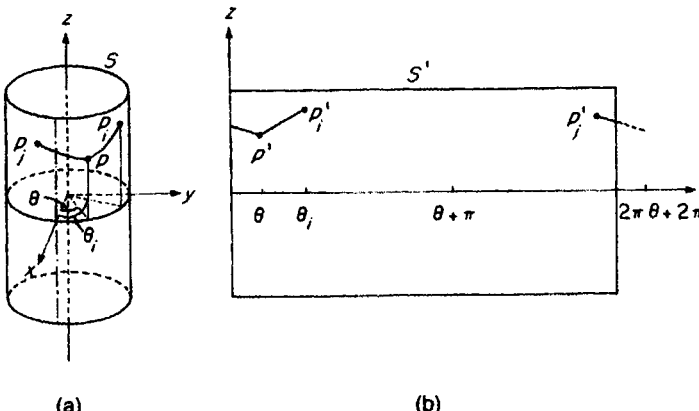


Figure 3.7.24 (a) A cylinder in \mathbb{R}^3 , and (b) its developed region in \mathbb{R}^2 .

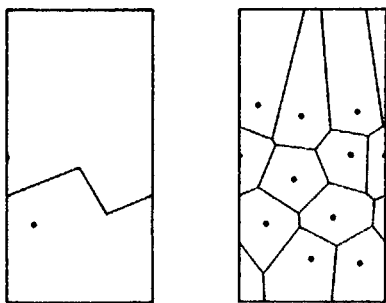


Figure 3.7.25 (a) A bisector on a cylinder, and (b) a cylindrical Voronoi diagram.

which we call the *cylindrical Voronoi diagram* on S generated by P (Figure 3.7.25(b)).

3.7.8 Voronoi diagrams on a cone

If a set $P = \{p_1, \dots, p_n\}$ of distinct points is placed on a cone, we may consider a Voronoi diagram on a cone. Suppose that a cone S is placed in \mathbb{R}^3 in such a way that the axis of the cone S is the z -axis of \mathbb{R}^3 , and the radius of the circle made by the intersection of the cone S with the x - y plane is unity (Figure 3.7.26(a)). Like a cylinder, a cone can be developed on a plane. If we cut the cone S along the line radiating from the top of the cone passing through $(1, 0, 0)$ and develop it on the plane, we get a fan-shaped region S' , as is shown in Figure 3.7.26(b). We can thus measure the distance between p and p_i on the cone S by the distance between p' and p'_i in the fan-shaped region S' . To write this distance mathematically, let (x_i, y_i, z_i) be the Cartesian coordinates of p_i in \mathbb{R}^3 ; θ_i be the counterclockwise angle (viewed from above the x - y plane, $z > 0$) from the x -axis to the half line radiating from the origin to the point $(x_i, y_i, 0)$; $\theta'_i = \theta_i \sin(\alpha/2)$, where α is the top angle of the cone (defined by the acute angle of the intersection lines made from the x - z plane and the cone); and

$$r_i = \sqrt{x_i^2 + y_i^2 + (z_i - \cot(\alpha/2))^2}, \quad (3.7.21)$$

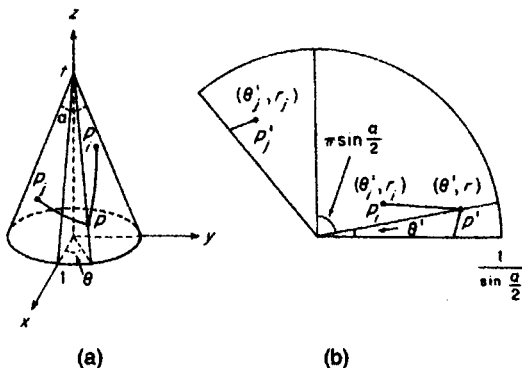


Figure 3.7.26 (a) A cone in \mathbb{R}^3 , and (b) its developed region in \mathbb{R}^2 .

which is the straight line distance from the top of the cone S to p_i . Then the point p_i on the cone S in \mathbb{R}^3 can be indicated by (θ_i, r_i) in the fan-shaped regions in \mathbb{R}^2 . Thus the distance between $p = (r, \theta)$ and p_i on the cone S is written as

$$d_{\text{cone}}(p, p_i) = \begin{cases} \sqrt{r^2 + r_i^2 - 2rr_i \cos(\theta'_i - \theta')} & \text{for } \theta'_i \leq \theta' + \pi \sin(\alpha/2), \\ \sqrt{r^2 + r_i^2 - 2rr_i \cos(\theta' + 2\pi \sin(\alpha/2) - \theta'_i)} & \text{for } \theta'_i > \theta' + \pi \sin(\alpha/2), \end{cases} \quad (3.7.22)$$

where $\theta' \leq \theta'_i$ is assumed without loss of generality (Figure 3.7.26(b)). The bisector defined with this distance consists of a chain of straight line segments which divides the fan-shaped region S' into two disjoint regions, as is shown in Figure 3.7.27(a). The chain of the bisector may form a circuit on S . The bisector is a circuit on S if and only if the top angle is less than $\pi/3$ (Dehne and Klein, 1987, Lemma 2). Since a circuit bisector as well as a non-circuit bisector is well-behaving, we can define a Voronoi diagram with this bisector. We call the resulting diagram the *conic Voronoi diagram* generated by P on S (Dehne and Klein, 1987; Klein, 1988; Klein and Wood, 1988). An example is depicted in Figure 3.7.27(b).

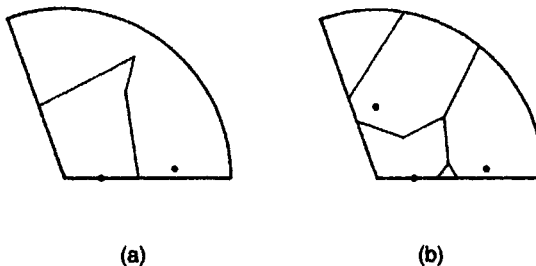


Figure 3.7.27 (a) A bisector in a cone, and (b) a conic Voronoi diagram.

3.7.9 Voronoi diagrams on a polyhedral surface

If the reader is interested in terrain navigation or a Voronoi diagram defined on uneven ground, a Voronoi diagram on an uneven surface in \mathbb{R}^3 may be useful. In most practical applications, a surface can be approximated by a polyhedral surface consisting of small polygonal faces. We can thus treat the above diagram as a Voronoi diagram on a polyhedral surface.

Let S be the surface of a polyhedron in \mathbb{R}^3 , and $P = \{p_1, \dots, p_n\}$ ($2 \leq n < \infty$) be a set of distinct points on S . A simple example is shown in Figure 3.7.28(a), where S is a tetrahedron. We measure the distance $d(p, p_i)$ from a point p on S to a point p_i by the length of the shortest path on S from p to p_i . A polyhedron can be developed into a region on a plane and

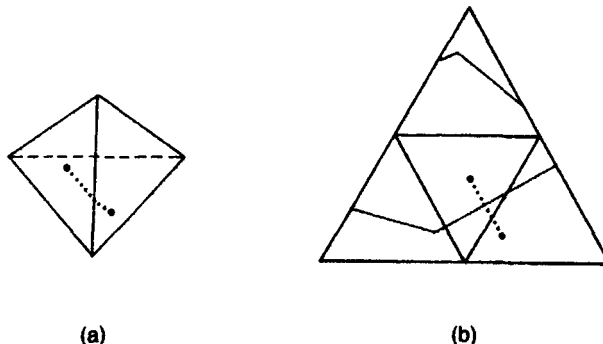


Figure 3.7.28 (a) A tetrahedron in \mathbb{R}^3 , and (b) its developed triangle in \mathbb{R}^2 where the heavy solid line shows a bisector.

we can measure this distance on the developed region. For instance, if we cut the tetrahedron in Figure 3.7.28(a) along three edges from the top, we obtain the triangle in Figure 3.7.28(b). The shortest path on the triangle is indicated by the dashed line in Figure 3.7.28. When the surface is given by a convex polyhedron, we may develop the surface on a plane without overlaps (Agarwal *et al.*, 1990a; Chen and Han, 1990; Aronov and O'Rourke, 1992). When the surface is given by a non-convex polyhedron, facets developed on a plane may overlap, and it is not straightforward to find the shortest path. In computational geometry, Mount (1985), Sharir and Schorr (1984), Sharir and Baltsan (1986) and Har-Peled *et al.* (1996) proposed several methods for finding the shortest path. Using these methods, we can define the bisector between p_i and p_j (the heavy solid line in the example of Figure 3.7.28(b)), and define a Voronoi diagram on the surface of a polyhedron. We call this diagram the *Polyhedral Voronoi diagram* generated by P (Figure 3.7.29).

3.7.10 Miscellany

In addition to the Voronoi diagrams with the above V-distances, we can find in the literature a few more Voronoi diagrams with other V-distances. We comment briefly on these diagrams.

A Voronoi diagram defined with the time-space distance is formulated by Seoung (1990), which will be shown in Chapter 8. A Voronoi diagram defined with the quadratic form distance is developed by Imai *et al.* (1985) (see also Section 18.2.2 in Boissonnat and Yvinec, 1995). A Voronoi diagram on a Riemannian manifold is investigated by Ehrlich and Im Hof (1979), Boissonnat and Yvinec (1995, Section 18.5.2) and Onishi and Takayama (1996). The geodesic distance, $d_{\text{Riemann}}(p_1, p_2)$, between $p_1 = (x_1, y_1)$ and $p_2 = (x_2, y_2)$ in the Riemannian manifold, called the upper half-plane, is given by

$$d_{\text{Riemann}}(p_1, p_2) = \left| \log \frac{A + \sqrt{A^2 - 4y_1^2 y_2^2}}{A - \sqrt{A^2 - 4y_1^2 y_2^2}} \right|, \quad (3.7.23)$$

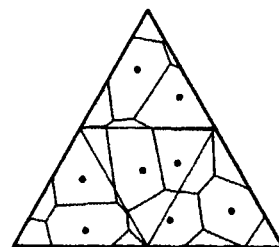


Figure 3.7.29 A polyhedral Voronoi diagram developed in \mathbb{R}^2 .

where $A = (x_1 - x_2)^2 + (y_1 + y_2)^2$. We call the Voronoi diagram defined with this distance the *Riemann Voronoi diagram*, which is alternatively called the (*hyperbolic*) *Voronoi diagram in the upper half-plane* by Onishi and Takayama (1996). An example is shown in Figure 3.7.30. In conjunction with the Riemann Voronoi diagram, we note that Onishi and Imai (1997) develop a Voronoi diagram for a set of points (each point correspond to a probability density function) in a statistical parametric space which is regarded as a Riemannian space.

A Voronoi diagram on a torus is referred to in conjunction with adjusting the boundary effect, which is discussed in Chapter 5 (or Upton and Fingleton, 1985, p. 72). It should be noted that this torus is a ‘quasi-torus’ in the sense that a distance between two points on the torus is not measured by the shortest path distance on the torus but by the Euclidean distance on the ‘developed’ rectangle from the torus. An example is shown in Figure 3.7.31(a), where generators are distributed over a unit square whose vertices are given by $(0,0)$, $(1,0)$, $(0,1)$ and $(1,1)$. Conceptually, we connect the edge \overline{ab} with the edge \overline{cd} and the edge \overline{ac} with the edge \overline{bd} in Figure 3.7.31 by deforming the square. Although we deform the square, we measure the distance between two points (x_i, y_i) and (x_j, y_j) by

$$\begin{aligned}
 d_{\text{torus}}(p, p_i) &= \min \left\{ \sqrt{(x_i - x_j)^2 + (y_i - y_j)^2}, \sqrt{(x_i - x_j + 1)^2 + (y_i - y_j)^2}, \right. \\
 &\quad \sqrt{(x_i - x_j)^2 + (y_i - y_j + 1)^2}, \sqrt{(x_i - x_j - 1)^2 + (y_i - y_j)^2}, \\
 &\quad \sqrt{(x_i - x_j)^2 + (y_i - y_j - 1)^2}, \sqrt{(x_i - x_j + 1)^2 + (y_i - y_j + 1)^2}, \\
 &\quad \sqrt{(x_i - x_j + 1)^2 + (y_i - y_j - 1)^2}, \sqrt{(x_i - x_j - 1)^2 + (y_i - y_j + 1)^2}, \\
 &\quad \left. \sqrt{(x_i - x_j - 1)^2 + (y_i - y_j - 1)^2} \right\}. \tag{3.7.24}
 \end{aligned}$$

This distance is readily obtained from the configuration which consists of nine squares with the same generators placed around the square, as shown in Figure 3.7.31(b). Then a Voronoi diagram on a quasi-torus is obtained as the solid lines in the central square in Figure 3.7.31(b).

When we can reach points only in a fan-shaped region, we may consider an ‘oriented Voronoi diagram’. To be explicit, let $C(p, \theta_1, \theta_2)$ be the fan-

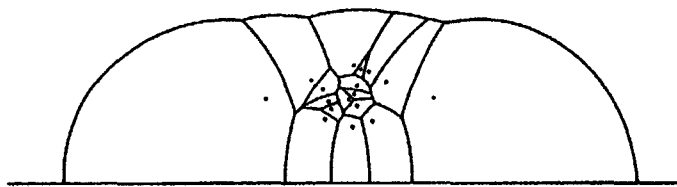


Figure 3.7.30 A Riemann Voronoi diagram. (Source: Onishi and Takayama, 1996).

shaped region with a vertex p and limiting angles θ_1 and θ_2 . Note that $C(p, \theta_1, \theta_2)$ includes its boundaries but excludes p , and $0 < \theta_2 - \theta_1 < \pi$ (the shaded area in Figure 3.7.32(a)). We define the *oriented distance* by

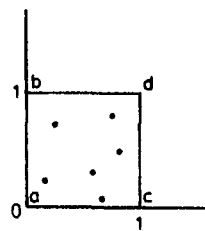
$$d_{\text{ori}}(p, p_i) = \begin{cases} \|x - x_i\| & \text{if } p \in C(p, \theta_1, \theta_2), \\ \infty & \text{if } p \notin C(p, \theta_1, \theta_2). \end{cases} \quad (3.7.25)$$

For example, in Figure 3.7.32(a), $d_{\text{ori}}(p, p_1)$ is the same as the Euclidean distance between p and p_1 but $d_{\text{ori}}(p, p_2)$ is infinity. This implies that the set of points from which the oriented distance to p_1 is finite is given by $C(p_1, \theta_1 + \pi, \theta_2 + \pi)$, the shaded area in Figure 3.7.32(b). For the two generator points p_1 and p_2 shown in Figure 3.7.32(c), the set of points satisfying $d_{\text{ori}}(p, p_1) \leq d_{\text{ori}}(p, p_2)$ is indicated by the shaded area (note that the broken line perpendicularly bisects the line segment $\overline{p_1 p_2}$).

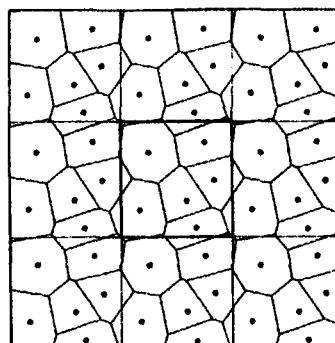
With the oriented distance, we define

$$V(p_i) = \{p \mid d_{\text{ori}}(p, p_i) \leq d_{\text{ori}}(p, p_j), j \in I_n \setminus \{i\}\}. \quad (3.7.26)$$

We call $V(p_i)$ the *oriented Voronoi polygon* associated with p_i . The resulting set $\{V(p_1), \dots, V(p_n)\}$ is a tessellation of $\bigcup_{i=1}^n C(p_i, \theta_1 + \pi, \theta_2 + \pi)$. We call



(a)



(b)

Figure 3.7.31 A Voronoi diagram on a quasi-torus.

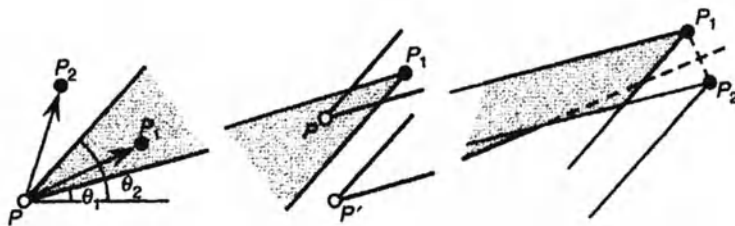


Figure 3.7.32 The oriented distance.

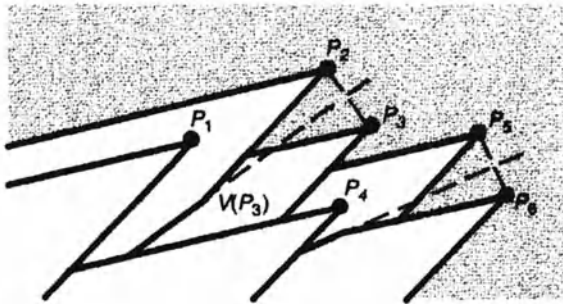


Figure 3.7.33 An oriented Voronoi diagram.

it the *oriented Voronoi diagram* generated by P (Chang *et al.*, 1990a; Georgakopoulos and Papadimitriou, 1987 (who call $V(p_i)$ the *oriented Dirichlet cell*)). An example of the oriented Voronoi diagram generated by six generator points is shown in Figure 3.7.33. In the special case where $\theta_1 = 0$ and $\theta_2 = \pi/2$, Chew and Fortune (1997) call the oriented Voronoi diagram the *right triangle distance Voronoi diagram*.

3.7.11 Applications

The Manhattan Voronoi diagram is used when movement is restricted to the north-south and the east-west directions. Applications are found in robot arm movements (Hwang, 1979; Lee and Wong, 1980), VLSI (Very Large Scale Integrated) circuit design (Li and Jabri, 1992; Guha, 1993; Tzionas *et al.* 1997), robot motion planning (Hague *et al.*, 1990; Tzionas *et al.*, 1997, for diamond-shaped robot) and market area analysis (Eaton and Lipsey, 1980). The rectangular Voronoi diagram is used for floor planning (Choi and Kyung, 1991).

The elliptic distance Voronoi diagram may represent a cell growth model, where the growth rate differs in directions, called *anisotropic growth* (Scheike, 1994). Suppose that the length of a line segment from o to a point on the boundary of an ellipse whose centre is placed on o indicates the growth rate in that direction in unit time, and that cells centred at p_1, \dots, p_n expand

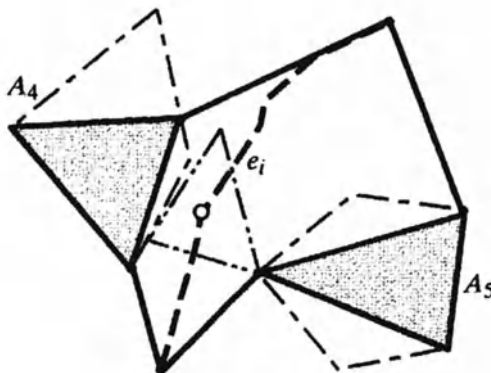


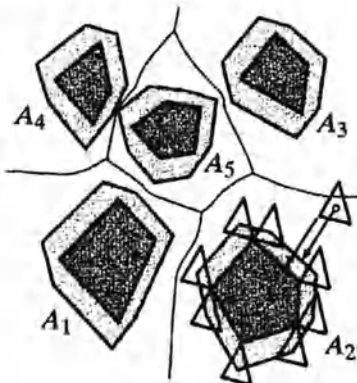
Figure 3.7.34 A bottleneck between two polygons in a spoke region in Figure 3.7.9.

simultaneously according to this growth rate (imagine that football shaped balloons (cells) are inflating with fixed centres). As the cells expand, they become tight and deformed; finally, the ‘packed’ cells form $\mathcal{V}_{\text{clip}}$ (a precise definition of the cell growth model is provided in Section 7.2). Figure 3.7.10(c) (the ordinary Voronoi diagram) shows the case in which the growth rate is the same in all directions; Figures 3.7.10(a) and (b) show the case in which the growth rate in the direction of the longer axis of the ellipse is twice as fast as that in the shorter axis. The elliptic distance Voronoi diagram is also used to analyse the growth of small fatigue cracks (Cox and Morris, 1988) and cluster analysis (Reyes and Adjouadi, 1995).

An application of the convex distance Voronoi diagram is found in robot motion planning, which is alternatively referred to as collision-free path planning (Lozano-Pérez and Wesley, 1979), the piano movers’ problem (Schwartz and Sharir, 1983a, b), the find path problem (Lozano-Pérez, 1983), the problem of moving a ladder (Ó'Dúnlaing *et al.*, 1986, 1987; Leven and Sharir, 1987), and the problem of moving a chair (Yap, 1987). *Robot motion planning* involves finding paths, called *collision-free paths*, on which a robot can move without colliding with obstacles A_1, \dots, A_n . If a robot moves under a translational motion and the robot can be represented by a convex polygon, $C(p, \bar{\lambda})$ (where $\bar{\lambda}$ is a fixed value), we can use $\mathcal{V}_{\text{conv}}$ to find collision-free paths.

To find the paths, consider a spoke region, and a point p on the Voronoi edge, e_i (the heavy broken line in Figure 3.7.34 in the spoke region). As p moves along e_i , the convex distance from p to the two polygons (A_4 and A_5 in Figure 3.7.34) changes, but the value has no plural local optimum (shown by McAllister *et al.*, 1996). The distance attains the minimum at a point on e_i (including the end points). Denote this point by p_i^* , and let a_{i1}^* and a_{i2}^* be attachment points of the spokes from p_i^* to the polygons whose Voronoi regions share e_i . We call the value $w_i^* = d_{\text{conv}}(p_i^*, a_{i1}^*)$ the *bottleneck width* of e_i . This implies that if the size $\bar{\lambda}$ of robot $C(p, \bar{\lambda})$ is less than the bottle-

Figure 3.7.35 An area Voronoi diagram for expanded obstacles (the densely shaded polygons are obstacles A_1, \dots, A_5 , and the shaded polygons are expanded obstacles $A_1^{+C}, \dots, A_5^{+C}$; the distance $d_{\min E}(C(p, \bar{\lambda}), A_i)$ from robot $C(p, \bar{\lambda})$ to obstacle A_i is the same as the distance $d_{\min E}(p, A_i^{+C})$ from the shrunken robot p to the expanded obstacle A_i^{+C} indicated by the two arrow line segments.



neck width w_i^* of e_i , robot $C(p, \bar{\lambda})$ can move on the path (edge) e_i without collision. Let w^{**} be the minimum value among w_i^* for all Voronoi edges. If the size $\bar{\lambda}$ of robot $C(p, \bar{\lambda})$ is less than the minimum bottleneck width w^{**} , robot $C(p, \bar{\lambda})$ can move on the Voronoi edges of $\mathcal{V}_{\text{conv}}$ without collision. These paths are optimal in the sense that robot $C(p, \bar{\lambda})$ is as far from obstacles as possible in terms of the convex distance. When the size $\bar{\lambda}$ is greater than the minimum bottleneck width w^{**} , robot $C(p, \bar{\lambda})$ can move freely on the Voronoi edges whose bottleneck width w_i^* is greater than $\bar{\lambda}$.

The collision-free paths may be obtained by a slightly different method, called the *retraction method*, using a different Voronoi diagram (the original idea was proposed by Lozano-Pérez and Wesley, 1979; Ó'Dúnlaing *et al.*, 1983; Ó'Dúnlaing and Yap, 1985; and Kedem and Sharir, 1985). In place of the convex distance $d_{\text{conv}}(B, A_i)$, the diagram is defined in terms of the distance given by

$$d_{\min E}(B, A_i) = \min_{p, q} \{d_E(p, q), p \in B, q \in A_i\}, \quad (3.7.27)$$

where $d_E(p, q)$ is the Euclidean distance between two points p and q . Note that $d_{\text{conv}}(B, A_i) \neq d_{\min E}(B, A_i)$ in general. As a generator polygon (an obstacle), we consider an *expanded polygon (obstacle)* defined by $A_i^{+C} = \{p \mid A_i \cap C(p) \neq \emptyset\}$ (the heavy line polygon in Figure 3.7.35) (Kedem and Sharir, 1985). At the same time, we consider a 'shrunken robot', i.e. robot $C(p, \bar{\lambda})$ is shrunk to the point $p = C(p, 0)$. For $C(p, \bar{\lambda})$, $C(p, 0)$, A and A^{+C} , a nice relation holds: the distance $d_{\min E}(C(p), A_i)$ from robot $C(p, \bar{\lambda})$ to obstacle A_i is the same as the distance $d_{\min E}(p, A_i^{+C})$ from the shrunken robot $C(p, 0)$ to the expanded obstacle A_i^{+C} (observe in Figure 3.7.35 that the lengths of the two arrows are the same). Thus the region in which robot $C(p, \bar{\lambda})$ can move without colliding with obstacles A_1, \dots, A_n is the same as the region in which the shrunken robot $C(p, 0)$ is in the complement of the expanded obstacles $A_1^{+C}, \dots, A_n^{+C}$.

For a set $A^{+C} = \{A_1^{+C}, \dots, A_n^{+C}\}$, as shown in Section 3.6, we can construct the area Voronoi diagram, \mathcal{V}_{exp} , with the Euclidean distance (note that when A_i^{+C} and A_j^{+C} overlap, we use $A_i^{+C} \cup A_j^{+C}$ as a generator polygon). We call

\mathcal{V}_{exp} , the *area Voronoi diagram for expanded obstacles* (Figure 3.7.35). The paths consisting of Voronoi edges of \mathcal{V}_{exp} are collision-free paths, which are optimal in the sense that the robot is as far from the obstacles as possible in terms of the distance d_{mine} . It should be noted that $\mathcal{V}_{\text{conv}}$ is not the same as \mathcal{V}_{exp} . Both diagrams provide optimal collision-free paths, but the optimality is evaluated in terms of different distances. Also note that a fast algorithm is developed by Rajasekaran and Ramaswami (1995) using a mesh-connected computer.

Robot motion planning becomes difficult when a robot is allowed not only to translate but also to rotate. This problem is discussed in Lozano-Pérez and Wesley (1979), Schwartz and Sharir (1983a,b) and Canny and Donald (1988) who propose the ‘simplified’ Voronoi diagram, and Takahashi and Schilling (1989) (a rectangular robot).

The spherical Voronoi diagram and the spherical Delaunay tessellation are used for spatial data management of terrestrial objects (Lukatela and Russell, 1992; Gold, 1997), meteorological modelling, shallow water equations (Augenbaum, 1984, 1985), interpolation on the globe (Renka, 1984a,b), point pattern matching in astronautics (Weber *et al.*, 1994), and minimum spanning trees and Steiner minimum trees on a sphere (Dolan *et al.*, 1991).

An application of the cylindrical Voronoi diagram is found in the locational optimization of facilities that open periodically (see Chapter 9) Hyman and Mayhew (1983) use the cylindrical, conic and polyhedral Voronoi diagrams for emergency service medical provision in cities.

The oriented Voronoi diagram is utilized in finding the shortest paths among polygonal obstacles (Mitchell, 1992), and the right triangle distance Voronoi diagram is utilized for sorting (Chew and Fortune, 1997).

3.8 NETWORK VORONOI DIAGRAMS

In Section 3.7 we showed that the Manhattan Voronoi diagram or the Karlsruhe Voronoi diagram were useful to investigate dominance regions in a grid street system or a radial–circular street system. Many actual streets are, however, not so regular. Even in Manhattan the streets do not completely form a grid. To deal with a Voronoi diagram in a more realistic street system, it may be worth formulating a Voronoi diagram on a general network.

We consider a planar geometric graph $G(N, L)$ consisting of a set of nodes $N = \{p_1, \dots, p_n, p_{n+1}, \dots, p_l\}$ and a set of links $L = \{l_1, \dots, l_k\}$ which form a connected component. For simplicity, we assume that $G(N, L)$ is a non-directed graph (the extension to a directed graph is not difficult). On $G(N, L)$ we define the distance from a point p on a link in L to a node p_i in N by the length of the shortest path from p to p_i . We call this distance the *network distance*, and denote it by $d_{\text{net}}(p, p_i)$. We call a geometric graph $G(N, L)$ with the network distance a *network*, and denote it by $\mathcal{N}(N, L)$. We assume without loss of generality that the generators are the first n elements of N , i.e. $P = \{p_1, \dots, p_n\}$.

3.8.1 The network Voronoi node diagram

We first consider that a space S is given by the node set N , called a *node space* (the unfilled circles, triangles and squares in Figure 3.8.1) of a network $\mathcal{N}(N, L)$ (the dashed lines with the nodes in Figure 3.8.1). Let

$$\text{Dom}(p_i, p_j) = \{p_k \mid p_k \in N; d_{\text{net}}(p_k, p_i) \leq d_{\text{net}}(p_k, p_j)\}, \quad i \neq j, \quad (3.8.1)$$

$$b(p_i, p_j) = \{p_k \mid p_k \in N; d_{\text{net}}(p_k, p_i) = d_{\text{net}}(p_k, p_j)\}, \quad i \neq j. \quad (3.8.2)$$

We call $\text{Dom}(p_i, p_j)$ the *dominance node set* of p_i over p_j , and $b(p_i, p_j)$ the *bisector node set* between p_i and p_j . The bisector node set may be empty. In fact, if no nodes are equally distant from any two nodes in N , the bisector node set is empty. Note that the bisector node set has quite different features from bisectors defined on a continuous plane (such as a bisector producing the ordinary Voronoi diagram), because the bisector node set is a set of discrete points, and so the concept of a boundary is meaningless. We can, however, develop a parallel concept for the bisector node set. When the bisector node set is empty or the shortest path from $p_k \in b(p_i, p_j)$ to p_i and that from $p_l \in b(p_i, p_j)$ to p_j do not have common links for $p_k \neq p_l$, we say that the bisector node set is *well-behaving*, and $\text{Dom}(p_i, p_j)$ is a well-behaving dominance node set.

For well-behaving dominance node sets, we define

$$V_{\text{node}}(p_i) = \bigcap_{j \in I_n \setminus \{i\}} \text{Dom}(p_i, p_j), \quad (3.8.3)$$

and let $\mathcal{V}(P, d_{\text{net}}, N) = \mathcal{V}_{nn} = \{V_{\text{node}}(p_1), \dots, V_{\text{node}}(p_n)\}$. We call the set \mathcal{V}_{nn} the *network Voronoi node diagram* generated by the node set P in the node space N , and call the set $V_{\text{node}}(p_i)$ the *Voronoi node set* associated with the node p_i (Iri and Koshizuka, 1986, Chapter 4). In Figure 3.8.1, three Voronoi node sets generated by p_1, p_2 , and p_3 are indicated by the sets of the unfilled circles, triangles and squares. It should be noted that to avoid lengthy treatments, we assume in the following analysis that the bisector node is empty.

The geometric properties of \mathcal{V}_{nn} appear quite different from those of the generalized Voronoi diagrams defined on a continuous space, because the node space N is discrete. We find, however, a few common properties. First,

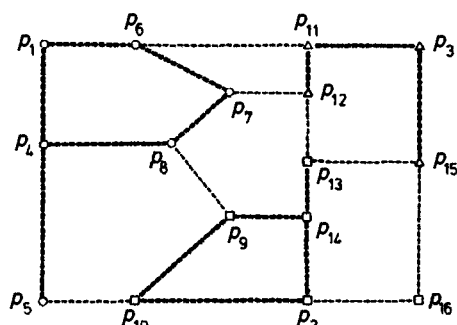


Figure 3.8.1 A network-node Voronoi diagram.

to discuss the ‘shape’ of the Voronoi node set, we consider the subgraph of the graph $G(N, L)$ in which the node set is given by $V_{\text{node}}(p_i)$ and the link set $L(p_i)$ is given by the links in L , both end points (nodes) of which are in $V_{\text{node}}(p_i)$. We denote this subgraph by $G(V_{\text{node}}(p_i), L(p_i))$. In Figure 3.8.1 the subgraphs $G(V_{\text{node}}(p_i), L(p_i)), i \in I_n$, are indicated by the heavy dashed lines. If the shortest path between any two nodes in $V_{\text{node}}(p_i)$ is embedded in $L(p_i)$ of $G(V_{\text{node}}(p_i), L(p_i))$, we say that the Voronoi node set $V_{\text{node}}(p_i)$ is *convex* (as an extension of convexity defined in Section 1.3). If the shortest path from any node in $V_{\text{node}}(p_i)$ to the generator node p_i is embedded in $L(p_i)$ of $G(V_{\text{node}}(p_i), L(p_i))$, we say that the Voronoi node set $V_{\text{node}}(p_i)$ is *star-shaped* (as an extension of star-shape defined in Section 1.3). In observing the shortest path between p_{12} and p_{15} in Figure 3.8.1, we notice that the shortest path is not embedded in $L(p_3)$ of $G(V(p_3), L(p_3))$. Thus, in general a Voronoi node set is not necessarily convex. We notice, however, that every Voronoi node set in \mathcal{V}_{nn} is star-shaped. To sum up, we obtain the following property.

Property NN1 No Voronoi node set $V_{\text{node}}(p_i)$ is empty. A Voronoi node set $V_{\text{node}}(p_i)$ is not necessarily convex, but it is star-shaped with respect to the generator node $p_i, i \in I_n$.

3.8.2 The network Voronoi link diagram

We next consider the space S given by points on links in L , i.e. $S = \bigcup_{i=1}^k l_i$, called a *link space*, and let

$$\text{Dom}(p_i, p_j) = \left\{ p \mid p \in \bigcup_{i=1}^k l_i, d_{\text{net}}(p, p_i) \leq d_{\text{net}}(p, p_j), j \in I_n \setminus \{i\} \right\}, \quad (3.8.4)$$

$$b(p_i, p_j) = \left\{ p \mid p \in \bigcup_{i=1}^k l_i, d_{\text{net}}(p, p_i) = d_{\text{net}}(p, p_j) \right\}, \quad i \neq j. \quad (3.8.5)$$

We call the set $\text{Dom}(p_i, p_j)$ the *dominance region* of p_i over p_j on links in L , and the set $b(p_i, p_j)$ the *bisector* between p_i and p_j on links in L . If the bisector consists of finite points, we say that the bisector $b(p_i, p_j)$ and the dominance region $\text{Dom}(p_i, p_j)$ are *well-behaving*. A well-behaving bisector implies that the shortest path from $p \in b(p_i, p_j)$ to p_i and that from $p \in b(p_i, p_j)$ to p_j does not share a positive length line segment. For well-behaving dominance regions, we define

$$V_{\text{link}}(p_i) = \bigcap_{j \in I_n \setminus \{i\}} \text{Dom}(p_i, p_j), \quad (3.8.6)$$

and let $\mathcal{V}(P, d_{\text{net}}, \bigcup_{i=1}^k l_i) = \mathcal{V}_{\text{nl}} = \{V_{\text{link}}(p_1), \dots, V_{\text{link}}(p_n)\}$. Since we define \mathcal{V}_{nl} for well-behaving dominance regions, elements in \mathcal{V}_{nl} are collectively exhaustive and mutually exclusive except for the finite number of points. We call this tessellation the *network Voronoi link diagram* generated by P on $N(N, L)$ and the set $V_{\text{link}}(p_i)$ the *Voronoi link set* associated with p_i . Hakimi *et al.* (1992) call \mathcal{V}_{nl} the *Voronoi partition*.

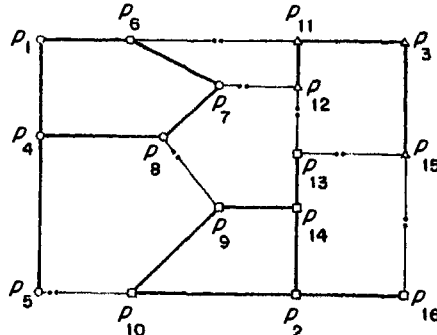


Figure 3.8.2 A network Voronoi link diagram.

Alternatively, we can define the set $V_{\text{link}}(p_i)$ with the subgraph $G(V_{\text{node}}(p_i), L(p_i))$ defined in Section 3.8.1. From the definition of the Voronoi node set, we note that if $p \in \cup_{j \in L(p_i)} l_j$, then $p \in V_{\text{link}}(p_i)$, i.e. a point on the heavy lines in Figure 3.8.2 is assigned to its generator. What is left to assign is a point on the links indicated by the light lines in Figure 3.8.2. We denote the k th link connecting a node in $V_{\text{node}}(p_i)$ and a node in $V_{\text{node}}(p_j)$ by l_{ijk} , $k \in I_{n_{ij}}$ (note that $I_{n_{ij}}$ may be empty for some pairs i and j). We divide the link l_{ijk} at the equally distant point from p_i and p_j and denote the resulting link connected to the node in $V_{\text{node}}(p_i)$ by l_{ijkl} , i.e.

$$l_{ijkl} = \{p \in l_{ijk} \mid d_{\text{net}}(p, p_i) \leq d_{\text{net}}(p, p_j)\} \quad (3.8.7)$$

(Figure 3.8.2). Then the set $V_{\text{link}}(p_i)$ given by equation (3.8.6) is written as

$$V_{\text{link}}(p_i) = \left[\bigcup_{l_i \in L(p_i)} l_i \right] \bigcup \left[\bigcup_{j \in I_n \setminus \{i\}} \bigcup_{k \in I_{n_{ij}}} l_{ijkl} \right]. \quad (3.8.8)$$

An actual network Voronoi link-diagram of roads is shown in Figure 3.8.3.

For the network Voronoi link diagram, almost the same property as in Property NN1 holds although a slight modification is necessary for the definition of convexity and star-shape. If the shortest path between any two points in $V_{\text{link}}(p_i)$ is embedded in $V_{\text{link}}(p_i)$, we say that the Voronoi link set is *convex*. If the shortest path from a point in $V_{\text{link}}(p_i)$ to the generator node p_i is embedded in $V_{\text{link}}(p_i)$, we say that the Voronoi link set $V_{\text{link}}(p_i)$ is *star-shaped*. Using these terms, we can state the following property.

Property NL1 No Voronoi node set $V_{\text{link}}(p_i)$ is empty. A Voronoi node set $V_{\text{link}}(p_i)$ is not necessarily convex, but it is star-shaped with respect to the generator node p_i , $i \in I_n$.

3.8.3 The network Voronoi area diagram

In the network Voronoi node diagram and link diagram, a point to be assigned to a generator is restricted to a point on a node or a link. In some



Figure 3.8.3 The network Voronoi link diagram of roads in the Nishinomiya district of Osaka (the large filled circles indicate generators and the small filled circles indicate the boundary points). (Source: Yomono, 1991, Figure 1.)

contexts, however, we find this restriction is too strong. For example, if we can access a network from any point in a region and take a path from the access point to a destination through links, every point (including a point on a node and a link) in a region should be assigned to a generator. To treat this assignment, we consider a Voronoi diagram formulated on \mathbb{R}^2 with a network $\mathcal{N}(N, L)$.

Let $P \subset N$ be a generator set on a network $\mathcal{N}(N, L)$ placed in \mathbb{R}^2 , and assume that the dominance region $\text{Dom}(p_i, p_j)$ defined by equation (3.8.4) is well-behaving for any $i, j \in I_l$, $i \neq j$. We first assign a point p in \mathbb{R}^2 to the nearest point, called the *access point*, on a link of L ; second, the access point is assigned to the nearest generator node p_i with respect to the network distance. To be precise, let $a(p)$ be the nearest point on $\bigcup_{i=1}^k l_i$ from p , i.e.

$$d_{\text{acc}}(p, a(p)) = \|x - x_a\| = \min_u \left\{ \|x - u\| \mid u \in \bigcup_{i=1}^k l_i \right\}, \quad (3.8.9)$$

where x , x_a , and u are the location vectors of points p , $a(p)$ and an arbitrary point on $\bigcup_{i=1}^k l_i$ (the dotted lines in Figure 3.8.4), respectively. We call the point $a(p)$ the *access point* of p to $N(N, L)$, and the distance $d_{\text{acc}}(p, a(p))$ the *access distance* from p . In terms of the access distance and the network distance, the distance from a point p in \mathbb{R}^2 to a node p_i in N is written as

$$d_{\text{acc-net}}(p, p_i) = d_{\text{acc}}(p, a(p)) + d_{\text{net}}(a(p), p_i) \quad (3.8.10)$$

(Okabe and Yomono, 1988). We should note that this distance is not always the shortest distance from a point p to a node p_i , because the access distance is determined locally by equation (3.8.9). With the distance of equation (3.8.10), we define

$$V_{\text{area}}(p_i) = \{p \mid d_{\text{acc-net}}(p, p_i) \leq d_{\text{acc-net}}(p, p_j), j \in I_n \setminus \{i\}\}. \quad (3.8.11)$$

This set is alternatively defined with the line Voronoi diagram defined in Section 3.5. First, recall that we can define $V_{\text{area}}(p_i)$ provided that the network Voronoi link diagram can be defined for $N(P, L)$. This means that $V_{\text{link}}(p_1), \dots, V_{\text{link}}(p_n)$ are mutually exclusive except at a finite number of points. If an access point $a(p)$ belongs to a link in $V_{\text{link}}(p_i)$, it follows from the definition of the network Voronoi link diagram that the point p is assigned to the generator p_i . Thus, a point p being assigned to p_i is equivalent to a point p being assigned to the nearest generator among the generators given by $\{V_{\text{link}}(p_1), \dots, V_{\text{link}}(p_n)\}$. This assignment is indeed the assignment of a point p in the line Voronoi diagram of $L = \{l_1, \dots, l_n\}$, where l_i is given by $V_{\text{link}}(p_i)$. The set $V_{\text{area}}(p_i)$ is hence written as $V_{\text{area}}(p_i) = V_L(V_{\text{link}}(p_i))$, where $V_L(V_{\text{link}}(p_i))$ is the line Voronoi region associated with the generator consisting of lines in $V_{\text{link}}(p_i)$. When we refer to this line Voronoi diagram in a network study, we call the set $\mathcal{V}(P, d_{\text{acc-net}}, \mathbb{R}^2) = \mathcal{V}_{\text{na}} = \{V_{\text{area}}(p_1), \dots, V_{\text{area}}(p_n)\}$ the *network Voronoi area diagram*.

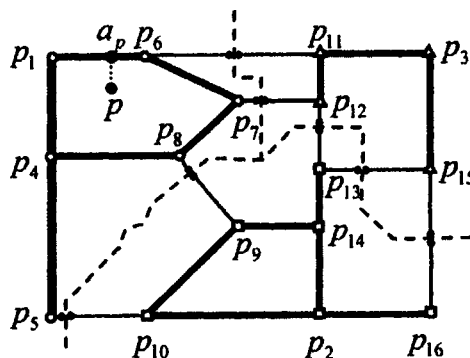


Figure 3.8.4 A network Voronoi area-diagram.

Since \mathcal{V}_{na} is exactly the same as the Voronoi line diagram, the properties of the network Voronoi area diagram are shared with those of the Voronoi link diagram.

3.8.4 Applications

As mentioned in Section 1.2, the earliest application of the network Voronoi diagram is found in Snow (1855) who studied spatial epidemiology on a street network around a water pump.

The network Voronoi diagram is implicitly used in multi-median problem (Hakimi, 1964, 1965), which is one of the central subjects in locational optimization on a network (Handler and Mirchandani, 1979). Yomono (1991) showed the network Voronoi line diagram with respect to stations in the Nishinomiya district of Osaka (Figure 3.8.3). Hakimi *et al.* (1992) consider the Voronoi p -centre problem (Section 9.2.8). Okabe and Okunuki (2000) use the network Voronoi area diagram to estimate market areas.

3.9 VORONOI DIAGRAMS FOR MOVING POINTS

In the preceding sections we assumed that the locations of generators are fixed over time. In this section we relax this assumption and consider a Voronoi diagram generated by a set of moving points over time or, more generally, a set of points whose locations are determined by one parameter.

3.9.1 Dynamic Voronoi diagrams

Let $\mathbf{x}_i(t)$ and $\mathbf{x}(t)$ be the location vectors of the i th generator point and an arbitrary point in \mathbb{R}^m at time t , respectively, and $P(t) = \{\mathbf{x}_1(t), \dots, \mathbf{x}_n(t)\}$. We assume that $\mathbf{x}_i(t)$ is continuous with respect to t in \mathbb{R}^m and no points collide. For a point (\mathbf{x}_i, t) in \mathbb{R}^{m+1} , we define a set $V(\mathbf{x}_i, t)$ of points (\mathbf{x}, t) in \mathbb{R}^{m+1} by

$$V(\mathbf{x}_i, t) = \{(\mathbf{x}, t) \mid \|\mathbf{x}(t) - \mathbf{x}_i(t)\| \leq \|\mathbf{x}(t) - \mathbf{x}_j(t)\|, j \in I_n \setminus \{i\}\}, \quad (3.9.1)$$

and let $\mathcal{V}(t) = \{V(\mathbf{x}_1, t), \dots, V(\mathbf{x}_n, t)\}$. We call the set $\mathcal{V}(t)$ the *dynamic (ordinary) Voronoi diagram* generated by $P(t)$ (Gowda *et al.*, 1983). Gold *et al.* (1997) call it the *kinematic Voronoi diagram*. Obviously, $\mathcal{V}(t)$ for a fixed point in time $t = t^*$, i.e. $\mathcal{V}(t^*)$, is the ordinary Voronoi diagram. In contrast to $\mathcal{V}(t)$, we call $\mathcal{V}(t^*)$ the *static (ordinary) Voronoi diagram*. An example of the dynamic Voronoi diagram in a two-dimensional space ($m = 2$) is shown in Figure 3.9.1 where four points move linearly with respect to t (the broken lines). Note that the dynamic Voronoi diagram defined here should be distinguished from that defined in the incremental method (Chapter 4) (Gowda *et al.*, 1983), that of Voronoi growth models (Section 5.6.2), that defined in astronomy (Zaninetti, 1989, 1990, 1995) and that defined in the dynamic maintenance of temporal maps (Gold *et al.*, 1996).

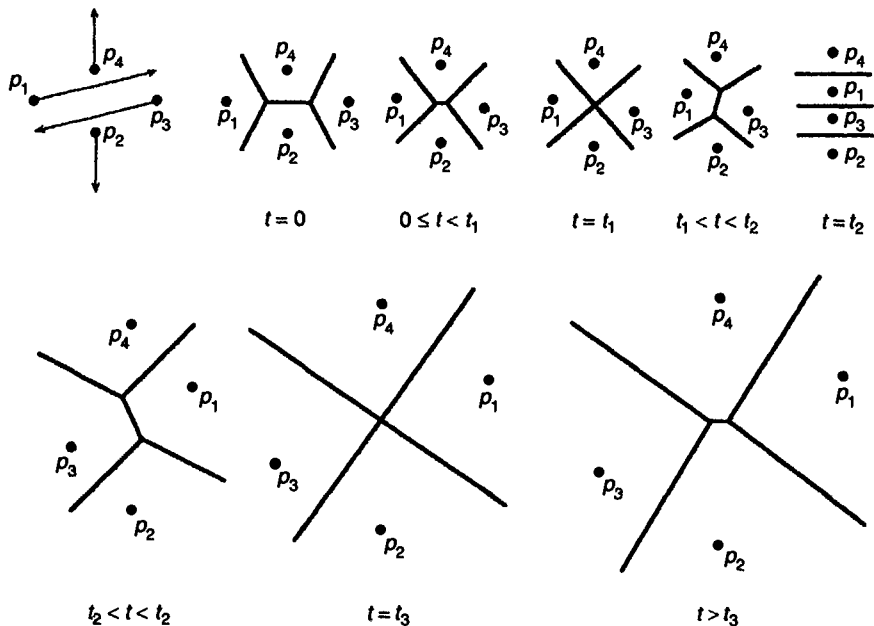


Figure 3.9.1 A dynamic Voronoi diagram in a two-dimensional space.

In Chapter 2 we defined a Delaunay triangulation as the dual of a Voronoi diagram. Similarly we can define a Delaunay triangulation as the dual of the dynamic Voronoi diagram. We call this triangulation the *dynamic Delaunay triangulation* (Devillers *et al.*, 1992). Rodin *et al.* (1992) call it the *flexible Delaunay triangulation*. Note that the dynamic Delaunay triangulation defined here should be distinguished from the Delaunay triangulation constructed by the incremental method (Devillers *et al.*, 1992), and cell growth models in crystallography (Section 7.2) or astrophysics (Zaninetti, 1990, 1995).

As is seen in Figure 3.9.1 (where four generator points move according to the arrows shown in the upper-left panel), the shape of $V(x_i)$ changes over time; in particular, a drastic change occurs when the topological configuration changes, i.e. at times t_1, t_2 and t_3 in Figure 3.9.1. We call these topological changes *topological events* (Fu and Lee, 1991; Albers and Roos, 1992). In Figure 3.9.1 three topological events occur. The number of topological events depends on the manner of motion of $P(t)$. A typical motion is given by $x_i(t) = \sum_{j=0}^k c_{ij} t_j$, where c_{ij} is an m -dimensional constant vector. This motion is called k -*motion* (Atallah, 1983), and 1-motion is called *linear motion*. The motion in Figure 3.9.1 is the linear motion, i.e. $x_i(t) = c_{i1} t + c_{i0} \in \mathbb{R}^2$. The number of topological events varies according to the values of the constants c_{i1} and c_{i0} . For instance, if c_{11}, c_{21}, c_{31} and c_{41} are all different, as in the above example, the number of topological events is three; if they are all the same, the number of topological events becomes zero, because all points move

rigidly and no topological events occur over time. In the study of dynamic Voronoi diagrams, one of the major concerns is with the possible maximum number of topological events for a given manner of motion, say the k -motion. This number is called the *topological complexity* (Huttenlocher *et al.*, 1992a) or *combinatorial complexity* (Imai and Imai, 1993a,b).

The topological complexity of a dynamic Voronoi diagram may be written in terms of a sequence, called the 'Davenport-Schinzel sequence'. To state it explicitly, consider a set $B = \{b_1, \dots, b_n\}$ of n different alphabet letters (or integers), and let S_B be a set of all possible sequences consisting of letters chosen from B (the length of a sequence is between 1 and n). For a sequence in S_B , say $(b_1 b_2 b_4 b_3 b_5 b_1 b_3 b_2)$, we consider a subsequence of the sequence containing two different letters, for example b_1, b_2, b_1, b_2 of the sequence $(b_1 b_2 b_4 b_3 b_5 b_1 b_3 b_2)$, and denote it by $[b_1 b_2 b_1 b_2]$. Let $\xi_{ij}^1 = [b_i b_j b_i]$; $\xi_{ij}^{2q} = [\xi_{ij}^{2q-1} b_j]$; $\xi_{ij}^{2q+1} = [\xi_{ij}^{2q} b_i]$, $q = 1, 2, \dots$. For example, $\xi_{25}^2 = [b_2 b_5 b_2 b_5]$, $\xi_{25}^3 = [b_2 b_5 b_2 b_5 b_2]$, $\xi_{25}^4 = [b_2 b_5 b_2 b_5 b_2 b_5]$, and so forth. Then we call an element of S_B an (n, s) *Davenport-Schinzel sequence*, denoted by $DS(n, s)$, if it satisfies the condition that: (i) sequences in $DS(n, s)$ do not contain a subsequence $(b_i b_i)$ (not $[b_i b_i]$), i.e. letters change every time; (ii) sequences in $DS(n, s)$ do not contain any ξ_{ij}^s as a subsequence, $i, j \in I_n$ (Davenport and Schinzel, 1965). An example of a sequence in $DS(6, 2)$ is $(b_1 b_6 b_2 b_4 b_5 b_1 b_3)$ (confirm that letters change every time in the sequence and the sequence does not contain any $[b_i b_i b_i]$).

The length of a sequence in $DS(n, s)$ is not constant, for example $(b_1 b_6 b_2 b_4 b_5 b_1 b_3)$, $(b_1 b_6 b_2 b_4 b_1)$ and $(b_1 b_2 b_3 b_5 b_6 b_5 b_4 b_2 b_1)$ are all in $DS(6, 2)$. We now ask: What is the maximum length, $\lambda(n, s)$, among the sequences in $DS(n, s)$? First, consider $\lambda(n, 1)$. Since a sequence in $DS(n, 1)$ does not contain $\xi_{ij}^1 = [b_i b_j b_i]$, the same letter does not appear in a sequence of $DS(n, 1)$. Thus the maximum length is achieved when a sequence is given by, for example, $(b_1 b_2 \dots b_n)$. Hence $\lambda(n, 1) = n$. Second, consider $\lambda(n, 2)$. Since a sequence in $DS(n, 2)$ does not contain any $\xi_{ij}^2 = [b_i b_j b_i b_j]$, a letter b_j between the same letters b_i does not appear after the second b_i in a sequence of $DS(n, 2)$. Thus the maximum length is achieved when a sequence is given by, for example, $(b_1 \dots b_{n-1} b_n b_{n-1} \dots b_1)$. Hence $\lambda(n, 2) = 2n - 1$. When $s \geq 3$, an explicit function of $\lambda(n, s)$ is difficult to derive. Here we only note that $\lambda(n, s)$ is of order $n \log^* n$ ($s \geq 3$), where $\log^* n$ means the number of taking logs that gives the first negative value, for example $\log 100 = 2$, $\log(\log 100) = 0.301 \dots$, $\log(\log(\log 100)) = -0.521 \dots$, and so $\log^* 100 = 3$. We also note that sharp upper and lower bounds of $\lambda(n, s)$ are shown by Agarwal *et al.* (1989b). In terms of $\lambda(n, s)$ we can state the following properties.

Property DV1 When generator points in $P(t) = \{x_1(t), \dots, x_n(t)\}$ move along continuous trajectories in \mathbb{R}^m , the topological complexity of the dynamic Voronoi diagram generated by $P(t)$ is of order $n^m \lambda(n, s)$, where s is a constant determined by the characteristic of the trajectories.

The proof is shown by Albers and Roos (1992). A slightly different theorem is proved by Roos (1993, Theorem 4.2).

The value of s in Property DV1 becomes explicit when the motion is explicitly stated. As a corollary to Property DV1, we have the following property.

Property DV2 When generator points in $P(t) = \{x_1(t), \dots, x_n(t)\}$ move in the linear motion in \mathbb{R}^2 , the topological complexity of the dynamic Voronoi diagram generated by $P(t)$ is of order $n^2 \lambda(n, 4)$.

The proof is shown by Guibas *et al.* (1991) and Imai and Imai (1990).

Huttenlocher *et al.* (1992a) show the topological complexity of $\mathcal{V}(t)$ in which subsets $P_1(t), \dots, P_q(t)$ of $P(t)$ move rigidly ($\bigcup_{i=1}^q P_i(t) = P(t)$, $P_i(t) \cap P_j(t) = \emptyset, i \neq j$). Guibas *et al.* (1991) and Roos (1994, 1997) show the topological complexity of $\mathcal{V}(t)$ in which only k points move while the other $n-k$ points are fixed.

In theory, all static generalized Voronoi diagrams shown in Sections 3.2–3.8 can be developed into *dynamic generalized Voronoi diagrams* by assuming that generators move over time. Actually Imai and Imai (1993a,b, 1998) formulate the *dynamic weighted Voronoi diagram* and the *dynamic kth order Voronoi diagram*.

3.9.2 Applications

A natural application of the dynamic Voronoi diagram is found in the dynamic configuration of service areas of mobile facilities. Consider a region in which mobile radio stations are moving under a certain time schedule. Receivers in the region want to catch the strongest wave among the waves transmitted from the mobile stations over time. Then a receiver at a location x at time t should use the mobile station whose Voronoi polygon $V(x_i, t)$ includes (x_i, t) , where $\mathcal{V}(t) = \{V(x_i, t), i \in I_n\}$ is the dynamic Voronoi diagram generated by the mobile stations. A similar application is shown by Devillers and Golin (1993) who extend the post-office problem (Section 2.3, Problem V3) of postmen (and a dog) moving with constant velocities. Blatov and Serezhkin (1997) investigate the connection between the topology of systems with many particles with the presence or absence of short-range or long-range order using the dynamic Voronoi diagram.

Another application is found in motion planning discussed in Section 3.7.11. The problem is to find a collision-free path or the safest path along which a robot moves among moving obstacles. Roos and Noltemeier (1991, 1992) solve this problem where a robot is represented by a disk. Rodin *et al.* (1992) apply the dynamic Voronoi diagram to implement a navigation system for an autonomous vehicle in an environment cluttered with both stationary and moving obstacles.

As noted in Section 3.9.1, t in $\mathcal{V}(t)$ does not necessarily represent time but a parameter. An application of $\mathcal{V}(t)$ with a non-time parameter is found in Problem FP3 discussed in Section 3.3.3 (the farthest-point Voronoi diagram).

The problem is to fit the configuration of points $P = \{p_{ij}, i \in I_{n_1}, j \in I_{n_2}\}$ placed at a square grid, i.e. $p_{ij} = (a(i-1), a(j-1))$, to a given configuration of points $Q = \{q_{ij}, i \in I_{n_1}, j \in I_{n_2}\}$ (see Figure 3.3.3) by translation and rotation in such a way that the distance between a point in P and a point in Q is minimized. In Section 3.3 we assumed that the configuration P moved through translation. Here we assume that the configuration P moves not only through translation but also rotation.

To solve the problem, let $p_{ij}(x_1, x_2, \theta)$ be the point p_{ij} that is translated by (x_1, x_2) and rotated by θ , i.e. $p_{ij}(x_1, x_2, \theta) = (x_1 + a(i-1) \cos \theta - a(j-1) \sin \theta, x_2 + a(i-1) \sin \theta + a(j-1) \cos \theta)$. Then the distance between $p_{ij}(x_1, x_2, \theta)$ and q_{ij} is given by

$$\begin{aligned} d(p_{ij}(x_1, x_2, \theta)) &= [((x_1 + a(i-1) \cos \theta - a(j-1) \sin \theta) - u_{ij})^2 \\ &\quad + ((x_2 + a(i-1) \sin \theta + a(j-1) \cos \theta) - v_{ij})^2]^{1/2} \\ &= [(x_1 - (u_{ij} - a(i-1) \cos \theta + a(j-1) \sin \theta))^2 \\ &\quad + (x_2 - (v_{ij} - a(i-1) \sin \theta - a(j-1) \cos \theta))^2]^{1/2}. \end{aligned} \quad (3.9.2)$$

Thus $d(p_{ij}(x_1, x_2, \theta))$ may be regarded as the distance between (x_1, x_2) and $o_{ij}(\theta) = (u_{ij} - a(i-1) \cos \theta + a(j-1) \sin \theta, v_{ij} - a(i-1) \sin \theta - a(j-1) \cos \theta)$. Let $O(\theta) = \{o_{ij}(\theta), i \in I_{n_1}, j \in I_{n_2}\}$. Then the problem is restated as: find the point (x_1, x_2) from which the distance to the farthest point in $O(\theta)$ is the shortest. This problem can be solved through the dynamic farthest-point Voronoi diagram generated by $O(\theta)$ where points move linearly with respect to θ (Imai *et al.*, 1989, 1998; Imai and Imai, 1998 (an extension using the dynamic weighted Voronoi diagram)).

The dynamic Voronoi diagram may be used to construct the line Voronoi diagram. Gold (1990) and Gold *et al.* (1995, 1997) show an incremental method in which a line segment is generated by a trajectory of a point moving from one end point to the other end point of the line segment. Huttenlocher *et al.* (1992b) apply the dynamic Voronoi diagram to the problem of finding the minimum Hausdorff distance between two sets in the plane under Euclidean motion.

CHAPTER 4

Algorithms for Computing Voronoi Diagrams

In this chapter we consider practical methods for constructing Voronoi diagrams. Here, we mainly concentrate our attention on the most basic case, namely the Voronoi diagram for points in a plane. In Section 4.1 we present a naive method which follows directly from the definition of the Voronoi diagram. The naive method is however inefficient, and many efforts have been made in the field of computational geometry to make efficient algorithms, which are also surveyed in this section. In Section 4.2 we present a typical data structure for representing the Voronoi diagram and thus make clear what is meant by the ‘construction’ of the Voronoi diagram. We also derive a lower bound of the time complexity for the construction of the Voronoi diagram. Then we present three typical algorithms, respectively, in Sections 4.3, 4.4 and 4.5. These algorithms are designed on the assumption that no numerical error takes place in the course of computation, so that a direct translation of such an algorithm to a computer program does not necessarily give a numerically valid program; such a program may fail because of geometric inconsistency caused by numerical errors. In order to make a practically valid computer program, we have to consider numerical errors. Hence, in Section 4.6 we present two typical techniques for avoiding inconsistency due to numerical errors. The last three sections, Sections 4.7, 4.8 and 4.9, are concerned with generalized Voronoi diagrams. In Section 4.7 we present a typical algorithm for constructing higher dimensional Voronoi diagrams, while in Section 4.8 we briefly touch upon algorithms for various kinds of generalized Voronoi diagrams in the plane. Finally in Section 4.9 we present approximation algorithms for generalized Voronoi diagrams.

4.1 COMPUTATIONAL PRELIMINARIES

As in the previous chapter, let $P = \{p_1, \dots, p_n\}$ be the set of generators, and $\mathcal{V} = \{V(p_1), \dots, V(p_n)\}$ denote the Voronoi diagram for P . The construction

of the Voronoi diagram is a procedure for generating \mathcal{V} from P . In the previous chapter we saw several equivalent conditions for characterizing the Voronoi diagram. Among them the characterization based on the half planes (Definition V3) directly gives us a naive method for constructing the diagram. The Voronoi polygon for the generator p_i is the intersection of all the half planes defined by the perpendicular bisectors of p_i and the other generators. According to this definition, we can construct the Voronoi polygons one by one. Thus we get the following method.

Naive method

Input: n generators p_1, p_2, \dots, p_n .

Output: Voronoi diagram $\mathcal{V} = \{V(p_1), V(p_2), \dots, V(p_n)\}$.

Procedure :

Step 1. For each i such that $i = 1, 2, \dots, n$, generate $n-1$ half planes $H(p_i, p_j)$, $1 \leq j \leq n, j \neq i$, and construct their common intersection $V(p_i)$.

Step 2. Report $\{V(p_1), V(p_2), \dots, V(p_n)\}$ as the output and stop.

In this chapter we present a number of geometric algorithms and name them with sequential numbers. However, we do not want to call the above method a practical ‘algorithm’, because it is ‘insufficient’. Let us see how ‘insufficient’ the above method is. To evaluate an algorithm, we have to consider at least correctness and efficiency, and if it involves numerical computation, we also have to consider robustness against numerical errors. The above method is correct, because it is a restatement of the definition of the Voronoi diagram. So, we consider the other two aspects.

First we consider efficiency. To construct the half plane $H(p_i, p_j)$ for two given points p_i and p_j requires only constant time. Hence for each p_i the time required for constructing $n-1$ half planes is proportional to $n-1$, say $a(n-1)$, where a is a positive constant. To construct the intersection of the half planes, let us consider the following simple procedure. First we construct the intersection of two half planes, obtaining a polygon with two sides; next construct the intersection of this polygon with the third half plane, and so on. In the k th step of this procedure, we have to find the intersection of a k -sided polygon (in the worst case) with another half plane, and this step requires time at least proportional to k if we check whether each of the k sides crosses the boundary line of the half plane. Thus, constructing the intersection of $n-1$ half planes requires time proportional to $1 + 2 + \dots + (n-2) = (n-2)(n-1)/2$, say $b(n-2)(n-1)$, where b is another positive constant. We have to repeat this process for all generators, and consequently the total time required by the naive method is

$$T(n) = n\{a(n-1) + b(n-2)(n-1)\} = O(n^3).$$

This means that for a computer program based on the above procedure, the time for processing becomes eight ($= 2^3$) times larger as the size of the input data becomes twice as large.

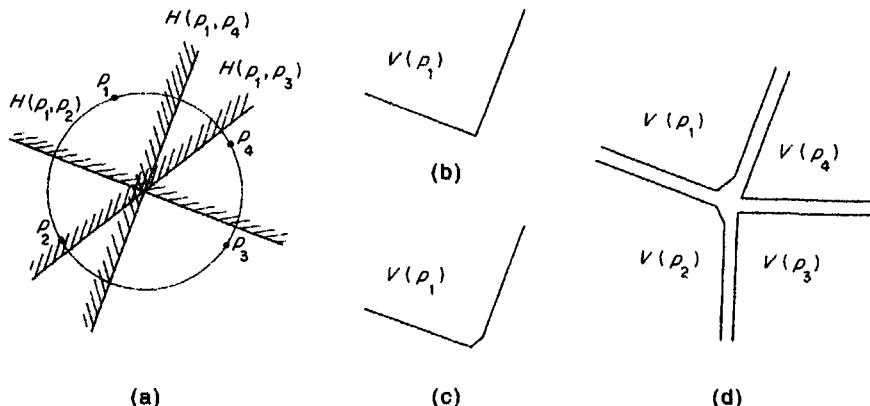


Figure 4.1.1 Inconsistency caused by numerical errors: (a) four generators on a common circle; (b) possible Voronoi polygon for p_1 ; (c) another possible Voronoi polygon for p_1 ; (d) inconsistent set of Voronoi polygons.

Employing a little more sophisticated technique, we can construct the intersection of $n-1$ half planes in $O(n \log n)$ time (Preparata and Shamos, 1985). Hence the time complexity of the naive method can be decreased to $O(n^2 \log n)$.

As we will see in the next section, any algorithm for constructing the Voronoi diagram requires at least $O(n \log n)$ time in the worst case, and at least $O(n)$ time on average. Moreover, there exist algorithms whose time complexities attain these lower bounds, and some of them actually run very fast even for small values of n (although the order itself represents the behaviour of the algorithm as n approaches infinity). The algorithm presented in Section 4.3 requires $O(n)$ time on average and $O(n^2)$ time in the worst case, while the algorithms presented in Sections 4.4 and 4.5 require $O(n \log n)$ time in the worst case. Compared with these algorithms, the naive algorithm is not very satisfactory from the time-complexity point of view.

Another important point of view for evaluating the algorithm is robustness against numerical errors. From this point of view too the naive method is not satisfactory. This can be understood by the following example. Suppose that there are only four generators p_1, p_2, p_3 and p_4 and they come very near to a common circle. Then, as shown in Figure 4.1.1(a), the three perpendicular bisectors between p_1 and the other generators pass near to the centre of the circle; if numerical error takes place, it is difficult to decide the relative locations of the points of intersections of these bisectors. Hence the result of intersecting the three half planes associated with p_1 may be a two-sided polygon as in (b) or a three-sided polygon as in (c); which result comes out depends on numerical errors. The other three Voronoi polygons have similar instability. In the naive method, each Voronoi polygon is computed independently, so that the result may become topologically inconsistent, as shown in Figure 4.1.1(d). This figure is contradictory, because the Voronoi

polygon $V(p_1)$ shows that there is a Voronoi edge between p_1 and p_3 , but the Voronoi polygon $V(p_3)$ shows that such a Voronoi edge does not exist; we cannot glue the boundaries of the Voronoi polygons together.

From a theoretical point of view all the Voronoi polygons give a tessellation of the plane, but in actual computation the output of the naive method does not necessarily give a tessellation of the plane. Thus the naive method, if translated to a computer program in a straightforward manner, is not robust against numerical errors. Its output may be topologically inconsistent. We need careful consideration in order to make a numerically robust algorithm. Basic techniques for this purpose will be presented in Section 4.6.

Here, we will briefly survey typical algorithms for constructing the ordinary Voronoi diagram in the plane. First of all, we should note that some algorithms are described in terms of the Voronoi diagram itself (e.g. Shamos and Hoey, 1975; Sibson, 1980a; Ohya *et al.*, 1984a), while others are described in terms of the Delaunay diagram (e.g. Lee and Schachter, 1980; Guibas and Stolfi, 1985). As we saw in Section 2.2, however, these two diagrams are duals of each other, and we can transform one to the other and vice versa. Moreover, the description of the algorithm itself can be transformed from Voronoi diagram terminology to Delaunay diagram terminology, and vice versa. Hence the choice of the terminology does not make any essential difference.

The naive method presented above is one of the easiest methods to understand (Rhynsburger, 1973) because it is a direct translation of the definition of the Voronoi diagram. Although this method is not recommended for general purposes, it may be used for some special types of simulation where the goal is not to construct the Voronoi diagram itself, but to generate many samples of Voronoi polygons to obtain statistical data such as the distribution of the number of edges per polygon (Crain, 1978; Boots and Murdoch, 1983; Quine and Watson, 1984). Bentley *et al.* (1980) combined this method with a bucketing technique and presented an algorithm that runs in $O(n)$ time on average, in which generators relevant to each Voronoi polygon are searched for from bucket to bucket in a spiral order (the bucketing technique will be described in Section 4.3). However, the output of the naive method is a simple collection of Voronoi polygons, and it does not include explicit information about the topological structure of the diagram. As we will see in more detail in the next section (Section 4.2), if we want to extract various kinds of information from the Voronoi diagram, the naive method is not suitable.

The second method, which is another naive method, can be categorized as a 'walking method', in which Voronoi vertices and Voronoi edges (or, equivalently, Delaunay polygons and Delaunay edges) are constructed one by one just in the order in which a traveller walks along the edges of the diagram. This method was described in Delaunay diagram terminology by Lawson (1977), and in Voronoi diagram terminology by Brassel and Reif (1979) and Cromley and Grogan (1985). While they did not consider the time complexity point of view, Maus (1984) utilized the bucketing technique to construct an

$O(n)$ algorithm in the average sense, in which the algorithm is described in terms of the Delaunay triangulation.

The third method may be called a 'flip method', in which an initial diagram is constructed first, and then it is modified step by step until it converges to the Voronoi diagram. Sibson (1978) showed that, starting with any triangulation of $\text{CH}(P)$, we can modify it to the Delaunay triangulation by flipping the diagonals of convex quadrilaterals according to the local max-min angle criterion, i.e. the diagonal of a convex quadrilateral is replaced by the other diagonal if the resulting pair of triangles gives a larger value for the minimum angle. As we saw in Section 2.4, Edelsbrunner (1988) gave an intuitive and simple interpretation of the procedure in the context of the lift-up transformation, and showed that $O(n^2)$ flipping of the diagonals is enough to obtain the Delaunay triangulation from any initial triangulation.

The fourth method, a simple but still very powerful method, is an incremental method, in which we start with a simple Voronoi diagram for two or three generators, and modify it by adding generators one by one; the method was presented in terms of the Voronoi diagram by Green and Sibson (1978), Sibson (1980a,b), Lee and Schachter (1980), Shapiro (1981), Tipper (1990a), and in terms of the Delaunay diagram by Watson (1981), Devijver and Dekesel (1982), Gowda *et al.* (1983), Correc and Chapuis (1987), Palacios-Velez and Renaud (1990), Jünger *et al.* (1991) and Tsai (1993). In the worst case, each addition of a generator requires time proportional to the number of generators added so far, and consequently the total time complexity is of $O(n^2)$. However, the average time complexity can be decreased to $O(n)$ by the use of special data structures such as buckets and a quaternary tree (Ohya, 1983; Iri *et al.*, 1984; Ohya *et al.*, 1984a; Maus, 1984). Randomization techniques are also useful to decrease the average time complexity (de Berg *et al.*, 1995; Guibas *et al.*, 1992). Also a numerically robust version of this method was proposed by Sugihara and Iri (1988, 1989b,d). Thus, this method is one of most practical from both the time-complexity and the robustness points of view. This method will be presented in detail in Section 4.3 and the numerically robust version will be shown in Section 4.6.

The fifth method, another typical method for constructing the Voronoi diagram, is the use of the divide-and-conquer paradigm, in which the set of generators is recursively divided into smaller subsets and the Voronoi diagrams for those subsets of generators are merged into the final diagram. This method was first proposed in terms of the Voronoi diagram by Shamos and Hoey (1975); an early attempt to implement this method was made, for example, by Horspool (1979). Later this method was written in a simpler form using Delaunay triangulation terminology by Drysdale and Lee (1978), Lee and Schachter (1980), Guibas and Stolfi (1985) and Elbaz and Spehner (1990). The worst-case time complexity of this method is $O(n \log n)$, which is the best possible as we will see in the next section. However, as was shown by Ohya *et al.* (1984a), the original divide-and-conquer method requires $O(n \log n)$ time also in the average sense. The average-case time complexity was lessened to $O(n \log \log n)$ by Dwyer (1987), and further to $O(n)$ by

Katajainen and Koppinen (1988). A robust version of the method was also constructed (Ooishi, 1990; Sugihara *et al.*, 1990; Ooishi and Sugihara, 1995). The divide-and-conquer method will be shown in Section 4.4.

The sixth method is the plane sweep method (Fortune, 1986, 1987). The plane sweep is one of fundamental techniques in computational geometry, by which a two-dimensional problem can be reduced to an almost one-dimensional problem. A vertical line, called a sweep line, is moved over the plane from left to right, and the Voronoi diagram is constructed along this line. This method also attains the worst-case optimal time complexity, $O(n \log n)$. This method will be presented in Section 4.5.

The seventh method may be called a ‘lift-up method’, which utilizes the relationship between a two-dimensional Voronoi diagram and a three-dimensional convex hull (Properties D7 and D8). In this method, first the generators in the plane are transformed to certain points in three-dimensional space, then their convex hull is generated, and finally the convex hull is inversely transformed to the original plane to obtain the Delaunay diagram. Brown (1979, 1980), Aurenhammer and Edelsbrunner (1984) and Buckley (1988) used a transformation from the plane to a sphere (Property D7), and Edelsbrunner and Seidel (1986) and O’Rourke *et al.* (1986) used a transformation from the plane to a paraboloid of revolution (Property D8). This method can be extended to any dimension, and hence we will see this method in the context of the construction of higher-dimensional Voronoi diagrams (Section 4.7).

Other directions of algorithmic research include the use of a matrix representation (Fang and Piegl, 1992), construction of the Voronoi diagram for convexly located generators (Agarwal *et al.*, 1989a), digital-image approximation of the Voronoi diagram (Toriwaki *et al.*, 1982; Mark, 1987; Yoshitake *et al.*, 1987), parallel computation of the Voronoi diagram (Lu, 1986; Saxena *et al.*, 1990; Adamatzky, 1993; Cole *et al.*, 1990, 1996; Evans and Stojmenovic, 1989; Garga and Bose, 1994; Goodrich *et al.*, 1993; Blelloch *et al.*, 1996), and constructing the dynamic Voronoi diagram (Tokuyama, 1988; Bajaj and Bouma, 1990; Fu and Lee, 1991; Huttenlocher *et al.*, 1992a; Devillers *et al.*, 1992; Roos, 1993). An attempt to decrease storage requirements was also studied by Kartashov and Folk (1995).

For a while (i.e. from Section 4.2 to Section 4.5) we make the following assumptions.

Assumption A4.1.1 Numerical computation is carried out in precise arithmetic.

Assumption A4.1.2 No four generators align on a common circle.

The first assumption is necessary to consider algorithms in a ‘theoretically closed world’, and has been adopted, implicitly or explicitly, in almost all discussions for designing geometric algorithms. The second assumption is to avoid degeneracy. Note that this assumption is not equivalent to the

non-cocircularity assumption; the non-cocircularity assumption avoids an empty circle passing through four points, whereas Assumption A4.1.2 avoids any circle passing through four points; Assumption A4.1.2 is stronger than the non-cocircularity assumption. This assumption is necessary to avoid degeneracy in the course of constructing the Voronoi diagram, because we treat many Voronoi diagrams generated by subsets of the generator set. Whether a case is special or not sometimes depends on which algorithm we consider. Indeed, we will make other assumptions when we discuss other algorithms.

In Section 4.6, on the other hand, we remove all such assumptions and construct algorithms that are valid in the real world.

4.2 DATA STRUCTURE FOR REPRESENTING A VORONOI DIAGRAM

Before starting our consideration of algorithms, we have to make clear what is meant by ‘construction of a Voronoi diagram’. Naively it might be thought that constructing a Voronoi diagram is equivalent to drawing it on a sheet of paper. Indeed, to draw the Voronoi diagram is a typical way to present it to the human eye. However, the drawn diagram itself, or a set of numerical data equivalent to the drawn diagram, does not convey enough information for many applications. Suppose that a computer program gives as output a list of line segments corresponding to the Voronoi edges. It is easy to draw the diagram from this list, but it is not easy to retrieve, for example, a sequence of Voronoi vertices on the boundary of one Voronoi polygon, or a set of Voronoi polygons contiguous to one Voronoi polygon. Thus, to ‘draw’ the Voronoi diagram is not enough in many applications. What we need to construct is a ‘richer structure’ from which we can extract a variety of information necessary for applications.

Another extremal way of representing the Voronoi diagram is to give all necessary data explicitly. For example, for each Voronoi polygon we may have the list of all Voronoi vertices on its boundary, the list of all Voronoi edges on its boundary, the list of all contiguous Voronoi polygons, and so on. However, this way of representation requires much space. Hence we have to choose some data structure in between which is concise but is still rich enough for us to retrieve various aspects of the diagram.

Here we choose one standard data structure, called a winged-edge data structure or a polygon data structure, which is common in geometric modelling and computer graphics (Baumgart, 1975; Ballard and Brown, 1982; Hoffmann, 1989; see also Guibas and Stolfi, 1985, for an alternative data structure). As will be shown in what follows, this data structure conveys explicit information about local incidence relations among Voronoi vertices, Voronoi edges and Voronoi polygons, so that a variety of information can be retrieved relatively easily.

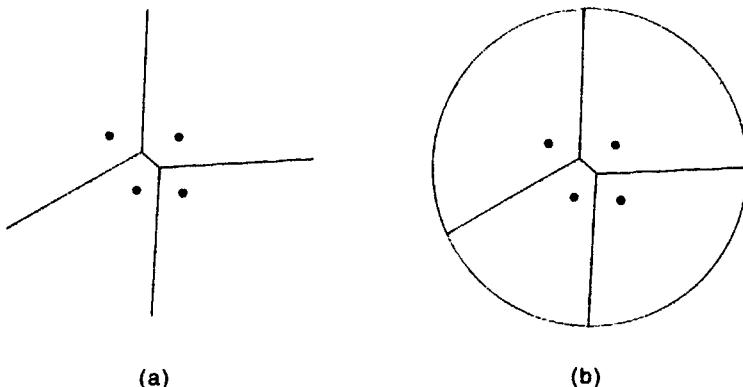


Figure 4.2.1 Voronoi diagram and the associated geometric graph: (a) Voronoi diagram; (b) geometric graph associated with the Voronoi diagram in (a).

The winged-edge data structure is a way of representing a geometric graph in the plane. However, the Voronoi diagram is slightly different from a geometric graph in that some Voronoi edges extend infinitely. To consider the Voronoi diagram as a geometric graph, we introduce a closed curve which is large enough to surround all the Voronoi vertices and consider that the infinite Voronoi edges have their terminal points on this closed curve. These terminal points are intuitively considered as points at infinity. By this convention, the Voronoi diagram shown in Figure 4.2.1(a) is converted to the diagram in (b). At these terminal points the closed curve itself is divided into curved line segments; these line segments are also considered as Voronoi edges. Thus, by this convention the Voronoi diagram is converted into a geometric graph. We call this geometric graph *the augmented geometric graph* associated with the Voronoi diagram. (Note that the augmented geometric graph is a little different from the geometric graph of the Voronoi diagram introduced in Section 2.3; in the geometric graph all the infinite Voronoi edges are connected to a common additional vertex, whereas in the augmented geometric graph infinite Voronoi edges are connected to mutually different vertices 'at infinity'. We adopt this structure because we want to store the direction of the infinite edges as the 'coordinates' of these vertices, as we will see soon.)

Consider the Voronoi diagram for the set $P = \{p_1, \dots, p_n\}$ of n generators. By the above convention the plane is divided into $n+1$ regions, n finite regions corresponding to the n Voronoi polygons and one outermost infinite region. We introduce a virtual generator, say p_∞ , and consider that the outermost infinite region is the Voronoi region of p_∞ . Thus the augmented geometric graph associated with the Voronoi diagram for P has $n+1$ regions, corresponding to p_1, p_2, \dots, p_n and p_∞ . Let n_e and n_v be the number of edges and vertices, respectively, of the augmented geometric graph. Since at least

three edges meet at a vertex, we get $3n_v \leq 2n_e$. From this inequality together with Euler's formula $(n + 1) - n_e + n_v = 2$, we get

$$n_e \leq 3n - 3 \quad \text{and} \quad n_v \leq 2n - 2, \quad (4.2.1)$$

where the equality holds when no degeneracy takes place. (Note that these inequalities are a little different from those in Property V11 in Section 2.3; this is because the 'pseudo' Voronoi edges and the 'pseudo' Voronoi vertices on the outermost closed curve are also counted here.)

To represent the augmented geometric graph associated with the Voronoi diagram, we create the winged-edge data structure in the following way. First, for each edge we choose and fix the direction of the edge arbitrarily, and thus convert the geometric graph to a directed geometric graph. Next we arbitrarily choose and fix a linear order from 1 to n_v to vertices, and similarly choose and fix a linear order from 1 to n_e to edges. Furthermore, we call the Voronoi polygon associated with p_i , *polygon i* ($i = 1, 2, \dots, n, \infty$). The incidence relations among vertices, edges and polygons are represented by ten integer-value arrays, one for polygons, one for vertices and eight for edges, which are defined in the following way.

For polygon i ($i = 1, 2, \dots, n, \infty$):

`edge.around.polygon[i]`: the ordinal number of an edge on the boundary of the polygon i .

For vertex j ($j = 1, 2, \dots, n_v$):

`edge.around.vertex[j]`: the ordinal number of an edge incident to the vertex j .

For each edge k ($k = 1, 2, \dots, n_e$) (Figure 4.2.2 shows the following eight geometric objects represented by these arrays for edge k):

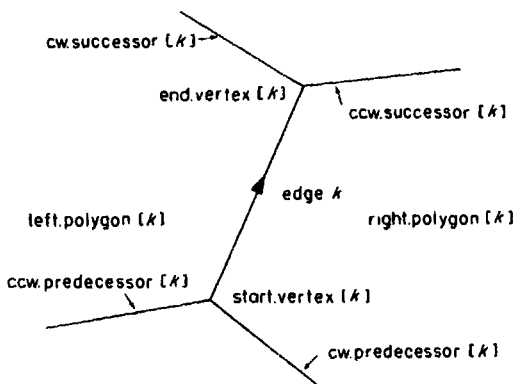


Figure 4.2.2 Geometric objects represented by the eight arrays associated with an edge.

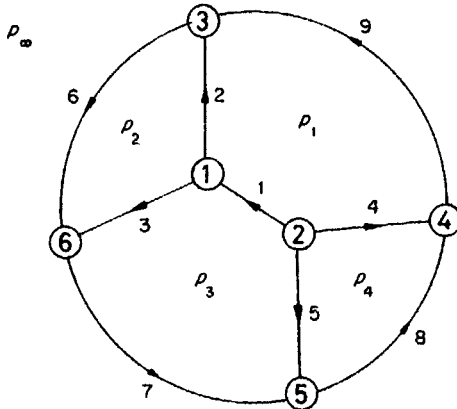


Figure 4.2.3 Directed augmented geometric graph associated with the Voronoi diagram in Figure 4.2.1.

right.polygon[k]: the ordinal number of the polygon that is to the right of the edge k ,
 left.polygon[k]: the ordinal number of the polygon that is to the left of the edge k ,
 start.vertex[k]: the ordinal number of the start vertex of the edge k ,
 end.vertex[k]: the ordinal number of the end vertex of the edge k ,
 cw.predecessor[k]: the ordinal number of the edge next to edge k clockwise around the start vertex,
 ccw.predecessor[k]: the ordinal number of the edge next to edge k counterclockwise around the start vertex,
 cw.successor[k]: the ordinal number of the edge next to edge k clockwise around the end vertex,
 ccw.successor[k]: the ordinal number of the edge next to edge k counterclockwise around the end vertex,

where cw and ccw indicate ‘clockwise’ and ‘counterclockwise’, respectively, and ‘predecessor’ and ‘successor’ represent edges around the start vertex and the end vertex, respectively. For each polygon i , we simply store in edge.around.polygon[i] one of the edges incident to the polygon, and similarly for each vertex j we store in edge.around.vertex[j] one of the edges incident to the vertex. Most information is stored in the eight arrays for edges (Figure 4.2.2).

Figure 4.2.3 shows a directed geometric graph obtained from the graph in Figure 4.2.1(b) by choosing directions arbitrarily and by ordering the vertices and the edges arbitrarily, and Table 4.2.1 shows the contents of the ten arrays representing this graph. Here we use the symbol ∞ to represent the outermost infinite region; this is simply because we want to emphasize that this region does not correspond to an actual Voronoi polygon, and in practical implementations the symbol ∞ may be replaced by the integer $n+1$.

The above ten arrays together represent the topological structure of the Voronoi diagram, but the metric aspect of the Voronoi diagram should also be represented. For this purpose, we use three more arrays, $w.\text{vertex}[j]$, $x.\text{vertex}[j]$ and $y.\text{vertex}[j]$, attached to the vertices. The array $w.\text{vertex}[j]$ represents one-bit information in such a way that

$$w.\text{vertex}[j] = \begin{cases} 1 & \text{if vertex } j \text{ is an ordinary point,} \\ 0 & \text{if vertex } j \text{ is a point at infinity.} \end{cases}$$

If vertex j is an ordinary point, $x.\text{vertex}[j]$ and $y.\text{vertex}[j]$ represent the x and the y coordinates of this vertex, while if vertex j is a point at infinity, $x.\text{vertex}[j]$ and $y.\text{vertex}[j]$ represent the x and the y components of the unit vector designating the direction in which the associated (infinite) Voronoi edge runs. Thus, each entry of the array $w.\text{vertex}$ requires one bit of memory space, while each entry of $x.\text{vertex}$ or $y.\text{vertex}$ requires one word to represent a floating-point number. The triple $(w.\text{vertex}[j], x.\text{vertex}[j], y.\text{vertex}[j])$ is a special case of what is usually called ‘homogeneous coordinates’, which are useful for representing ordinary points and points at infinity in a unified manner (e.g. Pedoe, 1970).

The collection of the above thirteen arrays is called the *winged-edge data structure*. In what follows by the construction of the Voronoi diagram $\mathcal{V}(P)$ we mean the construction of the winged-edge data structure for the augmented geometric graph associated with $\mathcal{V}(P)$.

In the augmented geometric graph associated with the Voronoi diagram, there are exactly $n+1$ polygons, and at most $3n-3$ edges and $2n-2$ vertices. Hence in total the winged-edge data structure requires memory space for $n+1 + (2n-2) + 8(3n-3) = 27n - 25$ integers, $2n-2$ bits and $2(2n-2)$

Table 4.2.1 Entries of the ten integer arrays in the winged-edge data structure associated with the augmented geometric graph shown in Figure 4.2.3.

k (edge number)	1	2	3	4	5	6	7	8	9
right.polygon[k]	1	1	2	4	3	∞	∞	∞	∞
left.polygon[k]	3	2	3	1	4	2	3	4	1
start.vertex[k]	2	1	1	2	2	3	6	5	4
end.vertex[k]	1	3	6	4	5	6	5	4	3
cw.predecessor[k]	4	1	2	5	1	9	6	7	8
ccw.predecessor[k]	5	3	1	1	4	2	3	5	4
cw.successor[k]	3	6	7	9	8	3	5	4	2
ccw.successor[k]	2	9	6	8	7	7	8	9	6
i (polygon number)	1	2	3	4	∞				
edge.around.polygon[i]	1	2	1	4	6				
j (vertex number)	1	2	3	4	5	6			
edge.around.vertex[j]	1	1	2	4	5	3			

$= 4n - 4$ floating-point numbers. To represent the Voronoi diagram completely, we also need $2n$ more floating-point numbers for the x and the y coordinates of the generators in P , which is not the output of the algorithm but the input to the algorithm.

Once we obtain the winged-edge data structure, we can easily retrieve a variety of fundamental information about the Voronoi diagram. For example, if we want to obtain the list of edges and polygons that are incident to vertex j , we can use the next algorithm. In the algorithm, a ‘list’ means data containing a sequence of items, and ‘to add an item to the tail of a list’ means to augment the list by adding the item as the last element of the sequence. For example, if we add b to the tail of list (b_1, b_2, \dots, b_k) , we get $(b_1, b_2, \dots, b_k, b)$.

Algorithm 4.2.1 (Retrieve the edges and polygons incident to a vertex)

Input: Winged-edge data structure of $\mathcal{V}(P)$ and vertex j .

Output: List L_e of edges and list L_r of polygons that surround vertex j counterclockwise.

Procedure:

- Step 1. $L_e \leftarrow$ empty list and $L_r \leftarrow$ empty list.
- Step 2. $k \leftarrow \text{edge.} \text{around.} \text{vertex}[j]$, and $kstart \leftarrow k$.
- Step 3. Add k to the tail of the list L_e .
- Step 4. If $j = \text{start.} \text{vertex}[k]$ then add $\text{left.} \text{polygon}[k]$ to the tail of L_r and $k \leftarrow \text{ccw.} \text{predecessor}[k]$,
else add $\text{right.} \text{polygon}[k]$ to the tail of L_r and $k \leftarrow \text{ccw.} \text{successor}[k]$.
- Step 5. If $k = kstart$ then return L_e and L_r , else go to Step 3.

In this description of the algorithm, we use several conventions common in computer science (Aho *et al.*, 1974). ‘ $x \leftarrow y$ ’ represents ‘replace the value of variable x by the value of y ’, ‘if C then X else Y ’ represents ‘do X if the condition C is true, and do Y otherwise’, and ‘return x ’ represents ‘report x as the output and exit from the procedure’.

In this algorithm, Steps 1 and 2 are done once, and Steps 3, 4 and 5 are repeated as many times as the number of edges (or, equivalently, the number of polygons) incident to vertex j . Hence, the total running time of this algorithm is proportional to the degree of vertex j .

If we want to get the list of edges and vertices that surround polygon i counterclockwise, we can use the next algorithm.

Algorithm 4.2.2 (Retrieve the edges and vertices surrounding a polygon)

Input: Winged-edge data structure of $\mathcal{V}(P)$ and polygon i .

Output: List L_e of edges and list L_v of vertices that surround polygon i counterclockwise.

Procedure:

- Step 1. $L_e \leftarrow$ empty list, and $L_v \leftarrow$ empty list.
- Step 2. $k \leftarrow \text{edge.} \text{around.} \text{polygon}[i]$, and $kstart \leftarrow k$.

- Step 3. Add k to the tail of list L_e .
 Step 4. If $i = \text{left.polygon}[k]$
 then add $\text{end.vertex}[k]$ to the tail of L_v and $k \leftarrow \text{cw.successor}[k]$,
 else add $\text{start.vertex}[k]$ to the tail of L_v and $k \leftarrow \text{cw.predecessor}[k]$.
 Step 5. If $k = k_{\text{start}}$ then return L_e and L_v , else go to Step 3.

This algorithm runs in time proportional to the number of edges on the boundary of polygon i , because Steps 1 and 2 are done once, and Steps 3, 4 and 5 are repeated as many times as the number of edges on the boundary of polygon i .

In particular, if polygon ∞ is chosen as the input polygon, this algorithm gives the list of edges and vertices on the boundary of the outermost infinite region, i.e. the list of edges and vertices on the boundary of the convex hull $\text{CH}(P)$ (recall Property V2).

Sometimes we want to retrieve the structure of the Delaunay diagram, the dual of the Voronoi diagram. The winged-edge data structure is also convenient for this purpose. Indeed, if we exchange the roles of the vertices and polygons, the winged-edge data structure for a geometric graph itself can be considered as the winged-edge data structure for the dual graph. For example, edge k corresponds to the Delaunay edge connecting two Delaunay vertices (i.e. generators) represented by $\text{right.polygon}[k]$ and $\text{left.polygon}[k]$, and the Delaunay polygon corresponding to the j th Voronoi vertex can be obtained as the output of Algorithm 4.2.1. Thus, what we have to do to retrieve information about the Delaunay diagram is simply to rename the geometric concepts by their dual concepts. That is, we consider that the edge k is a Delaunay edge connecting two generators $\text{right.polygon}[k]$ and $\text{left.polygon}[k]$, and that the Voronoi vertex i is a Delaunay triangle one of whose edges is $\text{edge.}.\text{around.vertex}[i]$, etc.

Before closing this section let us see the lower bound of the time complexity for constructing the Voronoi diagram. We can see that the lower bound of the worst-case time complexity for constructing the Voronoi diagram for n points is $O(n \log n)$. This lower bound can be derived from the well-known fact that any algorithm for sorting n real numbers in increasing order using comparisons requires at least $O(n \log n)$ time in the worst case (Aho *et al.*, 1974).

Let $X = \{x_1, x_2, \dots, x_n\}$ be a set of n real numbers. We create the set $P = \{(x_1, x_1^2), (x_2, x_2^2), \dots, (x_n, x_n^2)\}$ of n points in the plane and construct the Voronoi diagram for P . From this Voronoi diagram we obtain the cyclic sequence of points on the boundary of the convex hull $\text{CH}(P)$ by Algorithm 4.2.2 in $O(n)$ time. Since all the points in P are on the boundary of $\text{CH}(P)$, as shown in Figure 4.2.4, we obtain the increasing order of the n numbers in X . Thus, if the Voronoi diagram for P could be constructed faster than in $O(n \log n)$ time, then we could sort numbers in X faster than in $O(n \log n)$ time, which is a contradiction. Hence, any algorithm for constructing the Voronoi diagram for n points takes at least $O(n \log n)$ time in the worst case.

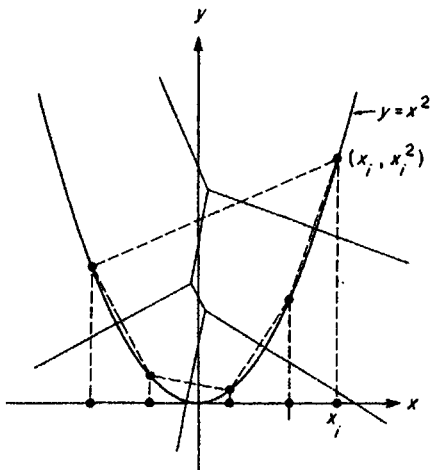


Figure 4.2.4 Relation between the sorting problem and the convex hull problem.

This proof also contains the proof of the property that any algorithm for constructing the cyclic sequence of points on the boundary of the convex hull of n points takes at least $O(n \log n)$ time in the worst case.

It may seem that some kind of ‘sorting’ is a bottleneck in constructing the Voronoi diagram. However, even if the sorted order of the generators in one direction is given, the construction of the Voronoi diagram still requires $O(n \log n)$ time (Djidjev and Lingas, 1995).

On the other hand, the lower bound of the average-case time complexity for constructing the Voronoi diagram is obviously $O(n)$; this is because any algorithm should create the winged-edge data structure whose size is $O(n)$.

As we will see, both of the lower bounds are tight in the sense that we can actually construct an algorithm whose worst-case time complexity is $O(n \log n)$ and an algorithm whose average-case time complexity is $O(n)$.

4.3 THE INCREMENTAL METHOD

The incremental method is one of the most important methods because it is conceptually simple and its average time complexity can be decreased to $O(n)$ by some algorithmic techniques. This method starts with a simple Voronoi diagram for a few generators, say two or three generators, and modifies the diagram by adding other generators one by one. For $l = 1, 2, \dots, n$, let \mathcal{V}_l denote the Voronoi diagram for the first l generators p_1, p_2, \dots, p_l . The main part of the incremental method is to convert \mathcal{V}_{l-1} to \mathcal{V}_l for each l .

Figure 4.3.1 shows an example of the addition of a generator. Suppose that we have already constructed the Voronoi diagram \mathcal{V}_{l-1} as shown by the solid lines, and that we now want to add a new generator p_l . First, we find the generator, say p_i , whose Voronoi polygon contains p_l , and draw the perpendicular bisector between p_l and p_i . The bisector crosses the boundary

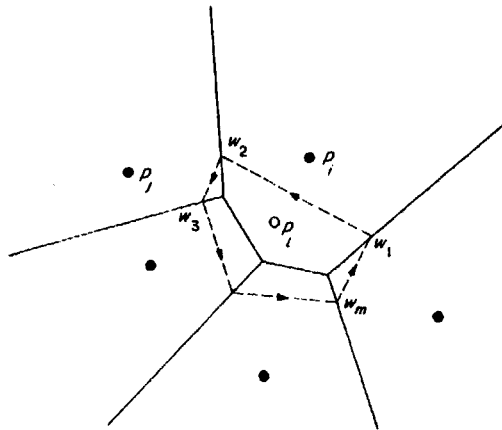


Figure 4.3.1 Addition of a new generator p_i .

of $\mathcal{V}(p_i)$ at two points; let the two points be w_1 and w_2 in such a way that p_i is to the left of the directed line segment $\overrightarrow{w_1w_2}$. The line segment $\overrightarrow{w_1w_2}$ divides the Voronoi polygon $V(p_i)$ into two portions, the one on the left belonging to the Voronoi polygon of p_i . Thus, we get a Voronoi edge on the boundary of the Voronoi polygon of p_i .

Starting with the edge $\overrightarrow{w_1w_2}$, we ‘grow’ the boundary of the Voronoi polygon of p_i by the following procedure, which we call the *boundary growing procedure*. The bisector between p_i and p_j crosses the boundary of $V(p_i)$ at w_2 , entering the adjacent Voronoi polygon, say $V(p_j)$. So, we next draw the perpendicular bisector between p_i and p_j , and find the point (other than w_2) at which the bisector crosses the boundary of $V(p_j)$; let this point be w_3 . In a similar way, we find the sequence of segments of perpendicular bisectors of p_i and the neighbouring generators until we reach the starting point w_1 . Let this sequence be $(\overrightarrow{w_1w_2}, \overrightarrow{w_2w_3}, \dots, \overrightarrow{w_{m-1}w_m}, \overrightarrow{w_mw_1})$. This sequence forms a counterclockwise boundary of the Voronoi polygon of the new generator p_i . Finally, we delete from \mathcal{V}_{i-1} the substructure inside the new Voronoi polygon, and thus obtain \mathcal{V}_i .

The above description is a rough sketch of the incremental method. To make an exact and efficient algorithm we must be careful at several points.

First, we have to take care that the boundary growing procedure works well only when the Voronoi polygon of the new generator p_i is finite, although a Voronoi polygon is not necessarily finite. An infinite region, if it happens, requires an exceptional branch of processing. However, such an exception can be avoided by a simple trick.

Recall that, in the Voronoi diagram \mathcal{V} for the generator set P , the Voronoi polygon $V(p_i)$ is infinite if and only if p_i is on the boundary of the convex hull of P (Property V2). Keeping this in mind, let us renumber the generators as p_4, p_5, \dots, p_n (now n is the number of generators plus three), and introduce three additional generators p_1, p_2 and p_3 in such a way that the

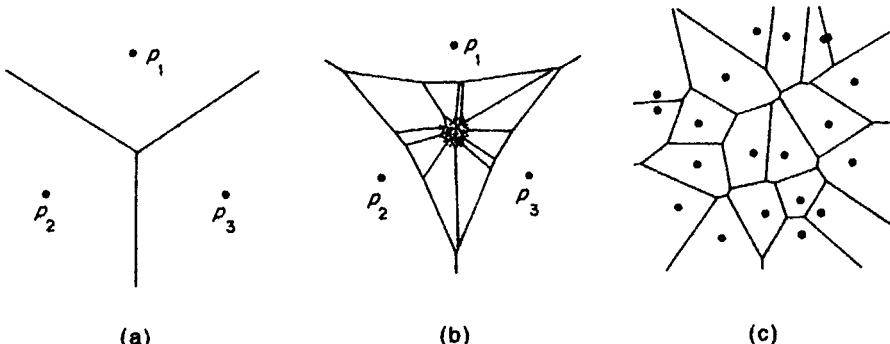


Figure 4.3.2 Avoidance of infinite Voronoi polygons: (a) Voronoi diagram for three additional generators; (b) Voronoi diagram for all the generators; (c) Voronoi diagram for the original generators.

triangle \$p_1p_2p_3\$ contains all the original generators \$p_4, p_5, \dots, p_n\$ in its interior. The Voronoi diagram for \$p_1, p_2\$ and \$p_3\$ is a simple one, as shown in Figure 4.3.2(a). We start with this Voronoi diagram, and add other generators \$p_4, p_5, \dots, p_n\$ one by one. The convex hull of \$p_1, p_2, \dots, p_l\$ is the triangle \$p_1p_2p_3\$ itself for any \$l = 4, 5, \dots, n\$, and consequently the Voronoi polygon of \$p_l\$ in the Voronoi diagram \$\mathcal{V}_l\$ is always finite, as shown in Figure 4.3.2(b). Thus, we can avoid the occurrence of an infinite Voronoi polygon in the boundary growing procedure.

The Voronoi diagram constructed in this way is not the same as the Voronoi diagram for the original generators. However, the difference due to the additional three generators can be eliminated substantially if a sufficiently large triangle is chosen. For example, if we magnify the central portion of Figure 4.3.2(b), we get (c), where the effect of the additional generators does not appear. Without loss of generality, let us assume that all the original generators \$p_4, p_5, \dots, p_n\$ are located in the unit square \$S = \{(x, y) | 0 \leq x, y \leq 1\}\$, and that we are interested in the Voronoi diagram in this square area. Then, we can choose the three additional generators, for example, by

$$\begin{aligned} p_1 &= (0.5, 3\sqrt{2}/2 + 0.5), \\ p_2 &= (-3\sqrt{6}/4 + 0.5, -3\sqrt{2}/4 + 0.5), \\ p_3 &= (3\sqrt{6}/4 + 0.5, -3\sqrt{2}/4 + 0.5). \end{aligned} \tag{4.3.1}$$

These three points form a sufficiently large regular triangle which contains the square area \$\{(x, y) | 0 \leq x, y \leq 1\}\$; see Figure 4.3.2(b). We can see that no boundary of the Voronoi polygon of the additional generators goes through the interior of the square \$S\$ unless the set of original generators is empty (actually, we can prove that no such boundary goes through the interior of the circle circumscribing \$S\$; the proof is left to the reader).

The second point we should take care over is the time complexity. The first task in the addition of a new generator \$p_l\$ is to find the old

generator p_i whose Voronoi polygon contains p_l . Obviously p_i satisfies $d(p_l, p_i) \leq d(p_l, p_j)$ for any $j = 1, 2, \dots, l-1$. Hence, p_i can be found if the distances from p_l to all the other generators are computed. However, this requires $O(l)$ time, so that the total time complexity will become $O(1 + 2 + \dots + (n-1)) = O(n^2)$.

A slightly more intelligent way is to start with an initial guess and to search its neighbours for a closer generator. This can be done using the next algorithm.

Algorithm 4.3.1 (Nearest neighbour search)

Input: l generators p_1, p_2, \dots, p_l , Voronoi diagram \mathcal{V}_{l-1} , and initial guess $p_i (1 \leq i \leq l-1)$.

Output: The generator (other than p_l) that is the closest to p_l .

Procedure:

Step 1. Among the generators adjacent to p_i , find the one, say p_j , with the minimum distance to p_l :

$$d(p_j, p_l) = \min_k d(p_k, p_l),$$

where the minimum is taken over all generators p_k whose Voronoi polygons are adjacent to $V(p_l)$.

Step 2. If $d(p_i, p_l) \leq d(p_j, p_l)$, return p_i , else $p_i \leftarrow p_j$ and go to Step 1.

The algorithm always terminates in a finite number of steps, because each replacement of p_i at Step 2 gives a closer generator than before. Moreover, the algorithm gives the closest generator as the output, because, if p_i is not closest to p_l , there always exists an adjacent generator closer to p_l (indeed, if we move from p_i in the direction to p_l , we cross the boundary of $V(p_i)$ and visit the neighbouring polygon, say the Voronoi polygon of p_j , which is closer to p_l ; the proof is left to the reader).

Note that the time required by the algorithm depends greatly on the initial guess p_i ; if it is near to the closest generator, we reach the closest generator quickly. Hence, it is important to make a good initial guess. For this purpose we employ a bucketing technique. Before describing this technique, however, we present another important point.

The final point we should be careful of is the size of the substructure to be deleted, because, if the substructure is large and complicated, we cannot find and delete it in constant time. As we have seen, the average number of edges on the boundary of a Voronoi polygon is six or less (recall Property V13 in Section 2.3). Consequently, we can expect that the average size of the substructure to be deleted is almost constant. However, we should not be too optimistic, because the average number of edges of a Voronoi polygon being six does not necessarily imply that the average number of edges of a 'new' Voronoi polygon will be six.

A counterexample is shown in Figure 4.3.3, where the generators align along a spiral and are numbered from outermost inward. The Voronoi polygon of the new generator, the innermost one, is adjacent to all the other

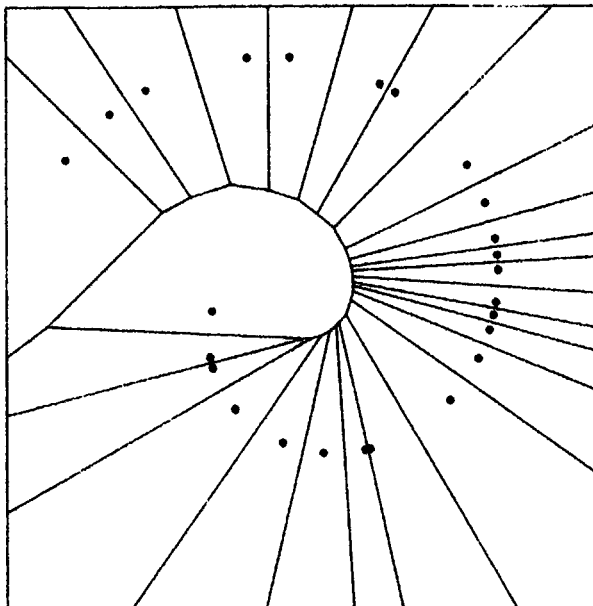


Figure 4.3.3 Voronoi diagram for points on a spiral.

polygons, so that the size of the substructure to be deleted is proportional to the number of generators added so far.

To restrict the average size of the substructure to be constant, the generators should be numbered in such a way that for any $l = 4, 5, \dots, n$, the generators p_4, p_5, \dots, p_l distribute as uniformly as possible. Hence before starting the incremental method, we have to reorder the generators to meet this property as nearly as possible. For this purpose also, we use the bucketing technique.

A *rooted tree* is a tree in which one node is specified as the *root* (see Figure 4.3.4). When we draw a rooted tree, we put the root at the top, and draw other nodes downward in such a way that nodes at the same distance from the root align horizontally (where the distance between two nodes is the number of links on the path connecting them). For each node u , the unique one-level upper node adjacent to u is called the *parent* of u , and one-level lower nodes adjacent to u (if any) are called *children* of u . The root is the only node that does not have a parent. A node without children is called a *leaf*. A node which is neither the root nor a leaf is called an *intermediate node*. If node u is on the path from node v to the root, u is called an *ancestor* of v and v a *descendant* of u . For any node u , the subgraph consisting of u and all its descendants is itself a rooted tree with the root u ; this subgraph is called the *subtree* rooted at u . A rooted tree is called a *quaternary tree* if every node other than a leaf has exactly four children.

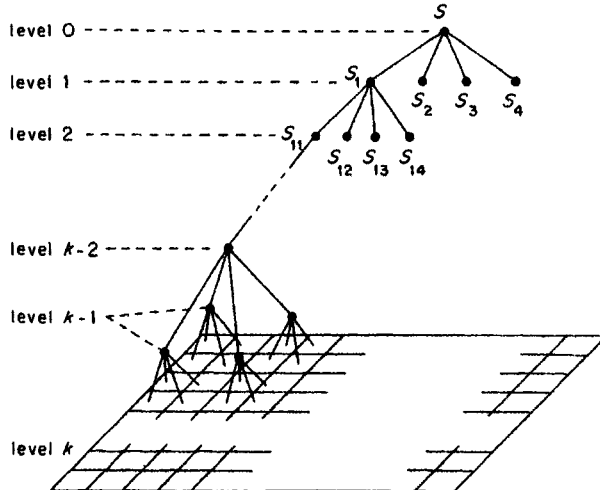
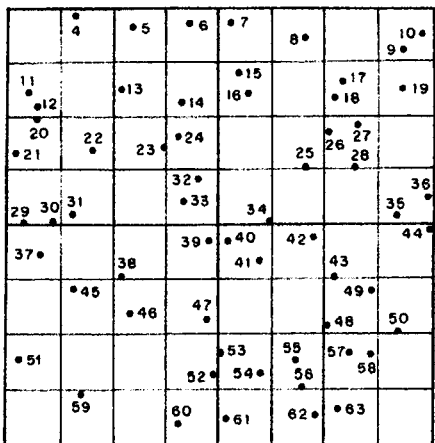


Figure 4.3.4 Quaternary tree with buckets as leaves.

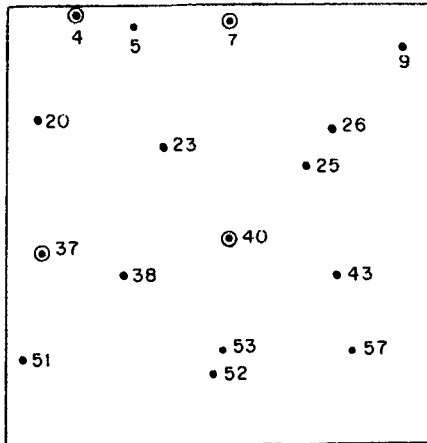
Let k be a positive integer such that 4^k is nearest to n . Let us divide the unit square S into four smaller squares, which we shall call quadrants; hence we divide the square into the left upper quadrant S_1 , the right upper quadrant S_2 , the left lower quadrant S_3 and the right lower quadrant S_4 . We repeat this process k times recursively. That is, first S is divided into S_1, S_2, S_3 and S_4 , and next S_i ($1 \leq i \leq 4$) is divided into S_{i1}, S_{i2}, S_{i3} and S_{i4} , and so on. The division procedure can be represented by a quaternary tree; the root corresponds to the entire region S , and for each node, its four child nodes correspond to the four smaller squares generated by the partition of the corresponding square, as shown in Figure 4.3.4. The first division process generates 4 level-one nodes, the second division process generates 4^2 level-two nodes, and so on; finally the k th process generates 4^k level- k nodes. The smallest squares, the squares corresponding to the level- k nodes, are called *buckets*.

This quaternary tree structure is useful both for finding a good initial guess for Algorithm 4.3.1 and for reordering the generators. For these purposes, we need a little more preprocessing.

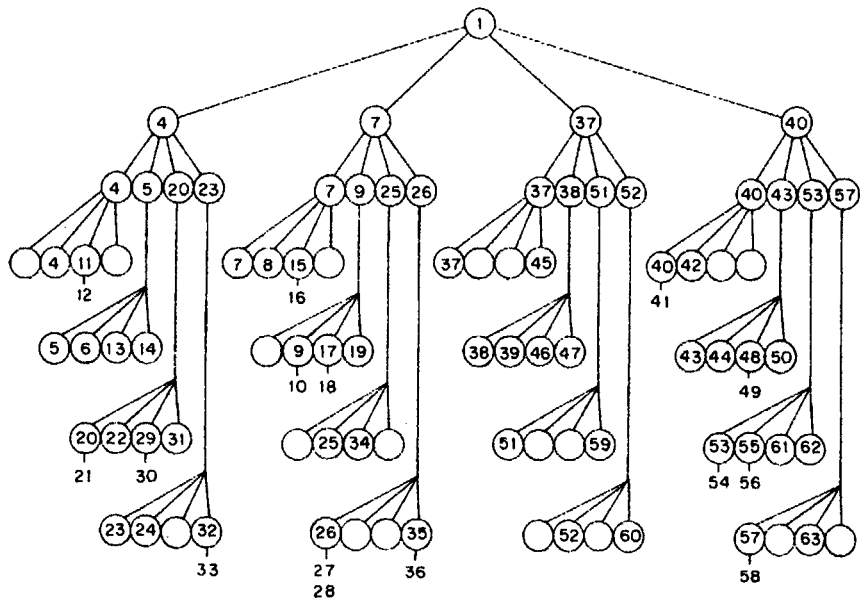
With each node u of the quaternary tree we associate a generator, say $g[u]$, according to the following procedure. First, for all $l = 4, 5, \dots, n$, we find the bucket containing p_l (since S is the unit square, the bucket containing p_l can be found from its coordinates by multiplying 2^k and then truncating off the fractional parts). Next, we put $g[u] \leftarrow p_1$ for the root node u . Thirdly, we visit the buckets one by one, and at each non-empty bucket we choose one generator, say p_i , contained in the bucket and put $g[u] \leftarrow p_i$ for all nodes u with $g[u]$ undefined on the path from this bucket to the root. This is all we have to do for the preprocessing.



(a)



(c)



(b)

Figure 4.3.5 Randomly distributed points and the associated quaternary tree: (a) 60 points distributed randomly in a square and 64 buckets covering the square; (b) quaternary tree associated with the points and the buckets in (a); (c) points added when the nodes with level two or less are scanned.

Figure 4.3.5 shows an example of the quaternary tree structure. Panel (a) shows 60 points randomly located in a square. Since 60 is near to 64 ($= 4^3$), the square region is divided into 64 buckets, and the points are numbered from 4 to 63 in the order in which we encounter them when we visit the buckets from the top row downward and from left to right at each row; points in the same buckets are numbered randomly. Scanning the buckets in the above order, we construct the quaternary tree, as shown in (b), where for each node the four child nodes correspond, from left to right, to the left upper quadrant, the right upper quadrant, the left lower quadrant and the right lower quadrant, respectively. The number attached to each node represents the generator number $g[u]$. For a bucket containing two or more generators, the corresponding leaf node contains one of them and the other generators are stored in an additional list attached to the node.

Note that some buckets may contain two or more generators and some buckets may contain no generator, and hence some generators may not be assigned to any node and $g[u]$ may not be defined for some node u . In the main processing of the incremental method, we visit the nodes of the quaternary tree from the level-one nodes to the leaves in a breadth-first manner, that is, we visit all the level- i nodes before visiting a level- $(i+1)$ node. Remember that we defined $g[u] = p_1$ for the root node, and that we start with the initial Voronoi diagram generated by p_1, p_2 and p_3 . Hence, we skip the root node, and start the addition at the level-one nodes. At each node u , if the associated generator $g[u]$ is new in the sense that we come across the generator $g[u]$ for the first time in the breadth-first visit, we add it to the current Voronoi diagram. Let u' be the parent node of u . Then the generator $g[u]$ is new if and only if $g[u] \neq g[u']$. If the visited node u is a bucket (i.e. a leaf node of the tree), and if the bucket contains generators other than $g[u]$, we add them to the current Voronoi diagram in an arbitrary order.

Adding generators in this order will keep the uniformness of the distribution of the generators relatively well, because at the end of visiting all the level- i nodes, exactly one generator is chosen from each non-empty square corresponding to that level. We call the above method for reordering *quaternary reordering*.

The quaternary tree is also useful for finding a good initial guess for Algorithm 4.3.1. Suppose that we are visiting node u . Let node u' be the parent of u . The generator $g[u]$ is added at this point if and only if $g[u] \neq g[u']$. We use $g[u']$ as the initial guess for Algorithm 4.3.1. If u is a leaf node and if the corresponding bucket contains two or more generators, we use $g[u]$ as the initial guess in the addition of the other generators in the bucket. This choice seems to give a good initial guess, because it lies either in the same square or in a one-level-larger square. We call this method for choosing the initial guess for Algorithm 4.3.1 *quaternary initial guessing*.

Figure 4.3.5(c) represents the points that are added by the end of scanning up to level-two nodes of the quaternary tree in (b). The four points designated by double circles are those added by the time the level-zero and level-one nodes are scanned, while the other points, represented by small

filled circles, correspond to those added in the scan of the level-two nodes. We can see that the 16 points shown in (c) are distributed relatively uniformly in the square.

Point 4 is used as the initial guess for the nearest neighbour search in the addition of points 5, 20 and 23, and similarly point 7 is used as the initial guess in the addition of points 9, 25 and 26, and so on. We see that the initial guess is either the nearest point itself or a point very near to the nearest point.

Summing up the above considerations, we obtain the next algorithm.

Algorithm 4.3.2 (Quaternary incremental method)

Input: Set $\{p_4, p_5, \dots, p_n\}$ of $n-3$ generators located in the unit square $S = \{(x, y) | 0 \leq x, y \leq 1\}$.

Output: Voronoi diagram \mathcal{V} for n generators $\{p_1, p_2, \dots, p_n\}$, where p_1, p_2 and p_3 are the additional generators defined by equation (4.3.1).

Procedure:

- Step 1. Find positive integer k such that 4^k is closest to n , divide S into 4^k square buckets, and construct the quaternary tree having the buckets as leaves.
- Step 2. Renumber the generators by the quaternary reordering, and let the resultant order be p_4, p_5, \dots, p_n .
- Step 3. Construct the Voronoi diagram \mathcal{V}_3 for the three additional generators p_1, p_2 and p_3 defined by equation (4.3.1), as shown in Figure 4.3.2(a).
- Step 4. For $l = 4, 5, \dots, n$, do 4.1, ..., 4.4.
 - 4.1. By Algorithm 4.3.1 with the initial guess given by the quaternary initial guessing, find the generator p_i ($1 \leq i \leq l-1$) closest to p_l .
 - 4.2. Find the points w_1 and w_2 of intersections of the perpendicular bisector of p_i and p_l with the boundary of $V(p_i)$.
 - 4.3. By the boundary growing procedure, construct the closed sequence $(\overline{w_1 w_2}, \overline{w_2 w_3}, \dots, \overline{w_{m-1} w_m}, \overline{w_m w_1})$ of segments of perpendicular bisectors forming the boundary of the Voronoi polygon of p_l .
 - 4.4. Delete from \mathcal{V}_{l-1} the substructure inside the closed sequence, and name the resultant diagram \mathcal{V}_l .
- Step 5. Return $\mathcal{V} = \mathcal{V}_n$.

This algorithm does not refer to the associated winged-edge data structure explicitly, but it is not difficult to understand how to create and modify the winged-edge data structure accordingly; the initial winged-edge data structure for \mathcal{V}_3 is created in Step 3 and is modified in Step 4.4. To describe Steps 3 and 4.4 in terms of the winged-edge data structure is left as an exercise. Obviously, Steps 1 and 2 are done in $O(n)$ time, and Steps 3 and 5 in $O(1)$ time. Because of the quaternary reordering and the quaternary initial guessing, we can expect that Steps 4.1, ..., 4.4 can be done in $O(1)$ time on

average for each l . Thus, in total, Algorithm 4.3.2 runs in $O(n)$ time on average if the generators are distributed at random in a square.

The use of buckets with the quaternary tree was proposed by Ohya, Iri and Murota (Ohya, 1983; Ohya *et al.*, 1984a,b), by which the average time complexity of the incremental method decreases from $O(n^2)$ to $O(n)$. They also recommended a certain specific order of visiting the buckets in the preprocessing and of visiting tree nodes in the main processing (see Ohya *et al.*, 1984a, for the details of their reordering). Guibas *et al.* (1992) and de Berg *et al.* (1995) studied the random-order insertion.

4.4 THE DIVIDE-AND-CONQUER METHOD

In this and the next sections we give two $O(n \log n)$ algorithms for constructing the Voronoi diagram, which are optimal in a worst-case sense. They are indeed important from a theoretical point of view. However, since we have in practice already obtained a more efficient method in the previous section, we describe only the basic ideas of these algorithms, skipping details for implementation.

'Divide-and-conquer' is one of the fundamental paradigms for designing efficient algorithms. In this paradigm the original problem is recursively divided into several simple subproblems of almost equal size, and the solution of the original problem is obtained by merging the solutions of the subproblems.

For our particular problem, the generators are sorted in increasing order of the x coordinates, and are represented by the 'list' $P = (p_1, p_2, \dots, p_n)$ (unlike the incremental method, we do not use any additional generators; p_1, \dots, p_n are all original generators). This can be done in $O(n \log n)$ time by any optimal sorting algorithm such as a heap sort or a merge sort (cf. Knuth, 1973, or Aho *et al.*, 1974). In addition to Assumptions A4.1.1 and A4.1.2, here we assume the following.

Assumption A4.4.1 No two generators align vertically.

Hence the order (p_1, p_2, \dots, p_n) is defined uniquely. Next, the divide-and-conquer paradigm is applied in the following way (we first state the algorithm formally and then give an example).

Algorithm 4.4.1 (Divide-and-conquer method)

Input: Number n of generators and list $P = (p_1, p_2, \dots, p_n)$ of the generators arranged in increasing order of the x coordinates.

Output: Voronoi diagram \mathcal{V} for P .

Procedure:

Step 1. If $n \leq 3$, then construct the Voronoi diagram \mathcal{V} for P directly and go to Step 3.

Step 2. Otherwise do the following.

- 2.1. Let t be the integral part of $n/2$, and divide P into $P_L = (p_1, \dots, p_t)$ and $P_R = (p_{t+1}, \dots, P_n)$.
- 2.2. Construct the Voronoi diagram \mathcal{V}_L for P_L by Algorithm 4.4.1.
- 2.3. Construct the Voronoi diagram \mathcal{V}_R for P_R by Algorithm 4.4.1.
- 2.4. Merge \mathcal{V}_L and \mathcal{V}_R into the Voronoi diagram \mathcal{V} for P (this can be done by Algorithm 4.4.3.).

Step 3. Return \mathcal{V} .

Note that the generators in P_L are to the left of the generators in P_R . We call elements of P_L *left generators* and those of P_R *right generators*. \mathcal{V}_L is called the *left Voronoi diagram* and \mathcal{V}_R the *right Voronoi diagram*.

The essential portion of this algorithm is Step 2.4, the step for merging two Voronoi diagrams. In what follows we consider how to do this step.

Suppose that we have obtained the left Voronoi diagram \mathcal{V}_L and the right Voronoi diagram \mathcal{V}_R , as shown in Figure 4.4.1, where the left generators are represented by filled circles, the right generators by unfilled circles, \mathcal{V}_L by dot-and-dash lines and \mathcal{V}_R by broken lines. Now we have to merge them by generating new Voronoi edges and new Voronoi vertices and by deleting superfluous portions from \mathcal{V}_L and \mathcal{V}_R . The new edges and the new vertices come from the interaction between left generators and right generators; that

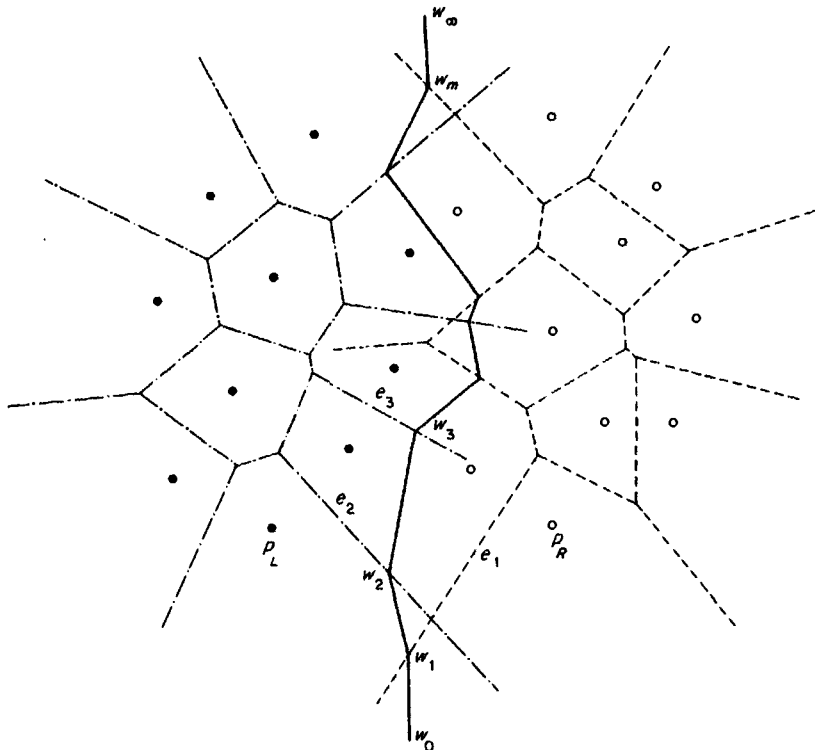


Figure 4.4.1 Merger of left and right Voronoi diagrams.

is, each new edge is part of the perpendicular bisector between a left generator and a right generator, and each new vertex is equidistant either from two left generators and one right generator or from one left generator and two right generators.

For any point p in the plane, let $d(p, P_L)$ denote the minimum distance from p to the generators in P_L , and $d(p, P_R)$ the minimum distance from p to the generators in P_R . Then, any point p on a new Voronoi edge satisfies $d(p, P_L) = d(p, P_R)$. Consider a point p that moves from left to right along an arbitrary horizontal line. Since P_L is to the left of P_R , there is a unique point p^* such that $d(p^*, P_L) = d(p^*, P_R)$ and $d(p, P_L) < d(p, P_R)$ before p reaches p^* and $d(p, P_L) > d(p, P_R)$ after p passes through p^* . As the horizontal line moves from the bottom upward, p^* moves continuously, tracing a polygonal line running between the left generators and the right generators. Our task is to construct this polygonal line and to remove from V_L and V_R the portions that lie to the right and to the left, respectively, of the polygonal line.

We construct the polygonal line from the bottom upward. To find the bottommost edge, we need one more preparation. We present an algorithmic tool for finding a line such that it touches two disjoint convex polygons and that all the other points of the polygons are on the same side of the line.

For any two points p and q , the directed line passing through p and q in this order is denoted by $L(p, q)$, and the directed line segment starting at p and ending at q is denoted by \overrightarrow{pq} .

Let U be a convex polygon defined by the cyclic list $(u_1, u_2, \dots, u_s, u_1)$ of vertices which surround the polygon counterclockwise. For the vertex u in U , let $cnext[u]$ and $ccnext[u]$ be the immediate predecessor and the immediate successor, respectively, of u in the list ($cnext[u]$ is the clockwise *next* vertex of u and $ccnext[u]$ is the counterclockwise *next* vertex of u).

Let U_L and U_R be two convex polygons, U_L being to the left of U_R , i.e. the x coordinates of vertices in U_L are smaller than the x coordinates of vertices in U_R . For the vertex u in U_L and the vertex w in U_R the line $L(u, w)$ is called a *common support* of U_L and U_R if all the nodes in U_L and U_R are on the same side of the line or on the line. U_L and U_R admit two common supports; the upper one is called the *upper common support* and the lower one the *lower common support*. For instance, for two polygons U_L and U_R represented by the solid lines in Figure 4.4.2, the lower common support is the line connecting the left vertex d and the right vertex g . The lower common support can be found by the next algorithm (an example of the behaviour of the algorithm follows the algorithm).

Algorithm 4.4.2 (Lower common support)

- Input:** Two convex polygons U_L and U_R such that the maximum x coordinate over all vertices in U_L is smaller than the minimum x coordinate over all vertices in U_R .
- Output:** Pair consisting of the vertex u in U_L and the vertex w in U_R such that $L(u, w)$ forms the lower common support of U_L and U_R .

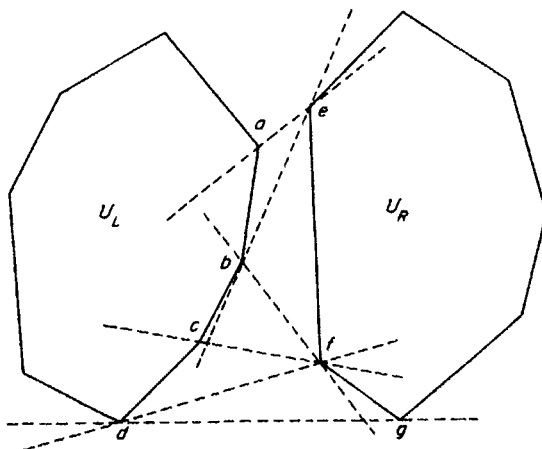


Figure 4.4.2 Search for the lower common support.

Procedure:

- Step 1. Find the vertex u in U_L with the largest x coordinate, and the vertex w in U_R with the smallest x coordinate.
- Step 2. Do 2.1 and 2.2 alternately until u and w are not changed any more.
 - 2.1. While vertex $\text{cnext}[u]$ is lower than $L(u, w)$, repeat $u \leftarrow \text{cnext}[u]$.
 - 2.2. While vertex $\text{ccnext}[w]$ is lower than $L(u, w)$, repeat $w \leftarrow \text{ccnext}[w]$.
- Step 3. Return $L(u, w)$.

An example of the behaviour of the algorithm is shown in Figure 4.2.2. First, the pair (u, v) is set to be (a, e) in Step 1. Next, the pair is changed to (b, e) in Step 2.1, to (b, f) in Step 2.2, through (c, f) to (d, f) in Step 2.1, and finally to (d, g) in Step 2.2.

This algorithm terminates in a finite number of steps and gives the lower common support as the output. This can be understood in the following way. Let $(u_1, u_2, \dots, u_s, u_1)$ be the list of vertices in U_L appearing counterclockwise on the boundary. Without loss of generality, suppose that u_1 is the vertex on the lower common support. Then, for any vertex w in U_R such that w is below the line $L(u_1, u_2)$, the vertex $\text{cnext}[u_1]$ is not lower than the line $L(u_1, w)$. Thus, once u reaches u_1 in Step 2.1, it will not be updated any more. Similarly, once w reaches the vertex on the common lower support in Step 2.2, it will not be updated. Therefore, Step 2 terminates in a finite number of repetitions. Moreover, the termination condition for Step 2 actually implies that $L(u, w)$ is the lower common support.

Let n denote the total number of vertices in U_L and U_R . In Step 1, the initial pair (u, w) can be found by scanning the lists of vertices. In Step 2, the total number of updates of the pair (u, w) does not exceed n . Hence,

Algorithm 4.4.2 runs in $O(n)$ time. Actually there is an $O(\log n)$ algorithm for finding the common support (Overmars and Leeuwen, 1981), but an $O(n)$ algorithm is enough for our purpose because the subproblem is not a bottleneck of the total time complexity.

Now we are ready to consider our main problem. We want to construct the polygonal line consisting of new Voronoi edges and new Voronoi vertices. As shown in Figure 4.4.1, let p_L and p_R be the pair of the left generator and the right generator forming the lower common support $L(p_L, p_R)$ of the convex hull of P_L and that of P_R , then $b(p_L, p_R)$, the perpendicular bisector of $\overline{p_L p_R}$, gives the bottommost edge of the polygonal line, because $\overline{p_L p_R}$ is an edge of the convex hull of $P_L \cup P_R$ but is not an edge of the convex hull of P_L or of P_R . Hence, we start with this pair (p_L, p_R) .

We consider a point w moving along the perpendicular bisector between p_L and p_R , from the bottom upward. If the y coordinate of the point w is sufficiently small, w belongs to both $V(p_L)$ and $V(p_R)$. Let w_0 be the point at infinity in the negative y direction along the bisector, and let w_1 be the point at which w crosses a Voronoi edge, say e_1 , of \mathcal{V}_L or \mathcal{V}_R for the first time (as in Figure 4.4.1). Then, the portion of the bisector along which w has moved so far, i.e. the half line $\overline{w_0 w_1}$, is the first new Voronoi edge, and w_1 is the first new Voronoi vertex.

At w_1 the moving point w changes the region either in \mathcal{V}_L or in \mathcal{V}_R , depending on whether e_1 is an edge of \mathcal{V}_L or of \mathcal{V}_R . If e_1 is an edge of \mathcal{V}_L , we replace p_L with the left generator that is on the other side of e_1 . If e_1 is an edge of \mathcal{V}_R (as in Figure 4.4.1), we replace p_R with the other right generator generating e_1 . Next, we draw the perpendicular bisector between the updated pair of p_L and p_R . This bisector has w_1 on it. Suppose that w moves from w_1 along the new bisector upward until it crosses a Voronoi edge of \mathcal{V}_L or \mathcal{V}_R again. Let the crossing point be w_2 . Thus we obtain the second new Voronoi vertex w_2 and the second new Voronoi edge $\overline{w_1 w_2}$.

We repeat similar procedures until we reach the pair (p_L, p_R) forming the upper common support. Thus, we obtain the next algorithm.

Algorithm 4.4.3 (Merger of two Voronoi diagrams)

Input: Two Voronoi diagrams \mathcal{V}_L and \mathcal{V}_R for generator sets P_L and P_R , respectively, such that the generators in \mathcal{V}_L have smaller x coordinates than those in \mathcal{V}_R .

Output: Voronoi diagram for $P_L \cup P_R$.

Procedure:

- Step 1. Construct the convex hull of P_L and that of P_R .
- Step 2. Find the lower common support $L(P_L, P_R)$ by Algorithm 4.4.2.
- Step 3. $w_0 \leftarrow$ the point at infinity downward on $b(p_L, p_R)$, and $i \leftarrow 0$.
- Step 4. While $L(p_L, p_R)$ is not the upper common support, repeat 4.1, ..., 4.4.
 - 4.1. $i \leftarrow i + 1$.
 - 4.2. Find the point a_L (other than w_{i-1}) of the intersection of $b(p_L, p_R)$ with the boundary of $V(p_L)$.

- 4.3. Find the point a_R (other than w_{i-1}) of the intersection of $b(p_L, p_R)$ with the boundary of $V(p_R)$.
- 4.4. If a_L has a smaller y coordinate than a_R ,
 - $w_i \leftarrow a_L$, and
 - $p_L \leftarrow$ the generator on the other side of the Voronoi edge containing a_L .
 Otherwise
 - $w_i \leftarrow a_R$, and
 - $p_R \leftarrow$ the generator on the other side of the Voronoi edge containing a_R .

Step 5. $m \leftarrow i$.

$w_{m+1} \leftarrow$ the point at infinity upward on $b(p_L, p_R)$.

Step 6. Add the polygonal line $(\overline{w_0 w_1}, \overline{w_1 w_2}, \dots, \overline{w_m w_{m+1}})$, and delete from \mathcal{V}_L the part to the right of the polygonal line and delete from \mathcal{V}_R the part to the left of the polygonal line. Return the resultant diagram.

Step 1 is done in $O(n)$ time because we have already obtained the Voronoi diagrams \mathcal{V}_L and \mathcal{V}_R (recall Algorithm 4.1.2). Step 2 is done in $O(n)$ time by Algorithm 4.4.2, and Step 3 in constant time. Step 4 is repeated at most $O(n)$ times, because there are at most $O(n)$ new Voronoi edges. Steps 4.1 and 4.4 require only constant time.

Steps 4.2 and 4.3 require time proportional to the number of edges on the boundary of $V(p_L)$ and to that of $V(p_R)$, respectively, which are not bounded by any fixed constant. However, we can decrease the total number of edges to be examined in Steps 4.2 and 4.3 over all repetitions of Step 4. For this purpose, we examine edges on the boundary of $V(p_L)$ counterclockwise, and those of $V(p_R)$ clockwise. Suppose that, in a certain repetition of Step 4, we have found the intersections a_L and a_R , as shown in Figure 4.4.3. Since a_L is lower than a_R in this example, p_L is replaced by p'_L ; as a result of this, the polygonal line bends to the right. Therefore, when we search for the intersection a'_R of $b(p'_L, p_R)$ with the boundary of $V(p_R)$, we need not examine the edges to the left of a_R ; we can start searching at a_R clockwise. Thus we can avoid the repeated check of irrelevant edges. Similarly, if a_R is lower than a_L , p_R is replaced and the polygonal line bends to the left, so that we can avoid unnecessary checks of edges by examining them counterclockwise. By doing so, we can execute Step 4 in $O(n)$ time.

Step 5 requires constant time. Step 6 requires $O(n)$ time. Hence, in total Algorithm 4.4.3 runs in $O(n)$ time.

Next, let us consider the time complexity of our main algorithm, Algorithm 4.4.1. The algorithm is recursive in the sense that the procedure calls itself at Steps 2.2 and 2.3. To evaluate the time complexity of such an algorithm, we first consider the other steps. Obviously, Steps 1, 2.1 and 3 can be done in constant time. Step 2.4 can be done in $O(n)$ time by Algorithm 4.4.3. Thus, all steps other than the recursive calls require $O(n)$ time.

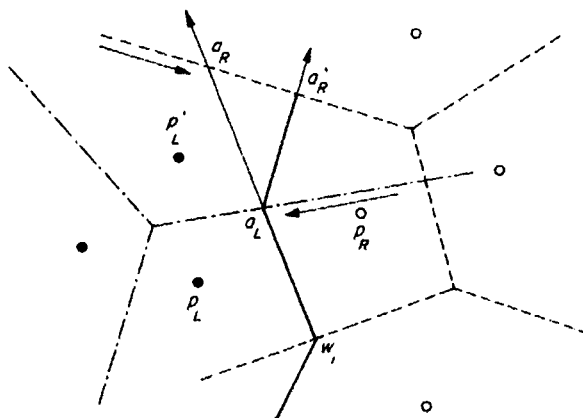


Figure 4.4.3 Search for the next Voronoi vertex on the boundary of the left and the right Voronoi diagrams.

Now, let $T(n)$ denote the time required by Algorithm 4.4.1 for n generators. Then, we get

$$T(n) = 2T(n/2) + O(n),$$

because the algorithm calls itself twice using half of the original input as the new input. With the consideration that $T(1)$ and $T(2)$ are constant, this equation implies that $T(n) = O(n \log n)$ (Aho *et al.*, 1974).

Recall that any algorithm for constructing a Voronoi diagram requires $O(n \log n)$ time in the worst case (Section 4.2). Thus, Algorithm 4.4.1 is optimal from the viewpoint of the worst-case time complexity.

The divide-and-conquer technique was first applied to this problem by Shamos and Hoey (1975); since then many variants have been proposed (Lee and Schachter, 1980; Guibas and Stolfi, 1985). It is also known that a divide-and-conquer method of this type actually requires $O(n \log n)$ time not only in the worst case but also on average (Ohya *et al.*, 1984a). Thus, in the average sense, this method is not optimal. Recently, quite different types of divide-and-conquer methods have been proposed; for uniformly distributed generators, the algorithm proposed by Dwyer (1987) runs in $O(n \log \log n)$ time on average, and the algorithm proposed by Katajainen and Koponen (1988) runs in $O(n)$ time on average.

4.5 THE PLANE SWEEP METHOD

'Plane sweep' is one of the fundamental techniques used to solve two-dimensional geometric problems. In this technique we use a special line called a *sweepline*, which is conventionally vertical, and sweep the plane with this line, say from left to right. As the sweepline moves, it hits geometric objects one by one. Each time an event happens, a portion of the problem is solved

on the sweepline. Thus, this technique enables us to solve two-dimensional problems by a sequence of almost one-dimensional processing. Hence, if successfully applied, the plane sweep technique gives a conceptually simple algorithm.

However, the plane sweep technique cannot be applied to our problem directly, because to construct Voronoi edges and Voronoi vertices on the sweepline we have to 'foresee' the locations of generators in the half plane that have not yet been swept; the sweepline reaches a Voronoi polygon before hitting the corresponding generator. If each generator p_i were to exist at the leftmost point of the Voronoi polygon $V(p_i)$, which is of course not the case, the plane sweep method could be applied. Indeed, there exists a transformation by which this 'dream' is realized (Fortune, 1986, 1987).

Suppose that the set $P = \{p_1, p_2, \dots, p_n\}$ of n generators is given. In addition to Assumptions A4.1.1, A4.1.2 and A4.4.1, here we make the following assumption.

Assumption A4.5.1 Any generator and any Voronoi vertex on its boundary do not align horizontally.

This assumption is not critical, but makes the description of the algorithm much simpler.

For any point p , we define $r(p) = \min \{d(p, p_i) \mid 1 \leq i \leq n\}$, i.e. $r(p)$ is the radius of the largest empty circle centred at p . Let $x(p)$ and $y(p)$ denote the x coordinate and the y coordinate, respectively, of p .

We define the map φ from \mathbb{R}^2 to itself by

$$\varphi(p) = (x(p) + r(p), y(p)) \quad (4.5.1)$$

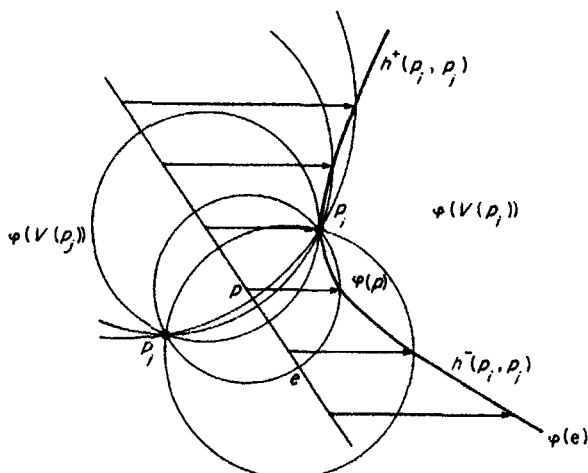


Figure 4.5.1 Perpendicular bisector and its image.

for point p (see Figure 4.5.1). If $p \in V(p_i)$, we get $\varphi(p) = (x(p) + d(p, p_i), y(p))$ because p_i is the nearest generator to p . $\varphi(p) = p$ if and only if p is a generator. For the Voronoi vertex q , the Voronoi edge e , the Voronoi polygon $V(p_i)$ and the Voronoi diagram \mathcal{V} , their images using φ are denoted by $\varphi(q)$, $\varphi(e)$, $\varphi(V(p_i))$ and $\varphi(\mathcal{V})$, respectively.

As shown in Figure 4.5.1, let p_i and p_j be two generators such that $x(p_i) > x(p_j)$, and let e be the Voronoi edge between p_i and p_j . Then, φ maps e to part of a curved line whose leftmost point is p_i . Indeed, it is an easy exercise to see that the image $\varphi(e)$ of e is part of a hyperbola open rightward with the leftmost point p_i . The image of each Voronoi polygon is a connected region surrounded by segments of hyperbolas.

The mapping φ can be interpreted in the context of ‘Voronoi diagrams in a river’ where the boat runs at the same speed as the water flow (Sugihara, 1992a). Suppose that the generators are point-like islands in a river, and each island has a boat of the same speed. Suppose that $p \in V(p_i)$. If there is no flow of water, the boat starting at island p_i reaches p faster than any other boat. Now assume that the water in the river flows from left to right (i.e. in the positive x direction) at the same speed as the boat. Then, during the sailing of the boat from p_i to p , the boat is carried to the right by the same distance as it sails; hence the boat reaches the point $\varphi(p) = (x(p) + r(p), y(p))$ instead of the point p . Thus, $\varphi(p)$ represents the point reached by the boat that leaves the island nearest to p facing toward p . Hence, $\varphi(\mathcal{V})$ can be interpreted as the tessellation on the surface of the river into ‘territories’ of the islands such that any point in a territory can be reached by the boat starting at the corresponding island faster than any other boat (see Section 3.7.5).

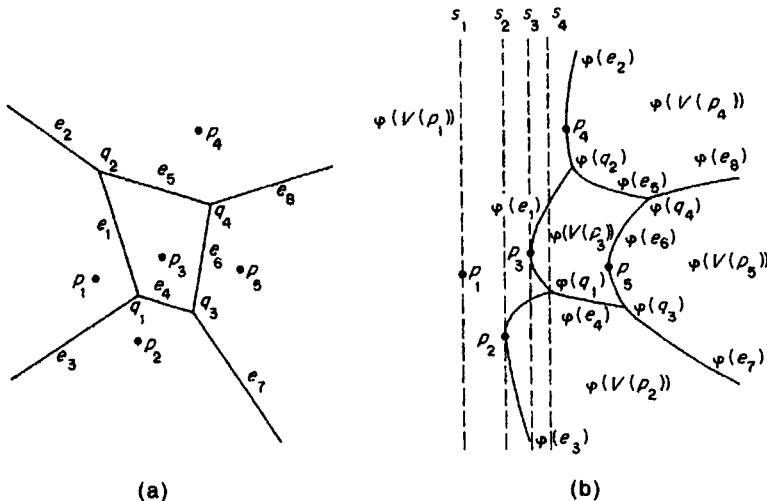


Figure 4.5.2 Voronoi diagram and its image: (a) Voronoi diagram \mathcal{V} for five generators; (b) its image $\varphi(\mathcal{V})$.

An example of the map ϕ applied to the Voronoi diagram is shown in Figure 4.5.2, where (a) is the Voronoi diagram for five points and (b) is its image by ϕ . (If we want to interpret diagram (b) as the tessellation on the surface of the river, the vertical line passing through p_1 , the broken line s_1 , is also necessary, because no boat can reach the region to the left of s_1 .)

Note that for any generator p_i other than the leftmost one, the point p_i is the farthest to the left in the transformed region $\phi(V(p_i))$. The images of all the Voronoi edges and Voronoi vertices related to p_i appear to the right of p_i . Hence we can apply the plane sweep technique for constructing $\phi(\mathcal{V})$.

In what follows we use the terminology for Voronoi diagrams to designate objects in $\phi(\mathcal{V})$. For instance, the image of a Voronoi vertex is called a Voronoi vertex of $\phi(\mathcal{V})$, and the image of a Voronoi edge is called a Voronoi edge of $\phi(\mathcal{V})$.

Let us note at this point that, because of Assumption A4.5.1, the image $\phi(q)$ of any Voronoi vertex q is not the leftmost point of any Voronoi region in $\phi(\mathcal{V})$, and consequently at $\phi(q)$ exactly one Voronoi edge extends to the right and the other two Voronoi edges extend to the left. For instance, at the vertex $\phi(q_1)$ in Figure 4.5.2(b), the edge $\phi(e_4)$ extends to the right and the edges $\phi(e_1)$ and $\phi(e_3)$ extend to the left.

The plane sweep method moves a vertical sweepline across the plane from left to right, and each time an event happens, the structure of the Voronoi diagram $\phi(\mathcal{V})$ is updated on the sweepline. There are two types of events. An event of the first type occurs when the sweepline hits a generator, as the lines s_1 , s_2 and s_3 in Figure 4.5.2(b). An event of the second type occurs when the sweepline hits a Voronoi vertex of $\phi(\mathcal{V})$, as the line s_4 in Figure 4.5.2(b).

Let p_i and p_j be two generators. The perpendicular bisector of p_i and p_j is transformed by ϕ to a hyperbola. Let us cut this hyperbola at the leftmost point, and let $h^+(p_i, p_j)$ and $h^-(p_i, p_j)$ be the upper part and the lower part, respectively, of the hyperbola; we call them the upper and lower half hyperbolas (see Figure 4.5.1). Note that $h^+(p_i, p_j) = h^+(p_j, p_i)$ and $h^-(p_i, p_j) = h^-(p_j, p_i)$.

To represent the structure of $\phi(\mathcal{V})$ along the sweepline, we use an alternating list L of regions and boundary edges which appear on the sweepline from the bottom to the top. We also use Q , which is a set of points in the plane. Q represents the potential points at which events may happen in future. At the beginning, Q is the set of all generators, and candidates of Voronoi vertices are added to Q whenever they are found. The algorithm is as follows (the example that follows the algorithm may help the reader to understand the algorithm).

Algorithm 4.5.1 (Plane sweep method)

Input: Set $P = \{p_1, p_2, \dots, p_n\}$ of n generators.

Output: Voronoi diagram $\phi(\mathcal{V})$.

Procedure:

Step 1. $Q \leftarrow P$.

Step 2. Choose and delete the leftmost point, say p_i , from Q .

- Step 3. $L \leftarrow$ the list consisting of a single region $\phi(V(p_i))$.
- Step 4. While Q is not empty, repeat 4.1, 4.2 and 4.3.
- 4.1. Choose and delete the leftmost point w from Q .
 - 4.2. If w is a generator, say $w = p_i$, do 4.2.1, 4.2.2 and 4.2.3.
 - 4.2.1. Find region $\phi(V(p_j))$ on L containing p_i .
 - 4.2.2. Replace $\phi(V(p_j))$ on L by the subsequence $(\phi(V(p_j)), h^-(p_j, p_i), \phi(V(p_i)), h^+(p_i, p_j), \phi(V(p_j)))$.
 - 4.2.3. Add to Q the intersection of $h^-(p_j, p_i)$ with the immediate lower half hyperbola on L , and the intersection of $h^+(p_i, p_j)$ with the immediate upper half hyperbola on L .
 - 4.3. If w is an intersection, say $w = \phi(q_i)$, do 4.3.1, ..., 4.3.4 (where we suppose that $\phi(q_i)$ is the intersection of $h^\pm(p_i, p_j)$ and $h^\pm(p_j, p_k)$).
 - 4.3.1. Replace subsequence $(h^\pm(p_i, p_j), \phi(V(p_j)), h^\pm(p_j, p_k))$ on L by $h = h^-(p_i, p_k)$ or $h = h^+(p_i, p_k)$ appropriately.
 - 4.3.2. Delete from Q any intersections of $h^\pm(p_i, p_j)$ or $h^\pm(p_j, p_k)$ with others.
 - 4.3.3. Add to Q any intersections of h with its immediate upper half hyperbola and its immediate lower half hyperbola on L .
 - 4.3.4. Mark $\phi(q_i)$ as a Voronoi vertex incident to $h^\pm(p_i, p_j)$, $h^\pm(p_j, p_k)$ and h .
- Step 5. Report all the half hyperbolas ever listed on L , all the Voronoi vertices marked in Step 4.3.4 and the incidence relations among them.

Steps 1, 2 and 3 are for initialization. In the example in Figure 4.5.2, Q is set to be $\{p_1, p_2, \dots, p_5\}$ in Step 1, $p_i = p_1$ is chosen and Q is changed to $\{p_2, \dots, p_5\}$ in Step 2, and L is set to be

$$L = (\phi(V(p_1)))$$

in Step 3. Steps 2 and 3 correspond to the event that the sweepline hits the leftmost generator (the vertical line s_1 in the figure). The list $L = (\phi(V(p_1)))$ implies that if we move along the sweepline from the bottom upward, we always lie in the Voronoi region for p_1 .

Step 4 is the main part of the algorithm. In Step 4.1 we choose a point at which the next event occurs. In the example shown in Figure 4.5.2, the algorithm goes in the following way. We have $Q = \{p_2, \dots, p_5\}$ at the end of Step 3, and hence at Step 4.1 point $w = p_2$ is chosen from Q and Q is changed to $Q = \{p_3, p_4, p_5\}$. This corresponds to the event that the sweepline hits p_2 , the sweepline being at s_2 in Figure 4.5.2(b).

According to the type of the event, Step 4.2 or 4.3 is done; Step 4.2 is for an event of the first type and Step 4.3 is for an event of the second type. Since $w = p_2$ is a generator, Step 4.2 is done. First, we find the region $\phi(V(p_2))$ containing the new generator p_2 in Step 4.2.1; next we create a new Voronoi

region $\varphi(V(p_i))$ and a new Voronoi edge consisting of $h^-(p_i, p_j)$ and $h^+(p_j, p_i)$ in Step 4.2.2; and finally we insert candidates of Voronoi vertices which may be end points of $h^-(p_i, p_j)$ and $h^+(p_i, p_j)$. In our example, in Step 4.2.1 $\varphi(V(p_i))$ is recognized as $\varphi(V(p_1))$, and in Step 4.2.2 L is changed to

$$L = (\varphi(V(p_1)), h^-(p_1, p_2), \varphi(V(p_2)), h^+(p_2, p_1), \varphi(V(p_1))).$$

The list L at this point implies that, if we move along the sweepline from the bottom upward, we traverse the region $\varphi(V(p_1))$, cross the edge $h^-(p_1, p_2)$, traverse the region $\varphi(V(p_2))$, cross the edge $h^+(p_2, p_1)$ and traverse the region $\varphi(V(p_1))$ in this order. This is the situation that we have immediately after the sweepline hits p_2 . Since there is no half hyperbola below $h^-(p_1, p_2)$ or above $h^+(p_2, p_1)$, nothing is done in Step 4.2.3.

In the second repeat of Step 4.1, $w = p_3$ is chosen and Q is changed to $Q = \{p_4, p_5\}$. This corresponds to the event that the sweepline hits p_3 (the line s_3 in Figure 4.5.2(b)). Hence, Step 4.2 is done again.

The generator p_3 lies above the upper hyperbola $h^+(p_1, p_2)$, and hence in Step 4.2.2 the second appearance of $\varphi(V(p_1))$ in L is replaced by the sublist $(\varphi(V(p_1)), h^-(p_1, p_3), \varphi(V(p_3)), h^+(p_3, p_1), \varphi(V(p_1)))$, which changes L to

$$L = (\varphi(V(p_1)), h^-(p_1, p_2), \varphi(V(p_2)), h^+(p_2, p_1), \\ \varphi(V(p_1)), h^-(p_1, p_3), \varphi(V(p_3)), h^+(p_3, p_1), \varphi(V(p_1))).$$

The new list L represents the situation obtained immediately after the sweepline hits p_3 . In L there is a half hyperbola $h^+(p_2, p_1)$, which is immediately below $h^-(p_1, p_3)$, and consequently in Step 4.2.3 the point $\varphi(q_1)$ of intersection of these two half hyperbolas is added to Q ; thus Q is changed to $Q = \{\varphi(q_1), p_4, p_5\}$.

In the third repeat of Step 4.1, $w = \varphi(q_1)$ is chosen and Q is changed to $Q = \{p_4, p_5\}$. This corresponds to the event that the sweepline comes to s_4 in Figure 4.5.2(b). Since $w = \varphi(q_1)$ is a Voronoi vertex, Steps 4.3.1–4.3.4 are done; throughout this step we should take the same superscript + or – for all appearances of $h^\pm(p_i, p_j)$ as we should do for all appearances of $h^\pm(p_j, p_k)$. In Step 4.3.1 the old region $\varphi(V(p_i))$ and its two boundaries $h^\pm(p_i, p_j)$ and $h^\pm(p_j, p_k)$ are deleted from L , and a new Voronoi edge h is inserted into L , where h is either $h^-(p_i, p_k)$ or $h^+(p_i, p_k)$, depending on the configuration around. At this point, $\varphi(q_1)$ is recognized as the end point of the edges $h^\pm(p_i, p_j)$ and $h^\pm(p_j, p_k)$. All the other candidates for the end points of them are deleted from Q in Step 4.3.2, and the candidates of the end point of the new edge h are added to Q in Step 4.3.3. In Step 4.3.4 the incidence structure around $\varphi(q_1)$ is recorded.

In our example, in Step 4.3.1 the subsequence $(h^+(p_2, p_1), \varphi(V(p_1)), h^-(p_1, p_3))$ is replaced by $h^-(p_2, p_3)$, changing L to

$$L = (\varphi(V(p_1)), h^-(p_1, p_2), \varphi(V(p_2)), h^-(p_2, p_3), \\ \varphi(V(p_3)), h^+(p_3, p_1), \varphi(V(p_1))).$$

Nothing is done in Step 4.3.2 because Q contains no point of intersection of two half hyperbolas. Nothing is done in Step 4.3.3, either, because the half hyperbola $h^-(p_2, p_3)$ has no point of intersection with $h^-(p_1, p_2)$ or with $h^+(p_3, p_1)$. In Step 4.3.4 the incidence relations among the Voronoi vertices, the Voronoi edges and the Voronoi regions around $\varphi(q_1)$ are registered.

The algorithm treats the other events one by one in a similar manner until Q becomes empty. The Voronoi diagram $\varphi(\mathcal{V}(P))$ is obtained by collecting all the half hyperbolas ever listed in L , all the Voronoi vertices marked in Step 4.3.4 and the incidence relations among them.

We can understand the correctness of the algorithm by noting that (i) the generator p_i , other than the leftmost one, lies at the leftmost point of the Voronoi region $\varphi(V(p_i))$; (ii) at each Voronoi vertex in $\varphi(\mathcal{V})$ exactly one edge emanates to the right and the other two edges to the left; and that (iii) for each Voronoi vertex in $\varphi(\mathcal{V})$, the two edges emanating to the left become neighbours on L at some time during the sweep (and hence the points inserted in Steps 4.2.3 and 4.3.3 include all the Voronoi vertices). See Fortune (1986, 1987) for the details of the proof.

To execute the procedure efficiently, we need some techniques in data structure. The basic operations on Q are the insertion of points and the deletion of the minimum point with respect to the x coordinate. A storage requiring these operations is called a *priority queue*, and can be implemented, for instance, by a data structure called a heap. Indeed, using a heap, we can carry out each of the above operations in $O(\log n)$ time, where n is the number of points stored in Q (Aho *et al.*, 1974). In Step 4.3.2 we also have to delete from Q some points that are not necessarily minimum in the x coordinate. However, these points can be accessed in constant time if we store and maintain pointers at the associated half hyperbolas, and can be deleted in $O(\log n)$ time in the same manner as the insertion and the minimum deletion.

The other important storage L is an alternating list of regions and half hyperbolas along the sweepline. The intersections of the regions with the sweepline give intervals on the sweepline, and the intersections of the half hyperbolas with the sweepline give boundary points of the intervals. The interval corresponding to each region $\varphi(V(p_i))$ changes as the sweepline moves. The basic operations in L are to search for a relevant interval in Step 4.2.1 and the deletion and insertion of substrings in Steps 4.2.2 and 4.3.1. A storage requiring these operations is called a *dictionary*, and is implemented efficiently by a data structure such as a 2–3 tree or an AVL tree (Aho *et al.*, 1974; AVL stands for the initials of the coauthors of the paper). With such a data structure, we can execute each operation in $O(\log n)$ time.

Employing those techniques in data structure, we can execute Algorithm 4.5.1 in $O(n \log n)$ time. Indeed, Step 1 requires $O(n \log n)$ time, Step 2 $O(\log n)$ time and Step 3 constant time. Note that the total number of elements ever listed on L is of $O(n)$; this is because the number of Voronoi edges and Voronoi vertices are both of $O(n)$. The total number of elements ever stored in Q is also of $O(n)$, because there are only $O(n)$ pairs of Voronoi

edges that ever become neighbours on L , and hence there are only $O(n)$ candidates for Voronoi vertices. Therefore, Steps 4.1, 4.2 and 4.3 require $O(\log n)$ time, and they are repeated $O(n)$ times in Step 4. Thus, the total time complexity is of $O(n \log n)$.

The plane sweep technique has been applied to many geometric problems, such as point location, the extraction of intersections between line segments or between polygons and the construction of an arrangement consisting of lines (Preparata and Shamos, 1985). Fortune (1986) was the first to apply this technique to the construction of Voronoi diagrams and obtained an algorithm equivalent to Algorithm 4.5.1. The plane sweep technique was also applied to a Voronoi diagram for line segments (Fortune, 1986, 1987; Section 3.5), to an additively weighted Voronoi diagram (Fortune, 1986, 1987; Section 3.1.2) and to a Voronoi diagram on a cone (Dehne and Klein, 1987; Section 3.7.8). Different types of sweep procedure are also used for the ordinary Voronoi diagrams (Dehne and Klein, 1987, 1988, 1997).

4.6 PRACTICAL TECHNIQUES FOR IMPLEMENTING THE ALGORITHMS

4.6.1 Inconsistency caused by numerical errors

So far we have assumed that neither degeneracy nor numerical error takes place in computation. However, algorithms designed in such an artificial world are not necessarily valid in practice, because in computers numerical values are treated only in finite-precision arithmetic. In degenerate or nearly degenerate cases, numerical error sometimes causes inconsistency in topological structures, and thus makes algorithms invalid.

An example of topological inconsistency we often encounter in the incremental method is shown in Figure 4.6.1. The boundary-growing procedure employed in the incremental method is based on the property that the boundary of a Voronoi polygon forms a closed sequence of segments of perpendicular bisectors. However, if the bisectors pass near to a Voronoi vertex, the topological relations between the boundaries and the Voronoi vertex are sometimes misjudged, resulting in a sequence in which the end point does not coincide with the start point, as shown in Figure 4.6.1. If such an inconsistency happens, the incremental algorithm cannot accomplish the task.

In this section, we remove all the assumptions, Assumptions A4.1.1, A4.1.2, A4.4.1 and A4.5.1, which we made for the sake of simplicity, and consider how to translate the incremental method into computer programs that work for any input data, degenerate or non-degenerate, in finite-precision computation. We present two quite different principles. The first one, presented in Section 4.6.2, is for constructing an error-free closed world in which all the topological structures are judged correctly. In this world, degeneracy is also detected exactly, so that we have another problem, i.e. the problem of

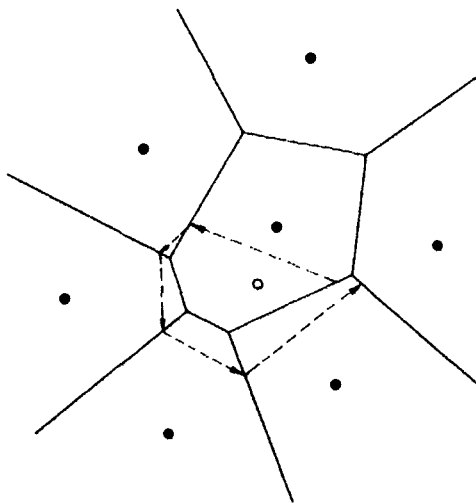


Figure 4.6.1 Unclosed boundary caused by numerical errors.

preparing complicated branches of exceptional procedure for treating degenerate cases. To circumvent this problem, we also present a method for avoiding degeneracy by symbolic perturbation. In Section 4.6.3, on the other hand, we consider a world with numerical errors and present the second principle, in which we avoid inconsistency by placing higher priority on topological structures than on numerical values. This principle automatically enables us to avoid degeneracy because it is impossible to detect degeneracy by computation with errors.

4.6.2 Construction of an error-free world

The first principle is to compute numerical values so precisely that they are good enough always to judge topological structures correctly.

Suppose that we fix the set $P = \{p_1, \dots, p_n\}$ of generators. Let (x_i, y_i) denote the coordinates of the generator p_i . Let us assume that the coordinates are represented by integers whose absolute values are not greater than a certain fixed integer K :

$$-K \leq x_i, y_i \leq K \quad \text{for } i = 1, 2, \dots, n. \quad (4.6.1)$$

This assumption is not unrealistic, because in a digital computer the coordinates are usually represented by a fixed number of bits, so that they can be transformed into integers if a sufficiently large-scale factor is multiplied.

Suppose that we have constructed a Voronoi diagram \mathcal{V}_{l-1} for the first $l-1$ generators p_1, p_2, \dots, p_{l-1} and now want to add a new generator p_l . For this purpose we need to find Voronoi vertices of \mathcal{V}_{l-1} that should be contained in the Voronoi polygon of the new generator.

Let q_{ijk} denote the Voronoi vertex incident to three Voronoi polygons $V(p_i)$, $V(p_j)$ and $V(p_k)$ counterclockwise in this order. For three generators p_i, p_j, p_k and a point $p = (x, y)$, let $H(p_i, p_j, p_k, p)$ be as defined by equation (2.4.10). The equation $H(p_i, p_j, p_k, p) = 0$ represents the circle that passes through p_i, p_j and p_k , and this circle contains p if and only if $H(p_i, p_j, p_k, p) < 0$. Recall that q_{ijk} belongs to the Voronoi polygon of the new generator p_l if and only if p_l is contained in this circle, which means that q_{ijk} belongs to $V(p_l)$ if and only if $H(p_i, p_j, p_k, p_l) < 0$.

Hence, what we have to do to find the points w_1, w_2, \dots, w_m in Step 4.3 of Algorithm 4.3.2 is to find Voronoi edges having $H(p_i, p_j, p_k, p_l)$ with opposite signs at their two end points.

Note that $H(p_i, p_j, p_k, p_l)$ is an integer, so that it can be computed correctly unless it overflows memory. From the Hadamard inequality (which says that the absolute value of the determinant of a matrix is not greater than the multiplication of the lengths of all the column vectors; see, for instance, Greub, 1975) and the assumption (4.6.1), we obtain

$$\begin{aligned} |H(p_i, p_j, p_k, p_l)| &\leq \sqrt{1^2 + 1^2 + 1^2 + 1^2} \sqrt{x_i^2 + x_j^2 + x_k^2 + x_l^2} \sqrt{y_i^2 + y_j^2 + y_k^2 + y_l^2} \\ &\quad \times \sqrt{(x_i^2 + y_i^2)^2 + (x_j^2 + y_j^2)^2 + (x_k^2 + y_k^2)^2 + (x_l^2 + y_l^2)^2} \quad (4.6.2) \\ &\leq 2 \cdot 2K \cdot 2K \cdot 4k^2 \\ &= 32K^4. \end{aligned}$$

If we compute the value of $H(p_i, p_j, p_k, p_l)$ according to the Laplace expansion of the right-hand side of equation (4.6.2), the absolute value of any number that appears in the course of computation does not exceed the bound $32K^4$, either. Hence the integer $H(p_i, p_j, p_k, p_l)$ can be computed without overflow if the computation is carried out so precisely that a number as large as $32K^4$ is representable.

Let $N = [\log_2(K + 1)]$, where $[x]$ is the smallest integer not less than x . Then each coordinate can be represented by $N+1$ bits, N bits for the absolute value and 1 bit for the sign. Any integer between $-32K^4$ and $32K^4$ can be represented by $4N+6$ bits, $4N+5$ bits for the absolute value and 1 bit for the sign. Hence, using $4N+6$ bits for computation, we can always correctly determine the Voronoi vertices to be deleted in the addition of the new generator. Thus we can avoid misjudgement in the topological structure of the Voronoi diagram.

For example, if we use 64 bits (2 words in an ordinary computer) to represent each integer appearing in the computation (i.e. 1 bit for the sign and 63 bits for the absolute value), we can represent integers as large as $M = 2^{63} - 1$. In this case, consequently, we can choose $K = 23\,170$, because

$$M = 2^{63} - 1 = 2^5 \times 2^{58} - 1 = 32(2^{14.5})^4 - 1 > 32(23170)^4,$$

which seems to give sufficient resolution for ordinary purposes in point pattern analysis.

By the above method we can indeed avoid misjudgement in topological structures, but we still have another problem, i.e. the treatment of degenerate cases. Degeneracy takes place when $H(p_i, p_j, p_k, p_l) = 0$. In this case the boundary of the Voronoi polygon of the new generator passes through the Voronoi vertex of \mathcal{V}_{l-1} , giving a Voronoi vertex with four or more edges. Such degeneracy usually requires exceptional branches of processing, which makes construction and maintenance of a computer program difficult.

Fortunately, however, we can avoid degeneracy by a very simple trick; intuitively, we 'shrink' the Voronoi polygon of the new generator infinitesimally and thus avoid creating degenerate Voronoi vertices.

From a topological point of view, the Voronoi diagram can be represented by an augmented geometric graph, a planar graph embedded in the plane; recall Section 4.2. Let G_i denote the augmented geometric graph associated with the Voronoi diagram \mathcal{V}_i for the first i generators. G_i represents the topological structure of \mathcal{V}_i . If no degeneracy takes place, the degree of any vertex (i.e. the number of edges incident to the vertex) in G_i is three. In the case of degeneracy, on the other hand, G_i has vertices with degree four or more.

To represent G_i , we adopt the convention that a vertex with degree four or more, if any, is replaced with a microstructure consisting of degree-three vertices and 'length-zero' edges. For example, if four generators p_i, p_j, p_k and p_l are on a common circle and give a degenerate Voronoi vertex with degree four, as shown in Figure 4.6.2(a), we generate two degree-three vertices and one length-zero edge, as shown in (b) or (c); we can choose either of the two alternative structures. This convention implies that we need not generate a vertex of degree more than three even if degeneracy takes place.

Our idea to avoid exceptional processing for degeneracy is just to treat the case where $H(p_i, p_j, p_k, p_l) = 0$ as if $H(p_i, p_j, p_k, p_l) > 0$. That is, we judge

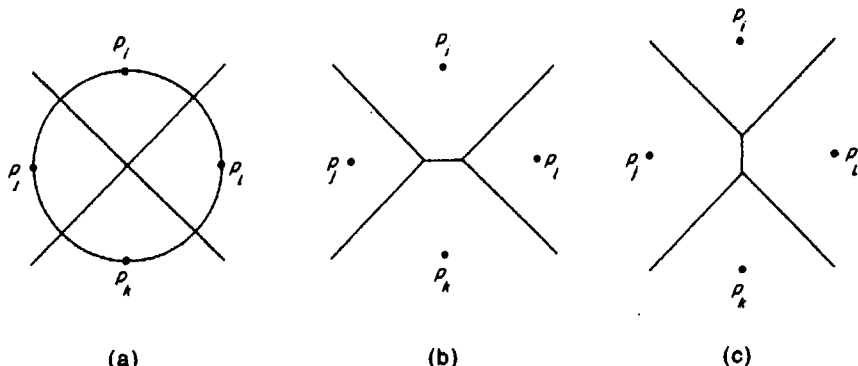


Figure 4.6.2 Degeneracy and perturbation: (a) four generators on a common circle; (b) introduction of a length-zero edge; (c) another way of introducing a length-zero edge.

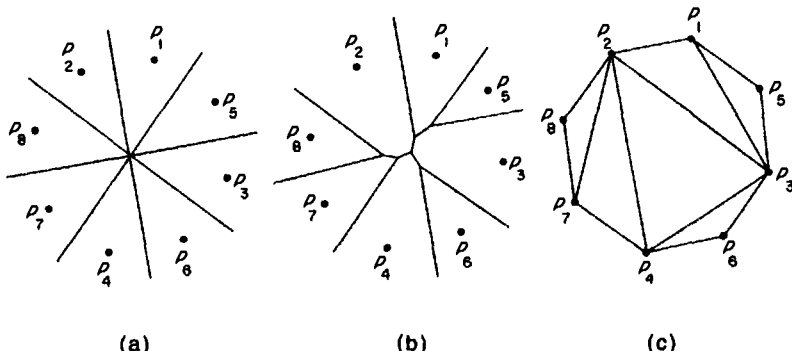


Figure 4.6.3 Degeneracy avoidance: (a) degenerate vertex of degree eight; (b) result of avoiding degeneracy; (c) the corresponding Delaunay triangulation.

that q_{ijk} is inside $V(p_i)$ if $H(p_i, p_j, p_k, p_l) < 0$, and outside if $H(p_i, p_j, p_k, p_l) \geq 0$; note that the latter inequality allows the equality. This strategy intuitively means that each time degeneracy takes place, we shrink the Voronoi polygon of the new generator only slightly so as not to disturb other parts of the Voronoi diagram. Hence every Voronoi vertex of G_{l-1} is judged either inside $V(p_l)$ or outside; no vertex is ‘on’ the boundary of $V(p_l)$.

Figure 4.6.3 shows an example of how our method avoids degeneracy. Here we assume that eight generators p_1, p_2, \dots, p_8 lie on a common circle, so that in an ordinary sense a Voronoi vertex of degree eight will appear, as shown in (a). Suppose that the generators p_1, p_2, \dots, p_8 are added in this order. Then the resultant topological structure will be as shown in (b), where the degenerate vertex is replaced by a tree structure consisting of six vertices and five length-zero edges. This structure is the result of our strategy. This may be understood more easily when we consider the Delaunay triangulation, dual to the Voronoi diagram, shown in (c). Since the primal diagram (b) consists of degree-three vertices, the dual diagram (c) is composed of triangles. These triangles are generated in such a way that every time a new generator is added, it is connected to the old generators to form a triangle. This is the interpretation of our shrink strategy in terms of the dual graph.

This strategy can avoid degeneracy because, if G_{l-1} is a geometric graph with degree three, then so is G_l . Moreover, the strategy does not disturb our original purpose in the sense that, when length-zero edges are contracted, the resulting diagram gives the correct topological structure of the Voronoi diagram.

Summing up the above considerations, we get the next principle for implementation.

Implementation Principle 4.6.1 (Error-free world) Choose and fix the upper bound K of the absolute values of the coordinates of the generators, and put $N = [\log_2(K + 1)]$. Represent the x and y coordinates of the generators by

$N+1$ bit integers (N bits for the absolute value and 1 bit for the sign), and compute the values of $H(p_i, p_j, p_k, p_l)$ in $4N+6$ bits. Judge that the Voronoi vertex q_{ijk} is inside the Voronoi polygon of the new generator p_l if $H(p_i, p_j, p_k, p_l) < 0$, and outside if $H(p_i, p_j, p_k, p_l) \geq 0$.

This principle is based on the recognition that ‘if the input data are represented by a finite number of bits, the sign of the result of an algebraic computation over the data can be determined correctly in a certain finite-precision arithmetic’. Recently this principle has gradually been recognized and utilized in several fields of computer sciences such as linear programming (Khachian, 1980), computational algebra (Lenstra, 1984) and solid modelling (Sugihara and Iri, 1989a).

The shrink strategy presented here is a kind of ‘symbolic perturbation’. Symbolic perturbation is a technique for avoiding degeneracy originally used in linear programming by Bland (1977). Recently the same idea was introduced in computational geometry, and general frameworks are discussed by Edelsbrunner and Mücke (1987) and Yap (1988), by which we can obtain a non-degenerate configuration that is topologically equivalent to a configuration resulting from some perturbation of the input numerical data. The strategy presented in this section can be considered as a symbolic perturbation in the context of the Voronoi diagram with the Laguerre metric (Sugihara, 1992b). The lift-up method was also implemented using the exact arithmetic and symbolic perturbation (Sugihara, 1997).

4.6.3 Topology-oriented approach

We next consider what we can do if we are not allowed to compute in sufficiently high precision. In poor precision arithmetic, numerical errors are inevitable, so that judgment based on numerical values cannot be relied upon; we can rely only on combinatorial computation. Hence, it is natural to place higher priority on topological structures than on numerical values. In this subsection we treat topological structures as higher-priority information than numerical values and thus make the incremental method robust against numerical errors.

As we saw in Section 4.2, the topological structure of the Voronoi diagram \mathcal{V}_l can be considered as the augmented geometric graph G_l . From a topological point of view, therefore, the main task in the incremental method is to convert G_{l-1} to G_l for $l = 4, 5, \dots, n$. We first characterize this task in terms of combinatorial computation only.

For $i = 3, 4, \dots, n$, let us define A_i as the set of augmented geometric graphs G satisfying the following conditions.

(C4.6.1) The degree of any vertex in G is exactly three.

(C4.6.2) G divides the plane into $i+1$ regions; let us call these regions cells.

- (C4.6.3)** Every cell except for the outermost infinite one is simply connected, i.e. it is connected and does not have a hole.
- (C4.6.4)** Two cells share at most one common edge.
- (C4.6.5)** The outermost circuit of G (i.e. the boundary of the outermost infinite cell) consists of exactly three edges and exactly three vertices.

If the Voronoi diagram \mathcal{V}_i is not degenerate, the augmented geometric graph G_i associated with \mathcal{V}_i belongs to A_i . Indeed, (C4.6.1) holds first because \mathcal{V}_i is non-degenerate so that all the Voronoi vertices are of degree three, and secondly because the infinite Voronoi edges were connected to the outermost closed curve (recall Section 4.2). Condition (C4.6.2) holds because \mathcal{V}_i divides the plane into i Voronoi polygons and we introduced the outermost closed curve to surround the diagram. (C4.6.3) and (C4.6.4) hold because Voronoi polygons are convex. To see that (C4.6.5) holds, recall that the additional three generators p_1, p_2 and p_3 were chosen in such a way that they formed a triangle containing all the original generators p_4, p_5, \dots, p_n . Hence as shown in Figures 4.3.2(a) and (b), only p_1, p_2 and p_3 have infinite Voronoi polygons; the three cells corresponding to these three Voronoi polygons only are incident to the outermost circuit of G . Thus, G_i satisfies (C4.6.5).

Let us represent the augmented geometric graph G_i by the triple $G_i = (W_i, E_i, C_i)$, where W_i, E_i and C_i are the set of vertices, edges and cells, respectively, of G_i . For any subset $T \subset W_i$, let $G_i(T)$ denote the subgraph of G_i consisting of vertices in T and those edges in E_i that connect two vertices in T . For any cell $c \in C_i$, let $W_i(c)$ denote the set of vertices on the boundary of the cell c . In the addition of a new generator p_l , the incremental method changes the topological structure of the Voronoi diagram from $G_{l-1} = (W_{l-1}, E_{l-1}, C_{l-1})$ to $G_l = (W_l, E_l, C_l)$. As shown by an example in Figure 4.6.4(a), this task can be done by first choosing a set T of vertices to be deleted (the vertices represented by filled circles in the figure), then creating new vertices (represented by unfilled circles) on all edges connecting a vertex in T and a vertex not in T , and new edges (represented by broken lines) forming a circuit enclosing T , and finally deleting the substructure inside the circuit.

Let $T (\subset W_{l-1})$ be the set of vertices that is deleted in the change from G_{l-1} to G_l . Then T should satisfy the following conditions.

- (C4.6.6)** T is non-empty.
- (C4.6.7)** T does not contain a vertex on the outermost circuit of G_{l-1} .
- (C4.6.8)** $G_{l-1}(T)$ is a tree, i.e. a connected acyclic graph.
- (C4.6.9)** For any $c \in C_{l-1}$, $G_{l-1}(T \cap W_{l-1}(c))$ is connected.

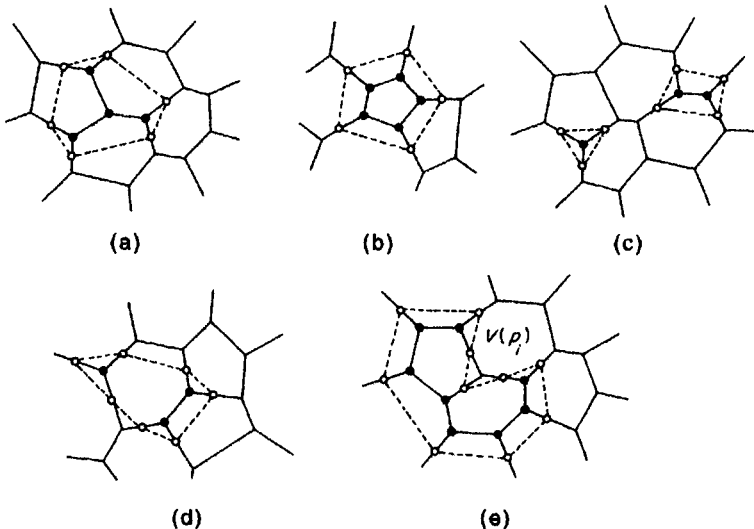


Figure 4.6.4 Topological aspect of the incremental method: (a) deletion of a tree; (b) deletion of a cycle; (c) deletion of two or more connected components; (d) another way of deleting two or more components; (e) deletion of a subgraph that violates condition (C4.6.9).

Condition (C4.6.6) is obvious because the new generator p_l should have its own non-empty Voronoi polygon. Condition (C4.6.7) holds because we introduced the three additional generators and hence the Voronoi polygon of p_l ($l = 4, 5, \dots, n$) is finite. If $G_{l-1}(T)$ has a circuit, then the Voronoi region of an old generator is removed entirely, as shown in Figure 4.6.4(b), which contradicts the basic property that every generator has its own non-empty region. If $G_{l-1}(T)$ is disconnected, then either the Voronoi region of p_l has two or more components, as shown in (c), or an old Voronoi region has two or more components, as shown in (d). Hence T satisfies (C4.6.8). If $G_{l-1}(T \cap W_{l-1}(c))$ is not connected as in (e) (where c corresponds to the boundary of Voronoi region $V(p_i)$), then the Voronoi regions $V(p_i)$ and $V(p_j)$ have two or more edges in common, which contradicts condition (C4.6.4). Thus, (C4.6.9) is satisfied.

Note that conditions (C4.6.6)–(C4.6.9) are written in terms of combinatorial properties only. Hence we can check the conditions by combinatorial computation; we need not employ numerical computation. Moreover, it is easy to see that if G_{l-1} belongs to A_{l-1} and T satisfies (C4.6.6)–(C4.6.9), then the augmented geometric graph G_l belongs to A_l .

However, there is freedom in the choice of the subset T . Hence we employ numerical computation to choose the most promising subset T , and for this purpose only. Thus we obtain the next algorithm for changing G_{l-1} to G_l , which should be used in place of the boundary-growing procedure.

Algorithm 4.6.1 (Tree expansion and deletion)

Input: Generators p_1, p_2, \dots, p_l and geometric graph G_{l-1} ($\in A_{l-1}$).

Output: Geometric graph G_l ($\in A_l$).

Procedure:

- Step 1. Find the generator p_i ($1 \leq i \leq l - 1$) such that $d(p_i, p_l)$ is minimum.
- Step 2. Among the Voronoi vertices q_{ijk} 's on the boundary of $V(p_l)$, find the one that gives the smallest value of $H(p_i, p_j, p_k, p_l)$. Let T be the set consisting of this Voronoi vertex alone.
- Step 3. Repeat 3.1 until T cannot be augmented any more.
 - 3.1. For each Voronoi vertex q_{ijk} that is connected by a Voronoi edge to an element of T , add q_{ijk} to T both if $H(p_i, p_j, p_k, p_l) < 0$ and if the resultant T satisfies conditions (C4.6.7)–(C4.6.9).
- Step 4. For every edge connecting a vertex in T with a vertex not in T , create a new vertex on the edge and thus divide the edge into two edges.
- Step 5. Create new edges connecting the vertices created in Step 4 in such a way that the new edges form a circuit enclosing the vertices in T .
- Step 6. Remove the vertices in T and the edges incident to them (and consider the interior of the circuit as the Voronoi polygon of p_l), and let the resultant geometric graph be G_l .

This algorithm corresponds to Steps 4.1–4.4 in Algorithm 4.3.2. More specifically, Step 1 in this algorithm is equivalent to Step 4.1 in Algorithm 4.3.2, Steps 2, 3 and 4 correspond to Steps 4.2 and 4.3, and Steps 5 and 6 correspond to Step 4.4. Hence if there is no numerical error, and if G_{l-1} corresponds to the Voronoi diagram \mathcal{V}_{l-1} , the output G_l correctly corresponds to the Voronoi diagram \mathcal{V}_l . The main difference is that in this algorithm the initial vertex found in Step 2 is used as a 'seed' from which a tree is expanded, while in the boundary-growing procedure the boundary enclosing this tree is traced. This difference is essential, because even if computed values of $H(p_i, p_j, p_k, p_l)$ contain numerical errors, the subset T obtained in the algorithm satisfies (C4.6.6)–(C4.6.9). We need not worry about inconsistency; the algorithm always carries out its task and the output G_l is consistent in the sense that it belongs to A_l .

Note that degeneracy can be avoided automatically in the algorithm. We judge the Voronoi vertex q_{ijk} as being inside the Voronoi polygon of the new generator if and only if $H(p_i, p_j, p_k, p_l) < 0$. This is equivalent to the shrink strategy presented in the previous subsection.

The conditions (C4.6.8) and (C4.6.9) can be checked efficiently in the following manner. We assign three labels, 'in', 'out' and 'undecided', to the Voronoi vertices; 'in' is assigned to the Voronoi vertices that are added to T , 'out' to the Voronoi vertices that are judged not to be added to T , and 'undecided' to the Voronoi vertices that are not yet judged. Also, we assign two labels 'incident' and 'non-incident' to the Voronoi polygons; 'incident' to the Voronoi polygons whose boundary has a vertex in T , and 'non-incident'

to the other Voronoi polygons. In Step 3.1, q_{ijk} is chosen among the Voronoi vertices that are labelled ‘undecided’ and that are adjacent to a vertex in T . Then, $G_{l-1}(T \cup \{q_{ijk}\})$ is a tree if and only if

(C4.6.10) q_{ijk} is not adjacent to two or more ‘in’ Voronoi vertices.

For any cell c of G_{l-1} , the subgraph $G_{l-1}((T \cup \{q_{ijk}\}) \cap W_{l-1}(c))$ is connected if and only if

(C4.6.11) for any ‘incident’ Voronoi polygon having q_{ijk} on its boundary, q_{ijk} is adjacent to an ‘in’ Voronoi vertex on this boundary.

Hence conditions (C4.6.8) and (C4.6.9) can be examined locally by checking the labels of the Voronoi polygons incident to q_{ijk} and those of the Voronoi vertices adjacent to q_{ijk} .

For the initial geometric graph G_3 , we assign ‘out’ labels to the three degree-one vertices, and these labels are permanently fixed. This is because the Voronoi polygon of a new generator is always finite, so that these three vertices should not belong to T . At the start of Algorithm 4.6.1 all the other Voronoi vertices are labelled ‘undecided’, and all the Voronoi polygons are labelled ‘non-incident’. Each time a Voronoi vertex is added to T , its label is changed from ‘undecided’ to ‘in’ and the labels of the Voronoi polygons incident to the Voronoi vertex, if they are ‘non-incident’, are changed to ‘incident’. Similarly, each time a Voronoi vertex is judged not to be added to T , its label is changed from ‘undecided’ to ‘out’. In Algorithm 4.6.1 the Voronoi vertices and the Voronoi polygons whose labels are changed are listed, and at the end of the algorithm these labels are cleared (that is, ‘in’ and ‘out’ are changed to ‘undecided’, and ‘incident’ is changed to ‘non-incident’). In this way Algorithm 4.6.1 can be executed in time proportional to the size of the substructure that is deleted for the addition of the new generator.

Thus, we obtain the next principle for implementing the incremental method.

Implementation Principle 4.6.2 (Topology-oriented approach)

We concentrate our attention on the construction of the topological structure G_n of the Voronoi diagram (that is, we replace $\mathcal{V}, \mathcal{V}_3, \mathcal{V}_{l-1}, \mathcal{V}_l$ and \mathcal{V}_n in Algorithm 4.3.2 with G, G_3, G_{l-1}, G_l and G_n , respectively), and replace Steps 4.1–4.4 in Algorithm 4.3.2 with Algorithm 4.6.1.

Once G_n is obtained, it is easy to draw the Voronoi diagram itself, because a Voronoi vertex is the centre of the circle passing through the three surrounding generators, and a Voronoi edge is the perpendicular bisector of the two side generators.

An example of the behaviour of the computer program constructed on the basis of this principle is shown in Figure 4.6.5, where (a) is the output constructed in single-precision floating point arithmetic for 20 generators

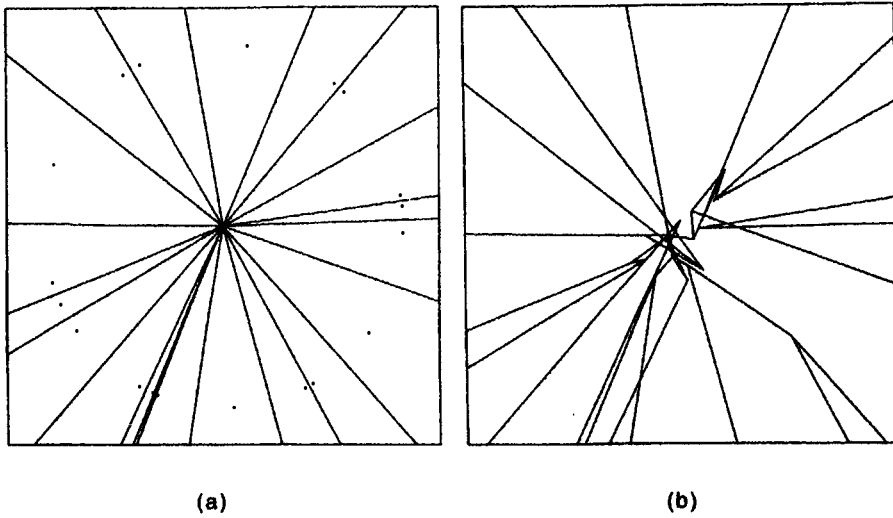


Figure 4.6.5 Behaviour of a computer program based on the topology-oriented approach: (a) output of the program for 20 generators; (b) central portion of (a) magnified by 10^5 .

placed at random on a common circle, and (b) represents the central portion of the same output magnified by 10^5 . The diagram in (a) seems a correct Voronoi diagram but, as (b) shows, the central portion of the output is far from the correct Voronoi diagram. This set of generators gives high degeneracy, and the criss-cross microstructure of this kind seems natural in single precision arithmetic. It should be noted that even for such a degenerate set of generators, the program carried out its task and gave an output, and that the output is topologically consistent in the sense that it belongs to A_n . A conventional computer program usually fails in processing such a degenerate set of generators.

We place higher priority on topological consistency than on numerical values, but this does not mean that numerical computation is less important. In our algorithm the most important numerical computation is that of $H(p_i, p_j, p_k, p_l)$ defined by (2.4.10). $H(p_i, p_j, p_k, p_l)$ can be rewritten in the following way:

$$H(p_i, p_j, p_k, p_l) = J_{ijk}^2(x_i - x_k) - J_{ijk}^3(y_i - y_k) + J_{ijk}^4((x_i - x_k)^2 + (y_i - y_k)^2), \quad (4.6.3)$$

where

$$J_{ijk}^2 = \begin{vmatrix} y_i - y_k & (x_i - x_k)^2 + (y_i - y_k)^2 \\ y_j - y_k & (x_j - x_k)^2 + (y_j - y_k)^2 \end{vmatrix}, \quad (4.6.4)$$

$$J_{ijk}^3 = \begin{vmatrix} x_i - x_k & (x_i - x_k)^2 + (y_i - y_k)^2 \\ x_j - x_k & (x_j - x_k)^2 + (y_j - y_k)^2 \end{vmatrix}, \quad (4.6.5)$$

$$J_{ijk}^4 = \begin{vmatrix} x_i - x_k & y_i - y_k \\ x_j - x_k & y_j - y_k \end{vmatrix}, \quad (4.6.6)$$

This expression shows that the value of $H(p_i, p_j, p_k, p_l)$ can be computed in terms of the coordinates of the generators with respect to the origin at p_k . The computation based on this expression is stable in a numerical sense, because the translation of the origin of the coordinate system to one of the relevant generators enables us to avoid dealing with unnecessarily large numbers. So this way of computation is recommended. Indeed, by this way of computation a Voronoi diagram for one million generators scattered at random in a unit square can be constructed in single precision arithmetic (Sugihara and Iri, 1989d, 1992).

The principle presented here was proposed by Sugihara and Iri (1988). A FORTRAN program called VORONOI2 was constructed on the basis of this principle, and is open for public use (Sugihara and Iri, 1989c; see Okabe, 1994, for a review).

There are still other algorithms that are robust in finite-precision arithmetic. They include a stable swapping algorithm (Fortune, 1992a, 1995), a topology-oriented divide-and-conquer algorithm (Oishi and Sugihara, 1995) and a topology-oriented lift-up algorithm using a three-dimensional convex hull (Minakawa and Sugihara, 1997).

4.7 ALGORITHMS FOR HIGHER-DIMENSIONAL VORONOI DIAGRAMS

A Voronoi diagram in a three- or higher-dimensional space is more complicated, at least in the sense that the size of the Voronoi diagram for n generators cannot be bounded by $O(n)$. It is known that the number of k -faces of the Voronoi diagram for n generators in an m -dimensional space is of $O(n^{\min\{m+1-k, [m/2]\}})$ for $0 \leq k \leq m$ (Klee, 1980).

In a three-dimensional space, for instance, the Voronoi diagram is a partition of the space into n convex polyhedra, but the total number of vertices of these polyhedra can be as many as $O(n^2)$. An example of such a situation is shown in Figure 4.7.1. Suppose that one half of n generators align on the x -axis and the other half align on the line passing through $(0,0,1)$ parallel to the y -axis. Recall that a Voronoi vertex, and hence its dual a Delaunay tetrahedron, is created by each set of those four generators whose circumscribing sphere is an empty sphere. Hence, each set of two consecutive generators on one line and two consecutive generators on the other line create a Delaunay tetrahedron as shown in the figure, giving $O(n^2)$ tetra-

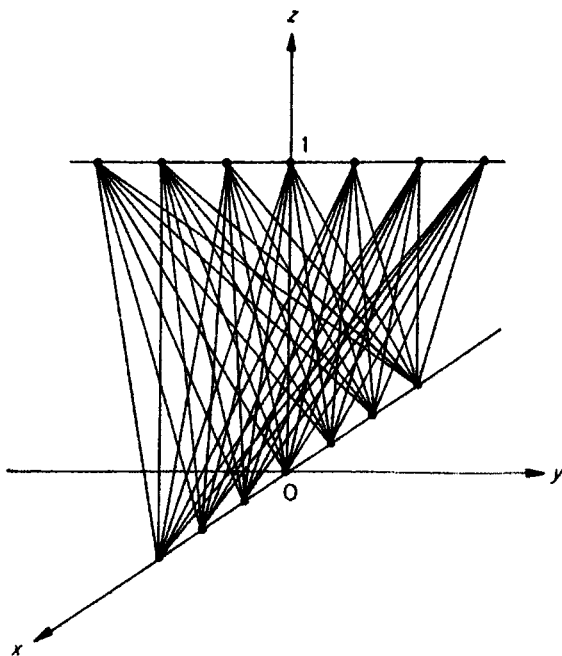


Figure 4.7.1 Three-dimensional Delaunay diagram with $O(n^2)$ tetrahedra.

hedra in total. Thus, $O(n^2)$ is a lower bound of the worst-case time complexity of an algorithm for constructing a Voronoi diagram in the three-dimensional space.

A simple and unifying approach to constructing an m -dimensional Voronoi diagram is to reduce the problem to a convex hull problem in an $(m+1)$ -dimensional space.

As we saw in Chapter 2, we can establish a correspondence between the Voronoi diagram in the plane and a convex polyhedron in the three-dimensional space through the lift-up transformation. A similar correspondence is established in any dimension, and this fact can be used to construct the Voronoi diagram in the following way.

Let $P = \{p_1, p_2, \dots, p_n\}$ be a set of n generators in an m -dimensional space, and $(x_{i1}, x_{i2}, \dots, x_{im})$ be the Cartesian coordinates of p_i . We consider the configuration of $t = m + 1$ generators. To avoid unnecessarily messy expressions, let us choose the first t generators p_1, p_2, \dots, p_t in P . These generators give a Voronoi vertex if and only if the hypersphere (a circle for $m = 2$, a sphere for $m = 3$, etc.) passing through them contains no other generators in its interior; actually the Voronoi vertex is the centre of this hypersphere.

The hypersphere S in an m -dimensional space that passes through p_1, p_2, \dots, p_t is represented by the equation

$$\begin{vmatrix} 1 & x_{11} & x_{12} & \cdots & x_{1m} & x_{11}^2 + x_{12}^2 + \cdots + x_{1m}^2 \\ 1 & x_{21} & x_{22} & \cdots & x_{2m} & x_{21}^2 + x_{22}^2 + \cdots + x_{2m}^2 \\ \vdots & \vdots & \vdots & \ddots & \vdots & \vdots \\ 1 & x_n & x_{n2} & \cdots & x_{nm} & x_{n1}^2 + x_{n2}^2 + \cdots + x_{nm}^2 \\ 1 & x_1 & x_2 & \cdots & x_m & x_1^2 + x_2^2 + \cdots + x_m^2 \end{vmatrix} = 0, \quad (4.7.1)$$

with the variable point $p = (x_1, x_2, \dots, x_m)$ (note that this equation is the extension of $H(p_i, p_j, p_k, p) = 0$, where $H(p_i, p_j, p_k, p)$ is defined in equation (2.4.10)). Hence the sign of the determinant in the left-hand side changes when the point p moves from inside S to outside.

Let p_i^* be the point in the t -dimensional space with coordinates

$$(x_{i1}, x_{i2}, \dots, x_{im}, x_{i1}^2 + x_{i2}^2 + \dots + x_{im}^2),$$

p^* be a variable point in the t -dimensional space with coordinates

$$(x_1, x_2, \dots, x_m, x_1^2 + x_2^2 + \dots + x_m^2),$$

and let $P^* = \{p_1^*, p_2^*, \dots, p_n^*\}$. As illustrated in Figure 4.7.2, which is the case where $m = 2$, p_i^* is obtained by lifting up p_i in the positive direction of the t th coordinate axis until we reach the surface of the paraboloid of revolution

$$x_t = x_1^2 + x_2^2 + \dots + x_m^2. \quad (4.7.2)$$

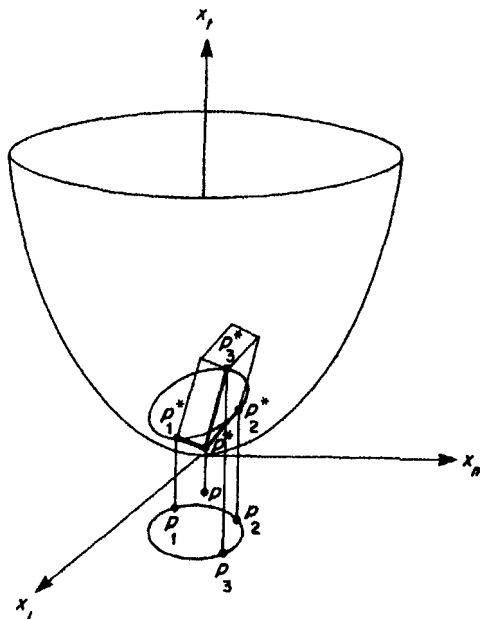


Figure 4.7.2 Lifting transformation that maps the plane to a hyperboloid of revolution.

Let S^* denote the hyperplane in the t -dimensional space that passes through $p_1^*, p_2^*, \dots, p_t^*$. Then, S coincides with the projection along the t th axis of the intersection of S^* with the surface defined by equation (4.7.2).

The determinant in the left-hand side of equation (4.7.1) can be considered as the signed volume of the t -dimensional parallelepiped defined by t edges $p^*p_1^*, p^*p_2^*, \dots, p^*p_t^*$. Since the t -dimensional region consisting of points above the surface defined by equation (4.7.2) is convex, we can see that the point p is in the interior of the sphere S in the m -dimensional space if and only if the point p^* is below the hyperplane S^* . This implies that the set of t generators p_1, p_2, \dots, p_t gives a Voronoi vertex (that is, p_1, \dots, p_t form the vertices of a Delaunay simplex) if and only if p_{t+1}^*, \dots, p_n^* are all above the hyperplane S^* . Thus, all the Voronoi vertices (equivalently, all the Delaunay simplices) can be obtained by constructing the convex hull $\text{CH}(P^*)$ of P^* in the t -dimensional space.

Suppose that $p_1^*, p_2^*, \dots, p_t^*$ form an m -dimensional face (m -face, for short) of the convex hull $\text{CH}(P^*)$ in the $(m+1)$ -dimensional space. There is a unique hyperplane passing through these points, and all the other points p_{t+1}^*, \dots, p_n^* are on the same side of the hyperplane. We call the m -face a *lower m-face* if the other points are above the hyperplane, and an *upper m-face* otherwise. As we have seen, p_1^*, \dots, p_t^* forming a lower m -face implies that the hypersphere passing through p_1, \dots, p_t contains no other generators in its interior. Thus, the lower m -faces of $\text{CH}(P^*)$ correspond to Voronoi vertices of $\mathcal{V}(P)$, or equivalently, the lower m -faces of $\text{CH}(P^*)$ correspond to Delaunay simplices.

If p_1^*, \dots, p_t^* form an upper m -face of $\text{CH}(P^*)$, the corresponding hypersphere in the m -dimensional space contains all the other generators p_{t+1}, \dots, p_n in its interior, which implies that p_1, \dots, p_t form a Voronoi vertex of the farthest-point Voronoi diagram for P .

Algorithm 4.7.1 (m -dimensional Voronoi diagram)

Input: Set $P = \{p_1, p_2, \dots, p_n\}$ of n generators in the m -dimensional space with the coordinates $(x_{i1}, x_{i2}, \dots, x_{im})$, $i = 1, 2, \dots, n$.

Output: Delaunay tessellation spanning P .

Procedure:

- Step 1. Create set $P^* = \{p_1^*, p_2^*, \dots, p_n^*\}$ of points in an $(m+1)$ -dimensional space, where the first m coordinates of p_i^* coincide with those of p_i and the $(m+1)$ st coordinate is $x_1^2 + x_2^2 + \dots + x_m^2$.
- Step 2. Construct the convex hull $\text{CH}(P^*)$ of P^* in the $(m+1)$ -dimensional space.
- Step 3. Project all the lower m -faces of $\text{CH}(P^*)$ in the direction parallel to the $(m+1)$ st coordinate axis onto the original m -dimensional space, and return the resulting diagram.

From the time-complexity point of view, the critical step is Step 2. There are many algorithms for constructing convex hulls in higher dimensions. One popular method is gift wrapping (Chand and Kapur, 1970; Preparata and

Shamos, 1985; Swart, 1985; Sugihara, 1994), where one supporting hyperplane is found initially and the neighbouring m -faces are found one by one just as we wrap the points using an elastic sheet. This method requires time proportional to $O(n^{[t/2]+1})$ for n points in the t -dimensional space, where $[x]$ represents the largest integer not greater than x .

Another popular method is an incremental method (which is sometimes called a beneath–beyond method) (Preparata and Shamos, 1985; Seidel, 1986; Edelsbrunner, 1987), where a convex hull of a small number of points is constructed initially and then the other points are added one by one. When a new point is added, the m -faces of the previous convex hull are divided into those visible from the new point and the others, and the former m -faces are replaced with new m -faces containing the new point as a vertex. This method requires $O(n^{[(t+1)/2]} + n \log n)$ time.

Other higher-dimensional convex hull algorithms include a shelling method, which runs in $O(n^{[t/2]} \log n)$ time (Seidel, 1987), and a divide-and-conquer method, which runs in $O(n \log n + n^{[t/2]})$ time (Buckley, 1988).

Therefore, the incremental method is optimal in the even-dimensional space, while the divide-and-conquer method is optimal in the odd-dimensional space. Hence, for example, the three-dimensional Voronoi diagram can be constructed in $O(n^2)$ time by Algorithm 4.7.1 using the incremental method for the four-dimensional convex hull.

The farthest-point Voronoi diagram (actually the dual diagram of the farthest-point Voronoi diagram) can be obtained if we project all the upper m -faces, instead of the lower m -faces, in Step 3 of Algorithm 4.7.1.

The reduction of the Voronoi diagram construction in the m -dimensional space to a convex hull construction in the $(m+1)$ -dimensional space was pointed out by Brown (1979, 1980), where another transformation called inversion (which maps the m -dimensional plane to a hypersphere in the $(m+1)$ -dimensional space) was used (see Figure 2.4.8 and equation (2.4.10)). That transformation was used by Aurenhanuner and Edelsbrunner (1984), Edelsbrunner (1987), Buckley (1988) and Mulmuley (1991). The transformation presented in this section (i.e. lift-up to the paraboloid of revolution) was used by Edelsbrunner and Seidel (1986), Edelsbrunner (1987) and Chan *et al.* (1997). This transformation can be considered as an extremal case of the inversion in which the centre of inversion is taken as a point at infinity.

It should be noted that the lift-up transformation can be used also for two-dimensional points (O'Rourke *et al.*, 1986). In this case the problem is converted to the construction of a three-dimensional convex hull, and hence this method runs in $O(n \log n)$ time if the divide-and-conquer method is applied (Preparata and Hong, 1977); this time complexity is optimal in the worst-case sense. The lift-up transformation gives also a linear-time algorithm for the Voronoi diagram for points forming a convex polygon (Agarwal *et al.*, 1989a).

Other algorithms for constructing higher-dimensional Voronoi diagrams include the naive method (Brostow *et al.*, 1978; Finney, 1979), a walking method (Avis and Bhattacharya, 1983), incremental methods (Bowyer, 1981;

Watson, 1981; Devijver and Dekesel, 1983; Tanemura *et al.*, 1983; Inagaki *et al.*, 1992; Borouchaki and Lo, 1995), a flipping method (Joe, 1991a), a randomized method (Dwyer, 1991; Facello, 1995), the bucketing method (Fang and Piegl, 1995), and others (Dwyer, 1991; Medvedev, 1986).

4.8 ALGORITHMS FOR GENERALIZED VORONOI DIAGRAMS

Let us return to two-dimensional Voronoi diagrams. As we saw in Chapter 3, there is a wide variety of generalizations of the concept of the Voronoi diagram. However, we do not have space to treat them individually. Hence we try to present a general framework for constructing Voronoi diagrams of various types.

To represent a generalized Voronoi diagram in a unified manner, we introduce the following notations. Let $\Gamma = \{A_1, A_2, \dots, A_n\}$ be the set of generators, and for any point z in the plane let $d(z, A_i)$ denote a ‘distance metric’ representing how far the point z is from the generator A_i (here we call d the ‘distance’ even if d does not satisfy the distance axiom). As in Chapter 3, we define the bisector of A_i and A_j by

$$b(A_i, A_j) = \{z \mid d(z, A_i) = d(z, A_j)\}, \quad (4.8.1)$$

and the dominance region of A_i over A_j by

$$(A_i, A_j) = \{z \mid d(z, A_i) \leq d(z, A_j)\}. \quad (4.8.2)$$

For any generator A_i , we define the Voronoi region for A_i with respect to the distance d by

$$V(A_i) = \bigcap_{i \neq j} \text{Dom}(A_i, A_j). \quad (4.8.3)$$

The collection of $V(A_1), V(A_2), \dots, V(A_n)$ is called the *Voronoi diagram for Γ with respect to d* .

For an ordinary Voronoi diagram, generators are distinct points, and d is the Euclidean distance. For a weighted Voronoi diagram, generators are distinct points, and d is an additively weighted, a multiplicatively weighted or a compoundly weighted distance. For a farthest-point Voronoi diagram, generators are distinct points, and $d(z, A_i)$ is a monotone decreasing function of the Euclidean distance between z and A_i ; for example, the inverse of the Euclidean distance between z and A_i can be used as $d(z, A_i)$. For a Voronoi diagram with obstacles, generators are distinct points, and $d(z, A_i)$ is the minimum length of the obstacle-avoiding path from A_i to z . For a Voronoi diagram of line segments or areas, generators are line segments or areas, respectively, and $d(z, A_i)$ is the minimum of the Euclidean distance from z to a point in A_i . For a Voronoi diagram with a non-Euclidean distance, generators are distinct points, and d is the associated non-Euclidean distance.

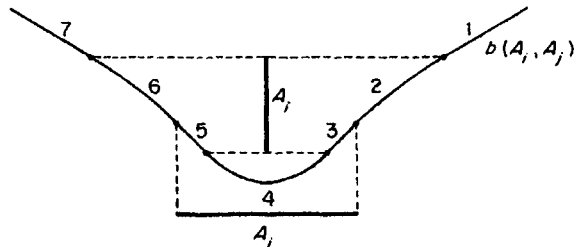


Figure 4.8.1 Bisector of two line segments.

We restrict our consideration to the case where every bisector $b(A_i, A_j)$ is a single curve without self-intersection, closed or extended infinitely in both directions, dividing the plane into two connected regions $\text{Dom}(A_i, A_j)$ and $\text{Dom}(A_j, A_i)$. This case includes almost all the generalized Voronoi diagrams listed in Chapter 3. An example of an exception is a bisector $b(A_i, A_j)$ with respect to an L_∞ -distance of two generators aligning horizontally or vertically, where $b(A_i, A_j)$ includes a two-dimensional region. A similar exception arises for the L_1 -distance Voronoi diagram and the convex-distance Voronoi diagram.

For an ordinary Voronoi diagram, $b(A_i, A_j)$ is the straight line forming the perpendicular bisector of $\overline{A_i A_j}$. For a Voronoi diagram with a power distance (i.e. a power diagram) and for a farthest-point Voronoi diagram, the bisector $b(A_i, A_j)$, if it exists, is a straight line. In general, however, $b(A_i, A_j)$ is a complicated curve. For instance, the bisector of $b(A_i, A_j)$ of two line segments A_i and A_j with respect to the Euclidean distance can be a concatenation of up to seven segments of parabolas and straight lines, as shown in Figure 4.8.1, where segments 1 and 7 are perpendicular bisectors of two terminal points, segments 2, 4 and 6 are parabolas with one generator being the directorix and a terminal point of the other generator being the focus, and segments 3 and 5 are bisectors of the angles formed by the two generators. The bisector $b(A_i, A_j)$ with respect to a multiplicatively weighted distance is a circle containing the generator with the smaller weight. The bisector $b(A_i, A_j)$ with respect to an additively weighted distance is a hyperbola with A_i and A_j being the foci. Thus, the bisector changes its type of line according to the generators and the distance. In what follows we assume that we can construct $b(A_i, A_j)$ for any pair of generators in constant time, and that we can find the points of intersection of two bisectors also in constant time.

The concepts of the bisector and the dominance region for a pair of generators can be extended to those for a pair of disjoint subsets of generators. Let Γ' and Γ'' be mutually disjoint subsets of Γ . We define

$$b(\Gamma', \Gamma'') = \{z \mid \min_{A_i \in \Gamma'} d(z, A_i) = \min_{A_j \in \Gamma''} d(z, A_j)\} \quad (4.8.4)$$

and call it the *bisector* of Γ' and Γ'' . Similarly, we define

$$\text{Dom}(\Gamma', \Gamma'') = \{z \mid \min_{A_i \in \Gamma'} d(z, A_i) \leq \min_{A_j \in \Gamma''} d(z, A_j)\} \quad (4.8.5)$$

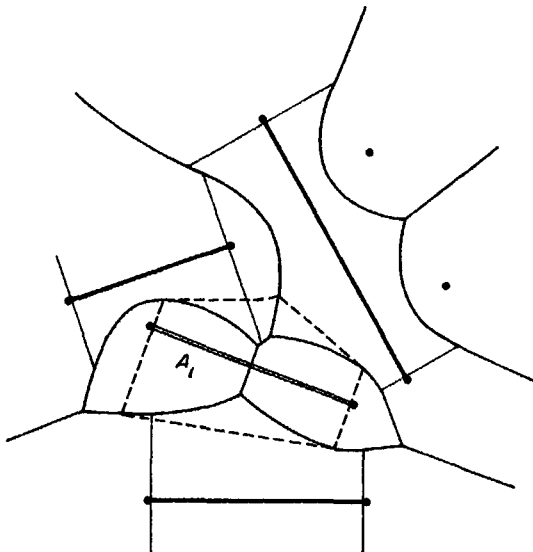


Figure 4.8.2 Incremental method for a Voronoi diagram for line segments.

and call it the *dominance region* of Γ' over Γ'' . $b(\{A_i\}, \Gamma')$ and $\text{Dom}(\{A_i\}, \Gamma'')$ are abbreviated to $b(A_i, \Gamma')$ and $\text{Dom}(A_i, \Gamma'')$, respectively.

In the incremental method, the Voronoi diagram $\mathcal{V}(\{A_1, \dots, A_l\})$ is constructed from the Voronoi diagram $\mathcal{V}(\{A_1, \dots, A_{l-1}\})$ for each l , where the main task is to find the bisector $b(A_l, \{A_1, \dots, A_{l-1}\})$. Let us assume that the Voronoi region $V(A_l)$ is simply connected. Then, for any $\Gamma' \subset \Gamma \setminus \{A_l\}$, $b(A_l, \Gamma')$ consists of a single connected curve, a closed curve or a curve extended infinitely in both directions. This is the case for an additively weighted Voronoi diagram, a power diagram, a farthest-point Voronoi diagram, a Voronoi diagram of lines or areas, and a Voronoi diagram with an L_p -metric for $1 < p < \infty$. For those types of Voronoi diagrams the following incremental method can be used.

Algorithm 4.8.1 (Incremental method for a generalized Voronoi diagram)

Input: Set $\Gamma = \{A_1, A_2, \dots, A_n\}$ of n generators and distance d .

Output: Voronoi diagram $\mathcal{V}(\Gamma) = \{V(A_1), V(A_2), \dots, V(A_n)\}$ for Γ with respect to the distance d .

Procedure:

Comment. Let $\Gamma_l = \{A_1, A_2, \dots, A_l\}$ for $1 \leq l \leq n$.

Step 1. Construct $\mathcal{V}(\Gamma_2)$.

Step 2. For $l = 3, 4, \dots, n$, do 2.1, 2.2 and 2.3.

2.1. Find a point on $b(A_l, \Gamma_{l-1})$.

2.2. Starting with the point found in 2.2, trace the whole bisector $b(A_l, \Gamma_{l-1})$.

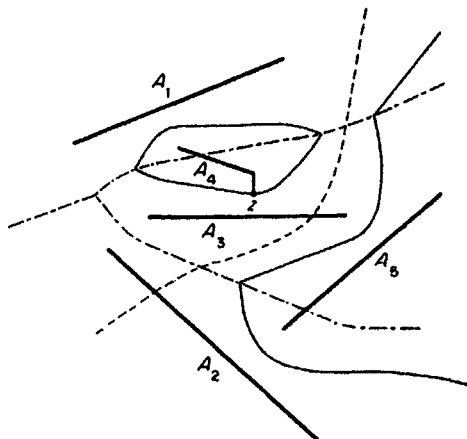


Figure 4.8.3 Merger of two Voronoi diagrams $\mathcal{V}(\{A_1, A_2, A_3\})$ and $\mathcal{V}(\{A_4, A_5\})$.

2.3. Construct $\mathcal{V}(\Gamma_i)$ by inserting $b(A_i, \Gamma_{i-1})$ to $\mathcal{V}(\Gamma_{i-1})$ and then deleting the substructure inside $\text{Dom}(A_i, \Gamma_{i-1})$.

Step 3. Return $\mathcal{V}(\Gamma) = \mathcal{V}(\Gamma_n)$.

An example of the addition of a generator is shown in Figure 4.8.2 for the case of a line Voronoi diagram. In this example each generator is partitioned into two terminal points and an open line segment, and they are treated as distinct generators. The Voronoi diagram for all the terminal points is generated first, and then open line segments are added one after another. The double line segment represents the new generator g_i and the broken lines represent $b(A_i, \Gamma_{i-1})$.

If the Voronoi region $V(A_i)$ contains the associated generator A_i , just as in the cases for a Voronoi diagram with a non-Euclidean metric and a Voronoi diagram for line segments or areas, the starter point in Step 2.2 can be found easily. All we have to do is first find the Voronoi region $V(A_i)$ containing at least one point in the new generator A_i and then find the point of the intersection of $b(A_i, A_i)$ with the boundary of $V(A_i)$. If $V(A_i)$ does not necessarily contain A_i , as is the case for a power diagram and a farthest-point Voronoi diagram, some non-trivial method should be constructed to find the starter point.

A randomized version of the incremental algorithm was studied by Mehlhorn *et al.* (1991) and Klein *et al.* (1990, 1993).

Next, let us consider the divide-and-conquer method. In this method two Voronoi diagrams $\mathcal{V}(\Gamma')$ and $\mathcal{V}(\Gamma'')$ are merged to $\mathcal{V}(\Gamma' \cup \Gamma'')$, where the main task is to find the bisector $b(\Gamma', \Gamma'')$.

For an ordinary Voronoi diagram the bisector $b(\Gamma', \Gamma'')$ is always a single connected curve (consisting of line segments). For a generalized Voronoi diagram, on the other hand, $b(\Gamma', \Gamma'')$ is not necessarily connected, but is a collection of a finite number of connected curves, some closed and the others are extended infinitely in both directions.

In Figure 4.8.3 an example of the situation where $b(\Gamma', \Gamma'')$ is disconnected is shown for the case of the Voronoi diagram for line segments, where $\Gamma' = \{A_1, A_2, A_3\}$ and $\Gamma'' = \{A_4, A_5\}$. Dot-and-dash lines represent $\mathcal{V}(\Gamma')$, broken lines represent $\mathcal{V}(\Gamma'')$ and solid lines represent $b(\Gamma', \Gamma'')$. Note that the partition of Γ into Γ' and Γ'' is not very sophisticated; we obtain this partition if we choose the leftmost points of the line segments as the representatives and divide them into a left set Γ' and a right set Γ'' .

To enumerate all the connected curves, we need a set of 'starters' from which we start tracing the curves. The set S of points is called a *starter set* of $b(\Gamma', \Gamma'')$ if any connected component of $b(\Gamma', \Gamma'')$ has at least one point in S . To trace the curves, S need contain only one point for each connected component. However, it is not always easy to tell the number of components of $b(\Gamma', \Gamma'')$ before we construct $b(\Gamma', \Gamma'')$. Hence, we put in S candidates of starter points that are enough to trace all components. Thus, a divide-and-conquer algorithm can be described in the following way.

Algorithm 4.8.2 (Divide-and-conquer method for a generalized Voronoi diagram)

Input: Set $\Gamma = \{A_1, A_2, \dots, A_n\}$ of n generators and distance d .

Output: Voronoi diagram $\mathcal{V}(\Gamma) = \{V(A_1), V(A_2), \dots, V(A_n)\}$ for Γ with respect to the distance d .

Procedure:

- Step 1. If $n \leq 2$, construct $\mathcal{V}(\Gamma)$ directly and return it. Otherwise, do Steps 2, 3, ..., 8.
- Step 2. Divide Γ into two disjoint subsets Γ' and Γ'' of almost the same size.
- Step 3. Construct $\mathcal{V}(\Gamma')$ by Algorithm 4.8.2.
- Step 4. Construct $\mathcal{V}(\Gamma'')$ by Algorithm 4.8.2.
- Step 5. Find a starter set S of $b(\Gamma', \Gamma'')$, and put $B \leftarrow \emptyset$.
- Step 6. While S is not empty, choose and delete an element s from S and if s is not on any curve in B , trace the connected component of $b(\Gamma', \Gamma'')$ containing s and put it in B .
- Step 7. Merge $\mathcal{V}(\Gamma')$ and $\mathcal{V}(\Gamma'')$ into $\mathcal{V}(\Gamma)$ by inserting all the curves in B and deleting the substructure inside $\text{Dom}(\Gamma', \Gamma'')$ from $\mathcal{V}(\Gamma'')$ and the substructure inside $\text{Dom}(\Gamma'', \Gamma')$ from $\mathcal{V}(\Gamma')$.
- Step 8. Return $\mathcal{V}(\Gamma)$.

The most difficult step in this algorithm is Step 5. We prefer a smaller starter set, but in general it is not easy to tell the number of components in $b(\Gamma, \Gamma'')$ unless we construct $b(\Gamma', \Gamma'')$ itself. For any $A_i \in \Gamma'$ and $A_j \in \Gamma''$, if point z with $d(z, A_i) = d(z, A_j)$ lies both in $V(A_i)$ of $\mathcal{V}(\Gamma')$ and in $V(A_j)$ of $\mathcal{V}(\Gamma'')$, then z is on $b(\Gamma', \Gamma'')$, and hence can be a starter point (Lee and Drysdale, 1981). For instance, the point z in Figure 4.8.3 satisfies the above condition; this point is the midpoint of the perpendicular line segment dropped from the rightmost point of A_4 to A_3 .

If the generators are points, we can partition Γ into a left generator set Γ' and a right generator set Γ'' , and in this case we can sometimes find the starter set easily. For a Voronoi diagram with the Laguerre metric, $b(\Gamma', \Gamma'')$ consists of a single curve extended infinitely, and the starter point can be found from the common support of Γ' and Γ'' just as in the case of an ordinary Voronoi diagram (Imai *et al.*, 1985). For a Voronoi diagram with an L_p -metric for $1 < p < \infty$, $b(\Gamma', \Gamma'')$ is not necessarily connected, but every connected component in $b(\Gamma', \Gamma'')$ extends infinitely and the starter set can be found in a similar way from the convex hulls of Γ' and Γ'' (Chew and Drysdale, 1985). Unifying studies of divide-and-conquer methods can be found in Chew and Drysdale (1985), Klein (1988, 1989), Klein and Wood (1988), and Klein *et al.* (1990).

There are a variety of other algorithms for individual types of generalized Voronoi diagrams. We briefly summarize them.

For the power diagram, Imai *et al.* (1985) proposed an incremental algorithm, which runs in $O(n^2)$ time in the worst case. On the other hand, Aurenhammer (1987a) pointed out that the power diagram in the plane can be obtained as the orthographic projection of the intersection of three-dimensional half spaces, and constructed a divide-and-conquer algorithm which runs in $O(n \log n)$ time. Gavrilova and Ronke (1996) also studied the construction of the power diagram. For the sectional Voronoi diagram, see Ash and Bolker (1986), Aurenhammer (1988b), Imai *et al.* (1985) and Sibson (1980a) (also see Section 3.1.5).

The construction of the multiplicatively weighted Voronoi diagram is studied by Aurenhammer and Edelsbrunner (1984), Ash and Bolker (1986), and Aurenhammer (1988b), and the additively weighted Voronoi diagram is studied by Ash and Bolker (1986), Fortune (1986, 1987) and Hanjoul *et al.* (1989).

Typical algorithms for the order- k Voronoi diagram and the ordered order- k Voronoi diagram in the plane are based on the arrangement of planes in the three-dimensional space. With each generator $p_i = (x_i, y_i)$, we associate the plane $z = 2x_i x + 2y_i y - (x_i^2 + y_i^2)$. Let A be the arrangement composed of such planes associated with all the generators. Property V17 can be restated that the ordinary Voronoi diagram is obtained as the orthographic projection of the uppermost layer of the arrangement A (note that the surface structure of the intersection of the upper half spaces bounded by these planes is nothing but the uppermost layer of A). The projection of the second layer of A corresponds to the order-2 Voronoi diagram, and the projection of the first and second layers together corresponds to the ordered order-2 Voronoi diagram. Similarly, the k th layer corresponds to the order- k Voronoi diagram, and the collection of the upper k layers corresponds to the ordered order- k Voronoi diagram (Aurenhammer, 1988b; Chazelle *et al.*, 1986; Mulmuley, 1991). In particular, the n th layer (the lowest layer) corresponds to the farthest-point Voronoi diagram (Brown, 1979; Buckley, 1988). Hence, the (ordered) order- k Voronoi diagram can be constructed through the arrangement A (Seidel, 1982; Chazelle and Edelsbrunner, 1985, 1987; Edelsbrunner

and Seidel, 1986; Aurenhammer, 1988b, 1990b; Boissonnat *et al.*, 1990, 1993). Aurenhammer and Schwarzkopf (1991) proposed a randomized incremental algorithm. A similar strategy using a slightly modified arrangement can be used for the order- k power diagram (Aurenhammer, 1987) and for the multiplicatively weighted Voronoi diagram (Aurenhammer and Edelsbrunner, 1984). Lee (1982b) studied a divide-and-conquer strategy. For the farthest-point Voronoi diagram, an incremental algorithm was also studied (Suzuki, 1989).

For the shortest-path Voronoi diagram, see El Gindy and Avis (1981), Lee (1983), Lee and Chen (1985), Imai *et al.* (1985), Chazelle and Guibas (1985), Asano and Asano (1987) and Seoung and Asano (1987). Algorithms for the Voronoi diagram for a simple polygon were proposed by Asano and Asano (1987) and Aronov (1987, 1989). An algorithm for the visibility Voronoi diagram was presented by Aurenhammer (1988b).

The Voronoi diagram for line segments can be constructed by the plane sweep method (Fortune, 1986, 1987), by the incremental methods (Kokubo, 1985; Imai *et al.*, 1985; Imai and Sugihara, 1994), by the divide-and-conquer method (Lee and Drysdale, 1981; Yap, 1987), and by other methods (Lee and Lin, 1986; Burnikel *et al.*, 1994; Gold *et al.*, 1995).

For the Voronoi diagram for polygons, see Preparata (1977), Lee (1982a), Aronov (1989), McAllister *et al.* (1996), Srinivasan and Nackman (1987) and Meshkat and Sakkas (1987), and for the Voronoi diagram for areas, see O'Dúnlaing *et al.* (1986), Leven and Sharir (1987) and Canny and Donald (1988). Chou (1995) studied an algorithm for the Voronoi diagram inside an arbitrary closed curve.

Variations in the distance are also studied from an algorithmic point of view. The Voronoi diagram for the Manhattan distance was studied by Carter *et al.* (1972), Hwang (1979), Lee (1980), Lee and Wong (1980), Chang *et al.* (1990a), Shute *et al.* (1991) and Sakakibara *et al.* (1996); for the Karlsruhe distance by Koshizuka and Kurita (1986) and Klein (1988); for the Hausdorff distance by Aurenhammer (1988b); for the elliptic distance by Nielson (1993); and for the general convex distance by Drysdale (1990) and Kao and Mount (1991). The shortest path on the surface of the three-dimensional object defines another type of distance. Distances of this type include the Voronoi diagram on a sphere (Miles, 1971; Brown, 1980; Paschinger, 1982; Ash and Bolker, 1985; Augenbaum and Peskin, 1985), on a cone (Dehne and Klein, 1987; Klein, 1988; Klein and Wood, 1988), and on a polyhedral surface (Aronov and O'Rourke, 1992).

The constrained Voronoi and Delaunay diagrams are another important direction of the generalizations. They are studied mainly from the mesh-generation point of view by Chew (1987, 1989b), Cline and Renka (1990), Du (1996), Fang and Piegl (1994), Borgers (1990), Lo (1989), Sloan (1993) and Zhou *et al.* (1990). Wang and Schubert (1987) constructed an optimal $O(n \log n)$ algorithm in which the Voronoi diagram for the end points was constructed first and then revised. Wang and Tsin (1990) showed that the complexity of the multiplicatively weighted Voronoi diagram is of $O(n^4)$. For

the purpose of finite element meshes, approximations of the constrained Delaunay diagrams are studied; see Section 6.5 for details.

Another important class of generalization is the dynamic Voronoi diagrams. There are two meanings to 'dynamic'. The first is that the generators move from time to time (Tokuyama, 1988; Roos, 1993), and the other is that the generators appear or disappear occasionally (Devillers *et al.*, 1992). Other generalizations include the oriented Voronoi diagram (Chang *et al.*, 1990a) and the Voronoi diagram in a river (Sugihara, 1992a).

4.9 APPROXIMATION ALGORITHMS

Sometimes we want to construct Voronoi diagrams for only a few different sets of generators. In such a situation we cannot ignore the time required in developing a computer program; the time for writing a program is often more serious than the running time itself. This problem might be solved by approximation schemes.

If generators are mutually disjoint sets of points (such as curves and areas) and if we want to construct a Voronoi diagram for them with respect to distance d , the problem can be reduced to the construction of a Voronoi diagram for points with respect to d in the following way. Given a set of generators, we first replace each generator with a finite number of points that approximate the original generator, then construct the Voronoi diagram for these points, and finally remove superfluous Voronoi edges and superfluous Voronoi vertices. Thus, we get the next algorithm.

Algorithm 4.9.1 (Approximation by points)

Input: Set $\Gamma = \{A_1, A_2, \dots, A_n\}$ of n disjoint figures in the plane.

Output: Approximation of the Voronoi diagram for Γ .

Procedure:

- Step 1. For each $i = 1, 2, \dots, n$, create a finite set P_i of points that approximates the boundary of A_i .
- Step 2. Construct the Voronoi diagram \mathcal{V} for the point set $P_1 \cup P_2 \cup \dots \cup P_n$.
- Step 3. Delete from \mathcal{V} those Voronoi edges whose generator points belong to the same original figure. Delete isolated Voronoi vertices, if any, from \mathcal{V} .
- Step 4. Return \mathcal{V} .

Figure 4.9.1 shows an example of this scheme applied to a set of generators containing different types of figures such as line segments, circular arcs and polygons; (a) represents the Voronoi diagram for 882 points located on the boundaries of the original figures, and (b) shows the approximation of the Voronoi diagram for the original figures obtained from (a).

To obtain a good approximation, we have to use many points to approximate the original generators. Hence, in general, the number of generators (= points)

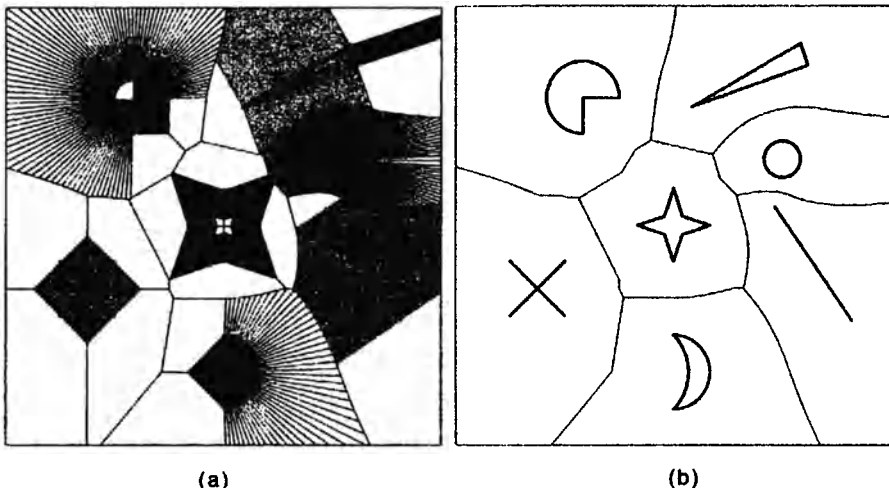


Figure 4.9.1 Approximation of generators by sets of points: (a) Voronoi diagram for 882 points that approximate seven generator figures; (b) approximation of the generalized Voronoi diagram obtained by deleting superfluous edges and superfluous vertices from (a).

becomes very large. Moreover, these points often give highly degenerate configurations. Therefore the approximation scheme is valid only when we can use a fast and robust algorithm, such as the one developed in Section 4.6. This approximation scheme can be extended to an m -dimensional generalized Voronoi diagrams directly, if an algorithm for Voronoi diagrams for points in the m -dimensional space is available.

Another, more brute-force approximation scheme is the use of digital image techniques. A digital image is a two-dimensional array, say $I(i, j)$, $1 \leq i, j \leq N$, where the entry $I(i, j)$ represents some property of the image at the point with coordinate (i, j) . Each point (i, j) is called a *pixel*, and $I(i, j)$ is called a *pixel value*. A pixel with a positive pixel value is called a *positive pixel*. The four-neighbour set of pixel (i, j) is defined by

$$\text{NB}_4(i, j) = \{(i, j-1), (i, j+1), (i-1, j), (i+1, j)\},$$

and the eight-neighbour set of pixel (i, j) is defined by

$$\text{NB}_8(i, j) = \text{NB}_4(i, j) \cup \{(i-1, j-1), (i-1, j+1), (i+1, j-1), (i+1, j+1)\},$$

where pixels outside the array are ignored. The four-neighbour set or the eight-neighbour set of (i, j) is simply called a neighbour set of (i, j) and is denoted by $\text{NB}(i, j)$.

In the next scheme, an approximation of a Voronoi diagram is constructed in the form of a digital image. First, each generator is replaced with a set of pixels, and then from these pixels the 'territories' of the generators are expanded simultaneously at the same speed until the territories collide with

one another. This can be done by repeating local parallel operations over the neighbours of pixels in the following way (an example of the behaviour of the algorithm immediately follows the algorithm).

Algorithm 4.9.2 (Approximation by a digital image)

Input: Integer N and set $\Gamma = \{A_1, A_2, \dots, A_n\}$ of n disjoint figures in the plane.

Output: Digital image $I(i, j)$ ($1 < i, j < N$) approximating the Voronoi diagram for Γ , where $I(i, j) = k > 0$ if pixel (i, j) belongs to the Voronoi region of A_k , and $I(i, j) = -1$ if pixel (i, j) is incident to two or more different Voronoi regions.

Procedure:

Step 1. For all $i < i, j < N$,

$I(i, j) \leftarrow k$ if there exists k such that $(i, j) \in A_k$,

$I(i, j) \leftarrow 0$ otherwise.

Step 2. Repeat 2.1 until pixel values are not changed any more.

2.1. For all (i, j) such that $I(i, j) = 0$, do the following simultaneously.

$I(i, j) \leftarrow k$ if all the positive pixels in $\text{NB}(i, j)$ have the same value k ,

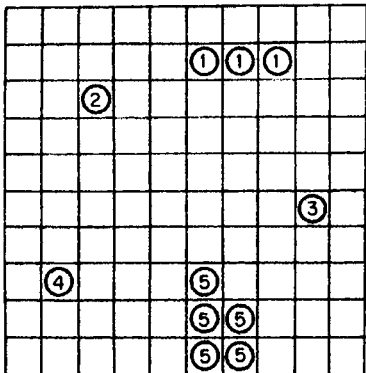
$I(i, j) \leftarrow -1$ if the positive pixels in $\text{NB}(i, j)$ admit two or more different values.

Step 3. Return the array $I(i, j)$.

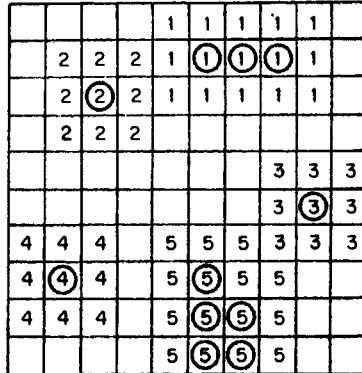
An example of the behaviour of the algorithm is shown in Figure 4.9.2. Panel (a) shows the initial value of the array, where the value i in a circle represents the ordinal number of the generator A_i to which the pixel belongs, and blank pixels represent those with value 0. The generators A_2 , A_3 and A_4 are represented by one pixel, whereas the generators A_1 and A_5 occupy more than one pixel. The array after the first, the second and the third execution of Step 2.1 are shown in (b), (c) and (d), respectively, where the eight-neighbour set $\text{NB}_8(i, j)$ is used as the neighbour set in the algorithm. After the third execution of Step 2.1 all the pixels have non-zero values, and hence the algorithm terminates. In (d), the boundaries of the Voronoi regions are represented by bold lines.

In Step 2.1 the pixel values are changed simultaneously; this is a kind of parallel procedure. To implement this procedure in the usual sequential computer, we use one more array, say $J(i, j)$, of the same size; we write the resulting pixel values in $J(i, j)$ in the first execution of Step 2.1, and switch the roles of these two arrays $I(i, j)$ and $J(i, j)$ every time we execute Step 2.1.

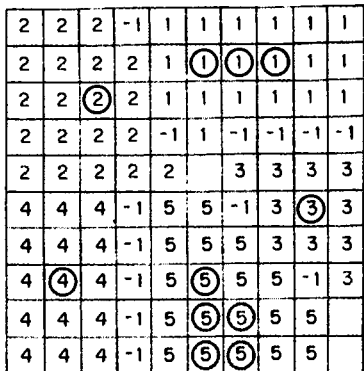
This approximation scheme is conceptually simple and does not require any exact algorithm for Voronoi diagrams for points, but is very time and space consuming. Moreover, the output of this algorithm is not a winged-edge data structure; the output merely gives us approximations of Voronoi regions and we need further processing to extract the incidence relations



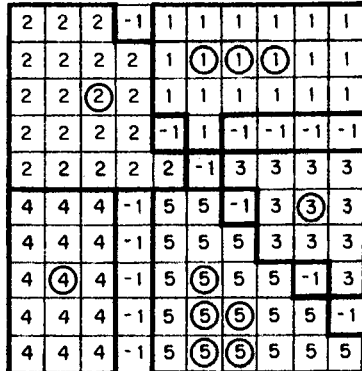
(a)



(b)



(c)



(d)

Figure 4.9.2 Approximation of the Voronoi diagram by a digital image: (a) digital image of five generators; (b) first execution of Step 2.1; (c) second execution of Step 2.1; (d) final result.

among the regions, the edges and the points. Furthermore, the distance is not Euclidean. If the four-neighbour set is used in Step 2.1, the 'territories' expand according to the L_1 -metric, while if the eight-neighbour set is used, they expand according to the L_∞ -metric. If these two kinds of the neighbour sets are used alternately in the repetition of Step 2.1, the output gives a slightly better approximation of a Euclidean-metric Voronoi diagram. Therefore this approximation scheme should be used only for special purposes such as for Voronoi diagrams with the L_1 - or L_∞ -metric or for very rough approximations of Voronoi diagrams.

On the other hand, if the original generators themselves are given in the form of a digital image, as is the case in digital pattern analysis, Algorithm 4.9.2 can be applied directly to various kinds of proximity analysis (Toriwaki *et al.*, 1982; Mark, 1987; Yoshitake *et al.*, 1987; Toriwaki and Yokoi, 1988).

CHAPTER 5

Poisson Voronoi Diagrams

In Section 2.1 we introduced the idea of a generator set $P = \{p_1, \dots, p_n\}$ as a set of n distinct points (i.e. no two or more points were spatially coincident) which generates the ordinary Voronoi diagram \mathcal{V} . For a finite Voronoi diagram the only condition imposed on P was that n was finite and greater than one. Other than this, no other aspects of the locations of the points in m -dimensional Euclidean space, \mathbb{R}^m , were specified. In this chapter we consider \mathcal{V} , its dual Delaunay tessellation \mathcal{D} , and some generalizations of \mathcal{V} when P contains countably infinitely many distinct points which generate the *infinite* Voronoi diagram. To avoid pathological cases, we assume that P is locally finite (i.e. there are only finitely many points inside a bounded region) and its points are *in the general quadratic position*, i.e. the points satisfy:

The Non-collinearity Assumption No $k+1$ points lie on a $(k-1)$ -dimensional hyperplane of \mathbb{R}^m , $k = 2, \dots, m$, and

The Non-cosphericity Assumption No $m+2$ points lie on the boundary of a sphere in \mathbb{R}^m .

(See Assumption D1 in Section 2.2 and Assumption V2 in Section 2.3). In particular, we concentrate on the case when the members of P are located in \mathbb{R}^m according to the homogeneous Poisson point process Θ_P discussed in Section 1.3.3, and refer to the resulting tessellation as the *Poisson Voronoi diagram* \mathcal{V}_P , and the *Poisson Delaunay tessellation* \mathcal{D}_P . We use the terms *Poisson Voronoi cell* (PVC) and *Poisson Delaunay cell* (PDC) to refer to the individual m -dimensional random polytopes ($m \geq 2$) of the respective tessellations. With probability 1, all PVCs and PDCs are bounded polygons (cf. Property V2 in Section 2.3). Most results concerning the Voronoi diagram and Delaunay tessellation generated by Θ_P or other random point processes discussed in this chapter hold only *almost surely* (i.e. they hold with probability 1). Nevertheless, for ease of presentation in what follows we omit the phrase ‘almost surely’.

Figure 5.0.1 shows a portion of \mathcal{V}_P in \mathbb{R}^2 , while a *typical* PVC in \mathbb{R}^3 is illustrated in Figure 5.0.2. A *typical* Voronoi cell refers to a random polytope which, loosely speaking, has the same distribution as a randomly chosen cell

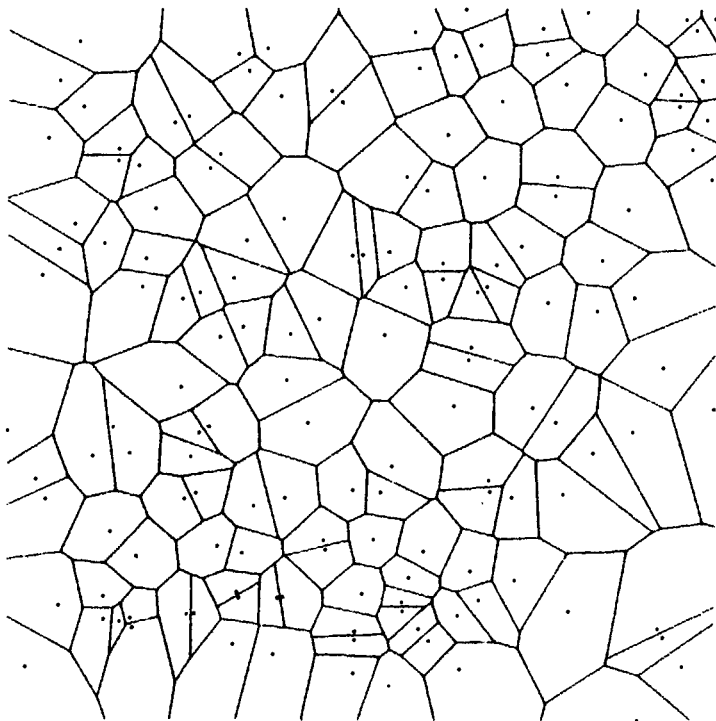


Figure 5.0.1 A portion of a planar Poisson Voronoi diagram.

from \mathcal{V} selected in such a way that every cell has the same chance of being sampled. However, such a uniform sampling scheme is in fact impossible to perform if P contains infinitely many distinct generators. The reason is that we are not able to choose with ‘equal probability’ from infinitely many cells. Nevertheless, a typical cell can be defined by using the ergodic theorem (Cowan, 1978, 1980) or the Palm distribution (Mecke, 1980; Møller, 1989, 1994) (see Section 1.3.3). If the generator set P is a realization of a simple stationary ergodic point process in \mathbb{R}^m , then these two methods are equivalent (see Section 1.3.3).

We first present the general properties of an infinite Voronoi diagram in \mathbb{R}^m in Section 5.1, and then begin our treatment of \mathcal{V}_P by considering its properties in Section 5.2. Some of these properties are inherited from properties of Θ_P by which the members of P are generated. Other properties of \mathcal{V}_P make it very attractive for use in a number of ways in an extensive range of empirical circumstances which are described in Section 5.3. In view of this widespread use of \mathcal{V}_P (and \mathcal{D}_P), there is great interest in obtaining information on both PVCs and PDCs. Such information includes moments, distributions and correlations of various characteristics such as the number of sides, area, perimeter (in \mathbb{R}^2), number of faces, volume and total edge

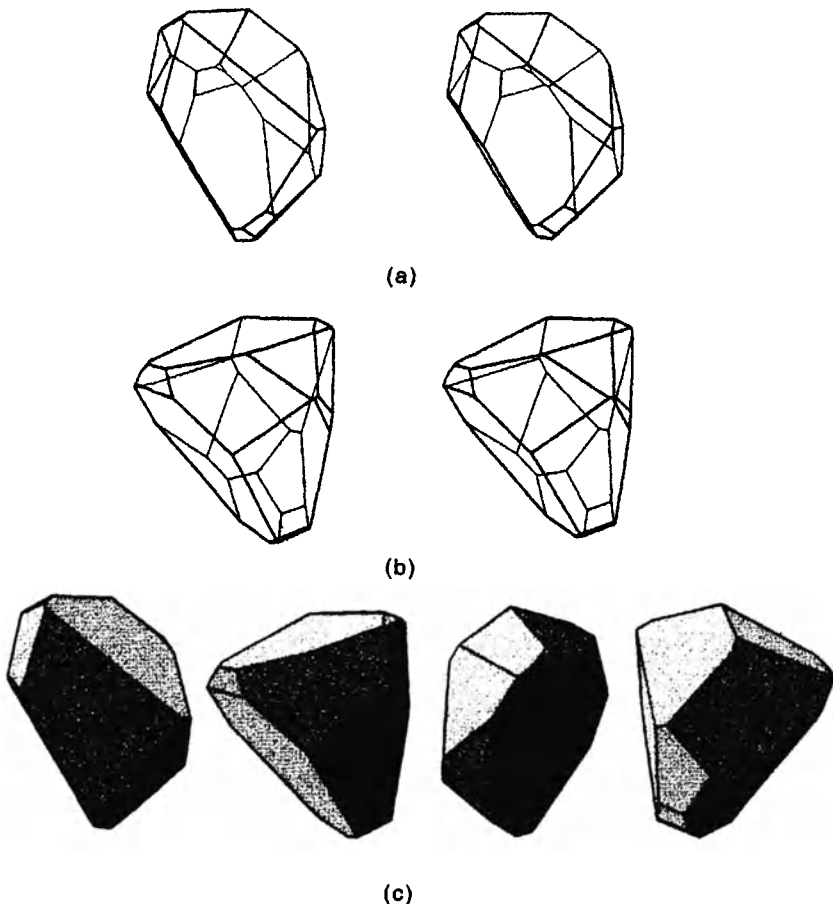


Figure 5.0.2 (a) Stereo pair of typical Poisson Voronoi cells in \mathbb{R}^3 . (b) The stereo pair after rotation of 90° about a fixed axis. (c) Cell shown after rotation of 0°, 90°, 180°, 270° about the fixed axis. (Source: Møller *et al.*, 1989.)

length (\mathbb{R}^3) of a typical cell. Considerable success has been achieved in deriving analytically the first-order moments of a variety of PVC and PDC characteristics, and these are reported in Sections 5.5.1 and 5.11, respectively. There is considerable interest in the conditional moments of PVC characteristics. Most of the 'equalities' are empirical laws obtained from simulation only. These are summarized in Sections 5.5.2 and 5.5.3.

In the first edition we stated that '*In principle it is also possible to derive integral formulae to obtain other moments of cell characteristics but often these are notoriously complicated, especially for PVCs. Consequently, many researchers have resorted to Monte Carlo approaches where the characteristics of cells are estimated by simulation*'. However, the scenery has changed. Integral formulae which are numerically tractable for the distributions of quite

a number of characteristics have been derived. These will be reported in Section 5.5.4. Nevertheless, the distributions of some important characteristics are still numerically intractable and have to be estimated by simulation. Several different simulation approaches are possible for both \mathcal{V}_P and \mathcal{D}_P and these are outlined in Section 5.4. Estimates obtained from such simulations of PVCs and PDCs are reported in Sections 5.5 and 5.11, respectively.

Poisson Voronoi diagrams induce many interesting stochastic processes, such as the point process of vertices. Some of these processes are discussed in Section 5.6.

In many applications involving \mathcal{V}_P in \mathbb{R}^3 , information concerning \mathcal{V}_P is not directly available but instead is acquired from planar sections or linear probes. Thus, such applications require information on sections of PVCs rather than the PVCs themselves. This information is reported in Section 5.7.

In Chapter 3 we described various ways of generalizing \mathcal{V} . Many of these generalizations can also be pursued when the generator set is a realization of a stationary point process. In fact, as noted in Section 3.1.5, the sectional Voronoi diagram of Section 5.7 can be considered as a type of weighted Voronoi diagram. Section 5.8 considers a particular type of additively weighted Poisson Voronoi diagram, more commonly known as the Johnson–Mehl model. This creates a dynamic version of the Poisson Voronoi model by associating with each generator point a weight which reflects the arrival time of the point in \mathbb{R}^m . Order- k and ordered order- k Voronoi diagrams and Voronoi diagrams on the surface of a sphere are discussed in Sections 5.9 and 5.10, respectively.

In general our knowledge of PDCs, particularly that derived by analytical methods, is greater than that of PVCs. This information, together with a brief treatment of sections of \mathcal{D}_P and \mathcal{D}_P on the surface of a sphere, is reported in Section 5.11.

For some applications the conditions involved in generating \mathcal{V}_P are inappropriate, perhaps because there are additional conditions influencing the locations of the members of P or because there are constraints on the sizes of the cells. In such circumstances modifications may be undertaken which produce other random tessellations. A selection of such tessellations is briefly surveyed in Section 5.12.

In view of the widespread interest in \mathcal{V}_P in empirical circumstances, considerable effort has been extended in many different disciplines in the pursuit of information on PVCs and PDCs and consequently the results of such endeavours are widely dispersed over a far-flung range of publications. In light of this it is not surprising that much duplication or near duplication has occurred because individual researchers (and reviewers and editors!) have been ignorant of similar, previous work of others. To reduce further duplication and in an attempt to synthesize previous activity, Sections 5.5–5.11 emphasize the reporting and reconciliation of the results of many previously disparate studies. Reviews on the mathematical theory for Poisson Voronoi diagrams can be found in Møller (1994, 1998, 1999).

5.1 PROPERTIES OF INFINITE VORONOI DIAGRAMS

As indicated in Section 2.1, no matter if P is finite or infinite, an m -dimensional Voronoi diagram, \mathcal{V} , constitutes a tessellation of \mathbb{R}^m ($m = 1, 2, \dots$) since the interiors of the individual cells of \mathcal{V} are non-overlapping and together with their boundaries are collectively space-filling. Denote by x_i the location vector of p_i and by $V(p_i)$ the Voronoi cell of p_i . The intersection of $k+1$ cells,

$$F(p_0, \dots, p_k) = \bigcap_{i=0}^k V(p_i),$$

lies on the hyperplane

$$G(p_0, \dots, p_k) = \{x \in \mathbb{R}^m \mid \|x - x_0\| = \dots = \|x - x_k\|\}.$$

The non-collinearity assumption is equivalent to one that such an affine subspace $G(p_0, \dots, p_k)$ is of $m-k$ dimensions for $k = 1, \dots, m$. The non-cosphericity assumption is equivalent to that $G(p_0, \dots, p_k) = \emptyset$ whenever $k > m + 1$. The general quadratic position and the local finiteness of the generator set P imply that $F(p_0, \dots, p_k)$ is either empty or of dimension $m-k$. A non-empty $F(p_0, \dots, p_k)$ is called an $(m-k)$ -face of the tessellation, and a cell an m -face. The boundary of an m -face consists of a hierarchy of s -dimensional polyhedra ($s = 0, 1, \dots, m$) which we term s -faces of a cell. In general, an s -face of a cell is not the same as an s -face of a tessellation. An s -face of a cell in a tessellation is the union of all s -faces of the tessellation which is contained in this s -face of a cell. For example, in \mathbb{R}^3 the 0-faces, 1-faces and 2-faces of a cell are the vertices, edges and faces of a cell. If an m -face is a polytope (i.e. a convex and bounded polyhedron), then all the s -faces on its boundary are s -dimensional polytopes. The 0-faces and m -faces of a tessellation coincide with the 0-faces and m -faces of the individual cells, respectively, but faces of other dimensions may not. A tessellation is called *regular* if the s -faces of the individual cells coincide with those of the tessellation for all s , $s = 0, \dots, m$. A typical s -face ($0 \leq s \leq m$) can be defined in the same way as a typical cell by using the ergodic theorem or the Palm distribution (see Sections 1.3.3 and 5.0). Note that a typical s -face ($0 \leq s < m$) and an s -face of a typical cell have different distributions.

Property IV1 (Møller, 1994, Proposition 2.1.2) The set of faces of cells is locally finite, i.e. there are only finitely many s -faces intersecting a bounded subset of \mathbb{R}^m , $s = 0, \dots, m$. Moreover, if P contains at least $m+1$ points, then \mathcal{V} contains faces of any dimensions s , $s = 0, \dots, m$.

Thus, if a Voronoi cell is bounded, then Property IV1 implies that it has only finitely many neighbours. This finiteness is essential for the discussion of the so-called *Aboav's law* and *Lewis' law* in Section 5.5.

Property IV2 (Møller, 1994, Proposition 2.1.3) A Voronoi cell $V(p_i)$ is bounded if and only if for all x_u (location vectors) on the surface of the unit

sphere in \mathbb{R}^m , there exists a generator $p \neq p_i$ with location vector x such that $(x - x_i)^T x_u > 0$.

(Cf. Property V2 in Section 2.3.) If $P = \{p_0, p_1, \dots\}$ is a realization of a non-empty stationary point process, then the condition of Property IV2 holds for all p_i (Møller, 1994, Proposition 3.1.1).

Property IV3 (Møller, 1994, Proposition 2.1.4) If a Voronoi cell $V(p_i)$ is bounded, then all its s -faces on the boundary coincide with those s -faces ($s = 0, \dots, m$) of the tessellation which are included in $V(p_i)$. Moreover, if all cells are bounded, then \mathcal{V} is regular.

A *normal* tessellation is one in which every s -face of the tessellation lies in the boundaries of $(m-s+1)$ cells ($0 \leq s \leq m-1$).

Property IV4 Every Voronoi diagram \mathcal{V} generated by points which are in the general quadratic position is a normal tessellation.

Equivalent terms to normal are ordinary or natural or in equilibrium state, all of which are used because empirical tessellations (for $1 \leq m \leq 3$) frequently possess this property. In terms of Section 2.1 (Assumption V1), \mathcal{V}_P is non-degenerate. Because of Property IV3 we may also express Property IV4 in terms of the constituent cells of the Voronoi diagram. Each s -face of a Voronoi cell lies in the s -dimensional hyperplane the points of which are equidistant from a set of $(m-s+1)$ generators in P . Thus, in \mathbb{R}^2 each vertex is shared by three cells and each edge is common to two cells. In \mathbb{R}^3 four cells meet at each vertex, each edge is shared by three cells and each face is common to two cells.

If in addition to the local finiteness and the general quadratic position assumptions, P is a realization of a stationary simple point process Θ in \mathbb{R}^m , then the Voronoi diagram generated, \mathcal{V}_Θ , is a random tessellation of \mathbb{R}^m . In view of Properties IV2, IV3 and IV4, we obtain an important property of such a random Voronoi diagram:

Property IV5 \mathcal{V}_Θ is a regular and normal random tessellation.

Reviews of theory and applications of general random tessellations can be found in Santaló (1988), Møller (1989, 1994) and Stoyan *et al.* (1995, Chapter 10). The most important class of random tessellations is the Poisson Voronoi diagram discussed in detail later in this chapter.

Once \mathcal{V}_Θ is generated by Θ , other point processes can be constructed from \mathcal{V}_Θ . Of particular interest are the stationary point processes Θ_s with intensities λ_s of the centroids of the s -faces of the cells of \mathcal{V}_Θ ($s = 0, \dots, m$) (see Section 5.6.1).

Property IV6 (Møller, 1989, Corollary 5.4) The intensity λ_s of the stationary point process Θ_s ($s = 1, \dots, m$) constructed from \mathcal{V}_Θ satisfies

$$[1 - (-1)^s] \lambda_s = \sum_{t=0}^{s-1} (-1)^t \binom{m-t+1}{s-t} \lambda_t. \quad (5.1.1)$$

Denote by λ the intensity of Θ . By definition, $\lambda = \lambda_m$ and so equation (5.1.1) yields

$$\begin{aligned} \lambda_0 &= 2\lambda, & \lambda_1 &= 3\lambda, & \lambda_2 &= \lambda, & \text{if } m = 2, \\ \lambda_1 &= 2\lambda_0, & \lambda_2 &= \lambda + \lambda_0, & \lambda_3 &= \lambda, & \text{if } m = 3. \end{aligned}$$

In fact, equation (5.1.1) holds for all regular and normal random tessellations.

For each $s = 0, 1, \dots, m$, the union of all s -faces of \mathcal{V}_Θ forms a stationary manifold process (see Section 1.3.3). In particular, it is known as a fibre process (consisting of the set of edges of \mathcal{V}_Θ) if $s = 1$ and a surface process (consisting of the set of facets of Voronoi cells) if $s = m - 1$ and $m \geq 3$. A Voronoi diagram is determined uniquely by its fibre or surface process.

Other relationships which hold for all stationary tessellations and which may be derived by either the ergodic theorem (see Section 1.3.3) (Miles, 1972a; Cowan, 1978, 1980) or the Palm distribution (see Section 1.3.3) (Radecke, 1980; Mecke, 1980, 1984; Møller, 1989), relate to the mean values of the cell characteristics. For \mathbb{R}^m general expressions are given by Møller (1989, Section 5) while specific relationships for $m = 2$ or $m = 3$ are given by Stoyan *et al.* (1995, pp. 317–318 and pp. 322–323, respectively). Furthermore, Mecke (1984) shows that for \mathbb{R}^2 these relationships can be expressed in terms of three parameters, λ_0 , λ_2 and L_A (the intensity of the fibre process of edges of the tessellation in \mathbb{R}^2 , i.e. the mean total edge length per unit area), while for \mathbb{R}^3 seven parameters are required (λ_0 , λ_3 , $\lambda_1 + \lambda_2$, L_V , S_V , T_V and Z_V , where L_V and S_V are the intensities of the fibre and surface processes of edges and facets, respectively, and T_V and Z_V are the intensities of the weighted vertex point process and the edge fibre process where the vertices and edges are weighted by the number of adjacent cells). In particular, for \mathcal{V}_Θ only two parameters $\lambda = \lambda_2$ and L_A and four parameters $\lambda = \lambda_3$, λ_0 , L_V and S_V are needed in \mathbb{R}^2 and \mathbb{R}^3 , respectively. The results are given in Table 5.1.1.

Both Miles (1972a) and Møller (1989) exploit these relationships in deriving many of the properties of PVC characteristics reported in Section 5.5. Møller also derives a series of relationships between the mean values of face and tessellation characteristics. Finally, since the intersection between an arbitrary p -dimensional hyperplane ($p = 1, \dots, m$) and \mathcal{V}_p in \mathbb{R}^m yields a random tessellation, the properties of such sections and their constituent cells can be generated from those of \mathcal{V}_p (Miles, 1972a, Section 2.5; 1972b; Møller, 1989, Section 6; Chiu *et al.*, 1996) and these are reported in Section 5.7.

The dual of an infinite Voronoi diagram is still a Delaunay tessellation. The non-empty intersection of Delaunay cells of dimension s is an s -face of

Table 5.1.1 The first moment of various characteristics of \mathcal{V}_Θ .

Characteristic	Mean
$m = 2$	
Area of a typical cell	$1/\lambda$
Perimeter of a typical cell	$2L_A/\lambda$
Number of vertices/edges of a typical cell	6
Length of a typical edge	$L_A/(3\lambda)$
$m = 3$	
Volume of a typical cell	$1/\lambda$
Surface area of a typical cell	$2S_V/\lambda$
Total length of all edges of a typical cell	$3L_V/\lambda$
Mean breadth (also known as the mean caliper diameter)*	$L_V/(4\lambda)$
Number of vertices of a typical cell	$4\lambda_0/\lambda$
Number of edges of a typical cell	$6\lambda_0/\lambda$
Number of faces of a typical cell	$2(1 + \lambda_0/\lambda)$
Area of a typical face	$S_V/(\lambda_0 + \lambda)$
Perimeter of a typical face	$3L_V/(\lambda_0 + \lambda)$
Number of vertices/edges of a typical face	$6/(1 + \lambda/\lambda_0)$
Length of a typical edge	$L_V/(2\lambda_0)$

L_A = intensity of the edge fibre process in \mathbb{R}^2 .

L_V = intensity of the edge fibre process in \mathbb{R}^3 .

S_V = intensity of the face, surface process in \mathbb{R}^3 .

λ_0 = intensity of the vertex point process.

λ = intensity of Θ .

* Mean length of the cell's projection onto an isotropic random line.

Source: Møller (1994, Proposition 3.3.1).

Table 5.1.2 The first moment of various characteristics of \mathcal{D}_Θ .

Characteristic	Mean
$m = 2$	
Area of a typical cell	$1/(2\lambda)$
Perimeter of a typical cell	L'_A/λ
Number of vertices/edges of a typical cell	3
Length of a typical edge	$L'_A/(3\lambda)$
$m = 3$	
Volume of a typical cell	$1/\lambda_0$
Surface area of a typical cell	$2S'_V/\lambda_0$
Area of a typical face	$S'_V/(2\lambda_0)$
Length of a typical edge	$L'_V/(\lambda_0 + \lambda)$

L'_A = intensity of the Delaunay edge fibre process in \mathbb{R}^2 .

L'_V = intensity of the Delaunay edge fibre process in \mathbb{R}^3 .

S'_V = intensity of the Delaunay face, surface process in \mathbb{R}^3 .

λ_0 = intensity of the Voronoi vertices/Delaunay cell centroids.

λ = intensity of Θ .

Source: Møller (1994, Remark 3.3.1).

the Delaunay tessellation ($s = 0, \dots, m$). An s -face of a Delaunay cell is the s -dimensional simplex which is the convex hull of $s+1$ distinct generators.

Property ID1 (Møller, 1994, Proposition 2.1.6) Delaunay tessellations are regular.

Denote by \mathcal{D}_Θ the dual of \mathcal{V}_Θ . \mathcal{D}_Θ is a stationary random Delaunay tessellation. The point processes of the centroids of the s -faces of \mathcal{D}_Θ are stationary and the intensities are simply λ_{m-s} ($s = 0, \dots, m$), because of the duality between \mathcal{D}_Θ and \mathcal{V}_Θ . The first moment of some characteristics, which depend on two and four parameters in \mathbb{R}^2 and \mathbb{R}^3 , respectively, are tabulated in Table 5.1.2.

5.2 PROPERTIES OF POISSON VORONOI DIAGRAMS

The results in Section 5.1 hold for any locally finite set P , the members of which are in the general quadratic position. In this section we discuss the Poisson Voronoi diagrams \mathcal{V}_P , which are generated by realizations of the homogeneous Poisson point process Θ_P .

Characteristics of \mathcal{V}_P and its constituent PVCs either derive from the procedure for generating Voronoi cells described in Section 2.1 or are inherited from the properties of Θ_P . The stationarity of \mathcal{V}_P yields the following two properties.

Property PV1 The cells of \mathcal{V}_P are polytopes (bounded and convex polyhedra).

(Cf. Property V1 in Section 2.3 and Property IV2 in Section 5.1.) Because all PVCs are bounded and the points of Θ_P are in the general quadratic position, by Property IV5 in Section 5.1 we have

Property PV2 \mathcal{V}_P is a regular and normal tessellation.

(See Møller, 1989, Example 1 and Proposition 7.1.) Thus, we need not distinguish an s -face of \mathcal{V}_P and an s -face of an individual cell of \mathcal{V}_P .

Properties which are inherited from Θ_P include the following.

Property PV3 \mathcal{V}_P is stationary and isotropic.

This means that its characteristics and those of its constituent PVCs are invariant under both translation and rotation about the origin in \mathbb{R}^m . Thus, \mathcal{V}_P can be considered a motion-invariant tessellation.

Property PV4 \mathcal{V}_P satisfies the strong mixing condition under the translation transformation.

The mixing condition means that spatially distant features of the tessellation are asymptotically independent as the distance tends to infinity (see Section 1.3.3).

5.3 USES OF POISSON VORONOI DIAGRAMS

Given the way in which the Poisson Voronoi diagram, \mathcal{V}_p , is generated and its resulting properties, there has been widespread interest in its use in a variety of empirical situations. Such uses of \mathcal{V}_p take two main forms. The most straightforward is as a model of a given empirical structure, while the other use is as a normative model against which other tessellations can be evaluated. Sometimes the distinction between these two uses becomes blurred because, once established as a structural model, \mathcal{V}_p is often subsequently used in a normative way.

An example of the direct use of \mathcal{V}_p is provided by Kumar and Kurtz (1994a) and Kumar and Singh (1995) who use the three-dimensional form as a microstructural model of a dense, single phase polycrystalline material in their investigations of thermal conductivity. They justify this by noting that the two structures are topologically equivalent and that the mean dihedral angle of 120° and the mean bond angle (i.e. the angle between edges) of 111.11° in \mathcal{V}_p are very close to those required by the minimum surface energy (120° and $109^\circ 28' 16''$, respectively), while the mean number of edges per face (5.228) is very similar to experimentally observed values. Further support for the use of \mathcal{V}_p as a model of single phase microstructures is provided by considering industrial standards. For single phase microstructures these deal only with the mean grain size as determined from the mean number of intercepts per unit length of test line or by the mean number of grain sections per unit area of test area. Mücklich *et al.* (1997) show that for the German standard DIN 50 601 these mean values are consistent with those of sectional Poisson Voronoi diagrams (see Section 5.7). \mathcal{V}_p has also been used as a microstructural model in simulating fatigue crack propagation (Cox and Morris, 1988) and plastic deformation (Seefeldt and Klimanek, 1997).

A specific example of a polycrystalline microstructure is zinc oxide (ZnO) varistors (multicomponent ceramic devices with highly non-linear current-voltage characteristics widely used as surge arresters), produced by sintering ZnO powder together with small amounts of other oxide additives. Thus varistors consist of semi-conducting ZnO grains surrounded by insulating barriers at the grain boundaries. To model the electrical transport properties of such material, Bartkowiak *et al.* (1996a,b,c) consider the cells of the two-dimensional \mathcal{V}_p to represent the grains of the ceramic and, using prescribed probabilities, randomly assign each Voronoi edge to one of three types; 'good' (high leakage resistance) and 'bad' (lower leakage resistance) electrically non-linear microjunctions, and ohmic (linear with low resistance) microjunctions. In this way, the behaviour of the material in response to changing proportions of microjunctions can be examined.

The same characteristics of \mathcal{V}_p that have made it popular as a microstructural model have also led to it being selected as a basis of a number of models that study the behaviour of time-varying phenomena. For example, Yuan and Edwards (1995) use it as the initial state in simulations of two-dimensional random foams in planar Poiseuille flow, while both Kermode and Weaire (1990) and Neubert and Schreckenberg (1997) adopt it as one of the initial configurations in their simulations of the coarsening of two-dimensional soap froth.

Another example of the direct use of \mathcal{V}_p is provided by Christ *et al.* (1982a,b,c), Friedberg and Ren (1984), Drouffe and Itzykson (1984), Ren (1984) and Itzykson and Drouffe (1989) in the investigation of quantum field theory. Here the traditional concept of a space-time continuum has been replaced by that of a discrete lattice. Initially, regular lattices were used since the links between individual nuclei (points) are clearly defined. However, such lattices are not motion invariant and thus do not possess properties assumed in the traditional concept. As we have seen, the homogeneous Poisson point process, Θ_p , does possess these properties (see Section 1.3.3) and so Christ *et al.* (1982a) propose using a random lattice in which the nuclei are generated by Θ_p and the links between the nuclei correspond to the adjacencies between the Voronoi regions of the Voronoi diagram of nuclei. Such a lattice is equivalent to the Poisson Delaunay tessellation, \mathfrak{D}_p . To distinguish it from other random lattices (see Section 5.12), this particular form is now often referred to as the *Poissonian random lattice* (PRL). Further support for the PRL is provided by the results of Monte Carlo simulations which demonstrate that the PRL displays the same behaviour as a regular lattice for both the Ising model (Espriu *et al.*, 1986; Janke *et al.*, 1993, 1994a,b) and the eight-state Potts model (Janke and Villanova, 1995).

The ability of the PRL to discretize space without introducing any form of anisotropy has led to its adoption in other contexts including modelling the statistical mechanics of membranes (David and Drouffe, 1988) and modelling the growth of sandpiles (Puhl, 1993). Lauritsen *et al.* (1993) have extended the basic concept by creating dynamic random lattices in which thermodynamic energy is distributed over the lattice on the basis of the topological properties of the Voronoi cells of the nuclei. Ostoja-Starzewski and Wang (1989, 1990), Ostoja-Starzewski (1990, 1993), and Ostoja-Starzewski *et al.* (1995) have proposed the two-dimensional PRL as a generic model of the microstructure of discrete granular media such as soils, powders and fibrous materials. In particular, they calculate the effective moduli of such materials by considering each Delaunay vertex as a joint and each Delaunay edge as a two-force member acting as a linear elastic spring of a directly specified length and of a deterministic or random spring constant. They also suggest that for some applications modified, less disordered forms of the PRL created by imposing a minimum edge length condition or by considering the Delaunay tessellation of the centroids of the cells of \mathcal{V}_p (Ostoja-Starzewski and Wang, 1990), may be more appropriate. The approach may also be extended to two-phase media by randomly assigning the vertices

of the PRL to either phase, subject to specified volume fractions (Ostoja-Starzewski *et al.*, 1995). Gasparini *et al.* (1996) use the PRL in a similar way to provide a network of truss or beam elements for use in simulating the behaviour of brittle materials such as concrete or ceramic. In this instance each Delaunay edge is assigned a truss element of the same deterministic axial stiffness and an independently, identically Weibull-distributed tensile strength.

\mathcal{V}_p has also been used in studies of conductivity and percolation in composites consisting of grains and associated pore space (void). When the concern is with movement through the material, the equivalent of the PRL has been proposed as a model of a topologically random network in both \mathbb{R}^2 (Jerauld *et al.*, 1984a) and \mathbb{R}^3 (Jerauld *et al.*, 1984b; Rivier *et al.*, 1985). Once the network is identified, the *bond percolation model* is obtained by choosing each edge to be present independently with a specified probability. The *site percolation model* is produced by choosing each vertex to be present independently with a specified probability and retaining those edges for which both endpoints are present. A third model, the *first-passage percolation (FPP) model*, is defined by independently assigning to each edge a non-negative travel time from a common probability distribution. The first-passage time between two vertices is then defined as the minimum travel time between the vertices over all paths connecting them. Vahidi-Asl and Wierman (1990, 1992) and Howard and Newman (1997) consider different FPP models in which the links are defined by the edges in \mathcal{V}_p or \mathcal{D}_p (see Section 5.6.4).

When the interest is in percolation through the void, the so-called *Swiss cheese model* may be used (Elam *et al.*, 1984; Halperin *et al.*, 1985; Feng *et al.*, 1987; van der Marck, 1996). In this model the pore space is represented by the complement of the union of a set of randomly located, overlapping spheres. Kerstein (1983) showed that when the spheres are of uniform size, the Voronoi diagram of the sphere centres (equivalent to \mathcal{V}_p) is a good representation of the void space since the Voronoi vertices can be considered as the sites (centres, nodes) of the void space and the Voronoi edges contained in the void space define the links over which flows can occur.

DiCenzo and Wertheim (1989) have also used \mathcal{V}_p in modelling the growth of clusters formed by a metal vapour deposited on amorphous substrates. The model is a two-step one in which first nucleation sites are distributed in \mathbb{R}^2 (\mathbb{R}^3) according to Θ_p and then atoms landing on the surface of the substrate are assigned to the nearest nucleation site. The number of atoms in a cluster formed at a nucleation site will be proportional to the area (volume) of the surface closest to the nucleation site which is equal to the area (volume) of the Voronoi cell of the nucleation site. Thus, the distribution of cell areas (volumes) can be used to derive the distribution of cluster sizes. Other studies involving \mathcal{V}_p have also focused on the distribution of cell areas (volumes). For example, it has been used to model the effects of variations in local density on variations in plant size (Miller and Weiner, 1989), the contribution from random noise in an algorithm for source detection in high-energy astrophysics (Ebeling and Wiedenmann, 1993), and particle size

distributions resulting from the abrupt or impulsive application of fracturing forces to a solid body (Grady and Kipp, 1985).

Foss and Zuyev (1996) used \mathcal{V}_p as a model for telecommunications networks. Think of stations as concentration points where cables meet or communications change their routes. They form a Poisson process on \mathbb{R}^2 . Each station serves its zone consisting of those locations that are closer to it than to any other stations, i.e. each station serves its own Voronoi cell. They considered further that subscribers to the telecommunication services form another independent Poisson process on \mathbb{R}^2 . Molchanov and Zuyev (1997) discussed the optimal intensity of stations so that the total connection cost would be minimized. If the connection cost is linearly proportional to the sum of the Euclidean distances between subscribers and stations, the optimal intensity of stations should be proportional to the intensity of subscribers raised to the power 2/3.

\mathcal{V}_p also forms the basis of another frequently used model of structure. This is a specific form of a random mosaic which we label the *Poisson Voronoi Random Mosaic* (PVRM). The creation of a random mosaic involves two steps (Schachter and Ahuja, 1979):

- Step 1: for some bounded region, B , of \mathbb{R}^m , tessellate B ;
- Step 2: independently assign one of k phases to each cell of the tessellation according to a fixed set of probabilities, p_1, \dots, p_k ; $\sum_{i=1}^k p_i = 1$.

In this way B is partitioned into subregions, B_1, \dots, B_k , each consisting of the union of all cells of phase k , so that $\bigcup_{i=1}^k B_i = B$. If the tessellation of Step 1 is the Poisson Voronoi diagram, we produce the PVRM. In ecology this model is referred to as the *S-Mosaic* (Pielou, 1977, p. 185).

The simplest PVRM is two-phase. Winterfield *et al.* (1981) have used such a mosaic as a model of a disordered composite in \mathbb{R}^2 which can be used for studying conduction and percolation in continuous media. The two phases are conducting and non-conducting (insulating). Using this approach they are able to study the effects on various conduction and percolation properties of the medium by varying the probabilities associated with each phase. Once established, they also use the two-phase PVRM as a normative model against which other mosaics involving tessellations composed of regular hexagonal and square cells are judged. The two-phase PVRM has also been used to model microemulsions in \mathbb{R}^3 (Talmon and Prager, 1978a,b; Kaler and Prager, 1982; Anderson *et al.*, 1989). Microemulsions are thermodynamically stable three-component systems consisting of an aqueous component, an oil component and a surfactant. The aqueous and oil components are the two phases of the mosaic (with probabilities p_a and p_o , respectively) and the surfactant is distributed over the resulting aqueous-oil interface (the boundaries of the subregions defined by the two phases). Such a model is capable of generating all three classes of microemulsion geometry: oil in water (small values of p_a/p_o), bicontinuous ($p_a/p_o \approx 1$) and water in oil (large values of p_a/p_o). Tipper (1990b) has suggested that the PVRM is also a useful

theoretical model for studying stratigraphic correlation where the phases can represent different lithologies (e.g. sand/shale).

A three-phase PVRM in \mathbb{R}^3 is used by Brumberger and Goodisman (1983) in the interpretation of small angle X-ray scattering observed for heterogeneous catalysts such as porous oxides (e.g. Al_2O_3 , S_iO_2) and oxide supported metals (e.g. $\text{Pt}/\text{Al}_2\text{O}_3$, $\text{Rh}/\text{S}_i\text{O}_2$). Here the three phases are void, support and metal, each of which is considered to contain an internally uniform electron density and whose associated probabilities are equal to the proportion of the total volume of the sample catalyst occupied by that phase.

A variant of the PVRM is described by Ahuja *et al.* (1985) and An *et al.* (1983) who use it in the representation of an image with k colours. A Poisson Voronoi tessellation is superimposed on the image and the individual cells of the tessellation are assigned the colour of the underlying image. In those cases where more than one colour occurs in a cell, the cell is assigned the colour that has the largest representation. The image can then be represented by the set of coordinates of the generators of the individual cells of the tessellation together with their associated colours. They suggest that such a representation is particularly useful for the secure transmission of images since, if the coordinates of the cell generators are produced by a pseudo-random number generator, only the seed for this generator and the colour of each cell need to be transmitted.

On those occasions when we observe a PVRM in a window we may be interested in statistical inference concerning the probabilities of the phases and the intensity of Θ_p . The latter is not straightforward since some of the edges of \mathcal{V}_p disappear as a result of the phase assignment process. Archambault and Moore (1995) provide estimates for the two-phase PVRM.

Although we have illustrated a number of empirical situations where our knowledge of the phenomenon suggests that \mathcal{V}_p may be an appropriate model, there are many other occurrences where such direct use may be unjustified. For instance, we may have little or no information on how a particular tessellation was generated or we may have sufficient information to suggest that it is unlikely that it was created under conditions analogous to those generating \mathcal{V}_p . In the former case our first concern might be to determine if the empirical tessellation differs from \mathcal{V}_p , while in the latter we may be interested in knowing in what ways the tessellation differs from \mathcal{V}_p . In both instances the results of our investigations may provide additional insight into the conditions under which the empirical tessellation was generated. In this way \mathcal{V}_p is used as a normative model against which other tessellations are compared. Such comparisons may be informal in nature or may involve the formal testing of hypotheses concerning the nature of the difference between the empirical tessellation and \mathcal{V}_p (see Section 5.12).

Numerous examples of the use of \mathcal{V}_p in this normative role occur for phenomena in both \mathbb{R}^2 and \mathbb{R}^3 in both the natural and the social sciences. In astronomy \mathcal{V}_p in \mathbb{R}^3 has been used to evaluate phenomena having a basic cellular topology (Pierre, 1990) such as Lyman Alpha absorbers at high redshifts (Pierre *et al.*, 1988) and galaxy distributions in \mathbb{R}^3 (Yoshioka and

Ikeuchi, 1989; Coles, 1990; Zaninetti, 1990, 1992; Ikeuchi and Turner, 1991; van de Weygaert, 1991, 1994; Goldwirth *et al.*, 1995; Doroshkevich *et al.*, 1997). \mathcal{V}_p in \mathbb{R}^2 can also be used if the galaxies are considered as either slices of the universe or as projections on the sky (Icke and van der Weygaert, 1987; Zaninetti, 1989). \mathcal{V}_p has also been used to evaluate the structure of several monatomic liquids and solids which may be modelled as sphere packings (Rahman, 1966; Finney, 1970a), as well as sections of geological (Crain, 1976) and metallurgical (Schwertel and Stamm, 1996) materials.

In animal ecology tessellations created by territorial units have been compared with \mathcal{V}_p in \mathbb{R}^2 (Hamilton, 1971; Hasegawa and Tanemura, 1976; Buckley and Buckley, 1977; Tanemura and Hasegawa, 1980). In geography Boots (1973, 1975a) has used \mathcal{V}_p in \mathbb{R}^2 to evaluate service areas associated with public bus services in parts of England and Wales, while Singh and Singh (1978) and Singh (1979) have used them in the evaluation of territories of villages in India.

All the above examples illustrate the use of \mathcal{V}_p as a normative model in the examination of empirical tessellations. However, it has also been used extensively as a normative model in the analysis of point patterns. This is because we can compare the characteristics of the Voronoi diagram generated by a given set of points (or, more frequently, the Delaunay tessellation) with those of \mathcal{V}_p (or \mathcal{D}_p). This provides an indirect way of comparing the empirical point pattern with one generated by Θ_p which provides the generators for \mathcal{V}_p . Such endeavours have received considerable attention and as a result are dealt with in more detail in Sections 8.1 and 8.2.

Poisson Voronoi diagrams in the above applications are constructed under the Euclidean distance. Many random *cellular automata* based on the *threshold growth mechanism* can be well approximated by Poisson Voronoi diagrams constructed under different measurements of distances (Gravner and Griffeath, 1997). An example of a cellular automaton is a model for excitable media in which rare 'pacemakers' emit waves that propagate until they encounter waves emanating from other sources (Fisch *et al.*, 1991). The meaning of the threshold growth mechanism can be illustrated in the following *multitype threshold vote automaton* (Durrett and Steif, 1993). Locations of voters are a regular lattice. Initially each voter adopts randomly one of many opinions. According to a deterministic discrete-time update (growth) rule, a voter changes affiliation to agree with the consensus of more than a threshold number of other voters in the voter's neighbourhood, but the voter's opinion remains unchanged in case of ambiguity. If the number of opinions is large, then high location concentrations of agreement have an advantage over their immediate surroundings, and so are able to grow until they encounter a large region controlled by another opinion.

5.4 SIMULATING POISSON VORONOI AND DELAUNAY CELLS

Simulations have been used frequently in studying the characteristics of PVCs, particularly for estimating the distribution of those characteristics. Tables 5.4.1 and 5.4.2 summarize those published studies involving more than 10 000 cells known to the authors, although there are doubtless some others. Although Icke and van de Weygaert (1987) involved only 100 cells, and Ohser and Mücklich (1995) have not reported the method and the number of cells in their simulation study, they are, to the best of our knowledge, the only simulation studies which involve the distances d_1 between a generator and

Table 5.4.1 Simulation studies of Poisson Voronoi cells in \mathbb{R}^2 .

Study	Method	Number of cells	Characteristics
Boots (1987)	R	30 000	L
Boots and Murdoch (1983)	R	50 000	A N P
Crain (1972, 1976)	T	5–11 000	A N P
Crain (1978)	T	25–59 000	A L N P
DiCenzo and Wertheim (1989)	A	~193 500	A
Drouffe and Itzykson (1984)	R	27 000	A N
Hinde and Miles (1980)	T	2 000 000	A N P α
Hutchings and Discombe (1986)	A	42 318	A N P
Icke and van de Weygaert (1987)	A	100	A L N P d_1 d_2 α
Janke <i>et al.</i> (1994a)	A	10 000	N
	A	80 000	N
Kumar and Kurtz (1993)	A	2 000 000	A L P
	A	650 000	N
Le Caër and Ho (1990)	A	600 696	A L N P
	A	1 001 500	A L N P
	A	1 020 800	A L N P
Marthinsen (1996)	A	100 000	A
Moore and Moore (1993)	A	100 000	L N
Moore and Angell (1993)	A	100 000	A N
Quine and Watson (1984)	R	50 000	A N P
Vincent <i>et al.</i> (1976, 1983)	A	10 000	N
Weaire <i>et al.</i> (1986)	A	79 400	A
	A	734 639	A
	A	929 070	A
	A	~96 500	N

Characteristics:

A = area

L = edge length

N = vertices (edges)

P = perimeter

d_1 = distance between a generator and a vertex

d_2 = perpendicular distance between a generator and an edge

α = interior angle

For definitions of methods, see the text.

a vertex and the perpendicular distance d_2 between a generator and an edge, and the maximum breadth (maximum length of the cell's projection onto a line) b_{\max} of a typical cell, respectively. Thus, we also included them in Tables 5.4.1 and 5.4.2.

As noted in Section 1.3.3, the homogeneous Poisson point process Θ_p is ergodic so that limiting distributions of the characteristics of the cells in a single, large Poisson Voronoi diagram V_p will coincide with those obtained from a sequence of individual, typical cells sampled from separate Poisson Voronoi diagrams. Consequently, two main simulation approaches are possible.

The first of these (referred to as method A in Tables 5.4.1 and 5.4.2) involves simply generating a large number of points inside a bounded region B according to Θ_p , constructing V_p and measuring the characteristics of all its cells. There are essentially two complications with this approach. The first is that, no matter how large V_p is, allowance must be made for edge effects introduced by those cells close to the boundary of B . One way to treat such edge effects is to exclude from consideration any cells of V_p in B for which a circle, centred at any vertex v of the cell and passing through the three

Table 5.4.2 Simulation studies of Poisson Voronoi cells in \mathbb{R}^3 .

Study	Method	Number of cells	Characteristics
Jerauld <i>et al.</i> (1984b)	A	10 184	F
Kiang (1966)	A	12 800	V
Kumar <i>et al.</i> (1992)	A	358 000	B F N S V
	A	102 000	A G L P S V
Kumar and Kurtz (1995)	A	377 000	A F L N P S V $\alpha_1 \alpha_2$
	A	165 000	B
Lorz (1990b, 1991)	R, A	82 870	A B F L M N P S V $\bar{b} \alpha_1 \alpha_2 \alpha_3$
Lorz and Hahn (1993)	R	1 081 945	F B S V $\bar{b} \alpha_3$
Marthinsen (1996)	A	~25 000	V
Møller (1994)	R	~10 000	V
Moore and Angell (1993)	A	50 000	V
Ohser and Mücklich (1995)	--	—	b_{\max}
Tanemura (1988)	A	100 000	F M S V
Thorvaldsen (1992)	R	250 000	F L M N S V
Yoshioka and Ikeuchi (1989)	A	64 000	V

Characteristics:

A = area/face

P = edge length/face

B = total edge length/cell

S = surface area/cell

C = full (Gabriel) neighbours

V = volume

F = faces/cell

\bar{b} = mean breadth/cell

G = face area/cell

b_{\max} = maximum breadth/cell

L = edge length

α_1 = face (dihedral) angle at an edge

M = vertices/cell

α_2 = interior angle of a face (bond angle)

N = edges/face

α_3 = face angle of a cell

Note that $M = 2F - 4$.

For definitions of methods, see the text.

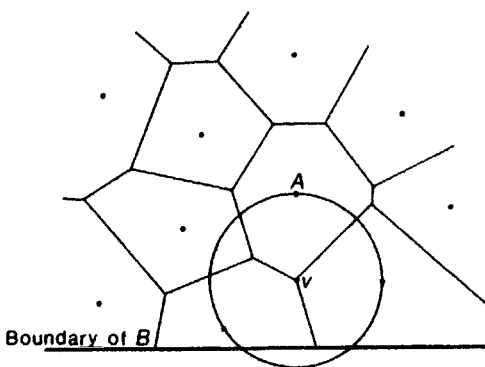


Figure 5.4.1 A procedure for identifying cells subject to edge effects.

points of Θ_p , which are equidistant from v , intersect the boundary of B (Kenkel *et al.*, 1989) (cell A in Figure 5.4.1 is such a cell). If B is a rectangle, an alternative procedure involves creating additional points outside of each edge of B which are translations of points of Θ_p inside the opposite edge of B (the points in the shaded polygons in Figure 5.4.2). The translated points are then used to complete the polygons of those points of \mathcal{V}_p whose polygons intersect the boundary of B . This procedure, which is usually referred to as a periodic boundary condition, is equivalent to converting B into a torus (see Section 3.7.10). The other complication arises because the characteristics of neighbouring cells are not independent (see Section 5.5.3). Thus, the number of cells in the aggregate must be sufficiently large to avoid any bias introduced by this source.

The second simulation approach involves generating a sequence of independent, typical PVCs, measuring the characteristics of each and then aggregating them to obtain the required distributions. The primary advantage of this approach over the previous one is that it avoids problems of edge effects. There are two variants of this approach. The first, method T in Table 5.4.1, involves repeatedly simulating Θ_p within a bounded region B , constructing \mathcal{V}_p and then identifying and measuring only the central cell. This approach involves two considerations: the choice of a single parameter λ (the intensity of Θ_p) and the number of replications n of the procedure. The selection of n is determined primarily by the degree of accuracy at a specified confidence level required of the simulation estimates. The choice of λ represents a compromise between two concerns. If λ is too small the central polygon may intersect the boundary of B or be subject to edge effects (see above), but if it is too large many points will be generated that have no effect on the construction of the central polygon. Estimates of the appropriate value of λ vary considerably even in the case when B is a unit square (for example, Crain, 1978, suggests $\lambda = 35$ is sufficient while Hinde and Miles, 1980, use $\lambda = 100$). Once the values of λ and n have been selected this simulation procedure involves two steps: generating a Poisson distributed variable k with mean $\lambda |B|$ (where $|B|$ is the size of B) and then generating

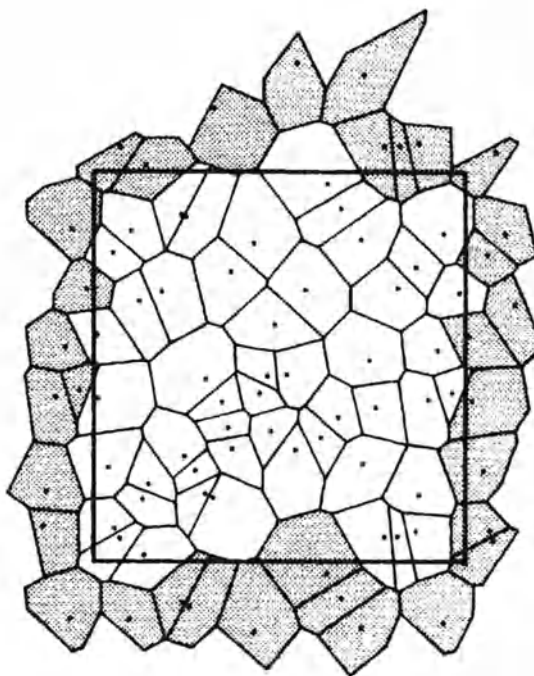


Figure 5.4.2 Periodic boundary condition to avoid edge effects.

k independent uniform random points in B . However, Hinde and Miles (1980) have suggested that, rather than selecting k independently, it is more efficient to choose the values deterministically as the $(i-1/2)/n$ quantiles ($i = 1, \dots, n$) of the Poisson distribution. While they indicate that this approach is superior to selecting the $i/(n+1)$ quantiles ($i = 1, \dots, n$), they make no claims for its optimality.

The second variant of the sequence approach, method R in Tables 5.4.1 and 5.4.2, was proposed by Boots and Murdoch (1983) and Quine and Watson (1984). It exploits the known joint distribution of ordered distances from the origin, o , in Θ_p , since a set of increasing distances with this distribution together with a sequence of random directions gives Θ_p . In two dimensions this simulation process begins by locating the first point, p_0 , at o ; additional points p_i ($i = 1, 2, \dots$) are then generated at random in increasing order of distance from p_0 . As p_i is generated the perpendicular bisector of $\overline{p_0 p_i}$ is drawn. After this step is repeated a number of times p_0 will be surrounded by a convex polygon, P_0 . Additional points are then generated until these points cease to influence the form of P_0 . This occurs when the distance from p_i exceeds the diameter of the smallest circle centred at p_0 containing P_0 . At that time the required characteristics of polygon P_0 are measured and the entire procedure repeated for the next polygon. Unlike method T this procedure is essentially scale invariant and so the choice of λ is no longer a

consideration. Also, since the number of points required to produce the final P_0 is usually about 15 to 20, this procedure is more efficient computationally than method T.

Quine and Watson (1984, p. 551) suggest that a modification of this procedure may be used to gain information about the tails of the distributions of the characteristics of the PVCs. This involves generating the polygon P_1 around p_1 , ignoring p_0 in the construction of P_1 . Thus, P_1 contains p_0 . Since it is known that, in any random tessellation such as \mathcal{V}_p the cell containing the origin is larger on average than other cells (Matheron, 1975, pp. 168–169; Stoyan, 1986; Mecke, 1999), polygons that result from this modified procedure will be larger than those generated by the basic procedure. Thus, knowledge of their characteristics will help to improve the estimates of the tails of the distributions. Drouffe and Itzykson (1984) use a refinement of this approach to ensure that only polygons with a specified number of sides are created.

In \mathbb{R}^3 Quine and Watson (1984) suggest it is easier to work with \mathcal{D}_p rather than \mathcal{V}_p . An initial very large simplex is established with its circumcentre at p_0 . This is subdivided to create a list of Delaunay simplices. As a new point is established this list is updated to include those simplices with the new point as a vertex. This process continues until the distance from p_0 to a new point exceeds twice the maximum circumradius of those simplices with a vertex at p_0 .

Relative to simulating \mathcal{V}_p , less effort has been expended in the simulation of \mathcal{D}_p . In part this is because analytical approaches (particularly the work of Miles, 1970a) have been successful in deriving more thorough knowledge of typical cells than is the case for \mathcal{V}_p . For example, Rathie (1992) derives the exact distribution for the length, area and volume of a typical PDC in \mathbb{R}^m for $m = 1, 2$ and 3 , respectively; Muche (1996b) establishes the distributions for the cell volume, the area and the perimeter of a face, the length of an edge, and an interior angle of a face in the case $m = 3$ (see Section 5.11 for the details). In addition, for $m \leq 3$ the methods of simulating \mathcal{V}_p are also efficient for constructing \mathcal{D}_p . Kumar and Kurtz (1994b) simulate 1.2 million PDCs in \mathbb{R}^3 . However, this is not the case for $m > 3$ and Kendall (1989, 1990) has developed a procedure for simulating individual cells which is particularly efficient in such circumstances. The approach is based on a theorem derived by Miles (1970a) (see equation (5.11.2)) which shows that the size and shape of a PDC are independent if the size is measured in terms of the radius r of its circumsphere and the shape by the angles at its vertices. Furthermore, since the distribution of r is known in terms of the dimensions m (see Section 5.11), the problem of simulation reduces to that of constructing the shape of the PDC. Kendall's approach involves creating a sequence of simplices, each of which consists of $(m+1)$ independent points in \mathbb{R}^m , from a standard normal distribution. For each simplex the values of r (the circumradius), and l , the square root of the sum of the squares of the distances of the $(m+1)$ points from their centroid, are used to create a shape variable, $\rho = r/l$. The j th such simplex in the sequence, with shape measure ρ_j , is retained and its shape recorded if and only if

$$U_j \leq 1 / (\alpha_m \rho_j^{m^2}),$$

where $\alpha_m = (m + 1)^{m^2/2}$ and U_j is the j th of an independent and identically distributed (i.i.d.) sequence of random variables uniformly distributed on the unit interval $[0, 1]$. Kendall (1990) proves that the sequence of recorded shapes will be an i.i.d. sequence of shapes of PDCs. The probability of accepting a simplex in this procedure is known exactly as a function of m (Kendall, 1990, equation (5)). As $m \rightarrow \infty$ this probability tends to zero, thus making the method impracticable for values of $m > 6$. Kendall (1983) has used such an approach to simulate the shapes of 5000 PDCs for $m = 2$ (see Section 5.11).

For larger values of m , Kendall (1988) has developed another simulation method which generates values of two regularity indices for the cells rather than the cells themselves. These indices are F , the volume of a PDC relative to the volume of a regular simplex having the same circumradius, and $\gamma = \log(1/F)$. For $m \geq 3$, Kendall obtains an expression for the expectation of the k th moments of F as the product of $2m$ beta functions. Since each of these beta functions is the $(k/2)$ th moment of a random variable on $[0, 1]$, F can be expressed as the square root of a product of $2m$ independent beta variables. Simulation procedures for such beta variables are available (Ripley, 1987) and so Kendall's method provides a means of simulating an i.i.d. sequence of F values. Initial results suggest that the approach produces useful results for values of m up to at least $m = 10\,000$.

5.5 PROPERTIES OF POISSON VORONOI CELLS

For the Poisson Voronoi diagram \mathcal{V}_P to be used in evaluating empirical tessellations, extensive knowledge of the characteristics of its constituent Poisson Voronoi cells (PVCs) is required. This information includes moments and distributions of individual characteristics of PVCs and correlations between pairs of characteristics.

5.5.1 Moments of the characteristics of Poisson Voronoi cells

Although in principle it should be possible to derive moments analytically, the derivation is notoriously complicated. Møller (1994, Section 4.2, pp. 88–103) demonstrates the complexity and laboriousness of deriving integrals for second-order moments. Several second moments and correlation coefficients of the characteristics of Poisson Voronoi cells in \mathbb{R}^2 and \mathbb{R}^3 have been derived from numerical integration by Gilbert (1962) and Brakke (1986, 1987a,b).

Here we begin by considering first-order moment measures. Many of these can be obtained from general expressions for \mathcal{V}_P in \mathbb{R}^m which can be derived by using either the ergodic theorem (Miles, 1970b, 1974) or the Palm distribution (Møller, 1989, 1994) (see Section 1.3.3).

The expected number of full neighbours of a typical PVC is 2^m (Møller, 1994, equation (4.2.18)), which does not depend on the intensity of the homogeneous Poisson point process. Two cells are full (or Gabriel) neighbours in \mathbb{R}^m if the line joining their generator points intersects their common $(m-1)$ -face (see Section 2.5).

Let λ denote the intensity of the homogeneous Poisson point process Θ_p in \mathbb{R}^m and Θ_{P_s} denote the point process of centroids of the s -faces of the cells of \mathcal{V}_p ($s = 0, \dots, m$) (see Section 5.1). Suppose that the intensity of Θ_{P_s} is λ_s . A main result (Møller, 1989, Theorem 7.2, p. 63) states that the expected value $\lambda_t E_t V_s$ of the total s -dimensional content V_s of the s -faces contained in a typical t -face of \mathcal{V}_p is

$$\lambda_t E_t V_s = \frac{\lambda^{(m-s)/m} 2^{m-s+1} \pi^{(m-s)/2} \Gamma\left(\frac{m^2 - sm + s + 1}{2}\right) \Gamma\left(\frac{m}{2} + 1\right)^{m-s+s/m} \Gamma\left(m - s + \frac{s}{m}\right)}{m (t-s)! (m-t+1)! \Gamma\left(\frac{m^2 - sm + s}{2}\right) \Gamma\left(\frac{m+1}{2}\right)^{m-s} \Gamma\left(\frac{s+1}{2}\right)} \quad (5.5.1)$$

$(0 \leq s \leq t \leq m),$

where E_t denotes expectation with respect to the Palm distribution of the random tessellation with respect to the typical t -face (see Møller, 1989, p. 47). That is to say, V_s is the s -dimensional content of the s -faces contained in a t -face which contains the origin o , and the expectation $E_t V_s$ is the expected value of V_s under the condition that the origin o is exactly the centroid of the t -face containing o (see Section 1.3.3 for the details of the Palm distribution). Note that we omit the parameter t from V_s , which can be written as $V_{s,t}$, in equation (5.5.1) because it already appears in E_t . The expected value $E(V_{s,t})$ is also well-defined; it is the average s -dimensional content of s -faces contained in a t -face which contains the origin o , but o is not necessarily the centroid. In general, $E(V_{s,t}) \geq E_t V_s = E_t V_s$ because a larger t -face has a higher chance of containing a fixed point o (size-biased sampling), and an explicit expression for $E(V_{s,t})$ is not yet known.

If we limit our attention to the m -dimensional polytopes of \mathcal{V}_p , $t = m$ and Θ_{P_m} is the set of centroids of the PVCs, so that $\lambda_m = \lambda$ and equation (5.5.1) reduces to

$$E_m V_s = \frac{2^{m-s+1} \pi^{(m-s)/2} \Gamma\left(\frac{m^2 - sm + s + 1}{2}\right) \Gamma\left(\frac{m}{2} + 1\right)^{m-s+s/m} \Gamma\left(m - s + \frac{s}{m}\right)}{\lambda^{s/m} m (m-s)! \Gamma\left(\frac{m^2 - sm + s}{2}\right) \Gamma\left(\frac{m+1}{2}\right)^{m-s} \Gamma\left(\frac{s+1}{2}\right)} \quad (5.5.2)$$

$(0 \leq s \leq m)$

(see also Miles, 1970b, 1974, equation (75)). Also for $s = 0$ the total s -dimensional content V_0 of the s -faces contained in a t -face is the number N_0 of o -faces (vertices) contained in the t -face, so that

$$\lambda_i E_i N_0 = \frac{\lambda 2^{m+1} \pi^{(m-1)/2} (m-1)! \Gamma\left(\frac{m^2+1}{2}\right)}{t! (m-t+1)! m \Gamma\left(\frac{m^2}{2}\right)} \left\{ \frac{\Gamma\left(\frac{m}{2}+1\right)}{\Gamma\left(\frac{m+1}{2}\right)} \right\}^m \quad (5.5.3)$$

(see Møller, 1989, p. 66, equation (7.6)). Furthermore, setting $t = 0$ in equation (5.5.3) yields

$$\lambda_0 = \frac{\lambda 2^{m+1} \pi^{(m-1)/2} \Gamma\left(\frac{m^2+1}{2}\right)}{m^2 (m+1) \Gamma\left(\frac{m^2}{2}\right)} \left\{ \frac{\Gamma\left(\frac{m}{2}+1\right)}{\Gamma\left(\frac{m+1}{2}\right)} \right\}^m, \quad (5.5.4)$$

so that using equation (5.1.1) from Section 5.1:

$$\lambda_1 = \frac{\lambda 2^m \pi^{(m-1)/2} (m-1)! \Gamma\left(\frac{m^2+1}{2}\right)}{m^2 \Gamma\left(\frac{m^2}{2}\right)} \left\{ \frac{\Gamma\left(\frac{m}{2}+1\right)}{\Gamma\left(\frac{m+1}{2}\right)} \right\}^m. \quad (5.5.5)$$

In accordance with our concern for empirical applications we present the values of equations (5.5.1)–(5.5.5) for $m = 2$ and $m = 3$ in Tables 5.5.1 and 5.5.2, respectively. To minimize the incidence of subscripts in the text, each of these values, $E_m V_s$, is given a simpler symbol which is identified in Tables 5.5.1 and 5.5.2. Many of these values were first obtained individually by Meijering (1953). Also included in Table 5.5.1 are numerical integration values for second moments of the number of vertices (edges) N , the perimeter P (Brakke, 1986, 1987a), and the cell area A (Gilbert, 1962; Hanson, 1983; Brakke, 1986, 1987a) of a typical cell, and the length L of a typical edge (Brakke, 1986, 1987a) and for the expected values of the products PA , NP and NA (Brakke, 1986, 1987a). The values of the last three second-order moments lead to the following correlation coefficients: $r(P, A) = 0.953$, $r(N, P) = 0.501$ and $r(N, A) = 0.568$. Similarly, Table 5.5.2 includes the second moments for the area A , the perimeter P , the number of vertices/edges N of a typical face, the total edge length B , the number of vertices M , edges E and faces F , the surface area S (Brakke, 1987b) and the volume V (Gilbert, 1962; Brakke, 1987b) of a typical cell of a \mathcal{V}_p in \mathbb{R}^3 and estimates of moments of other characteristics from Monte Carlo simulations by various researchers. Each estimate is taken from the study known to the authors which involves the largest number of cells. Each Voronoi cell satisfies the relation that $M + F - E = 2$ and $M = 2F - 4$. Thus, $M = 2E/3$. Note that the value of $E(N) = 6$ in Table 5.5.1 is a specific instance of a general result

$$E(N) = \frac{2\delta_v}{(\delta_v - 2)}, \quad (5.5.6)$$

where δ_v is the mean number of sides meeting at each vertex of the tessellation (i.e. the mean degree of each node when the tessellation is regarded

Table 5.5.1 The first and/or second-order moments of various characteristics of a Poisson Voronoi diagram in \mathbb{R}^2 .

Moment	Symbol	Exact value	Numerical value
Intensity of cell vertices	λ_0	2λ	
Intensity of mid-points of cell edges	λ_1	3λ	
Intensity of cell centroids	λ_2	λ	
Expected total edge length per unit area	L_A	$2\lambda^{1/2}$	
Expected number of vertices/edges of a typical cell [$E_2 N_0 / E_2 N_1$] and its second moment [$E_2(N_0^2) / E_2(N_1^2)$]	$E(N)$ $E(N^2)$	6 37.781	
Expected number of full neighbours of a typical cell	$E(C)$	4	
Expected area of a typical cell [$E_2 V_2$] and its second moment [$E_2(V_2^2)$]	$E(A)$ $E(A^2)$	λ^{-1} 1.280 λ^{-2}	
Expected perimeter of a typical cell [$E_2 V_1$] and its second moment [$E_2(V_1^2)$]	$E(P)$ $E(P^2)$	$4\lambda^{-1/2}$ 16.945 λ^{-1}	
Expected length of a typical edge [$E_1 V_1$] and its second moment [$E_1(V_1^2)$]	$E(L)$ $E(L^2)$	$2/(3\lambda^{1/2})$ 0.630 λ^{-1}	
Expected value of an angle at a typical vertex and its second moment	$E(X_1)$ $E(X_1^2)$	$2\pi/3$ $5\pi^2/9 - 5/6$	2.094 4.650
Expected product of the perimeter and the area of a typical cell [$E_2(V_1 V_2)$]	$E(PA)$	$4.491\lambda^{-32}$	
Expected product of the number of vertices/edges and the perimeter of a typical cell [$E_2(N_0 V_1) E_2(N_1 V_1)$]	$E(NP)$	24.651 $\lambda^{-1/2}$	
Expected product of the number of vertices/edges and the area of a typical cell [$E_2(N_0 V_2) E_2(N_1 V_2)$]	$E(NA)$	6.401 λ^{-1}	

$\lambda = \text{intensity of } \Theta_P$.

Sources: Meijering (1953), Gilbert (1962), Hanson (1983) and Brakke (1986, 1987a).

as an infinite graph, see Section 1.3.2), which holds for all homogeneous random planar tessellations (Matschinski, 1954). Coefficients of variation and the correlation coefficients derived from numerical integration by Brakke (1987b) or estimated from simulation studies are tabulated in Tables 5.5.3 and 5.5.4. The correlation coefficients will remain unchanged if M is replaced by F or E .

5.5.2 Conditional moments of the characteristics of Poisson Voronoi cells

For $m = 2$, in addition to the unconditional moments reported in Table 5.5.1, Quine and Watson (1984, Tables 1 and 2) also estimate the first four conditional moments for the area A and perimeter P , given the number of vertices (sides) N of a PVC. The conditional moments of A are also estimated by Crain (1978), Drouffe and Itzykson (1984), Le Caer and Ho (1990) and Kumar and Kurtz (1993). Crain (1978) and Kumar and Kurtz (1993) have also estimated the conditional moments of P . The conditional moments of the length of a cell edge L have been studied by Boots (1987) and Kumar and Kurtz (1993). Estimates of the first conditional moments obtained by them are summarized in Table 5.5.5. We also report estimates of the second conditional moments obtained by Kumar and Kurtz (1993) in Table 5.5.6. On the basis of the results for A , Quine and Watson (1984) conjectured that

$$E(A|N) = \frac{2N - 3}{9\lambda}, \quad (5.5.7)$$

where $E(A|N)$ is the conditional expectation of the area A , given that the number of vertices (sides) is N , which is consistent with $E(A) = \lambda^{-1}$, but they are unable to offer a proof. The values for $E(A|N)$ in Table 5.5.5 are also consistent with the so-called *Lewis' law* which describes a linear relationship between $E(A|N)$ and N of the form

$$E(A|N) = \frac{b}{\lambda} (N - 6) + \frac{1}{\lambda}, \quad (5.5.8)$$

where b is a constant. This relationship was originally observed for a variety of biological tessellations (including cucumber epidermis and pigmented epithelium of the retina) (Lewis, 1928, 1930, 1931, 1943, 1944). Rivier and Lissowski (1982) and Rivier (1985a) tried to derive equation (5.5.8) by using the maximum entropy argument, but their argument was shown to be incorrect by Chiu (1995a). Thus, equation (5.5.8) remains an empirical law. See Chiu (1995b) for a review.

Least squares fits of the data in Table 5.5.5 to equation (5.5.8) yield values of $b = 0.199$ (correlation coefficient $r = 0.9906$, Quine and Watson, 1984), 0.219 ($r = 0.9991$, Crain, 1978, assuming that the columns for the conditional average second moment of the perimeter and for the average area have been mistakenly transposed; otherwise $b = 0.178$ and $r = 0.9987$), 0.226 ($r = 0.9997$, Kumar and Kurtz, 1993), 0.228 ($r = 0.9999$, Le Caer and Ho, 1990), 0.257 ($r = 0.9998$, Drouffe and Itzykson, 1984). There is an obvious

Table 5.5.2 The first and/or second-order moments of various characteristics of a Poisson Voronoi diagram in \mathbb{R}^3 .

Moment	Symbol	Exact value	Numerical value	Estimate
Intensity of cell vertices	λ_0	$(24/35) \pi^2 \lambda$	6.768 λ	
Intensity of mid-points of cell edges	λ_1	$(48/35) \pi^2 \lambda$	13.535 λ	
Intensity of centroids of cell faces	λ_2	$(24\pi^2/35 + 1) \lambda$	7.768 λ	
Intensity of cell centroids	λ_3	λ		
Expected total face area per unit volume	S_V	$4(\pi/6)^{1/3} \Gamma(5/3) \lambda^{1/3}$	$2.910\lambda^{1/3}$	
Expected total edge length per unit volume	L_V	$(16/15)(3/4)^{1/3} \pi^{5/3} \Gamma(4/3) \lambda^{2/3}$	$5.832 \lambda^{2/3}$	
Expected number of vertices of a typical cell $[E_3 N_0]$ and its second moment $[E_3(N_0^2)]$	$E(M)$	$(96/35) \pi^2$	27.071	
Expected number of edges of a typical cell $[E_3 N_1]$ and its second moment $[E_3(N_1^2)]$	$E(M^2)$		776.823	
Expected number of faces of a typical cell $[E_3 N_2]$ and its second moment $[E_3(N_2^2)]$	$E(E)$	$(144/35) \pi^2$	40.606	
Expected number of full neighbours of a typical cell and its second moment	$E(F)$	$(48\pi^2/35) + 2$	1747.852	
Expected number of faces of a typical cell $[E_3 N_2]$ and its second moment $[E_3(N_2^2)]$	$E(F^2)$		15.535	
Expected number of full neighbours of a typical cell and its second moment	$E(C)$	8	252.348	
Expected volume of a typical cell $[E_3 V_3]$ and its second moment $[E_3(V_3^2)]$	$E(C^2)$		8	
Expected surface area of a typical cell $[E_3 V_2]$ and its second moment $[E_3(V_2^2)]$	$E(V)$	λ^{-1}	68.155 †	
Expected total edge length of a typical cell $[E_3 V_1]$ and its second moment $[E_3(V_1^2)]$	$E(V^2)$			
Expected number of vertices/edges of a typical face $[E_2 N_0 E_2 N_1]$ and its second moment $[E_2(N_0^2)/E_2(N_1^2)]$	$E(S)$	$(256\pi/3)^{1/3} \Gamma(5/3) \lambda^{-2/3}$	$1.180\lambda^{-2}$	
	$E(S^2)$		$5.821\lambda^{-2/3}$	
	$E(B)$	$(4\pi)^{5/3} \Gamma(1/3)/[5(9\lambda)^{1/3}]$	$36.070\lambda^{-4/3}$	
	$E(B^2)$		$17.496\lambda^{-1/3}$	
	$E(N)$	$144\pi^2/(24\pi^2 + 35)$	319.738 $\lambda^{-2/3}$	
	$E(N^2)$		5.228	
			29.825	

Table 5.5.2 continued

Moment	Symbol	Exact value	Numerical value	Estimate
Expected area of a typical face [$E_2 V_2$]	$E(A)$	$35(2)^{8/3} \pi^{1/3} \Gamma(2/3) / [(9\lambda)^{2/3} (24\pi^2 + 35)]$	$0.375\lambda^{-2/3}$	
and its second moment [$E_2(V_2^2)$]	$E(A^2)$		$0.283\lambda^{-4/3}$	
Expected total edge length of a typical face [$E_2 V_1$]	$E(P)$	$7(2)^{10/3} \pi^{5/3} \Gamma(1/3) / [(9\lambda)^{1/3} (24\pi^2 + 35)]$	$2.252\lambda^{-1/3}$	
and its second moment [$E_2(V_1^2)$]	$E(P^2)$		$6.540\lambda^{-2/3}$	
Expected length of a typical edge [$E_1 V_1$]	$E(L)$	$7 \Gamma(1/3) / [9(36\pi\lambda)^{1/3}]$	$0.431\lambda^{-1/3}$	
and its second moment [$E_1(V_1^2)$]	$E(L^2)$		$0.291\lambda^{-2/3}$	
Expected average breadth	$E(b)$	$[(16\pi)^2/243\lambda]^{1/3} [\Gamma(1/3)/5]$	$1.458\lambda^{-1/3}$	
and its second moment	$E(b^2)$		$2.156\lambda^{-2/3}\dagger$	
Expected value of a dihedral angle of a typical cell	$E(\alpha_i)$		2.068°	
and its second moment	$E(\alpha_i^2)$		4.456°	
Expected value of an interior angle of a typical face	$E(\alpha_e)$		1.940^*	
and its second moment	$E(\alpha_e^2)$		4.150^*	
Expected value of a dihedral angle on a typical edge	$E(\alpha_t)$	$2\pi/3$	2.094	
and its second moment	$E(\alpha_t^2)$	$\pi^2/2 - 3/8$	4.560	
Expected value of an angle at a typical vertex	$E(\gamma)$	$(48\pi^2 - 35)/(72\pi)$	1.940	
and its second moment	$E(\gamma^2)$	$(48\pi^2 - 175)/72$	4.149	

 $\lambda =$ intensity of Θ_P . \dagger Estimates from Monte Carlo simulation by Lorz and Hahn (1993).

* Estimates from Monte Carlo simulation by Quine and Watson (1984).

* Estimates from Monte Carlo simulation by Kumar and Kurtz (1995).

Sources of unmarked values: Gilbert (1962), Miles (1972a), Brakke (1987b) and Möller (1989*, 1994).
 * There are typos in the formulae for $E(S)$ [$E_3 V_2$], $E(P)$ [$E_2 V_1$] and $E(L)$ [$E_1 V_1$] in Möller (1989, p. 67).

Table 5.5.3 Coefficients of variation (c.v.) and correlation coefficients for various characteristics of a typical Poisson Voronoi cell in \mathbb{R}^3 .

	<i>V</i>	<i>S</i>	<i>B</i>	<i>M</i>	\bar{b}	α_3
c.v.	0.423*	0.254*	0.211*	0.246*	0.120†	0.204†
<i>V</i>	—	0.982*	0.938*	0.736*	0.945†	0.187†
<i>S</i>	—	—	0.924*	0.712*	0.987†	0.180†
<i>B</i>	—	—	—	0.875*	0.898†	0.222†
<i>M</i>	—	—	—	—	0.671†	0.247†
\bar{b}	—	—	—	—	—	0.170†

Characteristics:

V = volume*F* = number of faces/cell*S* = surface area/cell*M* = number of vertices/cell = $2F - 4 = 2E/3$ *B* = total edge length/cell \bar{b} = mean breadth/cell*E* = number of edges/cell α_3 = face angle of a cell

Sources: * Numerical values from Brakke (1987b) (see also Møller, 1994, Table 4.2.7).

† Estimates from Monte Carlo simulations by Lorz and Hahn (1993).

Table 5.5.4 Coefficients of variation (c.v.) and correlation coefficients for various characteristics of typical faces and edges of a Poisson Voronoi cell in \mathbb{R}^3 .

	<i>N</i>	<i>L</i>	<i>A</i>	<i>P</i>	α_2	α_1
c.v.	0.302*	0.753*	1.007*	0.538*	0.321†	0.199*
<i>N</i>	—	—	0.750*	0.746*	0.577†	—
<i>A</i>	—	—	—	0.928*	0.418†	—
<i>P</i>	—	—	—	—	0.456†	—
<i>L</i>	—	—	—	—	—	-0.000†

Characteristics:

N = number of vertices (edges)/face*P* = total edge length/face*L* = edge length α_2 = interior angle of a face*A* = area/face α_1 = face (dihedral) angle at an edge

Sources: * Numerical values from Brakke (1987b) (see also Møller, 1994, Table 4.2.6).

† Estimate from Monte Carlo simulations by Kumar and Kurtz (1995).

* Exact value = $\sqrt{1/8 - 27/(32\pi^2)}$.

† Estimates from Monte Carlo simulations by Lorz (1990b).

Table 5.5.5 Estimates of the first conditional moments of various characteristics of a typical Poisson Voronoi cell in \mathbb{R}^2 .

N	$\lambda E(A N)$					$\lambda^{1/2}E(P N)$			$\lambda^{1/2}E(L N)$		
	a	b	c	d	e	c	d	e	e	f	
3	0.342	0.342	0.359	0.360	0.342	2.803	2.828	2.747	0.916	0.910	
4	0.560	0.558	0.558	0.567	0.559	3.217	3.260	3.225	0.806	0.805	
5	0.777	0.774	0.778	0.773	0.774	3.650	3.660	3.647	0.729	0.733	
6	0.996	0.996	0.995	0.994	0.996	4.030	4.040	4.032	0.672	0.672	
7	1.228	1.222	1.223	1.214	1.222	4.382	4.396	4.385	0.627	0.625	
8	1.463	1.451	1.447	1.447	1.454	4.701	4.728	4.717	0.590	0.590	
9	1.693	1.688	1.661	1.710	1.688	4.981	5.068	5.029	0.559	0.553	
10	1.930	1.938	1.868	1.850	1.932	5.244	5.240	5.334	0.534	0.519	
11	2.155	2.16	2.063		2.173	5.475		5.625	0.512	0.512	
12	2.400	2.37	1.990		2.371	5.415		5.847	0.488	0.473	
13	2.691	2.6			2.555			6.049	0.465		
14	2.930								0.446		
15	3.200										
16	3.46										
18	4.00										
20	4.53										
25	5.84										
30	7.17										
35	8.42										
40	9.73										
45	11.02										
50	12.28										

λ = intensity of Θ_P .

Characteristics:

A = area of a cell

N = number of vertices (edges)

L = edge length

P = perimeter of a cell

Sources:

a Drouffe and Itzykson (1984, Table 1). Number of cells = 27 000.

b Le Caér and Ho (1990, Table 6). Numbers of cells = 600 696, 1 001 500 and 1 020 800.

c Quine and Watson (1984, Tables 1 and 2). Number of cells = 50 000.

d Crain (1978, Table III). Number of cells = 25 000.

e Kumar and Kurtz (1993, Tables 8, 9 and 10). Number of cells = 2 000 000.

f Boots (1987, Table 1). Number of cells = 30 000.

change in the slope in Drouffe and Itzykson (1984) for $n > 12$; their data for $n \leq 11$ yield $b = 0.228$ and $r = 0.9999$.

Szeto and Tam (1995) found in their study that *Feltham's law*, which states that $E(P|N)$ is linear in N , has a comparable but smaller statistical error than Lewis' law for PVCs. However, the correlation coefficients of $E(P|N)$ and N obtained from other studies (0.9835, Quine and Watson, 1984; 0.9959, Crain, 1978; 0.9941, Kumar and Kurtz, 1993) suggested the opposite, because these values are smaller than the corresponding correlation coefficients

Table 5.5.6 Estimates of the second conditional moments of various characteristics of a typical Poisson Voronoi cell in \mathbb{R}^2 .

N	$\lambda^2 E(A^2 N)$	$\lambda E(P^2 N)$	$\lambda E(L^2 N)$
3	0.161	8.208	0.952
4	0.399	11.064	0.806
5	0.730	13.965	0.710
6	1.168	16.921	0.637
7	1.717	19.899	0.578
8	2.386	22.919	0.530
9	3.172	25.974	0.489
10	4.096	29.125	0.456
11	5.131	32.321	0.428
12	6.007	34.791	0.392
13	6.897	37.068	0.366
14	—	—	0.309

λ = intensity of Θ_p .

Characteristics:

A = area of a cell

N = number of vertices (edges)

L = edge length

P = perimeter of a cell

Sources: Kumar and Kurtz (1993, Tables 8, 9 and 10). Number of cells = 2 000 000.

of $E(A|N)$ and N . Kumar and Kurtz (1993), on the basis of two million simulated PVCs in \mathbb{R}^2 (except for three-sided cells which are based on the simulation of one million cells), suggested empirically that

$$\lambda^{1/2} E(P|N) = 1.4879 N^{0.5519}.$$

Estimations of the correlations $r(A, P|N)$ between A and P , controlling for N , are given by Crain (1978, Table 3). His results show that in general $r(A, P|N)$ increases with N , indicating increasing 'circularity'.

For $m = 3$, the first four conditional moments of the volume V , the surface area S , the total edge length B , the mean breadth \bar{b} , and a randomly selected face (dihedral) angle α_3 of a typical PVC, the number of edges N and an interior angle α_2 of a typical face, and the length L of and the face angle α_1 at a typical edge, given the number of faces F , have been estimated from Monte Carlo simulation by various researchers (see Table 5.5.7). Also, the first two conditional moments of the face area A , the face perimeter P and an interior angle α_2 of a typical face, given the number of edges N , have been estimated. We report only the estimates for the first conditional moments of these characteristics (see Tables 5.5.8 and 5.5.9). Note that

$$E(N|F) = 6 - \frac{12}{F}$$

(see Zallen, 1983).

Table 5.5.7 Simulation studies for the conditional moments of various characteristics of Poisson Voronoi cells in \mathbb{R}^3 .

Study	Number of cells	Characteristics	
		Conditional on F	Conditional on N
Quine and Watson (1984)	2 500	$B S V$	
Lorz (1990b)	82 870	$B S V \bar{b} \alpha_3$	$A P \alpha_2$
Kumar <i>et al.</i> (1992)	358 000	N	
	102 000	$L S V$	$A L$
Kumar and Kurtz (1995)	377 000	$\alpha_1 \alpha_2$	$P \alpha_2$
	165 000	B	

Characteristics:

A = area/face

S = surface area/cell

B = total edge length/cell

V = volume

F = faces/cell

\bar{b} = mean breadth/cell

L = edge length

α_1 = face (dihedral) angle at an edge

N = edges/face

α_2 = interior angle of a face (bond angle)

P = edge length/face

α_3 = face angle of a cell

The values of the mean volume $E(V|F)$ of a typical cell conditional on its number of faces F in Table 5.5.8 show a reasonable fit with the three-dimensional version of Lewis' law (equation (5.5.8)) suggested by Rivier (1982, 1983a,b, 1985a, 1986a) and given by

$$E(V|F) = \frac{b}{\lambda}(F - E(F)) + \frac{1}{\lambda}, \quad (5.5.9)$$

where λ is the intensity of Θ_p and b is a constant. Similar to equation (5.5.8), equation (5.5.9) cannot be derived from the maximum entropy argument (Chiu, 1995a) and remains an empirical law. Values of Kumar *et al.* (1992), Lorz (1990b), and Quine and Watson (1984) in Table 5.5.8 lead to correlation coefficients and least squares estimates of $r = 0.9982$ and $b = 0.0942$, $r = 0.9897$ and $b = 0.095$, and $r = 0.9863$ and $b = 0.084$, respectively, for equation (5.5.9). Kumar *et al.* (1992) and Kumar and Kurtz (1995), based on their simulation studies, suggested empirically that

$$\begin{aligned} E(V|F) &= 0.0942F - 0.4338, \\ E(S|F) &= 0.3102F + 1.002, \\ E(B|F) &\approx 0.9647F + 2.5078, \\ E(A|N) &= 0.1812N - 0.5725, \\ E(P|N) &= 3.0534 \ln N - 2.7968. \end{aligned}$$

$$\begin{aligned} E(V|F) &= 0.0164F^{1.498}, \\ E(S|F) &= 0.5614F^{0.8526}, \\ E(B|F) &= 1.6552F^{0.8596}, \end{aligned}$$

Such equations are no more than a good empirical approximation and have not been theoretically justified.

Table 5.5.8 Estimates of the first conditional moments of various characteristics of a typical Poisson Voronoi cell in \mathbb{R}^3 .

F	$\lambda E(V F)$			$\lambda^{23} E(S F)$			$\lambda^{13} E(B F)$			$\lambda^{13} E(\bar{b} F)$			$\lambda^{13} E(L F)$			$E(\alpha_1 F)$		
F	a	b	c	a	b	c	d	b	b	d	b	b	d*	a	d*	a	d*	
4	-	-	-	-	-	-	-	-	-	-	-	-	-	-	-	-	-	
5	-	0.160	-	-	-	2.192	-	-	7.096	0.939	1.420	1.396	-	0.637	1.402	-	-	
6	0.216	0.225	0.179	2.426	2.628	7.855	8.046	1.042	1.571	1.571	0.365	0.365	1.543	1.543	1.543	1.543	1.543	
7	0.288	0.277	0.218	2.898	2.858	8.923	8.967	1.082	1.630	1.676	0.338	0.338	1.639	1.639	1.639	1.639	1.639	
8	0.350	0.342	0.356	3.243	3.183	9.977	9.861	1.127	1.770	1.745	0.348	0.348	1.726	1.726	1.726	1.726	1.726	
9	0.431	0.423	0.400	3.663	3.616	11.033	10.955	1.192	1.774	1.795	0.345	0.345	1.796	1.796	1.796	1.796	1.796	
10	0.507	0.511	0.507	4.009	4.018	12.058	12.074	1.246	1.864	1.833	0.342	0.342	1.857	1.857	1.857	1.857	1.857	
11	0.586	0.590	0.583	4.336	4.359	13.047	13.081	1.290	1.916	1.862	0.337	0.337	1.910	1.910	1.910	1.910	1.910	
12	0.669	0.670	0.697	4.683	4.686	14.066	14.049	1.331	1.952	1.885	0.334	0.334	1.956	1.956	1.956	1.956	1.956	
13	0.760	0.759	0.754	5.033	5.029	15.056	15.045	1.372	2.001	1.904	0.331	0.331	1.997	1.997	1.997	1.997	1.997	
14	0.852	0.844	0.834	5.371	5.340	16.055	15.999	1.408	2.032	1.920	0.328	0.328	2.034	2.034	2.034	2.034	2.034	
15	0.942	0.940	0.940	5.689	5.691	17.020	17.018	1.449	2.066	1.933	0.326	0.326	2.068	2.068	2.068	2.068	2.068	
16	1.034	1.031	1.040	5.994	5.996	17.989	17.970	1.483	2.093	1.945	0.323	0.323	2.099	2.099	2.099	2.099	2.099	
17	1.129	1.127	1.141	6.316	6.308	18.967	18.943	1.516	2.132	1.955	0.321	0.321	2.127	2.127	2.127	2.127	2.127	
18	1.225	1.225	1.218	6.615	6.620	19.902	19.898	1.549	2.154	1.964	0.318	0.318	2.153	2.153	2.153	2.153	2.153	
19	1.316	1.328	1.273	6.899	6.934	20.887	20.860	1.581	2.180	1.971	0.316	0.316	2.176	2.176	2.176	2.176	2.176	
20	1.426	1.429	1.463	7.230	7.234	21.822	21.860	1.611	2.209	1.978	0.315	0.315	2.199	2.199	2.199	2.199	2.199	
21	1.516	1.518	1.582	7.497	7.494	22.799	22.691	1.637	2.227	1.984	0.313	0.313	2.220	2.220	2.220	2.220	2.220	
22	1.622	1.636	1.603	7.790	7.836	23.711	23.725	1.671	2.235	1.990	0.311	0.311	2.239	2.239	2.239	2.239	2.239	
23	1.729	1.715	1.794	8.092	8.058	24.673	24.542	1.693	2.258	1.995	0.310	0.310	2.258	2.258	2.258	2.258	2.258	
24	1.854	1.822	1.861	8.422	8.334	25.478	25.519	1.717	2.283	1.999	0.308	0.308	2.275	2.275	2.275	2.275	2.275	
25	1.958	1.944	1.926	8.724	8.693	26.350	26.474	1.753	-	-	-	-	2.290	2.290	2.290	2.290	2.290	

Table 5.5.8 continued

F	$\lambda E(V F)$			$\lambda^{23} E(S F)$			$\lambda^{13} E(B F)$			$\lambda^{13} E(\bar{b} F)$			$E(\alpha_3 F)$			$\lambda^{13} E(L F)$			$E(\alpha_1 F)$				
	a	b	c				d	b				b				d'	a				d''		
				a	b	c			d	b	d		b	d	b			d	d	d			
26	2.062	1.988	1.885	8.969	8.787	27.653	27.063	1.761	2.321	2.007	0.311	2.307											
27	2.154	2.149	-	9.243	9.226	28.206	28.161	1.802	2.312	2.011	0.300	2.322											
28	2.247	2.285	-	9.538	9.575	29.500	29.390	1.833	2.366	2.014	0.304	2.333											
29	-	2.553	1.878	-	10.150	30.552	30.373	1.876	2.226	2.017	0.296	2.346											
30	-	2.106	-	-	9.010	-	29.881	1.773	2.229	2.020	0.309	2.352											
31	-	2.838	2.072	-	11.192	-	31.026	1.984	2.378	2.022	0.287	2.375											
32	-	-	-	-	-	-	-	-	-	-	-	-											

λ = intensity of Θ_F

Characteristics:

B = total edge length/cell

F = number of faces/cell

L = edge length

S = surface area/cell

V = volume

\bar{b} = mean breadth/cell
 α_1 = face (dihedral) angle at an edge
 α_2 = interior angle of a face (bond angle)
 α_3 = face angle of a cell

Sources:

a Kumar *et al.* (1992, Tables VI, VII and IX). Number of cells = 102 000.

b Lorz (1990b). Number of cells = 82 870.

c Quine and Watson (1984, Table 4). Number of cells = 2 500.

d Kumar and Kurtz (1995, Table 7). Number of cells = 165 000.

d' Kumar and Kurtz (1995, Tables 3 and 4). Number of cells = 377 000.

Table 5.5.9 Estimates of the first conditional moments of various characteristics of a typical face of a Poisson Voronoi cell in \mathbb{R}^3 .

N	$\lambda^{2/3} E(A N)$		$\lambda^{1/3} E(P N)$		$\lambda^{1/3} E(L N)$		$E(\alpha_2 N)$	
	a	c	b	c	a	b	c	
3	0.046	0.035	0.752	0.754	0.251	1.047	1.048	
4	0.139	0.136	1.531	1.528	0.382	1.571	1.571	
5	0.304	0.303	2.240	2.237	0.448	1.885	1.884	
6	0.505	0.504	2.833	2.831	0.473	2.095	2.095	
7	0.709	0.709	3.310	3.309	0.473	2.244	2.245	
8	0.907	0.908	3.696	3.699	0.462	2.357	2.358	
9	1.092	1.095	4.018	4.024	0.447	2.444	2.448	
10	1.263	1.260	4.279	4.278	0.429	2.513	2.512	
11	1.433	1.432	4.521	4.530	0.413	2.571	2.573	
12	1.561	1.537	4.721	4.665	0.393	2.618	2.632	
13	1.766	1.724	4.923	4.933	0.384	2.658	2.706	
14	1.839	1.807	5.141	5.152	0.364	2.693	2.639	
15	1.859	2.166	—	5.532	0.335	2.723	2.778	

λ = intensity of \mathcal{V}_p .

Characteristics:

A = area/face

P = total edge length/face

L = individual edge length

α_2 = interior angle of a face (bond angle)

N = number of vertices (edges)/face

Sources:

a Kumar *et al.* (1992, Table VIII). Number of cells = 102 000.

b Kumar and Kurtz (1995, Tables 5 and 6). Number of cells = 377 000.

c Lorz (1990b). Number of cells = 82 870.

5.5.3 Conditional moments of the characteristics of the neighbouring cells of a Poisson Voronoi cell

In some areas of application, particularly materials science and geography, there is considerable interest in how individual cells are arranged within \mathcal{V}_p . Although \mathcal{V}_p is an ergodic tessellation, we know that characteristics of an individual cell cannot be independent of those of contiguous cells. So far these dependences have been explored by examining the relationships between the value of a given characteristic for an individual cell and the mean value of that characteristic for contiguous cells. The most extensively studied characteristic is m_n , the first conditional moment of the number of edges of a randomly selected neighbouring cell of a typical PVC, given that the typical PVC has n edges. Aboav (1970) found empirically that in the cellular structure of a polycrystal,

$$m_n = 5 + \frac{8}{n}.$$

The value of the coefficient of n^{-1} is not always 8 but depends on the structure of the tessellation. Let N denote a random variable having the same

distribution as the random number of edges of a typical cell. Denote $\Pr\{N = n\}$ by p_n . Weaire (1974) showed that

$$\sum m_n np_n = \text{Var}(N) + 36, \quad (5.5.10)$$

where $\text{Var}(N)$ is the variance of N , and suggested semi-empirically that

$$m_n = 5 + \frac{6 + \text{Var}(N)}{n}. \quad (5.5.11)$$

Later Aboav (1980) proposed

$$m_n = 6 - a + \frac{6a + \text{Var}(N)}{n},$$

where a is a parameter which depends on the structure of the tessellation.

Numerous empirical studies of the relation between m_n and n have been done. See Chiu (1995b) for a review. Most of the studies suggested that $m_n n$ is linear in n with slope 5, where $m_n n$ is the conditional mean of the total number of edges of all neighbouring cells of a typical cell, given that it has n edges. However, deviations do exist. Peshkin *et al.* (1991) used a maximum entropy argument to 'prove' the linearity between $m_n n$ and n . Chiu (1994, 1995a) showed that their argument is incorrect and established the rigorous relation between m_n and n . Denote by $k(n, j)$ the average number of n -edged cells of a typical j -complex. A j -complex is the collection of a j -edged

Table 5.5.10 Estimates of m_n , the first conditional moments of the number of edges of a randomly selected neighbouring cell of a typical Poisson Voronoi cell in \mathbb{R}^2 , given that the typical cell has n edges.

Boots and Murdoch (1983)		Le Caër and Ho (1990)	Kumar and Kurtz (1993)
50 000 cells		1 020 800 cells	650 000 cells
		1 001 500 cells	
		600 696 cells	
n	m_n	m_n	m_n
3	7.013	7.009	7.017
4	6.731	6.718	6.719
5	6.493	6.492	6.485
6	6.312	6.315	6.312
7	6.169	6.171	6.167
8	6.048	6.050	6.044
9	5.932	5.948	5.948
10	5.841	5.859	5.850
11	5.779	5.78	5.774
12	5.655	—	5.703
13	5.615	—	5.615
14	5.5	—	—

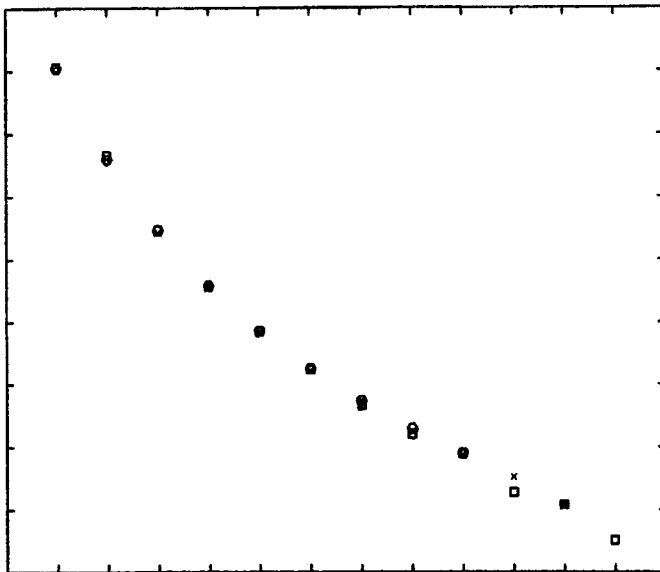


Figure 5.5.1 Values of m_n for Poisson Voronoi cells in \mathbb{R}^2 (values from: \square Boots and Murdoch, 1983; \times Le Caer and Ho, 1990; \circ Kumar and Kurtz, 1993).

cell and all its neighbouring cells. Let c_n denote the covariance between $k(n, N)$ and N . Chiu (1994) has shown that for a stationary regular tessellation in \mathbb{R}^2 ,

$$m_n = 5 + \frac{6 + c_n/p_n}{n}, \quad p_n > 0. \quad (5.5.12)$$

Note that if $p_n = 0$, then m_n is undefined. A general equation similar to equation (5.5.12) for a regular and normal stationary tessellation in \mathbb{R}^m has also been derived. Since in many natural two-dimensional tessellations, $3 \leq n \leq 8$ and both c_n and p_n do not vary too much with n , the ratio c_n/p_n may be well approximated by a constant or a linear function of n . Thus, equation (5.5.12) explains the empirical linearity between m_n , n and n . However, for Poisson Voronoi diagrams, theoretical values of c_n are unknown. Thus, it is desirable to find a good and simple approximation of m_n for \mathcal{V}_p . Table 5.5.10 and Figure 5.5.1 give the simulated values of m_n by Boots and Murdoch (1983), Le Caer and Ho (1990) and Kumar and Kurtz (1993).

Although the data show a reasonably good fit to

$$m_n = B_0 + \frac{B_1}{n}, \quad (5.5.13)$$

for some constants B_0 and B_1 , deviations do exist. Boots and Murdoch (1983) suggested the form

$$m_n = B_0 + \frac{B_1}{n} + \frac{B_2}{n^2}, \quad (5.5.14)$$

whilst Le Caér and Ho (1990) suggested

$$m_n = B_0 + \frac{B_1}{n} + B_3 n, \quad (5.5.15)$$

which means that m_n , n is not a linear but a quadratic function of n . The least squares estimates and the coefficients of determination are summarized in Table 5.5.11. Either equation (5.5.14) or (5.5.15) gives a higher coefficient of determination than equation (5.5.13). Kumar *et al.* (1994) used equation (5.5.29) to argue heuristically that

$$m_n = 4.942 + \frac{7.223}{n} - \frac{6.543}{n^2}, \quad (5.5.16)$$

which has the same form as equation (5.5.14) but the values of the parameters are rather different from those obtained in simulation studies (see Table 5.5.11). Aboav (1987) has also suggested the following equation, which is devoid of any arbitrary constants:

$$m_n = E(N) + \frac{2}{n} + \frac{E(N^{1/2}) - n^{1/2}}{2}, \quad (5.5.17)$$

although he offers no theoretical support for this form. Equation (5.5.17) is not valid for all Voronoi diagrams, since putting equation (5.5.17) into the sum rule given in equation (5.5.10) yields

$$\text{Var}(N) = 2 + \frac{E(6N^{1/2}) - E(N^{3/2})}{2},$$

which is approximately true for Poisson Voronoi diagrams but not for Voronoi diagrams generated by eigenvalues of random matrices (Le Caér and Ho, 1990).

The empirical Aboav's law and all its variations suggest that few-edged cells are more likely to be in contact with many-edged cells and vice versa, which was already observed in planar tessellations seen in epithelia by Lewis (1931). Moreover, the empirical Lewis' law given in equation (5.5.8) suggests that a many-edged cell is more likely to be a large cell. Hence, the area of a given cell and the areas of its neighbouring cells are negatively correlated (see, for example, Seul *et al.*, 1994, Figure 3).

Since the number of edges of a cell is influenced by its neighbouring cells, which in turn are under the influence of their neighbouring cells, *neighbours of higher orders* will also affect the number of edges of a cell. Fortes and Pina (1993) considered such higher order neighbouring relations. Let a typical cell be the zeroth-order neighbour and all its neighbouring cells be the first-order neighbours. The neighbouring cells of a first-order neighbour, excluding the zeroth-order and all other first-order neighbours, are the second-order neighbours. Inductively, the k th-order neighbours can be defined. Let the mean total number of k th-order neighbours of a typical cell, given that this typical cell has n edges, be denoted by $q_n^{(k)}$ and the number of edges of a randomly selected k th-order neighbour by $m_n^{(k)}$. Fortes and Pina (1993) found empirically that $q_n^{(k)}$ and $q_n^{(k)}m_n^{(k)}$ are linear in n for $k = 1, 2, 3$ and 4.

Table 5.5.11 Least squares regressions for various approximations of m_n and the corresponding coefficients of determination R^2 .

Boots and Murdoch (1983)		Le Caer and Ho (1990)		Kumar and Kurtz (1993)	
m_n	R^2	m_n	R^2	m_n	R^2
$5.251 + \frac{5.755}{n}$	0.959	$5.399 + \frac{5.012}{n}$	0.977	$5.312 + \frac{5.474}{n}$	0.971
$4.823 + \frac{11.428}{n} - \frac{14.724}{n^2}$	0.996	$5.010 + \frac{9.615}{n} - \frac{10.901}{n^2}$	1.000	$4.935 + \frac{10.270}{n} - \frac{12.181}{n^2}$	0.998
$6.165 + \frac{3.164}{n} - 0.063n$	0.999	$6.178 + \frac{3.094}{n} - 0.063n$	1.000	$6.100 + \frac{3.306}{n} - 0.057n$	1.000

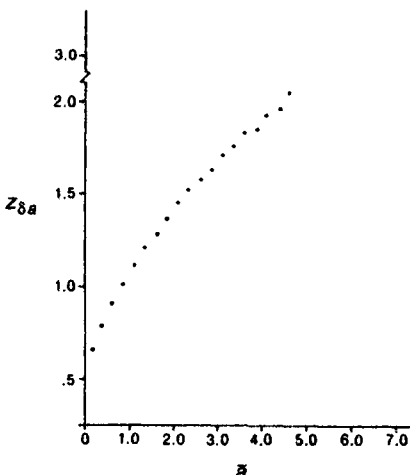


Figure 5.5.2 Values of $z_{\delta a}$ for Poisson Voronoi cells in \mathbb{R}^2 . (Source: Boots and Murdoch, 1983.)

Delannay *et al.* (1992) introduced the *topological correlation function* A_{kn} , which is defined as

$$A_{jn} = \frac{M_j(n)}{p_j},$$

where $M_j(n)$ is the average number of j -edged neighbouring cells of a typical n -edged cell. They used A_{jn} to compare the topological properties of tessellations which show different distributions of number of cell edges. Clearly, A_{jn} satisfies

$$A_{jn} = A_{nj}, \quad A_{jn} \geq 0,$$

$$\sum_j A_{jn} p_j = n, \quad \sum_j j A_{jn} = nm_n.$$

For Voronoi diagrams, since two 3-edged cells cannot share an edge without creating at least one non-convex cell, we have $A_{33} = 0$. Further discussions on A_{jn} can be found in Delannay *et al.* (1993, 1994) and Le Caer and Delannay (1993a,b).

Boots and Murdoch (1983) also estimate the relationships between neighbouring cells for the standardized measures of the area and perimeter of a PVC in \mathbb{R}^2 . Denote by $z_{\delta a}$ the average value of the standardized area λA of the neighbouring cells of a typical PVC, given that the standardized area of the typical PVC is in the interval δa . Values of $z_{\delta a}$ are illustrated in Figure 5.5.2. The relationship may be summarized by

$$z_{\delta a} = b_0 + b_1 \bar{a}^{1/2} + b_2 \bar{a}, \quad (5.5.18)$$

where $b_0 = 0.364$, $b_1 = 0.629$, $b_2 = 0.080$ and \bar{a} is the midpoint of the interval δa . Finally, denote by $r_{\delta p}$ the average value of the standardized perimeter $\lambda^{1/2} P/4$ for the neighbouring cells of a typical PVC, given that the standardized

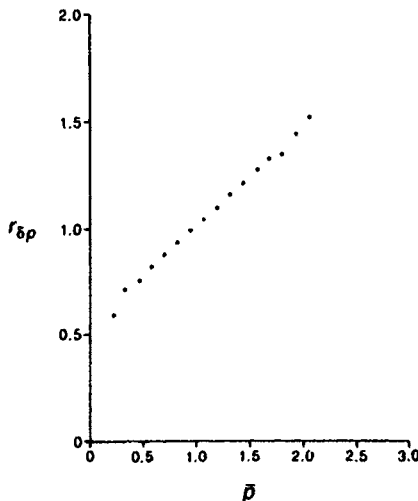


Figure 5.5.3 Values of $r_{\delta p}$ for Poisson Voronoi cells in \mathbb{R}^2 .
 (Source: Boots and Murdoch, 1983.)

perimeter of the typical PVC is in the interval δp . Values of $r_{\delta p}$ are shown in Figure 5.5.3. These values indicate a linear relationship described by

$$r_{\delta p} = b_0 + b_1 \bar{p}, \quad (5.5.19)$$

where $b_0 = 0.564$, $b_1 = 0.456$ and \bar{p} is the midpoint of the interval δp .

Stoyan and Hermann (1986) considered the cell pair of a typical edge. Let \mathcal{A}_1 and \mathcal{A}_2 be the areas of the individual cells of such a cell pair. On the basis of 1290 simulated cells, they obtained the following estimates: $E(\mathcal{A}_1) = 1.06$, $E(\mathcal{A}_1^2) = 1.42$, and $E(\mathcal{A}_1 \mathcal{A}_2) = 1.24$. Thus, the correlation coefficient of \mathcal{A}_1 and \mathcal{A}_2 is 0.39. Moreover, the values of $k_{mm}(r)$, the mean of the product of cell areas corresponding to two generating points of distance r apart, are estimated, which can be approximated by $0.28 + 0.72 [1 - \exp \{-r(0.4 + 1.1 r)\}]$ for $r \geq 0$.

For $m = 3$, relatively few investigations on the conditional moments of the characteristics of the neighbouring cells of a typical PVC have been done. Kumar *et al.* (1992) simulated 3729 PVCs and suggested that

$$m_f^{(3)} = 16.57 - 0.02f,$$

where $m_f^{(3)}$ is the mean number of faces of a randomly selected neighbouring cell of a typical cell in \mathbb{R}^3 , given that the typical cell has f faces. Using the same data set, Fortes (1993) proposed an equation similar to Aboav's law given in equation (5.5.13):

$$m_f^{(3)} = 15.95 + \frac{4.45}{f},$$

with correlation 0.865. Aboav (1991, 1992) found empirically that in a pure aluminium polycrystal, the three-dimensional version of the mean number m_n of edges of a randomly selected neighbouring face of a typical face, given that the typical face has n edges, can be expressed as

$$m_n = E(N) + \frac{\text{Var}(N)}{n},$$

where N has the same distribution as the number of edges of a typical face of a PVC in \mathbb{R}^3 . Chiu (1994) proved that for a regular and a normal stationary tessellation in \mathbb{R}^3

$$m_f^{(3)} = E(F) - 1 + \frac{E(F) + c'_f / p_f}{f},$$

$$m_n = E(N) + \frac{E(N) - n + c_n / p_n}{2n},$$

in which F , N , p_n and c_n are the same as defined above, $p_f = \Pr\{F = f\}$ and c'_f is the covariance of $k^{(3)}(f, F)$ and F , where $k^{(3)}(f, j)$ is the number of f -faced neighbouring cells of a typical three-dimensional j -complex. A three-dimensional j -complex is the collection of a j -faced cell and all its neighbouring cells.

5.5.4 Distributional properties

Since many of the moments and correlations of the characteristics for the PVCs given in Tables 5.5.1–5.5.6 and 5.5.8–5.5.9 may not differ greatly from the corresponding values for cells in tessellations where the generating set is located in \mathbb{R}^m according to point processes other than Θ_p (Hermann *et al.*, 1989), for empirical applications it is desirable to know the nature of the distributions of the PVC characteristics. Analytical expressions for the distributions of the length of a typical edge L (Brakke, 1987a,b; Muche, 1996a; Schlather 1999) and various angles (Miles, 1970a; Muche, 1996a, 1998) are known. The spherical and linear contact distributions have been obtained by Muche and Stoyan (1992). Simulation has been used to study the distributions of other characteristics. In particular most attention has been focused on the distributions of N and A in \mathbb{R}^2 and L and V in \mathbb{R}^3 , since the first of these is easy to measure manually and the second can be simply determined by image processing systems.

Mecke and Muche (1995) proved that the distribution of the length L of a typical edge of \mathcal{V}_p in \mathbb{R}^m has the same distribution as the length of an edge at a typical vertex. Using this result, Muche (1996a) showed that the distribution function F_L of L in \mathbb{R}^m is given by

$$F_L(l) = \int_0^\infty \int_0^\pi \left\{ 1 - \exp[-\lambda v_m(r, r_{l,\beta}, l)] \right\} f_\beta(\beta) f_R(r) d\beta dr, \quad (5.5.20)$$

where

$$r_{l,\beta} = \sqrt{r^2 + l^2 - 2lr \cos \beta}, \quad (5.5.21)$$

and $v_m(r, r_{l,\beta}, l)$ is the difference between the volume of an m -dimensional ball with radius $r_{l,\beta}$ and the volume of the intersection of this ball and another m -dimensional ball with radius r where the distance between the two centres is l . The explicit expressions for $v_m(r, r_{l,\beta}, l)$ are given in Muche (1996a,

equations (3.3) and (3.4)) (cf. equation (5.5.26)). The function f_R is the probability density function (pdf) of the distance from an arbitrary vertex to either one of its $m + 1$ nearest neighbouring generators, which is the generalized gamma distribution (Miles, 1970b, 1974):

$$f_R(r) = \frac{m(\lambda\omega_m)^m}{(m-1)!} r^{m^2-1} \exp(-\lambda\omega_m r^m), \quad r \geq 0, \quad (5.5.22)$$

where $\omega_m = \pi^{m/2}/\Gamma(m/2 + 1)$ is the volume of an m -dimensional sphere of unit radius. The function f_β is the pdf of the angle spanned by an edge emanating from a typical vertex and the line joining the typical vertex and the generator of a cell containing this edge. The result in Mecke and Muche (1995, equation (4.3)) implies that this density is the same as that given in equation (5.11.12) in the case $m = 2$:

$$f_\beta(\beta) = \frac{4}{3\pi} [(\pi - \beta) \cos \beta + \sin \beta] \sin \beta, \quad 0 \leq \beta < \pi. \quad (5.5.23)$$

Muche (1996a) gave explicitly the analytical expression of f_β for $m = 3, 4$ and 5 :

$$\begin{aligned} m=3, \quad f_\beta(\beta) &= \frac{105}{128} (1 + \cos \beta)^2 \sin^5 \beta, & 0 \leq \beta < \pi, \\ m=4, \quad f_\beta(\beta) &= \frac{2^{12}}{2145\pi} [3 \sin \beta - \sin^3 \beta + 3(\pi - \beta) \cos \beta] \sin^{11} \beta, & 0 \leq \beta < \pi, \\ m=5, \quad f_\beta(\beta) &= \frac{3380195}{3 \cdot 2^{21}} (3 - \cos \beta) (1 + \cos \beta)^3 \sin^{19} \beta, & \\ & & 0 \leq \beta < \pi. \end{aligned} \quad (5.5.24)$$

The densities are shown in Figure 5.5.4. Schlather (1999) gave a more complete general expression of F_L for \mathcal{V}_p in \mathbb{R}^m :

$$\begin{aligned} F_L(l) &= 1 - \frac{\frac{m^2 \Gamma\left(\frac{m^2}{2}\right)}{2} \pi^{\frac{(m^2-1)/2}{2}}}{2\Gamma\left(\frac{m^2+1}{2}\right) \Gamma(m-1)} \left[\frac{\lambda}{\Gamma\left(\frac{m+2}{2}\right)} \right]^m \\ &\times \int_0^\infty \int_0^\pi r^{m^2-1} \exp[-\lambda U_m(r, r_{l,\beta}, l)] \sin^{m^2-m-1} \beta \\ &\times \left(m \cos \beta \int_\beta^\pi \sin^m \phi d\phi + \sin^{m+1} \beta \right) d\beta dr, \quad l \geq 0, \end{aligned} \quad (5.5.25)$$

where $r_{l,\beta}$ is given in equation (5.5.21) and $U_m(r, r_{l,\beta}, l)$ denotes the volume of the union of two m -dimensional balls with radii r and $r_{l,\beta}$ and the distance between their centres is l :

$$U_m(r, r_{l,\beta}, l) = \omega_{m-1} \left[r^m I_m(\beta) + r_{l,\beta}^m I_m \left(\cos^{-1} \frac{l-r \cos \beta}{r_{l,\beta}} \right) \right], \quad (5.5.26)$$

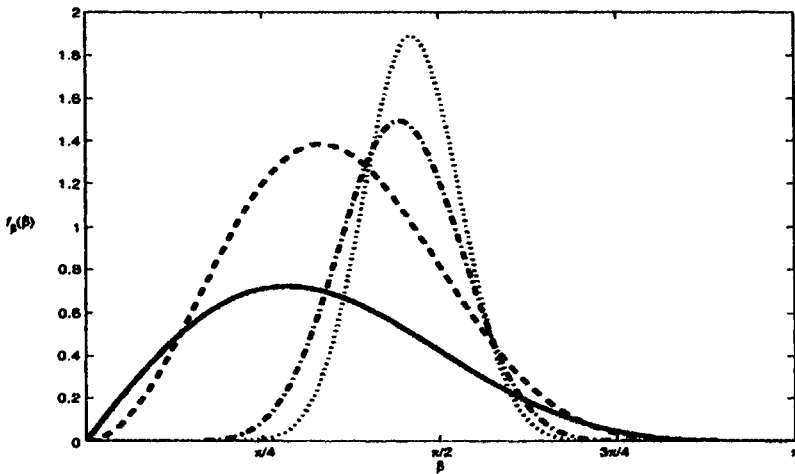


Figure 5.5.4 Probability density functions of the angle β spanned by an edge emanating from a typical vertex and the line joining the typical vertex and the generator of a cell containing this edge: — $m = 2$; - - $m = 3$; · - $m = 4$; · · · $m = 5$.

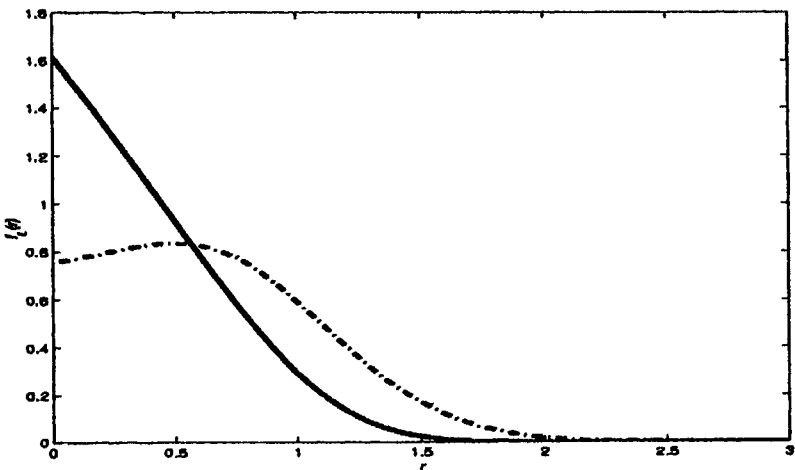


Figure 5.5.5 Probability density function of the length L of a typical edge in an m -dimensional Poisson Voronoi diagram with intensity $\lambda = 1$: — $m = 3$; · - $m = 2$ (values from Brakke, 1987a, b) (see also Muche, 1996a, Figure 1).

Table 5.5.12 Probability density functions for the length L of a typical edge in an m -dimensional Poisson Voronoi diagram with intensity $\lambda = 1$.

r	$f_L(r)$		r	$f_L(r)$	
	$m = 2$	$m = 3$		$m = 2$	$m = 3$
0.00	0.7545	1.6169	1.55	0.1413	0.0167
0.05	0.7636	1.5509	1.60	0.1171	0.0113
0.10	0.7732	1.4841	1.65	0.0962	0.0075
0.15	0.7831	1.4165	1.70	0.0782	0.0049
0.20	0.7933	1.3482	1.75	0.0631	0.0031
0.25	0.8035	1.2793	1.80	0.0504	0.0019
0.30	0.8133	1.2098	1.85	0.0399	0.0012
0.35	0.8222	1.1399	1.90	0.0312	0.0007
0.40	0.8295	1.0695	1.95	0.0243	0.0004
0.45	0.8344	0.9990	2.00	0.0187	0.0002
0.50	0.8361	0.9284	2.05	0.0143	0.0001
0.55	0.8340	0.8581	2.10	0.0108	0.0001
0.60	0.8274	0.7882	2.15	0.0081	0.0000
0.65	0.8156	0.7192	2.20	0.0060	0.0000
0.70	0.7985	0.6513	2.25	0.0044	0.0000
0.75	0.7758	0.5850	2.30	0.0032	0.0000
0.80	0.7478	0.5207	2.35	0.0023	0.0000
0.85	0.7147	0.4590	2.40	0.0017	0.0000
0.90	0.6770	0.4003	2.45	0.0012	0.0000
0.95	0.6356	0.3450	2.50	0.0008	0.0000
1.00	0.5911	0.2937	2.55	0.0006	0.0000
1.05	0.5446	0.2467	2.60	0.0004	0.0000
1.10	0.4970	0.2042	2.65	0.0003	0.0000
1.15	0.4492	0.1665	2.70	0.0002	0.0000
1.20	0.4021	0.1335	2.75	0.0001	0.0000
1.25	0.3564	0.1053	2.80	0.0001	0.0000
1.30	0.3129	0.0815	2.85	0.0001	0.0000
1.35	0.2721	0.0619	2.90	0.0000	0.0000
1.40	0.2343	0.0460	2.95	0.0000	0.0000
1.45	0.1998	0.0335	3.00	0.0000	0.0000
1.50	0.1688	0.0239	3.05	0.0000	0.0000

Source: Brakke (1987a, b).

with

$$I_m(x) = \int_x^\pi \sin^m \phi \, d\phi. \quad (5.5.27)$$

Brakke (1987a,b) has given equivalent expressions for the pdf of L in the case $m = 2$ and $m = 3$ and the values obtained from numerical integration are given in Table 5.5.12 and Figure 5.5.5.

The simulation studies by Le Caer and Ho (1990) and Moore and Moore (1993) suggested that in the case $m = 2$ the distribution of the standardized

length of a typical edge of a PVC ($3\lambda^{1/2}L/2$) is well approximated by a folded normal distribution, i.e. the distribution of the absolute value of a Gaussian variable with mean μ and variance σ^2 , with $\mu = 0.9144$ and $\sigma = 0.7623$. This result is consistent with that from the simulations of Boots (1987).

Denote by E^1 a typical edge. Let β_1 and β_2 be the angles spanned by E^1 and the lines joining one of the neighbouring generators and an endpoint of E^1 . These two angles are identically distributed. Denote by E^0 an edge emanating from a typical vertex. Mecke and Muche (1995, equation (4.3)) showed that β_1 and β_2 have the same joint distribution as the two angles spanned by E^0 and the lines passing one of the neighbouring generators and an endpoint of E^0 . Thus, β_1 and β_2 have the same marginal distribution f_β and is given in equations (5.5.23) and (5.5.24) when $m = 2, 3, 4$ and 5. Muche (1996a) derived the joint pdf of β_1 and β_2 for $m = 2$:

$$f_{\beta_1, \beta_2}(\beta_1, \beta_2) = \frac{16\pi}{3} \frac{[(\pi - \beta_1) \cos \beta_1 + \sin \beta_1][(\pi - \beta_2) \cos \beta_2 + \sin \beta_2] \sin^3 \beta_1 \sin^3 \beta_2}{[(\pi - \beta_1) \sin^2 \beta_2 + (\pi - \beta_2) \sin^2 \beta_1 + \sin \beta_1 \sin \beta_2 \sin(\beta_1 + \beta_2)]^3},$$

$$\beta_1 \geq 0, \beta_2 \geq 0, \beta_1 + \beta_2 < \pi,$$

and for $m = 3$:

$$f_{\beta_1, \beta_2}(\beta_1, \beta_2) = \frac{945}{2} \frac{(1 + \cos \beta_1)^2 (1 + \cos \beta_2)^2 \sin^8 \beta_1 \sin^8 \beta_2}{[(2 + (2 + \sin^2 \beta_2) \cos \beta_2) \sin^3 \beta_1 + (2 + (2 + \sin^2 \beta_1) \cos \beta_1) \sin^3 \beta_2]^4},$$

$$\beta_1 \geq 0, \beta_2 \geq 0, \beta_1 + \beta_2 < \pi.$$

Schlather (1999) gave the general expression of the joint pdf of β_1 and β_2 for \mathcal{V}_P in \mathbb{R}^m :

$$f_{\beta_1, \beta_2}(\beta_1, \beta_2) = \frac{2m\Gamma\left(\frac{m^2+2}{2}\right)\pi^{(m-1)/2}}{m(m+1)\Gamma\left(\frac{m^2-1}{2}\right)} \left(\frac{\Gamma\left(\frac{m+1}{2}\right)}{\Gamma\left(\frac{m+2}{2}\right)}\right)^m$$

$$\times \frac{(mI_m(\beta_1) \cos \beta_1 + \sin^{m+1} \beta_1)(mI_m(\beta_2) \cos \beta_2 + \sin^{m+1} \beta_2) \sin^{m^2-1} \beta_1 \sin^{m^2-1} \beta_2}{(I_m(\beta_1) \sin^m \beta_2 + I_m(\beta_2) \sin^m \beta_1)^{m+1}},$$

where I_m is given in equation (5.5.27).

In \mathbb{R}^2 , there are exactly three edges meeting at a typical vertex. The joint distribution of two randomly selected angles X_1 and X_2 spanned by these three edges is

$$f_{X_1, X_2}(x_1, x_2) = -\frac{8}{3\pi} \sin x_1 \sin x_2 \sin(x_1 + x_2), \quad \pi - x_1 \leq x_2 \leq \pi, \quad 0 \leq x_1 \leq \pi, \quad (5.5.28)$$

whilst the marginal density is

$$f_{X_1}(x) = \frac{4}{3\pi} (\sin x - x \cos x) \sin x, \quad 0 \leq x \leq \pi, \quad (5.5.29)$$

which gives $E(X_1) = 2\pi/3$ and $E(X_1^2) = (5\pi^2/9 - 5/6)$. The mode of the density given in equation (5.5.29) is at $x = 2.2467$ radians ($128^\circ 43' 36''$). In addition, $\Pr(X_1 < \pi/2) = 1/6$. The density f_{X_1} is shown in Figure 5.5.6. Hinde and Miles (1980, Figure 5) have also estimated the conditional density of X_1 , given the number of edges of the typical cell.

There is a complementarity in π between the interior angles X_1 and X_2 of the polygons at a typical vertex in an ordinary Voronoi diagram \mathcal{V} and the angles of a Delaunay triangle whose circumcentre is that vertex. Thus, equations (5.5.28) and (5.5.29) can be derived from equations (5.11.11) and (5.11.12), respectively. The joint distribution given in equation (5.5.28) also governs the distribution of the third angle X_3 , since $X_1 + X_2 + X_3 = 2\pi$. Let $X_{(1)} \leq X_{(2)} \leq X_{(3)}$ denote the order statistics of X_1, X_2 and X_3 . The marginal pdfs of them are:

$$f_{X_{(1)}}(x) = \begin{cases} \frac{4}{\pi} (\sin x - x \cos x) \sin x, & 0 \leq x < \frac{\pi}{2}, \\ \frac{4}{\pi} [-\sin 3x - (2\pi - 3x) \cos x] \sin x, & \frac{\pi}{2} \leq x < \frac{2\pi}{3}, \\ \frac{8}{\pi} [2 \sin^3 x - \sin x - (\pi - x) \cos x] \sin x, & \frac{2\pi}{3} \leq x < \pi \end{cases}$$

$$f_{X_{(2)}}(x) = \begin{cases} \frac{4}{\pi} (\pi - 2x + \sin 2x) \sin 2x, & \frac{\pi}{2} \leq x < \frac{2\pi}{3}, \\ \frac{8}{\pi} [2 \sin^3 x - \sin x - (\pi - x) \cos x] \sin x, & \frac{2\pi}{3} \leq x < \pi \end{cases}$$

$$f_{X_{(3)}}(x) = \frac{4}{\pi} [(2\pi - 3x) \cos x + \sin 3x] \sin x \quad \frac{2\pi}{3} \leq x < \pi$$

(cf. equations (5.11.13) to (5.11.15)). These densities are illustrated in Figure 5.5.6. The details of deriving these densities from Miles' formula (5.11.2) can be found in Muche (1998), who also successfully simplified Miles' formula for the case $m = 3$ and obtained the following densities. Let E^0 denote an edge emanating from a typical vertex and E^1 denote a typical edge. A result from Mecke and Muche (1995, equation (4.3)) implies that the distributional properties associated with E^0 are the same as those associated with E^1 . Suppose p_1, p_2 and p_3 are the three generators of the neighbouring cells of E^0 (or E^1) and p is the projection of p_1 onto E^0 (or E^1). Let Y_1 and Y_2 be the angles $\angle p_1 p p_2$ and $\angle p_2 p p_3$, respectively. The joint pdf of Y_1 and Y_2 is

$$f_{Y_1, Y_2}(y_1, y_2) = \frac{16}{3\pi^2} \left(\sin \frac{y_1}{2} \sin \frac{y_2}{2} \sin \frac{y_1 + y_2}{2} \right)^2, \quad 0 \leq y_2 < 2\pi - y_1, \quad 0 \leq y_1 < 2\pi, \quad (5.5.30)$$

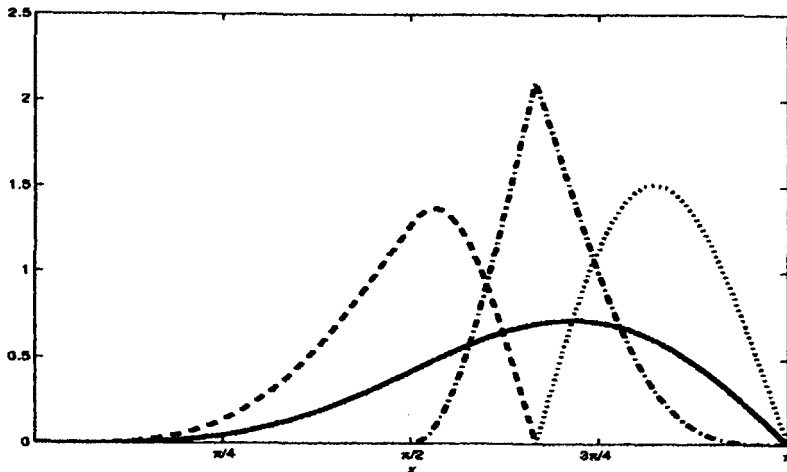


Figure 5.5.6 Probability density functions of angles at a typical vertex of a Poisson Voronoi diagram in \mathbb{R}^2 : — randomly selected angle X_1 ; - - - minimum $X_{(1)}$; · - middle $X_{(2)}$; . . . maximum $X_{(3)}$ of the three angles at a typical vertex (see also Muche, 1998, Figure 1).

and the marginal density is

$$f_{Y_1}(y) = \frac{[(2\pi - y)(2 + \cos y) + 3 \sin y](1 - \cos y)}{3\pi^2}, \quad 0 \leq y < 2\pi.$$

In \mathbb{R}^3 there are three faces meeting at an edge. Denote by X_1 , X_2 and X_3 the three face angles at a typical edge. These face angles, without loss of generality, can be expressed as $X_1 = \pi - Y_1/2$, $X_2 = \pi - Y_2/2$ and $X_1 + X_2 + X_3 = 2\pi$. Using these relationships, Muche (1998) derived from equation (5.5.30) the joint pdf of the face angles and the marginal pdfs of X_1 and their order statistics $X_{(1)} \leq X_{(2)} \leq X_{(3)}$:

$$f_{X_1, X_2}(x_1, x_2) = \frac{64}{3\pi^2} [\sin x_1 \sin x_2 \sin(x_1 + x_2)]^2, \quad \pi - x_1 \leq x_2 < \pi, \quad 0 \leq x_1 < \pi,$$

$$f_{X_1}(x) = \frac{8}{3\pi^2} [x(3 - 2 \sin^2 x) - 3 \sin x \cos x] \sin^2 x, \quad 0 \leq x < \pi,$$

$$f_{X_{(1)}}(x) = \begin{cases} \frac{8}{\pi^2} [x(3 - 2 \sin^2 x) - 3 \sin x \cos x] \sin^2 x, & x < \frac{\pi}{2}, \\ \frac{8}{\pi^2} [(2\pi - 3x)(3 - 2 \sin^2 x) + (9 - 16 \sin^4 x) \sin x \cos x] \sin^2 x, & \frac{\pi}{2} \leq x < \frac{2\pi}{3} \end{cases}$$

$$f_{X_{(2)}}(x) = \begin{cases} \frac{16}{\pi^2} [(2x - \pi)(3 - 2 \sin^2 x) + 2(4 \sin^4 x - 3) \sin x \cos x] \sin^2 x, & \frac{\pi}{2} \leq x < \frac{2\pi}{3}, \\ \frac{16}{\pi^2} [(\pi - x)(3 - 2 \sin^2 x) + (3 - 8 \sin^4 x) \sin x \cos x] \sin^2 x, & \frac{2\pi}{3} \leq x < \pi, \end{cases}$$

$$f_{X_{(3)}}(x) = \frac{8}{\pi^2} [(3x - 2\pi)(3 - 2 \sin^2 x) + (16 \sin^4 x - 9) \sin x \cos x] \sin^2 x, \quad \frac{2\pi}{3} \leq x < \pi.$$

These densities are illustrated in Figure 5.5.7. Let β denote the angle between E^0 (or E^1) and the line joining the typical vertex (or an endpoint of E^1) and a neighbouring generator. The pdf of β is given by the first density in equation (5.5.24) and

$$E(\cos^k \beta) = \begin{cases} \frac{105}{4} \frac{k+4}{(k+1)(k+3)(k+5)(k+7)} & \text{for even } k, \\ \frac{105}{4} \frac{1}{(k+2)(k+4)(k+6)} & \text{for odd } k. \end{cases}$$

Denote by γ the angle between two randomly chosen edges from a typical vertex. The pdf of it is:

$$f_\gamma(\gamma) = \frac{35}{16\pi^3} \int_{-1}^1 \int_{-(1-y_1^2)^{1/2}}^{(1-y_1^2)^{1/2}} \sqrt{1-y_1^2-y_2^2} \times \left\{ [(1-y_1^2-y_2^2) + 3(y_1 \sin \gamma + y_2 \cos \gamma)^2] \left[\frac{\pi}{2} - \tan^{-1} \frac{y_2}{\sqrt{1-y_1^2-y_2^2}} \right] \right. \\ - 3y_2 \sqrt{1-y_1^2-y_2^2} \left\{ 3(y_1 \sin \gamma + y_2 \cos \gamma) \sqrt{1-y_1^2-y_2^2} \right. \\ \left. + [(1-y_1^2-y_2^2) + 3(y_1 \sin \gamma + y_2 \cos \gamma)^2] \right\} \\ \times \left[\frac{\pi}{2} + \tan^{-1} \frac{y_1 \sin \gamma + y_2 \cos \gamma}{\sqrt{1-y_1^2-y_2^2}} \right] \left. \right\} \sin \gamma dy_2 dy_1, \quad 0 \leq \gamma \leq \pi$$

(see Figure 5.5.8) and the first two moments are

$$E(\gamma) = \frac{48\pi^2 - 35}{72\pi},$$

$$E(\gamma^2) = \frac{48\pi^2 - 175}{72}.$$

The density of the angle ζ between the lines from a typical vertex to two neighbouring generators chosen at random is

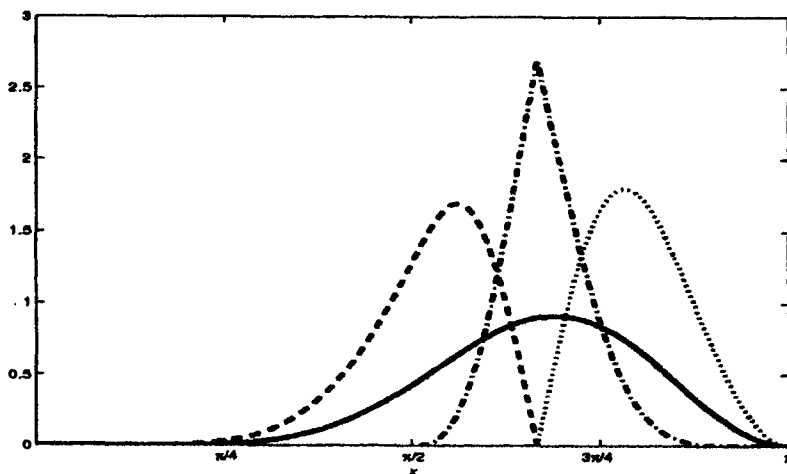


Figure 5.5.7 Probability density functions of face angles at a typical edge of a Poisson Voronoi diagram in \mathbb{R}^3 : — randomly selected angle X_1 ; - - minimum $X_{(1)}$; · - middle $X_{(2)}$; ··· maximum $X_{(3)}$ of the three face angles at a typical edge (see also Muche, 1998, Figure 2).

$$f_\zeta(\zeta) = \frac{35}{256} \left(8 + 8 \cos^2 \frac{\zeta}{2} - \cos^4 \frac{\zeta}{2} \right) \sin^2 \frac{\zeta}{2} \cos \frac{\zeta}{2}, \quad 0 \leq \zeta < \pi$$

(see Figure 5.5.8) and the first two moments are

$$E(\zeta) = \pi - \frac{4829}{3360},$$

$$E(\zeta^2) = \pi^2 - \frac{72598}{11025}.$$

Some other angular properties which are related to the Poisson Delaunay tessellation are discussed in Section 5.11.

A typical cell of V_p , using the definition of the Palm distribution approach, is the cell containing the origin o , which is also the generator of the cell. However, in general the cell P_o which contains the origin is not typical, since a larger cell has a higher chance of containing the origin (size-biased sampling). Mecke (1999) showed that all moments of the volume of a typical cell of a stationary tessellation in \mathbb{R}^m do not exceed the corresponding moments of the volume of P_o . Gilbert (1962) studied the distributions of the length of the longest line segment from the origin to the boundary of P_o in \mathbb{R}^m , which is known as the linear contact distribution function:

$$H_1(r) = 1 - A_m \lambda \int_0^\infty \int_0^\pi y^{m-1} \sin^{m-2} \beta \exp(-\lambda U_m(y, r_{y,\beta}, r)) d\beta dy, \quad r \geq 0, \quad (5.5.31)$$

where A_m is a normalizing constant, and $r_{y,\beta}$ and $U_m(y, r_{y,\beta}, r)$ have been defined in equations (5.5.21) and (5.5.26), respectively. Muche and Stoyan

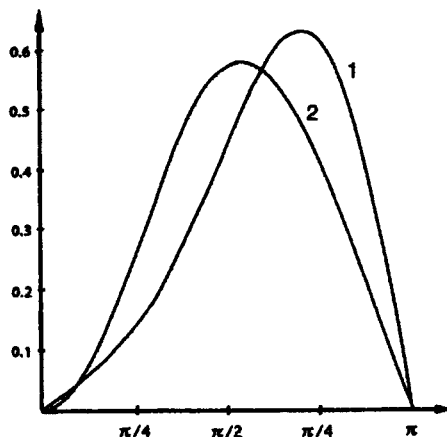


Figure 5.5.8 Probability density functions for (1) the angle γ spanned by two edges emanating from a typical vertex and (2) the angle ζ between the lines from a typical vertex to two neighbouring generators. (Source: Muche, 1998, Figure 3.)

(1992) derived the spherical contact distribution function in \mathbb{R}^2 and \mathbb{R}^3 , i.e. the distribution of the radius of the maximal ball lying completely within P_o and centred at the origin. For $m = 2$ the function is given by

$$H_s(r) = 1 - \frac{1}{2} \exp(-4\pi\lambda r^2) + \frac{1}{2} \exp(-6\pi\lambda r^2) \\ - 2\pi\lambda \int_r^\infty y \exp\left\{-\lambda\left[(4r^2 + 2y^2)\left(\pi - \cos^{-1}\frac{r}{y}\right) + 6r\sqrt{y^2 - r^2}\right]\right\} dy, \quad r \geq 0,$$

whilst for $m = 3$:

$$H_t(r) = 1 - 4\pi\lambda \int_0^r y^2 \exp\left[\frac{32\pi\lambda}{3} r(r^2 + y^2)\right] dy \\ - 4\pi\lambda \int_r^\infty y^2 \exp\left[\frac{4\pi\lambda}{3y} (r+y)^4\right] dy, \quad r \geq 0.$$

They also used the linear contact distribution to derive a numerically tractable expression for the chord length distribution (see Section 5.7).

Although Miles and Maillardet (1982, p. 108) have been able to derive an expression for the probability p_n that a PVC has n vertices (edges), this is computationally complex. Table 5.5.13 (see also Figure 5.5.9) gives the estimated values of p_n obtained by Hinde and Miles (1980), Drouffe and Itzykson (1984), Le Caér and Ho (1990) and Kumar and Kurtz (1993). Note that the largest value of n encountered amongst the two million polygons generated by Hinde and Miles is 14. On the basis of their estimates, Itzykson and Drouffe (1989, p. 745) suggested that asymptotically $p_n \sim n^{-\kappa n}$, where κ lies between 1 and 2.

Table 5.5.13 Estimates, \hat{p}_n , of the probability p_n that a typical Poisson Voronoi cell in \mathbb{R}^2 has n edges.

<i>n</i>	a		b		c		d
	\hat{p}_n	$\hat{\sigma}_n$	\hat{p}_n	$\hat{\sigma}_n$	\hat{p}_n	$\hat{\sigma}_n$	\hat{p}_n
3	0.01131	0.00007	0.01127	0.00894	0.0113	0.0002	0.011
4	0.1071	0.00022	0.1077	0.03316	0.1068	0.0002	0.107
5	0.2591	0.00031	0.258	0.04472	0.2595	0.0005	0.260
6	0.2944	0.00032	0.294	0.05477	0.2946	0.0003	0.294
7	0.1991	0.00028	0.198	0.05477	0.1986	0.0001	0.199
8	0.0902	0.00020	0.090	0.14142	0.0905	0.0003	0.090
9	0.0295	0.00012	0.0288	0.02646	0.0295	0.0003	0.030
10	0.00743	0.00006	0.00695	0.01414	0.0074	0.0001	0.007
11	0.00149	0.00003	0.00153	0.00949	0.00144	0.00003	0.0015
12	0.00025	0.00001	0.00024	0.00548			0.00023
13	0.000034	0.000004	0.000029	0.00224			0.00004
14	0.000005	0.0000016	0.0000028	0.00063			
15			2.6×10^{-7}	2.2×10^{-4}			
16			2.3×10^{-8}	5×10^{-5}			
18			1.3×10^{-10}	7.1×10^{-6}			
20			1.5×10^{-13}	2.8×10^{-7}			
25			9.6×10^{-21}	7.7×10^{-11}			
30			1.3×10^{-29}	3.3×10^{-15}			
35			3.6×10^{-40}				
40			2.4×10^{-50}				
45			2.0×10^{-63}				
50			1.5×10^{-75}				

$\hat{\sigma}_n$ = standard deviation of \hat{p}_n .

Sources:

- a Hinde and Miles (1980, Table III). Number of cells = 2 000 000.
- b Drouffe and Itzykson (1984, Table 1). Number of cells = 27 000.
- c Le Caér and Ho (1990, Table I). Number of cells = 600 696, 1 001 500, 1 020 800.
- d Kumar and Kurtz (1993, Table 3). Number of cells = 650 000.

Consider a three-parameter gamma probability density function of the form

$$f_3(x) = \frac{rb^{q/r} x^{q-1} \exp(-bx')}{\Gamma\left(\frac{q}{r}\right)}, \quad r > 0, b > 0, q > 0. \quad (5.5.32)$$

Hinde and Miles (1980) suggested a discretized three-parameter gamma distribution $\int_{n-1/2}^{n+1/2} f_3(x) dx$ with $r = 1.0186$, $b = 3.130$ and $q = 19.784$ to approximate p_n . Kumar and Kurtz (1993) used a discretized (two-parameter) gamma distribution. The general form of the pdf of a gamma distribution is that of equation (5.5.32) with $r = 1$:

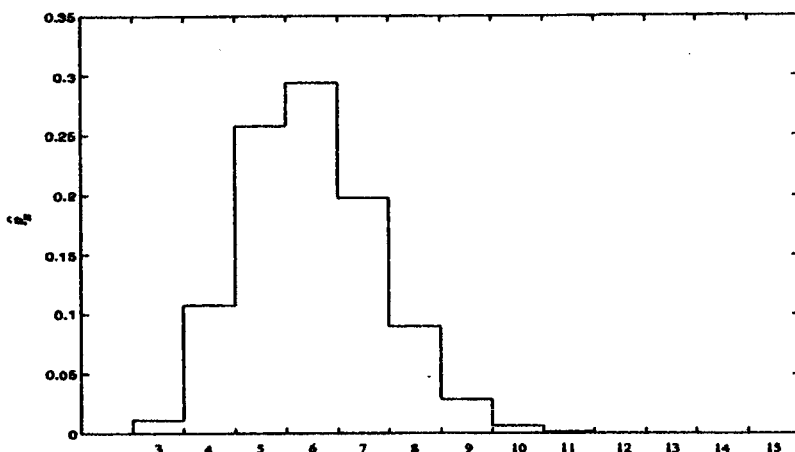


Figure 5.5.9 Normalized histogram of the number of edges N of a typical Poisson Voronoi cell in \mathbb{R}^2 (values from Drouffe and Itzykson, 1984).

$$f_2(x) = \frac{b^q x^{q-1} \exp(-bx)}{\Gamma(q)}, \quad b > 0, q > 0. \quad (5.5.33)$$

They suggested that $q = 21.199$ and $1/b = 0.283$, but the fit is rejected by the Kolmogorov-Smirnov test at the 0.01 significance level. Kumar and Kurtz (1993) also found that if the sample size is less than 50 000, a discretized lognormal distribution can be used to approximate the distribution of the number of edges. The reason has been given by Vaz and Fortes (1988): the difference between a gamma and a lognormal distribution with suitably chosen parameters is very small. Solomon and Stephens (1980) suggested using $(cw)^k$ to approximate the number of edges of a typical PVC, where $c = 4.457$, $k = 0.485$ and w has a χ^2 -distribution with 3.429 degrees of freedom. A χ^2 -distribution with p degrees of freedom is the gamma distribution given in equation (5.5.33) with $q = p/2$ and $b = 1/2$.

Turning to \mathbb{R}^3 , Hanson (1983), Quine and Watson (1984), Lorz (1990b, 1991) and Kumar *et al.* (1992) have estimated the distributions of the number of faces F per cell and the number of vertices (edges) N per face. Their estimates are reported in Tables 5.5.14 and 5.5.15 and illustrated in Figures 5.5.10 and 5.5.11, respectively. Kumar *et al.* (1992) suggested that the gamma distribution given in equation (5.5.33) with $q = 21.6296$ and $1/b = 0.7199$ can be used to describe the distribution of F , but again it is rejected by the Kolmogorov-Smirnov test at the 0.01 significance level.

Numerous researchers, including Kiang (1966), Crain (1972, 1978), Hinde and Miles (1980), Weaire *et al.* (1986), Icke and van de Weygaert (1987), DiCenzo and Wertheim (1989), Hermann *et al.* (1989), Kumar and Kurtz (1993), Quine and Watson (1984), Vaz and Fortes (1988), Zaninetti (1992), Moore and Angell (1993) and Marthinsen (1996), have produced estimates

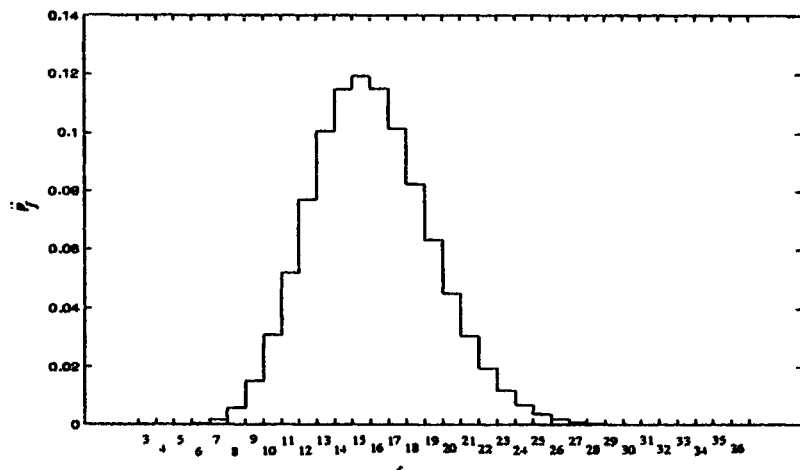


Figure 5.5.10 Normalized histogram of the number of faces F of a typical Poisson Voronoi cell in \mathbb{R}^3 (values from Kumar *et al.*, 1992).

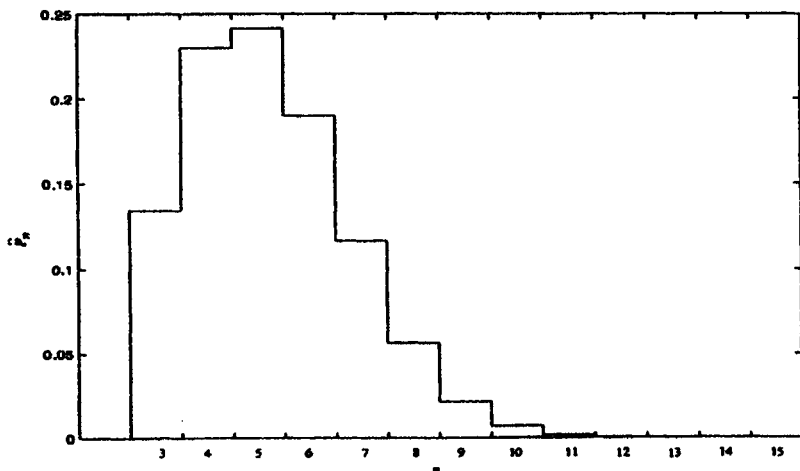


Figure 5.5.11 Normalized histogram of the number of edges (vertices) N of a randomly selected face of a typical Poisson Voronoi cell in \mathbb{R}^3 (values from Kumar *et al.*, 1992).

Table 5.5.14 Estimates, \hat{p}_f , of the probability p_f that a typical Poisson Voronoi cell in \mathbb{R}^3 has f faces.

f	\hat{p}_f		f	\hat{p}_f	
	a	b		a	b
4	0.0000055866	—	21	0.030620	0.02993
5	0.000027933	0.00006	22	0.019349	0.01895
6	0.00032682	0.00019	23	0.011640	0.01144
7	0.0015922	0.00193	24	0.0067207	0.00691
8	0.0058101	0.00578	25	0.0038156	0.00373
9	0.014936	0.01496	26	0.0018575	0.00215
10	0.030885	0.03102	27	0.00097486	0.00091
11	0.052115	0.05164	28	0.00050000	0.00042
12	0.076950	0.07806	29	0.00019832	0.00017
13	0.10041	0.09865	30	0.000061453	0.000048
14	0.11465	0.11492	31	0.000039106	0.000024
15	0.11927	0.12088	32	0.000013966	0.000012
16	0.11485	0.11418	33	0.0000027933	—
17	0.10144	0.10297	34	0.0000055866	—
18	0.082444	0.08219	35	0.0000027933	0.000012
19	0.063249	0.06287	36	0.0000027933	—
20	0.045232	0.04500			

*Sources:*a Kumar *et al.* (1992, Table III). Number of cells = 358 000.

b Lorz (1991). Number of cells = 82 870.

Table 5.5.15 Estimates, \hat{p}_n , of the probability p_n that a face of a typical Poisson Voronoi cell in \mathbb{R}^3 has n edges (vertices).

n	\hat{p}_n		n	\hat{p}_n	
	a	b		a	b
3	0.13448	0.1355	10	0.0068203	0.0068
4	0.23013	0.2301	11	0.0017689	0.0017
5	0.24161	0.2404	12	0.00038117	0.00038
6	0.19021	0.1900	13	0.000068471	0.000066
7	0.11646	0.1162	14	0.000010064	0.0000047
8	0.056384	0.0569	15	0.0000025160	0.0000039
9	0.021680	0.0220			

*Sources:*a Kumar *et al.* (1992, Table III). Number of cells = 358 000.

b Lorz (1991). Number of cells = 82 870.

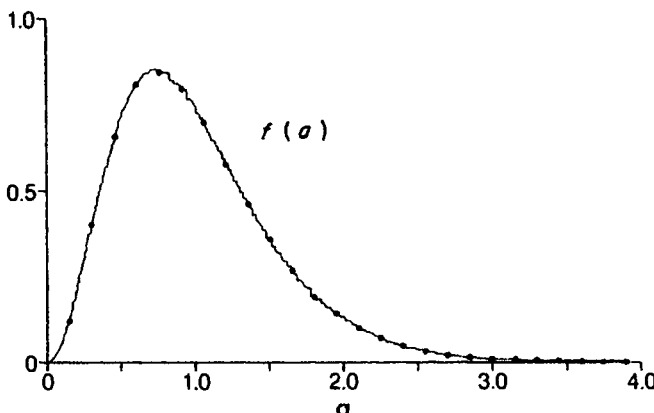


Figure 5.5.12 Normalized histogram of the standardized area λA of a typical Poisson Voronoi cell in \mathbb{R}^2 showing point values of the generalized gamma fit (5.5.32). (Source: Hinde and Miles, 1980 Figure 4.)

of the distribution f_A of the area of a typical PVC in \mathbb{R}^2 . The last five papers, as well as Hanson (1983), Andrade and Fortes (1988), Lorz (1990b, 1991), Kumar *et al.* (1992), Thorvaldsen (1992) and van de Weygaert (1994), also estimate the pdf f_V of the volume V of a typical PVC in \mathbb{R}^3 . Quine and Watson (1984) and Kumar and Kurtz (1993) have also examined the distribution of A conditioned by the number of edges N . Figure 5.5.12 shows the distribution of the standardized area λA (Hinde and Miles, 1980, Figure 4).

There has been considerable conjecture on the theoretical form of f_A . Hinde and Miles (1980, p. 219) fit a three-parameter generalized gamma function. Values obtained from equation (5.5.32) with $r = 1.0787$, $b = 3.0328\lambda'$ and $q = 3.3095$ are plotted in Figure 5.5.12. Visually this provides a good fit, although it is rejected by a χ^2 test. Tanemura (1988) follows Hinde and Miles and fits equation (5.5.32) to the volume of a typical cell in \mathbb{R}^3 . His estimates of the parameters are $r = 1.409$, $b = 2.813\lambda'$ and $q = 4.120$. He found that a three-parameter gamma distribution fits better than a two-parameter gamma. Solomon and Stephens (1980) used $(cw)^k$, where $c = 0.723$, $k = 0.445$ and w has a χ^2 -distribution with 1.855 degrees of freedom, to approximate A . Hermann *et al.* (1989, p. 194) claimed that Maxwell, lognormal and gamma distributions fit equally well the values of A derived from their simulations. Vaz and Fortes (1988) found that although lognormal and gamma distributions are very close, the description of the cell area or volume by a lognormal distribution is in general not as adequate as by a gamma distribution. On the basis of his simulations, Kiang (1966) suggests that the cell size (area if $m = 2$ and cell volume if $m = 3$) follows the gamma distribution given in equation (5.5.33) with $q = 2m$ and $b = 2m\lambda$. Both Rivier (1986b) and Weaire *et al.* (1986) offer some limited analytical support for A having a gamma distribution but the latter authors suggest values of $q = 3.61$ and $b = 3.61\lambda$.

Since the k th moments obtained from the gamma pdf given in equation (5.5.33) are $[\Gamma(q+k)\Gamma(q)]b^{-k}$, these values yield $E(A^2) = 1.277$, which is not consistent with Gilbert's value reported in Table 5.5.1. However, the fit to their observed values is excellent (Weaire *et al.*, 1986, p. L104). Other researchers also report an excellent fit of A to equation (5.5.33) with $q = 3.61$ and $b = 3.57\lambda$ (DiCenzo and Wertheim, 1989), $q = 3.61$ and $b = 3.61\lambda$ (Marthinsen, 1996), $q = 3.571$ and $b = 3.571\lambda$ (Vaz and Fortes, 1988), $q = 3.37$ and $b = 3.37\lambda$ (Zaninetti, 1992) and V to equation (5.5.33) with $q = 5.56$ and $b = 5.56\lambda$ (Andrade and Fortes, 1988; Vaz and Fortes, 1988; Thorvaldsen, 1992; Marthinsen, 1996), $q = 5.38$ and $b = 5.38\lambda$ (Zaninetti, 1992). Kumar and Kurtz (1993) and Kumar *et al.* (1992) estimated $q = 3.718$ and $b = 3.718\lambda$ for A and $q = 5.7869$ and $b = 5.7869\lambda$ for V , respectively, but each fit is rejected by the Kolmogorov-Smirnov test at the 0.01 significance level. Note that except for DiCenzo and Wertheim (1989), all these estimates fulfilled the condition that $E(A) = q/b = \lambda^{-1}$. A review of Kiang's conjecture and related simulation studies can be found in Moore and Angell (1993). Furthermore, Miles and Maillardet (1982, p. 101) considered that the conditional distribution of A , given that the number of edges is N . They suggested that if N is large, this conditional distribution can be approximated by the gamma distribution given in equation (5.5.33) with $q = N$ and $b = 4\lambda$. Quine and Watson (1984) estimated the conditional area of a typical cell with N edges in \mathbb{R}^2 and the conditional volume of a typical cell with F faces in \mathbb{R}^3 . Kumar and Kurtz (1993, Table 8) and Kumar *et al.* (1992, Table VI) also found that gamma distributions with suitably chosen parameters can be used to describe such conditional area and conditional volume distributions, respectively. Unlike the conditional perimeter discussed below, none of their fits has been rejected by the Kolmogorov-Smirnov test at the 0.05 significance level. Mulheran (1992) used a heuristic argument to derive an approximation of the distribution of the conditional area of a typical cell V_p in \mathbb{R}^2 , given that it has N edges, but simulation results are not well fitted by his approximation. For V_p in \mathbb{R}^m , Zuyev (1992, 1993) defined the *fundamental region* of a typical PVC to be the union of the m -dimensional spheres with centres at the vertices of the cell and containing the generator of the cell on their boundaries. He showed that given the number of $(m-1)$ -faces of a typical cell is $N (\geq m+1)$, the volume of its fundamental region has a gamma distribution with $q = N$ and $b = \lambda$ (see also Møller and Zuyev, 1996). Since the volume of a cell does not exceed $1/2^m$ of the volume of its fundamental region, a rough upper bound on the conditional distribution of the volume of a typical cell V , given that the number of $(m-1)$ -faces on its boundary is N , has been obtained:

$$\Pr(V > x | N) \leq \sum_{k=1}^N \frac{(2^m \lambda x)^k}{k!} e^{-2^m \lambda x},$$

for all $x > 0$.

Hinde and Miles (1980, Figure 3) have estimated the distribution of the standardized perimeter $(\sqrt{\lambda}/4)P$ of a typical cell (see Figure 5.5.13). They

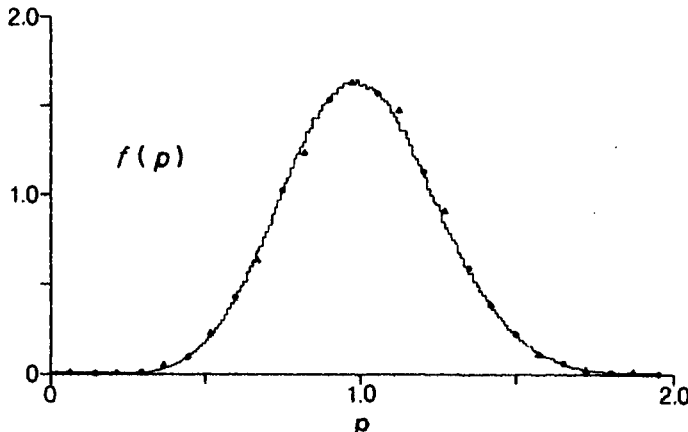


Figure 5.5.13 Normalized histogram of the standardized perimeter $\lambda^{1/2}P/4$ of a typical Poisson Voronoi cell in \mathbb{R}^2 showing point values for two fits: ● generalized gamma fit (5.5.32); ▲ normal fit. (Source: Hinde and Miles, 1980 Figure 3.)

again fit equation (5.5.32) to their data with $r = 2.3389$, $b = 2.9563$ and $q = 7.5579$. This fit is shown in Figure 5.5.13. As with the standardized cell area, while the visual impression is one of a good fit, it is rejected by a χ^2 test at the 0.05 significance level. They also note that, since their estimates of the coefficients of skewness and kurtosis of the standardized cell perimeter $(\sqrt{\lambda}/4)P$ are 0.193 and 2.983, respectively, $(\sqrt{\lambda}/4)P$ is approximately normally distributed with mean 1 and variance 0.0592. Values for this normal distribution are also plotted in Figure 5.5.13. Quine and Watson (1984, Figure 3) and Kumar and Kurtz (1993, Table 9) have studied the distribution of P conditioned on the number of edges N . The values can be described by gamma distributions with suitable parameters, although most of the fits are rejected by the Kolmogorov–Smirnov test at the 0.05 significance level.

The conditional number of edges of a randomly selected neighbouring cell of a typical cell with N edges can also be well described by gamma distributions and a lognormal distribution (Kumar and Kurtz, 1993, Table 6). In general, the lognormal distribution fits for this conditional number, as well as for the cell area A and perimeter P , are not as good as the gamma distribution fits (see Vaz and Fortes, 1988).

Quine and Watson (1984), Lorz (1990b) and Kumar *et al.* (1992) have estimated the distribution of the surface area S of a typical PVC in \mathbb{R}^3 . The last fits S to equation (5.5.33) and yields $q = 15.4847$ and $1/b = 0.3778 \lambda^{-2/3}$ and $q = 16.1576$ and $1/b = 0.3603 \lambda^{-2/3}$. The former is a better fit but the latter ensures $E(S) = 5.821 \lambda^{-2/3}$. Nevertheless, both fits are rejected by the Kolmogorov–Smirnov test at the 0.01 significance level. The conditional surface area, given that the typical cell has F faces, can also be well described by gamma distributions with suitably chosen parameters (Kumar *et al.*, 1992,

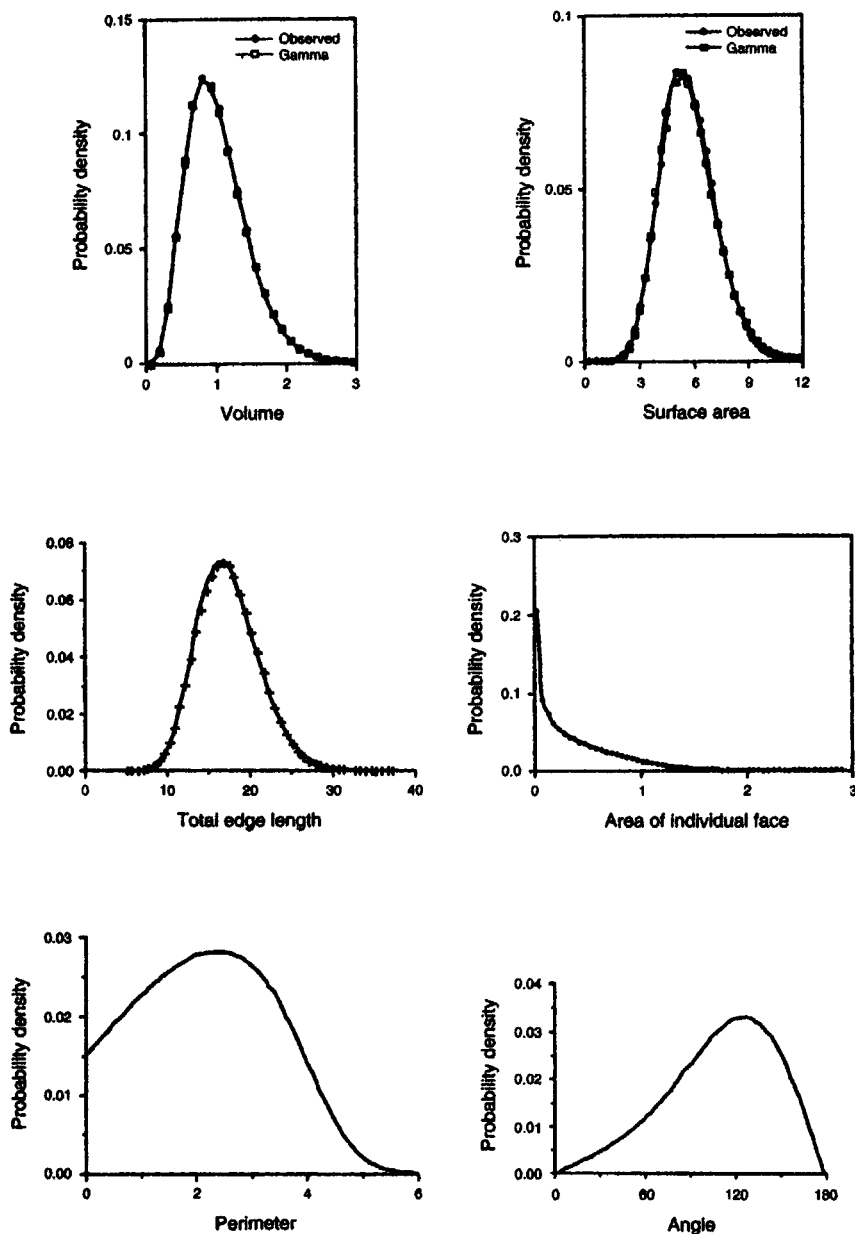


Figure 5.5.14 Normalized histograms of the volume V , surface area S and total edge length B of a typical Poisson Voronoi cell (with the best fit gamma distributions) and the area A , perimeter P and interior angle α_2 of a typical face of a Poisson Voronoi cell in \mathbb{R}^3 . (Sources: Kumar *et al.*, 1992, and Kumar and Kurtz, 1995.)

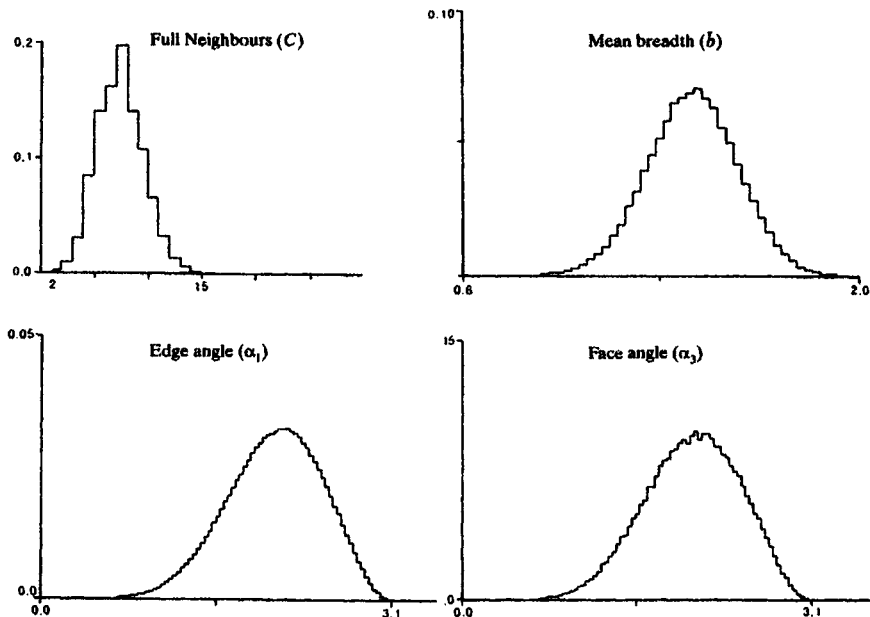


Figure 5.5.15 Normalized histograms of the number of full neighbours C , mean breadth \bar{b} , and face angle α_3 of a typical Poisson Voronoi cell and the face angle α_1 at a typical edge in \mathbb{R}^3 . (Sources: Quine and Watson, 1984, and Lorz, 1990b.)

Table VII) and all of them pass the Kolmogorov-Smirnov test at the 0.05 significance level.

Quine and Watson (1984), Lorz (1990b), Kumar *et al.* (1992) and Kumar and Kurtz (1995) also estimated the distributions of various characteristics of a PVC in \mathbb{R}^3 . The estimates are given in Figures 5.5.14 and 5.5.15. Kumar *et al.* (1992, Figures 12 and 13) also have estimated the conditional distribution of the area of a face of a typical PVC in \mathbb{R}^3 , given that the typical cell has F faces or that the face has N edges.

Avrami and Bertsimas (1993) have established central limit theorems for the total edge length of \mathcal{V}_P in $[0, 1]^2$ and \mathcal{D}_P in $[0, 1]^m$, as the intensity λ of the Poisson process tends to infinity. Let L_λ denote the total edge of \mathcal{V}_P in $[0, 1]^2$ or \mathcal{D}_P in $[0, 1]^m$. They showed that

$$\left| \Pr\left\{ \frac{L_\lambda - E(L_\lambda)}{\sqrt{\text{Var}(L_\lambda)}} \leq x \right\} - \int_0^x \frac{1}{\sqrt{2\pi}} e^{-z^2/2} dz \right| = O\left(\frac{(\log \lambda)^{1+3/(2m)}}{\lambda^{1/4}} \right),$$

where $m = 2$ for \mathcal{V}_P and $m \geq 2$ for \mathcal{D}_P . Heinrich (1994) provided a tool to show the asymptotic normality of the total length of \mathcal{V}_P in a very large m -dimensional cube.

5.6 STOCHASTIC PROCESSES INDUCED BY POISSON VORONOI DIAGRAMS

In addition to the point processes of centroids of faces mentioned in Section 5.1, there are also other stochastic processes induced by Poisson Voronoi diagrams. In this section we study the properties of some of these processes.

5.6.1 Point processes of centroids of faces

As indicated in Section 5.1 it is possible to generate other point processes from \mathcal{V}_P that share properties of the Poisson point process Θ_P , which generated \mathcal{V}_P . One such process with motion invariance is that of the centroids of s -faces of \mathcal{V}_P ($s = 0, \dots, m$), which is denoted by Θ_{P_s} . Suppose the intensity of Θ_{P_s} is λ_s . The relation between λ_s and λ is given by equations (5.1.1) and (5.5.4). Let $\lambda_0 = \kappa_m \lambda$. By equation (5.5.4),

$$\kappa_m = \frac{2^{m+1} \pi^{(m-1)/2} \Gamma\left(\frac{m^2 + 1}{2}\right)}{m^2(m+1) \Gamma\left(\frac{m^2}{2}\right)} \left\{ \frac{\Gamma\left(\frac{m}{2} + 1\right)}{\Gamma\left(\frac{m+1}{2}\right)} \right\}^m.$$

In particular, $\kappa_1 = 1$, $\kappa_2 = 2$ and $\kappa_3 = 24\pi^2/35$.

Consider a stationary point process Θ with intensity μ . The probability that an infinitesimally small disc of area dA_1 contains a point of Θ is μdA_1 . For two infinitesimally small discs of area dA_1 and dA_2 , with a distance r between their centres, the probability that both discs contain a point of Θ depends only on the distance r , because the point process Θ is stationary. Denote this probability by

$$\rho^{(2)}(r) dA_1 dA_2, \quad r \geq 0,$$

where $\rho^{(2)}$ is known as the *second-order product density*. This density is equal to λ^2 for a stationary Poisson point process of intensity λ . It is natural to divide $\rho^{(2)}$ by the square of the intensity of the point process as a normalization, which gives

$$g(r) = \frac{\rho^{(2)}(r)}{\mu^2}, \quad r \geq 0.$$

This is called the *pair correlation function* (see, for example, Stoyan and Stoyan, 1994, pp. 248–249). For Θ_P , $g(r) = 1$.

The pair correlation function for Θ_{P_0} , the point process of vertices of \mathcal{V}_P , is of particular interest. One reason is that Θ_{P_0} is also the point process of cell centroids of \mathcal{D}_P . For Θ_{P_0} of \mathcal{V}_P in \mathbb{R} :

$$g(r) = 1 + (2\lambda r - 1) e^{-2\lambda r}, \quad r \geq 0.$$

Heinrich and Muche (1994) have derived the general form of g for the point process of vertices Θ_{P0} of a Poisson Voronoi diagram \mathcal{V}_P in \mathbb{R}^m for $m \geq 2$:

$$g(r) = \frac{g_{0,m}^*(r)}{[(m+1)!]^2} + \sum_{j=0}^m \frac{g_{j,m}(r)}{j! [(m-j+1)!]^2}, \quad r \geq 0,$$

where

$$\begin{aligned} g_{0,m}^*(r) &= m^4(m+1)^2 \int_0^{(\lambda\omega_m)^{1/m}} \int_0^{r_1 - r(\lambda\omega_m)^{1/m}} \exp\{-(r_1^m + r_2^m)\} \\ &\quad \times r_1^{m^2-1} r_2^{m^2-1} dr_2 dr_1, \\ &= m^2(m+1)^2(m-1)! \int_0^{\lambda\omega_m r^m} f\left(\{r[\lambda\omega_m]^{1/m} - r_1^{1/m}\}^m\right) \\ &\quad \times e^{-r_1} r_1^{m-1} dr_1, \quad r \geq 0, \end{aligned} \tag{5.6.1}$$

with $\omega_m = \pi^{m/2}/\Gamma(1+m/2)$ being the volume of an m -dimensional sphere of unit radius, and

$$f(x) = \frac{1}{(m-1)!} \int_0^x y^{m-1} e^{-y} dy = 1 - e^{-x} \left\{ 1 + x + \dots + \frac{x^{m-1}}{(m-1)!} \right\}, \quad x \geq 0.$$

Explicit expressions for $g_{j,m}$ are known but messy. We state only the pair correlation function of Θ_{P0} in \mathbb{R}^m for $m = 2$ and $m = 3$.

For $m = 2$,

$$g(r) = \frac{g_{0,2}^*(r)}{36} + \frac{g_{0,2}(r)}{36} + \frac{g_{1,2}(r)}{4} + \frac{g_{2,2}(r)}{2}, \quad r \geq 0, \tag{5.6.2}$$

where $g_{0,2}^*$ can be obtained from equation (5.6.1):

$$\begin{aligned} g_{0,2}^*(r) &= 36 \int_0^{\lambda\pi r^2} \left\{ 1 - \left[1 + (r\sqrt{\lambda\pi} - \sqrt{y})^2 \right] \right. \\ &\quad \times \left. \exp[-(r\sqrt{\lambda\pi} - \sqrt{y})^2] \right\} y \exp(-y) dy, \end{aligned}$$

and

$$g_{2,2}(r) = \frac{\lambda^2 r^4}{2} \int_1^\infty \int_0^1 \exp\{-\lambda r^2 v_2(y_1, y_2)\} F_2(y_1, y_2) F_2(-y_1, y_2) dy_1 dy_2,$$

$$g_{1,2}(r) = \frac{\lambda^3 r^6}{4} \int_1^\infty \int_0^1 \frac{\exp\{-\lambda r^2 v_2(y_1, y_2)\}}{\sqrt{(1-y_1^2)(y_2^2-1)}} F_1(y_1, y_2) F_1(-y_1, y_2) dy_1 dy_2,$$

$$g_{0,2}(r) = \frac{9\lambda^4 r^8}{4} \int_1^\infty \int_0^1 \exp\{-\lambda r^2 v_2(y_1, y_2)\} F_0(y_1, y_2) F_0(-y_1, y_2) dy_1 dy_2.$$

The functions F_2 , F_1 , F_0 and v_2 are given by:

$$F_2(y_1, y_2) = (y_1 + y_2) \left[(1 + y_1 y_2) \left(\pi - \cos^{-1} \frac{1 + y_1 y_2}{y_1 + y_2} \right) \right. \\ \left. + \sqrt{(1 - y_1^2)(y_2^2 - 1)} \right],$$

$$F_1(y_1, y_2) = (y_1 + y_2) \left\{ [(y_1 + y_2)^2 + 2(1 + y_1 y_2)^2] \left(\pi - \cos^{-1} \frac{1 + y_1 y_2}{y_1 + y_2} \right) \right. \\ \left. + 3(1 + y_1 y_2) \sqrt{(1 - y_1^2)(y_2^2 - 1)} \right\},$$

$$F_0(y_1, y_2) = (y_1 + y_2) \left[(y_1 + y_2)^2 \left(\pi - \cos^{-1} \frac{1 + y_1 y_2}{y_1 + y_2} \right)^2 - 2(1 - y_1^2)(y_2^2 - 1) \right. \\ \left. - (1 + y_1 y_2) \sqrt{(1 - y_1^2)(y_2^2 - 1)} \left(\pi - \cos^{-1} \frac{1 + y_1 y_2}{y_1 + y_2} \right) \right],$$

$$v_2(y_1, y_2) = \frac{1}{2} \sqrt{(1 - y_1^2)(y_2^2 - 1)} + \frac{\pi}{2} (y_1^2 + y_2^2) \\ - \left(\frac{y_1 + y_2}{2} \right)^2 \cos^{-1} \frac{1 + y_1 y_2}{y_1 + y_2} - \left(\frac{y_2 - y_1}{2} \right)^2 \cos^{-1} \frac{1 - y_1 y_2}{y_2 - y_1}.$$

Table 5.6.1 Values of the pair correlation function g for the point process of vertices of \mathcal{V}_P in \mathbb{R}^2 .

r	$g(r)$	r	$g(r)$	r	$g(r)$
0.05	3.8263	1.05	1.0055	2.05	1.0190
0.10	2.0372	1.10	1.0289	2.10	1.0153
0.15	1.4503	1.15	1.0487	2.15	1.0121
0.20	1.1651	1.20	1.0648	2.20	1.0095
0.25	1.0017	1.25	1.0769	2.25	1.0074
0.30	0.9003	1.30	1.0854	2.30	1.0057
0.35	0.8356	1.35	1.0902	2.35	1.0043
0.40	0.7948	1.40	1.0920	2.40	1.0032
0.45	0.7712	1.45	1.0910	2.45	1.0024
0.50	0.7607	1.50	1.0877	2.50	1.0018
0.55	0.7606	1.55	1.0828	2.55	1.0013
0.60	0.7690	1.60	1.0766	2.60	1.0009
0.65	0.7844	1.65	1.0696	2.65	1.0007
0.70	0.8054	1.70	1.0622	2.70	1.0005
0.75	0.8307	1.75	1.0547	2.75	1.0003
0.80	0.8590	1.80	1.0474	2.80	1.0002
0.85	0.8892	1.85	1.0405	2.85	1.0001
0.90	0.9200	1.90	1.0342	2.90	1.0001
0.95	0.9503	1.95	1.0285	2.95	1.0001
1.00	0.9791	2.00	1.0234	≥ 3.00	1.0000

Source: Muche (1999).

Numerical values of $g(r)$ are given in Table 5.6.1 and Figure 5.6.1.

For $m = 3$,

$$g(r) = \frac{g_{0,3}^*(r)}{576} + \frac{g_{0,3}(r)}{576} + \frac{g_{1,3}(r)}{36} + \frac{g_{2,3}(r)}{8} + \frac{g_{3,3}(r)}{6}, \quad r \geq 0, \quad (5.6.2)$$

where $g_{0,3}^*$ can be obtained from equation (5.6.1):

$$\begin{aligned} g_{0,3}^*(r) = & 288 \int_0^{\frac{4\pi}{3}\lambda r^3} \left\{ 1 - \left[1 + \left(r \left(\frac{4\pi}{3} \right)^{1/3} - y^{1/3} \right)^3 + \frac{1}{2} \left(r \left(\frac{4\pi}{3} \right)^{1/3} - y^{1/3} \right)^6 \right] \right. \\ & \times \exp \left[- \left(r \left(\frac{4\pi}{3} \right)^{1/3} - y^{1/3} \right)^3 \right] \left. \right\} y^2 \exp(-y) dy, \end{aligned}$$

and for $j = 0, 1, 2$ and 3 ,

$$\begin{aligned} g_{j,3} = & \left(\frac{35}{96\pi^2} \right)^2 \left(\frac{r^3}{4} \right)^{6-j} \int_1^\infty \int_0^1 \exp \left\{ - \frac{\pi r^3}{12} [2y_2(3y_1^2 + y_2^2) + 3(y_1^2 + y_2^2 + y_1^2 y_2^2) - 1] \right\} \\ & \times (y_2^2 - y_1^2)^{8-j} \Delta_j(y_1, y_2) dy_1 dy_2. \end{aligned}$$

The functions Δ_j are given by

$$\Delta_0 = J_0 \left(\cos^{-1} \frac{1 + y_1 y_2}{y_2 + y_1} \right) J_0 \left(\cos^{-1} \frac{1 - y_1 y_2}{y_2 - y_1} \right),$$

$$\Delta_j = \int_{[-\pi, \pi]^j} J_j \left(\cos^{-1} \frac{1 + y_1 y_2}{y_2 + y_1}, \psi_1, \dots, \psi_j \right) J_j \left(\cos^{-1} \frac{1 - y_1 y_2}{y_2 - y_1}, \psi_1, \dots, \psi_j \right) d(\psi_1, \dots, \psi_j),$$

where

$$\begin{aligned} J_3(\alpha, \psi_1, \psi_2, \psi_3) = & \int_{[-\pi, \pi]} \int_{[\alpha, \pi]} \left| \det \begin{pmatrix} 1 & \sin \phi_1 \sin \varphi_1 & \cos \phi_1 \sin \varphi_1 & \cos \varphi_1 \\ 1 & \sin \psi_1 \sin \alpha & \cos \psi_1 \sin \alpha & \cos \alpha \\ 1 & \sin \psi_2 \sin \alpha & \cos \psi_2 \sin \alpha & \cos \alpha \\ 1 & \sin \psi_3 \sin \alpha & \cos \psi_3 \sin \alpha & \cos \alpha \end{pmatrix} \right| \\ & \times \sin \varphi_1 d\phi_1 d\varphi_1, \end{aligned}$$

$$\begin{aligned} J_2(\alpha, \psi_1, \psi_2) = & \int_{[-\pi, \pi]^2} \int_{[\alpha, \pi]^2} \left| \det \begin{pmatrix} 1 & \sin \phi_1 \sin \varphi_1 & \cos \phi_1 \sin \varphi_1 & \cos \varphi_1 \\ 1 & \sin \phi_2 \sin \varphi_2 & \cos \phi_2 \sin \varphi_2 & \cos \varphi_2 \\ 1 & \sin \psi_1 \sin \alpha & \cos \psi_1 \sin \alpha & \cos \alpha \\ 1 & \sin \psi_2 \sin \alpha & \cos \psi_2 \sin \alpha & \cos \alpha \end{pmatrix} \right| \\ & \times \sin \varphi_1 \sin \varphi_2 d(\phi_1, \varphi_1) d(\phi_2, \varphi_2), \end{aligned}$$

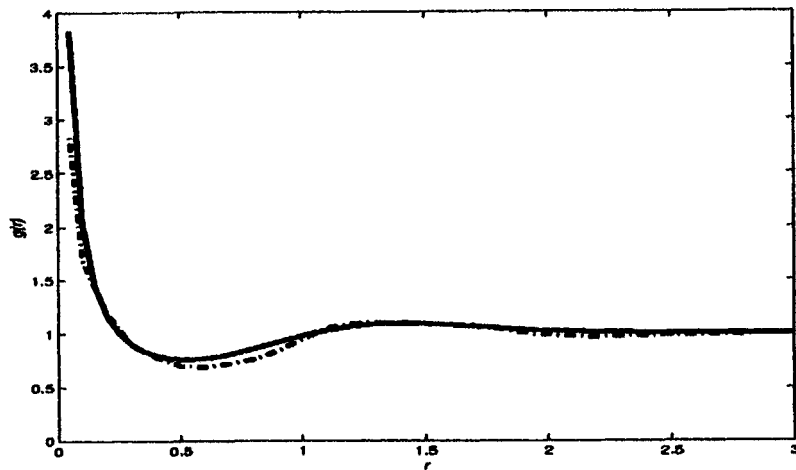


Figure 5.6.1 Pair correlation function g for the point process of vertices of \mathcal{V}_p in \mathbb{R}^2 (— numerical values from Muche, 1999; - - estimates from Stoyan and Stoyan, 1990).

$$\begin{aligned}
 J_1(\alpha, \psi_1) &= \int_{[-\pi, \pi]^3} \int_{[\alpha, \pi]^3} \left| \det \begin{pmatrix} 1 & \sin \phi_1 \sin \varphi_1 & \cos \phi_1 \sin \varphi_1 & \cos \varphi_1 \\ 1 & \sin \phi_2 \sin \varphi_2 & \cos \phi_2 \sin \varphi_2 & \cos \varphi_2 \\ 1 & \sin \phi_3 \sin \varphi_3 & \cos \phi_3 \sin \varphi_3 & \cos \varphi_3 \\ 1 & \sin \psi_1 \sin \alpha & \cos \psi_1 \sin \alpha & \cos \alpha \end{pmatrix} \right| \\
 &\quad \times \sin \phi_1 \sin \varphi_2 \sin \varphi_3 d(\phi_1, \phi_2, \phi_3) d(\psi_1, \phi_2, \phi_3), \\
 J_0(\alpha) &= 2\pi \int_0^\pi \int_0^\pi \int_0^{\pi/2} |\cos \psi - \cos \tau| T(\alpha, \varphi, \tau) U(\alpha, \varphi, \psi) \\
 &\quad \times \sin^5 \tau \sin \varphi \sin \psi d\tau d\varphi d\psi
 \end{aligned}$$

with

	$0 \leq b + c \leq a$ or $a + b + c \geq 2\pi$	$ b - c \geq a$	Otherwise
$T(a, b, c)$	0	$12\pi^3$	$S\left(\cos^{-1} \frac{\cos b \cos c - \cos a}{\sin b \sin c}\right)$
$U(a, b, c)$	0	2π	$2 \cos^{-1} \frac{\cos b \cos c - \cos a}{\sin b \sin c}$

Table 5.6.2 Values of the pair correlation function g for the point process of vertices of \mathcal{V}_P in \mathbb{R}^3 .

r	$g(r)$	r	$g(r)$	r	$g(r)$
0.01	764.2665	0.65	0.8984	1.65	1.0678
0.02	200.9408	0.70	0.8725	1.70	1.0614
0.03	91.7755	0.75	0.8562	1.75	1.0532
0.04	52.9836	0.80	0.8478	1.80	1.0443
0.05	34.8224	0.85	0.8462	1.85	1.0354
0.06	24.8332	0.90	0.8505	1.90	1.0272
0.07	18.7338	0.95	0.8599	1.95	1.0201
0.08	14.7256	1.00	0.8739	2.00	1.0143
0.09	11.9437	1.05	0.8917	2.05	1.0098
0.10	9.9299	1.10	0.9125	2.10	1.0064
0.15	5.0193	1.15	0.9355	2.15	1.0040
0.20	3.2034	1.20	0.9596	2.20	1.0025
0.25	2.3217	1.25	0.9838	2.25	1.0014
0.30	1.8230	1.30	1.0069	2.30	1.0008
0.35	1.5125	1.35	1.0277	2.35	1.0004
0.40	1.3065	1.40	1.0451	2.40	1.0002
0.45	1.1639	1.45	1.0584	2.45	1.0001
0.50	1.0623	1.50	1.0673	2.50	1.0001
0.55	0.9891	1.55	1.0715	2.55	1.0000
0.60	0.9361	1.60	1.0714	≥ 2.60	1.0000

Source: Heinrich *et al.* (1998, Table 9).

and $S(a) = 12a^3 - 3a \sin^2 2a - 24a \sin^2 a + 12 \sin 2a \sin^2 a$. The computation of $g_{j,3}$ is laborious and numerical values of $g_{0,3}^*(r)$ and $g_{j,3}(r)$ are presented in Heinrich *et al.* (1998, Tables 3–7, Figures 3–7). Numerical values of $g(r)$ is given in Table 5.6.2 (see Heinrich *et al.*, 1998, Tables 8–9, Figures 8–9) and Figure 5.6.2.

Heinrich and Muche (1994) showed that $\lim_{r \rightarrow 0} r^{m-1} g(r)$ exists and is non-zero. For example, if $m = 2$, $\lim_{r \rightarrow 0} r g(r) = 16/(9\pi^2\sqrt{\lambda})$. Therefore, g possesses a pole of order $m-1$ at $r = 0$.

The asymptotic behaviour of g for large r is governed by the following exponential bounds:

$$1 - \frac{g_{0,m}^*(r)}{[(m+1)!]^2} \leq 2 \exp\left(\frac{\lambda \omega_m r^m}{2^m}\right)^{m-1} e^{-\lambda \omega_m r^m / 2^m}, \quad r \geq 2(\omega_m \lambda)^{-1/m^2},$$

$$g_{j,m}(r) \leq c_m (\lambda r^m)^{2m-j-1} e^{-\lambda \omega_m r^m / 2^m}, \quad r \geq 2(\omega_m \lambda)^{-1/m},$$

$$j = 0, 1, \dots, m,$$

for some positive constant c_m . These bounds guarantee the existence of the integral $\int_0^\infty r^{m-1} [g(r) - 1] dr$, which is closely related to the variance of the following estimator of λ_0 .

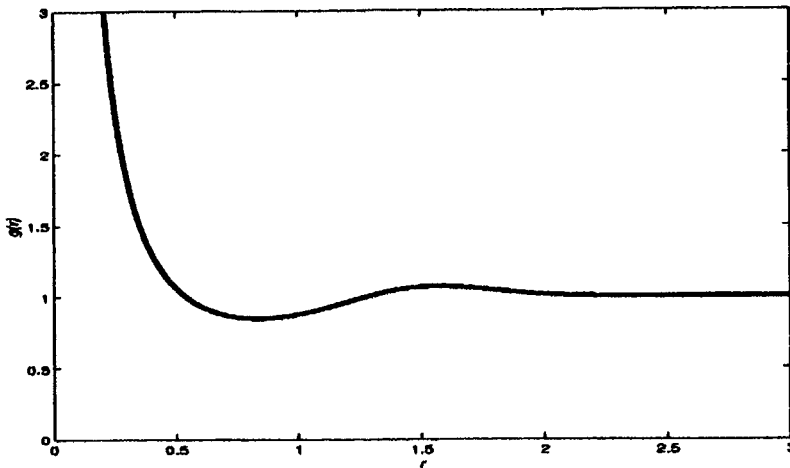


Figure 5.6.2 Pair correlation function g for the point process of vertices of \mathcal{V}_P in \mathbb{R}^3 (values from Heinrich *et al.*, 1998).

A natural unbiased estimator $\hat{\lambda}_{0,L}$ of λ_0 from point patterns observed within a cube $[0, L]^m$ in \mathbb{R}^m is

$$\hat{\lambda}_{0,L} = \frac{\Theta_{P_0} \cap [0, L]^m}{L^m},$$

where $\Theta_{P_0} \cap [0, L]^m$ is the number of points of Θ_{P_0} within $[0, L]^m$. A central limit theorem for $\Theta_{P_0} \cap [0, L]^m$ can be deduced from Heinrich (1994, Corollary of Theorem 2.3):

$$\frac{\hat{\lambda}_{0,L} L^m - \kappa_m \lambda L^m}{\sqrt{\lambda \kappa_m (1 + \kappa_m \sigma_m^2) L^m}} \longrightarrow Z \text{ in distribution as } L \rightarrow \infty,$$

where Z denotes a standard normal random variable and

$$\sigma_m^2 = m \omega_m \int_0^\infty r^{m-1} [g(r \lambda^{-1/m}) - 1] dr$$

is a constant depending only on m (Heinrich and Muche, 1994). In particular, $\sigma_2 = 0.744$ and $\sigma_3 = 2.255$ (Heinrich *et al.*, 1998). Central limit theorems for the fibre process of edges and other point processes associated with Poisson Voronoi diagrams and Voronoi diagrams satisfying a β -mixing (absolute regularity) condition (see Section 1.3.3) have also been established in Heinrich (1994).

Stoyan and Stoyan (1990) provide methods for estimating g and $\rho^{(2)}$ from point patterns observed within a bounded region in \mathbb{R}^2 . Using Monte Carlo simulation, they estimate g for Θ_{P_0} and Θ_{P_1} of \mathcal{V}_P in \mathbb{R}^2 . These functions are shown in Figures 5.6.1 and 5.6.3. The estimated pair correlation function for

the point process of a vertex is quite close to the theoretical form given in equation (5.6.2).

This approach may be developed further by considering marked point processes in which one or more values (or marks) are associated with each of the points. Stoyan and Stoyan (1990) considered the situation where each edge centre c_i is marked by the angle, $\alpha(c_i)$ between the line through the end points of the edge and a given fixed line ($0 \leq \alpha(c_i) \leq 2\pi$). They defined an angle correlation function g_α by

$$g_\alpha(r) = \frac{\rho_\alpha^{(2)}(r)}{\rho^{(2)}(r)}, \quad r \geq 0,$$

where $\rho_\alpha^{(2)}(r)$ is a product density defined as follows. Again consider two infinitesimally small discs of area dA_1 and dA_2 with distance r between their centres and suppose that $\rho^{(2)}(r) dA_1 dA_2$ is the probability that there is an edge centre in each of the discs. Define

$$f(u, v) = \min \{ |u - v|, 2\pi - |u - v| \}$$

as the minimum angle between the two lines, of directions u and v , containing the edge centres. Then $\rho_\alpha^{(2)}(r) = f(u, v) dA_1 dA_2$ and $g_\alpha(r)$ can be interpreted as the conditional mean of the angles between the two edges. Stoyan and Stoyan (1990) estimated g_α for the edge centres of \mathcal{V}_p and this is illustrated in Figure 5.6.4. Stoyan and Hermann (1986) considered marking c_i using the areas, A_1 and A_2 of the two cells on each side of the edge containing c_i , where A_1 is the area of the cell lying in the upper half of \mathbb{R}^2 defined by a line through the end points of the edge. Thus, A_1 and A_2 have the same distribution. Possible marks for c_i include $A_1 \cdot A_2$ and $(A_1 + A_2)$. They calculated the means and variances for these marks for \mathcal{V}_p .

It is also possible to mark the original generator points of \mathcal{V}_p . Stoyan and Hermann (1986) did this in terms of the area of the cell associated with the generator to define an area correlation function g_A analogous to g_α defined above, where $g_A(r)$ may be interpreted as the mean of the product of the areas of two cells with generators a distance r apart. They estimated g_A for \mathcal{V}_p using a Monte Carlo simulation approach.

5.6.2 Voronoi growth models

Voronoi diagrams can be regarded as the resultant structure of a growth process. Each generator starts generating a cell at the same time by growing radially in all directions in \mathbb{R}^m with the same non-zero speed. When two growing cells meet each other, they stop growing at the contact surface so that the cell associated with a point is fully grown when growth ceases in all directions. At the end of such a growth process the whole space is occupied by cells and the resultant structure is a Voronoi diagram. Such a Voronoi growth model is also known as the *cell model* (Meijering, 1953) or the *site saturation model* (Saetre *et al.*, 1986). Further discussion on growth models

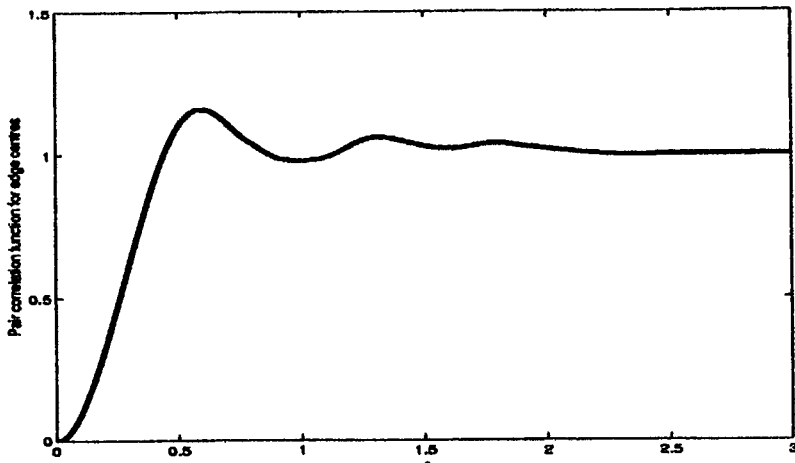


Figure 5.6.3 Pair correlation function for the edge centres of the Poisson Voronoi diagram in \mathbb{R}^2 (estimates from Stoyan and Stoyan, 1990).

can be found in Section 7.2. In Section 5.8 we will discuss a generalization of such a growth process in which generators do not start at the same time.

Chiu (1995c) studied the distribution of the *time of complete tessellation* T_L until a very large cube $[0, L]^m$ is completely occupied by cells of such a growth process, the generators of which form a Poisson point process of intensity λ . Assume that the growth starts at time 0 and suppose that the growth rate at time τ is v_τ . Chiu (1995c, Theorem 3) states that for each real number u ,

$$\Pr \left\{ \lambda \omega_m \left(\int_0^{T_L} v_\tau d\tau \right)^m - \log [\lambda L^m (\log \lambda L^m)^{m-1}] \leq u \right\} \rightarrow \exp(-\psi_m e^{-u})$$

as $L \rightarrow \infty$,

where $\omega_m = \pi^{m/2}/\Gamma(m/2 + 1)$ is the volume of an m -dimensional sphere of unit radius and

$$\psi_m = \frac{1}{m! \left\{ 2\Gamma\left(\frac{m+1}{2}\right) / m\sqrt{\pi} \Gamma\left(\frac{m}{2}\right) \right\}^{m-1}}. \quad (5.6.3)$$

Furthermore,

$$\frac{\lambda \omega_m \left(\int_0^{T_L} v_\tau d\tau \right)^m}{\log [\lambda L^m (\log \lambda L^m)^{m-1}]} \rightarrow 1 \text{ in probability as } L \rightarrow \infty.$$

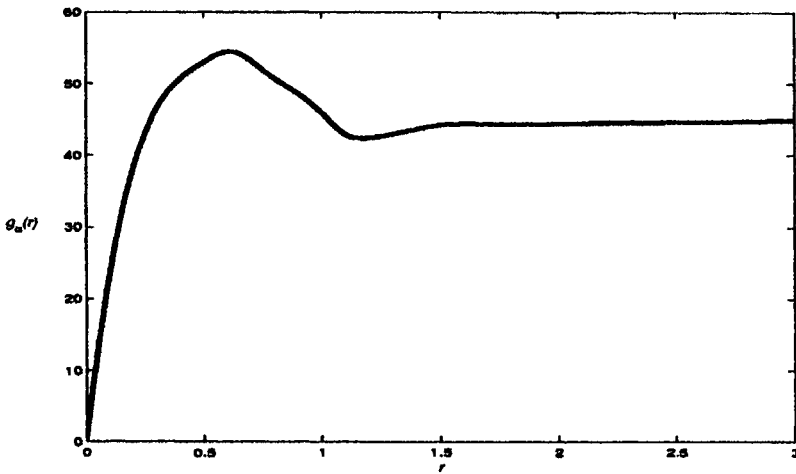


Figure 5.6.4 Angle correlation function g_a of the Poisson Voronoi diagram in \mathbb{R}^2 (estimates from Stoyan and Stoyan, 1990).

In particular, if v_t is equal to a constant v , then

$$T_L \simeq \left\{ \frac{\log [\lambda L^m (\log \lambda L^m)^{m-1}]}{\lambda \omega_m v^m} \right\}^{1/m} \quad \text{for large } L.$$

At any finite time t the space \mathbb{R}^m is not yet filled by cells and so we do not have a tessellation of the space. The union of all cells at time $t < \infty$ is called an *incomplete Voronoi diagram* (Muche, 1993). It is in fact a Boolean model (see, for example, Stoyan *et al.*, 1995, Chapter 3) with equal radius balls as grains. Muche (1993) has obtained the intensities $L_A(t)$ and $S_V(t)$ of the fibre process and the surface process of boundaries of cells at time t in \mathbb{R}^2 and in \mathbb{R}^3 , respectively:

$$L_A(t) = 4\lambda \int_0^t \exp(-\lambda \pi x^2) dx + (2\pi - 4)\lambda t \exp(-\lambda \pi t^2),$$

$$S_V(t) = \frac{16\pi\lambda}{3} \int_0^t x \exp\left(-\frac{4}{3}\pi\lambda x^3\right) dx + \frac{4}{3}\pi\lambda t^2 \exp\left(-\frac{4}{3}\pi\lambda t^3\right).$$

The linear and spherical contact distribution function (see Section 5.5.4) and the mean chord length (see Section 5.7) have also been derived.

Schulze *et al.* (1993) studied the normalized Euler characteristics of an incomplete Voronoi diagram at time t . The normalized Euler characteristic $\chi(t)$ is the mean of the difference of the number of connected components of the region occupied by cells in a square of area $1/\lambda$ and the number of connected components of the unoccupied region in the same square. Suppose the growth rate is a constant v , then

$$\chi(t) = (1 - \pi\nu^2 t^2) \exp(-\pi\nu^2 t^2).$$

Chiu (1995c) showed that as $t \rightarrow \infty$ in such a way that

$$\lambda L^m (\log \lambda L^m)^{m-1} e^{-\lambda \omega_m v^m t^m} \rightarrow e^{-u} \text{ as } L \rightarrow \infty,$$

for some real number u , then the number of connected components of the unoccupied region within $[0, L]^m$ follows a Poisson distribution with mean $\psi_m e^{-u}$ (see equation (5.6.3)), and such a component, after suitable normalization, converges essentially in distribution to a typical Poisson polyhedron formed by a stationary Poisson hyperplane process in \mathbb{R}^m (see Section 1.3.3) with intensity 1 (see also Hall, 1985).

5.6.3 The Stienen model

Stienen (1982) considered the maximal ball which can be inscribed in a Poisson Voronoi cell and centred at the generator of the cell. The union of these balls is now known as the *Stienen model*. It can also be regarded as the result of the following growth process: each generator starts growing radially in all directions. When two growing cells meet, these two cells stop growing. Thus, the Stienen model Ξ is the union of non-overlapping balls. The diameter of a typical sphere has the same distribution function D as the nearest neighbour distance of the Poisson point process, which is

$$D(r) = 1 - e^{-\lambda \omega_m r^m}, \quad r \geq 0.$$

This leads to the mean volume $1/(2^m \lambda)$. The covariance $C(r)$ is defined as $\Pr(o \in \Xi, r \in \Xi)$, where o is the origin and r a point at distance r from o . An analytical expression for $C(r)$ can be determined but the formula is very complicated except in the case when $m = 1$ (Schlather and Stoyan, 1997), which is given by

$$C(r) = \frac{1}{4} + 2e^{-3\lambda r/2} + \frac{e^{-2\lambda r}}{2} - \frac{2e^{-3\lambda r}}{5} + \left(\frac{\lambda r}{4} - \frac{21}{10}\right)e^{-4\lambda r/3} + \left(\frac{\lambda r}{12} + \frac{1}{4}\right)e^{-4\lambda r}$$

for $r \geq 0$. Wiencek and Stoyan (1993) have studied $C(r)$ for \mathcal{V}_P in \mathbb{R}^2 by simulation.

Another second-order statistic is $D_r(x, y)$, the probability that the diameter of a sphere at o is greater than x and the diameter of a sphere at r is greater than y , under the condition that there are sphere centres at o and r . In what follows we consider the Stienen model in \mathbb{R}^3 only. Stoyan (1990) showed that

$$D_r(x, y) = e^{-\lambda V(x, y, r)}, \quad r \geq 0,$$

where

$$V(x, y, r) = \begin{cases} \infty, & x \geq r \text{ or } y \geq r, \\ \frac{\pi}{3} [4x^3 + 4y^3 - (x-t)^2(2x+t) + (y+t-r)^2(2y-t+r)], & x+y > r, x < r \text{ and } y < r, \\ \frac{4}{3}\pi(x^3 + y^3), & x+y \leq r \end{cases}$$

and $t = (x^2 - y^2 + r^2)/(2r)$. A moment characteristic related to D_r is $k_{dd}(r)$, the mean of the product of the diameters of the spheres centred at o and r , where

$$k_{dd}(r) = \int_0^r \int_0^r e^{-\lambda V(x, y, r)} dx dy, \quad r \geq 0.$$

Note that $k_{dd}(0) = 0$ and $k_{dd}(\infty)$ is the square of the mean diameter of a typical sphere. The mean diameter is $[3/(4\pi)]^{1/3} \Gamma(4/3) \lambda^{-1/3} \approx 0.554 \lambda^{-1/3}$. Stoyan (1990) evaluated k_{dd} numerically. The values are reported in Table 5.6.3. The function k_{dd} is monotonic and $k_{dd}(2)$ is already very close to $k_{dd}(\infty)$. This indicates a short-range correlation.

5.6.4 Percolation on Poisson Voronoi diagrams and Poisson Delaunay tessellations

A *bond percolation model* is constructed from an infinite random lattice graph with periodic structure. Each edge will be assigned a value of 1 independently from the others with probability p and 0 with probability $1-p$. An edge assigned 0 will be deleted, whilst an edge assigned 1 will remain present. If instead of each edge we assign each vertex a value of 1 independently with probability p and 0 otherwise and retain those edges for which both endpoints have a value of 1, then a *site percolation model* is obtained. An important quantity in a percolation model is the critical or threshold probability p_c . If $p < p_c$, the expected cluster size is finite, and if $p > p_c$, there exists an infinite cluster with positive probability. The threshold probabilities for the bond and site percolation models on Poisson Voronoi diagrams and Poisson Delaunay tessellations in \mathbb{R}^2 and \mathbb{R}^3 are given in Table 5.6.4.

Table 5.6.3 Numerical values of the mean of the product of the diameters of two spheres whose centres are a distance r apart for the Stienen model in \mathbb{R}^3 .

r	0.1	0.2	0.3	0.4	0.5	0.6
$\lambda^{2/3} k_{dd}(r)$	0.010	0.039	0.085	0.141	0.196	0.243
r	0.7	0.8	0.9	1.0	2.0	
$\lambda^{2/3} k_{dd}(r)$	0.276	0.294	0.303	0.306	0.307	

Source: Stoyan (1990).

Table 5.6.4 The threshold probabilities for the bond and site percolation models on Poisson Voronoi diagrams and Poisson Delaunay tessellations in \mathbb{R}^m .

		Site	Bond
$m = 2$	Delaunay	0.5	0.347 [†]
	Voronoi	0.5	0.332*
$m = 3$	Voronoi	0.1453*	0.0822*

[†] Exact value = $2 \sin(\pi/18)$.

* Estimate.

Source: Jerauld *et al.* (1984a,b).

A *first-passage percolation*, originally suggested to model fluid flow in a random porous medium (Hammersly and Welsh, 1965), is a generalization of the bond percolation model in which each edge is independently assigned a non-negative random travel time from the same distribution, say F . The first-passage time between two vertices is the minimum travel time between the vertices over all paths connecting the vertices.

First-passage percolations on \mathcal{V}_p and \mathcal{D}_p in \mathbb{R}^2 were first suggested by Vahidi-Asl and Wierman (1990). They defined the first-passage time $t(u, v)$ in \mathcal{V}_p (\mathcal{D}_p) between two points u and v to be the minimum travel time between the vertices $p(u)$ and $p(v)$ which are the (almost surely unique) nearest vertices of u and v in \mathcal{V}_p (\mathcal{D}_p), respectively. Consider the first-passage time from the origin o to a point x . The limit $\lim_{\|x\| \rightarrow \infty} t(o, x)/\|x\| = \tau$ exists if and only if $\int_0^\infty [1 - F(t)]^3 dt < \infty$. Vahidi-Asl and Wierman (1992) established a shape theorem concerning the set $\mathcal{A}_t = \{x \in \mathbb{R}^2 : t(o, x) \leq t\}$ for $t > 0$. For all $\epsilon > 0$, the set \mathcal{A}_t contains a disc of radius $\tau^{-1}t(1 - \epsilon)$ and is contained in a disc of radius $\tau^{-1}t(1 + \epsilon)$ almost surely for all sufficiently large t if and only if $\int_0^\infty t[1 - F(t)]^3 dt < \infty$. Vahidi-Asl and Wierman (1993) studied the almost sure existence of the optimal path and the upper and lower bounds for the route length divided by the geometrical distance.

Howard and Newman (1997) suggested another first-passage percolation model on \mathcal{V}_p in \mathbb{R}^m . The distance between the two generators at locations x_1 and x_2 is defined to be $\|x_1 - x_2\|^\alpha$ for $\alpha \geq 0$. A route from a point u to v is the sequence (x_1, \dots, x_k) , where x_1 and x_k are the locations of the nearest generators of u and v , respectively; the length of this route is $\sum_{i=1}^{k-1} \|x_i - x_{i+1}\|^\alpha$ if $k \geq 2$ and zero otherwise. The first-passage time $t(u, v)$ from u to v is the length of the shortest route from u to v . Similar to Vahidi-Asl and Wierman (1990, 1992), they showed that the limit $\lim_{\|x\| \rightarrow \infty} t(o, x)/\|x\| = \tau_1$ exists and established a shape theorem for the set $\mathcal{B}_t = \{x \in \mathbb{R}^m : t(o, x) \leq t\}$ for $t > 0$. If $\alpha > 1$, then for each $\epsilon \in (0, \tau_1^{-1})$ the set \mathcal{B}_t contains an m -dimensional sphere of radius $\tau_1^{-1}t(1 - \epsilon)$ and is contained in an m -dimensional sphere of radius $\tau_1^{-1}t(1 + \epsilon)$ almost surely for all sufficiently large t .

5.7 SECTIONAL VORONOI DIAGRAMS

In many empirical situations involving tessellations in \mathbb{R}^3 it is not possible to observe the constituent cells directly. Instead the cells are examined by means of linear probes or planar sections. Indeed, the prevalence of such occurrences led to the development of the subject of stereology, which is concerned with drawing inferences about the geometric properties of three-dimensional material on the basis of observed, lower dimensional information.

We label the structure produced by the intersection between an s -dimensional hyperplane H_s ($1 \leq s \leq m$) and a Voronoi diagram \mathcal{V}_Θ generated by point process Θ in \mathbb{R}^m as the s -dimensional sectional Voronoi diagram denoted by $\mathcal{V}_s(s, m)$. In particular, if Θ is the stationary Poisson point process, then the corresponding sectional diagram is called the *s-dimensional sectional Poisson Voronoi diagram* and is denoted by $\mathcal{V}_P(s, m)$. Thus, \mathcal{V}_P in \mathbb{R}^3 is equivalent to $\mathcal{V}_P(3, 3)$. Also, the intersection of H_t with $\mathcal{V}_P(s, m)$ is equal to $\mathcal{V}_P(t, m)$, $t < s$ (Miles, 1986a, p. 153). Figure 5.7.1 shows a portion of $\mathcal{V}_P(2, 3)$. Since \mathcal{V}_P in \mathbb{R}^3 is homogeneous, isotropic and ergodic, $\mathcal{V}_P(s, m)$ has the same properties. Similarly, since \mathcal{V}_P is normal, so too is $\mathcal{V}_P(s, m)$. Nevertheless, a planar section of \mathcal{V}_P in \mathbb{R}^2 is not equivalent to a *Poisson Voronoi diagram* in \mathbb{R}^2 , because the mean values for the characteristics of $\mathcal{V}_P(2, 3)$ clearly deviate from the corresponding mean values of \mathcal{V}_P in \mathbb{R}^2 (Mecke, 1984). However,

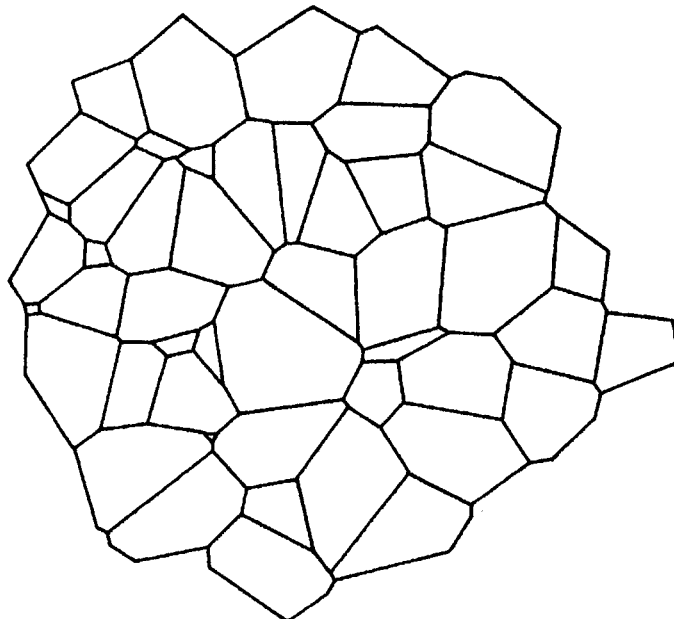


Figure 5.7.1 Portion of a two-dimensional sectional Poisson Voronoi diagram $\mathcal{V}_P(2, 3)$. (Source: Lorz, 1991.)

whether $\mathcal{V}_p(2, 3)$ is a Voronoi diagram generated by a *non-Poisson* point process cannot be answered by inspecting mean value formulae only. Chiu *et al.* (1996) proved that $\mathcal{V}_p(s, m)$ ($1 < s < m$) is *not* a Voronoi diagram, i.e. there does not exist any point process in \mathbb{R}^s ($1 < s < m$) the Voronoi diagram of which is the same as $\mathcal{V}_p(s, m)$. Moreover, almost surely each cell of $\mathcal{V}_p(s, m)$ is a *non-Voronoi cell*, i.e. a cell, together with all its neighbouring cells, is not possible to be present in a Voronoi diagram.

Only limited information about the characteristics of the individual cells of $\mathcal{V}_e(s, m)$ and $\mathcal{V}_p(s, m)$ has been obtained analytically and researchers have again resorted to Monte Carlo simulations as a source of supplementary information. General expressions paralleling those given in Table 5.1.1 for \mathcal{V}_e and equations (5.5.1)–(5.5.5) for \mathcal{V}_p may be derived by either the ergodic theorem (Miles, 1972a, 1984, 1986a) or the Palm distribution (Møller, 1989) (see Section 1.3.3). We use the same symbols employed in Section 5.5, and in addition use the superscript (s) to refer to the dimensionality of the hyperplane. Table 5.7.1 gives formulae for isotropic $\mathcal{V}_e(s, m)$, where $1 \leq s < m$ and $m = 2, 3$. The first moments given are only in terms of the intensities λ of the point process Θ , λ_0 of the point process of vertices, L_A and L_V of the fibre process of edges of \mathcal{V}_e for $m = 2$ and 3, respectively, and S_V of the surface process of cell faces of \mathcal{V}_e for $m = 3$. Since all these intensities for \mathcal{V}_p are known, explicit expressions for $\mathcal{V}_p(s, m)$, where $1 \leq s < m$ and $m = 2, 3$, can be derived (see Table 5.7.2). For an arbitrary m , Møller (1989) shows that the intensities of the vertices $\lambda_0^{(s)}$ and the midpoints of the edges of the cells $\lambda_1^{(s)}$ in $\mathcal{V}_p(s, m)$ are given by

$$\lambda_0^{(s)} = \frac{2}{s+1} \lambda_1^{(s)}, \quad (5.7.1)$$

$$\lambda_1^{(s)} = \frac{\lambda^{s/m} \pi^{s/2} \Gamma\left(\frac{ms+m-s+1}{2}\right) \Gamma\left(\frac{m}{2}+1\right)^{s+1-s/m} \Gamma\left(s+1-\frac{s}{m}\right)}{m \Gamma\left(\frac{s}{2}+1\right) \Gamma\left(\frac{ms+m-s}{2}\right) \Gamma\left(\frac{m+1}{2}\right)^{s+1}}. \quad (5.7.2)$$

Denote by $E_t^{(s)}$ the expectation with respect to the Palm distribution with respect to the typical t -faces of $\mathcal{V}_p(s, m)$ and by $E_t^{(s)} V_k$ the expected k -dimensional content of a k -face contained in a typical t -face of $\mathcal{V}_p(s, m)$. The expected length of a typical edge $E_1^{(s)} V_1$ in $\mathcal{V}_p(s, m)$ is

$$E_1^{(s)} V_1 = \frac{\Gamma\left(\frac{ms-s}{2}+1\right) \Gamma\left(\frac{ms+m-s}{2}\right) \Gamma\left(\frac{m+1}{2}\right) \Gamma\left(s-\frac{s-1}{m}\right)}{\lambda^{1/m} \Gamma\left(\frac{ms-s+1}{2}\right) \Gamma\left(\frac{ms+m-s+1}{2}\right) \Gamma\left(s-\frac{s}{m}+1\right) \Gamma\left(\frac{m}{2}+1\right)^{1-1/m}}. \quad (5.7.3)$$

For $s = 1$ and $m \geq 2$,

$$\lambda_0^{(1)} = \lambda_1^{(1)} = (\mathbf{E}_1^{(1)} V_1)^{-1} = \frac{2\lambda^{1/m} (m-1)! \Gamma\left(\frac{m}{2} + 1\right)^{2-1/m} \Gamma\left(2 - \frac{1}{m}\right)}{m \Gamma\left(m - \frac{1}{2}\right) \Gamma\left(\frac{m+1}{2}\right)^2}. \quad (5.7.4)$$

For $s = 2$ and $m \geq 3$,

$$\lambda_1^{(2)} = \frac{\lambda^{2/m} \pi \Gamma\left(\frac{3m-1}{2}\right) \Gamma\left(\frac{m}{2} + 1\right)^{3-2/m} \Gamma\left(3 - \frac{2}{m}\right)}{m \Gamma\left(\frac{3m}{2} - 1\right) \Gamma\left(\frac{m+1}{2}\right)^3},$$

$$\lambda_0^{(2)} = \frac{2}{3} \lambda_1^{(2)},$$

$$\lambda_2^{(2)} = \frac{1}{3} \lambda_1^{(2)},$$

$$\mathbf{E}_2^{(2)} V_0 = \mathbf{E}_2^{(2)} N_0 = \mathbf{E}_2^{(2)} N_1 = 6,$$

$$\mathbf{E}_2^{(2)} V_1 = \frac{6(m-1)! \Gamma\left(2 - \frac{1}{m}\right) \Gamma\left(\frac{3m}{2} - 1\right) \Gamma\left(\frac{m+1}{2}\right)}{\lambda^{1/m} \Gamma\left(\frac{m}{2} + 1\right)^{1-1/m} \Gamma\left(\frac{3m-1}{2}\right) \Gamma\left(m - \frac{1}{2}\right) \Gamma\left(3 - \frac{2}{m}\right)},$$

$$\mathbf{E}_1^{(2)} V_1 = \frac{(m-1)! \Gamma\left(\frac{3m}{2} - 1\right) \Gamma\left(\frac{m+1}{2}\right) \Gamma\left(2 - \frac{1}{m}\right)}{\lambda^{1/m} \Gamma\left(m - \frac{1}{2}\right) \Gamma\left(\frac{3m-1}{2}\right) \Gamma\left(3 - \frac{2}{m}\right) \Gamma\left(\frac{m}{2} + 1\right)^{1-1/m}},$$

$$\mathbf{E}_0^{(2)} V_1 = 3\mathbf{E}_1^{(2)} V_1.$$

Since our primary concern is with applications, the values of the above expressions for $s = 1, 2$ and $m = 2, 3$ are given in Table 5.7.2. As in Section 5.5, in order to avoid excessive use of subscripts, these values are given simpler symbols which are identified in the table. This table also includes a value for $\mathbf{E}^{(1)}(L_{1,2}^2)$ derived by numerical integration (Gilbert, 1962) and other moments estimated by Lorz (1990b, 1991) using Monte Carlo simulations. Lorz (1990b) has also estimated moments and correlation coefficients for the area, perimeter and a randomly chosen interior angle conditional on the number of edges for a typical cell of $\mathcal{V}_p(2, 3)$.

In addition to the exact mean sectional values given in Table 5.7.2, Miles (1972a, 1984) has derived asymptotic values as $m \rightarrow \infty$. These are reported in Table 5.7.3. Note that these mean values do not depend on the intensity

of the generators. Recall that the values for $\mathcal{V}_P(1, m)$ and $\mathcal{V}_P(2, m)$ are equivalent to the line sections of both $\mathcal{V}_P(3, m)$ and $\mathcal{V}_P(2, m)$ and the plane section of $\mathcal{V}_P(3, m)$, respectively.

A lemma due to Miles (1972a, p. 260) shows that an s -dimensional section of \mathcal{V}_P is stochastically equivalent to an s -dimensional section of a corresponding inhomogeneous $(s+1)$ -dimensional structure. In particular, let Θ_P^* be an inhomogeneous Poisson point process in \mathbb{R}^m with intensity $\lambda_m = \lambda_m(x_4, \dots, x_m)$ and \mathcal{V}_P^* be its associated Voronoi diagram. If ${}^0[3]$ is the three-dimensional subspace of \mathbb{R}^m defined by $x_4 = \dots = x_m = 0$, then since λ_m is functionally independent of (x_1, x_2, x_3) , the three-dimensional section of \mathcal{V}_P^* by ${}^0[3]$ is a homogeneous normal tessellation, denoted by $\mathcal{V}^*(3, m)$. Thus, $\mathcal{V}_P(3, m)$ is stochastically equivalent to $\mathcal{V}^*(3, 4)$ with respect to

$$\lambda_4(x_4) = \lambda x_4^{m-4} \left\{ \frac{2\pi^{(m-3)/2}}{\Gamma\left(\frac{m-3}{2}\right)} \right\} \quad (5.7.5)$$

(Miles, 1972a, pp. 260–261). This lemma extends from three-dimensional sections to general s -dimensional sections and Miles (1984) exploits it to derive a four-fold integral expression for the distribution of line segments when $s = 1$ but this is hardly tractable. However, Muche and Stoyan (1992) have derived numerically tractable double integral formulae for the chord length ($s = 1$) distribution functions, $F_{L_{1,2}}$ and $F_{L_{1,3}}$, in \mathbb{R}^2 and \mathbb{R}^3 , respectively. These distributions are derived from the linear contact distribution function $H_1(r)$ given in equation (5.5.31) (Gilbert, 1962) which gives the probabilities that a fixed line segment of length r , $r \geq 0$, with one end point in the origin, lies completely in the cell P_o containing the origin. The distribution of the chord length $L_{1,m}$ in $\mathcal{V}_P(1, m)$ and the linear contact distribution are linked by

$$H_1(r) = \frac{1}{E(L_{1,m})} \int_0^r [1 - F_{L_{1,m}}(x)] dx, \quad r \geq 0.$$

The mean chord length has been obtained by Gilbert (1962):

$$E(L_{1,m}) = \frac{\lambda^{-1/m} m \Gamma\left(\frac{m+1}{2}\right)^2 \Gamma\left(m - \frac{1}{2}\right)}{2(m-1)! \Gamma\left(2 - \frac{1}{m}\right) \Gamma\left(\frac{m}{2} + 1\right)^{(2m-1)/m}}.$$

The cumulative distributions of $L_{1,2}$ and $L_{1,3}$ as derived by Muche and Stoyan (1992) using numerical integration are given in Table 5.7.4. Explicit expressions for the pdf are given in equations (5.7.7) and (5.7.8), with $s = 1$. The densities for $2 \leq m \leq 7$ are illustrated in Figure 5.7.2.

The chord length distribution for $\mathcal{V}_P(1, m)$ is given in Schlather (1999), in which the distribution of the length $L_{s,m}$ of a typical edge in $\mathcal{V}_P(s, m)$ ($1 \leq s \leq m$) has also been given (cf. Muche, 1996a, p. 280):

Table 5.7.1 Moments of various characteristics of an s -dimensional homogeneous sectional Voronoi diagram $\mathcal{V}_\Theta(s, m)$.

Moment	Symbol	Exact value
$s = 1, m = 2$		
Intensity of vertices	$\lambda_0^{(1)}$	$2L_A/\pi$
Intensity of mid-points of line segments	$\lambda_1^{(1)}$	$2L_A/\pi$
Expected length of a typical line segment $[E_1^{(1)}V_1]$ and its third moment $E_1^{(1)}(V_1^3)$	$E^{(1)}(L_{1,2})$ $E^{(1)}(L_{1,2}^3)$	$\pi/(2L_A)$ $3\lambda E_2(V_2^2)/(2L_A)$
$s = 1, m = 3$		
Intensity of vertices	$\lambda_0^{(1)}$	$S_V/2$
Intensity of mid-points of line segments	$\lambda_1^{(1)}$	$S_V/2$
Expected length of a typical line segment $[E_1^{(1)}V_1]$, its third moment $[E_1^{(1)}(V_1^3)]$ and its fourth moment $[E_1^{(1)}(V_1^4)]$	$E^{(1)}(L_{1,3})$ $E^{(1)}(L_{1,3}^3)$ $E^{(1)}(L_{1,3}^4)$	$2/S_V$ $3L_V E^{(2)}(A^2)/(2\pi S_V)$ $6\lambda E_3(V_3^2)/(\pi S_V)$
$s = 2, m = 3$		
Intensity of vertices	$\lambda_0^{(2)}$	$L_V/2$
Intensity of mid-points of cell edges	$\lambda_1^{(2)}$	$3L_V/4$
Intensity of cell centroids	$\lambda_2^{(2)}$	$L_V/4$
Expected number of vertices of a typical cell $[E_2^{(2)}N_0]$ (edges of a typical cell $[E_2^{(2)}N_1]$)	$E^{(2)}(N)$	6
Expected area of a typical cell $[E_2^{(2)}V_2]$	$E^{(2)}(A)$	$4/L_V$
Expected perimeter of a typical cell $[E_2^{(2)}V_1]$	$E^{(2)}(P)$	$2\pi S_V/L_V$
Expected length of a typical edge $[E_2^{(2)}V_1]$ and its third moment $[E_1^{(2)}(V_1^3)]$	$E^{(2)}(L_{2,3})$ $E^{(2)}(L_{2,3}^3)$	$(\pi/3)(S_V/L_V)$ $(\lambda + \lambda_0) E_2(V_2^2)/L_V$

L_A = intensity of the fibre process of edges of \mathcal{V}_Θ in \mathbb{R}^2 .

L_V = intensity of the fibre process of edges of \mathcal{V}_Θ in \mathbb{R}^3 .

S_V = intensity of the surface process of faces of \mathcal{V}_Θ in \mathbb{R}^3 .

λ_0 = intensity of the point process of vertices of \mathcal{V}_Θ .

λ = intensity of Θ .

V_2 = area of a typical cell of \mathcal{V}_Θ in \mathbb{R}^2 /a typical face of \mathcal{V}_Θ in \mathbb{R}^3 .

V_3 = volume of a typical cell of \mathcal{V}_Θ in \mathbb{R}^3 .

Source: Møller (1994, Propositions 3.4.4 and 3.4.5).

Table 5.7.2 The first and/or second-order moments of various characteristics of an s -dimensional sectional Poisson Voronoi diagram.

Moment	Symbol	Exact value	Numerical value	Estimate*
$s = 1, m = 2$				
Intensity of vertices	$\lambda_0^{(1)}$	$4\lambda^{1/2}/\pi$	$1.273\lambda^{1/2}$	
Intensity of mid-points of line segments	$\lambda_0^{(1)}$	$4\lambda^{1/2}/\pi$	$1.273\lambda^{1/2}$	
Expected length of a typical line segment $[E_1^{(1)}V_1]$ and its second moment $E_1^{(1)}(V_1^2)$	$E_1^{(1)}(L_{1,2}^{(1)})$	$\pi/(4\lambda^{1/2})$	$0.785\lambda^{-1/2}$	
	$E_1^{(1)}(L_{1,2}^{(1)})$		$0.804\lambda^{-1}$	
$s = 1, m = 3$				
Intensity of vertices	$\lambda_0^{(1)}$	$\Gamma(2/3)(32\pi\lambda/81)^{1/3}$	$1.455\lambda^{1/3}$	
Intensity of mid-points of line segments	$\lambda_0^{(1)}$	$\Gamma(2/3)(32\pi\lambda/81)^{1/3}$	$1.455\lambda^{1/3}$	
Expected length of a typical line segment $[E_1^{(1)}V_1]$ and its second moment $E_1^{(1)}(V_1^2)$	$E_1^{(1)}(L_{1,3}^{(1)})$	$(32\pi\lambda/81)^{-1/3}\Gamma(2/3)^{-1}$	$0.687\lambda^{-1/3}$	
	$E_1^{(1)}(L_{1,3}^{(1)})$		$0.632\lambda^{-2/3}$	
$s = 2, m = 3$				
Intensity of vertices	$\lambda_0^{(2)}$	$2\Gamma(1/3)(16\pi\lambda^2/9)^{1/3}/15$	$2.916\lambda^{2/3}$	
Intensity of mid-points of cell edges	$\lambda_0^{(2)}$	$\Gamma(1/3)(16\pi\lambda^2/9)^{1/3}/5$	$4.374\lambda^{2/3}$	
Intensity of cell centroids	$\lambda_0^{(2)}$	$\Gamma(1/3)[16\pi\lambda^2/9]^{1/3}/15$	$1.458\lambda^{2/3}$	
Expected number of vertices of a typical cell $[E_2^{(2)}V_3]$ (edges of a typical cell $[E_2^{(2)}N_1]$ and its second moment $[E_2^{(2)}(N_0^2)]$)	$E_2^{(2)}(N)$	6	6	
Expected area of a typical cell $[E_2^{(2)}V_2]$ and its second moment $[E_2^{(2)}(V_2^2)]$	$E_2^{(2)}(A)$	$15/[\Gamma(1/3)(16\pi\lambda^2/9)^{1/3}]$	$0.686\lambda^{-2/3}$	
Expected perimeter of a typical cell $[E_2^{(2)}V_1]$ and its second moment $[E_2^{(2)}(V_1^2)]$	$E_2^{(2)}(A')$	$5/(6\pi)^{1/3}\Gamma(2/3)\lambda^{-1/3}/\Gamma(1/3)$	$0.699\lambda^{-4/3}$	
Expected length of a typical edge $[E_2^{(2)}V_1]$ and its second moment $[E_2^{(2)}(V_1^2)]$	$E_2^{(2)}(P)$	$5\Gamma(2/3)(36\pi\lambda)^{-1/3}/\Gamma(1/3)$	$3.136\lambda^{-1/3}$	
Expected value of an interior angle of a typical cell and its second moment	$E_2^{(2)}(P')$	$0.523\lambda^{-1/3}$	$11.308\lambda^{-2/3}$	
Expected value of an angle at a typical vertex and its second moment	$E_2^{(2)}(L_{2,3}^{(2)})$	$0.404\lambda^{-2/3}$	$0.404\lambda^{-2/3}$	
	$E_2^{(2)}(L_{2,3}^{(2)})$		2.094	2.094
	$E_2^{(2)}(\alpha_2)$	$2\pi/3$		4.349
	$E_2^{(2)}(\alpha_1)$			4.689
	$E_2^{(2)}(\alpha_1^2)$			

$\lambda =$ intensity of the m -dimensional Poisson point process Θ_p .

* Estimates from Monte Carlo simulation by Lorz (1990b, 1991).

Table 5.7.3 Asymptotic moments of various characteristics of an s -dimensional sectional Poisson Voronoi diagram $\gamma_p(s, m)$, as $m \rightarrow \infty$.

Symbol	Characteristic		Simpler symbol	Exact value	Numerical value
$s = 1$					
$E_1^{(1)}V_1$	Length of a typical line segment		$E^{(1)}(L_{1,\infty})$	$(2e)^{-1/2}$	0.429
$s = 2$					
$E_2^{(2)}N_6$ $(E_2^{(2)}N_1)$	Number of vertices of a typical cell (edges of a typical cell)	$E^{(2)}(N)$		6	6
$E_2^{(2)}V_2$	Area of a typical cell	$E^{(2)}(A)$	$3^{1/2}/(\pi e)$	0.203	
$E_2^{(2)}V_1$	Perimeter of a typical cell	$E^{(2)}(P)$	$(6/e)^{1/2}$	1.486	
$s = 3$					
$E_3^{(3)}N_6$	Number of vertices of a typical cell	$E^{(3)}(M)$	$1/\phi$	22.795	
$E_3^{(3)}N_1$	Number of edges of a typical cell	$E^{(3)}(E)$	$3/(2\phi)$	34.192	
$E_3^{(3)}N_2$	Number of faces of a typical cell	$E^{(3)}(F)$	$2 + 1/(4\phi)$	13.397	
$E_3^{(3)}N_6$ $(E_3^{(3)}N_1)$	Number of vertices of a typical face (edges of a typical face)	$E^{(3)}(N)$	$6/(4\phi + 1)$	5.104	
$E_3^{(3)}V_3$	Volume of a typical cell	$E^{(3)}(V)$	$1/(16\pi e^{3/2}\phi)$	0.101	
$E_3^{(3)}V_2$	Surface area of a typical cell	$E^{(3)}(S)$	$1/(2^{3/2}\pi e\phi)$	0.944	
$E_3^{(3)}V_1$	Total edge length of a typical cell	$E^{(3)}(B)$	$3/[4(3e)^{1/2}\phi]$	5.987	
$E_2^{(3)}V_2$	Area of a typical face	$E^{(3)}(A)$	$1/[2^{1/2}ne(4\phi + 1)]$	0.070	
$E_2^{(3)}V_1$	Total edge length of a typical face	$E^{(3)}(P)$	$(3e)^{1/2}/(4\phi + 1)$	0.894	
$E_3^{(3)}V_1$	Length of a typical edge	$E^{(3)}(L_{3,\infty})$	$1/[2(3e)^{1/2}]$	0.175	

$$\phi = 1/8 - [3/(4\pi)] \sin^{-1}(1/3).$$

Source: Miles (1972a, 1984).

Table 5.7.4 Chord length distributions for line segments $L_{1,2}$ for $\mathcal{V}_P(1, 2)$ and $L_{1,3}$ for $\mathcal{V}_P(1, 3)$.

r	$F_{L_{1,m}}(r)$		r	$F_{L_{1,m}}(r)$	
	$m = 2$	$m = 3$		$m = 2$	$m = 3$
0.00	0.000000	0.000000	1.65	0.969415	0.993309
0.05	0.021818	0.032205	1.70	0.975859	0.995651
0.10	0.044602	0.065057	1.75	0.981105	0.997247
0.15	0.068508	0.098591	1.80	0.985335	0.998305
0.20	0.093721	0.132843	1.85	0.988714	0.998985
0.25	0.120442	0.167850	1.90	0.991387	0.999410
0.30	0.148868	0.203651	1.95	0.993481	0.999667
0.35	0.179170	0.240286	2.00	0.995108	0.999818
0.40	0.211472	0.277787	2.05	0.996359	0.999903
0.45	0.245824	0.316178	2.10	0.997312	0.999950
0.50	0.282201	0.355461	2.15	0.998033	0.999975
0.55	0.320481	0.395611	2.20	0.998572	0.999988
0.60	0.360450	0.436560	2.25	0.998972	0.999995
0.65	0.401805	0.478188	2.30	0.999266	0.999998
0.70	0.444167	0.520312	2.35	0.999480	0.999999
0.75	0.487098	0.562677	2.40	0.999635	1.000000
0.80	0.530122	0.604958	2.45	0.999746	1.000000
0.85	0.572744	0.646764	2.50	0.999824	1.000000
0.90	0.614478	0.687650	2.55	0.999880	1.000000
0.95	0.654865	0.727139	2.60	0.999918	1.000000
1.00	0.693491	0.764751	2.65	0.999945	1.000000
1.05	0.730005	0.800029	2.70	0.999963	1.000000
1.10	0.764122	0.832570	2.75	0.999976	1.000000
1.15	0.795637	0.862056	2.80	0.999984	1.000000
1.20	0.824420	0.888273	2.85	0.999989	1.000000
1.25	0.850416	0.911122	2.90	0.999993	1.000000
1.30	0.873636	0.930625	2.95	0.999996	1.000000
1.35	0.894154	0.946912	3.00	0.999997	1.000000
1.40	0.912091	0.960209	3.05	0.999998	1.000000
1.45	0.927606	0.970813	3.10	0.999999	1.000000
1.50	0.940887	0.979067	3.15	0.999999	1.000000
1.55	0.952140	0.985333	3.20	1.000000	1.000000
1.60	0.961578	0.989969	3.25	1.000000	1.000000

Source: Muche and Stoyan (1990) and Muche (1999).

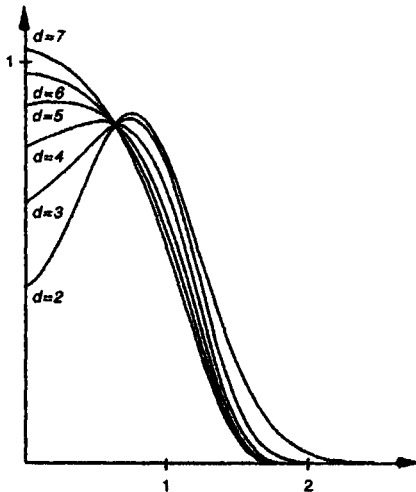


Figure 5.7.2 Probability density functions for the chord length $L_{1,m}$ in $\mathcal{V}_P(1, m)$ for $2 \leq m \leq 7$ ($\lambda = 1$). It should be noted that the six curves do not intersect at a common point. (Source: Muche and Stoyan, 1992, Figure 2.)

$$F_{L_{s,m}}(l) = 1 - \frac{m^2 \Gamma\left(\frac{ms-s+m}{2}\right) \pi^{(m-1)(s+1)/2}}{2\Gamma\left(\frac{ms+m-s+1}{2}\right) \Gamma\left(\frac{s(m-1)}{m}\right)} \left[\frac{\lambda}{\Gamma\left(\frac{m+2}{2}\right)} \right]^{(ms-s+m)/m} \\ \times \int_0^\infty \int_0^\pi r^{(m-1)(s+1)} \exp[-\lambda U_m(r, r_{l,\beta}, l)] \sin^{ms-s-1} \beta \\ \times \left(m \cos \beta \int_\beta^\pi \sin^m \varphi \, d\varphi + \sin^{m+1} \beta \right) d\beta \, dr, \quad l \geq 0, \quad (5.7.6)$$

where $r_{l,\beta}$ is given in equation (5.5.21) and $U_m(r, r_{l,\beta}, l)$ in equation (5.5.26), which denotes the volume of the union of two m -dimensional balls with radii r and $r_{l,\beta}$ and the distance between their centres is l . In particular, $F_{L_{s,m}}$ is the chord length distribution when $s = 1$ and the distribution of the length of a typical edge in \mathcal{V}_P given in equation (5.5.25) when $s = m$. Muche (1999) gave equivalent expressions of the pdf $f_{L_{s,m}}$ of $L_{s,m}$ for $1 \leq s \leq m \leq 3$:

$$f_{L_{s,2}}(l) = \frac{2s\lambda^{3/2}(\lambda\pi)^{(s+1)/2}}{\Gamma\left(\frac{s+3}{2}\right)} l^{s+3} \int_0^\pi \int_0^{\pi-\beta_1} \frac{\sin^{s+1} \beta_1 \sin^{s+1} \beta_2 [\sin \beta_1 + (\pi - \beta_1) \cos \beta_1]}{\sin^{s+4}(\beta_1 + \beta_2)} \\ \times [\sin \beta_2 + (\pi - \beta_2) \cos \beta_2] \exp\left(-\lambda l^2 \frac{\sin \beta_1 \sin \beta_2 \sin(\beta_1 + \beta_2)}{\sin^2(\beta_1 + \beta_2)}\right) \\ \times \exp\left(-\lambda l^2 \frac{(\pi - \beta_1) \sin^2 \beta_2 + (\pi - \beta_2) \sin^2 \beta_1}{\sin^2(\beta_1 + \beta_2)}\right) d\beta_2 \, d\beta_1, \quad l \geq 0, \quad (5.7.7)$$

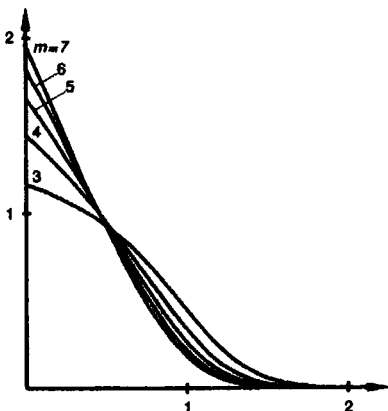


Figure 5.7.3 Probability density functions for the length $L_{2,m}$ of a typical edge in $V_p(2, m)$ for $3 \leq m \leq 7$ ($\lambda = 1$). (Source: Muche, 1996a, Figure 2.)

Table 5.7.5 Simulation studies of sectional Poisson Voronoi diagrams $V_p(2,3)$ and $V_p(1,3)$.

Study	Number of cells	Characteristics
Hahn and Lorz (1994)	400 000	m_n
Kumar and Kurtz (1993)	120 000	$N A_n m_n$
Lorz (1990b, 1991)	1 050 036	$A L_{2,3} N P \alpha_2 \alpha_1$
Lorz and Hahn (1993)	5 421 886	$A N P \alpha_2$
Mahin <i>et al.</i> (1980)	1 241	$A N L_{1,3}$
Marthinsen (1996)	25 000 – 100 000	$A L_{2,3} L_{1,3}$
van de Weygaert (1994)	–*	$A L_{2,3} N P \alpha_2 L_{1,3}$

* 20 planar sections of 1000 three-dimensional Poisson Voronoi cells.

Characteristics in $V_p(2,3)$:

A = area of a typical cell.

$L_{2,3}$ = edge length of a typical edge.

N = number of vertices (edges) of a typical cell.

P = perimeter of a typical cell.

α_2 = randomly selected interior angle of a typical sectional cell.

α_1 = angle of an edge at a typical vertex.

A_n = conditional area of a typical cell, given that it has n edges.

m_n = number of edges of a neighbouring cell of a typical cell, given that the typical cell has n edges.

Characteristics in $V_p(1,3)$:

$L_{1,3}$ = length of a line segment.

Table 5.7.6 Estimates, \hat{p}_n , of the probability that a typical polygon in a two-dimensional section of a Poisson Voronoi diagram in \mathbb{R}^3 has n edges (vertices).

n	\hat{p}_n	n	\hat{p}_n
3	0.0631	10	0.0178
4	0.1358	11	0.0051
5	0.2047	12	0.0012
6	0.2273	13	0.000263
7	0.1837	14	0.000042
8	0.1104	15	0.0000048
9	0.0506	16	0.00000095

Source: Lorz (1990b, 1991).

Table 5.7.7 Coefficients of variation (c.v.) and correlation coefficients for various characteristics of typical cells and edges in a two-dimensional section of a Poisson Voronoi diagram in \mathbb{R}^3 .

	N	A	P	$L_{2,3}$	α_2	α_1
c.v.	0.282*	0.695*	0.388*	0.691*	0.296†	—
N	—	0.753*	0.727*	-0.000*	0.566†	—
A	—	—	0.941*	0.221*	0.434†	—
P	—	—	—	0.264*	0.459†	—
$L_{2,3}$	—	—	—	—	—	-0.201‡

Characteristics:

A = area of a typical cell.

$L_{2,3}$ = edge length of a typical edge.

N = number of vertices (edges) of a typical cell.

P = perimeter of a typical cell.

α_2 = randomly selected interior angle of a typical sectional cell.

α_1 = angle of an edge at a typical vertex.

Sources: * Exact values from numerical integration by Brakke (1987b).

† Estimate from Monte Carlo simulations by Lorz and Hahn (1993).

‡ Estimate from Monte Carlo simulations by Lorz (1990b, 1991).

$$f_{L_{2,3}}(l) = \frac{27\Gamma\left(s + \frac{3}{2}\right)}{8\sqrt{\pi} \Gamma\left(\frac{2s}{3}\right) \Gamma(s+2)} \left(\frac{4\pi\lambda}{3}\right)^{2+2s/3} l^{2s+5} \int_0^\pi \int_0^{\pi-\beta_1} \frac{\sin^{2s+2}\beta_1 \sin^{2s+2}\beta_2}{\sin^{2s+6}(\beta_1 + \beta_2)} \\ \times (1 + \cos\beta_1)^2 (1 + \cos\beta_2)^2 \exp\left(-\frac{\lambda\pi l^3 [2 + (2 + \sin^2\beta_2) \cos\beta_2] \sin^3\beta_1}{3 \sin^3(\beta_1 + \beta_2)}\right) \\ \times \exp\left(-\frac{\lambda\pi l^3 [2 + (2 + \sin^2\beta_1) \cos\beta_1] \sin^3\beta_2}{3 \sin^3(\beta_1 + \beta_2)}\right) d\beta_2 d\beta_1, \quad l \geq 0. \quad (5.7.8)$$

The densities for $L_{2,m}$ for $3 \leq m \leq 7$ are illustrated in Figure 5.7.3.

As with \mathcal{V}_p , knowledge of such distributions is valuable in empirical work because existing evidence indicates that moment measures of many characteristics of individual cells of $\mathcal{V}_p(s, m)$ vary little from those cells in sectional tessellations where the set of generator points is not a realization of Θ_p (Lorz, 1990a). However, other distributions are all estimated from Monte Carlo simulations, and there have been far fewer reported simulation studies of $\mathcal{V}_p(s, m)$ than \mathcal{V}_p , all of which emphasize $\mathcal{V}_p(2, 3)$ (Mahin *et al.*, 1976, 1980; Lorz, 1990a,b, 1991; Lorz and Hahn, 1993; Kumar and Kurtz, 1993; Hahn and Lorz, 1994; van de Weygaert, 1994; Marthinsen, 1996). Of these the most extensive are Lorz (1990b, 1991) and Lorz and Hahn (1993) whose studies involved 1 050 036 and 5 421 886 cells, respectively. Table 5.7.5 summarizes these simulation studies. The distributions of characteristics in $\mathcal{V}_p(2, 3)$ are illustrated in Figure 5.7.4. The distribution of N for $\mathcal{V}_p(2, 3)$ is also reported in Table 5.7.6. Comparing Table 5.7.6 with Table 5.5.1 clearly reinforces the observation that $\mathcal{V}_p(2, 3)$ is not the same as \mathcal{V}_p in \mathbb{R}^2 . Table 5.7.7 gives the coefficients of variation and correlation of these characteristics obtained from numerical integration by Brakke (1987b) or from Monte Carlo simulations by Lorz and Hahn (1993) and Lorz (1990b, 1991). Conditional distributions of area, perimeter and interior angle, given the number of cell vertices (edges), have also been estimated by Lorz (1990b).

Kumar and Kurtz (1993) suggested the following empirical Aboav's law and Lewis' law in $\mathcal{V}_p(2, 3)$:

$$m_n = 5.09 + \frac{8.13}{n},$$

$$A_n = 0.2677n - 0.6064,$$

where m_n is the mean number of edges of a randomly selected neighbouring cell of a typical cell, under the condition that the typical cell has n edges, and A_n is the mean area of a typical cell, given that it has n edges.

Hahn and Lorz (1994) discussed how to use the statistics of a two-dimensional sectional diagram to estimate the parameters of the original three-dimensional tessellation and to test whether the original three-dimensional structure is a Poisson Voronoi diagram or not (see also Section 5.12).

5.8 ADDITIVELY WEIGHTED POISSON VORONOI DIAGRAMS: THE JOHNSON-MEHL MODEL

In Section 5.3 we discussed a variety of circumstances in which the Poisson Voronoi model could be used in a normative way in the examination of empirical tessellations. There are, however, other empirical tessellations for which it is not an appropriate model. One group of such tessellations consists of those in which the members of the generator set P are not

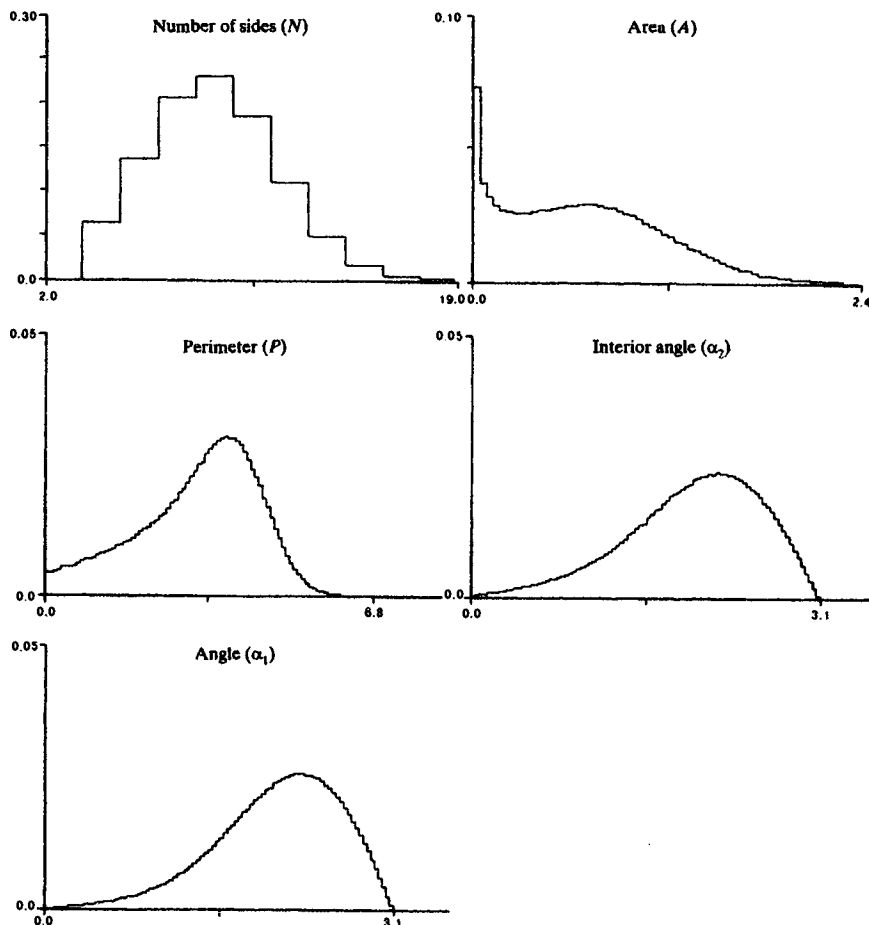


Figure 5.7.4 Normalized histograms of the number of vertices (edges) N , area A , perimeter P , interior angle α_2 of a typical sectional cell and the edge angle α_1 at a typical vertex for $\mathcal{V}_P(2, 3)$.

contemporaneous. In such instances we may assume that each generator p_i has both a location $x_i = (x_{i1}, x_{i2}, \dots, x_{im})$ in \mathbb{R}^m and an associated birth time, t_i (≥ 0). Once born, each point generates a cell which grows radially at a constant rate v . Interaction between growing cells is subject to the following conditions:

Condition JM1 If a point is born at a location which is already occupied by a growing cell, it disappears without trace.

Condition JM2 When radiating rays of two growing cells meet, both cease radiating so that the cell associated with a point is fully grown when growth ceases in all directions.

As we indicated in Section 3.1.2, this model can be considered equivalent to an (infinite) additively weighted Voronoi diagram in which the weight associated with p_i corresponds to t_i , since for the cell $C(p_i)$ that is generated by growth from p_i ,

$$C(p_i) = \left\{ \mathbf{x} \mid \left(t_i + \frac{\|\mathbf{x} - \mathbf{x}_i\|}{v} \right) \leq \left(t_j + \frac{\|\mathbf{x} - \mathbf{x}_j\|}{v} \right) \text{ for } p_j \in P, p_j \neq p_i \right\},$$

where $\|\mathbf{x} - \mathbf{x}_i\|$ and $\|\mathbf{x} - \mathbf{x}_j\|$ are the Euclidean distances from an arbitrary point p located at \mathbf{x} to p_i and p_j with location vectors \mathbf{x}_i and \mathbf{x}_j , respectively.

If we assume that both \mathbf{x}_i and t_i are generated by a Poisson point process, we have the *Johnson–Mehl* (J-M) (or *continuous nucleation*) model. This model was originally developed to study the growth of crystal aggregates (Kolmogorov, 1937; Johnson and Mehl, 1939; Avrami, 1939, 1940, 1941) and the surface film on metal (Evans, 1945). It has been independently rediscovered at least once since then (Glass, 1973, 1974; Armstrong, 1974; Jackson, 1974). The development of a tessellation over time in \mathbb{R}^2 according to the J-M model with a space–time homogeneous Poisson point process is illustrated in Figure 5.8.1. Such a tessellation is called a *Johnson–Mehl tessellation*. The rectangular window in Figure 5.8.1 was fully occupied by cells after 7 units of time. Suppose the intensity of the homogeneous Poisson point process is α per unit volume per unit time, i.e. the generators appear at a constant rate α . Chiu (1995c) showed that for each real number u , the time of complete tessellation T_L until the cube $[0, L]^m$ is fully occupied by cells of a J-M model (see Section 5.6.2) satisfies

$$\Pr \left\{ c^{m/(m+1)} (\alpha \omega_m v^m)^{1/(m+1)} T_L - c - \log \left[c^{1/(m+1)} \left(\frac{c + \log c}{m+1} \right)^{m-1} \right] \leq u \right\} \\ \rightarrow \exp \left(\psi_m \frac{(m+1)^{m-1}}{m^m} e^{-u} \right) \text{ as } L \rightarrow \infty,$$

where $c = \log(\alpha^m L^{m(m+1)} v^{-m} \omega_m^{-1})$, $\omega_m = \pi^{m/2}/\Gamma(m/2 + 1)$ is the volume of an m -dimensional sphere of unit radius and ψ_m is a constant given in equation (5.6.3). Furthermore,

$$\frac{\alpha \omega_m v^m T_L^{m+1}}{\log \alpha^m L^{m(m+1)}} \rightarrow 1 \text{ in probability as } L \rightarrow \infty.$$

Chiu also studied the time of complete tessellation for the following time-inhomogeneous Poisson point process. Suppose that the intensity measure of the Poisson point process on $\mathbb{R}^m \times [0, \infty)$ is $\ell \times \Lambda$, where ℓ is the Lebesgue measure in \mathbb{R}^m and Λ an arbitrary measure on $[0, \infty)$ such that $\Lambda([0, \infty)) > 0$ and

$$\lambda = \int_0^\infty \exp \left\{ -v^m \omega_m \int_0^\infty (t-s)^m \Lambda(ds) \right\} \Lambda(dt) < \infty.$$

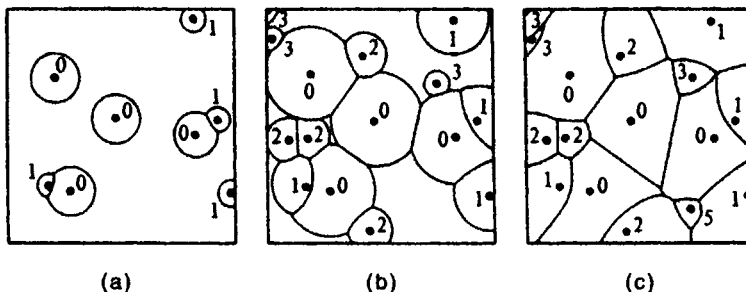


Figure 5.8.1 The Johnson–Mehl model for times (a) $t = 1$, (b) $t = 3$ and (c) $t = 7$.

The value λ is the intensity of cells formed according to the J–M model. Cowan *et al.* (1995) used $\Lambda(dt) = \alpha \gamma e^{-\gamma t} dt$ to model the mechanism of the replication of a DNA molecule. This form of Λ can be interpreted as follows. The generators form a Poisson point process on \mathbb{R}^m . Each one starts to grow after an independent exponentially distributed random time, provided that its location has not yet been occupied by other cells.

Chiu and Quine (1997) showed that the total number of cell generators remaining within $[0, L]^m$ in a J–M model, after suitable normalization, follows the standard normal distribution, as $L \rightarrow \infty$ (see also Quine and Robinson, 1990; Holst *et al.*, 1996; Chiu, 1997). Quine and Robinson (1992) and Chiu *et al.* (1999) discussed the estimation of Λ and v in the case $m = 1$ while Molchanov and Chiu (2000) proposed estimation methods for an arbitrary m .

At time t , the union of all growing cells is indeed a Boolean model (see, for example, Stoyan *et al.*, 1995, Chapter 3) of m -dimensional spheres. Thus, the volume fraction of the region occupied by cells at time t is

$$X(t) = 1 - \exp \left\{ -\omega_m v^m \int_0^t (t-s)^{m-1} \Lambda(ds) \right\}.$$

For a large class of Λ , such as $\Lambda(dt) = \alpha t^{\beta-1} dt$, where $\alpha, \beta > 0$, $X(t)$ can be written as

$$X(t) = 1 - \exp \{-kt^n\}, \quad (5.8.1)$$

where, the parameters k and n are independent of t . Equation (5.8.1) is known as the *Kolmogorov–Johnson–Mehl–Avrami* (KJMA, JMAK, JMA, AJM, or Avrami) equation in the materials science literature. The parameter n is known as the *Avrami exponent* or *Avrami index*. The KJMA equation has been the standard tool to study crystallization kinetics (see, for example, Weinberg *et al.*, 1997).

A typical cell of the J–M tessellation in \mathbb{R}^m has been studied in detail by Evans (1945), Gilbert (1962) and Meijering (1953) for $m = 1, 2$ and 3 and by Møller (1992, 1999) for $m \geq 2$. The moments of several characteristics

have been derived. A typical cell of a J-M tessellation is non-convex, unless Λ is concentrated at a singleton, which gives the Poisson Voronoi diagram. The non-empty intersection of $m-k+1$ cells is called a k -face. A k -face is not necessarily connected, because of the non-convexity of cells. A connected component of an k -face is called a k -interface, which is a vertex, an edge and a cell face for $k = 0, 1$ and 2 , respectively. For each of the cases (i) $0 < k = l \leq m$, (ii) $1 \leq k = l + 1 \leq m$, (iii) $k = m$ and $l = 1$, and (iv) $1 \leq k \leq m$ and $l = 0$, the mean $(k-l)$ -contents, $\mu_{k,k-l}$, of $(k-l)$ -interfaces per unit volume in a k -dimensional hyperplane is given by

$$\begin{aligned}\mu_{k,k-l} = & v^{lm+n} c_{kn} \int_0^\infty \left\{ \int_0^t (t-s)^{m-1} \Lambda(ds) \right\}^{l+1} \\ & \times \exp \left\{ -v^n \omega_m \int_0^\infty (t-s)^m \Lambda(ds) \right\} dt,\end{aligned}$$

where $n = m - l$ and

$$c_{kn} = \frac{2^{l+1} \pi^{(l+1)m/2} \Gamma\left(\frac{ml+n+1}{2}\right) \Gamma\left(\frac{k+1}{2}\right)}{(l+1)! \Gamma\left(\frac{ml+n}{2}\right) \Gamma\left(\frac{m+1}{2}\right)^{l+1} \Gamma\left(\frac{k-l+1}{2}\right)}$$

(Møller, 1992, equation (4.2)). The cases (i), (ii) and (iv) concern vertices, edges and k -interfaces in the k -dimensional hyperplane, respectively, whilst case (iii) concerns cell faces in \mathbb{R}^m . Meijering (1953) and Miles (1972a) obtained the same results for some special cases. Møller (1992) also gave formulae for the intensity $I_p^{(k)}$ of p -interfaces in a k -dimensional hyperplane and the mean number of q -interfaces $N_{pq}^{(k)}$ contained in a typical p -interface in the hyperplane and the mean q -dimensional content $V_{pq}^{(k)}$ of the union of such q -interfaces ($0 \leq q \leq p \leq k \leq m$):

$$I_p^{(k)} N_{pq}^{(k)} = \binom{k-q+1}{p-q} I_q^{(k)}, \quad (5.8.2)$$

$$I_p^{(k)} V_{pq}^{(k)} = \binom{k-q+1}{p-q} \mu_{k,q}, \quad (5.8.3)$$

$$I_2^{(2)} = I_1^{(2)} - I_0^{(2)}, \quad (5.8.4)$$

and for $0 < k \leq m \leq 3$,

$$\sum_{i=0}^k (-1)^i I_i^{(k)} = 0. \quad (5.8.5)$$

Equations (5.8.2) and (5.8.3) yield

$$\begin{aligned}
I_m^{(m)} &= \lambda, & N_{m0}^{(m)} &= \frac{m+1}{\lambda} \mu_{m,0}, & V_{mp}^{(m)} &= \frac{m-p+1}{\lambda} \mu_{m,p}, \\
I_0^{(k)} &= \mu_{k,0}, & I_1^{(1)} = I_1^{(1)} &= \mu_{1,0}, & N_{10}^{(1)} &= 2, \\
V_{11}^{(1)} &= \frac{1}{\mu_{1,0}}.
\end{aligned} \tag{5.8.6}$$

Since the edges in the hyperplane do not necessarily contain vertices, equations (5.8.2)–(5.8.4) and (5.8.6) lead to a series of inequalities:

$$\begin{aligned}
I_1^{(k)} &\geq \frac{k+1}{2} \mu_{k,0}, & N_{21}^{(k)} &\geq N_{20}^{(k)}, & N_{10}^{(k)} &\leq 2, \\
V_{11}^{(k)} &\leq \frac{2}{k+1} \frac{\mu_{k,1}}{\mu_{k,0}}, & I_2^{(2)} &\geq \frac{\mu_{2,0}}{2}, & N_{21}^{(2)} &\leq 6, \\
V_{21}^{(2)} &\leq \frac{4\mu_{2,1}}{\mu_{2,0}}, & V_{22}^{(2)} &\leq \frac{2}{\mu_{2,0}}.
\end{aligned} \tag{5.8.7}$$

Furthermore, for $m = 3$,

$$N_{32}^{(3)} \geq 2 + \frac{2\mu_{3,0}}{\lambda}, \quad N_{31}^{(3)} \geq \frac{6\mu_{3,0}}{\lambda}. \tag{5.8.8}$$

In particular, for $m = 2$, we have

$$\begin{aligned}
I_2^{(2)} &= \lambda, & I_1^{(2)} &= 3\lambda, & I_0^{(2)} &= 2\lambda, \\
I_1^{(1)} = I_0^{(1)} &= \mu_{1,0}, & N_{21}^{(2)} = N_{20}^{(2)} &= 6, & N_{10}^{(2)} = N_{10}^{(1)} &= 2, \\
V_{22}^{(2)} &= \lambda^{-1}, & V_{21}^{(2)} &= \frac{2\mu_{2,1}}{\lambda}, & V_{11}^{(2)} &= \frac{\mu_{2,1}}{3\lambda}, \\
V_{11}^{(1)} &= \frac{1}{\mu_{1,0}},
\end{aligned} \tag{5.8.9}$$

whilst for $m = 3$, we get

$$\begin{aligned}
I_3^{(3)} &= \lambda, & I_2^{(3)} &\geq \lambda + \mu_{3,0}, & I_1^{(3)} &\geq 2\mu_{3,0}, \\
I_0^{(3)} &= \mu_{3,0}, & I_2^{(2)} &\geq \frac{\mu_{2,0}}{2}, & I_1^{(2)} &\geq \frac{3\mu_{2,0}}{2}, \\
I_0^{(2)} &= \mu_{2,0}, & I_1^{(1)} = I_0^{(1)} &= \mu_{1,0}, & N_{30}^{(3)} &= \frac{4\mu_{3,0}}{\lambda}, \\
N_{21}^{(3)} &\geq N_{20}^{(3)}, & N_{20}^{(3)} &\leq \frac{6\mu_{3,0}}{\lambda + \mu_{3,0}}, & N_{10}^{(3)} &\leq 2,
\end{aligned}$$

$$\begin{aligned}
N_{20}^{(2)} \leq N_{21}^{(2)} \leq 6, & \quad N_{10}^{(2)} \leq 2, & \quad N_{10}^{(1)} = 2, \\
V_{33}^{(3)} = \lambda^{-1}, & \quad V_{32}^{(3)} = \frac{2\mu_{3,2}}{\lambda}, & \quad V_{31}^{(3)} = \frac{3\mu_{3,1}}{\lambda}, \\
V_{22}^{(3)} \leq \frac{\mu_{3,2}}{\lambda + \mu_{3,0}}, & \quad V_{21}^{(3)} \leq \frac{3\mu_{3,1}}{\lambda + \mu_{3,0}}, & \quad V_{11}^{(3)} \leq \frac{\mu_{3,1}}{2\mu_{3,0}}, \\
V_{22}^{(2)} \leq \frac{2}{\mu_{2,0}}, & \quad V_{21}^{(2)} \leq \frac{4\mu_{2,1}}{\mu_{2,0}}, & \quad V_{11}^{(2)} \leq \frac{2\mu_{2,1}}{3\mu_{2,0}}, \\
V_{11}^{(1)} = \mu_{1,0}^{-1},
\end{aligned} \tag{5.8.10}$$

with equality in any one of the inequalities if and only if Λ is concentrated at a singleton, which leads to the Poisson Voronoi diagram (see also Møller, 1999). The mean number of full neighbours of a typical cell is

$$\begin{aligned}
E(C) = & \frac{4\pi^{m/2} v^m}{\lambda \Gamma\left(\frac{m}{2}\right)} \int_0^\infty \int_0^t \int_0^t (2t - t_1 - t_2)^{m-1} \\
& \times \exp\left\{-v^m \omega_m \int_0^\infty (t-s)^m \Lambda(ds)\right\} \Lambda(dt_1) \Lambda(dt_2) dt
\end{aligned}$$

(Møller, 1992, Theorem 4.5). In particular, if $m = 2$, then $E(C) = 4$. The mean k -dimensional content $V^{(k)}$ of a typical k -dimensional face in a k -dimensional hyperplane is bounded above by

$$\begin{aligned}
V^{(k)} < & \left\{ \frac{2\pi^{(m-k)/2} v^{m-k}}{\Gamma\left(\frac{m-k}{2}\right)} \int_0^\infty \int_0^t (t-u)^{m-k-1} \right. \\
& \left. \times \exp\left\{-v^m \omega_m \int_0^\infty (t-s)^m \Lambda(ds)\right\} \Lambda(du) dt \right\}^{-1}.
\end{aligned}$$

This is a generalization of the results obtained by Miles (1972a) for a J-M tessellation in \mathbb{R}^3 .

Second-order moments are much more complicated. Gilbert (1962) obtained the variance of the volume of a typical cell of a J-M tessellation in \mathbb{R}^3 generated by a homogeneous Poisson point process, i.e. $\Lambda(dt) = \alpha dt$, by numerical integration. Second-order moments of other characteristics can also be derived, but the results are too complicated to evaluate. Møller (1992) showed that the coefficients of variation, $CV(\mathcal{C}_k)$ and $CV(\mathcal{F}_k)$, of the k -dimensional content of a typical k -interface and k -face, respectively, satisfy

$$CV(\mathcal{C}_k) = \sqrt{\frac{C_k}{V_{kk}^{(k)}} - 1},$$

$$CV(\mathcal{F}_k) = \sqrt{\frac{C_k}{V^{(k)} - 1}},$$

where

$$C_k = \frac{4\pi^{(m+k-1)/2} v^{m+k}}{\Gamma\left(\frac{m-1}{2}\right) \Gamma\left(\frac{k}{2}\right)} \iiint_{\Omega_1} s^{m+k-1} J(r_1, R_1) \\ \times \exp \left[\frac{2\pi^{(m-1)/2} v^m s^m}{\Gamma\left(\frac{m-1}{2}\right)} \iiint_{\Omega_2} J(r_2, R_2) dr_2 dR_2 \Lambda(dt_2) \right] \\ \times ds dr_1 dR_1 \Lambda(dt_1),$$

with

$$J(r, R) = rR \left(\frac{r^2 + R^2 + r^2 R^2}{2} - \frac{1 + r^4 + R^4}{4} \right)^{(m-3)/2}.$$

The integrations are over Ω_1 , which is the range of all $s, r_1, R_1, t_1 \geq 0$ such that $r_1 + R_1 > 1$ and $|r_1 - R_1| < 1$, and Ω_2 , which is the range of all $r_2, R_2, t_2 \geq 0$ such that $r_2 + R_2 > 1$, $|r_2 - R_2| < 1$ and either $sR_2 + t_2 < sR_1 + t_1$ or $sr_2 + t_2 < sr_1 + t_1$ or both.

These moments for the time-homogeneous case $\Lambda(dt) = \alpha dt$ are summarized in Table 5.8.1. In order to facilitate a comparison with similar moments reported in Tables 5.5.1 and 5.5.3 for the Poisson Voronoi diagram, the numerical values in Table 5.8.1 are given in terms of the density of generator points per unit space after all cell growth has ceased rather than in terms of the birth rate α and the growth rate v . Note that inequalities arise in Table 5.8.1 because it is possible that the common edge (in \mathbb{R}^2) or the common face (in \mathbb{R}^3) between two cells may be interrupted by one or more smaller cells. Frost and Thompson (1987a) and Heinrich and Schüle (1995) have estimated the distributions of area, edge length and number of edges (vertices) of a typical cell in the time-homogeneous case using information from 10 000 and 20 000 cells, respectively, from a computer simulation.

Horálek (1988, 1989) and Møller (1992) studied the case

$$\Lambda(dt) = \alpha t^{\beta-1} dt, \text{ where } \alpha, \beta > 0, \quad (5.8.11)$$

in detail. Note that $\beta = 1$ gives the time-homogeneous J-M model while as $\beta \rightarrow 0$ the tessellation approaches \mathcal{V}_p . Møller (1995) estimated the distributions of area, perimeter, numbers of vertices, 0-faces with two vertices contained in a typical cell and full neighbours and minimal and maximal angles of a typical vertex in \mathbb{R}^2 and volume and numbers of cell face, vertices and closed edges in \mathbb{R}^3 for the case of equation (5.8.11) from simulations of 10 000 cells.

Frost and Thompson (1987a) used a simulation approach to study the J-M model in \mathbb{R}^2 with

$$\Lambda(dt) = \alpha e^{-\beta t} dt, \text{ where } \alpha, \beta > 0.$$

Table 5.8.1 The first and/or second-order moments of various characteristics of a space-time homogeneous Johnson–Mehl model.

Moment	Symbol	Exact value	Numerical value	Estimate [†]
<i>Two-dimensions</i>				
Intensity of cell centroids	λ	$(3/\pi)^{1/3}\Gamma(4/3)(\alpha/\nu)^{2/3}$	$0.879(\alpha/\nu)^{2/3}$	
Expected number of vertices/edges of a typical cell and its second moment	$E(N)$ $E(N^2)$	6 –	6 –	41.916
Expected number of full neighbours of a typical cell and its second moment	$E(C)$ $E(C^2)$	4 –	4 –	18.731
Expected area of a typical cell and its second moment	$E(A)$ $E(A^2)$	$[(\pi/3)^{1/3}\Gamma(4/3)](\nu/\alpha)^{2/3}$ –	λ^{-1} –	$1.703\lambda^{-2}$
Expected perimeter of a typical cell and its second moment	$E(P)$ $E(P^2)$	$[4(3/\pi)^{1/3}\Gamma(5/3)/\Gamma(4/3)](\nu/\alpha)^{1/3}$ –	$3.734\lambda^{-1/2}$ –	$17.460\lambda^{-1}$
Expected length of an edge of a typical cell	$E(L)$	$< [2(3/\pi)^{1/3}\Gamma(5/3)/\Gamma(4/3)](\nu/\alpha)^{1/3}$	$< 0.623\lambda^{-1/2}$	
<i>Three-dimensions</i>				
Intensity of cell centroids	λ	$[4\Gamma(5/2)/\pi^{5/2}]^{1/4}\Gamma(5/4)(\alpha/\nu)^{3/4}$	$0.896(\alpha/\nu)^{3/4}$	
Expected number of vertices of a typical cell and its second moment	$E(M)$ $E(M^2)$	$16\pi^{2/7}$ –	22.559 –	740.213
Expected number of edges of a typical cell	$E(E)$	$> 24\pi^{2/7}$	> 33.839	
Expected number of faces of a typical cell and its second moment	$E(F)$ $E(F^2)$	$> 8\pi^{2/7} + 2$ –	> 13.280 –	13.002 226.305
Expected number of full neighbours of a typical cell	$E(C)$	7	7	

Table 5.8.1 continued

Moment	Symbol	Exact value	Numerical value	Estimate [†]
Expected area of a volume cell and its second moment	E(V) E(V ²)	$[(\pi/3)^{14}/\Gamma(5/4)](\nu/\alpha)^{3/4}$ —	λ^{-1} $2.236\lambda^{-2}$	
Expected surface area of a typical cell	E(S)	$[16\pi^{1/2}\Gamma(7/4)/[3^{3/2}\Gamma(5/4)]](\nu/\alpha)^{1/2}$	$5.143\lambda^{-2/3}$	
Expected total edge length of a typical cell	E(P)	$[3^{11/4}\pi^{9/4}/[5\Gamma(5/4)]](\nu/\alpha)^{1/4}$	$14.71\lambda^{-1/3}$	
Correlation between the number of vertices and faces	corr(M, F)	—	—	0.9986
<i>Sections</i>				
Expected area of typical cell	E ⁽²⁾ (A)	$\{3^{11/2}\Gamma(1/4)^{23}/[2^{43}\pi^2(5/4)^{23}]\}(\nu/\alpha)^{1/2}$	$0.816\lambda^{2/3}$	
Expected length of a typical line segment	E ⁽¹⁾ (L _{1,3})	$\{3^{11/4}\Gamma(1/4)^{13}/[2^{23}\pi^{1/4}\Gamma(3/4)\Gamma(5/4)^{13}]\}(\nu/\alpha)^{1/4}$	$0.778\lambda^{-1/3}$	

[†] Estimates from Monte Carlo simulation by Möller (1995).

α = birth rate.

ν = radial growth rate.

Sources: Evans (1945), Meijering (1953), Gilbert (1962) and Möller (1992, 1995).

In this case as $\beta \rightarrow 0$ we obtain the time-homogeneous J-M model, while $\beta \rightarrow \infty$ produces \mathcal{V}_p . Frost and Thompson (1987a) derived estimates of the distributions of the area, edge length and number of sides of a typical cell. They and Heinrich and Schüle (1995) also estimated the same distributions for situations in which the nucleation rate remains constant (i.e. time-homogeneous) but in which new generators are prohibited from being born at a distance δ from any edge of an existing cell (note that the Voronoi hard core models discussed in Section 5.12 may be considered as a limiting case of this modified J-M model). Heinrich and Schüle (1995) also estimated the distribution in the case when the generators form a cluster point process.

Another way to modify the J-M model to conform with certain empirical situations is to alter the growth rate v to vary over time. However, if v varies over time, we may have rather strange situations such as disconnected cells. Even worse, the resultant structure may not be a tessellation of \mathbb{R}^m at all. Chiu (1995c) showed such a pathological example in which the uncovered regions form a random fractal. Frost and Thompson (1987b) consider time-homogeneous situations in which the radial growth of a cell C_i at time t_i , $v_i(t)$, is proportional to a power of its radius $r_i(t)$ at that time. Thus,

$$v_i(t) \propto r_i(t)^\beta$$

which is equivalent to considering $r_i(t)$ as a function of the time elapsed $(t - t_i) = \Delta t$ since the birth of the cell's generator. In particular, they examine the distributions of the area and number of sides (vertices) of a typical cell in models with values of $\beta = -3, -2, -1, 0, 1$ (equivalent to Δt^ρ) ($\rho = 1/4, 1/3, 1/2, 1$) and $\exp(\Delta t)$, respectively. When $\beta = 0$ we have the basic J-M model while $\beta = -1$ yields a Voronoi power diagram (see Section 3.1.4) and $\beta = 1$ produces a multiplicatively weighted Voronoi diagram (see Section 3.1.1).

Because the J-M model has been of particular interest in materials science applications, there has been interest in the nature of one- and two-dimensional sections of the model in \mathbb{R}^3 . Horálek (1989, 1990) derived mean values for the length of the intercept through a typical cell and the area of a section of a typical cell for both the time-homogeneous J-M model and the J-M model with equation (5.8.11) (see Table 5.8.1 for these values for the time-homogeneous J-M model). Note that an exact value cannot be obtained for the area of a section of a typical cell because the star-shaped nature of the cells means that in two-dimensional sections it is possible to have subareas which are entirely surrounded by the planar section of an adjoining cell. Mahin *et al.* (1976, 1980) have used computer simulation to estimate the distribution of the cross-sectional area, intercept length and number of sides (vertices) of cells in sectional tessellations, while Saetre *et al.* (1986) have examined the distribution of the areas of cells in sections of J-M models with declining birth rates (a χ^2 distribution for t_i) and increasing birth rates (a Weibull distribution for t_i) and with growth rates declining over time.

Applications of the family of J-M models have been confined mainly to

the natural sciences and examples can be found in most of the references cited in this section. There are a huge number of studies of the application of the KJMA equation (5.8.1) and its generalizations or modifications on crystallization kinetics (see, for example, Christian, 1965; Crespo *et al.*, 1997; Weinberg *et al.*, 1997) and precipitation and the dissolution process (see, for example, Oguocha and Yannacopoulos, 1997). Hirsch *et al.* (1994) used the KJMA equation to study the kinetics of the mortality of fruit flies. The family of J-M models is also the basic framework of the geometric-probabilistic approach to heterogeneous chemical kinetics (Korobov, 1994, 1996). Additional astrophysical applications are presented by Zaninetti (1989, 1990, 1991b) who has used them in the study of supernovae explosions. Other applications include porphyroblasts (Carlson, 1991), microstructural evolution in thin films (Frost *et al.*, 1990), dynamic fragmentation (Grady and Kipp, 1985), plant ecology (Kenkel, 1990), recrystallization in cold rolled material (Marthinsen *et al.*, 1989; Furu *et al.*, 1990), and grain growth in metals (Srolovitz *et al.*, 1986). In the social sciences Boots (1973, 1975a) has used the models to explore the development of service areas associated with the provision of public, intercity bus services in England and Wales. These examples are applications of the J-M model in \mathbb{R}^2 and \mathbb{R}^3 . There are quite a number of biological applications of the J-M model in \mathbb{R} . Examples include unravelling the strands of a DNA molecule (Vanderbei and Shepp, 1988; Cowan *et al.*, 1995), release of neurotransmitter at neuromuscular synapses (Bennett and Robinson, 1990; Quine and Robinson, 1990, 1992), differentiation of cells into heterocysts in algae (Wolk, 1975) and lung carcinoma (Kayser and Stute, 1989).

5.9 HIGHER ORDER POISSON VORONOI DIAGRAMS

In Section 3.2 we generalized the basic concept of the ordinary Voronoi diagram by considering diagrams in which an individual cell is created with respect to a subset, $P_i^{(k)}$ of k points ($1 \leq k \leq n$) of the n points of P rather than an individual point of P . In the case of the order- k Voronoi diagram $\mathcal{V}^{(k)}$, an individual cell consists of all locations in \mathbb{R}^m for which the members of $P_i^{(k)}$ are the set of k nearest points while in the ordered order- k Voronoi diagram $\mathcal{V}^{(k)}$, we add the additional constraint that the k points are ordered so that all locations in a cell share the same first, second, ..., k th nearest points of P . When $\mathcal{V}^{(k)}$ and $\mathcal{V}^{(k)}$ are defined with respect to Θ_P we label them $\mathcal{V}_P^{(k)}$ and $\mathcal{V}_P^{(k)}$, respectively. Like \mathcal{V}_P , $\mathcal{V}_P^{(k)}$ is a normal tessellation while $\mathcal{V}_P^{(k)}$ is not. Figure 5.9.1 shows $\mathcal{V}_P^{(k)}$ in \mathbb{R}^2 for several different values of k .

Although Miles (1984, p. 311) has been able to derive an expression for the expectation $E_m V_s$ of the total s -dimensional content of the s -faces of an arbitrary cell of $\mathcal{V}_P^{(k)}$ in \mathbb{R}^m , which is analogous to expression (5.5.2) for \mathcal{V}_P , it has only proved possible to evaluate it for $m = 1, 2$. Thus, the known properties of $\mathcal{V}_P^{(k)}$ are limited to some first-order moments for $m = 2$. The same holds for $\mathcal{V}_P^{(k)}$. These values are given in Table 5.9.1.

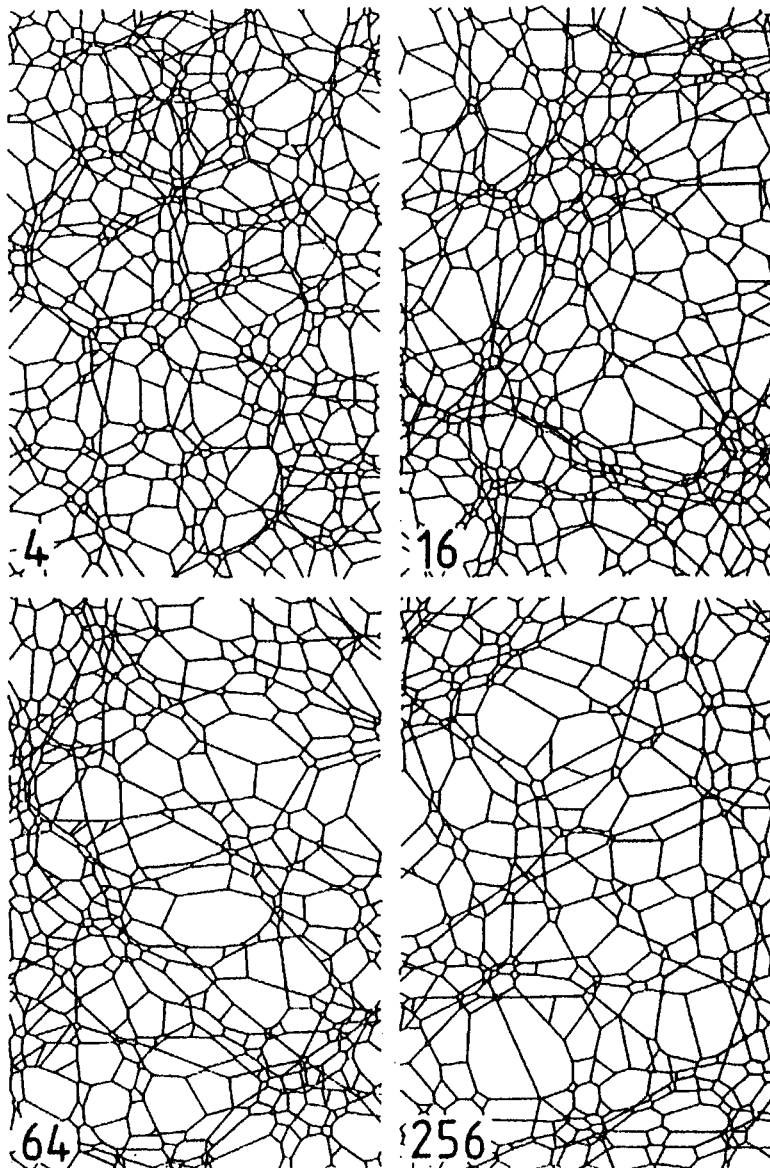


Figure 5.9.1 Portions of an order- k Poisson Voronoi diagram $\mathcal{V}_p^{(k)}$ for $k = 4, 16, 64, 256$. (Source: Miles and Maillardet, 1982, Figure 5.)

Table 5.9.1 The first and/or second-order moments of various characteristics of a typical cell of order- k and ordered order- k Poisson Voronoi diagrams in \mathbb{R}^2 .

Moment	Symbol	Exact value	Limit ($k \rightarrow \infty$)
<i>Order-k</i>			
Expected number of vertices (edges)	$E(N)$	6	
$E_2 N_0$ ($E_2 N_1$)	$E(C)$	4	
Expected number of full neighbours	$E(A)$	$\frac{1}{4}[(2k-1)\lambda]$	λ^{-1}
Expected area $E_2 V_2$	$E(P)$	$\frac{1}{(2k)!(k(k-1)!)^2}(2k-2)^{2k-3}\lambda^{1/2}$	$4/(\pi k\lambda)^{1/2}$
Expected perimeter $E_2 V_2$			
<i>Ordered order-k</i>			
Expected number of vertices (edges)	$E(N)$	$\frac{[54\pi^2 k + 256(k-1)(k-2)]}{\times [9\pi^2(2k-1) + 64(k-1)(k-2)]^{-1}}$	4
$E_2 N_0$ ($E_2 N_1$)	$E(N^2)$		$(\pi^2 + 24)/2$
and its second moment $E_2[N_0^2](E_2[N_1^2])$	$E(A)$	$1/[k[2k-1 + 64(k-1)(k-2)/(9\pi^2)]\lambda]$	$9\pi^2/(64k^3\lambda)$
Expected area $E_2 V_2$	$E(A^2)$		$81\pi^6/(2^{13}k^6\lambda^2)$
and its second moment $E_2[V_2^2]$	$E(P)$	$2\sum_{i=1}^k \{(2i)!/[i(i-1)!2^{i-2}]\} \times [k[2k-1 + 64(k-1)(k-2)/(9\pi^2)]\lambda^{1/2}]^{-1}$	$(3/4)[\pi^3/(\kappa^3)]^{1/2}$
Expected perimeter $E_2 V_1$			
and its second moment $E_2[V_1^2]$	$E(P^2)$		$9\pi^3(\pi^2 + 4)/(128k^3\lambda)$
λ	=	intensity of Θ_p	

Source: Miles (1964a, p. 904; 1970a, p. 114).

Note that for both diagrams $E(N)$ is a consequence of the general result given in equation (5.5.6). Similarly, $E(A)$ for $\mathcal{V}_p^{(k)}$ holds for any underlying point process which is homogeneous and ergodic (Miles, 1986b, p. 569). This value is also a specific instance of the more general relationship (Miles, 1984, 1986a)

$$E_m V_m^{(2)} = \frac{2E_m V_m^{(1)}}{E_m N_{m-1}^{(1)}}, \quad (5.9.2)$$

where (k) refers to the order of $\mathcal{V}_p^{(k)}$, and $\mathcal{V}_p^{(1)} = \mathcal{V}_p$, which holds because of the one-to-one correspondence between the cells of $\mathcal{V}_p^{(2)}$ and the $(m-1)$ -faces of \mathcal{V}_p .

The values of $E(A)$ for $\mathcal{V}_p^{(k)}$ and $\mathcal{V}_p^{<k>}$ can be combined to define the expectation of the multiplicity w of a cell of $\mathcal{V}_p^{(k)}$ as the number of cells of $\mathcal{V}_p^{<k>}$ it comprises so that

$$E(w) = k \left(1 + \frac{64(k-1)(k-2)}{9\pi^2(2k-1)} \right), \quad (5.9.2)$$

which is asymptotically equal to $32k^2/(9\pi^2)$ as $k \rightarrow \infty$ (Miles, 1970a, p. 119; Santaló, 1976, p. 20).

For $\mathcal{V}_p^{<k>}$ in \mathbb{R}^2 , as $k \rightarrow \infty$, the proportion of cells with four vertices tends to unity (Miles, 1970a, p. 118) and $\mathcal{V}_p^{<k>}$ tends to become equivalent to the tessellation \mathcal{L} formed by an isotropic Poisson line process (see Section 1.3.3) of intensity $\tau = (8/3)(\lambda k^3/\pi)^{1/2}$. Such a process involves defining lines in terms of their polar coordinates (r, θ) representing the perpendicular distance and direction from the origin, respectively, where the range of (r, θ) is taken as $\Pi = \{(r, \theta): -\infty < r < \infty, 0 \leq \theta < \pi\}$. Then for $\tau > 0$, the Poisson point process of intensity τ/π in Π induces the Poisson line process of intensity τ in \mathbb{R}^2 (see Section 1.3.3). Thus, any values for the characteristics of an arbitrary cell of \mathcal{L} carry over asymptotically for $\mathcal{V}_p^{<k>}$. Knowledge of such characteristics is quite extensive with all the first- and second-order moments, together with some higher order moments and the correlation coefficients being known for N , A and P (Miles, 1964a,b, 1973). Crain and Miles (1976) have also estimated the distributions of N , A and P using Monte Carlo methods. The values of the moment measures are given in Table 5.9.1.

Very little is known about the distributions of the various cell characteristics although Miles and Maillardet (1982, p. 108) have derived an integral expression for the probability distribution of N for an arbitrary cell in terms of its size and shape. There are no triangles in $\mathcal{V}_p^{(k)}$ and, as Miles and Maillardet (1982, p. 109) demonstrated empirically for a cell with $N = 4$ and Miles (1995) proved heuristically for a very large cell, as $k \rightarrow \infty$, the vertices tend to circularity, with the sums of their opposite interior angles tending to π . This tendency can be observed in Figure 5.9.1. They also show that, for any given shape, the conditional ergodic distributions of A and P of the cells of $\mathcal{V}_p^{(2)}$ are both mixtures of gamma distributions of the type given in expression (5.5.33).

Table 5.10.1 The first moment of various characteristics of a typical cell in a Poisson Voronoi diagrams on the surface of a sphere.

Characteristic	Symbol	Exact value
Number of vertices (edges)	$E(N)$	$6(1-2/n)$
Area	$E(A)$	$4\pi/n$
Perimeter	$E(P)$	$\pi(n-1)! \sum_{i=0}^{n/2-1} [2^{n+2i-3} \times i!(i+1)!(n-2i-2)!]^{-1}$

n = number of points in the generator set.

Source: Miles (1971).

Finally, there has been some consideration of the tessellation $\mathcal{V}_p^{(k)}(s, m)$, created by an s -dimensional section of $\mathcal{V}_p^{(k)}$ in \mathbb{R}^m . Miles (1984, p. 326) has been able to derive an integral expression for the moments of the volume of an arbitrary cell but this has proved resistant to evaluation.

5.10 POISSON VORONOI DIAGRAMS ON THE SURFACE OF A SPHERE

One of the instances of Voronoi diagrams involving spaces which are not the Euclidean space, which was examined in Section 3.7, was that in which the members of the generator set were located on the surface of a sphere S with unit radius, centred at the origin. In this case the distance between two points is defined in terms of the length of the lesser arc on the great circle passing through the two points (see equation (3.7.17), Section 3.7.6). If the generator set consists of n points selected at random on S , the resulting Voronoi diagram is a random Voronoi diagram which we label \mathcal{V}_s . Knowledge of \mathcal{V}_s is limited to the first-order moments derived by Miles (1971) which are given in Table 5.10.1. Note that as $n \rightarrow \infty$, $E(N)$ tends to 6, which corresponds to $E(N) = 6$ for \mathcal{V}_p in \mathbb{R}^2 .

5.11 PROPERTIES OF POISSON DELAUNAY CELLS

As demonstrated in Section 2.2 the Poisson Delaunay tessellation \mathcal{D}_p can be considered the dual tessellation of \mathcal{V}_p in \mathbb{R}^m . Each Poisson Delaunay cell (PDC) of \mathcal{D}_p is an $(m+1)$ -dimensional simplex whose vertices p_0, \dots, p_m are points of Θ_p . For $m = 2$ and $m = 3$ the PDCs are triangles and tetrahedra, respectively. Any s -face of \mathcal{D}_p is an $(s+1)$ -dimensional simplex with vertices p_0, \dots, p_s , also points of Θ_p . Alternatively, an s -face can be considered as the convex hull of p_0, \dots, p_s . There are $\binom{m+1}{s+1}$ s -faces contained in a PDC. Because of the duality between \mathcal{V} and \mathcal{D} , there is a simple relationship between the intensities of their s -faces (Møller, 1989, equation (7.31)).

If $\lambda_s(\mathcal{D})$ and $\lambda_s(\mathcal{V})$ are the intensities of the s -faces of \mathcal{D} and \mathcal{V} , respectively, then

$$\lambda_s(\mathcal{D}) = \lambda_{m-s}(\mathcal{V}), \quad s = 0, \dots, m. \quad (5.11.1)$$

The major result relating to PDCs was derived by Miles (1970b, 1974) (see also Møller, 1989, Section 7; 1994, Section 4.3). Let c and r be the circum-centre and circumradius, respectively, of an $(m+1)$ -dimensional PDC in \mathbb{R}^m . Then the $(m+1)$ vertices of the cell are the points $\{c + r u_i\}$ where $\{u_i\}$ are the unit vectors ($i = 0, \dots, m$). The ergodic probability distribution of \mathcal{D}_P is completely specified by the joint probability density function (pdf)

$$f(r, u_0, \dots, u_m) = a(\lambda, m) \Delta_m r^{m^2-1} \exp(-\lambda \omega_m r^m), \quad (5.11.2)$$

where Δ_m is the volume of the $(m+1)$ -simplex with vertices u_0, \dots, u_m , $\omega_m = \pi^{m/2}/\Gamma(m/2 + 1)$ and

$$a(\lambda, m) = \frac{\pi^{(m^2+1)/2} \Gamma(m^2/2) \{2\lambda \Gamma[(m+1)/2]\}^m}{m^{m-2} \Gamma(m/2)^{2m+1} \Gamma[(m^2+1)/2]}. \quad (5.11.3)$$

The marginal pdf of r is given in equation (5.5.22) in Section 5.5. Furthermore, r , which may be considered a measure of the size of the $(m+1)$ -simplex, is independent of $\{u_0, \dots, u_m\}$ which represents the shape of the simplex. It was this independence that was exploited by Kendall (1989) in deriving a method of simulating individual $(m+1)$ -dimensional simplices (see Section 5.4). The pdf of r is a generalized gamma function (equation (5.5.32)) with $r = m$, $q = m^2$ and $b = \lambda_m$. Miles (1974) shows that equation (5.11.2) can be used to derive a general expression for the k th moment of the volume V_m of a typical PDC in \mathbb{R}^m :

$$\begin{aligned} E_m V_m^k &= \frac{(m+k-1)! \Gamma\left(\frac{m^2}{2}\right) \Gamma\left(\frac{m^2+mk+k+1}{2}\right) \Gamma\left(\frac{m+1}{2}\right)^{m-k+1}}{(m-1)! \Gamma\left(\frac{m^2+1}{2}\right) \Gamma\left(\frac{m^2+mk}{2}\right) \Gamma\left(\frac{m+k+1}{2}\right)^{m+1} (2^m \pi^{(m-1)/2} \lambda)^k} \\ &\quad \times \prod_{i=2}^{m+1} \left\{ \Gamma\left(\frac{k+i}{2}\right) / \Gamma\left(\frac{i}{2}\right) \right\} \text{ for } k = 1, 2, \dots \end{aligned} \quad (5.11.4)$$

(see also Møller, 1989, Corollary 7.6), where E_m denotes expectation with respect to the Palm distribution of the random tessellation with respect to the typical cell (see Møller, 1989, p. 47). When $m = 2$, this reduces to

$$E_2 V_2^k = \frac{\Gamma\left(\frac{3k+5}{2}\right) \Gamma\left(\frac{k}{2}+1\right)}{3\Gamma\left(\frac{k+3}{2}\right)^2 2^k \pi^{k-1/2} \lambda^k} \text{ for } k = 1, 2, \dots, \quad (5.11.5)$$

while for $m = 3$,

Table 5.11.1 Moments of various characteristics of a Poisson Delaunay diagram in \mathbb{R}^2 .

Moment	Symbol	Exact value	Numerical value
Intensity of cell vertices	λ_0	λ	
Intensity of mid-points of cell edges	λ_1	3λ	
Intensity of cell centroids	λ_2	2λ	
Expected total edge length per unit area	L_A	$32\lambda^{1/2}/(3\pi)$	$3.395\lambda^{1/2}$
Expected number of edges at a typical vertex	$E(E)$	6	
Expected number of cells at a typical vertex	$E(M)$	6	
Expected number of cells at a typical edge	$E(N)$	2	
Expected area of a typical cell, its second moment	$E(A)$	$1/(2\lambda)$	$0.5\lambda^{-1}$
and its k th moment	$E(A^2)$	$35/(8\pi^2\lambda^2)$	$0.443\lambda^{-2}$
Expected perimeter of a typical cell and its second moment	$E(A^k)$	$\Gamma(3k+5)/2\Gamma(k/2+1)/[3\Gamma(k+3)^2/2\Gamma^{k-1/2}\lambda^k]$	—
Expected length of a typical edge, its second moment	$E(P)$	$32/(3\pi\lambda^{1/2})$	$3.395\lambda^{-1/2}$
and its second moment	$E(P^2)$	$125/(3\pi\lambda)$	$13.263\lambda^{-1}$
Expected circumradius, its second moment	$E(L)$	$32/(9\pi\lambda^{1/2})$	$1.132\lambda^{-1/2}$
and its k th moment	$E(L^2)$	$5/(\pi\lambda)$	$1.592\lambda^{-1}$
Expected inradius	$E(L^k)$	$2^{k+3}\Gamma(k+5)/2\Gamma(3(k+2)\pi^{(k+1)/2}\lambda^{k/2})$	—
and its second moment	$E(I)$	$1/(4\lambda^{1/2})$	$0.25\lambda^{-1/2}$
Expected circumradius, its second moment	$E(I^2)$	$1/(4\pi\lambda)$	$0.089\lambda^{-1}$
and its k th moment	$E(R)$	$3/(4\lambda^{1/2})$	$0.75\lambda^{-1/2}$
Expected angle spanned by two edges of a typical cell and its second moment	$E(R^2)$	$2/(\pi\lambda)$	$0.637\lambda^{-1}$
	$E(R^k)$	$\Gamma(k/2+2)/(\pi\lambda)^{k/2}$	—
	$E(\alpha)$	$\pi/3$	1.047
	$E(\alpha^2)$	$(4\pi^2 - 15)/18$	1.360

λ = intensity of Θ_p .

Sources: Martin (1965) and Miles (1970a).

Table 5.11.2 Moments of various characteristics of a Poisson Delaunay diagram in \mathbb{R}^3 .

Moment	Symbol	Exact value	Numerical value
Intensity of cell vertices	λ_0	λ	
Intensity of mid-points of cell edges	λ_1	$(24\pi^2/35 + 1)\lambda$	7.768 λ
Intensity of centroids of cell faces	λ_2	$(48/35)\pi^2\lambda$	13.535 λ
Intensity of cell centroids	λ_3	$(24/35)\pi^2\lambda$	6.768 λ
Expected total face area per unit volume	S_v	$(200/27)\Gamma(2/3)(\pi\lambda/6)^{13}$	8.085 λ^{13}
Expected total edge length per unit area	L_v	$(24\pi^2/35)\Gamma(2/3)(\pi\lambda/6)^{13}\Gamma(1/3)\lambda^{23}$	9.609 λ^{23}
Expected number of edges at a typical vertex	$E(E)$	$(3/4)^{13}\pi^{-13}\Gamma(1/3)\lambda^{23}$	
Expected number of faces at a typical vertex	$E(F)$	$(48\pi^2/35)^{+2}$	15.535
Expected number of cells at a typical vertex	$E(M)$	$(144/35)\pi^2$	40.606
Expected number of faces at a typical edge	$E(G)$	$(96/35)\pi^2$	27.071
Expected number of edges at a typical edge	$E(N)$	$(144\pi^2)/(24\pi^2 + 35)$	5.228
Expected number of edges of a typical cell	$E(V)$	$(144\pi^2)/(24\pi^2 + 35)$	5.228
Expected volume of a typical cell and its second moment	$E(V^2)$	$3.5/(24\pi^2\lambda^2)$	0.148 λ^{-1}
	$E(V')$	$105/(286\pi^2\lambda^2)$	0.037 λ^{-2}
		$35\pi^{12}(k+1)^(k+2)!(2k+4)!$	
		$\times [256\Gamma(k/2 + 2)^2\Gamma(9 + 3k)/2](16\pi\lambda)^k)^{-1}$	
Expected surface area of a typical cell and its second moment	$E(S)$	$[3500(3/4)^{25}\Gamma(2/3)]/[243\pi^{53}\lambda^{23}]$	2.389 λ^{-23}
Expected area of a typical face and its k th moment	$E(S^2)$	$-$	6.934 λ^{-43}
	$E(A)$	$[875(3/4)^{25}\Gamma(2/3)]/[243\pi^{53}\lambda^{23}]$	0.597 λ^{-23}
	$E(A^k)$	$[(35)(3/2\pi k)(k+4)\Gamma(2k/3 + 3)\Gamma(k+3)\Gamma(3k/2 + 4)]$	
		$\times [240\pi k + \pi^{2k/3 - 17}/\Gamma(k/2 + 2)\Gamma(k + 9/2)\lambda^{23}]^{-1}$	
Expected total edge length of a typical cell and its second moment	$E(B)$	$5(\pi/2)^8\Gamma(4/3)[6(\pi\lambda)^{13}]$	7.422 λ^{-13}
Expected perimeter of a typical face and its second moment	$E(P)$	$(5/27)(40 + 24/9\pi^2)\Gamma(5/3)[6(\pi\lambda)]^{23}$	57.760 λ^{-23}
Expected length of a typical edge and its k th moment	$E(L)$	$(1715/512)\Gamma(4/3)6^{13}(\pi\lambda)^{-13}$	3.711 λ^{-13}
	$E(L^k)$	$(3200/81)[128/(75\pi^2) + 3132]\Gamma(5/3)\cdot 6^{23}(\pi\lambda)^{-23}$	14.640 λ^{-23}
		$(1715/2304)(3/4)^{13}\pi^{-13}\Gamma(1/3)\lambda^{-13}$	1.237 λ^{-13}
		$(35/32)(k+8)(k+6)(k+7)(k+5)(k+3)]^{-1}$	
Expected mean breadth	$E(b)$	$\times \Gamma(3 + k/3)6^{43}(\pi\lambda)^{-k/3}$	—
Expected angle spanned by two edges of a typical face and its second moment	$E(\alpha)$	$\pi/3$	1.118 λ^{-13}
	$E(\alpha^2)$	$\pi^2/6 - 3/8$	1.047 1.270

λ = intensity of Θ_p .

Source: Miles (1970a), Muche (1999).

Table 5.11.3 The first moments of various characteristics of a Poisson Delaunay cell in \mathbb{R}^4 .

Characteristic	Exact first moment	Numerical value
Number of edges at a typical vertex	340/9	37.778
Number of triangles at a typical vertex	590/3	196.667
Number of tetrahedra at a typical vertex	2860/9	317.778
Number of cells at a typical vertex	1450/9	158.889
Number of triangles at a typical edge	177/17	10.412
Number of tetrahedra at a typical edge	429/17	25.235
Number of cells at a typical edge	286/17	16.824
Number of tetrahedra at a typical triangle	286/59	4.847
Number of cells at a typical triangle	286/59	4.487
Number of tetrahedra of a typical cell	2	2
Volume of a typical cell	$9/(286 \lambda)$	$0.031\lambda^{-1}$
Volume of a typical tetrahedron	$(2/\pi^2)^{3/4}(32/385)(14/13)^2(18!/17!)\Gamma(3/4)\lambda^{-3/4}$	$0.192\lambda^{-3/4}$
Area of a typical triangle	$2^{1/2}(2/13)(8/11)^2(17!/16!)\Gamma(1/2)\lambda^{1/2}$	$0.681\lambda^{-1/2}$
Length of a typical edge	$(2/\pi^6)^{1/4}(27/77)(16!/15!)\Gamma(1/4)\lambda^{-1/4}$	$1.3825\lambda^{-1/4}$

$\lambda =$ intensity of Θ_p .

Source: Christ et al. (1982a, Tables 1 and 2).

Table 5.11.4 Correlation coefficients for the characteristics of a typical Poisson Delaunay cell in \mathbb{R}^2 .

Characteristic		P	I	R
Area	A	0.916	0.921	0.783
Perimeter	P	—	0.878	0.936
Inradius	I	—	—	0.694
Circumradius	R	—	—	—

Source: Miles (1970a, p.113).

$$E_3 V_3^k = \frac{35\pi^{1/2}(k+1)!(k+2)!(2k+4)!}{256\Gamma\left(\frac{k}{2}+2\right)^3 \Gamma\left(\frac{9+3k}{2}\right)(16\pi\lambda)^k} \quad \text{for } k=1, 2, \dots \quad (5.11.6)$$

Values of $E_2 V_2^k$ and $E_3 V_3^k$ for $k = 1, 2$ are given in Tables 5.11.1 and 5.11.2, respectively.

For $m = 2$, Miles (1970a) has also derived the first- and second-order moments of a number of characteristics of a typical PDC (see Table 5.11.1). In addition, the relationship described in equation (5.11.1) allows the derivation of other moment measures for \mathcal{D}_P in \mathbb{R}^2 , \mathbb{R}^3 and \mathbb{R}^4 which are reported in Tables 5.11.1, 5.11.2 and 5.11.3, respectively. Correlation coefficients for pairs of selected characteristics of PDCs in \mathbb{R}^2 have also been obtained by Miles (1970a, Table 1) and are given in Table 5.11.4.

Probability distributions of PDC characteristics are mathematically more tractable than those of PVC characteristics considered in Section 5.5.

Rathie (1992) showed that the moments given in equation (5.11.4) determined the distribution of the volume of a typical PDC uniquely (see Rao, 1973, p. 106) and obtained the pdf $f_{\lambda V_m}$ for the standardized volume (λV_m) of a typical PDC:

$$f_{\lambda V_m}(v) = A_m (2\pi i v)^{-1} \int_Y \nabla_m(k) (B_m v^2)^{-k} dk, \quad v > 0, \quad (5.11.7)$$

where $i = \sqrt{-1}$, Y encloses all the poles of the integrand,

$$A_m = \frac{2^{m-1/2} (m+1)^{m^2/2} \Gamma\left(\frac{m^2}{2}\right) \Gamma\left(\frac{m+1}{2}\right)^m}{\pi m^{(m^2-1)/2} \Gamma(m) \Gamma\left(\frac{m^2+1}{2}\right) \prod_{i=2}^m \Gamma\left(\frac{i}{2}\right)},$$

$$B_m = \left[\frac{2^{m-1} \pi^{(m-1)/2} m^{m/2} \Gamma\left(\frac{m+1}{2}\right)}{(m+1)^{(m+1)/2}} \right]^2,$$

$$\nabla_m(k) = \frac{\prod_{r=2}^m \Gamma\left(\frac{r}{2} + k\right) \prod_{r=0}^m \Gamma\left[\frac{m^2 + 1 + 2r}{2(m+1)} + k\right]}{\prod_{r=1}^{m-1} \Gamma\left(\frac{m}{2} + \frac{r}{m} + k\right) \Gamma\left(\frac{m+1}{2} + k\right)^{m-1}}.$$

The integral in equation (5.11.7) can be evaluated as the sum of the residues at the poles of $\nabla_m(k)$. As a result, $f_{\lambda V_m}(v)$ can be expressed as an infinite series involving gamma, psi and zeta functions (see also Pederzoli, 1995). Rathie also developed a computer program for the numerical calculation of the density and the distribution functions.

In particular, when $m = 2$, the density given in equation (5.11.7) reduces to

$$f_{\lambda V_2}(v) = \left(\frac{8}{9}\right) \pi v K_{1/6}^2 \left(\frac{2\pi v}{3\sqrt{3}}\right), \quad v \geq 0, \quad (5.11.8)$$

where $K_{1/6}$ is the modified Bessel function of order 1/6:

$$K_{1/6}(x) = \sqrt{\pi} \left(\frac{x}{2}\right)^{1/6} \Gamma\left(\frac{2}{3}\right)^{-1} \int_1^\infty \exp(-xt)(t^2 - 1)^{-1/3} dt.$$

See Figure 5.11.1(a).

For $m = 3$, the density for the standardized volume derived from equation (5.11.7) involves a sequence of complicated analytical functions. Muche (1996b), using Miles' formula (5.11.2), obtained the following three-fold integral form for this density, which is more suitable for numerical evaluation:

$$f_{\lambda V_3}(v) = \frac{35}{2} \int_0^{2\pi} \int_0^{2\pi - \alpha_1} \int_0^\pi v \sin \beta \times \exp\left(\frac{-2\pi v}{g(\alpha_1, \alpha_2)(1 + \cos \beta) \sin^2 \beta}\right) d\beta d\alpha_2 d\alpha_1, \quad v \geq 0, \quad (5.11.9)$$

where

$$g(\alpha_1, \alpha_2) = \sin \frac{\alpha_1}{2} \sin \frac{\alpha_2}{2} \sin \frac{\alpha_1 + \alpha_2}{2}. \quad (5.11.10)$$

See Figure 5.11.1(b). He also obtained a two-fold integral expression for the density of the standardized area of a typical PDC in \mathbb{R}^2 given in equation (5.11.8):

$$f_{\lambda V_2}(v) = \frac{\pi v}{6} \int_0^{2\pi} \int_0^{2\pi - \alpha_1} \frac{1}{g(\alpha_1, \alpha_2)} \exp\left(\frac{-\pi v}{2g(\alpha_1, \alpha_2)}\right) d\alpha_2 d\alpha_1, \quad v \geq 0,$$

where the function g is given in equation (5.11.10). The equivalent radius R_m is defined to be the radius of an m -dimensional sphere with volume V_m . The pdfs of R_m for $m = 2$ and $m = 3$ are given in Muche (1996b):

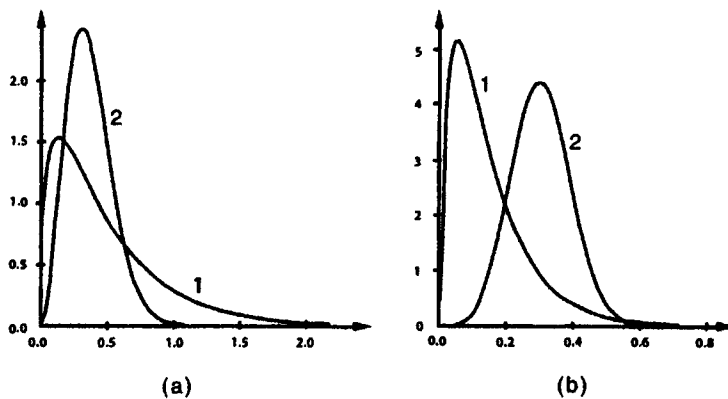


Figure 5.11.1 Probability density functions of (a) (1) the area V_2 and (2) the equivalent radius R_2 of a typical two-dimensional Poisson Delaunay cell; (b) (1) the volume V_3 and (2) the equivalent radius R_3 of a typical three-dimensional Poisson Delaunay cell ($\lambda = 1$). (Source: Muche, 1996b, Figures 1 and 5.)

$$f_{R_2}(r) = \frac{\pi^3 \lambda^2 r^3}{3} \int_0^{2\pi} \int_0^{2\pi - \alpha_1} \frac{1}{g(\alpha_1, \alpha_2)} \exp\left(\frac{-\lambda\pi^2 r^2}{2g(\alpha_1, \alpha_2)}\right) d\alpha_2 d\alpha_1, \quad r \geq 0,$$

$$f_{R_3}(r) = \frac{280\pi^2 \lambda^2 r^5}{3} \int_0^{2\pi} \int_0^{2\pi - \alpha_1} \int_0^\pi \sin \beta \times \exp\left(\frac{-8\pi^2 \lambda r^3}{3g(\alpha_1, \alpha_2)(1 + \cos \beta) \sin^2 \beta}\right) d\beta d\alpha_2 d\alpha_1, \quad r \geq 0,$$

respectively (see Figure 5.11.1). The k th moments are also obtained:

$$E_2 R_2^k = \frac{\Gamma\left(\frac{k+4}{4}\right) \Gamma\left(\frac{3k+10}{4}\right)}{3 \cdot 2^{k/2} \pi^{k-1/2} \Gamma\left(\frac{k+6}{4}\right)^2 \lambda^{k/2}},$$

$$E_3 R_3^k = \frac{35 \cdot 3^{k/3} \Gamma\left(\frac{k}{3} + 2\right) \Gamma\left(\frac{k}{3} + 3\right) \Gamma\left(\frac{2k}{3} + 5\right)}{2^{2k+8} \pi^{2k/3-1/2} \Gamma\left(\frac{k}{6} + 2\right)^3 \Gamma\left(\frac{k+9}{2}\right) \lambda^{k/3}}.$$

A *Gabriel edge* is an edge of a Delaunay cell which intersects the interface between the two Voronoi cells. The length of a typical Gabriel edge E follows a generalized gamma distribution, the density of which is:

$$f_L(l) = \frac{m\lambda\omega_m l^{m-1}}{2^m} \exp\left(-\frac{\lambda\omega_m l^m}{2^m}\right), \quad l > 0,$$

where $\omega_m = \pi^{m/2}/\Gamma(m/2 + 1)$ is the volume of an m -dimensional sphere of unit radius.

Knowledge of the probability distributions of other PDC characteristics is limited to $m = 3$ and $m = 2$. Miles' formula (5.11.2) plays a fundamental role in the derivation of them. For $m = 2$, the pdfs for the perimeter of a typical cell P (Muche, 1996b) and the length of a typical edge L (Collins, 1968; Muche, 1996b) are

$$\begin{aligned} f_P(p) &= \frac{\pi\lambda^2 p^3}{12} \int_0^{2\pi} \int_0^{2\pi-\alpha_1} \frac{g(\alpha_1, \alpha_2)}{\left(\sin \frac{\alpha_1}{2} + \sin \frac{\alpha_2}{2} + \sin \frac{\alpha_1 + \alpha_2}{2}\right)^4} \\ &\quad \times \exp\left(\frac{-\lambda\pi p^2}{4\left(\sin \frac{\alpha_1}{2} + \sin \frac{\alpha_2}{2} + \sin \frac{\alpha_1 + \alpha_2}{2}\right)^2}\right) d\alpha_2 d\alpha_1, \quad p \geq 0, \\ f_L(l) &= \frac{\lambda\pi l}{3} \left(\lambda^{1/2} l \exp\left(\frac{-\lambda\pi l^2}{4}\right) + \frac{2}{\sqrt{\pi}} \int_{(\lambda\pi)^{1/2} l/2}^{\infty} \exp(-x^2) dx \right), \quad l \geq 0, \end{aligned}$$

where g is given in equation (5.11.10). See Figure 5.11.2. The k th moments can now be evaluated:

$$\begin{aligned} E(P^k) &= \frac{2^{k+1} \Gamma\left(2 + \frac{k}{2}\right)}{3\pi^{k/2+1} \lambda^{k/2}} \int_0^{2\pi} \int_0^{2\pi-\alpha_1} g(\alpha_1, \alpha_2) \\ &\quad \times \left(\sin \frac{\alpha_1}{2} + \sin \frac{\alpha_2}{2} + \sin \frac{\alpha_1 + \alpha_2}{2}\right)^k d\alpha_2 d\alpha_1, \\ E(L^k) &= \frac{2^{k+1} (k+1)(k+3) \Gamma\left(\frac{k+1}{2}\right)}{3(k+2)\pi^{k+1/2} \lambda^{k/2}}. \end{aligned}$$

Mecke and Muche (1995) showed that the length of an edge emanating from a typical vertex has the same distribution as L . Drouffe and Itzykson (1984) have also estimated $E(L|N)$, the average length of an edge emanating from a vertex, as a function of the number of edges incident at the vertex, which they find grows approximately as $N^{1/2}$.

The joint pdf of the interior angles of a typical PDC was obtained by Miles (1970a):

$$f_{\alpha, \beta}(\alpha, \beta) = \frac{8\pi}{3} [\sin \alpha \sin \beta \sin(\alpha + \beta)], \quad \alpha \geq 0, \beta \geq 0, \alpha + \beta < \pi. \quad (5.11.11)$$

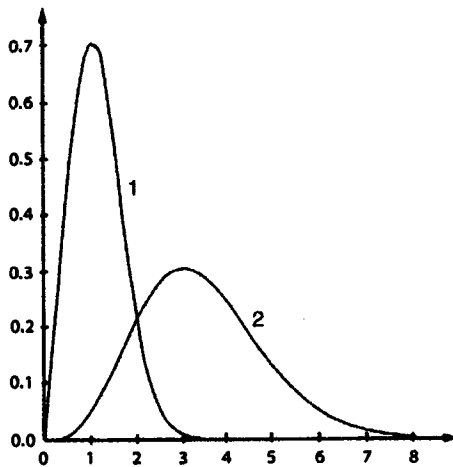


Figure 5.11.2 Probability density functions of (1) the length of an edge L and (2) the perimeter P of a typical two-dimensional Poisson Delaunay cell ($\lambda = 1$). (Source: Muche, 1996b, Figure 6.)

This density attains its maximum at $\alpha = \beta = \pi/3$, which indicates that the most likely triangle in \mathcal{D}_p is an equilateral one. From equation (5.11.11) the marginal density can be derived:

$$f_\alpha(\alpha) = \frac{4}{3\pi} [\sin \alpha + (\pi - \alpha) \cos \alpha] \sin \alpha, \quad 0 \leq \alpha < \pi, \quad (5.11.12)$$

which is the density of a randomly selected angle of a typical triangle of \mathcal{D}_p . This density is illustrated in Figure 5.11.3. Equation (5.11.12) was also obtained by Collins (1968), and the mode of it is at $\alpha = 0.89489$ radians ($51^\circ 16' 24''$). The first two moments are given in Table 5.11.1. Problems in using equation (5.11.12) in empirical applications led to the use of Miles' approach to derive both the densities of the minimum, middle and maximum angles, $f_{\alpha_{\min}}$, $f_{\alpha_{\text{mid}}}$ and $f_{\alpha_{\max}}$, respectively, of a typical PDC. Mardia *et al.* (1977) derived

$$f_{\alpha_{\min}}(\alpha) = \frac{2}{\pi} [(\pi - 3\alpha) \sin 2\alpha + \cos 2\alpha - \cos 4\alpha], \quad 0 \leq \alpha < \frac{\pi}{3}, \quad (5.11.13)$$

and Boots (1986) gave

$$f_{\alpha_{\max}}(\alpha) = \begin{cases} \frac{2}{\pi} [(3\alpha - \pi) \sin 2\alpha - \cos 2\alpha + \cos 4\alpha], & \frac{\pi}{3} \leq \alpha < \frac{\pi}{2}, \\ \frac{4}{\pi} [\sin \alpha + (\pi - \alpha) \cos \alpha] \sin \alpha, & \frac{\pi}{2} \leq \alpha < \pi. \end{cases} \quad (5.11.14)$$

Muche (1999) obtained that

$$f_{\alpha_{\text{mid}}}(\alpha) = \begin{cases} \frac{8}{\pi} [2 \sin^3 \alpha - \sin \alpha + \alpha \cos \alpha] \sin \alpha, & 0 \leq \alpha < \frac{\pi}{3}, \\ \frac{4}{\pi} [\pi - 2\alpha + \sin 2\alpha] \sin 2\alpha, & \frac{\pi}{3} \leq \alpha < \frac{\pi}{2}. \end{cases} \quad (5.11.15)$$

These densities are illustrated in Figure 5.11.3.

Further understanding of the angular properties of \mathcal{D}_p in \mathbb{R}^2 is provided by Kendall (1983) whose approach involves an examination of the shape of Delaunay triangles. Kendall's theory of shape involves associating a triad of labelled points from a pattern with a location in a shape space (for an overview of how this is achieved see Stoyan *et al.*, 1995, pp. 255–273 or Small, 1988, 1996). The particular shape space derived by Kendall is represented as a flat, curvilinear triangle referred to as the spherical blackboard. This is illustrated in Figure 5.11.4(a) which also shows triangles of representative shapes located at the appropriate positions. Figure 5.11.4(b) shows the shapes of 5000 PDCs obtained by Kendall using the simulation procedure described in Section 5.4. This clearly illustrates the dominance of more equilateral shapes.

For $m = 3$, Kumar and Kurtz (1994b) derived the pdf of the angle α in a typical face spanned by two of its edges:

$$f_\alpha(\alpha) = \frac{4}{3\pi^2} [2(\pi - \alpha)(2 + \cos 2\alpha) + 3 \sin 2\alpha] \sin^2 \alpha, \quad 0 \leq \alpha \leq \pi,$$

which was again obtained by Muche (1996b; 1999), who also derived the pdfs for the minimum, middle and maximum interior angles of a typical face, $f_{\alpha_{\min}}$, $f_{\alpha_{\text{mid}}}$ and $f_{\alpha_{\max}}$, respectively:

$$f_{\alpha_{\min}}(\alpha) = \frac{8}{\pi^2} [(\pi - 3\alpha)(3 - 2 \sin^2 \alpha) - (16 \sin^4 \alpha - 9) \sin \alpha \cos \alpha] \sin^2 \alpha, \quad 0 \leq \alpha < \pi/3,$$

$$f_{\alpha_{\text{mid}}}(\alpha) = \begin{cases} \frac{16}{\pi^2} [\alpha(3 - 2 \sin^2 \alpha) - (3 - 8 \sin^4 \alpha) \sin \alpha \cos \alpha] \sin^2 \alpha, & 0 \leq \alpha < \pi/3, \\ \frac{16}{\pi^2} [(\pi - 2\alpha)(3 - 2 \sin^2 \alpha) - 2(4 \sin^4 \alpha - 3) \sin \alpha \cos \alpha] \sin^2 \alpha, & \pi/3 \leq \alpha < \pi/2, \end{cases}$$

$$f_{\alpha_{\max}}(\alpha) = \begin{cases} \frac{8}{\pi^2} [(3\alpha - \pi)(3 - 2 \sin^2 \alpha) - (9 - 16 \sin^4 \alpha) \sin \alpha \cos \alpha] \sin^2 \alpha, & \pi/3 \leq \alpha < \pi/2, \\ \frac{8}{\pi^2} [(\pi - \alpha)(3 - 2 \sin^2 \alpha) + 3 \sin \alpha \cos \alpha] \sin^2 \alpha, & \pi/2 \leq \alpha < \pi. \end{cases}$$

These densities are illustrated in Figure 5.11.5.

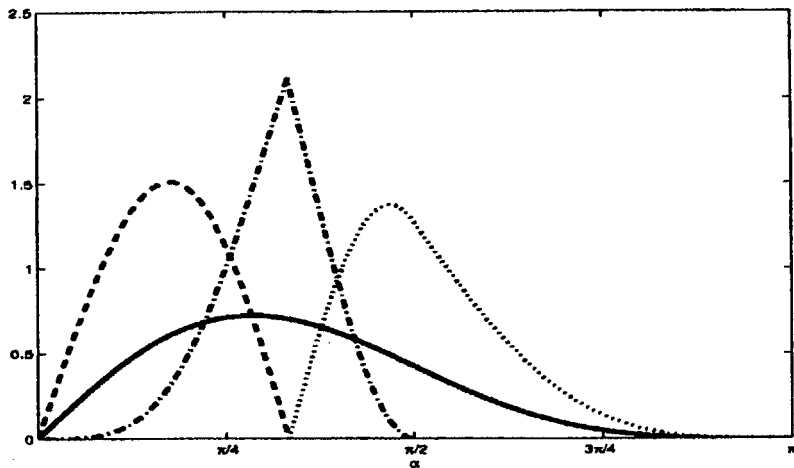


Figure 5.11.3 Probability density functions of interior angles of a typical PDC in \mathbb{R}^2 : — randomly selected angle α ; - - - minimum α_{\min} ; · - middle α_{mid} ; . . . maximum α_{\max} of the three angles of a typical cell.

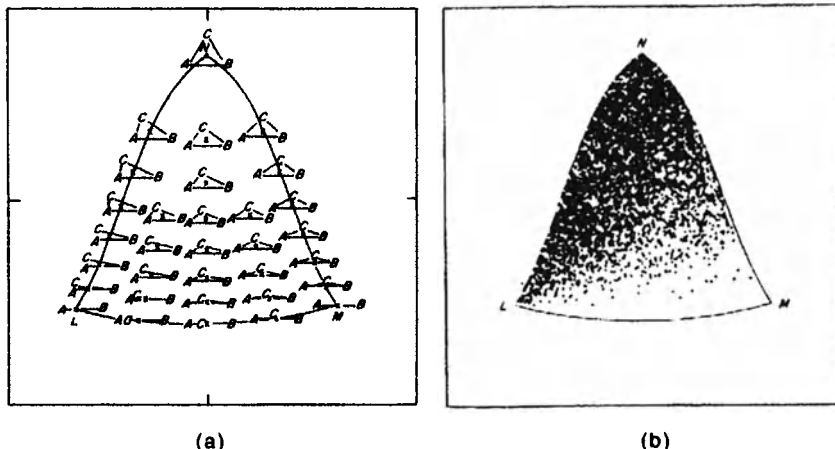


Figure 5.11.4 (a) The spherical blackboard showing 32 triangles located according to their shapes. (b) 5000 Poisson Delaunay cells in \mathbb{R}^2 located on the spherical blackboard. (Source: (a) Kendall, 1981; (b) Kendall, 1983.)

Muche (1996b, 1999) also established the pdfs for the surface area S , the total edge length B and the mean breadth \bar{b} of a typical PDC in \mathbb{R}^3 , the area A and the perimeter P of a typical face, and the length L of a typical edge. Denote by p_0, p_1, p_2 and p_3 the four vertices of a PDC in \mathbb{R}^3 and by c the centre of the sphere on whose surface the vertices lie. Consider the spherical coordinate system (distance, polar angle, amplitude). The locations of the vertices relative to c can be expressed in terms of seven parameters:

$$\begin{aligned} p_0 - c &= \left(r, \beta, -\frac{\alpha_1}{2} \right), & p_1 - c &= \left(r, \beta, \frac{\alpha_1}{2} \right), \\ p_2 - c &= \left(r, \beta, \frac{\alpha_1 + \alpha_2}{2} \right), & p_3 - c &= (r, \cos^{-1}(\cos \beta - h), \eta). \end{aligned}$$

Denote the corresponding unit vectors by $\mathbf{u}_i = (p_i - c)/r$. Let $t_{ij} = \|\mathbf{u}_i - \mathbf{u}_j\|$, $i, j = 0, 1, 2, 3$, $i \neq j$, be the distance between \mathbf{u}_i and \mathbf{u}_j , and $a_i = a_i(\mathbf{u}_i, \mathbf{u}_k, \mathbf{u}_l)$, where i, k, l are distinct elements from $\{0, 1, 2, 3\}$, be the area of the triangle spanned by $\mathbf{u}_i, \mathbf{u}_k, \mathbf{u}_l$. Furthermore, let κ_{ij} , $i, j = 0, 1, 2, 3$ and $i \neq j$, be the angle between the normal vectors of these two faces adjacent to the edge spanned by p_i and p_j . The pdfs are

$$\begin{aligned} f_S(s) &= \frac{70\lambda^3}{9} \int_0^{2\pi} \int_0^{2\pi-\alpha_1} \int_0^\pi \int_0^{2\pi} \int_0^{1+\cos\beta} \frac{hs^{7/2} g(\alpha_1, \alpha_2)^2 \sin^5 \beta}{(a_0 + a_1 + a_2 + a_3)^{9/2}} \\ &\quad \times \exp\left(-\frac{4\pi\lambda}{3} \frac{s^3/2}{(a_0 + a_1 + a_2 + a_3)^{3/2}}\right) dh d\eta d\beta d\alpha_2 d\alpha_1, \quad s \geq 0, \end{aligned}$$

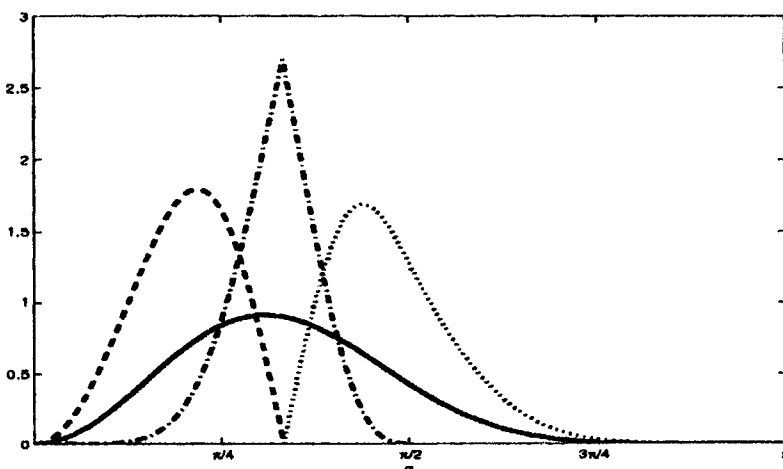


Figure 5.11.5 Probability density function of interior angles of a typical face of a PDC in \mathbb{R}^3 : — randomly selected angle α ; - - - minimum α_{\min} ; · · · middle α_{mid} ; · · · · maximum α_{\max} of the three interior angles of a typical face.

$$f_B(b) = \frac{140\lambda^3}{9} \int_0^{2\pi} \int_0^{2\pi-\alpha_1} \int_0^\pi \int_0^{2\pi} \int_0^{1+\cos\beta} \frac{hb^8 g(\alpha_1, \alpha_2)^2 \sin^5 \beta}{(\ell_{01} + \ell_{02} + \ell_{03} + \ell_{12} + \ell_{13} + \ell_{23})^9} \\ \times \exp\left(-\frac{4\pi\lambda}{3} \frac{b^3}{(\ell_{01} + \ell_{02} + \ell_{03} + \ell_{12} + \ell_{13} + \ell_{23})^3}\right) d\hbar d\eta d\beta d\alpha_2 d\alpha_1, \quad b \geq 0,$$

$$f_b(\bar{b}) = \frac{140(4\pi^9)\lambda^3}{9} \int_0^{2\pi} \int_0^{2\pi-\alpha_1} \int_0^\pi \int_0^{2\pi} \int_0^{1+\cos\beta} \frac{h(\bar{b})^8 g(\alpha_1, \alpha_2)^2 \sin^5 \beta}{\left(\sum_{i,j=0,\dots,3, i \neq j} t_{ij} \kappa_{ij}\right)^9} \\ \times \exp\left(-\frac{(4\pi)^4 \lambda}{3} \frac{(\bar{b})^3}{\left(\sum_{i,j=0,\dots,3, i \neq j} t_{ij} \kappa_{ij}\right)^3}\right) d\hbar d\eta d\beta d\alpha_2 d\alpha_1, \quad \bar{b} \geq 0,$$

$$f_A(a) = \frac{35\pi\lambda^3}{72\sqrt{2}} \int_0^{2\pi} \int_0^{2\pi-\alpha_1} \int_0^\pi \frac{a^{7/2} (1 + \cos \beta)^2}{g(\alpha_1, \alpha_2)^{5/2} \sin^4 \beta} \\ \times \exp\left(\frac{-\sqrt{2} \pi \lambda a^{3/2}}{3g(\alpha_1, \alpha_2)^{3/2} \sin^4 \beta}\right) d\beta d\alpha_2 d\alpha_1, \quad a \geq 0,$$

$$f_p(p) = \frac{35\pi\lambda^3}{2^7 \cdot 9} \int_0^{2\pi} \int_0^{2\pi-\alpha_1} \int_0^\pi \frac{p^8 g(\alpha_1, \alpha_2)^2 (1 + \cos \beta)^2}{\sin^4 \beta \left(\sin \frac{\alpha_1}{2} + \sin \frac{\alpha_2}{2} + \sin \frac{\alpha_1 + \alpha_2}{2}\right)^9} \\ \times \exp\left(\frac{-\lambda \pi p^3}{6 \sin^3 \beta \left(\sin \frac{\alpha_1}{2} + \sin \frac{\alpha_2}{2} + \sin \frac{\alpha_1 + \alpha_2}{2}\right)^3}\right) d\beta d\alpha_2 d\alpha_1, \quad p \geq 0,$$

$$f_L(l) = \frac{35\pi^2 \lambda^3}{2^7 \cdot 9} \int_0^{\pi/2} \int_0^{\pi/2} \frac{l^8 (2 - \sin^2 \beta) (3 - 2 \sin^2 \varphi)}{\sin^4 \beta \sin^7 \varphi} \\ \times \exp\left(\frac{\pi \lambda l^3}{6 \sin^3 \beta \sin^3 \varphi}\right) d\varphi d\beta, \quad l \geq 0,$$

where g is given in equation (5.11.10). See Figure 5.11.6.

Muche (1998) derived an equivalent one-fold integral form for f_L in the case $m = 3$:

$$f_L(l) = \frac{35\pi\lambda l^2}{2^8} \left[\left(\frac{\pi\lambda l^3}{4} + \frac{5}{2} \right) \exp\left(-\frac{\pi\lambda l^3}{6}\right) \right. \\ \left. - \frac{\pi\lambda l^2}{3} \int_{1/2}^{\infty} \left(1 + \frac{\pi\lambda l^2 x}{6} \right) \exp\left(-\frac{4\pi\lambda x^3}{3}\right) dx \right], \quad l \geq 0.$$

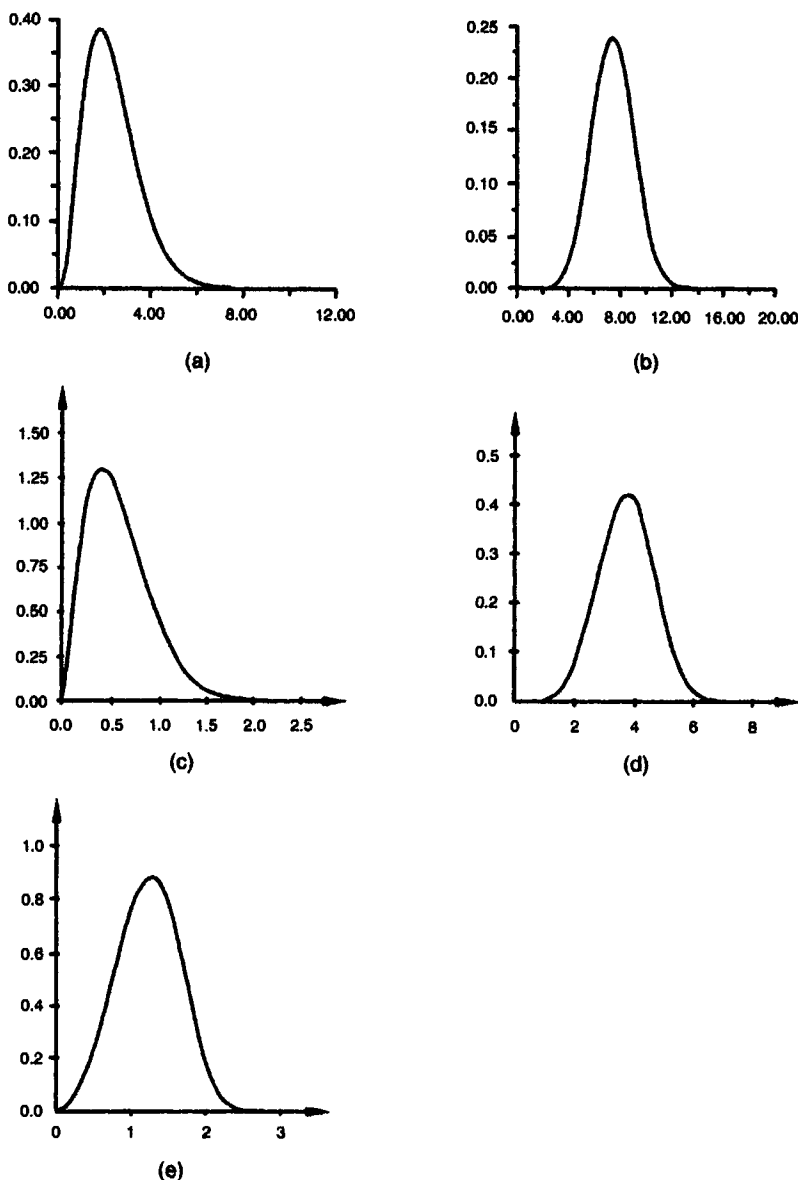


Figure 5.11.6 Probability density functions of (a) the total surface area S ; (b) the total edge length B of a typical cell; (c) the area A ; (d) the perimeter P of a typical face; (e) the length L of a typical edge of a three-dimensional Poisson Delaunay tessellation ($\lambda = 1$). (Sources: (a), (b) Muche, 1999; (c)–(e) Muche, 1996b, Figures 2, 3 and 4.)

The k th moments of A and L can be derived from their densities:

$$\begin{aligned} E(A^k) &= \frac{35 \cdot 3^{2k/3} (k+4) \Gamma\left(\frac{2k}{3} + 3\right) \Gamma(k+3) \Gamma\left(\frac{3k}{2} + 4\right)}{2^{10k/3+9} \pi^{2k/3-1/2} \Gamma\left(\frac{k}{2} + 2\right)^3 \Gamma\left(k + \frac{9}{2}\right) \lambda^{2k/3}}, \\ E(L^k) &= \frac{35}{32} \frac{(k+8)(k+6)}{(k+7)(k+5)(k+3)} \Gamma\left(3 + \frac{k}{3}\right) \left(\frac{6}{\pi\lambda}\right)^{k/3}, \end{aligned}$$

whilst the first and/or second moments of S , B , \bar{b} , P and α are given in Table 5.11.2. As in the case $m = 2$, the length of an edge emanating from a typical vertex has the same distribution as L (Mecke and Muche, 1995).

Kumar and Kurtz (1994b) simulated 1.2 million PDCs in \mathbb{R}^3 . They found that the distributions of the volume V and surface area S of a typical cell, and the face area A of a typical face, can be approximated by a gamma distribution, whilst those of the total edge length of a typical cell and the perimeter of a typical face can be approximated by a normal distribution.

With regard to an s -dimensional section of \mathcal{D}_p in \mathbb{R}^m , which is denoted by $\mathcal{D}_p(s, m)$, note that $\mathcal{D}_p(2, 3)$ consists of triangles and quadrilaterals while $\mathcal{D}_p(3, 4)$ consists of polyhedra with four and five faces and that the plane section of $\mathcal{D}_p(3, 4)$ contains polygons with three, four and five sides (Miles, 1986a, p. 153).

So far the only work on the nature of \mathcal{D} from the various generalizations of \mathcal{V} discussed in Section 3.7 has been that of Miles (1971) on the nature of the Delaunay tessellation \mathcal{D}_s for p random points distributed on the surface of a sphere of unit radius and centred at the origin o in \mathbb{R}^3 . In this case \mathcal{D}_s has $2p-4$ triangular faces and $3p-6$ edges. The expected area of a typical face $E(A)$ is given by

$$E(A) = \frac{2\pi}{p-2}. \quad (5.11.16)$$

In addition, Miles (1971, p. 167, equation (7.6)) derived an expression for the probability distribution of \mathcal{D}_s but was not able to evaluate it.

5.12 OTHER RANDOM VORONOI DIAGRAMS

If, as a result of comparing the characteristics of an empirical tessellation with those of the Poisson Voronoi diagram, \mathcal{V}_p , we determine that the latter is inappropriate as a model of the former or if we have other evidence that supports this viewpoint, we may wish to consider other random tessellations as models. One approach is to modify the properties of the homogeneous Poisson point process Θ_p (see Section 1.3.3) which provides the generator set for \mathcal{V}_p . For example, the independent scattering property of Θ_p means that

there is no constraint on interpoint distances, while in empirical situations inhibitive or repulsive effects may limit how closely individual points can be located with respect to others. If such limits are imposed, the locations of the points in \mathbb{R}^m are more dispersed than they would be in Θ_p . Following established convention in point pattern analysis (see Section 8.1), we label the resulting pattern of points as regular. In some areas of application in the natural sciences such patterns are also referred to as ordered. Alternatively, we may permit the intensity of the point process to vary spatially or randomly according to certain distributions, i.e. we consider an inhomogeneous point process or a compound point process (see Section 1.3.3). The resulting pattern of points is one in which there is a relative concentration of points in some regions of \mathbb{R}^m and a relative absence in others. Again following convention, we refer to such patterns as disordered.

In this section we briefly review different point processes which have been used to create generator sets for Voronoi diagrams. We do not report results for these diagrams although Table 5.12.1 provides a summary of the studies known to the authors together with a listing of the characteristics examined in them. We also note that, with the exception of those studies by Finney (1970a, 1975a), where the point locations are measured from laboratory models of sphere packings in \mathbb{R}^3 , and Lemaître *et al.* (1991, 1992, 1993) and Gervois *et al.* (1992) which involve hard discs moving on an air table, all studies report estimates from Monte Carlo simulations.

We begin by considering processes that produce point patterns which are more regular than those generated by Θ_p . A common feature of many of these processes is that a minimum interpoint distance r is specified. In one group of processes, collectively known as *hard core processes*, this constraint is imposed on points generated by Θ_p . The process is equivalent to a random packing of equal discs or spheres in \mathbb{R}^2 and \mathbb{R}^3 , respectively, if the resulting points are considered to be the centres of non-intersecting discs or spheres of diameter r (see Section 7.1). If we are concerned with a bounded region, B , of \mathbb{R}^3 , hard core processes terminate when either a previously specified number of points has been located in B or it is no longer possible to add more points in B without violating the minimum interpoint distance. The latter case is referred to as *complete random packing*. In either case the process can be characterized by the *packing density* which is the proportion of B that is occupied by discs or spheres. Hard core processes may take a variety of forms. In the *simple sequential inhibition (SSI) process* (Hasegawa and Tanemura, 1980; Tanemura and Hasegawa, 1980; Lotwick, 1982; Hanson, 1983) also referred to as *random sequential adsorption (or addition) (RSA)* (Feder, 1980), discs of fixed diameter r are located sequentially in B until the specified number of discs is obtained (or complete random packing is achieved). At each step the location of the centre of the next disc is chosen uniformly at random from those points which ensure that no two discs overlap. Voronoi diagrams of points located by SSI processes have been used in various applications. These include use as models of non-periodic micro-structure in examinations of the effects of defects on elastic and compressive

Table 5.12.1 Studies of other random Voronoi and Delaunay cells.

Study	R ^m	Model type	Characteristics
Boots (1977)	2	CP SSI	N
Boots (1982)	2	CP	N
Boots (1984)	2	DL	N
Burger <i>et al.</i> (1988)	2	CA DL	A N L _D
Finney (1970a)	3	HC	A F N V
Finney (1975a)	3	RA	R N
Fraser (1991)	2	RA	A L N
Fraser <i>et al.</i> (1990)	2	RA	L N
Fraser <i>et al.</i> (1991)	2	RA	L
Frost and Thompson (1987a)	2	SSI	A L N α
Frost and Thompson (1987b)	2	SSI	A N
Gervois <i>et al.</i> (1992)	2	RA	$A_n m_n$
Gotoh (1983)	3	RA SSI TL	A
Hanson (1983)	3	SSI	F M N V
Hasegawa and Tanemura (1980)	2	SSI	L _D
Heinrich and Schüle (1995)	2	PC TP	A N P
Hermann <i>et al.</i> (1989)	2	TP	A
Hutchings and Discombe (1986)	2	DL PC	A L _D
Icke and van de Weygaert (1987)	2	SSI SC	A L N P α
Kumar <i>et al.</i> (1997)	2	DL TP	N
	3	DL	F
Le Caér and Ho (1990)	2	RM	A L N P A _D L _D P _D
Lemaître <i>et al.</i> (1991)	2	RA	L _D α_D
Lemaître <i>et al.</i> (1992)	2	RA SSI	N
Lemaître <i>et al.</i> (1993)	2	RA	A N P
Lorz and Hahn (1993)	3	PC TP	B E F M N S V \bar{b} $f_3 g_3 \alpha_3$
Marcelpoil and Usson (1992)	2	DL	A P
Møller <i>et al.</i> (1989)	3	TP	M S V h
Moukarzel and Herrmann (1992)	2	DL	A N P L _D
Mulheran and Blackman (1995)	2	TP	A
Smalley (1966)	2	SSI	N
Szeto and Tam (1995)	2	DL	A P
Tanemura and Hasegawa (1980)	2	SSI	A N L P α
van de Weygaert (1994)	3	PC SSI	A B E F L M N P S V $j_2 j_3 \alpha_1 \alpha_3$
Vincent and Howarth (1982)	2	TP	N L _D α_D
Wilkinson (1988a)	2	CA	A
Zaninetti (1992)	2	RM SO	A
	3	SO	V
Zhang <i>et al.</i> (1996)	2	SSI	L _D

Model type:

CA Cluster amplification
 CP Compound Poisson
 DL Displaced lattice
 HC Hard core
 PC Poisson cluster
 RA Re-arrangement

RM Random matrix
 SC Sequential clustering
 SO Sobol
 SSI Simple sequential inhibition
 TL Thinned lattice
 TP Thinned Poisson

Table 5.12.1 cont.**Characteristics:***Three Dimensions*

Voronoi cells:

<i>A</i>	Area/face	<i>V</i>	Volume
<i>B</i>	Total edge length/cell	<i>b̄</i>	Mean breadth
<i>E</i>	Edges/cell	<i>h̄</i>	Mean height
<i>F</i>	Faces/cell	<i>f₃</i>	Cell shape factor $6V/(\pi b^3)$
<i>L</i>	Edge length	<i>g₃</i>	Cell shape factor $6\sqrt{\pi} V/S^{3/2}$
<i>M</i>	Vertices/cell	<i>j₂</i>	Face shape factor $4\pi A/S^2$
<i>N</i>	Edges/face	<i>j₃</i>	Cell shape factor $36\pi V^2/S^3$
<i>P</i>	Total edge length/face	α_1	Dihedral angle on a typical edge
<i>S</i>	Surface area	α_3	Randomly selected dihedral angle between adjacent faces

Two Dimensions

Voronoi cells:

<i>A</i>	Area
<i>L</i>	Edge length
<i>N</i>	Vertices
<i>P</i>	Perimeter
α	Interior angle
A_n	Area of an <i>n</i> -edged cell
m_n	Vertices of a neighbouring cell of an <i>n</i> -edged cell

Delaunay cells:

<i>A_D</i>	Area
<i>L_D</i>	Edge length
<i>P_D</i>	Perimeter
α_D	Interior angle

failure properties (Silva and Gibson, 1997; Silva *et al.*, 1995), granular structure of rocks in microfracturing (Malan and Napier, 1995), porous cellulose acetate membrane (Jafferali *et al.*, 1996), spatially non-differentiated tissue such as that found in the liver (Blackburn and Dunckley, 1996), and populations of anchorage-dependent animal cells developing on surfaces (Lim and Davies, 1990). Such Voronoi diagrams have also been used as initial states for two-dimensional models of soap froth (Weaire and Kermode 1984; Weaire and Lei, 1990; Kermode and Weaire, 1990) and dry foams (Herdle and Aref, 1992).

An alternative approach involves *thinning processes* in which first a specified number of points is generated in *B* using Θ_p and then points are removed in various ways until the minimum interpoint distance constraint is satisfied for all remaining points (Vincent and Howarth, 1982; Hermann *et al.*, 1989; Lorz and Hahn, 1993; Heinrich and Schüle, 1995).

Another hard core process involves a *re-arrangement process* (Finney, 1975a; Fraser, 1991). Initially, a set of points is generated by Θ_p . Then, for any pair of points separated by a distance less than *r*, the points are moved apart along a line passing through them until their interpoint distance is equal to *r*. This procedure is repeated until the minimum interpoint distance condition is met. Fraser *et al.* (1990, 1991) use a variant of this process to define the initial state for a solid-liquid transition model.

As discussed in Section 1.3.3, a Gibbs point process can produce a hard core process with minimum interpoint distance *r* if the pair potential is infinite when the distance between two points is less than *r*. Davy and Guild

(1988) use the Voronoi diagram generated by such a Gibbs point process to study composite materials consisting of spherical filler particles. Kuroda and Tanemura (1992) establish limit theorems for the Voronoi diagram generated by a more general Gibbs point process in which the pair potential function is non-negative.

Hasegawa *et al.* (1981) propose a variant of the SSI version of the hard core process which they label *Voronoi polygonal areal random packing*. It involves defining a minimum size, a , for the Voronoi polygon associated with a point. Initially, three points are located in B according to Θ_p . A new point is then selected at random and the Voronoi diagram of the points is generated. The new point is retained only if the sizes of individual Voronoi polygons exceed a . This procedure is continued until no additional points can be located in B without violating the minimum size constraint.

An alternative way of generating point patterns which are more regular than those resulting from Θ_p is to take a completely ordered situation such as the point lattices described in Section 8.1 and to introduce a random component. One way of doing this is to use a thinning process in which lattice points are deleted randomly according to a specified probability (Gotoh, 1993). Mulheran and Blackman (1995) use the Voronoi diagram of a randomly thinned square lattice to model the growth of a surface film.

Another way involves *displaced lattice processes*. If d is the distance separating neighbouring points on a lattice, a displaced lattice process involves moving each lattice point a distance $\alpha\beta d$ in a random direction ϕ ($0 \leq \phi < 2\pi$) where β is a displacement function and α is a random value ($0 < \alpha < 1$). As $\beta \rightarrow 1$, the points of the displaced lattice tend to Θ_p . Most applications of Voronoi diagrams for displaced lattice points involve triangular or square lattices in \mathbb{R}^2 and include using such structures in analyses of polycrystalline materials. For example, they have been used to explore the effects on such materials of monotonic and cyclic loadings (Cannmo *et al.*, 1995), to consider how disorder in local conductances and in local connectivity affects global conductance (Priolo *et al.*, 1992), to model zinc oxide varistors (Bartkowiak and Mahan, 1995), and as the basis of a two-phase model of ferritic-austenitic stainless duplex steel (Werner *et al.*, 1994). Applications involving lattices in \mathbb{R}^3 include the study of the large-scale distribution of galaxies (SubbaRao and Szalay, 1992) (see also Section 7.2).

Le Caer and Ho (1990) provide another point process in \mathbb{R}^2 which is more regular than Θ_p and which is associated with the eigenvalues of random matrices. For an ensemble of asymmetric $(n \times n)$ complex random matrices, M_n , in which the real and imaginary parts of the matrix elements are independently and identically distributed according to a Gaussian distribution with mean, μ , and standard deviation, $\sigma/\sqrt{2}$, the eigenvalues of $M_n/n^{1/2}$ are distributed uniformly over a disc of radius σ . The eigenvalues also display an inhibitive effect since the probability of finding two identical eigenvalues in such matrices is zero. Furthermore, this process is unique in the statistical sense, isotropic whatever the value of n and homogeneous when $n \rightarrow \infty$ (see Section 1.3.3 for a discussion of isotropy and homogeneity in point processes).

These properties led Le Caér and Ho (1990) to suggest that the resulting Voronoi diagram, which they label the *random matrix Voronoi diagram*, could be used in the same normative fashion as \mathcal{V}_p .

Another process which is more regular than Θ_p involves *Sobol points* (Zaninetti, 1992). The locations of the points are determined by a Sobol sequence which generates numbers between 0 and 1 directly as binary fractions of length w from a set of w special binary fractions, $V_i = 1, 2, \dots, w$, called *direction numbers*.

Less effort has been expended on Voronoi diagrams associated with point patterns more disordered than those resulting from Θ_p . Disordered point patterns can be generated by inhomogeneous or compound point processes. One example is provided by the *negative binomial process* in which the intensity of Θ_p is random and follows a gamma distribution. In such a process the number of points in a subarea follows a negative binomial distribution. We can further allow the intensity to vary spatially in a negative binomial process. Divide \mathbb{R}^m into many non-overlapping subsets. The random intensities in such subsets are independent and follow the same gamma distribution. Then the intensity of the point process varies spatially and in each arbitrary region the number of points still follows a negative binomial distribution. Boots (1977, 1982) reports on Voronoi diagrams for point processes generated in this way in \mathbb{R}^2 .

An alternative way of making Θ_p more disordered occurs in *Poisson cluster processes*. Such processes involve three steps. First, a set of locations for cluster centres in B is defined using Θ_p . Then a random variable describing the number of points in each cluster is generated from a specified probability distribution. Finally, the points in each cluster are distributed with respect to the cluster centre according to some spatial process. Hutchings and Discombe (1986), Hermann *et al.* (1989), Lorz and Hahn (1993), and Heinrich and Schüle (1995) describe characteristics of Voronoi diagrams for points generated by a Poisson cluster process where the number of points in a cluster has a Poisson distribution and where the points are distributed according to Θ_p over a circle (or sphere) of fixed radius centred on the cluster centre.

Burger *et al.* (1988) and Wilkinson (1988a) use the opposite of the thinning process described above to generate points which are more disordered than those of Θ_p . We label this a *cluster amplification process*. First a set of points is generated by Θ_p with intensity λ . Then any point which is farther than a critical distance, $\alpha\lambda^{1/2}$ ($0 < \alpha < 1$), from any other point is removed. The points removed in this way are replaced by an equivalent number of points located in B according to Θ_p . These steps are then repeated until the critical distance condition is satisfied. Note that as $\alpha \rightarrow 1$, the cluster amplification process tends to Θ_p .

Finally, we note that Icke and van de Weygaert (1987) describe a *sequential clustering process* in which an initial point is located at random in B and then each subsequent point is located at a distance $r = -\alpha \log d$ ($\alpha \geq 0$), where d is a random number ($0 \leq d \leq 1$), and a random direction ϕ ($0 \leq \phi < 2\pi$) from the previous point. As $\alpha \rightarrow \infty$, the process approaches Θ_p .

Voronoi diagrams generated by different point process are rather similar. For example, they are all regular and normal (see Property IV5 in Section 5.1). The first moments of cell characteristics may not vary too much (see Table 5.1.1 in Section 5.1). It may be desirable to have some statistical methods to distinguish different Voronoi diagrams. A natural way is to recognize the generator of each Voronoi cell by using Property V15 in Section 2.3 and then spatial point process statistics (see, for example, Diggle, 1983; Ripley, 1988; Cressie, 1991; Stoyan *et al.*, 1995) can be applied. However, empirical situations involving three-dimensional structures are often studied by means of planar sections (see Section 5.7). Since we are not able to construct the three-dimensional point process of the generators from a planar section of a Voronoi diagram, Krawietz and Lorz (1991) and Hahn and Lorz (1994) propose using stereological methods. Several tests are suggested to test whether a given Voronoi diagram is a Poisson Voronoi diagram or not. They find empirically that it is easier to distinguish a Poisson Voronoi diagram from a more disordered Voronoi diagram than from a more regular one. Among the tests they consider, the most powerful one is based on the variance of the cell areas of sectional Voronoi diagrams.

CHAPTER 6

Spatial Interpolation

In Chapter 2 the ordinary Voronoi diagram was defined with respect to a generator set of n distinct points, $P = \{p_1, \dots, p_n\}$, located in m -dimensional Euclidean space, \mathbb{R}^m . As with the bounded ordinary Voronoi diagram of Section 2.1, our concern here will be with a finite region S in \mathbb{R}^m . The location of each point p_i in S is indicated by $x_i = (x_{i1}, \dots, x_{im})^T$ and for the purposes of this chapter we label these points as *data sites*. Unlike Chapter 5 we make no assumption regarding how the data sites are located in S , although in most of the applications discussed below the data sites are irregularly spaced in S . In addition, for each data site we have a numerical observation z_i which we call the *data value*. If we assume that the data values represent observations from a surface defined by (x, z) , *spatial interpolation* involves finding a function $f(x)$ which best represents the entire surface and which predicts values of z for locations other than P in S . Such a function is referred to as an *interpolant*. The particular form we select for $f(x)$ depends on the type of measurement scale of z and the use to which the interpolated surface is put. However, we can make an immediate distinction between *exact* and *approximate interpolants* in terms of whether or not they reproduce the data values; i.e. for an exact interpolant, $f(x_i) = z_i$. Approximate interpolants may be considered a form of data smoothing which are more appropriate than exact interpolants if the data values are subject to inaccurate measurement or errors. This distinction is not of primary concern in this chapter although most of the interpolants discussed specifically are exact ones.

Various other characteristics may also be used to distinguish between interpolants. One which is relevant here is the difference between *global* and *local interpolants*. With the former the value of $f(x)$ at any given location in S depends on all the data values while the latter involves the use of only those values at ‘nearby’ points. Various definitions of nearby are provided below. In general, local interpolants involve partitioning S into s subdomains, $S_i; S = \cup_{i=1}^s S_i$ and then selecting a function of the form

$$f(x) = f_i(x), \quad x \in S_i, \quad i = 1, \dots, s. \quad (6.0.1)$$

Thus, global interpolants are affected by the addition or deletion of data values or by changing the location of data sites. For local interpolants such

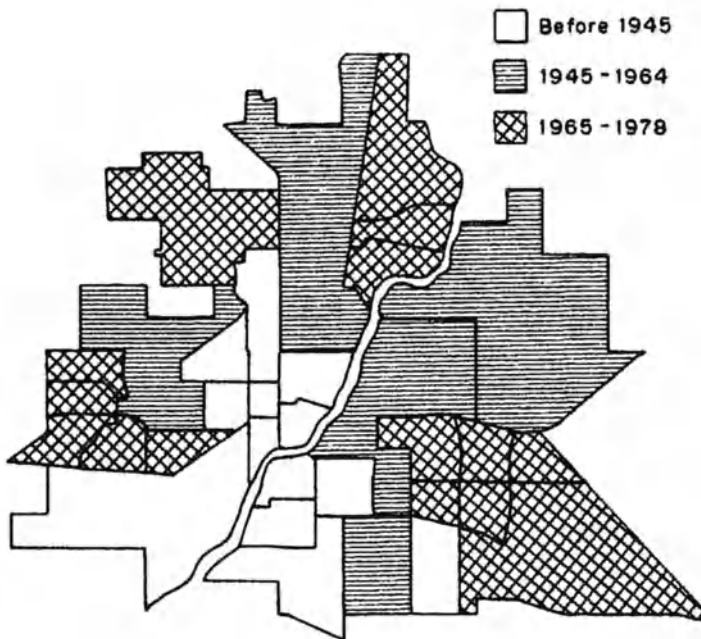


Figure 6.0.1 Choropleth map: Saskatoon Census Metropolitan Area, Canada. Time period of immigration of the majority of the immigrants by census tract, 1981.

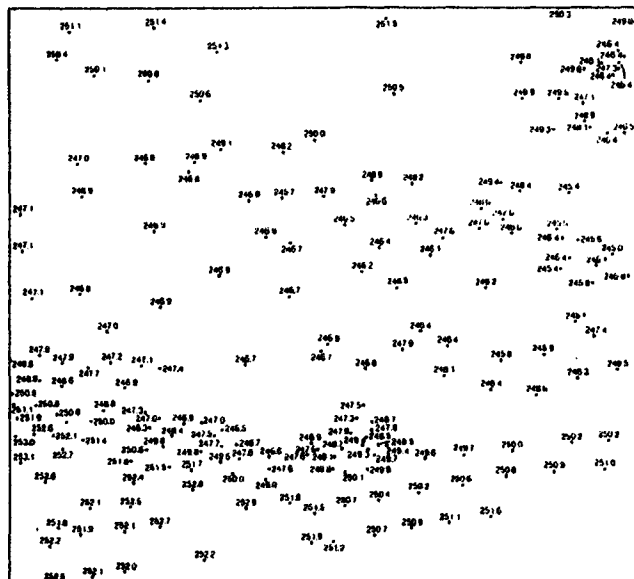
changes only produce effects at locations in the vicinity of the changes. Consequently, fairly large systems of equations are needed to evaluate $f(x)$ for global interpolants, which means that exact versions are not feasible when n is large, say in the order of 100–200 data sites. In contrast, local interpolants typically involve only small systems of equations although there may be a large number of these. In this chapter we consider local interpolants exclusively since global interpolants do not involve Voronoi diagrams.

We focus our discussion on \mathbb{R}^2 . Although the methods described can be extended in theory to \mathbb{R}^3 , complications created by the bounded nature of S quickly dominate the interpolation. Also the majority of applications relate to \mathbb{R}^2 . Typical examples of data values include soil and rock types, elevations of a geological strata, barometric pressure and thickness of an ore body or of a manufactured part. In such cases our choice of an interpolant (surface) will be influenced by the nature of the data values. Values measured on a nominal scale, such as rock and soil types, require a piecewise continuous surface which may be represented in two dimensions as a k -phase mosaic (or in cartographic terms, a choropleth map) (see Figure 6.0.1 where $k = 3$). Other values, such as elevation, which are continuous random variables, require at least a continuous surface. These can be represented in a number of ways including contour (isarithmic) maps, perspective views, hill shading and slope maps (see Figures 6.0.2(b), (c), (d) and (e), respectively). The nature

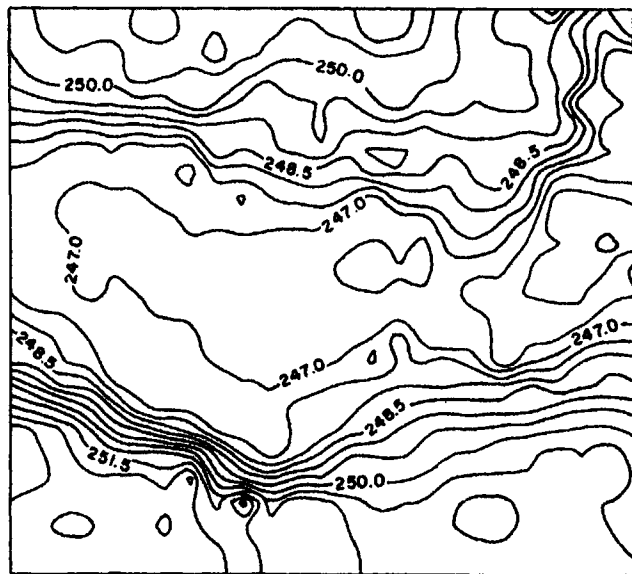
of the continuity of the interpolant (surface) is designated C^k which indicates that the k th or lower order derivatives of the interpolant are all continuous. Thus, for a C^0 interpolant the derivatives are in general discontinuous at the data sites so that a contour map produced from it will appear angular (see Figure 6.0.3). In contrast, a C^1 interpolant such as that used in Figure 6.0.2(b) produces smooth contours. For most practical applications, such as those listed below, C^1 interpolants are sufficient, particularly since, with the exception of special cases, higher order smoothness does not appear to be detectable by the human eye (Sibson, 1981, p. 22).

In terms of the uses of the interpolant, by far the most common is simply to produce a contour map or other visual representation of the surface. Other uses involve calculating some property of the surface at a specified location, calculating the volume under the surface, as in the estimation of ore bodies, and calculating global statistics for the surface, such as estimating the mean precipitation over a region.

This chapter considers only those interpolation procedures that involve Voronoi diagrams or Delaunay triangulations. We refer to these as *polygonal* and *triangular methods*, respectively, although in view of the duality between Voronoi diagrams and Delaunay triangulations, this distinction is one adopted primarily for the convenience of presentation. General reviews of spatial interpolants can be found in Rhind (1975), Schumaker (1976), Schut (1976), Barnhill (1977), Ripley (1981, Chapter 4), Franke (1982), Sabin (1982), Lam (1983), Gold (1989a), Franke and Nielson (1991) and Watson (1992). Section 6.1 deals with polygonal methods while triangular methods are the subject of Section 6.2. The methods described in Section 6.1 include both the use of the ordinary Voronoi diagram and the ordered order- k Voronoi diagram. The main thrust of Section 6.2 is a consideration of the merits of using triangular domains and the characteristics of different triangulations, including the Delaunay triangulation. Initially, this discussion assumes that S is convex, usually rectangular. Section 6.3 considers the modifications necessary to extend the Delaunay triangulation to situations in which S is neither convex nor simply connected. This section also considers ways of incorporating specific data features into the triangulation. In Section 6.4 we consider how the Delaunay triangulation can be used in approximating surfaces with a predefined level of accuracy. In Section 6.5 we concentrate on triangular and tetrahedral meshes that are useful for solving partial differential equations. Finally, in Section 6.6 we note that a tessellation may be considered an ordering of the data sites and we examine how the Voronoi and Delaunay tessellations can be used in this regard for multivariate data.

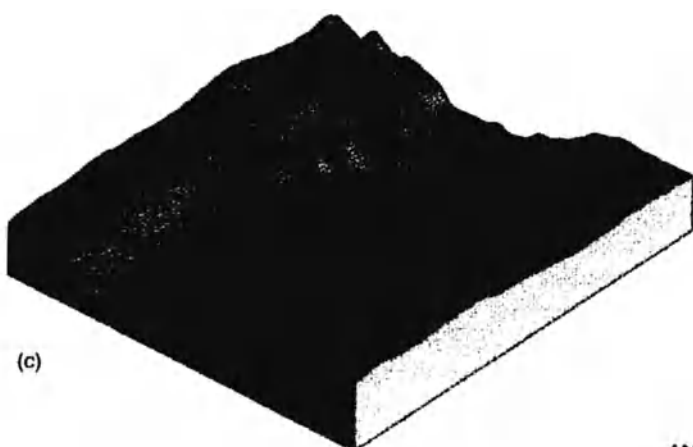


(a)



(b)

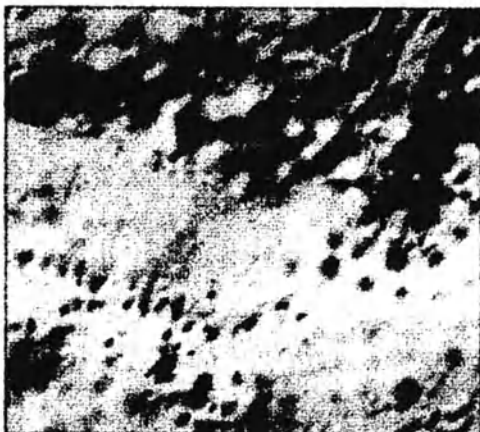
Figure 6.0.2 Different representations of a continuous surface. (a) Original data sites and data values. (b) Contour (isarithmic) map. [See facing page] (c) Perspective view. View direction (azimuth) = 45°; viewing angle = 30°. (d) Hill shading. Sun azimuth = 35°; sun elevation angle = 145°. (e) Slope. Classes: 1, 0–10%; 2, 10–20%; 3, 20–30%; 4, 30–40%; 5, 40–50%; 6, 50–60%.



(c)

ANALYTICAL
HILL-SHADING

sun azimuth = 315°
sun elevation angle = 30°



(d)

SLOPE CLASSES

0-10%	■
10-20%	■
20-30%	■
30-40%	■
40-50%	■
50-60%	■



(e)

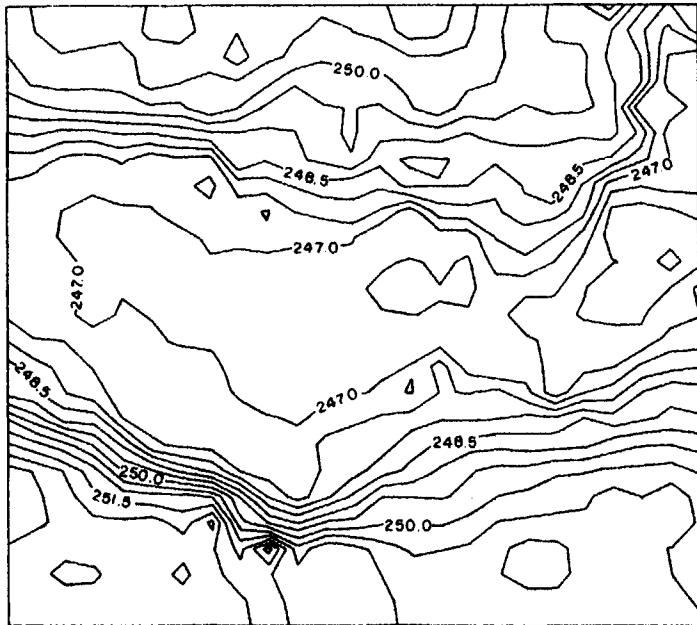


Figure 6.0.3 Contour map of data in Figure 6.0.2 (a) using a C^0 interpolant.

6.1 POLYGONAL METHODS

In general all local interpolants represent the value of the surface $f(\mathbf{x})$ at an arbitrary point p located at \mathbf{x} in S as a weighted, usually linear function of the values at a set of 'nearby' data sites, $D(p)$ ($D(p) \subset P$), so that

$$f(\mathbf{x}) = \sum_{i=1}^{n_D} w_i z_i, \quad p_i \in D(p), \quad (6.1.1)$$

where n_D is the number of nearby sites and w_i is the weight attached to p_i . Local interpolants differ in terms of how the nearby data sites are selected and how the weights are attached to the data values at those sites. The extent to which these two decisions are related may vary considerably in that different weighting schemes may be applied to the same set of nearby data sites. Since, with one exception (see Section 6.1.2), the weighting procedures do not involve concepts of Voronoi diagrams, our presentation will emphasize the methods of selecting nearby data sites. As Tobler (1975) indicated, there are many ways in which this can be performed. In this chapter we consider only those ways that involve either Voronoi diagrams or Delaunay triangulations.

6.1.1 Nearest neighbour interpolation

Perhaps the simplest means of defining $D(p)$ is to select only the nearest data site to p and assign the associated data value to z . Thus,

$$f(x) = z_i, \quad d(p, p_i) < d(p, p_j), \quad p_i \in P, j \neq i, \quad (6.1.2)$$

where $d(p, p_i)$ and $d(p, p_j)$ are the Euclidean distances between p and p_i and p and p_j , respectively. Note that this definition is essentially equivalent to that of an open Voronoi polygon given in Section 2.1. If x is equidistant from two or more members of P , $f(x)$ is undefined. Such locations correspond to the boundaries of the Voronoi polygons of $\mathcal{V}(P)$ so that the resulting surface is discontinuous. In this particular application the individual polygons are usually referred to as *proximal polygons* (Peucker and Chrisman, 1975).

Such an interpolant is most appropriate when z is measured on a nominal scale as with land use, soil, vegetation or rock type whose individual values form patches or phases over S . In such cases once the initial proximal polygons are formed, adjacent polygons with equal values can be merged to form larger patches (see Figure 6.1.1). Arnold and Milne (1984) used this approach to derive soil maps for Greece based on data values collected at data sites spaced every 50–200 m over the study area.

This application may be considered the equivalent of the nearest-point rule for pattern reconstruction in image analysis (Ahuja and Schachter, 1983, Section 1.4.3.3). Here the problem is one of reconstructing a continuous image from the colours observed at a number of fixed sample points. Under the nearest-point rule the colour assigned to each image element is that of the nearest sample point. A parallel procedure is also used in quantization which involves analog to digital conversion (Conway and Sloane, 1993, pp. 56–62) and has applications in digital measuring instruments or recording devices and in digital communications systems. Here the value at any location x is ‘rounded off’ to that of the closest data site.

Proximal polygon interpolation can also be used when z is not nominally scaled although it will not reproduce the underlying continuous surface. The application which gives rise to the term ‘Thiessen polygon’ is just such an example (Thiessen, 1911; Horton, 1917). Thiessen’s concern was to estimate the mean value \bar{z} of a surface (in his case, precipitation) over a bounded region for which data values z_i only existed for an irregularly spaced set of n data sites (precipitation gauges). Given the spatial distributions of gauges Thiessen felt it inappropriate to estimate \bar{z} simply as

$$\bar{z} = \sum_{i=1}^n z_i / n. \quad (6.1.3)$$

Instead he used

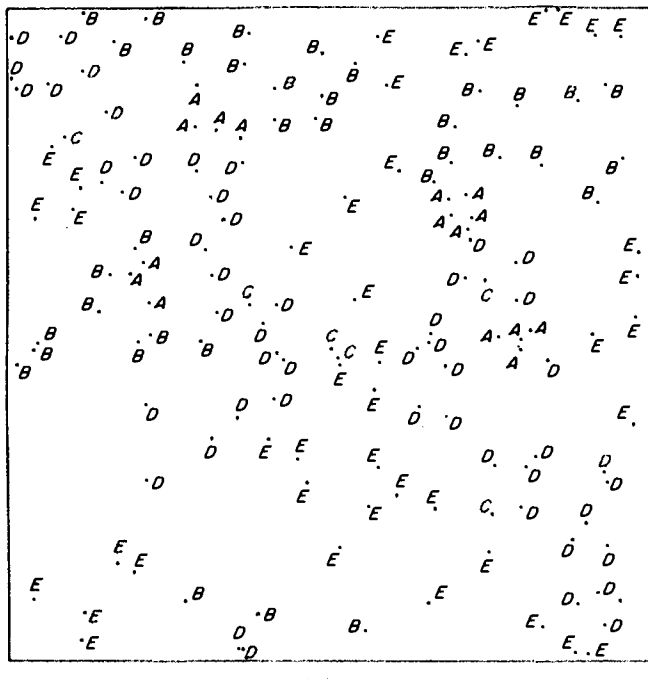
$$\bar{z} = \sum_{i=1}^n w_i z_i / \sum_{i=1}^n w_i, \quad (6.1.4)$$

where w_i is the area of the proximal polygon associated with p_i . This approach is very old, but it is still used in meteorology (Chakravarti and Archibald, 1993). This example is also discussed in Chapters 8 and 9.

The same approach is sometimes used in estimating the average grade of an ore deposit, although as befits a different application with different origins, the proximal polygons are usually termed *area of influence polygons* (Popoff, 1966; Reedman, 1979; Hayes and Koch, 1984). The approach involves representing the surface as a set of polygonal prisms whose heights reflect the thicknesses of the ore body (see Figure 6.1.2). The average grade \bar{z} is calculated using expression (6.1.4) with w_i equal to the volume of the prism associated with p_i and z_i equal to the ore grade (see Section 7.1 for more details and additional references).

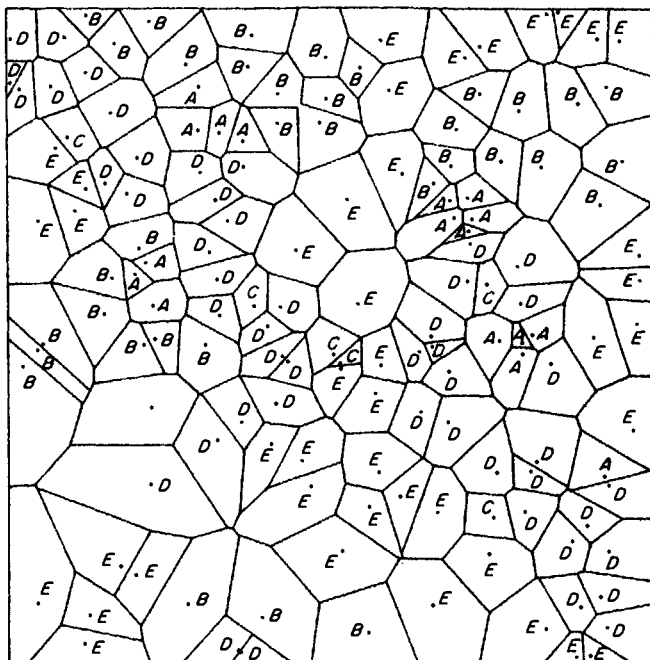
6.1.2 Natural neighbour interpolation

Another way of defining $D(p)$ for an arbitrary point p at location x in S is to identify those members of P which are Voronoi or, to use Sibson's term, 'natural' neighbours of p (Sibson, 1981; Watson and Philip, 1987). This involves generating the Voronoi diagram of $P \cup \{p\}$. Like all the members of P , p has its associated Voronoi region, $V(p)$ (the shaded polygon in Figure 6.1.3). Those points of P whose Voronoi regions are contiguous to $V(p)$ form

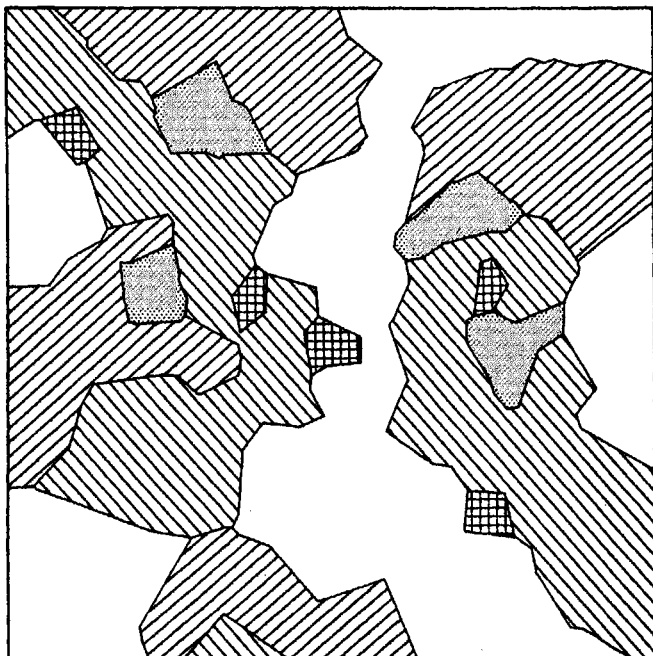


(a)

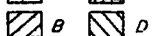
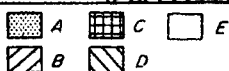
Figure 6.1.1 Creation of a discontinuous surface by nearest neighbour interpolation.
 (a) Data sites and data values. [See facing page] (b) Voronoi diagram (proximal polygons). (c) Final surface.



(b)



(c)



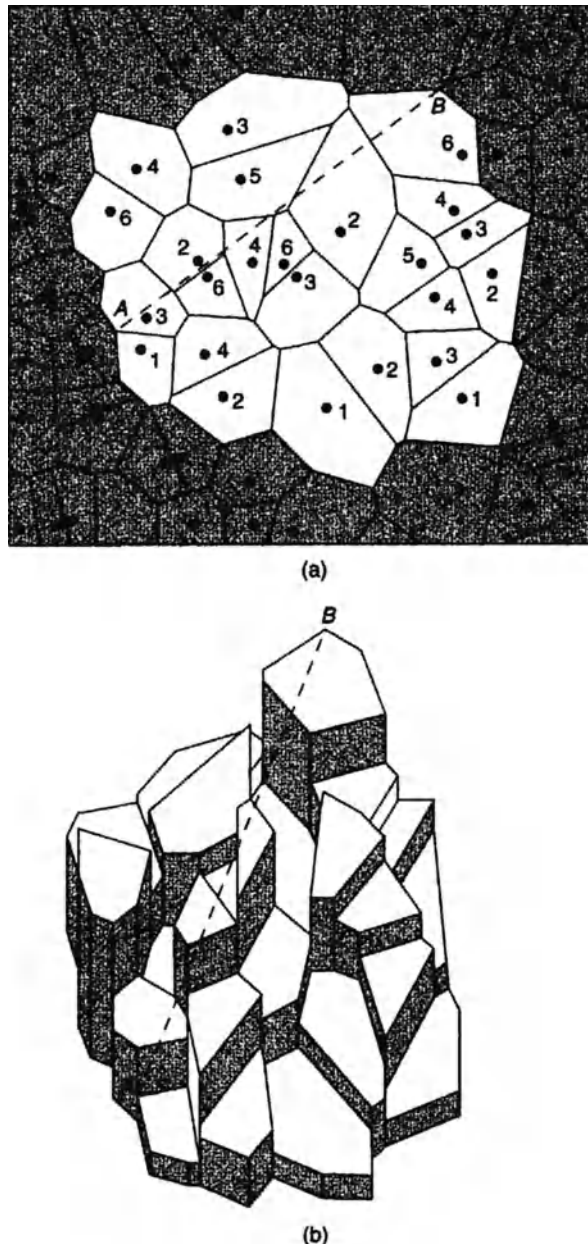


Figure 6.1.2 Representation of a surface as a set of polygonal prisms. (a) Voronoi diagram of data sites (value at data site represents thickness of ore body; shaded polygons are not represented in (b)). (b) Polygonal prisms. (Common dashed line AB is shown to facilitate comparison.)

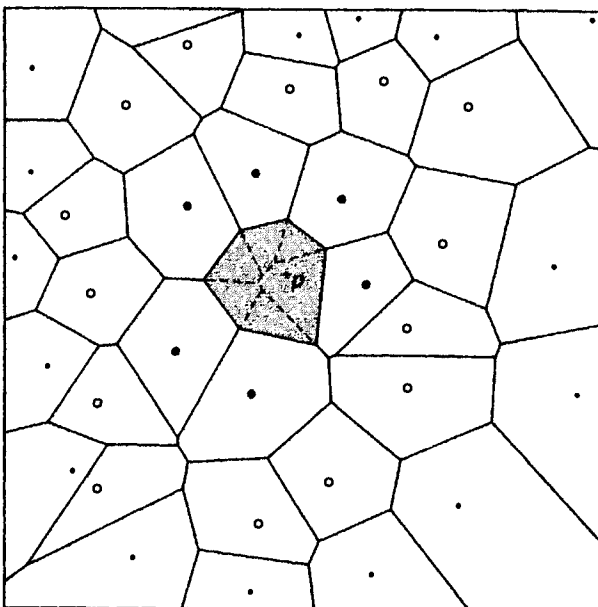


Figure 6.1.3 Voronoi diagram of $P \cup \{p\}$. Key: ●, natural neighbours of p ; points contributing to interpolated value at p using equation (6.1.9); ○, points contributing to interpolated values at p using equation (6.1.13); ·, other points of P .

the natural neighbours of p (the filled circles in Figure 6.1.3). The data values at the natural neighbours are then used in equation (6.1.1).

A special case of spatial interpolation is the missing value problem where the unknown value of a variable at a given location must be estimated from the known values of the variable at other locations. In their study of rainfall data for Kansas and Nebraska, U.S.A., Haining *et al.* (1984) used natural neighbours to identify which weather stations to use in estimating missing values at other stations.

There are also other situations besides interpolation where it may be necessary to identify nearby points and in which natural neighbours have been proposed as the solution (Besag, 1974, 1975; Ord, 1975). A particular instance is the study of spatial autocorrelation (Goodchild, 1986; Griffith, 1987; Odland, 1988). This involves measuring the extent of dependence in the values of a variable observed at nearby locations. Spatial autocorrelation measures ρ often have the general form

$$\rho = \sum_{i=1}^n \sum_{j=1}^n w_{ij} z_i z_j, \quad (6.1.5)$$

where z_i and z_j are the values of the variable at data sites p_i and p_j , respectively, and w_{ij} is a weight reflecting the spatial relationship between p_i and p_j . In a study of the grain handling system of the province of Manitoba in

Canada from 1943 to 1975, Griffith (1982) suggested setting $w_{ij} = 1$ in equation (6.1.5) if p_i and p_j are natural neighbours and $w_{ij} = 0$, otherwise. The same procedure was taken in a study of loblolly pine stands by Reed and Burkhardt (1985).

It is worth noting that the natural neighbour definition has also been frequently proposed as a way of identifying neighbours in a variety of other circumstances. In \mathbb{R}^3 these include identifying neighbouring atoms, molecules or particles in both crystalline and amorphous structures including monatomic liquids, solutions, metallic glasses, metals and alloys and for identifying neighbouring cracks in percolation structures. The definition of neighbouring capillaries in muscle tissue is an example involving two-dimensional sections of material in \mathbb{R}^3 , while the recognition of neighbours for plants and animals and for stores in competitive situations in ecology and retailing, respectively, are examples of the use for phenomena represented in \mathbb{R}^2 . Discussion of these uses together with the appropriate references is contained in Chapter 7.

If the members of P have associated weights (see Section 3.1) these may be combined with natural neighbour concepts to define other types of neighbour relationships. One example occurs in the field of spatial interaction modelling (Haynes and Fotheringham, 1984) which attempts to predict the movement of people, goods, information, etc. between places located in \mathbb{R}^2 . Typically, the amount of interaction I_{ij} between two places p_i and p_j with weights w_i and w_j , respectively (where the weights usually reflect some measure of the sizes of the places such as their populations), is considered to be directly proportional to the product of their weights and inversely proportional to the distance separating them so that

$$I_{ij} = k w_i w_j d(p_i, p_j)^{-\beta}, \quad (6.1.6)$$

where $d(p_i, p_j)$ is the distance between p_i and p_j , k is a constant, and β is the distance exponent ($\beta > 0$). A variant of this general interaction formulation, known as the intervening opportunity model, was proposed by Stouffer (1940). He replaced the direct measure of distance used in equation (6.1.6) by an indirect one and argued that

$$I_{ij} = k w_i w_j O_{ij}^{-1}, \quad (6.1.7)$$

where O_{ij} is the number of opportunities intervening in \mathbb{R}^2 between p_i and p_j which can be measured by

$$O_{ij} = \sum_{\substack{k=1 \\ k \neq i,j}}^l w_k \quad (6.1.8)$$

where l is the number of points in P which intervene between p_i and p_j . The problem with this modification is the definition of the intervening places. One way is to generate the Voronoi diagram $\mathcal{V}(P)$ of P and to consider the places intervening between p_i and p_j as those whose Voronoi polygons are intersected by the line segment, $\overline{p_i p_j}$. For example, in Figure 6.1.4(a) the

places intervening between p_{18} and p_{35} are p_6 , p_{13} and p_{30} . In those circumstances where w_i is recorded as on ordinal rank r_i (the larger the rank the more important the place), it is often suggested that interaction between p_i and p_j will only occur if no points with higher ranks intervene between the two. Thus, to determine which places interact, we can use the same procedure as above. In this case p_i and p_j will interact if the line segment $\overline{p_i p_j}$ does not intersect a Voronoi polygon of a point with a higher rank than either p_i or p_j . Thus, in Figure 6.1.4(a) if the numbers associated with the points represent their ranks, the points which interact with p_{18} are shown by the line segments linking them to p_{18} .

Elliott (1981, 1982, 1983, 1985) has proposed a further variant of this method. He labelled the set of places for which interaction occurs with p_i as the *surrounding larger neighbours* (SLNs) of p_i . The SLNs of p_i may be defined by generating $\mathcal{V}(P)$ (see Figure 6.1.4(a)) which in turn may be represented by the dual Delaunay triangulation, $\mathcal{D}(P)$ (see Figure 6.1.4(b)). If we consider $\mathcal{D}(P)$ as a graph (see Section 1.3.6) we can measure how far each point p_j is from p_i in terms of the number of edges e_j of $\mathcal{D}(P)$ (see Figure 6.1.4(b)). Point p_j is an SLN of p_i if it has a higher rank than p_i and a path of length e_j can be traced from p_j to p_i which does not pass through any other vertex of $\mathcal{D}(P)$ with a higher rank than p_j . Figure 6.1.4(c) shows the SLNs for p_{18} . These may be compared with the higher ranked places defined by the previous method (the solid lines in Figure 6.1.4(a)). Elliott (1983, 1985) made use of SLNs derived in this way in modelling inter-city airline passenger traffic in the United States.

Sibson (1981) has also proposed using the natural neighbour concept in deriving the appropriate weights used in equation (6.1.1). We know from our discussion of ordered order- k Voronoi diagrams in Section 3.2 (Property OOK2) that in the Voronoi diagram of $P \cup \{p\}$ the Voronoi region of p , $V(p)$, can be exhaustively subdivided into ordered order-2 regions $V((p, p_j))$, such that the first and second nearest points of $P \cup \{p\}$ from any location in $V((p, p_j))$ are p and p_j , respectively (see Figure 6.1.3). Let $\kappa(x, x_j)$ be the area of $V((p, p_j))$. In the special case $p = p_j$, we set $\kappa(x, x_j) > 0$ and $\kappa(x, x_i) = 0$ for $i \neq j$. Sibson used the normalized values $\lambda(x, x_j) = \kappa(x, x_j)/\sum_i \kappa(x, x_i)$ in deriving the weights for z_i in expression (6.1.1). These values have two fundamental properties

Property LCP1 $\lambda(x, x_j)$ is a continuous function of x which is continuously differentiable everywhere except for the data sites.

Property LCP2 Provided that $V(p)$ does not meet the boundary of S ,

$$\sum_j \lambda(x, x_j) x_j = x.$$

A proof of LCP2 is given by Sibson (1980a) (see Section 3.2.2, Property OOK7). In view of this representation of x , Sibson labelled the $\lambda(x, x_j)$'s the *local coordinates* of point p . If $V(p)$ meets the boundary of S , $\lambda(x, x_j)$ does not have any physically useful meaning because it is not independent of the

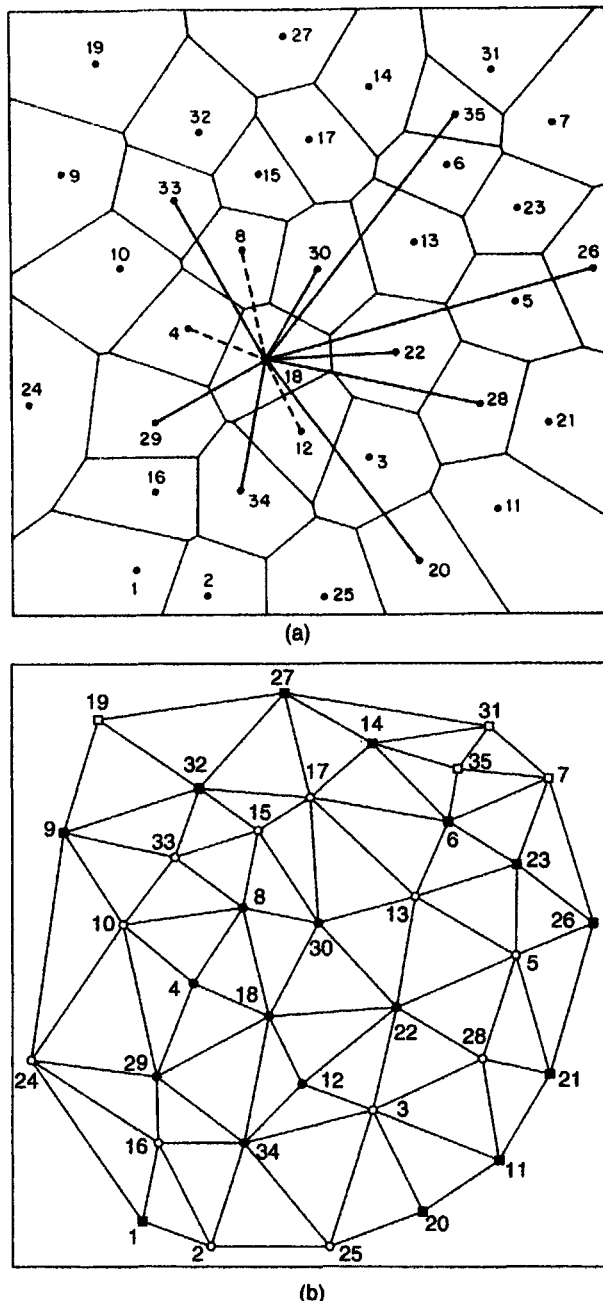


Figure 6.1.4 Definition of intervening opportunities. (a) Places interacting with p_{18} : —— higher ranked places; - - - lower ranked places. (b) Distance from p_{18} in terms of number of Delaunay edges; ●, 1; ○, 2; ■, 3; □, 4.

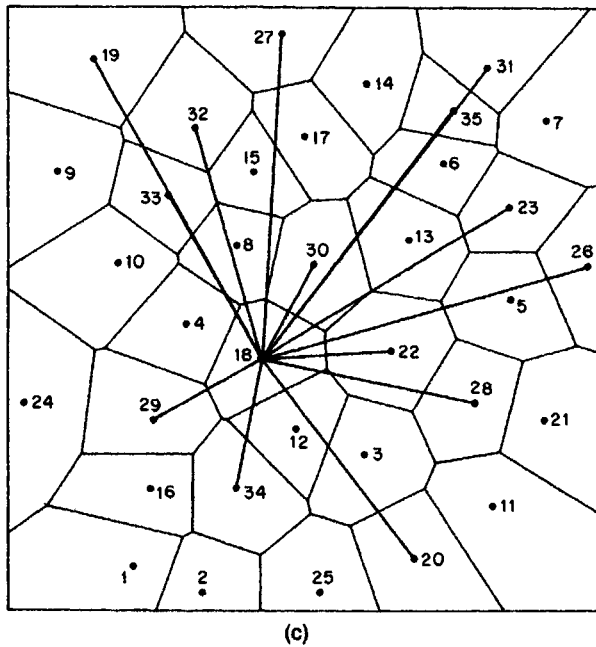


Figure 6.1.4 (c) Surrounding larger neighbours of p_{18} .

shape of region S . Indeed, in what follows we use the value of $\lambda(\mathbf{x}, \mathbf{x}_j)$ only for points p such that $V(p)$ does not meet the boundary of S .

A C^0 interpolant, $f_0(\mathbf{x})$, can be obtained by using the local coordinates directly so that

$$f_0(\mathbf{x}) = \sum_j \lambda(\mathbf{x}, \mathbf{x}_j) z_j. \quad (6.1.9)$$

Thus the data values that contribute to the interpolated values at p in Figure 6.1.3 are those for the points shown by filled circles. If the data values come from a linear function of the form

$$\mathbf{z} = \boldsymbol{\alpha} + \boldsymbol{\beta}^T \mathbf{x},$$

$f_0(\mathbf{x})$ correctly reproduces it, which can be shown as follows. Substituting

$$z_j = \boldsymbol{\alpha} + \boldsymbol{\beta}^T \mathbf{x}_j$$

in equation (6.1.9) gives

$$\begin{aligned} f_0(\mathbf{x}) &= \sum_j \lambda(\mathbf{x}, \mathbf{x}_j) (\boldsymbol{\alpha} + \boldsymbol{\beta}^T \mathbf{x}_j) \\ &= \boldsymbol{\alpha} + \boldsymbol{\beta}^T \sum_j \lambda(\mathbf{x}, \mathbf{x}_j) \mathbf{x}_j. \end{aligned}$$

Using Property LCP2,

$$z = \alpha + \beta^T \sum_i \lambda(\mathbf{x}, \mathbf{x}_i) \mathbf{x}_i.$$

Thus, $f_0(\mathbf{x}) = z$.

Sibson also used the local coordinates in deriving a C^1 interpolant. He fitted planes $\zeta(\mathbf{x}_i)$ for the value at \mathbf{x}_i , using a weighted least squares fit with weights

$$w(\mathbf{x}_i, \mathbf{x}_j) = \lambda(\mathbf{x}_i, \mathbf{x}_j) / d(\mathbf{x}_i, \mathbf{x}_j)^2, \quad (6.1.10)$$

where

$$d(\mathbf{x}_i, \mathbf{x}_j)^2 = (\mathbf{x}_j - \mathbf{x}_i)^T (\mathbf{x}_j - \mathbf{x}_i).$$

Explicitly, \mathbf{b}_i , the gradient at \mathbf{x}_i , is given by

$$\mathbf{b}_i = H_i^{-1} \mathbf{q}_i, \quad (6.1.11)$$

where

$$H_i = \sum_j w(\mathbf{x}_i, \mathbf{x}_j) (\mathbf{x}_j - \mathbf{x}_i)^T (\mathbf{x}_j - \mathbf{x}_i),$$

$$\mathbf{q}_i = \sum_j w(\mathbf{x}_i, \mathbf{x}_j) (\mathbf{x}_j - \mathbf{x}_i) (z_j - z_i).$$

Thus,

$$\zeta_i(\mathbf{x}) = z_i + \mathbf{b}_i^T (\mathbf{x} - \mathbf{x}_i)$$

is the linear function through (\mathbf{x}_i, z_i) with slope \mathbf{b}_i . Combining these functions with weights $W(\mathbf{x}, \mathbf{x}_i) = \lambda(\mathbf{x}, \mathbf{x}_i) / d(\mathbf{x}, \mathbf{x}_i)$, gives the interpolant

$$f^*(\mathbf{x}) = z_i = \mathbf{x}_i, \quad \text{if } \mathbf{x} = \mathbf{x}_i$$

$$f^*(\mathbf{x}) = \sum_j \left[W(\mathbf{x}, \mathbf{x}_j) \zeta_j(\mathbf{x}) \right] / \sum_j W(\mathbf{x}, \mathbf{x}_j) \quad \text{if } \mathbf{x} \neq \mathbf{x}_i. \quad (6.1.12)$$

The final C^1 interpolant, $f_1(\mathbf{x})$, is a linear combination of $f_0(\mathbf{x})$ and $f^*(\mathbf{x})$ chosen to ensure that it fits exactly restricted quadratic surfaces of the form

$$z = \alpha + \beta^T \mathbf{x} + \gamma \mathbf{x}^T \mathbf{x}.$$

Specifically,

$$f_1(\mathbf{x}) = \frac{\left\{ \left[\sum_i \lambda(\mathbf{x}, \mathbf{x}_i) d(\mathbf{x}, \mathbf{x}_i) \right] / \sum_i W(\mathbf{x}, \mathbf{x}_i) \right\} f_0(\mathbf{x}) + \sum_i [\lambda(\mathbf{x}, \mathbf{x}_i) d(\mathbf{x}, \mathbf{x}_i)^2] f^*(\mathbf{x})}{\left[\sum_i \lambda(\mathbf{x}, \mathbf{x}_i) d(\mathbf{x}, \mathbf{x}_i) \right] / \sum_i W(\mathbf{x}, \mathbf{x}_i) + \sum_i \lambda(\mathbf{x}, \mathbf{x}_i) d(\mathbf{x}, \mathbf{x}_i)^2}. \quad (6.1.13)$$

Note that while equation (6.1.9) is valid for all locations which satisfy the condition imposed in Property LCP2 above, equation (6.1.13) holds only for a more limited set of locations. This set consists of those locations p for which neither $V(p)$ nor any Voronoi polygon adjacent to $V(p)$ in the Voronoi

diagram $\mathcal{V}(P \cup \{p\})$ meets the boundary of S . The set of data values which contribute to the value of $f^*(x)$ at p in Figure 6.1.3 are those for the points shown by both filled and unfilled circles.

Sibson's basic interpolant, equation (6.1.9), has been studied further from several points of view. Farin (1990) considered its role in surface modelling. He notes that, if the number of the natural neighbours is four, Sibson's interpolant agrees with the classical bilinear interpolant. He also points out that Sibson's interpolant is not 'idempotent' in the following sense. Suppose that we generate Sibson's interpolant $f_0(x)$ using the height data z_i at n sites x_i , $i = 1, 2, \dots, n$, and next we add a new site x_{n+1} and the height $z_{n+1} = f_0(x_{n+1})$. If we generate Sibson's interpolant $f_0(x)'$ using the $n+1$ height data, we have $f_0(x) \neq f_0(x)'$ in general. This is a somewhat strange property for the interpolation system. Hence, we have to be careful in applications.

Piper (1993) gave an explicit expression of the gradient of Sibson's local coordinate together with its geometrical interpretation, while Sambridge *et al.* (1995) produce expressions for the derivatives of the interpolated function. Gross (1995) generalized Sibson's interpolant so that it can be used for the interpolation of continuously distributed height data along closed curves, where the Voronoi diagram for polygons plays an important role.

Finally, we note that Lowell (1994) uses order-2 Voronoi diagrams to interpolate nominal scale data, while Edwards (1993) and Edwards and Moulin (1995) use them to operationalize a wide range of linguistic spatial concepts such as 'between', 'behind' and 'close'. Watson (1985, 1988) extends the concept of natural neighbour order to n -component directional data, as normalized onto an n -dimensional sphere.

6.2 TRIANGULAR METHODS

In this approach interpolation of z at an arbitrary location p in S involves three steps. First, we construct a triangulation $\mathcal{T}(P)$ of the data sites in P using the data sites as vertices of the triangles. Next we identify the triangle $T(p)$ of $\mathcal{T}(P)$ which contains p and define the set of nearby points $D(p)$ as the vertices of $T(p)$. Finally, we compute z using the values of z_i ($i = 1, 2, 3$) for the members of $D(p)$.

The same procedure is also used in two other applications. One is in finite element methods, which will be discussed in Section 6.5. The other is the estimation of ore reserves where triangular prisms may be used in place of polygonal ones (see Section 6.1.1) (Harding, 1920–21, 1923; Popoff, 1966, pp. 78–84; Reedman, 1979, pp. 438–439).

In all of these application areas the methods used in the last two steps are independent of the nature of $\mathcal{T}(P)$ and since they do not involve Voronoi or Delaunay concepts, we confine our attention in this chapter to the construction of $\mathcal{T}(P)$. Reviews of different triangle based interpolants can be found in Barnhill (1977), Gold (1980), McCullagh (1981), Watson and Philip (1984a) and Watson (1992).

When the main purpose of interpolation is to create contours from data values at a set of data sites irregularly spaced over S , the triangulation approach possesses several advantages over the other most frequently used approach, the regular grid approach. An instance of this is a *digital terrain model* (DTM) where the data values are elevations of some region of a planetary surface. In this context $\mathcal{T}(P)$ is referred to as a *triangulated irregular network* (TIN). In the regular grid approach a regular, usually square grid is superimposed on S and values of z are estimated at the grid intersections on the basis of their spatial relationships to the data values for the members of P . There are a variety of ways that such an estimation can be performed (see Monmonier, 1982, pp. 58–65; Watson and Philip, 1985; Jones *et al.*, 1986, pp. 44–57 for reviews). The main advantage of the regular grid approach is that the set of grid intersections may be stored as a matrix in which both their locations and topological relationships are defined implicitly so that it is necessary only to store the z values assigned to them. In contrast, the topological relationships of the facets of a TIN must be stored explicitly, although this is not necessary if they are to be used only for hill shading. If the facets of the TIN are used as the units of storage, each facet requires six pointers, three for the vertices and three to identify the neighbouring triangles. Since the total number of triangles in a TIN is $2n - n_c - 2$, where n_c is the number of data sites on the boundary of the convex hull of P (see Property D11, Section 2.4), this scheme requires a total of $12n - 6n_c - 12$ pointers. Alternatively, we can list in a consistent order (e.g. clockwise from the north), the neighbouring data sites of each data site. This requires a total of $6n - 2n_c - 6$ pointers, equal to twice the number of edges in the TIN (see Property D11, Section 2.4) for about a 50% savings in storage.

Topographical surfaces are not stationary (see Section 1.3.3) since the variation in terrain height changes from one landform to another (compare a jagged mountain range with a coastal plain). Thus, the spacing of points of any regular grid superimposed on S must be adjusted to capture height changes in areas of greatest variability. This means that many of the grid points will be redundant in areas of constant relief. TINs with their natural variable resolution can easily adapt to such variations. Mark (1975) suggests that in a typical DTM 14 regular data points are required for each irregular data point to produce the same level of representation. Also it is much easier to incorporate linear and other required features (such as ridge and valley lines) in a TIN structure (see Section 6.3). In such circumstances Peucker *et al.* (1976) suggest that the ratio of regular to irregular data points rises to about 287:1. Furthermore, since the data sites are the vertices of the TIN, the data values will be interpolated exactly. It is unlikely that this will happen in the regular grid approach which, as a result, should more properly be considered a smoothing procedure rather than an interpolation one.

The facets of a TIN also avoid the ‘saddle point’ problem which can arise with the regular grid. If the data values associated with four neighbouring grid intersections take any of the forms in Figure 6.2.1(a), then the path of the contour through the grid square defined by the intersections is

unambiguous. However, if the data values are configured as in Figure 6.2.1(b), then several different paths for the contour are possible. Finally, TINs also appear to have advantages in terms of the computational effort and speed involved in calculating the final contours. Although there is little systematic information on this, at least one study (McCullagh and Ross, 1980) suggests that the identification of the TIN structure takes on average only one-tenth of the time required to compute the values of z at the grid intersections. The computing time for C^0 contours is approximately equal for the regular grid and the TIN while a C^1 interpolation on the former takes about two-thirds of the time taken on the latter. Nevertheless, this suggests that overall the TIN method is at least five times faster than the regular grid in this context. Computational speed for an actual contouring situation reported by Philip and Watson (1982) supports this suggestion. On the other hand, Kumler (1994) reaches an opposite conclusion when analysing twenty-five different physiographic maps of areas in the United States. He examines different ways of selecting points to construct TINs from regular grid map data, compares TINs and regular grids, and concludes that for the data he examined, TINs are never more efficient.

For n data sites in P , let E be the set of $n(n - 1)/2$ line segments (edges) joining all pairs of data sites. Then $\mathcal{T}(P)$ is a maximal subset of E in which no two edges intersect except at their end points. $\mathcal{T}(P)$ is not unique. The number of possible triangulations, $N[\mathcal{T}(P)]$, of P depends in part on the location of the members of P in S and no general expression exists for evaluating $N[\mathcal{T}(P)]$, although enumeration methods (Masada *et al.*, 1996b) and the upper bounds (Dey, 1993; Dey and Shah, 1995) are studied. However, each triangulation has $3(n - 1) - n_c$ edges and $2(n - 1) - n_c$ triangles (see Section 2.4).

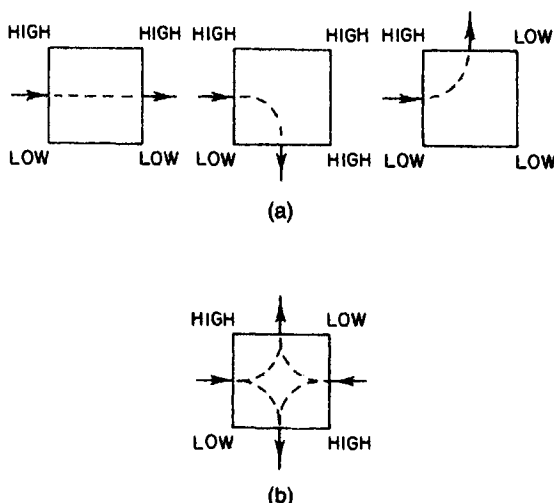


Figure 6.2.1 The saddle-point problem. (a) Unambiguous paths for the contour. (b) Ambiguous paths for the contour.

In the three areas of application mentioned above it is desirable that the triangulation selected avoids the occurrence of triangles with two highly acute interior vertex angles and that the triangles be as equiangular as possible. This is because elongated triangles involve greater separation of data sites and reduce the ability of the triangulation to reflect local variation in Z . Whitney (1929) appears to be the first to have recognized the importance of this consideration to spatial interpolation. In Section 2.4 (Property D15) we saw that the Delaunay triangulation, $\mathcal{D}(P)$, of P satisfies a local max-min angle criterion (also referred to as an equiangular criterion) in that the diagonal of every strictly convex quadrilateral, Q , in $\mathcal{D}(P)$ is chosen so that it maximizes the minimum interior angle of the two resulting triangles (see Figure 2.4.13 in Section 2.4). Sibson (1978) demonstrated that $\mathcal{D}(P)$ is the only triangulation with this property. Furthermore, as reported in Property D16 in Section 2.4.2, $\mathcal{D}(P)$ is also globally equiangular in that it maximizes the minimum angle occurring in $\mathcal{T}(P)$.

Lawson (1977, pp. 178–181) demonstrated that the equiangular criterion is equivalent to another, namely the circle criterion. If k is a circle passing through any three vertices of Q , and the fourth vertex is interior to k , we select the diagonal linking this vertex to the opposite vertex (see Figure 6.2.2(a)). If the fourth vertex is exterior to k we select the other diagonal (Figure 6.2.2(b)). If the fourth vertex is on k we select either diagonal (Figure 6.2.2(c)). This criterion avoids the selection of triangles with relatively large circumcircles and Watson and Philip (1984b) conjecture that $\mathcal{D}(P)$ is the $\mathcal{T}(P)$ which minimizes the mean circumcircle diameter. It is also known that from any triangulation $\mathcal{T}(P)$ we can reach $\mathcal{D}(P)$ by repeated application of local reconnections of diagonals (Cherfils and Hermeline, 1990; see also Property D16 in Section 2.4).

It has also been suggested (Lawson, 1977; De Floriani *et al.*, 1982, 1983, 1985) that the equiangular criterion of $\mathcal{D}(P)$ is equivalent to the ‘Pitteway’ criterion proposed by McLain (1976), which requires that any location within any triangle of $\mathcal{D}(P)$ should have one of the vertices of that triangle as its closest data point. However, Sabin (1976) and Ripley (1981, p. 40) show that there are some patterns of data sites for which no $\mathcal{T}(P)$ satisfies the Pitteway criterion. In Section 2.4 (Property D3) we give a necessary and sufficient condition for $\mathcal{D}(P)$ to satisfy the Pitteway criterion.

Additional speculation concerns the relationship of $\mathcal{D}(P)$ to other triangulations, in particular the *minimum length triangulation* (also known as the *minimum weight triangulation* and the *optimal triangulation*), $\text{MLT}(P)$, and the ‘greedy’ triangulation, $\text{GT}(P)$. Let $|\mathcal{T}(P)|$ denote the sum of the lengths of the edges in $\mathcal{T}(P)$. Then $\text{MLT}(P)$ is the $\mathcal{T}(P)$ which minimizes $|\mathcal{T}(P)|$. $\text{MLT}(P)$ is unique for general sites. This triangulation was originally proposed by Bengtsson and Nordbeck (1964) and Düppé and Gottschalk (1970). Steele (1982) showed that for n points ($1 \leq n \leq \infty$) located in a unit square according to a homogeneous planar Poisson point process (see Section 1.3.3), $|\text{MLT}(P)|/n^{1/2}$ tends to a constant as n tends to infinity.

The greedy triangulation $\text{GT}(P)$ is the triangulation obtained by consid-

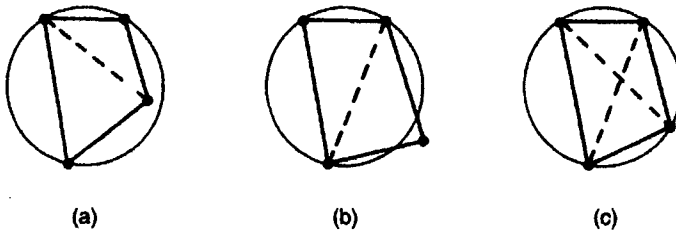


Figure 6.2.2 The circle criterion.

ering all possible edges in order of increasing length and inserting an edge provided that no edge already exists which properly intersects it. If no pair of edges has the same length $\text{GT}(P)$ is unique.

Often $\mathcal{D}(P)$, $\text{MLT}(P)$ and $\text{GT}(P)$ are identical (see Figure 6.2.3(a)). However they need not be (see Figure 6.2.3(b)) as was first noted by Lawson (1977) and Lloyd (1977). In most situations where $\mathcal{D}(P)$, $\text{MLT}(P)$ and $\text{GT}(P)$ are not identical, $\text{GT}(P)$ is a better approximator of $\text{MLT}(P)$ than $\mathcal{D}(P)$. For arbitrarily large n , Manacher and Zobrist (1979) constructed sets of n data sites P_1 and P_2 for which

$$|\mathcal{D}(P_1)|/|\text{MLT}(P_1)| \geq O(n/\log n) \quad (6.2.1)$$

and

$$|\text{GT}(P_2)|/|\text{MLT}(P_2)| > O(n^{1/3}) \quad (6.2.2)$$

where $|\cdot|$ is the length of the triangulation as defined above and $O(k)$ is the order of k (see Section 1.3.4). P_2 involves non-convex polygons. However, Lingas (1986a) constructed a positive real $\varepsilon < 1$ for which

$$|\text{GT}(P)|/|\text{MLT}(P)| < O(n^\varepsilon) \quad (6.2.3)$$

holds for any convex, planar point set P with n data sites.

Kirkpatrick (1980) identified arbitrarily large convex sets of n data sites P_3 for which

$$|\mathcal{D}(P_3)|/|\text{MLT}(P_3)| > O(n), \quad (6.2.4)$$

and so $\mathcal{D}(P_3)$ is asymptotically no better than an arbitrary triangulation in approximating $\text{MLT}(P_3)$. However, Lingas (1986b) proved that when P consists of data sites located in a unit square according to a homogeneous planar Poisson point process (see Section 1.3.3),

$$|\mathcal{D}(P)|/|\text{MLT}(P)| < O(\log n) \quad (6.2.5)$$

with probability of at least $1 - cn^\alpha$, where c and α are constants satisfying $c > 0$ and $\alpha > 1$. Furthermore, Chang and Lee (1984) showed that when the data points are located in this way the average length of $\mathcal{D}(P)$, $E(|\mathcal{D}(P)|)$, is of the same order as that of $\text{MLT}(P)$, $E(|\text{MLT}(P)|)$; more precisely they proved that

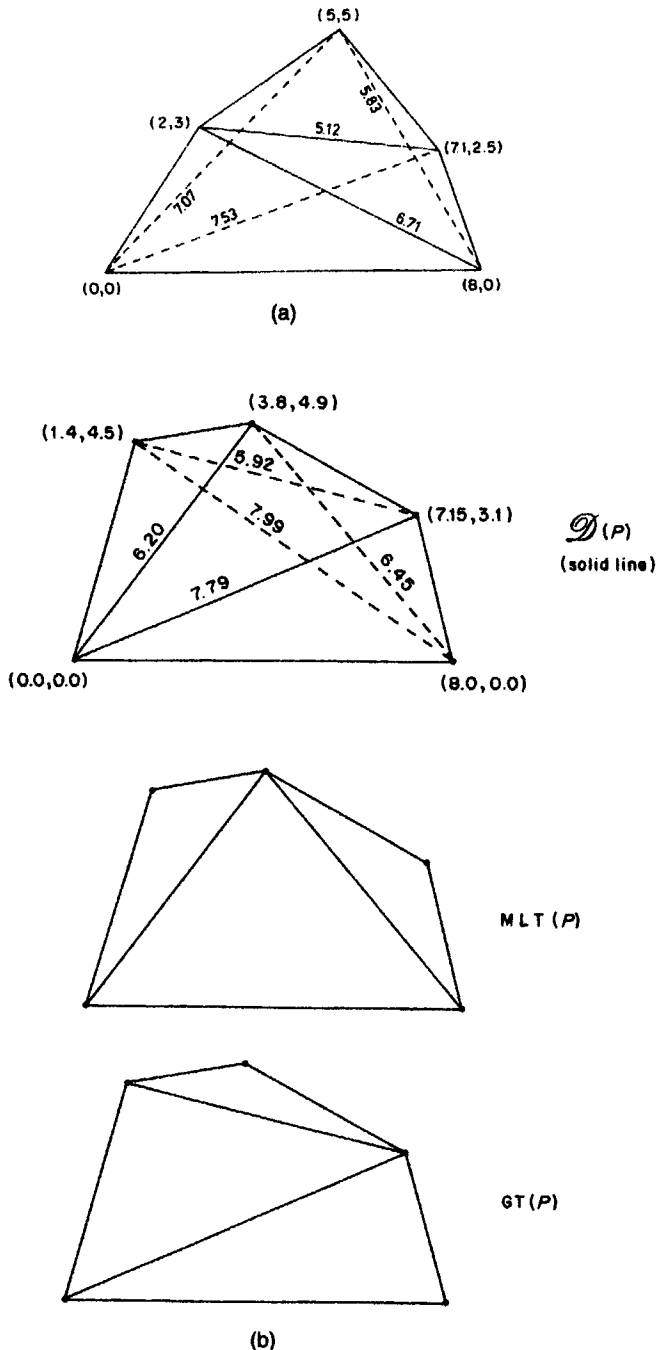


Figure 6.2.3 (a) A set of data sites in \mathbb{R}^2 for which $\mathcal{D}(P) = \text{MLT}(P) = \text{GT}(P)$ (solid line). (b) A set of data sites in \mathbb{R}^2 for which $\mathcal{D}(P) \neq \text{MLT}(P) \neq \text{GT}(P)$ (redrawn from material in Watson and Philip, 1984b).

$$E(|\mathcal{D}(P)|)/E(|MLT(P)|) < 64/9\pi. \quad (6.2.6)$$

$\mathcal{D}(P)$, $MLT(P)$ and $GT(P)$ are also proved to be good approximations of the complete graph spanning P in the sense that the length of the shortest path between any two vertices approximates the distance between the two points (Das and Joseph, 1989; Levcopoulos and Lingas, 1989; Keil and Gutwin, 1989; Dobkin *et al.*, 1990; see also Property D18 in Section 2.4).

Other triangulations have been suggested, but unlike $\mathcal{D}(P)$, $MLT(P)$ and $GT(P)$ these may be prone to problems such as lack of uniqueness and the creation of unnecessarily elongated triangles. Typically, these triangulations involve an iterative procedure in which first an initial triangulation is constructed and then this is 'optimized' according to specific criteria. Examples of such optimization criteria include (a) requiring that any location in a triangle must be closer to one of the vertices of that triangle than to any other vertex of the triangulation (i.e. the 'Pitteway' criterion discussed above) (McLain, 1976; Kleinstreuer and Holderman, 1980); (b) minimizing the length of the diagonal of the convex quadrilateral Q (Zienkiewicz and Phillips, 1971; Fraser and Van den Driessche, 1972; Fraser, 1977; Mirante and Weingarten, 1982); and (c) maximizing the minimum triangle height perpendicular to the proposed diagonal of Q (Gold *et al.*, 1977; Gold, 1980).

Another criterion for a good triangulation is related to the gradient of the interpolated surface. Let \mathcal{T} be a triangulation for a given set P of sites, and for $p \in CH(P)$ let $f(p)$ be the piecewise linear interpolant based on the triangulation \mathcal{T} , i.e. $f(p)$ be the height at p of the triangle determined by the given heights at the sites. The integration over $CH(P)$ of the square of the gradient of the interpolant is called the *roughness* of the interpolant. Rippa (1990) showed that the Delaunay triangulation attains the minimum roughness for any set of height data. In this sense, the Delaunay triangulation gives the best interpolant. Wilson *et al.* (1990) observed a similar property.

However, from a perceptual point of view, the interpolant based on the Delaunay triangulation is not always the best one. Sometimes we get a better interpolation by swapping some of the edges of the Delaunay triangulation. Suppose that we are given a continuous surface over $CH(P)$ and want to find the triangulation \mathcal{T} for P such that the piecewise linear interpolating surface based on \mathcal{T} is the closest to the given surface. One strategy to get this triangulation is to start with the Delaunay triangulation and to swap the edges in such a way that the resulting interpolating surface is closer to the given surface. Dyn *et al.* (1990), Brown (1991) and Schumaker (1993) showed that this strategy sometimes gives a better triangulation than the Delaunay triangulation.

Uniqueness and direct construction are particularly important to automated triangulation procedures. These characteristics of $\mathcal{D}(P)$ together with its equiangular property has led to it being proposed most frequently as a good triangulation for both spatial interpolation (Lewis and Robinson, 1977; Peucker *et al.*, 1978; Fowler and Little, 1979; McCullagh and Ross, 1980; De Floriani *et al.*, 1982, 1983, 1985; Philip and Watson, 1982; Watson and Philip,

1984b; Parker *et al.*, 1987; Jones 1989) and finite element methods (Bramble and Zlamal, 1970; Cavendish, 1974; Lawson, 1977; Akima, 1978; Joe, 1986), although in the latter area of application Babuska and Aziz (1976) argued that what is essential is not a minimum angle condition but a maximum angle (min-max) condition in which no angle is too close to 180°. Nielson and Franke (1983) showed that the min-max triangulation differs only slightly from the Delaunay triangulation, and Edelsbrunner *et al.* (1990b) have proposed an algorithm for generating the min-max triangulation.

6.3 MODIFYING DELAUNAY TRIANGULATIONS

One problem in using $\mathcal{T}(P)$ as the basis for interpolation over S is that $\mathcal{T}(P)$ is only defined in the interior of the convex hull $\text{CH}(P)$ of P and therefore $\mathcal{T}(P)$ does not usually cover S . Furthermore, particularly for irregularly spaced data sites, $\mathcal{T}(P)$ invariably contains some undesirable long, thin triangles associated with points on the boundary of $\text{CH}(P)$ regardless of the criterion used to define $\mathcal{T}(P)$. One way to extend a function defined over $\mathcal{T}(P)$ is to divide the area of S outside $\text{CH}(P)$, $S \setminus \text{CH}(P)$, into trapezoids and triangles by inserting perpendiculars to the exterior edges of $\text{CH}(P)$ at each of the vertices, as shown in Figure 6.3.1 (Akima, 1978; Ripley, 1981, pp. 42–43; Franke, 1982, p. 788). The value of the interpolant for any location in $S \setminus \text{CH}(P)$ is then obtained from the data values at one (triangular area) or two (trapezoidal area) nearest data sites. Strictly speaking such values should be considered extrapolations rather than interpolations.

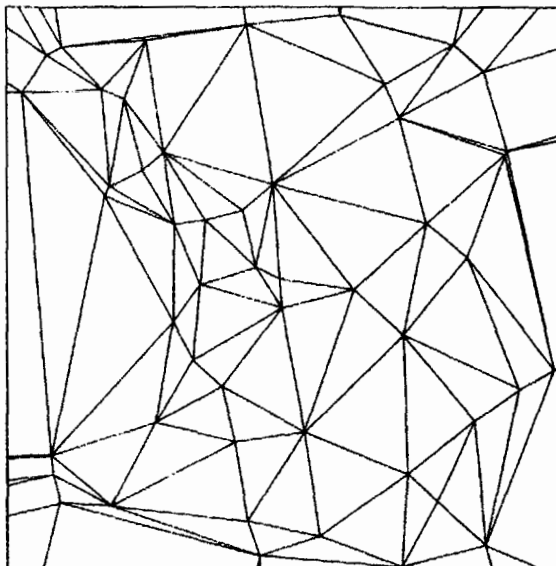


Figure 6.3.1 Extension of $\mathcal{D}(P)$ to cover S by constructing perpendiculars.

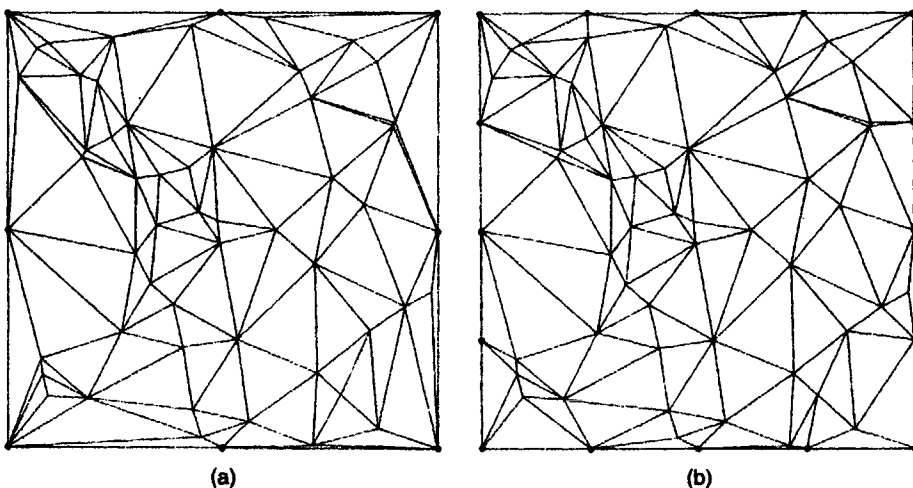


Figure 6.3.2 Extension of $\mathfrak{D}(P)$ to cover S by introducing imaginary points (filled circles): (a) 8 imaginary points; (b) 16 imaginary points.

Another procedure which completes coverage of S and reduces the incidence of elongated triangles is to introduce imaginary data sites on the boundary of S (McCullagh and Ross, 1980; Franke, 1982; Lasser and Stuttgen, 1996) as indicated by the filled circles in Figure 6.3.2. The impact of this procedure on $\mathcal{T}(P)$ depends on the number and spacing of such imaginary data sites (compare Figures 6.3.2(a) and 6.3.2(b)).

So far in this chapter we have assumed that S is a simply connected, convex region. We now consider the construction of $\mathfrak{D}(P)$ when S does not possess these properties as may be the case in some applications in digital terrain modelling (Yoeli, 1977; De Floriani *et al.*, 1982; Mirante and Weingarten, 1982) and finite element methods (Lewis and Robinson, 1977; Kleinstreuer and Holderman, 1980; Sadek, 1980) where non-convex and multiply connected regions may be encountered (for finite element methods, see Section 6.5). In such cases it is necessary to include edges of S as part of $\mathcal{T}(P)$. Another instance where specific edges must be incorporated into $\mathcal{T}(P)$ arises in digital terrain modelling when the data values refer to elevations. Although the data sites are usually irregular in terms of their location in the $x-y$ plane, often they are chosen to preserve both point features, such as pits and peaks, and linear features, such as ridges, valleys and fault lines, of special topographical significance (Peucker and Douglas, 1975; Yoeli, 1977; Fowler and Little, 1979; McCullagh, 1981; De Floriani *et al.*, 1985; Christensen, 1987; Buys *et al.*, 1991).

In all of the above instances we can consider the linear features as a set of non-intersecting edges L with end points in P , which together with P can be considered as a planar, straight line graph $G(P, L)$. Thus, the problem

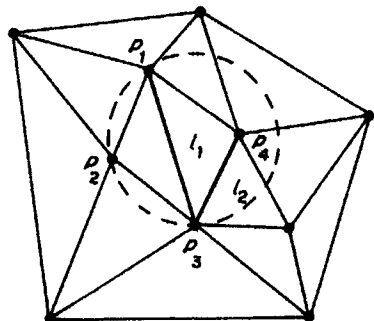


Figure 6.3.3 Illustration of criterion for defining edges in a constrained Delaunay triangulation.

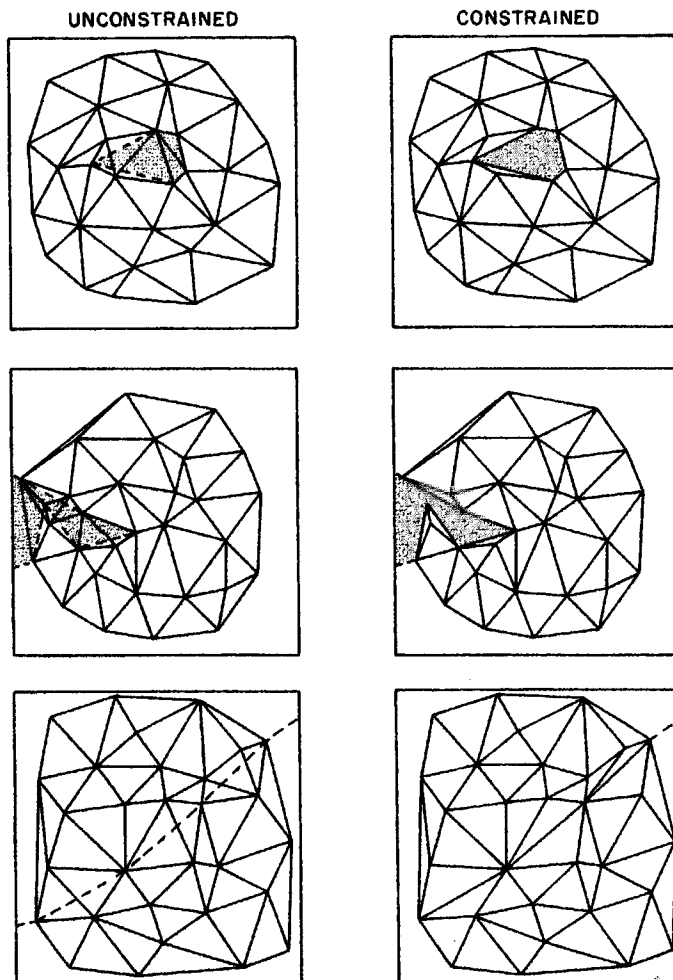


Figure 6.3.4 Examples of unconstrained and constrained triangulations for given sets of data sites. Bottom: - - -, ridge line.

becomes one of constructing a triangulation $\mathcal{T}(G)$ for $G(P, L)$. Our concern is extending the Delaunay criteria (see Section 6.2) to $\mathcal{T}(G)$ and we refer to the resulting triangulation as the *constrained Delaunay triangulation*, $\text{CDT}(G)$, of $G(P, L)$ (recall Section 3.4.3; see also Section 6.5).

The modifications of $\mathfrak{D}(P)$ which must be undertaken to create $\text{CDT}(G)$ arise because the presence of L in S affects the mutual visibility of members of P . Two sites in P , p_i and p_j , are said to be mutually visible if the line segment $\overline{p_i p_j}$ does not properly intersect any member of L . For example, in Figure 6.3.3 points p_1 and p_2 are mutually visible while points p_2 and p_4 are not. Let V be the set of edges joining those data sites which are mutually visible. Then $\text{CDT}(G)$ consists of L together with a subset of V in which the circumcentre of each triangle with vertices p_i, p_j and p_k does not contain in its interior any other data site which is visible from p_i, p_j and p_k . Thus, points p_1, p_2 and p_3 in Figure 6.3.3 form a triangle of $\text{CDT}(G)$ even though the circle passing through them contains p_4 because p_2 and p_4 are not mutually visible. If no four points of P are cocircular, $\text{CDT}(G)$ is unique. $\text{CDT}(G)$ is a subgraph of the visibility graph of $G(P, L)$ (see Section 3.4.1). For graphs $G(P, \emptyset)$, $\text{CDT}(G)$ is equal to $\mathfrak{D}(P)$. Figure 6.3.4 shows examples of $\text{CDT}(G)$ together with their unconstrained counterparts $\mathfrak{D}(P)$.

Like $\mathfrak{D}(P)$, $\text{CDT}(G)$ satisfies the local equiangular criterion since it applies to any strictly convex quadrilateral of $\mathcal{T}(G)$ and only one diagonal can be selected if a quadrilateral of $\mathcal{T}(G)$ is not convex or if one of the diagonals is a member of L . $\text{CDT}(G)$ also satisfies global equiangularity (see Lee and Lin, 1986, for a proof). Lee and Lin (1986) provide an $O(n^2)$ algorithm for computing $\text{CDT}(G)$ which reduces to $O(n \log n)$ when $G(P, L)$ is a simple polygon.

6.4 APPROXIMATING SURFACES

There are some applications where the number of data sites P may be extremely large. One instance is digital terrain modelling where the data sites may be in the form of a dense raster (grid) structure, particularly if they have been obtained by remote sensing (Fowler and Little, 1979; De Floriani *et al.*, 1983, 1985; Chen and Guevara, 1987). To capture the fundamental features of the surface being modelled while avoiding subsequent unnecessary time-consuming search and retrieval operations during its analysis and inefficiencies in its storage, it may be undesirable to use $\mathcal{T}(P)$ in deriving the function to represent the surface. Instead, we can select a representative subset P' of data sites in P which enables the surface to be represented with less than some predetermined level of error. P' should be generated so that only those members of P necessary to reduce the error level below the specified level are selected. Typically, this is achieved by an incremental procedure in which an initial set P' is defined and $\mathcal{T}(P')$ is generated. Further data sites are added to P' until the surface generated using $\mathcal{T}(P')$ no longer exceeds the specified error level. Such an incremental procedure is facilitated

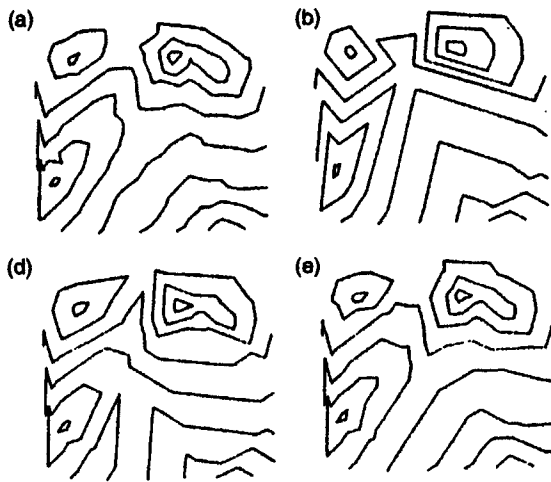


Figure 6.4.1 Estimating surfaces: (a) original surface; (b) 50% of error, obtained by selecting 20% of data sites; (c) 30% of error, obtained by selecting 30% of data sites; (d) 20% of error, obtained by selecting 50% of data sites. (Source: De Floriani *et al.*, 1985.)

by using the Delaunay triangulation $\mathcal{D}(P')$ to define $\mathcal{T}(P')$ since the local optimization character of $\mathcal{D}(P')$ ensures that an existing triangle is only affected if the new data site is added within the circumcircle defined by the vertices of the existing triangle.

A typical procedure is that used by De Floriani *et al.* (1983, 1985). The initial set P' is chosen so that it contains only those data sites necessary to define the boundary of the region under consideration, which may be the boundary of the convex hull $\text{CH}(P)$ of P or a modified form obtained using the procedures defined in Section 6.3. $\mathcal{D}(P')$ is then constructed. For each data site p''_i in the set P'' ($P'' = P \setminus P'$) of the data sites not in P' , we can define an associated error value $e(p''_i)$ as

$$e(p''_i) = |z''_i - f(p''_i)| / z''_i \quad (6.4.1)$$

where z''_i is the data value at p''_i and $f(p''_i)$ is the interpolated value (obtained using a specified interpolation procedure) at p''_i using $\mathcal{D}(P')$. The error associated with $\mathcal{D}(P')$, $e[\mathcal{D}(P')]$, is defined as

$$e[\mathcal{D}(P')] = \max_{p''_i \in P''} e(p''_i) \quad (6.4.2)$$

and can be used as a measure of the error. If $e[\mathcal{D}(P')]$ exceeds the predetermined error level the data site p''_i ($p''_i \in P'$) for which $e(p''_i) = e[\mathcal{D}(P')]$ is added to P' and $\mathcal{D}(P')$ is updated. The processes are repeated until $e[\mathcal{D}(P')]$ no longer exceeds the specified error level. Figure 6.4.1 shows a given surface at three different error levels when a C^0 interpolant is used in equation (6.2.5). Note that this procedure may be suboptimal since P' need not be

the minimal subset of P necessary to produce a surface with a specified error level.

Falcidieno and Pienovi (1990), Rippa (1992) and Fjällströn (1993) proposed similar data-selection strategies in the context of the data compression. Park and Kim (1995) also used the same strategy for the concise and fine representation of solid models using cubic triangular Bézier surfaces. A similar progressive refinement is also used to decrease the aliasing effect in computer graphics (Painter and Sloan, 1989).

De Floriani (1989a), De Floriani and Puppo (1992a) and De Floriani *et al.* (1996) proposed hierarchical data structures to represent a triangle-based surface in different resolutions, and De Floriani *et al.* (1993) constructed an algorithm for extracting the contour from these data structures.

6.5 DELAUNAY MESHES FOR FINITE ELEMENT METHODS

Finite element methods are used widely in modelling flow, diffusion, convection, heat transfer, mechanical oscillation and similar processes. Those methods can be considered as a kind of spatial interpolation since the solution of a partial differential equation is approximated by the values at discrete mesh sites or by the weights of trial functions defined locally on the mesh elements (Ho-Le, 1988; Schwarz, 1988; George, 1991; Bern and Eppstein, 1992b; Field, 1995; Babuska *et al.*, 1995; Klein and Cohen-Or, 1997).

The meshes used in the finite element methods are divided into two classes. One class consists of meshes composed of simplices (i.e. triangles in the two-dimensional space and tetrahedra in the three-dimensional space) while the other class is composed of non-simplex elements (such as quadrilaterals and hexahedra). One promising tool for the former class of meshes is the Delaunay tessellation, which we call the *Delaunay mesh*, and which we concentrate on in this section. However, we note that the medial axis and the medial surface (see Section 3.5.4) are sometimes used for the latter class (Tam and Armstrong, 1991; Srinivasan *et al.*, 1992; Price *et al.*, 1995; Price and Armstrong, 1997). For more information on this class, see Joe (1995b) for example. There is also another type of discretization of partial differential equations called finite volume methods, for which Voronoi diagrams are often used (Ghosh and Mukhopadhyay, 1993; Ghosh and Liu, 1995; Ghosh and Moorthy, 1995; Moorthy and Ghosh, 1996; Ball, 1996; Lee and Ghosh, 1996).

In this section we study mesh generation in two and three dimensions separately. While two-dimensional meshes can be generated relatively easily, there are difficult problems associated with three-dimensional meshes.

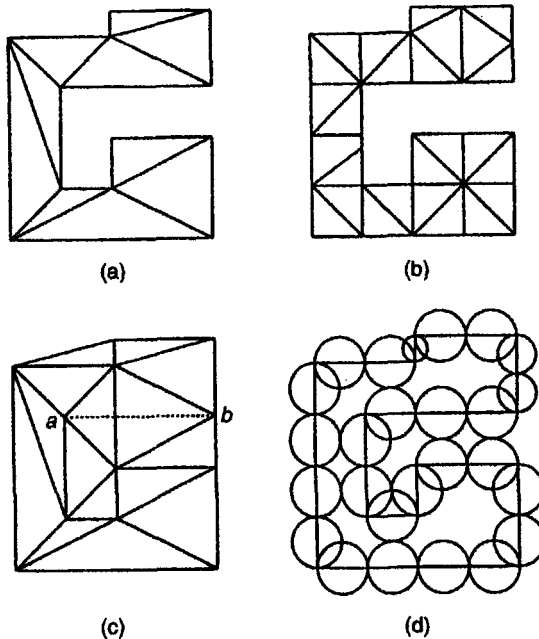


Figure 6.5.1 Triangulation inside a polygonal domain: (a) constrained Delaunay triangulation; (b) triangulation using additional points; (c) Delaunay triangulation for the same set of generators as in (a); (d) placement of additional points which guarantee the consistency of the Delaunay triangulation with the boundary of the domain.

6.5.1 Two-dimensional Delaunay meshes

Suppose that we are given a partial differential equation in a polygonal region S , and want to generate a triangular tessellation of S to solve the equation. According to the convention in finite element methods, we call this tessellation a *mesh* over S . Mesh generation differs from other Delaunay interpolations in two ways.

First, the set P of generators is not fixed. P should contain at least the vertices of the polygon S , but the number of other generators and their locations are not given *a priori*. We can use this freedom to get good meshes, to control mesh density, and for other purposes. For example, Figures 6.5.1(a) and (b) show two different meshes over the same polygonal region S . In (a) only the vertices of the polygon S are used, whereas in (b) many additional generators are used. Second, the mesh should be consistent with the boundary of S ; that is, the whole of the boundary of S should be realized as the edges of the triangles. This constraint makes the mesh generation a little difficult.

One strategy to generate the mesh may be first to compute the Delaunay triangulation and then to remove the triangles outside S . However, this strategy does not necessarily work. For example, if we compute the Delaunay triangulation for the vertices of S in Figure 6.5.1(a), we get the triangulation

as shown in (c). Note that in (c) the boundary edge ab is not realized as an edge of a triangle, and hence we cannot obtain a consistent mesh by this strategy.

There are two typical strategies to overcome this difficulty. One is to utilize the constrained Delaunay triangulation (Chew, 1989a) (see Section 3.4.3 and Section 6.3). This is also called the *domain Delaunay triangulation* (Sapidis and Perucchio, 1990). The constrained Delaunay triangulation can be constructed in $O(n \log n)$ time, where n is the number of vertices of S (Chew, 1989a; Moreau and Volino, 1993). Actually, the mesh in Figure 6.5.1(a) is obtained first by generating the constrained Delaunay triangulation with the boundary edges in S as the constraints, and then by removing the triangles outside S .

The other strategy is to place additional vertices so that the associated Delaunay triangulation realizes all the boundary of S . As shown in Figure 6.5.1(d), suppose that we place sufficiently many additional generators on the boundary of S in such a way that each circle having the consecutive generators as the diameter does not contain other generators. Then, the Delaunay triangulation of such generators realizes the whole boundary by the Delaunay edges (recall Property D5 in Section 2.4, i.e. the empty circle property). Such Delaunay triangulations are called *conforming Delaunay triangulations* (Edelsbrunner and Tan, 1993).

Edelsbrunner and Tan (1993) showed that this strategy always works by placing at most $O(m^2n)$ additional generators, where n is the number of vertices and m is the number of constraint edges. However, $O(m^2n)$ is for the worst case; a smaller number of additional generators is sufficient in many cases. Methods for the incremental addition of new points for this purpose were studied by Boissonnat (1988), Schroeder and Shephard (1988) and Sapidis and Perucchio (1991b).

Because of the lexicographical maximality of the small angles (recall Property D16 in Section 2.4), the Delaunay triangulation gives a good-quality mesh for the given set of generators. However, we have freedom in choosing the locations of the additional generators. This freedom enables us to get a better triangulation.

Figure 6.5.2(a) shows the mesh generated by the Delaunay triangulation. After generating this triangulation, we move the generators in the interior of the region to the centre of gravity of the adjacent generators simultaneously (this operation is called 'Laplacian smoothing' (Srinivasan *et al.*, 1992)), obtaining the triangulation shown in (b). This triangulation is better because their are fewer thin triangles than in (a).

Another strategy to improve the quality of a mesh is to insert additional generators. Chew (1989a), Dey (1990) and Dey *et al.* (1991, 1992a) recommended inserting new generators at the circumcentres of bad-quality triangles; see also Rebay (1993).

Mavriplis (1990) and Posenau (1993) pointed out that sometimes thin triangles, i.e. thin in some specific direction, are required rather than fat triangles, and Posenau (1993) showed that this requirement can be fulfilled using the

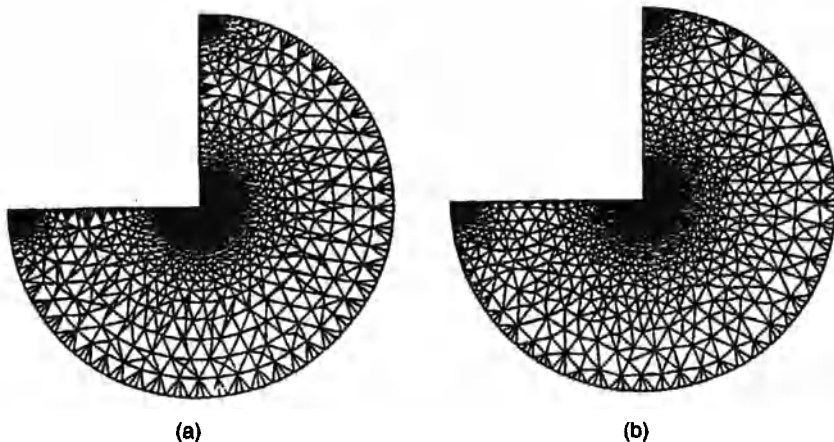


Figure 6.5.2 Mesh improvement with the displacement of points: (a) Delaunay mesh; (b) Laplacian smoothing.

Delaunay triangulation with respect to the elliptic distance. Srinivasan *et al.* (1992) used the Voronoi diagram of a polygon, particularly the medial axis, for placing vertices for both the triangular mesh and the quadrilateral mesh. Goodness of the mesh also depends on the partial differential equation to be solved. Hence, the *solution-adaptive mesh* is often used; that is, we first solve the equation using an initial mesh, and next modify the mesh adaptively in order to decrease the errors in the solution (Weatherill *et al.*, 1994, 1995; Marcum and Weatherill, 1995a,b; Medina *et al.*, 1996). For other two-dimensional, good-quality meshes, refer to Cendes *et al.* (1983), Lo (1985, 1989) and Baker *et al.* (1988), Bern *et al.* (1990), Cline and Renka (1990), Bern and Eppstein (1991, 1992a), Reichert *et al.* (1991), Melissaratos and Souvaine (1992), Weatherill (1992), Bern *et al.* (1995a,b), Borouchaki and George (1997) and Karamete *et al.* (1997).

6.5.2 Three-dimensional Delaunay meshes

Three-dimensional mesh generation is much more complicated than in two dimensions. One reason is that for a given polyhedral region S bounded by triangular faces and a given set P of generators, there might be no tetrahedral tessellation that satisfies the constraint.

For example, consider the polyhedron shown in Figure 6.5.3. This is a triangular prism whose boundary surface is partitioned into triangles by three vertex-disjoint diagonal edges. Suppose that the given generators are only the vertices of this polyhedron. Then, there is no tetrahedral tessellation, because any new line segment connecting two vertices lies outside the polyhedron.

It is still an open problem to judge in polynomial time whether a given constraint (specified by the region S and the generator set P) admits a tetra-

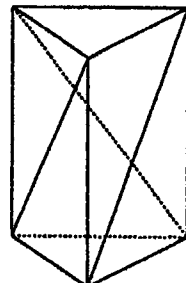


Figure 6.5.3 Polyhedral domain that cannot be partitioned into tetrahedra unless additional points are used.

hedral tessellation. Thus, no algorithm is known, for a given polyhedral region S bounded by triangular faces and a given set P of generators, to generate the constrained Delaunay tetrahedrization or to tell that it does not exist in $O(n)$ time. Hence, what we can do is to insert new generators in such a way that the augmented set of generators hopefully admits the consistent tetrahedral tessellation.

For the region in Figure 6.5.3, let us insert one new generator in the interior in such a way that all the corners of this polyhedron are visible from the new generator. Then, the region can be partitioned into tetrahedra, i.e. into triangular cones with the new generator as the apex and the triangular faces as the base triangles.

A typical strategy is to place sufficiently many additional generators on the boundary surface of S so that the resulting ordinary Delaunay tessellation realizes the whole boundary surface. To guarantee this property, we search for the placement of sufficiently many new generators on the faces of the boundary so that every Delaunay triangle in the two-dimensional Delaunay triangulation generated by the generators on each face admits a circumsphere that contains no other generators. If such a placement of new generators is found, then the ordinary Delaunay tetrahedrization realizes all the boundary faces, and consequently all we have to do is to remove the tetrahedra outside S . Methods for placing such new generators were studied by Dey *et al.* (1991, 1992a).

Another strategy is first to generate the Delaunay mesh for the set of generators (this is in general not consistent with the boundary of S), and then insert new generators one by one in order to eliminate tetrahedra that penetrate the boundary surface of the region S . This kind of incremental insertion was studied by George *et al.* (1990, 1991).

Another difficulty in three-dimensional mesh generation is the fact that Delaunay tetrahedra do not necessarily have good shape from the viewpoint of the finite element methods (Dey *et al.*, 1991, 1992a; Escobar and Montenegro, 1996). In two dimensions the goodness of the Delaunay triangles is supported by the max-min angle property (refer to Properties D15 and D16 in Section 2.4). In some sense, similar equiangularity properties also hold in three dimensions (and in higher dimensions) as shown by Rajan

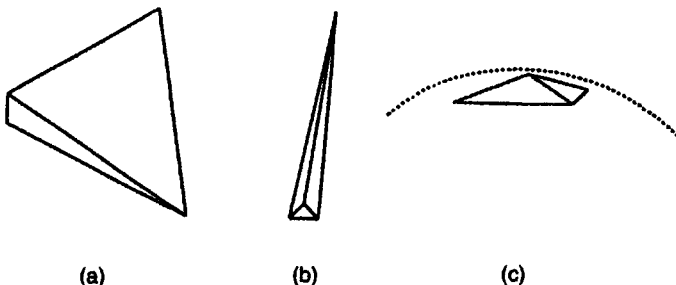


Figure 6.5.4 Bad tetrahedra that can be avoided by the Delaunay triangulation.

(1991, 1994) and Schmitt and Spehner (1993). However, there are different types of angles associated with a tetrahedron: angles of each face triangle, angles formed by two adjacent faces (which are called the *dihedral angles*), and solid angles at the vertices. In particular, the dihedral angles do not admit an equiangularity-type property. Indeed, the Delaunay tetrahedrization often contains smaller dihedral angles than other tetrahedrizations for the same set of generators.

Suppose that a tetrahedron t has the radius R of the circumscribing sphere, the longest edge length L and the shortest edge length l . According to Dey *et al.* (1992a), let us define ω and κ by $\omega = 2R/L$ and $\kappa = L/l$. Note that for any tetrahedron $1 \leq \omega$ and $1 \leq \kappa$. If κ is very large, the tetrahedron has either one short edge as in Figure 6.5.4(a) or three short edges as in Figure 6.5.4(b). They are bad tetrahedra, and hence a smaller κ is desirable. If ω is very large, the tetrahedron is very small compared with the circumsphere, as shown in Figure 6.5.4(c). This tetrahedron is also unsuitable for interpolation, and hence a smaller ω is desired. Recall that the circumsphere of every Delaunay tetrahedron is empty. A tetrahedron with large κ or large ω has a large circumsphere relative to the shortest edge length. As the sphere becomes larger, it is in general more likely to contain other generators. Therefore we can expect that the Delaunay mesh can avoid tetrahedra with large κ or large ω . However, even if both ω and κ are small, there may still be bad tetrahedra, as shown in Figure 6.5.5; this diagram consists of the pair of the top view and the front view. In this tetrahedron two dihedral angles are very large (nearly π) and the other four are very small. Such thin tetrahedra cause large numerical errors in finite element methods. However, tetrahedra of this type often appear in the Delaunay mesh because their circumspheres are not very large.

Thus, the Delaunay mesh is not always satisfactory; it may contain undesired slivers. Hence, some postprocessing is necessary to improve the quality of the mesh. Typical postprocessings proposed so far are based on heuristic local refinements, and there are three approaches.

The first approach is the local refinement using ‘flips’. Suppose that, as shown in Figure 6.5.6(a), two tetrahedra share a triangular face $v_1v_2v_3$, and their union forms a convex hexahedron. Let the other vertices be v_4 and v_5 ,

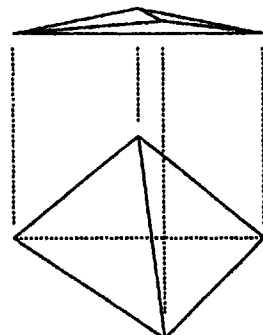


Figure 6.5.5 Bad tetrahedron with small ω and κ .

respectively. If we remove the face $v_1v_2v_3$ and add three faces $v_1v_4v_5$, $v_2v_4v_5$ and $v_3v_4v_5$, then this hexahedron is partitioned into three tetrahedra as shown in Figure 6.5.6(b). The change of the tetrahedrization from (a) to (b) or from (b) to (a) is called a *flip*. The flip operation is a three-dimensional counterpart of the swap operation for the two-dimensional triangulation.

If we have some criterion to judge whether a flip improves the quality of a mesh, then we can construct a local refinement procedure. An example of such a criterion is to maximize the minimum solid angle of the associated two or three tetrahedra; that is, we apply a flip operation if it makes the minimum solid angle larger (Joe, 1989, 1991b). Another criterion is to maximize the ratio of the radius of the inscribed sphere to that of the circumsphere (Joe, 1995a). Other criteria and a combination of two or more criteria are also proposed (Joe, 1995a). Nehl and Field (1991) and Zhu and Zienkiewicz (1997) proposed the adaptive subdivision of the mesh according to the errors in the finite element method. Kanaganathan and Goldstein (1991) showed experimentally that the Delaunay tetrahedrization still gives a better mesh than many other methods. If we use the empty-circumsphere criterion, then we can change any tetrahedral mesh to the Delaunay mesh by a sequence of flip operations (Joe, 1991a).

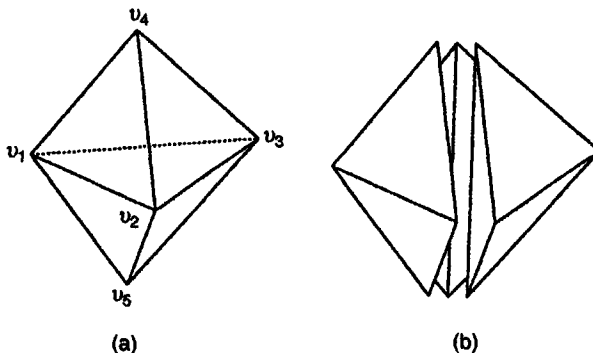


Figure 6.5.6 Flip operation for a hexahedron: (a) decomposition into two tetrahedra; (b) decomposition into three tetrahedra.

The second local refinement approach is the relocation of generators. By moving the vertices of the slivers or nearby vertices, we can improve the mesh quality (Cavendish *et al.*, 1985; George, 1997).

The third local-refinement approach is the insertion of new generators. Proposed heuristics include the insertion of the midpoints of edges (Liu and Joe, 1995), the insertion of new generators near the slivers (Baker, 1989), and the insertion of new generators at the centres of the circumspheres of the slivers (Yuen *et al.*, 1991). For other heuristics, see Morgan *et al.* (1991), Weatherill and Hassan (1992, 1994) and Yagawa *et al.* (1995).

Besides the Delaunay-mesh approaches, there are many other methods for quality-guaranteed mesh generation. For details, refer to the surveys by George (1991), Bern and Eppstein (1992b), Field (1995) and Babuska *et al.* (1995). The Delaunay mesh is also used in a domain including the time axis (Morgan *et al.*, 1994, 1996).

6.6 ORDERING MULTIVARIATE DATA

Unlike univariate data there is no unique way of ordering a set of multivariate data. However, if the individual cases are represented as a point set P in \mathbb{R}^m , the creation of either the Voronoi diagram, $\mathcal{V}(P)$, or the Delaunay tessellation, $\mathcal{D}(P)$, imposes a spatial structure on P . Thus, $\mathcal{V}(P)$ and $\mathcal{D}(P)$ are equivalent to a spatial ordering of the elements of P (Watson, 1985; Gold and Cormack, 1987). In this section we consider a number of situations where such ordering has been exploited.

When we are working with $\mathcal{D}(P)$, as in the digital terrain models discussed in Section 6.2, ordering the constituent triangles allows them to be processed incrementally, thus facilitating such tasks as isoline extraction, creating perspective views, and determining the visibility regions of arbitrary vertices. Gold and Maydell (1978), Gold (1987) and Gold and Cormack (1987) show that any triangulation may be represented as an ordered binary tree with respect to some viewpoint, thus permitting front-to-back or radially-outwards processing of the triangles and their associated data points. If the triangulation is a Delaunay triangulation, De Floriani (1989b) and De Floriani *et al.* (1991) show that it is possible to order the triangles with respect to any vertex in such a way that a ray from the vertex to an arbitrary target point inside any one of the triangles passes through only triangles which rank lower in the ordering than the triangle containing the target point. For example, in Figure 6.6.1 the ray from vertex v to target point t in triangle 10 passes in order through triangles 6 and 9. When the triangles are ordered in this way, each region R_k consisting of the union of triangles $1, 2, \dots, k$ is star shaped with respect to the vertex under consideration (see Figure 6.6.1). While this is a property of any Delaunay triangulation (see Property D19 in Section 2.4) it is not possessed by all planar triangulations. This ordering scheme has been generalized to \mathbb{R}^n for cell complexes whose faces are

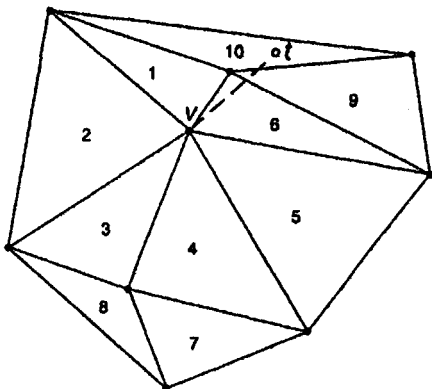


Figure 6.6.1 Ordering of Delaunay triangles with respect to vertex v .

obtained by orthogonal projections of the faces of a convex polytope in $m+1$ dimensions (Edelsbrunner, 1990).

The same spatial relations which give rise to the Voronoi diagram and the Delaunay tessellation can also be represented by the set of all empty (natural neighbour) spheres which define the Delaunay tessellation (see Figure 2.4.3). These natural neighbour spheres may be organized hierarchically to form a *natural tree* in \mathbb{R}^2 (Watson and Mees, 1996) or a *Delaunay tree* in \mathbb{R}^3 (Boissonnat and Teillaud, 1986) which corresponds to an incremental construction of the Delaunay tessellation (see Figure 6.6.2). Thus, the nodes of the tree are composites made up of groups of associated natural neighbour spheres and the clusters of data points which define them. As well

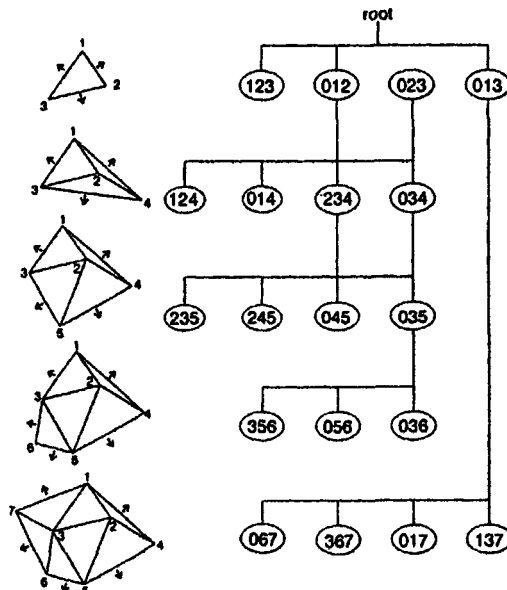


Figure 6.6.2 A Delaunay triangulation and its natural tree.

as providing an efficient means of generating Delaunay tessellations, especially when they are used for the study of dynamic systems in higher dimensions (Mees, 1991), natural trees have a wide range of applications in problems such as density estimation, interpolation, gradient estimation and classification.

Another means of organizing the data hierarchically is proposed by Okabe and Sadahiro (1996) who consider the situation in which each point p_i in P has an associated attribute value a_i measured on at least an ordinal scale (see Figure 6.6.3(a)). They begin by finding first-level local centres which are defined as those points whose attribute values are greater than or equal to

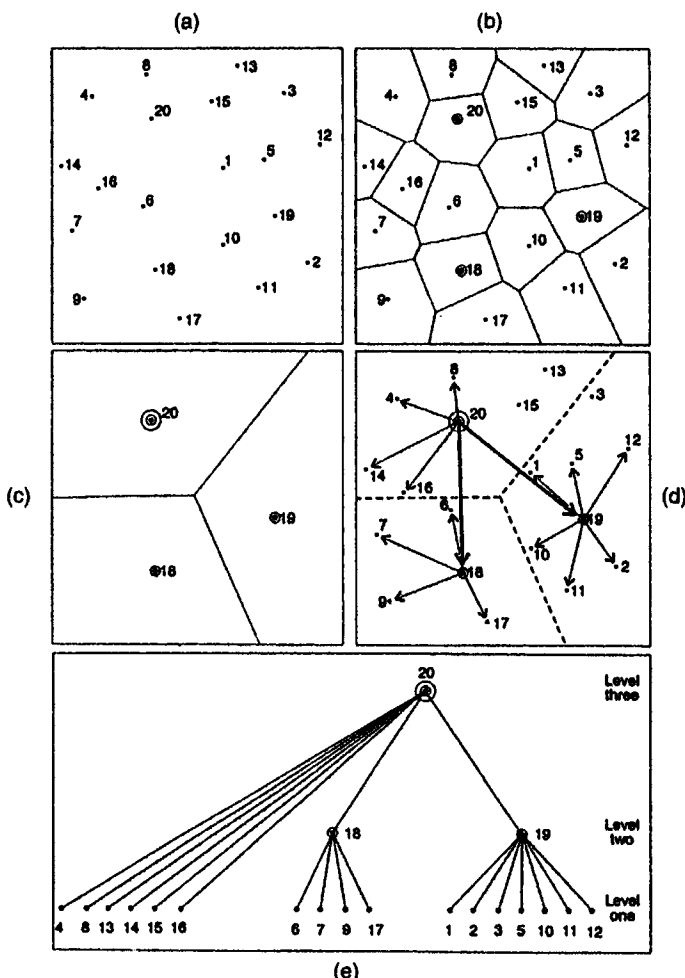


Figure 6.6.3 Hierarchical ordering of a set of points: (a) points and associated attribute values; (b) definition of first-level local centres; (c) definition of second-level local centres; (d) directed tree graph of relationships between points; (e) hierarchical order.

those of their Voronoi neighbours (see Figure 6.6.3(b)). In the same way, the Voronoi diagram of the first-level local centres is used to define second-level local centres (see Figure 6.6.3(c)). This procedure is repeated, with the Voronoi diagram of the k th-level local centres being used to define the $(k + 1)$ th-level local centres, until only one point is left. Finally, the hierarchical relationships between the points can be summarized by a directed tree graph (see Figures 6.6.3(d) and 6.6.3(e)) by determining for each k th-level local centre the $(k + 1)$ th level Voronoi polygon which contains it. Okabe and Sadahiro use this procedure to create a spatial hierarchy of 100 market-places in a 6 km-square residential area in Nishinomiya near Osaka.

Some problems may require considering more than one spatial structure simultaneously. For instance, the integration of remotely sensed data with cartographic data is usually achieved by transforming both the remotely sensed image and the cartographic data to a common base. Converting the remotely sensed data may require changing the origin, scale and orientation of the image, as well as correcting for any patterns of distortion in the data. This is done by collecting a set of *ground control points* (GCPs) at locations which are known to be coincident on both the image and the map (e.g. road intersections). The location of every GCP on both the image (x'_i) and the map (x_i) is then recorded and used to generate a polynomial which models the relationship between x'_i and x_i . The polynomial can then be used to predict x'_i for any x_i . As an alternative to this procedure, Devereux *et al.* (1990) suggest simultaneously constructing the Delaunay triangulation of the GCPs on both the image $\mathcal{D}(I)$ and the map $\mathcal{D}(M)$. Then, within each triangle in $\mathcal{D}(I)$ and $\mathcal{D}(M)$, generate a new GCP using the point of intersection formed by two lines which bisect any two triangle edges and their opposite angles. Add these secondary GCPs to the original GCPs and recompute $\mathcal{D}(I)$ and $\mathcal{D}(M)$. Examine the sizes of the triangles in $\mathcal{D}(I)$. If a triangle is less than some pre-specified threshold size, then it is no longer a source for new GCPs; if not, generate another new GCP in the above manner. The procedure terminates when every triangle in $\mathcal{D}(I)$ is less than the threshold size. While the final $\mathcal{D}(I)$ and $\mathcal{D}(M)$ will have the same topology, they will only have the same geometry if there is no distortion in the image. Distortion in the image can be corrected by matching the triangles of $\mathcal{D}(I)$ and $\mathcal{D}(M)$. Label the vertices of a triangle in $\mathcal{D}(M)$, and its corresponding triangle in $\mathcal{D}(I)$, ABC and $A'B'C'$, respectively. Since any two sides of the triangle ABC (say the shortest two, AB , AC) are linearly independent vectors, any pixel X inside triangle ABC can be linked to vertex A by vector \overrightarrow{AX} which can be expressed as a linear combination

$$\overrightarrow{AX} = \alpha \overrightarrow{AB} + \beta \overrightarrow{AC} \quad (0 \leq \alpha \leq 1; 0 \leq \beta \leq 1 - \alpha). \quad (6.6.1)$$

Equation (6.6.1) can be solved by two simultaneous equations and the values of the coefficients inserted into

$$\overrightarrow{A'X'} = \alpha \overrightarrow{A'B'} + \beta \overrightarrow{A'C'} \quad (6.6.2)$$

to find the image pixel location X' . Once found, the relevant pixel can be retrieved from the image and placed in the corrected output image at X . In studying the more general problem of matching a set of data points and a set of model points in the plane, Ogawa (1986), Finch and Hancock (1995), and Finch *et al.* (1997) generate the Delaunay triangulation of one of the point sets to provide a point–edge–face structure which is then checked for consistency with three-point subsets of the other point set.

Another kind of ordering arises in some multivariate two-sample tests. Suppose that we have two m -dimensional samples $X = \{x_1, x_2, \dots, x_n\}$ and $Y = \{y_1, y_2, \dots, y_m\}$, in each of which the points are independent and identically distributed and, without making any distributional assumptions, we wish to determine if the populations from which the samples are drawn are the same in some way. Friedman and Rafsky (1979, 1981) suggest defining a proximity graph G (see Section 2.5) on the pooled sample and examining the number of edges L in the graph which have one endpoint in each of the samples. When L is small, points in each sample tend to have neighbours in the same sample suggesting that the two samples are drawn from different populations. If the two samples are drawn from the same population, the mean of L is

$$\mathbb{E}(L | T) = gT \quad (6.6.3)$$

and the variance is

$$\text{Var}(L | C, T) = g \left\{ T(1 - gT)T + C + \frac{2(m-1)(n-1)}{(N-2)(N-3)} [T(T-1) - 2C] \right\} \quad (6.6.4)$$

where $N = n + m$ is the number of points in the pooled sample, T is the number of edges of G , C is the number of edge pairs which share a common vertex, and $g = 2mn/N(N-1)$. Friedman and Rafsky use the Euclidean minimum spanning tree (EMST) to define G and demonstrate that in this case the procedure is equivalent to a multivariate generalization of the Wald–Wolfowitz runs test. McIntosh (1988) uses the Delaunay tessellation instead of the EMST. He shows that while the test using L performs well when the populations being compared differ only in location, it performs poorly when the populations differ only in scale. In such situations, he proposes an alternative procedure in which each point in the pooled sample is assigned a rank according to the number of Delaunay tessellation edges that must be traversed to reach the point from the boundary of the convex hull ∂CH of the pooled sample. Ties in rankings are broken using the Euclidean distance from each point to the centroid of the points that are farthest from ∂CH , with points which are closer to the centroid receiving higher ranks. The ranks can then be assessed by means of either the standard Smirnov or Wilcoxon tests. Simulations show that when the underlying distributions are normal, the tests involving the Delaunay triangulation perform as well as or better than traditional tests.

The ranking procedure just described is related to *peeling* the data set. This is a form of data ordering which is useful in such procedures as the

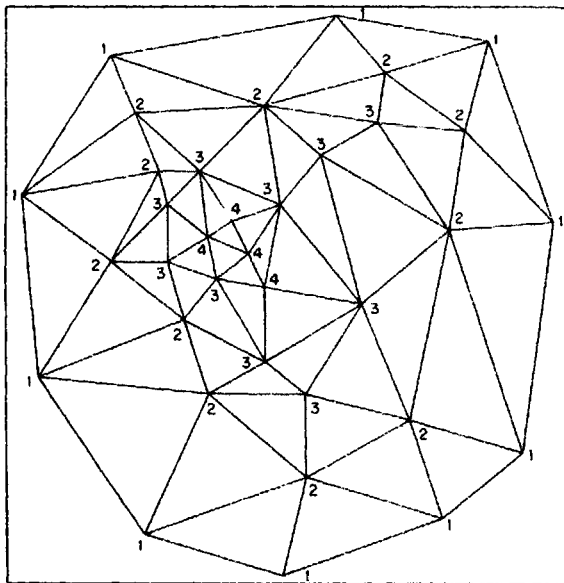


Figure 6.6.4 Peeling according to adjacencies defined by the Delaunay triangulation (numbers indicate the numbers of specific peels).

identification and treatment of outliers in P , establishing significance levels for Monte Carlo tests, estimating correlation and deriving measures of location (Green, 1981). In general, peeling involves an iterative process which begins by finding the smallest region, R , of a given form which contains P . The points on the boundary of R are assigned the index 1. These points are then discarded and R is redefined for the remaining points. This process is repeated until no points are left. Those points which are discarded on the j th iteration form the j th peel. Various suggestions have been proposed for the form of R including, in the bivariate case, rectangles, circles and ellipses. The first two take no regard of the joint distribution of the sample and may thus fail to identify outliers in strongly correlated data. The last two forms create peels that may not be nested spatially. Consequently, other forms of R have been proposed. One is the boundary of the convex hull of P , $\partial\text{CH}(P)$, (Bartlett, 1976) which as we saw in Section 2.3 is a subgraph of $\mathcal{D}(P)$. Another peel (Green, 1981) can be defined by the neighbour relationships in $\mathcal{V}(P)$ or $\mathcal{D}(P)$ as shown in Figure 6.6.4. Here those points on the boundary of $\partial\text{CH}(P)$ have the index 1 while their Delaunay neighbours have the index 2. The neighbours of these latter points are, in turn, indexed 3, and so on. So far there has been no analysis of the relative merits of the different peels in the various applications of data ordering mentioned above.

CHAPTER 7

Models of Spatial Processes

We have noted that the ordinary Voronoi diagram, $\mathcal{V}(P)$, of a set of n points, $P = \{p_1, \dots, p_n\}$, in \mathbb{R}^m is a tessellation of \mathbb{R}^m since it consists of a set of regions that do not overlap, except possibly at their boundaries, and which completely cover \mathbb{R}^m (see Section 2.3). Since there is a large number of empirical structures which also involve tessellations of \mathbb{R}^m , one of the most obvious direct applications of Voronoi concepts is in the modelling of such structures and the processes that generate them. Indeed, in Section 5.3 we have already shown how the Voronoi diagram associated with a set of points located in \mathbb{R}^m according to the homogeneous Poisson point process (the Poisson Voronoi diagram) can be used as a normative model to evaluate and compare various empirical structures. In this chapter we take a more general approach which does not limit the location of the members of P to a particular spatial pattern and consider other processes which result in tessellations. We shall refer to these as models of spatial processes of which several different types are presented. In Section 7.1 we consider models involving spatial assignment processes while in Section 7.2 we consider models involving concepts of growth.

The models presented in both these sections assume that once formed the regions remain unchanged and that the phenomenon associated with the regions is of a single type or belongs to a single group. In Section 7.3 we relax the first assumption by permitting the regions to change in form after their initial creation. Since such situations involve an explicit time dimension, we refer to them as spatial-temporal processes. The second assumption is relaxed in Section 7.4 by considering situations in which regions are associated with different phenomena which compete for space (e.g. crops and weeds in a field, prey and predators in an ecosystem).

For convenience, throughout this chapter we refer to the tessellation of \mathbb{R}^m associated with a particular phenomenon as a spatial pattern of that phenomenon. Also, since our concern is with modelling empirical structures, our treatment is limited to two- and three-dimensional Euclidean space.

7.1 ASSIGNMENT MODELS

These models describe processes which produce spatial patterns by allocating individual locations in \mathbb{R}^m ($m = 2, 3$) or a bounded region in \mathbb{R}^m (depending on the particular empirical circumstance) to a set of n points, $P = \{p_1, \dots, p_n\}$, at positions x_1, \dots, x_n , respectively, in the same space. If the following assumptions are made, the resulting set of regions is equivalent to the ordinary Voronoi diagram, $\mathcal{V}(P)$, of P :

Assumption VAM1 Each point, p_i ($i = 1, \dots, n$), is located simultaneously before any assignment procedure occurs.

Assumption VAM2 Each point p_i remains fixed at x_i throughout the assignment process.

Assumption VAM3 Each point p_i is of equal importance.

Assumption VAM4 Each location which is closer in terms of Euclidean distance to p_i than to any other member of P is assigned to p_i ; locations which are equidistant from two or more members of P are assigned to the boundaries of the regions of those points.

Collectively Assumptions VAM1–VAM4 define the *Voronoi Assignment Model*.

Given the simple assumptions of the Voronoi Assignment Model it is of no surprise that it has been evoked in a wide range of situations in an equally wide range of disciplines. One of the longer established areas of use is in modelling physical-chemical systems. Such systems are frequently considered to consist of a set of sites occupied by atoms, ions or molecules (depending on the specific application) which are represented as equal-sized spheres. When the sites are regularly arranged in \mathbb{R}^m , as they would be if they formed a lattice (see Figure 7.1.1(a)), then the structure is said to be *crystalline*. Such structures are also referred to as *periodic* or *ordered* since the physical situation at a given site is reproduced at other sites throughout the structure. Examples of such structures in \mathbb{R}^m are encountered frequently in inorganic chemistry (Wells, 1984). When the sites are no longer regularly arranged but the radii of the spheres are not negligible relative to the average distance between sites, we have a structure such as that illustrated in Figure 7.1.1(b), which is referred to as an *amorphous* (alternatively *non-crystalline*, *non-periodic* or *disordered*) structure (Yonezawa and Ninomiya, 1983). In such structures the size of the spheres has an inhibitive effect on how closely the sites may approach each other (no closer than the diameter of the spheres). Consequently, although amorphous structures lack the long-range order of crystalline structures, they may still exhibit some degree of short-range (local) order. Examples of such structures include monatomic liquids and metallic glasses (Zallen, 1979). Finally, if the sites are not regularly arranged and the

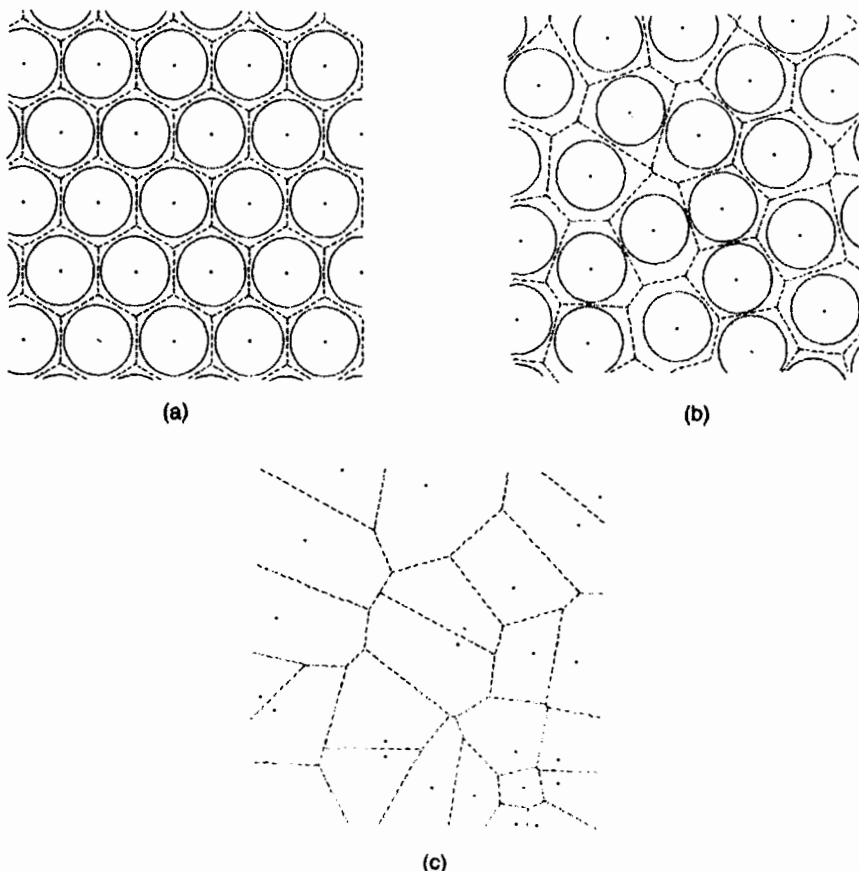


Figure 7.1.1 (a) Crystalline structure; sites and their associated spheres arranged on a lattice (dashed lines indicate Voronoi regions of sites). (b) Amorphous structure; sites and their associated spheres arranged irregularly (dashed lines indicate Voronoi regions of sites). (c) Ideal gas structure; sites located according to a homogeneous Poisson point process (dashed lines indicate Voronoi regions of sites).

radii of the spheres are considered negligible relative to the average inter-site distance, the inhibitive effect no longer occurs and the sites may occupy locations equivalent to those generated by a homogeneous Poisson point process (see Section 1.3.3) as shown in Figure 7.1.1(c). Such a structure is typical of many gasses and that in Figure 7.1.1(c) is often referred to as an *ideal gas* (Gil Montoro and Abascal, 1993). Both the crystalline and amorphous structures can thus be considered as consisting of closely spaced spherical atoms and it is in these situations that Voronoi concepts have been used extensively.

Regardless of how the sites are positioned in \mathbb{R}^m it is possible to assign each location in \mathbb{R}^m to the nearest site. The result is to produce the Voronoi diagram, $\mathcal{V}(P)$, of the sites (see Figure 7.1.1). Once this is done, the

characteristics of $\mathcal{V}(P)$ can be used to define various parameters of the atoms (ions, molecules) of the structure. One such property is the number of neighbours or *coordination number*, c_i , of the atom p_i which can be measured by the number of Voronoi regions adjacent to the Voronoi region, $V(p_i)$, of p_i (Frank and Kasper, 1958; Laves, 1967; Fischer and Koch, 1979; Allen *et al.*, 1983). The coordination number is considered a basic parameter on which many atomic properties, such as the atomic (ionic) radius, depend directly. The region with p_i as its centre and with vertices that are the sites whose Voronoi regions are adjacent to $V(p_i)$ is called the *coordination shell* (or *coordination polyhedron* in \mathbb{R}^m) of the site p_i (Frank and Kasper, 1958; Mackay, 1972; Loeb, 1976, p. 132). Examination of how the coordination polyhedra are connected together in space provides an alternative way of modelling the structure. However, for some amorphous structures, the coordination polyhedron of an individual atom p_i may include more distant members of P which are unlikely to interact with p_i . In such situations, various methods have been proposed for either weighting or discarding one or more faces of $\mathcal{V}(P)$ (Bernal, 1937; Brostow *et al.*, 1978; Hsu and Rahman, 1979b; O'Keefe, 1979; Medvedev, 1986; Rustad *et al.*, 1991a; Liška *et al.*, 1995a).

When the sites are regularly arranged they form a lattice. In this case each site has an identical environment in an identical orientation to every other site. More formally, in \mathbb{R}^m a lattice consists of the set of points with position vectors, \mathbf{p} , of the form

$$\mathbf{p} = l_1 \mathbf{a}_1 + l_2 \mathbf{a}_2 + l_3 \mathbf{a}_3 + \dots + l_m \mathbf{a}_m, \quad (7.1.1)$$

where $\mathbf{a}_1, \mathbf{a}_2, \mathbf{a}_3, \dots, \mathbf{a}_m$ are m linearly independent vectors and $l_1, l_2, l_3, \dots, l_m$ are integers. A lattice is infinite. For lattices the Voronoi regions of the sites are identical parallelotopes, convex polytopes with pairs of mirror equal opposite faces which fill space by being juxtaposed in parallel orientation. The upper limit for the number of facets F of a Voronoi parallelotope is $F \leq 2(2^m - 1)$ (Minkowski, 1897). Fedorov (1885) was the first to note that there are two types in \mathbb{R}^2 , the centrally symmetric convex hexagons and the

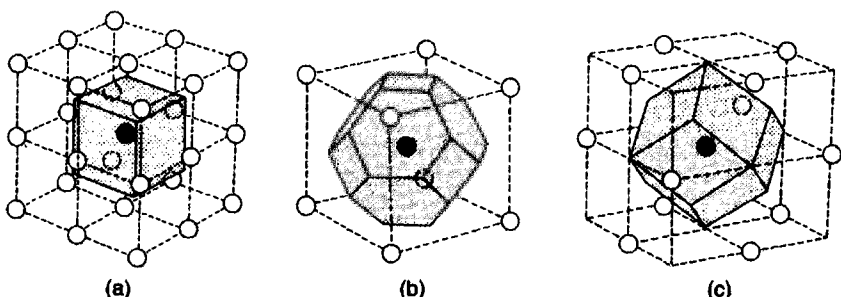


Figure 7.1.2 Some three-dimensional lattices and their associated Voronoi polyhedra: (a) simple cubic lattice, the Voronoi polyhedron is a cube; (b) body centred cubic lattice, the Voronoi polyhedron is a truncated octahedron; (c) face centred cubic lattice, the Voronoi polyhedron is a rhombic dodecahedron.

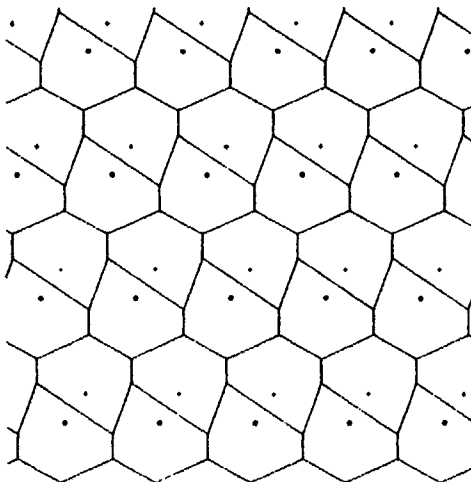
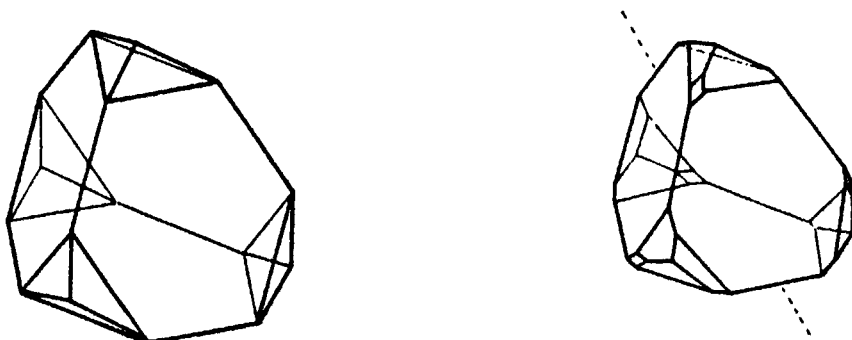


Figure 7.1.3 A lattice complex in \mathbb{R}^2 with sites of two different orientations.

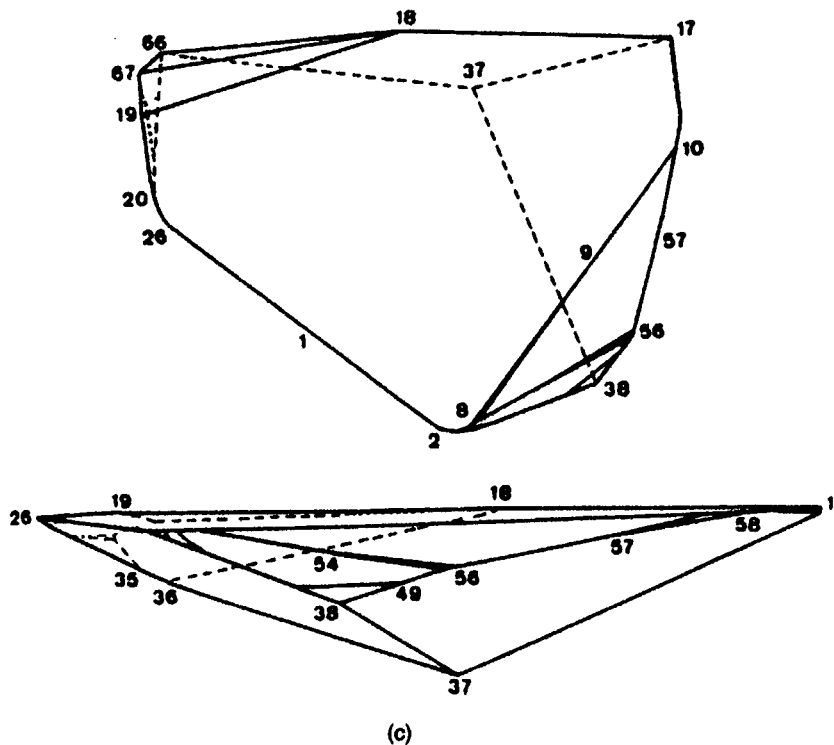
parallelograms, and five in \mathbb{R}^3 , the cube, hexagonal prism, rhombic dodecahedron, elongated dodecahedron, and truncated octahedron. Figure 7.1.2 shows the three types for which the corresponding point lattices are cubic. Forms with less symmetry can be obtained by distorting the basic five types by stretching or squeezing them along certain axes (Burzlaff and Zimmerman, 1977), yielding 24 classes of Voronoi regions (Bohm *et al.*, 1996). In \mathbb{R}^4 there are 52 types of Voronoi parallelotopes, 51 discovered by Delaunay (1929a, b) plus one more found by Stogrin (1973). The Voronoi region is also a primitive cell of the lattice. This is a bounded region which, when translated through all the vectors of the lattice, completely fills \mathbb{R}^m without overlap except possibly at boundaries. Although there is no unique way of defining the primitive cell of a lattice, the primitive cell defined by the Voronoi region of a site has the advantage that it has the same degree of symmetry as the lattice.

In some crystal structures the sites are not arranged on a lattice. One possibility is that all sites are equivalent with respect to other point group operations, besides that of translation involved in a lattice, such as rotation about an axis or reflection. Such sites are said to form a *lattice complex*. In such cases the environments of the sites are identical except for orientation and the Voronoi regions are congruent but with more than one orientation. An example of a lattice complex in \mathbb{R}^2 where the sites are of two different orientations is shown in Figure 7.1.3. For lattices and lattice complexes in \mathbb{R}^2 all the different types of Voronoi polygons have been determined (Laves, 1930, 1931; Delone *et al.*, 1980; see Grünbaum and Shephard, 1987, Table 9.1.5, for a summary).



(a)

(b)



(c)

Figure 7.1.4 (a) 16-faced space-filling Voronoi region obtained from the 'diamond lattice'. (Source: Grünbaum and Shephard, 1980, Figure 8.) (b) 20-faced space-filling Voronoi region obtained from a distorted 'diamond lattice'. (Source: Grünbaum and Shephard, 1980, Figure 9(a).) (c) Two views of a 38-faced Voronoi region (some of the vertices are labelled to facilitate recognition. (Source: Engel, 1981, Figure 4.)

In \mathbb{R}^3 the Voronoi polyhedra are sometimes called *plesiohedra* (Grünbaum and Shephard, 1980). As such they are members of a larger set of regions of equal shape called *stereohedra*, congruent copies of any one of which are capable of filling \mathbb{R}^3 without overlap except possibly for boundaries. There has been considerable interest in crystallography in determining the maximum number of $(m-1)$ -dimensional faces, F , of a stereohedron. Delone (1961) obtained the result that in m dimensions

$$F \leq 2^m (1 + h) - 2, \quad (7.1.2)$$

where h is the number of sets of sites with different orientations of their environments. For a lattice $h = 1$, and so for \mathbb{R}^3 , expression (7.1.2) gives an upper limit of 14 which is achieved by the Voronoi polyhedra of a body centred cubic lattice. The Voronoi polyhedra are truncated octahedra with six square faces and eight regular hexagonal faces; all edges are of the same length (see Figure 7.1.2(b)). For $m = 3$ and $h = 2$ the upper limit of F given by expression (7.1.2) is 22. A stereohedron with this number of faces has not been identified but $F = 16$ for the lattice complex consisting of two interpenetrating face centred cubic lattices is usually referred to as the diamond structure (since the carbon atoms in a diamond crystal take on this arrangement) (see Figure 7.1.4(a)). A simplified version of this polyhedron has been used by Grigorovici and Manaica (1967/8) and Grigorovici (1969) as a model for germanium. Smith (1965) has identified stereohedra with 20 faces which are Voronoi polyhedra of a slightly distorted version of the diamond structure (see Figure 7.1.4(b)). Other examples of Voronoi polyhedra with 20 faces have been identified by Stogrin (1968, 1973). The upper limit of F for $m = 3$ is 390 since the maximum value for h in \mathbb{R}^3 is 48 (Henry and Lonsdale, 1965).

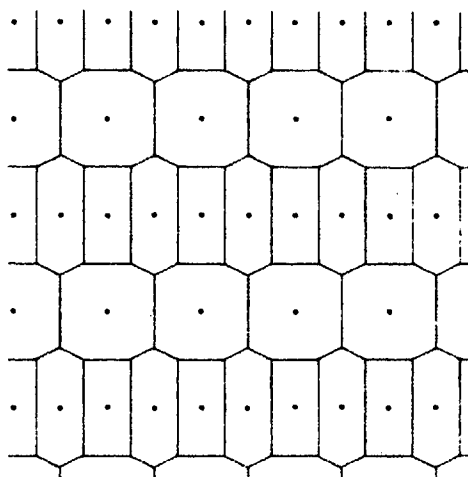


Figure 7.1.5 Voronoi diagram for sites belonging to three different sets of equivalent sites.

So far only a number of Voronoi polyhedra with 38 faces have been identified (Engel, 1981). One of these is illustrated in Figure 7.1.4(c). Other polyhedra with numbers of faces ranging from 17 to 37 have also been reported by a number of other researchers and these are reviewed in Grünbaum and Shephard (1980).

Conway and Sloane (1993, Chapter 21) extend the treatment of Voronoi regions for lattices in \mathbb{R}^m ($m \geq 4$). Interestingly, the Voronoi diagrams of these and other periodic structures can also be used to generate quasi-periodic tessellations, such as Penrose tilings, in lower dimensional space (Kramer and Schlottmann, 1989; Baake *et al.*, 1990). Their method, the Klotz construction, exploits a generalization of the projection described in Property D8 (see Sections 2.4 and 3.1.4) so that the resulting quasi-periodic tessellations are Laguerre tessellations (Schlottmann, 1993) (see Section 3.5).

Another alternative to a lattice which is sometimes encountered in crystallography occurs when the sites are not equivalent with respect to one or more point group operations but instead belong to k different sets of equivalent sites. In such instances the Voronoi regions form k different sets of mutually equivalent regions which together fill \mathbb{R}^m . An example in \mathbb{R}^2 for $k = 3$ is illustrated in Figure 7.1.5.

The lack of regularity and homogeneity in amorphous structures means that there is a much greater need to be able to characterize such materials at the individual atomic (ionic, molecular) level than for crystalline structures (Turnball and Polk, 1972; Jerauld *et al.*, 1984a). Since such structures often are modelled initially as collections of randomly packed spheres (or discs in \mathbb{R}^2), a related conceptualization is to consider them as packings of polyhedra by defining the Voronoi diagram of the set of sphere centres (see Figure 7.1.1(b)). While earlier work focused on non-overlapping (hard), equal-sized spheres, models involving overlapping (soft) spheres and variable-sized spheres have been developed. In the latter instance, the power diagram or Laguerre Voronoi diagram (see Sections 3.1.4 and 3.5.3) (Mackay, 1981, 1983, 1986; Gellatly and Finney, 1982b, 1982c; Richards, 1985; Baranyai and Ruff, 1986; Mackay and Klinowski, 1986; Rivier, 1987, 1991, 1993; Finney, 1991, 1993; Gervois and Bideau, 1993; Annic *et al.*, 1994; Aparicio and Cocks, 1995; Van der Marck, 1996), the Voronoi diagram for a set of circles (spheres) (see Section 3.5.3) (Medvedev, 1994; Anishchik and Medvedev, 1995; Goede *et al.*, 1997) and the multiplicatively-weighted Voronoi diagram (see Section 3.1.1) (Gerstein *et al.*, 1995) have been suggested as being more appropriate than the ordinary Voronoi diagram. Another alternative, known as *Richards' method B* (Richards, 1974), is encountered in protein studies where it is considered to be a 'Voronoi procedure' (Chothia, 1975; Gellatly and Finney, 1982b; Harpaz *et al.*, 1994; Gerstein *et al.*, 1993, 1995; Gerstein and Chothia, 1996). However, since the polyhedra are constructed using planes which perpendicularly bisect the line segment joining two sphere centres in proportion to their respective radii, small, unallocated tetrahedrons are created near each polyhedral vertex so that the resulting structure is not a tessellation.

Others have suggested that it is preferable to represent such packings by means of the dual Delaunay tessellation (e.g. Smith, 1964; Ogawa and Tanemura, 1974; Finney and Wallace, 1981; Hiwatari *et al.*, 1984), especially if the focus of investigation is on the nature of the pore space within the packing rather than on the atoms themselves (Medvedev and Naberukhin, 1987b; Medvedev *et al.*, 1988, 1989, 1990; Voloshin *et al.*, 1989; Medvedev, 1990; Finney, 1991; Bryant and Blunt, 1992).

Voronoi polyhedral models have been extensively applied, especially in the study of liquids, glasses, and proteins. Illustrative studies of both general and specific kinds are summarized in Table 7.1.1.

Once a structure is represented as either a Voronoi diagram or a Delaunay tessellation, various metric and topological characteristics of the constituent polyhedra or simplices, or measures derived from them (Gervois and Bideau, 1993; Blatov *et al.*, 1995) can be used to differentiate between structures. For example, polyhedron (or tetrahedron) volume V and surface area S are frequently examined either individually (e.g. Rapaport, 1983; Schnitker and Mausbach, 1990; Gotoh, 1993; Finney, 1993; Gil Montoro and Abascal, 1993; Shih *et al.*, 1994; Niemelä *et al.*, 1996; Jund *et al.*, 1997) or jointly in dimensionless measures (Kimura and Yonezawa, 1984; Nose and Yonezawa, 1986; Rigby and Roe, 1990; Ruocco *et al.*, 1991; Gil Montoro and Abascal, 1993; Shih *et al.*, 1994). For Voronoi polyhedra, Ruocco *et al.* (1991) and Shih *et al.* (1994) suggest using an asphericity measure defined by

$$\eta = \frac{S^3}{36\pi V^2}. \quad (7.1.3)$$

The minimum value ($\eta = 1$) occurs for a sphere while values for the Voronoi polyhedra of the three cubic lattices discussed above are 1.33 (body centred cubic, truncated octahedron), 1.35 (face centred cubic, rhombic dodecahedron), and 1.91 (simple cubic, cube).

The topological characteristics of Voronoi polyhedra include the number of faces/polyhedron F , the number of edges/face N and the full topological index proposed by Finney (1970a) (see also Tanemura *et al.*, 1977; Hsu and Rahman, 1979b; Cape *et al.*, 1981; Bushnell-Wye *et al.*, 1982; Kimura and Yonezawa, 1984; Medvedev *et al.*, 1986; Medvedev and Naberukhin, 1987a; Watanabe and Tsumuraya, 1987; Rigby and Roe, 1990; Finney, 1993; Tsumuraya *et al.*, 1993; Blatov and Serezhkin, 1997). This involves describing the local configuration of an atom a_i , with associated Voronoi polyhedron, $V(a_i)$, with f_i faces, by listing the number of faces, $n_3, n_4, n_5, \dots, n_j$, having $3, 4, 5, \dots, j$ edges, where $\sum_{k=3}^j n_k = f_i$. Re-analysis of previously published results relating to argon (Rahman, 1966; Finney, 1970b; Tanaka, 1986b; Medvedev and Naberukhin, 1987a), rubidium (Tanaka, 1986a), and super-cooled water (Ruocco *et al.*, 1991) led Kumar *et al.* (1997) to propose using the coefficient of variation of F as a descriptor of topological disorder which is particularly effective in studying solid-liquid-glass transitions.

For Delaunay simplices, measures such as volume (Voloshin *et al.*, 1989), circumradius (Hitawari *et al.*, 1984; Medvedev and Naberukhin, 1987b;

Table 7.1.1 Studies involving Voronoi diagrams of packing of spheres.

Application		Disc(2)/sphere(3) hard(h)/soft(s) equal(e)/variable(v)		Reference
General	2/3	h e		Ogawa and Tanemura (1974)
	3	h e/v		Medvedev (1994)
Dense packings	3	h e		Bernal and Finney (1967)
	3	h/s e		Medvedev and Naberukhin (1987b)
Lower density random packings	3	h e		Bernal and King (1967)
Different random configurations	2	h e		Gotoh (1993)
Air cushion table	2	h e		Lemaître <i>et al.</i> (1991, 1993)
	2	h v		Gervois <i>et al.</i> (1992)
				Lemaître <i>et al.</i> (1992)
Porous media	2	h e		Annic <i>et al.</i> (1994)
	3	h e		Chan and Ng (1988)
				Vretos <i>et al.</i> (1989a)
Percolation	3	s e		Roberts and Schwartz (1985)
	3	s v		Vretos <i>et al.</i> (1989b, 1990)
Hollow fibre modules	2	h e		Bryant and Blunt (1992)
Ostwald ripening	2	h e		Kerstein (1983)
Crystallization	3	h e		Van der Marck (1996)
	3	s e		Chen and Hlavacek (1994)
	3	s e		Rogers and Long (1997)
Melting	2	h e		Masbaum (1995)
	3	h e		Hsu and Rahman (1979b)
Entropy of melting	3	h e		Tanemura <i>et al.</i> (1977)
Liquids	3	h e		Cape <i>et al.</i> (1981)
				McTague <i>et al.</i> (1980)
Monatomic liquids	3	h e		Weber and Stillinger (1981)
	3	h e		Allen <i>et al.</i> (1983)
	3	h e		Hsu and Mou (1992)
High density liquids	3	h e		Rivier and Duffy (1982)
Supercooled liquids	2	h e		Kimura and Yonezawa (1984)
Liquid water	3	s e		Medvedev <i>et al.</i> (1988, 1989)
	3	h e		Gil Montoro and Abascal (1993)
				Bernal (1959, 1964)
	3	h e		Smith (1964)
	3	h e		Collins (1967)
	2/3	h e		Collins (1968, 1972)
	3	h/s e		Finney (1970a,b)
	3	h e		Brostow and Sicotte (1973)
	3	h e		Krishnamurthy <i>et al.</i> (1988)
	2	h e		Glaser and Clark (1990)
	3	s e		Tanemura <i>et al.</i> (1977)
	3	h e		Schnitker <i>et al.</i> (1986)
Liquid water, liquid hydrogen sulphide	3	h e		Schnitker and Mausbach (1990)
Supercooled water	3	h e		Shih <i>et al.</i> (1994)
Mobility of stretched SPC/E water	3	h e		Rapaport (1983)
Pure dimethylsulphide (DMSO), water-DMSO mixtures	3	h e		Vaisman <i>et al.</i> (1993)
Electrolyte solutions	3	h e		Vaisman and Berkowitz (1992)
Lennard-Jones system (argon)	3	h/s e		Gil Montoro <i>et al.</i> (1994)
				Barker <i>et al.</i> (1975)
				Medvedev <i>et al.</i> (1986)
				Nose and Yonezawa (1986)
				Medvedev and Naberukhin (1987a)
				Medvedev <i>et al.</i> (1988, 1989)
				Voloshin <i>et al.</i> (1989)

Table 7.1.1 cont.

Application		Disc(2)/sphere(3) hard(h)/soft(s) equal(e)/variable(v)		Reference
Liquid argon	3	h e		Brostow and Sicotte (1975) Tanaka (1986b)
Liquid and crystalline argon	3	h e		Galashev and Skripov (1980)
Liquid and quenched rubidium	3	h e		Hsu and Rahman (1979a,b) Tanaka (1986a,b) Medvedev (1990)
Molten rubidium chloride, lithium iodide	3	h v		Medvedev <i>et al.</i> (1990) Baranyai and Ruff (1986)
Molten cryolite (Na_3AlF_6)	3	h e		Liška <i>et al.</i> (1995)
Crystallization and glass formation in liquid sodium	3	h e		Watanabe and Tsumuraya (1987)
Liquids and glasses	3	h e		Finney (1975a)
Rapidly quenched liquids and glasses	3	h/s e		Hitawari <i>et al.</i> (1984)
Polymer liquid and glass	3	h e		Rigby and Roe (1990)
Glassy polysulfones	3	h e		Niemalà <i>et al.</i> (1996)
Glasses	3	h e		Rivier (1983a, 1985b)
Metallic glass	3	s e		Finney and Wallace (1981)
	3	h e		Rivier (1987)
Pd ₄ Si	3	h v		Troadec and Dodds (1993) Gellatly and Finney (1982c)
Silicon glass	3	h e		Tsumuraya <i>et al.</i> (1993)
Amorphous silicon or germanium	3	h e		Krishnamurthy <i>et al.</i> (1988)
Amorphous silica	3	h e		Rustad <i>et al.</i> (1991a,b)
Calcium aluminosilicate glasses	3	h e		Liška <i>et al.</i> (1995)
Glass transition	3	h e		Jund <i>et al.</i> (1997)
Granular media	2	h e/v		Gervois and Bideau (1993)
Sintering of fine particles	3	h e/v		Aparicio and Cocks (1995)
Densification of powders by cold compaction, hot-isostatic pressing and sintering	3	h e		Arzt (1982)
Zirconia nanocrystals	3	h v		Ogawa <i>et al.</i> (1996a, 1997)
Al-10% (by weight) Si binary alloy	2	h e		Brockenbrough <i>et al.</i> (1992)
Pd-Si alloys	3	h e		Ohkubo and Hirotsu (1996)
Cu ₅₇ Zr ₄₃ alloy	3	h e		Kobayashi <i>et al.</i> (1980)
Proteins	3	h e		Chothia (1975) Finney (1975b) Pontius <i>et al.</i> (1996)
Globular proteins	3	h e		Finney <i>et al.</i> (1980)
Lysozyme and ribonuclease S	3	h v		Richards (1974) Finney <i>et al.</i> (1980)
Ribonuclease S	3	h e		Finney (1978)
	3	h e/v		Gellatly and Finney (1982b)
Myoglobin	3	h e		Procacci and Scateni (1992)
	3	h v		Richards (1979)
Pancreatic trypsin inhibitor	3	h v		Richards (1979) Finney <i>et al.</i> (1980) Gerstein <i>et al.</i> (1995)
Lactoferrin	3	h v		Goede <i>et al.</i> (1977) Gerstein <i>et al.</i> (1993)
Protein-water interface	3	h v		Gerstein and Chothia (1996)
Protein folding	3	h v		Harpaz <i>et al.</i> (1994)

Note: Studies categorized as involving equal (e) spheres include those which recognize more than one type of sphere but which do not take this into account in constructing the Voronoi diagram (i.e. the ordinary Voronoi diagram is used rather than a generalized Voronoi diagram).

Voloshin *et al.* 1989; Medvedev *et al.*, 1990), edge lengths (Hiwatari *et al.*, 1984; Nose and Yonezawa, 1986; Finney, 1993; Masbaum, 1995), and solid angles (Kimura and Yonezawa, 1984) can be used. For instance, Hiwatari *et al.* (1984) propose characterizing the shape of a Delaunay simplex using an irregularity parameter

$$\delta = \frac{1}{6\bar{l}} \sum_{i=1}^6 l_i - \bar{l}, \quad (7.1.4)$$

where l_i is the length of the i th edge, and \bar{l} is the average edge length of the given simplex. However, since analyses of computer models of dense random packings of monotonic systems of spheres show that most Delaunay simplices are close in shape to either the perfect tetrahedron or a quarter of a perfect octahedron (Finney and Wallace 1981), Medvedev *et al.* (1988, 1989) (see also Medvedev and Naberukhin, 1987a,b; Voloshin *et al.*, 1989; Medvedev, 1990; Medvedev *et al.*, 1990; Vaisman and Berkowitz, 1992; Vaisman *et al.*, 1993, 1994) suggest focusing on measures such as

$$T = \frac{1}{15\bar{l}^2} \sum_{i>j} (l_i - l_j)^2 \quad (7.1.5)$$

and

$$O = \frac{1}{10\bar{l}^2} \sum_{i>j, i,j \neq m} (l_i - l_j)^2 + \frac{1}{5\bar{l}^2} \sum_{i \neq m} \left(l_i - \frac{l_m}{\sqrt{2}} \right)^2, \quad (7.1.6)$$

where l_m is the length of the maximum edge of the given simplex, which for an ideal octahedral simplex is $\sqrt{2}$ times longer than the rest of the equal edges. For a perfect tetrahedron $T = 0$, while $O = 0$ for a perfect octahedron.

In packings of hard spheres the proportion of the volume of the structure contained within the spheres is referred to as the *atomic volume* or the *packing fraction* of the material, or the *density of the packing*. A long believed but still unproven conjecture holds that the densest packing of equal sized spheres in \mathbb{R}^3 occurs when the sphere centres form a face centred cubic lattice (density = $\pi/\sqrt{18} = 0.74048$). In other situations it may be possible to increase the packing fraction of the initial packing. One way of doing this is to expand each sphere within the Voronoi region defined by its centre until the sphere touches one or more of the faces of the Voronoi region. Of course, the sizes of the resulting spheres are no longer equal. Anishchik and Medvedev (1995) present a more general sequential procedure for progressively increasing the packing fraction of variable-sized spheres. At each step, the locations of the centres of the new spheres are determined by the Voronoi vertices of the Voronoi diagram of existing spheres. Bieshaar *et al.* (1995) use a similar procedure to identify suitable locations to insert a non-overlapping test particle to calculate the excess chemical potential of a system of interacting particles. If the particles are represented by equal-sized spheres, each Voronoi vertex is simultaneously the circumcentre of the Delaunay simplex associated with the vertex and the centre of the largest sphere which can be inscribed inside the four spheres whose centres are the vertices of the

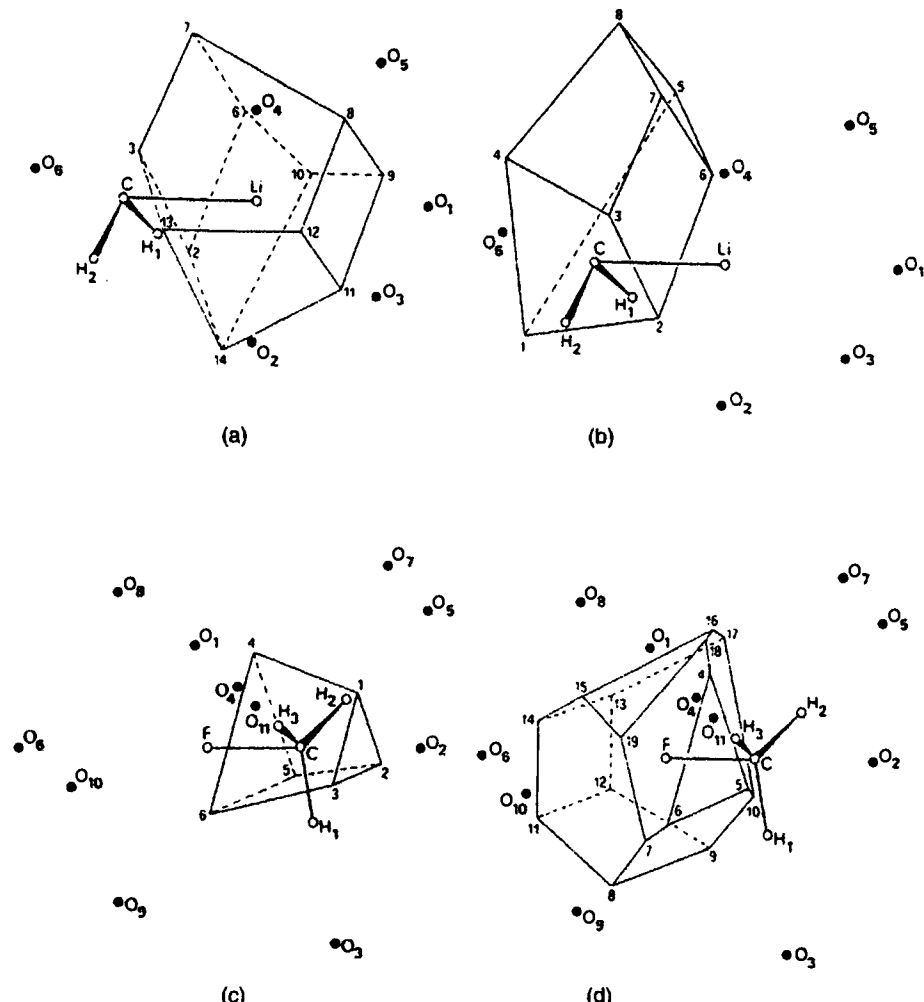


Figure 7.1.6 Voronoi polyhedra for different types of atoms in solvation structures: (a) lithium and (b) carbon atoms for $\text{CH}_2\text{Li}^+(\text{H}_2\text{O})_6$; (c) carbon and (d) fluorine atoms for $\text{CH}_3\text{F}(\text{H}_2\text{O})_{11}$. Filled circles represent the positions of oxygen atoms of water molecules. (Source: Bellagamba *et al.*, (1985, Figures 1 and 4.)

Delaunay simplex (Medvedev, 1994). Such locations are selected as test sites provided that there is sufficient free volume in the Delaunay simplex in which to insert a spherical test particle.

In Voronoi diagrams defined for centres of unit circles in the plane, the smallest Voronoi polygon is the regular hexagon and the smallest n -sided Voronoi polygon ($n \leq 6$) is a regular n -gon (superscribing a unit circle) with an area, a_n , of $n \tan(\pi/n)$. For $n > 6$, the smallest n -sided Voronoi polygon is not regular and there is no known formula for a_n . However, Muder (1990)

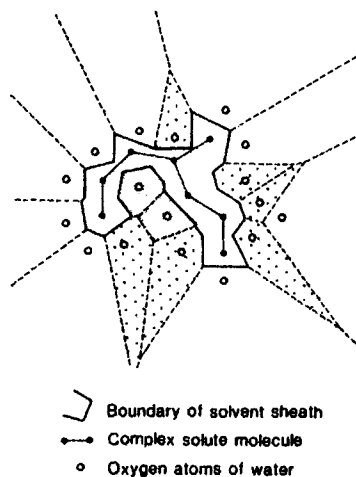


Figure 7.1.7 Identification of solvent accessible cleft regions of a solute. Stippled areas indicate molecules on the dimple region of the solvent; cross-hatched areas indicate molecules occupying a true cleft.

derives expressions for the upper and lower bounds on a_n from which he concludes that $a_n/n \rightarrow 1/\pi$. For packings of equal spheres in \mathbb{R}^3 , it is widely believed, but not proven, that the smallest Voronoi polyhedron is the regular pentagonal dodecahedron, although such polyhedra are incapable of filling space. Muder (1988) proves that the optimal face of a Voronoi polyhedron is a regular pentagon slightly smaller than the faces of the regular dodecahedron. He also shows that for the packing density to be maximized, the best three- and four-sided faces are regular triangles and quadrilaterals, respectively.

The Voronoi concepts used above to study monatomic liquids have also been extended to non-monatomic ones. One instance is the modelling of solution structures consisting of a combination of a solvent and a solute, with particular attention being given to aqueous solutions. Initially, David and David (1982b) proposed constructing the Voronoi polyhedron of each atom of the solute using the oxide anions of the solvent water and the other atoms of the solute. Later they extended the construction of the Voronoi polyhedra to include the protons of the solvent as well (David and David, 1982c). Once defined, the Voronoi polyhedra of the atoms of the solute can be used in a variety of ways. First, the union of the polyhedra of the atoms of the solute can be considered to be the *solvent sheath* (i.e. the region that contains the solute as its interior region) (see Figure 7.1.7). The volume of the solvent sheath so defined can be considered to be the co-volume of the solvent as measured by water while the area of its external faces measures the extent to which each solvent molecule coordinates each atom of the solute (David and David, 1983; Bellagamba *et al.*, 1985). The properties of

different solvents can be studied by examining the corresponding solvent sheaths (Bellagamba *et al.*, 1985) or differences in the shapes and volumes of the Voronoi polyhedra of the solute atoms (Bellagamba *et al.*, 1986). Figure 7.1.6 shows the Voronoi polyhedra for the different types of atoms for two different solvation structures.

The Voronoi diagram can also be used to divide the solvent into subsets. For example, in their study of highly polar fluids, Neumann *et al.* (1978, 1979) use Voronoi polyhedra to define two concentric regions around a giant dipole. Similarly, Abseher *et al.* (1996) investigate the influence exerted by the globular protein ubiquitin on the solvent dynamics in its vicinity using three subsets: a first solvation shell (equivalent to the solvent sheath), a second solvation shell consisting of the Voronoi polyhedra surrounding the first hydration shell, and the remaining bulk. Vaisman *et al.* (1994) establish a similar division when they use T , the tetrahedrality measure for Delaunay simplexes described in equation (7.1.5), to show how the structure of water changes with distance from methane and ammonium ions.

David and David (1982a) also propose using the Voronoi construction to determine if a given atom is a member of a set of solute atoms forming a single cluster in a solvate. An atom is considered to be a cluster member only if its Voronoi polyhedron, as defined using the other atoms of the set and the atoms of the solvent, is closed. David (1984) also suggests that the solvent accessible cleft regions of a solute can be identified using Voronoi concepts. The approach is illustrated in Figure 7.1.7, which for convenience shows a two-dimensional representation of a complex of solute molecules (shown by filled circles) solvated by water molecules (shown by unfilled circles). The union of the Voronoi polygons of the solute atoms constitutes the solvent sheath. If we consider the Voronoi polyhedra of the water molecules which are adjacent to the solvent sheath we observe that these may be either open or closed. The open Voronoi polygons can be considered as the surface solvating water molecules while the closed Voronoi polygons are of two types. Some (those shown stippled in Figure 7.1.7) exist because the molecule is, at least partially, on the dimple region of the solvent while others (those shown cross-hatched in Figure 7.1.7) occupy a true cleft of the solute molecules. Such clefts represent regions where solute molecules may come into contact as a result of the elimination of the intervening solvent. David (1986) suggests that this touching, the so-called 'docking problem' of biology, can be recognized when one or more of the faces of the Voronoi polyhedra of the solute molecules are shared with those of polyhedra of other solute molecules. This procedure is implemented in an application involving the insertion of a NAM-NAG-NAM molecule in the cleft of hen egg white lysozyme (David, 1988b). Lewis (1989) also uses clefts defined by the Voronoi diagram of the centres of atoms of a receptor to identify putative binding sites for use in computer-aided drug design.

Drug design is one instance of the more general problem of understanding the specific binding of small molecules to biological receptors. In this context Crippen and his associates (Crippen, 1984, 1987, 1995; Boulu and Crippen,

1989; Boulu *et al.*, 1990) have developed and refined a *Voronoi site model*. Given the observed binding energies for a series of compounds, the goal of the model is to attempt to deduce the structure and energies of a binding site. Specifically, the atoms of a ligand molecule are represented as a collection of points in space, and site geometry is modelled as the Voronoi regions of a set of generating points supplied by the investigator. Thus, every atom of the ligand molecule lies in one and only one Voronoi region and the orientation and internal configuration of a particular binding mode can be expressed by stating the Voronoi region in which each atom is found. Whenever a ligand atom lies in a Voronoi region of a site it is considered to be in contact and the contact makes an additive contribution to the total binding energy. Once all geometrically and conformationally allowed binding modes are identified, solutions with the minimal number of site points which simultaneously offer the greatest number of energetically satisfactory binding modes allowed for each molecule are searched for. Applications of the model to investigations of binding include studies of cocaine analogues at the cocaine receptor sites on the dopamine transport system (Srivastava and Crippen, 1993; Crippen, 1995), triazines and pyrimidines to *L. casei* dihydrofolate reductase (Bradley and Crippen, 1993), and steroid molecules to corticosteroid and testosterone-binding human globulin (Schnitker *et al.*, 1997).

Voronoi concepts have also been used extensively in modelling metallurgical structures. This is because one prevalent approach used in quantitative metallography involves the identification of microstructural characteristics, their measurement, and the deduction of empirical relationships linking these characteristics to the physical and mechanical properties of the material (Lantuejoul, 1980; Burger *et al.*, 1990). Furthermore, many of the processes which affect such structures operate at the local level. Examples include competition between heterogeneous flow and decohesion and the development of recrystallization nuclei during plastic flow (Burger *et al.*, 1988). In particular, the Voronoi Assignment Model has been employed to characterize the structure of second-order particles in metals by considering the particles as points and defining their Voronoi diagram (Wray *et al.*, 1983; Koken *et al.*, 1988; Stone and Tsakirooulos, 1995). Examples include sulphide inclusions and carbides in steels and graphite fibres in aluminium (Spitzig *et al.*, 1985) and non-metallic inclusions in Ti-V microalloyed steel under different conditions (Shehata and Boyd, 1988; Vander Voort, 1992). Pyrz (1994) uses the same approach to analyse the distribution of fibres in a glass/epoxy composite.

Another metallurgical application is involved in modelling the accumulation of structural damage in materials subjected to stress at elevated temperatures. In such situations, voids which nucleate on grain boundaries grow and subsequently coalesce causing fracture. One input parameter required by void growth models developed so far is the area, A_i , of the grain boundary affected by a given void, v_i , over which local stress occurs. Wilkinson (1988a, b) used the area of the Voronoi polygon of v_i as a measure of A_i .

The Voronoi Assignment Model has also been used in studies of submonolayer film growth, such as the epitaxial growth of semiconductors and metals and the non-epitaxial growth of metals on amorphous substrates. Here growth theories define initial regions in which the density of isolated atoms on the surface, called monomers, increases linearly with time until small islands begin to nucleate. As deposition continues, the density of the islands eventually exceeds that of the monomers. The process then enters an aggregation phase during which diffusing monomers are captured by existing islands. This process terminates once the islands start to coalesce. Following initial work by Venables and Ball (1971), Mulheran and Blackman (1995, 1996) and Blackman and Mulheran (1996) suggest that during the aggregation phase, the region from which an island acquires the monomers responsible for its growth, i.e. its capture zone, can be modelled by a Voronoi cell of the island. The particular form of the cell depends on whether the growth process is considered to be heterogeneous or homogeneous. In the former instance, the island can be represented by a central point and the ordinary Voronoi diagram is constructed, while in the latter it is represented as a circle whose radius is proportional to the number of monomers it has absorbed and the Voronoi diagram for a set of circles is constructed (see Section 3.5.3).

Ever since Honda *et al.* (1979) and Saito (1982) observed that Voronoi polygons closely approximate a variety of monolayer cells and epithelial cells in tissue, the Voronoi Assignment Model has been used increasingly in such applications. For example, Roudot *et al.* (1990) use the Voronoi diagram as the basis of a model of apple tissue while Weliky and Oster (1990) use it to determine the initial configuration of cell shapes and sizes in a model of morphogenesis in epithelial sheets. However, most applications involve animal and human tissues. These include modelling the distribution of both capillaries and fibres in transverse sections of muscle tissue. In the former, Voronoi polygons (here referred to as *capillary domains*) are defined with respect to capillaries represented as points (Hoofd *et al.*, 1985; Egginton *et al.*, 1988; Egginton and Ross, 1989b; Batra and Rakusan, 1991). Adjacencies of the Voronoi polygons in the resulting Voronoi diagram provide identification of neighbouring capillaries. A mean inter-capillary distance can then be defined for neighbouring capillaries which is a basic input parameter in models of oxygen transport in tissues (Egginton and Ross, 1989a; Egginton *et al.*, 1987). In this instance, the assumptions involved in the Voronoi Assignment Model are equivalent to assuming that the capillaries possess equal transport capacity and that they have equal levels of partially pressurized oxygen (Egginton, 1990). Thus, the models are most appropriate for muscle consisting of a single fibre type such as cardiac muscle (Turek *et al.*, 1986) and skeletal muscle for fish (Egginton *et al.*, 1987). Egginton (1990) provides a comprehensive review of this area of application.

Two types of fibre (slow-twitch and fast-twitch) occur within muscles and their spatial arrangement is considered to be an indicator of possible abnormalities. To follow this line of investigation it is necessary to determine which

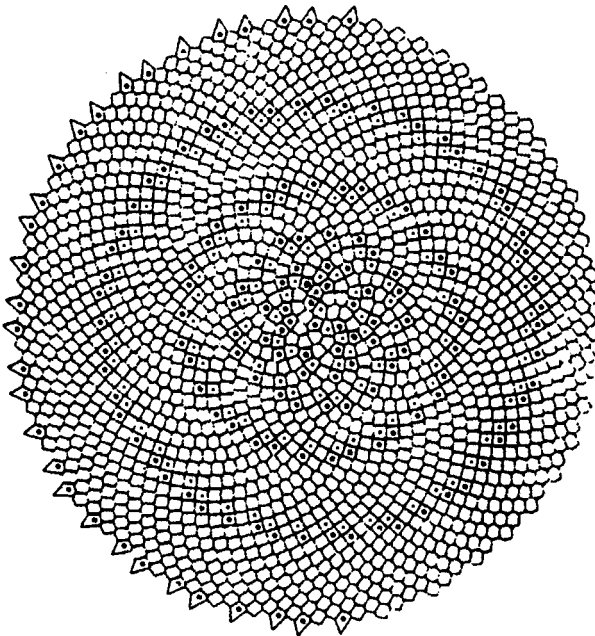


Figure 7.1.8 Simple daisy structure. (Source: Rivier *et al.*, 1984, Figure 6.)

fibres are neighbours. If the muscle fibres are represented as points located at fibre centroids, Paton and Zucker (1983) suggest that the Gabriel graph (see Section 2.5) be used to define neighbours, while Pernus (1988) proposes a spectrum of graphs which has the Gabriel graph and the Delaunay tessellation as its limits (see Section 8.4.2). Alternatively, Venema (1991) represents each fibre as a circle of equivalent area centred on the fibre centroid and uses the adjacency relationships in the power diagram (see Section 3.1.4) to define neighbours. Another possible indicator of abnormality is fibre shape, with healthy fibres being approximately hexagonal. Thus, Taylor *et al.* (1995) and Dryden *et al.* (1997) suggest generating the Delaunay triangulation of the fibre centroids and examining the degree to which the resulting triangles depart from equilateral ones (see Section 8.2).

Similar procedures have been used to investigate cancer cells. In a study of primary lung carcinoma, Kayser and Stute (1989) construct the Voronoi diagram of the geometric centres of cell nuclei in sections of surgical lung specimens and show that properties of the Voronoi polygons can be used to separate benign from malignant adenomatous tumours. Darro *et al.* (1993) use Voronoi diagrams defined in the same way to model the cell dynamics of human LOVO and HCT-15 colorectal neoplastic cell colonies growing in histological slides. Famiglietti (1992) also uses Voronoi polygons as one means of assessing the influence of the structural organization of Type 1 polyaxonal (PA1) amacrine cells in rabbit retina on their possible functionality.

We have already noted the use of Voronoi Assignment Models in studying periodic structures in chemistry. They have also been used in modelling a different type of periodicity which occurs in biology in phyllotaxis, the spiralling close packed arrangement of florets in composite plants such as daisies, asters and sunflowers and the scales of a pine cone or pineapple where successive florets are either identical or have a structure which can be obtained from the previous one. Rivier (1986c, 1988) and Rivier *et al.* (1984) have modelled the individual florets as Voronoi regions created with respect to points located on a parabolic spiral. Label the individual florets with positive integers ($i = 1, 2, \dots$) with the magnitude of the integer reflecting the age of the floret. If the stem is the origin of the coordinate system, the polar coordinates (r_i, θ_i) of the generator point of a floret are $r_i = ai^{1/2}$ and $\theta_i = 2\pi\alpha i$, where a is the average linear dimension of a floret (with area πa^2) and α ($0 < \alpha < 1$) is a parameter of the structure. Thus, the florets are generated at regular intervals from the stem and at a given angle $2\pi\alpha$ from each other. Rivier *et al.* (1984) and Rivier (1986c, 1988) prove that, in order to create florets which are as uniform as possible in terms of size and shape (expressed by the number of edges of the floret), α must be an irrational number (rational α produces a spider web-like structure) of the form

$$\alpha = 1 \{ q_1 + 1 / [q_2 + 1 / (q_3 \dots)] \},$$

where q_j are positive integers. The simplest solution occurs when $q_j = 1$ for all j and $\alpha \approx 0.618$ which is also equal to the reciprocal of the golden mean $([1 + \sqrt{5}]/2)$. This structure is illustrated in Figure 7.1.8.

There is also extensive use of the Voronoi Assignment Model in both plant and animal ecology. Indeed, this application represents yet another area in which Voronoi polygons were discovered independently; not once but twice! Brown (1965) defined what he called the *area potentially available* (APA) to a plant which, as Jack (1967) recognized, is equivalent to the Voronoi polygon of the plant. Later Mead (1966, 1967, 1971) defined the same region labelling it the *plant polygon*. The polygon adjacencies in the Voronoi diagram of a set of plants (or trees) are used to define the neighbours of a given plant (Reed and Burkhardt, 1985; Kenkel *et al.*, 1989), while the Voronoi polygon associated with an individual plant is considered an indicator of the portion of the environment available to that plant. Since interactions between plants are localized, the characteristics of the Voronoi polygons of a plant and its neighbours can be used in studying aspects of the plant's performance including survival rate, growth rate, size and weight (Kenkel, 1990). Examples of such studies are provided by Hasegawa *et al.* (1981), Liddle *et al.* (1982), Watkinson *et al.* (1983), Bulow-Olsen *et al.* (1984), Mithen *et al.* (1984), Hutchings and Waite (1985), Matlack and Harper (1986), Firbank and Watkinson (1987), Kenkel *et al.* (1989), Owens and Norton (1989), and Zhang and Hamill (1997). In a comparative evaluation of the ability of a wide range of competition measures to predict the growth of loblolly pine trees, Daniels *et al.* (1986) find that the Voronoi polygon approach performs at least as well

as the other measures and is particularly effective when other tree and stand characteristics are known.

Given the assumptions of the Voronoi Assignment Model the most appropriate applications are to monospecific stands of upright plants with simultaneous germination (Mithen *et al.*, 1984) especially in the first few months after germination when individual plant growth rates are most similar, thus ensuring that most plants are of approximately the same size (Matlack and Harper, 1986). When these conditions do not hold, a weighted Voronoi diagram may be appropriate with weights reflecting, for example, differences in tree diameters (Moore *et al.*, 1973; Zuuring *et al.*, 1984; Nance *et al.*, 1987), tree heights (Pelz, 1978), or plant germination times (Kenkel, 1991). Voronoi polygon models can also be used when more than one species of plant occupies the same environment, but since such models involve spatial competition, they are discussed in Section 7.4.

A variant of this use in plant ecology is provided by Hasegawa *et al.* (1981) in their study of the crown projection diagrams of trees in a forest. They propose that if identical trees develop uniformly in a uniform environment the crown projection diagram will be equivalent to a Voronoi diagram. To test this they construct the Voronoi diagram associated with the areal centres of gravity of the crowns of a stand of Japanese cedars (*Cryptomenia japonica*) and compare this with the actual crown projection diagram. A good measure of fit is found between the two diagrams, but some differences do exist because some degree of overlap and small unfilled areas are observed in the actual crown projection diagram which are not present in the Voronoi diagram.

Voronoi Assignment Models are also applicable to animal territories defined with respect to specific point locations such as nests, roosts and food caches (Tanemura and Hasegawa, 1980) while Byers (1992, 1996) uses Voronoi diagrams of points of entry to examine the spatial patterns of attack of different species of bark beetles on conifers.

Social scientists studying various types of territorial structures associated with humans have also made extensive use of Voronoi Assignment Models. Unlike many of their physical counterparts, human spatial patterns rarely show a high degree of regularity, although one celebrated instance occurs in geography in the context of *central place theory* (see King, 1984, for a review). This is concerned with explaining the size and spacing of nucleated settlements (central places) which provide goods and services to rural customers distributed over a geographical region. One aspect of this theory relates to the definition of the trade areas (areas of influence) associated with the central places for a specified good or service. In classical central place theory (Christaller, 1933; Lösch, 1954) the locations of the central places are assumed to form a triangular lattice (see Figure 8.2.2) and the rural population is assumed to be uniformly distributed over the region. In addition, it is assumed that

- (i) every central place provides the good or service under consideration;
- (ii) consumers travel to a central place to acquire the good or service;

- (iii) the market price, m , of the good or service is the same at all central places;
- (iv) the cost, c , to the consumer of acquiring the good or service is equal to the market price plus the cost of transportation, t , to the central place ($c = m + t$);
- (v) $t = rd$, where d is the Euclidean distance travelled by the consumer and r is the transportation rate per unit distance;
- (vi) customers minimize the cost of purchasing the good or service.

Taken collectively assumptions (ii)–(vi) imply that consumers will patronize the nearest central place. Thus, the trade areas are equivalent to the Voronoi polygons of the central places (Dacey, 1965) and in the case of classical central place theory they will be regular hexagons.

These concepts can be extended directly to situations involving any type of settlement spacing. Thus, Bogue (1949) and Snyder (1962) use the Voronoi Assignment Model to define Voronoi polygons around US metropolitan centres and Uruguayan urban centres, respectively, which are considered proxies for the real market areas of these centres. Ohji (1986) used them to define market areas for periodic markets in Kanataka State in southern India.

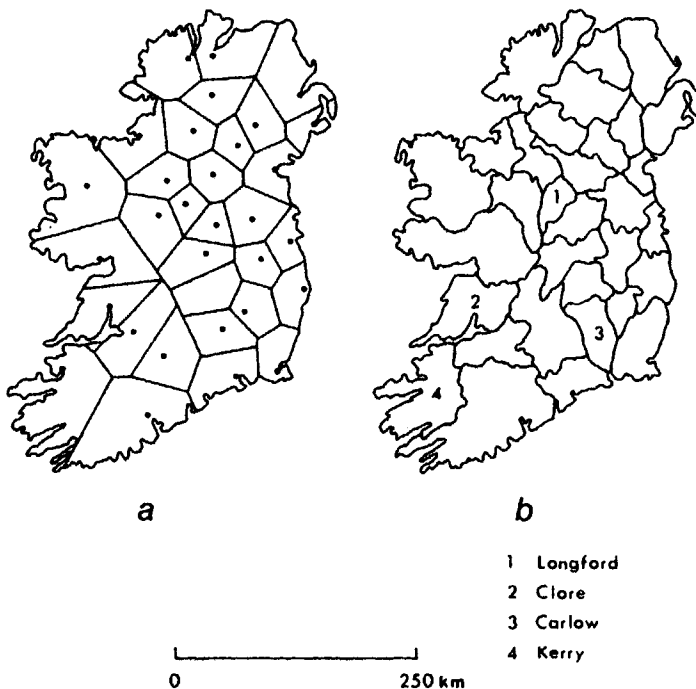


Figure 7.1.9 Counties of Ireland. (a) Theoretical partition created by the Voronoi diagram of county towns. (b) Actual counties. (Redrawn from data in Cox and Agnew, 1976.)

In each case the market areas so created correspond to areas over which the centres exercise a spatial monopoly. Identical concepts have been applied to a different geographic scale to model the trade areas of individual retail stores (West, 1981; Jones and Mock, 1984; West and von Hohenbalken, 1984; von Hohenbalken and West, 1984; Jones and Simmons, 1987). Polygon adjacencies in the Voronoi diagram of the stores can be used to identify which stores can be considered neighbours and thus are likely to be in direct competition.

Such considerations are also relevant in modelling the service areas of facilities providing public services. Suppose that we consider a set of facilities at fixed locations in a region which provide a service to a set of individual users distributed over the same region. The service may either be dispensed to the users at their locations or offered at the facility to which the users must travel. Obvious examples of such facilities are those providing public services such as health and education. If we assume that the facilities are identical, that there are no constraints on the number of people who can use a facility and that, in order to minimize costs of acquiring the service, users are served by the nearest facility, the service areas of the facilities will be equivalent to their Voronoi polygons (Goodchild and Massam, 1969; Keeney, 1972). Note that the last of these assumptions means that the aggregate distance travelled between users and facilities is minimized. This situation is usually referred to as the *unconstrained transportation problem* (Scott, 1971, p. 118; Keeney, 1972; Massam, 1972, pp. 9–10; 1975, pp. 59–60). While such a formulation may be unrealistic in empirical situations since facility constraints almost always occur and that, if allowed to choose, users do not always go to the nearest facility, the Voronoi diagram is often used as a normative structure against which the empirical or other proposed structures are evaluated. Goodchild and Massam (1969) follow such a strategy in evaluating the efficiency of electricity supply service areas in southern Ontario, Canada. Similarly, Cox and Agnew (1976) use the Voronoi diagram of the existing county towns of Ireland to create a theoretical partition (Figure 7.1.9(a)) against which the existing set of counties (Figure 7.1.9(b)) is compared. Using an information-theoretic measure, they determine that there is an overall spatial correspondence of 72% between the two structures. However, the measures of agreement between individual counties is quite variable being highest for large coastal counties such as Clare (92%) and Kerry (90%) and lowest for small inland counties such as Carlow (40%) and Longford (44%). Boyle and Dunn (1991) use Voronoi edges to approximate enumeration districts in England.

The Voronoi assignment model has also been used to determine various kinds of social boundaries. For example, Singh (1976, 1979), Singh and Singh (1975, 1977, 1978) and Callen and Stephan (1975) use the edges of the Voronoi diagram of village sites in the Middle Ghanga Valley in India and Bougainville Island in the Solomons, respectively, to simulate village boundaries. However, the most extensive work of this kind involves the identification of linguistic boundaries (isoglosses) and follows an approach

developed by Haag (1898) in a study of dialects in south-west Germany. He begins by generating the Voronoi diagram of a set of localities at which dialect data have been recorded. An edge of the Voronoi diagram is then 'decorated' if the two localities sharing the edge differ in terms of a dialect feature (e.g. the pronunciation of a particular word). In this way, highly decorated edges represent important linguistic divides and the resulting map is sometimes referred to as a *Kombinationskarte*. While the general idea of producing such a map (later called a *Wabenkarte* or *honeycomb*) became adopted widely, Haag's method of using the Voronoi diagram to determine the geographical location of the edges did not (see Handler and Wiegand, 1982, for review of the subsequent development of this approach). However, with the widespread availability of computer software for constructing the Voronoi diagram, Haag's method has experienced a resurgence in popularity (Goebl, 1981, 1983, 1987, 1993; Schlitz, 1996). Linguistic differences between neighbouring dialect data sites can also be represented by values attached to the edges of the Delaunay tessellation of these sites (Goebl, 1983). Oden *et al.* (1993) developed a procedure (categorical wombling) which uses several graph-theoretic statistics to determine if Delaunay edges linking dissimilar sites can be significantly configured into boundaries or if they tend to significantly enclose regions of homogeneous linguistic characteristics. Fortin (1994) has also employed this strategy to identify transition zones (ecotones) between adjacent communities in ecological data.

In archaeology, the Voronoi Assignment Model has been used to identify possible territorial structures of early civilizations by defining Voronoi polygons around significant sites. Examples include Iron Age (first century BC) southern England (Cunliffe, 1971; Lock and Harris, 1996), Minoan Crete (Renfrew, 1972), the Maya lowlands (Hammond, 1972, 1974), Roman Britain (Hodder, 1972), Malta (Renfrew, 1973b), Neolithic Wessex, England (Renfrew, 1973a), Mycenaean Greece and Etruria (Renfrew, 1975), the Late Archaic in the Savannah River valley of Georgia and South Carolina (Savage, 1990) and Aztec sites in the Basin of Mexico (Ruggles and Church, 1996). However, if the sites differ significantly, as would occur, for example, if they were part of a hierarchically organized social system, generalized Voronoi diagrams are more appropriate (see Section 3.1.6 for examples of such work).

The final application of the Voronoi Assignment Model to be discussed arises in the study of codes. In very general terms, coding involves the translation of a signal from one form to another (Agrell, 1997, p. v). In vector quantization the input signal has the form of a real valued vector x in m -dimensional Euclidean space \mathbb{R}^m and encoding involves examining a code book C , consisting of a finite set of codevectors c_i , to identify the codevector which best represents x (Agrell and Hedelin, 1994). This can be done by identifying the codevector which is geometrically closest to x , i.e. the one whose Voronoi region contains x . Since this procedure was labelled minimum distance or maximum likelihood coding (Shannon, 1959), when used in this context the Voronoi regions were originally referred to as *maximum likelihood regions* (Slepian, 1965, 1968). Essentially the same problem occurs in

decoding when a receiving device must search a set of possible transmitted signals to determine the one which underlies the observed signal (Landau, 1971). The most frequently used measure of the error resulting from quantization, the mean squared error, or distortion D , per vector can be expressed in terms of Voronoi regions (Agrell and Eriksson, 1998) as

$$D = \sum_{i=1}^N \int_{V(c_i)} \|x - c_i\| f_x dx, \quad (7.1.7)$$

where N is the number of codewords; $V(c_i)$ is the Voronoi region of c_i ; and $f_x dx$ is the probability density function of the input vectors x .

A well-known conjecture in quantization theory (Gersho, 1979) states that when the number of codevectors is sufficiently large, the optimal vector quantizer for a uniformly distributed x will consist of Voronoi regions almost all of which (the exceptions are due to edge effects) are congruent to some polytope H . Consequently, attention has focused on structured codes whose Voronoi regions possess this quality. Such codes include those based on modified lattices (Agrell and Eriksson, 1998; Baranovskii, 1991; Conway and Sloane, 1982, 1983, 1984, 1991, 1992, 1993; Eriksson and Agrell, 1996; Gersho, 1979, 1982; Moody and Patera, 1995; Viterbo and Biglieri, 1996; Worley, 1987, 1988) and block codes (Agrell, 1996, 1997; Shannon, 1959). Note that when a lattice is used as a vector quantizer for uniformly distributed input vectors, D in equation (7.1.7) is equal to the normalized second moment of inertia of the Voronoi cell of the lattice.

A (m, k) binary linear block code consists of 2^k codewords each of which is a block of m bits. When the values 0 and 1 are considered as coordinates, the codewords lie on the vertices of a hypercube, whose centre $(1/2, \dots, 1/2)$ is the one and only vertex of all Voronoi regions (i.e. the Voronoi regions are conical). In this case, all regions are the same shape and those that are Voronoi neighbours are also Gabriel (full) neighbours (Agrell, 1996, 1997). Binary linear block codes are part of a larger class of codes known as group codes (Slepian, 1965, 1968) which in turn are included in the class of geometrically uniform codes (Forney, 1991). This group also includes lattice-based codes and spherical codes (Gao *et al.*, 1988). General properties of the Voronoi regions of group codes and geometrically uniform codes are given by Slepian (1968) and Forney (1991), respectively.

The use of the Voronoi Assignment Model to address problems in coding can also be extended to conceptually similar situations such as re-sampling in remote sensing when values from spatially irregularly sampled sites must be converted to values at grid sites (Gotsman and Lindenbaum, 1995).

7.2 GROWTH MODELS

These models produce spatial patterns as the result of a simple growth process operating with respect to a set of n points (nucleation sites), $P = \{p_1, p_2, \dots, p_n\}$, at positions x_1, x_2, \dots, x_n , respectively, in \mathbb{R}^m or a bounded

region of \mathbb{R}^m ($m = 2, 3$). If we make the following assumptions, the resulting pattern will be equivalent to the ordinary Voronoi diagram, $\mathcal{V}(P)$, of P :

Assumption VGM1 Each point p_i ($i = 1, 2, \dots, n$) is located simultaneously.

Assumption VGM2 Each point p_i remains fixed at x_i throughout the growth process.

Assumption VGM3 Once p_i is established, growth commences immediately and at the same rate, l_i , in all directions from p_i .

Assumption VGM4 l_i is the same for all members of P .

Assumption VGM5 Growth ceases whenever and wherever the region growing from p_i comes into contact with that growing from p_j ($j \neq i$).

Collectively, assumptions VGM1–VGM5 define the *Voronoi Growth Model*. Figure 7.2.1 shows a series of stages in such a growth process.

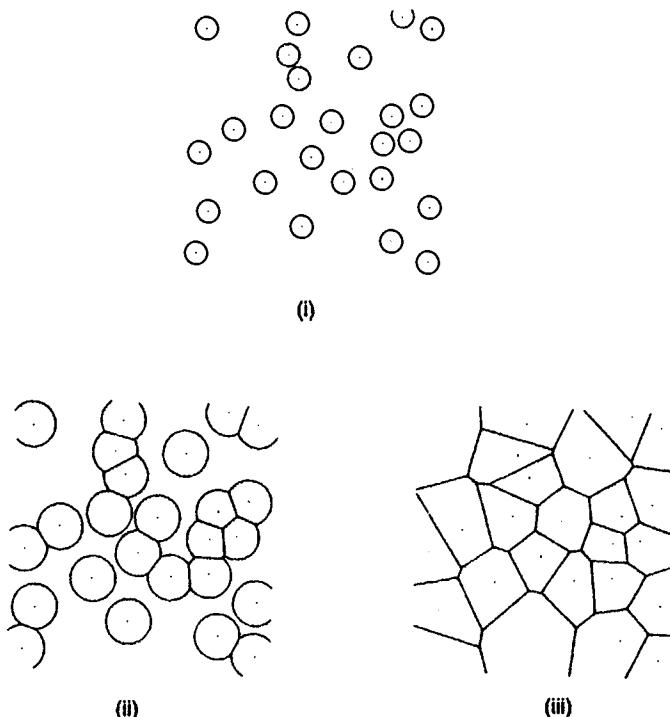


Figure 7.2.1 Stages (i), (ii) and (iii) of the Voronoi growth model.

Although the Voronoi Growth Model has been applied in a variety of different circumstances, the range of applications is not as great as that for the Voronoi Assignment Model and most are found in the natural sciences. One obvious application is to model crystal growth about a set of nucleation sites (Avrami, 1939; Leonyuk and Mal'tseva, 1980). Here Assumptions VGM3–VGM5 are equivalent to assuming an omnidirectional, uniform supply of crystallizing material to all faces of the growing crystal in the absence of any adsorbable impurities. Assumption VGM3 also implies that the rate of growth of the volume of a crystal will be proportional to its surface area. Steyer *et al.* (1990) suggest that in two dimensions a close analogy can be made between such crystallization and the growth of droplet condensation patterns, and so they use the Voronoi diagram to model the structure of the patterns of droplets that form when water condenses on the surface of paraffin oil, a liquid in which it is not soluble.

However, probably the most extensive use of growth models is in metallurgy. Here a major use is in modelling phase transitions involving the transformation of an isotropic, one-component solid through nucleation, and the isotropic growth of grains of a new or re-crystallized phase (Watson and Smith, 1975; Mahin *et al.*, 1980; Burger *et al.*, 1988; Vaz and Fortes, 1988; Marthinsen *et al.*, 1989). In this context the Voronoi Growth Model is sometimes referred to as the *cell model* (Meijering, 1953) or the *site saturation model* (Saetre *et al.*, 1986). Specific examples include covering a metallic surface with films or layers of a corrosive product (Evans, 1945) where the nucleation sites, P , might be surface imperfections such as impurities, points of intersection with bulk defects and surface pits (Frost and Thompson, 1987a). Another example is the growth of thin films of metal or semiconductors (Frost and Thompson, 1988). In these examples, if the thickness of the film is small relative to the spacing between the nucleation sites or if the grain boundaries are perpendicular to the plane of the film, a two-dimensional representation is appropriate.

An interesting application of the Voronoi Growth Model occurs in astronomy, where it has been used to describe the morphology of the large-scale structure of the universe. In one set of models (Matsuda and Shima, 1984; Icke and van der Weygaert, 1987, 1991; Coles and Barrow, 1990; Webster, 1998) it is suggested that a collection of slightly underdense regions in a primordial density field will act as the seeds of voids or expansion centres ('superbubble bubbles') from which matter will flow outwards until it encounters similar material flowing from another void. If the voids are created simultaneously, and the excess expansion is the same for all voids, we have the equivalent assumptions to those specified above for the Voronoi Growth Model. Once defined, the Voronoi diagram associated with the voids forms a skeleton around which the galaxies assemble during the evolution of the universe. In \mathbb{R}^3 the faces of the Voronoi polyhedra can be interpreted as the contact surfaces ('Pancakes'), their edges as elongated 'superclusters' and their nodes as virialized 'Abel clusters'. Van de Weygaert and Icke (1989) propose that the density at the facets of the Voronoi polyhedra of material

diffused from the voids is inversely proportional to the dimensionality of those facets so that over time galaxies tend to congregate at the highest density locations (the Abel clusters).

Another model, proposed by Yoshioka and Ikeuchi (1989), involves seed objects which explode simultaneously and with the same energy, thus forming shockwaves which expand into the intergalactic medium. The expanding shockwaves carry with them any mass particles which they encounter, thus concentrating the mass particles on the two-dimensional surfaces where the expanding shockwaves come into neutral contact. The result is again a Voronoi diagram in \mathbb{R}^3 .

A variety of different point processes (see Section 5.12) has been used to model the locations of the seeds of both the gravitational instability and explosion models including the homogeneous Poisson (Yoshioka and Ikeuchi, 1989; Coles, 1990; Ikeuchi and Turner, 1991; van de Weygaert, 1991, 1994; Zaninetti, 1990, 1992; Goldwirth *et al.*, 1995; Doroshkevich *et al.*, 1997), hard core (van de Weygaert, 1994; Ryden, 1995), Poisson cluster (van de Weygaert, 1994), displaced lattice (SubbaRao and Szalay, 1992), fractal (Martinez *et al.*, 1990; Zaninetti, 1991b, 1993), Sobol (Zaninetti, 1992) and the eigenvalues of random complex matrices (Zaninetti, 1992). The models have also been extended to consider other types of Voronoi diagram including the additively weighted (Johnson-Mehl) (Icke and van de Weygaert, 1991) with either random or Gaussian points (Zaninetti, 1991a; Molchanov *et al.*, 1997), and line (representing strings of seeds) (Zaninetti, 1991b).

The Poisson Voronoi diagram in \mathbb{R}^3 has also been used as the basis of a model to explore other astronomical phenomena where the overall structure has a basic cellular topology (Pierre, 1990) such as Lyman Alpha absorbers at high redshifts (Pierre *et al.*, 1988).

The Voronoi Growth Model has also been used in geology in several circumstances. One is in modelling crack patterns in general and cracking in basalt (lava flows), in particular, where the crack patterns result from the contraction of the material on cooling. An early application is provided by Stiny (1929) who proposed that, as a molten stream of basalt cools irregularly at its surface, the locations where hardening occurs first act as nuclei from which subsequent cooling extends in all directions throughout the material. Thus, tensile stress can be modelled as a set of expanding circles centred at the nuclei which, as they meet, develop lines along which cracking occurs. Smalley (1966) seems to have developed a similar model independently. He argues that if the basaltic material is of uniform temperature, the nuclei will appear simultaneously and form a regular spatial arrangement in the form of a triangular lattice (see Figure 8.2.2) so that growth centred on them produces hexagonal blocks of basalt. However, if uniformity of temperature does not occur, as is usually the case, the nuclei will not develop simultaneously and will not form a regular arrangement. Smalley (1966) suggests that in such circumstances the growth process should be applied to centres located according to a hard core process of the type described in Section 5.12, whereby centres are located at random subject to the constraint that centres

that are closer than some specified distance to an already existing centre cannot develop. He ran a number of simulations of this model and examined the frequency distribution of N , the number of neighbours (edges, vertices) of an individual Voronoi polygon (block of basalt). These frequencies were compared with those obtained from real world basalt patterns and found to differ in a statistically significant way. Smalley argues that such discrepancies could arise due to the difficulty of identifying very short edges in field counts of N . Thus, he ignored such small edges in his simulated patterns before recalculating the frequencies of N associated with them. These modified model frequencies provide a better fit to the empirical data than the original model frequencies but again the differences between the two sets are statistically significant. Further evidence for questioning the validity of the Stiny/Smalley model is provided by Stoyan and Stoyan (1980) who demonstrate that at least one empirical pattern of basalt blocks does not strongly approximate a Voronoi diagram.

Also in geology, Williams (1972, p. 152) has proposed that the Voronoi Growth Model is appropriate for modelling the polygonal depressions that develop in karst topography. Here the nuclei around which growth develops are stream sinkholes.

Ecological applications of the Voronoi Growth Model occur in the study of plant and animal territories where the Voronoi diagram defined with respect to a set of individuals, each with an associated fixed location in \mathbb{R}^2 , can be considered to represent ideal territories if the environment is ecologically uniform and the plants are even-aged and genotypically homogeneous (Galitsky, 1990) or the animals are of equal strength (Hasegawa and Tanemura, 1976; Gibson and Ashby, 1988). An example is provided by the territories of male mouthbreeder fishes (*Tilapia mossambica*) observed by Barlow (1974). These fish were kept in an outdoor pool with an initially uniform sandy bottom. The males excavate breeding pits by spitting sand away from fixed pit centres towards the pit centres of their neighbours. Reciprocal spitting results in sand parapets which act as territorial boundaries. Figure 7.2.2 shows such boundaries traced by Hasegawa and Tanemura (1976) from a photograph taken by Barlow (1974). Honda (1978) and Suzuki and Iri (1986a) (see Section 9.5.2) show that the pattern of such boundaries closely approximates the edges in the Voronoi diagram with the breeding pits as generators (see Figure 9.5.2).

Unlike the Voronoi Assignment Model, there have been far fewer applications of the Voronoi Growth Model to phenomena studied by social scientists. One example is provided by Boots (1973, 1975a) who used it to investigate patterns of service areas for bus companies as identified by Green (1955). In Britain bus services have their origins in the first few decades of the twentieth century when they first challenged the hegemony of the railways as the prime form of longer distance public transportation. The development of these services was not coordinated by any central agency and the process was a highly competitive one. Bus services tended to become established at the urban centres which already provided surrounding rural

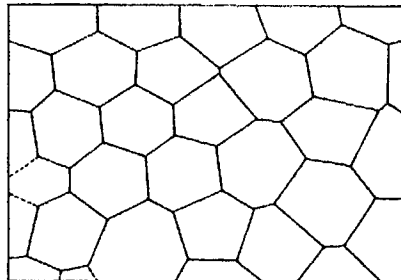


Figure 7.2.2 Schematic diagram of polygonal territories formed by male mouthbreeder fish replicated from a photograph in Barlow (1974). (Source: Hasegawa and Tanemura, 1976, Figure 1.)

areas with other goods and services. In areas away from the major urban agglomerations, such centres are relatively similar in size and so if the bus services were established at these places at approximately the same time, the Voronoi Growth Model could describe the service areas that arose under competition between centres. Although no formal statistical tests were undertaken, summary statistics for the characteristics of the bus service areas, such as number of neighbours, area and boundary length, were found to be similar to those expected for Voronoi polygons.

It is important to note that both the Voronoi Assignment and Growth Models can be modified to produce a whole set of extended models by changing one or more of their underlying assumptions. For instance, by changing Assumption VAM1 or VGM1 the points can be introduced into \mathbb{R}^m asynchronously, giving rise to Johnson-Mehl type models such as those described in Section 5.8. Changing Assumption VAM2 or VGM2 produces dynamic models of the type discussed in Section 7.5. Assumption VAM3 can be modified to consider unequal points by assigning to each point a weight which reflects its relative importance. Such differential weights might also be reflected in differences in the growth rates associated with individual points in the Voronoi Growth Model, thus revising Assumption VGM4. The weights could also be used in defining how the distance between a member of P and other locations in \mathbb{R}^m is measured, thus leading to assignment procedures which differ from those in Assumption VAM4. Such models and their applications are discussed in Chapter 3. Assumption VGM4 can also be modified to allow for growth to vary with direction from p_i . For instance, in the anisotropic Voronoi diagram proposed by Scheike (1994) (see Section 3.7.2), cells grow as ellipsoids, all with the same direction. Assumption VGM5 can be changed to allow for growth to terminate before the growing regions fill the space (e.g. before stage (iii) in Figure 7.2.1 is reached). Muche (1993) labels the resulting structure an incomplete Voronoi diagram (see Section 5.6.2). This structure has been extensively studied for the situation in which the points are located according to a homogeneous Poisson point process (see Section 1.3.3) in two dimensions (Schulze and Schwan, 1992, 1993; Schulze *et al.* 1989, 1993; Schulze and Wilbert, 1989b).

Finally, we note that while this section has described how the Voronoi Growth Model has been used to model physical systems, Tolmachiev and

Adamatzky (1996) propose a reversal of roles and suggest that an appropriate physical process can be used as an alternative way of computing a Voronoi diagram. First, they create a chemically active substrate by spreading a thin film of agar gel mixed with palladium chloride ($PdCl_2$) on a clear acetate film. Drops of potassium iodide liquid (KI) are then applied at sites corresponding to the Voronoi generator points. As the KI liquid diffuses over the film, it reacts with the $PdCl_2$ to produce PdI_2 as a precipitate, thus colouring the film black. However, at locations where waves of KI diffusing from different sites meet, the concentration of $PdCl_2$ is insufficient to be involved in the reaction. As a result, the interiors of the Voronoi cells appear black while their edges remain uncoloured (white). Antecedents of such chemical processors are found in the 'hardware models' of Morgan (1967). A simple model of his uses only ordinary pink blotting paper and a solvent of *N*-butanol. The solvent is supplied to the blotting paper by means of small wicks located at the generator points of the Voronoi diagram. As the solvent spreads out from each of the wicks, it carries with it some of the red pigment in the blotting paper, so that when the process is finished and the paper is dried, the limits of the solvent front are marked by thin red lines which represent the edges of the Voronoi diagram. For the specific case of the Poisson Voronoi diagram (see Chapter 5), Schulze and Schulze (1992) and Schulze and Wilbert (1989a, 1991a,b) show how this may be realized experimentally by heat treatment of polypropylene foil.

7.3 SPATIAL-TEMPORAL PROCESSES

In the preceding sections we dealt with spatial processes leading to Voronoi diagrams in which the locations of generators do not change over time. In this section we show some models of spatial processes in which the location of generators change over time.

7.3.1 Spatial competition models: the Hotelling process

In economics, in particular in spatial economics (or urban economics), a considerable number of studies have been carried out to examine market area stability (a review is provided, for example, by Gabszewicz *et al.*, 1986). Economic units, say firms, compete with each other to maximize their profits. In a spatial context, this competition takes the form of market area competition. If consumers buy products from the firm that offers the lowest price, each firm has its own market area. The market areas are different in size, yielding different profits, and firms with small profits move to alternative locations to gain more profits. Through this relocation process the configuration of firms may vary over time, or it may eventually reach an equilibrium configuration. The pioneering work on this market area stability was done by Hotelling (1929). A variety of models have been developed from his model, which we call Hotelling processes or, more broadly, spatial

competition processes. In this subsection we investigate spatial competition processes with the simplest Hotelling model, i.e. the Alonso version (Alonso, 1964) of the original Hotelling (1929) model.

Suppose that there are n firms located at x_1, \dots, x_n in a region S , and these firms are selling the same products with the same mill price (the price not including a delivery cost). We assume that the delivery cost from a firm at x_i to a consumer at x is proportional to the Euclidean distance $\|x_i - x\|$, and that consumers buy the products from the firm that quotes the lowest delivered price (the mill price plus the delivery cost). Under these assumptions, the configuration of n market areas is represented by the ordinary Voronoi diagram $V(P) = \{V(x_1), \dots, V(x_n)\}$, and the market area of firm i is represented by the Voronoi polygon $V(x_i)$. We further assume that the demand for the products is uniformly distributed over the region S ; the marginal cost of the products is the same for all firms; and the relocation cost is negligibly small. Then the profit of firm i is proportional to the area of $V(x_i)$. The firms compete in terms of their locations to maximize their profits. As a result, we observe a spatial competition process of n firms over time. We specify this process by the following behavioural assumptions.

Assumption HP1 (relocation timing) Each firm considers relocation once in every period, and the interval is equal over time periods.

Assumption HP2 (zero conjectural variation) In considering possible relocation, every firm conjectures that each firm will not change its location.

Let $X_{-i} = \{x_1, \dots, x_{i-1}, x_{i+1}, \dots, x_n\}$ be the set of locations of all firms except firm i , and x_i^* be the location of firm i that yields the maximum profit provided that the locations of the other firms are fixed at the present locations, i.e.

$$|V(x_i^*)| = \max_{x \in S} \left\{ |V(x)| \mid X_{-i} \text{ is fixed}, x \neq x_j, j \in I_n \setminus \{i\} \right\}, \quad (7.3.1)$$

where $|V(x)|$ indicates the area of $V(x)$. As is indicated by the condition in equation (7.3.1), firm i is not allowed to locate at the same location as any other firms.

We add one more behavioural assumption.

Assumption HP3 (relocation decision) Firm i moves to the location x_i^* (given by equation (7.3.1)) if the location x_i^* yields a greater profit than the present profit, i.e. $|V(x_i^*)| > |V(x_i)|$. Otherwise, firm i remains at the present location x_i .

We call the process characterized by the above assumptions the *Hotelling process*. Stated abstractly, the Hotelling process is the process in which each generator independently moves to maximize the area of its Voronoi polygon. Through the Hotelling process, the Voronoi diagram may change over time,

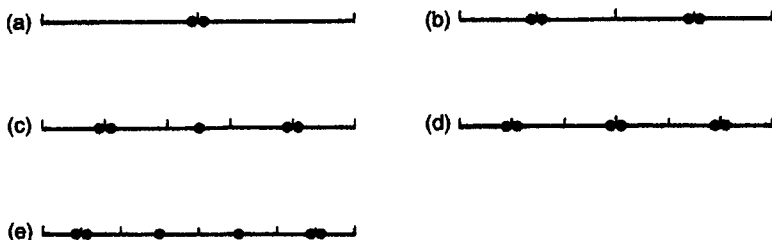


Figure 7.3.1 Global equilibrium configurations (Voronoi diagrams) of n firms on a bounded line market ($n = 2, 4, 5, 6$).

or it may eventually reach an equilibrium state in which all firms have no incentive to relocate. To be precise, the configuration of the n firms is in *global equilibrium* if and only if no firm can find a more profitable location than the present location; that is, the Voronoi diagram $\mathcal{V}^* = \{V(x_1^*), \dots, V(x_n^*)\}$ is in *global equilibrium* if and only if

$$|V(x_i^*)| > \max_{x_i \in S} |V(x_i)| \quad |X_{-i} = X_{-i}^*, x_i \neq x_j^*, j \in I_n \setminus [i]| \quad (7.3.2)$$

for any $i \in I_n$,

where $X_{-i}^* = \{x_1^*, \dots, x_{i-1}^*, x_{i+1}^*, \dots, x_n^*\}$.

When S is a bounded one-dimensional space, we can obtain the exact global equilibrium configurations \mathcal{V}^* (Eaton and Lipsey, 1975a), which are shown in Figure 7.3.1. For $n = 2, 4$ and 5 , we have the unique global equilibrium configuration; for $n = 3$, we have no global equilibrium; for $n \geq 6$, we have an infinite number of equilibrium configurations. Two extreme configurations are shown in panels (d) and (e).

The Hotelling process in a two-dimensional space was first studied by Eaton and Lipsey (1975a, b), followed by Shaked (1975), Okabe and Suzuki (1987), Okabe and Aoyagi (1991) and Aoyagi and Okabe (1993). Compared with the one-dimensional space, analytical examination becomes very difficult owing to complicated geometric calculations. We first show a few basic properties about the variation of the area of a Voronoi polygon. These properties are useful not only for the following analysis but also for locational optimization to be discussed in Chapter 9.

Consider a Voronoi diagram $\mathcal{V} = \{V(\mathbf{x}), V(x_1), \dots, V(x_{n-1})\}$, where $\mathbf{x}^T = (x, y)$ is the location of firm 0, and suppose that firms $1, \dots, m$ share their market boundaries with firm 0 (firms $1, \dots, m$ are indexed counterclockwise around firm 0). Let $\mathbf{u}_i^T = (u_i, v_i)$ be the Cartesian coordinates of the Voronoi vertex shared by $V(\mathbf{x})$, $V(x_i)$ and $V(x_{i+1})$. Recalling that a Voronoi vertex is the intersection of two bisectors (Chapter 2), we can write (u_i, v_i) in terms of \mathbf{x} , \mathbf{x}_i and \mathbf{x}_{i+1} , from which we can obtain the area of a Voronoi polygon $V(\mathbf{x})$. Since this quantity is frequently used in many applications, we state it as a formula.

The area of a Voronoi polygon

$$|V(x)| = \frac{1}{2} \sum_{i=1}^m (u_i(x, y)v_{i+1}(x, y) - u_{i+1}(x, y)v_i(x, y)), \quad (7.3.3)$$

where

$$\begin{aligned} u_i(x, y) &= \frac{(x_i^2 + y_i^2 - x^2 - y^2)(y - y_{i+1}) - (x_{i+1}^2 + y_{i+1}^2 - x^2 - y^2)(y - y_i)}{2 \{(x_i - x)(y_{i+1} - y) - (x_{i+1} - x)(y_i - y)\}}, \\ v_i(x, y) &= \frac{(x_i^2 + y_i^2 - x^2 - y^2)(x - x_{i+1}) - (x_{i+1}^2 + y_{i+1}^2 - x^2 - y^2)(x - x_i)}{2 \{(x_i - x)(y_{i+1} - y) - (x_{i+1} - x)(y_i - y)\}}, \end{aligned} \quad (7.3.4)$$

where $u_{m+1} = u_1$, $v_{m+1} = v_1$, $x_{m+1} = x_1$ and $y_{m+1} = y_1$.

From equations (7.3.3) and (7.3.4) we readily notice that $|V(x)|$ is continuous except at $x = x_i$ unless m changes. We should next examine whether or not $|V(x)|$ is continuous even if m changes (this question is closely related to a more general problem, called the *moving generator (particle) problem*; Cruz Orive, 1979). To consider this question, we depict Figure 7.3.2 where the filled circles show the fixed generators and the unfilled circle indicates the initial location, o , of the moving generator x . The initial shape of $V(x)$ at $x = \mathbf{0}$ is a hexagon (the heavy broken lines in Figure 7.3.2). Suppose that the generator x moves along a line radiating from o , indicated by the dash-dot line in Figure 7.3.2. When the generator x comes to the point indicated by the unfilled square, $V(x)$ becomes a septagon (the dotted lines in Figure 7.3.2). There must be a point between the unfilled circle and the unfilled square on the dash-dot line at which the shape of $V(x)$ changes from a hexagon to a septagon. The following property gives the answer to this question.

Property HP1 Consider a Voronoi diagram $\mathcal{V} = \{V(x), V(x_1), \dots, V(x_{n-1})\}$, where $V(x)$ is adjacent to $V(x_1), \dots, V(x_m)$ when $x = \mathbf{0}$. Suppose that as the generator x moves from $\mathbf{0}$ along a line L radiating from $\mathbf{0}$, a Voronoi vertex u_{m+1} appears between vertices u_i and u_{i+1} (or u_i and u_{i+1} degenerate into one vertex u_m). Let C be the circle that passes through points x_i, x_{i+1} and x_m , and x^* be a point at which the line L meets the circle C . Then x^* is the point at which $V(x)$ changes from an m -gon to an $(m+1)$ -gon (or $(m-1)$ -gon).

We can prove this property from the empty circle property (Property D5) in Chapter 2. The detailed derivation is shown by Cruz Orive (1979) for special lattice configurations and by Okabe and Aoyagi (1991) for general configurations.

Using Property HP1, we can determine regions for x in which $V(x)$ is an m -gon for a given configuration of generators. An example is shown in Figure 7.3.2, where generators are placed on regular triangular lattice points. (Note that generators are not necessarily spaced regularly.) The number in each region enclosed by circular arcs indicates m of $V(x)$.

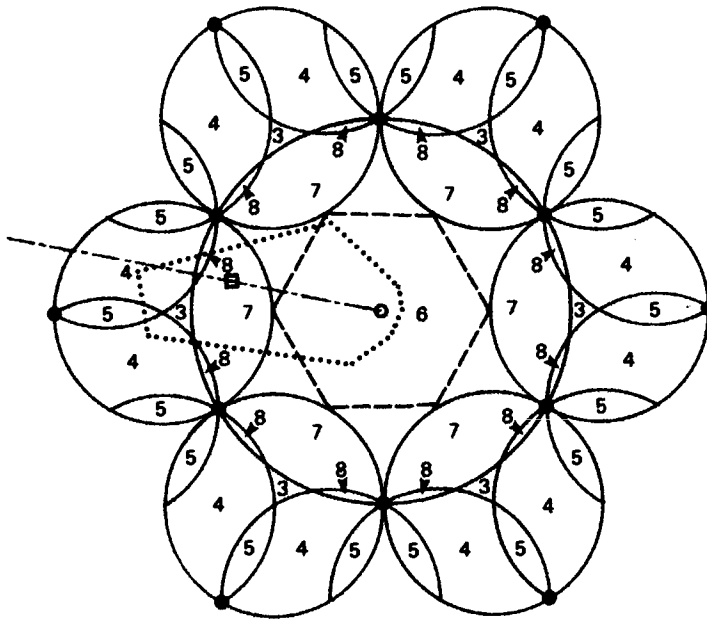


Figure 7.3.2 The shape of a Voronoi polygon $V(x)$ whose generator x moves on the plane where the other generators are fixed at regular triangular lattice points (the number m in each region enclosed by circular arcs indicates the number of vertices of $V(x)$ when x comes to that region).

From equations (7.3.3) and (7.3.4) with Property HP1, we can show, after a few steps of derivation, that $|V(x)|$ is continuous with respect to x ($\neq x_i$) not only when m does not change but also when m changes. In addition, we can show the following property.

Property HP2 For fixed x_1, \dots, x_{n-1} and $x \neq x_i \in I_{n-1}$

- (i) $|V(x)|$ is continuous with respect to x ;
- (ii) $\partial|V(x)|/\partial x$ exists and it is continuous with respect to x .

It is straightforward to obtain the first derivative of equation (7.3.3), from which we can easily notice that the derivative is continuous with respect to x unless m changes. If m changes, we can prove the continuity of the first derivatives using Property HP1. The detailed derivation is shown in Okabe and Aoyagi (1991). Note that the second derivatives are not necessarily continuous.

It follows from Property HP2 that a necessary condition for the global equilibrium in the Hotelling process is given by

$$\frac{\partial |V(x_i)|}{\partial x_{ik}} = 0, \quad \kappa = 1, 2 \text{ for } i = 1, \dots, n. \quad (7.3.5)$$

When this equation holds, we say that the configuration (Voronoi diagram) of the n firms is in *local equilibrium*.

When the region S is unbounded and firms are located on regular lattice points, it is left as an exercise to examine if the configuration of the firms is in local equilibrium. Using equations (7.3.3)–(7.3.5), we can show that the Voronoi diagram of regular triangular lattice points (Voronoi polygons are hexagons) and that of squares (Voronoi polygons are squares) are in local equilibrium, but the Voronoi diagram of regular hexagonal lattice points (Voronoi polygons are regular triangles) is not in local equilibrium. Furthermore, we can show a stronger property than this property.

Property HP3 The Voronoi diagram of regular triangular lattice points and that of square lattice points are in global equilibrium. The Voronoi diagram of regular hexagonal points is not in local equilibrium; consequently, it is not in global equilibrium.

We can prove this property by computing the Hessian matrix, which is too lengthy to show here (see Okabe and Aoyagi, 1991, in which REDUCE III (algebraic computation software) is used).

When the region S is bounded, analysis becomes extremely intractable except for $n = 2, 3$. Shaked (1975) shows the following property.

Property HP4 When region S is a disc, two firms paired at the centre of the disc are in global equilibrium; there is no local equilibrium for three firms.

See Shaked (1975) for the proof.

The analytical difficulty encountered in a bounded two-dimensional space with $n \geq 4$ firms results from the fact that the optimization problem of equation (7.3.1) is a non-linear, non-convex programming problem. As is shown in the brief review of the non-linear, non-convex programming problem in Chapter 9, it is almost impossible to obtain the global maximum by an analytical method; only a local maximum is obtainable by numerical methods. This intractability prevents analytical examination of the Hotelling process over time, not only in a bounded two-dimensional space but also in an unbounded two-dimensional space. At present it is difficult to say if firms on an unbounded two-dimensional space reach the global equilibrium configurations stated in Property HP3 for any initial configuration. Giving up analytical examination, Eaton and Lipsey (1975b) employed a naive numerical method to examine the Hotelling process for 17 firms in a disc. They conjectured from their numerical results that the global equilibrium configuration would not be achieved. Alternatively, Okabe and Suzuki (1987) imposed the following weaker assumption than Assumption HP3 and examined the Hotelling process over time with numerical simulations.

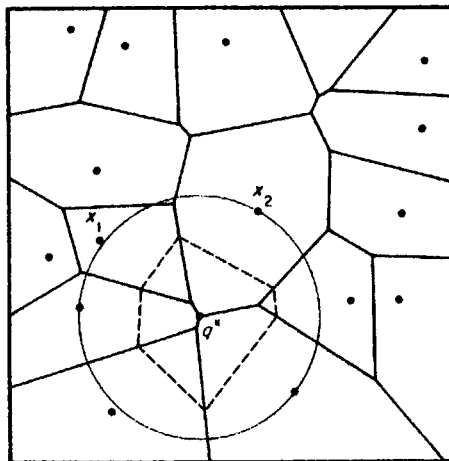


Figure 7.3.3 Searches for local maximum locations $|V(x_1)| < |V(q^*)|$ and $|V(x_2)| > |V(q^*)|$.

Assumption HP4 Let q^* be the centre of the largest empty circle in the Voronoi diagram $\mathcal{V} = \{V(x_1), \dots, V(x_n)\}$.

- (i) If $|V(x_i)| < |V(q^*)|$, firm i searches for a local maximum location x_i^* from q^* (for example, q^* in Figure 7.3.3). If $|V(x_i^*)| > |V(q^*)|$, firm i moves to x_i^* ; otherwise firm i moves to q^* .
- (ii) If $|V(x_i)| \geq |V(q^*)|$, firm i searches a local maximum location x_i^{**} from the present location (for example, x_2 in Figure 7.3.3). If $|V(x_i^{**})| > |V(x_i)|$, firm i moves to x_i^{**} ; otherwise firm i remains at the present location x_i .

Under Assumptions HP1, HP2 and HP4 with the steepest descent method (see Chapter 9), Okabe and Suzuki (1987) carried out the numerical simulation for 256 firms in a square over 100 periods (one period is defined by a period during which every firm makes the locational decision once). Part of the process is shown in Figure 7.3.4, where the filled circles, squares, triangles and stars indicate the change in profit (i.e. a market area) being less than 1%, 1–3%, 3–5%, and more than 5%, respectively. From these numerical results, they notice that although the configuration does not achieve the global equilibrium by the 100th period (observe peripheral firms in Figure 7.3.4), the configuration of inner firms is stable after a certain period of time.

From the simulation of $n = 17$ in Eaton and Lipsey (1975b) and that of $n = 256$ in Okabe and Suzuki (1987), we notice that the stability of the Hotelling process depends upon the number of firms. Moreover, the shape of region S crucially affects the stability. These effects are investigated by Aoyagi and Okabe (1993) theoretically as well as numerically.

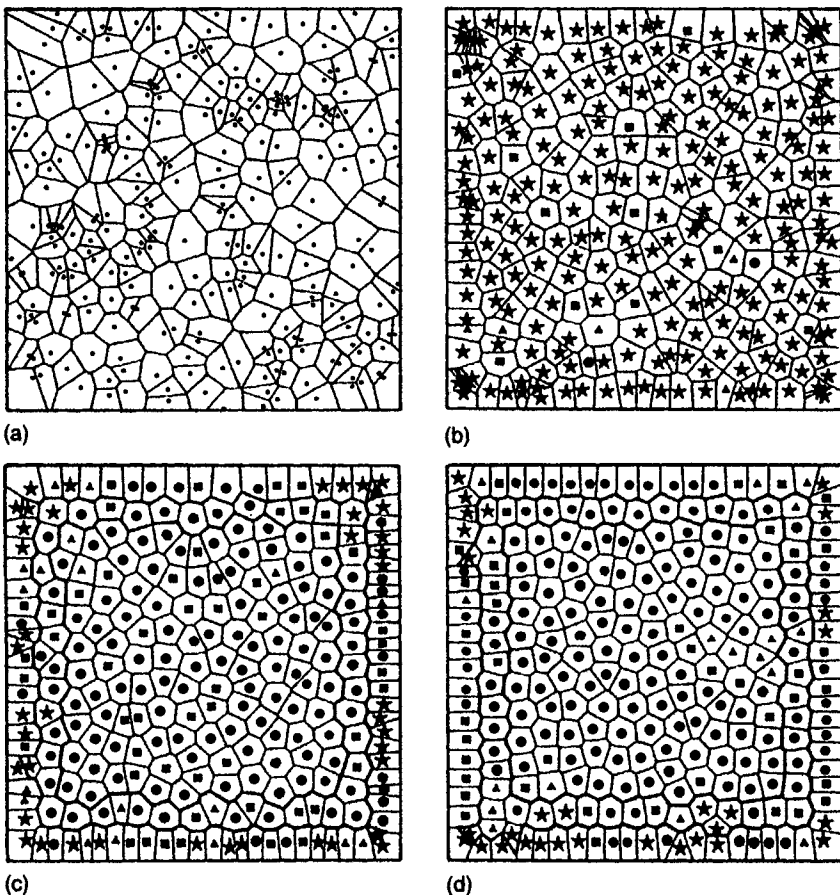


Figure 7.3.4 The Hotelling process of 256 firms in a square region: (a) the initial configuration (uniformly random); (b) the first period; (c) the tenth period; (d) the hundredth period. (The filled circles, squares, triangles and stars indicate the change in profit (i.e. a market area) being less than 1%, 1–3%, 3–5%, and more than 5%, respectively.) (Source: Okabe and Suzuki, 1987, Figure 5.)

7.3.2 Adjustment models

Spatial-temporal processes are investigated not only in economic behaviour as we discussed above, but also in animal behaviour. One well-known process is the adjustment process (Hasegawa and Tanemura, 1976). Consider individual animals settled down in a region. In the initial stage, the individuals are fairly independent. As time goes by, however, the individuals interact with each other and each individual tends to occupy its territory in such a way that the individual is as distant from its neighbours as possible. Through this interaction process the territories of the individuals are mutually adjusted until a stable configuration is achieved.

To formulate this process mathematically, let $\mathbf{x}_1^{(t)}, \dots, \mathbf{x}_n^{(t)}$ be the location of n individuals in a region S , $t = 0, 1, \dots$. We assume that the initial locations, i.e. $\mathbf{x}_1^{(0)}, \dots, \mathbf{x}_n^{(0)}$, are uniformly randomly distributed over S . We next assume that a location in S is dominated by the nearest individual. It follows from this assumption that the territory of individual i at time t is given by the Voronoi polygon $V(\mathbf{x}_i^{(t)})$ in the Voronoi diagram $\mathcal{V}^{(t)} = \{V(\mathbf{x}_1^{(t)}), \dots, V(\mathbf{x}_n^{(t)})\}$. We further assume that individual i moves its location toward the gravitational centre of its territorial area. To be explicit, let $\mathbf{u}_{ij}^{(t)} = (u_{ij}^{(t)}, v_{ij}^{(t)})^T$, $j \in I_n$, be Voronoi vertices of $V(\mathbf{x}_i^{(t)})$ which are indexed counterclockwise. Then the gravitational centre, $\mathbf{x}_{gi}^{(t)} = (x_{gi}^{(t)}, y_{gi}^{(t)})^T$, of $V(\mathbf{x}_i^{(t)})$ is given by

$$\begin{aligned} x_{gi}^{(t)} &= \frac{1}{6|V(\mathbf{x}_i^{(t)})|} \sum_{j=1}^{n_i} (v_{ij}^{(t)} - v_{j-1}^{(t)}) \left\{ (u_{ij}^{(t)} + u_{j-1}^{(t)})^2 - u_{ij}^{(t)} u_{j-1}^{(t)} \right\}, \\ y_{gi}^{(t)} &= \frac{1}{6|V(\mathbf{x}_i^{(t)})|} \sum_{j=1}^{n_i} (u_{ij}^{(t)} - u_{j-1}^{(t)}) \left\{ (v_{ij}^{(t)} + v_{j-1}^{(t)})^2 - v_{ij}^{(t)} v_{j-1}^{(t)} \right\}. \end{aligned} \quad (7.3.6)$$

In these terms, the above behavioural assumption may be written as follows.

Assumption AP1 (adjustment move)

$$\mathbf{x}_i^{(t+1)} = \mathbf{x}_i^{(t)} + \frac{1}{\alpha} (\mathbf{x}_{gi}^{(t)} - \mathbf{x}_i^{(t)}), \quad t = 0, 1, 2, \dots, \quad (7.3.7)$$

where $\alpha \geq 1$ is a behavioural constant.

We call the process in which all individuals follow Assumption AP1 the *adjustment process* or *adjustment model* (Hasegawa and Tanemura, 1976, 1980, 1986) (Figure 7.3.5). When $\mathbf{x}_{gi}^{(t)} = \mathbf{x}_i^{(t)}$ for all $i \in I_n$, we say that the configuration of territories is *stable*. If region S is one-dimensional, such as a river side or a beach side, the limiting configuration can be obtained analytically (Hasegawa and Tanemura, 1976; Saito, 1982). In the limit, the configuration becomes stable and all territories become the same size. If region S is two-dimensional, analytical examination is intractable. Hasegawa and Tanemura (1976), employing numerical simulations, concluded from the simulations that the adjustment model leads to a stable configuration and this configuration is fairly close to the configuration of the territories of mouthbreeder fish observed by Barlow (1974) (see Section 7.2).

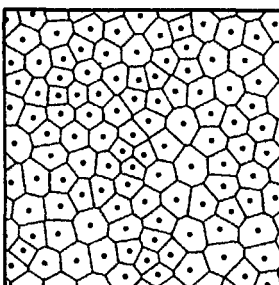


Figure 7.3.5 The adjustment process: ($t = 500$) configuration. (Source: Hasegawa and Tanemura, 1981, Figure 1.)

7.4 TWO-SPECIES MODELS

In Section 7.3 we showed the models of territories formed through the interaction within the same kinds of behavioural units. In the real world we also find another type of territories which are formed not only through the interaction within the same kind of behavioural units but also through the interaction between different kinds of behavioural units. In this section we show a few Voronoi-type models that attempt to explain such phenomena.

In animal ecology, many prey-predator relations are known, such as cows and lions, and it is reported that prey tend to form herds or flocks. To explain this tendency, Hamilton (1971) proposes a model which may be called the *selfish herd model*. Consider, as an example, cows and lions in grassland, and suppose that the cows are grazing and the lions are hiding in the grass to catch a cow. Lions tend to catch the cow nearest to their hiding site. Then a Voronoi polygon associated with a cow represents the 'domain of danger' (Hamilton, 1971) of that cow. To be explicit, let $\mathcal{V} = \{V(p_1), \dots, V(p_n)\}$ be the Voronoi diagram generated by a set of sites of n cows. If a lion happens to be in $V(p_i)$, the cow at p_i will be a prey of the lion. Thus the area of $V(p_i)$ represents the magnitude of danger of the cow at p_i . When a cow senses the presence of a lion, the cow tends to move to the nearest cow. As a result, cows form a herd and each cow wants to be surrounded by the other cows. Actually, the domain of danger of a cow that is tightly surrounded by the other cows becomes small and the cow is less likely to be a prey of a lion. Since every cow wants to be tightly surrounded by the other cows, the configuration of cows within a herd is unstable, but as a whole, a herd guarantees more or less safety. With this model, Hamilton (1971) emphasizes that the selfish avoidance of a predator can lead to aggregation.

The area of a Voronoi polygon has a negative implication for a cow, but it may have a positive implication for certain kinds of insects. As an example Cannings and Cruz Orive (1975) referred to signalling females in relation to mobile males. Consider wingless females scattered over a region. Females send signals to males to be fertilized. Suppose that the intensity of the signal is inversely proportional to the distance from a female and the intensity of the signal is the same for all females. If males respond to the strongest signals and males are distributed fairly uniformly over the region, then the probability of a female being fertilized is proportional to the area of the Voronoi polygon of the female. Each female tries to maximize the probability of being fertilized by moving her location. As a result, the configuration of females changes over time and eventually it may reach an equilibrium configuration. Recalling the profit maximization behaviour in Section 7.3, we notice that this problem is similar to the problem considered in the Hotelling process. Cannings and Cruz Orive (1975) examined whether or not a slight move of a female was profitable provided that the other females were placed on regular hexagonal, square or triangular lattice points. This problem is in fact the same as the problem of the Hotelling process in an unbounded plane,

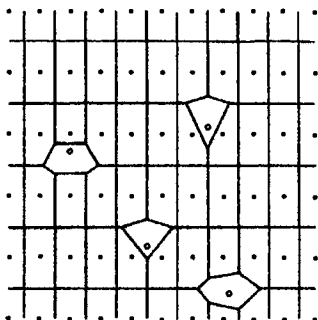


Figure 7.4.1 Two-species model (filled circles indicate crop plants and unfilled circles indicate weeds).

and the answer is shown in Property HP3. This problem is also investigated theoretically by Cruz Orive (1979).

In plant ecology, the prey-predator relationship may correspond to the relationship between crop plants and weeds. This relationship is studied by Fischer and Miles (1973) with a Voronoi diagram. Usually crop plants are planted at rectangular lattice points (the filled circles with $a \times b$ intervals in Figure 7.4.1), whereas weeds are distributed randomly, i.e. the distribution of weeds follows a Poisson process (the unfilled circles in Figure 7.4.1). Suppose that crop plants and weeds emerge simultaneously and expand with equal rates. Ultimately, as we saw in Section 7.2, each plant establishes its individual zone of exploitation, and collectively these form a Voronoi diagram. To estimate the yield of the crop, it is useful to know the expected area $\mu_c(\rho)$ of each crop plant domain (the mean area of each Voronoi polygon) when the density ρ of weeds and intervals a and b are given. Fischer and Miles (1973) obtain this value as

$$\mu_c(\rho) = \frac{4}{\rho} \Psi\left(\sqrt{\frac{\pi\rho}{2}} a\right) \Psi\left(\sqrt{\frac{\pi\rho}{2}} b\right), \quad (7.4.1)$$

where

$$\Psi(x) = \frac{1}{2\pi} \int_0^x e^{-z^2/2} dz. \quad (7.4.2)$$

Fischer and Miles (1973) also examine the cases of simultaneous emergence and different expansion rates, and different emergence and different expansion rates.

We may also find the prey-predator relationship in economic behaviour. Von Hohenbalken and West (1984) and West and Von Hohenbalken (1984) surveyed the entry and withdrawal of stores in Edmonton, Canada, during 1959–1973 to test Kreps and Wilson's (1982) economic predation theory. The predation process assumed by Kreps and Wilson may be summarized as follows.

Suppose that an established firm operates a set of stores in a region and a firm is entering this region with new stores.

- (i) The new stores of the entrant are challenged by the neighbourhood stores of the established firm.
- (ii) The established firm locates new stores to force losses on the entrant's new stores.
- (iii) The entrant stops constructing new stores.
- (iv) Eventually, the entrant withdraws from the region.

Von Hohenbalken and West (1984) assume that a set of market areas is represented by a Voronoi diagram and the neighbourhood stores of a store, say store i , are given by stores whose Voronoi polygons are adjacent to the Voronoi polygon of store i . With these assumptions, they investigated empirically the above predation process in Edmonton. They conclude that generally the data support the Kreps and Wilson predation process.

CHAPTER 8

Point Pattern Analysis

A common concern that runs through a wide range of disciplines is the examination of the spatial occurrence of a particular phenomenon. Illustrative examples, which also reflect the extensive range of scales covered by such phenomena, include the location of sulphide inclusions in a steel (metallurgy), artefacts over a site (archaeology), nest sites of bird species in a habitat (ecology), towns in a state (geography), seismic events in a continent (geology) and galaxies of stars in the universe (astronomy). In each of these instances it is possible to represent individual incidences of the phenomenon as a set of n distinct points, $P = \{p_1, p_2, \dots, p_n\}$, in a bounded region, B , in either \mathbb{R}^2 or \mathbb{R}^3 . We call such representations, empirical point patterns. Note that while the individual objects themselves are not points, such representations are possible because the physical sizes of the objects are very small relative to both the distances between them and the extent of the region in which they occur.

Empirical point patterns are examined for a variety of reasons. A major one is the expectation that a pattern represents one source of evidence that may be useful in learning more about the process responsible for creating it. If our ideas concerning a phenomenon are sufficiently developed, we may be able to build an explanatory model of it. We can use such models to derive hypotheses concerning the locational behaviour of the phenomenon. Support for such hypotheses, and thus the models from which they are derived, can be obtained by analysing empirical point patterns of the phenomenon. Sometimes such analysis focuses on the relative locations of individual points of P or on the spatial distribution of P over B . Such situations are dealt with in Sections 8.1 and 8.2. At other times we may be interested in how the members of P are located with respect to other objects, not members of P , also located in B . These objects may be represented as points, lines or areas, or some combination of all three. We examine such circumstances in Section 8.3 which is further subdivided in terms of the dimensionality of the other objects.

When our knowledge of the phenomenon represented by the point pattern is more rudimentary, modelling may be less appropriate. Then analysis takes on a more exploratory form as we seek to identify fundamental characteristics of the point pattern. Sections 8.4–8.6 discuss some exploratory analyses involving shape, spatial intensity, and segmentation of point patterns which have been pursued using concepts of Voronoi diagrams and related

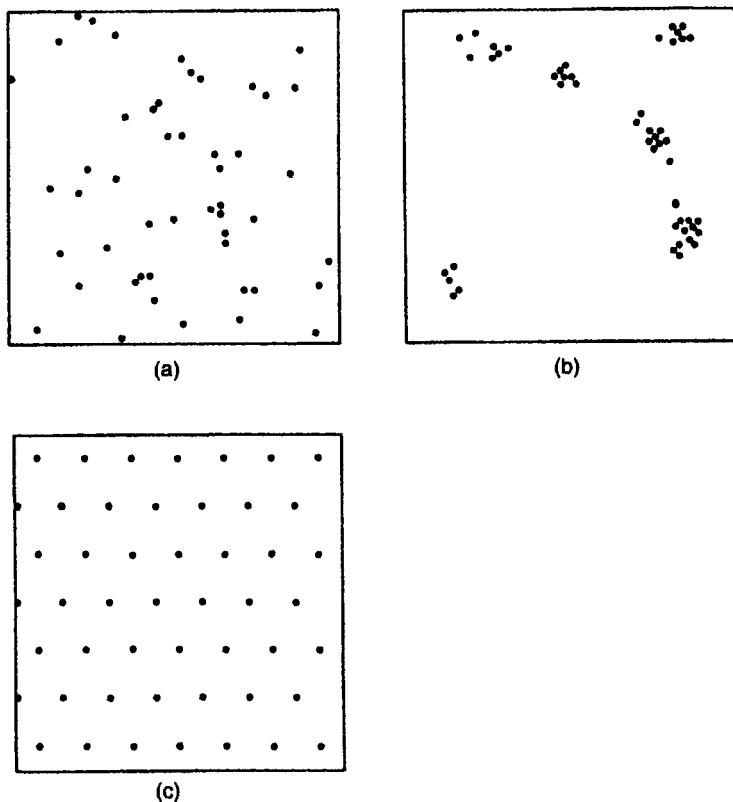


Figure 8.0.1 Classes of point patterns: (a) complete spatial randomness; (b) clustered; (c) regular.

structures. Finally, in Section 8.7 we show how such concepts can also be used to generate point processes with specific properties.

In those circumstances where our primary concern is with modelling and our analysis is limited to a consideration of only the members of P , it is usual to adopt an approach that involves establishing a theoretical point pattern with respect to which other patterns are compared. The theoretical point pattern chosen is that which results from the operation of the homogeneous Poisson point process, Θ_P , described in Section 1.3.3. A pattern that results from such a process can be considered one that would arise by chance in a completely undifferentiated environment. Following Diggle (1983) we call such a point pattern *complete spatial randomness* (CSR). Figure 8.0.1(a) shows such an example of CSR. In view of the conditions involved in generating such a pattern, it is unlikely that true CSR occurs in any empirical situations. Instead, our concern with CSR is primarily for its role as an idealized standard. The two conditions that are assumed to exist when CSR results provide a simple model that can be useful in several circumstances. For

instance, if we know little about the process responsible for a particular empirical point pattern, we can begin by testing a hypothesis that the pattern is CSR. This allows for exploration of the empirical point pattern. Whether or not the initial hypothesis relating to CSR is rejected, a description of the empirical point pattern remains. If CSR cannot be rejected, further analysis is unwarranted, otherwise the results of the test can be used as an aid in formulating new hypotheses regarding the empirical point pattern.

Classes of point patterns can be recognized using CSR as a benchmark. *Clustered* point patterns are those in which the points are significantly more grouped in B than they are in CSR (see the example in Figure 8.0.1(b)) whereas *regular* patterns (sometimes also called uniform or dispersed point patterns) are those in which the points are more spread out over B than they would be in CSR (see Figure 8.0.1(c)). Clustered and regular patterns can arise as the result of changing one or more of the postulates of Θ_p identified in Section 1.3.3.

Homogeneity may be relaxed by differentiating subareas of B in some way. Environmental inhomogeneity implies that some subareas of B are less likely to receive a point than other subareas, or might even be prohibited from receiving a point. In such circumstances we would expect to find more points in the favoured subareas of B than elsewhere, thereby producing a clustered pattern.

One way of relaxing independent scattering is to permit interaction among points. Points may either attract or repulse one another. Attraction may result from processes such as agglomeration, association, and some types of diffusion and competition. In each instance the result is a clustered pattern. Such situations, where different processes result in similar types of point patterns, are not unusual in point pattern analysis. When they occur, if the only evidence we have is the pattern itself, further analysis is necessary to determine the conditions responsible for the observed clustering. Instead of points attracting each other, in some instances, such as diffusion or competition, points may repel each other. Repulsion will likely produce regular patterns. The types of models that produce non-CSR outcomes are reviewed by Haggett *et al.* (1977, Chapter 13), Getis and Boots (1978), Ripley (1981), Cliff and Ord (1981), Diggle (1983), Upton and Fingleton (1985), Cressie (1991), Stoyan and Stoyan (1994) and Stoyan *et al.* (1995) (see also Sections 1.3.3 and 5.12).

In general, the hypothesis of CSR (or any other hypothesis concerning the spatial nature of the empirical point pattern) is tested by comparing measures of selected characteristics of the empirical point pattern with those of the hypothesized pattern. The most frequently used approaches are quadrat analysis, nearest neighbour analysis, and second-order analysis (see Boots and Getis, 1988, for details). Quadrat analysis involves defining a set of spatial sampling units (quadrats) of consistent size and shape which, depending on the specific approach adopted, may or may not overlap and which, collectively, may or may not completely cover B . A frequency array, $f(x)$, is generated by counting the number of quadrats containing $x = 0, 1, 2, \dots$

points, $f(x)$ can then be compared with the corresponding distribution, $p(x)$, expected under CSR with the same intensity as the empirical pattern, using a χ^2 goodness-of-fit test.

Nearest neighbour analysis involves measuring the distance between each point in P and the nearest other point. The nearest neighbour distances so obtained are compared with those expected under CSR with the same intensity as the empirical pattern using a variety of tests. Second-order analysis extends this approach by examining the distances between all pairs of points in P . These interpoint distances are compared with the CSR expectations, again taking into consideration the intensity of the points in the empirical pattern.

8.1 POLYGON-BASED METHODS

8.1.1 Direct approach

If we represent the empirical point pattern as a set, $P = \{p_1, p_2, \dots, p_n\}$ of n distinct points in a bounded region, B , of \mathbb{R}^m , we can define the bounded Voronoi diagram, $\mathcal{V}(P)$, of P (see Section 2.1). For each polygon of $\mathcal{V}(P)$ we can measure the values of selected characteristics. For $\mathcal{V}(P)$ in \mathbb{R}^2 the most obvious characteristics in terms of dimensionality from zero to two are the number of sides (vertices) N of a polygon, the perimeter P , and the area A , although several measures of shape have also been considered (Burger *et al.*, 1990; Marçalpoil and Usson, 1992). We can compare the values of these characteristics with those of polygons of the Voronoi diagram defined for a hypothesized point process. Since edge effects influence the values for polygons around the boundary of B , some allowance must be made for this. One approach (already considered in Section 5.4) is to exclude values for any polygon for which a circle, centred at any vertex, v , of the polygon and passing through the three points of P which are equidistant from v , intersects the boundary of B .

The polygonal approach was originally proposed by Evans (1967), but despite being advocated by a number of researchers (Haggett *et al.*, 1977, pp. 436–439; Matérn, 1979; Cormack, 1979, pp. 171–175; Ripley, 1981, p. 149; Cliff and Ord, 1981, p. 110; Thomas, 1981), it was not widely developed until later. One reason for this delay is that the properties of N , by far the most studied and most easily measured characteristic initially, do not always vary strongly amongst Voronoi diagrams defined for patterns generated by different processes. Recall that in Section 5.5 (equation (5.5.6)) we noted that the average value of N , $E(N)$, is always 6 for any normal, planar tessellation. Furthermore, Boots (1977) demonstrates that the frequency distribution of N for at least one set of clustered patterns is not significantly different from that of CSR. Vincent and Howarth (1982) reach a similar conclusion for a set of regular patterns, although Burger *et al.* (1990) suggest that the standard deviation of N is a strong indicator of the level of regu-

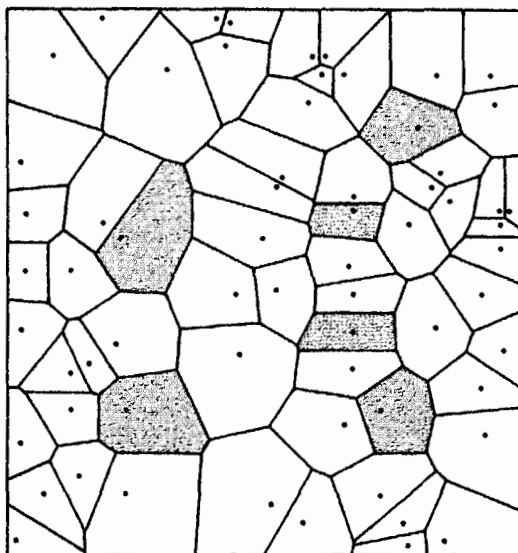


Figure 8.1.1 Voronoi diagram of Japanese black pine saplings (shaded polygons are those used in calculating U_k in equation (8.1.1)). (Redrawn from data in Upton and Fingleton, 1985, Figures 1.39a and 1.42a.)

larity in some point patterns encountered in metalgraphy. Krawietz and Lorz (1991) also explore tests using moments of N and find that a variance test is the most powerful of these in general, although a skewness test is more sensitive in detecting regularity.

When, as is usually the case initially, the theoretical pattern we are comparing with the empirical one is CSR, the values for the polygons are those reported for the Poisson Voronoi cells (PVCs) in Section 5.5. Recall that these polygons comprise the Voronoi tessellation defined for points located according to a homogeneous Poisson point process, Θ_p . For PVCs the distribution of P , the perimeter of a polygon, was estimated by Hinde and Miles (1980) to be approximately normal with mean $4\lambda^{-1/2}$ and variance $0.9472\lambda^{-1}$, where λ is the intensity of Θ_p (see Table 5.5.1). This led Upton and Fingleton (1985, p. 99) to propose the statistic U_k as a test of CSR where

$$U_k = \frac{1}{0.9472} \hat{\lambda} \sum_{i=1}^k (P_i - 4\hat{\lambda}^{-1/2})^2 \quad (8.1.1)$$

and P_1, P_2, \dots, P_k , are the perimeters of a sample of k of the n polygons of $\mathcal{V}(P)$ and $\hat{\lambda} = n/|B|$ (where $|B|$ is the area of B) is the sample estimate of λ . When the k polygons are selected following certain conditions, the distribution of U_k for CSR will be approximately χ^2 with k degrees of freedom. These conditions involve avoiding both edge effects as discussed above and dependence between the k polygons. As noted by Boots and Murdoch (1983) (see equation (5.5.19)) the lengths of the perimeters of neighbouring PVCs

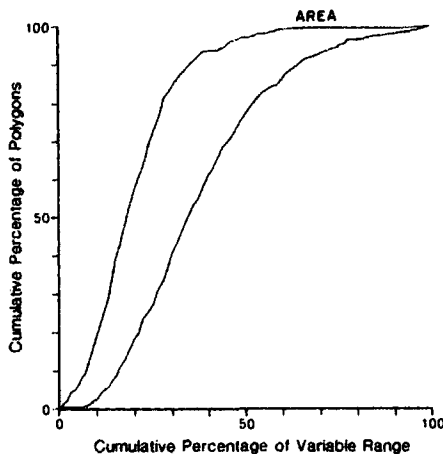


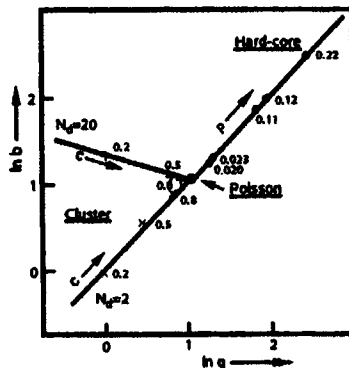
Figure 8.1.2 Standardized cumulative frequency histogram for the areas of Voronoi polygons of points in a CSR pattern. The curves are the limits to an envelope describing the standardized cumulative frequency histograms for a family of simulations of 500 points. (Source: Hutchings and Discombe, 1986, Figure 2.)

are not independent and so the k polygons must be selected so that no two are adjacent.

To illustrate this approach consider Figure 8.1.1, which shows the Voronoi diagram for a set of 65 Japanese black pine saplings (Upton and Fingleton, 1985, Figures 1.39a and 1.42a). In this example $k = 6$ (the shaded polygons of Figure 8.1.1) and U_k is calculated to be 4.17. Since $\chi^2_{0.05,6} = 12.59 > 4.17$, the pattern of pines is not considered significantly different from CSR.

Because the dependence between the lengths of the perimeters of neighbouring PVCs also applies to other polygon characteristics such as area and number of sides (see equations (5.5.18) and (5.5.19), respectively), Hutchings and Discombe (1986) propose an analytical approach using Monte Carlo simulation tests. This involves generating a number of patterns, typically 100, using a known spatial point process (e.g. the homogeneous Poisson point process which produces CSR) containing the same number of points as the empirical pattern being investigated. The Voronoi diagram is generated for each simulated pattern and the values of the desired characteristics of all polygons not subject to edge effects (as defined above) are measured. These values are then formed into a cumulative percentage frequency histogram in which the class intervals are set equal to 1% of the range between the smallest and largest values in the set of measurements. The use of percentages avoids the problem of different numbers of polygons in each of the simulations. A curve is produced by plotting the histogram class interval against the cumulative percentage frequency. If the curves for all simulations are superimposed, an envelope of values is created which contains all the values from the simulated patterns (see Figure 8.1.2). A similar frequency curve can be generated for the values of the polygons of the Voronoi diagram

Figure 8.1.3 Values of b and q of gamma distributions fitted to the density functions of areas of Voronoi polygons for sets of points generated by different point processes. For cluster processes, N_{cl} is the mean number of points per cluster and c characterizes the distance of the points from the cluster centre, which is inversely proportional to c . For hard core processes, p characterizes the degree of order which increases with increasing p .
 (Source: Hermann *et al.*, 1989, Figure 4(c).)



of the empirical pattern. If this empirical curve lies entirely within the envelope of simulated values, the hypothesis that the process which generated the simulated patterns is also responsible for the empirical one is not rejected.

Using this approach Hutchings and Discombe (1986) suggest that the best single polygon characteristic for distinguishing both regular and clustered empirical patterns from a hypothesized pattern of CSR is area, while perimeter is sensitive to clustering only. In view of this conjecture it is not surprising that recent work has emphasized examining distributions of polygon areas (Shehata and Boyd, 1988; Hermann *et al.*, 1989; Burger *et al.*, 1990; Byers, 1992, 1996; Duyckaerts *et al.*, 1994; Horizoe *et al.*, 1995; Itoh *et al.*, 1995; Stone and Tsakiroopoulos, 1995; Bertram and Wendrock, 1996).

Recall from Section 5.5.4 that the distribution of areas for PVCs follows a two parameter gamma distribution (see equation (5.5.33)). The same distribution has also been found to fit Voronoi polygon area distributions in a number of empirical situations (e.g. Zaninetti, 1991b, 1992; Gotoh, 1993; Lemaître *et al.*, 1993; Le Caér and Delannay, 1993b; Itoh *et al.*, 1995; Mulheran and Blackman, 1996). This finding led Hermann *et al.* (1989) to suggest that the estimates of b and q in equation (5.5.33) can be used to define a two dimensional parameter space which can be used to classify patterns. As Figure 8.1.3 shows, clustered and regular (hard core) patterns each occupy distinct regions of the parameter space. Since both Maxwell and lognormal distributions have also been shown to provide good fits to Voronoi polygon areas, Hermann *et al.* (1989) suggest that other two-dimensional parameter spaces created by using the estimated parameters of these distributions or the values of the extremes of the distributions (the 5th and 95th quantiles) may also prove useful.

Marcelpoin and Usson (1992) adopt a similar approach but instead create a three-dimensional graph by using a measure of the variation in cell areas

$$AD = 1 - (1 + \sigma_A / \mu_A)^{-1}, \quad (8.1.2)$$

where μ_A and σ_A are the mean and standard deviation of the polygon areas, respectively, together with two measures which use the 'roundness factor',

$RF_i = 4\pi A_i/L_i^2$, where L_i and A_i are the perimeter and area of polygon i , respectively. These measures are the average roundness factor

$$RF_{AV} = \frac{1}{N} \sum_{i=1}^N RF_i \quad (8.1.3)$$

and the roundness factor homogeneity

$$RFH = (1 + \sigma_{RF}/RF_{AV})^{-1}, \quad (8.1.4)$$

where σ_{RF} is the standard deviation of RF . All three of these measures are defined on the interval $[0, 1]$. Bertin *et al.* (1992) propose parallel measures for points located in \mathbb{R}^3 using cell volume and 'sphericity'.

Despite the number of analyses using Voronoi polygon areas, there has been little investigation of the statistical power of the procedures involved relative to each other or to other analytical procedures. Myles *et al.* (1995) examine two statistics which use empirical distribution functions. These are

$$H_M = \max_{0 \leq r \leq r_0} |\hat{H}(r) - \hat{E}[\hat{H}(r)]| \quad (8.1.5)$$

and

$$H_I = \int_0^{r_0} (\hat{H}(r) - \hat{E}[\hat{H}(r)])^2 dr, \quad (8.1.6)$$

where $\hat{H}(r) = U(r)/n$, $U(r)$ is the total number of Voronoi polygons with areas less than r and $\hat{E}[\hat{H}(r)]$ is the estimated value for a CSR pattern. Their results suggest that H_I is almost always the more powerful of the two statistics against clustering while neither test is better than the other with respect to regularity. When other analytical procedures are considered, they find that against clustering quadrat tests perform best, Voronoi and second order tests are essentially equal, and all three are considerably better than nearest neighbour. However, against regularity it is the second order test which is best, followed in order by the nearest neighbour, Voronoi, and quadrat tests.

Wallet and Dussert (1997) examined the three parameters AD , RF_{AV} and RFH described in equations (8.1.2)–(8.1.4) and found that AD performed best against both clustering and regularity. Relative to other analytical procedures considered (nearest analysis, second-order, quadrat, and edge lengths of minimum spanning trees), the Voronoi measures were again found to be more successful against clustering than regularity.

8.1.2 Indirect approaches

In addition to their direct use, the characteristics of $\mathcal{V}(P)$ may be exploited to implement other procedures for analysing point patterns. This subsection describes two such procedures, one based on information theory and the other on rearranging the points.

Information theory attempts to measure the degree of organization in a given system. Shannon (1948a, b) applied this idea to a set of probabilities by measuring organization using the entropy statistic, H , given by

$$H = \sum_{i=1}^n p_i \ln \frac{1}{p_i}, \quad (8.1.7)$$

where p_i is the probability of a random variable, x , taking the value x_i ($i = 1, \dots, n$) and

$$\sum_{i=1}^n p_i = 1 \quad (p_i \geq 0). \quad (8.1.8)$$

Originally, in communications theory, logarithms to the base 2 were used, but in applications elsewhere these have been replaced by natural logarithms to the base e, as in equation (8.1.7).

If the system being investigated is an empirical point pattern consisting of a set $P = \{p_1, p_2, \dots, p_n\}$ of n distinct points in a bounded region, B , of \mathbb{R}^m , one way the level of organization will be reflected is by the variation in the frequency with which points occur in subregions of B . To operationalize this concept in \mathbb{R}^2 , Chapman (1970) defines the Voronoi diagram of P , $\mathcal{V}(P)$, and sets $p_i = A_i / \sum_{i=1}^n A_i$ ($i = 1, \dots, n$), where A_i is the area of the polygon associated with p_i . Edge effects are avoided by disregarding any member of P which does not meet the criterion described at the beginning of Section 8.1.1.

In fact, H is more properly considered as a measure of disorder since its maximum value, H_{\max} , occurs when there is no information other than n and the area of B , $|B|$. In this case, \hat{A}_i , the best estimate of A_i for any member p_i of P , would be $\hat{A}_i = |B|/n$. This would mean that \hat{A}_i would equal $1/n$ for each of the n points so that

$$H_{\max} = n \left(\frac{1}{n} \ln \frac{1}{1/n} \right) = \ln n. \quad (8.1.9)$$

However, there are problems in using H directly to evaluate empirical point patterns (Chapman, 1970, pp. 320–321; Lenz, 1979, pp. 376–377). In particular, although H decreases as the extent of clustering in the pattern increases, maximum regularity (members of P located on a triangular grid, see Figure 8.2.2) also yields H_{\max} . Also as n gets very large the value of H for CSR also approaches H_{\max} thus making the interpretation of H for an empirical point pattern almost impossible. In addition, since $\ln n$ increases as n increases, patterns generated by the same process but with different intensities will not produce the same value of H .

These problems with H can be overcome by using Thiel's redundancy measure, R^* , given by

$$R^* = \sum_{i=1}^n p_i \ln \frac{p_i}{1/n} = H_{\max} - H. \quad (8.1.10)$$

For a regular pattern, $R^* = 0$, while R^* increases with increasing clustering of points. In addition, R^* is less sensitive to variations in n .

If we wish to test an empirical point pattern against a hypothesis of CSR we need both the expected value, $E(R^*)$, and the variance, $\text{Var}(R^*)$, of R^* for CSR. Recall that the area A of a Poisson Voronoi cell (PVC) has a gamma distribution,

Table 8.1.1 Estimates of the expected value and variance of Thiel's redundancy measure R^* for CSR.

n	$E(R^*)$	$\text{Var}(R^*)$
15	0.124	0.001875
30	0.129	0.001225
60	0.131	0.000660
90	0.132	0.000412
180	0.132	0.000204
360	0.132	0.000090
∞	0.134	0

Source: Lenz (1979).

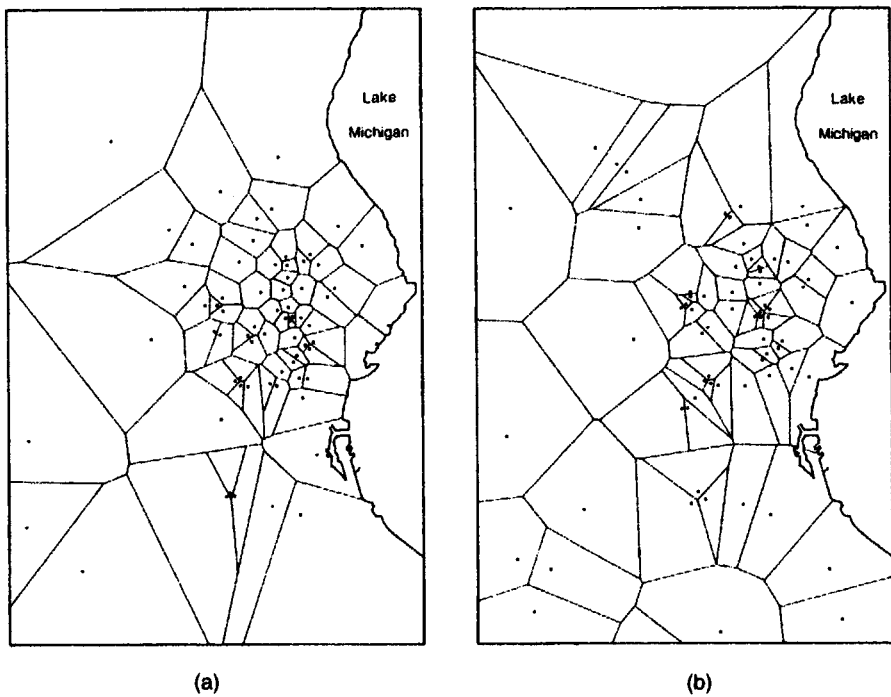


Figure 8.1.4 City of Milwaukee, 1975: (a)Voronoi diagram of locations of personal robberies; (b)Voronoi diagram of locations of victims' addresses (Source: Lenz, 1979, Figures 3 and 4.)

$$f(A, \alpha) = [\alpha(\alpha A)^{\alpha-1} e^{-\alpha A}] / \Gamma(\alpha), \quad (8.1.11)$$

for which $\alpha = 3.57$ if the variance of $A = 0.280\lambda^{-2}$. The best fit to the data in Table 8.1.1 yields

$$\text{Var}(R^*) = 0.2157 / \sqrt[1.9]{n}, \quad (8.1.12)$$

which can be used to estimate $\text{Var}(R^*)$ for values of n not given in Table 8.1.1.

Lenz (1979) shows that when $n \geq 15$, R^* is approximately normally distributed for CSR so that we may use the variate of the standard normal curve

$$z = [R_{\text{obs}}^* - E(R^*)] / \text{Var}(R^*)^{1/2}, \quad (8.1.13)$$

where R_{obs}^* is the value of R^* for the empirical point pattern, as a test statistic.

Since R^* is independent of n we can also use it to compare two empirical point patterns, for example of the same phenomenon at different times or different phenomena in the same region. An example is provided by Lenz who compares the pattern of personal robbery locations in the city of Milwaukee in 1975 with the pattern of victims' addresses (see Figure 8.1.4). Values of R_{obs}^* indicate that the former pattern shows more clustering than the latter, which leads Lenz to conclude that victims contribute to the occurrence of personal robberies by exposing themselves to high crime risk districts of the city.

Another set of procedures, based on rearranging the points, has been developed by Perry (1995). In summary, this involves moving the points of the pattern simultaneously until the pattern converges on a regular one and then comparing the locations of the points in the initial and final patterns. The procedure involves four steps. The first step is to construct $V(P)$. In step two, each point whose Voronoi polygon does not include part of the boundary ∂B of the study area B is relocated to a new position which is the centroid of the locations of its Voronoi neighbours weighted by the lengths of the shared Voronoi polygon edges. Thus, if the initial coordinates of the q neighbours of a point p_i are (x_j, y_j) , $j = 1, \dots, q$, and the length of the common edge between $V(p_i)$ and $V(p_j)$ is l_j , the new coordinates for p_i are given by

$$\left(\frac{\sum_{j=1}^q l_j x_j}{\sum_{j=1}^q l_j}, \frac{\sum_{j=1}^q l_j y_j}{\sum_{j=1}^q l_j} \right). \quad (8.1.14)$$

When one or more of the edges of the Voronoi polygon of a point are parts of ∂B , a temporary, imaginary point is located at the mid-point of each boundary edge and assigned a weight of $4/\sqrt{3}$ times the edge length. This value is derived from the situation where the points are located on a triangular grid (see Figure 8.2.2). The imaginary points are removed once the point has been re-located. Step three is to construct a new Voronoi diagram using the new set of point locations. The final step is to assess if the new

pattern of points has achieved a sufficient degree of regularity. If the variation in the areas of the Voronoi polygons for the current pattern is smaller than that of the previous pattern and differs from it by less than some specified value, the process ends; if not, steps two through four are repeated.

If d_i is the Euclidean distance between the initial and final locations of p_i , Perry proposes Monte Carlo test procedures involving either the empirical distribution function of d_i or

$$D = \sum_{i=1}^n d_i. \quad (8.1.15)$$

By applying these tests to some of the same data sets analysed by Diggle (1983), Perry suggests that they have power which is comparable with that of quadrat, nearest neighbour and second-order tests, especially for detecting clustering.

8.2 TRIANGLE-BASED METHODS

If an empirical point pattern consists of a set $P = \{p_1, p_2, \dots, p_n\}$ of n distinct points in a bounded region, B , of \mathbb{R}^m , this approach involves defining the Delaunay tessellation of P , $\mathcal{D}(P)$, measuring properties of the polytopes of $\mathcal{D}(P)$ and comparing these with the properties of the polytopes of a Delaunay tessellation defined for a hypothesized point pattern. As with all areas of point pattern analysis, the hypothesized pattern which has been emphasized is CSR. Such patterns correspond to those produced when P is generated according to a homogeneous Poisson point process (see Section 1.3.3). Known results relating to this model are reported in Section 5.5 and several of them are used here.

In \mathbb{R}^2 the probability density function (pdf), $f(\alpha)$, of α , a random angle of a randomly selected triangle of $\mathcal{D}(P)$ when P is CSR, was derived by Miles (1970a) (see equation (5.11.12)). Boots (1974, 1975b) and later Vincent *et al.* (1976, 1977, 1983) argued that a test for CSR can be obtained by integrating equation (5.11.12) for chosen class intervals to obtain a set of expected frequencies which can be compared with the empirical frequencies using a Pearson goodness-of-fit test. The probability $F_\alpha(x)$ that $\alpha \leq x$ derived by integrating equation (5.11.12) is

$$\begin{aligned} F_\alpha(x) &= \int_0^x f(\alpha) d\alpha \\ &= (1/3) \left[2 \sin^2 \alpha + \left\{ \alpha \cos 2\alpha - (3 \sin 2\alpha)/2 + 2\alpha \right\} \pi^{-1} \right]_0^x. \end{aligned} \quad (8.2.1)$$

Both Boots (1975b) and Vincent *et al.* (1977) use this procedure to analyse patterns of urban settlements in various parts of the United States and demonstrate that, in this context, the procedure is more effective than the nearest neighbour approach (see Section 8.1) in correctly rejecting a null hypothesis of CSR.

However, since this approach requires that we take a random sample of triangles from $\mathcal{D}(P)$, Mardia *et al.* (1977) have argued that it is wasteful of the available information. They propose instead using the marginal density of the minimum angle, α_{\min} , of all triangles in $\mathcal{D}(P)$. The pdf of α_{\min} for CSR is given in equation (5.11.13). Mardia *et al.* assume that the values of α_{\min} are independent for the triangles of $\mathcal{D}(P)$. Integrating equation (5.11.13) we get

$$F_{\alpha_{\min}}(x) = \left[1 + \frac{1}{2} \pi \{ (6\alpha_{\min} - 2\pi) \cos 2\alpha_{\min} - \sin 2\alpha_{\min} - \sin 4\alpha_{\min} \} \right] \quad (8.2.2)$$

$(0 < x \leq \pi/3)$

as the probability that $\alpha_{\min} \leq x$.

Boots (1986) has proposed that a similar argument may also be made in favour of the use of the maximum angle, α_{\max} , of the triangles of $\mathcal{D}(P)$. When P is CSR the marginal density of α_{\max} is given by equation (5.11.14) which yields

$$F_{\alpha_{\max}}(x) = \frac{1}{2} \pi [\sin 4x + \sin 2x + 2\pi \cos x - 6x \cos 2x] \quad (8.2.2)$$

$(\pi/3 \leq x \leq \pi/2)$

and

$$F_{\alpha_{\max}}(x) = \frac{1}{2} \pi [2x \cos 2x - 2\pi \cos 2x - 3 \sin 2x + 4x - 2\pi] \quad (8.2.3)$$

$(\pi/2 \leq x \leq \pi)$

as the probability that $\alpha_{\max} \leq x$.

Preliminary investigations by Boots (1986) using both empirical and simulated patterns containing different degrees of regularity or clustering suggest that α_{\min} has the best overall ability to reject a null hypothesis of CSR against both regular and clustered alternatives, although there is some indication that α_{\max} is able to detect instances of clustering not discernible by α_{\min} . In view of these findings we illustrate this procedure using α_{\min} for a pattern of settlements in an area of southeastern Montana, USA, in 1973 (see Figure 8.2.1).

For each triangle in $\mathcal{D}(P)$ in Figure 8.2.1 we identify and measure α_{\min} . These values are used to determine the number of values, $G(\alpha_{\min})$, of α_{\min} in a specified interval. In calculating $G(\alpha_{\min})$ we must account for edge effects produced by the bounded nature of $\mathcal{D}(P)$. Mardia (1989) (see also the discussion in Kendall, 1989, p. 110) proposes doing this by discounting any triangle for which the circumcentre does not lie in B (recall from Section 2.3 (Property V7) that the circumcentres are vertices of the Voronoi diagram of P). This procedure was followed in this example and such discounted triangles are shaded in Figure 8.2.1. The values of $G(\alpha_{\min})$ so obtained are compared with the corresponding values, $F(\alpha_{\min})$, for CSR obtained from equation (8.2.2) using a χ^2 goodness-of-fit test (see Table 8.2.1). Following usual statistical convention, categories for which the expected values are less than five are combined with adjacent categories. Since the value of $\chi^2 = 11.198$ which results has a probability of less than 0.05 of occurring for a χ^2_4 distribution, we reject the hypothesis of CSR for this settlement pattern.

Table 8.2.1 Analysis of locations of settlements in southeastern Montana using the minimum angle technique.

Minimum angle, α_{\min} (degrees)	Observed frequency, $G(\alpha_{\min})$	Expected frequency, $F(\alpha_{\min})$
0–10	1	2.468
11–20	1 } 2	6.973 }
21–30	15	10.007
31–40	8	10.521
41–50	15 } 16	8.023 }
51–60	1	3.008 }
		11.031

$$\chi^2_4 = 11.198.$$

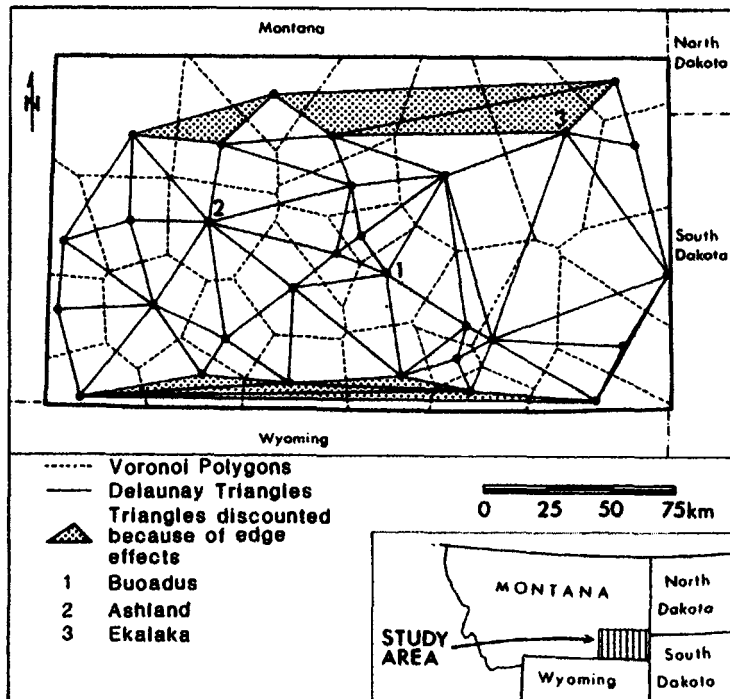


Figure 8.2.1 Voronoi diagram and Delaunay triangulation for a pattern of settlements in an area of Montana, USA, in 1973. Re-drawn from data in Boots and Getis (1988, Figure 4.3).

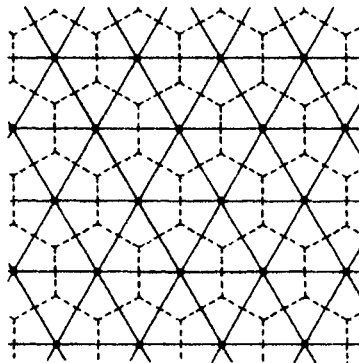


Figure 8.2.2 Voronoi polygons (indicated by dashed lines) and Delaunay triangles (indicated by solid lines) for points located on a triangular grid.

However, can we proceed further beyond this result? Currently, the answer is a tentative yes. If the points of P are arranged in a perfectly regular way on a triangular grid such as that shown in Figure 8.2.2, all the Voronoi polygons (indicated by dashed lines) will be regular hexagons and all the Delaunay triangles in $\mathcal{D}(P)$ (indicated by solid lines) will be equilateral so that all angles would be equal to $\pi/3$. Thus, if for an empirical point pattern there is an excess of values (relative to the number expected for CSR) at the upper tail of $G(\alpha_{\min})$, a regular pattern is indicated. However, in Section 5.11 we noted that there will also be a high proportion of nearly equilateral triangles in $\mathcal{D}(P)$ under CSR so that the excess referred to might prove difficult to detect. If the points are located on a square grid (see Figure 8.2.3) the resulting Voronoi polygons (indicated by dashed lines) will be squares and the Delaunay triangles of $\mathcal{D}(P)$ (indicated by the solid lines) will be right-angled so that $\alpha_{\min} = \pi/4$. A significant excess of such angles would indicate a point pattern with affinities to a square grid. In contrast, a pattern in which points are clustered in distinct groups will have some edges of $\mathcal{D}(P)$ which correspond to links between points on the peripheries of different clusters (see Figure 8.2.4). Many of the triangles formed by such edges will be elongated so that their minimum angles will be small. Thus, a distribution of empirical values of α_{\min} with a significant excess of small angles is suggestive of a pattern of clustered points.

On the basis of these speculations and noting that the greatest differences between the frequencies for the observed angles and the CSR expectations occur in the ranges of 0–20 degrees (where there is a deficit of minimum angles relative to CSR) and 41–50 degrees (where there is an excess) (see Table 8.2.1), we may conclude that the pattern of settlements in Figure 8.2.1 shows a significant degree of regularity. Furthermore, it appears that this regularity is more consistent with the expectations of a regular square grid than with a triangular one.

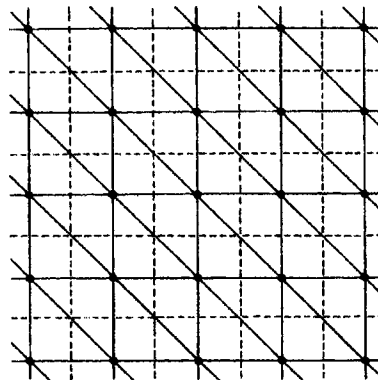


Figure 8.2.3 Voronoi polygons (indicated by dashed lines) and Delaunay triangles (indicated by solid lines) for points located on a square grid.

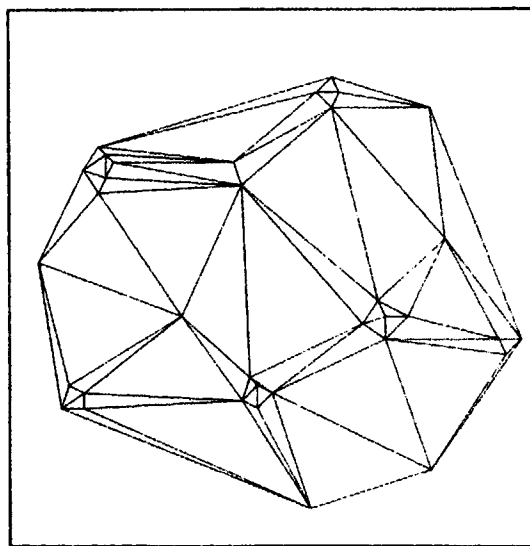


Figure 8.2.4 Delaunay triangulation for a clustered pattern of points.

An alternative to considering individual angles of triangles in $\mathcal{D}(P)$ is to focus on triangle shape. Mardia (1989) has proposed a test which involves comparing the positions of the triangles of $\mathcal{D}(P)$ in Kendall's shape space (see Section 5.11 and Figure 5.11.12) with the positions of those expected under CSR. When testing if an empirical point pattern is significantly different from a regular one, Taylor *et al.* (1995) and Dryden *et al.* (1995, 1997) define test statistics that incorporate the Procrustes shape distance from each triangle in $\mathcal{D}(P)$ to an equilateral triangle. An example of such a

measure is the Riemannian shape distance $(\cos \rho)^2$ between two triangles $((x_i, y_i)$ and $(\alpha_i, \beta_i), i = 1, 2, 3$), where

$$(\cos \rho)^2 = \frac{(S_{x\alpha} + S_{y\beta})^2 + (S_{x\beta} - S_{y\alpha})^2}{(S_{xx} + S_{yy})(S_{\alpha\alpha} + S_{\beta\beta})}, \quad (8.2.4)$$

where $S_{xy} = \sum_{i=1}^3 (x_i - \bar{x})(y_i - \bar{y})$, $\bar{x} = (\sum_{i=1}^3 x_i)/3$ and $\bar{y} = (\sum_{i=1}^3 y_i)/3$.

Other characteristics of triangles can also be examined. So far most attention has been paid to N the number of edges incident at a vertex in $\mathcal{D}(P)$ and L , the length of an edge of $\mathcal{D}(P)$ (Vincent *et al.*, 1976, 1977, 1983; Pyrz, 1994; Bertram and Wendrock, 1996). Because of the duality between $\mathcal{D}(P)$ and the ordinary Voronoi diagram of P , N is also the number of edges (vertices) of the Voronoi polygon associated with the vertex in $\mathcal{D}(P)$ and L is the distance between a pair of Voronoi neighbours.

For CSR the pdf of $L, f(L)$, is given by equation (5.11.3), while pdfs for other processes whose realizations are either clustered (Pyrz, 1994; Bertram and Wendrock, 1996) or regular patterns (Vincent and Howarth, 1982; Pyrz, 1994; Bertram and Wendrock, 1996) have been approximated using Monte Carlo procedures. Using the Monte Carlo simulation test procedure described in Section 8.1.1, Hutchings and Discombe (1986) suggest that L is effective in distinguishing both regular and clustered patterns from those of CSR. Bertram and Wendrock (1996) reach a similar conclusion. They also consider a local average of L for each point p_i given by

$$L_i = \frac{1}{N_i} \sum_{j=1}^{N_i} L_{ij}, \quad (8.2.5)$$

where L_{ij} is the length of the edge between point i and point j , and N_i is the number of edges incident at point p_i , and demonstrate that the coefficient of variation (cv) of L_i , $cv(L_i)$, can be used together with $cv(N)$ to create a two-dimensional parameter space in which different patterns are shown to occupy different locations. L_i has also been used in empirical investigations of metals (Wray *et al.*, 1983; Spitzig *et al.*, 1985; Shehata and Boyd, 1988; Burger *et al.*, 1990; Stone and Tsakirooulos, 1995) and unidirectional composites (Pyrz, 1994) where it is usually referred to as the *near neighbour distance*.

Finney (1991, 1993) also uses L to construct a classification for individual cells in three-dimensional simplexes. Depending on its length relative to a specified threshold, each edge is designated as either short or long. Since each simplicial cell has six edges, it can be assigned to one of seven classes depending on the number of its short and long edges. The complete structure is summarized by the frequency distribution of the classes and by a table showing the adjacencies between cells of a given class. Such summary measures can then be compared with model expectations.

Rather than considering individual characteristics of the triangles of $\mathcal{D}(P)$ independently, both Mardia *et al.* (1977) and Kendall (1989) propose pursuing them jointly. For CSR a lemma due to Miles (1970a) (see equation (5.11.2)) demonstrates that the size (measured by the circumradius, r) and the shape

(measured by the joint orientation of the edges) of an individual triangle are independent with the distribution of both characteristics being known. Using this information Kendall (1989) suggests the following test. First, sort the triangles of $\mathcal{D}(P)$ in terms of their shapes into three groups: those that are 'nearly equilateral', those that are highly 'splinter shaped', and the remainder. Then for the first and last of these groups, examine the departures from independence and from the known distribution of r .

8.3 NEAREST NEIGHBOUR DISTANCE METHODS

In this section we show the nearest neighbour distance method, abbreviated to the NND method. The NND method is a statistical method which examines the effect of physical objects located in a region upon the distribution of point-like elements over the region. The effect of nuclear power stations on the distribution of abnormal plants, the locational dependency of fast food stores on arterial streets, the spatial association of firms producing integrated circuits around airports, etc. can be investigated with the NND method. We should note that the NND method discussed here is different from the ordinary nearest neighbour distance method referred to in biology, geography and ecology (Bartlett, 1975; Pielou, 1977; Getis and Boots, 1978). The ordinary nearest neighbour method also deals with the distribution of point-like elements but it does not deal directly with physical objects affecting the distribution of the point-like elements. In this section we focus on the NND method because this method is an application of the Voronoi diagram which is the major concern of this text. The reader who wishes to study the ordinary nearest neighbour distance method in depth should consult Diggle (1983), Upton and Fingleton (1985) and Cressie (1991).

To fix a general setting for the analysis, let us consider a region in which m physical objects (such as power stations, arterial streets and airports referred to above) are located in a region, and n point-like elements (such as plants, stores and firms) are distributed over the region excluding the area occupied by the objects. A set of the m objects in the region is represented by a set of points, lines or areas in a bounded region S in \mathbb{R}^2 , which is denoted by $O = \{O_1, \dots, O_m\}$ ($1 \leq m < \infty$), where $O_i \cap O_j = \emptyset$, $i \neq j$, $i, j \in I_n$. A set of the n point-like elements is represented by a set of points distributed over $S_0 = S \setminus \bigcup_{i=1}^m O_i$, which is denoted by $P = \{p_1, \dots, p_n\}$ ($1 \leq n < \infty$) with the set of their location vectors $\{\mathbf{x}_1, \dots, \mathbf{x}_n\}$.

Given O and P , we define the distance from a point p_i in \mathbb{R}^2 to an object O_j by

$$d(p_i, O_j) = \min_{\mathbf{u}_j} \{ \| \mathbf{x}_i - \mathbf{u}_j \| \mid \mathbf{u}_j \in O_j \}, \quad (8.3.1)$$

where $\| \mathbf{x}_i - \mathbf{u}_j \|$ is the Euclidean distance between $\mathbf{x}_i \in S_0$ and $\mathbf{u}_j \in O_j$. With $d(p_i, O_j)$, we next define the distance from a point p_i to the nearest object in O by

$$d(p_i, O) = \min_j \{d(p_i, O_j) \mid j \in I_n\}. \quad (8.3.2)$$

We call this distance the *nearest neighbour distance*, or briefly the *NN-distance* from p_i to O . Third, we define the NN-distance averaged across the n points, i.e.

$$\bar{t} = \frac{1}{n} \sum_{i=1}^n d(p_i, O). \quad (8.3.3)$$

We call \bar{t} the *average nearest neighbour distance* or the *average NN-distance* for short.

In the NND method, several indices are proposed to measure or to test the effect of objects O on the distribution of points P . To formulate one of the simplest indices, let us consider the hypothesis that points P are independently and randomly distributed according to the uniform distribution over S_0 . This hypothesis implies that objects O do not affect the distribution of points P . Under this hypothesis, the NN-distance $t_i = d(p_i, O)$ is a random variable; consequently \bar{t} of equation (8.3.3) is also a random variable. We define an index by

$$R = \frac{\bar{t}}{E(\bar{t})}, \quad (8.3.4)$$

where $E(\bar{t})$ is the expected value of \bar{t} (cf. Pielou's index, 1977, p.155). Since \bar{t} is the average of independent random variables having the same distribution with a finite mean, the central limit theorem guarantees that the distribution of \bar{t} asymptotically approaches the normal distribution with mean $E(\bar{t}) = E(t)$ and variance $\text{Var}(\bar{t}) = \text{Var}(t)/n$, where $t = d(p, O)$ is the NN-distance from a random point p to O . It follows from this property that the random variable R asymptotically follows the normal distribution with $E(R) = 1$ and $\text{Var}(R) = \text{Var}(\bar{t})/(n E(t)^2)$ as n increases. With this test statistic we may conclude that if the observed value \hat{R} is less than a lower critical value of R , then the points P are more closely distributed around objects O than they would be in the random distribution. If \hat{R} is greater than an upper critical value of R , we may infer that the points P are more sparsely distributed around objects O than they would be in the random distribution.

We should make one remark on the boundary effect often discussed in the related literature. The nature of the boundary effect of the NND method is different from that of the ordinary nearest neighbour method. Since the NND method is based upon a uniform distribution over a bounded region and a random NN-distance t_i is a distance from a random point to a fixed object (not a random object), in theory the NND method is not bothered by the boundary effect. In practice, the boundary effect may appear if we apply the NND method to a subregion of a region in which points P are distributed, because we usually ignore objects outside the subregion that affect the distribution of P . In this case we can overcome the boundary effect by considering the objects outside the subregion whose Voronoi regions (generated by O) overlap the subregion.

When we use the index R in practice, we have to compute $d(p_i, O)$, $E(\bar{t}) = E(t)$ and $\text{Var}(\bar{t}) = \text{Var}(t)/n$. The latter two values are obtained from the probability distribution function, $F(t)$, of t . Since a point is placed according to the two-dimensional uniform distribution over S_0 , the probability of the point being placed in a subregion in S_0 is given by the ratio of the area of the subregion to that of the whole region S_0 (recall Section 1.3.3). As a subregion, we consider the region $S(t)$ in which the NN-distance from any point p in $S(t)$ to O is less than or equal to t , i.e.

$$S(t) = \{p \mid d(p, O) \leq t, p \in S_0\}. \quad (8.3.5)$$

We call this region the *buffer zone* of objects O with distance t . Since the value of $F(t)$ is the probability that the NN-distance from a random point to O is less than or equal to t , $F(t)$ is given by

$$F(t) = \frac{|S(t)|}{|S_0|}, \quad (8.3.6)$$

where $|S(t)|$ indicates the area of $S(t)$. At first glance, the exact form of the function $|S(t)|$ or $F(t)$ is difficult to obtain. Fortunately, however, if we use a Voronoi diagram, we can exactly obtain the function $|S(t)|$. Since the computational method differs according to the shape of objects O , we deal with the NND methods for point-like objects, line-like objects, and area-like objects, separately.

8.3.1 Nearest neighbour distance method for point-like objects

When the area occupied by an object O_i is very small relative to the whole region S_0 , we may regard O_i as a point, and O as a set of points. We call the NND method for this set the *NND method for point-like objects*. Using this method, we may examine the effect of point-like objects O on the distribution of point-like elements P . For example, we may examine the effect of firms (O) polluting the air with smoke on the distribution of patients (P) suffering from asthma, and the association of news stands (P) around stations (O). An actual application was carried out by Okabe and Miki (1984) who examined the effect of railway stations (O) on the distribution of several kinds of retail stores (P) in Toshima, Tokyo. Figure 8.3.1 shows the distribution of book stores (the filled circles) with respect to railway stations (the unfilled circles).

As we mentioned above, when we use the index R in practice, we have to calculate the value of $d(p_i, O)$ and the moments of $t = d(p, O)$, i.e. $E(t)$ and $\text{Var}(t) = E(t^2) - E(t)^2$. Recalling Problem P3 in Section 2.3, we notice that $d(p_i, O)$ can be efficiently computed using the ordinary Voronoi diagram. First, we generate the Voronoi diagram $\mathcal{V} = \{V(O_1), \dots, V(O_n)\}$ with point-like objects O (indicated by continuous lines in Figure 8.3.1). Second, we find in which Voronoi polygon a point p_i is located. This search problem is known as the *point-location problem*, and several efficient computational methods are proposed (see Chapter 4). Once $p_i \in V(O_j)$ is known, $d(p_i, O)$

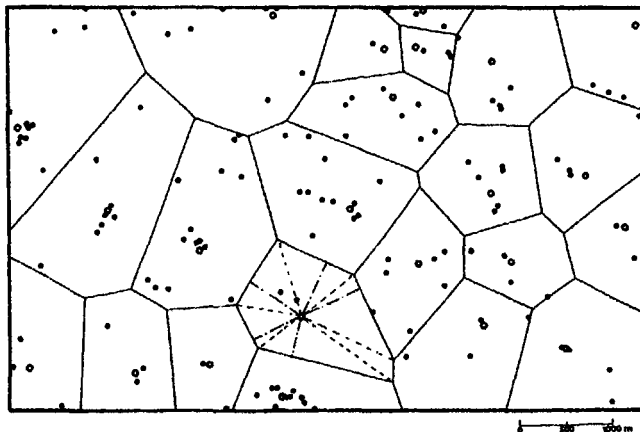


Figure 8.3.1 The location of the railway stations (the unfilled circles), the distribution of book stores (the filled circles) in Toshima and the Voronoi diagram generated by the railway stations. (Source: Miki, 1983, Figure 3.7.)

is readily given by $d(p_i, O_j)$. Substituting this value into equation (8.3.3), we obtain the value of \bar{t} in equation (8.3.4).

The moments of the NN-distance to point-like objects (the moments of the distance from a random point to the nearest generator point) We next show the procedure for calculating the moments of t . First, we generate the Voronoi diagram \mathcal{V} with point-like objects O . We next triangulate each Voronoi polygon by the line segments connecting generator O_i and Voronoi vertices (indicated by the broken lines in Figure 8.3.1). We further partition the resulting triangle by the line passing through O_i perpendicular to the facing edge if the line crosses the edge (indicated by the dash-dotted lines in Figure 8.3.1). As a result, the whole region S is partitioned into a set of obtuse or right angle triangles $S = \{S_1, \dots, S_k\}$, where $S = S_1 \cup \dots \cup S_k$.

Figure 8.3.2 depicts a triangle S_i in S , where the vertex O_i is placed on the v -axis and the other two vertices are placed on the u -axis. Let θ_{ii} , θ_{iz} , u_{ii} , u_{iz} , v_{io} , t_{ii} and t_{iz} be those indicated in Figure 8.3.2, respectively, and $S_i(t) = S(t) \cap S_i$. Then the probability distribution function of equation (8.3.6) is written as

$$F(t) = \frac{1}{|S_0|} \sum_{i=1}^k |S_i(t)|. \quad (8.3.7)$$

With the help of Figure 8.3.2, we obtain $|S_i(t)|$ as

$$|S_i(t)| = \begin{cases} \frac{1}{2} t^2 (\theta_{iz} - \theta_{ii}) & \text{for } 0 \leq t \leq t_{ii}, \\ \frac{1}{2} v_{io} \left(\sqrt{t^2 - v_{io}^2} - u_{ii} \right) + \frac{1}{2} t^2 \left(\theta_{iz} - \arccos \frac{v_{io}}{t} \right) & \text{for } t_{ii} \leq t \leq t_{iz}, \\ \frac{1}{2} v_{io} (u_{iz} - u_{ii}) & \text{for } t_{iz} \leq t. \end{cases} \quad (8.3.8)$$

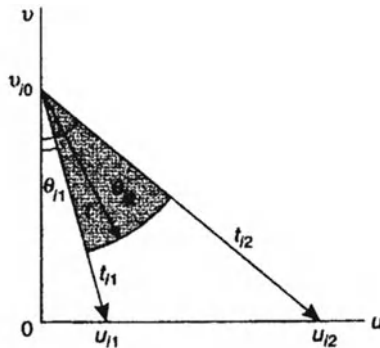


Figure 8.3.2 A triangle in the triangulated Voronoi diagram shown in Figure 8.3.1.

Thus we can explicitly obtain the probability distribution function $F(t)$ by substituting equation (8.3.8) into equation (8.3.7).

The probability density function $f(t)$ of $F(t)$ is obtained from

$$f(t) = \frac{dF(t)}{dt} = \frac{1}{|S_0|} \frac{d|S(t)|}{dt} = \frac{1}{|S_0|} \sum_{i=1}^k \frac{d|S_i(t)|}{dt} = \frac{1}{|S_0|} \sum_{i=1}^k s_i(t). \quad (8.3.9)$$

The r th moment of t is given by

$$E(t^r) = \int_0^\infty t^r f(t) dt = \frac{1}{|S_0|} \sum_{i=1}^k \int_0^\infty t^r s_i(t) dt. \quad (8.3.10)$$

After several steps of calculation, we obtain the second integral in equation (8.3.10) as:

if r is even ($r = 2q - 2$, $q \geq 1$),

$$\begin{aligned} \int_0^\infty t^r s_i(t) dt &= \frac{(2q-2)!!}{2q(2q-1)!!} \sum_{j=0}^{q-1} \frac{(2j-1)!!}{(2j)!!} \\ &\times \left[u_{i2}(u_{i2}^2 + v_{i0}^2)^j - u_{i1}(u_{i1}^2 + v_{i0}^2)^j \right] v_{i0}^{2q-2j-1}; \end{aligned} \quad (8.3.11)$$

if r is odd ($r = 2q - 1$, $q \geq 1$),

$$\begin{aligned} \int_0^\infty t^r s_i(t) dt &= \frac{(2q-1)!!}{(2q+1)(2q)!!} \\ &\times \left\{ \sum_{j=0}^{q-1} \frac{(2j)!!}{(2j+1)!!} \left[u_{i2}(u_{i2}^2 + v_{i0}^2)^{j+1/2} - u_{i1}(u_{i1}^2 + v_{i0}^2)^{j+1/2} \right] v_{i0}^{2q-2j-1} \right. \\ &\left. + v_{i0}^{2q+1} \ln \left(\frac{\sqrt{v_{i0}^2 + u_{i2}^2} + u_{i2}}{\sqrt{v_{i0}^2 + u_{i1}^2} + u_{i1}} \right) \right\} \end{aligned} \quad (8.3.12)$$

(Okabe, 1987; Yoshikawa, 1989). Substituting this equation into equation (8.3.10), we can explicitly obtain the expected value $E(t)$ and the variance

$\text{Var}(t) = E(t^2) - E(t)^2$. Okabe and Miki (1984) calculated the value of R for book stores in Figure 8.3.1 with these equations, and obtained $R = 0.727$. Since this value was smaller than unity with significance level 0.05, they rejected the null hypothesis that the book stores were independently and uniformly distributed over Toshima. The book stores tended to gather around railway stations.

Besides the NND method, the moments of the NN-distance are also used in the quantizing problem encountered in applications to analog-to-digital conversion (Conway and Sloane, 1993, Chapter 22). This problem asks how to place points in space so that the average second moment of their Voronoi polygons is as small as possible. This problem is discussed with the second moments of the NN-distance of m -dimensional Voronoi diagrams generated by several types of lattice points. These moments are shown in Conway and Sloane (1993, Chapter 22) (see also a related discussion in Section 7.1).

8.3.2 Nearest neighbour distance method for line-like objects

When the area occupied by an object O_i is very narrow and long relative to the whole region S_0 , we may regard the object as a line segment, and O as a set of line segments. We call the NND method for this set the *NND method for line-like objects*.

Applications of the NND method for line-like objects are shown by Okabe and Fujii (1984) and Okabe and Yoshikawa (1989). Figure 8.3.3 illustrates the distribution of high-class apartment buildings (the dots) and arterial streets (the continuous lines) in Kohto-Sumida, Tokyo. Okabe and Yoshikawa

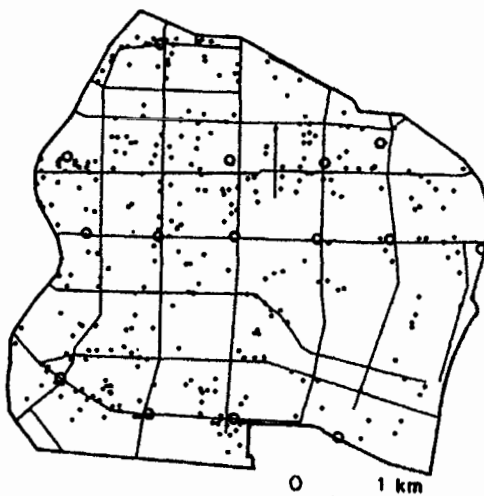


Figure 8.3.3 The distribution of high-class apartment buildings (dots) and the arterial streets (continuous lines) in Kohto-Sumida, Tokyo. (Source: Okabe and Yoshikawa, 1989, Figure 9.)

(1989) asked whether or not the distribution of high-class apartment buildings was affected by arterial streets. This question can be examined by the NND method for line-like objects.

To carry out this statistical examination, we have to calculate $d(p_i, O)$ and the moments of $t = d(p, O)$. First, to gain computational tractability, we assume that a set of line-like objects O is represented by a set of chains of straight line segments. A curved line is approximated by the chain of connected small straight line segments. If this modification is made, the procedure is essentially the same as that of the NND method for point-like objects. We construct the Voronoi diagram $\mathcal{V} = \{V(O_1), \dots, V(O_n)\}$ generated by the decomposed set of the line generator set O (see Section 3.5). We next find in which Voronoi region a point p_i is placed. Once $p_i \in V(O_j)$ is known, the NN-distance $d(p_i, O)$ is given by $d(p_i, O_j)$.

The moments of the NN-distance to line-like objects (the moments of the distance from a random point to the nearest generator line) We next show the procedure for calculating the moments of t . This procedure is similar to that in Section 8.3.1. We first generate the Voronoi diagram \mathcal{V} . Second, when a generator is a point O_i , we join the vertices of $V(O_i)$ and O_i by line segments (the broken lines in Figure 8.3.4). Third, when a generator is a line segment O_i , we consider the line that passes through a vertex of $V(O_i)$ and is perpendicular to the generator line O_i . If this line crosses the generator line O_i other than its end points (the dash-dotted lines), we partition $V(O_i)$ by that line. As a result, S_0 is partitioned into subregions and these subregions are classified into four types, three of which are shown in Figure 8.3.5 and the other one is shown in Figure 8.3.2. Let S_{ij} be the j th subregion of type i , $j = 1, \dots, k_i$, $i = 1, \dots, 4$, and $S_{ij}(t) = S_{ij} \cap S(t)$, i.e. the buffer zone in S_{ij} . Then the probability distribution function $F(t)$ of equation (8.3.6) is written as

$$F(t) = \frac{|S(t)|}{|S_0|} = \frac{1}{|S_0|} \sum_{i=1}^4 \sum_{j=1}^{k_i} |S_{ij}(t)|. \quad (8.3.13)$$

To give the explicit form of $S_{ij}(t)$, let $u_{j1}, u_{j2}, t_{j1}, t_{j2}, a, \theta_{j1}$ and θ_{j2} be those indicated in Figure 8.3.5, respectively. Then, $S_{ij}(t)$ is given by

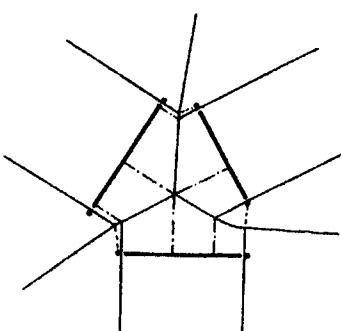


Figure 8.3.4 The partition of a Voronoi diagram generated by a set of lines for calculating the moments of t .

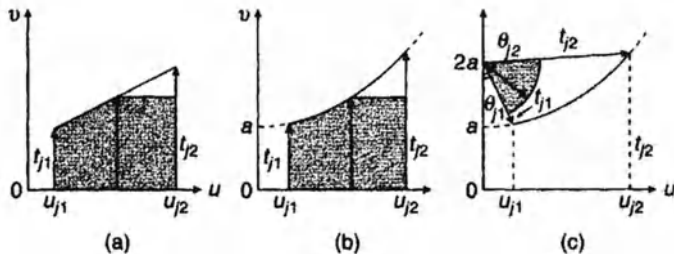


Figure 8.3.5 Four types of subregions constituting a Voronoi diagram generated by a set of line segments (three types are shown here; the fourth type is shown in Figure 8.3.2).

$$|S_{ij}(t)| = \begin{cases} (u_{j2} - u_{j1})t & \text{for } 0 \leq t \leq t_{j1}, \\ -\frac{(u_{j2} - u_{j1})(t - t_{j1})^2}{2(t_{j2} - t_{j1})} + (u_{j2} - u_{j1})t, & \text{for } t_{j1} \leq t \leq t_{j2}, \\ \frac{1}{2}(u_{j2} - u_{j1})(t_{j2} + t_{j1}) & \text{for } t_{j2} \leq t; \end{cases} \quad (8.3.14)$$

$$|S_{2j}(t)| = \begin{cases} (u_{j2} - u_{j1})t & \text{for } 0 \leq t \leq t_{j1}, \\ -\frac{4}{3}\sqrt{a}(t-a)^{3/2} - \frac{u_{j1}^3}{12a} - au_{j1} + u_{j2}t & \text{for } t_{j1} \leq t \leq t_{j2}, \\ a(u_{j2} - u_{j1}) + \frac{u_{j2}^3 - u_{j1}^3}{12a} & \text{for } t_{j2} \leq t; \end{cases} \quad (8.3.15)$$

$$|S_{3j}(t)| = \begin{cases} \frac{1}{2}(\theta_{j2} - \theta_{j1})t^2 & \text{for } 0 \leq t \leq t_{j1}, \\ \frac{1}{3}\sqrt{a}(t+2a)\sqrt{t-a} - \frac{1}{2}au_{j1} - \frac{u_{j1}^3}{24a} + \frac{1}{2}t^2\left[\theta_{j2} - \arccos\left(\frac{2a}{t}-1\right)\right] & \text{for } t_{j1} \leq t \leq t_{j2}, \\ \frac{u_{j2}^3 - u_{j1}^3}{24a} + \frac{1}{2}a(u_{j2} - u_{j1}) & \text{for } t_{j2} \leq t. \end{cases} \quad (8.3.16)$$

Notice that $S_{4j}(t)$ is given by $S_j(t)$ of equation (8.3.8).

The probability density function $f(t)$ of $F(t)$ is obtained from

$$f(t) = \frac{dF(t)}{dt} = \frac{1}{|S_0|} \frac{d|S(t)|}{dt} = \frac{1}{|S_0|} \sum_{i=1}^4 \sum_{j=1}^{k_i} \frac{d|S_{ij}(t)|}{dt} = \frac{1}{|S_0|} \sum_{i=1}^4 \sum_{j=1}^{k_i} s_{ij}(t). \quad (8.3.17)$$

The r th moment of t is given by

$$E(t^r) = \int_0^\infty t^r f(t) dt = \frac{1}{|S_0|} \sum_{i=1}^4 \sum_{j=1}^{k_i} \int_0^\infty t^r s_{ij}(t) dt. \quad (8.3.18)$$

Differentiating equations (8.3.8) and (8.3.14)–(8.3.16) with respect to t and evaluating the integral in equation (8.3.18), we obtain

$$\int_0^\infty t' s_{1j}(t) dt = \frac{(u_{j2} - u_{j1})(t_{j2}^{r+2} - t_{j1}^{r+2})}{(t_{j2} - t_{j1})(r+1)(r+2)}, \quad (8.3.19)$$

$$\int_0^\infty t' s_{2j}(t) dt = \frac{1}{r+1} \sum_{i=1}^{r+1} \binom{r+1}{i} \frac{a^{r+1-2i} (u_{j2}^{2i+1} - u_{j1}^{2i+1})}{2^{2i}(2i+1)}, \quad (8.3.20)$$

$$\int_0^\infty t' s_{3j}(t) dt = \frac{1}{r+2} \sum_{i=0}^{r+1} \binom{r+1}{i} \frac{a^{r+1-2i} (u_{j2}^{2i+1} - u_{j1}^{2i+1})}{2^i(2i+1)} \quad (8.3.21)$$

(Yoshikawa, 1989). Notice that $\int_0^\infty t' s_{4j}(t) dt$ is given by equations (8.3.11) and (8.3.12). Substituting equations (8.3.11), (8.3.12) and (8.3.19)–(8.3.21) into equation (8.3.18), we can explicitly obtain the values of $E(t)$ and $\text{Var}(t)$.

Through the above procedure, Okabe and Yoshikawa (1989) calculated the statistic R and showed that high-class apartment buildings tended to locate along arterial streets in Kohto-Sumida, Tokyo (Figure 8.3.3).

8.3.3 Nearest neighbour distance method for area-like objects

When we cannot ignore the area of object O_j , we should apply the NND method for area-like objects. Figure 8.3.6 shows its typical application provided by Okabe *et al.* (1988). In the figure, the area-like objects O indicated by shaded polygons are big parks in Setagaya, Tokyo, and the point-like elements P indicated by the unfilled circles are high-class apartment buildings. They examined whether or not the distribution of high-class apartment buildings was affected by big parks.

The procedure of the the NND method for area-like objects is just the same as that for line-like objects, and so we do not repeat it here. Through that procedure, Okabe *et al.* (1988) calculated the statistic R and came to the conclusion that the distribution of high-class apartment buildings being independent of the location of big parks could not be rejected with significance level 0.05 in Setagaya, Tokyo.



Figure 8.3.6 The distribution of high-class apartment buildings (the unfilled circles) and big parks (the shaded polygons) in Setagaya, Tokyo. (Source: Okabe *et al.*, 1988, Figure 1.)

8.3.4 Multi nearest neighbour distance method

In the above three subsections we showed the methods that examined the effect of only one type of objects O on the distribution of point-like elements P . In the real world, the effect is likely to be compounded; more than one type of objects, $O_{(j)}, j \in I_m$, compoundly affect the distribution of point-like objects P . For instance, as is shown in Figure 8.3.3, it is likely that the distribution of high-class apartment buildings is compoundly affected by subway stations (the unfilled circles) and arterial streets (the solid lines).

To examine this compound effect, Okabe and Yoshikawa (1989) generalize the above univariate index R into the multivariate index

$$R = \left(\frac{\bar{t}_{(1)}}{E(\bar{t}_{(1)})}, \dots, \frac{\bar{t}_{(m)}}{E(\bar{t}_{(m)})} \right), \quad (8.3.22)$$

where $\bar{t}_{(i)}$ is the average NN-distance defined by equation (8.3.3) for objects $O_{(i)}, i \in I_m$. With this multivariate index, we can examine the compound effect of several kinds of objects, $O_{(1)}, \dots, O_{(m)}$, on the distribution of point-like elements P . Using this index, Okabe and Yoshikawa (1989) found that there was a compound effect of arterial streets and subway stations on the distribution of high-class apartment buildings in Kohto-Sumida, Tokyo (see Okabe and Yoshikawa, 1989, for a detailed discussion).

8.4 THE SHAPE OF A POINT PATTERN

There is no single precise definition of the term shape. Instead, exact meanings are context dependent (for example, see Section 5.11). The shape of a point pattern is the geometric form produced by identifying and linking ‘essential’ members of a point set $P = \{p_1, p_2, \dots, p_n\}$ in \mathbb{R}^m (Kirkpatrick and Radke, 1985; Radke, 1988). Essential points are defined in terms of their spatial relationships with other members of P . Since there is no unique way of either selecting or joining essential points, more than one shape can be defined for P . However, most of the resulting shapes are either linear or polygonal structures. Following Kirkpatrick and Radke (1985) and Jaromczyk and Toussaint (1992), we refer to these as internal and external shapes, respectively, although the terms endo-skeleton and exo-skeleton (Radke, 1988) and skeleton and shape hull (Toussaint, 1980b) are also used elsewhere. In this section we describe measures that use features of Voronoi diagrams or related structures, with the emphasis placed on point sets in \mathbb{R}^2 .

8.4.1 Internal shape

We begin by noting that each shape defined in the above way is equivalent to a graph whose vertices are a subset of P and whose edges join points that are related in some sense. Since the Delaunay triangulation of P , $\mathcal{D}(P)$, can be considered a maximal planar description of the internal structure of P ,

attention has focused on using subgraphs of $\mathfrak{D}(P)$ described in Section 2.5 as measures of internal shape, in particular the Euclidean minimum spanning tree EMST(P), the relative neighbourhood graph RNG(P), and the Gabriel graph GG(P) which provide, respectively, increasingly more detailed descriptions of the internal shape of P .

Fairfield (1983) also proposes using subgraphs of $\mathfrak{D}(P)$ generated using a threshold value t . His method involves examining paths of $\mathcal{V}(P)$. A path is a connected series of segments of $\mathcal{V}(P)$. For any location s on the path, the spread angle of the path is the angle defined by p_i and p_j where p_i and p_j are the two closest points to s on either side of the path. Then define the internal concavity of the path as the difference between the spread angle of the first and last points on the path as it is traversed in a given direction. A path is said to be t -increasing if it contains a subpath of concavity $\geq t$ and it contains no subpath of concavity $\leq -t$. A maximal t -increasing path is a t -increasing path which is contained within a no longer t -increasing path. Once all of the maximal t -increasing paths of $\mathcal{V}(P)$ have been found, they are 'cut' into pieces of internal concavity less than t , using the minimal number of cuts. When a path is cut on a Voronoi edge e , the edge of $\mathfrak{D}(P)$ which corresponds to e is drawn. The set of all such Delaunay edges so drawn constitutes the internal shape of P . Note that $t = 0$ gives $\mathfrak{D}(P)$ and as t increases, smaller subsets of $\mathfrak{D}(P)$ are produced (see Figure 8.4.1).

Recall from Section 2.5 that the links in RNG(P) and GG(P) can be defined in terms of empty spindles and empty circles, respectively. Kirkpatrick and Radke (1985) generalize this idea to produce a spectrum of internal shapes. They do this by defining two points p_i and p_j in P , distance $d(p_i, p_j)$ apart, as β -neighbours if their neighbourhood or region of influence $N(p_i, p_j, \beta)$ contains no other points of P , where β is a positive real valued parameter whose magnitude reflects the size of the neighbourhood. The β -skeleton of P is the set of edges joining the β -neighbours of P . They consider two different ways of operationalizing the neighbourhoods. In the first, for

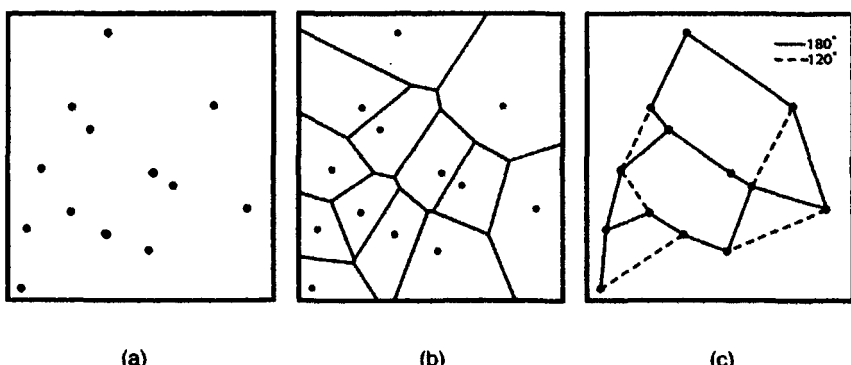


Figure 8.4.1 Defining an internal shape of a point pattern using Voronoi diagram concavity: (a) point pattern; (b) Voronoi diagram; (c) internal shape for two different values of t . (Source: Fairfield, 1983, Figure 4.)

$\beta \geq 1$, $N(p_i, p_j, \beta)$ is the intersection of the two circles of radius $\beta d(p_i, p_j)/2$ centred at locations $[(1 - \beta/2)p_i + (\beta/2)p_j]$ and $[(\beta/2)p_i + (1 - \beta/2)p_j]$, respectively, while for $0 < \beta < 1$, $N(p_i, p_j, \beta)$ is the intersection of two circles of radius $d(p_i, p_j)/(2\beta)$ passing through both p_i and p_j . When $\beta = 1, 2$, the β -skeleton is identical to $GG(P)$ and $RNG(P)$, respectively. An alternative is to define $N(p_i, p_j, \beta)$ for $\beta \geq 1$ as the union of the two circles of radius $\beta d(p_i, p_j)/2$ which pass through both p_i and p_j and for $0 < \beta < 1$ as the intersection of the two circles of radius $d(p_i, p_j)/2\beta$ that pass through p_i and p_j . In this case, when $\beta = 1$ the β -skeleton again corresponds to $GG(P)$.

8.4.2 External shape

One of the simplest measures of this type is provided by the convex hull $CH(P)$ of P (see Section 2.5 and Figure 8.4.2(b)). Simple extensions of this measure have been proposed to accommodate specific features of the spatial distribution of P such as concavities. For example, Jarvis (1977) suggests defining n subsets of P consisting of each point of P and its k ($1 \leq k \leq n$) nearest neighbours, generating the convex hull of each subset, and overlaying them. The external shape is defined by the union of the free edges of the union of convex hulls. Thus, as $k \rightarrow n$, this shape approaches $CH(P)$. Figure 8.4.2(c) shows this shape hull for $k = 3$. Toussaint (1980) proposes the *Gabriel hull* which involves removing from $CH(P)$ any edge which does not intersect the dual Voronoi diagram edge and replacing it with two new edges, one of which extends from one of the vertices of the removed edge to the generator point of the first Voronoi polygon traversed by the removed edge (see Figure 8.4.2(d)).

Edelsbrunner *et al.* (1983) generalize the notion of a convex hull to produce a spectrum of shapes which they call *α -hulls*. For an arbitrary real number α , they define a generalized disc of radius $1/\alpha$ as a disc of radius $1/\alpha$ if $\alpha > 0$, the complement of a disc of radius $|1/\alpha|$ if $\alpha < 0$, and a half plane if $\alpha = 0$. The α -hull of P is the intersection of all closed generalized discs of radius $1/\alpha$ that contain all points of P (see Figures 8.4.2(e) and (f)). If α is sufficiently large, the α -hull is the smallest enclosing circle of P ; if $\alpha = 0$ it is $CH(P)$; and if α is sufficiently small it is P itself. Furthermore, they define a point p_i in P as α -extreme if there exists a closed generalized disc of radius $|1/\alpha|$ such that p_i lies on its boundary and it contains all points of P . If for two α -extreme points, p_i and p_j , there exists a closed generalized disc of radius $|1/\alpha|$ with both points on its boundary and which contains all other points of P , p_i and p_j are said to be α -neighbours. Then the α -shape of P is a straight line graph whose vertices are the α -extreme points and whose edges connect the respective α -neighbours. As the value of α decreases, the α -shapes provide increasingly more detailed descriptions of the external shape of P . Edelsbrunner *et al.* (1983) show that when $\alpha \geq 0$, any α -shape is a subgraph of the Delaunay triangulation of the farthest point Voronoi diagram of P (see Section 3.3.1), while for $\alpha \leq 0$ it is a subgraph of $\mathfrak{D}(P)$. Edelsbrunner and Mücke (1994) extend the concepts of α -hulls and

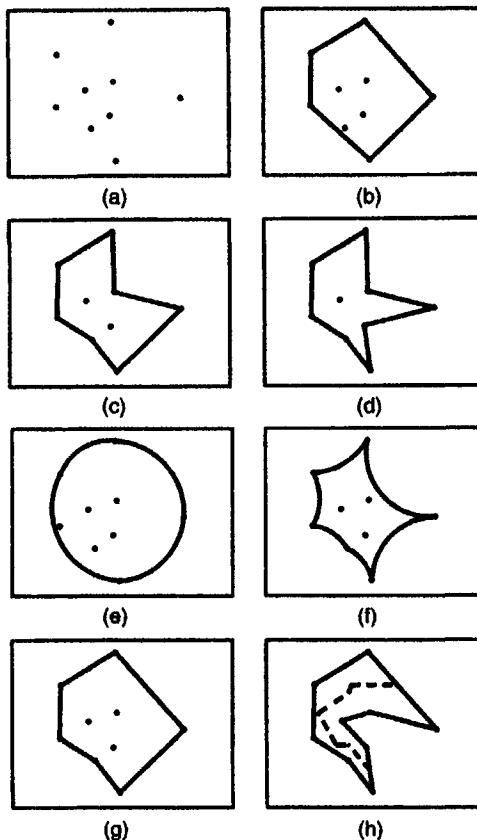


Figure 8.4.2 Different external shapes of a point pattern: (a) point pattern; (b) convex hull; (c) union of convex hulls of subsets of points; (d) Gabriel hull; (e) α -hull ($\alpha > 0$); (f) α -hull ($\alpha < 0$); (g) Pernus's circles of influence; (h) 'natural' simple polygon (the dashed line is the minimal spanning Voronoi tree).

α -shapes to finite point sets in \mathbb{R}^3 , while Saito *et al.* (1991) extend the concept of the α -hull to sets of figures of different shapes and sizes located in a digitized picture plane, labelling the resulting structure the *extended digital α -hull*, ED α -hull. They also consider different distance metrics in addition to Euclidean with the disc being replaced by a rhombus or a square for the Manhattan metric (L_1) and the supremum metric (L_∞) (see Section 3.7.1), respectively.

Pernus (1988) proposes a method combining aspects of both the Gabriel hull and the α -shape which involves circles of influence similar to those used by Kirkpatrick and Radke (1985) to develop the β -skeletons discussed in the previous section. For two points p_i and p_j located at (x_i, y_i) and (x_j, y_j) , respectively, a distance $d(p_i, p_j)$ apart, and a parameter t ($0 \leq t \leq \infty$), the circles of influence are the set of circles with centres

at $([x_i + x_j]/2 - [y_j - y_i]t, [y_i + y_j]/2 + [x_j - x_i]t)$ and radius $d(p_i, p_j)(1 + 4t^2)^{1/2}/2$. The method begins by generating $\mathcal{D}(P)$. Then for each pair of points p_i and p_j which are the end points of an edge of $\text{CH}(P)$ we examine their circle of influence for the specified value of t . If that circle is empty, the edge between p_i and p_j is retained; if not, the edge is removed. This process is repeated until no further edges are removed (see Figure 8.4.2(g)). The resulting shapes decrease in detail from the Gabriel hull ($t = 0$) to $\text{CH}(P)$ ($t = \infty$).

Another way to summarize the shape of P is with a simple polygon. Since the complete graph of P consists of $\binom{n}{2}$ edges, to create a simple polygon we need to choose $\left(\frac{\binom{n}{2}}{n}\right)$ edges. The magnitude of this search can be reduced by considering $\mathcal{D}(P)$ which has at most $(3n-6)$ edges (Property V11). The problem then becomes a search for a subgraph of $\mathcal{D}(P)$ which is a simple polygon. Furthermore, since the polygonal path must touch each and every vertex just once, it must be a Hamiltonian cycle. O'Rourke *et al.* (1987) note that the set of Delaunay triangles forming a simple polygon is also associated with a tree in $\mathcal{V}(P)$. In light of this, their choice for the most 'natural' simple polygon is that associated with the minimal spanning Voronoi tree of P which they define as the shortest subgraph of $\mathcal{V}(P)$ whose corresponding collection of Delaunay triangles forms the triangulation of a simple polygon which spans every point of P (see Figure 8.4.2(h)).

Boissonnat (1984) generates a simple polygon by sculpting $\text{CH}(P)$. He begins by defining $\mathcal{D}(P)$ and then eliminating sequentially triangles that have one or more edges forming part of $\text{CH}(P)$ or its subsequently sculpted form. The procedure continues until all members of P are located on the sculptured $\text{CH}(P)$. However, these simple polygon approaches will only be successful if $\mathcal{D}(P)$ contains a Hamiltonian cycle, which, although highly probable, is not universally true (Kantrabutra, 1983; Dillencourt, 1987a,b, 1990c, 1996a,b). Unfortunately, Dillencourt (1996a) shows that it is an NP-complete (Section 1.3.4) problem to determine if there is a Hamiltonian cycle in a non-degenerate Delaunay triangulation.

8.5 SPATIAL INTENSITY

When the point pattern under investigation is not homogeneous, we may wish to explore how the intensity of the phenomenon represented by the points varies over the study area. If we generate the Voronoi diagram of the point set $P = \{p_1, p_2, \dots, p_n\}$ and measure the area A_i of each polygon p_i , we can consider $1/A_i$ as an indicator of the local intensity of the point pattern at p_i (Duyckaerts *et al.*, 1994). In order to visualize variations in local intensity, Dahlberg (1967) suggests that we may represent each polygon as a prism whose height is inversely proportional to the area of the polygon (see Section 6.1.1 for a similar procedure). However, other characteristics of the Voronoi polygons besides area also reflect changes in spatial intensity. For example,

Voronoi polygons are elongated in a direction perpendicular to that of increasing intensity, while their generator points are increasingly displaced from their centres of gravity in the direction of increasing density (Ahuja and Tuceryan, 1989).

In some situations, instead of being concerned with local variations in intensity, the focus of our investigation is on estimating the intensity for the entire pattern. Such instances arise in forestry where estimates of the intensity of a particular tree species may be used in deriving expected timber yields, or in metallurgy where intensities of impurities in a given material above a specified level may invalidate its use for a particular purpose.

The obvious way of obtaining an estimate $\hat{\rho}$ of ρ , the spatial intensity of a point process, is to use

$$\hat{\rho} = n / |B|, \quad (8.5.1)$$

where $|B|$ is the area of B , or alternatively, to count the number, n_b , of the members of P in some bounded subregion, b of B of area $|b|$ and use

$$\hat{\rho} = n_b / |b|. \quad (8.5.2)$$

However, ρ may also be estimated using any of the techniques mentioned above such as quadrat, nearest neighbour and second-order methods. (See Upton and Fingleton, 1985, Chapter 2, for a review of the use of such methods in estimating intensity.) Voronoi polygons may also be used in this role.

If ρ is the intensity or number of points per unit of area, then the area per point is ρ^{-1} . Recognition of this provides an alternative way of estimating ρ . If we select a sample of m polygons from $\mathcal{V}(P)$ which satisfy the avoidance of edge effects and the independence conditions specified in Section 8.1.1, then the mean area \bar{A} of the sample polygons is given by

$$\bar{A} = \frac{1}{m} \sum_{i=1}^m A_i. \quad (8.5.3)$$

Brown (1965) suggests that the intensity may be estimated from

$$\hat{\rho} = 1 / \bar{A}. \quad (8.5.4)$$

However, this estimate is only asymptotically unbiased. To provide an unbiased estimate of ρ Ord (1978) uses the reciprocal of A_i so that the intensity estimate is given by

$$\hat{\rho} = \frac{1}{m} \sum_{i=1}^m (A_i^{-1}). \quad (8.5.5)$$

If we wish to provide a range for the above estimates, for equation (8.5.4) we need the variance $\text{Var}(A_i)$ of the sample areas given by

$$\text{Var}(A_i) = \frac{1}{m-1} \left[\sum_{i=1}^m (A_i^2) - \frac{1}{m} \left(\sum_{i=1}^m A_i \right)^2 \right], \quad (8.5.6)$$

and for equation (8.5.5) the variance $\text{Var}(A_i^{-1})$ of the reciprocals given by

$$\text{Var}(A_i^{-1}) = \frac{1}{m-1} \left[\sum_{i=1}^m (A_i^{-2}) - \frac{1}{m} \left(\sum_{i=1}^m A_i^{-1} \right)^2 \right]. \quad (8.5.7)$$

Thus, a two-standard-deviation range for \bar{A} in equation (8.5.4) is given by $\{\bar{A} \pm [\text{Var}(A_i)/m]^{1/2}\}$ while that for the mean of the reciprocals is given by $\{(\sum_{i=1}^m A_i^{-1})/m \pm [\text{Var}(A_i^{-1})/m]^{1/2}\}$. In general, the size of the range reflects the nature of the point pattern. If it is regular, there is little variation in the areas of the Voronoi polygons and so the variances in equations (8.5.6) and (8.5.7) are small leading to a small range. Conversely, clustered patterns produce Voronoi polygons of greatly varying sizes, thus producing large variances in equations (8.5.6) and (8.5.7) and large ranges.

When intensities are estimated in the field, as often arises in forest inventories, it is more practical to use the areas of Delaunay triangles defined by trees enclosing sampling sites (Ward, 1991), in which case a factor of 2 is included in the denominator and numerator of equations (8.5.4) and (8.5.5), respectively. Simulation studies undertaken by Ward suggest that using triangle areas produces more accurate estimates of intensity than either the quadrat or nearest neighbour methods, regardless of whether the distribution of trees is random, regular or clustered.

8.6 SEGMENTING POINT PATTERNS

For those patterns where there is marked spatial variation in the local intensity of points, we may wish to attempt to segment the pattern into component parts. Ahuja (1982) and Ahuja and Tuceryan (1989) suggest that individual points may be considered to belong to one of five types; isolated points, members of a curvilinear structure, members of a cluster with an empty interior, or members of either the boundary or the interior of a cluster with a non-empty interior (see Figure 8.6.1). They suggest that various geometric properties of the Voronoi polygons of a point and its neighbours (compactness, area, elongation, and eccentricity) and ratio measures involving the associated Delaunay edges can be used to determine to which group a point belongs. For example, the Voronoi polygons of points in the interior of a homogeneous cluster will all be compact, have approximately equal areas, small eccentricities, and little elongation. In contrast, in the interior of a non-homogeneous cluster, the areas, eccentricities and elongation of the Voronoi polygons all change with respect to the direction of density changes. David (1988a) illustrates the utility of such an approach by using volumes and adjacencies of Voronoi polyhedra of atoms to identify channels in macromolecular assemblies.

Tuceryan and Jain (1990) extend this approach to texture segmentation in images. This is the process of identifying regions in an image with similar texture and separating regions with different textures. Textures are defined in terms of tokens, which may take the form of either points or more complex primitives such as triangles or arrows, extracted from grey level images. They

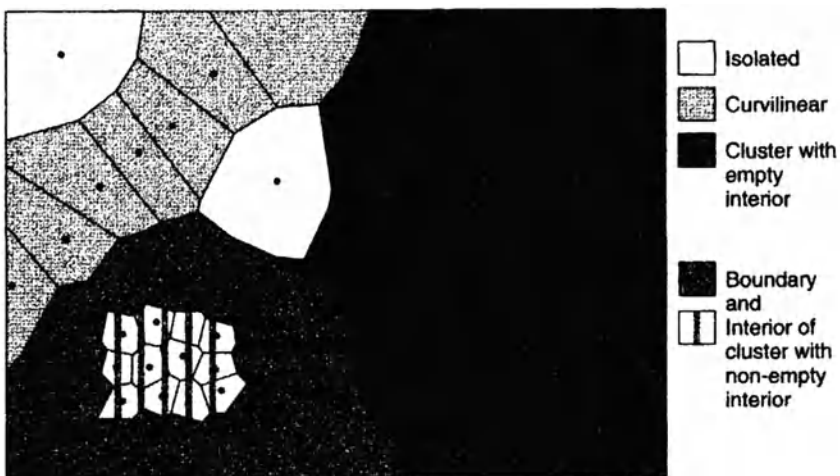


Figure 8.6.1 Segmenting a point pattern into component parts.

generate both the Voronoi diagram and the Delaunay tessellation of the set of image tokens and measure various order moments of each Voronoi region. A neighbour of token t_i is defined as any token whose Voronoi region is contiguous to the Voronoi region of t_i , $V(t_i)$, or contiguous to a Voronoi region which is contiguous to $V(t_i)$. If e_{ij} is the Delaunay edge linking tokens t_i and t_j , and N_i and N_j are the sets of neighbouring tokens for t_i and t_j , respectively, when e_{ij} lies in a single texture region the properties of N_i and N_j should be similar. Thus a 'break probability' can be assigned to e_{ij} in terms of the similarity of the order moments of the Voronoi regions of N_i and N_j .

If we are only interested in identifying clusters within a point pattern it may be possible to focus on just one characteristic. For instance, Yokoi and Toriwaki (1986) suggest defining a neighbourhood graph such as one of those described in Section 2.5 and then removing any point for which the average length of edges incident at the point exceeds some threshold value. The remaining connected points then constitute the clusters. A specific example of this approach is provided by Zahn (1971) who uses the Euclidean minimum spanning tree (see Section 2.5) and deletes any edge whose length is significantly longer than the average of those edges on both sides of the edge. Duyckaerts *et al.* (1994) propose a three-step iterative method for cluster identification which uses the areas of the Voronoi polygons of the points. The first step involves identifying the smallest polygon in the Voronoi diagram of the points which is designated the reference polygon. Step two examines the polygons which are contiguous to the reference polygon and adds to it those polygons whose areas do not exceed that of the reference polygon by more than some pre-specified proportion. This step is repeated until all newly examined polygons exceed the threshold. In the third step, the cluster so defined is removed from the pattern and the three steps are

repeated for the remaining polygons until no further clusters result. Isaac and Wyatt (1997) adopt a similar strategy to automatically segment multi-modal wave spectra into the individual modes present when the spectra are sampled by means of a set of sampling points. They show that the Voronoi diagram approach is particularly effective when the sampling points are non-uniformly distributed as they are for wave spectra extracted by the inversion of high-frequency radar backscatter.

8.7 MODELLING POINT PROCESSES

In this section we turn our attention away from the ways in which characteristics of Voronoi diagrams, Delaunay tessellations and related structures can be used in both exploring and modelling of point patterns to considerations of their use in constructing point processes. Most of this work focuses on *Markov point processes*.

A Markov point process on B is one in which the conditional distribution on A (a subset of B), given its behaviour in $B \setminus A$, depends only on its behaviour in $E(A) \setminus A$, where $E(A)$ is the environment of A given by means of a neighbourhood relation \sim on B (Stoyan *et al.*, 1995, p. 175). $E(A)$ is defined by

$$E(A) = \{x : x \sim y \text{ for some } y \in A\} \quad (8.7.1)$$

One possible definition of \sim is

$$x \sim y \text{ if and only if } \|x - y\| < r, \quad (8.7.2)$$

so that interaction occurs between all pairs of points within a fixed, predetermined range. Building on a suggestion by Ord (1977), Baddeley and Møller (1989) offer an alternative approach in which the neighbourhood relationships are defined in terms of the configuration of the points. One possibility is that a pairwise interaction occurs between points which are Voronoi neighbours. Another is to consider the interaction between triples of points whose Voronoi polygons share a common vertex. As an example, consider the simple sequential inhibition process mentioned in Section 5.12. In this process points are located sequentially at random in B subject to the constraint that a new point is at least some fixed distance r from any existing point. Weaker inhibitory effects can be produced by replacing this constraint with one in which a new point is realized if the area of its Voronoi polygon exceeds some pre-specified threshold size (Ord, 1977) or if the distance of a point to each of the vertices of its Voronoi polygon exceeds some pre-specified value (Baddeley and Møller, 1989).

Markov point processes may also be applicable in situations where the points in the pattern consist of more than one type so that a mark can be attached to each point indicating its type. Brown *et al.* (1981) describe a class of *two-type point processes* where the marginal process of both types of point is Poisson and an interaction occurs between points of different types.

In particular, they focus on the situation of inhibition between the two types. Such a process may be constructed in the following way. First, generate a Poisson Voronoi diagram. Then, for each Poisson Voronoi cell generate the number of events of each type, e_1 and e_2 , based on the marginal distributions of the processes and level of their correlation, and the area of the cell. Finally, locate the e_1 and e_2 events uniformly in the cell. The resulting process is stationary under rigid motions, ergodic, and mixing. Since this approach can be extended to any random partition, the Poisson Delaunay tessellation may be used instead of the Poisson Voronoi diagram.

In those situations where we wish to consider the phenomenon represented by the points at more than one scale, *fractal set models* may be appropriate, especially if the scales span several orders of magnitude. A set A has a fractal dimension d if the number of points inside a sphere of radius r is given by $N(A, r) = cr^d$ for some positive constant c (Zaninetti, 1991b). In an application in astronomy, Martinez *et al.* (1990) describe a stochastic point process in \mathbb{R}^3 which results in clustered patterns with multifractal properties very similar to those of real galaxies. This process involves generating a Poisson Voronoi diagram, then using the vertices of this diagram to generate a second Voronoi diagram whose vertices constitute the realization of the process.

CHAPTER 9

Locational Optimization Through Voronoi Diagrams

Voronoi diagrams are useful not only for the spatial analyses shown in the preceding chapters, but also for spatial optimization. In this chapter we discuss four classes of locational optimization problems which can be solved with the aid of Voronoi diagrams. The chapter consists of five sections. Section 9.1 is a preliminary section in which we briefly show a few non-linear non-convex optimization methods to be used in this chapter. The reader who is familiar with these methods can skip this preliminary section.

In Section 9.2 we deal with the locational optimization of points. In general, the problem is to determine the location of points so that the average distance (more generally, the average cost) to the nearest points is minimized. The problem varies slightly according to the nature of the points. We consider six kinds of points: point-like facilities used by independent individuals (e.g. public mail boxes); point-like facilities used by groups (e.g. tennis courts); a hierarchical facility (e.g. the main library and branch libraries); observation points for estimating some spatial quantities (e.g. pluviometers); service points of a mobile facility (e.g. a bookmobile) and nodes through which users go to a central point (e.g. bus stops for commuters). We show that these locational optimization problems can be solved with the ordinary and weighted Voronoi diagrams.

In Section 9.3 we discuss the locational optimization of lines. We deal with three types of lines. The first type of lines is a service route of a mobile facility (e.g. an ice-cream vendor). The optimization problem is to determine a service route to minimize the average distance (or cost) to the nearest point on a service route provided that the total length of the service route is given. The second type of lines is a network (e.g. a railway network). The optimization problem is to determine the location of nodes (stations) and links (railways) to minimize the total flow cost (or transportation cost) between any two points on a plane provided that the total length of a network and the flow density between any two points in a region are given. The third type of lines is the Steiner tree. The problem is to approximately obtain a big Steiner tree which cannot be obtained from combinatorial methods. We

show that the locational optimization problems of these types of lines can be solved with the help of the ordinary Voronoi diagram, the line Voronoi diagram and the Delaunay triangulation.

In Section 9.4 we consider two types of space-time optimization problem. The first type of problem is to optimize the location of point-like facilities that are constructed over multiple time-stages. The optimization is to minimize the distance (or cost) to the nearest facility averaged over users in a region as well as over time. The second type of problem is to determine the location of facilities which open periodically (e.g. marketplaces open every Sunday) so that the average distance (or cost) to the nearest facilities and the waiting time is minimized. We show that these two types of problems can be solved with the aid of the space-time Voronoi diagram and the Voronoi diagram on a cylinder.

In Section 9.5 we show a method for fitting a Voronoi diagram to a given polygonal tessellation. With this method we can see to what extent a Voronoi diagram fits a given tessellation. Moreover, we can apply this method to the locational optimization problem of point-like facilities whose use is spatially restricted.

9.1 PRELIMINARIES

In solving the locational optimization problems mentioned above, we meet a certain type of mathematical optimization problem, called the non-linear, non-convex programming problem. In this section we briefly present a few computationally feasible methods to solve this problem. The reader who wants to know the full details of non-linear programming methods should consult, for example, Fiacco and McCormick (1968), Gill *et al.* (1981), and Konno and Yamashita (1978).

9.1.1 The non-linear, non-convex programming problem

The *programming problem* referred to in the mathematical optimization literature is the problem in which we seek to determine n variables x_1, \dots, x_n which satisfy m_1 inequalities and/or m_2 equations, and, in addition, minimize a function of the n variables. Mathematically, the programming problem is written as

Problem OPT1 (the general programming problem)

$$\min_{x_1, \dots, x_n} F(x_1, \dots, x_n), \quad (9.1.1)$$

subject to

$$\begin{aligned} g_i(x_1, \dots, x_n) &\leq 0, \quad i = 1, \dots, m_1, \\ g_i(x_1, \dots, x_n) &= 0, \quad i = m_1 + 1, \dots, m_1 + m_2. \end{aligned} \quad (9.1.2)$$

We call the function in expression (9.1.1) an *objective function*. In this chapter we assume that the objective function has at least the first derivative and it is bounded below, i.e. $F(x) > K > -\infty$. We call relations (9.1.2) *constraints* and the functions in the constraints *constraint functions*. The programming problems with constraints ($m_1 + m_2 \geq 1$) and without constraints ($m_1 + m_2 = 0$) are called the *constrained programming problem* and the *unconstrained programming problem*, respectively. For simplicity, $F(x_1, \dots, x_n)$ and $g_i(x_1, \dots, x_n)$ are written as $F(\mathbf{x})$ and $g_i(\mathbf{x})$, where $\mathbf{x}^T = (x_1, \dots, x_n)$ is a vector in the n -dimensional Euclidean space \mathbb{R}^n . Note that since the maximization of $F(\mathbf{x})$ is equivalent to the minimization of $-F(\mathbf{x})$, we consider only the minimization problem; since $g_i(\mathbf{x}) \geq 0$ is equivalent to $-g_i(\mathbf{x}) \leq 0$, we consider only the two relations \leq and $=$ in the constraints of relation (9.1.2). In Figure 9.1.1 a simple example is depicted, where the objective function is a univariate function, $F(x) = x(x - 1)(x - 2)(x - 4)(x - 8)(x - 10) + 3000$, and the constraints are $g_1(x) = -x \leq 0$ and $g_2(x) = x \leq 10$ ($m_1 = 2, m_2 = 0$).

The constraints in relation (9.1.2) determine a region in \mathbb{R}^n , which is given by

$$S = \{\mathbf{x} \mid g_i(\mathbf{x}) \leq 0, i = 1, \dots, m_1; g_i(\mathbf{x}) = 0, i = m_1 + 1, \dots, m_1 + m_2\}. \quad (9.1.3)$$

We call the set S a *feasible region*, and $\mathbf{x} \in S$ a *feasible solution*. In the above example the feasible region is given by $S = \{\mathbf{x} \mid 0 \leq x \leq 10\}$, which is indicated by the heavy solid line in Figure 9.1.1. In this feasible region we notice three basins around the points indicated by x^*, x'^* and x^{**} . We call the bottom points in these basins *local minima*. To be precise, let $N_\varepsilon(x^*) = \{\mathbf{x} \mid \|\mathbf{x} - x^*\| < \varepsilon\}$ be an open ball centred at x^* with radius ε . If there exist a positive ε and $x^* \in S$ for which the relation $F(x^*) \leq F(\mathbf{x})$ holds for $\mathbf{x} \in S \cap N_\varepsilon(x^*)$, we call x^* a *local minimum (optimum)*. In the example of Figure 9.1.1, local minima are x^*, x'^* and x^{**} . Among them, the bottom

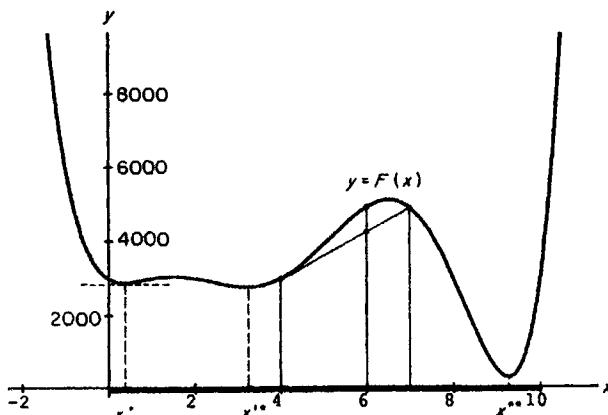


Figure 9.1.1 A feasible region, local minima, and the global minimum $F(x) = x(x - 1)(x - 2)(x - 4)(x - 8)(x - 10) + 3000, g_1(x) = -x \leq 0, g_2(x) = x \leq 10$.

at x^{**} is the lowest. We call such a bottom point the *global minimum*. Mathematically, if there exists $x^{**} \in S$ that satisfies $F(x^{**}) \leq F(x)$ for $x \in S$, we call x^{**} the *global minimum (optimum)*.

Since the functions $F(\mathbf{x})$ and $g_i(\mathbf{x})$ are general functions, programming problems subsumed under Problem OPT1 are various, but we can classify them into two classes: the linear programming problem and the non-linear programming problem. The *linear programming problem* is the programming problem in which each of the functions $F(\mathbf{x})$ and $g_i(\mathbf{x})$, $i \in I_{m_1+m_2}$, is a linear function, i.e. $F(x_1, \dots, x_n) = c_1x_1 + \dots + c_nx_n$, and $g_i(x_1, \dots, x_n) = a_{i1}x_1 + \dots + a_{in}x_n + b_i$. The *non-linear programming problem* is the programming problem in which either $F(\mathbf{x})$, or at least one of the functions $g_i(\mathbf{x})$, $i \in I_{m_1+m_2}$, is a non-linear function, such as $F(x_1, \dots, x_n) = c_1x_1^2 + \dots + c_nx_n^2$.

We can further classify the non-linear programming problem into two subclasses: the non-linear convex programming problem, and the non-linear, non-convex programming problem. If for any two points \mathbf{x}_1 and \mathbf{x}_2 in \mathbb{R}^n and for all $0 \leq \lambda \leq 1$, the following relation holds

$$F[\lambda\mathbf{x}_1 + (1 - \lambda)\mathbf{x}_2] \leq \lambda F(\mathbf{x}_1) + (1 - \lambda)F(\mathbf{x}_2), \quad (9.1.4)$$

we call the function $F(\mathbf{x})$ a *convex function*; otherwise, we call it a *non-convex function* (an alternative definition is given in Section 1.3.1). The function shown in Figure 9.1.1 is a non-convex function, because the relation (9.1.4) does not hold, for example, $F(0.5 \times 4 + 0.5 \times 7) > 0.5 F(4) + 0.5 F(7)$ (observe the two filled circles in Figure 9.1.1). If every non-linear function in the non-linear programming problem is convex, we call such a programming problem the *non-linear convex programming problem*; if at least one non-linear function in the non-linear programming problem is non-convex, we call it the *non-linear, non-convex programming problem*. As will be seen below, the programming problems encountered in the proceeding sections are the non-linear, non-convex programming problems.

9.1.2 The descent method

Let us first consider the unconstrained case of Problem OPT1, i.e.

Problem OPT 2 (the unconstrained programming problem)

$$\min_{x_1, \dots, x_n} F(x_1, \dots, x_n). \quad (9.1.5)$$

As is indicated by the horizontal broken line in Figure 9.1.1, the necessary condition for a local minimum of a univariate function is that the line tangential to the curve given by $y = F(x)$ at x^* is horizontal. Algebraically, this necessary condition is written as $dF(x)/dx = 0$. Similarly, the necessary condition of a multivariate function $F(x_1, \dots, x_n)$ for a local minimum is that the hyperplane tangential to the surface given by $y = F(\mathbf{x})$ at \mathbf{x}^* is horizontal. Algebraically, this condition is written as

$$\begin{aligned} \frac{\partial F(x^*)}{\partial x_1} &= 0, \\ &\vdots \\ \frac{\partial F(x^*)}{\partial x_n} &= 0. \end{aligned} \tag{9.1.6}$$

When the function $F(x)$ is a non-linear, non-convex function, we usually encounter analytical difficulty in solving the simultaneous equations of equation (9.1.6). It is almost impossible to obtain not only the global minimum but also a local minimum with the analytical method, or the so-called classical method. To overcome this difficulty, we may alternatively use a numerical method which gives a solution close to a local minimum with a certain precision level.

The difficulty in solving the non-linear programming problem may be intuitively understood by imagining the difficult situation in which we are lost in a rolling mountainous region (Figure 9.1.2(a)) covered with mist, and we are looking for the bottom of a basin in the region without a contour map (Figure 9.1.2(b)). Since we are surrounded by mist, we can see only the small area around us ($x^{(k)}$ in Figure 9.1.2(b)). What we can do therefore is to walk down observing the slope in this small area. First, we decide in which direction ($d^{(k)}$ in Figure 9.1.2(b)) we should walk down (Step 1). Once the direction is determined (the arrow in Figure 9.1.2(b)), we traverse straight in this direction (the straight line in Figure 9.1.2). Second, we decide at which point we should stop on this line (Step 2); third, when we reach that point ($x^{(k+1)}$ in Figure 9.1.2(b)), we reconsider the direction and repeat the same procedure from that point (Step 3); finally, if we reach a flat place, we stop

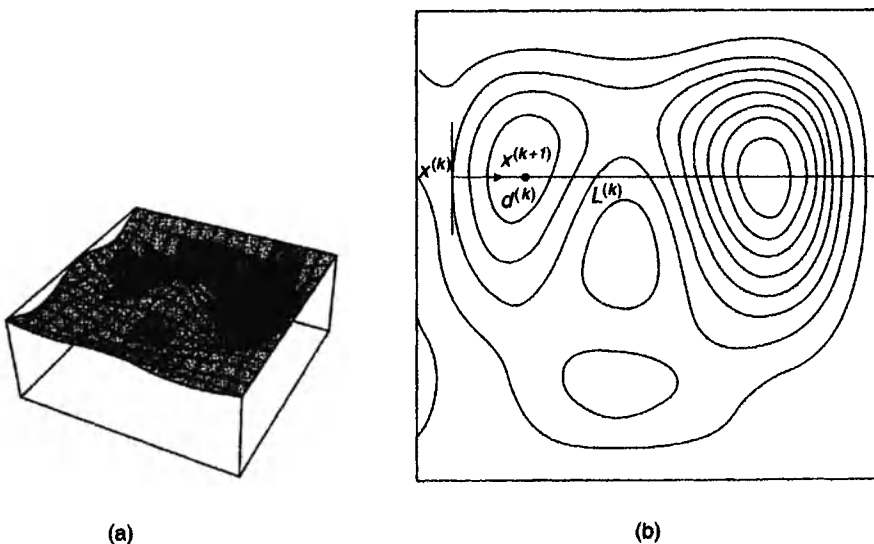


Figure 9.1.2 The descent method: (a) the surface of a function $F(x_1, x_2)$ and (b) its contour lines.

at that point (Step 4). We consider that the reached point is a bottom point (a local minimum). Since we do not know how many bottoms exist in the region, we only know that the reached bottom is one of the many bottoms (local minima). If we are lucky enough, the bottom may be the lowest bottom (the global minimum) in the region. The above search method is called the *descent method*, and its computational procedure is written algorithmically as follows.

Algorithm OPT1 (a prototype of the descent method)

- Step 0. Choose an arbitrary point $\mathbf{x}^{(0)} \in \mathbb{R}^n$, and substitute 0 for k (denoted by $k \leftarrow 0$).
- Step 1. Determine a direction vector $\mathbf{d}^{(k)}$ at the point $\mathbf{x}^{(k)}$.
- Step 2. Determine a step size $\alpha^{(k)}$ at the point $\mathbf{x}^{(k)}$.
- Step 3. $\mathbf{x}^{(k+1)} \leftarrow \mathbf{x}^{(k)} + \alpha^{(k)} \mathbf{d}^{(k)}$.
- Step 4. If $\|\mathbf{x}^{(k+1)} - \mathbf{x}^{(k)}\| < \varepsilon \approx 0$, report $\mathbf{x}^{(k+1)}$; otherwise, $k \leftarrow k+1$ and go to Step 1.

The descent method has several variations in the choice of direction vector $\mathbf{d}^{(k)}$ (Step 1). When the direction vector is given by the steepest direction, i.e.

$$\mathbf{d}^{(k)^T} = -\nabla F(\mathbf{x}^{(k)}) = -\left(\frac{\partial F(\mathbf{x}^{(k)})}{\partial x_1^{(k)}}, \dots, \frac{\partial F(\mathbf{x}^{(k)})}{\partial x_n^{(k)}}\right), \quad (9.1.7)$$

the descent method is called the *steepest descent method*. In the example of Figure 9.1.3, the steepest direction is shown by the solid arrow (note that the steepest direction is orthogonal to the contour line of $F(\mathbf{x})$). The steepest descent method has an advantage in that it requires only the first derivatives. On the other hand, it has a disadvantage in that the convergence to a local optimum solution is not always fast (compare the zig-zag solid line with the broken line in Figure 9.1.3). To overcome this disadvantage, the *Newton method* is proposed, in which the direction vector is given by

$$\mathbf{d}^{(k)^T} = -[\nabla^2 F(\mathbf{x}^{(k)})]^{-1} \nabla F(\mathbf{x}^{(k)}), \quad (9.1.8)$$

where $\nabla^2 F(\mathbf{x}^{(k)})$ is the Hessian matrix of $F(\mathbf{x}^{(k)})$, i.e.

$$\nabla^2 F(\mathbf{x}) = \begin{bmatrix} \frac{\partial^2 F}{\partial x_1^2} & \cdots & \frac{\partial^2 F}{\partial x_1 \partial x_n} \\ \vdots & \ddots & \vdots \\ \frac{\partial^2 F}{\partial x_n \partial x_1} & \cdots & \frac{\partial^2 F}{\partial x_n^2} \end{bmatrix}. \quad (9.1.9)$$

In the example of Figure 9.1.3, this direction is indicated by the broken arrow. The calculation of the Hessian matrix is, however, sometimes difficult. To diminish this difficulty, we may use a direction vector

$$\mathbf{d}^{(k)^T} = -[H^{(k)}]^{-1} \nabla F(\mathbf{x}^{(k)}), \quad (9.1.10)$$

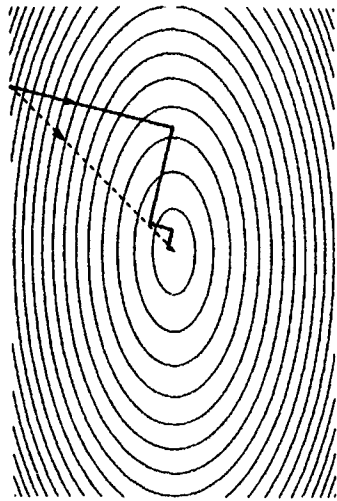


Figure 9.1.3 Direction vectors: the steepest direction (the solid arrow) and the direction used in the Newton method (the broken line).

where $H^{(k)}$ is a ‘simple’ approximation of the Hessian matrix in the sense that the matrix operation with $H^{(k)}$ is simpler than that with $\nabla^2 F(\mathbf{x})$. For example, $H^{(k)}$ is given by the matrix in which the diagonal elements are given by those of $\nabla^2 F(\mathbf{x})$ and the off-diagonal elements are zeros. We call this alternative method the *quasi-Newton method*. Formally, if $H^{(k)} = I$, the quasi-Newton method becomes the steepest descent method; if $H^{(k)} = \nabla^2 F(\mathbf{x}^{(k)})$, the method becomes the Newton method.

Having determined the direction vector $\mathbf{d}^{(k)}$ at the point $\mathbf{x}^{(k)}$ (Step 1), we next consider the straight line $L^{(k)}$ radiating from $\mathbf{x}^{(k)}$ in the direction $\mathbf{d}^{(k)}$, and search a point $\mathbf{x}^{(k+1)}$ on $L^{(k)}$ at which we reconsider the direction (Step 2). We call this search the *line search*. In the example of Figure 9.1.2(b), the direction vector $\mathbf{d}^{(k)}$ and the line $L^{(k)}$ are indicated by the arrow and the hair line, respectively. In the literature, several rules are proposed for the line search, for example, Curry’s rule, Altman’s rule, and Goldstein’s rule. Among them, Goldstein’s rule has an advantage in that we can always terminate the line search in a finite number of steps.

To show Goldstein’s rule explicitly, let α be the distance from $\mathbf{x}^{(k)}$ along the line $L^{(k)}$ toward the direction $\mathbf{d}^{(k)}$, and

$$h^{(k)}(\alpha) = F(\mathbf{x}^{(k)} + \alpha \mathbf{d}^{(k)}). \quad (9.1.11)$$

The function $h^{(k)}(\alpha)$ shows the value of $F(\mathbf{x})$ along the line $L^{(k)}$ (see $\beta = h^{(k)}(\alpha)$ on the α - β plane in Figure 9.1.4 obtained from $L^{(k)}$ in Figure 9.1.2(b)). The line tangential to $\beta = h^{(k)}(\alpha)$ at $\alpha = 0$ is given by

$$\tau^{(k)}(\alpha) = h^{(k)}(0) + \frac{\partial h^{(k)}(0)}{\partial \alpha} \alpha \quad (9.1.12)$$

(see $\beta = \tau^{(k)}(\alpha)$ in Figure 9.1.4). We now consider two lines passing through the point $(0, h^{(k)}(0))$ which are slightly flatter than the line of equation (9.1.12) (see Figure 9.1.4). Mathematically, these lines are written as

$$\eta_i^{(k)}(\alpha) = h^{(k)}(0) + \mu_i \frac{\partial h^{(k)}(0)}{\partial \alpha} \alpha, \quad i=1,2, \quad (9.1.13)$$

where $0 < \mu_1 \leq \mu_2 < 1$ (in practice, $\mu_1 = 0.4$ and $\mu_2 = 0.6$ are often used). With this function, we define the set

$$M^{(k)} = \{ \alpha \mid \eta_2^{(k)}(\alpha) \leq h^{(k)}(\alpha) \leq \eta_1^{(k)}(\alpha) \} \quad (9.1.14)$$

(see the heavy solid line segment on the α -axis in Figure 9.1.4). The set $M^{(k)}$ is always finite because $F(x)$ is assumed to be bounded below. Goldstein's rule is the rule in which we choose $\alpha^{(k)}$ in $M^{(k)}$. We can find such an $\alpha^{(k)}$ in a finite number of steps using the following algorithm.

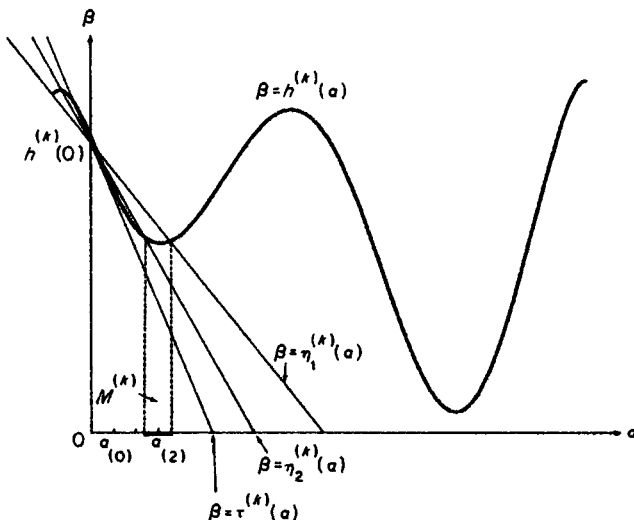


Figure 9.1.4 Goldstein's rule.

Algorithm OPT2 (Goldstein's rule)

- Step 0. Choose an arbitrary initial value $\alpha_{(0)} > 0$, and $i \leftarrow 0$.
- Step 1. $\alpha_{(i)} \leftarrow (i+1)\alpha_{(0)}$.
- Step 2. If $\eta_2^{(k)}(\alpha_{(i)}) \leq h^{(k)}(\alpha_{(i)})$, then go to Step 3; otherwise, $i \leftarrow i+1$ and go to Step 1.
- Step 3. If $h^{(k)}(\alpha_{(i)}) \leq \eta_1^{(k)}(\alpha_{(i)})$, then report $\alpha_{(i)}$; otherwise, $\alpha_{(i)} \leftarrow \frac{1}{2}\{\alpha_{(i)} + \alpha_{(i-1)}\}$, and go to Step 2 (where $\alpha_{(-1)} = 0$).

9.1.3 The penalty function method

The descent method is developed for the unconstrained non-linear programming problem (Problem OPT2); it cannot be directly applied to the constrained non-linear programming problem (Problem OPT1, $m_1 + m_2 \geq 1$). To solve the latter problem, we can use the 'transformation method'. The

essential idea is that we first transform a constrained non-linear programming problem into an unconstrained non-linear programming problem (Problem OPT2); next we solve this unconstrained programming problem with a method that solves the unconstrained programming problem, say the descent method. The transformation method has several variations, such as the penalty function method and the multiplier method. In this subsection we show the penalty function method, because this method is one of the most basic methods and many other methods are developed from this method.

In the constrained programming problem of Problem OPT1, we have to find a local minimum in the feasible region S determined by the relation (9.1.2). In the process of searching a local minimum, however, we may choose an infeasible solution. In such a case we are supposed to pay a penalty. If this penalty is extremely high, we give up that solution and try to find another solution. In the end, we may reach the local minimum in the feasible region S .

To state this method a little more precisely, suppose that a penalty $R_1(\mathbf{x})$ for an infeasible solution is given by

$$R_1(\mathbf{x}) = \begin{cases} +\infty & \text{if } \mathbf{x} \notin S, \\ 0 & \text{if } \mathbf{x} \in S, \end{cases} \quad (9.1.15)$$

and let $L(\mathbf{x}) = F(\mathbf{x}) + R_1(\mathbf{x})$. Noticing that $L(\mathbf{x})$ coincides with $F(\mathbf{x})$ for any feasible solution and it is $+\infty$ for any infeasible solution, we can restate the constrained programming problem (Problem OPT1) as the unconstrained programming problem:

$$\min_{\mathbf{x}} L(\mathbf{x}) = \min_{\mathbf{x}} [F(\mathbf{x}) + R_1(\mathbf{x})]. \quad (9.1.16)$$

In principle, this idea appears to work well, but we have a difficulty in implementing this method in practice. In the descent method, we assume that the objective function has at least the first derivative. The objective function $L(\mathbf{x})$ is, however, discontinuous at the boundary of the feasible region S , even if $+\infty$ is replaced by a very large number.

To overcome this difficulty, we approximate the penalty function $R_1(\mathbf{x})$ by a smooth function whose value (i.e. the penalty) smoothly increases as \mathbf{x} moves farther from the feasible region S . For instance,

$$R_2(\mathbf{x}) = \sum_{i=1}^{m_1} [\max \{g_i(\mathbf{x}, 0)\}]^2 + \sum_{l=m_1+1}^{m_1+m_2} g_l(\mathbf{x})^2. \quad (9.1.17)$$

To show how this penalty function works well, let us consider an illustrative example: $F(x) = (x+1)^2$, $g_1(x) = -x$ and $g_2(x) = x-1$, which are depicted in Figure 9.1.5. In this case, the penalty function of equation (9.1.17) is written as

$$R_2(x) = [\max \{-x, 0\}]^2 + [\max \{x-1, 0\}]^2, \quad (9.1.18)$$

which is shown in Figure 9.1.5(b). Then the transformed function is given by $L(x) = F(x) + R_2(x)$, which is depicted in Figure 9.1.5(c).

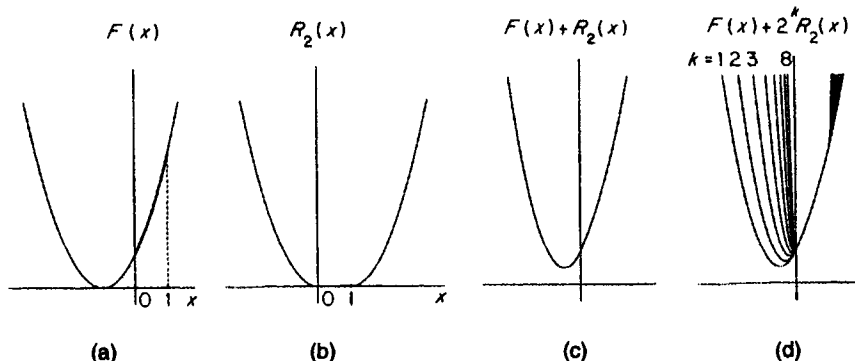


Figure 9.1.5 The penalty function method: (a) $F(x) = (x+1)^2$, $g_1(x) = -x \leq 0$, $g_2(x) = x-1 \leq 0$; (b) $R_2(x) = [\max\{-x, 0\}]^2 + [\max\{x-1, 0\}]^2$; (c) $L(x) = F(x) + R_2(x)$; (d) $L(x^{(k)}) = F(x) + 2^k R_2(x)$.

In this example we can analytically obtain the global minimum of $L(x)$, and the solution is $x^* = -0.5$. Obviously, this solution violates the constraint $g_1(x) = -x \leq 0$. This violation suggests that the penalty should be higher. We do not know in advance, however, how high the penalty should be. We hence increase the penalty from low to high according to $2^k R_2(x)$, $k = 0, 1, \dots$. As a result, we obtain a series of solutions, $-0.50, -0.33, -0.20, -0.11, -0.05, -0.03, -0.02, -0.01$ for $k = 0, \dots, 8$ (Figure 9.1.5(d)). As is easily noticed in Figure 9.1.5(a), the minimum is 0. The above series appears to approach this minimum.

In general, with the penalty function of equation (9.1.17), we can transform the constrained programming problem of Problem OPT1 into the unconstrained programming problem

$$\min_x L^{(k)}(x) = \min_x [F(x) + r_0^k R_2(x)], \quad (9.1.19)$$

where $r_0 > 1$. It is shown that if there exists a local optimum $x^{*(k)}$, for this unconstrained programming problem, then there exists a series $x^{*(0)}, x^{*(1)}, x^{*(2)}, \dots, x^{*(k)}, \dots$, that converges to a local minimum of the constrained programming problem, Problem OPT1. Hence, as we expected, the series in the above example actually converges to 0. This technique is called the *sequential unrestrained minimization technique* (Fiacco and McCormick, 1968).

We call the above method the *penalty function method* or, more specifically, the *exterior penalty function method*. With this method we can solve the constrained programming problems in the following sections. Of course we can use alternative methods which are modified from the exterior penalty function method, such as the *interior penalty function method* and the *mixed penalty function method*. Furthermore, to gain fast convergence, we may use the *multiplier method*. The reader who wishes to use these alternative methods should see, for example, Gill *et al.* (1981, Chapters 4–6).

9.2 LOCATIONAL OPTIMIZATION OF POINTS

Using the computational methods in Section 9.1, we now wish to solve the locational optimization problems mentioned in the introduction. We first discuss the locational optimization of points in a plane or in a space, where the points represent point-like facilities, service points, observation points, nests of birds, crystallites, points from which some influential power is generated, and so forth.

The study of locational optimization of point-like facilities may date back to Launhardt (1882) or Weber (1909) (the so-called Weberian problem; a historical review is provided by Wesolowsky, 1993), but the study has been rapidly progressed since Hakimi (1964) in Operations Research. The recent progress can be seen, for example, in Handler and Mirchandani (1979), the *European Journal of Operations Research* (1985, Vol. 20, No. 3), Love *et al.* (1988), Mirchandani and Francis (1990) and Drezner (1995). It should be noted that the problem dealt with there is mostly locational optimization on

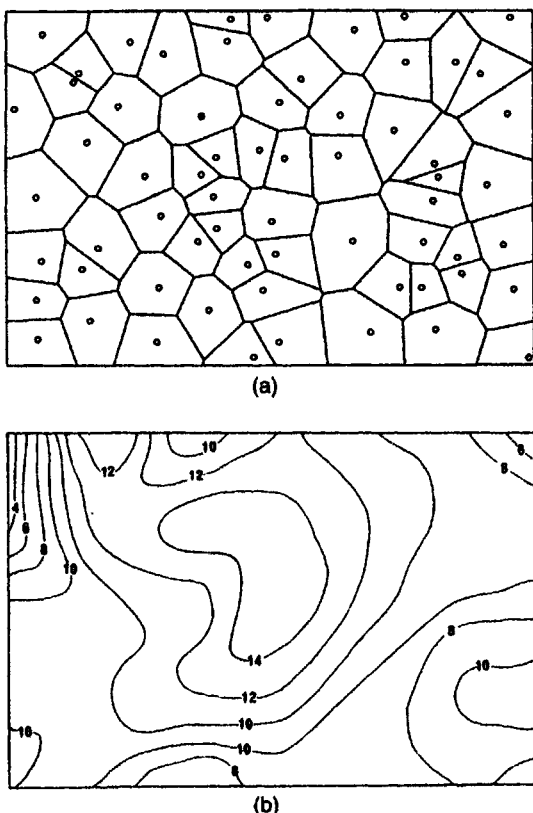


Figure 9.2.1 (a) Public mail boxes in Koganei district in Tokyo and (b) the distribution of population ($\times 10/\text{ha}$).

a network where the demand for services supplied by facilities is supposed to arise only on nodes of the network.

Compared with this rapid progress, progress was slow in the study of locational optimization in a continuous plane where demand arises at any point in a plane and feasible locations of facilities are any point in the plane. This slow progress was due to the lack of efficient computational methods for managing complicated geometrical calculation on a plane. In fact, the computational method in the 1960s could deal with less than twenty facilities, e.g. Leamer (1968). In the 1980s, however, computational geometry (Preparata and Shamos, 1985), in particular efficient computational methods for constructing a Voronoi diagram (Chapter 4), have been rapidly developed to overcome this difficulty (Iri *et al.*, 1984; Sugihara and Iri, 1992). We can now practically solve locational optimization problems of a large number of points in a continuous plane or space with Voronoi diagrams (see the review by Okabe and Suzuki, 1997).

9.2.1 Locational optimization of point-like facilities used by independent users

We first consider the locational optimization of point-like facilities which are used by independent users. A good example of such a facility is a public mail box. For illustrative purposes, we show an actual example in Figure 9.2.1 where the empty circles and the filled circle indicate the locations of public mail boxes in Koganei, Tokyo. Our concern is with whether or not the configuration of those mail boxes is 'optimal'; if not, to what extent we can improve the configuration by relocating the mail boxes?

To answer these questions, we should explicitly define what is 'optimal'. To define it, let us discuss two factors: the cost borne by the post office and the cost borne by users. Regarding the former cost, the major cost is the cost of collecting the mail. In Koganei, the mail boxes are managed by the main post office indicated by the filled circle in Figure 9.2.1. A collector wagon starts from this office, visits all mail boxes successively, and returns to the office. We have to take this cost into account. However, since a public organization is supposed to minimize the user's cost or maximize the user's convenience instead of maximizing profit, the primary factor is the user's convenience rather than the cost borne by the post office. For the moment, let us consider the primary factor. The secondary factor will be taken into account later (see the locational optimization of service points of a mobile facility in Section 9.3.1).

The user's cost or user's convenience may be measured in terms of the distance from a user to a mail box. Since mail boxes are indifferent, most users go to their nearest mail box. As a result, every mail box, say a mail box $i \in I_n = \{1, \dots, n\}$, has its own catchment area or the area in which the nearest mail box from any point in this area is the mail box i . Recalling Property V6 in Chapter 2, we notice that this region is indeed the Voronoi polygon (strictly speaking, since users use streets, this region is given by the

Voronoi region of the network area-Voronoi diagram defined in Section 3.8.3) associated with the mail box i .

Obviously, a street distance is different from a crow-flight distance (the Euclidean distance). This difference is empirically examined by Kobayashi (1983), Koshizuka and Kobayashi (1983), and Love *et al.* (1988, Chapter 10). At first glance, this difference appears very big, but according to Koshizuka and Kobayashi (1983), this difference is not so large as we might expect. If this difference is allowable in practice, the catchment areas of mail boxes can be approximated by the ordinary Voronoi diagram. The solid lines in Figure 9.2.1 indicate the ordinary Voronoi diagram generated by the mail boxes in Koganei.

As mentioned above, we measure the cost of a user by the Euclidean distance from the user to his/her nearest mail box. The cost of users as a whole is hence measured by the average nearest neighbour distance, i.e. the distance to the nearest mail box averaged over all users in a region. In these terms, we can say that the optimal configuration of mail boxes implies the configuration which provides the minimum average nearest neighbour distance.

To formalize the above model mathematically, let S be a closed subset of \mathbb{R}^2 representing a region; $\mathbf{x}_1, \dots, \mathbf{x}_n$ be n points (location vectors) in S indicating the locations of n facilities; $\phi(\mathbf{x})$ be the density of users over region S , where the integral of $\phi(\mathbf{x})$ over S is assumed to be unity without loss of generality; and $\mathcal{V}_{\cap S} = \{V_1 \cap S, \dots, V_n \cap S\}$ be the Voronoi diagram generated by $P = \{\mathbf{x}_1, \dots, \mathbf{x}_n\}$ bounded by S . For simplicity, we write $\mathcal{V} = \{V_1, \dots, V_n\}$ for $\mathcal{V}_{\cap S} = \{V_1 \cap S, \dots, V_n \cap S\}$.

The Euclidean distance from a user at \mathbf{x} to a mail box at \mathbf{x}_i is written as $\|\mathbf{x} - \mathbf{x}_i\|$. More generally, we can consider the travel cost from a user at \mathbf{x} to a facility at \mathbf{x}_i as a function of the Euclidean distance or the squared Euclidean distance, $f(\|\mathbf{x} - \mathbf{x}_i\|^2)$ (note that we use the squared Euclidean distance simply for analytical convenience). One of the simplest cost functions is $f(\|\mathbf{x} - \mathbf{x}_i\|^2) = c \sqrt{\|\mathbf{x} - \mathbf{x}_i\|^2} = c \|\mathbf{x} - \mathbf{x}_i\|$. With this cost function, the objective function discussed above is written as

$$F(\mathbf{x}_1, \dots, \mathbf{x}_n) = \sum_{i=1}^n \int_{V_i} f(\|\mathbf{x} - \mathbf{x}_i\|^2) \phi(\mathbf{x}) d\mathbf{x}. \quad (9.2.1)$$

Note that since the total number of users is assumed to be unity, the total travel cost is the same as the average cost.

When $f(\|\mathbf{x} - \mathbf{x}_i\|^2) = \|\mathbf{x} - \mathbf{x}_i\|$, and $\phi(\mathbf{x}) = 1/S$ (the density of users is uniform over S), we can calculate the integral in equation (9.2.1). The explicit form is shown in Section 8.3.

In terms of the objective function given by equation (9.2.1), we can formally state the locational optimization problem of public mail boxes as the following programming problem.

Problem OPT3 (minimization of the average travel cost to the nearest points without constraints)

$$\min_{x_1, \dots, x_n} \sum_{i=1}^n \int_{V_i} f(\|x - x_i\|^2) \phi(x) dx. \quad (9.2.2)$$

The network problem corresponding to Problem OPT3 is called the *multi-median problem*. In this problem, permissible locations are only on nodes and a distance is given by the shortest path distance on a network. When a network density is dense, we may expect that the solution of Problem OPT3 is close to the solution of the multi-median problem. This approximation is quite useful when a network is huge, because the multi-median problem on a huge network is hard to solve.

The function F of equation (9.2.1) is apparently non-linear, and moreover it is non-convex. We can see the latter property from the following fact. If $(x_1^*, \dots, x_i^*, \dots, x_j^*, \dots, x_n^*)$ is a local minimum of F , then $(x_1^*, \dots, x_i^*, \dots, x_i^*, \dots, x_n^*)$ is also a local minimum of F , because the equation $F(x_1^*, \dots, x_i^*, \dots, x_j^*, \dots, x_n^*) = F(x_1^*, \dots, x_i^*, \dots, x_i^*, \dots, x_n^*)$ holds (confirm this equation in equation (9.2.1)). This implies that we have multiple local minima unless $x_1^* = \dots = x_n^*$. The solution, $x_1^* = \dots = x_n^*$, means that all facilities are located at the same place. Obviously, this solution does not give a minimum. Therefore the function F has multiple local minima, implying that the function F is non-convex.

Because of this non-convex property, as we mentioned in Section 9.1, we have to use a numerical method. If we employ the steepest descent method, we need the first derivatives of F . To derive them, suppose that the i th generator point slightly changes its location from x_i to $x_i + \delta x_i$ ($\|\delta x_i\| \approx 0$) provided that all other generator points remain at the same location. Let \mathcal{V} be the Voronoi diagram generated by $\{x_1, \dots, x_i, \dots, x_n\}$ and \mathcal{V}' be that generated by $\{x_1, \dots, x_i + \delta x_i, \dots, x_n\}$; V_i be the Voronoi polygon of the i th generator in \mathcal{V} and V'_i be that in \mathcal{V}' ; and J_i be the set of indices of the Voronoi polygons adjacent to V_i . Owing to the slight move δx_i , the Voronoi diagram slightly changes, but, as is indicated by the broken lines in Figure 9.2.2, this change occurs only in V_i and its adjacent Voronoi polygons, i.e. $V_j, j \in J_i$. Moreover, the Voronoi edges between adjacent Voronoi polygons V_j and V_k , $j, k \in J_i$, and the Voronoi edges between adjacent Voronoi polygons V'_j and V'_k , $j, k \in J_i$, are on the same line. From this property and equation (9.2.1), we obtain

$$\begin{aligned} \Delta F &= F(x_1, \dots, x_i + \delta x_i, \dots, x_n) - F(x_1, \dots, x_i, \dots, x_n) \\ &= \int_{V'_i} f(\|x_i + \delta x_i - x\|^2) \phi(x) dx - \int_{V_i} f(\|x_i - x\|^2) \phi(x) dx \\ &\quad + \sum_{j \in J_i} \left[\int_{V'_j} f(\|x_j - x\|^2) \phi(x) dx - \int_{V_j} f(\|x_j - x\|^2) \phi(x) dx \right]. \end{aligned} \quad (9.2.3)$$

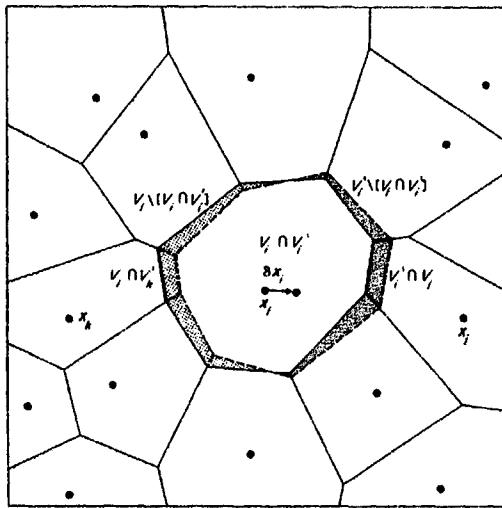


Figure 9.2.2 Variation in a Voronoi polygon.

Since the equations $V_i = (V_i \cap V'_i) \cup (V_i \setminus (V_i \cap V'_i))$, $V'_i = (V_i \cap V'_i) \cup (V'_i \setminus (V'_i \cap V_i))$, $V_j = (V_j \cap V'_j) \cup (V'_j \cap V_j)$ and $V'_j = (V'_j \cap V_j) \cup (V'_j \setminus (V'_j \cap V_j))$ hold, (see Figure 9.2.2), equation (9.2.3) is written as

$$\begin{aligned} \Delta F = & \int_{V'_i \cap V_i} [f(\|x_i + \delta x_i - x\|^2) - f(\|x_i - x\|^2)] \phi(x) dx \\ & + \int_{V'_i \setminus (V_i \cap V'_i)} f(\|x_i + \delta x_i - x\|^2) \phi(x) dx \int_{V_i \setminus (V_i \cap V'_i)} f(\|x_i - x\|^2) \phi(x) dx \\ & + \sum_{j \in J_i} \left[\int_{V_j \cap V'_i} f(\|x_j - x\|^2) \phi(x) dx - \int_{V'_i \cap V_j} f(\|x_j - x\|^2) \phi(x) dx \right]. \quad (9.2.4) \end{aligned}$$

In Figure 9.2.2 the integral domains $V'_i \setminus (V_i \cap V'_i)$ and $V_i \setminus (V_i \cap V'_i)$ are indicated by the sparsely and densely shaded regions, respectively; the integral domains $V'_i \cap V_j$ and $V_i \cap V'_j$ are indicated by the regions surrounded by the heavy lines (note that $V_i \cap V'_j$ or $V'_i \cap V_j$ may be empty or may not, but at least one of the two is non-empty). Observing in Figure 9.2.2 that the lightly shaded region $V'_i \setminus (V_i \cap V'_i)$ consists of subregions $V_i \cap V'_k$, $k \in J_i$ (one of which is indicated by the heavy solid lines on the left-hand side), and the densely shaded region $V_i \setminus (V_i \cap V'_i)$ consists of subregions $V'_i \cap V_j$, $j \in J_i$ (one of which is indicated by the heavy solid lines on the right-hand side), we notice that the following equations hold:

$$V'_i \setminus (V_i \cap V'_i) = \sum_{j \in J_i} V'_i \cap V_j, \quad V_i \setminus (V_i \cap V'_i) = \sum_{j \in J_i} (V_i \cap V'_j). \quad (9.2.5)$$

Using these equations, equation (9.2.4) is written as

$$\begin{aligned}\Delta F = & \int_{V'_i \cap V_j} \left\{ f(\|x_i + \delta x_i - x\|^2) - f(\|x_i - x\|^2) \right\} \phi(x) dx \\ & + \sum_{j \in J_i} \int_{V'_i \cap V_j} \left\{ f(\|x_i + \delta x_i - x\|^2) - f(\|x_i - x\|^2) \right\} \phi(x) dx \\ & + \sum_{j \in J_i} \int_{V_i \cap V'_j} \left\{ f(\|x_j - x\|^2) - f(\|x_i - x\|^2) \right\} \phi(x) dx.\end{aligned}\quad (9.2.6)$$

As δx_i approaches zero, the integral domains $V_i \cap V'_j$ and $V'_i \cap V_j$ in equation (9.2.6) reduce to the Voronoi edge shared by V_i and V_j , and

$$\lim_{\delta x_i \rightarrow 0} |V'_i \cap V_j| = 0, \quad \lim_{\delta x_i \rightarrow 0} |V_i \cap V'_j| = 0. \quad (9.2.7)$$

From this property and the property that the equation $\|x_i - x\| = \|x_j - x\|$ (or $\|x_i + \delta x_i - x\| = \|x_j - x\|$) holds if the point x is on the Voronoi edge shared by V_i and V_j (or V'_i and V'_j), we have the following relations:

$$\begin{aligned}\|x_i - x\| &\approx \|x_j - x\|, \quad x \in V_i \cap V'_j, \quad j \in J_i, \\ \|x_i + \delta x_i - x\| &\approx \|x_j - x\|, \quad x \in V'_i \cap V_j, \quad j \in J_i,\end{aligned}\quad (9.2.8)$$

for sufficiently small δx_i . From this equation and the assumption that $f(\|x_i - x\|)$ and $\phi(x)$ are continuous, the value of $|f(\|x_i + \delta x_i - x\|^2) - f(\|x_i - x\|^2)| \phi(x)$ is of order $\|\delta x_i\|$, denoted by $O(\|\delta x_i\|)$, for $x \in V'_i \cap V_j$. From equation (9.2.7), the area of the integral domain $V'_i \cap V_j$ is also $O(\|\delta x_i\|)$ for sufficiently small δx_i . Hence, $|V'_i \cap V_j| [f(\|x_i + \delta x_i - x\|^2) - f(\|x_i - x\|^2)] \phi(x)$ is $O(\|\delta x_i\|^2)$. Similarly, $|V_i \cap V'_j| [f(\|x_i - x\|^2) - f(\|x_j - x\|^2)] \phi(x)$ is $O(\|\delta x_i\|^2)$. Therefore, equation (9.2.6) is written as

$$\Delta F = \int_{V'_i \cap V_j} \left\{ f(\|x_i + \delta x_i - x\|^2) - f(\|x_i - x\|^2) \right\} \phi(x) dx + O(\|\delta x_i\|^2), \quad (9.2.9)$$

from which we obtain

$$\begin{aligned}\frac{\partial F}{\partial x_{i\kappa}} &= \lim_{\delta x_{i\kappa} \rightarrow 0} \frac{\Delta F}{\delta x_{i\kappa}} \\ &= \lim_{\delta x_{i\kappa} \rightarrow 0} \left[\int_{V'_i \cap V_j} \frac{f(\|x_i + \delta x_i - x\|^2) - f(\|x_i - x\|^2)}{\delta x_{i\kappa}} \phi(x) dx \right. \\ &\quad \left. - + \frac{O(\|\delta x_i\|^2)}{\delta x_{i\kappa}} \right], \quad \kappa = 1, 2.\end{aligned}\quad (9.2.10)$$

Therefore, we obtain the first derivatives as

$$\frac{\partial F}{\partial x_{i\kappa}} = \int_{V_i} 2(x_{i\kappa} - x_\kappa) f'(\|x_i - x\|^2) \phi(x) dx, \quad \kappa = 1, 2. \quad (9.2.11)$$

Note that this result holds not only for $x_i^T = (x_{i1}, x_{i2}), x^T = (x_1, x_2) \in \mathbb{R}^2$, but also for $x_i^T = (x_{i1}, \dots, x_{i\kappa}, \dots, x_{im})$ and $x^T = (x_1, \dots, x_\kappa, \dots, x_m) \in \mathbb{R}^m$. In the latter case, $\kappa = 1, 2$ is simply replaced by $\kappa = 1, \dots, m$.

Using the steepest descent method with this derivative, we can obtain a local optimal solution. Alternatively, as mentioned in Section 9.1, we may use the Newton method to gain faster convergence. For this use, we need the second partial derivatives of F . The derivation of the second partial derivatives is much more lengthy than the above derivation. Since space is limited, we show only the result here. The detailed derivation is given by Suzuki (1987) and Asami (1991). Using the notation $\mathbf{x}_i^T = (x_{i1}, \dots, x_{ik}, \dots, x_{i\lambda}, \dots, x_{im})$ and $\mathbf{x}^T = (x_1, \dots, x_k, \dots, x_\lambda, \dots, x_m) \in \mathbb{R}^m$, the second partial derivatives are written as

$$\begin{aligned} \frac{\partial^2 F}{\partial x_{ik} \partial x_{i\lambda}} &= \int_{V_i} \left[2\delta(\kappa, \lambda) f'(\|\mathbf{x}_i - \mathbf{x}\|^2) + 4(x_{ik} - x_\kappa)(x_{i\lambda} - x_\lambda) f''(\|\mathbf{x}_i - \mathbf{x}\|^2) \phi(\mathbf{x}) \right] d\mathbf{x} \\ &\quad - \sum_{j \in J_i} \int_{V_i \cap V_j} \frac{2}{\|\mathbf{x}_j - \mathbf{x}_i\|^2} (x_{ik} - x_\kappa)(x_{i\lambda} - x_\lambda) f'(\|\mathbf{x}_i - \mathbf{x}\|^2) \phi(\mathbf{x}) d\mathbf{x}, \end{aligned} \quad (9.2.12)$$

where

$$\delta(\kappa, \lambda) = \begin{cases} 1 & \text{if } \kappa = \lambda, \\ 0 & \text{if } \kappa \neq \lambda, \kappa, \lambda \in I_m, \end{cases} \quad (9.2.13)$$

$$\begin{aligned} \frac{\partial^2 F}{\partial x_{ik} \partial x_{j\lambda}} &= \int_{V_i \cap V_j} \frac{2}{\|\mathbf{x}_j - \mathbf{x}_i\|} (x_{ik} - x_\kappa)(x_{j\lambda} - x_\lambda) \\ &\quad \times f'(\|\mathbf{x}_i - \mathbf{x}\|^2) \phi(\mathbf{x}) d\mathbf{x}, \quad j \neq i, j \in J_i, \kappa, \lambda \in I_m, \end{aligned} \quad (9.2.14)$$

$$\frac{\partial^2 F}{\partial x_{ik} \partial x_{j\lambda}} = 0, \quad j \neq i, j \notin J_i, \quad (9.2.15)$$

(note that $V_i \cap V_j$ is the Voronoi edge shared by V_i and V_j). Although we may use the Newton method with these second derivatives, the calculation of the Hessian becomes time consuming for a large number of facilities when the density $\phi(\mathbf{x})$ is not uniform. To reduce computing time, Iri *et al.* (1984) recommend, based upon their numerical experiment, using the quasi-Newton method with the diagonal matrix, H , whose diagonal elements are given by the first term in equation (9.2.12). Using this quasi-Newton method, we can solve Problem OPT3 in practice for a large number of facilities. (Note that when $\phi(\mathbf{x})$ is not uniform, Iri *et al.*, 1984, carry out the integration in equations (9.2.11)–(9.2.15) using the numerical integration formula shown in Abramowitz and Stegun, 1964.)

Figure 9.2.3 shows the optimal configuration of $n = 128$ points in a square S for the three different density functions $\phi(\mathbf{x})$ (Iri *et al.*, 1984).

Using the same method, we can obtain the local optimal configuration of public mail boxes in Koganei. The result is shown in Figure 9.2.4. It is of interest to compare this local optimal configuration with the present configuration shown in Figure 9.2.1(a).

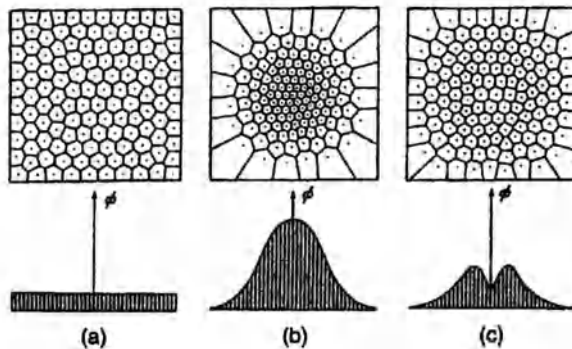


Figure 9.2.3 Optimal location of 128 points in a square for: (a) the density function $\phi(x)$ given by $\phi(x) = c, x \in S$; (b) the density function $\phi(x)$ given by $\phi(x) = c \exp(-25 \|x\|^2), x \in S$; and (c) the density function $\phi(x)$ given by $\phi(x) = c \exp(-\|x\| (25 \|x\| - 10)), x \in S$. (Source: Iri et al., 1984, Figures 1 and 2.)

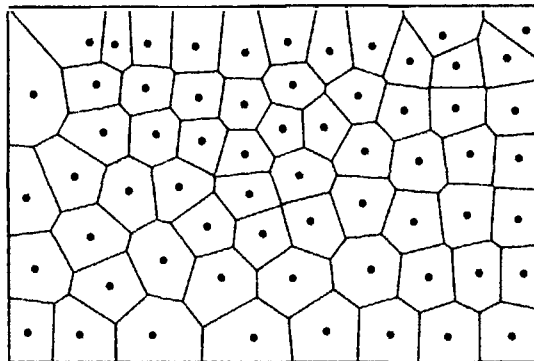


Figure 9.2.4 Locational optimization of public mail boxes in Koganei, Tokyo.

9.2.2 Locational optimization of points in a three-dimensional space

In the above example we formulated Problem OPT3 in the plane \mathbb{R}^2 . We can also formulate the same problem in the space \mathbb{R}^3 and can solve the problem almost in the same manner using the three-dimensional Voronoi diagram. Figure 9.2.5 shows the optimal configuration of 16 points in a cube where the density function $\phi(x)$ is given by the uniform distribution (Takeda, 1985). This result is quite suggestive for crystallography. It is shown in Rogers (1964) that Voronoi polyhedra become truncated octahedra when generators are given by cubic lattice points in an infinite space (see also Chapter 7).

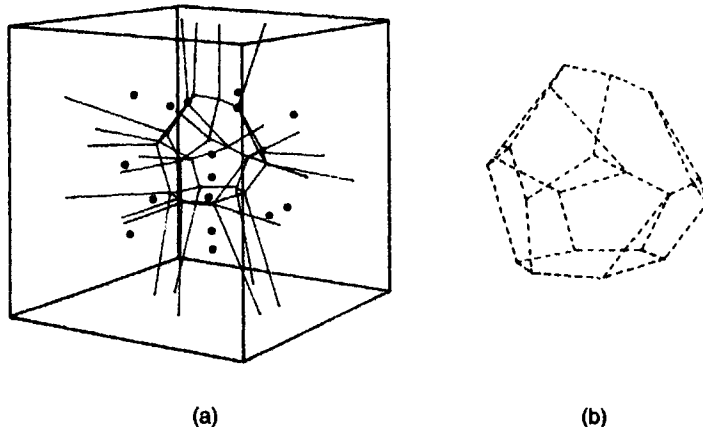


Figure 9.2.5 Optimal location of 16 points in a cube: (a) the Voronoi diagram of the optimized points; (b) a Voronoi polyhedron in (a). (Source: Takeda, 1985, Figure 3.7.)

9.2.3 Locational optimization of point-like facilities used by groups

Facilities are not always used by independent users; some kinds of facilities are used by groups of users. For example, a tennis court is used by at least a pair of players; a convention hall is used by groups of certain members. This type of locational optimization problem is examined by Ohsawa and Suzuki (1987), upon which this subsection is based.

Suppose that there are n facilities located at x_1, \dots, x_n in region S , and that every group consists of m members. Groups are distributed over S according to a density function $\phi(y_1, \dots, y_m)$, where y_1, \dots, y_m indicate the locations of m members. The value of $\phi(y_1, \dots, y_m) dy_1, \dots, dy_m$ indicates the number of groups whose members $1, \dots, m$ are in a small region dy_1 around y_1, \dots, m in a small region dy_m around y_m , respectively. Since m members in a group use the same facility, say facility i , the total travel cost of the group is given by the sum of the travel costs of the m members from their locations to facility i , i.e. $\sum_{j=1}^m f(\|y_j - x_i\|^2)$.

We make two assumptions. First, every group chooses the facility that gives the minimum total travel cost, i.e. $\min_i \sum_{j=1}^m f(\|y_j - x_i\|^2)$. Second, every group uses the facility α times per unit time regardless of the travel cost to their nearest facility. For convenience, $\alpha = 1$ without loss of generality. Under these assumptions, the total travel cost of groups over region S is given by

$$F(x_1, \dots, x_n) = \int_S \min_i \sum_{j=1}^m f(\|y_j - x_i\|^2) \phi(y_1, \dots, y_m) dy_1 \dots dy_m. \quad (9.2.16)$$

The locational optimization problem is hence to minimize this objective function with respect to x_1, \dots, x_n . This problem is difficult to solve for a general travel cost function. The problem, however, becomes tractable in a specific

case where the travel cost function is given by $f(\|\mathbf{y}_j - \mathbf{x}_i\|^2) = \|\mathbf{y}_j - \mathbf{x}_i\|^2$. For this travel cost function, the following equation holds:

$$\sum_{j=1}^m \|\mathbf{y}_j - \mathbf{x}_i\|^2 = m \|\bar{\mathbf{y}} - \mathbf{x}_i\|^2 + \sum_{j=1}^m \|\mathbf{y}_j - \bar{\mathbf{y}}\|^2, \quad (9.2.17)$$

where $\bar{\mathbf{y}}$ is the centroid of m members, i.e. $\bar{\mathbf{y}} = \sum_{i=1}^m \mathbf{y}_i / m$. Substituting equation (9.2.17) into equation (9.2.16), we obtain

$$\begin{aligned} F(\mathbf{x}_1, \dots, \mathbf{x}_n) &= \int_S \min_i \sum_{j=1}^m f(\|\mathbf{y}_j - \mathbf{x}_i\|^2) \phi(\mathbf{y}_1, \dots, \mathbf{y}_m) d\mathbf{y}_1 \dots d\mathbf{y}_m \\ &\approx \int_S \min_i \left[m \|\bar{\mathbf{y}} - \mathbf{x}_i\|^2 + \sum_{j=1}^m f(\|\mathbf{y}_j - \bar{\mathbf{y}}\|^2) \right] \phi(\mathbf{y}_1, \dots, \mathbf{y}_m) d\mathbf{y}_1 \dots d\mathbf{y}_m. \end{aligned} \quad (9.2.18)$$

The first term, $\min_i m \|\bar{\mathbf{y}} - \mathbf{x}_i\|^2$, implies the distance to the nearest facility from the centroid of m members (multiplied by m). Obviously, if the centroid $\bar{\mathbf{y}}$ is in the Voronoi polygon V_i , the nearest facility is the facility at \mathbf{x}_i . The second term, $\min_i \sum_{j=1}^m \|\mathbf{y}_j - \bar{\mathbf{y}}\|^2$, is the total cost from m members to their centroid, which is independent of i , and so $\min_i \sum_{j=1}^m \|\mathbf{y}_j - \bar{\mathbf{y}}\|^2 = \sum_{j=1}^m \|\mathbf{y}_j - \bar{\mathbf{y}}\|^2$. Thus, equation (9.2.18) is written as

$$F(\mathbf{x}_1, \dots, \mathbf{x}_n) = m \sum_{i=1}^n \int_{V_i} \|\bar{\mathbf{y}} - \mathbf{x}_i\|^2 \phi_g(\bar{\mathbf{y}}) d\bar{\mathbf{y}} + c, \quad (9.2.19)$$

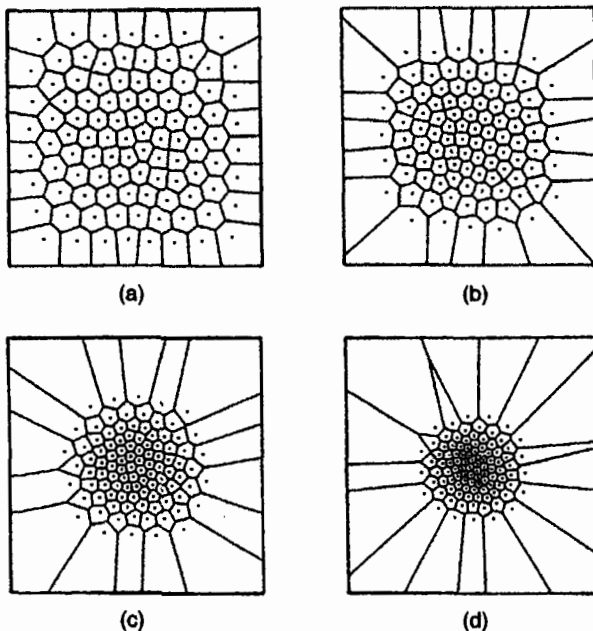


Figure 9.2.6 Optimal locations of 100 facilities used by a group of (a) $m = 2$ members, (b) $m = 4$ members, (c) $m = 8$ members, (d) $m = 16$ members. (Source: Ohsawa and Suzuki, 1987, Figure 3.)

where $\phi_g(\bar{y})$ is the density function of \bar{y} obtained from $\phi(y_1, \dots, y_m)$, and c is a constant. Note that when $\phi(y_1, \dots, y_m)$ is uniform over a unit square region, $\phi_g(\bar{y}) = \phi_g(\bar{y}_1, \bar{y}_2)$ is written as

$$\begin{aligned}\phi_g(\bar{y}_1, \bar{y}_2) &= \frac{m^2}{\{(m-1)!\}^2} \sum_{i=1}^{[m\bar{y}_1]} \frac{(-1)^i i! (m\bar{y}_1 - i)^{m-1}}{m! (m-i)!} \\ &\quad \times \sum_{j=1}^{[m\bar{y}_2]} \frac{(-1)^j j! (m\bar{y}_2 - j)^{m-1}}{m! (m-j)!},\end{aligned}\quad (9.2.20)$$

where $[m\bar{y}_i]$ is the maximum integer less than or equal to $m\bar{y}_i$ (Mood *et al.*, 1974).

Comparing equation (9.2.19) with equation (9.2.2), we notice that the objective function of equation (9.2.19) is the same as that of equation (9.2.2) except that $f(\|\mathbf{x} - \mathbf{x}_i\|^2)$ is replaced by $\|\mathbf{x} - \mathbf{x}_i\|^2$. Therefore, we can apply the same computational method used for Problem OPT3 to this locational optimization problem. Actually, using that method, Ohsawa and Suzuki (1987) solved the problem for $n = 100$ facilities used by groups of $m = 2, 4, 8, 16$ members. The results are shown in Figure 9.2.6. We notice from Figure 9.2.6 that facilities tend to gather near the centre as the number of members constituting a group increases.

9.2.4 Locational optimization of a hierarchical facility

We implicitly assumed above that all facilities supply the same quality service, or that facilities are indifferent, like public mail boxes. This assumption is not always appropriate for some kinds of facilities. For example, in Japan,

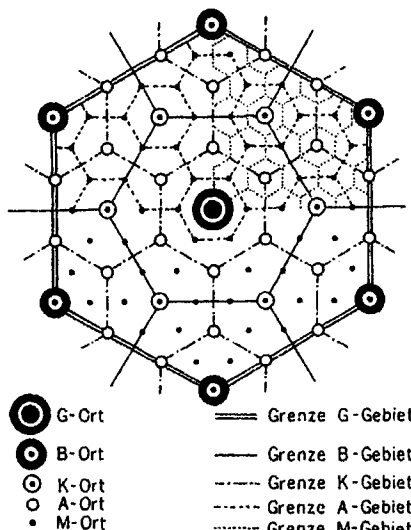


Figure 9.2.7 Hierarchical system of cities. (Source: Christaller, 1933, Figure 2.)

post offices are ranked from the first to the third according to the level of postal service; a university library system usually consists of the main library and a few branch libraries. We call such a set of facilities a *hierarchical facility*.

Besides a hierarchical facility, we also observe a hierarchy in a set of cities in a country. The study of this hierarchy, which has been investigated in spatial economics since Christaller (1933) and Lösch (1940), is worth noting in conjunction with Voronoi diagrams. Christaller (1933) formulates hierarchical systems of cities with Voronoi diagrams generated by triangular lattice points. A few examples are shown in Figures 9.2.7 and 9.2.10 (which will be discussed with the optimal configurations obtained in Figure 9.2.9).

The locational optimization of a hierarchical facility has been studied mainly in Operations Research. Dokmeci (1973) solves this problem for discrete demand with the integer programming. Moore and ReVelle (1982) viewed a hierarchical facility from a covering problem. Tien *et al.* (1983) dealt with the problem of a hierarchical health facility for discrete demand. O'Kelley and Storbeck (1984) took probabilistic allocation into account. Narula (1984) examined the characteristics of several hierarchical facilities and classified the types of hierarchy. Hodgson (1984) solved a multi-level locational problem with the gravity model. Mirchandani (1987) generalized the Tien *et al.* (1983) model.

As is noticed in those articles, most of the models are formulated on a network; few models are formulated on a continuous plane. Recalling the computational method used in Problem OPT3, we notice that the same method can be applied to the above problem. In fact, T. Suzuki (1989) and Okabe *et al.* (1997) have applied that method to the locational optimization problem of a hierarchical facility on a continuous plane. In this subsection we follow T. Suzuki's (1989) model.

Suppose that there are n facilities in a region S , and those facilities are ranked from 1 to m . Let n_i be the number of facilities of rank i , ($\sum_{i=1}^m n_i = n$),

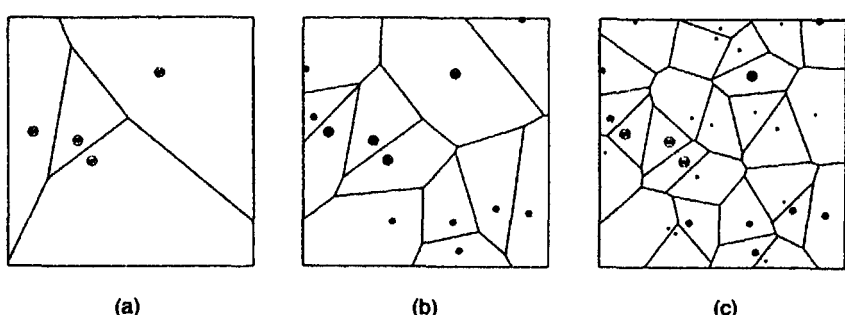


Figure 9.2.8 A nested hierarchical facility: (a) the Voronoi diagram $V^{(1)}$ generated by the locations of facilities supplying service s_1 (facilities of rank 1); (b) the Voronoi diagram $V^{(2)}$ generated by the locations of facilities supplying service s_2 (facilities of rank 1 and rank 2); (c) the Voronoi diagram $V^{(3)}$ generated by the locations of facilities supplying service s_3 (facilities of ranks 1, 2 and 3).

and $\mathbf{x}_1, \dots, \mathbf{x}_n$ be the locations of n facilities. For convenience, the first n_1 locations of $\mathbf{x}_1, \dots, \mathbf{x}_n$ are those of rank 1 facilities; the next n_2 locations are those of rank 2 facilities, and so forth.

Suppose next that the n facilities supply k kinds of services, s_1, \dots, s_k . Service s_j may be supplied by all facilities or may be supplied by facilities of certain ranks. First, we consider the case in which facilities of rank i supply services s_i, \dots, s_m , implying that facilities of rank i supply their proper service as well as the services supplied by facilities of lower ranks $i+1, \dots, m$. This type of hierarchy is called a *successively inclusive hierarchy* (Tien et al., 1983) or a *nested hierarchy* (Banerji and Fisher, 1974).

We make two assumptions. First, a user who needs service s_j goes to the nearest facility among the facilities supplying service s_j (the facilities of rank $1, \dots, j$). As a result, service areas of the facilities supplying service s_j are given by the Voronoi diagram $\mathcal{V}^{(j)} = \{V_1^{(j)}, \dots, V_{n_1+\dots+n_{j-1}+1}^{(j)}\}$, generated by $\{\mathbf{x}_1, \dots, \mathbf{x}_{n_1+\dots+n_j}\}$. An example of $m = 3$ is depicted in Figure 9.2.8. Second, every user consumes α_j units of service s_j , $j \in I_k$, per unit time regardless of the Euclidean distance to the facilities. For convenience, the α_i 's are standardized as $\sum_{j=1}^k \alpha_j = 1$.

Under these assumptions the average travel cost of users over the region S is written as

$$F(\mathbf{x}_1, \dots, \mathbf{x}_n) = \sum_{i=1}^k \alpha_i \sum_{j=n_1+\dots+n_{i-1}+1}^n \int_{V_j^{(i)}} \|\mathbf{x}_j - \mathbf{x}\| \phi(\mathbf{x}) d\mathbf{x}. \quad (9.2.21)$$

The computational method for minimizing this objective function is the same as that of Problem OPT3. Using that method, T. Suzuki (1989) obtained the optimal configurations for $n = 37$, $m = 2$ and $\alpha_1 = \alpha_2 = 0.5$. The results are shown in Figure 9.2.8 where $n_1 = 6, 7, 10$.

As is noticed from Figure 9.2.9, the optimal configuration varies according to the ratio of n_2 to n_1 . This ratio, K , is an important parameter in Christaller's (1933) model. In Figure 9.2.9, the K values are 5.2 in (a), 4.3 in (b), and 2.7 in (c). Christaller (1933) refers to $K = 3, 4, 7$ (Figure 9.2.10) as the hierarchical systems resulting from the market principle, the transportation principle, and the administrative principle, respectively. Since Christaller

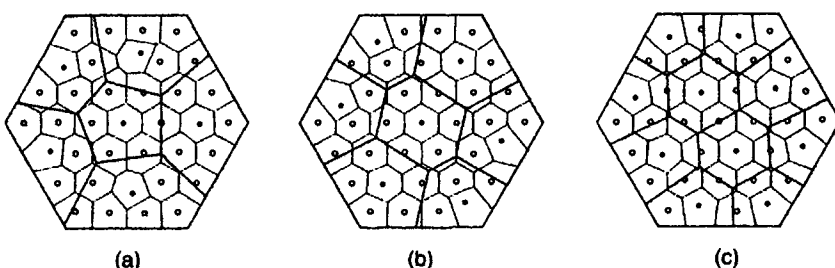


Figure 9.2.9 Optimal configurations of a hierarchical facility, $n = 37$, $m = 2$, $\alpha_1 = \alpha_2 = 0.5$: (a) $n_1 = 6$, (b) $n_1 = 7$, (c) $n_1 = 10$. (Source: T. Suzuki, 1989, Figure 4.10.)

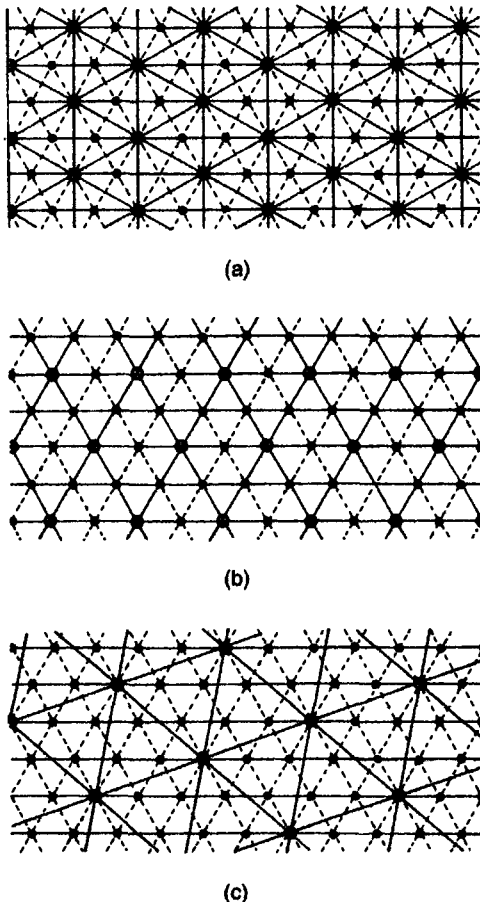


Figure 9.2.10 Christaller's (1933) hierarchical systems of cities: (a) $K = 3$; (b) $K = 4$; (c) $K = 7$.

(1933) formulated the model on an unbounded plane, whereas T. Suzuki (1989) formulated it on a bounded plane, we cannot directly compare their results. Figure 9.2.9, however, provides a new look at hierarchical systems of cities from an optimization viewpoint (see also Okabe and Sadahiro, 1996, who studied the problem from a statistical viewpoint).

In the above model, optimization is achieved with respect to the locations of facilities provided that the number of rank i facilities are given. We may relax this condition and optimize not only the locations but also the number of rank i facilities, provided that the total number of all rank facilities is fixed. This relaxation is made by Okabe *et al.* (1997).

A hierarchy is not always nested; it may be partially nested or successively exclusive. We can formulate the optimization problems of such a hierarchical facility almost in the same manner as in the above, and can solve them with

the descent method. The reader who is interested in this problem should consult T. Suzuki (1989).

9.2.5 Locational optimization of observation points for estimating the total quantity of a spatial variable continuously distributed over a plane

As we mentioned in Chapter 1, the Voronoi diagram is alternatively called the Thiessen diagram. The original use of the Thiessen diagram was to estimate the total precipitation in a region S . To be explicit, suppose that there are n pluviometers placed at x_1, \dots, x_n in the region S . Let $z(x_i)$ be the precipitation at x_i , and V_i be the Voronoi polygon associated with a pluviometer at x_i . Thiessen (1911) estimated the true total precipitation in the region S , i.e.

$$Z = \int_S z(x) dx = \sum_{i=1}^n \int_{V_i} z(x) dx, \quad (9.2.22)$$

by

$$\hat{Z} = \sum_{i=1}^n |V_i| z(x_i). \quad (9.2.23)$$

In Thiessen (1911), the locations of pluviometers are fixed, and no locational optimization problem is discussed (see also Lebel *et al.*, 1987). However, if we can freely choose those locations, we have a locational optimization problem to minimize the estimation error. A similar problem is considered by Hori and Nagata (1985), who obtain the optimal configuration of monitor points to estimate NO_x in a region.

To formulate the above optimization problem, let $z(x)$ be a random variable at x in a region S given by

$$z(x) = m(x) + \varepsilon(x), \quad (9.2.24)$$

where $m(x)$ is a continuous function of x , which is constant for a given x , and $\varepsilon(x)$ is a random variable whose expected value is given by $E[\varepsilon(x)] = 0$. From equation (9.2.24) and $E[\varepsilon(x)] = 0$, we obtain $E[z(x)] = m(x)$, which indicates the average trend of the variable z over S . To measure the estimation error, we consider the expected squared error over the region S , i.e.

$$F(x_1, \dots, x_n) = E \left[\sum_{i=1}^n \int_{V_i} \{z(x) - z(x_i)\}^2 dx \right]. \quad (9.2.25)$$

Upon substituting equation (9.2.24) into equation (9.2.25), we obtain

$$\begin{aligned} F(x_1, \dots, x_n) &= \sum_{i=1}^n \int_{V_i} E[(m(x) - m(x_i))^2] \\ &\quad + E[\varepsilon(x)^2] + E[\varepsilon(x_i)^2] - 2E[\varepsilon(x)\varepsilon(x_i)] \\ &\quad + 2E[\varepsilon(x)\{m(x) - m(x_i)\}] + 2E[\varepsilon(x_i)\{m(x) - m(x_i)\}] dx. \end{aligned} \quad (9.2.26)$$

The first term, $E[(m(x) - m(x_i))^2]$, is written as $\{m(x) - m(x_i)\}^2$ because $m(x)$ is constant for a given x . The second and third terms are variances, which

are denoted by $\sigma(\mathbf{x})$ and $\sigma(\mathbf{x}_i)$, respectively. The fourth term is written as $E[\varepsilon(\mathbf{x}) \varepsilon(\mathbf{x}_i)] = \sigma(\mathbf{x})\sigma(\mathbf{x}_i) \text{Cov}(\mathbf{x}, \mathbf{x}_i)$ where $\text{Cov}(\mathbf{x}, \mathbf{x}_i)$ is the covariance. The fifth and sixth terms are zero, because $E[\varepsilon(\mathbf{x}) \{m(\mathbf{x}) - m(\mathbf{x}_i)\}] = \{m(\mathbf{x}) - m(\mathbf{x}_i)\} E[\varepsilon(\mathbf{x})] = 0$. Thus, equation (9.2.26) is written as

$$F(\mathbf{x}_1, \dots, \mathbf{x}_n) = \sum_{i=1}^n \int_{V_i} [\{m(\mathbf{x}) - m(\mathbf{x}_i)\}^2 + \{\sigma(\mathbf{x}) - \sigma(\mathbf{x}_i)\}^2 + 2\sigma(\mathbf{x})\sigma(\mathbf{x}_i)\{1 - \text{Cov}(\mathbf{x}, \mathbf{x}_i)\}] d\mathbf{x}. \quad (9.2.27)$$

The locational optimization problem is hence to minimize F of equation (9.2.27) with respect to $\mathbf{x}_1, \dots, \mathbf{x}_n$.

First, let us consider the case in which the variance $\sigma(\mathbf{x})$ is independent of \mathbf{x} , and constant for all points in the region S , i.e. $\sigma(\mathbf{x}) = \sigma$; the change in the average trend, $m(\mathbf{x})$, is small compared with the variance σ . In this case, equation (9.2.27) is approximated by

$$F(\mathbf{x}_1, \dots, \mathbf{x}_n) = \sum_{i=1}^n \int_{V_i} 2\sigma^2 \{1 - \text{Cov}(\mathbf{x}, \mathbf{x}_i)\} d\mathbf{x}. \quad (9.2.28)$$

Empirically, the covariance $\text{Cov}(\mathbf{x}, \mathbf{x}_i)$ tends to decrease monotonically as $\|\mathbf{x} - \mathbf{x}_i\|$ increases, and so $1 - \text{Cov}(\mathbf{x}, \mathbf{x}_i)$ increases monotonically as $\|\mathbf{x} - \mathbf{x}_i\|$ increases. Let $f(\|\mathbf{x} - \mathbf{x}_i\|)$ be this increasing function. Then, the optimization problem reduces to

$$\min_{\mathbf{x}_1, \dots, \mathbf{x}_n} \sum_{i=1}^n \int_{V_i} 2\sigma^2 \{1 - \text{Cov}(\mathbf{x}, \mathbf{x}_i)\} d\mathbf{x} = \min_{\mathbf{x}_1, \dots, \mathbf{x}_n} \sum_{i=1}^n \int_{V_i} f(\|\mathbf{x} - \mathbf{x}_i\|) d\mathbf{x}. \quad (9.2.29)$$

We readily notice from equation (9.2.2) that the problem given by expression (9.2.29) is a special case of Problem OPT3.

Let us next consider the case in which the variance $\sigma(\mathbf{x})$ is small compared with the change in the average trend, $m(\mathbf{x})$. In this case, equation (9.2.27) is approximated by

$$F(\mathbf{x}_1, \dots, \mathbf{x}_n) = \sum_{i=1}^n \int_{x \in V_i} \{m(\mathbf{x}) - m(\mathbf{x}_i)\}^2 d\mathbf{x}. \quad (9.2.30)$$

The locational optimization problem is to minimize this function with respect to $\mathbf{x}_1, \dots, \mathbf{x}_n$. The exact solution of this minimization problem is difficult to obtain for a general function, $m(\mathbf{x})$. We may, however, obtain a solution which is possibly close to the optimal solution from the following relation. For a given V_i , the following relation holds:

$$\int_{V_i} \{m(\mathbf{x}) - m(\mathbf{x}_i)\}^2 d\mathbf{x} \geq \int_{V_i} \{m(\mathbf{x}) - m_i\}^2 d\mathbf{x}, \quad (9.2.31)$$

where

$$m_i = \frac{1}{|V_i|} \int_{V_i} m(\mathbf{x}) d\mathbf{x}. \quad (9.2.32)$$

We notice from this relation that if $m(\mathbf{x}_i)$ happens to be equal to m_i , that is, if the value of $m(\mathbf{x}_i)$ at the generator \mathbf{x}_i of the Voronoi polygon V_i happens to be equal to the average value of $m(\mathbf{x})$ over V_i , the value on the left-hand

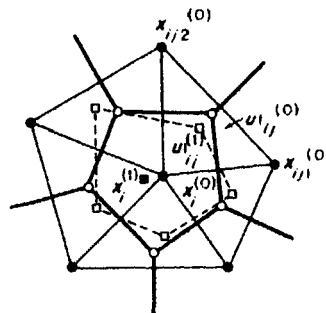


Figure 9.2.11 A heuristic method for searching for $m(\mathbf{x}_i) = m_r$.

side of equation (9.2.31) achieves the minimum value. This property suggests that the solution may be given by a set $\{\mathbf{x}_1, \dots, \mathbf{x}_n\}$ that satisfies $m(\mathbf{x}_i) = m_i$ (or $m(\mathbf{x}_i) \approx m_i$ in practice). To find such a set, Hori and Nagata (1985) propose the following heuristic or crude method.

First, we construct the Voronoi diagram $\{V_1^{(0)}, \dots, V_n^{(0)}\}$ (the heavy solid lines in Figure 9.2.11) generated by an initial generator set $\{\mathbf{x}_1^{(0)}, \dots, \mathbf{x}_n^{(0)}\}$ (the filled circles in Figure 9.2.11). Hori and Nagata (1985) recommend using the initial generator set given by the optimal solution of Problem OPT3, where $f(\|\mathbf{x} - \mathbf{x}_i\|^2) = \|\mathbf{x} - \mathbf{x}_i\|^2$, $\phi(\mathbf{x}) = m(\mathbf{x})$. Second, we construct the Delaunay triangulation for this Voronoi diagram (the light solid lines in

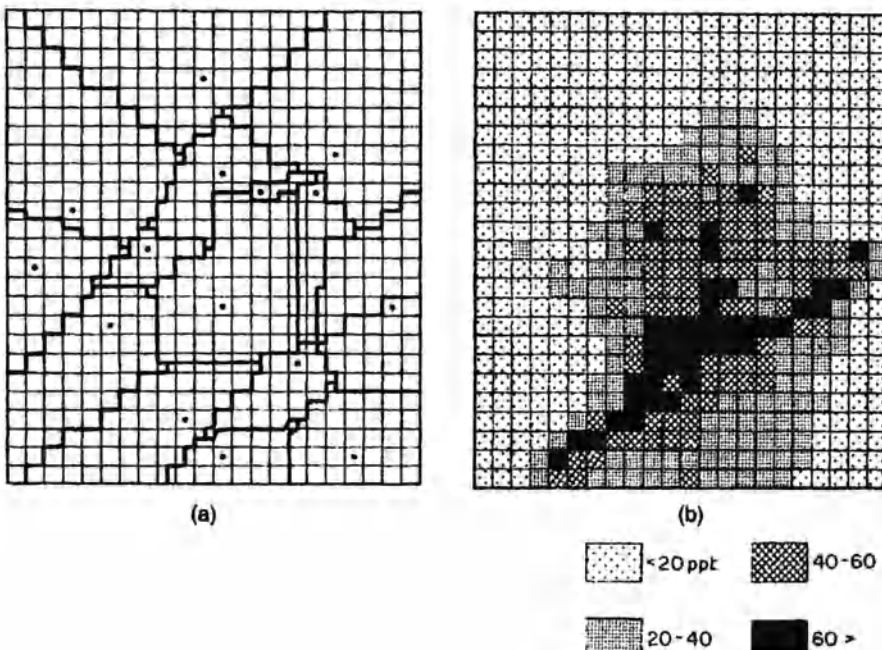


Figure 9.2.12 (a) The optimal configuration of 16 observation points, and (b) density of NO_x in Kyoto. (Source: Hori and Nagata, 1985, redrawn from Figures 6 and 7.)

Figure 9.2.11). Let $\mathbf{u}_{ij}^{(0)}, j \in I_{n_i}$, be the Voronoi points of the Voronoi polygon $V_i^{(0)}$, where n_i is the number of Voronoi vertices of $V_i^{(0)}$ (the unfilled circles in Figure 9.2.11); $T_{ij}^{(0)}$ be a Delaunay triangle which corresponds to the vertex $\mathbf{u}_{ij}^{(0)}$; and $\mathbf{x}_{ij1}^{(0)}$ and $\mathbf{x}_{ij2}^{(0)}$ be two vertices of $T_{ij}^{(0)}$ other than $\mathbf{x}_i^{(0)}$. Third, we find a point $\mathbf{u}_{ij}^{(1)}$ in $T_{ij}^{(0)}$ or in the circumcircle of $T_{ij}^{(0)}$ that satisfies $m(\mathbf{u}_{ij}^{(1)}) = \{m(\mathbf{x}_i^{(0)}) + m(\mathbf{x}_{ij1}^{(0)}) + m(\mathbf{x}_{ij2}^{(0)})\}/3$ (if such a point does not exist, we find a point $\mathbf{u}_{ij}^{(0)}$ in such a way that $m(\mathbf{u}_{ij}^{(1)})$ is close to $\{m(\mathbf{x}_i^{(0)}) + m(\mathbf{x}_{ij1}^{(0)}) + m(\mathbf{x}_{ij2}^{(0)})\}/3$) (the unfilled squares in Figure 9.2.11). Fourth, we construct the polygon V'_i whose vertices are given by $\mathbf{u}_{ij}^{(1)}, j \in I_{n_i}$ (the broken lines in Figure 9.2.11). Fifth, in this polygon we find a point $\mathbf{x}_i^{(1)}$ that satisfies equation (9.2.33) where $m_i = m(\mathbf{x}_i^{(1)})$, $V_i = V'_i$ (if we cannot find such a point, we find a point $\mathbf{x}_i^{(1)}$ in such a way that $m(\mathbf{x}_i^{(1)})$ is close to the left-hand-side of equation (9.2.33)) (the filled square in Figure 9.2.11). Last, we generate a Voronoi diagram with $\{\mathbf{x}_1^{(1)}, \dots, \mathbf{x}_n^{(1)}\}$. We continue this procedure until $\mathbf{x}_i^{(k)}, i \in I_n$ converges. It should be noted, however, that this procedure does not guarantee convergence.

According to Hori and Nagata (1985), the variance in the density of NO_x is fairly small. Hori and Nagata (1985) hence optimize the objective function given by equation (9.2.31) with the above heuristic method. Figure 9.2.12(a) shows the near-optimal configuration of 16 monitor points placed in Kyoto provided that $m(x)$ is given by Figure 9.2.12(b).

9.2.6 Locational optimization of service points of a mobile facility

Facilities are not always fixed at the same locations. Some kinds of facilities are mobile and stop at several points in a region to provide service. An example is a bookmobile (Takeda, 1985). A bookmobile offers a library service at some fixed points in a region for a certain length of time. Library users go to their nearest service points when the bookmobile stops at those points. If the bookmobile could stop at every house, the user's convenience would be maximum. Because of a time constraint, however, the sum of the library service time and travel time should be not greater than a certain limit. The locational optimization problem is hence to minimize the average distance (or cost) of users to their nearest service points provided that the number of service points and the total travel distance of the bookmobile are given.

The mathematical formulation of this locational optimization problem is almost the same as that of Problem OPT3 except for constraints. The objective function is given by equation (9.2.1). If we assume that the total travel distance of the bookmobile is given by the sum of the Euclidean distance between the successive service points, the bookmobile problem is formulated as follows.

Problem OPT4 (minimization of the average travel cost to the nearest points provided that the length of a line successively connecting those service points is not greater than a certain limit)

$$\min_{x_1, \dots, x_n} \sum_{i=1}^n \int_{V_i} f(\|\mathbf{x} - \mathbf{x}_i\|^2) \phi(\mathbf{x}) d\mathbf{x}, \quad (9.2.33)$$

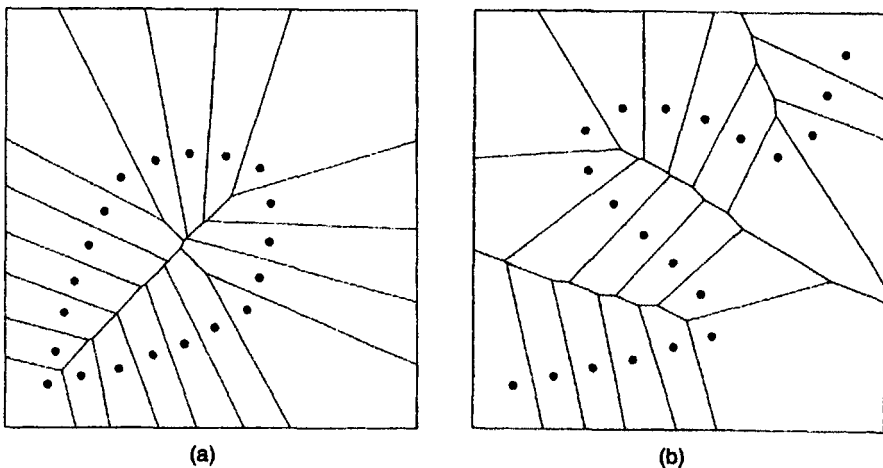


Figure 9.2.13 Locational optimization of $n = 20$ service points: (a) $d^{**} = 0.1$, $x_1^T = (0.1, 0.1)$, $x_{20}^T = (0.9, 0.9)$; (b) $d^{**} = 0.1$, $x_1^T = x_{20}^T = (0.15, 0.15)$. (Source: Takeda, 1985, Figure 5.3.)

subject to

$$\sum_{i=1}^{n-1} d(\mathbf{x}_i, \mathbf{x}_{i+1}) \leq d^*. \quad (9.2.34)$$

An alternative constraint is that every distance between service points is not greater than $d^{**} = d^*/n$, i.e.

$$d(\mathbf{x}_i, \mathbf{x}_{i+1}) \leq d^{**}, \quad i = 1, \dots, n-1. \quad (9.2.35)$$

Obviously, this constraint is stronger than the constraint of equation (9.2.34).

We may also add the constraint that the starting and finishing points are fixed, or that those points are the same and fixed, i.e.

$$\mathbf{x}_1 = \mathbf{c}, \quad \mathbf{x}_n = \mathbf{c}' (\mathbf{c} \neq \mathbf{c}') \quad \text{or} \quad \mathbf{x}_1 = \mathbf{x}_n = \mathbf{c}. \quad (9.2.36)$$

In this case, the variables in expression (9.2.33) are $\mathbf{x}_2, \dots, \mathbf{x}_{n-1}$.

Problem OPT4 is a constrained non-linear, non-convex programming problem. As we showed in Section 9.1, we can solve this problem using the penalty function method. Note that when n is large, the penalty function method is not efficient. Alternatively, we may use the multiplier method.

Figure 9.2.13 shows the optimal configuration of $n = 20$ service points obtained by Takeda (1985).

9.2.7 Locational optimization of terminal points through which users go to the central point

On a network we have terminal facilities, such as stations on a railway network, bus stops on a bus route, access points of a communication network,

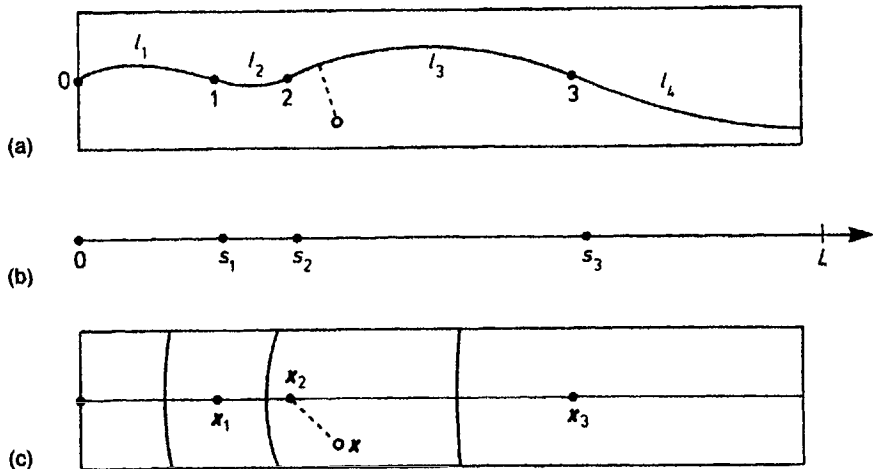


Figure 9.2.14 Bus stops on a bus route.

and so forth. Such networks sometimes have central points. For example, consider a bus route in a residential area. Commuters walk from their homes to bus stops, and take a bus to a railway station, from which they go to their places of work. In this case the central point is the railway station at which a bus terminates. Obviously, commuters want to reach the station as fast as possible. The problem is thus to seek a set of the locations of bus stops that minimizes the average travel time of commuters. This type of optimization problem is examined by Lesley (1976), Vaughan and Cousins (1977), Wirasinghe and Ghoneim (1981), and T. Suzuki (1987), among others.

To formulate the above problem mathematically, let us consider a bus route, L , in a region S (Figure 9.2.14), on which n bus stops are placed. Those bus stops are indexed from 1 to n from the station. Let l_i be the route distance from bus stop i to bus stop $i+1$, $i = 0, 1, \dots, n$. Note that bus stop 0 is fixed at the station, and l_{n+1} is the distance from bus stop n to the end of the bus route L from which a bus departs (a bus garage). The location of a point on the route L can be represented by a route distance, s , from the station. The location of bus stop i is hence indicated by $s = s_i = \sum_{j=1}^i l_j$. Commuters are distributed over S according to a density function $\phi(x)$.

First, we assume that every commuter walks from his/her home (the unfilled circle in Figure 9.2.14(a)) to the nearest point (called an access point) on the bus route L , and then walks from this access point to a bus stop along the bus route L . Under this assumption, the choice of a bus stop depends upon only the distances from the access point to alternative bus stops; the choice does not depend upon the distance from his/her home to the access point. Hence, the two-dimensional problem reduces to a one-dimensional problem (Figure 9.2.14(b)). To be explicit, let $\phi_L(s)$ be the density of

commuters whose nearest point on the bus route L from their homes is a point s . Once $\phi_L(s)$ is obtained from $\phi(x)$ (the density of commuters on a plane), the problem becomes the problem of optimizing n bus stops on the line segment L over which commuters are distributed with the density function $\phi_L(s)$.

Let v_b be the speed of a bus, v_w be walking speed, and b be the time spent at every bus stop. We assume that every commuter has a time schedule and arrives at a bus stop when a bus just reaches it. Then, the total travel time from a point s to bus stop i on foot and from this bus stop to the station by bus is given by $|s - s_i|/v_w + s_i/v_b + ib$. Obviously, the relation

$$b + \frac{l_i}{v_b} < \frac{l_i}{v_w} \quad (9.2.37)$$

should be satisfied; otherwise, walking is faster than taking a bus. Since every commuter minimizes the travel time, commuters at the point s choose the bus stop that gives the minimum travel time, i.e. $\min_i \{ |s - s_i|/v_w + s_i/v_b + ib \}$. As a result, every bus stop has its catchment area, which is given by

$$V_i = \left\{ s \mid \frac{|s - s_i|}{v_w} + \frac{s_i}{v_b} + ib \leq \frac{|s - s_j|}{v_w} + \frac{s_j}{v_b} + jb, \text{ for } j \in I_n \setminus \{i\} \right\}. \quad (9.2.38)$$

As we defined in Chapter 3, this region is the weighted Voronoi region generated on the line L .

From equation (9.2.38), the total travel time of all commuters in the region L (or S) is given by

$$F(l_1, \dots, l_n) = \sum_{i=0}^n \int_{V_i} \left\{ \frac{|s - s_i|}{v_w} + \frac{s_i}{v_b} + ib \right\} \phi_L(s) ds. \quad (9.2.39)$$

The optimization problem is hence written as

$$\min_{l_0, \dots, l_n} \sum_{i=0}^n \int_{V_i} \left\{ \frac{|s - s_i|}{v_w} + \frac{s_i}{v_b} + ib \right\} \phi_L(s) ds, \quad (9.2.40)$$

subject to

$$b + \frac{l_i}{v_b} < \frac{l_i}{v_w} \quad \text{for } i \in I_n, \quad (9.2.41)$$

$$\sum_{i=1}^n l_i \leq L, \quad (9.2.42)$$

$$l_i > 0 \quad \text{for } i \in I_{n+1}. \quad (9.2.43)$$

This problem is a constrained non-linear programming problem, which can be solved, as shown in Section 9.1, by use of the penalty function method. When the density function $\phi_L(s)$ is the uniform distribution, the objective function is explicitly written as

$$\begin{aligned}
 F(l_1, \dots, l_n) = & \frac{1}{4v_b^2 v_w} (v_b^2 + 2v_b v_w - v_w^2) \sum_{i=1}^n l_i + \frac{1}{v_b} \sum \sum_{i \neq j} l_i l_j \\
 & + b \sum_{i=1}^n (i-1)l_i + \frac{v_b - v_w}{2v_b} b \sum_{i=1}^n l_i - \frac{v_w b^2}{4} n \\
 & + \frac{l_{n+1}}{v_b} \sum_{i=1}^n l_i + nb l_{n+1} + \frac{l_{n+1}^2}{2v_w}.
 \end{aligned} \quad (9.2.44)$$

In this case, the problem becomes a constrained quadratic programming problem (a special case of the constrained non-linear programming problem).

In the above, we assumed that commuters first go to the nearest point on the route L . Instead, if we assume that commuters take the Euclidean path to a bus stop (the broken line in Figure 9.2.14(c)), the problem cannot be reduced to the one-dimensional problem; the problem should be formulated on a plane. Essentially, the formulation is the same as in the one-dimensional case. In place of equation (9.2.38), the catchment area of the bus stop at s_i is given by

$$V_i = \left\{ \mathbf{x} \mid \frac{\|\mathbf{x} - \mathbf{x}_i\|}{v_w} + \frac{s_i}{v_b} + i b \leq \frac{\|\mathbf{x} - \mathbf{x}_j\|}{v_w} + \frac{s_j}{v_b} + j b, \quad j \neq i, j \in I_n \right\}. \quad (9.2.45)$$

An example is shown in Figure 9.2.14(c). The objective function is thus given by

$$F(l_1, \dots, l_n) = \sum_{i=0}^n \int_{V_i} \left\{ \frac{\|\mathbf{x} - \mathbf{x}_i\|}{v_w} + \frac{s_i}{v_b} + i b \right\} \phi(\mathbf{x}) d\mathbf{x}. \quad (9.2.46)$$

The constraints are the same as those given by relations (9.2.37), (9.2.41), (9.2.42) and (9.2.43).

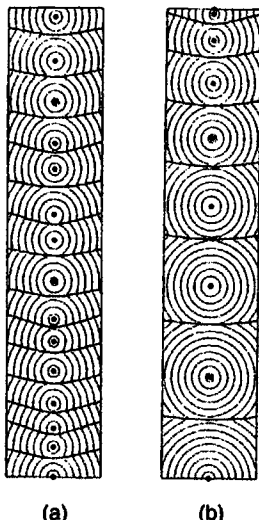


Figure 9.2.15 Locational optimization of bus stops on the Motoyahata–Takatsuka line: (a) the present location of bus stops; (b) the optimal location of bus stops. (Source: T. Suzuki, 1987, Figure 8.)

The calculation of the integral in equation (9.2.46) is fairly complex, but we can carry it out in practice. In particular, when the density $\phi(x)$ is uniform, this integral is explicitly obtained. The result is, however, extremely lengthy, and so it is omitted here (see T. Suzuki, 1987, who obtained the results with the help of REDUCE-III).

T. Suzuki (1987) applies the above optimization problem to the Motoyahata-Takatsuka bus line in Ichikawa. This line is chosen because it is mainly used for commuting to Motoyahata station; the bus route is almost straight; and the population density $\phi(x)$ is fairly uniform. From the empirical survey, the parameter values are observed as $v_b = 8.00$ m/s, $v_w = 1.20$ m/s, $b = 30$ s, $L = 4865.7$ m. T. Suzuki (1987) obtained the optimal solutions for $n = 2, \dots, 34$. These solutions indicate that the total travel time is minimized when $n = 8$. The optimal locations of the eight bus stops are depicted in Figure 9.2.15(b). It is of interest to compare this figure with the actual locations of bus stops shown in Figure 9.2.15(a). The travel time in the optimal solution is shorter than the actual travel time by 2 min on average. Obviously, the optimal solution depends upon an objective function. Instead of minimizing the total travel time, we may maximize the profit of a bus company. This alternative optimization (including other criteria) is discussed in T. Suzuki (1987).

9.2.8 Locational optimization of points on a continuous network

In the preceding subsections we dealt with locational optimization problems on a continuous plane. In this subsection we deal with those on a continuous network (i.e. point-like facilities are locatable on any point on the network (including nodes)).

In Section 3.8.2 we introduced the network Voronoi link-diagram, $V_{\text{link}} = \{V_{\text{link}}(p_1), \dots, V_{\text{link}}(p_n)\}$ generated by $\{p_1, \dots, p_n\}$ on a network $N(N, L)$, where N denotes the set of nodes and L denotes the set of links forming the network. To measure the Voronoi link set $V_{\text{link}}(p_i)$, Hakimi *et al.* (1992) define the 'size' of $V_{\text{link}}(p_i)$. To be explicit, let $w(q_i)$ be the weight of the i th node in N . Then the size, $s(V_{\text{link}}(p_i))$, of $V_{\text{link}}(p_i)$ is defined by $s(V_{\text{link}}(p_i)) = \sum_{q_i \in V_{\text{link}}(p_i)} w(q_i)$. In terms of $s(V_{\text{link}}(p_i))$, we consider the following problem.

Problem OPT5 (Voronoi p -centre problem) Find a set P of points such that

$$\min_{p_1, \dots, p_n} \max \{s(V_{\text{link}}(p_1)), \dots, s(V_{\text{link}}(p_n))\}. \quad (9.2.47)$$

Hakimi *et al.* (1992) show that the Voronoi p -centre problem is NP-hard (Section 1.3.4). They also develop an algorithm to solve this problem.

In the study of market area delineation, one of the most popular models is the Huff model (1963). Originally this model assumed the Euclidean distance. This assumption, however, is not always acceptable when we deal with market area delineation in a small district, such as the market areas of

fast food stores in a down town district. To deal with such market area delineation, we use the Huff model on a continuous network of streets (Miller, 1994; Okabe and Kitamura, 1996). Okabe and Okunuki (1999) attempt to optimize the location of one store to maximize its profit provided that the other stores are fixed and the choice behaviour of consumers is given by the Huff model.

9.3 LOCATIONAL OPTIMIZATION OF LINES

In the previous section we discussed the locational optimization of points. In this section, extending the method developed there, we consider the locational optimization of lines. We deal with three types of lines: a service route (Section 9.3.1), a network (Section 9.3.2) and an Euclidean Steiner minimum tree (Section 9.3.3).

9.3.1 Locational optimization of a service route

We first consider the locational optimization of a service route. Generally, the problem is to seek an optimal service route of a mobile facility that provides some service at any point on the service route. Such mobile services are numerous in Japan. The well-known example is a wagon collecting old newspapers. The wagon travels a route calling with a loudspeaker, 'we are exchanging old newspapers for tissue paper'. Hearing that call, a resident who wants to sell old newspapers goes to the nearest service route to catch the wagon. The wagon then comes to the resident's home and the resident gets tissue paper in exchange for old newspapers. More traditional examples in Japan are an ice-cream vendor riding on a bicycle with a bell, a bean card (tofu) vendor pulling a cart blowing a bugle, a fermented soybeans (natto) vendor calling 'natto' with a resonant voice, and so forth. The problem of these vendors is to find the optimal service route in a region that yields the maximum profit.

To discuss the above problem more precisely, let us consider, for example, an optimal service route of an ice-cream vendor. We suppose, for simplicity, that only one ice-cream vendor exclusively sells ice-cream in a region, and that a service route can be freely placed in a region (a road network is so dense that the route can be almost freely placed in a region). The starting point and the finishing point of the service route may be the same or may not. We assume that every customer buys ice-cream at the nearest point on the service route; the demand for ice-cream is inversely proportional to the average travel cost from all customers to their nearest points on the service route; the ice-cream vendor can satisfy all demand; and the marginal cost of a unit amount of ice-cream is constant. Under these assumptions, the profit maximization problem reduces to the problem of minimizing the average travel cost. Obviously, as the length of the service route becomes long, the average travel cost becomes shorter, and the profit increases. Because of a

time constraint, however, the vendor cannot walk infinitely; the travel distance in a day is limited. The problem is hence to determine the service route to minimize the average travel cost provided that the length of the service route is not greater than a certain limit.

To formulate the above problem mathematically, we represent a service route in a region S by the chain of straight line segments (a curved line is approximated by the chain of small straight line segments). Let $\mathbf{x}_1, \dots, \mathbf{x}_n$ be the end points of the straight line segments; $\overline{\mathbf{x}_i \mathbf{x}_{i+1}}$ be the open straight line segment connecting points \mathbf{x}_i and \mathbf{x}_{i+1} ; and $\{V(\mathbf{x}_1), \dots, V(\mathbf{x}_n), V(\overline{\mathbf{x}_1 \mathbf{x}_2}), \dots, V(\overline{\mathbf{x}_{n-1} \mathbf{x}_n})\}$ be the line Voronoi diagram generated by $\{\mathbf{x}_1, \dots, \mathbf{x}_n, \overline{\mathbf{x}_1 \mathbf{x}_2}, \dots, \overline{\mathbf{x}_{n-1} \mathbf{x}_n}\}$ (Section 3.5). From the definition of the line Voronoi diagram, if a point \mathbf{x} is in the Voronoi region $V(\mathbf{x}_i)$, the Euclidean distance from the point \mathbf{x} to the nearest point on the service route is given by $\|\mathbf{x} - \mathbf{x}_i\|$; if a point \mathbf{x} is in the Voronoi region $V(\overline{\mathbf{x}_i \mathbf{x}_{i+1}})$, the Euclidean distance $d_i(\mathbf{x}, \overline{\mathbf{x}_i \mathbf{x}_{i+1}})$ from the point \mathbf{x} to the nearest point on the service route is given by the Euclidean distance from the point \mathbf{x} to the line segment $\overline{\mathbf{x}_i \mathbf{x}_{i+1}}$, which is explicitly given by

$$d_i(\mathbf{x}, \overline{\mathbf{x}_i \mathbf{x}_{i+1}}) = \left[\|\mathbf{x} - \mathbf{x}_i\|^2 - \frac{(\mathbf{x} - \mathbf{x}_i)^T (\mathbf{x}_{i+1} - \mathbf{x}_i)^2}{\|\mathbf{x}_{i+1} - \mathbf{x}_i\|^2} \right]^{1/2}. \quad (9.3.1)$$

Let $\phi(\mathbf{x})$ be the demand density at \mathbf{x} ; and $f(\|\mathbf{x} - \mathbf{x}_i\|^2)$ be a strictly increasing travel cost function of the squared Euclidean distance, $\|\mathbf{x} - \mathbf{x}_i\|^2$. Note that the total demand is assumed to be unity without loss of generality.

In these terms, the average travel cost to the service route is written as

$$\begin{aligned} F(\mathbf{x}_1, \dots, \mathbf{x}_n) &= \sum_{i=1}^n \int_{V(\mathbf{x}_i)} f(\|\mathbf{x} - \mathbf{x}_i\|^2) \phi(\mathbf{x}) d\mathbf{x} \\ &\quad + \sum_{i=1}^{n-1} \int_{V(\overline{\mathbf{x}_i \mathbf{x}_{i+1}})} f(d_i(\mathbf{x}, \overline{\mathbf{x}_i \mathbf{x}_{i+1}})^2) \phi(\mathbf{x}) d\mathbf{x}. \end{aligned} \quad (9.3.2)$$

When $f(\|\mathbf{x} - \mathbf{x}_i\|^2) = \|\mathbf{x} - \mathbf{x}_i\|$, and the demand density is uniform, i.e. $\phi(\mathbf{x}) = 1/S$ over S , we can explicitly obtain the value of equation (9.3.2) for given $\mathbf{x}_1, \dots, \mathbf{x}_n$ (see Section 8.3).

With the above objective function, we can formulate the optimal service route problem as follows.

Problem OPT6 (minimization of the average travel cost to the nearest point on a service line provided that the length of the service line is not greater than a certain limit)

$$\begin{aligned} \min_{\mathbf{x}_1, \dots, \mathbf{x}_n} & \left[\sum_{i=1}^n \int_{V(\mathbf{x}_i)} f(\|\mathbf{x} - \mathbf{x}_i\|^2) \phi(\mathbf{x}) d\mathbf{x} \right. \\ & \left. + \sum_{i=1}^{n-1} \int_{V(\overline{\mathbf{x}_i \mathbf{x}_{i+1}})} f(d_i(\mathbf{x}, \overline{\mathbf{x}_i \mathbf{x}_{i+1}})^2) \phi(\mathbf{x}) d\mathbf{x} \right] \end{aligned} \quad (9.3.3)$$

subject to

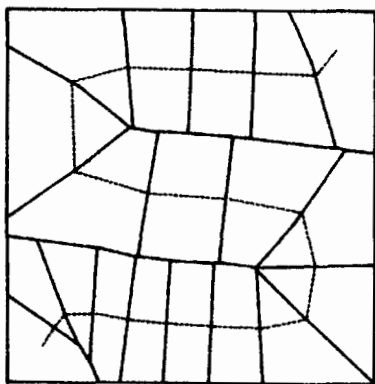
$$\sum_{i=1}^{n-1} \| \mathbf{x}_i - \mathbf{x}_{i+1} \| \leq d^*. \quad (9.3.4)$$

We may add the constraints $\mathbf{x}_1 = \mathbf{c}$, $\mathbf{x}_n = \mathbf{c}'$, or $\mathbf{x}_1 = \mathbf{x}_n = \mathbf{c}$, where \mathbf{c} and \mathbf{c}' ($\mathbf{c} \neq \mathbf{c}'$) are constants. In this case the variables in expression (9.3.3) are $\mathbf{x}_2, \dots, \mathbf{x}_{n-1}$.

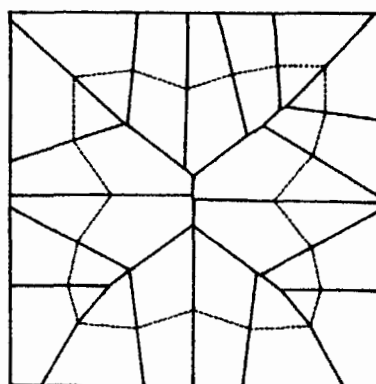
Like Problem OPT3, Problem OPT6 is a non-linear, non-convex programming problem. To solve this problem, as mentioned in Section 9.1, we should use a numerical method, such as the penalty function method. If we adopt the steepest descent method in the unconstrained programming problem transformed from the constrained programming problem of Problem OPT3 (recall Section 9.1.3), we need the first derivative. The derivation of the first derivative is almost the same as was shown in Problem OPT3 (equation (9.2.2)). The slight move of \mathbf{x}_i produces the changes in the Voronoi regions $V(\mathbf{x}_i)$, $V(\overline{\mathbf{x}_{i-1}\mathbf{x}_i})$ and $V(\overline{\mathbf{x}_i\mathbf{x}_{i+1}})$, and their adjacent Voronoi regions. Since the changes in the integral domains are cancelled out (recall the derivation from equation (9.2.3) to equation (9.2.11)), the first derivative is obtained from the first-order derivative of the integrand,

$$\begin{aligned} \frac{\partial F}{\partial x_{i\kappa}} &= \int_{V(x_i)} \frac{\partial}{\partial x_{i\kappa}} f(\|\mathbf{x} - \mathbf{x}_i\|^2) \phi(\mathbf{x}) d\mathbf{x} \\ &+ \int_{V(\overline{\mathbf{x}_{i-1}\mathbf{x}_i})} \frac{\partial}{\partial x_{i\kappa}} f(d_l(\mathbf{x}, \overline{\mathbf{x}_{i-1}\mathbf{x}_i})^2) \phi(\mathbf{x}) d\mathbf{x} \\ &+ \int_{V(\overline{\mathbf{x}_i\mathbf{x}_{i+1}})} \frac{\partial}{\partial x_{i\kappa}} f(d_l(\mathbf{x}, \overline{\mathbf{x}_i\mathbf{x}_{i+1}})^2) \phi(\mathbf{x}) d\mathbf{x}, \quad \kappa = 1, 2. \end{aligned} \quad (9.3.5)$$

Since $d_l(\mathbf{x}, \overline{\mathbf{x}_i\mathbf{x}_{i+1}})$ is explicitly given by equation (9.3.1), and the function $f(\mathbf{x})$ is assumed to be differentiable, we can calculate the integrals in equation



(a)



(b)

Figure 9.3.1 Locally optimal service routes in a unit square. Parameter values are: $d^* = \sqrt{2}/10$, $\phi(\mathbf{x}) = 1$, $f(\|\mathbf{x} - \mathbf{x}_i\|^2) = \|\mathbf{x} - \mathbf{x}_i\|^2$; $n = 20$ in (a), $n = 21$ in (b). (Source: Takeda, 1985, Figure 5.10.)

(9.3.5) once the function $f(\mathbf{x})$ is explicitly given (the first integral is the same as equation (9.2.11)).

Using the penalty function method and the steepest descent method with this derivative, we can solve Problem OPT6. Actually, Takeda (1985) solved this problem with a slight modification (the quasi-Newton method) for $f(\|\mathbf{x} - \mathbf{x}_i\|^2) = \|\mathbf{x} - \mathbf{x}_i\|^2$, $n = 20$, $\phi(\mathbf{x})$ being uniform over a unit square, $d^* = \sqrt{2}/10$ and $\mathbf{x}_1^T = (0.1, 0.1)$, $\mathbf{x}_{20}^T = (0.9, 0.9)$; $n = 21$, $\mathbf{x}_1^T = \mathbf{x}_{21}^T = (0.15, 0.15)$. The results are depicted in Figure 9.3.1.

9.3.2 Locational optimization of a network

In most of network optimization problems the location of nodes and links, or at least the location of links, is fixed (for example, recall the bus stop problem in Section 9.2.1). The locational optimization of both nodes and links was rarely studied because of complicated geometrical computation. The recent progress in the Voronoi diagrams, however, provides a clue to this difficult problem. In fact, using the Voronoi diagram, Suzuki and Iri (1986c) attempted to solve the optimization problem in which the locations of both nodes and links were to be optimized so that the total travel time was minimized provided that the connection of links of the network and the traffic volumes between origins and destinations were given.

Let us consider a railway network in a region S in which nodes are stations, and links are railways connecting the stations. We assume that the speed of a train on this railway network is controlled as follows: first, the speed is accelerated from a station with α until it reaches v_{\max} ; next, the speed is kept constant at v_{\max} ; last, the speed is decelerated with $-\alpha$ until it becomes zero at the next station. To avoid unnecessary complicated equations, we assume that the distance between two adjacent stations is greater than v_{\max}^2/α , implying that a train achieves the maximum speed between stations.

When a traveller makes a trip from an origin \mathbf{x}_0 to a destination \mathbf{x}_d , we assume that the traveller first walks to the nearest station, $\mathbf{x}^*(\mathbf{x}_0)$, from the origin \mathbf{x}_0 at walking speed v_w (since the traveller knows the time schedule of trains, he/she reaches the station just when a train arrives there); next, the traveller takes a train from station $\mathbf{x}^*(\mathbf{x}_0)$ to station $\mathbf{x}^*(\mathbf{x}_d)$, which is the nearest station from the destination \mathbf{x}_d ; last, the traveller walks from the station $\mathbf{x}^*(\mathbf{x}_d)$ to the destination \mathbf{x}_d at walking speed v_w . To obtain the total travel time of this trip, let $N[\mathbf{x}^*(\mathbf{x}_0), \mathbf{x}^*(\mathbf{x}_d)]$ be the number of stations between station $\mathbf{x}^*(\mathbf{x}_0)$ and station $\mathbf{x}^*(\mathbf{x}_d)$; $d_{\text{net}}(\mathbf{x}^*(\mathbf{x}_0), \mathbf{x}^*(\mathbf{x}_d))$ be the railway distance between station $\mathbf{x}^*(\mathbf{x}_0)$ and the station $\mathbf{x}^*(\mathbf{x}_d)$; and b be the time spent at each station. A train runs a distance v_{\max}^2/α while it is accelerating and decelerating, and the train runs a distance $d_{\text{net}}(\mathbf{x}^*(\mathbf{x}_0), \mathbf{x}^*(\mathbf{x}_d)) - N[\mathbf{x}^*(\mathbf{x}_0), \mathbf{x}^*(\mathbf{x}_d)]v_{\max}^2/\alpha$ while it maintains a constant speed v_{\max} . Since it takes $2v_{\max}/\alpha$ (minutes) for acceleration and deceleration, the total travel time from the origin \mathbf{x}_0 to the destination \mathbf{x}_d is given by

$$\begin{aligned}
T(\mathbf{x}_o, \mathbf{x}_d) = & \frac{1}{v_w} \left\{ \| \mathbf{x}_o - \mathbf{x}^*(\mathbf{x}_o) \| + \| \mathbf{x}_d - \mathbf{x}^*(\mathbf{x}_d) \| \right\} \\
& + \left(\frac{v_{\max}}{\alpha} + b \right) \{ N[\mathbf{x}^*(\mathbf{x}_o), \mathbf{x}^*(\mathbf{x}_d)] + 1 \} \\
& + \frac{1}{v_{\max}} d_{\text{net}}(\mathbf{x}^*(\mathbf{x}_o), \mathbf{x}^*(\mathbf{x}_d)).
\end{aligned} \tag{9.3.6}$$

To consider the traffic volume between two points in S , suppose that a traveller in a small region around \mathbf{x}_o makes trips to see friends who are distributed over the region S . The number of friends in a small region ($d\mathbf{x}$) around \mathbf{x}_d is proportional to the number of inhabitants there. In terms of the density function of inhabitants, $\phi(\mathbf{x}_d)$, this number is given by $c_1 \phi(\mathbf{x}_d) d\mathbf{x}$, where c_1 is a constant. We assume that the traveller makes $c_1 \phi(\mathbf{x}_d) d\mathbf{x}$ trips to a small region around \mathbf{x}_d during a unit period of time. We also assume that the number of trip-makers in a small region around \mathbf{x}_o is proportional to the number of inhabitants there, i.e. $c_2 \phi(\mathbf{x}_o) d\mathbf{x}$, where c_2 is a constant. Thus the number of trips from a small region around \mathbf{x}_o to a small region around \mathbf{x}_d is given by $c_1 c_2 \phi(\mathbf{x}_o) \phi(\mathbf{x}_d) d\mathbf{x}_o d\mathbf{x}_d = \phi(\mathbf{x}_o) \phi(\mathbf{x}_d) d\mathbf{x}_o d\mathbf{x}_d$, where we fix $c_1 c_2 = 1$ without loss of generality. In the region S , the total round travel time of all travellers in a unit period of time is given by

$$F(\mathbf{x}_1, \dots, \mathbf{x}_n) = 2 \int_S T(\mathbf{x}_o, \mathbf{x}_d) \phi(\mathbf{x}_o) \phi(\mathbf{x}_d) d\mathbf{x}_o d\mathbf{x}_d. \tag{9.3.7}$$

The nearest stations, $\mathbf{x}^*(\mathbf{x}_o)$ and $\mathbf{x}^*(\mathbf{x}_d)$, are readily obtained from the Voronoi diagram, $\{V_1, \dots, V_n\}$, generated by a set of the n stations at $\mathbf{x}_1, \dots, \mathbf{x}_n$. Obviously, if $\mathbf{x}_o \in V_i$, then $\mathbf{x}^*(\mathbf{x}_o) = \mathbf{x}_i$; if $\mathbf{x}_d \in V_j$, then $\mathbf{x}^*(\mathbf{x}_d) = \mathbf{x}_j$. We hence write $N[\mathbf{x}^*(\mathbf{x}_o), \mathbf{x}^*(\mathbf{x}_d)]$ as $N[\mathbf{x}_i, \mathbf{x}_j]$ for $\mathbf{x}_o \in V_i, \mathbf{x}_d \in V_j$, and equation (9.3.7) is written as

$$\begin{aligned}
F(\mathbf{x}_1, \dots, \mathbf{x}_n) = & 2 \sum_{i=1}^n \int_{V_i} \frac{1}{v_w} \| \mathbf{x}_o - \mathbf{x}_i \| \phi(\mathbf{x}_o) d\mathbf{x}_o \\
& + 2 \sum_{j=1}^n \int_{V_j} \frac{1}{v_w} \| \mathbf{x}_o - \mathbf{x}_j \| \phi(\mathbf{x}_d) d\mathbf{x}_d \\
& + 2 \sum_{i=1}^n \sum_{\substack{j=1 \\ j \neq i}}^n \left\{ \left(\frac{v_{\max}}{\alpha} + b \right) (N[\mathbf{x}_i, \mathbf{x}_j] + 1) + \frac{1}{v_{\max}} d_{\text{net}}(\mathbf{x}_i, \mathbf{x}_j) \right\} \\
& \times \int_{V_i} \phi(\mathbf{x}_o) d\mathbf{x}_o \int_{V_j} \phi(\mathbf{x}_d) d\mathbf{x}_d.
\end{aligned} \tag{9.3.8}$$

The first term is the round travel time from (to) origins in the region V_i to (from) the station \mathbf{x}_i . The second term is the round travel time from (to) the station \mathbf{x}_j to (from) destinations in the region V_j . The last term is the round travel time from (to) the station \mathbf{x}_i to (from) the station \mathbf{x}_j . Notice that the first term and the second term are the same.

To sum up, the network locational optimization problem is formulated as follows.

Problem OPT7 (locational optimization of a network by minimizing the total travel time)

$$\begin{aligned} \min_{x_1, \dots, x_n} & \left[\sum_{i=1}^n \int_{V_i} \frac{1}{v_w} \|x - x_i\| \phi(x) dx \right. \\ & + \sum_{i=1}^n \sum_{j \geq i+1}^n \left\{ \left(\frac{v_{\max}}{\alpha} + b \right) (N[x_i, x_j] + 1) + \frac{1}{v_{\max}} d_{\text{net}}(x_i, x_j) \right\} \\ & \times \int_{V_i} \phi(x) dx \int_{V_j} \phi(x) dx \left. \right] \end{aligned} \quad (9.3.9)$$

(note that the factor 4 is omitted in expression (9.3.9)). We may add the constraints that $x_1 = c$ and $x_n = c'$, or $x_1 = x_n = c$ ($c \neq c'$).

Again, Problem OPT7 is a non-linear, non-convex programming problem. We may solve it with the steepest descent method. The first-order derivative is obtained from

$$\begin{aligned} \frac{\partial}{\partial x_{i\kappa}} F(x_1, \dots, x_n) = & \int_{V_i} \frac{1}{v_w} \frac{\partial}{\partial x_{i\kappa}} \|x - x_i\| \phi(x) dx \\ & + \sum_{i=1}^n \sum_{j \geq i+1}^n \frac{1}{v_{\max}} \left\{ \frac{\partial}{\partial x_{i\kappa}} d_{\text{net}}(x_i, x_j) \right\} \int_{V_i} \phi(x) dx \int_{V_j} \phi(x) dx \\ & + \sum_{i=1}^n \sum_{j=i+1}^n \left\{ \left(\frac{v_{\max}}{\alpha} + b \right) (N[x_i, x_j] + 1) + \frac{1}{v_{\max}} d_{\text{net}}(x_i, x_j) \right\} \\ & \times \left\{ \int_{V_i} \phi(x) dx \frac{\partial}{\partial x_{i\kappa}} \int_{V_i} \phi(x) dx + \int_{V_i} \phi(x) dx \frac{\partial}{\partial x_{i\kappa}} \int_{V_j} \phi(x) dx \right\}, \quad \kappa = 1, 2. \end{aligned} \quad (9.3.10)$$

The first term is the same as equation (9.3.5). The second term indicates the change in the railway distance due to the slight move of the station x_i . If the railway is assumed to be a chain of lines connecting stations with straight line segments, the value of this term is obtained from

$$\frac{\partial}{\partial x_{i\kappa}} d_{\text{net}}(x_i, x_j) = \frac{\partial}{\partial x_{i\kappa}} \{ \|x_{i-1} - x_i\| + \|x_i - x_{i+1}\| \}, \quad \kappa = 1, 2. \quad (9.3.11)$$

The last term in equation (9.3.10) treats the change in the area of Voronoi polygons. The derivation is almost the same as that in Section 9.3.1 (we will also refer to this derivation in Section 9.5).

Using the steepest descent method with this derivative, we can solve Problem OPT7. An actual computation is carried out by Suzuki and Iri (1986c) with a modified method (the quasi-Newton method). Figure 9.3.2 shows one of their results where $n = 16$, $S = \{(x_1, x_2) \mid -0.5 \leq x_1, x_2 \leq 0.5\}$, $x_1^T = (-0.1, -0.1)$, $x_{16}^T = (0.9, 0.9)$, $v_{\max} = 0.01$, $\alpha = 0.002$, $v_w = 0.001$, and

$$\phi(x) = \begin{cases} \exp(-25\|x\|) & \text{if } x \in S, \\ 0 & \text{if } x \notin S. \end{cases} \quad (9.3.12)$$

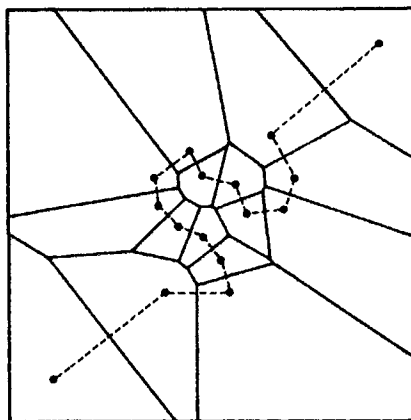


Figure 9.3.2 A locally optimal railway stations $n = 16$, $S = \{(x_1, x_2) | -0.5 \leq x_1, x_2 \leq 0.5\}$, $x_1^T = (-0.1, -0.1)$, $x_{16}^T = (0.9, 0.9)$, $v_{\max} = 0.01$, $\alpha = 0.002$, $v_w = 0.001$, and $\phi(x)$ is given by equation (9.3.12). (Source: Suzuki and Iri, 1986c, Figure 1.)

9.3.3 Euclidean Steiner minimal tree

In Section 2.5 we referred to a Euclidean minimum spanning tree (EMST). As is noticed from the term ‘minimum’, the EMST problem may be regarded as a locational optimization problem of lines, and this problem can be solved with the Delaunay triangulation (Property D23). In this subsection we show another locational optimization problem of lines, called the Steiner problem, which can also be solved with the Delaunay triangulation.

To give an example of the Steiner problem, suppose that there are three factories on a plane where we can freely lay out roads (Figure 9.3.3(a)). The problem is to construct a network of roads connecting these factories with the minimum length of roads, provided that roads are directly connected between these factories. Recalling the definition of Euclidean minimum spanning trees in Section 2.5, we realize that the solution is given by a Euclidean minimum spanning tree for the three points at which the factories are located (Figure 9.3.3(b)). This solution, however, is not optimal if we are allowed to add a new point (an empty circle in Figure 9.3.3(c)). The problem is to find the fourth point that minimizes the length of roads connecting the three

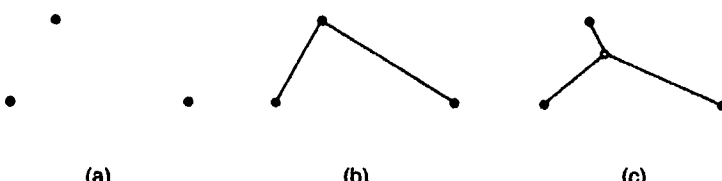


Figure 9.3.3 An example of a Euclidean minimum spanning tree (b) and an Euclidean Steiner minimal tree (c).

factories and the fourth point. The solution is shown in Figure 9.3.3(c). The length of the roads of Figure 9.3.3(c) is shorter than that of Figure 9.3.3(b).

According to Kuhn (1974), the above problem dates back to Fermat in the seventeenth century, and was introduced by Courant and Robbins (1941, VII, §6) as the Steiner (Steiner's) problem. Since then, the Steiner problem has been generalized in various directions. In this subsection we consider the following generalized problem.

Problem OPT8 (Euclidean Steiner minimal tree problem) Suppose that a certain number of points are fixed in the Euclidean plane (space). We wish to minimize the length of line segments connecting the given points. We can add new points (through which the given points are connected) if the additional points reduce the length. The problem is to find the number of additional points and their locations that minimize the length of the line segments connecting the given points and the additional points.

We call the collection of line segments of this solution a *Euclidean Steiner minimal tree*, and the additional points *Steiner points*.

To discuss the above problem mathematically, let P be a set $\{x_1, \dots, x_m\}$ of m ($2 \leq m < \infty$) distinct points which are fixed in \mathbb{R}^2 ; Q_n be a set of n additional points where n and their locations $\{x_{m+1}, \dots, x_{m+n}\}$ are variables; $C_{m+n} = [c_{ij}]$ be the $(m+n) \times (m+n)$ adjacency matrix of points in $P \cup Q_n$ where $c_{ij} = 1$ if nodes x_i and x_j are connected by a line segment and $c_{ij} = 0$ if they are not connected; $c_i = \sum_{j=1, j \neq i}^{m+n} c_{ij}$ be the degree of node i (the number of links connected to node i); l_{ij} be $\overline{x_i x_j}$ (the line segment joining nodes x_i and x_j) if $c_{ij} = 1$ and $l_{ij} = \emptyset$ if $c_{ij} = 0$; $L_{m+n} = \{l_{ij} \mid i \neq j, i, j \in I_{m+n}\}$; and \mathcal{G} be all possible connected geometric graphs of $G(P \cup Q_n, L_{m+n})$ for $n = 0, 1, \dots$ and $x_{m+1}, x_{m+2}, \dots \in \mathbb{R}^2$. In these terms, Problem OPT8 is written mathematically as

$$\min_{n, x_{m+1}, \dots, x_{m+n}} \sum_{i=1}^{m+n} \sum_{j=i+1}^{m+n} c_{ij} \|x_i - x_j\|, \text{ subject to } G(P \cup Q_n, L_{m+n}) \in \mathcal{G}. \quad (9.3.13)$$

To solve this problem, we first solve its subproblem. We fix n and the adjacency matrix C_{m+n} , and consider a set, $\mathcal{G}(C_{m+n})$, of all possible geometric graphs whose adjacency matrix is given by C_{m+n} . The subproblem is written as

$$\min_{x_{m+1}, \dots, x_{m+n}} \sum_{i=1}^{m+n} \sum_{j=i+1}^{m+n} c_{ij} \|x_i - x_j\|, \text{ subject to } G(P \cup Q_n, L_{m+n}) \in \mathcal{G}(C_{m+n}). \quad (9.3.14)$$

We call the tree of this solution the *relatively minimal tree*. Gilbert and Pollak (1968) show that the relatively minimal tree is uniquely determined for a given C_{m+n} . Figure 9.3.4 depicts relatively minimal trees for different adjacency matrices. Obviously, a Euclidean Steiner minimal tree is one of the relatively minimal trees including points P .

Euclidean Steiner minimal trees have many interesting properties, which are discussed by Courant and Robbins (1941), Melzak (1961), Chang (1972),

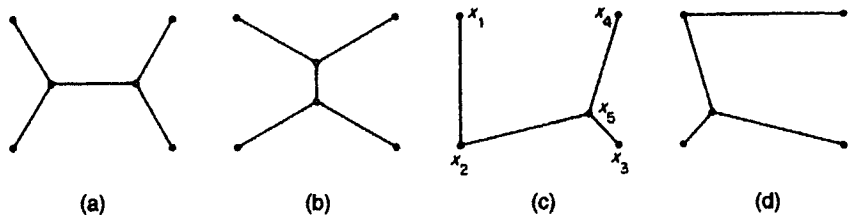


Figure 9.3.4 (a) Euclidean Steiner minimal tree; (a)(b) Euclidean Steiner trees; (a)–(d) relatively minimal trees.

Gilbert and Pollak (1968), Megiddo (1978), Smith *et al.* (1981), Winter (1985), among others. We refer to only three of them which are to be used here.

Property ST1 Exactly three links meet at every Steiner point, and the three angles ($\alpha_{i1}, \alpha_{i2}, \alpha_{i3}$) made by those links at any Steiner point are all 120° (i.e. $c_i = 3$ and $\alpha_{i1} = \alpha_{i2} = \alpha_{i3} = 120^\circ$).

Property ST2 At most three links meet at every point of P ($c_i \leq 3$). If exactly three links meet at a point in P ($c_i = 3$), then $\alpha_{i1} = \alpha_{i2} = \alpha_{i3} = 120^\circ$. If exactly two links meet at a point in P ($c_i = 2$), then $\alpha_{i1} \geq 120^\circ$, where α_{i1} and α_{i2} are angles at a point of degree 2, and $\alpha_{i1} \leq \alpha_{i2}$.

Property ST3 The number n^* of Steiner points is less than or equal to the number of given points minus 2, i.e. $n^* \leq m - 2$.

We call the relatively minimal tree satisfying these three properties a *Euclidean Steiner tree*. Figures 9.3.4(a) and (b) are Euclidean Steiner trees. A *Euclidean Steiner minimal tree* is the Euclidean Steiner tree whose length is minimum among all Euclidean Steiner trees (Figure 9.3.4(a)).

To obtain Euclidean Steiner minimal trees, several combinatorial methods are proposed in the literature, for example Chang (1972), Gilbert and Pollak (1968), Megiddo (1978), and Winter (1985). In practice, however, their methods can hardly solve the problem with more than twenty points ($m > 20$). In fact, Garey *et al.* (1977) show that the Steiner problem is NP-hard (Section 1.3.4). For a large number of points, it is almost impossible to obtain a Euclidean Steiner minimal tree. We may, however, obtain an approximate Euclidean minimal Steiner tree with a computational method. A few heuristic methods are proposed in the literature, for example Smith *et al.* (1981) and Suzuki and Iri (1986b). We show the latter method here, because it is more efficient than the former.

A clue to the problem is shown in Figure 9.3.5. Figure 9.3.4(c) is a relatively minimal tree, but not a Euclidean Steiner tree, because the links at x_2 do not satisfy Property ST2. To avoid such a point, we *split* (Gilbert and Pollak, 1968) the point as follows. First, we add a new point, x_6 , in the close neighbourhood of x_2 (see Figure 9.3.5(a)); second we connect x_2 with x_6 ,

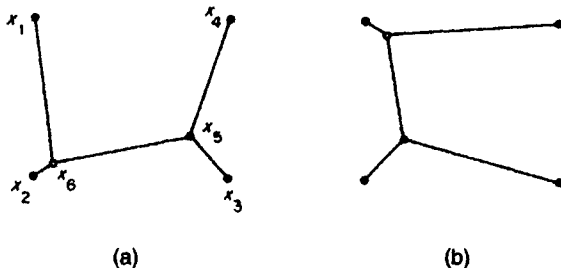


Figure 9.3.5 Splitting a point in relatively minimal trees.

x_6 with x_1 , and x_6 with x_5 . As a result (Figure 9.3.5a), the adjacency matrix of the resulting network becomes the same as that of the Euclidean Steiner tree in Figure 9.3.4(a). Solving the optimization problem given by expression (9.2.14), we obtain Figure 9.3.4(a), which is one of the Euclidean Steiner trees. Similarly, we obtain another Euclidean Steiner tree (Figure 9.3.4(b)) from the relatively minimal tree in Figure 9.3.4(d) through splitting shown in Figure 9.3.5(b).

We now formulate the above procedure as the following algorithm.

Algorithm OPT1 (Euclidean Steiner tree algorithm)

- Step 1. Choose an arbitrary number n larger than $m-2$, and place the n points Q_n randomly in the convex hull of the given points P .
 - Step 2. Construct the Delaunay triangulation for points $P \cup Q_n$.
 - Step 3. Obtain the minimum spanning tree from the Delaunay triangulation using, for example, Cheriton-Tarjan's method (Cheriton and Tarjan, 1976).
 - Step 4. Given the adjacency matrix of this minimum spanning tree, solve the problem of expression (9.3.14) with the descent method.
 - Step 5. Delete the points of degree $c_i \leq 2$ in Q_n of the resulting relatively minimal tree, and place a new point in the close neighbourhood of each point of degree $c_i \geq 4$ in Q_n (as a result, n changes).
 - Step 6. For each point of degree $c_i = 2$ in P (denoted by x_i^*), place a new point in the close neighbourhood of each x_i^* inside the angle $\alpha_{ii} < 120^\circ$ in the direction of the bisector of angle α_{ii} .
 For each point of degree $c_i > 3$ in P and each point of degree $c_i = 3$ in P that does not satisfy $\alpha_{ii} = \alpha_{il} = \alpha_{fl} = 120^\circ$ (denoted by x_i^{**}), place a new point in the close neighbourhood of each x_i^{**} inside the smallest angle $\alpha_i^* = \min\{\alpha_{ij}, j \in I_{ci}\}$ in the direction of the bisector of the angle α_i^* .
 - Step 7. If there is no point that can be deleted or added in Steps 5 and 6, report n and x_{m+1}, \dots, x_{m+n} . Else, go to Step 2.

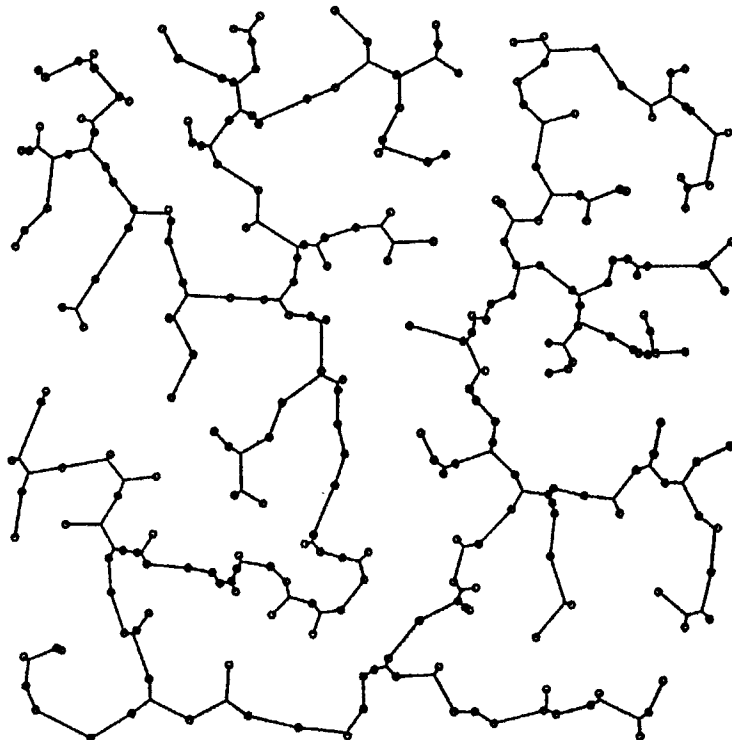


Figure 9.3.6 An approximate Euclidean Steiner tree. (Source: Suzuki and Iri, 1986b, Figure 9.)

Step 5 is the procedure to satisfy Property ST1, and Step 6 is the procedure to satisfy Property ST2. Step 4 is to solve the non-linear, non-convex optimization problem of expression (9.3.14). The objective function is given by $F(\mathbf{x}_{m+1}, \dots, \mathbf{x}_{m+n}) = \sum_{i=1}^{m+n} \sum_{j=i+1}^{m+n} c_{ij} \|\mathbf{x}_i - \mathbf{x}_j\|$. The first-order derivative is given by

$$\frac{\partial F}{\partial \mathbf{x}_{ik}} = \sum_{j \in \{ik, j \neq 0\}} \frac{\partial}{\partial \mathbf{x}_{ik}} \|\mathbf{x}_i - \mathbf{x}_j\|, \quad \kappa = 1, 2. \quad (9.3.15)$$

The second-order derivatives are also obtained from this equation. Using the steepest descent method or the (quasi-)Newton method, we can solve the problem in Step 4.

With Algorithm OPT1, we can obtain a Euclidean Steiner tree. In the case of Figure 9.3.4, we have only two Euclidean Steiner trees. Hence, comparing those trees, we can obtain a Euclidean Steiner minimal tree (Figure 9.3.4(a)). In the case of a large number of given points, we can hardly find all Euclidean Steiner trees. We hence obtain a computationally feasible number of Euclidean Steiner trees and find the minimum tree among them. Obviously, this tree is not guaranteed to be a Euclidean Steiner minimal tree, but it may be close to it.

Figure 9.3.6 shows an approximate Euclidean Steiner minimal tree obtained by Suzuki and Iri (1986b) for $m = 2^8$ points.

Recalling that Section 9.2 dealt with the locational optimization of points, and Section 9.3 dealt with that of lines, the reader might expect that the next section will deal with the locational optimization of areas. At present, however, few papers deal with this problem except for an initial attempt. Shiode (1995) considers the locational optimization of a park in a region to minimize the average distance to the boundary of the park provided that the area of the park and the length of the boundary of the park are fixed.

9.4 LOCATIONAL OPTIMIZATION OVER TIME

In the preceding sections we formulated the locational optimization problems without considering the time dimension. In this section we take this dimension into account.

9.4.1 Multi-stage locational optimization

In Section 9.2 we implicitly assumed that all facilities can be constructed at the same time. This assumption, however, is not always acceptable in reality. One reason is the budget constraint. The number of facilities that can be constructed in a year is sometimes limited because of the budget constraint; we have to construct the required number of facilities over years. Another reason is inefficiency. When the density of users is expected to increase from low density to high density, it is inefficient to construct all facilities in the early stage; the facilities should be constructed in accordance with the increase of users. Because of these reasons, we sometimes meet the problem in which the location of facilities is to be optimized not only over a region but also over time. The problems related to this locational optimization are studied by several researchers in Operations Research, for example Love (1976), Erlenkotter (1981), Van Roy and Erlenkotter (1982), Gunawardane (1982) and Scott (1975). Among them, the problems considered by Scott (1971) and Suzuki *et al.* (1991) are the closest to the above problem. The former model is formulated on a network, whereas the latter model is formulated on a continuous plane. We show the latter model here, because it is formulated with the Voronoi diagram.

Suppose that we construct n facilities in a region S , and that we can construct only one facility in one stage. Consequently it takes n stages to construct all the facilities. The length of the i th stage (referred to as stage i) is τ_i , which may be the same constant like a year ($\tau_i = 1$) or may not. The n facilities are indexed according to the order of construction; facility i is constructed at the beginning of stage i . Thus, facilities $j = 1, \dots, i$ are usable in stage i . We assume that once a facility is located, the facility remains there; it cannot be replaced (Figure 9.4.1).

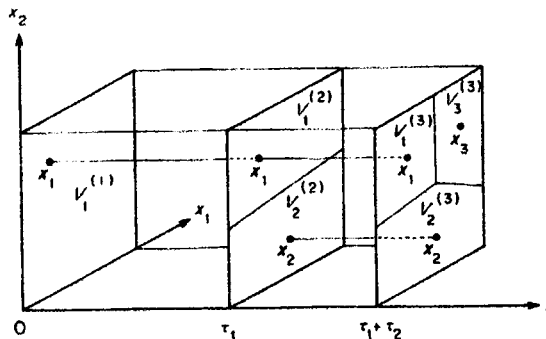


Figure 9.4.1 Locating facilities over many stages.

We further assume, as in Section 9.2, that every user uses the nearest facility with respect to the Euclidean distance. Let $\mathcal{V}^{(i)} = \{V_1^{(i)}, \dots, V_j^{(i)}\}$ be the Voronoi diagram generated by a set $\{x_1, \dots, x_i\}$ of points. Obviously, $\mathcal{V}^{(1)} = S$. In stage i , users in $V_j^{(i)}$ use facility j ; in stage $i+1$, users in $V_j^{(i+1)}$ use facility j (Figure 9.4.1). Let $f(\|x - x_j\|^2)$ be the travel cost function of the squared Euclidean distance, which is assumed to be strictly increasing and differentiable, and $\phi_i(x)$ be the density of users at x in stage i . We assume that $\phi_i(x)$ is constant in stage i (note that $\phi_i(x) \neq \phi_{i+1}(x)$ in general).

In the above terms, the travel cost averaged over region S and over n stages is written as

$$F(x_1, \dots, x_n) = \sum_{i=1}^n \tau_i \sum_{j=1}^i \int_{V_j^{(i)}} f(\|x - x_j\|^2) \phi_i(x) dx. \quad (9.4.1)$$

With this objective function, we formulate the above problem as the following mathematical programming problem.

Problem OPT9 (minimization of the average travel cost to the nearest points over many stages)

$$\min_{x_1, \dots, x_n} \left[\sum_{i=1}^n \tau_i \sum_{j=1}^i \int_{V_j^{(i)}} f(\|x - x_j\|^2) \phi_i(x) dx \right]. \quad (9.4.2)$$

In conjunction with this far-sighted locational optimization problem, it may be of interest to compare a near-sighted locational optimization problem. In the latter problem, we optimize the location of facility 1 in stage 1; in stage 2, provided that the location of facility 1 is fixed at x_1 obtained in stage 1, we optimize the location of facility 2; in stage 3, provided that locations of facilities 1 and 2 are fixed at x_1 and x_2 obtained in stages 1 and 2, we optimize the location of facility 3; ... ; in stage i , provided that the locations of the facilities $j = 1, \dots, i-1$ are fixed at x_1, \dots, x_{i-1} obtained in stages 1, ..., $i-1$, we optimize the location of facility i without considering the facilities $j = i+1, \dots, n$ to be located in the future. Mathematically, this optimization problem is written as

Problem OPT10 (myopic locational optimization problem)

$$\min_{x_i} \left[\sum_{j=1}^i \int_{V_j^{(0)}} f(\|x - x_j\|^2) \phi_i(x) dx \right], \quad (9.4.3)$$

where x_1, \dots, x_{i-1} are fixed and obtained from

$$\min_{x_{i-1}} \left[\sum_{j=1}^{i-1} \int_{V_j^{(0-1)}} f(\|x - x_j\|^2) \phi_i(x) dx \right], \quad (9.4.4)$$

for $k = 2, 3, \dots, i$, where, $V_j^{(0)} = S$.

The computational methods for Problems OPT9 and OPT10 are almost the same as that for Problem OPT3. Regarding Problem OPT10, the first derivative of the objective function in expression (9.4.3) is just the same as that of equation (9.2.11). Regarding Problem OPT9, the first derivative of equation (9.4.1) is given by

$$\frac{\partial F}{\partial x_{j\kappa}} = \sum_{i=j}^n \tau_i \int_{V_i^{(0)}} \frac{\partial}{\partial x_{j\kappa}} f(\|x - x_i\|^2) \phi_i(x) dx, \quad \kappa = 1, 2. \quad (9.4.5)$$

Each term in the summation is the same as equation (9.2.11). We can thus solve Problem OPT9 using the descent method with the derivatives obtained from equation (9.4.5). (Note that Voronoi diagrams $V^{(i)}$, $i = 1, \dots, n$, are efficiently obtained from the incremental method shown in Chapter 4.) Figure 9.4.2 shows the locally optimal locations of $n = 3, \dots, 8$ facilities obtained by T. Suzuki *et al.* (1991) for the uniform distribution over a unit square and $f(\|x - x_i\|^2) = \|x - x_i\|$. The filled circles in panel (a) show the locally optimal locations of Problem OPT9 for equal time intervals ($\tau_i = 1$, $i = 1,$

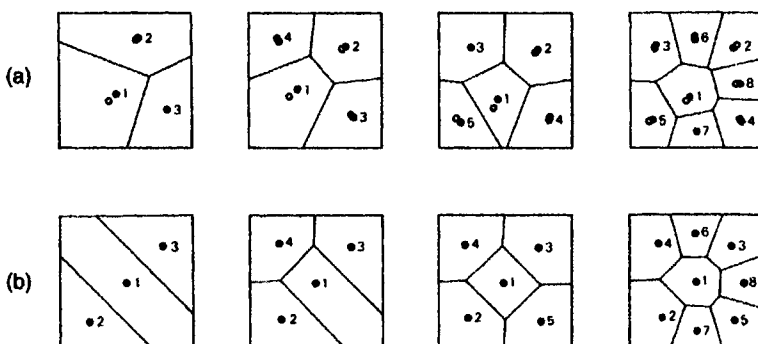


Figure 9.4.2 Locally optimal locations of $n = 1, \dots, 8$ firms in a unit square region with a uniform distribution and $f(\|x - x_i\|^2) = \|x - x_i\|$: (a) locally optimal locations for Problem OPT9 (optimized over time) $\tau_i = 1$ for filled circles and $\tau_i = i$ for unfilled circles; (b) locally optimal locations for Problem OPT10 (optimized at each time stage). (Source: T. Suzuki *et al.*, 1991, Figure 4.)

\dots, n), and the unfilled circles in the same panel show those for linearly increasing time intervals ($\tau_i = i$, $i = 1, \dots, n$). The numbers associated with the filled and unfilled circles indicate the time of construction. As is noticed from these circles, the difference appears quite small. Panel (b) shows the locally optimal locations of facilities under the myopic location policy. Compared with panel (a), the configurational difference is large for a small number of facilities, but it becomes small as the number of facilities increases. In fact, T. Suzuki *et al.* (1991) show that the difference in the average nearest neighbour distance over time is within only 3% for $n = 8$, implying that the myopic location policy is not as bad as expected for this case.

9.4.2 Periodic locational optimization

A few hundreds years ago, market places were open periodically. In Japan, we can find such traces in the names of places, for instance 3rd-Day-Market, 7th-Day-Market, etc. In a 3rd-Day-Market, the market opened on the 3rd, 13th, and 23rd of each month. Nowadays, there are few such old-style markets, but we still have such periodic services, for example a monthly mobile clinic visiting several places in a region. In this subsection we consider the locational optimization of facilities that open periodically.

Suppose that there are n market places, $i = 1, \dots, n$, in a region $S \subset \mathbb{R}^2$ and these market places are located at $x_1, \dots, x_n \in S$, respectively. Market place i is open at $t_i + jT$, $j = 0, 1, \dots$, where $t_1 < t_2 < \dots < t_n < T$ is assumed without loss of generality. A market opens for a certain length of time, but we assume that this time is very short compared with $t_i - t_{i-1}$. Under this assumption, market i located at x_i and open at t_i is represented by the point (x_i, t_i) in \mathbb{R}^3 . Let $t_i^*(t)$ be the length of time from time t to the nearest time when market i opens, i.e.

$$t_i^*(t) = \min_j \{t_i + jT \mid t_i + jT \geq t\}. \quad (9.4.6)$$

Suppose that at time t a consumer at a location x plans to go to a market. If the consumer chooses market place i , he/she has to wait for $t_i^*(t)$ days and walk $\|x - x_i\|$ km; if the consumer chooses market place k , he/she has to wait for $t_k^*(t)$ days and walk $\|x - x_k\|$ km. If the waiting time for market i is shorter than that for market k and the walking distance to market i is shorter than market k , the consumer's decision is simple; he/she decides to go to market i . If the former inequality holds, but the latter inequality does not hold (or vice versa), the consumer's decision becomes slightly complex; he/she makes a decision by trading off between waiting time and walking distance. To be explicit, let α be this trade-off rate, that is, the patience of waiting for one day is equivalent to that of walking α km, and

$$d((x, t), (x_i, t_i^*(t))) = \sqrt{\|x - x_i\|^2 + \alpha^2 (t - t_i^*(t))^2} \quad (9.4.7)$$

(recall that this distance is equivalent to the space-time distance defined in Chapter 3). If a consumer does not mind waiting, then $\alpha = 0$. If a consumer

dislikes waiting, α is very large. In terms of this distance, the above choice assumption is written as: a consumer at x who considers to go to a market at time t chooses the market which is the nearest with respect to the distance of equation (9.4.7), i.e. $\min_i [\sqrt{\|x - x_i\|^2 + \alpha^2(t - t_i^*(t))^2}]^{1/2}$.

With the distance of equation (9.4.7), we can define the Voronoi diagram $\{V_1, \dots, V_n\}$ generated by points (x_i, t_i) , $i \in I_n$, in the space given by $\{(x, t) | x \in S, 0 \leq t \leq T\}$. We can see the consumer's choice from this Voronoi diagram. If (x, t) is in the Voronoi polygon V_i , the market place at i is chosen. This Voronoi polygon can be depicted on a plane if S is given by a line segment. In this case the Voronoi diagram becomes the space-time Voronoi diagram on a cylinder (Chapter 3), which is extendable on a plane (Figure 9.4.3(a)).

The optimization problem is to place n market places so that the average space-time distance to the nearest market places is minimized. Mathematically, this problem is written as follows.

Problem OPT11 (minimization of the average space-time distance to the nearest points)

$$\min_{x_1, \dots, x_n} \sum_{i=1}^n \int_{V_i} \sqrt{\|x - x_i\|^2 + \alpha^2(t - t_i^*(t))^2} \phi(x, t) dx dt. \quad (9.4.8)$$

The computational method for this problem is almost the same as that for Problem OPT3. Figure 9.4.3 shows a locally optimal solution in the simplest case in which two market places are placed in a unit line segment with $\phi(x, t) = 1$, $t_1 = 0.4$, $t_2 = 0.8$ and $\alpha = 1$ (Seoung, 1990). Obviously, the solution changes according to the value of α . When $\alpha = 0$ (implying that consumers do not mind waiting), the optimization problem in $\{(x, t) | x \in S, 0 \leq t \leq T\}$ reduces to the optimization problem in S (Problem OPT3). The solution is given by $x_1 = 0.25$ and $x_2 = 0.75$. When α is very large (implying that consumers do not mind walking to a market place), the solution is given by $x_1 = x_2 = 0.5$. As is shown in Figure 9.4.3(b), the locations of market places approach the centre as the value of α increases. Note that

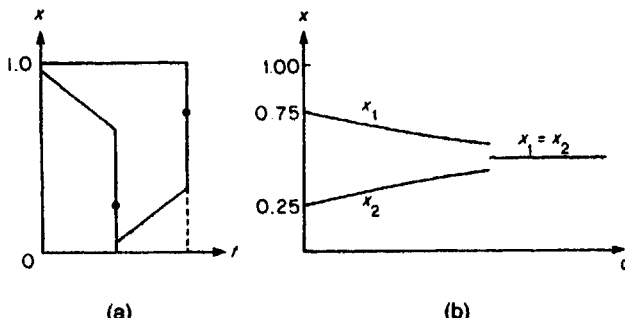


Figure 9.4.3 Local optimal locations of two market places ($n = 2$) for $\phi(x, t) = 1$, $t_1 = 0.5$, $t_2 = 1.0$: (a) $\alpha = 1$; (b) local optimal locations with respect to α .

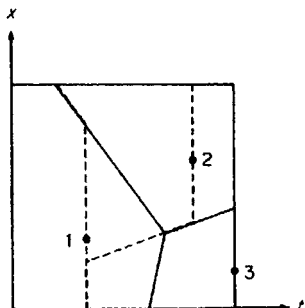


Figure 9.4.4 The difference between the space-time Voronoi diagram (dashed lines) and the ordinary Voronoi diagram (solid lines).

this change is not continuous; after α exceeds a certain value, both market places locate at the centre.

The case of a two-dimensional region S is studied by Takeda (1985) with a slightly different distance, i.e. equation (9.4.7) is replaced by

$$t_i^*(t) = \min_j \{ \| t_i + jT - t \| \mid j = 0, 1, \dots \}. \quad (9.4.9)$$

An example of the Voronoi diagram with this distance is depicted by the solid lines in Figure 9.4.4. In the same figure, the space-time Voronoi diagram is shown by the broken lines. The difference is, as is seen in Figure 9.4.4, distinct, and so their implications of time should be different. To consider a possible implication, suppose that a consumer wants to eat fresh fish on every Friday. If a fish market opens on every Friday, the consumer is happy. If a fish market opens on every Sunday, the consumer eats fish on Sunday, because he or she does not want to eat refrigerated fish. In this case, the consumer has to wait two days, and hence the degree of dissatisfaction may be measured as two days. If the market opens on every Thursday, the degree of dissatisfaction may be measured as one day. Under this understanding, the distance

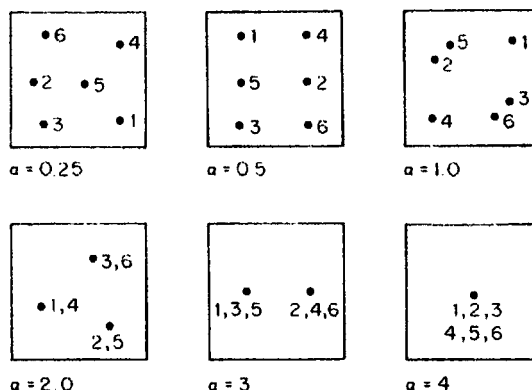


Figure 9.4.5 Locally optimal locations of six market places in a unit square with a uniform distribution. (Source: Takeda, 1985, Figure 4.5.)

of equation (9.4.9) may be regarded as the measure of dissatisfaction with respect to time.

Figure 9.4.5 shows the local optimal locations of six market places in a unit square obtained by Takeda (1985). The numbers associated with the filled circles indicate t_i . For $\alpha \leq 1$, market places open at six different places, but for $\alpha = 2.0, 3.0$ and 4.0 , they open at three, two and one place, respectively.

9.5 VORONOI FITTING AND ITS APPLICATION TO LOCATIONAL OPTIMIZATION PROBLEMS

In Chapter 7 we observed that the territories of mouthbreeder fish looked like a Voronoi diagram, and discussed how to measure the fitness of a polygonal tessellation to a Voronoi diagram. In this section we show another method in which we seek to find a Voronoi diagram that gives the ‘best’ fit to a given polygonal tessellation. We also show that this method is applicable to some locational optimization problems.

9.5.1 Method of fitting a Voronoi diagram to a polygonal tessellation

Let S_1, \dots, S_n be a finite number of closed polygons in $S \subset \mathbb{R}^2$ satisfying $[S_i \setminus \partial S_i] \cap [S_j \setminus \partial S_j] \neq \emptyset$ for $i \neq j$, $i, j \in I_n$ and $\bigcup_{i=1}^n S_i = S$. Then, $\mathcal{S} = \{S_1, \dots, S_n\}$ forms a tessellation of S (the dash-dot lines in Figure 9.5.1). Our objective is to fit a Voronoi diagram to the tessellation \mathcal{S} . To this end, we first choose an arbitrary point x_i in S_i and generate the Voronoi diagram $\mathcal{V} = \{V_1, \dots, V_n\}$ by the set $\{x_1, \dots, x_n\}$ of points (the solid lines in Figure 9.5.1). Since we are concerned with the Voronoi diagram in S , the Voronoi diagram should be bounded by S , i.e. $\{V_1 \cap S, \dots, V_n \cap S\}$, which is written, for notational simplicity, as $\{V_1, \dots, V_n\}$. In general, we can treat a non-convex S using the shortest-path Voronoi diagram (Section 3.4), but we assume, for simplicity, that S is convex.

The similarity between the Voronoi diagram \mathcal{V} and the tessellation \mathcal{S} may be measured in terms of the intersection area $\sum_{i=1}^n |S_i \cap V_i|$ (the shaded regions in Figure 9.5.1). Obviously, if this value is large (i.e. close to $|S|$), we can say that the tessellation \mathcal{S} is close to the Voronoi diagram \mathcal{V} . Mathematically, this intersection area is written as

$$F(x_1, \dots, x_n) = \sum_{i=1}^n \int_{V_i \cap S_i} dx. \quad (9.5.1)$$

This function may be slightly generalized as

$$F(x_1, \dots, x_n) = \sum_{i=1}^n \int_{V_i \cap S_i} \phi(x) dx, \quad (9.5.2)$$

where $\phi(x)$ indicates a weight (an explicit meaning will be given in Section 9.5.2). With this generalized objective function, the Voronoi fitting problem is formulated as follows.

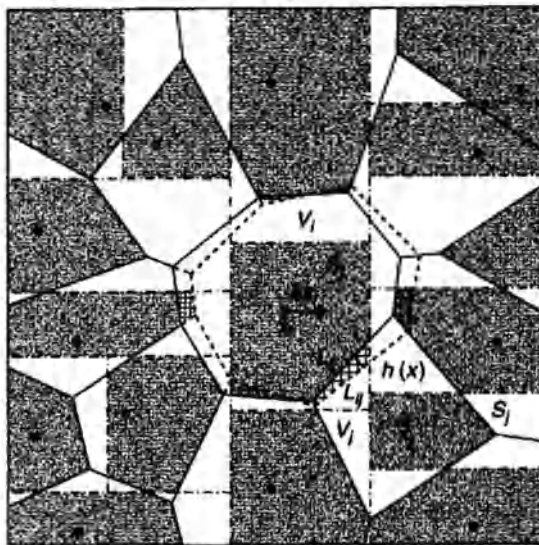


Figure 9.5.1 Change in $V_i \cap S_j$ produced by a slight move of x_i .

Problem OPT12 (maximization of the common area between a given tessellation and a Voronoi diagram)

$$\max_{x_1, \dots, x_n} \sum_{i=1}^n \int_{V_i \cap S_i} \phi(x) dx. \quad (9.5.3)$$

The computational method for this maximization problem is almost the same as that in expression (7.3.1) in Section 7.3. As is seen in Figure 9.5.1, a slight move, δx_i , of x_i produces the changes in $V_i \cap S_j$, $j \in J_i = \{j \mid V_i \cap S_j \neq \emptyset, j \in I_n\}$ (the shaded areas in Figure 9.5.1). To measure these changes, let V'_i be the Voronoi polygon of the point $x_i + \delta x_i$; $L_{ij} = (V_i \cap V_j) \cap S_i$ (the Voronoi edge shared with Voronoi polygons V_i and V_j included in S_i); $L'_{ij} = (V'_i \cap V_j) \cap S_i$; and $h(x)$ be the length of the perpendicular line segment from a point on L'_{ij} to the foot point, $x^T = (x_1, x_2)$, on L_{ij} (see Figure 9.5.1). After a few steps of calculation (Suzuki and Iri, 1986b), $h(x)$ is obtained as

$$h(x) = \frac{(x_{i1} - x_1) \delta x_{i1}}{\|x_i - x_j\|} + \frac{(x_{i2} - x_2) \delta x_{i2}}{\|x_i - x_j\|}. \quad (9.5.4)$$

The change in the area of $V_i \cap S_j$ (the grid area in Figure 9.5.1) is obtained from the integral of $h(x)$ along the line L_{ij} . Thus, the first derivative of equation (9.5.2) is given by

$$\begin{aligned} \frac{\partial F}{\partial x_{ik}} &= \sum_{j \in J_i} \left\{ \int_{L_{ij}} h(x) \phi(x) dx - \int_{L_{ij}} h(x) \phi(x) dx \right\} \\ &= \sum_{j \in J_i} \left\{ \int_{L_{ij}} \frac{x_{ik} - x_k}{\|x_i - x_j\|} \phi(x) dx - \int_{L_{ij}} \frac{x_{ik} - x_k}{\|x_i - x_j\|} \phi(x) dx \right\}. \end{aligned} \quad (9.5.5)$$

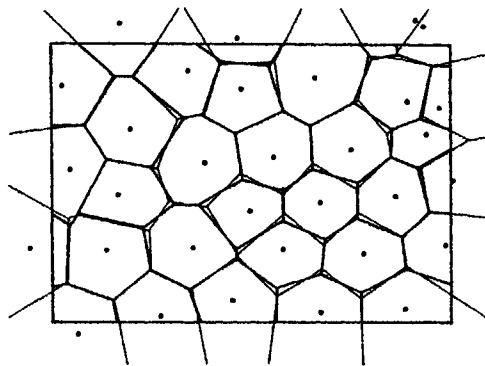


Figure 9.5.2 Fitting a Voronoi diagram to the territories of mouthbreeder fish. (Source: Suzuki and Iri, 1986a, Figure 13.)

Using the steepest descent method with this derivative, we can solve Problem OPT12. Figure 9.5.2 illustrates an actual application carried by Suzuki and Iri (1986b) who fit a Voronoi diagram (the heavy solid lines) to the territories of mouthbreeder fish studied by Barlow (1974) (followed by Hasegawa and Tanemura, 1976, and Honda, 1978). Suzuki and Iri (1986a) also fitted a Voronoi diagram to basaltic columnar jointing studied by Koch (1974), Stoyan and Stoyan (1980) and Stoyan and Hermann (1986). Judging from

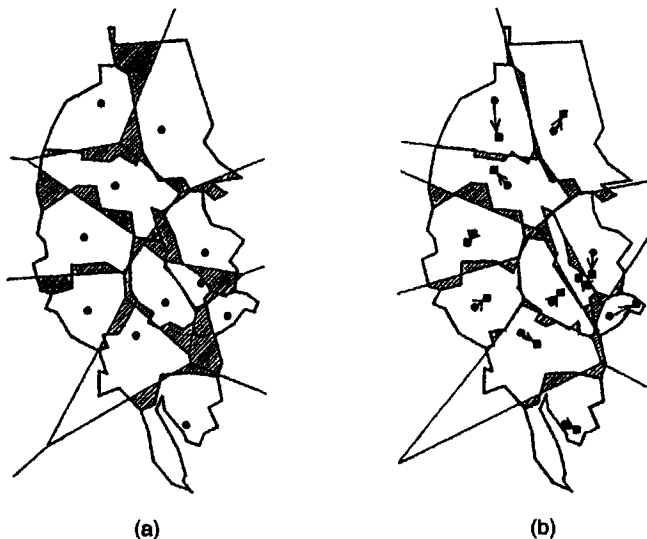


Figure 9.5.3 School districts in Tsukuba: (a) school districts and the present sites of schools (filled circles), the students in the shaded region cannot go to their nearest schools; (b) school sites (filled squares) that minimize the area in which students cannot go to their nearest schools. (Source: Suzuki and Iri, 1986a, Figure 14.)

their examination, the Voronoi diagrams appear to give a good fit to these phenomena.

9.5.2 Locational optimization for minimizing restricted areas

The method of fitting a Voronoi diagram to a given tessellation is also useful to solve the locational optimization of facilities whose use is spatially restricted. An example is the locational optimization of schools constrained by school districts. Figure 9.5.3(a) shows the districts of junior high schools in Tsukuba (the filled circles indicate the locations of the schools). In Japan, students in a school district are supposed to go to the school assigned to that district. As a result, students in some areas have to go to the school which is farther than the nearest school. If we assume that students can take the Euclidean path in Figure 9.5.3, the area in which students cannot go to their nearest schools is given by the hatched region in Figure 9.5.3(a), where the polygons are the Voronoi diagram generated by the school sites. The locational optimization problem is to relocate the schools so that the number of students who cannot go to their nearest schools is minimized. This minimization problem is equivalent to the maximization problem of expression (9.5.3), where $\phi(x)$ is given by the density of students. Figure 9.4.5 shows the locally optimal locations obtained by Suzuki and Iri (1986a). The area in which students cannot go to their nearest schools reduces from 20% to 10% by this relocation.

References

- Abellanas, M., G. Hernandez, R. Klein, V. Neumann-Lara and J. Urrutia (1995) Voronoi diagrams and containment of families of convex sets on the plane *Proceedings of the 11th ACM Conference on Computational Geometry, Vancouver, B.C., Canada*, 71–78. [3.7.2]
- Abellanas, M., G. Hernandez, R. Klein, V. Neumann-Lara and J. Urrutia (1997) A combinatorial property of convex sets *Discrete and Computational Geometry*, **17**(3), 307–318. [3.7.2]
- Abellanas, M., F. Hurtado and P.A. Ramos (1994) Redrawing a graph within a geometric tolerance *Graph Drawing DIMACS International Workshop, GD '94, Proceedings*, 246–253 [2.4]
- Aboav, D.A. (1970) The arrangement of grains in a polycrystal *Metallography*, **3**, 383–390. [5.5.3]
- Aboav, D.A. (1980) The arrangement of cells in a net *Metallography*, **13**, 43–58. [5.5.3]
- Aboav, D.A. (1987) Contiguous polygons in a random Voronoi tessellation – an approximate topological formula *Acta Stereologica*, **6**(3), 371–373. [5.5.3]
- Aboav, D.A. (1991) The stereology of the intergranular surface of a metal *Acta Stereology*, **10**(1), 43–54. [5.5.3]
- Aboav, D.A. (1992) The topology of a polycrystal in three dimensions *Materials Science Forum*, **94–96**, 275–280. [5.5.3]
- Abramowitz, M. and I.A. Stegun (eds) (1964) *Handbook of Mathematical Functions with Formulas, Graphs, and Mathematical Tables* New York: Dover. [9.2.1]
- Abseher, R., H. Schreiber and O. Steinhauser (1996) The influence of a protein on water dynamics in its vicinity investigated by molecular dynamics simulation *Proteins: Structure, Function, Genetics*, **25**, 366–378. [7.1]
- Adamatzky, A.I. (1993) Massively parallel algorithms for inverting Voronoi diagram *Neural Networks World*, **4**(3), 385–392. [2.3, 4.1]
- Adamatzky, A.I. (1994) Constructing a discrete generalized Voronoi diagram in reaction-diffusion media *Neural Networks World*, **4**(6), 635–644. [2.1]
- Adamatzky, A.I. (1996) Voronoi-like partition of lattice in cellular automata *Mathematical and Computer Modelling*, **23**(4), 51–66. [2.1]
- Agarwal, P.K., B. Aronov, J. O'Rourke and C. Chevon (1990a) Star unfolding of a polytope with applications. In: J.R. Gilbert and R. Karlsson (eds) *Lecture Notes in Computer Science*, **447** (Proceedings of the Second Scandinavian Workshop on Algorithm Theory) Berlin: Springer-Verlag, 251–263. [3.7.9]
- Agarwal, P.K., M.D. Berg and J. Matousek (1994) Constructing levels in arrangements and higher order Voronoi diagrams *Proceedings of the 10th Annual Symposium on Computational Geometry, June 6–8, 1994, Stony Brook, N.Y.*, 67–75. [3.2]
- Agarwal, P.K., H. Edelsbrunner, O. Schwarzkopf and E. Welzl (1990b) Euclidean minimum spanning trees and biochromatic closest pairs *Proceedings of the 6th ACM Symposium on Computational Geometry*, 203–210. [2.5]
- Agarwal, P.K., L. Guibas, J. Saxe and P.W. Shor (1989a) A linear-time algorithm for computing the Voronoi diagram of a convex polygon *Discrete and Computational Geometry*, **4**(6), 591–604. [2.4, 3.4.3, 3.4.4, 4.1, 4.7]
- Agarwal, P.K. and J. Matousek (1992) Relative neighbourhood graphs in three dimensions *Computational Geometry: Theory and Applications*, **2**, 1–14. [2.5]
- Agarwal, P.K., M. Sharir and P. Shor (1989b) Sharp upper and lower bounds on the length

- of general Davenport-Schinzel sequences *Journal of Combinatorial Theory, Series A*, **52**, 228–274. [3.9.1]
- Agrell, E. (1996) Voronoi regions for binary linear block-codes *IEEE Transactions on Information Theory*, **42**(1), 310–316. [7.1]
- Agrell, E. (1997) Voronoi-based coding *Chalmers University of Technology, School of Electrical and Computer Engineering, Technical Report*, 303. [Ack, 1.0, 7.1]
- Agrell, E. and T. Eriksson (1998) Optimization of lattices for quantization *IEEE Transactions on Information Theory*, **44**(5), 1814–1828. [7.1]
- Agrell, E. and P. Hedelin (1994) How to evaluate search methods for vector quantization *Proceedings of the Nordic Signal Processing Symposium, Ålesund, Norway, June 1994*, 258–263. [7.1]
- Aho, A.V., J.E. Hopcroft and J.D. Ullman (1974) *The Design and Analysis of Computer Algorithms* Reading: Addison-Wesley. [1.3.4, 4.2, 4.4, 4.5]
- Ahuja, N. (1982) Dot pattern processing using Voronoi neighbourhoods *IEEE Transactions on Pattern Analysis and Machine Intelligence*, **PAMI-4**(3), 336–343. [8.6]
- Ahuja, N., B. An and B. Schachter (1985) Image representation using Voronoi tessellation *Computer Vision, Graphics, and Image Processing*, **29**(3), 286–295. [5.3]
- Ahuja, N. and B.J. Schachter (1983) *Pattern Models* New York: John Wiley. [1.0, 6.1.1]
- Ahuja, N. and M. Tuceryan (1989) Extraction of early perceptual structure in dot patterns: integrating region, boundary and component Gestalt *Computer Vision, Graphics and Image Processing*, **48**, 304–356. [8.5, 8.6]
- Aichholzer, O. and F. Aurenhammer (1996) Straight skeletons for general polygonal figures in the plane *Lecture Notes in Computer Science*, **1090** (Proceedings of the Second Annual International Conference on Computing and Combinatorics COCOON '96) Berlin: Springer-Verlag, 117–126. [3.5.4]
- Akima, H. (1978) A method of bivariate interpolation and smooth surface fitting for irregularly distributed data points *ACM Transactions on Mathematical Software*, **4**(2), 148–159. [6.2, 6.3]
- Albers, G. and T. Roos (1992) Voronoi diagrams of moving points in higher dimensional spaces *Lecture Notes in Computer Science*, **621** (Proceedings of the Third Scandinavian Workshop on Algorithm Theory SWAT '92) Berlin: Springer-Verlag 399–409. [3.9.1]
- Allen, M.P., D. Frenkel, W. Gignac and J.P. McTague (1983) A Monte Carlo simulation study of the two-dimensional melting mechanism *Journal of Chemical Physics*, **78**(6), 4206–4222. [6.6, 7.1]
- Alonso, W. (1964) Location theory. In: J. Friedmann and A.W. Alonso (eds) *Regional Development and Planning: A Reader* Cambridge: Cambridge University Press. [7.3.1]
- Alt, H. and O. Schwarzkopf (1995) The Voronoi diagram of curved objects *Proceedings of the 11th Annual Symposium on Computational Geometry, June 5–12, Vancouver, B.C., Canada*, 89–97. [3.5.4]
- Amato, N.M. and E.A. Ramos (1996) On computing Voronoi diagrams by divide-prune-and-conquer *Proceedings of the Twelfth Annual Symposium on Computational Geometry, FCRC '96*, 166–175. [3.0, 3.1.4]
- An, B.H., N. Ahuja and B. Schachter (1983) Representation of images using Voronoi tessellation *Proceedings of the IEEE Computer Society Conference on Computer Vision and Pattern Recognition*, **2**, 188–189. [5.3]
- Anderson, D.M., H.T. Davis and L.E. Scriven (1989) Mean and Gaussian curvatures of randomly decorated Voronoi and cubic tesselations *Journal of Chemical Physics*, **91**(5), 3246–3251. [5.3]
- Andrade, P.N. and M.A. Fortes (1988) Distribution of cell volumes in a Voronoi partition *Philosophical Magazine B*, **58**(6), 671–674. [5.5.4]
- Anglada, M.V. (1997) An improved incremental algorithm for constructing restricted Delaunay triangulations *Computers and Graphics*, **21**(2), 215–223. [3.4.3]
- Anishchik, S.V. and N.N. Medvedev (1995) Three-dimensional Appollonian packing as a model for dense granular systems *Physical Review Letters*, **75**(23), 4314–4317. [3.5.5, 7.1]
- Annic, C., J.P. Troadec, A. Gervois, J. Lemaître, M. Ammi and L. Oger (1994) Experimental study of radical tessellations of assemblies of disks with size distribution *Journal de Physique I*, **4**(1), 115–125. [7.1]

- Aoyagi, M. and A. Okabe (1993) Spatial competition of firms in a bounded two-dimensional market *Regional Science and Urban Economics*, **23**, 259–289. [7.3.1]
- Aonuma, H., H. Imai, K. Imai and T. Tokuyama (1990) Maximin locations of convex objects in a polygon and related dynamic Voronoi diagrams *Computational Geometry, Proceedings of the Sixth Annual Symposium*, 225–234. [3.7.2]
- Aparicio, N.D. and A.C.F. Cocks (1995) On the representation of random packings of spheres for sintering simulations *Acta Metallurgica et Materialia*, **43**(10), 3873–3884. [1.2, 7.1]
- Arcelli, C. and G.S. Baja (1993) Euclidean skeleton via centre-of-maximal-disc extraction *Image and Vision Computing*, **11**(3), 163–173. [3.5.4]
- Archambault, S. and M. Moore (1995) Statistical inference for Voronoi images *Canadian Journal of Statistics*, **23**(1), 11–20. [5.3]
- Armstrong, R.A. (1974) Dynamics of expanding inhibitory fields *Science*, **183**, 444–445. [5.8]
- Arnold, D.B. and W.J. Milne (1984) The use of Voronoi tessellations in processing soil survey results *IEEE Computer Graphics and Applications*, **4**, 22–28. [6.1.1]
- Aronov, B. (1987) On the geodesic Voronoi diagram of point sites in a simple polygon *Proceedings of the ACM Symposium on Computational Geometry, Waterloo, Ontario*, 39–49. [4.8]
- Aronov, B. (1989) On the geodesic Voronoi diagram of point sites in a simple polygon *Algorithmica*, **4**(1), 109–140. [3.4.1, 3.4.4, 4.8]
- Aronov, B., S. Fortune and G. Wildfang (1993) The furthest-site geodesic Voronoi diagram *Discrete and Computational Geometry*, **9**(3), 217–255. [3.4.1]
- Aronov, B. and J. O'Rourke (1992) Nonoverlap of the star unfolding *Discrete and Computational Geometry*, **8**(3), 219–250. [3.7.9, 4.8]
- Aronov, B. and M. Sharir (1994) On translational motion planning in 3-space *Proceedings of the 10th Annual Conference on Computational Geometry, June 6–8, 1994, Stony Brook, N.Y.*, 21–30. [3.6.2]
- Arzt, E. (1982) The influence of an increasing particle coordination on the densification of spherical powders *Acta Metallurgica*, **30**, 1883–1890. [7.1]
- Asami, Y. (1991) A note on the derivation of the first and second derivatives of objective functions on geographical optimization *Journal of the Faculty of Engineering, University of Tokyo*, **XLI**, 1–13. [9.2.1]
- Asano, T. and T. Asano (1987) Voronoi diagram for points in a simple polygon. In: D.S. Johnson, T. Nishizeki, A. Nozaki and H.S. Wilf (eds) *Discrete Algorithms and Complexity, Perspectives in Computing*, **15** New York: Academic Press. [3.4.1, 3.4.4, 4.8]
- Asano, T., T. Asano, L. Guibas, J. Herschberger and H. Imai (1986) Visibility of disjoint polygons *Algorithmica*, **1**, 49–63. [3.4.1]
- Asano, T. and G. Toussaint (1987) Computing the geodesic center of a simple polygon. In: W. Rheinboldt and D. Siewiorek (eds) *Perspectives in Computing: Discrete Algorithms and Complexity, Proceedings of the Japan-US Joint Seminar, June 4–6, 1986, Kyoto, Japan* Boston: Academic Press Inc., 65–79. [3.4.1, 3.4.5]
- Ash, P.F. and E.D. Bolker (1985) Recognizing Dirichlet tessellations *Geometriae Dedicata*, **19**, 175–206. [2.3, 2.6, 3.7.6, 4.8]
- Ash, P.F. and E.D. Bolker (1986) Generalized Dirichlet tessellations *Geometriae Dedicata*, **20**, 209–243. [3.1.1, 3.1.2, 3.1.5, 4.8]
- Atallah, M.J. (1983) Dynamic computational geometry (preliminary version) *IEEE 24th Symposium on Foundations of Computer Science*, 92–99. [3.9.1]
- Augenbaum, J.M. (1984) A Lagrangian method for the shallow water equations based on a Voronoi mesh – one dimensional results *Journal of Computational Physics*, **53**, 240–265. [3.7.11]
- Augenbaum, J.M. (1985) A Lagrangian method for the shallow water equations based on a Voronoi mesh-flows on a rotating sphere *Lecture Notes in Physics*, **238**, (Proceedings of the First International Conference on Free-Lagrange Methods) Berlin: Springer-Verlag, 54–86. [3.7.11]
- Augenbaum, J.M. and C.S. Peskin (1985) On the construction of the Voronoi mesh on a sphere *Journal of Computational Physics*, **59**, 177–192. [3.7.6, 3.7.11, 4.8]
- Aurenhammer, F. (1987a) Power diagrams: properties, algorithms and applications *SIAM Journal of Computing*, **16**, 78–96. [3.1.6, 3.2.1, 4.8]

- Aurenhammer, F. (1987b) Recognizing polytopial cell complexes and constructing projection polyhedra. *Journal of Symbolic Computation*, **3**, 249–255. [2.6.1]
- Aurenhammer, F. (1988a) Voronoi diagrams – a survey. *Institute for Information Processing, Technical University of Graz, Report*, **263**. [1.0, 3.1.2, 3.1.4, 3.1.5, 3.4.2, 3.5.3, 3.7.4]
- Aurenhammer, F. (1988b) Improved algorithms for discs and balls using power diagrams. *Journal of Algorithms*, **9**, 151–161. [3.5.3, 4.8]
- Aurenhammer, F. (1990a) Voronoi diagrams – a survey of a fundamental data structure. *Free University of Berlin, Department of Mathematics, Technical Report*, **B-90-09**. [1.0]
- Aurenhammer, F. (1990b) A new duality result concerning Voronoi diagrams. *Discrete and Computational Geometry*, **5**, 243–254. [3.2, 3.2.1, 4.8]
- Aurenhammer, F. (1991) Voronoi diagrams – a survey of a fundamental data structure. *ACM Computing Surveys*, **23**(3), 345–405. [1.0, 3.0, 3.1.4, 3.4.2, 3.5.4]
- Aurenhammer, F. and H. Edelsbrunner (1984) An optimal algorithm for constructing the weighted Voronoi diagram in the plane. *Pattern Recognition*, **17**, 251–257. [3.1.1, 4.1, 4.7, 4.8]
- Aurenhammer, F. and O. Schwarzkopf (1991) A simple on-line randomized incremental algorithm for computing higher order Voronoi diagrams. *Proceedings of the Seventh Annual ACM Symposium on Computational Geometry*, 142–151. [3.2, 4.8]
- Avis, D. and B.K. Bhattacharya (1983) Algorithms for computing d -dimensional Voronoi diagrams and their duals. *Advances in Computing Research*, **1**, 159–180. [2.2, 4.7]
- Avrami, M. (1939) Kinetics of phase change: general theory. *Journal of Chemical Physics*, **7**, 1103–1112. [5.8, 7.2]
- Avrami, M. (1940) Kinetics of phase change II. *Journal of Chemical Physics*, **8**, 212–224. [5.8]
- Avrami, M. (1941) Kinetics of phase change III. *Journal of Chemical Physics*, **9**, 177–184. [5.8]
- Avrami, F. and D. Bertsimas (1993) On central limit theorems in geometrical probability. *The Annals of Applied Probability*, **3**(4), 1033–1046. [5.5.4]
- Baake, M., P. Kramer, M. Schlottmann and D. Ziedler (1990) Planar patterns with fivefold symmetry as sections of periodic structures in 4-space. *International Journal of Modern Physics B*, **4**(15/16), 2217–2268. [7.1]
- Babuska, I. and A.K. Aziz (1976) On the angle condition in the finite element method. *SIAM Journal on Numerical Analysis*, **13**, 214–226. [6.2]
- Babuska, I., J.E. Flaherty, W.D. Henshaw, J.E. Hopcroft, J.E. Oliker and T. Tezduyar (eds) (1995) *Modeling, Mesh Generation, and Adaptive Numerical Methods for Partial Differential Equations. The IMA Volumes in Mathematics and Its Applications*, **75**. New York: Springer-Verlag. [6.5, 6.5.2]
- Baddeley, A. and J. Møller (1989) Nearest-neighbor Markov point processes and random sets. *International Statistical Review*, **57**(2), 89–121. [8.7]
- Bajaj, C.L. and W.J. Bouma (1990) Dynamic Voronoi diagrams and Delaunay triangulations. *Abstracts of the Second Canadian Conference on Computational Geometry, Ottawa, August 1990*, 273–277. [4.1]
- Baker, B.S., E. Grosse and C.S. Rafferty (1988) Nonobtuse triangulation of polygons. *Discrete and Computational Geometry*, **3**, 147–168. [6.5.1]
- Baker, T. (1989) Automatic mesh generation for complex 3-dimensional regions using a constrained Delaunay triangulation. *Engineering with Computers*, **5**(3–4), 161–175. [6.5.2]
- Baker, T. (1992) Tetrahedral mesh generation by a constrained Delaunay triangulation. In: E.N. Houstis and J.R. Rice (eds) *Artificial Intelligence, Expert Systems and Symbolic Computing. Selected and Revised Papers from the IMACS 13th World Congress*. Amsterdam: Elsevier Science Publishers, B.V. 223–234. [3.4.3, 3.4.5, 6.5]
- Ball, G.J. (1996) A free-Lagrangian method for unsteady compressible flow: simulation of a confined cylindrical blast wave. *Shock Waves*, **5**, 311–325. [6.5]
- Ballard, D.H. and C.M. Brown (1982) *Computer Vision*. Englewood Cliffs, N.J.: Prentice-Hall. [4.2]
- Banerji, A. and H.B. Fisher (1974) Hierarchical location analysis for integrated area planning in rural India. *Papers of the Regional Science Association*, **33**, 177–194. [9.2.4]

- Baranovskii, E.P. (1991) Tilings of Euclidean spaces with L-polytopes of some perfect lattices *Trudy Matematicheskogo Instituta imeni V.A. Steklova*, **196**, 27–46. [7.1]
- Baranyai, A. and I. Ruff (1986) Statistical geometry of molten alkali halides *Journal of Chemical Physics*, **85**(1), 365–373. [1.2, 7.1]
- Barker, J.A., M.A. Hoare and J.L. Finney (1975) Relaxation of the Bernal model *Nature*, **257**, 120–122. [7.1]
- Barlow, G.W. (1974) Hexagonal territories *Animal Behaviour*, **22**, 876–878. [7.2, 7.3.2, 9.5.1]
- Barnhill, R.E. (1977) Representation and approximation of surfaces. In: J.R. Rice (ed) *Mathematical Software III* New York: Academic Press, 69–120. [6.0, 6.2]
- Bartkowiak, M. and G.D. Mahan (1995) Nonlinear currents in Voronoi networks *Physical Review B: Condensed Matter*, **51**(6), 10825–10832. [2.1, 5.12]
- Bartkowiak, M., G.D. Mahan, F.A. Modine and M.A. Alim (1996a) Influence of ohmic grain boundaries in ZnO varistors *Journal of Applied Physics*, **79**(1), 273–281. [5.3]
- Bartkowiak, M., G.D. Mahan, F.A. Modine and M.A. Alim (1996b) Multiple-peaked structure in the nonlinearity coefficient of ZnO varistors *Japanese Journal of Applied Physics – Letters*, **35**, L414–L417. [5.3]
- Bartkowiak, M., G.D. Mahan, F.A. Modine, M.A. Alini, R. Lauf and A. McMillan (1996c) Voronoi network model of ZnO varistors with different types of grain boundaries *Journal of Applied Physics*, **80**(11), 6516–6522. [5.3]
- Bartle, R. G. (1964) *The Elements of Real Analysis* New York: John Wiley. [1.3]
- Bartlett, M.S. (1975) *The Statistical Analysis of Spatial Pattern* London: Chapman and Hall. [1.3.3, 8.3]
- Bartlett, V. (1976) The ordering of multivariate data (with discussion) *Journal of the Royal Statistical Society, Series A*, **139**, 318–354. [6.6]
- Bass, L.J. and S.R. Schubert (1967) On finding the disc of minimum radius containing a given set of points *Mathematics of Computation*, **21**, 712–714. [3.3.1]
- Batra, S. and K. Rakusan (1991) Capillarization of the hypertrophic heart: discrepancy of the results obtained by the triangulation and domain methods *Journal of Cardiovascular Pharmacology*, **17** (Supplement 2), S151–S153. [7.1]
- Battista, G.D. and L. Vismara (1993) Angles of planar triangular graphs *Proceedings of the 25th Annual Symposium on Theory of Computing*, 431–437. [2.6, 6.5]
- Baumgart, B. (1975) A polyhedron representation for computer vision *IFIPS Conference Proceedings*, **44**, 589–596. [4.2]
- Beasley, J.E. and F. Goffinet (1994) A Delaunay triangulation based heuristic for the Euclidean Steiner problem *Networks*, **24**, 215–224. [2.5]
- Beckmann, M. (1971) Market share, distances, and potential *Regional Science and Urban Economics*, **1**, 1–18. [3.1.6]
- Bellagamba, V., R. Ercoli, A. Gamba and M. Simonetta (1985) An introduction to the use of Voronoi polyhedra in the study of organic reactions in solution *Theochem (Netherlands)*, **24**(3–4), 383–389. [7.1]
- Bellagamba, V., R. Ercoli, A. Gamba and M. Simonetta (1986) Theoretical investigation on the role of solvent in solvolytic reactions. Part 7. The enhancement of solvolysis of fluoromethane viewed by Voronoi polyhedra *Journal of the Chemical Society, Perkin Transactions*, **2**, 1127–1132. [7.1]
- Bengtsson, B-E. and S. Nordbeck (1964) Construction of isorhythms and isarithmic maps by computer *BIT*, **4**, 87–105. [6.2]
- Bennett, M.R. and J. Robinson (1990) Probabilistic secretion of quanta at the neuromuscular junction: non-uniformity, autoreceptors and the binomial hypothesis *Proceedings of the Royal Society of London, Series B*, **239**, 329–358. [5.8]
- Bentley, J.L. and H.A. Maurer (1979) A note on Euclidean near neighbor searching in the plane *Information Processing Letters*, **8**, 133–136. [3.2]
- Bentley, J.L., B.W. Weide and A.C. Yao (1980) Optimal expected-time algorithms for closest point problems *ACM Transactions on Mathematical Software*, **6**, 563–580. [2.3, 4.1]
- Bern, M., D. Dobkin and D. Eppstein (1995a) Triangulating polygons without large angles *International Journal of Computational Geometry and Applications*, **5**, 171–192. [6.5.1]
- Bern, M. and D. Eppstein (1991) Polynomial-size nonobtuse triangulation of polygons *Proceedings of the ACM Symposium on Computational Geometry*, 342–350. [6.5.1]

- Bern, M. and D. Eppstein (1992a) Polynomial-size nonobtuse triangulation of polygons *International Journal of Computational Geometry and Applications*, **2**(3), 241–255. [6.5.1]
- Bern, M. and D. Eppstein (1992b) Mesh generation and optimal triangulation. In: F.K. Hwang and D-Z. Du (eds) *Computing in Euclidean Geometry* Singapore: World Scientific. [6.5, 6.5.2]
- Bern, M., D. Eppstein and J.R. Gilbert (1990) Provably good mesh generation *Proceedings of the 31st IEEE Symposium on Foundations of Computer Science*, 231–241. [2.4, 6.5.1]
- Bern, M., D. Eppstein and F. Yao (1991) The expected extremes in a Delaunay triangulation *International Journal of Computational Geometry and Applications*, **1**(1) 79–91. [2.4]
- Bern, M., S. Mitchell and J. Ruppert (1995b) Linear-size nonobtuse triangulation of polygons *Discrete and Computational Geometry*, **14**(4), 411–428. [6.5.1]
- Bernal, J.D. (1937) An attempt at a molecular theory of liquid structure *Transactions of the Faraday Society*, **33**, 27–45. [7.1]
- Bernal, J.D. (1959) A geometrical approach to the structure of liquids *Nature*, **183**(4655), 141–147. [7.1]
- Bernal, J.D. (1964) The structure of liquids *Proceedings of the Royal Society, Series A*, **280**, 299–322. [7.1]
- Bernal, J.D. and J.L. Finney (1967) Random close-packed hard-sphere model II. Geometry of random packing of hard spheres *Discussions, Faraday Society*, **43**, 62–69. [7.1]
- Bernal, J.D. and S.V. King (1967) Random close-packed hard-sphere model I. Effect of introducing holes *Discussions, Faraday Society*, **43**, 60–62. [7.1]
- Bertin, E., R. Marcelpoil and J.M. Chassery (1992) Morphological algorithms based on Voronoi and Delaunay graphs: microscopic and medical applications *SPIE 1769 Image Algebra and Morphological Image Processing III*, 356–367. [8.1.1]
- Bertin, E., F. Parazza and J.M. Chassery (1993) Segmentation and measurement based on Voronoi diagram: application to confocal microscopy *Computerized Medical Imaging and Graphics*, **17**(3), 175–182. [2.2]
- Bertram, M. and H. Wendrock (1996) Characterization of planar local arrangement by means of the Delaunay neighbourhood *Journal of Microscopy*, **181**(1), 45–53. [8.1.1, 8.2]
- Besag, J. (1974) Spatial interaction and the statistical analysis of lattice systems (with discussion) *Journal of the Royal Statistical Society, Series B*, **36**, 192–236. [6.1.2]
- Besag, J. (1975) Statistical analysis of non-lattice data *The Statistician*, **24**, 179–196. [6.1.2]
- Bhattacharya, B.K. and G.T. Toussaint (1985) On geometric algorithms that use furthest-point Voronoi diagram. In: G.T. Toussaint (ed) *Computational Geometry* Amsterdam: North-Holland. 43–61. [3.4.1]
- Bhavsar, S.P. and N. Line (1988) Are the filaments real? *The Astrophysical Journal (Letters)*, **331**, L63–L68. [2.5]
- Billia, B., H. Jamgotchian and H. N. Thi (1991) Statistical analysis of the disorder of two-dimensional cellular arrays in directional solidification *Metallurgical Transactions A*, **22A**, 3041–3050. [2.5, 3.1.6]
- Bieshaar, R., A. Geiger and N.N. Medvedev (1995) Calculation of chemical potentials by a novel Delaunay-simplex sampling technique for particle insertion *Molecular Simulation*, **15**, 189–196. [7.1]
- Blackburn, C.G. and L. Dunckley (1996) The application of Voronoi tessellations in the development of 3D stochastic models to represent tumour growth *Zeitschrift für Angewandte Mathematik und Mechanik*, **76**(Supplement 3), 335–338. [5.12]
- Blackman, J.A. and P.A. Mulheran (1996) Scaling behavior in submonolayer film growth: a one-dimensional model *Physical Review B*, **54** (16), 11681–11692. [7.1]
- Bland, R.G. (1977) New finite pivoting rules for the simplex method *Mathematics of Operations Research*, **2**, 103–107. [4.6.2]
- Blatov, V.A. and V.N. Serezhkin (1997) Order and topology in systems with many particles *Acta Crystallographica Section A*, **53**(2), 144–160. [3.9.2, 7.1]
- Blatov, V.A., A.P. Shevchenko and V.N. Serezhkin (1995) Crystal space analysis by means of Voronoi-Dirichlet polyhedra *Acta Crystallographica Section A*, **51**(6), 909–916. [1.2, 7.1]

- Bleloch, G.E., G.L. Miller and D. Talmer (1996) Developing a practical projection-based parallel Delaunay algorithm *Proceedings of the 12th Annual Symposium on Computational Geometry*, 186–195. [4.1]
- Blum, H. (1967) A transformation for extracting new descriptors of shape. In: W. Wathen-Dunn (ed) *Symposium on Models for the Perception of Speech and Visual Form* Cambridge: M.I.T. Press, 362–380. [3.5.4, 3.5.5]
- Blum, H. (1973) Biological shape and visual science (Part I) *Journal of Theoretical Biology*, **38**, 205–287. [3.5.4, 3.5.5]
- Blum, H. and R.N. Nagel (1978) Shape description using weighted symmetric axis features *Pattern Recognition*, **10**, 167–180. [3.5.4, 3.5.5]
- Boiggs, S.W. (1951) Delimitation of seaward areas under national jurisdiction *American Journal of International Law*, **45**, 240–266. [3.6.2]
- Bogue, D.J. (1949) *The Structure of the Metropolitan Community: A Study of Dominance and Subdominance*. Ann Arbor: Horace M. Rackham School of Graduate Studies, University of Michigan. [1.2, 7.1]
- Bohm, J., M. Bohm and R.B. Meimann (1996) Voronoi polyhedra: a useful tool to determine the symmetry and Bravais class of crystal lattices *Crystal Research and Technology*, **31**(8), 1069–1075. [7.1]
- Boissonnat, J.-D. (1984) Geometric structures for three-dimensional shape representation *ACM Transactions on Graphics*, **3**(4), 266–286. [8.4.2]
- Boissonnat, J.D. (1988) Shape reconstruction from planar cross sections *Computer Vision, Graphics and Image Processing*, **44**, 1–29. [3.4.5, 6.5.1]
- Boissonnat, J.D., O. Devillers and M. Teillaud (1990) A dynamic construction of higher order Voronoi diagrams and its randomized analysis *Institut National de Recherche en Informatique et Automatique, Research Report*, 1207. [4.8]
- Boissonnat, J.D., O. Devillers and M. Teillaud (1993) A semidynamic construction of higher-order Voronoi diagrams and its randomized analysis *Algorithmica*, **9**, 329–356. [4.8]
- Boissonnat, J.D., O.D. Faugeras and E. Le Bras-Mehlman (1988) Representing stereo data with the Delaunay triangulation *Proceedings of the International Conference on Robotics and Automation*, 24–29. [3.4.3]
- Boissonnat, J.-D. and P. Kofakis (1985) Use of the Delaunay triangulation for the identification and the localization of objects *IEEE Conference on Computer Vision and Pattern Recognition*, 398–401. [3.5.4]
- Boissonnat, J.-D., M. Sharir, B. Tagansky and M. Yvinec (1995) Voronoi diagrams in higher dimensions under certain polyhedral distance functions *Proceedings of the Eleventh Annual Symposium on Computational Geometry, June 5–12, 1995, Vancouver, B.C., Canada*, 79–88. [3.7.1]
- Boissonnat, J.-D. and M. Teillaud (1986) A hierarchical representation of objects: the Delaunay tree *Proceedings of the Second Annual ACM Symposium on Computational Geometry*, 260–268. [6.6]
- Boissonnat, J.-D., and M. Yvinec (1995) *Géométrie Algorithmique* Paris: Edisciences International [in French]. Translated by H. Brönnimann (1988) *Algorithmic Geometry* Cambridge: Cambridge University Press; [3.7.10]
- Boots, B.N. (1973) Some models of the random subdivision of space *Geografiska Annaler*, **55B**, 34–48. [5.3, 5.8, 7.2]
- Boots, B.N. (1974) Delaunay triangles: an alternative approach to point pattern analysis *Proceedings Association of American Geographers*, **6**, 26–29. [1.2, 8.2]
- Boots, B.N. (1975a) Some observations on the structure of socioeconomic cellular networks *The Canadian Geographer*, **19**, 107–120. [5.3, 5.8, 7.2]
- Boots, B.N. (1975b) Patterns of urban settlements revisited. *The Professional Geographer*, **27**, 426–431. [8.2]
- Boots, B.N. (1977) Contact number properties in the study of cellular networks *Geographical Analysis*, **9**(4), 379–387. [5.12, 8.1.1]
- Boots, B.N. (1980) Weighting Thiessen polygons *Economic Geography*, **56**, 248–259. [3.1.6]
- Boots, B.N. (1982) The arrangement of cells in 'random' networks *Metallography*, **15**, 53–62. [5.12]
- Boots, B.N. (1984) Comments on 'Aboav's Rule' for the arrangement of cells in a network *Metallography*, **17**, 411–418. [5.12]

- Boots, B.N. (1986) Using angular properties of Delaunay triangles to evaluate point patterns *Geographical Analysis*, **18**(3), 250–260. [5.11, 8.2]
- Boots, B.N. (1987) Edge length properties of random Voronoi polygons *Metallography*, **20**, 231–236. [5.4, 5.5.2, 5.5.4]
- Boots, B. (1994) Visualizing spatial autocorrelation in point data *Geographical Systems*, **1**, 255–266. [3.1.6]
- Boots, B.N. and A. Getis (1988) *Point Pattern Analysis* Sage Scientific Geography Series, **8**. Newbury Park: Sage Publications Inc. [8.0]
- Boots, B.N. and D.J. Murdoch (1983) The spatial arrangement of random Voronoi polygons *Computers and Geosciences*, **9**, 351–365. [4.1, 5.4, 5.5.3, 8.1.1]
- Boots, B. and R. South (1997) Modelling retail trade areas using higher-order, multiplicatively weighted Voronoi diagrams *Journal of Retailing*, **73**(4), 519–536. [3.2.3]
- Borgers, C. (1990) Generalized Delaunay triangulations of non-convex domains *Computers and Mathematics with Applications*, **20**(7), 45–49. [4.8]
- Borouchaki, H. and P.L. George (1997) Aspects of 2-D Delaunay mesh generation *International Journal for Numerical Methods in Engineering*, **40**, 1957–1975. [6.5.1]
- Borouchaki, H. and S.H. Lo (1995) Fast Delaunay triangulation in three dimensions *Computer Methods in Applied Mechanics and Engineering*, **128**(1–2), 153–167. [2.2, 4.7]
- Boulu, L.G. and G.M. Crippen (1989) Voronoi binding site models: calculation of binding modes and influence of drug binding data accuracy *Journal of Computational Chemistry*, **10**, 673–682. [7.1]
- Boulu, L.G., G.M. Crippen, H.A. Barton, H. Kwon and M.A. Marletta (1990) Voronoi binding site model of a polycyclic aromatic hydrocarbon binding protein *Journal of Medicinal Chemistry*, **33**(2), 771–775. [7.1]
- Bowyer, A. (1981) Computing Dirichlet tessellations *The Computer Journal*, **24**, 162–166. [2.1, 2.2, 4.7]
- Boyle, P.J. and C.E. Dunn (1991) Redefinition of enumeration district centroids: a test of their accuracy using Thiessen polygons *Environment and Planning A*, **23**, 1111–1119. [7.1]
- Bradley, M.P. and G.M. Crippen (1993) Voronoi modeling: the binding of triazines and pyrimidines to *L. casei* dihydrofolate reductase *Journal of Medicinal Chemistry*, **36**(21), 3171–3177. [7.1]
- Brady, M. (1983) Criteria for representations of shape. In: J. Beck, B. Hope and A. Rosenfeld (eds) *Human and Machine Vision* New York: Academic Press, 39–84. [3.5.5]
- Brakke, K.A. (1986) Plane Voronoi tessellation second order statistics *Abstracts of the American Mathematical Society*, **7**(2), 235–236. [5.5.1]
- Brakke, K.A. (1987a) Statistics of random plane Voronoi tessellations *Technical Report*, Department of Mathematical Sciences, Susquehanna University, Selinsgrove. [5.5.1, 5.5.4]
- Brakke, K.A. (1987b) Statistics of three dimensional random Voronoi tessellations *Technical Report*, Department of Mathematical Sciences, Susquehanna University, Selinsgrove. [5.5.1, 5.5.4, 5.7]
- Bramble, J.H. and M. Zlamal (1970) Triangular elements in the finite element method *Mathematics of Computation*, **24**(112), 809–820. [6.2]
- Brandt, J.W. (1994) Convergence and continuity criteria for discrete approximations of the continuous planar skeleton *Computer Vision, Graphics Image Processing: Image Understanding*, **59**(1), 116–124. [3.5.4]
- Brandt, J.W. and V.R. Algazi (1991) Computing a stable, connected skeleton from discrete data *Proceedings 1991 IEEE Computer Society Conference on Computer Vision and Pattern Recognition*, 666–667. [3.5.4]
- Brandt, J. and V.R. Algazi (1992) Continuous skeleton computation by Voronoi diagram *Computer Vision, Graphics and Image Processing: Image Understanding*, **55**(3), 329–338. [3.5.4]
- Brassel, K.E. and D. Reif (1979) A procedure to generate Thiessen polygons *Geographical Analysis*, **11**, 289–303. [4.1]
- Brillouin, L. (1953) *Wave Propagation in Periodic Structures: Electric Filters and Crystal Lattices* (second edition) New York: Dover Publications. [3.2.3]

- Brockenbrough, J.R., W.H. Hunt Jr and O. Richmond (1992) A reinforced material model using actual microstructural geometry *Scripta Metallurgica et Materialia*, **27**, 385–390. [7.1]
- Brostow, W., J.-P. Dussault and B.L. Fox (1978) Construction of Voronoi polyhedra *Journal of Computational Physics*, **29**, 81–92. [4.7, 7.1]
- Brostow, W. and Y. Sicotte (1973) Some properties of the informational model of the liquid state *Journal of Statistical Physics*, **9**(4), 339–349. [7.1]
- Brostow, W. and Y. Sicotte (1975) Coordination number in liquid argon *Physica*, **80A**, 513–522. [7.1]
- Brown, G.S. (1965) Point density in stems per acre *New Zealand Forestry Service Research Notes*, **38**, 1–11. [1.2, 7.1, 8.5]
- Brown, J.L. (1991) Vertex based data dependent triangulations *Computer Aided Geometric Design*, **8**, 239–251. [6.4, 6.5]
- Brown, K.Q. (1979) Voronoi diagrams from convex hulls *Information Processing Letters*, **9**(5), 223–228. [2.4, 4.1, 4.7, 4.8]
- Brown, K.Q. (1980) Geometric Transforms for Fast Geometric Algorithms. Ph.D. Thesis, Report, CMU-CS-80-101, Carnegie-Mellon University, Pittsburgh, Pennsylvania. [2.4, 3.7.6, 4.1, 4.7, 4.8]
- Brown, T.C., B.W. Silverman and R.K. Milne (1981) A class of two-type point processes *Zeitschrift für Wahrscheinlichkeitstheorie und verwandte Gebiete*, **58**, 299–308. [8.7]
- Brumberger, H. and J. Goodman (1983) Voronoi cells: an interesting and potentially useful cell model for interpreting the small-angle scattering of catalysts *Journal of Applied Crystallography (Denmark)*, **16**, 83–88. [5.3]
- Bruzzone, E., M. Cazzanti, L. De Floriani and F. Mangili (1992) Applying two-dimensional Delaunay triangulation to stereo data interpolation *Lecture Notes in Computer Science*, **372** (Proceedings of the Second European Conference on Computer Vision – ECCV '92) Berlin: Springer-Verlag, 368–372. [3.4.5]
- Bruzzone, E., G. Garibotto and F. Mangili (1991) Three-dimensional surface reconstruction using Delaunay triangulation in the image plane *Visual Form*, **92**, 99–108. [3.4.5]
- Bryant, S. and M. Blunt (1992) Prediction of relative permeability in simple porous media *Physical Review A*, **46**, 2004–2011. [7.1]
- Buckley, C.E. (1988) A divide-and-conquer algorithm for computing 4-dimensional convex hulls *Lecture Notes in Computer Science*, **333** (International Workshop on Computational Geometry, Wurzburg, March 1988) Berlin: Springer-Verlag, 113–135. [4.1, 4.7, 4.8]
- Buckley, P.A. and F.G. Buckley (1977) Hexagonal packing of Royal Tern nests *The Auk*, **94**, 36–43. [5.3]
- Bulow-Olsen, A., N.R. Sackville Hamilton and M.J. Hutchings (1984) A study of growth form in genets of *Trifolium repens L.* as affected by intra- and interplant contacts *Oecologia (Berlin)*, **71**, 383–387. [7.1]
- Burge, M. and G. Monagan (1995a) Using the Voronoi tessellation for grouping words and multi-part symbols in documents. In: R.A. Melter, A.Y. Wu, F.L. Bookstein and W.D.K. Green (eds) *Proceedings of SPIE* 2573, 116–126. [3.6.2]
- Burge, M. and G. Monagan (1995b) Extracting words and multi-part symbols in graphics rich documents. In: C. Braccini, L. DeFloriani and G. Vernazza (eds) *Lecture Notes in Computer Science*, **974** (Proceedings of the 8th International Conference on Image Analysis and Processing ICIAP '95 San Remo, Italy, September 13–15, 1995) Berlin: Springer-Verlag, 533–538. [3.6.2]
- Burger, G., J.D. Embury and D.S. Wilkinson (1990) The characterization of microstructures using tessellations and their application to deformation processes. In: M.P. Anderson and A.D. Rollett (eds) *Simulation and Theory of Evolving Microstructures* Warrendale: The Minerals, Metals and Materials Society, 199–209. [7.1, 8.1.1, 8.2]
- Burger, G., E. Koken, D.S. Wilkinson and J.D. Embury (1988) The influence of spatial distribution on metallurgical processes. In: J.D. Embury and G.R. Purdy (eds) *Advances in Phase Transition* Oxford: Pergamon Press, 247–262. [5.12, 7.1, 7.2]
- Burnikel, C., K. Melhorn and S. Schirra (1994) How to compute the Voronoi diagram of

- line segments: theoretical and experimental results *Lecture Notes in Computer Science*, **855** (Proceedings of the Second Annual European Symposium on Algorithms ESA '94), Berlin: Springer-Verlag, 227–239. [3.5, 4.8]
- Burzlaff, H. and H. Zimmerman (1977) *Symmetrielehre* Stuttgart: Georg Thieme Verlag. [7.1]
- Busacker, R.G. and T.L. Saaty (1965) *Finite Graphs and Networks: An Introduction with Applications* New York: McGraw-Hill. [1.3]
- Bushnell-Wye, G., J.L. Finney and J.E. Quinn (1982) An annotated atlas of glass, crystal and interface Voronoi polyhedra. In: T. Masumoto and K. Suzuki (eds) *Proceedings of the Fourth International Conference on Rapidly Quenched Metals*, Sendai, Japan Sendai, Japan: The Japan Institute of Metals, 271–273. [7.1]
- Buyss, J., H.J. Messerschmidt and J.F. Botha (1991) Including known discontinuities directly into a triangular irregular mesh for automatic contouring purposes *Computers and Geosciences*, **17**(7), 875–881. [6.3]
- Byers, J.A. (1992) Dirichlet tessellation of Bark Beetle spatial attack points *Journal of Animal Ecology*, **61**(3), 759–768. [7.1, 8.1.1]
- Byers, J.A. (1996) Correct calculation of Dirichlet polygon areas *Journal of Animal Ecology*, **65**, 528–529. [7.1, 8.1.1]
- Calabi, L. and W.E. Hartnett (1968) Shape recognition, prairie fires, convex deficiencies, and skeletons *American Mathematical Monthly*, **75**, 335–342. [3.5.4, 3.5.5]
- Callen, J.S. and G.E. Stephan (1975) Siwai line-villages: Thiessen polygons and the size-density hypothesis *Field Museum of Natural History, Solomon Island Studies in Human Biogeography*, **4**. [7.1]
- Cannings, C. and L.M. Cruz Orive (1975) On the adjustment of the sex ratio and the gregarious behaviour of animal populations *Journal of Theoretical Biology*, **55**, 115–136. [7.4]
- Cannmo, P., K. Runesson and M. Ristinmaa (1995) Modelling of plasticity and damage in a polycrystalline microstructure *International Journal of Plasticity*, **11**(8), 949–970. [5.12]
- Canny, J. and B. Donald (1988) Simplified Voronoi diagram *Discrete and Computational Geometry*, **3**, 219–236. [3.7.11, 4.8]
- Cape, J.N., J.L. Finney and L.V. Woodcock (1981) An analysis of crystallization by homogeneous nucleation in a 4000-atom soft-sphere model *Journal of Chemical Physics*, **75**(5), 2366–2373. [7.1]
- Carlson, W.D. (1991) Competitive diffusion-controlled growth of porphyroblasts *Mineralogical Magazine*, **55**(380), 317–330. [5.8]
- Carter, G.M., J.M. Chaiken and E. Ignall (1972) Response areas for two emergency units *Operations Research*, **20**, 571–594. [3.7.1, 4.8]
- Cavendish, J.C. (1974) Automatic triangulation of arbitrary planar domains for the finite element method *International Journal for Numerical Methods in Engineering*, **8**, 679–696. [6.2]
- Cavendish, J.C., D.A. Field and W.H. Frey (1985) An approach to automatic three-dimensional finite element mesh generation *International Journal for Numerical Methods in Engineering*, **21**, 329–347. [6.5.2]
- Cendes, Z.J., D. Shenton and H. Shahnasser (1983) Magnetic field computation using Delaunay triangulation and complimentary finite element method *IEEE Transactions on Magnetics*, **MAG19**, 2551–2554. [6.5.1]
- Chakrabarti, A.K. and O.W. Archibald (1993) Patterns of diurnal variation of growing season precipitation on the Canadian Prairies: a harmonic analysis *The Canadian Geographer*, **37**(1), 16–28. [6.1.1]
- Chan, S.K. and K.M. Ng (1988) Geometrical characteristics of the pore space in a random packing of equal spheres *Powder Technology*, **54**, 147–155. [7.1]
- Chan, T.M., J. Snoeyink and C-K. Yap (1995) Output sensitive construction of polytopes in four dimensions and clipped Voronoi diagram *Proceedings of the 6th Annual ACM-SIAM Symposium on Discrete Algorithms*, 282–291. [3.1.4, 3.1.5]
- Chan, T.M., J. Snoeyink and C-K. Yap (1997) Primal dividing and dual pruning: output-sensitive construction of four-dimensional polytopes and three-dimensional Voronoi diagrams *Discrete and Computational Geometry*, **18**, 433–454. [4.7]

- Chand, D. R. and S. S. Kapur (1970) An algorithm for convex polytopes *Journal of the ACM*, **17**, 78–86. [4.7]
- Chang, M.S., N-F. Huang and C-Y. Tang (1990a) An optimal algorithm for constructing oriented Voronoi diagrams and geographic neighborhood graphs *Information Processing Letters*, **35**(5), 255–260. [3.7.10, 4.8]
- Chang, M.S., C.Y. Tang and R.C.T. Lee (1990b) 20-Relative neighborhood graphs are Hamiltonian *Proceedings of the International Symposium of SIGAL '90, August*, 53–65. [2.5]
- Chang, M., C. Tang and R. Lee (1992) Solving the Euclidean bottleneck matching problem by k -relative neighborhood graphs *Algorithmica*, **8**, 177–194. [2.5]
- Chang, R.C and R.C.T. Lee (1984) On the average length of Delaunay triangulations *BIT*, **24**, 269–273. [6.2]
- Chang, S-K. (1972) The generation of minimal trees with a Steiner topology *Journal of the Association for Computing Machinery*, **19**, 699–711. [9.3.3]
- Chapman, G.P. (1970) The application of information theory to the analysis of population distributions in space *Economic Geography*, **46**, 317–331. [8.1.2]
- Chassery, J. and M. Melkemi (1990) A segmentation method using Voronoi diagrams in a split and merge environment *Progress in Image Analysis and Processing, Proceedings of the 5th International Conference on Image Analysis and Processing, 1989, Positano, Italy* Singapore: World Scientific, 44–48. [3.5.5]
- Chazelle, B. (1983) The polygon containment problem *Advances in Computing Research*, **1**, 1–33. [3.7.2]
- Chazelle, B. (1985) How to search in history *Information and Control*, **64**, 77–99. [3.2.3, 3.3.3]
- Chazelle, B., R. Cole and F.P. Preparata (1986) New bounds for neighbor searching *Information and Control*, **68**, 105–124. [3.2, 4.8]
- Chazelle, B. and H. Edelsbrunner (1985). An improved algorithm for constructing k th order Voronoi diagrams *First ACM Symposium on Computational Geometry, Baltimore, June*, 228–234. [4.8]
- Chazelle, B. and H. Edelsbrunner (1987) An improved algorithm for constructing k th-order Voronoi diagrams *IEEE Transactions on Computers*, **11**(36), 1349–1354. [3.2, 4.8]
- Chazelle, B., H. Edelsbrunner, L.J. Guibas, J.E. Hershberger, R. Seidel and M. Sharir (1990) Slimming down by adding; selecting heavily covered points *Proceedings of the Sixth Annual Symposium on Computation Geometry, June 6–8, 1990, Berkeley*, 116–127. [2.4]
- Chazelle, B. and L.J. Guibas (1985) Visibility and intersection problems in plane geometry *Proceedings of the ACM Symposium on Computational Geometry, Baltimore*, 135–146. [3.4.1, 4.8]
- Chen, J. and Y. Han (1990) Shortest paths on a polyhedron *Proceedings of the Sixth Annual Symposium on Computational Geometry, June 6–8, 1990, Berkeley*, 360–369. [3.7.9]
- Chen, V. and M. Hlavacek (1994) Application of Voronoi tessellation for modeling randomly packed hollow-fiber bundles *A.I.Ch.E. Journal*, **40**(4), 606–612. [7.1]
- Chen, Z-T. and J.A. Guevara (1987) Systematic selection of very important points (VIP) from digital terrain model for constructing triangular irregular networks *Proceedings of Auto-Carto*, **8**, 50–56. [6.4]
- Cherifis, C. and F. Hermeline (1990) Diagonal swap procedures and characterizations of 2d-Delaunay triangulations *Mathematical Modelling and Numerical Analysis*, **24**(5), 613–625. [6.2]
- Cheriton, D. and R. E. Tarjan (1976) Finding minimum spanning trees *SIAM Journal on Computing*, **5**, 724–742. [2.5, 9.3.3]
- Chew, L.P. (1986) There is a planar graph almost as good as the complete graph *Proceedings of the Second ACM Symposium on Computational Geometry, Yorktown Heights, N.Y.*, 169–177. [3.4.3]
- Chew, L.P. (1987) Constrained Delaunay triangulations *Proceedings of the Third Annual Symposium on Computational Complexity*, 215–222. [3.4.3, 3.4.5, 4.8]
- Chew, L.P. (1989a) Guaranteed-quality triangular meshes *Technical Report, TR-89-983, Cornell University, Ithaca*. [3.4.3, 3.4.5, 6.5]

- Chew, L.P. (1989b) Constrained Delaunay triangulations *Algorithmica*, **4**, 97–108. [3.4.3, 3.4.5, 4.8]
- Chew, L.P. and R. Drysdale, III (1985) Voronoi diagrams based on convex distance functions *Proceedings of the ACM Symposium on Computational Geometry, Baltimore, June 1985*, 235–244. [3.7.2, 4.8]
- Chew, L.P. and S. Fortune (1997) Sorting helps for Voronoi diagrams *Algorithmica*, **18**(2), 217–228. [3.7.10, 3.7.11]
- Chew, L.P. and K. Kedem (1993) A convex polygon among polygonal obstacles: placement and high-clearance motion *Computational Geometry: Theory and Applications*, **3**, 59–89. [3.7.2]
- Chew, L.P., K. Kedem, M. Sharir, B. Tangansky and E. Welzl (1995) Voronoi diagrams of lines in 3-space under polyhedral convex distance functions *Proceedings of the 6th Annual ACM-SIAM Symposium on Discrete Algorithms*, 197–204. [3.5, 3.7.2]
- Chiu, S.N. (1994) Mean-value theorems for the neighbourhood of the typical cell of a random tessellation *Advances in Applied Probability*, **26**, 565–576. [5.5.3]
- Chiu, S.N. (1995a) A comment on Rivier's maximum entropy method of statistical crystallography *Journal of Physics A: Mathematical and General*, **28**, 607–615. [5.5.2, 5.5.3]
- Chiu, S.N. (1995b) Aboav-Weaire's and Lewis' laws – a review *Materials Characterization*, **34**, 149–165. [5.5.2, 5.5.3]
- Chiu, S.N. (1995c) Limit theorems for the time of completion of Johnson–Mehl tessellations *Advances in Applied Probability*, **27**, 889–910. [5.6.2, 5.8]
- Chiu, S.N. (1997) A central limit theorem for linear Kolmogorov's birth-growth models *Stochastic Processes and their Applications*, **66**, 97–106. [5.8]
- Chiu, S.N. and M.P. Quine (1997) Central limit theory for the number of seeds in a growth model in \mathbb{R}^d with inhomogeneous Poisson arrivals *The Annals of Applied Probability*, **7**(3), 802–814. [5.8]
- Chiu, S.N., M.P. Quine and M. Stewart (1999) Nonparametric and parametric estimation for a linear germination–growth model Preprint, Hong Kong Baptist University. [5.8]
- Chiu, S.N., R. van de Weygaert and D. Stoyan (1996) The sectional Poisson Voronoi tessellation is not a Voronoi tessellation *Advances in Applied Probability*, **28**, 356–376. [3.1.5, 5.1, 5.7]
- Choi, H-K., E. Bengtsson, T. Jarkrans, J. Vasko, K. Wester, P-U. Malmstrom and C. Busch (1995) Minimum spanning trees (MST) as a tool for describing tissue architecture when grading bladder carcinoma. In: C. Braccini, L. DeFloriani and G. Vernazza (eds) *Lecture Notes in Computer Science*, **974** (Proceedings of the 8th International Conference on Image Analysis and Processing ICIAP '95 San Remo, Italy, September 13–15, 1995) Berlin: Springer-Verlag, 613–620. [2.5]
- Choi, S-G. and C-M. Kyung (1991) A floorplanning algorithm using rectangular Voronoi diagram and force-directed block shaping 1991 *IEEE International Conference on Computer-Aided Design. Digest of Technical Papers*, 56–59. [3.7.1, 3.7.11]
- Cholera Inquiry Committee (1855) *Report on the Cholera Outbreak in the Parish of St. James, Westminster, During the Autumn of 1854* London: J. Churchill. [1.2, 3.8.4]
- Chothia, C. (1975) Structural invariants in protein folding *Nature*, **254**, 304–308. [7.1]
- Chou, J.J. (1995) Voronoi diagrams for planar shapes *IEEE Magazines: Computer Graphics and Applications*, **15**(2), 52–59. [3.5.4, 4.8]
- Christ, N.H., R. Friedberg and T.D. Lee (1982a) Random lattice field theory: general formulation *Nuclear Physics*, **B202**, 89–125. [1.2, 5.3, 5.11]
- Christ, N.H., R. Friedberg and T.D. Lee (1982b) Gauge theory on a random lattice *Nuclear Physics*, **B210**[FS6], 310–336. [5.3]
- Christ, N.H., R. Friedberg and T.D. Lee (1982c) Weights of links and plaquettes in a random lattice *Nuclear Physics*, **B210**, 337–346. [5.3]
- Christaller, W. (1933) *Die Zentralen Orte in Suddeutschland* Jena: Fisher. (Translated by C. Baskin, *The Central Places of Southern Germany* Englewood Cliffs: Prentice-Hall, 1966). [7.1, 9.2.4]
- Christensen, A.H.J. (1987) Fitting a triangulation to contour lines *Proceedings of Auto-Carto*, **8**, 57–67. [6.3]
- Christian, J.W. (1965) The theory of transformation in metals and alloys. In: R.W. Cahn (ed) *Physical Metallurgy* Amsterdam: North-Holland, 443–539. [5.8]

- Chynoweth, S. (1996) Generalised Voronoi/Delaunay duality, with applications *Zeitschrift für Angewandte Mathematik und Mechanik*, **76**(Supplement 3), 339–342. [2.4]
- Chynoweth, S. and M.J. Sewell (1990) Mesh duality and Legendre duality *Proceedings of the Royal Society of London, Series A*, **428**, 351–377. [2.4, 6.5]
- Cigoni, P., D. Laforenza, C. Montani, R. Perego and R. Scopigno (1995) Evaluation of parallelization strategies for an incremental Delaunay triangulation in E^3 *Currency: Practice and Experience*, **7**, 61–80. [2.2]
- Cimikowski, R.J. (1990) Finding Hamiltonian cycles in certain planar graphs *Information Processing Letters*, **35**, 249–254. [2.5]
- Clarkson, K.L. and P.W. Shor (1989) Applications of random sampling in computational geometry, II *Discrete and Computational Geometry*, **4**, 387–421. [3.3.1, 3.5]
- Cliff, A.D. and J.K. Ord (1981) *Spatial Processes: Models and Applications* London: Pion. [1.3.3, 8.0, 8.1.1]
- Cline, A.K. and R.J. Renka (1990) A constrained two-dimensional triangulation and the solution of closest node problems in the presence of barriers *SIAM Journal on Numerical Analysis*, **27**(5), 1305–1321. [3.4.3, 3.4.5, 4.8, 6.5.1]
- Cole, R., M. Goodrich and C. O'Dunlaing (1990) Merging free trees in parallel for efficient Voronoi diagram construction *Lecture Notes in Computer Science*, **443** (Proceedings of the 17th International Colloquium on Automata, Languages and Programming) Berlin: Springer-Verlag, 432–445. [4.1]
- Cole, R., M.T. Goodrich and C. O'Dunlaing (1996) A nearly optimal deterministic parallel Voronoi diagram algorithm *Algorithmica*, **16**, 569–617. [4.1]
- Coles, P. (1990) Understanding recent observations of the large-scale structure of the universe *Nature*, **346**, 446–447. [5.3]
- Coles, P. and J.D. Barrow (1980) Microwave background constraints on the Voronoi model of large-scale structure *Monthly Notices of the Royal Astronomical Society*, **244**, 557–562. [7.2]
- Collins, R. (1967) Statistical geometry and thermodynamics of liquids. In: P.S. Rudman, J. Stringer and R.J. Jaffee (eds) *Phase Stability in Metals and Alloys* New York: McGraw-Hill, 499–522. [7.1]
- Collins, R. (1968) A geometrical sum rule for two-dimensional fluid correlation functions *Journal of Physics C: Solid State Physics (London)*, **Series 2**, **1**, 1461–1471. [5.11, 7.1]
- Collins, R. (1972) Melting and statistical geometry of simple liquids. In: C. Domb and M.S. Green (eds) *Phase Transitions and Critical Phenomena* New York: Academic Press, 271–303. [7.1]
- Conway, J.H. and N.J.A. Sloane (1982) Voronoi regions of lattices, second moments of polytopes, and quantization *IEEE Transactions on Information Theory*, **28**(2), 211–226. [7.1]
- Conway, J.H. and N.J.A. Sloane (1983) A fast encoding method for lattice codes and quantizers *IEEE Transactions on Information Theory*, **IT-29**(6), 820–824. [7.1]
- Conway, J.H. and N.J.A. Sloane (1984) On the Voronoi regions of certain lattices *SIAM Journal on Algorithms and Discrete Mathematics*, **5**(3), 294–305. [7.1]
- Conway, J.H. and N.J.A. Sloane (1991) The cell structures of certain lattices. In: P. Hilton, F. Hirzebruch and R. Remmert (eds) *Miscellanea Mathematica* New York: Springer-Verlag, 71–107. [7.1]
- Conway, J.H. and N.J.A. Sloane (1992) Low-dimensional lattices. 6. Voronoi reduction of 3-dimensional lattices *Proceedings of the Royal Society of London, Series A*, **436**, 55–68. [1.2, 7.1]
- Conway, J.H. and N.J.A. Sloane (1993) *Sphere Packings, Lattices and Groups* (second edition) New York: Springer-Verlag. [6.1.1, 7.1, 8.3.1]
- Cormack, R.M. (1979) Spatial aspects of competition between individuals. In: R.M. Cormack and J.K. Ord (eds) *Spatial and Temporal Analysis in Ecology* Fairland: International Co-operative Publishing House, 151–212. [8.1.1]
- Correc, Y. and E. Chapuis (1987). Fast computation of Delaunay triangulations *Advances in Engineering Software*, **9**(2), 77–83. [4.1]
- Courant, R. and H. Robbins (1941) *What is Mathematics?* New York: Oxford University Press. [9.3.3]

- Cover, T.M. and P.E. Hart (1967) Nearest neighbor pattern classification *IEEE Transactions, Information Theory*, **IT-13**, 21–27. [3.2.3, 3.3.3]
- Cowan, R. (1978) The use of ergodic theorems in random geometry *Advances in Applied Probability*, **10**(Supplement), 47–57. [1.3.3, 5.0, 5.1]
- Cowan, R. (1980) Properties of ergodic random mosaic processes *Mathematische Nachrichten*, **97**, 89–102. [1.3.3, 5.0, 5.1]
- Cowan, R., S.N. Chiu and L. Holst (1995) A limit theorem for the replication time of a DNA molecule *Journal of Applied Probability*, **32**, 296–303. [5.8]
- Cox, B.N. and W.L. Morris (1988) Monte-Carlo simulations of the growth of small fatigue cracks *Engineering Fracture Mechanics*, **31**(4), 591–610. [3.7.11, 5.3]
- Cox, K.R. and J.A. Agnew (1974) Optimal and non-optimal territorial partitions: a possible approach toward conflict *Papers of the Peace Science Society (International)*, **23**, 123–138. [3.1.6]
- Cox, K.R. and J.A. Agnew (1976) The spatial correspondence of theoretical partitions *Discussion Paper*, Syracuse University, Department of Geography, **24**. [7.1]
- Crain, I.K. (1972) Monte-Carlo simulation of the random Voronoi polygons: preliminary results *Search*, **3**(6), 220–221. [5.4, 5.5.4]
- Crain, I.K. (1976) Statistical analysis of geotectonics. In: D.F. Merriam (ed) *Random Processes in Geology* New York: Springer-Verlag, 3–15. [5.3, 5.4]
- Crain, I.K. (1978) The Monte-Carlo generation of random polygons *Computers and Geosciences*, **4**, 131–141. [4.1, 5.4, 5.5.2, 5.5.4]
- Crain, I.K. and R.E. Miles (1976) Monte Carlo estimates of the distribution of the random polygons determined by random lines in a plane *Journal of Statistical Computation and Simulation*, **4**, 293–325. [1.3.3, 5.9]
- Crespo, D., T. Pradell, N. Clavaguera and M.T. Clavaguera-Mora (1997) Kinetic theory of microstructural evolution in nucleation and growth processes *Materials Science and Engineering A*, **238**, 160–165. [5.8]
- Cressie, N. (1991) *Statistics for Spatial Data* Chichester: John Wiley. [1.2, 1.3.3, 5.12, 8.0, 8.3]
- Crippen, G.M. (1984) Deduction of binding site structure from ligand binding data *Annals New York Academy of Sciences*, **439**, 1–11. [7.1]
- Crippen, G.M. (1987) Voronoi binding site models *Journal of Computational Chemistry*, **8**, 943–955. [7.1]
- Crippen, G.M. (1995) Intervals and the deduction of drug binding site models *Journal of Computational Chemistry*, **16**, 486–500. [7.1]
- Cromley, R.G. and D. Grogan (1985) A procedure for identifying and storing a Thiessen diagram within a convex boundary *Geographical Analysis*, **17**(2), 167–175. [4.1]
- Cruz Orive, L.-M. (1979) Distortion of certain Voronoi tessellations when one particle moves *Journal of Applied Probability*, **16**, 95–103. [7.3.1, 7.4]
- Cunliffe, B. (1971) Some aspects of hillforts and their cultural environments. In: D. Hill and M. Jesson (eds) *The Iron Age and its Hillforts* Southampton: Millbrook Press, 53–69. [7.1]
- Dacey, M.F. (1965) The geometry of central place theory *Geografiska Annaler*, **47B**, 111–124. [1.2, 7.1]
- Dahlberg, R.E. (1967) Towards the improvement of the dot map *Internationales Jahrbuch für Kartographie*, **7**, 157–166. [8.5]
- Dai, W.W.-M. (1991) Performance driven layout for thin-film multichip modules *International Journal of High Speed Electronics*, **2**, 287–317. [3.4.3, 3.4.5]
- Daley, D.J. and D. Vere-Jones (1988) *Introduction to the Theory of Point Processes* New York: Springer-Verlag. [1.3.3]
- Daniels, R.F., H.E. Burkhardt and T.R. Clason (1986) A comparison of competition measures for predicting growth of loblolly pine trees *Canadian Journal of Forest Research*, **16**, 1230–1237. [7.1]
- Darro, F., A. Kruczynski, C. Etievant, J. Martinez, J.-L. Pasteels and R. Kiss (1993) Characterization of the differentiation of human colorectal cancer cell lines by means of Voronoi diagrams *Cytometry*, **14**(7), 783–792. [7.1]
- Das, G. and D. Joseph (1989) Which triangulations approximate the complete graph? In:

- H. Djidjev (ed) *Lecture Notes in Computer Science: Optimal Algorithms*, 401 Berlin: Springer-Verlag, 168–192. [6.2]
- Datta, A. (1996) Computing minimum spanning circle by self-organization *Neurocomputing*, 13, 75–83. [3.3.1]
- Davenport, H. and A. Schinzel (1965) A combinatorial problem connected with differential equations *American Journal of Mathematics*, 87, 684–694. [3.9.1]
- David, C.W. (1984) Voronoi polyhedra and cleft recognition in aquated macromolecules *Computers and Chemistry*, 8(3), 225–226. [7.1]
- David, C.W. (1986) Voronoi polyhedra and the docking problem *Computers and Mathematics with Applications*, 12B(3/4), 763–766. [7.1]
- David, C.W. (1988a) Voronoi polyhedra as structure probes in large molecular systems – VII. Channel identification *Computers and Chemistry*, 12(3), 207–208. [8.6]
- David, C.W. (1988b) Voronoi polyhedra as structure probes in large molecular systems *Biopolymers*, 27, 339–344. [7.1]
- David, E.E. and C.W. David (1982a) Voronoi polyhedra and cluster recognition *Journal of Chemical Physics*, 77(6), 3288–3289. [7.1]
- David, E.E. and C.W. David (1982b) Voronoi polyhedra as a tool for studying solution structures *Journal of Chemical Physics*, 76(9), 4611–4614. [7.1]
- David, E.E. and C.W. David (1982c) Voronoi polyhedra and solvent structure for aqueous solutions (III) *Journal of Chemical Physics*, 77(12), 6251–6254. [7.1]
- David, E.E. and C.W. David (1983) Voronoi polyhedra for studying solvation structure (IV) *Journal of Chemical Physics*, 78(3), 1459–1464. [7.1]
- David, F. and J-M. Drouffe (1988) Monte-Carlo simulations of random rigid surfaces with random lattices *Nuclear Physics B (Proceedings Supplement)* 4, 83–87. [5.3]
- Davies, G.A. and D.J. Bell (1996) Voronoi tessellations to describe pattern structures in science and technology *Zeitschrift für Angewandte Mathematik und Mechanik*, 76(Supplement 3), 343–346. [1.2]
- Davy, P.J. and F.J. Guild (1988) The distribution of interparticle distance and its application in finite-element modelling of composite materials *Proceedings of the Royal Society, London Series A*, 418, 95–112. [5.12]
- Dearholt, D.W., N. Gonzales and G. Kurup (1988) Monotonic search networks for computer vision databases *Proceedings of the 22nd Asilomar Conference on Signals, Systems, and Computers*, 548–553. [2.5]
- de Berg, M., K. Dobrindt and O. Schwarzkopf (1995) On lazy randomized incremental construction *Discrete and Computational Geometry*, 14, 261–286. [4.1, 4.3]
- de Berg, M., M. van Kreveld, M. Overmars and O. Schwarzkopf (1997) *Computational Geometry: Algorithms and Applications* Berlin: Springer-Verlag. [1.0]
- De Floriani, L. (1989a) A pyramidal data structure for triangle-based surface description *IEEE Computer Graphics and Applications*, 9(2), 67–78. [6.4]
- De Floriani, L. (1989b) Two algorithms for radial ordering of Delaunay triangles *Abstracts of the First Canadian Conference on Computational Geometry, Montreal, Quebec*, 40. [6.6]
- De Floriani, L., B. Falcidieno, G. Nagay and C. Pienovi (1991) On sorting triangles in a Delaunay triangulation *Algorithmica*, 6, 522–532. [6.6]
- De Floriani, L., B. Falcidieno and C. Pienovi (1982) Triangulated irregular networks in geographical data processing. In: S. Rinaldi (ed) *Environmental Systems Analysis and Management* Amsterdam: North-Holland, 801–811. [6.2, 6.3]
- De Floriani, L., B. Falcidieno and C. Pienovi (1983) A Delaunay-based method for surface approximation. In: P.J.W. ten Hagen (ed) *Eurographics '83* Amsterdam: Elsevier Science Publishers B.V., 333–350. [6.2, 6.4]
- De Floriani, L., B. Falcidieno and C. Pienovi (1985) Delaunay-based representation of surfaces defined over arbitrarily shaped domains *Computer Vision, Graphics and Image Processing*, 32, 127–140. [6.2, 6.3, 6.4]
- De Floriani, L., P. Marzano and E. Puppo (1996) Multiresolution models for topographic surface description *The Visual Computer*, 12(7), 317–345. [3.4.3, 6.4]
- De Floriani, L., D. Mirra and E. Puppo (1993) Extracting contour lines from a hierarchical surface model *Computer Graphics Forum (EUROGRAPHICS '93 Conference Issue)*, 12(3), 249–260. [6.4]

- Dc Floriani, L. and E. Puppo (1988) Constrained Delaunay triangulation for multi-resolution surface description *Proceedings of the 9th International Conference on Pattern Recognition, 14–17 November 1988, Rome, Italy*, Vol. I Washington: IEEE Computer Society Press, 566–569. [3.4.3]
- De Floriani, L. and E. Puppo (1992a) A hierarchical triangle-based model for terrain description. In: A.U. Frank, I. Campari and U. Formentini (eds) *Lecture Notes in Computer Science: Theories and Methods of Spatio-Temporal Reasoning in Geographic Space*, 639 Berlin: Springer-Verlag, 236–251. [6.4]
- De Floriani, L. and E. Puppo (1992b) An on-line algorithm for constrained Delaunay triangulation *Computer Vision, Graphics and Image Processing*, 54, 290–300. [3.4.3]
- Dehne, F. (1982) An optimal algorithm to construct all Voronoi diagrams for k nearest neighbor searching in the Euclidean plane *Proceedings Twentieth Annual Allerton Conference on Communication, Control, and Computing*, 85–93. [3.2]
- Dehne, F. (1989) Computing digitized Voronoi diagrams on a systolic screen and applications to clustering. In: H. Djidjev (ed) *Optimal Algorithms, Lecture Notes in Computer Science*, 401 Berlin: Springer-Verlag, 14–24. [2.1]
- Dehne, F., A-L. Hassenklover, J-R. Sack and N. Santoro (1991) Computational geometry algorithms for the systolic screen *Algorithmica*, 6 (5), 724–761. [2.1, 3.5.1]
- Dehne, F. and R. Klein (1987) An optimal algorithm for computing the Voronoi diagram on a cone *Report, SCS-TR-122*, School of Computer Science, Carleton University, Ottawa, Canada. [3.7.8, 4.5, 4.8]
- Dehne, F. and R. Klein (1988) A sweepcircle algorithm for Voronoi diagrams. In: H. Gottler and H.J. Schneider (eds) *Lecture Notes in Computer Science: Graph Theoretic Concepts in Computer Science*, 314 (WG '87) Berlin: Springer-Verlag, 59–70. [4.5]
- Dehne, F. and R. Klein (1997) 'The Big Sweep': On the power of the wavefront approach to Voronoi diagrams *Algorithmica*, 17, 19–32. [3.5.4, 4.5]
- Delannay, R., G. Le Caér and M. Khatun (1992) Random cellular structures generated from a 2D Ising ferromagnet *Journal of Physics A: Mathematical and General*, 25, 6193–6210. [5.5.3]
- Delannay, R., G. Le Caér and A. Steir (1993) Topological correlations in 2D random cellular structures. In: A. Mohammad-Djafari and G. Demoments (eds) *Maximum Entropy and Bayesian Methods* Dordrecht: Kluwer, 357–362. [5.5.3]
- Delannay, R., N. Ito, M. Khatun and G. Le Caér (1994) Exact two-cell correlations in random cellular structures generated from a 2D Ising ferromagnet *Physica A*, 212, 1–11. [5.5.3]
- Delaunay, B. (1928) Sur la sphère vide *Proceedings of the International Mathematical Congress held in Toronto, August 11–16* Toronto: University of Toronto Press, 695–700. [1.2]
- Delaunay, B. (1929a) Sur la partition régulière de l'espace à 4 dimensions. Première partie *Bulletin de L'Academie des Sciences de L'URSS, Classe des Sciences Mathématiques et Naturelles*, 1, 79–110. [1.2]
- Delaunay, B. (1929b) Sur la partition régulière de l'espace à 4 dimensions. Deuxième partie *Bulletin de L'Academie des Sciences de L'URSS, Classe des Sciences Mathématiques et Naturelles*, 1, 147–164 [1.2]
- Delaunay, B. (1932) Neue Darstellung der geometrischen krystallographie *Zeitschrift für Krystallographie*, 84, 109–149. [1.2]
- Delaunay, B. (1934) Sur la sphère vide *Bulletin de L'Academie des Sciences de L'URSS, Classe des Sciences Mathématiques et Naturelles*, Series 7(6), 793–800. [1.2]
- Delone, B.N. (1961) Proof of the fundamental theorem in the theory of stereohedra *Soviet Mathematics*, 2, 812–815. [7.1]
- Delone, B.N., N.P. Dolbilin and M.I. Stogrin (1980) Combinatorial and metric theory of planigons *Proceedings of the Steklov Institute of Mathematics*, Issue 4, 111–141. [7.1]
- Deng, X. and B. Zhu (1996) A randomized algorithm for Voronoi diagram of line segments on coarse grained multiprocessors *Proceedings of the 10th International Parallel Processing Symposium IPPS '96*, 192–198. [3.5]
- Devereux, B.J., R.M. Fuller, L. Carter and R.J. Parsell (1990) Geometric correction of airborne scanner imagery by matching Delaunay triangles *International Journal of Remote Sensing*, 11(12), 2237–2251. [6.6]

- Devijver, P.A. and M. Dekesel (1982) Insert and delete algorithms for maintaining dynamic Delaunay triangulations *Pattern Recognition Letters*, **1**, 73–77. [4.1]
- Devijver, P.A. and M. Dekesel (1983) Computing multidimensional Delaunay tessellations *Pattern Recognition Letters*, **1**, 311–316. [4.7]
- Devillers, O. (1992) Randomization yields simple $O(n \log^* n)$ algorithms for difficult $\Omega(n)$ problems *International Journal of Computational Geometry and Applications*, **2**(1), 97–111. [3.5.4]
- Devillers, O. and M. Golin (1993) Dog bites postman: point location in the moving Voronoi diagram and related problems *Proceedings of the First Annual European Symposium on Algorithms – ESA '93*, 133–144. [3.9.2]
- Devillers, O., S. Meiser and M. Teillaud (1992) Fully dynamic Delaunay triangulation in logarithmic expected time per operation *Computational Geometry: Theory and Applications*, **2**(2), 55–80. [3.9.1, 4.1, 4.8]
- Devroye, L. (1988) The expected size of some graphs in computational geometry *Computers and Mathematics with Applications*, **15**, 53–64. [2.5]
- Dewdney, A.K. and J.K. Vranch (1977) A convex partition of \mathbb{R}^3 with applications to Crum's problem and Knuth's post-office problem *Utilitas Mathematica*, **12**, 193–199. [2.3]
- Dey, T. (1990) Good triangulations in planes *Proceedings of the Second Canadian Conference on Computational Geometry*, 102–106. [6.5]
- Dey, T.K. (1993) On counting triangulations in d dimensions *Computational Geometry: Theory and Applications*, **3** 315–325. [6.2]
- Dey, T.K., C.L. Bajaj and K. Sugihara (1991) On good triangulations in three dimensions *Proceedings of the ACM Symposium on Solid Modeling, Foundations and CAD/CAM Applications, June 5–7, 1991, Austin, Texas*, 431–441. [6.5.1, 6.5.2]
- Dey, T., C.L. Bajaj and K. Sugihara (1992a) On good triangulations in three dimensions *International Journal of Computational Geometry and Applications*, **2**, 75–95. [6.5.1, 6.5.2]
- Dey, T.K. and N.R. Shah (1995) On the number of simplicial complexes in \mathbb{R}^d *Proceedings of the Seventh Canadian Conference on Computational Geometry*, 31–36. [6.2]
- Dey, T.K., K. Sugihara and C.L. Bajaj (1992b) Delaunay triangulations in three dimensions with finite precision arithmetic *Computer Aided Geometric Design*, **9**, 457–470. [2.2]
- DiCenzo, S.B. and G.K. Wertheim (1989) Monte Carlo calculation of the size distribution of supported clusters *Physical Review B*, **39** (10), 6792–6796. [5.3, 5.4, 5.5.4]
- Dickerson, M.T. and R.L.S. Drysdale (1990) Fixed-radius near neighbors search algorithms for points and segments *Information Processing Letters*, **35**(5), 269–273. [2.3]
- Dickerson, M.T. and R.L.S. Drysdale (1991) Enumerating k distances for n points in the plane *Proceedings of the Seventh Annual ACM Symposium on Computational Geometry*, 234–238. [2.5]
- Dickerson, M.T., R.L.S. Drysdale and J.R. Sack (1992) Simple algorithms for enumerating interpoint distances and finding k nearest neighbors *International Journal of Computational Geometry and Applications (Singapore)*, **2**(3), 221–239. [2.3]
- Dickerson, M.T. and D. Eppstein (1996) Algorithms for proximity problems in higher dimensions *Computational Geometry: Theory and Applications*, **5**(5), 277–291. [2.3]
- Diggle, P.J. (1983) *Statistical Analysis of Spatial Point Patterns* New York: Academic Press. [1.3.3, 5.12, 8.0, 8.1.2, 8.3]
- Dijkstra, E. (1959) A note on two problems in connection with graphs *Numerische Mathematik*, **1**, 269–271. [3.4.1]
- Dillencourt, M.B. (1987a) A non-Hamiltonian, non-degenerate Delaunay triangulation *Information Processing Letters*, **25**(3), 149–151. [2.5, 8.4.2]
- Dillencourt, M.B. (1987b) Traveling salesman cycles are not always subgraphs of Delaunay triangulations or of minimum weight triangulations *Information Processing Letters*, **25**(5), 339–342. [8.4.2]
- Dillencourt, M.B. (1990a) Toughness and Delaunay triangulations *Discrete and Computational Geometry*, **5**, 573–601. [2.4, 2.6]
- Dillencourt, M.B. (1990b) Realizability of Delaunay triangulations *Information Processing Letters*, **33**(6), 283–287. [2.4, 2.6]

- Dillencourt, M.B. (1990c) Hamiltonian cycles in planar triangulations with no separating triangles *Journal of Graph Theory*, **14**(1), 31–40. [8.4.2]
- Dillencourt, M.B. (1996a) Finding Hamiltonian cycles in Delaunay triangulations is NP-complete *Discrete Applied Mathematics*, **64**(3), 207–217. [2.5, 8.4.2]
- Dillencourt, M.B. (1996b) Polyhedra of small order and their Hamiltonian properties *Journal of Combinatorial Theory, Series B*, **66** (1), 87–122. [8.4.2]
- Dirichlet, G.L. (1850) Über die Reduction der positiven quadratischen Formen mit drei unbestimmten ganzen Zahlen *Journal für die Reine und Angewandte Mathematik*, **40**, 209–227. [1.2]
- Djidjev, H. and A. Lingas (1991) On computing the Voronoi diagram for restricted planar figures *Lecture Notes in Computer Science*, **519** (Proceedings of the Second Workshop on Algorithms and Data Structures WADS '91), 54–64. [3.4.2]
- Djidjev, H.N. and A. Lingas (1995) On computing Voronoi diagrams for sorted point sets *International Journal of Computational Geometry and Applications*, **5**, 327–337. [4.1, 4.2]
- Dobkin, D.P., S.J. Friedman and K.J. Supowit (1990) Delaunay graphs are almost as good as complete graphs *Discrete and Computational Geometry*, **5**, 399–407. [2.4, 6.2]
- Dodge, C. (1972) *Euclidean Geometry and Transformation*, Reading: Addison-Wesley. [2.4]
- Dokmeci, V.F. (1973) An optimization model for a hierarchical spatial system *Journal of Regional Science*, **13**, 3, 439–451. [9.2.4]
- Dolan, J., R. Weiss and J. MacGregor Smith (1991) Minimal length tree networks on the unit sphere *Annals of Operations Research*, **33**(1–4), 503–535. [3.7.11]
- Doroshkevich, A.G., S. Gottlöber and S. Madsen (1997) The accuracy of parameters determined with the core-sampling method: application to Voronoi tessellations *Astronomy and Astrophysics Supplement Series*, **123**, 495–506. [5.3, 7.2]
- Drezner, Z. (ed) (1995) *Facility Location, A Survey of Application and Methods* New York: Springer-Verlag. [9.2]
- Drouffe, J.M. and C. Itzykson (1984) Random geometry and the statistics of two-dimensional cells *Nuclear Physics*, **B235**, 45–53. [5.3, 5.4, 5.5.2, 5.5.4, 5.11]
- Dryden, I.L., M.R. Faghihi and C.C. Taylor (1995) Investigating regularity in spatial point patterns using shape analysis. In: K.V. Mardia and C.A. Gill (eds) *Proceedings in Current Issues in Statistical Shape Analysis* Leeds: Leeds University Press, 40–48. [8.2]
- Dryden, I.L., M.R. Faghihi and C.C. Taylor (1997) Procrustes shape analysis of planar point sets *Journal of the Royal Statistical Society B*, **59**(2), 353–374. [7.1, 8.2]
- Drysdale, R.L. (1979) Generalized Voronoi Diagrams and Geometric Searching. Ph.D. Thesis, Department of Computer Science, Stanford University. [3.5]
- Drysdale, R.L. (1990) A practical algorithm for computing the Delaunay triangulation for complex distance functions *Proceedings of the First Annual ACM-SIAM Symposium on Discrete Algorithms*, 159–168. [4.8]
- Drysdale, R.L. and D-T. Lee (1978) Generalized Voronoi diagram in the plane *Proceedings of the 16th Annual Allerton Conference on Communications, Control and Computing*, 833–842. [3.0, 3.5, 4.1]
- Du, C. (1996) An algorithm for automatic Delaunay triangulation of arbitrary planar domains *Advances in Engineering Software*, **27**, 21–26. [4.8]
- Düppé, R.D. and H.J. Gottschalk (1970) Automatische Interpolation von Isolinien bei willkuerlich verteilten Stuetzpunkten *Allgemeine Vermessungs-Nachrichten*, **129**(10), 423–426. [6.2]
- Durrett, R. and J. Steif (1993) Fixation results for threshold voter systems *The Annals of Probability*, **21**, 232–247. [5.3]
- Dussert, C., G. Rasigni, M. Rasigni, J. Palmari and A. Llebaria (1986) Minimal spanning tree: a new approach for studying order and disorder *Physical Review B*, **34**(5), 3528–3531. [2.5]
- Dussert, C., M. Rasigni, J. Palmari, G. Rasigni, A. Llebaria and A. Marty (1987) Minimal spanning tree analysis of biological structures *Journal of Theoretical Biology*, **125**, 317–323. [2.5]
- Duyckaerts, C., G. Godefroy and J-J. Hauw (1994) Evaluation of neuronal density by Dirichlet tessellation *Journal of Neuroscience Methods*, **51**(1), 47–69. [8.1.1, 8.5, 8.6]

- Dwyer, R.A. (1987) A faster divide-and-conquer algorithm for constructing Delaunay triangulations *Algorithmica*, **2**, 137–151. [4.1, 4.4]
- Dwyer, R.A. (1991) Higher-dimensional Voronoi diagrams in linear expected time *Discrete and Computational Geometry*, **6**, 343–367. [4.7, 4.8]
- Dwyer, R.A. (1997) Voronoi diagrams of random lines and flats *Discrete and Computational Geometry*, **17**(2), 123–136. [3.5]
- Dyn, N., D.N. Levin and S. Rippa (1990) Data dependent triangulations for piecewise linear interpolation *IMA Journal of Numerical Analysis*, **10**(1), 137–154. [6.2]
- Eaton, B.C. and R.G. Lipsey (1975a) The principle of minimum differentiation reconsidered: some new developments in the theory of spatial competition *Review of Economic Studies*, **42**, 27–49. [7.3.1]
- Eaton, B.C. and R.G. Lipsey (1975b) The non-uniqueness of equilibrium in the Löschian location model *The American Economic Review*, **66**, 77–93. [7.3.1]
- Eaton, B.C. and R.G. Lipsey (1980) The block metric and the law of markets *Journal of Urban Economics*, **7**, 337–347. [3.7.11]
- Ebeling, H. and G. Wiedenmann (1993) Detecting structure in two dimensions combining Voronoi tessellation and percolation *Physical Review E*, **47**(1), 704–710. [5.3]
- Edelsbrunner, H. (1986) Edge-skeletons in arrangements with applications *Algorithmica*, **1**, 93–109. [3.1.4, 3.2]
- Edelsbrunner, H. (1987) *Algorithms in Combinatorial Geometry*. Berlin: Springer-Verlag. [2.4, 4.7]
- Edelsbrunner, H. (1988) The computational geometry column *EATCS (European Association for Theoretical Computer Science) Bulletin*, **37**, 109–116. [2.4, 4.1]
- Edelsbrunner, H. (1990) An acyclicity theorem for cell complexes in d dimensions *Combinatorica*, **10**, 251–260. [6.6]
- Edelsbrunner, H., D. Kirkpatrick and R. Seidel (1983) On the shape of a set of points in the plane *IEEE Transactions on Information Theory*, **IT-29**(4), 551–559. [8.4.2]
- Edelsbrunner, H. and E.P. Mücke (1987) Simulation of simplicity – A technique to cope with degenerate cases in geometric algorithms *Technical Report, UIUCDCS-R-87-1393*, Department of Computer Science, University of Illinois at Urbana-Champaign. [4.6.2]
- Edelsbrunner, H. and E.P. Mücke (1994) Three-dimensional alpha shapes *ACM Transactions on Graphics*, **13**(1), 43–72. [8.4.2]
- Edelsbrunner, H., F.P. Preparata and D.B. West (1990a) Tetrahedrizing point sets in three dimensions *Journal of Symbolic Computation*, **10**, 335–347. [2.2]
- Edelsbrunner, H. and R. Seidel (1986) Voronoi diagrams and arrangements *Discrete Computational Geometry*, **1**, 25–44. [2.4, 3.0, 4.1, 4.7, 4.8]
- Edelsbrunner, H. and N.R. Shah (1994) Triangulating topological spaces *Proceedings of the 10th Annual Symposium on Computational Geometry*, 285–292. [2.2]
- Edelsbrunner, H. and N.R. Shah (1996) Incremental topological flipping works for regular triangulations *Algorithmica*, **15**, 223–241. [3.1.4]
- Edelsbrunner, H. and M. Sharir (1990) A hyperplane incidence problem with applications to counting distances *Lecture Notes in Computer Science*, **450** (Proceedings of the International Symposium on Algorithms) Berlin: Springer-Verlag, 419–428. [3.3.1]
- Edelsbrunner, H. and T.S. Tan (1993) An upper bound for conforming Delaunay triangulations *Discrete and Computational Geometry*, **10**(2), 197–213. [2.4, 3.4.3, 6.5.1]
- Edelsbrunner, H., T.S. Tan and R. Waupotitsch (1990b) An $O(n^2 \log n)$ time algorithm for the minmax angle triangulation *Proceedings of the Sixth Annual Symposium on Computational Geometry, Berkeley, California*, 44–52. [6.2]
- Edwards, G. (1993) The Voronoi model and cultural space: applications to the social sciences and humanitites. In: A.U. Frank and I. Campari (eds) *Spatial Information Theory – A Theoretical Basis for GIS* Berlin: Springer-Verlag, 202–214. [3.6.2, 6.1.2]
- Edwards, G., G. Ligozat, A. Gryl, L. Fraczak, B. Moulin and C.M. Gold (1996) A Voronoi-based pivot representation of spatial concepts and its application to route descriptions expressed in natural language. In: M.J. Kraak and M. Molenaar (eds) *Proceedings of the 7th International Conference on Spatial Data Handling, Delft, Netherlands, August 12–16*, 7B1–7B15. [3.6.2]

- Edwards, G. and B. Moulin (1995) Towards the simulation of spatial mental images using the Voronoi model *Proceedings of the International Joint Conference on Artificial Intelligence, Montreal*, 63–73. [6.1.2]
- Egginton, S. (1990) Morphometric analysis of tissue capillary supply. In: R.G. Boutilier (ed) *Advances in Comparative and Environmental Physiology*, 6 Berlin: Springer-Verlag, 73–141. [7.1]
- Egginton, S. and H.F. Ross (1989a) Quantifying capillary distribution in four dimensions *Advances in Experimental Medicine and Biology*, 248, 271–280. [7.1]
- Egginton, S. and H.F. Ross (1989b) Influence of muscle phenotype on local capillary supply *Advances in Experimental Medicine and Biology*, 248, 281–291. [7.1]
- Egginton, S., Z. Turek and L. Hoofd (1987) Morphometric analysis of sparse capillary networks. In: J.A. Silver and A. Silver (eds) *Oxygen Transport to Tissue IX* New York: Plenum, 1–12. [7.1]
- Egginton, S., Z. Turek and L. Hoofd (1988) Differing patterns of capillary distribution in fish and mammalian skeletal muscle *Respiration Physiology*, 74, 383–396. [7.1]
- Ehrlich, P.E. and H.C. Im Hof (1979) Dirichlet regions in manifolds without conjugate points *Commentarii Mathematici Helvetici*, 54, 642–658. [3.7.10]
- Elam, W.T., A.R. Kerstein and J.J. Rehr (1984) Critical properties of the void percolation problem for spheres *Physical Review Letters*, 52(17), 1516–1519. [5.3]
- Elbaz, M. and J-C. Spehner (1990) Construction of Voronoi diagrams in the plane by using maps *Theoretical Computer Science*, 77, 331–343. [2.2, 2.3, 4.1]
- El Gindy, H.A. and D. Avis (1981) A linear algorithm for computing the visibility polygon from a point *Journal of Algorithms*, 2, 186–197. [3.4.1, 4.8]
- El Gindy, H.A. and G.T. Toussaint (1988) Computing the relative neighbour decomposition of a simple polygon. In: G.T. Toussaint (ed) *Computational Morphology* Amsterdam: Elsevier Science Publishers B.V., 53–70. [2.5]
- El Gindy, H. and L. Wetherall (1995) An L_1 Voronoi diagram algorithm for a reconfigurable mesh *IEEE First International Conference on Algorithms and Architectures for Parallel Processing ICAPP 95*, 1, 442–451. [3.7.1]
- Elliott, H.M. (1981) Macrocalifornia and the urban gradient *The California Geographer*, 21, 1–17. [6.1.2]
- Elliott, H.M. (1982) The Pacific nearest larger neighbor gradient *Yearbook, Association of Pacific Coast Geographers*, 44, 29–45. [6.1.2]
- Elliott, H.M. (1983) Surrounding larger neighbors and the Atlantic Coast cardinal neighbor gradient *Economic Geography*, 59(4), 426–444. [6.1.2]
- Elliott, H. (1985) Cardinal place geometry *Geographical Analysis*, 17(1), 16–35. [6.1.2]
- Embrechts, H. and D. Roose (1996) A parallel Euclidean distance transformation algorithm *Computer Vision and Image Understanding*, 63(1), 15–26. [2.1]
- Engel, P. (1981) Über Wirkungsbereichsteilungen von kubischer Symmetrie *Zeitschrift für Kristallographie*, 154, 199–215. [7.1]
- Eppstein, D. (1992) The furthest point Delaunay triangulation minimizes angles *Computational Geometry, Theory and Applications*, 1(3), 43–48. [3.3.1]
- Eppstein, D. and J. Erickson (1998) Raising roofs, crashing cycles, and playing pool: applications of a data structure for finding pairwise interactions *12th ACM Symposium on Computational Geometry, Minneapolis*, 58–67. [3.5.5]
- Eriksson, T. and E. Agrell (1996) Lattice-based quantization, Part II *Technical Report*, 18, Department of Information Theory, Chalmers University of Technology, Goteborg, Sweden. [7.1]
- Erlenkotter, D. (1981) A comparative study of approaches to dynamic location problems *European Journal of Operations Research*, 6, 133–143. [9.4.1]
- Escobar, J.M. and R. Montenegro (1996) Several aspects of three-dimensional Delaunay triangulation *Advances in Engineering Software*, 27, 27–39. [2.2, 6.5.2]
- Espriu, D., M. Gross, P.E.L. Rakow and J.F. Wheater (1986) Continuum limit on a 2-dimensional random lattice *Nuclear Physics*, B265 [FS15], 92–112. [5.3]
- Evans, D.J. and S.M. Jones (1987) Detecting Voronoi (area of influence) polygons *Mathematical Geology*, 19(6), 523–537. [2.5]
- Evans, D.J. and I. Stojmenovic (1989) On parallel computation of Voronoi diagrams *Parallel Computing*, 12(1), 121–125. [4.1]

- Evans, I.S. (1967) The properties of patterns of points, measured by space filling and angular relationships *Geographical Articles (Cambridge)*, **8**, 63–77. [1.2, 8.1.1]
- Evans, U.R. (1945) The laws of expanding circles and spheres in relation to the lateral growth of surface films and the grain-size of metals *Transactions of the Faraday Society*, **41**, 365–374. [5.8, 7.2]
- Facello, M.A. (1995) Implementation of a randomized algorithm for Delaunay and regular triangulations in 3 dimensions *Computer Aided Geometric Design*, **12**(4), 349–370. [4.7, 4.8]
- Fairfield, J. (1983) Segmenting dot patterns by Voronoi diagram concavity *IEEE Transactions on Pattern Analysis and Machine Intelligence*, **PAMI-5**, 104–110. [8.4.1]
- Falcidieno, B. and C. Pienovi (1990) Natural surface approximation by constrained stochastic interpolation *Computer-Aided Design*, **22**(3), 167–172. [6.4]
- Famiglietti, E.V. (1992) Polyaxonal amacrine cells of rabbit retina: size and distribution of PA1 cells *The Journal of Comparative Neurology*, **316**, 406–421. [7.1]
- Fang, T.P. and L.A. Piegl (1992) Algorithm for Delaunay triangulation and convex-hull computation using a sparse matrix *Computer-Aided Design*, **24**, 425–436. [4.1, 4.8]
- Fang, T.P. and L.A. Piegl (1994) Algorithm for constrained Delaunay triangulation *Visual Computer*, **10**(5), 255–265. [3.4.3, 4.1, 4.8]
- Fang, T.-P. and L.A. Piegl (1995) Delaunay triangulation in three dimensions *IEEE Computer Graphics and Applications*, **15**(5), 62–69. [2.2, 4.7]
- Farin, G. (1990) Surfaces over Dirichlet tessellations *Computer Aided Geometric Design*, **7**, 281–292. [6.1.2]
- Farouki, R.T. and J.K. Johnstone (1994) The bisector of a point and a plane parametric curve *Computer Aided Geometric Design*, **7**, 117–151. [3.5.2]
- Faugeras, O.D., E. Le Bras-Mehlman and J.D. Boissonnat (1990) Representing stereo data with the Delaunay triangulation *Artificial Intelligence*, **44**(1–2), 41–87. [3.4.5]
- Feder, J. (1980) Random sequential adsorption *Journal of Theoretical Biology*, **87**, 237–254. [5.12]
- Fedorov, E.S. (1885) Elemente der Lehre von den Figuren *Verhandlungen Russisch-Kaiserliche Mineralogische Gesellschaft zu St. Petersburg*, **21**, 1–279. [1.2]
- Feller, W. (1957) *An Introduction to Probability Theory and its Applications* (second edition). New York: John Wiley. [1.3]
- Feng, S., B.I. Halperin and P.N. Sen (1987) Transport properties of continuum systems near the percolation threshold *Physical Review B*, **35**(1), 197–214. [5.3]
- Fetter, F.A. (1924) The economic law of market areas *Quarterly Journal of Economics*, **38**, 520–529. [3.1.6]
- Fiacco, A.V. and G.P. McCormick (1968) *Nonlinear Programming: Sequential Unconstrained Minimization Technique* New York and Toronto: John Wiley. [9.1, 9.1.3]
- Field, D.A. (1986) Implementing Watson's algorithm in three dimensions *Proceedings of the 2nd ACM Symposium on Computational Geometry*, 246–259. [2.2]
- Field, D.A. (1995) The legacy of automatic mesh generation from solid modeling *Computer Aided Geometric Design*, **12**, 651–673. [6.5, 6.5.2]
- Finch, A.M. and E.R. Hancock (1995) Matching Delaunay graphs. In: C. Braccini, L. DeFloriani and G. Vernazza (eds) *Lecture Notes in Computer Science: Image Analysis and Processing*, **974** (Proceedings of the 8th International Conference, ICIAP '95 San Remo, Italy, September 13–15, 1995) Berlin: Springer-Verlag, 56–61. [6.6]
- Finch, A.M., R.C. Wilson and E.R. Hancock (1997) Matching Delaunay graphs *Pattern Recognition*, **30**(1), 123–140. [6.6]
- Finney, J.L. (1970a) Random packings and the structure of simple liquids. I. The geometry of random close packing *Proceedings of the Royal Society of London A*, **319**, 479–493. [5.3, 5.12, 7.1]
- Finney, J.L. (1970b) Random packings and the structure of simple liquids. II. The molecular geometry of simple liquids *Proceedings of the Royal Society of London A*, **319**, 495–507. [7.1]
- Finney, J.L. (1975a) The structures of laboratory and computer built random packing *Journal de Physique, Colloque C2*, **36**(4 Supplement), C2–1–C2–11. [5.12, 7.1]
- Finney, J.L. (1975b) Volume occupation, environment and accessibility in proteins *Journal of Molecular Biology*, **96**, 721–732. [7.1]

- Finney, J.L. (1978) Volume occupation, environment, and accessibility in proteins. Environment and molecular area of RNase-S *Journal of Molecular Biology*, **119**, 415–441. [7.1]
- Finney, J.L. (1979) A procedure for the construction of Voronoi polyhedra *Journal of Computational Physics*, **32**, 137–143. [4.7]
- Finney, J.L. (1991) Short range order in non-crystalline packing of spheres. In: D. Bideau and J.A. Dodds (eds) *Physics of Granular Media* New York: Nova Science. [1.2, 7.1, 8.2]
- Finney, J.L. (1993) Local structure of disordered hard sphere packings. In: D. Bideau and A. Hansen (eds) *Disorder and Granular Media* Amsterdam: Elsevier Science Publishers B.V., 35–54. [7.1, 8.2]
- Finney, J.L., B.J. Gellatly, I.C. Golton and J. Goodfellow (1980) Solvent effects and polar interactions in structural stability and dynamics of globular proteins *Biophysical Journal*, **32**(1), 17–33. [7.1]
- Finney, J.L. and J. Wallace (1981) Interstice correlation functions: a new, sensitive characterisation of non-crystalline packed structures *Journal of Non-Crystalline Solids*, **43**, 165–187. [7.1]
- Firbank, L.G. and A.R. Watkinson (1987) On the analysis of competition at the level of the individual plant *Oecologia (Berlin)*, **71**, 308–317. [7.1]
- Fisch, R., J. Gravner and D. Griffeath (1991) Threshold-range scaling for the excitable cellular automata *Statistics and Computing*, **1**, 23–39. [5.3]
- Fischer, R.A. and R.E. Miles (1973) The role of spatial pattern in the competition between crop plants and weeds. A theoretical analysis *Mathematical Biosciences*, **18**, 335–350. [7.4]
- Fischer, W. and E. Koch (1979) Geometrical packing analysis of molecular compounds *Zeitschrift für Kristallographie*, **150**, 245–260. [3.1.6, 7.1]
- Fjällström, P.O. (1993) Evaluation of a Delaunay-based method for surface approximation *Computer-Aided Design*, **25**(2), 711–719. [6.4]
- Forney, G.D., Jr (1991) Geometrically uniform codes *IEEE Transactions on Information Theory*, **37**(5), 1241–1260. [7.1]
- Fortes, M.A. (1993) Applicability of Aboav rule to a 3-dimensional Voronoi partition *Philosophical Magazine Letters*, **68**(2), 69–71. [5.5.3]
- Fortes, M.A. and P. Pina (1993) Average topological properties of successive neighbours of cells in random networks *Philosophical Magazine B*, **67**(2), 263–276. [5.5.3]
- Fortin, M.-J. (1994) Edge detection algorithms for two-dimensional ecological data *Ecology*, **75**(4), 956–965. [7.1]
- Fortune, S. (1985) A fast algorithm for polygon containment by translation *Lecture Notes in Computer Science*, **194** Berlin: Springer-Verlag, 189–198. [3.7.2]
- Fortune, S. (1986) A sweepline algorithm for Voronoi diagrams *Proceedings of the 2nd Annual ACM Symposium on Computational Geometry, Yorktown Heights, June 1986*, 313–322. [3.5, 4.1, 4.5, 4.8]
- Fortune, S. (1987) A sweepline algorithm for Voronoi diagrams *Algorithmica*, **2**, 153–174. [4.1, 4.5, 4.8]
- Fortune, S. (1992a) Numerical stability of algorithms for 2-d Delaunay triangulations and Voronoi diagrams *Proceedings of the Eighth Annual ACM Symposium on Computational Geometry*, 83–92. [4.6.3]
- Fortune, S. (1992b) Voronoi diagrams and Delaunay triangulations. In: D-Z. Du and F. Hwang (eds) *Computing in Euclidean Geometry* River Edge: World Scientific, 193–234. [4.6]
- Fortune, S. (1993) A note on Delaunay diagonal flips *Pattern Recognition Letters*, **14**(9), 723–726. [2.4]
- Fortune, S. (1995) Numerical stability of algorithms for 2-d Delaunay triangulations *International Journal of Computational Geometry and Applications*, **5**, 193–213. [4.6.3]
- Foss, S.G. and S.A. Zuyev (1996) On a Voronoi aggregative process related to a bivariate Poisson process *Advances in Applied Probability*, **28**, 965–981. [5.3]
- Fowler, R.S. and J.J. Little (1979) Automatic extraction of irregular network digital terrain models *Computer Graphics*, **13**, 199–207. [3.4.5, 6.2, 6.3, 6.4]

- Frank, F.C. and J.S. Kasper (1958) Complex alloy structures regarded as sphere packings. I. Definitions and basic principles *Acta Crystallographica*, **11**, 184–190. [1.2, 7.1]
- Franke, R. (1982) Scattered data interpolation: tests of some methods *Mathematics of Computation*, **38**(157), 181–200. [6.0, 6.3]
- Franke, R. and G.M. Nielson (1991) Scattered data interpolation and applications: a tutorial and survey. In: H. Hagen and D. Roller (eds) *Geometric Modeling* Berlin: Springer-Verlag, 131–160. [6.0]
- Franklin, W.R., V. Akman and C. Verrilli (1985) Voronoi diagrams with barriers and on polyhedra for minimal path planning *The Visual Computer – International Journal on Computer Graphics*, **1**, 133–150. [3.4.1, 3.4.4]
- Fraser, A.R. (1977) Triangle based probability polygons for forest sampling *Forest Science*, **23**, 111–121. [6.2]
- Fraser, A.R. and P. Van den Driessche (1972) Triangles, density and pattern in point populations *Proceedings of the Third Conference of the Advisory Group of Forest Statisticians, Jouy en Josas, France*, 277–286. [6.2]
- Fraser, D.P. (1991) Voronoi statistics of hard-core systems *Materials Characterization*, **26**, 73–83. [5.12]
- Fraser, D., M.J. Zuckermann and O.G. Mouritsen (1990) Simulation technique for hard-disk models in two dimensions *Physical Review A*, **42**(6), 3186–3195. [5.12]
- Fraser, D., M.J. Zuckermann and O.G. Mouritsen (1991) Theory and simulations for hard-disk models of binary mixtures of molecules with internal degrees of freedom *Physical Review A*, **43**, 6642–6656. [5.12]
- Freund, J. E. (1962) *Mathematical Statistics* Englewood Cliffs: Prentice-Hall. [1.3]
- Friedberg, R. and H-C. Ren (1984) Field theory on a computationally constructed random lattice *Nuclear Physics*, **B235** [FS11], 310–320. [5.3]
- Friedman, J.H. and L.C. Rafsky (1979) Multivariate generalizations of the Wald–Wolfowitz and Smirnov two-sample tests *The Annals of Statistics*, **7**(4), 696–717. [2.5, 6.6]
- Friedman, J.H. and L.C. Rafsky (1981) Graphics for the multivariate two-sample problem *Journal of the American Statistical Association*, **76**(374), 277–295. [2.5, 6.6]
- Frost, H.J. and C.V. Thompson (1987a) The effect of nucleation conditions on the topology and geometry of two-dimensional grain structures *Acta Metallurgica*, **35**(2), 529–540. [5.8, 5.12, 7.2]
- Frost, H.J. and C.V. Thompson (1987b) Development of microstructure in thin films *Proceedings of SPIE – The International Society for Optical Engineering*, **821**, 77–87. [5.8, 5.12]
- Frost, H.J. and C.V. Thompson (1988) Computer simulation of microstructural evolution in thin-films *Journal of Electronic Materials*, **17**(5), 447–458. [7.2]
- Frost, H.J., C.V. Thompson and D.T. Walton (1990) Grain growth stagnation and abnormal grain growth in thin films. In: M.P. Anderson and A.D. Rollett (eds) *Simulation and Theory of Evolving Microstructures* Warrendale: The Minerals, Metals and Materials Society, 31–39. [5.8]
- Fu, J-J. and R.C.T. Lee (1991) Voronoi diagrams of moving points in the plane *International Journal of Computational Geometry and Applications*, **1**(1), 23–32. [3.9.1, 4.1]
- Fujii, A. (1976) Activity Contour Lines. Ph.D. Thesis, Department of Architecture, University of Tokyo [in Japanese]. [3.5.5]
- Fujii, A. (1983) Geometrical models for regional analysis *Review of City Planning*, **126**, 93–98 [in Japanese]. [3.6.2]
- Fujii, A. and K. Oikawa (1986) Simulation models of domain division based on the allocation of urban facilities *Monthly Journal of the Institute of Industrial Science, University of Tokyo*, **38**, 418–421 [in Japanese]. [3.6.2]
- Fukunaga, K. and P.M. Narendra (1975) A branch and bound algorithm for computing k -nearest neighbor *IEEE Transactions on Computers*, **C-24**, 750–753. [3.2.3, 3.3.3]
- Fukushima, S. (1997) Division-based analysis of symmetry and its application *IEEE Transactions on Pattern Analysis and Machine Intelligence*, **19**(2), 144–148. [3.5.4]
- Fukushima, S. and T. Okumura (1991) Estimating the three-dimensional shape from a silhouette by geometrical division of the plane *Proceedings IIECON '91. 1991 International Conference on Industrial Electronics, Control and Instrumentation*, **3**, 1773–1778. [3.5.4]

- Furu, T., K. Marthinsen and E. Nes (1990) Modelling recrystallisation *Materials Science and Technology*, **6**, 1093–1102. [5.8]
- Gabriel, K. R. and R. R. Sokal (1969) A new statistical approach to geographic variation analysis *Systematic Zoology*, **18**, 259–278. [2.5]
- Gabszewicz, J.J., J-F. Thisse, M. Fujita and U. Schweizer (1986) *Location Theory* Switzerland: Harwood Academic Publishers. [7.3.1]
- Galashev, A.E. and V.P. Skripov (1980) Molecular-dynamic study of the structures of liquid and crystalline argon *Journal of Structural Chemistry*, **21**, 158–162. [7.1]
- Galitsky, V.V. (1990) Dynamic 2-d model of plant communities *Ecological Modelling*, **50**, 95–105. [7.2]
- Gambini, R., D.L. Huff and G.F. Jenks (1967) Geometric properties of market areas *Papers and Proceedings of the Regional Science Association*, **20**, 85–92. [3.1.6]
- Gao, J., L.D. Rudolph and C.R.P. Hartmann (1988) Iteratively maximum likelihood decodable spherical codes and a method for their construction *IEEE Transactions on Information Theory*, **34**(3), 480–485. [7.1]
- Garey, M.R., R.L. Graham and D.S. Johnson (1977) The complexity of computing Steiner minimal trees *SIAM Journal on Applied Mathematics*, **32**, 835–859. [9.3.3]
- Garga, A.K. and N.K. Bose (1994). A neural-network approach to the construction of Delaunay tessellation of points in R(D) *IEEE Transactions on Circuits and Systems I – Fundamental Theory and Applications*, **41**(9), 611–613. [4.1]
- Gasparini, D.A., P. Bonacuse, L. Powers and A. Romeo (1996) Stochastic parallel-brittle networks for modeling materials *Journal of Engineering Mechanics*, **12**(2), 130–137. [5.3]
- Gavrilova, M. and J. Ronke (1996) An efficient algorithm for construction of the power diagram from the Voronoi diagram in the plane *International Journal of Computer Mathematics*, **61**, 49–61. [4.8]
- Gellatly, B.J. and J.L. Finney (1982a) Characterisation of models of multicomponent amorphous metals: the radical alternative to the Voronoi polyhedron *Journal of Non-Crystalline Solids*, **50**, 313–329. [3.1.6]
- Gellatly, B.J. and J.L. Finney (1982b) Calculation of protein volumes: an alternative to the Voronoi procedure *Journal of Molecular Biology*, **161**(2), 305–322. [3.1.6, 7.1]
- Gellatly, B.J. and J.L. Finney (1982c) The radical alternative to the Voronoi polyhedron. In: T. Masumoto and K. Suzuki (eds) *Proceedings of the Fourth International Conference on Rapidly Quenched Metals* Sendai, Japan: The Japan Institute of Metals, 275–277. [3.5.3, 3.5.5, 7.1]
- Gen, E. (1983) Algorithms for High Dimensional Voronoi diagrams. Bachelor's Thesis, Department of Mathematical Engineering and Information Physics, University of Tokyo [in Japanese]. [2.1, 2.2]
- Georgakopoulos and C.H. Papadimitriou (1987) The 1-Steiner tree problem *Journal of Algorithms*, **8**, 122–130. [3.7.10]
- George, P.L. (1991) *Automatic Mesh Generation. Applications to Finite Element Methods* Chichester: John Wiley. [6.5, 6.5.2]
- George, P.L. (1997) Improvements on Delaunay-based three-dimensional automatic mesh generator *Finite Elements in Analysis and Design*, **25**, 297–317. [6.5.2]
- George, P.L., F. Hecht and E. Saltel (1990) Automatic 3D mesh generation with specified boundary *IEEE Transactions on Magnetics*, **26**, 771–774. [6.5, 6.5.2]
- George, P.L., F. Hecht and E. Saltel (1991) Automatic mesh generator with specified boundary *Computer Methods in Applied Mechanics and Engineering*, **92**, 269–288. [6.5.2]
- Gersho, A. (1979) Asymptotically optimal block quantization *IEEE Transactions on Information Theory*, **IT-25**(4), 373–380. [7.1]
- Gersho, A. (1982) On the structure of vector quantizers *IEEE Transactions on Information Theory*, **IT-28**(2), 157–166. [7.1]
- Gerstein, M., B.F. Anderson, G.E. Norris, E.N. Baker, A.M. Lesk and C. Chothia (1993) Domain closure in lactoferrin: two hinges produce a see-saw motion between alternative close-packed interfaces *Journal of Molecular Biology*, **234**, 357–372. [7.1]
- Gerstein, M. and C. Chothia (1996) Packing at the protein-water interface *Proceedings of the National Academy of Science, USA*, **93**, 10167–10172. [7.1]

- Gerstein, M., J. Tsai and M. Levitt (1995) The volume of atoms on the protein surface: calculated from simulation, using Voronoi polyhedra *Journal of Molecular Biology*, **249**, 955–966. [1.2, 3.1.6, 3.5.5, 7.1]
- Gervois, A. and D. Bideau (1993) Some geometrical properties of two-dimensional hard disk packings. In: D. Bideau and A. Hansen (eds) *Disorder and Granular Media* Amsterdam: Elsevier Science Publishers B.V., 1–34. [7.1]
- Gervois, A., J.P. Troadec and J. Lemaître (1992) Universal properties of Voronoi tessellations of hard discs *Journal of Physics A: Mathematical and General*, **25**(23), 6169–6177. [5.12]
- Getis, A. and B. Boots (1978) *Models of Spatial Processes: An Approach to the Study of Point, Line and Area Patterns* Cambridge: Cambridge University Press. [1.3.3, 8.0, 8.3]
- Ghosh, S. and Y. Liu (1995) Voronoi cell finite element model based on micropolar theory of thermoelasticity for heterogeneous materials *International Journal for Numerical Methods in Engineering*, **38**(8), 1361–1398. [6.5]
- Ghosh, S. and S. Moorthy (1995) Elastic-plastic analysis of arbitrary heterogeneous materials with Voronoi cell finite element method *Computational Methods in Applied Mechanics and Engineering*, **121**, 373–409. [6.5]
- Ghosh, S.K. and D. Mount (1991) An output sensitive algorithm for computing visibility graphs *SIAM Journal on Computing*, **20**, 888–910. [3.4.1]
- Ghosh, S. and S.N. Mukhopadhyay (1993) A material based finite element analysis of heterogeneous media involving Dirichlet tessellations *Computer Methods in Applied Mechanics and Engineering*, **104**(2), 211–247. [6.5]
- Gibson, I.J. and M.F. Ashby (1988) *Cellular Solids* Oxford: Pergamon. [7.2]
- Gilbert, E.N. (1962) Random subdivisions of space into crystals *Annals of Mathematical Statistics*, **33**, 958–972. [5.5.1, 5.5.4, 5.7, 5.8, 8.1.2]
- Gilbert, E.N. and H.O. Pollack (1968) Steiner minimum trees *SIAM Journal of Applied Mathematics*, **16**(1), 1–29. [9.3.3]
- Gil Montoro, J.C. and J.L.F. Abascal (1993) The Voronoi polyhedra as tools for structure determination in simple disordered systems *Journal of Physical Chemistry*, **97**, 4211–4215. [7.1]
- Gil Montoro, J.C. F. Bresme and J.L.F. Abascal (1994) Ionic association in electrolyte solutions: a Voronoi polyhedra analysis *Journal of Chemical Physics*, **101**, 10892–10898. [7.1]
- Gill, P.E., W. Murry and M.H. Wright (1981) *Practical Optimization* London: Academic Press. [9.1, 9.1.3]
- Glaser, M.A. and N.A. Clark (1990) Melting and liquid structure in two dimensions. In: I. Prigogine and S.A. Rice (eds) *Advances in Chemical Physics I* New York: John Wiley. [7.1]
- Glass, L. (1973) Stochastic generation of regular distributions *Science*, **180**, 1061–1063. [5.8]
- Glass, L. (1974) Dynamics of expanding inhibitory fields *Science*, **183**, 446. [5.8]
- Goebel, H. (1981) Éléments d'analyse dialectométrique (avec application à l'AIS) *Revue de Linguistique Romane*, **45**, 349–420. [7.1]
- Goebel, H. (1983) Parquet polygonal et treillis triangulaire. Les deux versants de la dialectométrie interponctuelle *Revue de Linguistique Romane*, **47**, 353–412. [7.1]
- Goebel, H. (1987) Encore un coup d'œil dialectométrique sur les *Tableaux phonétiques des patois suisses romans (TPPSR)* *Vox Romanica*, **46**, 91–125. [7.1]
- Goebel, H. (1993) Dialectometry: a short overview of the principles and practice of quantitative classification of linguistic atlas data. In: R. Kohler and B.B. Rieger (eds) *Contributions in Quantitative Linguistics* Dordrecht: Kluwer Academic Publishers, 277–315. [7.1]
- Goede, A., R. Preissner and C. Frommel (1997) Voronoi cell: new method for allocation of space among atoms: elimination of avoidable errors in calculation of atomic volume and density *Journal of Computational Chemistry*, **18**(9), 1113–1123. [1.2, 7.1]
- Gold, C.M. (1980) Triangulation-based terrain modelling – where are we now? *Proceedings of Auto-Carto 4*, Volume II, 104–111. [6.2, 6.5]
- Gold, C.M. (1987) Spatial ordering of Voronoi networks and their use in terrain data base measurement *Proceedings, Auto-Carto 8, Baltimore*, 185–194. [6.6]

- Gold, C.M. (1989a) Surface interpolation, spatial adjacency and GIS. In: J. Raper (ed) *Three Dimensional Applications in Geographical Information Systems* London: Taylor and Francis, 21–35. [3.6.2, 6.0]
- Gold, C.M. (1989b) Spatial adjacency – general approach *Proceedings, Auto-Carto 9, Baltimore, April 1989*, 298–312 [3]
- Gold, C.M. (1990) Spatial data structures – the extension from one to two dimensions. In: L.F. Pau (ed) *Mapping and Spatial Modelling for Navigation NATO ASI Series F 65* Berlin: Springer-Verlag, 11–39. [3.9.2]
- Gold, C.M. (1992) An object-based dynamic spatial model, and its application in the development of a user-friendly digitizing system *Proceedings, Fifth International Symposium on Spatial Data Handling, Charleston, August*, 495–504. [3.6.2]
- Gold, C.M. (1997) Simple topology generation from scanned maps *Proceedings of the ACSM/ASPRS – Auto-Carto 13*, 5, 337–346. [3.5.5, 3.7.11]
- Gold, C.M., T.D. Charters and J. Ramsden (1977) Automated computer mapping using triangular element data structures and an interpolant over each irregular triangular domain *Computer Graphics*, 11, 170–175. [6.2]
- Gold, C.M. and S. Cormack (1987) Spatially ordered networks and topographic reconstructions *International Journal of Geographical Information Systems*, 1(2), 137–148. [6.6]
- Gold, C.M. and U.M. Maydell (1978) Triangulation and spatial ordering in computer cartography *Proceedings, Third Annual Meeting, Canadian Cartographic Association, Vancouver, B.C., 8–10 June 1978*, 69–81. [6.6]
- Gold, C.M., J. Nantel and W. Yang (1996) Outside-in: an alternative approach to forest map digitizing *International Journal of Geographical Information Systems*, 10(3), 291–310. [3.5.5, 3.9.1]
- Gold, C.M., P.R. Remmeli and T. Roos (1995) Voronoi diagrams of line segments made easy *Proceedings of the 7th Canadian Conference on Computational Geometry*, 223–228. [3.9.2, 4.8]
- Gold, C.M., P.R. Remmeli and T. Roos (1997) Voronoi methods in GIS *Lecture Notes in Computer Science*, 1340 Berlin: Springer-Verlag, 21–35. [3.9.1, 3.9.2]
- Goldak, J.A., X. Yu, A. Knight and L. Dong (1991) Constructing discrete medial axis of 3-D objects *International Journal of Computational Geometry and Applications*, 1(3), 327–339. [3.5.4]
- Goldwirth, D.S., L.N. Da Costa and R. Van de Weygaert (1995) The two-point correlation function and the structure of voids *Monthly Notices, Royal Astronomical Society*, 275, 1185–1194. [5.3, 7.2]
- Golias, N.A. and R.W. Dutton (1997) Delaunay triangulation and 3D adaptive mesh generation *Finite Elements in Analysis and Design*, 25(3–4), 331–341. [2.2]
- Goodchild, M.F. (1986) *Spatial Autocorrelation. Concepts and Techniques in Modern Geography*, 47, Norwich: Geo Books. [6.1.2]
- Goodchild, M.F. and B.H. Massam (1969) Some least-cost models of spatial administrative systems in southern Ontario *Geografiska Annaler*, 52B, 86–94. [7.1]
- Goodrich, M.T., C. O'Dunlaing and C.K. Yap (1993) Constructing the Voronoi diagram of a set of line segments in parallel *Algorithmica*, 9(2), 128–141. [3.5, 4.1]
- Gotoh, K. (1993) Comparison of random configurations of equal disks *Physical Review E*, 47(1), 316–318. [5.12, 7.1, 8.1.1]
- Gotsman, C. and M. Lindenbaum (1995) Euclidean Voronoi labelling on the multidimensional grid *Pattern Recognition Letters*, 16 (4), 409–415. [7.1]
- Gowda, I.G., D.G. Kirkpatrick, D.T. Lee and A. Naamad (1983) Dynamic Voronoi diagrams *IEEE Transactions on Information Theory*, IT-29(5), 724–731. [3.9.1, 4.1]
- Gower, J.C., and G.J.S. Ross (1969) Minimum spanning trees and single linkage cluster analysis *Applied Statistics*, 18, 54–64. [2.5]
- Grady, D.E. and M.E. Kipp (1985) Geometric statistics and dynamic fragmentation *Journal of Applied Physics*, 58(3), 1210–1222. [5.3, 5.8]
- Gravner, J. and D. Griffeath (1997) Multitype threshold growth: convergence to Poisson-Voronoi tessellations *The Annals of Applied Probability*, 7, 615–647. [5.3]
- Green, F.H.W. (1955) *Local Accessibility*, Chessington: Director General of the Ordnance Survey. [7.2]

- Green, P.J. (1981) Peeling bivariate data. In: V. Barnett (ed) *Interpreting Multivariate Data* New York: John Wiley, 3–19. [6.6]
- Green, P.J. and R. Sibson (1978) Computing Dirichlet tessellations in the plane *The Computer Journal*, **21**, 168–173. [4.1]
- Greub, W. (1975) *Linear Algebra* (fourth edition) New York: Springer-Verlag. [4.6.2]
- Griffith, D.A. (1982) Dynamic characteristics of spatial economic systems *Economic Geography*, **58**, 177–196. [6.1.2]
- Griffith, D.A. (1987) *Spatial Autocorrelation: A Primer* Washington: Association of American Geographers. [6.1.2]
- Grigorovici, R. (1969) Short-range order in amorphous semiconductors *Journal of Non-Crystalline Solids*, **1**, 303–325. [7.1]
- Grigorovici, R. and R. Manaila (1967/8) Structural model for amorphous germanium layers *Thin Solid Films*, **1**, 343–352. [7.1]
- Gross, L.M. (1995) Transfinite Surface Interpolation over Voronoi Diagrams, Ph.D. Dissertation, Arizona State University. [6.1]
- Gruber, P.M. and C.G. Lekkerkerker (1987) *Geometry of Numbers* (second edition) Amsterdam: North-Holland. [1.2]
- Grünbaum, B. and G.C. Shephard (1980) Tilings with congruent tiles *Bulletin (New Series) of the American Mathematical Society*, **3**(3), 951–973. [1.2 7.1]
- Grünbaum, B. and G.C. Shephard (1987) *Tilings and Patterns* New York: W.H. Freeman and Company. [7.1]
- Guha, S. (1993) An optimal parallel algorithm using exclusive read/writes for the rectilinear Voronoi diagram *Computational Geometry: Theory and Applications*, **3**(1), 37–52. [3.7.1, 3.7.11]
- Guha, S. (1994) An optimal mesh computer algorithm for constrained Delaunay triangulation *Proceedings Eighth International Parallel Processing Symposium*, 102–109. [3.4.3]
- Guha, S. and I. Suzuki (1997) Proximity problems for points on a rectilinear plane with rectangular obstacles *Algorithmica*, **17**, 281–307. [3.4.1]
- Guibas, L., J. Hershberger, D. Leven, M. Sharir and R.E. Tarjan (1987) Linear-time algorithms for visibility and shortest path problems inside triangulated simple polygons *Algorithmica*, **2**, 209–233. [3.4.1]
- Guibas, L.J., D.E. Knuth and M. Sharir (1992) Randomized incremental construction of Delaunay and Voronoi diagrams *Algorithmica*, **7**, 381–413. [4.1, 4.3]
- Guibas, L., J.S.B. Mitchell and T. Roos (1991) Voronoi diagrams of moving points in the plane. In: G. Schmidt and R. Berghammer (eds) *Lecture Notes in Computer Science*, **570** (Proceedings of the 17th International Workshop on Graph-theoretic Concepts in Computer Science) New York: Springer-Verlag, 113–125. [3.9.1]
- Guibas, L. and J. Stolfi (1985) Primitives for the manipulation of general subdivisions and the computation of Voronoi diagrams *ACM Transactions on Graphics*, **4**(2), 74–123. [4.1, 4.4]
- Gunawardane, G. (1982) Dynamic versions of set covering type public facility location problems *European Journal of Operations Research*, **10**, 190–195. [9.4.1]
- Gürsoy, H.N. and N.M. Patrikalakis (1991) Automated interrogation and adaptive subdivision of shape using medial axis transform *Advances in Engineering Software*, **13**(5/6), 287–302. [3.5.4]
- Gürsoy, H.N. and N.M. Patrikalakis (1992) An automatic coarse and fine surface mesh generation scheme based on medial axis transform. Part II: Implementation *Engineering with Computers*, **8**, 179–186. [3.5.4, 3.5.5]
- Haag, C. (1898) *Die Mundarten des oberen Neckar- und Donaulandes (Schwäbisch-alemannisches Grenzgebiet: Baarmundarten)* Reutlingen: Hutzler. [1.2, 7.1]
- Haag, F. (1911) Die regelmäßigen Planteilungen *Zeitschrift für Kristallographie*, **49**, 360–369. [1.2]
- Haag, F. (1923) Die regelmäßigen Planteilungen und Punktsysteme *Zeitschrift für Kristallographie*, **58**, 478–489. [1.2]
- Haag, F. (1924) Die pentagonalen Anordnungen von sich berührenden Kreisen in der Ebene *Zeitschrift für Kristallographie*, **61**, 339. [1.2]
- Haag, F. (1925) Die Planigone von Fedorow *Zeitschrift für Kristallographie*, **63**, 179–186. [1.2]

- Hagggett, P., A.D. Cliff and A. Frey (1977) *Locational Methods* London: Edward Arnold. [1.3.3, 8.0, 8.1.1]
- Hague, T., M. Brady and S. Cameron (1990) Using moments to plan paths for the Oxford AGV Proceedings 1990 IEEE International Conference on Robotics and Automation, 1, 210–215. [3.7.11]
- Hahn, U. and U. Lorz (1994) Stereological analysis of the spatial Poisson–Voronoi tessellation *Journal of Microscopy*, **175**, 176–185. [5.7, 5.12]
- Hai, T. and T.S. Huang (1996) Multi-scale image warping using weighted Voronoi diagram *Proceedings, International Conference on Image Processing*, **1**, 241–244. [3.1.6]
- Haining, R., D.A. Griffith and R. Bennett (1984) A statistical approach to the problem of missing spatial data using a first-order Markov model *The Professional Geographer*, **36**, 338–345. [6.1.2]
- Hakimi, S.L. (1964) Optimal locations of switching centers and the absolute centers and medians of a graph *Operations Research*, **12**, 450–475. [3.8.4, 9.2]
- Hakimi, S.L. (1965). Optimum distribution of switching centers in a communication network and some related graph theoretic problems *Operations Research*, **13**, 462–475. [3.8.4]
- Hakimi, S.L., M. Labbe and E. Schmeichel (1992) The Voronoi partition of a network and its implications in location theory *ORSA Journal on Computing*, **4**(4), 412–417. [3.8.2, 3.8.4, 9.2.8]
- Haldar, C. and L.M. Patnaik (1990) Oracle complexities for computational geometry of semi-algebraic sets and Voronoi diagrams *Information Processing Letters*, **36**, 95–102. [3.5.2]
- Hall, P. (1985) Distribution of size, structure and number of vacant regions in a high-intensity mosaic *Zeitschrift für Wahrscheinlichkeitstheorie und verwandte Gebiete*, **70**, 237–261. [5.6.2]
- Halperin, B.I., S. Feng and P.N. Sen (1985) Differences between lattice and continuum percolation transport exponents *Physical Review Letters*, **54**(22), 2391–2394. [5.3]
- Hama, T. and H. Etoh (1997) Topological routing path search algorithm with incremental routability test *Proceedings of the Asia and South Pacific Design Automation Conference 1997 ASP-DAC '97*, 645–648. [3.4.5]
- Hamann, B. and P.Y. Tsai (1996) A tessellation algorithm for the representation of trimmed NURBS surfaces with arbitrary trimming curves *Computer-Aided Design*, **28**(6–7), 461–472. [3.0]
- Hamilton, W.D. (1971) Geometry for the selfish herd *Journal of Theoretical Biology*, **31**, 295–311. [5.3, 7.4]
- Hammersly, J.M. and D.J.A. Welsh (1965) First-passage percolation, subadditive processes, stochastic networks and generalized renewal theory. In: J. Neyman and L. Le Cam (eds) *Bernoulli, Bayes, Laplace Anniversary Volume* Berlin: Springer-Verlag, 61–110. [5.6.4]
- Hammond, N.D.C. (1972) Locational models and the site of Lubaantun: a classic Maya centre. In: D.L. Clarke (ed) *Models in Archaeology* London: Methuen, 757–799. [7.1]
- Hammond, N. (1974) The distribution of Late Classic Maya major ceremonial centres in the Central Area. In: N. Hammond (ed) *Mesoamerican Archaeology: New Approaches* Austin: University of Texas Press, 313–334. [7.1]
- Handler, G.Y. and P.B. Mirchandani (1979) *Location on Networks, Theory and Algorithms* Cambridge: The MIT Press. [3.8.4, 9.2]
- Handler, H. and H.E. Wiegand (1982) Das Konzept der Isoglosse: methodische und terminologische Probleme. In: W. Besch, U. Knoop, W. Putschke, H.E. Wiegand and E. Halbwand (eds) *Dialektologie. Ein Handbuch zur deutschen und allgemeinen Dialektforschung* Berlin: Walter de Gruyter, 501–527. [7.1]
- Hanjoul, P., H. Beguin and J-C. Thill (1989) Advances in the theory of market areas *Geographical Analysis*, **21**(3), 185–196. [3.1.2, 3.1.6, 4.8]
- Hanjoul, P. and J-C. Thisse (1987) Elements of planar analysis in spatial competition *Regional Science and Urban Economics*, **17**, 423–439. [3.1.6]
- Hanson, H.G. (1983) Voronoi cell properties from simulated and real random spheres and points *Journal of Statistical Physics (USA)*, **30**(3), 591–605. [5.5.1, 5.5.4, 5.12]

- Harding, J.E. (1920-21) Calculation of ore tonnage and grade from drill-hole samples *Transactions of the American Institute of Mining Engineers*, **66**, 117-126. [1.2, 6.2]
- Harding, J.E. (1923) How to calculate tonnage and grade of an ore body *Engineering and Mining Journal Press*, **116**(11), 445-448. [1.2, 6.2]
- Harpaz, Y., M. Gerstein and C. Chothia (1994) Volume changes on protein folding *Structure*, **2**, 641-649. [7.1]
- Har-Peled, S., M. Sharir and K.R. Varadarajan (1996) Approximating shortest paths on a convex polytope in three dimensions *Proceedings of the 12th Annual Symposium on Computational Geometry, May 24-26, 1996, Philadelphia, PA., USA*, 329-338. [3.7.9]
- Hartvigsen, D. (1992) Recognizing Voronoi diagrams with linear programming *ORSA Journal on Computing*, **4**(4), 369-374. [2.6]
- Hasegawa, M. and M. Tanemura (1976) On the pattern of space division by territories *Annals of the Institute of Statistical Mathematics*, **28**, Part B, 509-519. [5.3, 7.2, 7.3.2, 9.5.1]
- Hasegawa, M. and M. Tanemura (1980) Spatial patterns of territories. In: K. Matusita (ed) *Recent Developments in Statistical Inference* Amsterdam: North-Holland, 73-78. [5.12, 7.3.2]
- Hasegawa, M. and M. Tanemura (1986) *Ecology of Territories: Statistics of Ecological Models and Spatial Patterns* Tokyo: Tokai University Press. [7.3.2]
- Hasegawa, M., M. Tanemura and S. Takiguchi (1981) Spatial patterns in ecology *International Roundtable Congress - The 50th Anniversary of the Japan Statistical Society*, 146-161. [5.12, 7.1]
- Hayes, W.B. and G.S. Koch (1984) Constructing and analyzing area-of-influence polygons by computer *Computers and Geosciences*, **10**(4), 411-430. [1.2, 6.1.1]
- Haynes, K.E. and A.S. Fotheringham (1984) *Gravity and Spatial Interaction Models*. Sage Scientific Geography Series, 2. Beverly Hills: Sage Publications. [6.1.2]
- Hazlewood, C. (1993) Approximating constrained tetrahedrizations *Computer Aided Geometric Design*, **10**, 67-87. [3.4.3]
- Hearn, D.W. and J. Vijay (1982) Efficient algorithms for the (weighted) minimum circle problem *Operations Research*, **30**, 777-795. [3.3.1]
- Heath, D. and S. Kasif (1993) The complexity of finding minimal Voronoi covers with applications to machine learning *Computational Geometry: Theory and Applications*, **3**(5), 289-305. [2.3]
- Heinrich, L. (1994) Normal approximation for some mean-value estimates of absolutely regular tessellations *Mathematical Methods of Statistics*, **3**(1), 1-24. [1.3.3, 5.5.4, 5.6.1]
- Heinrich, L., R. Körner, N. Mehlhorn and L. Muche (1998) Numerical and analytical computation of some second-order characteristics of spatial Poisson-Voronoi tessellations *Statistics*, **31**, 235-259. [5.6.1]
- Heinrich, L. and L. Muche (1994) On the pair correlation function of the point process of nodes in a Voronoi tessellation Preprint, TU Bergakademie Freiberg. [5.6.1]
- Heinrich, L. and E. Schüle (1995) Generation of the typical cell of a non-Poissonian Johnson-Mehl tessellation *Communications in Statistics. Stochastic Models*, **11**(3), 541-560. [5.8, 5.12]
- Held, M. (1991) On the computational geometry of pocket machining *Lecture Notes in Computer Science*, **500** Berlin: Springer-Verlag. [3.5.5]
- Held, M. (1993) A fast incremental algorithm for computing the Voronoi diagram of a planar shape *Communicating with Virtual Worlds (CGI '93), Switzerland, June 21-25, 1993*, 318-329. [3.5.4, 3.5.5]
- Henry, N.F.M. and K. Lonsdale (eds) (1965) *International Tables for X-ray Crystallography. Volume 1: Symmetry Groups* Birmingham: Kynoch Press. [7.1]
- Herdle, T. and H. Aref (1992) Numerical experiments on two-dimensional foam *Journal of Fluid Mechanics*, **241**, 233-260. [5.12]
- Hermann, H., H. Wendrock and D. Stoyan (1989) Cell-area distributions of planar Voronoi mosaics *Metallography*, **23**, 189-200. [5.5.4, 5.12, 8.1.1]
- Hinde, A.L. and R.E. Miles (1980) Monte Carlo estimates of the distributions of the random polygons of the Voronoi tessellation with respect to a Poisson process *Journal of Statistical Computation and Simulation*, **10**, 205-223. [5.4, 5.5.4, 8.1.1]

- Hiroshima, T. and K. Sugihara (1994) Polynomial-time algorithm for recognizing Delaunay graphs *Technical Report, METR94-15*, Department of Mathematical Engineering and Information Physics, University of Tokyo. [2.6]
- Hiroshima, T. and K. Sugihara (1996) Recognition of Delaunay graphs *Proceedings of the Korea-Japan Joint Workshop on Algorithms and Computation, Taijon*, 102–109. [2.6]
- Hirsch, A.G., R.J. Williams and R. Mechl (1994) Kinetics of medfly mortality *Experimental Gerontology*, **29**, 197–204. [5.8]
- Hiwatari, Y., T. Saito and A. Ueda (1984) Structural characterization of soft-core and hard-core glasses by Delaunay tessellation *Journal of Chemical Physics*, **81**(12), 6044–6050. [7.1]
- Hobby, J.D. (1993) Generating automatically tuned bitmaps from outlines *Journal of the Association for Computing Machinery*, **40**(1), 48–94. [3.5.5]
- Hodder, I.R. (1972) Locational models and the study of Romano-British settlement. In: D.L. Clarke (ed) *Models in Archaeology* London: Methuen. [7.1]
- Hodder, I.R. and C. Orton (1976) *Spatial Analysis in Archaeology* Cambridge: Cambridge University Press. [3.1.6]
- Hodgson, C.D., I. Rivin and W.D. Smith (1992) A characterization of convex hyperbolic polyhedra and of convex polyhedra inscribed in the sphere *Bulletin of the American Mathematical Society*, **27**, 246–251. [2.6]
- Hodgson, M. (1984) Alternative approaches to hierarchical location-allocation systems *Geographical Analysis*, **16**, 275–281. [9.2.4]
- Hoffman, C.M. (1989) *Geometric and Solid Modeling – An Introduction* San Mateo: Morgan Kaufmann. [4.2]
- Hogg, A.H.A. (1971) Some applications of surface fieldwork. In: D. Hill and M. Jesson (eds) *The Iron Age and Its Hillforts* Southampton: Millbrook Press, 105–125. [3.1.6]
- Ho-Le, K. (1988) Finite element mesh generation methods: a review and classification *Computer Aided Design*, **20**, 27–38. [6.5]
- Holst L., M.P. Quine and J. Robinson (1996) A general stochastic model for nucleation and linear growth *The Annals of Applied Probability*, **6**(3), 903–921. [5.8]
- Honda, H. (1978) Description of cellular patterns by Dirichlet domains: the two-dimensional case *Journal of Theoretical Biology*, **72**, 523–543. [7.2, 9.5.1]
- Honda, H., T. Morita and A. Tanabe (1979) Establishment of epidermal cell columns in mammalian skin: computer simulation *Journal of Theoretical Biology*, **81**, 745–759. [7.1]
- Hoofd, L., Z. Turek, K. Kubat, B.E.M. Ringnalda and S. Kazda (1985) Variability of inter-capillary distance estimated on histological sections of rat heart *Advances in Experimental Medicine and Biology*, **191**, 239–247. [1.2, 7.1]
- Horálek, V. (1988) A note on the time-non-homogeneous Johnson-Mehl tessellation *Advances in Applied Probability*, **20**, 684–685. [5.8]
- Horálek, V. (1989) The Johnson–Mehl tessellation with time dependent nucleation intensity in view of basic 3-d tessellations *Mathematical Research*, **51**, 111–116. [5.8]
- Horálek, V. (1990). On ASTM grain-size model and related random tessellation models *Metallography*, **25**, 263–284. [5.8]
- Hori, H. and M. Nagata (1985) Examples of optimization methods for environment monitoring systems *Report, B-266-R-53-2*, Environmental Sciences, Ministry of Education, Japan, 18–29 [in Japanese]. [9.2.5]
- Horizoe, M., R. Itoh and K. Gotoh (1995) Uniform dispersion of fine particles in a magnetic fluid and its evaluation *Advanced Powder Technology*, **6**(2), 139–148. [8.1.1]
- Horspool, R.N. (1979) Constructing the Voronoi diagram in the plane *Technical Report, SOCS 79.12*, McGill University. [4.1]
- Horton, R.E. (1917) Rational study of rainfall data makes possible better estimates of water yield *Engineering News-Record*, **79**, 211–213. [1.2, 6.1.1]
- Hoschek, J. (1985) Offset curves in the plane *Computer-Aided Design*, **17**, 77–82. [3.5.5]
- Hotelling, H. (1929) Stability in competition *Economic Journal*, **39**, 41–57. [7.3.1]
- Howard, C.D. and C.M. Newman (1997) Euclidean models of first-passage percolation *Probability Theory and Related Fields*, **108**, 153–170. [5.3, 5.6.4]
- Hsu, C.S. and A.J. Rahman (1979a) Crystal nucleation and growth in liquid rubidium *Journal of Chemical Physics*, **70**(11), 5234–5240. [7.1]

- Hsu, C.S. and A.J. Rahman (1979b) Interaction potentials and their effect on crystal nucleation and symmetry *Journal of Chemical Physics*, **71**(12), 4974–4986. [7.1]
- Hsu, T.-J. and C-Y. Mou (1992) Molecular dynamics of liquid-solid transition of dense Lennard-Jones liquid *Molecular Physics*, **75**(6), 1329–1344. [7.1]
- Hubbard, R. (1970) The spatial pattern and market areas of urban settlement in Jamaica *University of the West Indies, Department of Geography, Research Notes*, **1**. [3.1.6]
- Huff, D.L. (1963) A probabilistic analysis of shopping center trade area *Land Economics*, **39**, 81–90. [9.2.8]
- Huff, D.L. (1973) The delineation of a national system of planning regions on the basis of urban spheres of influence *Regional Studies*, **7**, 323–329. [3.1.6]
- Huff, D.L. and C.F. Jenks (1968) A graphic interpretation of the friction of distance in gravity models *Annals, Association of American Geographers*, **58**, 814–824. [3.1.6]
- Huff, D.L. and J.M. Lutz (1979) Ireland's urban hierarchy *Economic Geography*, **55**, 196–212. [3.1.6]
- Hutchings, M.J. and R.J. Discombe (1986) The detection of spatial pattern in plant populations *Journal of Biogeography*, **13**, 225–236. [5.4, 5.12, 8.1.1, 8.2]
- Hutchings, M.J. and S. Waite (1985) Cohort behaviour and environmental determination of life histories within a natural population of *Plantago coronopus* L. In: J. Haeck and J.W. Woldendorp (eds) *Structure and Functioning of Plant Populations* 2 Amsterdam: North-Holland. [7.1]
- Huttenlocher, D.P., K. Kedem and J.M. Kleinberg (1992a) Voronoi diagrams of rigidly moving sets of points *Information Processing Letters*, **43**(4), 217–223. [3.9.1, 4.1]
- Huttenlocher, D.P., K. Kedem and J.M. Kleinberg (1992b) On dynamic Voronoi diagrams and the minimum Hausdorff distance for point sets under Euclidean motion in the plane *Proceedings of the Eighth Annual Symposium on Computational Geometry, June 10–12, 1992, Berlin, Germany*, 110–119. [3.9.2]
- Huttenlocher, D.P., K. Kedem and M Sharir (1993) The upper envelope of Voronoi surfaces and its application *Discrete and Computational Geometry*, **9**(3), 267–291. [2.1, 3.3.3]
- Hwang, T.Y. (1979) Decoding linear block codes for minimizing word error rate *IEEE Transactions on Information Theory*, **IT-25**(6), 733–737. [3.7.1, 3.7.11, 4.8]
- Hyman, G.M. and L.D. Mayhew (1983) On the geometry of emergency service medical provision in cities *Environment and Planning A*, **15**, 1669–1690. [3.7.11]
- Hyson, C.D. and W.P. Hyson (1950) The economic law of market areas *Quarterly Journal of Economics*, **64**, 319–327. [3.1.6]
- Ichino, M. and J. Sklansky (1985) The relative neighborhood graph for mixed feature variables *Pattern Recognition*, **18**(2), 161–167. [2.5]
- Icke, V. and R. van de Weygaert (1987) Fragmenting the universe. I Statistics of two-dimensional Voronoi foams *Astronomy and Astrophysics*, **184**, 16–32. [1.2, 2.1, 5.3, 5.4, 5.5.4, 5.12, 7.2]
- Icke, V. and R. van de Weygaert (1991) The galaxy distribution as a Voronoi foam *Quarterly Journal of the Royal Astronomical Society*, **32**(2), 85–112. [Foreward, 7.2]
- Icking, C., R. Klein, N-M. Le and L. Ma (1995) Convex distance functions in 3-space are different *Fundamenta Informaticae*, **22**(4), 331–352. [3.7.2]
- Ikeuchi, S. and E.L. Turner (1991) Quasi-periodic structures in the large scale galaxy distribution and three-dimensional Voronoi tessellation *Monthly Notices of the Royal Astronomical Society*, **250**, 519–522. [5.3, 7.2]
- Ilg, M. (1990) Knowledge-based interpretation of road maps *Proceedings of the 4th International Symposium on Spatial Data Handling, Zurich*, 25–34. [3.5.5]
- Illeris, S. (1967) Funktionelle regioner i Danmark omkring 1960 *Geografisk Tidsskrift*, **66**, 225–251. (English translation reprinted in B.J.L. Berry and F.E. Horton (eds) *Geographic Perspectives on Urban Systems with Integrated Readings* Englewood Cliffs: Prentice-Hall, 200–207. [3.1.6]
- Imai, H and K. Imai (1990) Voronoi diagrams for moving points *Proceedings of International Computer Symposium, Hsinchu, Taiwan*, 600–606. [3.9.1]
- Imai, H., M. Iri and K. Murota (1985) Voronoi diagram in the Laguerre geometry and its applications *SIAM Journal of Computing*, **14**(1), 93–105. [3.1.4, 3.1.5, 3.4.1, 3.5, 3.5.3, 3.7.10, 4.8]

- Imai, K. and H. Imai (1993a) On weighted dynamic Voronoi diagrams *The 6th Karuizawa Workshop on Circuits and Systems*, 103–108. [3.9.1]
- Imai, K. and H. Imai (1993b) Higher-order dynamic Voronoi diagrams and its applications *Transactions of the Information Processing Society of Japan*, **34**(12), 2458–2463. [3.9.1]
- Imai, K. and H. Imai (1998) Dynamic weighted Voronoi diagrams and weighted minimax matching of two corresponding point sets. *Optimization Methods and Software*, **10**(12), 261–274. [3.9.1, 3.9.2]
- Imai, K., S. Sumino and H. Imai (1989) Minimax geometric fitting of two corresponding sets of points *Proceedings of the 5th Annual ACM Symposium on Computational Geometry*, 266–275. [3.3.3, 3.9.2]
- Imai, K., S. Sumino and H. Imai (1998) Minimax geometric fitting of two corresponding sets of points and dynamic furthest Voronoi diagrams *IEICE Transactions on Information and Systems*, **E81-D(11)**, 1161–1171. [3.7.2, 3.9.2]
- Imai, T. (1996) A topology-oriented algorithm for the Voronoi diagram of polygons. *Canadian Conference on Computational Geometry. CCCG '96, Proceedings of the 8th Canadian Conference on Computational Geometry*, 107–112. [3.5.4]
- Imai, T. and K. Sugihara (1994) A failure-free algorithm for constructing Voronoi diagrams of line segments *Transactions of the Information Processing Society of Japan*, **35**(10), 1966–1977. [4.8]
- Inaba, M., N. Katoh and H. Imai (1994) Applications of weighted Voronoi diagrams and randomization to variance-based k -clustering *Proceedings of the 10th Annual Symposium on Computational Geometry, June 6–8, 1994, Stony Brook, N.Y.*, 332–339 [3.1.6]
- Inagaki, H., N. Sugie and K. Sugihara (1992) Numerically robust incremental algorithm for constructing three-dimensional Voronoi diagrams *Proceedings of the 4th Canadian Conference on Computational Geometry*, 334–339. [4.6, 4.7]
- Ip, H.H.S. and B.W.C. Lam (1995) Three dimensional structural texture modeling and segmentation *Pattern Recognition*, **29**, 1299–1319. [3.6.2]
- Iri, M. and T. Koshizuka (eds) (1986) *Computational Geometry and Geographical Information Processing* Tokyo: Kyoritsu [in Japanese]. [1.0, 3.8.1]
- Iri, M., K. Murota and T. Ohya (1984) A fast Voronoi-diagram algorithm with applications to geographical optimization problems. In: P. Throft-Christensen (ed) *Lecture Notes in Control and Information Science System*, **59** (Modelling and Optimization, Proceedings of the 11th IFIP Conference Copenhagen) Berlin: Springer-Verlag, 273–288 [9.2, 9.2.1]
- Isaac, F.E. and L.R. Wyatt (1997) Segmentation of high-frequency radar-measured directional wave spectra using the Voronoi diagram *Journal of Atmospheric and Oceanic Technology*, **14**, 950–959. [8.6]
- Itoh, R., M. Horizoe and K. Gotoh (1995) A method for measuring two-dimensional dispersed state of particles *Advanced Powder Technology*, **6** (2), 81–89. [8.1.1]
- Itzykson, C. and J.-M. Drouffe (1989) *Statistical Field Theory. Volume 2. Strong Coupling, Monte Carlo Methods, Conformal Field Theory, and Random Systems* Cambridge: Cambridge University Press. [5.3, 5.5.4]
- Jack, W.H. (1967) Single tree sampling in even-aged plantations for survey and experimentation *International Union of Forestry Research Organisations, XIV. IUFRO-Kongress, Munchen, Papers VI*, Section 25, 379–403. [1.2, 7.1]
- Jackson, J.L. (1974) Stochastic generation of regular distributions: some analytical results *Science*, **183**, 445–446. [5.8]
- Jafferali, R., N.M. Jackson, D.J. Bell and G.A. Davies (1996) Analysis of the structure of porous polymeric membranes *Zeitschrift für Angewandte Mathematik und Mechanik*, **76**(Supplement 3), 351–353. [5.12]
- Janke, W., M. Katoot and R. Villanova (1993) Ising model universality for two-dimensional lattices *Physics Letters B*, **315**, 412–416. [5.3]
- Janke, W., M. Katoot and R. Villanova (1994a) Single-cluster Monte Carlo study of the Ising model on two-dimensional random lattices *Physical Review B*, **49**(14), 9644–9657. [5.3, 5.4]
- Janke, W., M. Katoot and R. Villanova (1994b) Ising model on 2D random lattices *Nuclear Physics Section B*, (Proceedings Supplements), **34**, 698–701. [5.3]

- Janke, W. and R. Villanova (1995) Two-dimensional eight-state Potts model on random lattices: a Monte Carlo study *Physics Letters A*, **209**, 179–183. [5.3]
- Jaromczyk, J.W. and M. Kowaluk (1987) A note on relative neighborhood graphs *Proceedings of the Third Annual Symposium on Computational Geometry (Waterloo, Canada)*, June 8–10, 233–241. [2.5]
- Jaromczyk, J.W. and M. Kowaluk (1991) Constructing the relative neighborhood graph in 3-dimensional Euclidean space *Discrete Applied Mathematics*, **31**, 181–192. [2.5]
- Jaromczyk, J.W. and G.T. Toussaint (1992) Relative neighborhood graphs and their relatives *Proceedings of the IEEE*, **80**(9), 1502–1517. [2.5, 8.4]
- Jarvis, R.A. (1977) Computing the shape hull of points in the plane *Proceedings of the IEEE Computing Society Conference on Pattern Recognition and Image Processing*, 231–241. [8.4.2]
- Jennings, E. and A. Lingas (1992) On the relationship among constrained geometric structures *Lecture Notes in Computer Science*, **650** Berlin: Springer-Verlag, 289–298. [2.5, 6.5]
- Jcong, C.S. (1991) Parallel Voronoi diagram in L_1 (L_∞) metric on a mesh connected computer *Parallel Computing*, **17**(2–3), 241–252. [3.7.1, 4.1, 4.8]
- Jerauld, G.R., J.C. Hatfield and H.T. Davis (1984a) Percolation and conduction on Voronoi and triangular networks: a case study in topological disorder *Journal of Physics C: Solid State Physics (London)*, **17**(9), 1519–1529. [5.3, 5.6.4, 7.1]
- Jerauld, G.R., L.E. Scriven and H.T. Davis (1984b) Percolation and conduction on the 3D Voronoi and regular networks: a second case study in topological disorder *Journal of Physics C: Solid State Physics (London)*, **17**(19), 3429–3439. [5.3, 5.4, 5.6.4]
- Jian-ming, Z., S. Ke-ran, Z. Ke-ding and Z. Qiong-hua (1990) Computing constrained triangulation and Delaunay triangulation: a new algorithm *IEEE Transactions on Magnetics*, **26**, 649–697. [3.4.3]
- Joe, B. (1986) Delaunay triangular meshes in convex polygons *SIAM Journal on Scientific and Statistical Computing*, **7**(2), 514–539. [6.2]
- Joe, B. (1989) Three dimensional triangulations from local transformations *SIAM Journal on Scientific and Statistical Computing*, **10**, 718–741. [2.4, 6.5.2]
- Joe, B. (1991a) Construction of three dimensional triangulations using local transformations *Computer Aided Geometric Design*, **8**, 123–142. [2.2, 2.4, 4.7, 6.5.2]
- Joe, B. (1991b) Delaunay versus max-min solid angle triangulations for three-dimensional mesh generation *International Journal for Numerical Methods in Engineering*, **31**, 987–997. [6.5.2]
- Joe, B. (1993) Construction of k -dimensional Delaunay triangulations using local transformations *SIAM Journal on Scientific Computing*, **14**(6), 1415–1436. [2.2]
- Joe, B. (1995a) Construction of three-dimensional improved quality triangulations using local transformations *SIAM Journal on Scientific Computing*, **16**(6), 1292–1307. [2.2, 2.4, 6.5.2]
- Joe, B. (1995b) Quadrilateral mesh generation in polynomial regions *Computer-Aided Design*, **27**(3), 209–222. [6.5]
- Joe, B. and A.C. Wang (1993) Duality of constrained Voronoi diagrams and Delaunay triangulations *Algorithmica*, **9**(2), 142–155. [3.4.2, 3.4.3]
- Johnson, S.C. (1967) Hierarchical clustering schemes *Psychometrika*, **32**(3), 241–254. [2.5]
- Johnson, W.A. and R.F. Mehl (1939) Reaction kinetics in processes of nucleation and growth *Transactions of the American Institute of Mining, Metallurgical and Petroleum Engineers*, **135**, 410–458. [3.1.6, 5.8]
- Jones, K.G. and D.R. Mock (1984) Evaluating retail trading performance. In: R.L. Davies and D.S. Rogers (eds) *Store Location and Store Assessment Research* New York: John Wiley, 333–360. [7.1]
- Jones, K. and J. Simmons (1987) *Location, Location, Location. Analyzing the Retail Environment* Toronto: Methuen. [7.1]
- Jones, M. (1991) A non-uniqueness theorem on the theory of Voronoi sets *International Journal of Mathematics and Mathematical Science*, **14**(4), 817–820. [3.6.1]
- Jones, T.A. (1989) The three faces of geological computer contouring *Mathematical Geology*, **21**(3), 271–283. [6.2]
- Jones, T.A., D.E. Hamilton and C.R. Johnson (1986) *Contouring Geologic Surfaces with the Computer* New York: Van Nostrand Reinhold. [6.2]

- Jund, P., D. Caprion and R. Jullien (1997) Local investigation of the glass transition: molecular dynamics and Voronoï tessellation *Europhysics Letters*, **37**(8), 547–552. [7.1]
- Jünger, M., G. Reinelt and D. Zepf (1991) Computing correct Delaunay triangulations *Computing*, **47**, 43–49. [2.2, 4.1]
- Kaler, E.W. and S. Prager (1982) A model of dynamic scattering by microemulsions *Journal of Colloid and Interface Science*, **86**(2), 359–369. [5.3]
- Kallenberg, O. (1983) *Random Measures* (3rd edition, revised and enlarged) London: Academic Press. [1.3.3]
- Kanaganathan, S. and N.B. Goldstein (1991) Comparison of 4-point adding algorithms for Delaunay-type 3-dimensional mesh generators *IEEE Transactions on Magnetics*, **27**(3), 3444–3451. [6.5.2]
- Kantabutra, V. (1983) Traveling salesman cycles are not always subgraphs of Voronoi duals *Information Processing Letters*, **16**(1), 11–12. [2.5, 8.4.2]
- Kao, T.C. and D.M. Mount (1991) An algorithm for computing compacted Voronoi diagrams defined by convex distance functions *Proceedings of the Third Canadian Conference on Computational Geometry (Simon Fraser University)*, 104–109. [4.8]
- Karamete, B.K., T. Tokdemir and M. Ger (1997) Unstructured grid generation and a simple triangulation algorithm for arbitrary 2-D geometries using object oriented programming *International Journal for Numerical Methods in Engineering*, **40**, 251–268. [6.5.1]
- Karlin, S. (1969) *A First Course in Stochastic Processes* New York: Academic Press. [1.3, 1.3.3]
- Kartashov, A. and R. Folk (1995) Delaunay triangulations in the plane with $O(N^{1/2} \log N)$ storage requirements *International Journal of Modern Physics C*, **6**(5), 639–649. [4.1]
- Katajainen, J. (1988) The region approach for computing relative neighbourhood graphs in the L_p metric *Computing*, **40**, 147–161. [2.5]
- Katajainen, J. and M. Koppinen (1988) Constructing Delaunay triangulations by merging buckets in quadtree order *Fundamental Informatica*, **11**, 275–288. [4.1, 4.4]
- Katajainen, J. and O. Nevalainen (1986) Computing relative neighborhood graphs in the plane *Pattern Recognition*, **19**(3), 221–228. [2.5]
- Kawashima, M., R. Tokunaga and Y. Hirai (1994) Fast algorithm for parallel contour map information processing by using Voronoi diagram and inverse square field *Transactions of the Institute of Electronics, Information and Communication Engineers D-II*, **J77D-II**(7), 1219–1225. [3.5.5]
- Kayser, K., K. Sandau, J. Paul and G. Weisse (1992) An approach based on two-dimensional graph theory for structural cluster detection and its histopathological application *Journal of Microscopy*, **165**(2), 281–288. [2.5]
- Kayser, K. and H. Stute (1989) Minimum spanning tree, Voronoi's tessellation and Johnson–Mehl diagrams in human lung carcinoma *Pathology, Research and Practice*, **185**(5), 729–734. [2.5, 5.8, 7.1]
- Kedem, K. and M. Sharir (1985) An efficient algorithm for planning collision-free translational motion of a convex polygonal object in 2-dimensional space amidst polygonal objects *Journal of the Association for Computing Machinery*, 75–80. [3.6.2, 3.7.11]
- Keeney, R.L. (1972) A method for districting among facilities *Operations Research*, **20**, 613–618. [3.2.3, 3.3.3, 7.1]
- Keil, J.M. and C.A. Gutwin (1989) The Delaunay triangulation closely approximates the complete Euclidean graph *Proceedings of the First Workshop on Algorithms and Data Structures*, 47–56. [2.4, 6.2]
- Kendall, D.G. (1981) The statistics of shape. In: V. Barnett (ed) *Interpreting Multivariate Data* Chichester: John Wiley. [5.11]
- Kendall, D.G. (1983) The shape of Poisson–Delaunay triangles. In: M.C. Demetrescu and M. Iosifescu (eds) *Studies in Probability and Related Topics* Montreal: Nagard, 321–330. [5.4, 5.11]
- Kendall, D.G. (1988) Delone simplexes in many dimensions Paper presented at 18th EMS, Berlin, DDR, 24 August 1988. [5.4]
- Kendall, D.G. (1989) A survey of the statistical theory of shape *Statistical Science*, **4**(2), 87–120. [5.4, 5.11, 8.2]
- Kendall, D.G. (1990) Random Delaunay simplexes in \mathbb{R}^m *Journal of Statistical Planning and Inference*, **25**, 225–234. [5.4]

- Kenkel, N.C. (1990) Spatial competition models for plant populations *Coenoses*, **5**(3), 149–158. [5.8, 7.1]
- Kenkel, N.C. (1991) A weighted tessellation model for studying [sic] plant population dynamics *Coenoses*, **6**(3), 143–149. [7.1]
- Kenkel, N.C., J.A. Hoskins and W.D. Hoskins (1989) Local competition in a naturally established jack pine stand *Canadian Journal of Botany*, **67**, 2630–2635. [5.4, 7.1]
- Kermode, J. and D. Weaire (1990) 2D-FROTH: a program for the investigation of 2-dimensional froths *Computer Physics Communications*, **60**, 75–109. [1.2 5.3 5.12]
- Kerstein, A.R. (1983) Equivalence of the void percolation problem for overlapping spheres and a network problem *Journal of Physics A: Mathematical and General*, **16**, 3071–3075. [5.3 7.1]
- Khachian, L.G. (1979) A polynomial algorithm in linear programming *Doklady Akademii Nauk SSSR*, **244**, 1093–1096. [2.6.1]
- Khachian, L.G. (1980) Polynomial algorithms in linear programming *USSR Computational Mathematics and Mathematical Physics*, **20**, 53–72. [2.6.1, 4.6.2]
- Kiang, T. (1966) Random fragmentation in two and three dimensions *Zeitschrift für Astrophysik*, **64**, 433–439. [5.4, 5.5.4]
- Kim, D-S., I-K. Hwang and B-J. Park (1995) Representing the Voronoi diagram of a simple polygon using rational quadratic Bezier curves *Computer-Aided Design*, **27**(8), 605–614. [3.5.2]
- Kimura, M. and F. Yonezawa (1984) Nature of amorphous and liquid structures – computer simulations and statistical geometry *Journal of Non-Crystalline Solids*, **61&62**, 535–540. [7.1]
- King, L.J. (1984) *Central Place Theory* Scientific Geography Series, **1**, Beverly Hills: Sage Publications. [7.1]
- Kingman, J.F.C. (1993) *Poisson Processes* Oxford: Oxford University Press. [1.3.3]
- Kirkpatrick, D.G. (1979) Efficient computation of continuous skeletons *Proceedings of the 20th Annual IEEE Symposium on Foundations of Computer Science*, 18–27. [3.5, 3.5.4]
- Kirkpatrick, D.G. (1980) A note on Delaunay and optimal triangulations *Information Processing Letters*, **10**(3), 127–128. [2.4, 6.2]
- Kirkpatrick, D.G. and J.D. Radke (1985) A framework for computational morphology. In: G.T. Toussaint (ed) *Computational Geometry* Amsterdam: Elsevier Science B.V., 217–248. [8.4, 8.4.1, 8.4.2]
- Kishimoto, K. (1978) An algorithm for the optimal triangulation *Information Processing*, **19**, 211–218 [in Japanese]. [2.4]
- Klec, V. (1980) On the complexity of d -dimensional Voronoi diagrams *Archiv de Mathematik*, **34**, 75–80. [2.3, 4.7]
- Klein, R. (1988) Abstract Voronoi diagrams and their applications *Lecture Notes in Computer Science*, **333** (International Workshop on Computational Geometry, Wurzburg, March 1988) Berlin: Springer-Verlag, 148–157. [3.0, 3.7.3, 3.7.8, 4.8]
- Klein, R. (1989) Concrete and abstract Voronoi diagrams *Lecture Notes in Computer Science*, **400** Berlin: Springer-Verlag [3.0, 3.7.3, 4.8]
- Klein, R. and D. Cohen-Or (1997) Incremental view-dependent multiresolution triangulation of terrain *Proceedings of the 5th Pacific Conference on Computational Geometry and Applications*, Seoul, 127–136. [6.5]
- Klein, R. and A. Lingas (1992) Manhattan proximity in a simple polygon *International Journal of Computational Geometry and Applications*, **5**(1–2), 53–74. [3.4.2, 3.4.4]
- Klein, R. and A. Lingas (1993) A linear-time randomized algorithm for the bounded Voronoi diagram of a simple polygon *Proceedings of the 9th Annual ACM Symposium on Computational Geometry*, 124–132. [3.4.4]
- Klein, R. and A. Lingas (1995) Fast skeleton construction *Lecture Notes in Computer Science*, **979** (Proceedings of the Third Annual European Symposium) Berlin: Springer-Verlag, 582–595. [3.5.4]
- Klein, R., K. Melhorn and S. Meiser (1990) On the construction of abstract Voronoi diagrams II. In: T. Asano, T.I. Doraki, H. Imai and T. Nishizeki (eds) *Proceedings of the International Symposium SIGAL '90*, 138–154. [4.8]
- Klein, R., K. Mehlhorn and S. Meiser (1993) Randomized incremental construction of abstract Voronoi diagrams *Computational Geometry*, **3**, 157–184. [4.8]

- Klein, R. and D. Wood (1988) Voronoi diagrams based on general metrics in the plane *Proceedings of the 5th Annual Symposium on Theoretical Aspects of Computer Science, Bordeaux, February 1988, Lecture Notes in Computer Science, 294* Berlin: Springer-Verlag, 281–291. [3.7.8, 4.8]
- Kleinsteuer, C. and J.T. Holderman (1980) A triangular finite element mesh generation for fluid dynamic systems of arbitrary geometry *International Journal for Numerical Methods in Engineering*, **15**, 1325–1334. [6.2, 6.3]
- Knuth, D.E. (1968) *The Art of Computer Programming: Volume I Fundamental Algorithms* Reading: Addison-Wesley. [1.3, 1.3.4]
- Knuth, D.E. (1973) *The Art of Computer Programming: Volume III Sorting and Searching* Reading: Addison-Wesley. [2.3, 4.4]
- Kobayashi, J. (1983) Road Distance and the Euclidean Distance. Master's Thesis, University of Tsukuba [in Japanese]. [9.2.1]
- Kobayashi, S., K. Maeda and S. Takeuchi (1980) Computer simulation of atomic structure of Cu₅₇Zr₄₃ amorphous alloy *Journal of the Physical Society of Japan*, **48**(4), 1147–1152. [7.1]
- Koch, R.A. (1974) Zur Frage der quantitativen Klüfterklassierung von saulig absonderndem Eruptivgestein (Nephelinbasalt von Stolzenberg) *Abhandlungen des Staatlichen Museums für Mineralogie und Geologie zu Dresden*, **21**, 1–37. [9.5.1]
- Koken, E., N. Chandrasekaran, J.D. Embury and G. Berger (1988) The role of particle distribution in recrystallization in two-phase alloys *Materials Science and Engineering*, **A104**, 163–168. [7.1]
- Kokubo, I. (1985) Computational Methods of Generalized Voronoi Diagrams. Master's Thesis, Department of Mathematical Engineering and Information Physics, University of Tokyo [in Japanese]. [3.5, 4.8]
- Kolars, J.F. and J.D. Nyquist (1974) *Human Geography* New York: McGraw-Hill. [2.5]
- Kolmogorov, A.N. (1937) On statistical theory of metal crystallization *Izvestia Akademii Nauk SSSR, Seria Matematicheskaya*, **3**, 355–360. [5.8]
- Konno, H. and H. Yamashita (1978) *Nonlinear Programming Methods* Tokyo: Nikka Giken [in Japanese]. [9.1]
- Kopec, R.J. (1963) An alternative method for the construction of Thiessen polygons *The Professional Geographer*, **15**, 24–26. [1.2]
- Korobov, A. (1994) A geometric-probabilistic approach to heterogeneous chemical kinetics with respect to the IKP ambiguity *Thermochimica Acta*, **243**, 79–93. [5.8]
- Korobov, A. (1996) Solid-phase reaction kinetics: towards deeper insight through a discrete description *Heterogeneous Chemistry Reviews*, **3**, 477–497. [5.8]
- Koshizuka, T. and J. Kobayashi (1983) Road distances and straight line distances *Papers of the Annual Conference of the City Planning Institute of Japan*, **18**, 43–48 [in Japanese]. [9.2.1]
- Koshizuka, T. and O. Kurita (1986) A theoretical study on the role of a circular part of radial-circular networks *Papers of the Annual Conference of the City Planning Institute of Japan*, **21**, 217–222 [in Japanese]. [3.7.3, 4.8]
- Kramer, P. and M. Schlotmann (1989) Dualisation of Voronoi domains and Klotz construction: a general method for the generation of proper space fillings *Journal of Physics A: Mathematics and General*, **22**, L1097–L1102. [7.1]
- Krawietz, R. and U. Lorz (1991) Stereological model tests for the spatial Poisson-Voronoi tessellation: I *Acta Stereologica*, **10**(2), 203–212. [5.12, 8.1.1]
- Kreps, D.M. and R. Wilson (1982) Reputation and imperfect information *Journal of Economic Theory*, **27**, 253–279. [7.4]
- Krishnamurthy, V., W. Brostow and J.S. Sochanski (1988) Representation of properties of materials by Voronoi polyhedra *Materials Chemistry and Physics*, **20**, 451–469. [7.1]
- Krozel, J. and D. Andrisanu II (1989) Navigation path planning for autonomous aircraft: Voronoi diagram approach *Journal of Guidance, Control, and Dynamics*, **13**(6), 1152–1154. [3, 6.2]
- Kübler, O., F. Klein, R. Ogniewicz and U. Kienholz (1990) Isolation and identification of abutting and overlapping objects in binary images *Proceedings of the 5th International Conference on Image Analysis and Processing. Progress in Image Analysis and Processing*, 340–347. [3.5.5]

- Kuhn, H.W.(1974) Steiner's problem revisited. In: G.B. Dantzig and B.C. Evans (eds) *Studies in Optimization*, **10**, 52–70. [9.3.3]
- Kumar, S. and S.K. Kurtz (1993) Properties of a two-dimensional Poisson–Voronoi tessellation: a Monte-Carlo study *Materials Charaterization*, **31**, 55–68. [5.4, 5.5.2, 5.5.3, 5.5.4, 5.7]
- Kumar, S. and S.K. Kurtz (1994a) Simulation of material microstructure using a 3D Voronoi tessellation: calculation of effective thermal-expansion coefficient of polycrystalline materials *Acta Metallurgica et Materialia*, **42**(12), 3917–3927. [5.3]
- Kumar, S. and S.K. Kurtz (1994b) A Monte-Carlo study of size and angular properties of a three-dimensional Poisson–Delaunay cell *Journal of Statistical Physics*, **75**(3), 735–747. [5.4, 5.11]
- Kumar, S. and S.K. Kurtz (1995) Monte-Carlo study of angular and edge length distribution in a three-dimensional Poisson–Voronoi tessellation *Materials Characterization*, **34**, 15–27. [5.4, 5.5.2]
- Kumar, S., S.K. Kurtz, J.R. Banavar and M.G. Sharma (1992) Properties of a three-dimensional Poisson–Voronoi tessellation: a Monte Carlo study *Journal of Statistical Physics*, **67**(3), 523–551. [5.4, 5.5.2, 5.5.3, 5.5.4]
- Kumar, S., S.K. Kurtz and M. Cieplak (1997) Topological disorder in cellular microstructures *Philosophical Magazine B*, **75**(5), 669–679. [5.12, 7.1]
- Kumar, S., S.K. Kurtz and D. Weaire (1994) Average number of sides for the neighbours in a Poisson–Voronoi tessellation *Philosophical Magazine B*, **69**(2), 431–435. [5.5.3]
- Kumar, S. and R.N. Singh (1995) Thermal conductivity of polycrystalline materials *Journal of the American Ceramic Society*, **78**(3), 728–736. [5.3]
- Kumler, M.P. (1994) An intensive comparison of triangulated irregular networks (TINs) and digital elevation models (DEMs) Monograph 45 *Cartographica*, **31**(2), 1–99. [6.2]
- Kuroda, K. and H. Tanemura (1992) Limit theorem and large deviation principle for the Voronoi tessellation generated by a Gibbs point process *Advances in Probability*, **24**, 103–128. [5.12]
- Lam, N. S-N. (1983) Spatial interpolation methods: a review *The American Cartographer*, **10**(2), 129–149. [6.0]
- Lam, S.W.C. and H.H.S. Ip (1994) Structural texture segmentation using irregular pyramid *Pattern Recognition Letters*, **15**, 691–698 [3, 6.2]
- Lambregts, C.A.H., F.L.M. Delbressine, W.A.H. de Vries and A.C.H. van der Wolf (1996) An efficient automatic tool path generator for 2½D free-form pockets *Computers in Industry*, **29**, 151–157. [3.5.5]
- Landau, H.J. (1971) How does a porcupine separate its quills? *IEEE Transactions on Information Theory*, **IT-17**(2), 157–161. [7.1]
- Lang, R.J. (1996) A computational algorithm for origami design *Proceedings of the 12th ACM Symposium on Computational Geometry*, 98–105. [3.5.5]
- Lantuejoul, C. (1980) Skeletonization in quantitative metallography. In: R.M. Haralick and J.C. Simon (eds) *Issues in Digital Image Processing* Alphen aan der Rijn: Sijthoff and Noordhoff, 107–135. [7.1]
- Lantuejoul, C. and F. Maisonneuve (1984) Geodesic methods in quantitative image analysis *Pattern Recognition*, **17**, 177–187. [3.5.5]
- Lasser, D. and T. Stuttgen (1996) Boundary improvement of piecewise linear interpolants defined over Delaunay triangulations *Computers and Mathematics with Applications*, **32**(10), 430–458. [6.3]
- Latombe, J.-C. (1991) *Robot Motion Planning* Boston: Kluwer Academic Publishers. [3.6.2]
- Launhardt, W. (1882) Die Bestimmung des zweckmässigsten Standortes einer gewerblichen Anlage *Zeitschrift des Deutscher Ingenieure*, **26**, 768. [3.1.6, 9.2]
- Lauritsen, K.B., C. Moukarzel and H.J. Herrmann (1993) Statistical laws and mechanics of Voronoi random lattices *Journal de Physique I France*, **3**(9), 1941–1951. [5.3]
- Lavender, D., A. Bowyer, J. Davenport, A. Wallis and J. Woodwork (1992) Voronoi diagrams of set-theoretic solid models *IEEE Computer Graphics and Applications*, **12**(5), 69–77. [3.0, 3.5.4]
- Laves, F. (1930) Ebeneneinteilung in Wirkungsbereich *Zeitschrift für Kristallographie*, **76**, 277–284. [7.1]

- Laves, F. (1931) Ebeneneinteilung und Koordinationszahl *Zeitschrift für Kristallographie*, **78**, 208. [7.1]
- Laves, F. (1967) Space limitations on the geometry of the crystal structures of metals and intermetallic compounds. In: P.S. Rudman, J. Stringer and R.I. Jaffee (eds) *Phase Stability in Metals and Alloys* New York: McGraw-Hill, 85–99. [7.1]
- Lawson, C.L. (1977) Software for C^1 surface interpolation. In: J. Rice (ed) *Mathematical Software III* New York: Academic Press, 161–194. [2.4, 4.1, 6.2]
- Lê, N.-M. (1996) On Voronoi diagrams in the L_p metric in \mathbb{R}^d *Discrete and Computational Geometry*, **16**(2), 177–196. [3.7.1]
- Lê, V.B. and D.T. Lee (1991) Out-of-roundness problem revisited *IEEE Transactions on Pattern Analysis and Machine Intelligence*, **13**(3), 217–223. [3.3.3]
- Leamer, E.E. (1968) Locational equilibria *Journal of Regional Science*, **8**(2), 229–242. [9.2]
- Lebel, T., G. Bastin, C. Obled and J.D. Creutin (1987) On the accuracy of areal rainfall estimation: a case study *Water Resources Research*, **23**(11), 2123–2134. [9.2.5]
- Le Caër, G. and R. Delannay (1993a) Correlations in topological models of 2D random cellular structures *Journal of Physics A: Mathematical and General*, **26**, 3931–3954. [5.5.3]
- Le Caër, G. and R. Delannay (1993b) The administrative divisions of mainland France as 2D random cellular structures *Journal de Physique, I France*, **3**, 1777–1800. [5.5.3, 8.1.1]
- Le Caër, G. and J.S. Ho (1990) The Voronoi tessellation generated from eigenvalues of complex random matrices *Journal of Physics A: Mathematical and General*, **23**, 3279–3295. [5.4, 5.5.2, 5.5.3, 5.5.4, 5.12]
- Lechat, P., G. Le Mestre and D. Pele (1997) An approach for scene reconstruction from the analysis of a triplet of still images *Proceedings of the SPIE – The International Society for Optical Engineering (USA)*, **3023**, 169–179. [3.4.5]
- Lee, D.T. (1980) Two-dimensional Voronoi diagrams in the L_∞ -metric *Journal of the Association for Computing Machinery*, **27**, 604–618. [3.7.1, 4.8]
- Lee, D.T. (1982a) Medial axis transformation of a planar shape *IEEE Transactions on Pattern Analysis and Machine Intelligence*, **4**, 363–369. [3.5.4, 3.5.5, 4.8]
- Lee, D.T. (1982b) On k -nearest neighbor Voronoi diagrams in the plane *IEEE Transactions on Computers*, **C-31**(6), 478–487. [3.2, 3.2.1, 4.8]
- Lee, D.T. (1983) Visibility of a simple polygon *Computer Vision, Graphics, and Image Processing*, **22**, 207–211. [3.4.1, 4.8]
- Lee, D.T. and I.M. Chen (1985) Display of visible edges of a set of convex polygons. In: G.T. Toussaint (ed) *Computational Geometry* Amsterdam: North-Holland, 249–266. [3.4.1, 4.8]
- Lee, D.T. and R.L. Drysdale, III (1981) Generalization of Voronoi diagrams in the plane *SIAM Journal of Computing*, **10**, 73–87. [3.5, 3.5.3, 4.8]
- Lee, D.T. and A.K. Lin (1986) Generalized Delaunay triangulations for planar graphs *Discrete Computational Geometry*, **1**, 201–217. [2.4, 3.4.3, 4.8, 6.3]
- Lee, D.T. and F.P. Preparata (1984) Euclidean shortest paths in the presence of rectilinear barriers *Networks*, **14**, 393–410. [3.4.1]
- Lee, D.T. and B.J. Schachter (1980) Two algorithms for constructing the Delaunay triangulation *International Journal of Computer and Information Sciences*, **9**(3), 219–242. [2.4, 4.1, 4.4]
- Lee, D.T. and C.K. Wong (1980) Voronoi diagrams in L_1 (L_∞) metrics with 2-dimensional storage applications *SIAM Journal of Computing*, **9**, 200–211. [3.7.1, 3.7.11, 4.8]
- Lee, F. and R. Jou (1995) Efficient parallel geometric algorithms on a mesh of trees *Proceedings of the 33rd Annual Southeast Conference*, 213–218. [2.2]
- Lee, K. and S. Ghosh (1996) Small deformation multi-scale analysis of heterogeneous materials with the Voronoi cell finite element model and homogenization theory *Computational Materials Science*, **7**, 131–146. [6.5]
- Lefkovitch, L.P. (1984) A nonparametric method for comparing dissimilarity matrices, a general measure of biogeographical distance, and their applications *The American Naturalist*, **123**(4), 484–499. [2.5]
- Lefkovitch, L.P. (1985) Further nonparametric tests for comparing dissimilarity matrices based on the relative neighborhood graph *Mathematical Biosciences*, **73**, 71–88. [2.5]

- Lefkovitch, L.P. (1987) Species associations and conditional clustering: clustering with or without pairwise resemblances. In: P. Legendre and L. Legendre (eds) *Developments in Numerical Ecology* (NATO ASI Series, Vol. G14) New York: Springer-Verlag, 309–331. [2.5]
- Lemaître, J., A. Gervois, D. Bideau, J-P. Troadec and M. Ammi (1992) Distribution du nombres de côtés des cellules de mosaïques bidimensionnelles (Distribution of cell edges in two-dimensional mosaics) *Compte Rendus De l'academie Des Sciences, Paris, Serie II*, **315**(1), 35–38. [5.12]
- Lemaître, J., A. Gervois, J.P. Troadec, N. Rivier, M. Ammi, L. Oger and D. Bideau (1993) Arrangement of cells in Voronoi tessellations of monosize packing of discs *Philosophical Magazine B*, **67**(3), 347–362. [5.12 8.1.1]
- Lemaître, L., J.P. Troadec, A. Gervois and D. Bideau (1991) Experimental study of densification of disc assemblies *Europhysics Letters*, **14**(1), 77–83. [5.12]
- Lenstra, A. K. (1984) Polynomial factorization by root approximation *Lecture Notes in Computer Science*, **174** Berlin: Springer-Verlag, 272–276. [4.6.2]
- Lenz, R. (1979) Redundancy as an index of change in point pattern analysis *Geographical Analysis*, **11**, 374–388. [8.1.2]
- Leonyuk, N.I. and L.I. Mal'tseva (1980) Use of the Wulff–Delaunay method to assess the habitats of crystals *Soviet Physics – Crystallography*, **25**(5), 524–527. [7.2]
- Lesley, L.J.S. (1976) Optimum bus-stop spacing: part 1 *Traffic Engineering Control*, **17**, 399–401. [3.1.6, 9.2.7]
- Levcopoulos, C. and D. Krznaric (1996) Tight lower bounds for minimum weight triangulation heuristics *Information Processing Letters*, **57**, 129–135. [2.4]
- Levcopoulos, C. and A. Lingas (1989) There are planar graphs almost as good as the complete graphs and as short as minimum spanning trees. In: H. Djidjev (ed) *Lecture Notes in Computer Science: Optimal Algorithms*, **401** Berlin: Springer-Verlag, 9–13. [2.4, 6.2]
- Levcopoulos, C. and A. Lingas (1992) There are planar graphs almost as good as the complete graphs and almost as cheap as minimum spanning trees. *Algorithmica*, **8**, 251–256. [2.4]
- Leven, D. and M. Sharir (1987) Planning a purely translational motion for a convex polygonal object in two dimensional space using generalized Voronoi diagrams *Discrete and Computational Geometry*, **2**, 9–31. [3.0, 3.7.2, 3.7.11, 4.8]
- Lewis, B.A. and J.S. Robinson (1977) Triangulation of planar regions with applications *The Computer Journal*, **21**(4), 324–332. [6.2, 6.3]
- Lewis, F.T. (1928) The correlation between cell division and the shapes and sizes of prismatic cells in the epidermis of *Cucumis* *Anatomical Record*, **38**, 341–376. [5.5.2]
- Lewis, F.T. (1930) A volumetric study of growth and cell division in two types of epithelium – the longitudinally prismatic cells of *Tradescantia* and the radially prismatic epidermal cells of *Cucumis* *Anatomical Record*, **47**, 59–99. [5.5.2]
- Lewis, F.T. (1931) A comparison between the mosaic of polygons in a film of artificial emulsion and in cucumber epidermis and human amnion *Anatomical Record*, **50**, 235–265. [5.5.2, 5.5.3]
- Lewis, F.T. (1943) The geometry of growth and cell division in epithelial mosaics *American Journal of Botany*, **30**, 766–776. [5.5.2]
- Lewis, F.T. (1944) The geometry of growth and cell division in columnar parenchyma *American Journal of Botany*, **31**, 619–629. [5.5.2]
- Lewis, R.A. (1989) Determination of clefts in receptor structures *Journal of Computer-Aided Molecular Design*, **3**, 133–147. [7.1]
- Leymarie, F. and M.D. Levine (1992) Simulating the grass-fire transform using an active contour model *IEEE Transactions on Pattern Analysis and Machine Intelligence*, **PAMI14**(1), 56–75. [3.5.4]
- Li, Y.M. and M.A. Jabri (1992) A zero-skew clock routing scheme for VLSI circuits 1992 *IEEE/ACM International Conference on Computer-Aided Design. Digest of Technical Papers*, 458–463. [3.7.11]
- Liddle, M.J., C.S.J. Budd and M.J. Hutchings (1982) Population dynamics and neighbourhood effects in establishing swards of *Festuca rubra* *Oikos*, **38**, 52–59. [7.1]

- Lim, J.H.F. and G.A. Davies (1990) A stochastic model to simulate the growth of anchorage dependent cells on flat surfaces *Biotechnology and Bioengineering*, **36**, 547–562. [5.12]
- Lin, Z. and C. Lu (1996) *Limit Theory for Mixing Dependent Random Variables* Dordrecht: Kluwer Academic Publishers. [1.3.3]
- Lingas, A. (1986a) An approximation behaviour and implementation of the greedy triangulation for convex planar point sets *Proceedings of the 2nd Symposium of Computational Geometry, Yorktown Heights, New York*. [1.2, 6.2]
- Lingas, A. (1986b) The greedy and the Delaunay [sic] triangulations are not bad in the average case *Information Processing Letters*, **22**, 25–31. [1.2, 6.2]
- Lingas, A. (1989) Voronoi diagrams with barriers and the shortest diagonal problem *Information Processing Letters*, **32**(4), 191–198. [3.4.2]
- Linhart, J. (1981) Die Beleuchtung von Kugeln *Geometriae Dedicata*, **10**, 145–154. [3.1.6]
- Líška, M., P. Perichta and B. Hatálová (1995a) The structure of molecular dynamics simulated oxide glasses viewed through Voronoi polyhedra tesselation *Journal of Non-Crystalline Solids*, **192 & 193**, 249–252. [7.1]
- Líška, M., P. Perichta and L.T. Nagy (1995b) The structure of MD simulated cryolite melt *Journal of Non-Crystalline Solids*, **192 & 193**, 309–311. [7.1]
- Liu, A. and B. Joe (1995) Quality local refinement of tetrahedral meshes based on bisection *SIAM Journal on Scientific and Statistical Computing*, **6**, 1269–1291. [6.5.2]
- Lloyd, E.L. (1977) On triangulations of a set of points in the plane *Proceedings of the 18th Annual IEEE Conference on the Foundations of Computer Science, Providence, R.I.*, 228–240. [2.4, 6.2]
- Lo, S.H. (1985) A new mesh generation scheme for arbitrary planar domains *International Journal for Numerical Methods in Engineering*, **21**, 1403–1426. [6.5.1]
- Lo, S.H. (1989) Delaunay triangulation of non-convex planar domains *International Journal for Numerical Methods in Engineering*, **28**, 2695–2707. [4.8, 6.5, 6.5.1]
- Lock, G.R. and T.M. Harris (1996) Danebury revisited: an English Iron Age hillfort in a digital landscape. In: M. Aldenderfer and H.D.G. Maschner (eds) *Anthropology, Space, and Geographic Information Systems* New York: Oxford University Press. [7.1]
- Loeb, A.L. (1976) *Space Structures – Their Harmony and Counterpoint* Reading: Addison-Wesley. [2.5, 7.1]
- Loftsgaarden, D.O. and D.P. Quesenberry (1965) A nonparametric density function *Annals of Mathematical Statistics*, **36**, 1049–1051. [3.2.3, 3.3.3]
- Longmate, N. (1966) *King Cholera: The Biography of a Disease* London: Hamish Hamilton. [1.2]
- Lorz, U. (1990a) Cell-area distributions of planar sections of spatial Voronoi mosaics *Materials Characterization*, **25**(3), 297–309. [5.7]
- Lorz, U. (1990b) Personal Communication. [5.4, 5.5.2, 5.5.4, 5.7]
- Lorz, U. (1991) Distributions of cell characteristics of the spatial POISSON-VORONOI tessellation and plane sections. In: U. Eckhardt, A. Hubler, W. Nagel and G. Werner (eds) *Geometrical Problems of Image Processing. Research in Information Series*, **4** Berlin: Akademie-Verlag, 171–178. [5.4, 5.5.4, 5.7]
- Lorz, U. and U. Hahn (1993) Geometric characteristics of random spatial Voronoi tessellations and planar sections *Preprint*, TU Bergakademie Freiberg [5.4, 5.5.2, 5.7, 5.12]
- Lösch, A. (1940) *Die raumliche Ordnung der Wirtschaft*. Jena: Fisher. (Translated by W.H. Woglom and W.F. Stolper, *The Economics of Location* New Haven: Yale University Press, 1954). [7.1, 9.2.4]
- Lotwick, H.W. (1982) Simulation of some spatial hard core models, and the complete packing problem *Journal of Statistical Computation and Simulation*, **15**, 295–314. [5.12]
- Love, R.F. (1976) One-dimensional facility location-allocation using dynamic programming *Management Science*, **22**, 614–617. [9.4.1]
- Love, R.F., J.Q. Morris and G.O. Wesolowsky (1988) *Facilities Location* New York: North-Holland. [9.2, 9.2.1]
- Lowell, K. (1994) A fuzzy surface cartographic representation for forestry based on Voronoi diagram area stealing *Canadian Journal of Forest Research*, **24**, 1970–1980. [6.1.2]
- Lozano-Pérez, T. (1981) Automatic planning of manipulator transfer movement *IEEE Transactions on Systems, Man and Cybernetics*, **10**(11), 681–698. [3.6.2]

- Lozano-Pérez, T. (1984) Spatial planning configuration space approach *IEEE Transactions on Computers*, **32**, 108–120. [3.7.11]
- Lozano-Pérez, T. and M.A. Wesley (1979) An algorithm for planning collision free paths among polyhedral obstacles *Communications of the ACM*, **22**(10), 560–570. [3.7.11]
- Loze, M.K. and R. Saunders (1993) Two simple algorithms for constrained Delaunay triangulation *Applied Numerical Mathematics*, **11**, 403–418. [3.4.3]
- Lu, M. (1986). Constructing the Voronoi diagram on a mesh connected computer *Proceedings of the International Conference on Parallel Processing*, 806–811. [4.1, 4.8]
- Lu, Y. and W.W-M. Dai (1991) A numerical stable algorithm for constructing constrained Delaunay triangulation and application to multichip module layout *Proceedings of the China 1991 International Conference on Circuits and Systems*, **2**, 644–647. [3.4.3, 3.4.5]
- Lukatela, H and J. Russell (1992) Spatial data and the Voronoi tessellation *Dr. Dobb's Journal of Software for the Pro*, **17**, 18–25. [3.7.11]
- Mackay, A.L. (1972) Stereological characteristics of atomic arrangements in crystals *Journal of Microscopy*, **95**(2), 217–227. [7.1]
- Mackay, A.L. (1981) De nive quinquaungula: on the pentagonal snowflake *Soviet Physics Crystallography*, **26**(5), 517–522. [7.1]
- Mackay, A.L. (1983) The numerical geometry of biological structures. In: M.J. Geisow and A.N. Barrett (eds) *Computing in Biological Science* Amsterdam: Elsevier Biomedical Press, 349–392. [7.1]
- Mackay, A.L. (1986) Generalized crystallography *Computers and Mathematics with Applications*, **12B**(1/2), 21–37. [7.1]
- Mackay, A.L. and J. Klinowski (1986) Towards a grammar of inorganic structure *Computers and Mathematics with Applications*, **12B**(3/4), 803–824. [7.1]
- Mahin, K.W., K. Hanson and J.W. Morris, Jr. (1976) The computer simulation of homogeneous nucleation and growth processes *Computer Simulation for Materials Applications, Nuclear Metallurgy*, **20**, 39–50. [5.7, 5.8]
- Mahin, K.W., K. Hanson and J.W. Morris, Jr. (1980) Comparative analysis of the cellular and Johnson–Mehl microstructures through computer simulation *Acta Metallurgica*, **28**, 443–453. [5.7, 5.8, 7.1]
- Mahoney, M.S. (1979) *Rene Descartes. Le Monde, ou Traité de la lumière* (Translation and introduction) New York: Abaris Books. [1.1]
- Malan, D.F. and J.A.L. Napier (1995) Computer modelling of granular material microfracturing *Tectonophysics*, **248**, 21–37. [5.12]
- Manacher, G.K. and A.L. Zobrist (1979) Neither the greedy triangulation nor the Delaunay triangulation of a planar point set approximates the optimal triangulation *Information Processing Letters*, **9**(1), 31–34. [2.4, 6.2]
- Marcelpoil, R. and Y. Usson (1992) Methods for the study of cellular sociology: Voronoi diagrams and parametrization of the spatial relationships *Journal of Theoretical Biology*, **154** 359–369. [5.12, 8.1.1]
- Marcum, D.L. and N.P. Weatherall (1995a) Aerospace applications of solution adaptive finite element analysis *Computer Aided Geometric Design*, **12**, 709–731. [6.5.1]
- Marcum, D.L. and N.P. Weatherall (1995b) A procedure for efficient generation of solution adapted unstructured grids *Computer Methods in Applied Mechanics and Engineering*, **127**(1–4), 259–268. [6.5.1]
- Mardia, K.V. (1989) Shape analysis of triangles through directional techniques *Journal of the Royal Statistical Society, Series B*, **51**(3), 449–458. [8.2]
- Mardia, K.V., R. Edwards and M.L. Puri (1977) Analysis of central place theory *Bulletin of the International Statistical Institute*, **47**, 93–110. [5.11, 8.2]
- Mark, D.M. (1975) Computer analysis of topography: a comparison of terrain storage methods *Geografiska Annaler*, **57A**, 179–188. [6.2]
- Mark, D.M. (1987) Recursive algorithm for determination of proximal (Thiessen) polygons in any metric space *Geographical Analysis*, **19**(3), 264–272. [4.1, 4.9]
- Marston, R.E. and J.C. Shih (1995) Modified quaternary tree bucketing for Voronoi diagrams with multi-scale generators *IEEE Colloquium 'Multiresolution Modelling and Analysis in Image Processing and Computer Vision'*, **70**, 11/1–6. [3.5.4]

- Marthinsen, K. (1996) Comparative analysis of the size distributions of linear, planar, and spatial Poisson Voronoi cells *Materials Characterization*, **36**, 53–63. [5.4, 5.5.4, 5.7]
- Marthinsen, K., O. Lohne and E. Nes (1989) The development of recrystalline microstructures studied experimentally and by computer simulation *Acta Metallurgica*, **37**, 135–145. [5.8, 7.2]
- Martin, J.L. (1965) Solution to problem 62–8 *SIAM Review*, **7**, 132–134. [5.11]
- Martinetz, T. and K. Schulten (1994) Topology representing networks *Neural Networks*, **7**(3), 507–522. [2.1]
- Martinez, V.J., B.J.T. Jones, R. Dominguez-Tenreiro and R. van de Weygaert (1990) Clustering paradigms and multifractal measures *Astrophysical Journal*, **357**, 50–61. [2.5, 7.2, 8.7]
- Masada, T., H. Imai and K. Imai (1996a) Enumeration of regular triangulations *Proceedings of the Twelfth Annual Symposium on Computational Geometry, FCRC '96*, 224–233. [3.1.4]
- Masada, T., K. Imai and H. Imai (1996b) Enumeration of regular triangulations with computational results *Zeitschrift für Angewandte Mathematik und Mechanik*, **76**, 187–190. [6.2]
- Masbaum, N. (1995) Simulation of Ostwald ripening in two dimensions: spatial and nearest neighbor correlations *Journal of Physics I, France*, **5**, 1143–1159. [7.1]
- Massam, B.H. (1972) The spatial structure of administrative systems *Association of American Geographers, Commission on College Geography, Resource Paper*, **12**. [7.1]
- Massam, B.H. (1975) *Location and Space in Social Administration* London: Edward Arnold. [7.1]
- Matérn, B. (1979) The analysis of ecological maps as mosaics. In: R.M. Cormack and J.K. Ord (eds) *Spatial and Temporal Analysis in Ecology* Fairland: International Co-operative Publishing House, 271–278. [8.1.1]
- Matheron, G. (1975) *Random Sets and Integral Geometry* New York: John Wiley. [1.3.3, 5.4]
- Matlack, G.R. and J.L. Harper (1986) Spatial distribution and the performance of individual plants in a natural population of *Silene dioica* *Oecologia (Berlin)*, **70**, 121–127. [7.1]
- Matschinski, M. (1954) Considération statistique sur les polygones et les polyèdres *Université de Paris, Publications de l'Institut Statistique*, **3**, 179–201. [5.5.1]
- Matsuda, T. and E. Shima (1984) Topology of supercluster-void structure *Progress in Theoretical Physics*, **71**(4), 855–857. [7.2]
- Matthes, K., J. Kerstan and J. Mecke (1978) *Infinitely Divisible Point Processes* Chichester: John Wiley. [1.3.3]
- Matula, D.W. and R.R. Sokal (1980) Properties of Gabriel graphs relevant to geographic variation research and the clustering of points in the plane *Geographical Analysis*, **12**, 205–222. [2.5]
- Matzke, E.B. and J. Nestler (1946) Volume–shape relationships in variant foams. A further study of the role of surface forces in three-dimensional cell shape determination *American Journal of Botany*, **33**, 130–144. [3.1.6]
- Maus, A. (1984) Delaunay triangulation and the convex hull of n points in expected linear time *BIT*, **24**, 151–163. [4.1]
- Mavriplis, D.J. (1990) Adaptive mesh generation for viscous flows using Delaunay triangulation *Journal of Computational Physics*, **90**(2), 271–291. [6.5.1]
- Maxwell, J.C. (1864) On reciprocal diagrams and diagrams of forces *Philosophical Magazine*, **4**(27), 250–261. [2.4]
- Mayya, N. and V.T. Rajan (1996) Voronoi diagrams of polygons: a framework for shape representation *Journal of Mathematical Imaging and Vision*, **6**(4), 355–378. [3.5.4]
- McAllister, M., D. Kirkpatrick and J. Snoeyink (1996) A compact piecewise-linear Voronoi diagram for convex sites in the plane *Discrete and Computational Geometry*, **15**, 73–105. [3.7.2, 3.7.11, 4.8]
- McAllister, M. and J. Snoeyink (1994) The spoke diagram: a compact approximate Voronoi diagram for spatial computation *GIS '94 (Vancouver)*. [3.7.2]
- McCullagh, M.J. (1981) Creation of smooth contours over irregularly distributed data using local surface patches *Geographical Analysis*, **13**(1), 51–63. [6.2, 6.3]

- McCullagh, M.J. and C.G. Ross (1980) Delaunay triangulation of a random data set for isarithmic mapping *The Cartographic Journal*, **17**(2), 93–99. [6.2, 6.3]
- McIntosh, A.A. (1988) Non-parametric two-sample tests based on the Delaunay triangulation *ASA Proceedings of Statistical Computing Section*, 99–104. [2.5, 6.6]
- McLain, D.H. (1976) Two dimensional interpolation from random data *The Computer Journal*, **19**(2), 178–181. [2.4, 6.2]
- McTague, J.P., D. Frenkel and J.P. Allen (1980) Simulation studies of the 2-D melting mechanisms. In: S.K. Sinha (ed) *Ordering in Two Dimensions* New York: North-Holland. [7.1]
- Mead, R. (1966) A relationship between individual plant-spacing and yield *Annals of Botany, N.S.*, **30**, 301–309. [1.2]
- Mead, R. (1967) A mathematical model for the estimation of inter-plant competition *Biometrics*, **23**, 189–205. [7.1]
- Mead, R. (1971) Models for interplant competition in irregularly distributed populations. In: G.P. Patil, E.C. Pielou and W.E. Waters (eds) *Statistical Ecology Volume 2: Sampling and Modeling Biological Populations and Population Dynamics* University Park: The Pennsylvania State University Press, 15–30. [7.1]
- Meade, M.S., J.W. Florin and W.M. Gesler (1988) *Medical Geography* New York: Guilford Press. [1.2]
- Mecke, J. (1980) Palm methods for stationary random mosaics. In: R.V. Ambartzumian (ed) *Combinatorial Principles in Stochastic Geometry* Erevan: Armenian Academy of Sciences. 124–132. [5.0, 5.1]
- Mecke, J. (1981) Stereological formulas for manifold processes *Probability and Mathematical Statistics*, **2**, 31–35. [1.3.3]
- Mecke, J. (1984) Parametric representation of mean values for stationary random mosaics *Mathematische Operationsforschung und Statistik. Series Statistik*, **15**, 437–442. [5.1, 5.7]
- Mecke, J. (1995) Inequalities for the anisotropic Poisson polytope *Advances in Applied Probability*, **27**, 56–62. [1.3.3]
- Mecke, J. (1999) On the relationship between the 0-cell and the typical cell of a stationary random tessellation. *Pattern Recognition*, **32**(9), 1645–1648. [1.3.3, 5.4, 5.5.4]
- Mecke, J. and L. Muche (1995) The Poisson Voronoi tessellation I. A basic identity *Mathematische Nachrichten*, **176**, 199–208. [5.5.4, 5.11]
- Medina, J., M. Picasso and J. Rappaz (1996) Error estimates and adaptive finite elements for nonlinear diffusion-convection problems *Mathematical Models and Methods in Applied Sciences*, **6**(5), 689–712. [6.5.1]
- Medvedev, N.N. (1986) The algorithm for the three-dimensional Voronoi polyhedra *Journal of Computational Physics*, **67**, 223–229. [4.7, 7.1]
- Medvedev, N.N. (1990) Aggregation of tetrahedral and quartoctahedral Delaunay simplices in liquid and amorphous rubidium *Journal of Physics: Condensed Matter*, **2**, 9145–9154. [7.1]
- Medvedev, N.N. (1994) Application of the Voronoi-Delone method to description of structure of intersphere space in polydisperse systems *Doklady Physical Chemistry*, **337**(1–6), 157–161. [1.2, 3.5.5, 7.1]
- Medvedev, N.N., A. Geiger and W. Brostow (1990) Distinguishing liquids from amorphous solids: percolation analysis on the Voronoi network *Journal of Chemical Physics*, **93**(11), 8337–8342. [7.1]
- Medvedev, N.N. and Y.I. Naberukhin (1987a) Study of the structure of simple liquids and amorphous solids by statistical geometry methods *Journal of Structural Chemistry*, **28**(3), 433–446. [7.1]
- Medvedev, N.N. and Y.I. Naberukhin (1987b) Shape of the Delaunay simplices in dense random packings of hard and soft spheres *Journal of Non-Crystalline Solids*, **94**, 402–406. [7.1]
- Medvedev, N.N., V.P. Voloshin and Y.I. Naberukhin (1986) Local environmental geometry of atoms in the Lennard-Jones systems *Materials Chemistry and Physics*, **14**, 533–548. [7.1]
- Medvedev, N.N., V.P. Voloshin and Y.I. Naberukhin (1988) Structure of simple liquids as

- a percolation problem on the Voronoi network *Journal of Physics A: Mathematical and General*, **21**, L247-L252. [2.1, 7.1]
- Medvedev, N.N., V.P. Voloshin and Y.I. Naberukhin (1989) Structure of simple liquids as a problem of percolation in the Voronoi grid *Journal of Structural Chemistry*, **30**(2), 253–260. [7.1]
- Mees, A.I. (1991) Dynamical systems and tessellations: detecting determinism in data *International Journal of Bifurcation and Chaos*, **1**(4), 777–794. [6.6]
- Megiddo, N. (1978) Cost allocation for Steiner trees *Networks*, **8**, 1–6. [9.3.3]
- Mehlhorn, K., St. Meiser and C. O'Dunlaing (1991) On the construction of abstract Voronoi diagrams *Discrete and Computational Geometry*, **6**(3), 211–224. [3.0, 4.8]
- Meijering, J.L. (1953) Interface area, edge length, and number of vertices in crystal aggregates with random nucleation *Philips Research Reports*, **8**, 270–290. [1.2, 5.5.1, 5.6.2, 5.8, 7.2]
- Melachrinoudis, E. and T.P. Cullinane (1986) Locating an obnoxious facility within a polygonal region *Annals of Operations Research*, **6**, 137–145. [3.1.6]
- Melachrinoudis, E. and J.M. Smith (1995) An $O(mn^2)$ algorithm for the Maximin problem in E^2 . *Operations Research Letters*, **18**, 25–30. [3.1.6]
- Melissaratos, E.A. and D.L. Souvaine (1992) Coping with inconsistencies: a new approach to produce quality triangulations of polygonal domains with holes *Proceedings of the 8th Annual Symposium on Computational Geometry*, 202–211. [6.5.1]
- Melkemi, M. and J.M. Chassery (1992) Edge region segmentation process based on generalized Voronoi diagram representation *Proceedings of the 11th ICPR IAPR International Conference on Pattern Recognition, 1 August–4 September 1992, The Hague. Vol. III. Conference C: Image, Speech and Signal Analysis*, **32**. [3.0]
- Melkemi, M. and Vandorpe, D. (1994) An iterative algorithm for computing the shape of a finite set of points *Proceedings of the SPIE – The International Society for Optical Engineering*, **2315**, 592–603. [2.1]
- Melter, R.A. and I. Stojmenović (1995) Constant time BSR solutions to L_1 metric and digital geometry problems *Journal of Mathematical Imaging and Vision*, **5**(2), 119–127. [2.1, 3.7.1]
- Melville, R.C. (1985) An implementation study of two algorithms for the minimum spanning circle problem. In: G.T. Toussaint (ed) *Computational Geometry* Amsterdam: North-Holland, 267–294. [3.3.1]
- Melzak, Z.A. (1961) On the problem of Steiner *Canadian Mathematical Bulletin*, **4**, 143–148. [9.3.3]
- Meng, A. C-C. (1987) Flight path planning under uncertainty for robotic air vehicles *IEEE National Aerospace and Electronics Conference, Institute of Electrical and Electronics Engineers, New York, May*, 359–366. [3.6.2]
- Meshkat, S.N. and C.M. Sakkas (1987) Voronoi diagram for multiply-connected polygonal domains, II – Implementation and application *IBM Journal of Research and Development*, **31**, 373–381. [3.5.4, 3.5.5, 4.8]
- Miki, F. (1983) A Study of the Distribution of Convenience Goods Stores. Ph.D. Thesis, Department of Urban Engineering, University of Tokyo [in Japanese]. [8.3.1]
- Miles, R.E. (1964a) Random polygons determined by random lines in a plane: I *Proceedings of the National Academy of Sciences (USA)*, **52**, 901–907. [1.3.3, 5.9]
- Miles, R.E. (1964b) Random polygons determined by random lines in a plane: II *Proceedings of the National Academy of Sciences (USA)*, **52**, 1151–1160. [1.3.3, 5.9]
- Miles, R.E. (1970a) On the homogeneous planar Poisson point process *Mathematical Biosciences*, **6**, 85–127. [3.2, 5.4, 5.5.4, 5.9, 5.11, 8.1.2]
- Miles, R.E. (1970b) A synopsis of 'Poisson flats in Euclidean spaces' *Izvestiya Akademii Nauk Armianskoi SSR Matematika*, **5**(3), 263–285. [5.5.1, 5.5.4, 5.11]
- Miles, R.E. (1971) Random points, sets and tessellations on the surface of a sphere *Sankhyā: The Indian Journal of Statistics, Series A*, **33**(2), 145–174. [3.7.6, 4.8, 5.10, 5.11]
- Miles, R.E. (1972a) The random division of space *Advances in Applied Probability*, **4**(Supplement), 243–266. [1.3.3, 5.1, 5.7, 5.8]
- Miles, R.E. (1972b) Multi-dimensional perspectives on stereology *Journal of Microscopy*, **95**, 181–195. [5.1]

- Miles, R.E. (1973) The various aggregates of random polygons determined by random lines in the plane *Advances in Mathematics*, **10**, 256–290. [1.3.3, 5.9]
- Miles, R.E. (1974) A synopsis of ‘Poisson flats in Euclidean spaces’. In: E.F. Harding and D.G. Kendall (eds) *Stochastic Geometry* New York: John Wiley, 202–227. [5.5.1, 5.5.4, 5.11]
- Miles, R.E. (1984) Sectional Voronoi tessellations *Revista de la Union Mathematica Argentina*, **29**, 310–327. [5.7, 5.9]
- Miles, R.E. (1986a) Spatial tessellations and their stereology. In: Y. Kato, R. Takaki and J. Toriwaki (eds) *Science on Form: Proceedings of the First International Symposium for Science on Form* Tokyo: KTK Scientific Publishers, 147–155. [5.7, 5.9, 5.11]
- Miles, R.E. (1986b) Random tessellations. In: S. Kotz and N.L. Johnson (eds) *Encyclopedia of Statistical Sciences*, Volume 7 New York: John Wiley, 567–572. [5.9]
- Miles, R. (1995) A heuristic proof of a long-standing conjecture of D.G. Kendall concerning the shapes of certain large random polygons *Advances in Applied Probability*, **27**, 397–417. [1.3.3, 5.9]
- Miles, R.E. and R.J. Maillardet (1982) The basic structures of Voronoi and generalized Voronoi polygons *Journal of Applied Probability*, **19A**, 97–111. [3.0, 3.2, 3.2.1, 5.5.4, 5.9]
- Miller, H. (1994) Market area delineation within networks using geographic information systems *Geographical Systems*, **1**, 157–175. [9.2.8]
- Miller, T.E. and J. Weiner (1989) Local density variation may mimic effects of asymmetric competition on plant size variability *Ecology*, **70**, 1188–1191. [5.3]
- Minakawa, T. and K. Sugihara (1997) Topology oriented vs. exact arithmetic – experience in implementing the three-dimensional convex hull algorithm. In: H.W. Leong, H. Imai and S. Jain (eds) *Lecture Notes in Computer Science*, **1350** (Proceedings of the 8th International Symposium on Algorithms and Computation) Berlin: Springer-Verlag, 273–282. [4.6.3]
- Minkowski, H. (1897) Allgemeinelehrsätze über die konvexen Polyeder *Nachrichten Gesellschaft der Wissenschaften zu Goettingen. Mathematisch-Physikalische Klasse*, 198–219. [*Gesammelte Abhandlungen*, Vol. 2 (New York: Chelsea, 1967), 103–121] [1.2]
- Mirante, A. and N. Weingarten (1982) The radial sweep algorithm for constructing triangulated irregular networks. *IEEE Computer Graphics and Applications*, **2**(3), 11–21. [6.2, 6.3]
- Mirchandani, P.B. (1987) Generalized hierarchical facility locations *Transportation Science*, **21**(2), 123–125. [9.2.4]
- Mirchandani, P.B. and R.L. Francis (1990) *Discrete Location Theory* New York: John Wiley. [9.2]
- Mirzaian, A. (1993) Minimum weight Euclidean matching and weighted relative neighborhood graphs *Lecture Notes in Computer Science*, **709** (The Third Workshop on Algorithms and Data Structures WADS '93), 506–517. [3.1.2]
- Mitchell, J.S.B. (1991) A new algorithm for shortest paths among obstacles in the plane *Annals of Mathematics and Artificial Intelligence*, **3**, 83–106. [3.4.1]
- Mitchell, J.S.B. (1992) L_1 shortest paths among polygonal obstacles in the plane *Algorithmica*, **8**(1), 55–88. [3.4.1, 3.7.11]
- Mitchell, J.S.B. (1993) Shortest paths among obstacles in the plane *Proceedings of the 9th Annual ACM Symposium on Computational Geometry, 19–21 May, 1993, San Diego*, 308–317. [3.4.1]
- Mitchell, J.S.B. (1996) Shortest paths among obstacles in the plane *International Journal of Computational Geometry and Applications*, **6**(3), 309–332. [3.4.1]
- Mitchell, J.S.B., D.M. Mount and C.H. Papadimitriou (1987) The discrete geodesic problem *SIAM Journal on Computing*, **16**, 647–668. [3.4.1]
- Mithen, R., J.L. Harper and J. Weiner (1984) Growth and mortality of individual plants as a function of ‘available area’ *Oecologia (Berlin)*, **62**, 57–60. [7.1]
- Mizutani, N., T. Watanabe, Y. Yoshida and N. Okabe (1993) Extraction of contour lines by identification of neighbor relationships *Systems and Computers in Japan*, **24**(1), 57–68. [3.5.5]

- Mohan, S. and J.-F. Lee (1993) Three-dimensional finite element mesh generation using Delaunay triangulation *IEEE Antennas and Propagation Society International Symposium 1993, Digest*, **1**, 312–315. [2.2]
- Molchanov, I. and S.N. Chiu (2000) Smoothing techniques and estimation methods for non-stationary Boolean models with applications to coverage processes *Biometrika*, to appear. [5.8]
- Molchanov, I. and S. Zuyev (1997) Variational analysis of functionals of a Poisson process *INRIA Research Reports*, **3302**. [5.3]
- Molchanov, S.A., D. Surgailis and W.A. Woyczyński (1997) The large-scale structure of the universe and quasi-Voronoi tessellation of shock fronts in forced Burgers turbulence in \mathbb{R}^d *The Annals of Probability*, **7**(1), 200–228. [7.2]
- Møller, J. (1989) Random tessellations in \mathbb{R}^d *Advances in Applied Probability*, **21**, 37–73. [5.0, 5.1, 5.2, 5.5.1, 5.7, 5.11]
- Møller, J. (1992) Random Johnson–Mehl tessellations *Advances in Applied Probability*, **24**, 814–844. [3.1.5, 5.8]
- Møller, J. (1994) *Lectures on Random Voronoi Tessellations Lecture Notes in Statistics*, **87** New York: Springer-Verlag. [1.0, 2.3, 5.0, 5.1, 5.4, 5.5.1, 5.5.2, 5.7, 5.11]
- Møller, J. (1995) Generation of Johnson–Mehl crystals and comparative analysis of models for random nucleation *Advances in Applied Probability*, **27**(2), 367–383. [5.8]
- Møller, J. (1998) A review on probabilistic models and results for Voronoi tessellations. In: P. Engel and H. Syta (eds) *Voronoi's Impact on Modern Science Book 1* Kyiv: Institute of Mathematics, National Academy of Sciences, Ukraine, 254–265. [5.0]
- Møller, J. (1999) Topics in Voronoi and Johnson–Mehl tessellations. In: O.E. Barndorff-Nielsen, W.S. Kendall and M.N.M. Van Lieshaut (eds) *Stochastic Geometry. Likelihood and Computation*. Boca Raton: Chapman and Hall, 173–198. [5.0, 5.8]
- Møller, J., E.B. Jensen, J.S. Petersen and H.J.G. Gundersen (1989) Modelling an aggregate of space-filling crystals from sectional data *University of Aarhus, Department of Theoretical Statistics, Research Report*, **182**. [5.0, 5.12]
- Møller, J. and S. Zuyev (1996) Gamma-type results and other related properties of Poisson processes *Advances in Applied Probability*, **28**, 662–673. [5.5.4]
- Monmonier, M.S. (1982) *Computer-Assisted Cartography. Principles and Prospects* Englewood Cliffs: Prentice-Hall. [6.2]
- Monmonier, M. (1996) *How to Lie with Maps* Chicago: University of Chicago Press. [1.2]
- Montanari, U. (1968) A method of obtaining skeletons using a quasi-Euclidean distance *Journal of the ACM*, **15**, 600–624. [3.5.4]
- Montanari, U. (1969) Continuous skeletons from digitized images *Journal of the Association for Computing Machinery*, **16**(1), 534–549. [3.5.4]
- Mood, A.M., F.A. Graybill and D.C. Boes (1974) *Introduction to the Theory of Statistics* New York: McGraw-Hill. [9.2.3]
- Moody, R.V. and J. Patera (1995) Voronoi domains and dual cells in the generalized kaleidoscope with applications to root and weight lattices *Canadian Journal of Mathematics*, **47**(3), 573–605. [7.1]
- Moore, G.C. and C. ReVelle (1982) The hierarchical service location problem *Management Science*, **28**(7), 775–780. [9.2.4]
- Moore, G.S.M. and R.E.M. Moore (1993) The side-lengths of Voronoi polygons for random nuclei *Physica A*, **196**, 6–11. [5.4, 5.5.4]
- Moore, J.A., C.A. Budelsky and R.C. Schlesinger (1973) A new index representing individual tree competitive status *Canadian Journal of Forest Research*, **3**, 495–500. [7.1]
- Moore, R.E.M. and I.O. Angell (1993) Voronoi polygons and polyhedra *Journal of Computational Physics*, **105**, 301–305. [5.4, 5.5.4]
- Moorthy, S. and S. Ghosh (1996) A model for analysis of arbitrary composite and porous microstructures with Voronoi cell finite elements *International Journal for Numerical Methods in Engineering*, **39**, 2363–2398. [6.5]
- Moreau, J.-M. and P. Volino (1993) Constrained Delaunay triangulation revisited *Proceedings of the 5th Canadian Conference on Computational Geometry*, 340–345. [6.5]

- Morgan, K., O. Hassan and J. Peraire (1994) An unstructured grid algorithm for the solution of Maxwell's equations in the time domain *International Journal of Numerical Methods in Fluids*, **19**, 849–863. [6.5.2]
- Morgan, K., O. Hassan and J. Peraire (1996) A time domain unstructured grid approach to the simulation of electromagnetic scattering in piecewise homogeneous media *Computer Methods in Applied Mechanics and Engineering*, **134**, 17–36. [6.5.2]
- Morgan, K., J. Peraire, J. Peiro and O. Hassan (1991) The computation of three-dimensional flows using unstructured grids *Computer Methods in Applied Mechanics and Engineering*, **87**, 335–352. [6.5.2]
- Morgan, M. (1967) Hardware models in geography. In: R.J. Chorley and P. Haggett (eds) *Models in Geography* London: Methuen, 727–774. [7.2]
- Moukarzel, C. (1993) Voronoi foams *Physica A*, **199**, 19–30. [1.2, 3.1.6]
- Moukarzel, C. (1995) Two-dimensional foams are (sectional multiplicative) Voronoi partitions, *Preprint*. [3.1.5, 3.1.6]
- Moukarzel, C. and H.J. Herrmann (1992) A vectorizable random lattice *Journal of Statistical Physics*, **68**(5/6), 911–923. [5.12]
- Mount, D.M. (1985) Voronoi diagrams on the surface of a polyhedron *Report*, **1496**, University of Maryland. [3.7.9]
- Muche, L. (1993) An incomplete Voronoi tessellation *Applicationes Mathematicae*, **22**(1), 45–53. [5.6.2, 7.2]
- Muche, L. (1996a) The Poisson Voronoi tessellation II. Edge length distribution functions *Mathematische Nachrichten*, **178**, 271–283. [5.5.4, 5.7]
- Muche, L. (1996b) Distributional properties of the three-dimensional Poisson Delaunay cell *Journal of Statistical Physics*, **84**, 147–167. [5.4, 5.11]
- Muche, L. (1998) The Poisson Voronoi tessellation III. Miles' Formula *Mathematische Nachrichten*, **191**, 247–267. [5.5.4, 5.11]
- Muche, L. (1999) Private communications. [5.6.1, 5.7, 5.11]
- Muche, L. and D. Stoyan (1992) Contact and chord length distributions of the Poisson–Voronoi tessellation *Journal of Applied Probability*, **29**, 467–471. [5.5.4, 5.7]
- Mücke, E.P., I. Sais and B. Zhu (1996) Fast randomized point location without preprocessing in two- and three-dimensional Delaunay triangulations *Proceedings of the Twelfth Annual Symposium on Computational Geometry, May 24–26, 1996, Philadelphia*, 274–283. [2.3]
- Mücklich, J., J. Osher and G. Schneider (1997) Die Charakterisierung homogener polyedrischer Gefüge mit Hilfe des räumlichen Poisson–Voronoi-Mosaiks und der Vergleich zur DIN 50 601 (The characterization of homogeneous polyhedral microstructures applying the spatial Poisson–Voronoi tessellation compared to the standard DIN 50 601) *Zeitschrift für Metallkunde*, **88**(1), 27–32. [5.3]
- Muder, D.J. (1988) Putting the best face on a Voronoi polyhedron *Proceedings of the London Mathematical Society*, (3), **56**, 329–348. [7.1]
- Muder, D.J. (1990) How big is an n -sided Voronoi polygon? *Proceedings of the London Mathematical Society*, (3), **61**, 91–108. [7.1]
- Mulheran, P.A. (1992) On the statistical properties of the two-dimensional random Voronoi network *Philosophical Magazine Letters*, **66**(5), 219–224. [5.5.4]
- Mulheran, P.A. and J.A. Blackman (1995) The origins of island size scaling in heterogeneous film growth *Philosophical Magazine Letters*, **72**(1), 55–60. [5.12, 7.1]
- Mulheran, P.A. and J.A. Blackman (1996) Capture zones and scaling in homogeneous thin-film growth *Physical Review B*, **53**(15), 10261–10267. [7.1, 8.1.1]
- Mulmuley, K. (1991) On levels in arrangements and Voronoi diagrams *Discrete and Computational Geometry*, **6**, 307–338. [4.7, 4.8]
- Myles, J.P., E.C. Flenley, N.R.J. Fieller, H.V. Atkinson and H. Jones (1995) Statistical tests for clustering of second phases in composite materials *Philosophical Magazine A*, **72**(2), 515–528. [8.1.1]
- Nackman, L.R. and S.M. Pizer (1985) Three-dimensional shape description using the symmetric axis transformation, I. Theory *IEEE PAMI*, **7**(2), 187–202. [3.5.4]
- Nackman, L.R. and V. Srinivasan (1994) Point placement algorithms for Delaunay triangulation of polygonal domains *Algorithmica*, **12**(1), 1–17. [3.4.3]

- Näf, M., G. Szekely, R. Kikinis, M.E. Shenton and O. Kubler (1997) 3D Voronoi skeletons and their usage for the characterization and recognition of 3D organ shape *Computer Vision and Image Understanding*, **66**(2), 147–161. [3.5.4]
- Nair, K.P.K. and R. Chandrasekaran (1971) Optimal location of a single service center of certain types *Naval Research Logistics Quarterly*, **18**, 503–510. [3.3.1]
- Nance, W.L., J.E. Grissom and W.R. Smith (1987) A new competition index based on weighted and constrained area potentially available. In: A.R. Ek, S.R. Shifley and T.E. Burk (eds) *Forest Growth Modelling and Prediction*, Volume 1 (Proceedings of the IUFRO Conference August 23–27, 1987, Minneapolis, Minnesota. Society of American Foresters Publication SAF-87.12), 134–142. [7.1]
- Narula, S.C. (1984) Hierarchical location-allocation problems: a classification scheme *European Journal of Operational Research*, **15**, 93–99. [9.2.4]
- Nehl, T.W. and D.A. Field (1991) Adaptive refinement of first order tetrahedral meshes for magnetostatics using local Delaunay subdivisions *IEEE Transactions on Magnetics*, **27**(5), 4193–4196. [6.5.2]
- Neubert, L. and M. Schreckenberg (1997) Numerical simulation of two-dimensional soap froth *Physica A*, **240**, 491–502. [5.3]
- Neumann, M., F.J. Vesely, O. Steinhauser and P. Schuster (1978) Solvation of large dipoles I. A molecular dynamics study *Molecular Physics*, **35**(3), 841–855. [7.1]
- Neumann, M., F.J. Vesely, O. Steinhauser and P. Schuster (1979) Solvation of large dipoles. A molecular dynamics study II *Molecular Physics*, **37**(6), 1725–1743. [7.1]
- Neumann-Lara, V. and J. Urrutia (1988) A combinatorial result on points and circles on the plane *Discrete Mathematics*, **69**, 173–178 [3.7.2]
- Nielson, G.M. (1993) A characterization of an affine invariant triangulation *Computing Supplement*, **8**, 191–210. [4.8, 6.5]
- Nielson, G.M. and R. Franke (1983) Surface construction based upon triangulations. In: R.E. Barnhill and W. Boehm (eds) *Surfaces in Computer Aided Design* Amsterdam: North-Holland, 163–177. [6.2]
- Niemelä, S., J. Leppänen and F. Sundholm (1996) Structural effects on free volume distribution in glassy polysulfones: molecular modelling of gas permeability *Polymer*, **37**(18), 4155–4165. [7.1]
- Niggli, R. (1927) Die topologische strukturanalyse I *Zeitschrift für Kristallographie*, **65**, 391–415. [1.2]
- Ninomiya, T. and Y. Nakagawa (1991) Precise position detection of a mesh-backed printing screen based on the smallest enclosing circle detection *IEICE Transactions*, **E74**(10), 3484–3491. [3.3.3]
- Nose, S. and F. Yonezawa (1986) Isothermal-isobaric computer simulations of melting and crystallization of a Lennard-Jones system *Journal of Chemical Physics*, **84**, 1803–1814. [7.1]
- Nowacki, W. (1933) Der Begriff ‘Voronoiischer Bereich’ *Zeitschrift für Kristallographie* **85**, 331–332. [1.2]
- Nowacki, W. (1976) Über allgemeine Eigenschaften von Wirkungsbereichen *Zeitschrift für Kristallographie*, **143**, 360–385. [1.2]
- Oden, N.L., R.R. Sokal, M.-J. Fortin and H. Goebel (1993) Categorical wombling: detecting regions of significant change in spatially located categorical variables *Geographical Analysis*, **25**(4), 315–336. [Ack, 7.1]
- Odland, J. (1988) *Spatial Autocorrelation*. Scientific Geography Series, **9** Newbury Park: Sage Publications. [6.1.2]
- Ó'Dúnlaing, C., M. Sharir and C. Yap (1983) Retraction: a new approach to motion planning *Proceedings of the 15th Annual ACM Symposium on Theory of Computation*, 207–220. [3.7.11]
- Ó'Dúnlaing, C., M. Sharir and C. Yap (1986) Generalized Voronoi diagrams for moving a ladder. I: Topological analysis *Communications on Pure and Applied Mathematics*, **39**, 423–483. [3.0, 3.7.11, 4.8]
- Ó'Dúnlaing, C., M. Sharir and C. Yap (1987) Generalized Voronoi diagrams for moving a ladder. II: Efficient construction of the diagram *Algorithmica*, **2**, 27–59. [3.7.11]
- Ó'Dúnlaing, C. and C.K. Yap (1985) A ‘reaction’ method for planning the motion of a disk *Journal of Algorithms*, **6**, 104–111. [3.5.4, 3.6.2, 3.7.11]

- Ogawa, H. (1986) Labelled point pattern matching by Delaunay triangulation and maximal cliques *Pattern Recognition*, **19**(1), 35–40. [6.6]
- Ogawa, H., N. Sawaguchi and F. Wakai (1996a) Molecular dynamics simulation on the grain boundary structure of polycrystalline zirconia *Transactions of the Materials Research Society of Japan*, **20**, 807–810. [7.1]
- Ogawa, H., N. Sawaguchi and F. Wakai (1997) High temperature deformation of ceramics simulated by molecular dynamics *Materials Science Forum*, **243–245**, 351–356. [7.1]
- Ogawa, H., F. Wakai and Y. Waseda (1996b) Molecular dynamics simulation of the model grain boundary structure of polycrystalline materials *Molecular Simulation*, **18**, 179–192. [3.1.6]
- Ogawa, T. and M. Tanemura (1974) Geometrical considerations on hard core problems *Progress in Theoretical Physics*, **51**(2), 399–417. [7.1]
- Ogniewicz, R. and M. Ilg (1992) Voronoi skeletons: theory and applications *Proceedings of the 1992 IEEE Computer Society Conference on Computer Vision and Pattern Recognition, Champaign, Illinois, June*, 63–69. [3.5.4; 3.5.5]
- Ogniewicz, R.L. and O. Kübler (1995) Hierarchic Voronoi skeletons *Pattern Recognition*, **28**(3), 343–359. [3.5.4]
- Oguocha, I.N.A. and S. Yannacopoulos (1997) Precipitation and dissolution kinetics in Al–Cu–Mg–Fe–Ni alloy 2618 and Al–alumina particle metal matrix composite *Materials Science and Engineering*, **A231**, 25–33. [5.8]
- Ohji, T. (1986) Normative approach to the study of periodic markets in South India *Human Geography*, **38**(4), 289–315 [in Japanese]. [7.1]
- Ohkubo, T. and Y. Hirotsu (1996) Molecular dynamics simulation of local atomic structure in amorphous Pd–Si alloys *Materials Science and Engineering*, **A217/218**, 388–391. [7.1]
- Ohsawa, Y. and A. Imai (1997) Degree of locational freedom in a single facility euclidean minimax location model *Location Science*, **5**(1), 29–45. [3.3.3]
- Ohsawa, Y. and A. Suzuki (1987) Location-allocation problem of multi-person facility *Journal of the Operations Research Society of Japan*, **30**, 368–395 [in Japanese]. [9.2.3]
- Ohser, J. and F. Mücklich (1995) Stereology for some classes of polyhedrons *Advances in Applied Probability*, **27**(2), 384–396. [5.4]
- Ohya, T. (1983) On Efficient Algorithms for the Voronoi Diagram. Master's Thesis, Department of Mathematical Engineering and Information Physics, University of Tokyo [in Japanese]. [4.1, 4.3]
- Ohya, T., M. Iri and K. Murota (1984a) Improvements of the incremental method for the Voronoi diagram with computational comparisons of various algorithms *Journal of the Operations Research Society of Japan*, **27**, 306–336. [4.1, 4.3, 4.4]
- Ohya, T., M. Iri and K. Murota (1984b) A fast Voronoi-diagram algorithm with quaternary tree bucketing *Information Processing Letters*, **18**(4), 227–231. [4.3]
- Oikawa, K. (1986) A study on the optimal partitioning model with distributed facilities *Papers of the Annual Conference of the City Planning Institute of Japan*, **21**, 235–240 [in Japanese]. [3.6.2]
- Okabe, A. (1987) Exact higher moments of the nearest neighbor distance *Journal of the Faculty of Engineering, University of Tokyo*, **39**, 1–6. [8.3.1]
- Okabe, A. (1994) Software review of VORONOI2 *Geographical Systems* **1**, 347–347. [4.6]
- Okabe, A. and M. Aoyagi (1991) Existence of equilibrium configurations of competitive firms on an infinite two-dimensional space *Journal of Urban Economics*, **29**, 349–370. [7.3.1]
- Okabe, A. and A. Fujii (1984) The statistical analysis through a computational method of a distribution of points in relation to its surrounding network *Environment and Planning A*, **16**, 107–114. [3.5.5, 8.3.2]
- Okabe, A. and M. Kitamura (1996) A computational method for market area analysis on a network *Geographical Systems*, **28**, 330–349. [9.2.8]
- Okabe, A. and F. Miki (1984) A conditional nearest-neighbor spatial association measure for the analysis of conditional locational interdependence *Environment and Planning A*, **16**, 163–171. [8.3.1]

- Okabe, A. and K. Okunuki (2000) A computational method for estimating the demand of retail stores on a street network and its implementation in GIS *Transactions in GIS*, (to appear) [9.2.8]
- Okabe, A., K. Okunuki and T. Suzuki (1997) A computational method for optimizing the hierarchy and spatial configuration of successively inclusive facilities on a continuous plane *Location Science*, **5**(4), 255–267. [9.2.4]
- Okabe, A. and Y. Sadahiro (1996) An illusion of spatial hierarchy: spatial hierarchy in a random configuration *Environment and Planning A*, **28**, 1533–1552. [6.6, 9.2.4]
- Okabe, A. and A. Suzuki (1987) Stability of spatial competition for a large number of firms on a bounded two-dimensional space *Environment and Planning A*, **19**, 1067–1082. [7.3.1]
- Okabe, A. and A. Suzuki (1997) Locational optimization problems solved through Voronoi diagrams *European Journal of Operational Research*, **98**, 445–456. [3.3.3, 9.2]
- Okabe, A. and H. Yomono (1988) Statistical methods for evaluating the geometrical hierarchy of a network *Geographical Analysis*, **20**(2), 122–139. [3.8.3]
- Okabe, A. and T. Yoshikawa (1989) The multi nearest neighbor distance method for analyzing the compound effect of infrastructural elements on the distribution of activity points *Geographical Analysis*, **21**(3), 216–235 [3.5.5, 8.3.2, 8.3.4]
- Okabe, A., T. Yoshikawa, A. Fujii and K. Oikawa (1988) The statistical analysis of a distribution of activity points in relation to surface-like elements *Environment and Planning A*, **20**, 609–620. [3.6.2, 8.3.3]
- O'Keefe, M. (1979) A proposed rigorous definition of coordination number *Acta Crystallographica*, **A35**, 772–775. [7.1]
- O'Kelly, M.E. and H.J. Miller (1989) A synthesis of some market area delimitation models *Growth and Change*, **20**, 14–33. [3.1.6]
- O'Kelly, M.E. and J.E. Storbeck (1984) Hierarchical location models with probabilistic allocation *Regional Studies*, **18**(2), 121–129. [9.2.4]
- Oloufa, A.A. (1991) Triangulation applications in volume calculation *Journal of Computers in Civil Engineering*, **5**, 103–119. [3.4.3]
- Onishi, K. and H. Imai (1997) Voronoi diagram in statistical parametric space by Kullback–Liebler divergence *Proceedings of the Thirteenth ACM Symposium in Computational Geometry*, 463–467. [3.7.10]
- Onishi, K. and N. Takayama (1996) Construction of Voronoi diagram on the upper half plane *IEICE Transactions on Fundamentals of Electronics, Communications and Computer Sciences*, **E79-A**(4), 533–539. [3.7.10]
- Ooishi, T. (1990) Numerically Robust Implementation of the Divide-and-Conquer Algorithm for Constructing Voronoi Diagrams. Bachelor's Thesis, Department of Mathematical Engineering and Information Physics, Faculty of Engineering, University of Tokyo [in Japanese]. [4.1]
- Ooishi, T. and K. Sugihara (1995) Topology-oriented divide-and-conquer algorithm for Voronoi diagrams *Graphical Models and Image Processing*, **57**(4), 303–314. [4.1, 4.6]
- Ord, J.K. (1975) Estimation methods for models of spatial interaction *Journal of the American Statistical Society*, **70**, 120–126. [6.1.2]
- Ord, J.K. (1977) Discussion of Dr. Ripley's paper *Journal of the Royal Statistical Society, Series B*, **39**, 199. [8.7]
- Ord, J.K. (1978) How many trees in a forest? *Mathematical Scientist*, **3**, 23–33. [8.5]
- O'Rourke, J. (1982) Computing the relative neighborhood graph in the L_1 and L_∞ metrics *Pattern Recognition*, **15**(3), 189–192. [2.5]
- O'Rourke, J., H. Booth and R. Washington (1987) Connect-the-dots: a new heuristic *Computer Vision, Graphics and Image Processing*, **39**(2), 258–266. [8.4.2]
- O'Rourke, J., S.R. Kosaraju and N. Megiddo (1986) Computing circular separability *Discrete and Computational Geometry*, **1**, 105–113. [2.4, 4.1, 4.7]
- Osteen, R.E. and P.P. Lin (1974) Picture skeletons based on eccentricities of points of minimum spanning trees *SIAM Journal on Computing*, **3**, 23–40. [2.5]
- Ostoja-Starzewski, M. (1990) Bounds on constitutive response for a class of random material microstructures *Computers and Structures*, **37**, 163–167. [5.3]
- Ostoja-Starzewski, M. (1993) Random fields and processes in mechanics of granular media *Mechanics of Materials*, **16**, 55–64. [5.3]

- Ostoja-Starzewski, M. and C. Wang (1989) Linear elasticity of planar Delaunay networks: random field characterization of effective moduli *Acta Mechanica*, **80**, 61–80. [5.3]
- Ostoja-Starzewski, M. and C. Wang (1990) Linear elasticity of planar Delaunay networks. Part II: Voigt and Reuss bounds, and modification for centroids *Acta Mechanica*, **84**, 47–61. [5.3]
- Ostoja-Starzewski, M., K. Alzebdeh and I. Jasiuk (1995) Linear elasticity of planar Delaunay networks. III. Self-consistent approximations *Acta Mechanica*, **110**(1–4), 57–72. [5.3]
- Overmars, M.H. and J. van Leeuwen (1981) Maintenance of configurations in the plane *Journal of Computing and System Sciences*, **34**, 166–204. [4.4]
- Owens, M.K. and B.E. Norton (1989) The impact of ‘available area’ on *Artemisia tridentata* seedling dynamics *Vegetatio*, **82**, 155–162. [7.1]
- Painter, J. and K. Sloan (1989) Antialiased raytracing by adaptive progressive refinement *Computer Graphics*, **23**(3), 281–288. [6.4]
- Palacios-Velez, O. and B.C. Renaud (1990) A dynamic hierarchical subdivision algorithm for computing Delaunay triangulations and other closest-point problems *ACM Transactions on Mathematical Software*, **16**(3), 275–292. [4.1]
- Papadopoulou, E. and D.T. Lee (1995) Efficient computation of the geodesic Voronoi diagram of points in a simple polygon *Algorithms – ESA 95. Third Annual European Symposium Proceedings*, 238–251. [3.4.1]
- Park, H. and K. Kim (1995) An adaptive method for smooth surface approximation to scattered 3D points *Computer-Aided Design*, **27**(12), 929–939. [3.4.5, 6.4]
- Parker, R.L., L. Shure and J.A. Hildebrand (1987) The application of inverse theory to seamount magnetism *Reviews of Geophysics*, **25**(1), 17–40. [6.2]
- Parr, J.B. (1995a) Alternative approaches to market-area structure in the urban system *Urban Studies*, **32**(8), 1317–1329. [1.2]
- Parr, J.B. (1995b) The economic law of market areas: a further discussion *Journal of Regional Science*, **35**, 599–615. [1.2]
- Parr, J.B. (1997a) The law of market areas and the size distribution of urban centers *Papers in Regional Science: The Journal of the RSAI*, **76**(1), 43–68. [1.2]
- Parr, J.B. (1997b) The law of retail gravitation: insights from another law *Environment and Planning A*, **29**, 1477–1492. [1.2]
- Paschinger, I. (1982) Konvexe Polytope und Dirichletsche Zellenkomplexe, Dissertation, Institut für Mathematik, University of Salzburg, Austria. [3.7.6, 4.8]
- Paton, K. and S.W. Zucker (1983) Spatial pattern in sections of human muscle *Pattern Recognition Letters*, **2**, 53–57. [7.1]
- Pederzoli, G. (1995) Volumetric distributions for random tessellations *Supplemento ai Rendiconti del Circolo Matematico di Palermo*, **38**, 77–82. [5.11]
- Pedoe, D. (1970) *Geometry* New York: Dover Publications. [4.2]
- Peleg, S. and A. Rosenfeld (1981) A mini-max medial axis transformation *IEEE Transactions on Pattern Analysis and Machine Intelligence*, **3**, 208–210. [3.5.4]
- Pelz, D.R. (1978) Estimating individual tree growth with tree polygons. In: J. Freis, H.E. Burkhardt and T.A. Max (eds) *Growth Models for Long-term Forecasting of Timber Yields* Virginia Polytechnical Institute and State University, School of Forestry and Wildlife Resources, Publications FWS-1–78, 172–178. [7.1]
- Pernus, F. (1988) The Delaunay triangulation and the shape hull as tools in muscle fibre analysis *Pattern Recognition Letters*, **8**, 197–202. [7.1, 8.4.2]
- Perry, J.N. (1995) Spatial analysis by distance indexes *Journal of Animal Ecology*, **64**(3), 303–314. [8.1.2]
- Peshkin, M.A., K.J. Strandburg and N. Rivier (1991) Entropic predictions for cellular networks *Physical Review Letters*, **7**, 1803–1806. [5.5.3]
- Peucker, T.K. and N. Chrisman (1975) Cartographic data structures *The American Cartographer*, **2**(1), 55–69. [6.1.1]
- Peucker, T.K. and D.H. Douglas (1975) Detection of surface-specific points by local parallel processing of discrete terrain elevation data *Computer Graphics and Image Processing*, **4**, 375–387. [6.3]

- Peucker, T.K., R.J. Fowler, J.J. Little and D.M. Mark (1976) Digital representation of three-dimensional surfaces by triangulated irregular networks (TIN) *Technical Report, 10*, Department of Geography, Simon Fraser University. [6.2]
- Peucker, T.K., R.J. Fowler, J.J. Little and D.M. Mark (1978) The triangulated irregular network *Proceedings of the Digital Terrain Models Symposium, American Society of Photogrammetry, St. Louis*, S16–540. [6.2]
- Pfaltz, J.L. and A. Rosenfeld (1967) Computer representation of planar regions by their skeletons *Communications of the ACM*, **10**(2), 119–125. [3.5.4]
- Philbrick O. (1968) Shape recognition with the medial axis transform. In: G.C. Cheng, R.S. Ledley, D.K. Pollock and A. Rosenfeld (eds) *Pictorial Pattern Recognition* Washington: Thompson Book Company. [3.5.5]
- Philip, G.M. and D.F. Watson (1982) A precise method for determining contoured surfaces *Journal of the Australian Petroleum and Exploration Association*, **22**, 205–212. [6.2]
- Pielou, E. (1977) *Mathematical Ecology* New York: Wiley-Interscience. [1.3.3, 2.5, 5.3, 8.3]
- Pierre, M. (1990) Probes for large scale structures *Astronomy and Astrophysics*, **229**, 7–16. [5.3, 7.2]
- Pierre, M., P. Shaver and A. Iovino (1988) Void structure in the Lyman alpha forest *Astronomy and Astrophysics*, **197**, L3–L6. [5.3, 7.2]
- Piper, B. (1993) Properties of local coordinates based on Dirichlet tessellations *Computing (Supplementum)*, **8**, 227–239. [3.2.2, 6.1.2, 6.5]
- Pollack, R., M. Sharir and G. Rote (1989) Computing the geodesic center of a simple polygon *Discrete and Computational Geometry*, **4**, 611–626. [3.4.1, 3.4.5]
- Pontius, J., J. Richelle and S.J. Wodak (1996) Deviations from standard atomic volumes as a quality measure for protein crystal structures *Journal of Molecular Biology*, **264**, 121–136. [7.1]
- Popoff, C.C. (1966) Computing reserves of mineral deposits: principles and conventional methods *U.S. Department of the Interior, Bureau of Mines, Information Circular*, 8283. [6.1.1, 6.2]
- Posenau, M.A.K. (1993) Approaches to high aspect ratio triangulation *Proceedings of the 5th Canadian Conference on Computational Geometry*, 30–35. [6.5.1]
- Power, P.L. (1992) Minimal roughness property of the Delaunay triangulation: a shorter approach *Computer-Aided Geometric Design*, **9**, 491–494. [2.4]
- Preparata, F.P. (1977) The medial axis of a simple polygon. In: *Proceedings of the 6th Symposium, Mathematical Foundation of Computer Science*, **53** New York: Springer-Verlag, 443–450. [3.5.4, 4.8]
- Preparata, F.P. and S.J. Hong (1977) Convex hulls of finite sets of points in two and three dimensions *Communications of the ACM*, **20**(2), 87–93. [4.7]
- Preparata, F.P. and M.I. Shamos (1985) *Computational Geometry – An Introduction* New York: Springer-Verlag. [1.0, 1.3.2, 3.3.1, 4.1, 4.5, 4.7, 9.2]
- Price, M.A. and C. Armstrong (1997) Hexahedral mesh generation by medial surface subdivision. Part 2. Solids with flat and concave edges *International Journal for Numerical Methods in Engineering*, **40**(1), 111–136. [3.5.4, 3.5.5, 6.5]
- Price, M.A., C.G. Armstrong and M.A. Sabin (1995) Hexahedral mesh generation by medial surface subdivision: Part 1. Solids with convex edges *International Journal for Numerical Methods in Engineering*, **38**, 3335–3359. [3.5.4, 3.5.5, 6.5]
- Prim, R. (1957) Shortest connection networks and some generalizations *Bell Systems Technical Journal*, **36**, 1389–1401. [2.5]
- Priolo, A., H.M. Jaeger, A.J. Dammers and S. Radelaar (1992) Conductance of two-dimensional disordered Voronoi networks *Physical Review B. Condensed Matter*, **46**(22), 14889–14892. [5.12]
- Procacci, P. and R. Scatenni (1992) A general algorithm for computing Voronoi volumes: applications to the hydrated crystal of myoglobin *International Journal of Quantum Chemistry*, **42**(5), 1515–1528. [7.1]
- Puhl, H. (1993) Sandpiles on random lattices *Physica A*, **197**, 14–22. [5.3]
- Pyrz, R. (1994) Quantitative description of the microstructure of composites. Part I: Morphology of unidirectional composite systems *Composites Science and Technology*, **50**, 197–208. [7.1, 8.2]

- Quin, C., S. Cameron and A. McLean (1995) Towards efficient motion planning for manipulators with complex geometry *Proceedings. IEEE International Symposium on Assembly and Task Planning*, 207–212. [3.6.2]
- Quine, M.P. and J. Robinson (1990) A linear random growth model *Journal of Applied Probability*, **27**, 499–509. [5.8]
- Quine, M.P. and J. Robinson (1992) Estimation for a linear growth model *Statistics and Probability Letters*, **15**, 293–297. [5.8]
- Quine, M.P. and D.F. Watson (1984) Radial generation of n -dimensional Poisson processes *Journal of Applied Probability*, **21**, 548–557. [4.1, 5.4, 5.5, 5.5.2, 5.5.4]
- Radecke, W. (1980) Some mean value relations on stationary random mosaics in the space *Mathematische Nachrichten*, **97**, 203–210. [5.1]
- Radke, J.D. (1988) On the shape of a set of points. In: G.T. Toussaint (ed) *Computational Morphology* Amsterdam: Elsevier Science Publishers B.V., 105–136. [2.5, 8.4]
- Rahman, A. (1966) Liquid structure and self diffusion *Journal of Chemical Physics*, **45**(7), 2585–2592. [5.3, 7.1]
- Rajan, V.T. (1991) Optimality of the Delaunay triangulation in \mathbb{R}^d *Proceedings of the Seventh Annual ACM Symposium on Computational Geometry*, 357–363. [6.5.2]
- Rajan, V.T. (1994) Optimality of the Delaunay triangulation in \mathbb{R}^d *Discrete and Computational Geometry*, **12**, 189–202. [2.2, 6.5.2]
- Rajasekaran, S. and S. Ramaswami (1994) Optimal parallel randomized algorithms for the Voronoi diagram of line segments in the plane and related problems. *Proceedings of the 10th Annual Symposium on Computational Geometry*, 57–66. [3.5, 4.1, 4.8]
- Rajasekaran, S. and S. Ramaswami (1995) Optimal mesh algorithms for the Voronoi diagram of line segments and motion planning in the plane *Journal of Parallel and Distributed Computing*, **26**(1), 99–115. [3.4.1, 3.5, 3.7.11]
- Rao, C.R. (1973) *Linear Statistical Inference and its Applications* (second edition) New York: John Wiley. [5.11]
- Rao, N.S.V., N. Stoltzfus and S.S. Iyengar (1991) A ‘retraction’ method for learned navigation in unknown terrains for a circular robot *IEEE Transactions on Robotics and Automation*, **7**(5), 699–707. [3.6.2]
- Rapaport, D.C. (1983) Density fluctuations and hydrogen bonding in supercooled water *Molecular Physics*, **48**(1), 23–31. [7.1]
- Rapaport, D. (1992) A convex hull algorithm for discs, and applications *Computational Geometry: Theory and Applications*, **1**(3), 171–187. [3.6.1]
- Rathie, P.N. (1992) On the volume distribution of the typical Poisson–Delaunay cell *Journal of Applied Probability*, **29**, 740–744. [5.4, 5.11]
- Rau, K. (1841) Report to the Bulletin of the Belgian Royal Society. In: W. Baumol and S. Goldfield (eds) *Precursors in Mathematical Economics: An Anthology* London: London School of Economics and Political Science, 181–182. [3.1.6]
- Rebay, S. (1993) Efficient unstructured mesh generation by means of Delaunay triangulation and Bowyer–Watson algorithm *Journal of Computational Physics*, **106**(1), 125–138. [6.5.1]
- Recuero, A. and P.J. Gutiérrez (1993) Sloped roofs for architectural CAD systems *Microcomputers in Civil Engineering*, **8**, 147–159 [3.5.5]
- Reddy, J.M. and G.M. Turkiiyah (1995) Computation of 3D skeletons using a generalized Delaunay triangulation technique *Computer Aided Design*, **27**(9), 677–694. [3.5.1, 3.5.4]
- Reed, D.D. and H.E. Burkhart (1985) Spatial autocorrelation in individual tree characteristics in loblolly pine stands *Forest Science*, **31**, 575–587. [6.1.2, 7.1]
- Reedman, J.H. (1979) *Techniques in Mineral Exploration* London: Applied Science Publishers. [6.1.1, 6.2]
- Rees, M.D. and K.W. Morton (1991) Moving point, particle, and free-Lagrange methods for convection-diffusion equations *SIAM Journal on Scientific and Statistical Computing*, **12**(3), 547–572. [2.4]
- Reichert, K., J. Skoczylas and T. Tarnhuvud (1991) Automatic mesh generation based on expert-system-methods *IEEE Transactions on Magnetics*, **27**(5), 4197–4200. [6.5.1]
- Reiss, R-D. (1993) *A Course on Point Processes* Berlin: Springer-Verlag. [1.3.3]
- Ren, H-C. (1984) Monte Carlo study of U(1) and SU(2) gauge fields on four-dimensional random lattices *Nuclear Physics*, **B235** [FS11], 321–330. [5.3]

- Renfrew, C. (1972) *The Emergence of Civilization* London: Methuen. [7.1]
- Renfrew, C. (1973a) Monuments, mobilization and social organization in neolithic Wessex. In: C. Renfrew (ed) *The Explanation of Culture Change: Models in Prehistory* Pittsburgh: University of Pittsburgh Press, 539–558. [7.1]
- Renfrew, C. (1973b) *Before Civilization. The Radiocarbon Revolution and Prehistoric Europe* London: Jonathan Cape. [7.1]
- Renfrew, C. (1975) Trade as action at a distance: questions of integration and communication. In: J.A. Sabloff and C.C. Lamberg-Karlovsky (eds) *Ancient Civilization and Trade* Albuquerque: University of New Mexico Press, 3–59. [7.1]
- Renka, R.J. (1984a) Interpolation of data on the surface of a sphere *ACM Transactions on Mathematical Software*, **10**, 417–435. [3.7.6]
- Renka, R.J. (1984b) Algorithm 623: interpolation on the surface of a sphere *ACM Transactions on Mathematical Software*, **10**(4), 437–439. [3.7.6, 3.7.11]
- Renka, R.J. (1996) Algorithm 751: TRIPACK: a constrained two-dimensional Delaunay triangulation package *ACM Transactions on Mathematical Software*, **22**(1), 1–8. [3.4.3]
- Renka, R.J. and A.K. Cline (1992) Scattered data fitting using a constrained Delaunay triangulation *Artificial Intelligence, Expert Systems and Symbolic Computing. Selected and Revised Papers from the IMACS 13th World Congress*, 208–214. [3.4.3]
- Reyes, C. and M. Adjouadi (1995) A clustering technique for random data classification *1995 IEEE International Conference on Systems, Man and Cybernetics. Intelligent Systems for the 21st Century*, **1**, 316–321. [3.7.11]
- Reyes, C. and M. Adjouadi (1997) A directional clustering technique for random data classification *Cytometry*, **27**, 126–135. [3.5.5]
- Rhind, D. (1975) A skeletal overview of spatial interpolation techniques *Computer Applications*, **2**, 293–309. [6.0]
- Rhynsburger, D. (1973) Analytic delineation of Thiessen polygons *Geographical Analysis*, **5**, 133–144. [4.1]
- Richards, F.M. (1974) The interpretation of protein structures: total volume, group volume distributions and packing density *Journal of Molecular Biology*, **82**, 1–14. [7.1]
- Richards, F.M. (1979) Packing defects, cavities, volume fluctuations, and access to the interior of proteins. Including some general comments on surface area and protein structure *Carlsberg Research Communications*, **44**, 47–63. [7.1]
- Richards, F.M. (1985) Calculation of molecule volumes and areas for structures of known geometry *Methods in Enzymology*, **115**, 440–464. [7.1]
- Ricketts, P. (1986) Geography and international law: the case of the 1984 Gulf of Maine boundary dispute *The Canadian Geographer*, **30**(3), 194–205. [3.6.2]
- Rigby, D. and R.J. Roe (1990) Molecular dynamics simulation of polymer liquid and glass. 4. Free-volume distribution *Macromolecules*, **23**, 5312–5319. [7.1]
- Ripley, B.D. (1981) *Spatial Statistics* New York: John Wiley. [3.2.3, 6.0, 6.2, 6.3, 8.0, 8.1.1]
- Ripley, B.D. (1987) *Stochastic Simulation* New York: John Wiley. [5.4]
- Ripley, B.D. (1988) *Statistical Inference for Spatial Processes* Cambridge: Cambridge University Press. [1.3.3, 5.12]
- Rippa, S. (1990) Minimal roughness property of the Delaunay triangulation *Computer Aided Geometric Design*, **7**(6), 489–497. [2.4, 6.2, 6.4]
- Rippa, S. (1992) Adaptive approximation by piecewise linear polynomials on triangulations of subsets of scattered data *SIAM Journal on Scientific and Statistical Computing*, **13**(5), 1123–1141. [6.4]
- Rippa, S. and B. Schiff (1990) Minimum energy triangulations for elliptic problems *Computer Methods in Applied Mechanics and Engineering*, **84**(3), 257–274. [2.4]
- Rivier, N. (1982) Recent results on the ideal structures of glasses *Journal de Physique (Colloque C9)*, **43**(12, Supplement), C9–91–C9–95. [5.5.2]
- Rivier, N. (1983a) Topological structure of glasses. In: V. Vitek (ed) *Amorphous Materials: Modeling of Structure and Properties* New York: American Institute of Mining, Metallurgical and Petroleum Engineers, 81–98. [5.5.2, 7.1]
- Rivier, N. (1983b). On the structure of random tissues or froths, and their evolution *Philosophical Magazine B*, **47**(5), L45–L49. [5.5.2]

- Rivier, N. (1985a) Statistical crystallography: structure of random cellular networks *Philosophical Magazine B*, **52**(3), 795–819. [5.5.2]
- Rivier, N. (1985b) Theory of glass *Revista Brasileira de Fisica*, **15**. [7.1]
- Rivier, N. (1986a) Structure of random cellular networks and their evolution *Physica*, **23D**, 129–137. [5.5.2]
- Rivier, N. (1986b) Distributions of shapes and sizes by maximum entropy methods *Annals, Israel Physical Society*, **8**, 560. [5.5.4]
- Rivier, N. (1986c) A botanical quasicrystal *Journal de Physique (Colloque C3)*, **47**(7, Supplement), C3–299-C3–308. [7.1]
- Rivier, N. (1987) Continuous random networks. From graphs to glasses *Advances in Physics*, **36**(1), 95–134. [7.1]
- Rivier, N. (1988) Crystallography of spiral lattices *Modern Physics Letters B*, **2**(8), 953–960. [7.1]
- Rivier, N. (1991) Geometry of random packings and froths. In: D. Bideau and J.A. Dodds (eds) *Physics of Granular Media* New York: Nova Science, 3–25. [7.1]
- Rivier, N. (1993) Order and disorder in packings and froths. In: D. Bideau and A. Hansen (eds) *Disorder and Granular Media* New York: Elsevier Science Publishers B.V., 55–102 [7.1]
- Rivier, N. and D.M. Duffy (1982) On the topological entropy of atomic liquids and the latent heat of fusion *Journal of Physics C: Solid State Physics*, **15**, 2867–2874. [7.1]
- Rivier, N., E. Guyon and E. Charlaix (1985) A geometrical approach to percolation through random fractured rocks *Geological Magazine*, **122**(2), 157–162. [5.3]
- Rivier, N. and A. Lissowski (1982) On the correlation between sizes and shapes of cells in epithelial mosaics *Journal of Physics A: Mathematical and General*, **15**, L143-L148. [5.5.2]
- Rivier, N., R. Occelli, J. Pantaloni and A. Lissowski (1984) Structure of Benard convection cells, phyllotaxis and crystallography in cylindrical symmetry *Journal de Physique*, **45**, 49–63. [7.1]
- Roberts, J.N. and L.M. Schwartz (1985) Grain consolidation and electrical conductivity in porous media *Physical Review B*, **31**(9), 5990–5997. [7.1]
- Rodin, E.Y., S.M. Amin and C. Ruan (1992) Collision avoidance and low-observable navigation in a dynamic environment *Mathematical and Computer Modelling*, **16**(5), 77–98. [3.9.1, 3.9.2]
- Rogers, C.A. (1964) *Packing and Covering* Cambridge Tracts in Mathematics and Mathematical Physics No.54, Cambridge: Cambridge University Press. [1.2, 9.2.2]
- Rogers, J.D. and R.L. Long Jr (1997) Modeling hollow fiber membrane contactors using film theory, Voronoi tessellations, and facilitation factors for systems with interface reactions *Journal of Membrane Science*, **134**, 1–17. [7.1]
- Rohlb, F.J. (1973) Hierarchical clustering using the minimum spanning tree *The Computer Journal*, **16**, 93–95. [2.5]
- Roos, T. (1989) k -nearest-neighbour Voronoi diagrams for sets of convex polygons, line segments and points. In: M. Nagl (ed) *Lecture Notes in Computer Science*, **411** (Proceedings of the 15th International Workshop on Graph-Theoretic Concepts in Computer Science WG '89) Berlin: Springer-Velag, 330–340. [3.2.1, 3.6.1]
- Roos, T. (1993) Voronoi diagrams over dynamic scenes *Discrete Applied Mathematics*, **43**(3), 243–259. [3.9.1, 4.1, 4.8]
- Roos, T. (1994) Maintaining Voronoi diagrams in parallel *Proceedings of the Twenty-Seventh Hawaii International Conference on System Sciences. Vol.II: Software Technology*, 179–186. [3.9.1]
- Roos, T. (1997) New upper bounds on Voronoi diagrams of moving points *Nordic Journal of Computing*, **4**, 167–171. [3.9.1]
- Roos, T. and H. Noltemeier (1991) Dynamic Voronoi diagrams in motion planning *Lecture Notes in Computer Science*, **553** Berlin: Springer-Verlag, 227–236. [3.9.2]
- Roos, T. and H. Noltemeier (1992) Dynamic Voronoi diagrams in motion planning *Lecture Notes in Control and Information Science*, **180** Berlin: Springer-Verlag, 102–111. [3.9.2]
- Rosenberger, H. (1991) Order- k Voronoi diagrams of sites with additive weights in the plane *Algorithmica*, **6**, 490–521. [3.2.1, 4.8]

- Rosenfeld, A. (1979) Digital topology *American Mathematical Monthly*, **86**, 621–630. [3.5.5]
- Rosenfeld, A. and J.L. Pfaltz. (1966) Sequential operations in digital picture processing *Journal of the ACM*, **15**, 471–494. [3.5.4]
- Rosenkrantz, D. J., R. E. Stearns and P. M. Lewis II (1977) An analysis of several heuristics for the traveling salesman problem *SIAM Journal on Computing*, **6**, 563–581. [2.5]
- Roudot, A.C., F. Duprat and E. Pictri (1990) Simulation of a penetrometric test on apples using Voronoi-Delaunay tessellation *Food Structure*, **9**(3), 215–222. [7.1]
- Rouns, T.N., J.M. Fridy, K.B. Lippert and O. Richmond (1990) Quantitative characterization and modeling of second phase populations through the use of tessellations. In: M.P. Anderson and A.D. Rollett (eds) *Simulation and Theory of Evolving Microstructures* Warrendale: The Minerals, Metals and Materials Society, 269–275. [3.5.5]
- Roy, U. and X. Zhang (1994) Development and application of Voronoi diagram in the assessment of roundness error in an industrial environment *Computers and Industrial Engineering*, **26**(1), 11–26. [3.3.3]
- Royden, H.L. (1963) *Real Analysis* New York: Macmillan. [1.3]
- Ruggles, A.J. and R.L. Church (1996) An analysis of Late-Horizon settlement patterns in the Teotihuacan-Temascalapa basins: a location-allocation and GIS-based approach. In: M. Aldenderfer and H.D.G. Maschner (eds) *Anthropology, Space, and Geographic Information Systems* New York: Oxford University Press, 155–174. [7.1]
- Ruocco, G., M. Sampoli and R. Valluri (1991) Molecular dynamics simulations of liquid water: Voronoi polyhedra and network typology *Journal of Molecular Structure*, **250**, 259–270. [7.1]
- Ruppert, J. (1995) A Delaunay refinement algorithm for quality 2-dimensional mesh generation *Journal of Algorithms*, **18**(3), 548–585. [3.4.3]
- Ruprecht, D. and H. Müller (1995) Image warping with scattered data interpolation *IEEE Computer Graphics and Applications*, **15**(2), 37–43. [3.4.5]
- Rustad, J.R., D.A. Yuen and F.J. Spera (1991a) Molecular dynamics of amorphous silica at very high pressures (135 GPa): thermodynamics and extraction of structures through analysis of Voronoi polyhedra *Physical Review B*, **44**(5), 2108–2121. [7.1]
- Rustad, J.R., D.A. Yuen and F.J. Spera (1991b) The statistical geometry of amorphous silica at lower mantle pressures: implications for melting slopes of silicates and anharmonicity *Journal of Geophysical Research*, **96**(B12), 19665–19673. [7.1]
- Ryden, B.S. (1995) Measuring q_0 from the distortion of voids in redshift space *The Astrophysical Journal*, **452**, 25–32. [7.2]
- Saalfeld, A. (1991) Delaunay edge refinements *Proceedings of the Third Canadian Conference on Computational Geometry*, 33–36. [3.4.3]
- Saaty, T. L (1970) *Optimization in Integers and Related Extremal Problems* New York: McGraw-Hill. [2.5]
- Sabin, M.A. (1976) Errata *The Computer Journal*, **19**, 384. [6.2]
- Sabin, M.A. (1982) Contouring – a review of methods for scattered data. In: K.W. Brodie (ed) *Mathematical Methods in Computer Graphics and Design* London: Academic Press, 63–86. [6.0]
- Sadek, E.A. (1980) A scheme for automatic generation of triangular finite elements *International Journal for Numerical Methods in Engineering*, **15**, 1813–1822. [6.3]
- Saetre, T.O., O. Hunderi and E. Nes (1986) Computer simulation of primary recrystallization microstructures. The effects of nucleation and growth kinetics *Acta Metallurgica*, **34**(6), 981–987. [5.6.2, 5.8, 7.2]
- Saito, N. (1982) Asymptotic regular pattern of epidermal cells in mammalian skin *Journal of Theoretical Biology*, **95**, 591–599. [7.1, 7.3.2]
- Saito, T. and J-I. Toriwaki (1992) Algorithms of three dimensional Euclidean distance transformation and extended digital Voronoi diagram, and analysis of human liver section images *Journal of the Institute of Image Electronics Engineers of Japan*, **21**(5), 468–474. [3.6.2]
- Saito, T., J-I. Toriwaki and S. Yokoi (1991) Properties of extended digital α -hull with applications to shape feature analysis of a figure set *Forma*, **6**, 9–25. [8.4.2]
- Sakakibara, K., K. Matsuyama and A. Suzuki (1996) Error free $L1$ -Voronoi diagram construction algorithm and its application to p -median problem of $L1$ distance in a

- unit square *International Symposium of Location Decision, VII, Alberta, 26 June-3 July, Studies on Location Science*, 113–116. [4.8]
- Sakamoto, M. and M. Takagi (1987) Weighted Voronoi tessellations *Denshi Joho Tsushin Gakkai*, **PRU87-49**, 21–30 [in Japanese]. [3.1.6]
- Sambridge, M., J. Braun and H. McQueen (1995) Geophysical parameterization and interpolation of irregular data using natural neighbours *Geophysical Journal International*, **122**, 837–857. [6.1.2]
- Santaló, L.A. (1976) *Integral Geometry and Geometric Probability* Reading, Ma.: Addison-Wesley. [1.3.3, 5.9]
- Santaló, L.A. (1988) Random mosaics *Revista de la Real Academia de Ciencias Exactas, Fisicas y Naturales de Madrid*, **82**, 483–522. [5.1]
- Santos, F. (1996) On Delaunay oriented matroids for convex distance functions *Discrete and Computational Geometry*, **16**, 197–210. [2.3]
- Sapidis, N. and R. Perucchio (1991a) Domain Delaunay tetrahedrization of solid models *International Journal of Computational Geometry and Applications*, **1**(3), 299–325. [3.4.3]
- Sapidis, N. and R. Perucchio (1991b) Delaunay triangulation of arbitrarily shaped planar domains *Computer-Aided Geometric Design*, **8**(6), 421–437. [3.4.3, 6.5.1]
- Sapidis, N. and R. Perucchio (1992) Solid/solid classification operations for recursive spatial decomposition and domain triangulation of solid models *Computer Aided Design*, **24**(10), 517–529. [3.4.3]
- Savage, S.H. (1990) Modelling the Late Archaic social landscape. In: K.M.S. Allen, S.W. Green and E.B.W. Zubrow (eds) *Interpreting Space: GIS and Archaeology* London: Taylor and Francis, 330–355. [7.1]
- Saxena, S., P.C.P. Bhatt and V.C. Prasad (1990) Efficient VLSI parallel algorithm for Delaunay triangulation on orthogonal tree network in two and three dimensions *IEEE Transactions on Computers*, **39**(3), 400–404. [4.1]
- Schachter, B. and N. Ahuja (1979) Random pattern generation processes *Computer Graphics and Image Processing*, **10**, 95–114. [5.3]
- Schraudt, B.F. and R.L. Drysdale (1991) Multiplicatively weighted crystal growth Voronoi diagrams *Proceedings of the Seventh Annual ACM Symposium on Computational Geometry, June*, 214–223. [3.1.2]
- Scheike, T.H. (1994) Anisotropic growth of Voronoi cells *Advances in Applied Probability*, **26**(1), 43–53. [3.7.2, 3.7.11, 7.2]
- Schlather, M. (1999) A formula for the edge length distribution function of the Poisson Voronoi tessellation *Muthematische Nachrichten*, to appear. [5.5.4, 5.7]
- Schlather, M. and D. Stoyan (1997) Covariance of Stienen model. In: D. Jeulin (ed) *Advances in Theory and Applications of Random Sets* Singapore: World Scientific, 157–174. [5.6.3]
- Schlitz, G. (1996) German dialectometry. In: H-H. Bock and W. Polasek (eds) *Data Analysis and Information Systems. Statistical and Conceptual Approaches* Berlin: Springer-Verlag. [7.1]
- Schlottmann, M. (1993) Periodic and quasi-periodic Laguerre tilings *International Journal of Modern Physics B*, **7**(6–7), 1351–1363. [2.5, 3.1.4, 7.1]
- Schmitt, D. and J-C. Spehner (1993) On equiangularity of Delaunay diagrams in every dimension *Proceedings of the Fifth Canadian Conference on Computational Geometry*, 346–351. [6.5.2]
- Schmit, M. (1988) Some examples of algorithms analysis in computational geometry by means of mathematical morphology techniques. In: J-D. Boissonnat and J-P. Laumond (eds) *Lecture Notes in Computer Science: Geometry and Robotics*, **391** Berlin: Springer-Verlag, 225–245. [3.5.4]
- Schnitker, J., R. Gopalaswamy and G.M. Crippen (1997) Objective models for steroid binding sites of human globulins *Journal of Computer-Aided Molecular Design*, **11**, 93–110. [7.1]
- Schnitker, J. and P. Mausbach (1990) Voronoi polyhedra analysis and order-disorder transition of a tetrahedrally ordered liquid *Zeitschrift für Angewandte Mathematik und Mechanik*, **70**(4), T266-T269. [7.1]

- Schnitker, J., P.J. Rossky and G.A. Kenny-Wallace (1986) Electron localization in liquid water: a computer simulation study of microscopic trapping sites *Journal of Chemical Physics*, **85**, 2986–2998. [7.1]
- Schoenflies, A. (1891) *Krystallsysteme und Krystallstruktur* Leipzig: B.G. Teubner. [1.2]
- Schoenflies, A. (1923) *Krystallsysteme und Krystallstruktur* Zweite Auflage Berlin: Gebr. Borntraeger [1.2]
- Schroeder, W.J. and M.S. Shephard (1988) Geometry-based fully automatic mesh generation and the Delaunay triangulation *International Journal of Numerical Methods in Engineering*, **26**, 2530–2545. [6.5.1]
- Schulze, G.E.W. and W.A. Schulze (1992) Chord intercepts in a two-dimensional cell growth model: Part III. Chord intercepts in an experiment *Journal of Materials Science*, **27**, 947–955. [7.2]
- Schulze, G.E.W. and L.O. Schwan (1992) Die Zwickel im wachsenden 2D Zellenmodell *Zeitschrift für Metallkunde*, **83**, 208–211. [7.2]
- Schulze, G.E.W. and L.O. Schwan (1993) The normalized numbers of grain boundaries, triple points and growth fronts in a circular growing two-dimensional Voronoi tessellation with Poisson-distributed points *Journal of Materials Science*, **28**(10), 2706–2714. [7.2]
- Schulze, G.E.W., L.O. Schwan and P. Franke (1993) The mean normalized Euler characteristic of a simultaneously starting and growing 2D Voronoi tessellation with Poisson-distributed nuclei *Philosophical Magazine B*, **68**(2), 149–170. [5.6.2, 7.2]
- Schulze, G.E.W., L.O. Schwan and R. Willers (1989) Chord intercepts in a two-dimensional cell growth model: Part II. Chord intercepts of the grains *Journal of Materials Science*, **24**, 3107–3112. [7.2]
- Schulze, G.E.W. and H-P. Wilbert (1989a) Thermic marking of spherulitic growth fronts *Journal of Materials Science Letters*, **8**, 71–74. [7.2]
- Schulze, G.E.W. and H-P. Wilbert (1989b) Chord intercepts in a two-dimensional cell growth model: Part I. Chord intercepts of the diminishing phase *Journal of Materials Science*, **24**, 3101–3106. [7.2]
- Schulze, G.E.W. and H-P. Wilbert (1991a) Experimenteller Nachweis der Poissonverteilung von Keimen beim Phasenübergang flüssig-fest in einer Ebene *Zeitschrift für Metallkunde*, **82**, 713–717. [7.2]
- Schulze, G.E.W. and H-P. Wilbert (1991b) The definition of the two-dimensional ‘cell model’ in experiment *Journal of Materials Science Letters*, **10**, 770–771. [7.2]
- Schumaker, L.L. (1976) Fitting surfaces to scattered data. In: G.G. Lorentz, C.K. Chui and L.L. Schumaker (eds) *Approximation Theory II* New York: Academic Press, 203–268. [6.0]
- Schumaker, L.L. (1993) Triangulations in CAGD *IEEE Computer Graphics and Applications*, **13**, 47–52. [6.2, 6.5]
- Schut, G.H. (1976) Review of interpolation methods for digital terrain models *The Canadian Surveyor*, **30**(5), 389–412. [6.0]
- Schwarz, H.R. (1988) *Finite Element Methods* London: Academic Press. [6.5]
- Schwartz, J.T. and M. Sharir (1983a) On the piano movers’ problem I. The Case of a two-dimensional rigid polygonal body moving amidst polygonal barriers *Communications on Pure and Applied*, **36**, 345–398. [3.7.11]
- Schwartz, J.T. and M. Sharir (1983b) On the movers’ problem. II. General techniques for computing topological properties of real algebraic manifolds *Advances in Applied Mathematics*, **4**, 298–351. [3.7.11]
- Schwarzkopf, O. (1989) Parallel computation of discrete Voronoi diagrams *Lecture Notes in Computer Science* (STACS ‘89), **349** Berlin: Springer-Verlag, 193–204. [2.1, 2.4]
- Schwertel, J. and H. Stamm (1996) Analysis and modelling of tessellations by means of image analysis methods *Journal of Microscopy*, **186**(2), 198–209. [5.3]
- Scott, A.J. (1971) *Combinatorial Programming, Spatial Analysis and Planning* London: Methuen. [7.1, 9.4.1]
- Scott, A.J. (1975) Discrete dynamic location systems: notes on a structural framework. In: A. Karlqvist, L. Lundqvist, F. Snickars (eds) *Dynamic Allocation of Urban Space* Westmead Farnborough: Saxon House, 121–160. [9.4.1]

- Seefeldt, M. and P. Klimanek (1997) Interpretation of plastic deformation by means of dislocation-disclination reaction kinetics *Materials Science and Engineering*, **A234-236**, 758–761. [5.3]
- Seidel, R. (1982) On the size of closest point Voronoi diagrams *Institute for Information Processing, Technical University of Graz, Report, F94*. [3.3.1, 4.8]
- Seidel, R. (1986) Constructing higher-dimensional convex hulls at logarithmic cost per face *Proceedings of the 18th Annual ACM Symposium on Theory of Computing*, 404–413. [4.7]
- Seidel, R. (1987) Output-size Sensitive Algorithms for Constructional Problems in Computational Geometry. Ph.D. Thesis, Cornell University. [4.7]
- Seidel, R. (1991) Exact upper bounds for the number of faces in d -dimensional Voronoi diagrams *DIMACS Series in Discrete Mathematics and Theoretical Computer Science, Volume 4, Applied Geometry and Discrete Mathematics: The Victor Klee Festschrift* Providence: The American Mathematical Society, 517–530. [2.3, 3.3.1]
- Seoung, Y.M. (1990) A Study on Optimal Location Problems of Facilities Using the Voronoi Diagram. Master's Thesis, Department of Urban Engineering, University of Tokyo [in Japanese]. [3.7.10, 9.4.2]
- Seoung, Y.M. and T. Asano (1987) Facility location problems with obstacles *Proceedings of the 1987 Joint Technical Conference on Circuits and Systems (JTC-CAS'87)*, 237–242. [3.4.4, 4.8]
- Seul, M., N.Y. Morgan and C. Sire (1994) Domain coarsening in a two-dimensional binary mixture: growth dynamics and spatial correlations *Physical Review Letters*, **73**(17), 2284–2287. [5.5.3]
- Sewell, M.J. (1987) *Maximum and Minimum Principle – A Unified Approach with Applications* Cambridge: Cambridge University Press. [2.4]
- Shaked, A. (1975) The non-existence of equilibrium for the two-dimensional three-firms problem *Review of Economic Studies*, **42**, 51–55. [7.3.1]
- Shamos, M.I. (1978) Computational Geometry. Ph.D. Thesis, Yale University. [3.2, 3.2.2]
- Shamos, M.I. and D. Hoey (1975) Closest-point problems *Proceedings of the 16th Annual IEEE Symposium on Foundations of Computer Science*, 151–162. [1.2, 2.4, 3.2, 4.1, 4.4]
- Shannon, C.E. (1948a) A mathematical theory of communication *Bell System Technical Journal*, **27**(3), 379–423. [1.2, 8.1.2]
- Shannon, C.E. (1948b) A mathematical theory of communication *Bell System Technical Journal*, **27**(4), 623–656. [1.2, 8.1.2]
- Shannon, C.E. (1949) Communication in the presence of noise *Proceedings of the I.R.E.*, **37**, 10–21. [1.2]
- Shannon, C.E. (1959) Probability of error for optimal codes in a Gaussian channel *Bell System Technical Journal*, **38**(3), 611–656. [1.2, 7.1]
- Shapiro, M. (1981) A note on Lee and Schachter's algorithm for Delaunay triangulation *International Journal of Computer and Information Sciences*, **10**, 413–418. [4.1]
- Sharir, M. (1985) Intersection and closest-pair problems for a set of planar discs *SIAM Journal on Computing*, **14**, 448–468. [3.5, 3.5.3]
- Sharir, M. and A. Baltan (1986) On shortest paths amidst convex polyhedra *Proceedings of the Second Annual ACM Symposium on Computational Geometry*, 193–206. [3.7.9]
- Sharir, M. and A. Schorr (1984) On shortest paths in polyhedral spaces *Proceedings of the 16th ACM Annual Symposium on Theory of Computing*, 144–153. [3.4.1, 3.7.9]
- Shehata, M.T. and J.D. Boyd (1988) Measurement of spatial distribution of inclusions. In: R. Rungta (ed) *Inclusions and Their Influence on Material Behavior* Metals Park: ASM International, 123–131. [7.1, 8.1.1, 8.2]
- Sheehy, D.J., C.G. Armstrong and D.J. Robinson (1996) Shape description by medial surface construction *IEEE Transactions on Visualization and Computer Graphics*, **2**(1), 62–72. [3.5.4]
- Sheng, X. and B.E. Hirsch (1992) Triangulation of trimmed surfaces in parametric space *Computer Aided Design*, **24**(8), 437–444. [3.4.3]
- Sherbrooke, E.C., N.M. Patrikalakis and E. Brisson (1996) An algorithm for the medial axis transform of 3D polyhedral solids *IEEE Transactions on Visualization and Computer Graphics*, **2**(1), 44–61. [3.5.4]

- Shieh, Y-N. (1985) K.H. Rau and the economic law of market areas *Journal of Regional Science*, **25**(2), 191–199. [1.2, 3.1.6]
- Shih, J-P., S-Y. Sheu and C-Y. Mou (1994) A Voronoi polyhedra analysis of structures of liquid water *Journal of Chemical Physics*, **100**(3), 2202–2212. [7.1]
- Shiode, T. (1995) A Study on Optimization of the Shape of Spatial Facilities. Bachelor's Thesis, Department of Urban Engineering, University of Tokyo [in Japanese]. [9.3.3]
- Shute, G.M., L.L. Deneen and C.D. Thomborson (1991) An $O(n \log n)$ plane-sweep algorithm for L_1 and L_∞ Delaunay triangulations *Algorithmica*, **6**(2), 207–221. [3.7.1, 4.8]
- Sibson, R. (1978) Locally equiangular triangulations *The Computer Journal*, **21**, 243–245. [2.4, 4.1, 6.2]
- Sibson, R. (1980a) A vector identity for the Dirichlet tessellation *Mathematical Proceedings of the Cambridge Philosophical Society*, **87**, 151–155. [3.1.5, 3.2, 3.2.2, 3.2.3, 4.1, 4.8, 6.1.2]
- Sibson, R. (1980b) The Dirichlet tessellation as an aid in data analysis *Scandinavian Journal of Statistics*, **7**, 14–20. [3.2.2, 4.1]
- Sibson, R. (1981) A brief description of natural neighbour interpolation. In: V. Barnett (ed) *Interpreting Multivariate Data* New York: John Wiley, 21–36. [6.0, 6.1.2]
- Siersma, D. (1998) Voronoi diagrams and Morse theory of the distance function. In: O.E. Barndorff-Nielsen and E.B.V. Jensen (eds) *Geometry in Present Day Science* Singapore: World Scientific. [2.1, 3.1.6]
- Silva, M.J. and L.J. Gibson (1997) The effects of non-periodic microstructure and defects on the compressive strength of two-dimensional cellular solids *International Journal of Mechanical Sciences*, **39**(5), 549–563. [5.12]
- Silva, M.J., L.J. Gibson and W.C Haynes (1995) The effects of non-periodic microstructure on the elastic properties of two-dimensional cellular solids *International Journal of Mechanical Sciences*, **37**(11), 1161–1177. [5.12]
- Singh, R.L. and R.P.B. Singh (1975) Shape analysis in rural settlement geography: qualitative vs. quantitative approach. In: R.L. Singh (ed) *Readings in Rural Settlement Geography* Varanasi: National Geographical Society of India, 444–452. [7.1]
- Singh, R.L. and R.P.B. Singh (1977) Spatial and structural analysis of the rural market network and its relation to society in an Indian environment *National Geographical Journal of India*, **23**, 151–159. [7.1]
- Singh, R.P.B. (1976) A note on the transformation of village shapes into Thiessen polygons and hexagons *Geographical Review of India*, **38**, 50–53. [7.1]
- Singh, R.P.B. (1979) Poisson process and cell model properties of village shape in Middle Ganga valley, India: a comparative study of locational pattern *National Geographical Journal of India*, **25**, 154–166. [5.3, 7.1]
- Singh, R.P.B. and U.P. Singh (1978) Structural characteristics and transformation of village shape in spatial matrix (case of Gorakpur district) *National Geographer*, **13**, 143–154. [5.3, 7.1]
- Skyum, S. (1991) A simple algorithm for computing the smallest enclosing circle *Information Processing Letters*, **37**(3), 121–125. [3.3.1]
- Slepian, D. (1965) Permutation modulation *Proceedings of the IEEE*, **53**(3), 228–236. [1.2, 7.1]
- Slepian, D. (1968) Group codes for the Gaussian channel *Bell System Technical Journal*, **47**(4), 575–602. [1.2, 7.1]
- Slivnyak, I.M. (1962) Some properties of stationary flows of homogeneous random events *Theory of Probability and its Applications*, **7**, 336–341. [1.3.3]
- Sloan, S.W. (1993) A fast algorithm for generating constrained Delaunay triangulations *Computers and Structures*, **47**, 441–450. [3.4.3, 4.8]
- Small, C.G. (1988) Techniques of shape analysis on sets of points *International Statistical Review*, **56**(3), 243–257. [5.11]
- Small, C.G. (1996) *The Statistical Theory of Shape* New York: Springer-Verlag. [5.11]
- Smalley, L.J. (1966) Contraction crack networks in basalt flows *Geological Magazine*, **103**, 110–114. [5.12, 7.2]
- Smirnov, V.I., A.P. Prokof'yev and others (1960) Podschet Zapasov Mestorozhdenii Poleznykh Iskopaemykh (Reserve Computations of Mineral Deposits) Moscow: Gosgeoltekhnizdat (State Scientific and Technical Publishers for Mining Literature) [1.2]

- Smith, C.S. (1954) The shape of things *Scientific American*, **190**(1), 58–64. [3.1.6]
- Smith, F.W. (1964) The structure of aggregates and the molecular kinematics of the viscosity of a Bernal liquid *Canadian Journal of Physics*, **42**, 304–320. [1.2, 7.1]
- Smith, F.W. (1965) The structure of aggregates – a class of 20-sided space-filling polyhedra *Canadian Journal of Physics*, **43**, 2052–2055. [1.2, 7.1]
- Smith, J.M., D.T. Lee and J.S. Liebman (1981) An $O(n \log n)$ heuristic for Steiner minimal tree problems on the Euclidean metric *Networks*, **11**, 23–39. [9.3.3]
- Smith, J.M., R. Weiss and M. Patel (1995) An $O(N^2)$ heuristic for Steiner minimal trees in E^3 *Networks*, **25**, 273–289. [2.5]
- Smith, R.W. (1987) Computer processing of line images: a survey *Pattern Recognition*, **20**(1), 7–15. [3.5.4, 3.5.5]
- Snow, J. (1855) *On the Mode of Communication of Cholera* (second edition) London: Churchill Livingstone. [1.2, 3.8.4]
- Snyder, D.E. (1962) Urban places in Uruguay and the concept of a hierarchy *Festschrift: C.F. Jones, Northwestern University, Studies in Geography*, **6**, 29–46. [1.2, 7.1]
- Snyder, D.L. and M.I. Miller (1991) *Random Point Processes in Time and Space* (second edition) New York: Springer-Verlag. [1.3.3]
- Solomon, H. and M.A. Stephens (1980) Approximations to densities in geometric probability *Journal of Applied Probability*, **17**, 145–153. [5.5.4]
- Speiser, A. (1927) *Die Theorie der Gruppen von endlicher Ordnung* (zweite Auflage) Berlin: Springer-Verlag. [1.2]
- Spitzig, W.A., J.F. Kelly and O. Richmond (1985) Quantitative characterization of second-phase populations *Metallography*, **18**, 235–261. [7.1, 8.2]
- Srinivasan, V. and L.R. Nackman (1987) Voronoi diagram for multiply-connected polygonal domains, I – Algorithm *IBM Journal of Research and Development*, **31**, 361–372. [3.5.4, 4.8]
- Srinivasan, V., L.R. Nackman, J.M. Tang and S.N. Meshkat (1992) Automatic mesh generation using the symmetric axis transformation of polygonal domains *Proceedings of the IEEE*, **80**(9), 1485–1501. [3.5.4, 3.5.5, 6.5.1]
- Srivastava, S. and G.M. Crippen (1993) Analysis of cocaine receptor site ligand binding by three-dimensional Voronoi site modeling approach *Journal of Medicinal Chemistry*, **36**(23), 3572–3579. [7.1]
- Srolovitz, D.J., G.S. Grest and M.P. Anderson (1986) Computer simulation of recrystallization – I. Homogeneous nucleation and growth *Acta Metallurgica*, **34**(9), 1833–1845. [5.8]
- Stamp, L.D. (1964) *The Geography of Life and Death* New York: Cornell University Press. [1.2]
- Steele, M. (1982) Optimal triangulation of random samples in the plane *The Annals of Probability*, **10**(3), 548–553. [6.2]
- Steinitz, E. (1906) Polyeder und Raumteilungen *Enzyklopädie der Mathematischen Wissenschaften III. AB*, **12**. Leipzig: Teubner, 1–139. [1.2]
- Steyer, A., P. Guenoun, D. Beyens and C.N. Knobler (1990) Two-dimensional ordering during droplet growth on a liquid surface *Physical Review B*, **42**(1), 1086–1089. [7.2]
- Stienen, H. (1982) Die Vergrößerung von Karbiden in reinen Eisen-Kohlenstoff-Stählen *Dissertation RWTH Aachen*. [5.6.3]
- Stifter, S. (1991) An axiomatic approach to Voronoi-diagrams in 3D *Journal of Computer and System Sciences*, **43**(2), 361–379. [3.0]
- Stiny, J. (1929) *Technische Gesteinskunde für Bauingenieure, Kulturtechniker Land- und Forstwirte, sowie für Steinbruchtechniker* Vienna: Julius Springer-Verlag. [7.2]
- Stogrin, M.I. (1968) Regular Dirichlet-Voronoi partitions for the second triclinic group *Soviet Mathematics Doklady* **9**, 1479–1482. [7.1]
- Stogrin, M.I. (1973) Regular Dirichlet-Voronoi partitions for the second triclinic group *Proceedings of the Steklov Institute of Mathematics* **123**. [7.1]
- Stone, I.C. and P. Tsakiroopoulos (1995) Characterisation of spatial distribution of reinforcement in powder metallurgy route Al/SiC_p metal matrix composites. Part 1 – Techniques based on microstructure *Materials Science and Technology*, **11**, 213–221. [7.1, 8.1.1, 8.2]

- Storer, J.A. and J.H. Reif (1994) Shortest paths in the plane with polygonal obstacles *Journal of the Association for Computing Machinery*, **41**(5), 982–1012. [3.4.1]
- Stouffer, S.A. (1940) Intervening opportunities: a theory relating mobility and distance *American Sociological Review*, **5**, 845–867. [6.1.2]
- Stoyan, D. (1986) On generalized planar random tessellations *Mathematische Nachrichten*, **128**, 215–219. [5.4]
- Stoyan, D. (1990) Stereological formulae for a random system of non-intersecting spheres *Statistics*, **21**(1), 131–136. [5.6.3]
- Stoyan, D. and H. Hermann (1986) Some methods for statistical analysis of planar random tessellations *Statistics*, **17**(3), 407–420. [5.5.3, 5.6.1, 9.5.1]
- Stoyan, D., W.S. Kendall and J. Mecke (1987) *Stochastic Geometry and its Applications* New York: John Wiley. [1.0]
- Stoyan, D., W.S. Kendall and J. Mecke (1995) *Stochastic Geometry and its Applications* (second edition) New York: John Wiley. [1.3.3, 5.1, 5.6.2, 5.8, 5.11, 5.12, 8.0, 8.7]
- Stoyan, D. and H. Stoyan (1980) Gedanken zur Entstehung der Selenformen bei Basalten *Zeitschrift für Geologischen Wissenschaften*, **8**, 1529–1537. [7.2, 9.5.1]
- Stoyan, D. and H. Stoyan (1990) Exploratory data analysis for planar tessellations: structural analysis and point process models *Applied Stochastic Models and Data Analysis*, **6**, 13–25. [5.6.1]
- Stoyan, D. and H. Stoyan (1994) *Fractals, Random Shapes and Point Fields: Methods of Geometrical Statistics* New York: John Wiley. [5.6.1, 8.0]
- Su, T-H. and R-C. Chang (1990) The k -Gabriel graphs and their applications *Proceedings International Symposium, SIGAL '90, August*, 66–75. [2.5]
- Su, T. and R. Chang (1991a) Computing the constrained relative neighborhood graphs and constrained Gabriel graphs in Euclidean plane *Pattern Recognition*, **24**(3), 221–230. [2.5]
- Su, T. and R. Chang (1991b) Computing the k -relative neighborhood graphs in Euclidean plane *Pattern Recognition*, **24**(3), 231–239. [2.5]
- SubbaRao, M.U. and A.S. Szalay (1992) Statistics of pencil beams in Voronoi foams *The Astrophysical Journal*, **391**(2), 483–493. [5.12, 7.2]
- Sugihara, K. (1986) *Machine Interpretation of Line Drawings* Cambridge: MIT Press. [2.4]
- Sugihara, K. (1992a) Voronoi diagrams in a river *International Journal of Computational Geometry and Applications*, **2**(1), 29–48. [3.7.5, 4.5, 4.8]
- Sugihara, K. (1992b) A simple method for avoiding numerical errors and degeneracy in Voronoi diagram construction *IEICE Transactions. Fundamentals*, **E75-A**(4), 468–477. [4.6.2]
- Sugihara, K. (1994) Robust gift wrapping for the three-dimensional convex hull *Journal of Computer and System Sciences*, **49**, 391–407. [4.7]
- Sugihara, K. (1997) Experimental study on acceleration of an exact-arithmetic geometric algorithm *Proceedings of the 1997 International Conference on Shape Modeling and Applications, Aizu-Wakamatsu, Japan, March 3–6, 1997*, IEEE Computer Society, 160–168. [3.7.6, 4.6.2, 4.7]
- Sugihara, K. and M. Iri (1988) Geometric algorithms in finite-precision arithmetic *Abstracts of the 13th International Symposium on Mathematical Programming, Tokyo, August 1988*, 196. [4.1, 4.6.3]
- Sugihara, K. and M. Iri (1989a) A solid modelling system free from topological inconsistency *Journal of Information Processing*, **12**, 380–393. [4.6.2]
- Sugihara, K. and M. Iri (1989b) Two design principles of geometric algorithms in finite-precision arithmetic *Applied Mathematics Letters*, **2**, 203–206. [4.1, 4.6.3]
- Sugihara, K. and M. Iri (1989c) VORONOI2 reference manual – Topology-oriented version for the incremental method for constructing Voronoi diagrams *Research Memorandum, RMI 89-04*, Department of Mathematical Engineering and Information Physics, Faculty of Engineering, University of Tokyo. [4.6.3]
- Sugihara, K. and M. Iri (1989d) Construction of the Voronoi diagram for one million generators in single precision arithmetic, Paper presented at the First Canadian Conference on Computational Geometry, August 21–25, 1989, Montreal, Canada. [4.1]
- Sugihara, K. and M. Iri (1992) Construction of the Voronoi diagram for ‘one million’ generators in single-precision arithmetic *Proceedings of the IEEE*, **80**(9), 1471–1484. [9.2]

- Sugihara, K., Y. Ooishi and T. Imai (1990) Topology-oriented approach to robustness and its applications to several Voronoi-diagram algorithms *Abstracts of the 2nd Canadian Conference on Computational Geometry, Ottawa, August 1990*, 36–39. [4.1]
- Supowit, K.J. (1983) The relative neighborhood graph with an application to minimum spanning trees *Journal of ACM*, **30**, 428–447. [2.5]
- Suri, S. (1989) Computing geodesic furthest neighbors in simple polygons *Journal of Computer and System Sciences*, **39**, 220–235. [3.4.5]
- Sutherland, W.R.S. (1990) The offsets of a convex polygon *Methods of Operations Research*, **62**, 33–41. [3.5.5]
- Suzuki, A. (1989) An incremental algorithm for the farthest Voronoi diagram *Abstracts of The Fifth Canadian Conference on Computational Geometry, Montreal, August 1989*, 43. [4.8]
- Suzuki, A. and M. Iri (1986a) Approximation of a tessellation of the plane by a Voronoi diagram *Journal of the Operations Research Society of Japan*, **29**, 69–96. [7.2, 9.5.1, 9.5.2]
- Suzuki, A. and M. Iri (1986b) A heuristic method for the Euclidean Steiner problems as a geometrical optimization problem *Asia-Pacific Journal of Operational Research*, **3**(2), 109–122. [9.3.3, 9.5.1]
- Suzuki, A. and M. Iri (1986c) Location problems for railroad-minimizing total travel times *Abstract of Operations Research Society of Japan, Spring*, **2-C-9**, 210–211. [9.3.2]
- Suzuki, T. (1987) Optimum locational patterns of bus-stops for many-to-one travel demand *Papers of the Annual Conference of the City Planning Institute of Japan*, **22**, 247–252 [in Japanese]. [9.2.1, 9.2.7]
- Suzuki, T. (1989) Study on Locational Optimization of Facilities on a Plane with Socially Optimal Criteria. Master's Thesis, Department of Urban Engineering, University of Tokyo [in Japanese]. [9.2.4]
- Suzuki, T., Y. Asami and A. Okabe (1991) Sequential allocation of public facilities in one- and two-dimensional space: comparison of several policies, *Journal of Mathematical Programming Series B*, **52**, 125–146. [9.4.1]
- Swart, G. (1985) Finding the convex hull facet by facet *Journal of Algorithms*, **6**, 17–48. [4.7]
- Szeto, K.Y. and W.Y. Tam (1995) Lewis' law versus Feltham's law in soap froth *Physica A*, **221**, 256–262. [5.5.2, 5.12]
- Tagare, H.D., F.M. Vos, C.C. Jaffe and J.S. Duncan (1995) Arrangement: A spatial relation between parts for evaluating similarity of tomographic section *IEEE Transactions on Pattern Analysis and Machine Intelligence*, **17**(9), 880–893. [3.6.2]
- Takahashi, O. and R.J. Schilling (1989) Motion planning in a plane using generalized Voronoi diagrams *IEEE Transactions on Robotics and Automation*, **5**(2), 143–150. [3.7.11]
- Takeda, S. (1985) On Geographical Optimization and Dynamic Facility Location Problem. Master's Thesis, Department of Mathematical Engineering and Information Physics, University of Tokyo [in Japanese]. [3.5.5, 9.2.2, 9.2.6, 9.3.1, 9.4.2]
- Takizawa, H., Y. Shirai and J. Miura (1996) Selective refinement of 3-D scene description by attentive observation for mobile robot *Robotics and Autonomous Systems (Netherlands)*, **17**(1–2), 15–23. [3.4.5]
- Talmon, Y. and S. Prager (1978a) Statistical mechanics of microemulsions *Nature*, **267**, 333–335. [5.3]
- Talmon, Y. and S. Prager (1978b) Statistical thermodynamics of phase equilibria in microemulsions *Journal of Chemical Physics*, **69**(7), 2984–2991. [5.3]
- Tam, T.K.H. and C.G. Armstrong (1991) 2D finite element mesh generation by medial axis subdivision *Advances in Engineering Software*, **13**(5/6), 313–324. [3.5.5, 6.5]
- Tan, T.S. (1996) An optimal bound for high-quality conforming triangulations *Discrete and Computational Geometry*, **15**, 169–193. [2.4]
- Tanaka, M. (1986a) Statistics of Voronoi polyhedra in rapidly quenched monatomic liquids. I. Changes during the rapid-quenching process *Journal of the Physical Society of Japan*, **55**(9), 3108–3116. [7.1]
- Tanaka, M. (1986b) Statistics of Voronoi polyhedra in rapidly quenched monatomic liquids.

- II. Comparison between argon and rubidium *Journal of the Physical Society of Japan*, **55**(10), 3428–3436. [7.1]
- Tanemura, M. (1988) Random packing and random tessellation in relation to the dimension of space *Journal of Microscopy*, **151**(3), 247–255. [5.4, 5.5.4]
- Tanemura, M. and M. Hasegawa (1980) Geometrical models of territory, I. Models for synchronous and asynchronous settlement of territories *Journal of Theoretical Biology*, **82**, 477–496. [5.3, 5.12, 7.1]
- Tanemura, M., Y. Hiwatari, H. Matsuda, T. Ogawa, N. Ogita and A. Ueda (1977) Geometrical analysis of crystallization of the soft core model *Progress of Theoretical Physics*, **58**(4), 1079–1095. [7.1]
- Tanemura, M., T. Ogawa and N. Ogita (1983) A new algorithm for three-dimensional Voronoi tessellation *Journal of Computational Physics*, **51**, 191–207. [2.2, 4.7]
- Taniguchi, T., K.-P. Holz and T. Ohta (1992) Grid generation for 2D flow problems *International Journal of Numerical Methods in Fluids*, **15**(9), 985–997. [3.4.5]
- Tao, H. and T.S. Huang (1996) Multi-scale image warping using weighted Voronoi diagram *Proceedings of the International Conference on Image Processing*, **1**, 241–244. [3.1.6]
- Taylor, C.C., M.R. Faghghi and I.L. Dryden (1995) An understanding of muscle fibre images. In: C. Braccini, L. DeFloriani and G. Vernazza (eds) *Lecture Notes in Computer Science: Image Analysis and Processing*, **974** (Proceedings of 8th International Conference, ICIAP '95 San Remo, Italy, September 13–15, 1995) Berlin: Springer-Verlag, 223–228. [7.1, 8.2]
- Telly, H., Th.M. Liebling, A. Mocellin and F. Righetti (1992) Simulating and modelling grain growth as the motion of a weighted Voronoi diagram *Materials Science Forum*, **94–96**(1), 301–306. [3.1.6, 3.5.3, 3.5.5]
- Telly, H., T.M. Liebling and A. Mocellin (1996) The Laguerre model of grain growth in two dimensions. I. Cellular structures viewed as dynamical Laguerre tessellations *Philosophical Magazine B (Physics of Condensed Matter, Electronic, Optical and Magnetic)* **73**, 395–408. [3.5.3]
- Teng, Y.A., F. Sullivan, I. Beichl and F. Puppo (1993) A data-parallel algorithm for three-dimensional Delaunay triangulation and its implementation *Proceedings SUPER-COMPUTING '93*, 112–121. [2.2]
- Thiessen, A.H. (1911) Precipitation averages for large areas *Monthly Weather Review*, **39**, 1082–1084. [1.2, 6.1.1, 9.2.4]
- Thomas, R.W. (1981) Point pattern analysis. In: N. Wrigley and R.J. Bennett (eds) *Quantitative Geography* Henley-on-Thames: Routledge and Kegan Paul, 166–176. [8.1.1]
- Thorvaldsen, A. (1992) Simulation of 3-D Voronoi polygons *Materials Science Forum*, **94–96**, 307–312. [5.4, 5.5.4]
- Thrower, N.J.W. (1972) *Maps and Civilization: Cartography in Culture and Society* Chicago: University of Chicago Press. [1.2]
- Tien, J.M., K. El-Tell and G.R. Simons (1983) Improved formulations to the hierarchical health facility location-allocation problem *IEEE Transactions on Systems, Man, and Cybernetics*, **13**(6), 1128–1132. [9.2.4]
- Tiller, W. and E.G. Hanson (1984) Offsets of two-dimensional profiles *IEEE Computer Graphics and Applications*, **4**, 36–46. [3.5.5]
- Tipper, J.C. (1990a) A straightforward iterative algorithm for the planar Voronoi diagram *Information Processing Letters*, **34**(3), 155–160. [4.1]
- Tipper, J.C. (1990b) Correlation in mosaic environments *Journal of the Geological Society London*, **147**, 487–494. [5.3]
- Tobler, W.R. (1975) Linear operators applied to real data. In: J.C. Davis and M.J. McCullagh (eds) *Display and Analysis of Spatial Data* London: John Wiley, 14–37. [6.1]
- Tokuyama, T. (1988) Deformation of merged Voronoi diagrams with translation *TRL Research Report, TR-88-0049*, IBM Tokyo Research Laboratory. [4.1, 4.8]
- Tolmachiev, D. and A. Adamatzky (1996) Chemical processor for computation of Voronoi diagram *Advanced Materials for Optics and Electronics*, **6**, 191–196. [7.2]
- Toriwaki, J., K. Mase, Y. Yashima and T. Fukumura (1982) Modified Voronoi diagram and relative neighbors on a digitized picture and their applications to tissue image analysis

- Proceedings of the IEEE First International Symposium on Medical Imaging and Image Interpretation*, 362–367. [4.1 4.9]
- Toriwaki, J.I. and S. Yokoi (1988) Voronoi and related neighbors on digitized two dimensional space with application to texture analysis. In: G.T. Toussaint (ed) *Computational Morphology* Amsterdam: Elsevier Science Publishers B.V., 207–228. [2.1, 2.5, 4.9]
- Toussaint, G.T. (1980a) The relative neighbourhood graph of a finite planar set *Pattern Recognition*, **12**, 261–268. [2.5]
- Toussaint, G.T. (1980b) Pattern recognition and geometrical problems *Proceedings of the Fifth International Conference on Pattern Recognition, Miami Beach*, **2**, 1324–1347. [2.5, 8.4, 8.4.2]
- Toussaint, G.T. (1988) A graph-theoretical primal sketch. In: G.T. Toussaint (ed) *Computational Morphology* Amsterdam: Elsevier Science Publishers B.V., 229–260. [2.5]
- Troadec, J.R. and J.A. Dodds (1993) Global geometrical description of homogeneous hard sphere packings. In: D. Bideau and A. Hansen (eds) *Disorder and Granular Media* Amsterdam: Elsevier Science Publishers B.V., 133–163. [7.1]
- Tsai, V.J.D. (1993) Fast topological construction of Delaunay triangles and Voronoi diagrams *Computers and Geosciences*, **19**(10), 1463–1474. [4.1]
- Tsin, Y.H. and C.A. Wang (1996) Geodesic Voronoi diagrams in the presence of rectilinear barriers *Nordic Journal of Computing*, **3**, 1–26. [3.4.1]
- Tsumuraya, K., K. Ishibashi and K. Kusunoki (1993) Statistics of Voronoi polyhedra in a model of silicon glass *Physical Review B, Condensed Matter*, **47**(14), 8552–8557. [7.1]
- Türcyan, M. and T. Chorzempa (1991) Relative sensitivity of a family of closest point graphs in computer vision applications *Pattern Recognition*, **25**, 361–373. [2.5]
- Türcyan, M. and A.K. Jain (1990) Texture segmentation using Voronoi polygons *IEEE Transactions on Pattern Analysis and Machine Intelligence*, **12**(2), 211–216. [8.6]
- Tuominen, O. (1949) Das Einflussgebeit der Stadt Turku im System der Einflussgebiete SW-Finnlands Finnia, **71**, 1–38. [3.1.6]
- Turek, Z., L. Hoofd and K. Rakusan (1986) Myocardial capillaries and tissue oxygenation *Canadian Journal of Cardiology*, **2**, 98–103. [7.1]
- Turkiyyah, G.M., D.W. Storti, M. Ganter, H. Chen and M. Vimawala (1997) An accelerated triangulation method for computing the skeletons of free form solid models *Computer Aided Design*, **29**(1), 5–19. [3.5.4]
- Turnball, D. and D.E. Polk (1972) Structure of amorphous semiconductors *Journal of Non-Crystalline Solids*, **8–10**, 19–35. [7.1]
- Tzionas, P., A. Thanailakis and P. Tsalides (1997) An efficient algorithm for the largest empty figure problem based on a 2D cellular automaton architecture *Image and Vision Computing*, **15**(1), 35–45. [3.7.11]
- Upton, G. and B. Fingleton (1985) *Spatial Data Analysis by Example. Volume 1: Point Pattern and Quantitative Data* Chichester: John Wiley. [1.3.3, 3.7.10, 8.0, 8.1.1, 8.3, 8.5]
- Urquhart, R.B. (1982) Some properties of the planar Euclidean relative neighbourhood graph *Pattern Recognition Letters*, **1**(5), 317–322. [2.5]
- Vahidi-Asl, M.Q. and J.C. Wierman (1990) First-passage percolation on the Voronoi tessellation and Delaunay triangulation. In: M. Karonski, J. Jaworski and A. Rucinski (eds) *Random Graphs '87* New York: John Wiley, 341–359. [5.3, 5.6.4]
- Vahidi-Asl, M.Q. and J.C. Wierman (1992) A shape result for first-passage percolation on the Voronoi tessellation and Delaunay triangulation. In: A. Frieze and T. Luczak (eds) *Random Graphs Volume 2* New York: John Wiley, 247–262. [5.3, 5.6.4]
- Vahidi-Asl, M.Q. and J.C. Wierman (1993) Upper and lower bounds for the route length of first-passage percolation in Voronoi tessellations. *Iranian Mathematical Society Bulletin*, **19**(1), 15–28. [5.6.4]
- Vaisman, I.I. and M.L. Berkowitz (1992) Local structural order and molecular associations in water-DMSO mixtures. Molecular dynamics study *Journal of the American Chemical Society*, **114**, 7889–7896. [7.1]
- Vaisman, I.I., F.K. Brown and A. Tropsha (1994) Distance dependence of water structure around model solutes *Journal of Physical Chemistry*, **98**, 5559–5564. [7.1]
- Vaisman, I.I., L. Perera and M.L. Berkowitz (1993) Mobility of stretched water *Journal of Chemical Physics*, **98**(12), 9859–9862. [7.1]

- Vanderbei, R.J. and L.A. Shepp (1988) A probabilistic model for the time to unravel a strand of DNA *Communication in Statistics. Stochastic Models*, **4**, 299–314. [5.8]
- van der Marck, S.C. (1996) Network approach to void percolation in a pack of unequal spheres *Physical Review Letters*, **77**(9), 1785–1788. [5.3, 7.1]
- Vander Voort, G.F. (1992) Computer-aided microstructural analysis of specialist steels *Materials Characterization*, **27**(4), 241–260. [7.1]
- van de Weygaert, R. (1991) Quasi-periodicity in deep redshift surveys *Monthly Notices Royal Astronomical Society*, **249**, 159–163. [5.3]
- van de Weygaert, R. (1994) Fragmenting the universe III. The construction and statistics of 3-D Voronoi tessellations *Astronomy and Astrophysics*, **283**, 361–406. [3.1.6, 5.3, 5.5.4, 5.7, 5.12]
- van de Weygaert, R. and V. Icke (1989) Fragmenting the universe II. Voronoi vertices as Abell clusters *Astronomy and Astrophysics*, **213**, 1–9. [7.2]
- Van Roy, T.J. and D. Erlenkotter (1982) A dual-based procedure for dynamic facility location *Management Science*, **28**, 1091–1105. [9.4.1]
- Vaughan, R.J. and E.A. Cousins (1977) Optimum location of stops on a bus route *Proceedings of the Seventh International Symposium on Transportation and Traffic Theory*, 697–716. [3.1.6, 9.2.7]
- Vaz, M.F. and M.A. Fortes (1988) Grain size distribution: the lognormal and the gamma distribution functions *Scripta Metallurgica*, **22**, 35–40. [5.5.4, 7.1]
- Venables, J.A. and D.J. Ball (1971) Nucleation and growth of rare-gas crystals *Proceedings Royal Society of London, Series A*, **322**, 331–354. [1.2, 7.1]
- Venema, H.W. (1991) Determination of nearest neighbours in muscle fibre patterns using a generalized version of the Dirichlet tessellation *Pattern Recognition Letters*, **12**(7), 445–449. [3.1.6, 3.5.3, 3.5.5, 7.1]
- Vincent, P.J., R. Collins, J. Griffiths and J. Howarth (1983) Statistical geometry of geographical point patterns *Geographia Polonica*, **45**, 109–125. [5.4, 8.2]
- Vincent, P.J. and J. Howarth (1982) A theoretical note on spatial pattern of discs and properties of simplicial graph *Forest Science*, **28**(1), 181–186. [5.12, 8.1.1, 8.2]
- Vincent, P.J., J.M. Howarth, J.C. Griffiths and R. Collins (1976) The detection of randomness in plant patterns *Journal of Biogeography*, **3**, 373–380. [5.4, 8.2]
- Vincent, P.J., J. Howarth, J. Griffiths and B. Collins (1977) Urban settlement patterns and the properties of the simplicial graph *The Professional Geographer*, **29**, 21–25. [8.2]
- Viterbo, E. and E. Biglieri (1996) Computing the Voronoi cell of a lattice: The diamond-cutting algorithm *IEEE Transactions on Information Theory*, **42**(1), 161–171. [7.1]
- Voigtmann, A., L. Becker and K. Hinrichs (1994) Hierarchical surface representations using constrained Delaunay [sic] triangulations. In: T.C. Waugh and R.G. Healey (eds) *Advances in GIS Research: Proceedings of the 6th International Symposium* London: Taylor and Francis, 848–867. [1.2, 3.4.5]
- Voloshin, V.P., Y.I. Naberukhin and N.N. Medvedev (1989) Can various classes of atomic configurations (Delaunay simplices) be distinguished in random dense packings of spherical particles? *Molecular Simulation*, **4**, 209–227. [7.1]
- Von Hohenbalken, B. and D.S. West (1984a) Predation among supermarkets: an algorithmic locational analysis *Journal of Urban Economics*, **15**, 244–257. [3.1.6, 7.1, 7.4]
- Voronoi, G. (1907) Nouvelles applications des paramètres continus à la théorie des formes quadratiques. Premier Mémoire: Sur quelques propriétés des formes quadratiques positives parfaites *Journal für die Reine und Angewandte Mathematik*, **133**, 97–178. [1.2]
- Voronoi, G. (1908) Nouvelles applications des paramètres continus à la théorie des formes quadratiques. Deuxième Mémoire: Recherches sur les paralléléloèdres primitifs *Journal für die Reine und Angewandte Mathematik*, **134**, 198–287. [1.2]
- Voronoi, G. (1909) Nouvelles applications des paramètres continus à la théorie des formes quadratiques. Deuxième Mémoire: Recherches sur les paralléléloèdres primitifs. Second partie. Domaines de formes quadratiques correspondant aux différents types de paralléléloèdres primitifs *Journal für die Reine und Angewandte Mathematik*, **136**, 67–181. [1.2]
- Vrettos, N.A., H. Imakoma and M. Okazaki (1989a) Characterization of porous media by

- means of the Voronoi-Delaunay tessellation *Chemical Engineering Process*, **25**, 35–45. [7.1]
- Vrettos, N.A., H. Imakoma and M. Okazaki (1989b) Transport properties of porous media from the microgeometry of a three-dimensional Voronoi network *Chemical Engineering Process*, **26**, 237–246. [7.1]
- Vrettos, N.A., H. Imakoma and M. Okazaki (1990) Effective medium approximation of 3-D Voronoi networks *Journal of Applied Physics*, **67**(7), 3249–3253. [7.1]
- Wallet, F. and C. Dussert (1997) Multifactorial comparative study of spatial point pattern analysis methods *Journal of Theoretical Biology*, **187**, 437–447. [8.1.1]
- Walters, P. (1982) *An Introduction to Ergodic Theory* New York: Springer-Verlag. [1.3.3]
- Wang, C. (1993) Efficient updating constrained Delaunay triangulations, *BIT*, **33**, 238–252. [3.4.3]
- Wang, C.A. and F. Chin (1995) Finding the constrained Delaunay triangulation and constrained Voronoi diagram of a simple polygon in linear-time *Algorithms – ESA 95. Third Annual European Symposium. Proceedings*, 280–294. [3.4.2]
- Wang, C.A. and L.K. Schubert (1987) An optimal algorithm for constructing the Delaunay triangulation of a set of line segments *Proceedings of the Third ACM Symposium on Computational Geometry*, 223–232. [3.4.2, 4.8]
- Wang, C.A. and P.Y. Tsin (1990) Finding constrained and weighted Voronoi diagrams in the plane *Proceedings of the Second Canadian Conference in Computational Geometry*, 200–203. [3.4.2, 4.8]
- Ward, D. (1991) Triangular tessellation: a new approach to forest inventory *Forest Ecology and Management*, **44**, 285–290. [8.5]
- Ware, J.M., C.B. Jones and G.L. Bundy (1995) A triangulated spatial model for cartographic generalisation of areal objects *International Conference on Spatial Information Theory COSIT 95*, 173–192. [3.4.5]
- Watanabe, T. and S. Murashima (1996) A method to construct a Voronoi diagram on 2-D digitized space in O(1) computing time *Transactions of the Institute of Electronics, Information and Communication Engineers D-I, J79D-I*(3), 114–122. [2.1]
- Watanabe, M.S. and K. Tsumuraya (1987) Crystallization and glass formation processes in liquid sodium: a molecular dynamics study *Journal of Chemical Physics*, **87**(8), 4891–4900. [7.1]
- Watkinson, A.R., W.M. Lonsdale and L.G. Firbank (1983) A neighbourhood approach to self-thinning *Oecologica (Berlin)*, **56**, 381–384. [7.1]
- Watson, D.F. (1981) Computing the n -dimensional Delaunay tessellation with application to Voronoi polytopes *The Computer Journal*, **24**, 167–172. [2.2, 4.1, 4.7]
- Watson, D.F. (1985) Natural neighbor sorting *Australian Computer Journal*, **17**, 189–193. [2.4, 6.1.2, 6.6]
- Watson, D.F. (1988) Natural neighbor sorting on the n -dimensional sphere *Pattern Recognition*, **21**(1), 63–67. [6.1.2]
- Watson, D.F. (1992) *Contouring: A Guide to the Analysis and Display of Spatial Data* Oxford: Pergamon Press. [6.0, 6.2]
- Watson, D.F. and A.I. Mees (1996) Natural trees – neighbourhood-location in a nutshell *International Journal of Geographical Information Systems*, **10**(5), 563–572. [6.6]
- Watson, D.F. and G.M. Philip (1984a) Triangle based interpolation *Journal of the International Association for Mathematical Geology*, **16**(8), 779–795. [6.2]
- Watson, D.F. and G.M. Philip (1984b) Systematic triangulations *Computer Vision, Graphics and Image Processing*, **26**, 217–233. [6.2 6.5]
- Watson, D.F. and G.M. Philip (1985) A refinement of inverse distance weighted interpolation *Geo-Processing*, **2**, 315–327. [6.2]
- Watson, D.F. and G.M. Philip (1987) Neighbourhood-based interpolation *Geobyte*, **2**(2), 12–16. [6.1.2]
- Watson, D.F. and F.G. Smith (1975) A computer simulation and study of grain shape *Computers and Geosciences*, **1**, 109–111. [7.2]
- Weaire, D. (1974) Some remarks on the arrangement of grains in a polycrystal *Metallography*, **7**, 157–160. [5.5.3]
- Weaire, D. and J.P. Kermode (1984) Computer simulation of two-dimensional soap froth II. Analysis of results *Philosophical Magazine B*, **50**(3), 379–395. [5.12]

- Weaire, D., J.P. Kermode and J. Wejchert (1986) On the distribution of cell areas in a Voronoi network *Philosophical Magazine B*, **53**, L101–L105. [5.4, 5.5.4]
- Weaire, D. and H. Lei (1990) A note on the statistics of the mature two-dimensional soap froth *Philosophical Magazine Letters*, **62**(6), 427–430. [5.12]
- Weaire, D. and N. Rivier (1984) Soap, cells and statistics – random patterns in two dimensions *Contemporary Physics*, **25**, 59–99. [3.1.6, 3.5.3]
- Weatherill, N.P. (1988) A method for generating irregular computational grids in multiply connected planar domains *International Journal for Numerical Methods in Fluids*, **8**, 181–197. [3.4.5]
- Weatherill, N.P. (1990) The integrity of geometrical boundaries in the two-dimensional Delaunay triangulation *Communications in Applied Numerical Methods*, **6**(2), 101–109. [3.4.3]
- Weatherill, N.P. (1992) Delaunay triangulation in computational fluid dynamics *Computers and Mathematics with Applications*, **24**(5/6), 129–150. [6.5.1]
- Weatherill, N.P., K.P. Gaither and J.A. Gaither (1995) Building unstructured grids for computational fluid dynamics *Computational Fluid Dynamics Journal*, **4**(1), 1–28. [6.5.1]
- Weatherill, N.P. and O. Hassan (1992) Efficient three-dimensional grid generation using the Delaunay triangulation *Computational Fluid Dynamics Journal*, **2**, 961–968. [6.5.2]
- Weatherill, N.P. and O. Hassan (1994) Efficient three-dimensional Delaunay triangulation with automatic point creation and imposed boundary constraints *International Journal for Numerical Methods in Engineering*, **37**, 2005–2039. [2.2, 6.5.2]
- Weatherill, N.P., M.J. Marchant, O. Hassan and D.L. Marcum (1994) Grid adaptation using a distribution of sources applied to inviscid compressible flow simulations *International Journal for Numerical Methods in Fluids*, **19**, 739–764. [6.5.1]
- Weber, A. (1909) *Über den Standort der Industrien, Reine Theorie des Standorts*. Tubingen: Erster Teil (English translation by C.J. Friedrich (1957) *Theory of the Location of Industries* Chicago: Chicago University Press). [9.2]
- Weber, G., L. Knipping and H. Alt (1994) An application of point pattern matching in astronautics *Journal of Symbolic Computation*, **17**(4), 321–340. [3.7.11]
- Weber, T.A. and F.H. Stillinger (1981) Gaussian core model in two dimensions. II. Solid and fluid phase topological distribution functions *Journal of Chemical Physics*, **74**(7), 4020–4028. [7.1]
- Webster, A. (1998) Callan's canyons and Voronoi's cells *Nature*, **391**, 430. [7.2]
- Weinberg, M.C., D.P. Birnie III and V.A. Shneidman (1997) Crystallization kinetics and the JMAK equation *Journal of Non-Crystalline Solids*, **219**, 89–99. [5.8]
- Weliky, M. and G. Oster (1990) The mechanical basis of cell rearrangement *Development*, **109**, 373–388. [7.1]
- Wells, A.F. (1984) *Structural Inorganic Chemistry* (fifth edition) Oxford: Clarendon Press. [7.1]
- Welzl, E. (1985) Constructing the visibility graph for n line segments in $O(n^2)$ time *Information Processing Letters*, **20**, 167–171. [3.4.1]
- Werner, E., T. Siegmund, H. Weinhandl and F.D. Fischer (1994) Properties of random polycrystalline two-phase materials *Applied Mechanics Reviews*, **47**(1), Part 2, S231–S240. [5.12]
- Wesolowsky, G.O. (1993) The Weber problem: history and perspectives *Location Science*, **1**, 5–23. [9.2]
- West, D.S. (1981) Testing for market preemption using sequential location data *Bell Journal of Economics*, **12**, 129–143. [7.1]
- West, D.S. and B. Von Hohenbalken (1984) Spatial predation in Canadian retail oligopoly *Journal of Regional Science*, **24**(3), 415–427. [7.1, 7.4]
- Whitney, E.N. (1929) Areal rainfall estimates *Monthly Weather Review*, **57**, 462–463. [1.2, 6.2]
- Wiencek, K. and D. Stoyan (1993) Spatial correlations in metal structures and their analysis II: the covariance *Materials Characterization*, **31**, 47–53. [5.6.3]
- Wigner, E. and F. Seitz (1933) On the constitution of metallic sodium *Physical Review*, **43**, 804–810. [1.2]

- Wilkinson, D.S. (1988a) The effect of a non uniform void distribution on grain boundary void growth during creep *Acta Metallurgica*, **36**(8), 2055–2063. [5.12, 7.1]
- Wilkinson, D.S. (1988b) Modelling the effect of material inhomogeneity on grain boundary creep fracture *Proceedings of Ashby Symposium, World Materials Congress*, TMS-AIME. [7.1]
- Wilks, S.S. (1962) *Mathematical Statistics* New York: John Wiley. [1.3]
- Williams, P.W. (1972) The analysis of spatial characteristics of karst terrain. In: R.J. Chorley (ed) *Spatial Analysis in Geomorphology* New York: Harper and Row, 135–163. [7.2]
- Williams, R.E. (1968) Space-filling polyhedron: its relation to aggregates of soap bubbles, plant cells, and metal crystallites *Science*, **161**, 276–277. [3.1.6]
- Wilson, F.W., R.K. Goodrich and W. Spratte (1990) Lawson's triangulation is nearly optimal for controlling error bounds *SIAM Journal of Numerical Analysis*, **27**(1), 190–197. [6.2]
- Winter, P. (1985) An algorithm for the Steiner problem in the Euclidian plane *Networks*, **15**, 323–345. [9.3.3]
- Winterfield, P.H., L.E. Scriven and M.T. Davis (1981) Percolation and connectivity of random two-dimensional composites *Journal of Physics C: Solid State Physics*, **14**, 2361–2376. [5.3, 5.4]
- Wirasinghe, S.C. and N.S. Ghoneim (1981) Spacing of bus-stops for many travel demand *Transportation Science*, **15**(3), 210–221. [3.1.6, 9.2.7]
- Wolk, C.P. (1975) Formation of one-dimensional patterns by stochastic processes and by filamentous blue-green algae *Developmental Biology*, **46**, 370–382. [5.8]
- Wood, L.J. (1974) Spatial interaction and partitions of rural market space *Tijdschrift voor Economische en Sociale Geografie*, **65**(1), 23–34. [3.1.6]
- Worley, R.T. (1987) The Voronoi region of E^k *Journal Australian Mathematical Society Series A*, **48**, 268–278. [7.1]
- Worley, R.T. (1988) The Voronoi region of E^k *SIAM Journal on Discrete Mathematics*, **1**, 134–141. [7.1]
- Wray, P.J., O. Richmond and H.L. Morrison (1983) Use of the Dirichlet tessellation for characterizing and modeling nonregular dispersions of second-phase particles *Metallography*, **16**, 39–58. [7.1, 8.2]
- Wu, Y-F., P. Widmayaer, M.D.F. Schlag and C.K. Wong (1987) Rectilinear shortest paths and minimum spanning trees in the presence of rectilinear obstacles *IEEE Transactions on Computers*, **C-36**, 3(Mar.), 321–331. [3.4.1]
- Wulff, G. (1908) Zur Theorie des Krystallhabitus *Zeitschrift für Kristallographie*, **45**, 433–472. [1.2]
- Xia, Y. (1989) Skeletonization via the realization of the fire front's propagation and extinction in binary shapes *IEEE Transactions on Pattern Recognition and Machine Intelligence*, **11**(10), 1076–1086. [3.5.4]
- Xie, S. (1990) View planning for mobile robots *Proceedings 1990 IEEE International Conference on Robotics and Automation*, **2**, 748–754. [3.4.5]
- Yagawa, G., S. Yoshimura and K. Nakao (1995) Automatic mesh generation of complex geometries based on fuzzy knowledge processing and computational geometry *Integrated Computer-Aided Engineering*, **2**(4), 265–280. [6.5.2]
- Yamamoto, H., S. Uchiyama and H. Tamura (1995) The Delaunay triangulation for accurate three-dimensional graphic model *Transactions of the Institute of Electronics, Information and Communication Engineers D-II*, **J78D-II**(5), 745–753. [3.4.5]
- Yap, C.K. (1987) An $O(n \log n)$ algorithm for the Voronoi diagram of a set of simple curve segments *Discrete and Computational Geometry*, **2**, 365–393. [3.5, 3.7.11, 4.8]
- Yap, C.-K. (1988) A geometric consistency theorem for a symbolic perturbation scheme *Proceedings of the 4th Annual ACM Symposium on Computational Geometry, Urbana-Champaign, June 1988*, 134–142. [4.6.2]
- Yao, C. and J. Rokne (1991) A straightforward algorithm for computing the medial axis of a simple polygon *International Journal of Computer Mathematics*, **39**(1–2), 51–60. [3.5.4]
- Yoeli, P. (1977) Computer executed interpolation of contours into arrays of randomly distributed height-points *The Cartographic Journal*, **14**(2), 103–108. [6.3]

- Yokoi, S. and J. Toriwaki (1986) Adjacency relations among figures on a digitized image plane with applications to texture analysis. In: S. Ishizaka (General ed), Y. Kato, R. Takaki and J. Toriwaki (eds) *Science on Form: Proceedings of the First International Symposium for Science on Form* Tokyo: KTK Scientific Publishers, 431–439. [8.6]
- Yomono, H. (1991) The Voronoi diagram on a network *Technical Report, 91–09–02, Nippon System Co.*, Tokyo [in Japanese]. [3.8.3, 3.8.4]
- Yonezawa, F. and T. Ninomiya (1983) Introduction. In: F. Yonezawa and T. Ninomiya (eds) *Topological Disorder in Condensed Matter* Berlin: Springer-Verlag. [7.1]
- Yoshikawa, T. (1989) Moments of the nearest neighbor distance from a random point to line segments or polygons *Comprehensive Urban Studies, Special Edition, Tokyo Metropolitan University*, 25–33 [in Japanese]. [8.3.1, 8.3.2]
- Yoshikawa, T. and A. Okabe (1991) A statistical analysis of the compound effect of urban infra-structures on the spatial distribution of apartment buildings with the multi-nearest neighbor distance method *Papers of the Annual Conference of the City Planning Institute of Japan*, 27, 523–528 [in Japanese]. [3.5.5]
- Yoshikawa, T., A. Okabe, A. Fujii and K. Oikawa (1987) A statistical method of analyzing the distribution of urban activities in relation to the locations of infrastructural elements *Papers of the Annual Conference of the City Planning Institute of Japan*, 22, 241–246 [in Japanese]. [3.6.2, 4.9]
- Yoshioka, S. and S. Ikeuchi (1989) The large scale structure of the universe and the division of space *The Astrophysical Journal*, 341, 16–25. [5.3, 5.4, 7.2]
- Yoshitake, T., K. Sugihara and M. Sugie (1987) Recognition of three-dimensional objects by means of regular pattern projection *Proceedings of the IEEE International Workshop on Industrial Applications of Machine Vision and Machine Intelligence, Tokyo*, 229–234. [4.1]
- Yu, X., J.A. Goldak and L.D. Ling (1991) Constructing 3-D discrete medial axis *Proceedings. Symposium on Solid Modeling Foundations and CAD/CAM Applications*, 481–489. [3.5.4]
- Yuan, X.F. and S.F. Edwards (1995) Flow behaviour of two-dimensional random foams *Journal of Non-Newtonian Fluid Mechanics*, 60, 335–348. [5.3]
- Yuen, M.M.F., S.T. Tan and K.Y. Hung (1991) A hierarchical approach to finite element mesh generation *International Journal for Numerical Methods in Engineering*, 32, 501–525. [6.5.2]
- Zahn, C.T. (1971) Graph-theoretical methods for detecting and describing gestalt clusters *IEEE Transactions on Computers*, C-20(1), 68–86. [8.6]
- Zallen, R. (1979) Stochastic geometry: aspects of amorphous solids. In: E.W. Montroll and J.L. Lebowitz (eds) *Studies in Statistical Mechanics. Volume VII Fluctuation Phenomena* Amsterdam: North-Holland Publishing Company. [7.1]
- Zallen, R. (1983) *The Physics of Amorphous Solids* New York: John Wiley. [5.5.2]
- Zaninetti, L. (1989) Dynamical Voronoi tessellation. I The two-dimensional case *Astronomy and Astrophysics*, 224, 345–350. [3.9.1, 5.3, 5.8]
- Zaninetti, L. (1990) Dynamical Voronoi tessellation. II The three-dimensional case *Astronomy and Astrophysics*, 233, 293–300. [3.9.1, 5.3, 5.8]
- Zaninetti, L. (1991a) About the time evolving Voronoi tessellation *Journal of Computational Physics*, 97, 559–565. [7.2]
- Zaninetti, L. (1991b) Dynamical Voronoi tessellation III. The distribution of galaxies *Astronomy and Astrophysics*, 246, 291–300. [3.5.5, 5.8, 7.2, 8.1.1, 8.7]
- Zaninetti, L. (1992) The Voronoi tessellation generated from different distributions of seeds *Physics Letters A*, 165, 143–147. [5.3, 5.5.4, 5.12, 7.2, 8.1.1]
- Zaninetti, L. (1993) Dynamical Voronoi tessellation IV. The distribution of the asteroids *Astronomy and Astrophysics*, 276, 255–260. [7.2]
- Zaninetti, L. (1995) Dynamical Voronoi tessellation V. Thickness and incompleteness *Astronomy and Astrophysics Supplement Series*, 109(1), 71–77. [3.9.1]
- Zhang, J.H. and A.S. Hamill (1997) Seed weight, intraspecific competition, and plant performance in *Abutilon theophrasti* *Canadian Journal of Botany*, 75(9), 1614–1620. [7.1]
- Zhang, Z.P., A.B. Yu and R.B.S. Oakeshott (1996) Effect of packing method on the randomness of disc packings *Journal of Physics A: Mathematical and General*, 29, 2671–2685. [5.12]

- Zhou, J.M., K.R. Shao, K.D. Zhou and L.R. Li (1993) A new approach to automatic quadrilateral mesh generation *IEEE Transactions on Magnetics (USA)*, **29**(2), 1910–1913. [3.4.5]
- Zhou, J., K. Shao, K. Zhou and Q. Zhen (1990) Computing constrained triangulation and Delaunay triangulation: a new algorithm *IEEE Transactions on Magnetics*, **26**(2), 694–697. [3.4.3, 4.8]
- Zhou, J.M., K.D. Zhou and K.R. Shao (1992) Automatic generation of 3D meshes for complicated solids *IEEE Transactions on Magnetics (USA)*, **28**(2), 1759–1762. [3.4.5]
- Zhu, J.Z. and O.C. Zienkiewicz (1997) A posteriori error estimation and three-dimensional automatic mesh generation *Finite Elements in Analysis and Design*, **25**, 167–184. [6.5.2]
- Zienkiewicz, O.C. and D.V. Phillips (1971) An automatic mesh generation scheme for plane and curved surfaces by isoparametric co-ordinates *International Journal for Numerical Methods in Engineering*, **3**, 519–528. [6.2]
- Zuuring, H.R., S.D. Tesch and J.L. Faurot (1984) Past tree spacing levels estimated by current stand conditions and past radial growth rates *Forest Science*, **30**(1), 209–218. [7.1]
- Zuyev, S.A. (1992) Estimates for distributions of the Voronoi polygon's geometric characteristics *Random Structures and Algorithms*, **3**(2), 149–162. [5.5.4]
- Zuyev, S.A. (1993) Russo's formula for Poisson point fields and its applications *Discrete Mathematics and Applications*, **3**(2), 63–73. [5.5.4]

Index

- 2-3 tree 263
2-connected 107
- Aboav's law 295, 324, 325, 330, 374
absolute regularity 38, 356
abstract graph 25
access distance 223
access point 222, 223
additional generator 244, 271
additively weighted (AW) distance 123
additively weighted Poisson Voronoi diagram 376
additively weighted power diagram 129
additively weighted power distance 128
additively weighted Voronoi diagram 9, 123, 124, 285, 376, 479
additively weighted Voronoi region 124
adjacency matrix 28, 565
adjacent 46
adjacent link 28
adjacent node 28
adjustment model 489, 490
adjustment process 489, 490
algorithm 229
all nearest neighbour 60
alloys 8
almost surely 291
 α -mixing 38, 299
 α -mixing coefficient 38
 α -extreme 523
 α -hull 523
 extended digital 524
 α -neighbour 523
 α -shape 523
amorphous 454
amorphous structure 454, 460
amorphous substrate 302
ancestor 246
angle variable 108
angle vector 92
anisotropic growth 215
APA (area potentially available) 9, 471
Apollonius circle 120, 122
approximate interpolant 411
approximation algorithm 287
- area 475
 market 10, 224, 473, 482
 restricted 584
 service 134, 305, 385, 480
 trade 472
area-like object 514, 520
area of a Voronoi polygon 298, 314, 319–321, 343, 345, 347, 485
area of influence polygon 8, 418
area potentially available (APA) 9, 471
area-preserving transformation 34
area Voronoi diagram 186, 188
area Voronoi diagram for expanded obstacles 218
area Voronoi region 186
assignment model
 Voronoi 454
assignment rule 113
 V- 115
 Voronoi generation 115
astronomy 9, 305, 478, 530
astrophysics 225, 302
atomic volume 464
attachment point 195
augmented geometric graph 236
AVL tree 263
Avrami equation 376
Avrami exponent 376
Avrami index 376
Avrami-Johnson-Mehl (AJM) equation 376–384
- basalt 479
 β -mixing 356
 β -mixing coefficient 37
 β -neighbour 522
 β -skeleton 522
bisecting curve 117
binomial distribution 31
binomial point process 31
bisector 47, 116, 220, 280
bisector node set 219
Blum's transform 182
bond percolation model 302, 360
border 50

- bottleneck width 189, 216
 bound
 lower 21, 226, 241
 upper 21, 226
 boundary 16
 lower 80
 village 474
 boundary growing procedure 243
 boundary point 16
 boundary Voronoi polygon 47
 boundary Voronoi region 47
 bounded 21
 bounded above 21
 bounded below 21
 bounded distance 163
 bounded Voronoi diagram 47, 164
 Brillouin zone 51
 bucket 247
 buffer zone 185, 514
- cancer 470
 capillary domain 9, 469
 c-facing 109
 cc-facing 109
 ccw (counterclockwise) 238
 C-diagram 199
 CDT (constrained Delaunay triangulation) 165, 437, 441
 cell
 Poisson Delaunay 291–294, 310, 311, 389–404
 Poisson Voronoi 291, 293–294, 299, 306–349, 359, 499
 cell model 8, 357, 478
 cellular automata 305
 central limit theorem 349, 354, 356
 central place theory 472
 chain
 simple 29
 children 246
 chi-square distribution 342, 384
 cholera 9
 choropleth map 412
 circle
 Apollonius 120, 122
 empty 61, 74, 80
 largest empty 63, 74
 smallest enclosing 154
 circular Dirichlet tessellation 122
 circuit
 simple 29
 city-block distance 189
 classification 151
 class NP 42
 class NP-complete 42
 class P 42
 clearance disc 181
 clipped Voronoi diagram 133
 closed 16
 closed ball 116
 closed disc 16
 closed half plane 19
 closed half space 19
 closed Voronoi polygon 46
 closest pair 60
 closest pair problem 60
 closure 16
 cluster amplification process 406, 409
 clustered point pattern 497, 498, 509, 511
 codes 8–9, 475
 coefficient
 mixing 37
 collision-free path 27, 118, 216
 combinatorial complexity 226
 combinatorial recognition problem 103
 common support 253
 complete random packing 405
 complete spatial random pattern 35
 complete spatial randomness (CSR) 35, 496, 499, 503, 506, 511
 complex 325
 component 29, 359
 compound point process 405, 406
 compound Poisson point process 38, 406
 compoundly weighted (CW) distance 127
 compoundly weighted Voronoi diagram 127
 compoundly weighted Voronoi region 127
 computational geometry 11
 conduction 303
 conforming Delaunay triangulation 167, 441
 connected
 strongly 29
 conic Voronoi diagram 211
 constrained Delaunay triangulation 165, 437, 441
 constrained programming problem 533, 559, 561
 constraint 533
 constraint function 533
 continuous nucleation 376
 continuous nucleation model 376
 continuous skeleton 189
 contour map 412
 convex 20, 211
 convex distance function 194
 convex function 21, 534
 convex hull 20, 21, 70, 97, 299, 389, 523
 convex set
 strictly 20
 convex spherical polygon 207
 coordination number 456
 coordination polyhedron 456

- coordination shell 456
 core 198
 correlation function
 angle 356, 357
 area 356, 357
 pair 350–357, 358
 topological 329
 cosmic fragmentation 6
 Cox point process 39
 crack pattern 479
 criterion
 empty circumcircle 74
 local max-min angle 87, 88, 92
 Pitteway 430
 Crum's problem 66
Cryptomenia japonica 472
 crystal aggregates 376
 crystal growth 376, 478
 crystalline 454
 crystalline structure 134, 185, 454
 crystallization 462
 crystallography 6, 225, 459, 460
 CSR (complete spatial randomness) 35,
 496, 499, 503, 506, 511
 cw (clockwise) 238
 cycle
 simple 29
 cylindrical Voronoi diagram 210, 218

 data site 411
 data structure 235
 data value 411
 Davenport–Schinzel sequence 226
 decision problem 42
 decomposed generator set 172
 degeneracy 268
 degenerate 46
 degenerate Delaunay triangulation 54, 267
 degree
 negative 28
 positive 28
 Delaunay cell 297, 298, 299
 Poisson 291–294, 295, 310, 311,
 389–404
 Delaunay circle 74
 Delaunay diagonal flip 91
 Delaunay diagram
 (additively) weighted 124
 Delaunay edge 55, 73, 82
 external 56, 70, 82
 internal 55, 71
 Delaunay graph 81, 97
 Delaunay mesh 439
 Delaunay oriented matroid 70
 Delaunay pretriangulation 54, 55
 Delaunay refinement 167
 Delaunay simplex 11, 299, 389, 390
 m -dimensional 56, 299, 389, 390
 Delaunay simplicial complex 56
 Delaunay sphere 74
 Delaunay surface 83
 Delaunay tessellation 52, 291, 299, 305,
 470
 m -dimensional 52, 291, 299
 Poisson 291, 292, 294, 298, 302, 305,
 362, 389, 391, 392
 spherical 218
 Delaunay tetrahedrization 56, 82, 83, 443
 Delaunay tree 447
 Delaunay triangle 55, 82, 336, 399
 Delaunay triangulation 52, 54, 55, 56, 70,
 77, 80, 81, 97, 470, 521, 523
 conforming 167, 441
 constrained 167, 437
 degenerate 54
 domain 168, 441
 dynamic 225
 farthest-point 523
 flexible 225
 generalized 166, 172
 hierarchical 168
 Minkowski 193
 modifying 434
 restricted 166
 spherical 207, 218
 Delaunay vertex 56, 73, 82, 302
 density of packing 405, 464
 descendant 246
 descent method 534, 536
 steepest 536
 dialectology 10
 diameter 153
 dictionary 263
 digital image 289
 digital terrain model (DTM) 428
 digital Voronoi diagram 51
 digitized Voronoi diagram 50
 dihedral angles 300, 307, 317, 318, 320,
 321, 322, 444
 directed graph 27
 direction number 409
 Dirichlet tessellation
 circular 122
 hyperbolic 124
 disconnected 17, 29, 384
 discrete Manhattan Voronoi diagram 191
 discrete medial axis 183
 discrete Voronoi diagram 51
 disordered 405, 409, 410, 454
 displaced lattice process 406, 408, 479
 distance 118, 280
 access 223
 additively weighted 123
 additively weighted power 128
 boat-on-a-river 205
 bounded 163

- city-block 189
 compoundly weighted 127
 Euclidean 16, 99
 geodesic 159
 great circle 207, 389
 Hausdorff 202, 208, 286
 multiplicatively weighted 120
 near neighbour 511
 nearest neighbour (NN-) 360, 513
 network 218
 oriented 214
 power 128
 quadratic form 212
 shortest-path 159
 space-time 212, 578, 579
 spherical Laguerre 208
 taxi-cab 189
 V- 118
 visibility-shortest-path 163
 Voronoi generation 118
 weighted 119
 distance metric 118
 distribution
 binomial 32
 chi-square 342, 345, 384
 gamma 341, 342, 346, 347
 generalized gamma 332, 341, 345
 lognormal 342, 345, 347
 Maxwell 345
 normal 347, 404
 Palm 36, 292, 295, 297, 311, 312, 339,
 364, 390
 standard normal 310, 356, 377
 divide-and-conquer method 233, 251, 284
 domain Delaunay triangulation 168, 441
 dominance metric 189
 dominance node set 219
 dominance region 48, 116, 220, 282
 domaine de Dirichlet 6
 domain of an atom 8
 doubly stochastic Poisson point process 39
 drug design 467
 DTM (digital terrain model) 428
 dual graph 31, 81

 ecology 303, 305, 385, 471, 475
 economic predation theory 492
 edge
 Delaunay 53, 73, 82
 external Delaunay 56
 Gabriel 97, 396
 inner 108
 internal Delaunay 55
 outer 108
 Voronoi 46, 49, 50, 73
 edge effect 306, 308–310, 498, 503, 507
 empirical point pattern 305, 495
 eight-neighbour set 288

 empty circle 61, 74, 80
 empty circumcircle criterion 74
 empty circumcircle theorem 74
 EMST (Euclidean minimum spanning tree) 99, 450, 522, 528
 end point 18, 28
 entropy 315, 321, 325, 502
 epigraph 21
 equilibrium state 296
 ergodic 36, 292, 307, 324, 363, 388, 390
 ergodic theorem 292, 295, 297, 311, 364
 ergodicity 35
 error-free world 265, 268
 estimating spatial intensity 526
 Euclidean distance 16, 99
 Euclidean minimum spanning tree 450,
 522, 528
 Euclidean space 16, 291, 389
 Euclidean Steiner minimal tree 571, 572
 Euclidean Steiner tree 572
 Euclidean Steiner tree algorithm 573
 Euler's formula 30, 63, 82
 Euler-Poincaré's formula 30, 64, 82
 Euler-Schaeffer formula 30
 exact interpolant 411
 expanded polygon obstacle 217
 extended digital α -hull 524
 exterior penalty function method 540
 external Delaunay edge 56

 face
 $(m - 1)$ - 23, 295, 296
 of a cell 295, 296
 of a J-M tessellation 378
 of a tessellation 295, 296
 facet
 lower 80
 Voronoi 49, 50
 facility
 hierarchical 551, 552
 mobile 227
 point-like 542, 549
 far-side triangle 154
 farthest pair 153
 farthest-point Voronoi diagram 151, 152
 farthest-point Voronoi polygon 151, 152
 farthest-site Voronoi diagram with
 the geodesic distance 163
 feasible region 533
 feasible solution 533
 Feltham's law 319
 finer 67
 finite element method 439
 finite graph 25
 finite region 21
 first-order simplex 21
 first-passage percolation (FPP) model
 302, 362

- fixed radius nearest neighbour search 61
 flip 233, 444
 forestry 526
 four-neighbour set 288
 FPP (first-passage percolation) 302, 362
 fractal set models 530
 free configuration space 188
 free placement 188
 full neighbour 307, 312, 314, 316, 349,
 380–381, 391
 fundamental area 7
 fundamental region 346
 Fundamentalbereich 7
- Gabriel edge 97, 396
 Gabriel graph (GG) 97, 470, 476, 522
 Gabriel hull 523
 galaxies 134, 185, 304–305, 408
 general Poisson point process 39
 general position 62
 general quadratic position 62, 291, 295,
 296, 299
 general programming problem 532
 generalized additively weighted distance
 126
 generalized gamma function 332, 341,
 345
 generalized sectional Voronoi diagram
 133
 generalized Voronoi/Delauney duality 81
 generalized Voronoi diagram 115, 139,
 280, 475
 generalized Voronoi region 115
 generator 45
 generator point 45
 generator recognition problem 66, 68,
 126
 generator set 45, 113, 291, 292, 295,
 374–375, 389, 404
 geodesic centre 169
 geology 479
 geometric graph 26, 83
 geometric recognition problem 103
 germanium 459
 GG (Gabriel graph) 97, 470, 476, 522
 Gibbs point process 39, 407
 global equilibrium 484, 487
 global interpolant 411
 global minimum 534
 global minimum (optimum) 534
 globular protein 134, 467
 golden mean 471
 Goldstein's rule 538
 granular composites 301, 463
 graph
 abstract 25
 Delaunay 81
 directed 27
- dual 30
 finite 25
 Gabriel 97, 470, 476, 522
 geometric 26, 83
 nearest neighbour 100
 non-planar 27
 planar 27
 planar straight-line 26
 primal 30
 proximity 450
 relative neighbourhood 99, 522
 simplicial 11
 tree 29
 undirected 25
 visibility 160
 Voronoi 63
- great circle distance 207, 389
 greedy triangulation (GT) 430
 ground control point (GCP) 449
 growth model
 Voronoi 357–360, 477
 GT (greedy triangulation) 430
- Hadamard inequality 266
 half hyperbola 260
 half line 18, 59
 Hamilton cycle 47, 102, 525
 hard core process 39, 405, 407–408, 479
 Hausdorff area Voronoi diagram 203
 Hausdorff distance 158, 202, 228, 286
 Hausdorff line Voronoi diagram 203
 hierarchical facility 551, 552
 higher-dimensional Voronoi diagram 275
 higher-order Poisson Voronoi diagram 385
 higher-order Voronoi diagram 134, 385
 hill shading 412
 homogeneous 34
 homogeneous normal tessellation 366
 homogeneous Poisson point process 38,
 291, 299, 301, 307, 312, 376, 380, 404,
 455, 479, 481, 496, 499, 506
- homogeneous tessellation 315, 363
 honeycomb 475
 Hotelling process 482, 483, 491
 Huff model 563
 hull
 convex 20, 21, 299, 389, 523
 Gabriel 523
- hyperbolic arc 126, 128
 hyperbolic Dirichlet tessellation 124
 hyperbolic Voronoi diagram 213
 hyperplane 19
 hyperplane process 40, 360
- ideal gas 455
 illumination of ball 134
 image 50, 304, 527
 image processing 185, 331, 527

- imaginary data site 435
incomplete Voronoi diagram 359, 481
incremental method 225, 228, 233, 242,
 282, 577
incidence mapping 27
incident
 negatively 28
 positively 28
independent scattering 33, 35, 39
independent user 542
independently identically distributed
 (i.i.d.) 311
infinite region 21
infinite Voronoi diagram 45, 291, 292,
 295, 297
infinitely countable set 291
infimum 21
information retrieval system 151, 188
information theory 502
information theory approach 502
inhomogeneous Poisson point process
 366, 376
initial node 28
inner cell 106
inorganic chemistry 454
intensity 525
 estimating spatial 526
 spatial 525
interaction energy function 40
interface 378
interior penalty function method 540
interior point 16
intermediate node 246
internal Delaunay edge 55
interpolant 411
 approximate 411
 exact 411
 global 411
 local 411
interpolation 81
 natural neighbour 418
 nearest neighbour 417
 proximal polygon 417
 spatial 151, 416
 triangle based 427
intervening opportunities model 422
inversion transformation 76, 77
invertible 35
inverting the Voronoi diagram 66
Ireland 474
isarithmic map 412
isolated node 28
isomorphic 27, 86
isotropic 35
- j*-complex 326
Johnson-Mehl-Avrami (JMA) equation
 377–385
- Johnson-Mehl-Avrami-Kolmogorov
 (JMAK) equation 377–383
Johnson-Mehl (J-M) model 125, 134,
 374–385
 one- and two-dimensional sections of
 384
 time inhomogeneous 376
Johnson-Mehl tessellation 376–385
J-M (Johnson-Mehl) 374–385
- Karlsruhe metric 201
Karlsruhe-metric Voronoi region 202
Karlsruhe Voronoi diagram 202
karst 480
kernel 23
k-face 378
k-interface 378
Klotz Construction 460
k-motion 225
KNP (*k*th nearest point) 156
Kolmogorov-John-Mehl-Avrami
 (KJMA, JMAK, JMA, AJM) 377–383
Kolmogorov-John-Mehl-Avrami
 equation 377–383
Kombinationskarte 475
*k*th nearest-point Voronoi diagram 155,
 156
*k*th nearest-point Voronoi region 156
- L*-partition 11
*L*₁-metric 290
la partition de l'espace en tetraedres *L* 11
Laguerre diagram 180, 460
Laguerre Voronoi diagram 129, 180, 185,
 460
Laplacian smoothing 441
largest convex polygon contained in a
 simple polygon 199, 200
lattice 301, 456, 476
 body centred cubic 456, 459, 461
 diamond 458
 primitive cell of a 457
 random 301, 302, 361, 408
 square 408, 515
 triangular 472, 479, 503, 505, 509
lattice complex 457
leaf 246
left generator 252
left Voronoi diagram 252
Legendre dual function 81
l'ensemble *L* de simplex 11
Lewis' law 295, 315, 319, 321, 327,
 374
lexicographically greater 93
lexicographically maximum triangulation
 theorem 93
lift-up 68
lift-up method 234

- lift-up transformation 68, 79, 81
 line
 Voronoi 50
 straight 18
 linear motion 225, 227
 linear programming problem 534
 linear time 41
 linearly dependent 13
 linearly independent 13, 14
 line-like object 514, 517, 518
 line search 537
 line segment
 straight 59
 line Voronoi diagram 170, 185, 228, 532
 line Voronoi region 170, 175
 linguistics 475
 link
 adjacent 28
 parallel 28
 link space 220
 liquid 280, 462
 monatomic 305, 454, 462
 local coordinate property 150, 426
 local coordinates 423
 local equilibrium 487
 local interpolant 411
 local(ly) optimal procedure 91
 local max-min angle criterion 87, 88, 89, 92
 local max-min angle theorem 89
 local minimum 533
 local transformation procedure 92
 locally equiangular triangulation 91
 locally finite 32, 291, 295, 299
 location vector 13
 locational optimization of a network
 567, 569
 locational optimization of lines 564
 locational optimization of points 564
 loop 28
 lower bound 226, 241
 lower bound of the time complexity 241
 lower boundary 80
 lower common support 253
 lower facet 80, 278
 lower *m*-face 278
- $(m - 1)$ -dimensional Voronoi face 50
 Manhattan metric 163, 168, 189
 Manhattan-metric Voronoi diagram 190, 191, 215
 Manhattan-metric Voronoi polygon 191
 manifold 41, 297
 map
 choropleth 412
 contour 414
 isarithmic 412
 slope 412
 soil 417
- marked point process 357
 market area 10, 224, 473, 482
 Markov point process 529
 matrix
 adjacency 28, 571
 Hessian 536
 random 327, 406, 408
 maximal disk 181
 maximal sphere 182, 360
 maximum entropy 312, 322, 326
 maximum likelihood regions 9, 475
m-dimensional Delaunay pre tessellation 56
m-dimensional Delaunay simplex 56, 299, 389, 390
m-dimensional Delaunay tessellation 56, 291, 299
m-dimensional ordinary Voronoi diagram 49, 276, 278
m-dimensional ordinary Voronoi polyhedron 49
 measure 35
 measure space 35
 measurable 35
 measurable space 35
 measure-preserving transformation
 35
 medial axis 181, 182, 185
 medial (axis) surface 182
 medial axis transform 182
 mesh 440
 Delaunay 439
 solution-adaptive 442
 metal 385, 468
 oxide supported 304
 second-order particles in 468
 surface film on 376, 478
 metal vapour 302
 metallic glass 134, 456, 463
 metallurgy 468, 478, 499
 meteorology 8, 417
 method A 307
 method R 309
 method T 308
 metric 117
 distance 117
 dominance 189
 Karlsruhe 201
 L_1 - 290
 L_∞ - 290
 Manhattan 163, 168, 189
 Minkowski power 189
 Moscow 201
 supremum 189
 microemulsions 303
 minimum length triangulation 430
 minimum weight (length) criterion 94

- minimum weight length triangulation
 94, 430
 Minkowski power metric 189
 mixed dimensional set 172
 mixed penalty function method 540
 mixing 37–38
 α - 37
 strongly 37, 299
 mixing coefficient 38
 α - 38
 β - 38
 mixing condition 299–300
 ($m - k$)-face of the tessellation 295
 MLT (minimum length triangulation)
 430
 mobile facility 227, 558, 564
 modifying Delaunay triangulation 434
 moments of the nearest neighbour
 distance to line-like objects 518
 moments of the nearest neighbour
 distance to point-like objects 515
 monatomic liquid 305, 454, 462
 monotone with respect to ray shooting
 95
 mosaic 303
 k -phase 412
 Poisson Voronoi random 303–304
 random 303
 S - 303
 Moscow metric 201
 motion invariant 33
 motion invariant tessellation 299
 mouthbreeder fish 480
 moving generator (particle) problem 485
 multi-median problem 224, 544
 multiplicatively weighted distance 120
 multiplicatively weighted Voronoi
 diagram 9, 120, 121, 285, 384, 460
 multiplicatively weighted Voronoi region
 122
 multiplier method 540
 multiply connected polygonal domain 181
 multi-stage locational optimization 575
 multitype threshold vote automaton 305
 multivariate density estimation 151, 158
 muscle tissue 469
 myopic locational optimization 577

 naive method 230
 natural neighbour 74
 natural neighbour interpolation 418
 natural tree 447
 nearest neighbour (NN) 360, 418
 nearest neighbour analysis 497, 502, 506,
 526
 nearest neighbour distance (NND)
 average 360, 513
 nearest neighbour distance method 510

 nearest neighbour distance method
 for area-like objects 520
 nearest neighbour distance method
 for line-like objects 517
 nearest neighbour distance method
 for point-like objects 514
 nearest neighbour graph (NNG) 100
 nearest neighbour interpolation 417
 nearest neighbour rule 117
 nearest neighbour search 245
 nearest-point Voronoi diagram 151
 near neighbour distance 511, 513
 near-side triangle 77, 154
 negative binomial process 409
 negative degree 28
 negatively incident 28
 neighbourhood
 ε - 16
 neighbour 188
 neighbours of higher orders 327
 nested hierarchy 553
 network 218
 topologically random 302
 triangulated irregular (TIN) 428
 network distance 218
 network Voronoi area-diagram 10, 221,
 223
 network Voronoi diagram 218
 network Voronoi link-diagram 220, 563
 network Voronoi node-diagram 219
 Neyman–Scott process 39
 Newton method 548
 NN (nearest neighbour) 360, 418
 NND (nearest neighbour distance) 513
 NNG (nearest neighbour graph) 100
 node
 adjacent 28
 initial 28
 intermediate 246
 isolated 28
 terminal 28
 node set
 bisector 219
 dominance 219
 Voronoi 219
 node space 219
 non-cocircularity 62
 non-collinearity 53, 291, 295
 non-convex function 21, 534
 non-cosphericity 62, 291, 295
 non-crystalline 454
 non-degenerate 46, 47, 175, 296
 non-degenerate tessellation 296
 non-linear convex programming problem
 534
 non-linear, non-convex programming
 problem 524, 534, 569
 non-linear programming problem 534

- non-periodic 405, 454
- non-planar graph 27
- non-Poisson 364
- non-Voronoi cell 364
- norm 13
- normal 296
- normal distribution 347, 404
- normal tessellation 296, 297, 299, 326, 363, 385, 410
 - homogeneous 366
- NP-complete 42, 525
- NP-hard 42, 68, 563, 572
- nucleation site 302

- object
 - area-like 514, 520
 - line-like 514, 517, 518
 - point-like 514, 515
- objective function 533
- observation point 555
- offset problem 185
- open 16
- open ball 161, 533
- open disk 16
- open Voronoi polygon 46
- optimal triangulation 430
- order 41, 405, 408
- ordered 405, 408, 454
- ordered minimum angle vector 92
- ordered order-2 Voronoi diagram 285
- ordered order- k Voronoi diagram 144, 285, 385, 387
- ordered order-2 Voronoi polygon 145
- ordered order- k Voronoi polygon 146
- ordered product 27
- ordering multivariate data 446
- order- k power diagram 139, 286
- order-2 Voronoi diagram 136, 139, 285
- order- k Voronoi diagram 135, 285, 385, 386, 387
- order-2 Voronoi polygon 136
- order- k Voronoi polygon 139
- ordinary Voronoi diagram 43, 49
- ordinary Voronoi polygon 44, 48, 454
- ore reserves 8
 - estimation of 8, 418
- oriented Dirichlet cell 215
- orthogonal 14
- orthogonal projection 14, 131
- orthographic projection 14, 70, 80, 278, 285

- packing
 - complete random 405
 - random 405
 - Voronoi polygonal areal random 408
- packing density 405
- packing fraction 464

- pair correlation function 348–360
- pair potential 40, 407
- Palm distribution 36, 292, 295, 297, 311, 312, 339, 364, 390
- parallel link 28
- parent 246
- path
 - simple 29
- pattern recognition 185
- p-centre 563
- PDC (Poisson Delaunay cell) 291, 292, 293, 294, 310, 311, 389–404
- pdf (probability density function) 332–347, 390–404
- peeling 450
- peeling data 450
- peeper's Voronoi diagram 164
- penalty function method 538, 540
- Penrose tiling 460
- percolation 462
 - first-passage 302, 362
- percolation model
 - bond 302, 361
 - first-passage 302, 362
 - site 302, 361
- periodic 454
- periodic boundary condition 308, 309
- periodic locational optimization 578
- perpendicular projection 14
- phase transition 478
- phyllotaxis 471
- Pielou's index 513
- Pitteway criterion 430
- Pitteway triangulation 71
- Pitteway triangulation theorem 71
- pixel 288
 - positive 288
- pixel value 288
- planar graph 27, 82
- planar ordinary Voronoi diagram 44, 45, 48
- planar stochastic point process 32
- planar straight-line graph (PSLG) 26
- planar tessellation 24, 315, 327
- plane sweep method 234, 257, 260
- plant polygon 9, 471
- plastic flow 468
- plesiohedron 7, 459
- point 12
- point-like facility 543, 549
- point-like object 514, 515
- point-location problem 60, 514
- point pattern 356, 405, 408, 495
- point process
 - binomial 31
 - compound 405, 409
 - compound Poisson 39, 406

- Cox 39
 doubly stochastic Poisson 39
 general Poisson 39
 Gibbs 39, 407
 homogeneous Poisson 39, 291, 299, 301, 307, 312, 376, 380, 404
 inhomogeneous Poisson 366, 376
 marked 357
 Markov 529
 non-Poisson 364
 planar stochastic 32
 Poisson 350, 358, 360, 363, 376, 388
 spatial stochastic 31
 spatial-temporal stochastic 31
 stochastic 31, 35
 two-type 529
 point vector 13
 Poisson cluster process 39, 406, 409, 479
 Poisson Delaunay cell (PDC) 291, 293, 294
 properties of 389–404
 shape of 310, 390
 simulating 310, 311
 Poisson Delaunay tessellation 291, 292, 294, 298, 302, 305, 362, 389, 391, 392
 s -dimensional sections of 404
 Poisson Delaunay tessellation on the surface of a sphere 404
 Poisson hyperplane process 40, 360
 Poisson hyperplane tessellation 40
 Poisson line process 40, 388
 Poisson point process 350, 358, 360, 363, 376, 388
 compound 405, 409
 doubly stochastic 39
 general 39
 homogeneous 39, 299, 301, 307, 312, 376, 380, 404
 inhomogeneous 366, 376
 Poisson Voronoi cell (PVC) 291, 293–294, 499
 properties of 311–349
 simulating 306–311
 typical 291
 Poisson Voronoi diagram 291
 additively weighted 374
 higher order 385
 properties of 295–300
 s -dimensional section of higher order 389
 s -dimensional sectional 363
 sectional 363
 uses of 300
 Poisson Voronoi diagram on the surface of a sphere 389
 Poisson Voronoi random mosaic (PVRM) 303–304
 Poissonian random lattice 301
 polygon
 area of influence 8, 418
 convex spherical 207
 plant 471
 proximal 417
 simple 22, 525
 Thiessen 8, 417
 polygonal containment 199
 polygon-based method 413, 416
 polyhedral Voronoi diagram 212
 polyhedron
 coordination 456
 Voronoi
 polynomial time 41
 polytope 23, 291, 295, 299, 312
 porous oxides 304
 positive degree 28
 positive pixel 288
 positively incident 28
 post office problem 60, 227
 power diagram 128, 129, 132, 285, 460, 470
 additively weighted 129
 order- k 139, 286
 power distance
 additively weighted 128
 power Voronoi polygon 129
 prey–predator relations 491, 492
 primal graph 30
 priority queue 263
 probability density function (pdf) 332–347, 390–404
 probability space 35
 problem
 offset 185
 process
 adjustment 489, 490
 cluster amplification 406, 409
 hard core 39, 405, 407–408
 Hotelling 482, 483, 491
 hyperplane 40, 360
 negative binomial 40, 409
 Neyman–Scott 39
 non-Poisson point 364
 Poisson cluster 39, 406, 409, 479
 Poisson hyperplane 40, 360
 Poisson line 40, 388
 re-arrangement 406, 407
 sequential clustering 406, 409
 simple sequential inhibition (SSI) 405, 406
 stochastic fibre 41, 297
 stochastic line 40, 388
 stochastic manifold 41, 297
 thinning 407, 408, 409
 programming problem 532

- projection
 orthogonal 14, 31
 orthographic 14, 70, 80, 278, 285
 perpendicular 14
- properties of the Voronoi diagram 295–299
- proteins 463, 467
- proximal polygon 417
- proximity graph 102
- PVC (Poisson Voronoi cell) 291, 293–295, 299, 306–349, 360
- PVRM (Poisson Voronoi random mosaic) 303, 304
- quadrat analysis 497, 502, 506, 526
- quadratic form distance 212
- quantization 475
- quantizing problem 517
- quantum field theory 301
- quasi-Newton method 537, 547
- quaternary incremental method 250
- quaternary initial guessing 249
- quaternary reordering 249
- quaternary tree 246
- radius function 182
- random matrix 327, 406, 408
- random matrix Voronoi diagram 327, 406, 409
- random packing 405
 complete 405
 Voronoi polygonal areal 408
- random sequential addition 405
- random sequential adsorption 405
- random set 35
- ray-shoot monotone 95
- realizability 82
- re-arrangement process 406, 407
- reciprocal farthest-pair 153
- reciprocal figure 82
- reciprocal (nearest) pair 60
- redundancy measure 503
- refinement 147, 173
- regular 295, 405
- regular point pattern 497, 498
- regular pattern 405, 408
- regular tessellation 295, 296, 299, 326, 331, 410
- relative flow velocity 204
- relative neighbour graph (RNG) 99, 522
- relatively minimal tree 571
- relocation decision 483
- relocation timing 483
- restricted area 584
- retail stores 474, 514
- retraction method 217
- Richard's method B 460
- Riemannian manifold 212
- right generator 252
- right Voronoi diagram 252
- RNG (relative neighbourhood graph) 99, 522
- robot motion planning 189, 215
- root 246
- rooted tree 246
- rotation 23, 299
- roughness 433
- saddle point problem 428
- s*-dimensional sectional Poisson Voronoi diagram 363
- s*-faces 295, 296
- s*-faces of a cell 295, 296
- second-order analysis 497, 502, 506, 526
- second-order product density 350
- sectional Poisson Voronoi diagram 363
- sectional Voronoi diagram 131, 363
- sectional Voronoi polygon 131
- selfish herd model 491
- sequential clustering process 406, 409
- service point 558
- service route 564
- set
 decomposed generator 172
 eight-neighbour 288
 four-neighbour 288
 generator 45, 113, 291, 292, 295, 374–375, 389, 404
 infinitely countable 291
 invariant 36
 starter 284
- settlement pattern 506
- shape 310, 362, 388, 390, 399, 521
 theory of 399
- shape space 399, 510
- shortest obstacle-free path 159
- shortest-path (SP) distance 159
- shortest-path Voronoi diagram 158, 161, 286
- significance level 451
- simple 32, 33, 292, 296
- simple chain 29
- simple path 29
- simple polygon 22
- simple sequential inhibition (SSI) process 405, 406
- simplex 439
 Delaunay 11, 299, 389, 390
 first-order 21
l'ensemble L de 11
m-dimensional Delaunay 56, 299, 389, 390
 second-order 21
 third-order 21
 zeroth order 21
- simplicial graph 11

- sinkholes 480
 site percolation model 302, 361
 site saturation model 357, 478
 site 45, 302, 411
 size 83, 563
 size-biased sampling 312, 339
 skeletal point 182
 skeletonization 182
 slope map 412
 smallest enclosing circle 154
 S-mosaic 303
 Sobol points 406, 409, 479
 solution-adaptive mesh 442
 solvent sheath 466
 space-time distance 212, 578, 579
 space-time Voronoi diagram 529, 579
 spanning circle
 - minimum radius 154
 - short minimum 154
 spatial autocorrelation 134
 spatial competition model 483
 spatial intensity 525
 spatial interaction 422
 spatial interpolation 151, 411
 spatial-temporal process 482
 spatial-temporal stochastic point process
 - 31
 sphere of influence 7
 spherical power (Voronoi) diagram 208
 spherical Voronoi diagram 207, 218
 spherical Voronoi polygon 207
 split 572
 spoke diagram 198
 spoke region 198
 SSI (simple sequential inhibition) 405, 406
 stable 490
 standard normal distribution 310, 356, 377
 standard position 194
 star-shaped 23, 126, 221, 384
 starter set 284
 stations 303
 stationary 34, 36, 292, 296, 299, 326, 331, 339
 stationary tessellation 297, 299, 326, 331, 339
 steepest descent method 536
 Steiner point 571
 stereohedron 7, 459
 stick figure 182
 Stienen model 360–361
 stochastic point process 31, 32, 35–36
 stochastic fibre process 41, 297
 stochastic line process 40, 388
 stochastic manifold process 41, 297
 straight line segment 18
 straight skeleton 184, 185
 strictly convex set 20
 strongly mixing 37, 299
 subgraph 25
 subtree 246
 successively inclusive hierarchy 553
 supremum 21
 supremum metric 189
 surrounding larger neighbour (SLN) 423
 swapping procedure 90, 91, 92
 sweepline 257
 Swiss cheese model 302
 symbolic perturbation 269
 symmetric axis 182
 symmetric axis transform 182
 taxi-cab distance 189
 terminal node 28
 terminal point 559
 territory 133, 581, 583
 - animal 305, 472, 480
 - village 305
 tessellation
 - homogeneous normal 366
 - m -dimensional Delaunay 56, 291, 299
 - motion invariant 299
 - normal 296, 297, 299, 326, 331, 363, 385, 410
 - planar 24, 315, 327
 - Poisson hyperplane 40
 - radical axis 187
 - regular 295, 296, 299, 326, 331, 410
 - stationary 297, 299, 326, 331, 339
 tetrahedrization
 - domain 168
 - domain Delaunay 168
 Thiessen polygon 8, 417
 thinning process 407, 408, 409
 third-order simplex 21
 threshold growth mechanism 305
 TIJ-M (time inhomogeneous J-M)
 - 376–377*Tilapia mossambica* 480
 time complexity 41
 time of complete tessellation 358, 376
 TIN (triangulated irregular network) 428
 tissue 407, 469
 topological complexity 226, 227
 topological correlation function 329
 topological event 225
 topology-oriented approach 269, 273
 torus 213, 308
 trade area 472
 transformation
 - area-preserving 34
 - inversion 76, 77
 - lift-up 68, 79, 81
 - measure-preserving 35
 - volume-preserving 34

- translation 33, 299
 transportation problem
 unconstrained 472
 traveling salesperson problem 42
 tree 29–30
 2-3 263
 AVL 263
 crown projection diagram of a 472
 Delaunay 447
 Euclidean minimum spanning 99, 450,
 522, 528
 Euclidean Steiner 572
 Euclidean Steiner minimal 571, 572
 natural 447
 quaternary 246
 relatively minimal 571
 rooted 246
 tree expansion 272
 triangle
 far-side 154
 Delaunay 55, 82, 336, 399
 near-side 77, 154
 triangle-based interpolant 427
 triangle-based method 427
 triangular method 413, 427
 triangulated irregular network (TIN) 428
 triangulation
 constrained Delaunay (CDT) 165, 441
 degenerate Delaunay 54, 267
 Delaunay 52, 54, 55, 56, 70, 77, 80, 81
 domain 167
 domain Delaunay 168, 441
 greedy 430
 lexicographically maximum 93
 locally equiangular 91
 minimax length 94, 430
 minimum energy 94
 minimum length 430
 minimum roughness 94
 minimum weight 430
 Minkowski Delaunay 193
 modifying Delaunay 434
 optimal 437
 Piteway 71
 radical axis 181
 regular 131
 trivial generalization 118
 Turning machine
 deterministic 41
 non-deterministic 41
 two-dimensional Voronoi face 50
 two-type point process 529
 typical Poisson Voronoi cell 291
 typical Voronoi cell 37, 291, 292
 unbounded 21, 58, 141, 148, 176
 unconstrained programming problem
 533, 534
 unconstrained transportation problem
 474
 undirected graph 25
 unordered product 25
 unrealizability 86
 upper bound 167, 226
 upper common support 253
 upper m -face 278
 value 411
 vertex 23, 24
 Delaunay 56, 73, 82, 301
 inner 108
 outer 108
 Voronoi 46, 49, 50, 73, 302
 V-assignment rule 115
 V-distance 118
 village boundary 474
 visibility graph 160
 visibility polygon 159
 visibility-shortest-path (VSP) distance
 163
 visibility-shortest-path Voronoi diagram
 163, 164
 visibility-shortest-path Voronoi polygon
 163
 volume-preserving 34
 volume-preserving transformation 34
 Voronoi assignment model 454
 Voronoi cell 49
 Poisson 291, 293–294, 299, 306–349,
 360, 499
 typical 291, 292
 Voronoi cover 68
 Voronoi diagram 44, 49, 291
 abstract 177
 additively weighted Poisson 376
 additively weighted 9, 123, 124, 285,
 376, 479
 additively weighted order-k 143
 anisotropic 481
 area 186, 188
 B- 196
 bounded 47, 164
 clipped 133
 closest covered set 200
 compact 198
 compact piecewise-linear 198
 compoundly weighted 127
 conic 211
 constrained 164, 286
 constrained and weighted 165
 convex distance 196, 216
 cylindrical 210, 218
 digital 51
 digitized 50, 287
 discrete 51
 discrete Manhattan 191

- dynamic (ordinary) 224, 287
 dynamic generalized 227
 dynamic k th order 227
 dynamic weighted 227, 228
 elliptic distance 196, 215
 farthest-point SP- 161
 farthest-point 151, 152
 farthest-site geodesic 163
 fitting a 581
 generalized 115, 139, 280
 generalized sectional 133
 generalized weak 115
 geodesic 161
 geodesic farthest-point 163
 Hausdorff line 203
 higher-dimensional 275
 higher-order 134, 385
 higher-order Poisson 385
 incomplete 359, 481
 infinite 45, 291, 292, 295, 297
 Karlsruhe (-metric) 202
 kinematic 224
 k th nearest-point 155, 156
 k th order 139
 Laguerre 129, 180, 185, 460
 line 170, 185, 228, 532
 Manhattan (-metric) 191, 215
 m -dimensional 65, 276, 278, 295
 m -dimensional ordinary 49
 Minkowski (-metric) 57, 193
 multiplicatively weighted 9, 120, 121, 285, 384, 460
 nearest-point 151
 nearest-site geodesic 161
 network 218
 order-2 285
 ordered order-2 145, 285
 ordered order- k 144, 146, 285, 385, 387
 order- k 135, 285, 385, 386, 387
 order- k area 187
 ordinary 43, 49, 454
 oriented 215, 218
 peeper's 164
 planar ordinary 44, 45, 48
 planar ordinary digitized 50
 Poisson 291
 polyhedral 212
 properties of 295–299
 properties of Poisson 295–300
 radical axis 181, 185
 random 296, 389, 404
 random matrix 327, 406, 409
 rectangular 194, 215
 Riemann 213
 right 252
 right triangle distance 215, 218
 s -dimensional sectional Poisson 363
 sectional 131, 363
 sectional additively weighted 133
 sectional Johnson–Mehl 133, 384
 sectional multiplicatively weighted 133
 sectional Poisson 301, 363
 shortest-path 158, 161, 286
 shortest-path multiplicatively weighted 125
 simplified 218
 solid object 188, 189
 space-time 532, 579
 spherical 207, 218
 spherical Laguerre 208
 static (ordinary) 224
 supremum-metric 191, 193
 visibility-shortest-path (VSP) 163, 164
 weighted 119, 120, 531
 weighted area 188
 weighted visibility-shortest-path 165
 Voronoi diagram based on a convex distance function 196
 Voronoi diagram bounded by S 47
 Voronoi diagram clipped to 133
 Voronoi diagram for area 186
 Voronoi diagram for lines 50, 479
 Voronoi diagram on a river 204, 205, 206, 259
 Voronoi diagram of order k 139
 Voronoi diagram on a cone 210
 Voronoi diagram on a cylinder 209, 532, 529
 Voronoi diagram on a polyhedral surface 211
 Voronoi diagram on a sphere 206, 389, 404
 Voronoi diagram with barriers 164
 Voronoi diagram with obstacles 158
 Voronoi edge 46, 50, 73
 Voronoi face 50, 64, 155
 $(m - 1)$ -dimensional 50
 $(m - 2)$ -dimensional 50
 one-dimensional 50
 two-dimensional 50
 zero-dimensional 50
 Voronoi facet 49, 50
 Voronoi fitting 581
 Voronoi foams 49
 Voronoi-G tessellation 197
 Voronoi generation assignment rule 115
 Voronoi generation distance 118
 Voronoi graph 63
 Voronoi growth model 477
 Voronoi honeycomb 9
 Voronoi line 50
 Voronoi link set 220
 Voronoi medial axis 183
 Voronoi network 46
 Voronoi node set 219

- Voronoi partition 220
Voronoi polygon 44
area of a 298, 314, 315, 319–320, 321,
342, 345, 346
boundary 47, 314
closed 46
digital 51
farthest-point 151, 152
Manhattan-metric 191
open 46
order-2 145
order- k 146
ordered order-2 136
ordered order- k 139
ordinary 44, 48
oriented 214
planar ordinary 45
power 129
sectional 131
spherical 207
visibility-shortest-path 163
Voronoi polygonal areal random packing
408
Voronoi polytope 58
Voronoi region
additively weighted 124
area 186
boundary 47
compoundly weighted 127
digitized 50
generalized 115
Karlsruhe (-metric) 202
 k th nearest-point 186
line 170, 175
multiplicatively weighted 122
weighted 120, 561
Voronoi site model 468
Voronoi skeleton 183
Voronoi surface 52
Voronoi vertex 46, 49, 50, 73, 301
Voronoi'scher Bereich 6
Wabenkarte 475
walking method 232
weakly mixing 37
Weberian problem 541
weighted area Voronoi diagram 188
weighted distance 119
weighted Voronoi diagram 119, 120, 472,
531
weighted Voronoi region 120, 561
well-behaving 117, 219, 220
Wigner–Seitz region 8
winged-edge data structure 235, 239
Wirkungsbereich 7
X-ray scattering 304
zero conjectural variation 483
zero-dimensional Voronoi face 50
zeroth order simplex 21
zone 303

WILEY SERIES IN PROBABILITY AND STATISTICS
ESTABLISHED BY WALTER A. SHEWHART AND SAMUEL S. WILKS

Editors

*Vic Barnett, Noel A. C. Cressie, Nicholas I. Fisher, Iain M. Johnstone,
J. B. Kudane, David W. Scott, Bernard W. Silverman,
Adrian F. M. Smith, Jozef L. Teugels, Ralph A. Bradley, Emeritus,
J. Stuart Hunter, Emeritus, David G. Kendall, Emeritus*

Probability and Statistics Section

- *ANDERSON · The Statistical Analysis of Time Series
ARNOLD, BALAKRISHNAN, and NAGARAJA · A First Course in Order Statistics
ARNOLD, BALAKRISHNAN, and NAGARAJA · Records
BACCELLI, COHEN, OLSDER, and QUADRAT · Synchronization and Linearity: An Algebra for Discrete Event Systems
BARNETT · Comparative Statistical Inference, *Third Edition*
BASILEVSKY · Statistical Factor Analysis and Related Methods: Theory and Applications
BERNARDO and SMITH · Bayesian Theory
BILLINGSLEY · Convergence of Probability Measures
BOROVKOV · Asymptotic Methods in Queueing Theory
BOROVKOV · Ergodicity and Stability of Stochastic Processes
BRANDT, FRANKEN, and LISEK · Stationary Stochastic Models
CAINES · Linear Stochastic Systems
CAIROLI and DALANG · Sequential Stochastic Optimization
CONSTANTINE · Combinatorial Theory and Statistical Design
COOK · Regression Graphics
COVER and THOMAS · Elements of Information Theory
CSÖRGÖ and HORVÁTH · Weighted Approximation in Probability Statistics
CSÖRGÖ and HORVÁTH · Limit Theorems in Change Point Analysis
DETTE and STUDDEN · The Theory of Canonical Moments with Applications in Statistics, Probability, and Analysis
*DOOB · Stochastic Processes
DUPUIS and ELLIS · A Weak Convergence Approach to the Theory of Large Deviations
ETHIER and KURTZ · Markov Processes: Characterization and Convergence
FELLER · An Introduction to Probability Theory and Its Applications, Volume 1, *Third Edition*, Revised; Volume II, *Second Edition*
FULLER · Introduction to Statistical Time Series, *Second Edition*
FULLER · Measurement Error Models
GHOSH, MUKHOPADHYAY, and SEN · Sequential Estimation
GIFI · Nonlinear Multivariate Analysis
GUTTORP · Statistical Inference for Branching Processes
HALL · Introduction to the Theory of Coverage Processes

*Now available in a lower priced paperback edition in the Wiley Classics Library.

Probability and Statistics Section (Continued)

- HAMEL · Robust Statistics: The Approach Based on Influence Functions
HANNAN and DEISTLER · The Statistical Theory of Linear Systems
HUBER · Robust Statistics
HUŠKOVÁ, BERAN, and DUPAČ · Collected Works of Jaroslav Hájek—With Commentary
IMAN and CONOVER · A Modern Approach to Statistics
JUREK and MASON · Operator-Limit Distributions in Probability Theory
KASS and VOS · The Geometrical Foundations of Asymptotic Inference
KAUFMAN and ROUSSEEUW · Finding Groups in Data: An Introduction to Cluster Analysis
KELLY · Probability, Statistics, and Optimization
KENDALL, BARDEN, CARNE, and LE · Shape and Shape Theory
LINDVALL · Lectures on the Coupling Method
McFADDEN · Management of Data in Clinical Trials
MANTON, WOODBURY, and TOLLEY · Statistical Applications Using Fuzzy Sets
MARDIA and JUPP · Directional Statistics
MORGENTHALER and TUKEY · Configural Polysampling: A Route to Practical Robustness
MUIRHEAD · Aspects of Multivariate Statistical Theory
OLIVER and SMITH · Influence Diagrams, Belief Nets, and Decision Analysis
*PARZEN · Modern Probability Theory and Its Applications
PRESS · Bayesian Statistics: Principles, Models, and Applications
PUKELSHEIM · Optimal Experimental Design
RAO · Asymptotic Theory of Statistical Inference
RAO · Linear Statistical Inference and Its Applications, *Second Edition*
RAO and SHANBHAG · Choquet-Deny Type Functional Equations with Applications to Stochastic Models
ROBERTSON, WRIGHT, and DYKSTRA · Order Restricted Statistical Inference
ROGERS and WILLIAMS · Diffusions, Markov Processes, and Martingales, Volume I: Foundations, *Second Edition*, Volume II: Itô Calculus
RUBINSTEIN and SHAPIRO · Discrete Event Systems: Sensitivity Analysis and Stochastic Optimization by the Score Function Method
RUZSA and SZEKELEY · Algebraic Probability Theory
SCHEFFÉ · The Analysis of Variance
SEBER · Linear Regression Analysis
SEBER · Multivariate Observations
SEBER and WILD · Nonlinear Regression
SERFLING · Approximation Theorems of Mathematical Statistics
SHORACK and WELLNER · Empirical Processes with Applications to Statistics
SMALL and MCLEISH · Hilbert Space Methods in Probability and Statistical Inference
STAPLETON · Linear Statistical Models
STAUDTE and SHEATHER · Robust Estimation and Testing
STOYANOV · Counterexamples in Probability
TANAKA · Time Series Analysis: Nonstationary and Noninvertible Distribution Theory
THOMPSON and SEBER · Adaptive Sampling
WELSH · Aspects of Statistical Inference
WHITTAKER · Graphical Models in Applied Multivariate Statistics
YANG · The Construction Theory of Denumerable Markov Processes

*Now available in a lower priced paperback edition in the Wiley Classics Library.

Applied Probability and Statistics Section

- ABRAHAM and LEDOLTER · Statistical Methods for Forecasting
AGRESTI · Analysis of Ordinal Categorical Data
AGRESTI · Categorical Data Analysis
ANDERSON, AUQUIER, HAUCH, OAKES, VANDAELE, and WEISBERG · Statistical Methods for Comparative Studies
ARMITAGE and DAVID (editors) · Advances in Biometry
*ARTHANARI and DODGE · Mathematical Programming in Statistics
ASMUSSEN · Applied Probability and Queues
*BAILEY · The Elements of Stochastic Processes with Applications to the Natural Sciences
BARNETT and LEWIS · Outliers in Statistical Data, *Third Edition*
BARTHOLOMEW, FORBES, and MCLEAN · Statistical Techniques for Manpower Planning, *Second Edition*
BATES and WATTS · Nonlinear Regression Analysis and Its Applications
BECHHOFER, SANTNER, and GOLDSMAN · Design and Analysis of Experiments for Statistical Selection, Screening, and Multiple Comparisons
BELSLEY · Conditioning Diagnostics: Collinearity and Weak Data in Regression
BELSLEY, KUH, and WELSCH · Regression Diagnostics: Identifying Influential Data and Sources of Collinearity
BHAT · Elements of Applied Stochastic Processes, *Second Edition*
BHATTACHARYA and WAYMIRE · Stochastic Processes with Applications
BIRKES and DODGE · Alternative Methods of Regression
BLISCHKE and PRABHAKAR MURTHY · Reliability: Modeling, Prediction, and Optimization
BLOOMFIELD · Fourier Analysis of Time Series: An Introduction
BOLLEN · Structural Equations with Latent Variables
BOULEAU · Numerical Methods for Stochastic Processes
BOX · Bayesian Inference in Statistical Analysis
BOX and DRAPER · Empirical Model-Building and Response Surfaces
BOX and DRAPER · Evolutionary Operation: A Statistical Method for Process Improvement
BUCKLEW · Large Deviation Techniques in Decision, Simulation, and Estimation
BUNKE and BUNKE · Nonlinear Regression, Functional Relations, and Robust Methods: Statistical Methods of Model Building
CHATTERJEE and HADI · Sensitivity Analysis in Linear Regression
CHERNICK · Bootstrap Methods: A Practitioner's Guide
CHILÈS and DELFINER · Geostatistics: Modeling Spatial Uncertainty
CHOW and LIU · Design and Analysis of Clinical Trials
CLARKE and DISNEY · Probability and Random Processes: A First Course with Applications, *Second Edition*
*COCHRAN and COX · Experimental Designs, *Second Edition*
CONOVER · Practical Nonparametric Statistics, *Second Edition*
CORNELL · Experiments with Mixtures, Designs, Models, and the Analysis of Mixture Data, *Second Edition*
*COX · Planning of Experiments
CRESSIE · Statistics for Spatial Data, *Revised Edition*
DANIEL · Applications of Statistics to Industrial Experimentation
DANIEL · Biostatistics: A Foundation for Analysis in the Health Sciences, *Sixth Edition*
DAVID · Order Statistics, *Second Edition*
*DEGROOT, FIENBERG, and KADANE · Statistics and the Law
*DODGE · Alternative Methods of Regression

*Now available in a lower priced paperback edition in the Wiley Classics Library.

Applied Probability and Statistics (Continued)

- DOWDY and WEARDEN · Statistics for Research, *Second Edition*
DRYDEN and MARDIA · Statistical Shape Analysis
DUNN and CLARK · Applied Statistics: Analysis of Variance and Regression, *Second Edition*
ELANDT-JOHNSON and JOHNSON · Survival Models and Data Analysis
EVANS, PEACOCK, and HASTINGS · Statistical Distributions, *Second Edition*
FLEISS · The Design and Analysis of Clinical Experiments
FLEISS · Statistical Methods for Rates and Proportions, *Second Edition*
FLEMING and HARRINGTON · Counting Processes and Survival Analysis
GALLANT · Nonlinear Statistical Models
GLASSERMAN and YAO · Monotone Structure in Discrete-Event Systems
GNANADESIKAN · Methods for Statistical Data Analysis of Multivariate Observations. *Second Edition*
GOLDSTEIN and LEWIS · Assessment: Problems, Development, and Statistical Issues
GREENWOOD and NIKULIN · A Guide to Chi-squared Testing
*HAHN · Statistical Models in Engineering
HAHN and MEEKER · Statistical Intervals: A Guide for Practitioners
HAND · Construction and Assessment of Classification Rules
HAND · Discrimination and Classification
HEDAYAT and SINHA · Design and Inference in Finite Population Sampling
HEIBERGER · Computation for the Analysis of Designed Experiments
HINKELMAN and KEMPTHORNE · Design and Analysis of Experiments, Volume 1: Introduction to Experimental Design
HOAGLIN, MOSTELLER, and TUKEY · Exploratory Approach to Analysis of Variance
HOAGLIN, MOSTELLER, and TUKEY · Exploring Data Tables, Trends and Shapes
HOAGLIN, MOSTELLER, and TUKEY · Understanding Robust and Exploratory Data Analysis
HOCHBERG and TAMHANE · Multiple Comparison Procedures
HOCKING · Methods and Applications of Linear Models: Regression and the Analysis of Variables
HOGG and KLUGMAN · Loss Distributions
HOLLANDER and WOLFE · Nonparametric Statistical Methods
HOSMER and LEMESHOW · Applied Logistic Regression
HØYLAND and RAUSAND · System Reliability Theory: Models and Statistical Methods
HUBERTY · Applied Discriminant Analysis
HUNT and KENNEDY · Financial Derivatives in Theory and Practice
JACKSON · A User's Guide to Principal Components
JOHN · Statistical Methods in Engineering and Quality Assurance
JOHNSON · Multivariate Statistical Simulation
JOHNSON & KOTZ · Distributions in Statistics
Continuous Multivariate Distributions
JOHNSON, KOTZ, and BALAKRISHNAN · Continuous Univariate Distributions, Volume 1, *Second Edition*
JOHNSON, KOTZ, and BALAKRISHNAN · Continuous Univariate Distributions, Volume 2, *Second Edition*
JOHNSON, KOTZ, and BALAKRISHNAN · Discrete Multivariate Distributions
JOHNSON, KOTZ, and KEMP · Univariate Discrete Distributions, *Second Edition*
JUREČKOVÁ and SEN · Robust Statistical Procedures: Asymptotics and Interrelations
KADANE · Bayesian Methods and Ethics in a Clinical Trial Design
KADANE and SCHUM · A Probabilistic Analysis of the Sacco and Vanzetti Evidence
KALBFLEISCH and PRENTICE · The Statistical Analysis of Failure Time Data

*Now available in a lower priced paperback edition in the Wiley Classics Library.

Applied Probability and Statistics (Continued)

- RYAN · Statistical Methods for Quality Improvement
SCHUSS · Theory and Applications of Stochastic Differential Equations
SCOTT · Multivariate Density Estimation: Theory, Practice, and Visualization
*SEARLE · Linear Models
SEARLE · Linear Models for Unbalanced Data
SEARLE, CASELLA, and McCULLOCH · Variance Components
STOYAN, KENDALL, and MECKE · Stochastic Geometry and Its Applications,
Second Edition
STOYAN and STOYAN · Fractals, Random Shapes, and Point Fields: Methods of
Geometrical Statistics
THOMPSON · Empirical Model Building
THOMPSON · Sampling
THOMPSON · Simulation: A Modeler's Approach
TIJMS · Stochastic Modeling and Analysis: A Computational Approach
TIJMS · Stochastic Models: An Algorithmic Approach
TITTERINGTON, SMITH, and MARKOV · Statistical Analysis of Finite Mixture
Distributions
UPTON and FINGLETON · Spatial Data Analysis by Example, Volume I: Point Pattern
and Quantitative Data
UPTON and FINGLETON · Spatial Data Analysis by Example, Volume II: Categorical and
Directional Data
VAN RIJKEVORSEL and DE LEEUW · Component and Correspondence Analysis
VIDAKOVIC · Statistical Modeling by Wavelets
WEISBERG · Applied Linear Regression, *Second Edition*
WESTFALL and YOUNG · Resampling-Based Multiple Testing: Examples and
Methods for *p*-Value Adjustment
WHITTLE · Systems in Stochastic Equilibrium
WOODING · Planning Pharmaceutical Clinical Trials: Basic Statistical Principles
WOOLSON · Statistical Methods for the Analysis of Biomedical Data
WU and HAMANDA · Experiments: Planning, Analysis, and Parameter Design
Optimization
*ZEELNER · An Introduction to Bayesian Inference in Econometrics

Texts and References Section

- AGRESTI · An Introduction to Categorical Data Analysis
ANDERSON · An Introduction to Multivariate Statistical Analysis, *Second Edition*
ANDERSON and LOYNES · The Teaching of Practical Statistics
ARMITAGE and COLTON · Encyclopedia of Biostatistics. 6 Volume set
BARTOSZYNSKI and NIEWIADOMSKA-BUGAJ · Probability and Statistical Inference
BENDAT and PIERSOL · Random Data: Analysis and Measurement Procedures, *Third
Edition*
BERRY, CHALONER, and GEWEKE · Bayesian Analysis in Statistics and
Econometrics: Essays in Honor of Arnold Zellner
BHATTACHARYA and JOHNSON · Statistical Concepts and Methods
BILLINGSLEY · Probability and Measure, *Second Edition*
BOX · R. A. Fisher, the Life of a Scientist
BOX, HUNTER, and HUNTER · Statistics for Experimenters: An Introduction to
Design, Data Analysis, and Model Building
BOX and LUCEÑO · Statistical Control by Monitoring and Feedback Adjustment

*Now available in a lower priced paperback edition in the Wiley Classics Library.

Texts and References Section (Continued)

- BROWN and HOLLANDER · Statistics: A Biomedical Introduction
CHATTERJEE and PRICE · Regression Analysis by Example, *Second Edition*
COOK and WEISBERG · An Introduction to Regression Graphics
COOK and WEISBERG · Applied Regression Including Computing and Graphics
COX · A Handbook of Introductory Statistical Methods
DILLON and GOLDSTEIN · Multivariate Analysis: Methods and Applications
DODGE and ROMIG · Sampling Inspection Tables, *Second Edition*
DRAPER and SMITH · Applied Regression Analysis, *Third Edition*
DUDEWICZ and MISHRA · Modern Mathematical Statistics
DUNN · Basic Statistics: A Primer for the Biomedical Sciences, *Second Edition*
FISHER and VAN BELLE · Biostatistics: A Methodology for the Health Sciences
FREEMAN and SMITH · Aspects of Uncertainty: A Tribute to D. V. Lindley
GROSS and HARRIS · Fundamentals of Queueing Theory, *Third Edition*
HALD · A History of Probability and Statistics and their Applications Before 1750
HALD · A History of Mathematical Statistics from 1750 to 1930
HELLER · MACSYMA for Statisticians
HOEL · Introduction to Mathematical Statistics, *Fifth Edition*
HOLLANDER and WOLFE · Nonparametric Statistical Methods, *Second Edition*
HOSMER and LEMESHOW · Applied Survival Analysis: Regression Modeling of Time to Event Data
JOHNSON and BALAKRISHNAN · Advances in the Theory and Practice of Statistics: A Volume in Honor of Samuel Kotz
JOHNSON and KOTZ (editors) · Leading Personalities in Statistical Sciences: From the Seventeenth Century to the Present
JUDGE, GRIFFITHS, HILL, LÜTKEPOHL, and LEE · The Theory and Practice of Econometrics, *Second Edition*
KHURI · Advanced Calculus with Applications in Statistics
KOTZ and JOHNSON (editors) · Encyclopedia of Statistical Sciences. Volumes 1 to 9 with Index
KOTZ and JOHNSON (editors) · Encyclopedia of Statistical Sciences: Supplement Volume
KOTZ, REED, and BANKS (editors) · Encyclopedia of Statistical Sciences: Update Volume 1
KOTZ, REED, and BANKS (editors) · Encyclopedia of Statistical Sciences: Update Volume 2
LAMPERTI · Probability: A Survey of the Mathematical Theory, *Second Edition*
LARSON · Introduction to Probability Theory and Statistical Inference, *Third Edition*
LE · Applied Categorical Data Analysis
LE · Applied Survival Analysis
MALLOWS · Design, Data, and Analysis by Some Friends of Cuthbert Daniel
MARDIA · The Art of Statistical Science: A Tribute to G. S. Watson
MASON, GUNST, and HESS · Statistical Design and Analysis of Experiments with Applications to Engineering and Science
MURRAY · X-STAT 2.0 Statistical Experimentation, Design Data Analysis, and Nonlinear Optimization
PURI, VILAPLANA, and WERTZ · New Perspectives in Theoretical and Applied Statistics
RENCHER · Methods of Multivariate Analysis
RENCHER · Multivariate Statistical Inference with Applications
ROSS · Introduction to Probability and Statistics for Engineers and Scientists
ROHATGI · An Introduction to Probability Theory and Mathematical Statistics
RYAN · Modern Regression Methods

*Now available in a lower priced paperback edition in the Wiley Classics Library.

Texts and References Section (Continued)

- SCHOTT · Matrix Analysis for Statistics
SEARLE · Matrix Algebra Useful for Statistics
STYAN · The Collected Papers of T. W. Anderson: 1943–1985
TIERNEY · LISP-STAT: An Object-Oriented Environment for Statistical Computing and Dynamic Graphics
WONNACOTT and WONNACOTT · Econometrics, *Second Edition*

WILEY SERIES IN PROBABILITY AND STATISTICS

ESTABLISHED BY WALTER A. SHEWHART AND SAMUEL S. WILKS

Editors

*Robert M. Groves, Graham Kalton, J. N. K. Rao, Norbert Schwarz,
Christopher Skinner*

Survey Methodology Section

BIEMER, GROVES, LYBERG, MATHIOWETZ, and SUDMAN · Measurement Errors in Surveys

COCHRAN · Sampling Techniques, *Third Edition*

COUPER, BAKER, BETHLEHEM, CLARK, MARTIN, NICHOLLS and O'REILLY (editors) · Computer Assisted Survey Information Collection

COX, BINDER, CHINNAPPA, CHRISTIANSON, COLLEDGE, and KOTT (editors) · Business Survey Methods

*DEMING · Sample Design in Business Research

DILLMAN · Mail and Telephone Surveys: The Total Design Method

GROVES · Survey Errors and Survey Costs

GROVES and COUPER · Nonresponse in Household Interview Surveys

GROVES, BIEMER, LYBERG, MASSEY, NICHOLLS, and WAKSBERG · Telephone Survey Methodology

*HANSEN, HURWITZ, and MADOW · Sample Survey Methods and Theory, Volume I: Methods and Applications

*HANSEN, HURWITZ, and MADOW · Sample Survey Methods and Theory, Volume II: Theory

KASPRZYK, DUNCAN, KALTON, and SINGH · Panel Surveys

KISH · Statistical Design for Research

*KISH · Survey Sampling

LESSLER and KALSBECK · Nonsampling Error in Surveys

LEVY and LEMESHOW · Sampling of Populations: Methods and Applications

LYBERG, BIEMER, COLLINS, de LEEUW, DIPPO, SCHWARZ, TREWIN (editors) · Survey Measurement and Process Quality

SIRKEN, HERRMANN, SCHECHTER, SCHWARZ, TANUR and TOURNANGEAU (editors) · Cognition and Survey Research

SKINNER, HOLT and SMITH · Analysis of Complex Surveys

*Now available in a lower priced paperback edition in the Wiley Classics Library.



9 780471 986355